



NAPLES Hotel Royal Continental

9 > 11 December, 2019

EUROPEAN FUEL CELL

CONFERENCE & EXHIBITION



Proceedings

of the 8th European Fuel Cell
Piero Lunghi Conference



ATENA
FUTURE TECHNOLOGY

ENEA

Agenzia nazionale per le nuove tecnologie,
l'energia e lo sviluppo economico sostenibile



UNIVERSITÀ
DEGLI STUDI
DI NAPOLI
"PARTHENOPE"



UNIVERSITÀ
DEGLI STUDI
DI PERUGIA



**EUROPEAN
FUEL CELL**
CONFERENCE & EXHIBITION

EFC 19 Proceedings

OF THE 8TH EUROPEAN FUEL CELL PIERO LUNGI CONFERENCE

To Piero Lunghi. We miss you a lot. To you our gratitude for ever.

This book is dedicated to the memory of Piero Lunghi, creator of the European Fuel Cell Technology and Applications Conference, dear friend and colleague, who prematurely passed away in a car accident on damned November 9, 2007.

Piero made significant contributions in the field of fuel cells in the course of his too short career. He was the leading figure in the formation of the fuel cell research group at the University of Perugia and several activities and research projects initiated by him are still ongoing. This means that, thanks to Piero, many young people are working in this exciting research field and are coming to Naples to present their results. Therefore, Piero's memory is in the conference name but Piero's contribution is still in the contents of this book.

The memory of our friend Piero, his great personal generosity and energy, survives in our hearts, his contribution and his tenacity survive in the work of young people who carry on his vision throughout the world.

Give them your passion, your strength, and make all necessary effort to realize them. There is no greater satisfaction than seeing one's ideas become reality and become part of the future of our world. Piero strongly desired this, and constantly followed this through with conviction, passion and dedication.

For a better future, we need young researchers of this kind.



EUROPEAN FUEL CELL

CONFERENCE & EXHIBITION

NAPLES Hotel Royal Continental

9 > 11 December, 2019

edited by
Viviana Cigolotti

2019

ENEA

ITALIAN NATIONAL AGENCY FOR NEW TECHNOLOGIES, ENERGY
AND SUSTAINABLE ECONOMIC DEVELOPMENT

Lungotevere Thaon di Revel, 76 / 00196 / Rome

ISBN 978-88-8286-386-9



ATENA
FUTURE TECHNOLOGY

ENEA

Agenzia nazionale per le nuove tecnologie,
l'energia e lo sviluppo economico sostenibile



UNIVERSITÀ
DEGLI STUDI
DI NAPOLI
"PARTHENOPE"



UNIVERSITÀ
DEGLI STUDI
DI PERUGIA

Supporting Institutions



EFC19 Special Issue



AppliedEnergy

Authors of selected extended abstracts will be invited to submit a full paper for publication within the special issues of the International Journal of Hydrogen Energy and Applied Energy fully dedicated to EFC15



EUROPEAN FUEL CELL

CONFERENCE & EXHIBITION

Organizers



**Angelo
Moreno**

CHAIRMAN
ATENA Scarl - Italy



**Viviana
Cigolotti**

SCIENTIFIC PROGRAM MANAGER
ENEA - Italy



**Stephen
McPhail**

ENEA - Italy



**Elio
Jannelli**

Dept. of Engineering
University of Naples "Parthenope"
ATENA Scarl Italy



**Ludovica
Cosentino**

ATENA Scarl Italy



**Adele
Pianese**

University of Naples "Parthenope"

Committee

INTERNATIONAL ADVISORY BOARD

Australia Andrew Dicks **Austria** Günter R. Simader, Austrian Energy Agency **Brasil** Paulo Emilio Valadao de Miranda, Universidade Federal do Rio de Janeiro **China** Min-Fang Han, China University of Mining and Technology (CUMT) **Finland** Jari Kiviaho, VTT Technical Research Center of Finland **France** Laurent Antoni, CEA, President of the New European Research Grouping on fuel cells and Hydrogen **Germany** Detlef Stolten, Forschungszentrum Jülich GmbH **Greece** Tsiakaras Panagiotis, University of Thessaly **India** Onkar Nath Srivastava, Banaras Hindu University **Italy** Aristide Massardo / Università degli Studi di Genova, Alberto Ravagni / SOLIDPower Spa, Alberto Dossi / H2IT, Marcello Capra / Ministero dello Sviluppo Economico **Japan** Kenchiro Ota, Yokohama National University **Poland** Jakub Kupecki, Institute of Power Engineering - IPE **Spain** Emilio Nieto Gallego, Centro Nacional del Hidrógeno (CNH2) **South Africa** Dmitri G Bessarabov / North-West University, Vladimir M Linkov / University of the Western Cape **South Korea** Tae-Hoon Lim / Korea Institute of Science & Technology (KIST), Jonghee Han / Korea Institute of Science & Technology (KIST) **Turkey** Atilla Ersoz / TUBITAK Marmara Research Center, Isil Isik Gulsac / TUBITAK Marmara Research Center

SCIENTIFIC COMMITTEE

Bulgaria Daria Vladikova / Institute of Electrochemistry and Ebergy Systems - IEES **Czech Republic** Karel Bouzek / University of Chemistry and technology **Finland** Olli Himanen / Technical Research Center of Finland (VTT) **France** Michel Cassir / Chimie Paris Tech (ENSCP) **Germany** Ludger Blum / Forschungszentrum Jülich (FZJ), Ludwig Jörissen / ZSW, Olaf Jedicke / KIT, Can Samsun / Forschungszentrum Jülich (FZJ), Thanos Stubos / NCSR **Italy** Mauro Scagliotti / RSE Spa, Stefano Ubertini / Università della Toscana, Marcello Baricco / Università di Torino, Luigi Crema / Fondazione Bruno Kessler, Mariagiovanna Minutillo / Università di Napoli "Parthenope", Alessandra Perna / Università degli Studi di Cassino, Umberto Desideri / Università degli Studi di Pisa, Angelo Basile / CNR - ITM, Vincenzo Palma / Università degli Studi di Salerno, Barbara Bosio / University of Genoa, Rodolfo Taccani / University of Trieste, Pierluigi Leone / Polytechnic of Turin, Nicola Massarotti / University of Naples Parthenope, Andrea Casalegno / Polytechnic of Milan, Massimo Santarelli / Polytechnic of Turin, Domenico Borello / Università di Roma "La Sapienza", Linda Barelli / Università degli Studi di Perugia, Marcello Romagnoli / Università di Modena e Reggio Emilia, Vincenzo Antonucci / CNR ITAE, Giuseppe Spazzafumo / Università degli Studi di Cassino, Pierangela Cristiani / RSE - Ricerca sul Sistema Energetico S.P.A., Antonino Aricò / CNR ITAE, Gaetano Squadrito / CNR ITAE **Japan** Koichi Eguchi / Kyoto University, Hiroyuki Uchida / University of Yamanashi **Netherlands** Kas Hemmes / Delft University of Technology - TU Delft, P.V. Aravind / TU Delft **Poland** Marcin Bresznowski / Institute of Power Engineering - IPE **Portugal** Carmen Rangel / LNEG - National Laboratory of Energy and Geology **South Korea** Jaeyoung Lee / GIST **Spain** Javier Brey Sanchez / H2B2, David Sanchez / University of Sevilla, Justo Lobato Bajo / University of Castilla-La Mancha **Sweden** Bin Zhu / Royal Institute of Technology, Martin Andersson / Lund University, Carina Lagergren / KTH, **Switzerland** Olivier Bucheli / Solid Power **Turkey** Fehmi Akgun / TUBITAK Marmara Research Center, Cigdem Karadag / TUBITAK Marmara Research Center **USA** Whitney Colella / Gaia Energy Research Institute

Exhibitors

Fiaxell

SOFC Technologies™

Fiaxell SOFC Technologies

Located in the Science Park of the Swiss federal institute of technology (EPFL) in Lausanne, Fiaxell is manufacturing components for SOFC and SOEC research such as the Open Flanges test Set-Up™, short stack, gold, crofer 22H and nickel M_Grid™, Cell-Connex™ for current collection and gas diffusion. We are also retailer for H2 generator, potentiostat/galvanostat/EIS analyzer and mass flow controller.

For more info, please consult : fiaxell.com



thasar

Technology is our playground

Thasar

Independent Italian distributor of high performance research solutions for electrochemistry, materials and renewable energy applications.

Our customers include researchers and manufacturers in applications such as sensors, corrosion, coatings, catalysts, fuel cells, batteries and super capacitors.

We offer a wide range of laboratory and portable potentiostats and EIS / impedance solutions: femtoamps to over 120 Amps, single channel to 256+ channel systems, including fuel cells, fuel cell test systems (FCTS), membrane test systems, electronic loads, test jigs, materials and accessories.

For more info, please consult : thasar.com

Main Sponsor



Leading the way
to greener and
smarter mobility,
worldwide



Alstom - Mobility by Nature

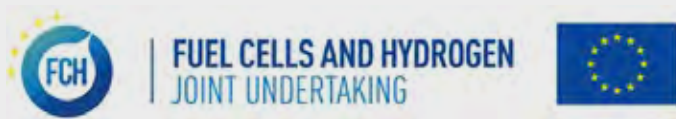
Leading the way to greener and smarter mobility worldwide, Alstom develops and markets integrated systems that provide the sustainable foundations for the future of transportation. Alstom offers a complete range of equipment and services, from high-speed trains, metros, trams and e-buses to integrated systems, customised services, infrastructure, signalling and digital mobility solutions. Alstom recorded sales of €8.1 billion and booked orders of €12.1 billion in the 2018/19 fiscal year.

Headquartered in France, Alstom is present in over 60 countries and employs 36,300 people.

Deeply rooted in the Italian railway tradition, Alstom in Italy has been manufacturing trains for 160 years, signalling equipment for 90 years and traction systems for 60 years. Today, with 8 sites throughout Italy and 3000 employees, Alstom is a strong local employer recognised as one of the leaders on the Italian market.

For more info, please consult : alstom.com

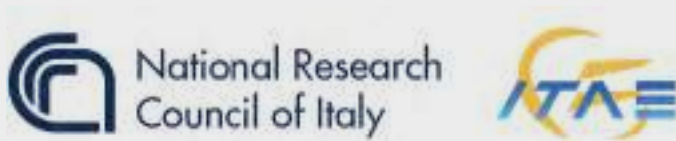
Sponsors



FCH JU – Fuel Cells and Hydrogen Joint Undertaking

The Fuel Cells and Hydrogen Joint Undertaking (FCH JU) is a unique public private partnership supporting research, technological development and demonstration (RTD) activities in fuel cell and hydrogen energy technologies in Europe. Its aim is to accelerate the market introduction of these technologies, realising their potential as an instrument in achieving a carbon-clean energy system. Fuel cells, as an efficient conversion technology, and hydrogen, as a clean energy carrier, have a great potential to help fight carbon dioxide emissions, to reduce dependence on hydrocarbons and to contribute to economic growth. The objective of the FCH JU is to bring these benefits to Europeans through a concentrated effort from all sectors. The three members of the FCH JU are the European Commission, fuel cell and hydrogen industries represented by Hydrogen Europe and the research community represented by Hydrogen Europe Research.

For more info, please consult : fch.europa.eu



ITAE

ITAE develops and promotes innovative energy technologies able to conjugate the deep knowledge on electrochemical, catalytic and adsorption processes with the ability to design materials, components and energy systems. The energy technologies based on renewable sources play a central role in the novel energy system scenario, in which the distributed generation will be supported by actions towards the improvement of energy efficiency, also exploiting synergies with the information and telecommunication technologies (ITC). The novel ITAE research topics are part of this new framework, which includes current needs for a sustainable development. Accordingly, the “Energetic Sustainability” represents the common target of all the different research areas of the institute: **1.** Technologies for storage and conversion of renewable thermal energy **2.** Sustainable technologies for production and storage of electrical energy **3.** Technologies for hydrogen production and storage, eco-friendly energy vectors and CO2 recycling **4.** Integrated systems and technologies application for energy efficiency – Smart Energy Technologies **5.** Socio-economic and environmental impact of energy technologies.



HySchool - Hydrogen teaching resources made for teachers, by teachers

The Hydrogen In Schools (HySchools) project is an Erasmus+ project that aims to deliver hydrogen education in schools. Educational and online resources have been created for use in secondary schools across the European partner countries, aimed at providing teachers with increased confidence to teach students about Hydrogen Fuel Cell Technology (HFCT).

HySchools aims to help schools enhance the quality of HFCT teaching to equip students with the future skills required by this growing sector.

For more info, please consult : hyschools.eu



EUROPEAN FUEL CELL

CONFERENCE & EXHIBITION

NAPLES Hotel Royal Continental

9 > 11 December, 2019

Proceedings



ATENA
FUTURE TECHNOLOGY



Agenzia nazionale per le nuove tecnologie,
l'energia e lo sviluppo economico sostenibile



UNIVERSITÀ
DEGLI STUDI
DI NAPOLI
"PARTHENOPE"



UNIVERSITÀ
DEGLI STUDI
DI PERUGIA

DESIGN AND DEVELOPMENT OF A H₂ PRODUCTION SYSTEM BASED ON SOLID OXIDE ELECTROLYSIS TECHNOLOGY

David Abad*, José María Olavarrieta*, Emilio Nieto*, Fernando Vega **, Benito Navarrete**, Francesca Ferrara***

*National Hydrogen Center, Puertollano (Ciudad Real), Spain

**Chemical and Environmental Engineering Department, School of Engineering, University of Seville, (Seville), Spain

*** Sotacarbo SpA, Grande Miniera di Serbariu, Carbonia, Italy

Abstract - The scope of this work extends to the design and development of a H₂ pilot plant which is coupled to a Power to Liquid system to produce clean fuels. This facility involves the BoP and its integration with the SOEC stack. Technical specifications must be based on parameters such as a SOEC power of 1000 W, high operating temperature (above 800°C) and the ability to reach high pressures.

Increasing pressure from atmospheric levels to 60bar_g represents the biggest challenge from the BoP engineering point of view. SOEC stacks operate optimally under atmospheric pressure. At the same time, specific pressure conditions must be obtained at the outlet of the system.

For this purpose, detailed engineering has been developed, including mass and energy balances, PFD diagram and 3D construction drawing.

Index Terms – hydrogen production, solid oxide electrolysis system, high temperature electrolyzer, test bench.

I. NOMENCLATURE

BoP: Balance of plant

SOEC: Solid oxide electrolysis cells

PFD: Process and flow diagram

II. INTRODUCTION

SOEC is the most promising solution for efficient and cost-effective H₂ production and storage/re-use. This technology demands heat and electricity, and offers the possibility to work in a reversible way and in CO-electrolysis mode [1].

Most of SOEC development efforts are focused on finding optimal materials to avoid thermal degradation and on developing predictive mathematical models of their

performance. Nevertheless, few studies are concentrating on improving the integration of the stack within the BoP.

III. METHODS

A. Pilot plant technical requirements

The pilot plant designed aims at H₂ by using SOEC (non-mature technology) with specific outlet conditions for coupling to a methanol synthesis reactor, such as: gas pressure of 30 bar_g, ambient temperature and completely dry and constant H₂ gas flow up to 0,5 NI/min. In addition, the pilot plant must be able to self-supply the H₂ produced for the correct operation of the stack. Being a wheeled structure, it can be moved for the H₂ to be used in other applications in different laboratories.

B. Design considerations [2], [3]

- SOEC technology must work at high temperature, and the gas flow speed must be low enough so that the residence time in the piping gets extended. The motivation is not only to increase the temperature before and during the stage of H₂ production, but also at the stage of cooling down and drying the gas when it leaves the electrolyzer.

- Due to the high operating temperature, it is not feasible to work in repeated start/stop cycles, so the plant must work continuously for at least a long period of time and be able to store enough H₂ so as to make the electrolysis system independent of the methanol synthesis system.

- Air is used as sweep gas and as a thermal manager. An operation in approximately thermo-neutral regime is expected.

- H₂ outlet has very high temperature and humidity ratio, so appropriate devices to cooling down and drying must be implemented.

- H₂ leaves the stack around atmospheric pressure and low gas flow. According to the technical requirements, the final pressure must reach at least 30 bar_g, so compression stages must be included. It should be noted that, commercial H₂ compressors capable of reaching this pressure need to start operating from 1 bar_g, so an

additional compression step (pump) must be provided. H₂ is then stored at 60 bar_g to increase storage.

After considering the above, the conceptual, basic and detailed engineering was carried out, obtaining the following results.

IV. RESULTS

C. Pilot plant description

Figure 1, Table 1 and Table 2 shows a flow and process diagram (PFD), main equipment and main technical specifications of stack, respectively.

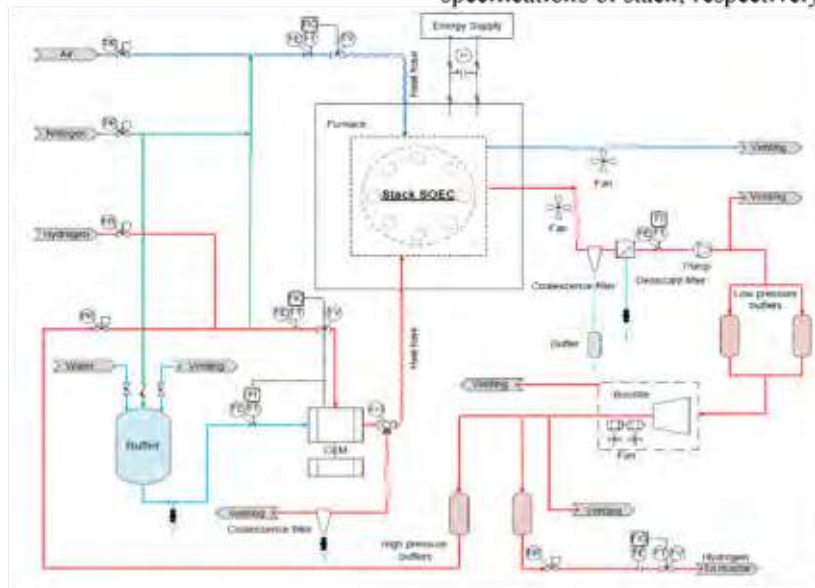


Fig. 1. SOEC system PFD

TABLE I. MAIN EQUIPMENTS

CEM (Controller Evaporator Mixer)	SOEC stack
Furnace	Three buffers (one deionized water and two H ₂ gas)
Pump	Electrical Booster
Heat exchangers with fan	Coalescence and desiccant filters

TABLE II. MAIN OPERATIONAL CONDITIONS INVOLVED IN STACK

	H ₂ /steam inlet	Air inlet	H ₂ outlet	Oxygen outlet	
Gas flow	10 – 12	20 – 30	10 – 12	5 – 6	
Pressure	0,5 – 1	0,5 – 1	0,5 – 1	0,5 – 1	
Temperature	100 – 120	20 – 25	800 – 900	800 – 900	
Expected cell voltage	~1,2	Nominal current density	0,5	Temperature	800
Power	~ 870	Pressure	atmospheric		

D. Pilot plant 3D design

A 3D design of the SOEC electrolyzer system has been developed as a template used for the definitive configuration of the plant.

IV. UNITS

Gas flow	Nl/min	Voltage	V
Working gas pressure	bar _g	Current density	A/cm ²
Working gas temperature	°C	Power	W

V. CONCLUSIONS

CNH₂ is able to design different SOEC system, in order to meet multiple requirements and operating conditions of each of the devices, so they can work as a part of a larger system.

REFERENCES

- [1] M. Preininger, J. Wurm, V. Subotić, R. Schauerpl, and C. Hochenaucr, "Performance characterization of a solid oxide cell stack with chromium-based interconnects (CFY)," *Int. J. H₂ Energy*, vol. 42, no. 48, pp. 28653–28664, 2017.
- [2] A. Electrolyser, H. Production, and R. E. Sources, "Specification and preliminary design of demonstrator," no. 256755, 2014.
- [3] J. E. O'Brien, X. Zhang, G. K. Housley, K. Dewall, L. Moore-McAteer, and G. Tao, "High Temperature Electrolysis Pressurized Experiment Design, Operation and Results" Idaho National Laboratory. September, p. 15, 2012.

A REDUCED ORDER MODEL OF PROTON CONDUCTING SOLID OXIDE FUEL CELL: A PROPOSAL

J. Milewski

Faculty of Power and Aeronautical Engineering, Warsaw University
 of Technology, Institute of Heat Engineering, 21/25 Nowowiejska
 Street, Warsaw (Poland)

Abstract - This paper presents a mathematical model of the Proton Conducting Solid Oxide Fuel Cell (H⁺SOFC), proposing a new approach for modeling the voltage of H⁺SOFC. Electrochemical, thermal, electrical and flow parameters are collected in an 0-D mathematical model. The aim is to combine all cell working conditions in as a low number of factors as possible and to have the factors relatively easy to determine. A validation process for various experimental data was carried out and the results are shown. The model was validated for various fuel mixtures across relatively wide ranges of parameters. A distinction is made between design-point and off-design operation.

Index Terms - Fuel cells; Proton-conducting SOFC; Numerical modeling.

I. INTRODUCTION

Mathematical modeling is now the basic method for analyzing fuel cells [1] and most often a zero-dimensional approach is used for modeling the H⁺SOFC. Generally speaking, H⁺SOFC working principles are based on partial hydrogen pressure differences between the anode and cathode side (see Fig. 1), which forces protons to pass from the anode side to the cathode. Hydrogen partial pressure on the cathode side must be very low (10⁻²⁰ MPa) to obtain practical voltage values with a single cell, which can be achieved through the oxidization of fuel on the cathode side.

The main processes occurring during H⁺SOFC operation and indicated in Fig. 1 can be described by adequate flows of ions and electrons, which gives an adequate equivalent electric circuit of the fuel cell see Fig. 2. The current i_1 indicates total flow of electrons transported by solid electrolyte (H⁺), then the electrons are divided into two circuits, the electrons which pass through the electrolyte layer in the same direction as the protons (see Fig. 2) due to the presence of electronic conductivity. The detailed description about the used set of equations can be found in our

previous works [1, 2]. By solving them, an equation for cell voltage is obtained:

$$E_{H^+SOFC} = \frac{E_{\max} - \eta \cdot i_{\max} \cdot r_1}{\frac{r_1}{r_2} \cdot (1 - \eta) + 1} \quad (1)$$

The meaning of the used variables are also included in the other publications as well as the detailed explanation of them.

For proton conducting solid oxide fuel cells, the general form of Nernst's equation is used to estimate the maximum voltage of H⁺SOFC.

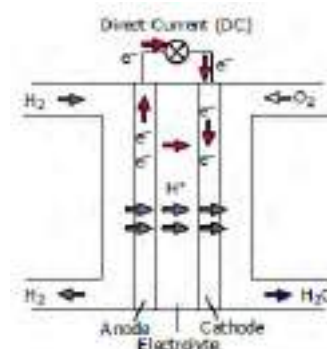


Figure 1: Working principles of Proton Conducting Solid Oxide Fuel Cell

The way to calculate the partial pressure especially at cathode is also explained in our works about oxygen conducting SOFCs. Based on the researchers' own calculations, which were based on data taken from [3] i_{\max} of 3.18 A/cm² was determined.

The generation of water vapor on the cathode side increases the hydrogen partial pressure. Therefore, overall system efficiency increases with respect to the classical SOFC. The main advantage of electrolyte made with proton-conducting material is the high ionic conductivity at an intermediate range

of temperatures (sufficient performances are reported in the literature at 600 .. 700°C [4]). The most popular type of material for solid state proton conductors are perovskite-type oxides structures which, in the presence of a wet atmosphere and elevated temperatures, exhibit high protonic conductivity [5]. Total protonic resistance of the cell is a function of many parameters. The H⁺SOFC consists of electrolyte sandwiched between anode and cathode layers. Those layers influence protonic conductivity as well (e.g., triple boundary phase processes). The material used, porosity and design of the electrodes affect fuel cell voltage significantly. Additionally, both electrolyte and electrodes can be built as multi-layers. Based on data gathered by the authors from [3], adequate factors were obtained, as shown in Fig. 3.

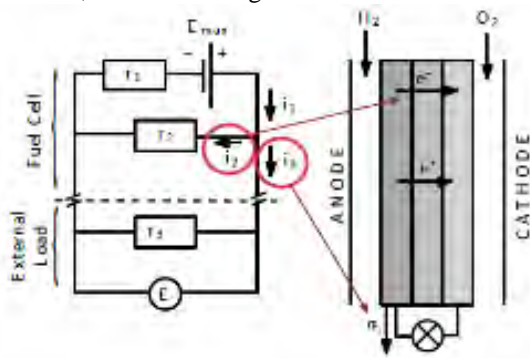


Figure 2: Equivalent electric circuit of a Proton Conducting Solid Oxide Fuel Cell

II. CONCLUSIONS

The present study shows the Reduced Order model of a proton conducting solid oxide fuel cell. Based on our experience of using this way of describing electrochemical devices, we built a model which rivals the classic way of modeling H⁺SOFC. Our model was validated based on two different sets of experimental data, giving acceptable coherence. The model is based on a combination of electric laws, gas flow relationships, solid materials properties and electrochemical correlations.

The paper describes clearly how the model was obtained and provides all details required to understand its validity. The model contains only physically explained parameters (with the minimum number of required factors possible) and takes into account all important thermal flow as well as architecture parameters.

The presented model is very stable and can be used for both simulations and H⁺SOFC system optimization procedures during which both material and thermal flow parameters are changed. The parameters can be changed across the whole, practically achieved range, which is in stark contrast to models based on the Butler Volmer and diffusion equations (they are very sensitive to input parameters and very often generate non physical results).

The proposed model was validated for various temperatures, fuel mixtures and oxidant mixtures across relatively wide ranges.

Based on the presented equations, a fuel cell model was created and compared against experimental data.

A separation is made between the design-point and o -design operation modes (by using the factor of maximum current density). The design point model can be used to select fuel cell size according to other system elements (gas turbine, heat exchangers, etc.). In those situations, a fuel/oxidant utilization factor is equivalent to current density and the cell characteristics can be drawn as a voltage fuel/oxidant utilization factor curve instead of a voltage current density curve (which is correlated to o -design operation). For instance, the parameter i_{max} for data taken from [6] is 4.88 A/cm² and regards the amount of oxygen delivered (hydrogen is not a limiting factor here). The same factor for data given by [3] is 2.75 A/cm² (also for oxidant electrode). Thus, the second fuel cell is not ten times worse, as can be read just from current density, but only partially due to the fact that less oxidant and fuel are delivered. In actual fact, the fuel cell used by [3] has a maximum efficiency of 3.32% whereas [6] is slightly better at 4.14%.

Not all of the model parameters are estimated in depth: further work is required and will be done (e.g., area specified internal electronic resistance, the influence of layer porosity, etc.).

It should be underlined that the proposed model is very light and serviceable for system level performance prediction, but may be less reliable for detailed H⁺SOFC prediction or cell optimization.

REFERENCES

- [1] J. Milewski, K. Świrski, M. Santarelli, P. Leone, Advanced Methods of Solid Oxide Fuel Cell Modeling, 1st Edition, Springer-Verlag London Ltd., 2011.
- [2] J. Milewski, M. Wołowicz, A. Miller, R. Bernat, A reduced order model of molten carbonate fuel cell: A proposal, International Journal of Hydrogen Energy 38 (26) (2013) 11565 – 11575.
- [3] G. Taillades, J. Dailly, M. Taillades-Jacquín, F. Mauvy, A. Essouhmi, M. Marrony, C. Lalanne, S. Fourcade, D. Jones, J.-C. Grenier, et al., Intermediate temperature anodesupported fuel cell based on base0. 9y0. 1o3 electrolyte with novel pr2nio4 cathode, Fuel Cells 10 (1) (2010) 166–173.
- [4] F. Lefebvre-Joud, G. Gauthier, J. Mougín, Current status of proton-conducting solid oxide fuel cells development, J Appl Electrochem 39 (2009) 535–543.
- [5] R. Hariharan, T. Prasanna, P. Gopalan, Novel perovskite based proton conductor for solid oxide fuel cells, Scripta Materialia 66 (2012) 658–661.
- [6] A. Zhu, G. Zhang, T. Wan, T. Shi, H. Wang, M. Wu, C. Wang, S. Huang, Y. Guo, H. Yu, et al., Evaluation of srsc0. 175nb0. 025co0. 8o3-δ perovskite as a cathode for proton conducting solid oxide fuel cells: The possibility of in situ creating protonic conductivity and electrochemical performance, Electrochimica Acta 259 (2018) 559–565.

INTEGRATION OF A SOLID OXIDE FUEL CELL FOR THE SUSTAINABLE POWER GENERATION FROM WASTES IN A WINERY INDUSTRY

Rubén Beneito*, Daniel Vilaplana*, Juan Antonio Micó*, and
Joaquín Juan*

*Asociación de Investigación de la Industria del juguete, conexas y
afines (AIJU), Avenida de la industria 23, 03440 Ibi (Alicante),
(Spain)

Abstract - In the framework of the LIFE ECOELECTRICITY project (LIFE15 CCM/ES/000080), a Solid Oxide Fuel Cell (SOFC) has been evaluated for the sustainable production of power to be used in an alcohol treatment company. This project consists on the optimization of a pilot plant operating with reforming gas to produce 3 kW of net electricity for both, to partially supply the energy demand of the garage of the company, as well as for recharging the batteries of a cleaning vehicle used at the company facilities.

The reforming gas fed in the SOFC is produced in a previous stage by using alcoholic wastes with very low commercial value. As by-products, the SOFC only generates heat in the form of hot streams at the outlet of the cathode and anode, which are addressed to the reforming process to provide it with the thermal energy that it needs. In this work, the SOFC was first operated with synthetic gas mimicking the composition of hydrogen in the reforming gas to define the operation methodology and the control system for the correct, reliable and safety functioning of the SOFC. Afterwards, the SOFC was run with the reforming gas to optimize the power production process in the temperature region between 600-700 °C.

Index Terms – Alcoholic waste treatment, Solid Oxide Fuel Cell (SOFC), sustainable production of energy.

I. INTRODUCTION

Hydrogen production is currently based on methane and/or oil reforming processes (78%) and coal gasification (18%) and, thus, hydrogen used in energy purposes mainly comes from non-renewable sources [1-2]. Motivated by the transition towards a more sustainable production and consumption, it would be advantageous to increase hydrogen supply from low-carbon footprint materials, such as residual biomass. In that sense, distilleries and

winery industries generate ethanolic waste streams with low added value that could be exploited as sources of hydrogen for subsequent sustainable energy generation.

LIFE ECOELECTRICITY project (LIFE15 CCM/ES/000080) arises with the challenge of designing, assembling and optimizing a pilot plant in which ethanolic wastes from industrial streams are upgraded by catalytic reforming into hydrogen-enriched gas that then feeds a 3-kW SOFC to produce electricity and heat.

In order to achieve an energy production process as much efficient as possible, the pilot plant is formed by heat exchangers situated at the hotbox outlet. The recirculation gases will allow the reduction of electrical consumption of the heaters located at the hotbox inlet once reached the stationary state, and therefore, it will improve the overall performance of the pilot plant.

II. SOFC DESCRIPTION AND PILOT PLANT DESIGN

The commercial SOFC to be integrated in the demonstrative pilot plant to be run with the reforming gas produced from ethanolic wastes is the Elcogen E3000 (Elcogen AS, Finland). This fuel cell is composed of the stack (119 unit cells), compression system to secure gas tightness and electrical contact, gas delivery system, current collection system and instrumentation system.

The gas delivery system of the fuel cell is coupled with side inlet and outlet pipes to distribute the gases within the stack. Inside the fuel cell, the stack is an open air structure with a co-flow type configuration. Within the project, the manifold structure was designed and constructed for the distribution of the air through the cells and to ensure a uniform temperature within the stack. Additionally, the

structure that house the Elcogen E3000 fuel cell in the pilot plant, which is called hot box, was designed and constructed within the project as well. The main purpose of the hot box is to heat-isolate the stack and to minimize energy losses in the form of heat (lower than 200 W). Homogeneous thermal surrounding is critical for stack performance and reliability in order to minimize the thermal gradients inside the stack and avoid the breakage of the SOFC.

The instrumentation system of the pilot plant mainly includes pressure regulators, flow and temperature controllers, temperature and pressure sensors and flow control valves. Regarding equipment, several heat exchangers were introduced in order to reuse the heat of the SOFC outlet streams, minimize energy requirements of the full process and maximize the energy efficiency of the pilot plant. Hence, two heat exchangers were included in the exhausted combustion gases line to pre-heat inlet gases, whereas seven heat exchangers were included in the air line to pre-heat in-let gases, as well as to provide thermal energy to the catalytic reforming process. Additionally, two electrical heaters were integrated to compensate heat shortcomings when necessary, especially during the start-up of the pilot plant, in which hydrogen and nitrogen mixtures in different ratios will be supplied to the SOFC (Figure 1).



Figure 1: Pilot plant.

As a result of the heat reutilization, the current energy requirement of the pilot plant is 2.3 kW. Nevertheless, this rate could be improved by utilizing the hydrogen content in the SOFC outlet stream, since almost the 40% of the H₂ produced is currently unused.

III. PRELIMINARY RESULTS

With the purpose of adjust (calibrate) the control system of the pilot plant, a first test has been performed, where the temperature was progressively incremented up to about 500 °C in the inlet cathode and 450 °C inside the Hotbox. Despite the presence of small heat losses between

the gas heater outlet and the cathode inlet, it was possible to prove that the Hotbox was perfectly thermal isolated from the outside as a first result. Furthermore, it has been demonstrated that the heaters are correctly inserted to supply the heat power required by the Hotbox to reach the operating temperature, as can be seen in figure 2.

Finally, during the course of the control test, voltage measurements were registered in each of the cells of the stack, confirming the reproducibility of the results provided by the SOFC cell supplier for each given temperature.

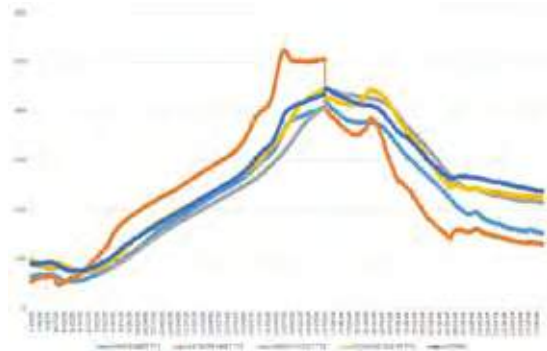


Figure 2: Temperatures corresponding to the first control test.

IV. CONCLUSION

A pilot plant has been developed in which, a solid oxide fuel cell (SOFC) has been integrated for electrical generation. Several tests have been carried out to verify the control and stability of the plant proving that it is able to reach temperatures close to nominal temperature.

On the other hand, it has been validated that the voltage values generated by the SOFC at different temperatures are well in accordance with those given by the supplier.

Therefore, it can be stated that the Hot Box and the heaters, are correctly designed, while the control system is adequately implemented.

ACKNOWLEDGMENT

This work (LIFE15 CCM/ES/000080) has been partially funded by the European Commission, within the framework of the LIFE programme.

REFERENCES

- [1] Godat J., Marechal, F., Optimization of a fuel cell system using process integration techniques, *Journal of Power Sources*, Volume 118, 2003, pp. 411-423
- [2] Pukrushpan J., Stefanopoulou, A., Varigonda, S., Eborn, J., Haugsteretter, C., Control-Oriented Model of Fuel Processor for Hydrogen Generation in Fuel Cell Applications, *Control Engineering Practice*, Volume 14, Issue 3, 2006, pp. 277-293.

DEVELOPMENT OF STANDARDIZED TEST METHODS FOR IN-SITU VALIDATION OF SYSTEM MATERIALS FOR THE USE IN AUTOMOTIVE FUEL CELL SYSTEMS

U. Misz*, P. Beckhaus*, T. Notthoff*, L. Kühnemann*, A. Heinzl*

*ZBT GmbH, Carl-Benz-Str. 201, 47057 Duisburg, (Germany)

Abstract - Balance of plant costs have risen in importance with decreasing fuel cell stack costs. In addition to further cost reductions of stacks intensive attention is therefore focused on cheaper system components and materials. So far high quality components and materials have been used to minimize negative impact on performance and durability. To include cheaper materials in fuel cell systems their harmfulness has to be validated. In order to achieve this target, a test chamber has been developed for testing different materials regarding suitability in fuel cell systems. The test chamber filled with material samples is integrated upstream of a test fuel cell, so that material outgassing is led directly to the cell. The functionality of the test chamber was successfully tested by performing tests with two peroxide cross-linked ethylene propylene diene monomer (EPDM).

Index Terms – fuel cell system, quality tests, durability, EPDM

I. INTRODUCTION

Beside degradation effects due to operating conditions external supplied contaminants originated from air, fuel or system materials could also have a negative effect on the performance and lifetime of a fuel cell. With a view to series production and high price pressure on fuel cell systems, however, significantly cheaper system components will have to be used in the future. Nevertheless, quality must be guaranteed in order to achieve the required durability.

Exemplary the National Renewable Energy Laboratory (NREL) has invested a lot of work in the field of researching materials for suitability in fuel cell systems system [1-3]. An extensive database was created, which, however, was not maintained after the project activities had expired.

So far there is no standardized test method that can determine the suitability of materials for fuel cell systems. In a joint research project (German BMWi funded) Volkswagen AG, SGS INSTITUT FRESENIUS GmbH and ZBT GmbH are developing uniform test methods for the qualification of new

materials for fuel cell applications.

ZBT focusses on the development of standardized test methods with a test chamber for in-situ analyses. The test chamber is integrated upstream of the anode or cathode inlet of a test fuel cell and can be flowed through with different gases (air, H₂) at different temperatures, pressures and relative humidity. The structure of the rack inside the chamber enables the stacking of a significant number of material samples to overflow a large sample surface with gas, Fig. 1.

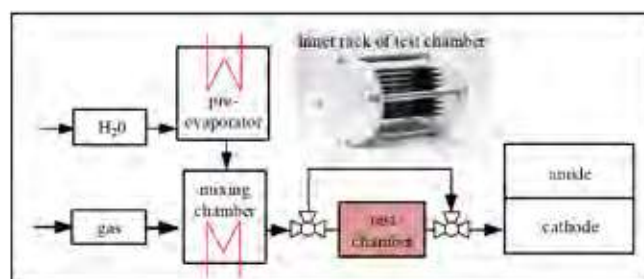


Fig. 1. Test setup with test chamber on the cathode side

If harmful substances are emitted within the chamber, the influence on the fuel cell can be determined. Electrochemical measuring methods are used for the determination of the contamination mechanisms.

Due to the large surface area of material samples in relation to the small active area of the membrane electrode assembly (MEA), the procedure can be used as a rapid test for material suitability.

II. EXPERIMENT

In a first test series two peroxide cross-linked EPDMs and their effect on the test cell were compared. The technical designations of the EPDMs are E628 and E9614. The materials differ only marginally in terms of density, shore hardness, and

other characteristics. 27 material samples were placed in the chamber. Tests were performed at cathode side. The temperature in the chamber was 90 °C, while the test fuel cell was operated at 80 °C. Current density during all tests was 1.4 A cm⁻² at an absolute pressure of 2 bar and a cathode dew point of 65 °C. All tests started with a MEA characteristic and a 25 h operation in bypass to determine reference degradation, followed by 25 h test with the integrated chamber. Afterwards, the fuel cell was again operated for 25 hours in bypass mode to identify the possibility of regeneration.

III. RESULTS AND DISCUSSION

In advance of each material test a reference measurement of the chamber without any sample content was carried out in order to determine the basic degradation. A new MEA was used for each experiment. Figure 2 displays a comparison of EPDM E628 and E9614 within first 240 minutes in the test chamber. The course of the cell voltage due to the outgassing of the materials is shown.

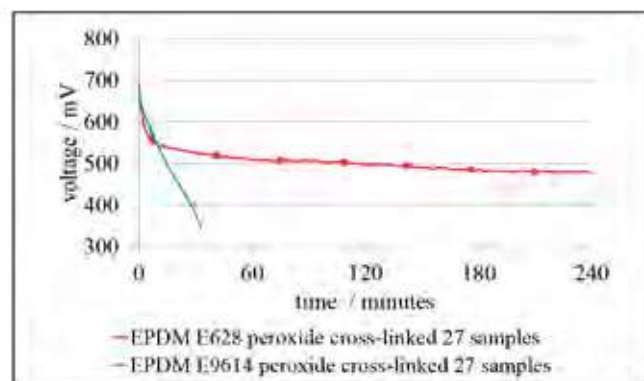


Fig. 2. Voltage course of test fuel cell during EPDM material outgassing in test chamber

Although both materials have almost identical properties, the fuel cell is much more sensitive to E9614. Nevertheless, considerable voltage losses occur due to both materials. One reason for these results is the extremely large exposed surface of the tested materials compared to the small active area of the MEA. In subsequent regeneration with bypass mode a complete recovery of the test cell was unexpectedly achieved after contamination with E9614. In contrast, the cell voltage was permanently reduced after outgassing of E628.

The results of the in-situ investigations with the test chamber are compared with parallel ex-situ analyses performed by SGS. The main degassing product of both EPDM materials was a 4-pyridone, which is an organic compound with the molecular formula C₅H₅NO. It belongs to the group of pyridones. However, a large number of other volatile hydrocarbons have been identified using ex-situ methods, which differ depending on the EPDM and may have a negative influence on the cell.

The first test series indicated that the number of samples was

too high. Accordingly, the test was repeated with E628 using only three material samples. Fig. 3 displays the voltage course by operating the chamber with different number of test samples.

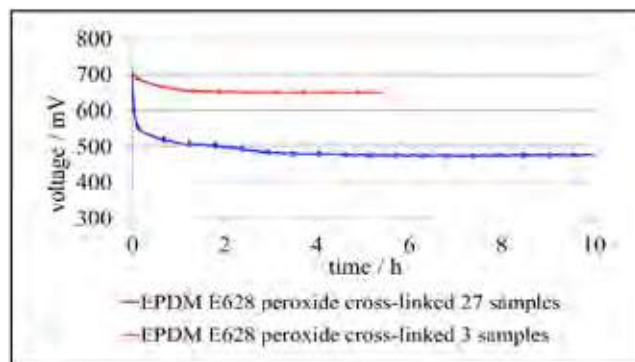


Fig. 3. Comparison of voltage loss due to different number of E628 samples in test chamber

It was possible to determine a direct connection between the surface size of the test material and voltage loss of the test cell. Further investigations and the transfer of the results to components in real fuel cell applications are necessary.

IV. CONCLUSION

The development and verification of an in-situ test chamber to investigate materials for suitability in fuel cell systems has been successfully implemented. Since the investigations showed that nearly identical materials emitted different volatile hydrocarbons, the development of a new chamber is focused on an additional investigation on additives. In addition, the new chamber can be constructed much more compactly on the basis of the first results, as a smaller number of samples is needed.

ACKNOWLEDGMENT

The authors thank the German Federal Ministry for Economic Affairs and Energy for supporting the project VALIDATE (03ETB001C).

REFERENCES

- [1] Mehrabadi, B., Dinh, N., Bender, G., Weidner, J., Effect of System Contaminants on the Performance of a Proton Exchange Membrane Fuel Cell, *Journal of the Electrochemical Society* 163 (2016): F1527-F1534.
- [2] Opu, M., Bender, G., Macomber, C., Van Zee, J., Dinh, H., Understanding the Effects of PEMFC Contamination from Balance of Plant Assembly Aids Materials: In Situ Studies, *Journal of the Electrochemical Society* 162 (2015): F1011-F1019.
- [3] Yu, P., Bonn, E., Lakshmanan, B., Impact of Structural Plastics as Balance of Plant Components on Polymer Electrolyte Membrane Fuel Cell Performance, *ECS Transactions* 58 (2013): 665-680.

CFD MODEL FOR TUBULAR SOFC CELLS FED DIRECTLY BY BIOMASS – A COMPLETE INTEGRATED SYSTEM

D. Papurello* **, D. Ferrero*, V. Somano*, D. Canuto* and
M. Santarelli*

* Politecnico di Torino, DENERG, Corso Duca degli Abruzzi 24 -
10129, Torino (Italy)

**Energy Center Laboratory, Address, (Italy)

Abstract - In this work, an innovative solution under development in the DB-SOFC project to produce electrical power from a SOFC stack feed by syngas obtained from the gasification of residual biomass inside the stack is presented. Firstly, the CFD model of a single SOFC tubular cell was developed. Secondly, the model was applied to simulate the operation of a 25-cells stack feed by syngas in two different configurations (square, circular) and with two different cooling systems (air, water). The results show the squared stack cooled by air is able to reach the 200 W target power of the project. The circular stack configuration provides lower power in all the investigated conditions because of the difficult management of the current collection of the cells that have different current outputs, limiting the total current inside the stack, demonstrating the higher potential of a squared configuration.

Index Terms – biomass, CFD model, SOFC, stack

I. INTRODUCTION

Among the technologies and the possible energy sources, the coupling of fuel cells and biomass is becoming interesting, considering the high electrical efficiency of fuel cells and the low environmental impact of biomass. The potentiality in the Mediterranean area of exploiting residues from the cultivation of olives and grapes was assessed in the DB-SOFC project, investigating the possibility of directly gasifying the biomass in a SOFC stack made of tubular cells, with the target of realizing a 200 W stack – schematic shown in Figure 1 – able to operate with pre-treated biomass as input. The cells are YSZ-electrolyte supported with a length of 16 cm, designed to reach a target power of 8 W each, being 25 cells the target number for a stack. To assess the feasibility of the system, a CFD model of the single cell operating with biomass-derived syngas has been developed and different stack configuration have been analyzed

to verify the possibility to reach the 200 W target of the stack.

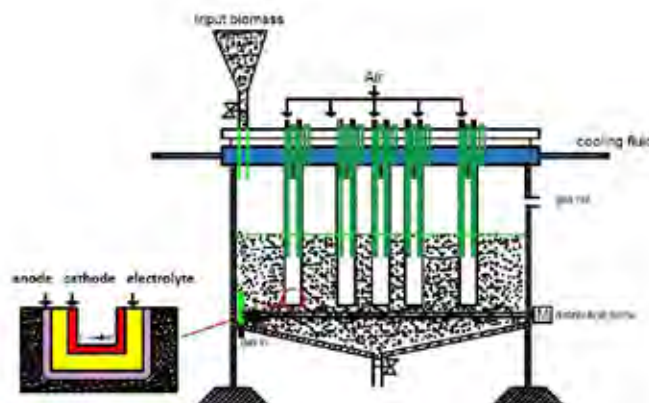


Fig. 1. Schematic of direct-biomass stack concept

II. METHODS

The CFD models of the tubular SOFC cell and stack have been developed using Comsol Multiphysics™. Firstly, the axial symmetrical 2D model of the cell has been implemented, using an electrochemical model based on equilibrium potentials at the electrodes, Ohm's law for ions conduction in the electrolyte and a linearized Butler-Volmer equation adopted to estimate the activation overvoltages, with a fixed cathodic potential set to 0.7 V as operating voltage. An advection-diffusion equation combined with Fick's law has been implemented for modeling the flow and transport of species in flow channels. The electrodes have been assumed to be dimensionless, thus as boundary layers on the electrolyte. The energy conservation has been imposed in the simulated domains, taking into account the heat sources related to electrochemical reactions, overpotentials

and the heat of reaction of steam methane reforming and water gas shift occurring in the syngas flow at the anode of the cell [1]. The operation of the cell has been simulated with syngas derived by the gasification of biomass pre-heated at 800°C (dry composition in volume: CO₂ 54%, CO 44.8%, CH₄ 0.01%, H₂ 1.19%). After the single cell, simulations have been performed modeling the stack in squared and circular (rhombic shaped) configurations with two different types of cooling system at the top of cell, one based on water and the other with air. The squared stack is composed by a 5x5 matrix of cells (distance between the centers of them of 5 cm). The circular geometry of the stack has been build distributing the cell on a diameter of around 35 cm.

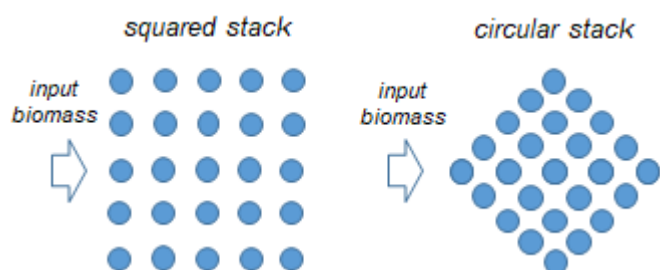


Fig. 2. Stack configurations

Subsequently, it has been estimated the power output of the stacks introducing three different inlet syngas temperature distributions (linear) along the stack, decreasing from the biomass inlet to gas outlet (ie., left to right in Figure 1). Connection between the cells has been done by putting in series cells with similar generated current, which are the column cells for the square stack configuration that operates exactly in the same conditions.

III. RESULTS

The single cell simulation under isothermal conditions (800 °C) shows that the cell is able to produce 8.66 W at 0.7 V with the selected syngas. The simulation has been repeated in non-isothermal conditions by considering the same syngas input at 800 °C, with both air and water cooling. The cell cooled by water could provide 11.57 W, instead the air cooled cell is able to generate 12.63 W, in both cases above the fixed target of reaching 8 W per cell at 800°C. The analysis of temperature inside the model highlighted that with the water cooling system the maximum temperature is slightly lower than in the case of the air one, but the top zone of the cell is thermally inhibited and could be subjected to degradation due to low temperature and thermal gradients with the bottom part of the cell. For this reason, an air-cooled option is selected.

The stack simulations have been performed with three different linear temperature distributions for the inlet syngas (850-700°C, 800-700°C, 800-650°C) for the squared and circular configurations. The results in term of total stack output power

(at 0.7 V) are shown in Table I for the two stack configurations, showing always a higher output for the squared stack. The simulations highlighted that a circular stack is limited by the connection in series of cells with different current outputs, while in the square configuration a row of cells has the same current as it can operate in the same conditions even in the presence of an inhomogeneous temperature of the inlet syngas. The power output for each cell in a row of the squared stack is shown in Figure 3. The power decreases with the temperature as expected, as the temperature has a strong influence especially on the ohmic losses, as the cell is electrolyte-supported.

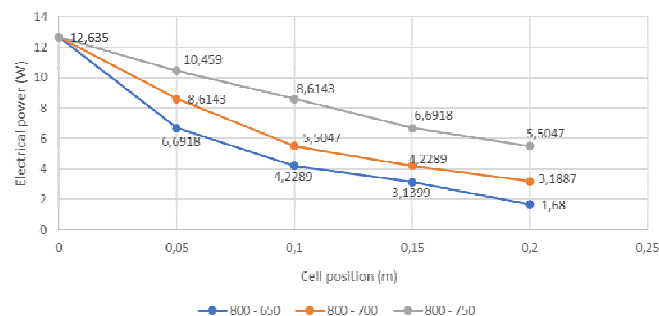


Fig. 3. Power distribution of air-cooled stack (squared, 0.7 V each cell)

TABLE I. STACK POWER OUTPUT

Temperature profile (inlet syngas)	Squared stack	Circular stack
800 °C – 750 °C	219 W	204 W
800 °C – 700 °C	171 W	141 W
800 °C – 650 °C	142 W	106 W

IV. CONCLUSION

The CFD simulation of the syngas-fed tubular cell showed that at 800°C it is possible to reach and go above the 8 W of power output target. The results also showed that a water cooling system is not feasible because the temperature on the top of the cell becomes too small for a SOFC and that an air-cooling system is even more performing. The complete stack simulations highlighted that a circular stack is limited by the inhomogeneity of currents, while a squared stack is able to overcome this issue and achieve a higher power output. In future works, the validation of the temperature distribution inside the stacks, the effects of carbon deposition and inhibition of the cells due to the solid biomass will be investigated.

ACKNOWLEDGMENT

The DB-SOFC project has received funding from the European Union under the ERANETMED 2-72-246.

REFERENCES

- [1] Ferrero, D., Lanzini, A., Santarelli M., Solid Oxide Fuel Cells Modeling, in Advances in Medium and High Temperature Solid Oxide Fuel Cell Technology. Springer, Cham, 2017, pp. 291-342.

GREEN HYDROGEN AND ADVANCED PEFCs WITHOUT NPGM AND CARBON FOR OUR SUSTAINABLE GROWTH

K. Ota*, T. Nagai*, Y.Kuroda*, K. Matsuzawa*, S. Mitsushima***, A. Ishihara**

Yokohama National University,

*Green Hydrogen Research Center, **the Institute of Advanced Sciences

79-5 Tokiwadai, Hodogaya-ku, Yokohama, 240-8501 (JAPAN)

Abstract - Considering our future sustainable growth, renewable energies should be the primary energy. So, we need technologies to store and transport renewable energies. Green Hydrogen is the hydrogen from water using renewable energies. The environmental impact factor was defined as a ratio of an annual quantity of materials produced by the energy consumption of mankind to a natural movement on the earth. By the comparison of environmental impact factor, the Green Hydrogen could keep our environment more than 2 orders of magnitude cleaner compared to that of fossil fuels. With using Green Hydrogen, we could produce clean electricity effectively through fuel cells without any pollutants. A stable non-precious metal oxide cathode with stable metal oxide support might be the final goal for the cathode of PEFCs. We are developing non precious metal oxide cathode with metal oxide support using group 4 and 5 metal oxides. The highest onset potential of was over 1.1 V vs. RHE and stable even after potential cycles.

Index Terms -cathode catalyst, non PGM catalyst, polymer electrolyte fuel cell, transition metal oxide

I. INTRODUCTION

More than 200 years has passed after the industrial revolution and we are using many technologies in order to have a wealthy life. We are using energy to apply these technologies. Now we are going to use a huge amount of energy to keep our life style or to get a higher life, so that we need more energy. Many people are anxious about the global warming caused by the large usage of fossil fuels.

II. GREEN HYDROGEN AND EIF[1]

The water cycle caused by the hydrogen energy system on the earth was compared with the carbon cycle which is caused by the usage of fossil fuels. The ratio of the energy consumption of human beings to the movement from

atmosphere of water is more than two orders of magnitude less than that of carbon. The water cycle is superior to the carbon cycle.

The Green Hydrogen is the hydrogen made from water using renewable energies. In order to evaluate energy carriers from the point of the environmental effect, more quantitative analysis is important. Considering the dynamic flow of energy carriers, we can define the environmental impact factor (EIF) of carbon and hydrogen as follows.

$$\text{EIF of Carbon} = \frac{[\text{CO}_2 \text{ from fuel usage}]}{[\text{Natural CO}_2 \text{ Circulation}]} \quad (1)$$

$$\text{EIF of Hydrogen} = \frac{[\text{H}_2\text{O from H}_2 \text{ Usage}]}{[\text{Natural Water Circulation}]} \quad (2)$$

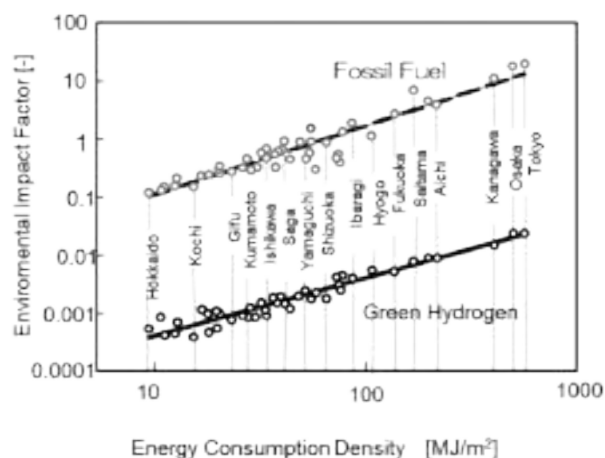


Fig.1 Dependence of EIF on Consumption Density (2004-2013)

The EIF for carbon on the earth in average can be calculated to be 0.036. This means that the EIF of energy carriers should be less than 0.036 to obtain a sustainable growth of human beings.

Figure 1 show the local EIF of prefectures in Japan relating to the density of energy consumption. The difference of EIF for fossil fuels and the green hydrogen is roughly 2 orders of magnitude at any energy consumption density. This means that the Green Hydrogen Energy System might be more than 100 times cleaner compared to the present fossil energy system. Considering the sustainable growth of human beings in the future, the "Green Hydrogen" might be only one solution.

III. NON PGM OXIDE CATHODE

Polymer electrolyte fuel cells (PEFCs) are using Pt cathode. However, the estimated amount of Pt reserve is limited and its cost is high. The dissolution of Pt cathode might be the final problem to be solved related to the stability in the present PEFC system. Additionally, the instability of carbon support is also a big problem especially for fuel cell vehicles. Carbon including graphite is thermochemically unstable even at room temperature in air or oxygen containing atmosphere.

In the future energy system fuel cells may be operated at 120 °C or higher for PEFCs. At these high potential and temperature, Pt and carbon are no more stable. We need new materials, such as metal oxides that are stable in acid and oxygen atmosphere.

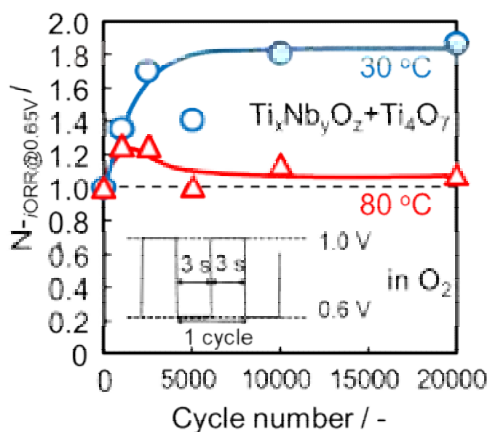


Fig.2 Normalized $i_{ORR}@0.65V$ during rectangular cycling.

We have reported that partially oxidized group 4 and 5 metal oxides, or the oxides with containing carbon or nitrogen are stable in an acid solution and have the definite catalytic activity for the oxygen reduction reaction (ORR) [2-4]. The highest onset potential of the $Ti_xNb_yO_z + Ti_4O_7$ was over 1.1 V vs. RHE at 80 °C [5]. No degradation of the ORR

performance of $Ti_xNb_yO_z + Ti_4O_7$ was observed during both start-stop cycles and load cycles tests as shown in Fig.2. Considering these factors, we could improve the ORR activity of group 4 and 5 metal oxide cathodes with oxide support [6].

Recently, we have proposed titanium oxide-based cathodes without carbon to obtain high durable catalysts [7] because a stable non-precious metal oxide cathode with stable metal oxide support might be the final goal for the cathode of PEFCs of fuel cell vehicles. In addition, we are investigating the factors which affect the ORR activity using thin film model electrodes [8]. The oxide composition and the metal defects are important to get high activity.

IV. CONCLUSION

In the future energy system fuel cells should be operated at higher efficiencies such as 60 % (HHV) since their theoretical efficiency is more than 80% even at room temperature. To obtain this high efficiency, fuel cells should be operated at 0.9 V or higher. We need new materials for the ORR catalyst system, ORR catalysts and their supports. Group 4 and Group 5 metal oxides might be good candidates for the future ORR system of PEFCs.

ACKNOWLEDGMENT

The authors wish to thank to the New Energy and Industrial Technology Development Organization (NEDO) for their financial support.

REFERENCES

- [1]. K. Ota, et al., *Advances in Hydrogen Production, Storage and Distribution*, p.32, Woodhead publishing, UK (2014)
- [2]. A. Ishihara, M. Tamura, Y. Ohgi, M. Matsumoto, K. Matsuzawa, S. Mitsushima, H. Imai, and K. Ota, *J. Phys. Chem. C*, 117, 18837 (2013).
- [3]. A. Ishihara, M. Chisaka, Y. Ohgi, K. Matsuzawa, S. Mitsushima and K. Ota, *Phys. Chem. Chem. Phys.*, 17, 7643 (2015).
- [4]. M. Chisaka, A. Ishihara, H. Morioka, T. Nagai, S. Yin, Y. Ohgi, K. Matsuzawa, S. Mitsushima, and K. Ota, *ACS Omega*, 2, 678 (2017).
- [5]. K. Ota, T. Nagai, K. Matsuzawa, Y. Kuroda, S. Mitsushima and A. Ishihara, *Polymer Electrolyte Fuel Cells 16 (ECS Trans. 75(14))*, 875- 883 (2016).
- [6]. K. Ota, T. Nagai, K. Matsuzawa, Y. Kuroda, S. Mitsushima and A. Ishihara, *Polymer Electrolyte Fuel Cells and Electrolyzers 18 (ECS Trans. 86(13))*, 549-558 (2018)
- [7]. A. Ishihara, M. Hamazaki, M. Arai, M. Matsumoto, H. Imai, Y. Kohno, K. Matsuzawa, S. Mitsushima, K. Ota, *J. Electrochem. Soc.*, 163, F603 (2016).
- [8]. A. Ishihara, Y. Tamura, Y. Kohno, K. Matsuzawa, S. Mitsushima, K. Ota, *Catalysts*, 5, 1289 (2015).

COMPACT AND ROBUST DIESEL FUEL PROCESSING SYSTEMS WITH QUICK-START CAPABILITY FOR 5-10 KW HT-PEFC SYSTEMS

R.C. Samsun*, M. Prawitz*, A. Tschauder*, J. Pasel*,
R. Peters* and D. Stolten* **

* Forschungszentrum Jülich GmbH, Institute of Electrochemical
Process Engineering, 52425, Jülich (Germany)

** Chair for Fuel Cells, RWTH Aachen University, 52072, Aachen
(Germany)

Abstract - This work deals with the experimental characterization of two fuel processor generations for diesel and jet fuel for HT-PEFC systems. Firstly, the start-up is optimized based on thermal and electrical start strategies. Secondly, operation strategy is optimized focusing on steady state operation under full load, load change performance as well as shut-down and regeneration. The start time could be reduced to 14 min using an electrical start. For each fuel used, ideal operation parameters were identified to maximize the conversion and minimize the by-products. The results from this study are used to develop the next generation HT-PEFC system based on diesel in the 7.5 kW power class.

Index Terms – auxiliary power unit, diesel reforming, fuel cell system, fuel processor.

I. INTRODUCTION

As a complement to hydrogen being the ideal fuel for fuel cells, reformat-based operation offers the possibility for the wider utilization of fuel cells in a broad range of applications. This work deals with the reforming of liquid fuels such as diesel and jet fuel on a systems level. The reforming of diesel and jet fuel remains a major challenge due to the complicated chemical structure of these hydrocarbon mixtures and the resulting stability issues [1, 2]

We report on the recent advances at the Forschungszentrum Jülich with examples from two fuel processing systems developed for fuel cell-based auxiliary power units. The focus is given 1) to the optimization of system start-up comparing a thermal and an electrical strategy, 2) steady-state operation minimizing the amount of undesired higher hydrocarbons in the produced gas, 3) load change strategy without exceeding the

target carbon monoxide concentration in the produced gas under transient mode and 4) shut-down combined with a regeneration to achieve constant system performance at each operation. The core components are an autothermal reformer, a water-gas shift reactor and a catalytic burner, in which several functions are integrated. The findings from this work serve for closing the gap between research and application.

II. EXPERIMENTAL

The developed fuel processors of the fifth and sixth generation can be classified based on their start strategy. The fifth generation fuel processor utilizes a diesel burner to heat the system upon start, which is referred to as thermal start-up. In the sixth generation, electrical wires are included inside the reformer and the shift reactor, therefore this concept enables an electrical start-up. In both generations, the start-up strategy also includes a glow plug placed at the catalytic burner inlet.

Both systems are developed to deliver a hydrogen rich reformat for a high temperature PEFC stack. The thermal system power is defined as 28 kW_{th}. However, based on recent findings on the activity and stability of shift reactors in diesel fuel processors, the residence time in the shift stages is increased in the fifth generation, which limited the maximum load of the system to 14 kW_{th}. The sixth generation, however, includes a new shift reactor, so that the maximum load can be achieved with this system. Considering possible operation points in coupled system operation, the fifth generation fuel processor can be used in 5 kW_e fuel cell systems, whereas the sixth generation for up to 10 kW_e. Further details on the system designs and components can be found in Samsun et al., as well as detailed discussions on the developed start-up strategies for

each system [3, 4].

III. RESULTS

The experiments with the fifth generation fuel processor focused on the start-up. Using the hot exhaust gas from a diesel burner and a glow plug, the fuel processor could commence operation after 20 min and the start-up could be completed after approximately 30 min, as the desired reformat quality (< 1 vol.%) was achieved. Fig. 1 shows the development of temperatures at selected locations in the autothermal reformer (ATR), high and low temperature shift reactors (HTS and LTS) and the catalytic burner (CAB) on the left axis. On the right axis, concentrations of hydrogen, carbon monoxide and carbon dioxide in the produced reformat at the outlet of the shift reactor, namely the anode inlet, are displayed.

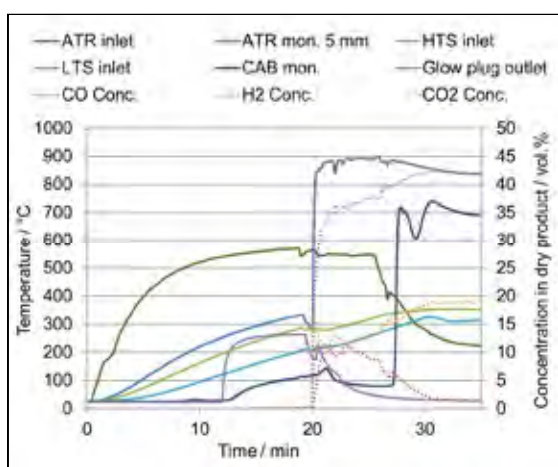


Fig. 1. Selected temperatures in the fuel processor and concentrations of CO, H₂ and CO₂ in the dry product gas at the water-gas shift reactor outlet during start experiment using thermal start strategy using a diesel burner assisted by a glow plug.

Building on the findings with this system, a further fuel processor in the 10 kW_e power class was developed based on an electrical start-up strategy. Using this system, the start-up period could even be reduced to 14 min. As displayed in Fig. 2, reformer operation commences already in 8.5 min. Within 14 min, autarkic system operation is achieved at full load, and the CO concentration is reduced to less than 1 vol.%, so that, the reformat can be fed into an HT-PEFC for electricity production. This result shows that the electrical start concept can strongly accelerate the start-up of a diesel fuel processor.

Further experiments with the sixth generation system focused on the following aspects, which will be presented in the EFC19 for the first time. 1) Steady state performance: In this part, the operation parameters of the system are optimized for different diesel and jet fuels, so that the produced reformat contains very low levels of unwanted by-products and can be fed into the HT-PEFC anode. 2) Load change performance: With all fuels, it was possible to keep the CO concentration at

less than 1 vol.% during load change experiments based on pre-defined load levels for a period of 1.5 h. 3) Shut-down performance: The developed quick system shut-down using air as purge gas could eliminate temperature peaks and by-products completely, preparing the components for the next stable system operation at the same time, thanks to the integrated regeneration strategy.

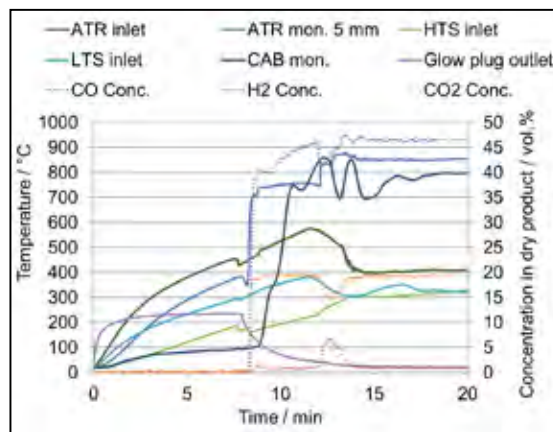


Fig. 2. Selected temperatures in the fuel processor and concentrations of CO, H₂ and CO₂ in the dry product gas at the water-gas shift reactor outlet during start experiment using electrical start strategy.

IV. CONCLUSION

Based on the findings using the thermal start strategy, a new fuel processor system was developed using new reactors and an electrical start, with which the start period could be reduced strongly. This system proved its performance in further experiments, in which the operation strategy is optimized for steady state, load change, shut-down and regeneration. Based on these scientific findings, a complete fuel cell APU was developed in Jülich, which will also be presented during the conference talk.

REFERENCES

- [1] Bae, J., Lee, S., Kim, S., Oh, J., Choi, S., Bae, M., Kang, I., Katikaneni, S. P., Liquid fuel processing for hydrogen production: A review, *Int. Journal of Hydrogen Energy*, 41(44), 2016, pp. 19990-20022.
- [2] Specchia, S., Fuel processing activities at European level: A panoramic overview, *International Journal of Hydrogen Energy*, 39(31), 2014, pp. 17953-17968.
- [3] Samsun, R. C., Prawitz, M., Tschauder, A., Pasel, J., Pfeifer, P., Peters, R., Stolten, D., An integrated diesel fuel processing system with thermal start-up for fuel cells, *Applied Energy*, 226, 2008, pp.145-159.
- [4] Samsun, R. C., Prawitz, M., Tschauder, A., Pasel, J., Peters, R., Stolten, D., An autothermal reforming system for diesel and jet fuel with quick start-up capability, *Int. Journal of Hydrogen Energy*, 44, 2019, pp. 27749-27764.

HYACINTH PROJECT: CASES OF STUDIES THROUGHOUT SAMT TOOL

E. Nieto, G. Alcalde

Centro Nacional del Hidrógeno, Prolongación Fernando el Santo
S/N. 13500, Puertollano, Ciudad Real, (Spain).

Abstract –HYACINTH aim has been to achieve a greater understanding of the social acceptance of fuel cell and hydrogen (FCH) technologies & applications at European level such as Fuel Cell Electric Vehicles (FCEV) and micro-Combined Heat and Power system (micro-CHP). In addition, the project has developed a tool to facilitate the product development and market introduction being better aimed to the target audience, giving better response to the expectations and reducing the risks & barriers to their acceptance. The tool comprises two studies carried out in the project, Public awareness and acceptance of FCH technologies and Stakeholder acceptance of FCH technologies across Europe both. This study analyses the results provided by the tool carrying out a comparison between European Union (EU) and Germany (DE) in both applications previously mentioned. The results show that, even there is not a great awareness and experience in these applications, there is a high acceptance.

Index Terms – European Union, Fuel Cell Electric Vehicle, Hydrogen Technologies, General Acceptance, micro Combined Heat and Power system, awareness, stakeholders.

I. INTRODUCTION

It is deemed by stakeholders that public acceptance plays a key role in the implementation process of a new technology such as hydrogen technologies. Stationary and mobile applications, supply infrastructures, HRS or industries based on hydrogen will be close to general public -as customers or users- so it is needed to know their attitudes towards this technology.

Previous researchs on social acceptance carried out point out the general levels of public understanding of FCH technologies in specific countries i.e *Percepción y Aceptación Pública de las Tecnologías del Hidrógeno. Un Estudio Exploratorio* (PSE H2RENOV project) [1] or *Influencing factors to the acceptance process of FCH technologies in public transport* (CHIC project) [2], but there is a limited systematic evidence on the acceptance of FCH technologies throughout Europe, which is the main objective of HYACINTH project.

The aim of this project has been to achieve a greater understanding of the social acceptance of hydrogen & fuel cell technologies and applications at European level as well as developing a tool (SAMT) to facilitate the product development and market introduction being better aimed to the target

audience, giving better response to the expectations and deducted the risks or barriers to their acceptance.

II. METHODOLOGY

The main HYACINTH methodology used to collect the information has been based on 2 studies developed among more than 7000 citizens & 350 stakeholders. Those have been carried out through surveys and interviews to general public and stakeholders from different EU countries: *Public awareness and acceptance of FCH technologies across EU* [3] and *Stakeholder acceptance of FCH technologies across EU* [4].

It is needed to understand what factors could have a direct influence in general public awareness and acceptance, and Government Policies could be a relevant issue.

This document contains the results on general acceptance on FCEV and micro-CHP between the EU and DE considering that this country has a policy to support FCH technologies.

A. The performance of SAMT

The SAMT has been implemented to provide several themes such as Knowledge & Experience, Trust, Positive & Negative Affects, Perceived Effects-Costs, Risks & Benefits, Perceived Consequences, Attitude, Initial Acceptance & Acceptance. It also provides advice to stakeholders about FCH technologies introduction within an application in the following countries and their regions: Spain, Germany, France, United Kingdom, Slovenia, Norwegian and Belgium.

In the initial stage, the SAMT's user is asked to choose his preference related to general public information and technology "Filtering Questions" such as F1: Which technology are you interested in? F5: Which country do you want the general public responses from? F6: Are you interested in energy awareness? being possible to filter the results accordingly. Once all questions have been chosen, the SAMT provides a report with the results of the previously mentioned studies.

B. Themes and Preferences

This study uses SAMT for assessing the differences between themes like **Acknowledge and Experience** and on the other

hand, **Acceptance** between EU vs DE in two different applications, FCEV and micro-CHP.

From the preferences “Filtering Questions”, data have been obtained choosing both applications, male & female views, age range selected 16-100, region DE or All, interested in energy awareness & lifestyle activities and finally, depending the application chosen, interest on typology of cars and housing.

III. RESULTS

A. Results on FCEV application

It can be found that, in relation to Knowledge & Experience of FCH technologies, for the general public in the EU vs DE, the level of awareness in DE has better results due to people who responded have heard something about hydrogen technologies (58% DE vs 46% EU); it is also DE stakeholders who have a coherent view with the results on the level of awareness of the general public. Related to the question about awareness of any hydrogen refuelling station in your region, the results show a low ratio (2.85% DE vs 5.51% EU).

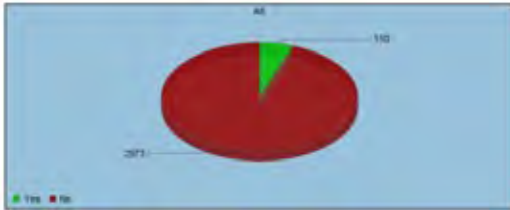


Fig. 1. EU Respondents. Awareness on HRS in their region.

However, the Acceptance of these technologies regarding the analysis of the response to the willingness to purchase a FCEV in the same previous sample, and comparing the result EU vs DE, it is observed that the acceptance of respondents would be similar in both samples under similar conditions of cost & autonomy to current vehicles (75% DE vs 72% EU). Similar values are obtained for those who would not be willing or at all willing to purchase the vehicle (6% DE vs 7% EU).

B. Results on micro-CHP application

Another relevant application within hydrogen and technologies sector such as micro-CHP shows rates quite different than described before for FCEV in the same places. The percentages related to knowledge & Experience for general public in EU and DE have similar values (6% both), and the micro-CHP awareness has a low percentage. Nevertheless, regarding the Acceptance of this application in DE compared to EU, the values are completely different. The majority of participants are likely or very likely in DE, being lower percentage in EU (80% DE vs 67% EU).

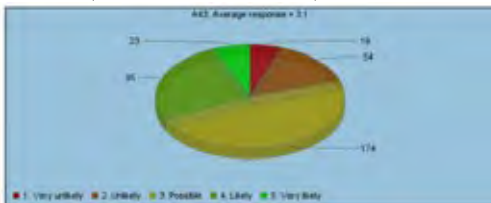


Fig. 2. DE Respondents. Participants are willing to install micro-CHP.

According the obtained results, participants were asked about what tenancy were they interested, among different options like Home owners, rented or others. In DE there is less knowledge & experience than EU average regarding micro-CHP application (4,61% DE vs 6,24% EU). However, this lower value does not have relevant influence in acceptance due to Home Owners that are willing to install a hydrogen fuel cell system as a heating & electricity source (84% DE vs 66.88% EU), and better than results obtained when is also being considered as participant end users.

IV. CONCLUSIONS

The results obtained from both applications show a high level of acceptance for buying and installing FCEV and micro-CHP respectively, although low level of awareness. On the other hand, the comparison carried out between DE and EU shows that acceptance is higher for micro-CHP than FCEV application.

A. Abbreviations and Acronyms

European Union (EU), Germany (DE), Fuel Cell Electric Vehicle (FCEV), Fuel Cell and Hydrogen (FCH), HYdrogen Acceptance IN the Transition pHase (HYACINTH), Hydrogen Refueling Station (HRS), micro Combined Heat and Power system (micro-CHP), Social Acceptance Management Toolbox (SAMT).

ACKNOWLEDGMENT

This project has received funding from the Fuel Cells and Hydrogen Joint Undertaking (FCH-JU) under Grant Agreement N° 621228. HYACINTH goals have been reached thanks to the Consortium team and their commitment from the following entities: University of Sunderland, RCVT, NORSTAT, ABERDEEN COUNCIL, Cidaut, Fraunhofer, IplusF, CIEMAT, University of Leeds and CNH2.

REFERENCES

- [1] Percepción y Aceptación Pública de las Tecnologías del Hidrógeno. Un Estudio Exploratorio, <http://documenta.ciemat.es>.
- [2] Influencing factors to the acceptance process of FCH technologies in public transport (CHIC project) <http://chic-project.eu/>.
- [3] HYACINTH-D5_2-General-findings-on-public-acceptance_V1, <http://hyacinthproject.eu/>.
- [4] HYACINTH-D5_1-Report-on-results-of-the-stakeholders-survey_V1, <http://hyacinthproject.eu/>.
- [5] HYACINTH EHEC2018: Recommendations for deployment the fuel cell and hydrogen market.

GRAPHENE OXIDE-BASED COMPOSITE MEMBRANES AS NOVEL ELECTROLYTES FOR PEM FUEL CELLS

A. Basso Peressut*, S. Latorrata*, L. Brambilla*,
C. Castiglioni*, and G. Dotelli*

*Department of Chemistry, Materials and Chemical Engineering
“Giulio Natta”, Politecnico di Milano, piazza Leonardo da Vinci, 32,
20133 Milan, (Italy)

Abstract – A novel approach is presented for the production of self-assembling sulfonated graphene oxide membranes, with the aim of evaluating them as an alternative to Nafion® for the application in PEMFCs as proton-conducting electrolytes. The functionalization has been performed by reacting a commercial aqueous dispersion of graphene oxide (GO) with different volumes of sulfuric acid, studying their effect on both structure and degree of sulfonation of the membranes. The specimens have been characterized from the morphological viewpoint by ATR-FTIR, XRD and SEM-EDX spectroscopies, thermogravimetric analysis, optical microscopy and static contact angle measurements. Their water uptake, ion exchange capacity and degree of sulfonation have been evaluated as well, and the relationship among them allowed the identification of an optimal acid-to-GO molar ratio for the sulfonation reaction. These tests resulted in an improved behavior compared to both Nafion® and pristine GO, while promising results have been obtained from a preliminary fuel cell test.

Index Terms – Electrolyte, graphene oxide, PEM fuel cells, sulfonation.

I. NOMENCLATURE

SGO-X: sulfonated graphene oxide membranes prepared with an acid-to-GO molar ratio equal to X (1, 20 or 200).

II. INTRODUCTION

One of the fundamental components of proton exchange membrane fuel cells (PEMFCs) is the proton-conducting electrolyte, nowadays commonly based on Nafion®, a perfluorosulfonate ionomer produced by DuPont. This membrane material is characterized by hydrophilic lateral substituents containing sulfonic acid groups ($-\text{SO}_3\text{H}$), which are responsible for its high proton

conductivity ($> 0.1 \text{ S cm}^{-1}$) under humidified conditions. However, Nafion® is expensive and suffers both a rapid performance drop and a physical degradation at low relative humidity ($< 50\%$) and elevated temperatures ($> 80 \text{ }^\circ\text{C}$). Therefore, huge research efforts have been deployed for the development of new materials able to operate at such conditions, which would significantly enhance both kinetics and efficiency of the redox reaction, while simplifying water management and cell design [1,2].

Among the possible approaches, graphene oxide (GO) has gained a lot of interest because of the presence of several oxygenated functionalities, which are responsible for the self-assembling properties that make it an ideal candidate for the production of freestanding membranes. However, previous works displayed a poor performance and durability of GO-based electrolytes [3]. Thus, the aim of this work has been to improve the properties of GO by exploiting an innovative approach consisting in its functionalization with sulfonic acid groups analogous to those of Nafion®. The obtained membranes have been extensively characterized from both morphological and operative points of view, providing promising results.

III. MEMBRANES PRODUCTION

The sulfonation of GO has been performed by developing a reaction between sulfuric acid and a commercial water-based dispersion of GO (4 mg mL^{-1}) acquired from Graphenea. Three tentative acid volumes have been defined according to a sulfonation procedure proposed in literature [4], and they correspond to three different acid-to-GO molar ratios (1, 20 and 200). The latter have been calculated by considering a structural

formula of GO ($C_{1.5}H_{0.2}N_{0.01}S_{0.03}O$), which has been roughly estimated from the elemental analysis of the commercial dispersion.

IV. MORPHOLOGICAL AND OPERATIVE CHARACTERIZATION

The effectiveness of the proposed sulfonation method has been confirmed by ATR-FTIR and SEM-EDX spectroscopies. The latter demonstrated an increase in the weight percentages of oxygen and sulfur after the functionalization reaction, while the former allowed to identify the characteristic bands corresponding to the stretching vibrations of O=S=O ($1143-1153\text{ cm}^{-1}$) and S-O ($870-880\text{ cm}^{-1}$) in sulfonic acid groups, as displayed in Fig. 1. In addition, with respect to the infrared spectrum of virgin GO, in those of SGO membranes we witnessed the vanishing of the bands corresponding to carboxyl moieties ($1300-1400\text{ cm}^{-1}$) and to less stable oxygenated functions (981 cm^{-1}), such as lactols and peroxides. Along with the appearance of the stretching mode (1580 cm^{-1}) of C=C bonds in sp^2 , unoxidized, graphitic domains, this suggested that the functionalization reaction has induced a probable reduction and amorphization of the structure of GO. These findings have been verified by X-ray diffraction and thermogravimetric analyses as well.

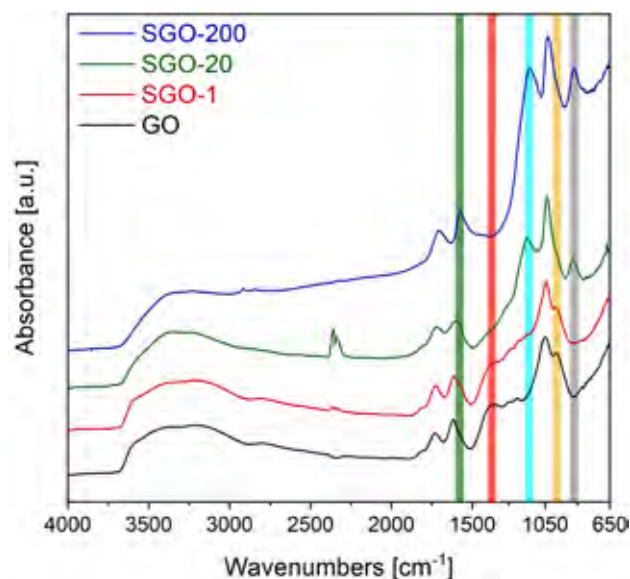


Fig. 1. ATR-FTIR spectra of GO and SGO-X membranes; colored bands point out the characteristic vibrations of S-O (gray), O=S=O (cyan) and C=C (green) bonds, as well as those of carboxyl (red) and less stable (yellow) moieties that are lost after sulfonation.

Water uptake tests have been carried out in a small-scale humid chamber by exploiting an oil bath to control the temperature between 20 and 100 °C, while deionized water or a saturated solution of $Mg(NO_3)_2$ have been employed to vary the level of humidification between 95% and 53%, respectively. Sulfonation resulted in an improved water uptake behavior as against both virgin GO and Nafion[®], in particular at reduced humidification and elevated temperature. However, the rising of the

acid-to-GO molar ratio caused a significant increase in the swelling ratio, symptom of a reduced structural stability. The ion exchange capacity has been enhanced as well by the functionalization with sulfonic acid moieties, with values higher than 1 meq g^{-1} for SGO-X membranes, almost twice the one measured for a reference sample of Nafion[®] 212 (about 0.7 meq g^{-1}). The best results have been achieved with $X = 20$, suggesting that the optimal sulfonation ratio probably lies close to this value.

The preliminary test in a hydrogen-fed fuel cell performed on a specimen of SGO-1 demonstrated a promising compression resistance and a practically absent contamination by carbon residues coming from the gas diffusion electrode, which are a typical issue in the case of Nafion and a sign of degradation of the catalyst. The open circuit voltage has been significantly improved with respect to virgin GO (0.63 vs 0.24 V), but it is still too low for practical applications, most likely because of hydrogen crossover issues. However, morphological and thermal characterization performed after the test demonstrated a fair stability of the functionalization to the fuel cell environment, especially in the bulk, while major changes took place on the surface, with the loss of less stable moieties.

V. CONCLUSION

A simple and effective method has been developed for the sulfonation of graphene oxide, and the resulting membranes have shown a promising behavior under different testing conditions, in particular from the point of view of water uptake and ion exchange capacity. These results confirmed the potential of freestanding sulfonated graphene oxide for the application in PEMFCs as an alternative electrolyte to Nafion[®]. Future developments of these components should address some stability issues concerning the introduced functionalities, in order to make the sulfonation process more efficient and to improve the cohesion of the membrane.

REFERENCES

- [1] Barbir, F., Introduction – in PEM Fuel cells – 2nd ed., Academic Press, 2013, pp. 1-16.
- [2] Li, Q., He, R., Jensen, J.O., Bjerrum, N.J., Approaches and recent development of polymer electrolyte membranes for fuel cells operating above 100 °C, Chemistry of Materials, Volume 15, 2003, Issue 26, pp. 4896-4915.
- [3] Bayer, T., Bishop, S., Nishihara, M., Sasaki, K., Lyth, S. M., Characterization of a graphene oxide membrane fuel cell, Journal of Power Sources, Volume 272, 2014, pp. 239-247.
- [4] Cheng, T., Feng, M., Huang, Y., Liu, X., SGO/SPEN-based highly selective polymer electrolyte membranes for direct methanol fuel cells, Ionics, Volume 23, 2017, Issue 8, pp. 2143-2152.

ENHANCEMENT OF OXYGEN REDUCTION REACTION ACTIVITY ON PHOSPHOR AND NITROGEN CO-DOPED TiO₂ CATALYST FOR POLYMER ELECTROLYTE FUEL CELL CATHODES

M. Chisaka*

*Hirosaki University, 3 Bunkyo-cho, Hirosaki, Aomori 036-8561
(Japan)

Abstract – The catalysts free from both platinum group metals and carbon supports are attractive for the use in polymer electrolyte fuel cell cathodes. Carbon support free titanium oxide based catalysts have suffered from the low activity. Recent attempts to enhance the activity by doping a new element, phosphor, will be presented at the meeting.

Non-platinum catalyst, Oxygen Reduction Reaction, PEFC, Titania

I. INTRODUCTION

Polymer electrolyte fuel cells (PEFCs) have been expected to replace internal combustion engines in vehicles which operate over 300 miles or carry high loads of buses and trucks [1]. Despite the worldwide trend to regulate vehicle emissions, the widespread use of PEFC-powered vehicles has not yet been recorded.

The rate for oxygen reduction reaction (ORR) at the cathode is much slower than that for hydrogen oxidation reaction (HOR) at the anode and currently ca. 4 times larger amount of platinum group metals (PGMs) is needed at the cathode [2]. As a result, the usage of high cost and scarce PGMs in PEFCs is still one order of magnitude larger than conventional internal combustion engines [3] and thus the reduction of PGMs is urgently needed for the widespread use of PEFCs. Besides, carbon supports for the PGM catalysts are easily oxidized during the start-up/shut-down of the vehicles. Non carbon supports are also needed to decrease the cost of automotive PEFCs.

The highly oxidative conditions of PEFC cathodes, i.e., (i) the strong acidity in which pH is less than 1 [4], (ii) high operating voltage between 0.6 and 1.0 V [5], and (iii) low operating temperature (typically ~353 K [5]), have limited the choice of non-PGM catalyst types. We developed a new non-PGM catalyst,

nitrogen-doped rutile TiO₂ covered on conductive nitride, TiN in the last three years. The activity has been enhanced by replacing the carbon black support [6] to Ti₄O₇ fiber [7], and even without using supports [8]. However, the maximum activity was still lower than the state-of-the-art non PGM catalyst, so-called Fe/N/C whose volume is mostly graphitic carbon with abundant micro pores. One of the reasons was the lower surface area when compared with that of Fe/N/C and thus high catalyst loading, 2.0 mg cm⁻² was necessary even for the half cell tests to form catalyst layers without “catalyst islands”. To enlarge the surface area and to reduce the catalyst loading, a new element, phosphor was doped into the carbon-support-free nitrogen-doped rutile TiO₂ catalysts recently [9]. The mass activity has been successfully improved by a factor of two with reduced catalyst loading, 0.86 mg cm⁻² owing to the phosphor doping.

In this study, some attempts have been made to further enhance the activity of recently developed phosphor and nitrogen codoped rutile TiO₂ catalysts.

II. EXPERIMENTS

The carbon-support-free TiO₂ based catalysts were synthesized using a recently developed facile combustion method [9] with some modifications including using a new precursor, introducing the new mixing method etc. The obtained catalysts were characterized using field emission scanning electron microscopy (FE-SEM), transmission electron microscopy (TEM), X-ray diffraction (XRD) analyses, Raman spectroscopy and X-ray photoelectron spectroscopy (XPS). The activity and selectivity were evaluated in 0.1 mol dm⁻³ H₂SO₄ solution.

III. RESULTS

The Raman and XP spectra indicate that the surface was rutile TiO_2 doped with pentavalent phosphor and nitrogen atoms. The activity has been successfully enhanced by increasing the surface phosphor content when compared with the previously best catalysts [9]. The chemical states of surface titanium and nitrogen atoms did not change significantly, which indicate that phosphor atoms played an important role to increase the activity.

IV. CONCLUSION

The low activity, which is critical to use oxide-based catalysts has been improved without using carbon supports, which should degrade the performance during start-up/shut-down of the cell. The mechanism will be presented at the conference.

ACKNOWLEDGMENT

The author acknowledges Dr Kohei Okitsu, Prof Hojun Im and Mr Yusei Tsushima for providing assistance in obtaining the XP spectra, Raman spectra and microscopy images, respectively. This work was partially supported by a Grant-in-Aid for Scientific Research (C) (17K06180) from the Ministry of Education, Culture, Sports, Science, and Technology (MEXT) of Japan; a research grant from Iketani Science and Technology Foundation, Japan; a research grant from SEI Group CSR Foundation in Japan and a research grant from the Salt Science Research Foundation in Japan. The X-ray photoelectron spectra were acquired with the support by Nanotechnology Platform of the MEXT of Japan.

REFERENCES

- [1] Eberle, U., von Helmolt, R., Sustainable Transportation Based on Electric Vehicle Concepts: A Brief Overview, *Energy & Environmental Science*, Volume 3, 2010, pp. 689-699.
- [2] Kongkanand, A., Mathias, M. F., The Priority and Challenge of High-Power Performance of Low-Platinum Proton-Exchange Membrane Fuel Cells, *Journal of Physical Chemistry Letters*, Volume 7, 2016, pp. 1127-1137.
- [3] Chisaka, M., in *Electrocatalysts for Low Temperature Fuel Cells: Fundamentals and Recent Trends*, T. Maiyalagan and V. S. Saji (Eds); Wiley-VCH, 2017, p.423-441.
- [4] Jaouen, F., Herranz, J., Lefèvre, M., Dodelet, J. P., Kramm, U. I., Herrmann, I., Bogdanoff, P., Maruyama, J., Nagaoka, T., Garsuch, A., Dahn, J. R., Olson, T., Pylypenko, S., Atanassov, P., Ustinov, E. A., Cross-Laboratory Experimental Study of Non-Noble-Metal Electrocatalysts for

the Oxygen Reduction Reaction, *ACS Applied Materials & Interfaces*, Volume 1, 2009, pp. 1623-1639.

- [5] Ohma, A., Shinohara, K., Iiyama, A., Yoshida, T., Daimaru, A., Membrane and Catalyst Performance Targets for Automotive Fuel Cells by FCCJ Membrane, Catalyst, MEA WG, *Electrochemical Society Transactions*, Volume 41, 2011, pp. 775-784
- [6] Chisaka, M., Ando, Y., Itagaki, N., Activity and Durability of the Oxygen Reduction Reaction in a Nitrogen-Doped Rutile-Shell on TiN-Core Nanocatalysts Synthesised via Solution-Phase Combustion, *Journal of Materials Chemistry A*, Volume 4, 2016, pp. 2501-2508.
- [7] Chisaka, M., Ando, Y., Yamamoto, Y., Itagaki, N., A Carbon-Support-Free Titanium Oxynitride Catalyst for Proton Exchange Membrane Fuel Cell Cathodes, *Electrochimica Acta*, Volume 214, 2016, pp. 165-172.
- [8] Chisaka, M., Creation of Oxygen Reduction Reaction Active Sites on Titanium Oxynitride Without Increasing the Nitrogen Doping Level, *Physical Chemistry Chemical Physics*, Volume 20, 2018, pp. 15613-15617.
- [9] Chisaka, M., Morioka, H. Phosphor and Nitrogen Co-doped Rutile TiO_2 Covered on TiN for Oxygen Reduction Reaction in Acidic Media, *Catalysis Science & Technology*, Volume 9, 2019, pp. 611-619.

MODELLING AND VALIDATION OF A SMALL-SCALE HYBRID PHOTOVOLTAIC-BATTERY-ELECTROLYZER SYSTEM

M. A. Ancona, M. Bianchi, L. Branchini, F. Catena, A. De Pascale, F. Melino, A. Peretto
 DIN – Università di Bologna, Viale del Risorgimento 2, 40136 Bologna (Italy)

Abstract – In this study, the behaviour of a small-scale hybrid energy system is predicted by means of a developed calculation model. In more detail, the experimental setup consists of photovoltaic panels, batteries and an electrolyzer; the mathematical sub-models for each device are provided. These sub-models have been validated by means of experimental data, recorded during laboratory tests. The results show that each sub-model reproduces very well the experimental data and then the whole system model can be applied to identify the optimal management strategy of a solar-to-hydrogen micro-scale system.

Index Terms – photovoltaic; hydrogen; battery; experimental setup.

I. INTRODUCTION

The study analyses a micro-scale hybrid photovoltaic/battery/hydrogen system, installed at the “micro-grid and storage” laboratory test facility of the University of Bologna. The main components of the analyzed integrated system are photovoltaic (PV) panels, batteries and an electrolyzer. This paper represents a prosecution of Author’s previous study [1], in which the system experimental arrangement was described in detail, and the aim is to model the components in order to simulate the behavior of the whole system. To this purpose, literature models for the PV panels and the batteries are here used, adapted to the system and integrated with experimental data; the electrolyzer, instead, is modelled directly using experimental data recorded during laboratory tests.

II. COMPONENTS SUB-MODEL DESCRIPTION AND RESULTS OF THE VALIDATION

Fig.1 shows the block diagram of the whole system model. It is made up of three main sub-systems that will be described in the following paragraphs: the PV sub-model (yellow block), the battery sub-model (green block) and the electrolyzer sub-model (blue block).

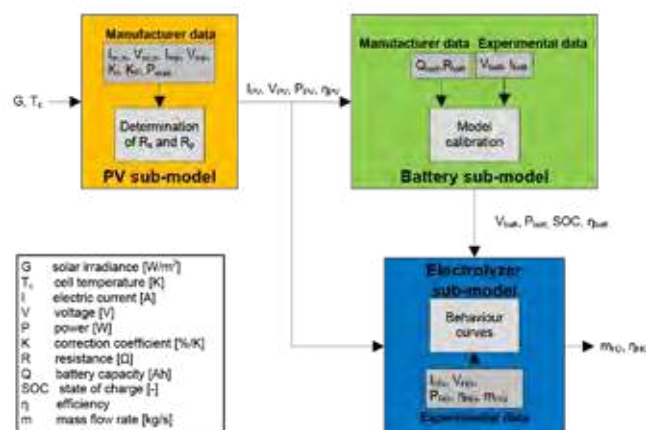


Fig. 1. Block diagram of the whole system model.

A. PV panels

A mathematical model that describes the behaviour of a PV panel has to take into account the performances variation caused by changes in operating conditions. The main parameters affecting the PV panel performances are the solar radiation and the module temperature, besides the operating voltage and the electric current. The sub-model employed in this paper is described in [2]. This PV model is based on data commonly available on the PV panel datasheet and it can be applied to any solar module. Fig. 2 shows the electric current production of the PV panels with respect to the cell voltage. The values obtained from the sub-model (red dots in Fig. 2) properly fit the experimental values (black dots in Fig. 2).

B. Batteries

The sub-model chosen to simulate the battery behaviour is described in [3]. It is a semi-empirical model which has been calibrated and adapted by means of available experimental data. As the model is based on the dependence of the battery voltage on the input or output electric current, targeted laboratory tests have been carried out, aimed at identifying the charging and discharging curves.

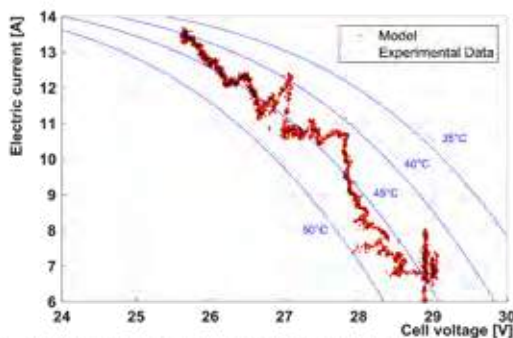


Fig. 2. Electric current produced by the PV panels with respect to the cell voltage as a function of the cell temperature.

The comparison between the experimental data and the calibrated models, is shown in Fig. 3. The discharging model is in good agreement with the experimental data in the battery operating field, showing a maximum error equal to 1.48 %. Also the charging phase shows a good agreement between the experimental data and the model, with a maximum error equal to 1.51 %.

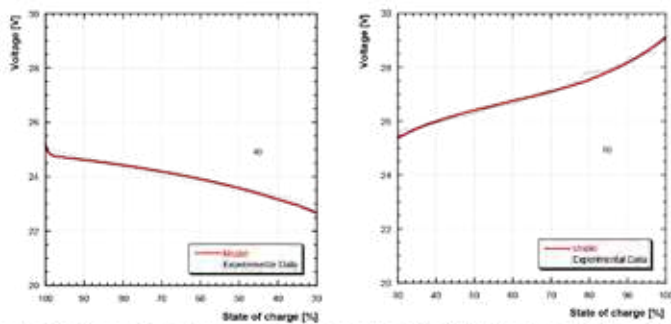


Fig. 3. Comparison between experimental data (in black) and model (in red): (a) discharging phase, (b) charging phase.

C. Electrolyzer

In order to reproduce the electrolyzer behaviour within the system, two possible operating strategies have been considered: (1) fixed-voltage mode and (2) variable-voltage mode. In the first case a constant input voltage feeds the electrolyzer, while in the second case the electrolyzer is able to work within a voltage supply range. Several experimental tests have been carried out in order to characterize the electrolyzer when operated in the two modes in its operating field (from 120 W up to 200 W). The results of the test campaign are shown in Fig. 4. It can be observed that even if the efficiency should be almost constant with a constant input voltage (Fig. 4a), there's a slight variation due to the micro-scale of the device. In variable-voltage mode (Fig. 4b), instead, the efficiency varies from a value of about 0.50 (for an input power equal to about 200 W) to a maximum value of about 0.83 (for an input power equal to about 120 W). These results can be explained considering that the electrolyzer efficiency is proportional to a constant factor per applied voltage, as shown in [4]. In both cases, the efficiency can be modelled by a third-degree polynomial

function.

III. CONCLUSION

In this study, sub-models of photovoltaic panels, batteries and an electrolyzer have been proposed. These models have been adapted to an experimental setup, consisting in a micro-scale hybrid system composed by PV panels, batteries and an electrolyzer. The models have been validated with experimental data, recorded during targeted laboratory test. The sub-models results show an excellent fitting between models' response and experimental data. Then, the whole system model has been applied to identify the optimal management strategy of a solar-to-hydrogen micro-scale system with the aim to maximize the total conversion efficiency (from irradiance to produced H_2). The considered strategies differ on the several operation modes of each component of the system. Depending on adopted management strategy, results show values of the total conversion efficiency ranging from less than 1% up to a maximum of 4.6%.

This evidence strongly demonstrates that the optimal management of all the components and their appropriate interaction is the key for the maximization of hydrogen production from solar source.

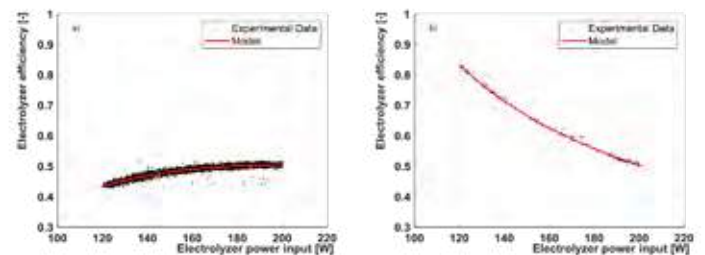


Fig. 4. Trend of the electrolyzer efficiency as a function of the input power for the two operating modes: a) fixed-voltage mode; b) variable-voltage mode.

REFERENCES

- [1] Ancona, M. A., Bianchi, M., Branchini, L., De Pascale, A., Melino, F., Peretto, A., ... & Scarponi, L. B. (2017). From solar to hydrogen: Preliminary experimental investigation on a small scale facility. *International Journal of Hydrogen Energy*, 42(33), 20979-20993.
- [2] Villalva, M. G., Gazoli, J. R., & Ruppert Filho, E. (2009). Comprehensive approach to modeling and simulation of photovoltaic arrays. *IEEE Transactions on power electronics*, 24(5), 1198-1208.
- [3] Tremblay, O., & Dessaint, L. A. (2009). Experimental validation of a battery dynamic model for EV applications. *World electric vehicle journal*, 3(2), 289-298.
- [4] Gruber, M., Weinbrecht, P., Biffar, L., Harth, S., Trimis, D., Brabandt, J., ... & Blumentritt, R. (2018). Power-to-Gas through thermal integration of high-temperature steam electrolysis and carbon dioxide methanation-Experimental results. *Fuel Processing Technology*, 181, 61-74.

H2PORTS. HYDROGEN REFUELLING SYSTEM DEVELOPMENT IN THE PORT OF VALENCIA

C. Ballester* and C. Fúnez*

*Hydrogen National Centre (CNH2), Prolongación Fernando el Santo s/n, 13500 Puertollano (Ciudad Real), Spain.

Abstract - Hydrogen is an energy carrier with great potential for clean, efficient power in transport applications. Hydrogen can be obtained from different sources, which in combination with fuel cells it can improve energy efficiency. This project tries to introduce hydrogen as an alternative fuel in the port industry.

The H2Ports project is an Action aligned with the needs and objectives of the European Commission and the port industry. The aim is to provide efficient solutions to facilitate a fast evolution from a fossil fuel based industry towards a low carbon and zero-emission sector.

H2Ports aims to test and validate hydrogen-powered solutions in the port-machinery industry with the target of having applicable and real solution without affecting port operations while producing zero local emissions. The project involves a mobile hydrogen refueling system which supplies hydrogen to two different heavy duty vehicles. The port machineries are a reach stacker and a yard tractor. Both vehicles are in two different terminals, MSC and Grimaldi.

Because ports regulation, the port machinery cannot leave their terminals so the solution that has been developed is a mobile refueling station which will travel along the port to supply hydrogen to the heavy duty vehicles in their terminals. The facility will be based in the port of Valencia allocated near both terminals.

Index Terms – Hydrogen refueling station, mobile hydrogen station, decarbonation of maritime ports.

I. INTRODUCTION

Maritime transport and the port sector are a powerful source for job creation and economic welfare. The increase of foreign trade in European ports has led the expansion and improvements of many of them from many perspectives. This evolution has provided remarkable benefits in the society boosting global trade and facilitating the access to goods worldwide. However, the increase of infrastructure, services and logistics have important negative impacts on the environment, especially on the cities located nearby ports.

The intensive consumption of energy during port operations, with a significant part coming from fossil fuels, leads to the release of pollutants and greenhouse gases. This has motivated port authorities from all around the world to become cleaner and more efficient, and

the Port of Valencia has a clear strategy in this sense in which the use of hydrogen plays an important role. This is aligned with Regulation 2014/94/EU of the European Parliament related to the implementation of an infrastructure for alternative fuels, hydrogen is called to be one of the alternative fuels to current fossil-based ones.

The main tool that the European Commission has deployed to promote the hydrogen sector is the FCH 2 JU, a unique public private partnership supporting research, technological development and demonstration (RTD) activities in fuel cell and hydrogen energy technologies in Europe.

In 2017, the FCH 2 JU launched the initiative entitled "Fuel Cells and Hydrogen for Green Energy in European Cities and Region" to support regions and cities reducing emissions and favoring their energy transition. Port applications were identified in the study as one having high environmental benefit even though their low Technological Readiness Level. FCH 2 JU's Annual Work Plan 2018, promoted the development of vehicles in port operations and selected H2Ports project in order to demonstrate that hydrogen is a feasible alternative and cleaner energy source to take into account in the port-maritime sector.

The H2Ports Project aims to develop, deploy, test and to benchmark industrial heavy duty port cargo-handling equipment powered with Fuel Cells (FC) to be used in real port operation. A Yard tractor and a Reach stacker have been selected as those specially fitted to the use of FC in port facilities.

H2Ports helps to facilitate a fast decarbonation of the port-logistic industry applying hydrogen technologies already used in other sectors but not adopted yet in the European port sector. So this project is a novelty idea to be implemented in more ports in the future. H2Ports is a highly ambitious project, aiming to deploy port equipment working with hydrogen as a fuel, in the Port of Valencia (Spain) as a test and demonstration site.

II. HYDROGEN REFUELLING SYSTEM

A. Process Introduction

The facility will be based in the port of Valencia allocated near both terminals [1]; it will have four main parts:

- Reception hydrogen storage
- Compressor
- Cascade pressure system
- Dispenser

Due to port regulations the vehicles cannot leave the terminals so the refueling station should move along the port and the terminals to refill the vehicle tanks. Therefore, the installation will have two different parts:

- Mobile unit: the dispenser and the cascade pressure vessels
- Static part: the compressor and the storage tank.

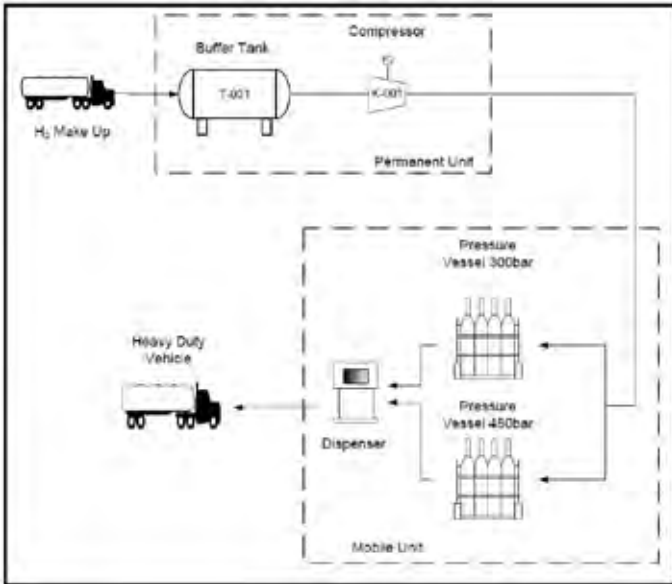


Figure 1. Hydrogen Refueling Station Schematic

B. Process Description

The hydrogen refueling system (HRS) facility has been configured in such a way that the set of two heavy duty vehicles will be able to refuel fuel hydrogen within their terminals [2].

The HRS receives the hydrogen gas from the gas supplier and it is stored in the buffer tank. This deposit is connected to the compression part where the gas will be compressed up to 450bar. Once the hydrogen has been compressed, it is connected to a cascade pressure tank system which has a dispenser integrated. The pressure system is a cascade pressure system and has 2 levels of pressure. 300 bar and 450 bar.

This entire unit is a mobile unit and it will move from the HRS facility to the terminals to refuel the vehicles which have been mentioned previously.

C. Facility Details

Buffer Tank: The storage tank will receive the hydrogen gas from the supplier and will store the pressured gas at 40bar. The storage tank is a horizontal vessel with a volume of 50m³ at 40bar.

Compressor: The compressor will receive the hydrogen gas from the buffer tank at a minimum of 10bar and maximum

40bar. The compressor will be able to compress the gas up to 300bar and 450bar due to the FC vehicle admit the gas at 350bar.

Cascade pressure system: The high pressure storage facility on this project is a cascade storage system. This system has two pressure vessels which are medium pressure (300bar) and high pressure (450bar). There have been studies showing a better performance over the buffer systems and it is considered as the most appropriate configuration for the storage system [3]. This configuration allows the facility to start the refueling with the lowest pressure vessel. When the flow rate gets the set point value the flow will come from the highest pressure level till the tank in the heavy duty vehicle is completely full

Dispenser: Hydrogen dispenser will supply hydrogen to the heavy duty vehicle up to 350bar. During filling, the vehicle hydrogen tank is first connected to the lowest pressure vessel up to reach equal pressure level; afterwards, hydrogen will be supplied through the highest pressure vessel up to get 350 bar in the on-board tank. Regarding standard regulation the supply should be done at 3.6kg/min as maximum flow rate [4].

III. CONCLUSION

H2Ports sorts out the issue of refueling final user where the access to a hydrogen fuelling system is not as easy as in a standard refueling station. This mobile unit solution allows to heavy duty vehicles do not leave their terminals to be refueled due to Maritime Port's regulations.

ACKNOWLEDGMENT

This project has received funding from the Fuel Cells and Hydrogen 2 Joint Undertaking under grant agreement No (826339). This Joint Undertaking receives support from the European Union's Horizon 2020 research and innovation program, Hydrogen Europe and Hydrogen Europe research. The authors would also like to thank to all the participants within the consortium of the H2Ports project.

REFERENCES

- [1] Royal Decree 656/2017, of June 23, Whereby the Approving the Technical Regulation for the Storage of Chemical Products and its complementary technical instructions
- [2] Argonne National Laboratory: Hydrogen Refueling Analysis of Fuel Cell Heavy-Duty Vehicles Fleet.
- [3] Mahmood Farzaneh-Gord: "Effects of storage types and conditions on compressed hydrogen fuelling stations performance". International Journal of Hydrogen Energy 37 (2012) 3500-3509
- [4] SAE J2601-2 "Surface Vehicle Technical Information. Fueling Protocol for Gaseous Hydrogen Powered Heavy Duty Vehicles".

ESTIMATING TEMPERATURE IN THE CATALYST LAYER OF THE PEM FUEL CELL

A. Stoilova^{1,2}, F. Barbir^{1,2}, and Ž. Penga^{1,2}

¹ Center of Excellence for Science and Technology – Integration of Mediterranean Region (STIM-REI) at University of Split, Poljicka cesta 35, 21000 Split, (Croatia)

² Faculty of Electrical Engineering, Mechanical Engineering and Naval Architecture (FESB), University of Split, R. Boskovicica 32, 21000 Split, (Croatia)

Abstract - Temperature has an important role in the degradation of polymer electrolyte membrane (PEM) fuel cells. Prolonged operation at high temperature conditions may lead to morphological changes in ionomer surrounding the most active catalyst sites, i.e., where the local current density is the highest. Insertion of even the smallest thermocouples in the catalyst layer or even at the interface between the catalyst layer and the gas diffusion layer would change the flow distribution patterns and, therefore, the current density distribution and the temperature distribution. By inserting an S++ segmented sensor plate between the cathode bipolar plate and the collecting plate, it is possible to measure current distribution in an 11×11 array and the temperature distribution in a 6×6 array. The obtained current and temperature distribution data is then used as a boundary condition for a computational fluid dynamics (CFD) model which in turn can calculate the temperatures inside the catalyst layer.

Index Terms – catalyst layer, current and temperature distribution, local temperatures, S++ segmented current measurement sensor plate.

I. INTRODUCTION

Distribution of current density and temperature along the surface of polymer electrolyte membrane (PEM) is of paramount importance for life time of the cell. Non-uniform current density and temperature distribution can often cause starvation or localized corrosion of the membrane-electrode assembly (MEA) on the cathode side of the cell, potentially initiating and enhancing irreversible degradation. The membrane must be characterized by sufficient chemical and mechanical resistance in the specific fuel cell environment, and since the protonic conductivity, i.e. membrane water content of the membrane has direct influence on PEM fuel cell efficiency, temperature variations inside the MEA must be carefully addressed. Insufficient heat removal from the electrochemical reaction sites, i.e. triple-phase boundaries, can often result in the occurrence of high temperatures inside the cathode catalyst

layer, potentially causing morphological changes in the polymer electrolyte. Since the operating environment inside the catalyst layer is specific – thickness of ca. 10 micrometers it is impossible to measure or monitor the local temperature distributions on such a small scale with intrusive methods due to significant alteration of the operating conditions. For this reason, 3D computational fluid dynamics (CFD) model was developed to give insight in the spatially resolved temperature and current density distribution inside the MEA.

II. EXPERIMENTAL

A segmented S++ current measurement sensor plate, sandwiched between the bipolar plate and the current collecting plate, was used to examine the current and temperature distribution on the cathode side of the PEM fuel cell. The bipolar plate has 4 parallel channel serpentine design configuration. Silicone gaskets (415 μm thick) were employed for both electrodes to provide the required compression ratio. Measurements were performed on a single 50 cm² cell (50 μm) MEA at 80 °C and under 100 % relative humidity at various operation points. Current was adjusted at the desired values preselected for the study. Other relevant details regarding measurement are available in Table I.

TABLE I

OPERATING CONDITIONS FOR THE EXPERIMENT

Stoichiometry (Anode/Cathode)	2 of H ₂ / 4 of Air		
Anode backpressure (g)	0.2		
Cathode backpressure (g)	0.2		
Anode inlet relative humidity	100 %		
Cathode inlet relative humidity	100 %		
Cell temperature	80 °C		
Current	10 A	20 A	30 A
Anode reactant flow rate	0.15 L min ⁻¹	0.29 L min ⁻¹	0.44 L min ⁻¹
Cathode reactant flow rate	0.66 L min ⁻¹	1.34 L min ⁻¹	2.02 L min ⁻¹

The segmented plate consists of 11x11 segments for current and 6x6 segments for temperature distribution. During each operating point, current and temperature distribution data were collected every 0,5 seconds, during a two-hour period.

III. RESULTS AND DISCUSSION

Obtained results during the measurements were shown to be repeatable on every default current, with the maximum deviation close to inlet and outlet at given locations on the sensor plate. In Fig.1 the currents are shown on chosen segments, i.e. 4, 30, 49, 85 and 104, instead of showing the entire data set to avoid overcrowding the diagram with data. It can be seen that the currents shown in the diagram have periodic disturbances, this is due to the current interrupt being activated in the background.

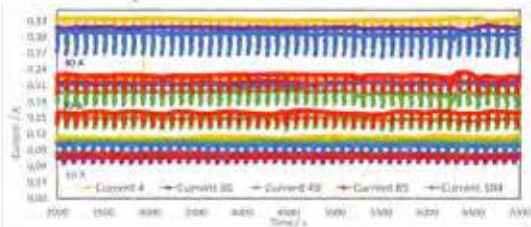


Fig. 1. Current distribution on the cathode side of the fuel cell at 10 A, 20 A and 30 A.

In Fig. 2 it can be seen that the temperatures on the segments are different from the cell temperature, i.e. the temperature of the thick end plates, and this difference is highest for the low current case (10 A), and lowest for the high current case (30 A). The difference in the temperatures is a result of heat losses. It is clearly visible that the differences are minimized at higher currents as a consequence of the released heat during the electrochemical reactions inside the fuel cell.

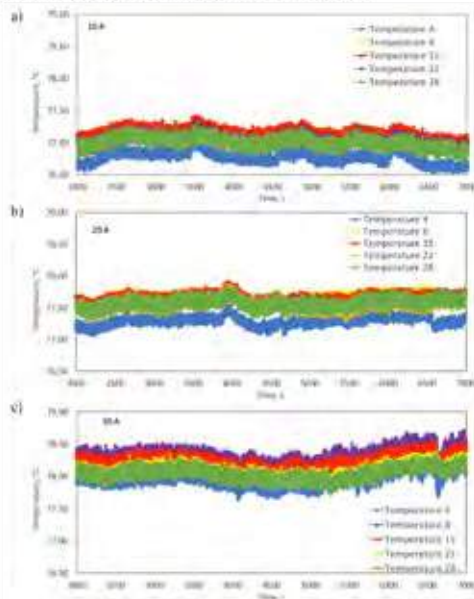


Fig. 2 Temperature distribution on the cathode side of the fuel cell at a) 10 A; b) 20 A and c) 30 A.

Fig. 3 shows temperatures profiles estimated by the 3D CFD model on the terminals and inside the catalyst layer for the cathode side for a similar flow field (triple serpentine). The difference between the maximal temperature at the current collectors and the catalyst layers is ca. 7 °C at current density of 500 mA cm⁻² and ca. 18 °C at current density of 1000 mA cm⁻², which is very significant for the membrane degradation.

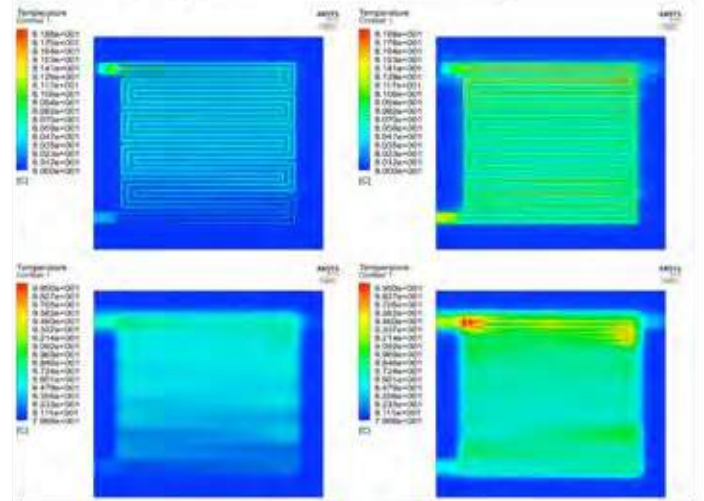


Fig. 3. Temperature contours along the mid-surface between the terminal and cathode channels (above) and in the middle of the cathode catalyst layer (below) for at current density of 500 mA cm⁻² (left) and 1000 mA cm⁻² (right) obtained by the 3D CFD model.

IV. CONCLUSION

The objective of this work was to estimate the temperature inside the cathode catalyst layer of PEM fuel cell at different operating currents. The experimental investigation is conducted using segmented cell and the results of current density distribution and temperature distribution show uniform distribution along the entire flow field. Since it is not possible to measure the temperature directly inside the catalyst layer, 3D CFD model is developed using similar boundary conditions and similar flow field to estimate the temperature inside the cathode catalyst layer. The results of the CFD analysis show that the difference between the maximal temperature inside the current collectors and the catalyst layers is ca. 7 °C at current density of 500 mA cm⁻² and ca. 18 °C at current density of 1000 mA cm⁻², which is very significant for the membrane degradation and should be studied in more details in the future. Since the current density and temperature distributions for this particular case were uniform, in a future study partially humidified operating conditions will also be considered to determine the influence of non-uniform effects on the cell performance and compare it with the CFD model results.

ACKNOWLEDGMENT

The research was supported under the project Center of Excellence for Science and Technology – integration of Mediterranean region (STIM-REI), (KK.01.1.1.01.0003), which is funded by the ERDF - OPCC 2014-2020.

Synthesis and Characterization of $\text{Ca}_2\text{Fe}_{1.95}\text{Mg}_{0.05}\text{O}_5$: Innovative Low Cost Material for Reversible Solid Oxide Cell

E. Squizzato*, G. Carollo*, and A. Glisenti* **

*Università degli Studi di Padova, Dipartimento di Scienze
Chimiche, Padova, 35131, (Italy)

** CNR-ICMATE, INSTM

The creation of Reversible Solid Oxide Cells (Re-SOCs) is able to reduce costs and to increase the reliability of SOFCs. Recent studies have shown interesting properties on brownmillerites, oxygen defective double-perovskites. In this contribution, we focus on $\text{Ca}_2\text{Fe}_{1.95}\text{Mg}_{0.05}\text{O}_5$ (CFMO). The synthesis was carried out by an auto-combustion based citrate procedure (Marcilly method) and characterized by different techniques (XRD, H_2 -TPR, XPS, EDX, SEM) to evaluate its suitability as a SOFC electrode. The material was electrochemically characterized as a cathode by EIS, obtaining low ASR values ($0.19 \Omega\text{cm}^2$ at 800°C). EIS investigation of CFMO was carried out at different oxygen partial pressures to verify stability under different atmospheres. Further enhancement of electrocatalytic performance was obtained by building nanocomposites of the type FeO_x/CFMO . To this purpose both exsolution and wet impregnation (10-15 wt. %) have been used and compared. The obtained results indicate that $\text{Ca}_2\text{Fe}_{1.95}\text{Mg}_{0.05}\text{O}_5$ can be a possible low cost solution as cathode material for SOFCs.

Brownmillerite, Innovative low cost material, Reversible Solid Oxide Fuel Cell, Sustainable energy.

I. INTRODUCTION

All of us knows fossil fuels related problems and the importance of finding new green and cheap alternative technologies for energy production. Solid Oxide Fuel Cells (SOFCs) can be a valid support in pursuing sustainable development. A way to reduce costs and to increase the reliability and life span of a SOFC is the creation of a Reversible Solid Oxide Cell (Re-SOC). Recent studies have shown interesting properties on brownmillerite compounds, which make them suitable as electrode materials for Re-SOCs. A brownmillerite is an oxygen defective double-perovskite, with a structure $\text{A}_2\text{B}_2\text{O}_5$. Their oxygen vacancies are able to

enhance the material ionic conductivity.^[1] In this contribution, we focus on $\text{Ca}_2\text{Fe}_{1.95}\text{Mg}_{0.05}\text{O}_5$ (CFMO). Magnesium doping was carried out to emphasize $\text{Fe}^{3+}/\text{Fe}^{4+}$ redox couple and thus electronic conductivity.^[2]

II. EXPERIMENT PROCEDURE

A. Synthesis

$\text{Ca}_2\text{Fe}_{1-x}\text{Mg}_x\text{O}_5$ (CFMO) powders were synthesized by citrate route.^[3] Stoichiometric quantities of calcium carbonate (CaCO_3 Sigma-Aldrich 99%, powder), magnesium hydroxide ($\text{Mg}(\text{OH})_2$ Sigma-Aldrich 95%) and iron (Sigma-Aldrich 99.98%, chips) were dissolved in deionized water and nitric acid with a molar ratio of 1.9:1 with respect to the total amount of cations. Citric acid ($\text{C}_6\text{H}_8\text{O}_7$ Sigma-Aldrich $\geq 99.0\%$) is added as complexing agent under stirring and then the solution is lead to neutral pH by dropwise addition of ammonia hydroxide. Then, the solution was heated overnight allowing the formation of a gel, which burned by heating at 400°C . The formed powders were calcinated at 1150°C for 6 hours. Trying to improve the performances, other two electrodes alternatives were tested. In the first case, the electrode is made by an exsolution of magnetite (Fe_3O_4) particles, inserting the corresponding additional amount of iron (50% mol) during the citrate synthesis. The second one consists on the electrode infiltration of α -hematite (Fe_2O_3). Finally, the composite electrode was done by infiltration, adding drop by drop an aqueous solution containing the desired cation mass percentage on the already deposited electrode (10-15% wt).

B. Material Chemical and Physical characterization:

XRD diffractograms show a marked crystallinity of the powders; the comparison between the patterns of different batches, confirmed the good reproducibility of the synthesis. The TPR analysis has shown a hydrogen consumption higher than the theoretical value (calculated considering only Fe^{3+} cations), supporting the idea that different oxidation states for iron cations are present. The XPS semi-quantitative analysis has confirmed the absence of calcium or iron segregation on the powders' surface. The correct stoichiometry was confirmed also by EDX analysis. SEM images have shown the globular morphology of particles and a good porosity was also confirmed by BET analysis. The determined surface area is in good correspondence with typical perovskitic and brownmilleritic values present in literature ($4.6 \pm 0.1 \text{ m}^2 \cdot \text{g}^{-1}$).

C. Electrochemical characterization results:

CFMO: To verify stability and behavior of the material in different atmosphere conditions, a study of CFMO cathode performances in different partial pressures of oxygen was performed. The measurements were carried out at steady state condition (zero DC current) in the frequency range of 10^{-2} - 10^6 Hz and with signal amplitude of 50 mV. In air the impedance spectra show a semicircle at 800°C , which becomes larger when temperature decreases (thermo-activate process). Its frequency and capacitance make possible the attribution of this signal to oxygen adsorption/dissociation on the surface of the electrode material. Under 750°C , the oxygen reduction reaction semicircle compares and its resistance increases with the decrease of temperature. The appearance of a second semicircle at high temperatures characterizes the spectra at lower partial pressure of oxygen (Fig. 1). This signal increases when the oxygen concentration decreases. Its frequency and capacitance suggest its attribution to chemical capacitance. When temperature decreases ($\leq 700^\circ\text{C}$) this signal is covered by the semicircles of the oxygen adsorption/dissociation and reduction.

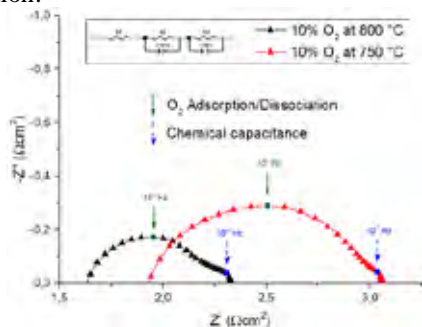


Fig. 1. EIS spectra for CFMO at 800°C - 750°C

CFMO-based nanocomposite To compare the effect of iron oxides on the electrocatalytic behavior of CFMO three other electrode materials have been prepared and tested: an electrode is composed by CFMO and magnetite particles obtained by exsolution; two electrodes were prepared by wet impregnation

of Fe_2O_3 in increasing amounts (10% - 15% wt. related to the electrode mass). Unlike CFMO electrode, they present a second semicircle at high temperatures ($800 - 750^\circ\text{C}$) even in air conditions. The stimulating frequency and capacitance suggest also in this case the presence of chemical capacitance processes. This process produces another contribution to resistance, determining higher ASRs for the nanocomposite, but it is noteworthy that the performances for oxygen adsorption/dissociation and reduction are improved.

	CFMO	CFMO + Fe_2O_3 10%	CFMO + Fe_2O_3 15%	CFMO + Fe_3O_4
T ($^\circ\text{C}$)	ASR (Ωcm^2)	ASR (Ωcm^2)	ASR (Ωcm^2)	ASR (Ωcm^2)
800	0.19	0.19	0.17	0.29
750	0.43	0.44	0.52	0.61

Tab. I. ASR values for the different cathodic solutions

III. CONCLUSION

In this work, a low cost brownmillerite material ($\text{Ca}_2\text{Fe}_{1.95}\text{Mg}_{0.05}\text{O}_5$) was synthesized and studied to understand its properties and performances as a cathode for Re-SOCs. EIS analysis was performed, obtaining promising ASR values ($0.19 \Omega\text{cm}^2$ at 800°C). $\text{Ca}_2\text{Fe}_{1.95}\text{Mg}_{0.05}\text{O}_5$ preliminary response as cathode material at high temperatures is very promising, considering its low cost compared to other state-of-art materials. All steps of device realization have been investigated and improved to increase adhesion and reduce electrode resistance (ink composition, thermal treatment, etc.). A chemical capacitance signal is observed at high temperatures. Three nanocomposites of the type FeO_x/CFMO have been prepared to see the effects of Fe_2O_3 (10 and 15 wt.%) and Fe_3O_4 on the electrochemical performance. These nanocomposites were prepared by exsolution and wet impregnation, to enhance the comparison. The presence of chemical capacitance was confirmed also in those electrodes. It would be important to reduce its resistance contribution, especially for composite electrodes that present lower values for adsorption and reduction resistances (Best result: $0.17 \Omega\text{cm}^2$ for 15% wt Fe_2O_3 infiltration).

REFERENCES

- [1] D. Hirabayashi, T. Yoshikawa, K. Mochizuki, K. Suzuki, and Y. Sakai, Formation of brownmillerite type calcium ferrite ($\text{Ca}_2\text{Fe}_2\text{O}_5$) and catalytic properties in propylene combustion, *Catal. Letters*, vol. 110, no. 3-4, pp. 269-274, 2006.
- [2] E. Asenath-Smith, I. N. Lokuhewa, S. T. Misture, and D. D. Edwards, p-Type thermoelectric properties of the oxygen-deficient perovskite $\text{Ca}_2\text{Fe}_2\text{O}_5$ in the brownmillerite structure, *J. Solid State Chem.*, vol. 183, no. 7, pp. 1670-1677, 2010.
- [3] C. Marcilly, P. Courty, and B. Delmon, Preparation of highly dispersed mixed oxides and oxide solid solutions, *J. Am. Ceram. Soc.*, vol. 53, no. 1, p. 56, 1970.

DEVELOPMENT OF CATHODE COOLING FINNS WITH A MULTI-HOLE STRUCTURE FOR OPEN-CATHODE POLYMER ELECTROLYTE MEMBRANE FUEL CELLS

Kyung Don Baik, Eun Hye Lee, and Sung Ho Yang
Agency for Defense Development, Daejeon, 305-152,
(Republic of Korea)

Abstract - The open-cathode polymer electrolyte membrane fuel cell (OC-PEMFC) system are generally adopted into drones or unmanned aerial vehicle as a power source due to the advantages of light weight. In this study, novel cathode cooling fins with a multi-hole structure (MHS) in the rib regions is developed to improve the stack performance. Results show that the OC-PEMFC with a MHS produces the higher stack performance than that with conventional design. Furthermore, the OC-PEMFC with conventional cooling fin design usually has a difficulty in maintaining a uniform temperature distribution within the stack, which is exacerbated with an increase in power density, which is one of the common problems in OC-PEMFC. The OC-PEMFC stack using a cooling fan with a MHS shows relatively uniform temperature distribution comparing with the conventional stack configuration due to the large flow path from MHS.

Index Terms - Open-cathode polymer electrolyte membrane fuel cell, Cooling fin, Multi-hole structure, Stack performance

I. INTRODUCTION

The polymer electrolyte membrane fuel cell (PEMFC) system is highly efficient and quiet operation and has been suggested as a promising alternative for future power generation systems. Currently, the PEMFC system is adopted as a power source such as an unmanned aerial vehicles (UAVs) or drones because it results in a longer flight duration compared with conventional battery propulsion systems.

Among the PEMFC system configuration of PEMFC, an air-cooled, open-cathode PEMFC (OC-PEMFC) type is widely adopted to the UAVs or drones due to its light weight and simple balance-of-plant (BOP) concept. The OC-PEMFC only uses fans in an open cathode flow path to supply external air and cool it so OC-PEMFC system does not need an air blower and liquid cooling system such as liquid pump and heat exchanger etc. Furthermore, OC-PEMFC system is a self-

humidifying system using water generated through the reaction so the external humidifier is not needed. Consequently, the OC-PEMFC can be simplified to adopt to the UAVs and drones due to its advantages [1].

Despite the many advantages of OC-PEMFC system, there are several problems to adopt the actual platform. Generally, it uses the supplying air as fuel (i.e., oxygen as an oxidant) and cooling gas at the same time when the outside air is supplied to the OC-PEMFC by the fans, which makes it difficult to ensure stable performance [2]. Thus, it is important to develop the new materials for the stable stack performance.

In this study, a new cooling fin with a MHS in the rib region for OC-PEMFC stack is developed for improving and stable stack performance. Here, we represent the results of current-voltage (I-V) polarization performance.

II. MATERIALS AND METHODS

A 20-cell OC-PEMFC stack was used for testing. A commercially available perfluorinated sulfonic acid membrane electrode assembly (MEA) with an active area of 30 cm² was used. Both the anode and cathode of the MEA were composed of typical Pt/C catalysts, and the Pt loadings of the anode and cathode were 0.1 and 0.4 mg Pt cm⁻², respectively. Both electrodes had GDLs (JNT20-A3, JNTG, Korea) with a substrate and MPL on one side.

The novel cooling fins have a multi-hole structure (MHS) in the rib regions. For the stack with the novel cooling fins, the additional air through the MHS in the rib regions can be supplied to the MEA. This makes it possible to supply additional gas in the rib regions, which results in a uniform gas concentration distribution. The overall structure of cooling fins is a parallel flow design. Aluminum with a thickness of 0.1 mm

was used as the substrate material.

The electrochemical performances of the OC-PEMFC stack was measured with a commercial fuel cell tester (G-60, Greenlight Innovation, Canada). The dry hydrogen was supplied to the anodes in through-flow mode and the ambient air was blown by two fans to the open cathode channels. The hydrogen flow rate was controlled with mass flow controller to be 4.5 SLPM. An activation process was conducted first to activate the fresh OC-PEMFC stack. After the activation process, the stack was characterized by measuring the I-V polarization performance.

III. RESULTS AND DISCUSSION

The electrochemical I-V & P-V performance of the OC-PEMFC stack under the supply of dry hydrogen is represented in Fig. 1. The stack with MHS in the rib regions showed no significant voltage drops. A voltage drop occurred at high currents when the general cooling fins with conventional rib/channel structure were used because of depleted oxygen supply to the catalyst in the rib regions. However, oxygen can be easily supplied through the MHS in the case of an OC-PEMFC stack with MHS. As a results, the power of OC-PEMFC stack was about 210 W at a current of 19 A. Fig. 2 showed the cell voltages of OC-PEMFC stack under the two different current conditions. The uniform distribution of cell voltages was observed.

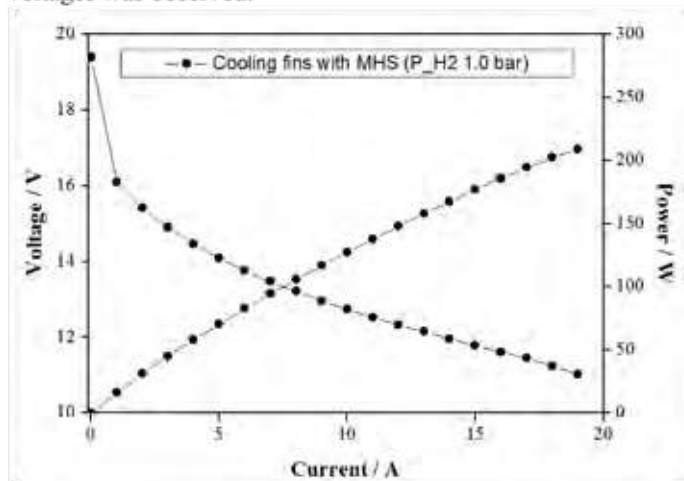


Fig. 1. The electrochemical I-V & P-V performance of the OC-PEMFC stack.

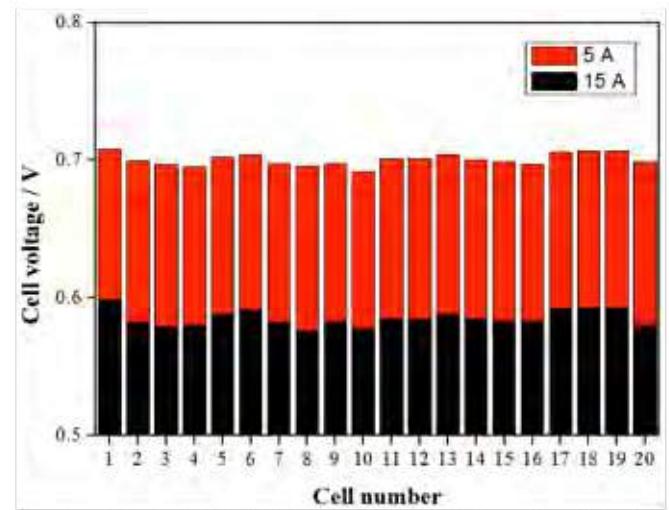


Fig. 2. Cell voltages of OC-PEMFC stack under the different currents.

IV. CONCLUSION

In this study, a new cooling fin with a MHS in the rib region for the OC-PEMFC stack was developed to improve performance. The OC-PEMFC stack with MHS cooling fins showed no significant voltage drop due to the MHS in the rib regions, resulting in the performance of about 210 W at a current of 19 A. The uniform cell voltage distribution was also observed.

ACKNOWLEDGMENT

The supports by the Defense Acquisition Program Administration and by the Agency for Defense Development of the Republic of Korea are greatly appreciated.

REFERENCES

- [1] Meyer, Q., Himeur, A., Ashton, S., Curnick, O., Clague, R., Reisch, T., et al. System-level electro-thermal optimisation of air-cooled open-cathode polymer electrolyte fuel cells: Air blower parasitic load and schemes for dynamic operation, *International Journal of Hydrogen Energy*, Volume 40, 2015, Pages 16760-16766.
- [2] De LHA., Vivas, FJ., Segura, F., Andújar, JM., How the BoP configuration affects the performance in an air-cooled polymer electrolyte fuel cell. Keys to design the best configuration, *International Journal of Hydrogen Energy*, Volume 42, 2017, Pages 12841-12855.

CHARACTERISTICS OF ACTIVATED CARBON-SUPPORTED CO-B AND CO-P-B AS A CATALYST FOR HYDROGEN GENERATION BY NaBH_4 HYDROLYSIS

E. H. Lee, K. D. Baik, and S. H. Yang

*Agency for Defense Development, Daejeon, (Republic of Korea)

Abstract – Characteristics of activated carbon-supported Co-B (Co-B/C) and Co-P-B (Co-P-B/C) catalysts for hydrogen generation using NaBH_4 hydrolysis were investigated under various experimental conditions. Hydrogen generation using Co-B/C at a mixed solution of 20 wt% NaBH_4 and 0.5 wt% NaOH improved with an increase of sonication time. In the case of Co-P-B/C, a rise of ratio of ethanol in solvent, molar concentration of $\text{CoCl}_2 \cdot 6\text{H}_2\text{O}$, and sonication time increased hydrogen generation. In the condition of 15 ~ 23 wt% in NaBH_4 concentration, Co-P-B/C showed lower catalyst loss and higher hydrogen yield than Co-B/C.

Index Terms – Activated carbon support, Co-based catalyst, Hydrogen generation, Sodium borohydride

I. INTRODUCTION

NaBH_4 has been much attention as one of promising materials for hydrogen storage and generation due to the relatively high gravimetric H_2 density of 10.8 wt%.[1] Since NaBH_4 reacts with water in room temperature and generates hydrogen, no effort to manage high temperature is needed. NaBH_4 is also non-flammable and relatively stable in the air. The byproduct NaBO_2 is non-toxic and it does not have a side effect in operating polymer membrane fuel cells. Due to these merits, hydrogen generation from a NaBH_4 aqueous solution has been steadily studied and it will be able to be one of the feasible methods for military applications. However, extra water is required in a real-life hydrolysis reaction and in the case of vehicles it could be a critical issue because it increases the system weight and volume. In military applications such as unmanned aerial vehicles, submarines and unmanned underwater vehicles, the increase of system weight can cause decrease of operational time and lead to mission failure. One of the solutions is to increase the ratio of NaBH_4 in the NaBH_4 solution. The high concentration of NaBH_4 , however, can cause severe loss of catalyst and deteriorate durability. In this study, characteristics of activated carbon-supported Co-B (Co-B/C)

and Co-P-B (Co-P-B/C) tested in the relatively high concentrations of the NaBH_4 solution were investigated.

II. EXPERIMENT

For fabrication of Co-B/C and Co-P-B/C, the molar concentration of $\text{CoCl}_2 \cdot 6\text{H}_2\text{O}$, ratio of ethanol in solvent, and sonication time were changed in the range of 0.075 ~ 0.2 M, 0 ~ 75%, and 40 ~ 210 min, respectively. In order to improve dispersion, ethanol was added to deionized water as a solvent. The activation energies of Co-B/C and Co-P-B/C were calculated by Arrhenius plots of the hydrogen generation at 50 ~ 80 °C. A mixed solution of 20 wt% NaBH_4 and 0.5 wt% NaOH was used for hydrogen generation except the experimental set of NaBH_4 concentration. A catalyst loss and hydrogen yield of Co-B/C, Co-P-B/C were investigated in NaBH_4 concentration 15 ~ 27 wt% (0.5 wt% NaOH was also added).

III. RESULT AND DISCUSSION

The parametric analysis of the fabrication process of Co-B/C and Co-P-B/C catalysts was conducted. As shown in Table I, hydrogen generation of Co-B/C only depended on the sonication time. With an increase of sonication time from 40 min to 100 min, a Brunauer-Emmett-Teller (BET) surface area and hydrogen generation were improved together.

TABLE I
BET SURFACE AREA AND HYDROGEN GENERATION OF CO-B/C AT A FEW CONDITIONS OF SONICATION TIME

Experimental conditions		BET surface area (m^2/g)	Hydrogen generation (L/min)
Sonication time (min)	40	469.11	2.1
	80	524.08	2.14
	100	552.54	2.23

Table II presents the trend on hydrogen generations of Co-P-B/C in the various experimental conditions. Unlike Co-B/C catalysts, hydrogen generation of Co-P-B/C was increased with a rise of the ratio of ethanol, molar concentration of $\text{CoCl}_2 \cdot 6\text{H}_2\text{O}$ as well as sonication time. However, in the case of Co-P-B/C, correlation between a BET surface area and hydrogen generation was not found.

TABLE II
HYDROGEN GENERATION OF Co-P-B/C UNDER VARIOUS EXPERIMENTAL CONDITIONS

Experimental conditions		Hydrogen generation (L/min)
Ratio of ethanol (%)	0	2.26
	25	2.31
	50	2.35
	75	2.46
Molar concentration of $\text{CoCl}_2 \cdot 6\text{H}_2\text{O}$ (M)	0.075	2.03
	0.1	2.16
	0.2	2.31
Sonication time (min)	90	2.1
	150	2.14
	210	2.23

In order to investigate catalytic activity of Co-B/C and Co-P-B/C, samples with the highest BET surface area were selected among those which showed hydrogen generation of about 2 L/min. The BET surface areas of Co-B/C (#1) and Co-P-B/C (#2) were $571.73 \text{ m}^2/\text{g}$ and $682.27 \text{ m}^2/\text{g}$, respectively. The activation energies of #1 and #2 were 57.95 kJ/mol and 61.31 kJ/mol , respectively, which showed that Co-B/C is more reactive than Co-P-B/C (not shown). However, the hydrogen yield of #2 was better than that of #1, though the activation energy of #1 was lower. The reason that relatively less reactive Co-P-B/C had better hydrogen yield is that the catalyst loss of Co-P-B/C was lower than that of Co-B/C.

For Co-B/C (#1) and Co-P-B/C (#2) catalysts mentioned above, the trends on hydrogen yield and catalyst loss were observed in the NaBH_4 concentrations of 15 ~ 27 wt%. Fig. 1 and Fig. 2 present the hydrogen yields and catalyst losses of two kinds of samples, respectively. There was not clear correlation between the hydrogen yield and catalyst loss in the NaBH_4 concentrations over 23 wt% and the hydrogen yield was less than 90%. However, in the NaBH_4 concentration of 15 ~ 23 wt%, Co-P-B/C showed lower catalyst loss and higher hydrogen yield than Co-B/C. These results indicate that the maximum NaBH_4 concentration keeping more than 90% in hydrogen yield is 23 wt% and the reduction of catalyst loss can lead to higher hydrogen yield.

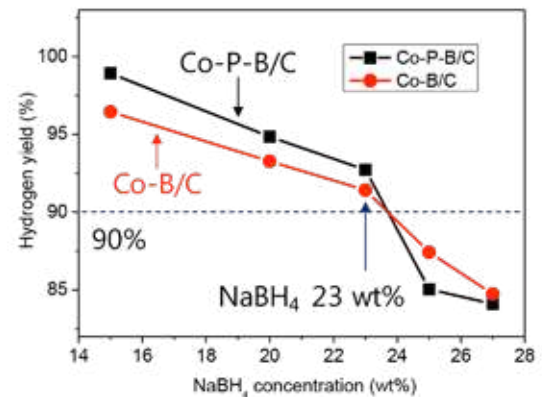


Fig. 1. Hydrogen yield of Co-B/C and Co-P-B/C in NaBH_4 concentration 15 ~ 23 wt%

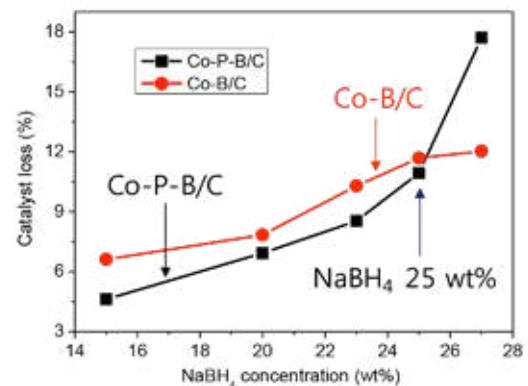


Fig. 2. Catalyst loss of Co-B/C and Co-P-B/C in NaBH_4 concentration 15 ~ 23 wt%

IV. CONCLUSION

Characteristics of Co-B/C and Co-P-B/C catalysts for hydrogen generation were investigated under various experimental conditions. For the analysis of the process parameters, the hydrogen generation of Co-B/C only depended on the sonication time, while that of Co-P-B/C increased with a rise of the ratio of ethanol, molar concentration of $\text{CoCl}_2 \cdot 6\text{H}_2\text{O}$, and sonication time. Co-P-B/C showed lower catalyst loss and higher hydrogen yield than Co-B/C in NaBH_4 concentration 15 ~ 23 wt%, indicating that improving durability of catalyst such as a reduction of catalyst loss can lead to higher hydrogen yield.

ACKNOWLEDGMENT

This study was supported by the Agency for Defense Development, Republic of Korea.

REFERENCES

- [1] U. B. Demirci, O. Akdim, J. Andrieux, J. Hannauer, R. Chamoun, P. Miele, Sodium Borohydride Hydrolysis as Hydrogen Generator: Issues, State of the Art and Applicability Upstream from a Fuel Cell, Fuel Cells, Volume 10, 2010, pp. 335-350.

ESTIMATING THE HYDROGEN PURGING TIME FOR A PEM FUEL CELL WORKING IN A CLOSED ENVIRONMENT

Ariel Chiche, Göran Lindbergh, Ivan Stenius, and
 Carina Lagergren

KTH Royal Institute of Technology, Stockholm, Sweden

Abstract - Fuel cells are promising technologies for zero emission energy conversion. Proton Exchange Membrane Fuel Cells (PEMFC) use hydrogen and oxygen to produce electricity, water and heat. Hydrogen supply is crucial for such systems and using the fuel cell in dead-end mode, meaning the hydrogen is trapped in the cell, is a solution to save hydrogen. However, water and impurities accumulate inside and the cell needs to be purged. A Design of Experiment approach, with fuel cell's performance and time between two purges as studied responses, was conducted on an air breathing PEMFC in a closed environment. The studied parameters were the relative humidity (RH), the current load, the convection, the oxygen inlet frequency, the voltage drop trigger criteria for the purge and the hydrogen inlet pressure. Results show that the most influential parameters are the RH, the current load and the voltage trigger criteria, interactions between them are also highlighted.

Index Terms – fuel cell, dead-end, purge, hydrogen.

I. INTRODUCTION

Fuel cells represent an interesting zero-emission solution for energy storage and generation in stationary and automotive applications. The Proton exchange membrane fuel cell (PEMFC) is the most commonly used fuel cell since it works at relatively low temperatures (50–80 °C). It consumes hydrogen and oxygen (H₂ at the anode and O₂ at the cathode) as reactants in order to produce electricity, water and heat. In order to save H₂ and ensure 100 % H₂ utilization, closing the anode outlet is a popular solution, named the dead-end anode (DEA). However, accumulation of water and impurities in the different layers of the Membrane Electrode Assembly (MEA) leads to voltage drop of the fuel cell stack. Purging the anode channel is therefore necessary to ensure proper fuel cell operation.

Planned purging strategies with frequent purges have been studied and showed that dead-end mode is a suitable solution for PEMFC [1][2] and can ensure a certain fuel cell stack efficiency and limit its degradation [3][4]. With a varying current load, the time between two purges has to be modified [5][6]. This study investigates the purging behavior of a small PEMFC stack in a

closed environment using a Design of Experiment (DoE) approach.

II. DESIGN OF EXPERIMENT AND EXPERIMENTAL PROCEDURE

A PEMFC stack composed of 6 cells in series was implemented in a set-up simulating a closed environment, Fig. 1. A DoE was performed in order to quantify the impact of each considered parameter, Table I, on the time between two purges and the performance of the stack. Each experiment lasted at least for 40 purges.

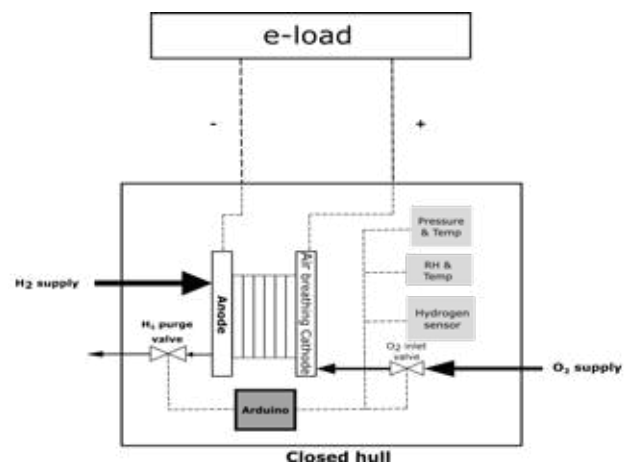


Fig. 1. Scheme of the experimental set-up.

TABLE I
 CONSIDERED PARAMETERS AND MESH

	Parameter	+1	-1	0
P1	Relative Humidity (RH)	> 95 %	< 50 %	65–75 %
P2	Current	500 mA	300 mA	400 mA
P3	Convection	Fan max	Fan off	Fan on
P4	Oxygen supply frequency	300 s	30 s	120 s
P5	Voltage drop trigger	10 %	30 %	20 %
P6	Hydrogen inlet pressure	0.5 BAR	0.3 BAR	1.4 BAR

The voltage drop trigger criteria is the accepted voltage drop from the steady state fuel cell voltage at the given current load.

Matrix (1) shows the experiments ran according to the DoE (each column corresponds to one parameter and each row is an experiment). This first round of experiments highlights which parameters that have more influence on the studied phenomenon.

$$\begin{pmatrix} 1 & 1 & 1 & 1 & 1 & 1 \\ -1 & 1 & -1 & 1 & -1 & 1 \\ 1 & -1 & -1 & 1 & 1 & -1 \\ -1 & -1 & 1 & 1 & -1 & -1 \\ 1 & 1 & 1 & -1 & -1 & -1 \\ -1 & 1 & -1 & -1 & 1 & -1 \\ 1 & -1 & -1 & -1 & -1 & 1 \\ -1 & -1 & 1 & -1 & 1 & 1 \end{pmatrix} \quad (1)$$

III. RESULTS

The designed DoE were conducted on an air breathing PEMFC working in a closed environment in order to estimate the purging time of the system. The set-up was successfully built and controlled.

The voltage of the entire stack was monitored during the experiments, as shown in Fig. 2. Voltage drops and hydrogen purges are visible. The voltage recovers almost instantly when the purge valve opens. The median value of the time between two purges is considered as a result of the DoE analysis.

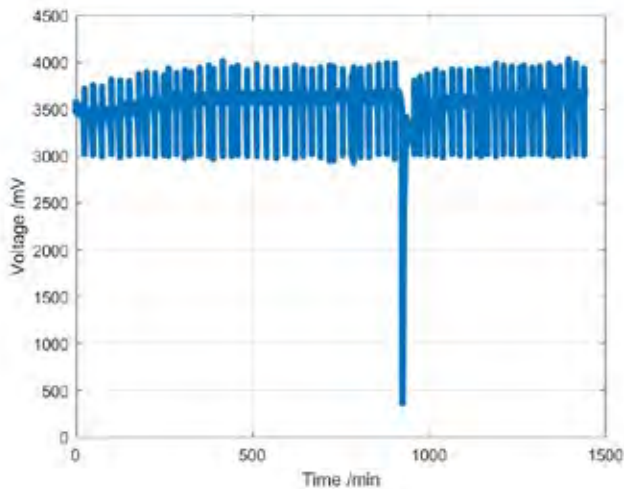


Fig. 2. Fuel cell stack voltage over 24h corresponding to the experiment 1 1 -1 -1 -1.

The 8 experiments were performed using the described set-up and results highlighted the relative humidity, the current and the voltage drop trigger as the parameters with the most influence on both the cell performance and the time between two purges. When increasing the current load, the time between two purges decreases, which was expected since the amount of produced water also increases with the current load. When the RH increases, the time between purges decreases and the performance increases. When the voltage drop trigger criteria is

high (30 %), it was observed that the performance of the stack decreases with time. This parameter has a low impact though on the time between two purges. The three other considered parameters show less impact on the studied responses.

IV. CONCLUSION

Results show that the main parameters affecting the time between purges are the current load, the relative humidity and the voltage drop trigger. The optimal way to run a fuel cell seems to be at high RH with a low voltage drop trigger criteria. A too high voltage drop trigger can accelerate the degradation of the cell and reduce the performance of the stack and its lifetime.

Interactions between the three cited parameters exist. However, more experiments, using the same set-up, need to be performed to highlight and quantify them.

ACKNOWLEDGEMENT

This work was supported by Swedish foundation for strategic research (SSF) through the Swedish Maritime Robotic Centre (SMaRC (IRC 15-0046)).

REFERENCES

- [1] K. Nikiforow, H. Karimäki, T. Keränen and J. Itonen, "Optimization study of purge cycle in proton exchange membrane fuel cell system," *Journal of Power Sources*, vol. 238, pp. 336 - 344, 2013.
- [2] F. Migliardini, T. D. Palma, M. Gaele and P. Corbo, "Hydrogen purge and reactant feeding strategies in self-humidified PEM fuel cell systems," *International Journal of Hydrogen Energy*, vol. 42, pp. 1758-1765, 2017.
- [3] S. Strahl, A. Husar and J. Riera, "Experimental study of hydrogen purge effects on performance and efficiency of an open-cathode Proton Exchange Membrane fuel cell system," *Journal of Power Sources*, vol. 248, pp. 474 - 482, 2014.
- [4] Z. Hu, G. Wang, X. Chen, P. Chen and J. Chen, "Anode purge strategy optimization of the polymer electrode membrane fuel cell system under the dead-end anode operation," *Journal of Power Sources*, vol. 320, pp. 68 - 77, 2016.
- [5] A. Gomez, A. P. Sasmitho and T. Shamim, "Investigation of the purging effect on a dead-end anode PEM fuel cell-powered vehicle during segments of a European driving cycle," *Energy Conversion and Management*, vol. 106, pp. 951-957, 2015.
- [6] C.-Y. Hung, H.-S. Huang, S.-W. Tsai and Y.-S. Chen, "A purge strategy for proton exchange membrane fuel cells under varying-load operations," *International Journal of Hydrogen Energy*, vol. 41, pp. 12369 - 12376, 2016.

SYSTEM LEVEL MODELLING AND SIMULATION OF TRANSIENT BEHAVIOR FOR POLYMER ELECTROLYTE FUEL CELLS

Yuanxin Qi^a, Mayken Espinoza-Andaluz^b, Marcus Thern^a,
Martin Andersson^{a,*}

^aLund University, P.O.Box 118, Lund 22100, Sweden

^bEscuela Superior Politécnica del Litoral, P.O.Box 09-01-5683,
Guayaquil 090902, Ecuador

Abstract - In this paper, a system level model for a polymer electrolyte fuel cell (PEFC) system, which is capable of characterizing transient behavior using the control volume method, is developed. Three different cases based on different mass transfer assumptions in the cathode channel are explicitly discussed considering the presence of 1) only oxygen, 2) both oxygen and nitrogen or 3) oxygen as well as nitrogen and water vapor in the cathode control volume. The analysis illustrates that the model developed predict in adequate manner the dynamic behavior of a PEFC system. It is demonstrated that the presence of nitrogen and water vapor in the cathode volume significantly affects the PEFC's overall performance.

Index Terms – System level modelling, transient behavior, PEFCs.

I. INTRODUCTION

Polymer electrolyte fuel cells (PEFCs) have become one of the most promising power sources with a wide range of applications due to its high electrical efficiency, fast start-up, no emission of pollutants and low operation temperature [1]. A dynamic system model helps to test the PEFC system's overall performance, improve the coordination between each subsystem and optimize the system's real time control design in practical automotive applications [2].

Various models have been proposed to study the specific aspects of PEFCs and have laid down a solid foundation for PEFCs' system level dynamic modelling. Pukrushpan et al [3] developed a fuel cell system dynamic model suitable for control studies, but neglecting the reactant gases' flow rate and pressure changes during the operation. Xue et al [4] proposed a fuel cell model that could predict the dynamic behaviour using control volume approach, but the presence of the water vapour

in the cathode volume was neglected. Pathapati et al [5] established a mathematical model to simulate the transient phenomena in a PEFC system but water vapor in the cathode side was still neglected. The above mentioned studies provide a comprehensive understanding of PEFC system modelling. However, they do not address the PEFC model at a fully dynamic system scale.

The aim of this paper is to develop a complete system scale dynamic PEFC model, addressing the difference in the system performance when different mass transfer in cathode control volume are studied.

II. MODELLING METHODOLOGY

In this study, the control volume approach is used to develop the system level dynamic PEFC model [6].

A. Model 1

Oxygen is supplied as the reactant gas, and is assumed as the only specie in the cathode channel. Its continuity and energy equations could be extracted from [6].

B. Model 2

Air is supplied to the PEFC system and the mole ratio of O₂/N₂ is defined to 21/79, i.e., both oxygen and nitrogen are considered in the cathode control volume. Its mass and energy conservation equations are extracted from [6].

C. Model 3

Obviously, there is water produced at the cathode side due to the electrochemical reaction. Also, there exists a well-known phenomenon called electro-osmotic drag inside a PEFC, which means that some water molecules would be dragged to the

cathode side from the anode channel along with the hydrogen protons traveling through the membrane. Its mass and energy conservation equations are extracted from [6].

III. SIMULATION RESULTS

Figure 1 presents the step changes of the current load. The current is initially 5 A during the first 33333 s, then it increases to 40 A, which remains until 66666 s and finally it drops to 20 A until the end. Figure 2 shows the stack voltage response corresponding to the current changes. Noticeably, Model 1 gives the highest voltage. At 33333 s, the stack voltage drops from 29.2 to 17.4 V and then increases to 24.6 V at 66666 s. It is also observable that Model 3 has the lowest voltage. The gradual decrease of the voltage from Model 1 to Model 3 is because the presence of nitrogen and water vapour in the cathode channel lowers the oxygen partial pressure. Figure 3 shows the temperature profiles of the fuel cell body. To clarify, the cooling system is not considered in our model. As it can be seen, Model 2 and Model 3 have the same temperature profile. The temperature gradually increases to 301 K during the first 33333 s due to the heat generated by the electrochemical reaction. Then it keeps increasing to 360 K during the second stage (33333 s - 66666 s) due to the increase of the output power when current goes up to 40 A. Finally, the temperature slowly drops to 323 K when the load current is decreased. It is clear that the presence of water vapour in the cathode control volume has no impact on the stack temperature. The temperature of Model 2 and Model 3 are higher than Model 1 as a result of the extra heat added to the PEFC system when the nitrogen enters the channel.

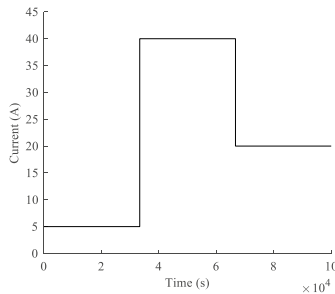


Figure 1. Current load

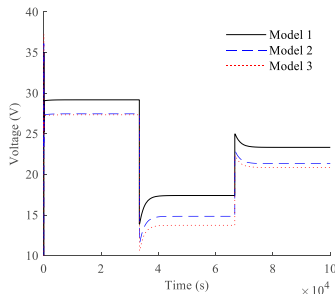


Figure 2. Voltage response

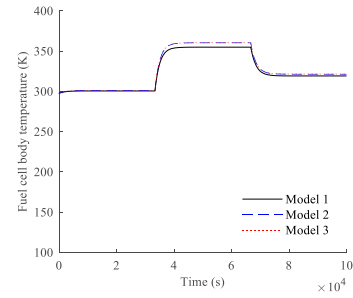


Figure 3. Stack temperature

IV. CONCLUSION

In this paper, a system scale dynamic model for a PEFC system is developed. The developed models stress a comparison on the system performance concerning the different mass transfer when different assumptions are made about the species in the cathode control volume. It was found the presence of nitrogen and water vapor in the cathode channel would decrease the output voltage of the PEFC. And the nitrogen would bring extra heat to the PEFC system when it enters the cathode channel, which will finally lead to an increase on the system temperature.

ACKNOWLEDGMENT

The authors would like to acknowledge support from the Chinese Scholarship Council, grant number: 201706080005 as well as from Åforsk project 17-331.

REFERENCES

- [1] M. Andersson, V. Vukčević, S. Zhang, Y. Qi, H. Jasak, S.B. Beale, W. Lehnert, Modeling of droplet detachment using dynamic contact angles in polymer electrolyte fuel cell gas channels, *International Journal of Hydrogen Energy*, 44 (2019) 11088-11096.
- [2] J. Baschuk, X. Li, Modelling of polymer electrolyte membrane fuel cells with variable degrees of water flooding, *Journal of power sources*, 86 (2000) 181-196.
- [3] J.T. Pukrushpan, H. Peng, A.G. Stefanopoulou, Simulation and analysis of transient fuel cell system performance based on a dynamic reactant flow model, in: *ASME 2002 International Mechanical Engineering Congress and Exposition*, American Society of Mechanical Engineers, 2002, pp. 637-648.
- [4] X. Xue, J. Tang, A. Smirnova, R. England, N. Sammes, System level lumped-parameter dynamic modeling of PEM fuel cell, *Journal of Power Sources*, 133 (2004) 188-204.
- [5] P. Pathapati, X. Xue, J. Tang, A new dynamic model for predicting transient phenomena in a PEM fuel cell system, *Renewable energy*, 30 (2005) 1-22.
- [6] S.M. Sharifi Asl, S. Rowshanzamir, M.H. Eikani, Modelling and simulation of the steady-state and dynamic behaviour of a PEM fuel cell, *Energy*, 35 (2010) 1633-1646.

TOWARDS COMPOSITE BIPOLAR PLATES MADE BY INJECTION MOLDING FOR PEMFC APPLICATION: FORMULATION, COMPOUNDING AND PHYSICAL PROPERTIES

B. Huitorel*, M. Ramage*, T. Laguionie*, J. Bigarré*
* Laboratoire de Synthèse et de Transformation des Polymères,
CEA-DAM Le Ripault 37260 MONTS, (France)

Abstract – The hydrogen technologies are currently being widely deployed in Europe. For the Proton Exchange Membrane Fuel Cell (PEMFC) market, it implies the need of higher quantities and durability of the components at the lowest cost. In this context, the development of cheaper materials and processes for the manufacturing of composite bipolar plates is critical. Therefore, a previous technology of composite bipolar plate developed at CEA Le Ripault needs to evolve in order to be compatible with mass production and reduction of costs.

Index Terms – Bipolar plates, Graphite composites, Injection molding, Proton Exchange Membrane Fuel Cell

I. INTRODUCTION

Since the middle of the 2000s, CEA Le Ripault has developed materials and processes for the manufacture of composite bipolar plates for PEMFC by compression molding process.[1] These plates are easily processable and present good performance and durability in PEMFC environment. They are of interest for applications needing long period of use such as in heavy vehicles (trucks and trains for instance). The material used at CEA Le Ripault is a poly(vinylidene fluoride) (PVDF)/graphite composite which has been optimized for compression molding. However, the need of reducing the cost production of the bipolar plates turns the manufacture process towards higher rates and quantities. Therefore, going from compression molding to injection molding becomes necessary. For this purpose, new materials are developed for the fabrication of composite bipolar plates based on our knowledge about PVDF/graphite composites.

The goal is to define new compositions with high carbon loading for good thermal and electrical conductivities and low viscosity for the ease of the injection molding process.

II. BIPOLAR PLATES IN PEMFC

The bipolar plates are components of a PEMFC stack. Their main goals are the distribution of the fluids as well as the collection of the electrons and their transportation from an electrode to the next one. Cooling, gas and fluids separation and mechanical behavior of the stack are also ensured by these plates.

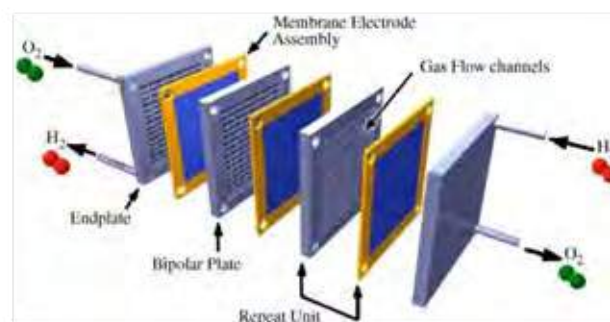


Fig. 1. Components of a PEMFC stack [2]

Bipolar plates play many roles in a PEMFC stack. To do so, they need several physical properties such as:

- High electrical conductivity
- Corrosion resistance
- Good mechanical properties
- High thermal conductivity
- Low gas permeability
- Thermal and chemical stability
- Low coefficient of thermal expansion

Low density of the plates is an advantage too because it gives higher density of energy to a stack.

Metallic bipolar plates are widely used, especially for the automotive market, because they offer excellent conductivities, mechanical properties and very low gas permeability. However, these plates are very sensitive to corrosion which shortens their lifetime. For some application needing long time of use, such as in heavy vehicles for instance, composite materials become an interesting choice thanks to their good corrosion resistance. But today, the costs of composite bipolar plates still need to be reduced while keeping good physical properties in order to make this technology competitive.

III. PROCESSES AND MATERIALS

A. From compression molding to injection molding

Previously developed composite bipolar plates at CEA Le Ripault satisfy the U.S. Department of Energy (DoE) technical targets for 2020 (see Table 1). These plates are made of a PVDF/graphite composite and manufactured by compression molding process.

TABLE I
PHYSICAL PROPERTIES OF CEA BIPOLAR PLATES MADE BY COMPRESSION MOLDING COMPARED WITH DOE TECHNICAL TARGETS FOR 2020.

	Electrical conductivity (S/cm)	Flexural strength (MPa)	Density
U.S. Department of Energy Technical targets for 2020	> 100	> 25	< 2
CEA bipolar plate (compression molding)	95 (+15)	32,1 (+1)	2,0

Nevertheless, for the production of high quantities, the cost of such bipolar plates is too high to be competitive. The main way to reduce this cost is to go to a more continuous process such as injection molding. [3-4]

B. Polymer matrices

The materials which have been developed for making bipolar plates by compression molding have a too high viscosity to be shapes directly by injection molding. For this purpose, PVDF has been replaced by polypropylene (PP) as the matrix of the composite. Indeed, PP has sufficient thermal and chemical stability to be used in a PEMFC environment. Moreover, PP is ten times cheaper than PVDF, it has also a lower density and the risks related to the decomposition gases of this polymer during the process are far less hazardous than the ones of PVDF.

Another advantage of the PP is the availability of various polymer grades and specific grades for injection molding. Homopolymers, block copolymers, random copolymers and metallocene grades of PP have been investigated as matrices for bipolar plates.

PP/graphite composites with filler weight percentage around 80% have been compounded with a twin-screw extruder (ThermoFisher). The electrical conductivities measured on

these materials are around 10 S/cm which could be greatly improved by increasing the of the filler content or by changing the nature and the shape of the fillers.

IV. CONCLUSION

The next generation of composite bipolar plates is driven by their production cost. In order to make bipolar plates cheaper, the processes have to support higher production rates. This makes the injection molding process more competitive than the compression molding process. However, changing a process implies to change the material and so the physical properties of the final object. First experiments with several PP matrices have been carried out leading to a compound with medium electrical conductivity. The influence of the PP grade (homopolymer, copolymer ...) on the physical properties of a final composite plate is currently being investigated.

Additional studies would be necessary to go deeper in the understanding of the relationships between the microstructure, the chemical nature of the components of the plates and their final physical properties as well as the understanding of the rheological behavior of highly charged polymers.

ACKNOWLEDGMENT

The authors thank the Région Centre-Val-de-Loire for the financial support of this work (LAVOISIER 2 program).

REFERENCES

- [1] Buvat P, Toneguzzo P, Dagaz S and Page B, Method for manufacturing a composite bipolar plate, composite bipolar plate, uses thereof and fuel cell comprising such a composite bipolar plate, European Patent EP3149795B1, 2015
- [2] Li X. and Sabir I, Review of bipolar plates in PEM fuel cells : Flow-field designs, International Journal of Hydrogen Energy, Volume 30, 2005, Pages 359-371
- [3] Heinzel A, Mahlendorf F, Niemzig O and Kreuz C, Injection moulded low cost bipolar plates for PEM fuel cells, Journal of Power Sources, Volume 131, 2004, Pages 35-40
- [4] Müller A, Kauranen P, von Ganski A and Hell B, Injection moulding of graphite composite bipolar plates, Journal of Power Sources, Volume 154, 2006, Pages 467-471

EFFECT OF THE CYCLIC FROST EXPOSURE ON THE PERFORMANCE OF PEM FUEL CELLS

S. Gorelkov, S. Palecki, J. Wartmann and A. Heinzl

The hydrogen and fuel cell center (ZBT GmbH), Carl-Benz-Straße 201,
D-47057 Duisburg (Germany)

Abstract - In this study, the behaviour of Polymer-Electrolyte Membrane (PEM) single cells with different types of MEA systems have been studied under thermal cycling with respect to structural and electrochemical changes. The cells have been insulated and exposed to repeated freeze-thaw cycles with a minimum temperature of -40°C inside an environmental chamber. To some extent, great differences between the degrees of damage could be found for the various types of MEA systems (e.g. catalyst coated membrane (CCM), catalyst coated substrate (CCS)).

Index Terms – cyclic frost exposure, testing methodology, performance degradation

I. INTRODUCTION

Commercially available fuel cell systems have to ensure an adequate performance level at least for the duration of the specified product lifetime. During its exploitation, the polymer electrolyte membrane fuel cells (PEMFCs) could be exposed to a wide range of extreme conditions, which in turn may considerably shorten their lifespan. One of those acute stress scenarios occurs when PEMFCs are exposed to cold environments when the ambient temperature falls below 0°C and passes the freezing point of water. Freezing of residual water inside and between the individual components of the membrane electrode assembly (MEA) leads under certain circumstances to severe performance degradation of a PEM fuel cell. Due to phase transitions and the corresponding volumetric changes of water and ice, the physical as well as chemical properties of the MEA components could alter, resulting in more or less significant performance losses. Based on findings made on other porous materials under freeze-thaw exposure such as concrete or cementitious materials, the damage and transport mechanisms within the porous MEA components could be explained [1]. In accordance with physical theories the redistribution of residual water during the freezing process and shrinkage effects of smaller pores are important factors for the

frost behaviour of porous materials. It comes obvious that the composition and manufacturing of the separate MEA layers could significantly influence the water uptake and hence the frost resistance of such systems. Therefore, the impact of material variation on the freeze/thaw behaviour has been investigated in detail in this study by using a defined test procedure with fixed boundary test conditions.

II. EXPERIMENTAL

A. Design, components and assembly of fuel cell stacks

The tested fuel cell stacks have been assembled manually, using components of the basic design developed by ZBT GmbH. The used MEA systems of different types - catalyst coated membrane (CCM) and catalyst coated substrate (CCS) - have been acquired separately. The experiments have been conducted using liquid-cooled single cell PEMFC stacks with an active area of 50 cm^2 .

B. Applied testing approach and thermal cycle

In this study, single cells with a lateral thermal insulation were arranged inside a climate chamber and exposed to a defined freeze-thaw cycle (ftc) with cooling and heating rate of 10 K/h as well as a minimum temperature of -40°C , which is required by the Department of Energy (DOE). To this state of analysis, the shutdown procedure did not include any appropriate operation conditions or purging procedure with respect of water reduction. With other words, the maximum amount of water remained within the stack before frost exposure starts. The described conditions have been regarded as worst-case scenario within the frame of this scientific study.

III. RESULTS AND DISCUSSION

Under the applied worst-case scenario conditions, with high contents of residual water inside the stack, a measurable

performance degradation with increasing number of freeze-thaw cycles could be observed for both MEA systems. The individual MEA types show different frost resistance abilities, which can be assessed by the degrees of performance degradation with progressing ftc. For both systems, a measurable voltage drop has been observed at high current densities. The reason for such behaviour is presumably the increase in both the charge and mass transfer resistances, resulting from the ice formation, which led to the corresponding structural changes of the individual MEA components.

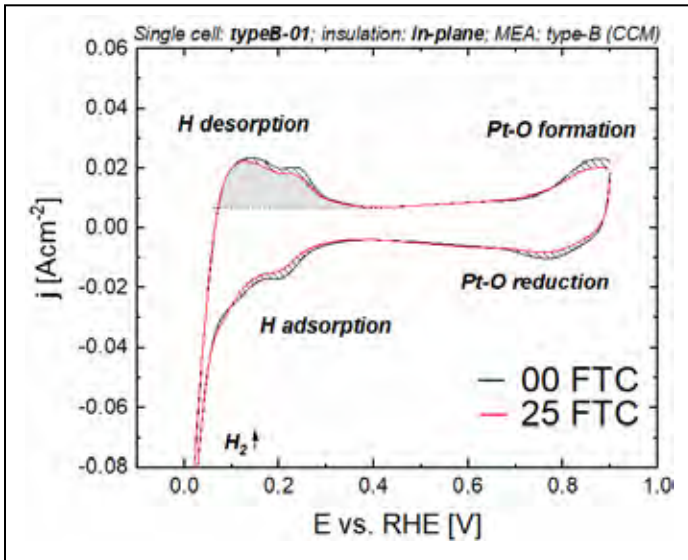


Fig. 1. Cyclic voltammograms for frost-resistant MEA system: CCM at different stages of frost exposure (initial state & after 25 ftc).

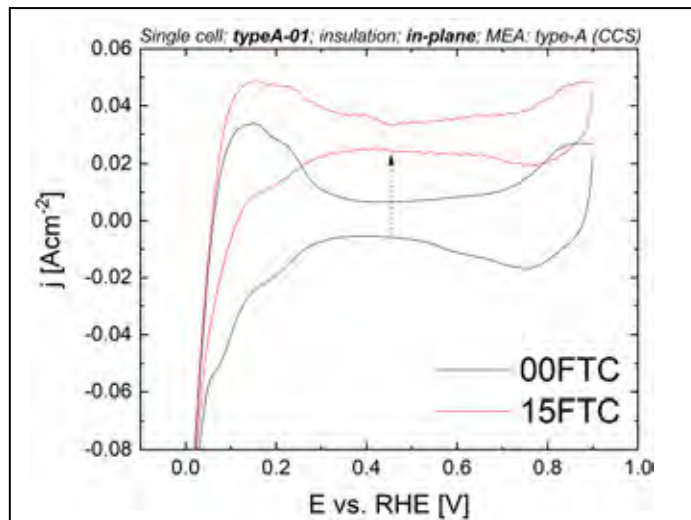


Fig. 2. Cyclic voltammograms for frost-prone MEA system: CCS at different stages of frost exposure (initial state & after 15 ftc).

Figure 1 shows the corresponding CV measurements for different stages of frost exposure, which have been performed to assess the potential reduction in electrochemical surface area (ECSA) with growing number of freeze/thaw cycles. The ECSA of the electrodes has been estimated by the area under the hydrogen desorption peaks (shaded area) (Fig.1).

For the CCM system only a slight reduction of ECSA have been measured after 25 ftc, while for the CCS assembly great changes have been observed already after 15 cycles. The latter shows also a vertical translation of the CV curve, which is a typical sign of a possible reactant crossover between the anode and the cathode (Fig.2). This behaviour indicates damages within the membrane such as pinholes or cracks, which in turn can lead to the formation of free radicals and the corresponding chemical degradation of the membrane material.

IV. CONCLUSION AND OUTLOOK

Performance and electrochemical kinetic losses have been observed to different extent when diverse MEA systems (CCS/CCM) assembled in a single cell were subjected to multiple freeze-thaw cycles with high amount of residual water, since no purging was performed. ECSA estimated from hydrogen desorption peak decreased to different degrees for individual MEA systems. In this context, a greater reduction of the ECSA for CCS systems could be measured by cyclic voltammetry (CV). Ac impedance spectroscopy (EIS) measurements indicate an increase in mass transport resistance, which may presumably have been caused by the structural changes of the gas diffusion layer. In contrast to these results, the CCM systems show less structural damages and great frost resistance even under such worst-case conditions.

For overall statements concerning the influence of material properties and manufacturing effects on the frost resistance of MEAs the spectrum of tested components have to be increased. Nevertheless, with the applied test assembly it is possible to assess the frost durability of MEA systems in advance so that damages i.e. performance losses due to freeze-thaw cycling could be presumably prevented in the future.

ACKNOWLEDGMENT

This work has been carried out with the financial support of the German Federation of Industrial Research Associations (AiF) within the frame of the research project No. 18224N.

REFERENCES

- [1] Palecki, S., Gorelkov, S., Wartmann, J., & Heinzl, A., Frost induced damages within porous materials-from concrete technology to fuel cells technique, Journal of Power Sources, Volume 372, 2017, pp.204-211.

(Put paper number here) EFC19022

IMPEDANCE STUDIES OF ARTIFICIALLY AGED NI-YSZ ANODE FOR ACCELERATED STRESS TESTS

D. Vladikova*, B Burdin*, D. Montinaro**, P. Piccardo***,
M. Rolland**, R. Spotorno***

* Institute of Electrochemistry and Energy Systems – Bulgarian Academy of Sciences, 10 Acad. G. Bonchev, 1113 Sofia, (Bulgaria)

** SOLIDpower S.p.A, Viale Trento 117, 38017 Mezzolombardo, (Italy)

*** Dipartimento di Chimica e Chimica Industriale – University of Genova, via Dodecaneso 31, I-16146 Genoa, (Italy)

Abstract - This work aims at development of procedure for artificially *ex-situ* and *in-situ* accelerated degradation of a single component - anode in solid oxide fuel cell. The selected approach ensures opportunity for recognizing the influence of critical cell/stack components degradation in the total behavior of the system. The *ex-situ* accelerated aging is tested on YSZ/Ni samples sintered at up to 100°C higher temperature in respect to the standard one, or exposed to a series of redox cycles. The *in situ* artificial acceleration of the anode degradation in a button cell is based on redox cycling before operation. A methodology for direct impedance monitoring of the processes that take place in the anode during reduction and redox cycling is developed. It is combined with post mortem microstructural analysis. The results are promising. A definition of levels of anode degradation based on microstructural comparison with long term tested cells is under development.

Index Terms – accelerated stress tests, anode degradation, artificial aging of single components, solid oxide fuel cells.

I. INTRODUCTION

Durability is a severe hurdle towards deployment of solid oxide fuel cells (SOFC) which are regarded as a promising technology for economic power generation due to their high efficiency and large fuel flexibility. The numerous and important studies for deeper insight into the degradation sources and life time improvement meet one and the same barrier - the long term testing needed for initial accumulation of reliable data. Long tests are neither appropriate as information source for further optimization, nor convenient for implementation. The problem solving approach, which is under active

development, is the introduction of accelerated stress tests [1] and sophisticated performance/degradation models to quantify the accelerating impact. One effective direction which could distinguish the influence of critical cell/stack components degradation in the total behavior of the system is their artificial *ex-situ* aging which should reproduce a given degradation state faster than if obtained at normal test conditions. The artificially aged component could be further integrated and tested in a new cell/stack. This approach can give information about the response of the whole tested system when affected by the targeted degradation process. Another approach could be *in-situ* accelerated degradation of a single component in the test set up before operation. Both approaches need preliminary deep research for validation and justification of the experimental conditions which is the aim of this work.

II. RESULTS AND DISCUSSION

Two approaches were selected for artificial aging of YSZ/Ni anode. Since the degradation behavior of the anode support is found to be more sensitive to temperature than to polarization [2], the *ex-situ* accelerated aging is checked on micro-samples starting from YSZ/NiO layers sintered at conventional and at up to 100°C higher temperature. The *in situ* artificial acceleration is based on redox cycling before operation of a button cell with anode, sintered at standard technological conditions. The electrochemical behavior is monitored by Electrochemical Impedance Spectroscopy in combination with current-voltage characterization for the cell tests. The changes in the porosity

and in the Ni microstructure are registered by SEM/EDX analysis and by measurements of the gases permeability.

A methodology for direct impedance monitoring of the processes that take place in the anode during reduction and redox cycling is applied. It ensures direct measurement of a “bare” green anode positioned between two Ni meshes. This approach eliminates the necessity for data analysis via separation of the contributions coming from different processes occurring in the tested cell. The measurement is sensitive only to the electronic conductivity of the Ni network when connectivity between the reduced particles appears, grows or decreases. The impedance fingerprint for the formation of the Ni network is registered with the inductive behavior of the diagram (Fig. 1).

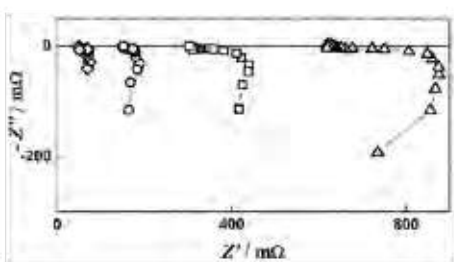
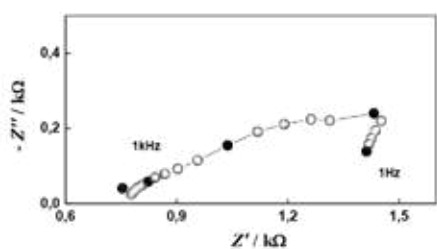


Fig. 1. Impedance diagrams of anode sample measured during the first reduction: 0 minutes reduction (upper figure); 6,5 minutes reduction (Δ); 7,5 minutes reduction (\square); 8,5 minutes reduction; (\circ) 10,5 minutes reduction (\diamond) (figure down)

Fig. 2 shows that the changes in the anode electrochemical behavior during redox cycling caused by partial oxidation of the Ni network can be successfully registered by impedance measurements. The deepness of the oxidation can be also controlled by the change in the Ni network resistance and the shape of the diagram. It was registered that oxidation is much slower than reduction.

The redox cycling on button cell level is performed by chemical oxidation which is a mild process that distributes in the whole volume of the anode and can be controlled with the air flow. The level of oxidation is well registered by impedance and can be controlled.

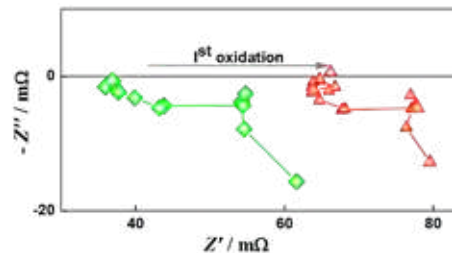


Fig. 1. Impedance diagram of anode sample measured before and after the first oxidation cycle

III CONCLUSION

The first experiments on the development of a procedure for artificially accelerated aging of single component (anode) in SOFC applying *ex situ* and *in-situ* procedures show promising results. Two approaches are selected for testing: artificial aging of separate anode by increased sintering temperature and redox cycling of cell before operation. A procedure for monitoring and quantitative control by impedance spectroscopy is developed. The next step of the accelerating algorithm is the definition of levels of degradation based on microstructural comparison with long term tested cells.

ACKNOWLEDGMENT

The research leading to these results received funding from the Fuel Cells and Hydrogen 2 Joint Undertaking under grant agreement No 825027. This Joint Undertaking receives support from the European Union’s Horizon 2020 research and innovation program, Hydrogen Europe and Hydrogen Europe Research. The experiments were performed with equipment supported by the Bulgarian Ministry of Education and Science under the National Roadmap for Research Infrastructure 2017-2023 “Energy storage and hydrogen energetics (ESHER)”, approved by DCM # 354/29.0862017.

In memory of Prof. Zdravko Stoykov who inspired those studies.

REFERENCES

- [1] Ploner, A., Hagen, A., Hauch, A., Study of Operating Parameters for Accelerated Anode Degradation in SOFCs, Fuel Cells, Volume 17 (4), 2017, Pages 498-507
- [2] Hagen, A., Barfod R., Hendriksen P.V., Liu Y.-L., Degradation of Anode Supported SOFCs as a Function of Temperature and Current Load, Journal of the Electrochemical Society, Volume 153(6), 2006. Pages A1165-A1171.

NUMERICAL MODELING AND PERFORMANCE OPTIMIZATION OF A HYBRID DESICCANT COOLING SYSTEM INTEGRATED WITH SOLID OXIDE FUEL CELL SYSTEM

Yulho Lee*, Sungjin Park*, Sanggyu Kang**

*Department of Mechanical and System Design Engineering,
Hongik Univ., Seoul, 04066 (Korea)

**Mechanical Engineering, Gwangju Institute of Science and
Technology, Gwangju, 61005 (Korea)

Abstract - The parametric study of the desiccant cooling system model has been conducted by varying the operating parameters such as outdoor temperature, outdoor relative humidity, regeneration temperature from the SOFC system. The system model is simulated by employing the actual weather conditions of world city for the development of the optimal system design and control. At abnormal days under temperature higher than 35°C and relative humidity higher than 40%, the electric heat pump has to be operated for compensating the indirect cooler to satisfy the target cooling performance. This study is useful to determine the optimal system design and control strategy for the desiccant hybrid cooling system at various actual weather conditions.

Index Terms – Hybrid Desiccant Cooling System, Solid Oxide Fuel Cell System, Numerical Modeling, Air Conditioning System.

I. INTRODUCTION

World energy consumption for space cooling in buildings was 2100TWh in 2016 [1]. According to World energy perspectives, Building should shrink energy consumption by increasing efficiency [2, 3]. To increase an efficiency of air conditioning system, a desiccant cooling system could be a solution. Especially for residential cooling, 99% of residential types of Air Conditioning (AC) is single unit Electric Heat Pump (EHP) [1]. Desiccant cooling system consumes only 60% electric power of EHP [4]. Also, CO₂ emission of desiccant cooling system is 60% that of conventional air conditioning system exhaust [4]. A solid desiccant evaporative cooling system as small space air conditioner has several advantages: 1) It uses heat energy that system can utilize exhaust waste heat from power generation system. 2) It saves a source energy likes electric and fuel by utilizing waste heat. 3) It can control indoor supply air humidity separate to sensible heat

II. MODELING

As shown in Fig. 1, Hybrid desiccant cooling system (HDC) use two coolers which are indirect evaporative cooler and heat pump evaporator. Schematic of HDC has cooling components combination of electric heat pump and indirect evaporative cooler. HDC system make use of heat from the condenser of electric heat pump. While an evaporator of electric heat pump cooldown a supply air. A Solid Oxide Fuel Cell system is integrated as suppling exhaust heat as waste heat for HDC system.

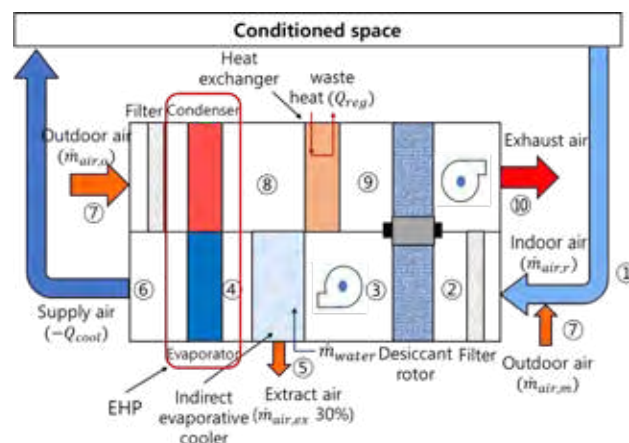


Fig. 1. Schematic of hybrid desiccant cooling system (HDC)

III. SIMULATION & RESULTS

In various simulation conditions, the HDC system is simulated to verify a cooling ability and system characteristic. The outdoor conditions of simulation are range of from 24°C, RH 100% to 50°C, RH 4%. Each condition is based on climate data of city as shown as table I, II [5, 6]. According to weather

data of cities there is high humidity of over 10g/kg until outdoor temperature 40°C, while, when outdoor temperature is too high likes a 45°C, 50°C, because of too high temperature, a relative humidity doesn't reach high. Based on the climate data of table I, II, the system parameter study is conducted. The flow rate is settled at maximum flow rate of the system. Also, based on Fig. 2, the optimal regeneration temperature is figured out at 70°C.

TABLE I
TEMPERATURE AND HUMIDITY CONDITIONS OF OUTDOOR (LOW HUMIDITY)

T outdoor (°C)	RH outdoor (%)	AH outdoor (g/kg)	City	Country	date
50	4	3.04	Ahvaz	Iran	2012-08-02 16:30
45	8	4.72	Phoenix	USA	2018-07-05 16:00
30	6	2.72	Phoenix	USA	2018-07-02 14:00
36	8	2.92	Phoenix	USA	2018-07-02 21:00
30	13	3.39	Phoenix	USA	2018-07-01 23:00
26	17	3.51	Phoenix	USA	2017-07-01 05:00

TABLE II
TEMPERATURE AND HUMIDITY CONDITIONS OF OUTDOOR (HIGH HUMIDITY)

T outdoor (°C)	RH outdoor (%)	AH outdoor (g/kg)	City	Country	date
50	9	6.85	Ahvaz	Iran	2012-08-02 16:00
44	15	8.87	Ahvaz	Iran	2012-08-02 11:30
40	27	12.32	Phoenix	USA	2018-07-19 19:00
35	53	18.5	Bangkok	Thailand	2015-07-02 11:30
30	79	20.84	Bangkok	Thailand	2015-07-02 17:30
24	100	18.52	Phoenix	USA	2018-07-11 23:00

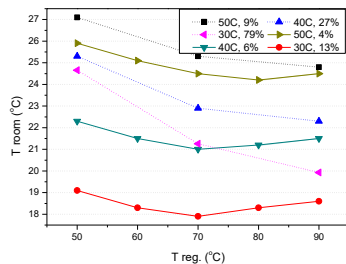


Fig. 2. Regeneration temperature parameter study effect on room cooled temperature of indirect cooler desiccant cooling system

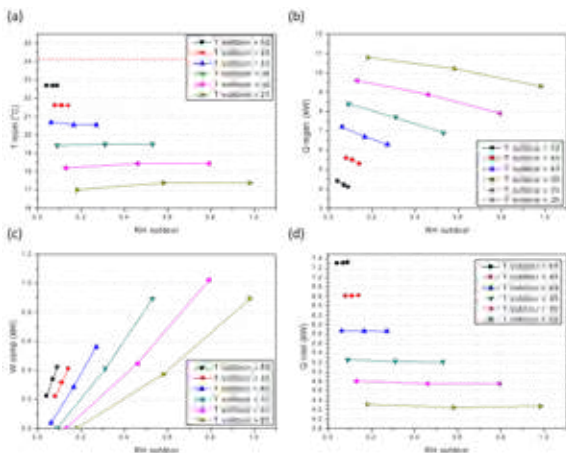


Fig. 3. Parameter study based on world outdoor climate conditions effect on (a) room cooled temperature, (b) regeneration heat consumption, (c) electric power consumption of electric heat pump, (d) cooling capacity of hybrid desiccant cooling (HDC) system

IV. CONCLUSION

In this study, desiccant cooling system model is developed. With developed model, system room cooled temperature, regeneration heat consumption, electric heat consumption, cooling capacity are simulated in various climate cases. The climate data is based on world climate conditions: USA west-south region, Iran and Thailand that data varies from 50°C, RH 9% to 40°C, RH 27%. HDC has sufficient cooling ability in any climates even 50°C climates while the heat consumption is only 4~10kW with electric power consumption 0~1kW. HDC system needs only 5~10 kW regeneration heat because the condenser of heat pump supplements a heat with an electric heat pump consumption under 1kW. As a result, while a heat energy is not sufficient as heat energy supply is equivalent to cooling demand, HDC is best cooling system that can apply to any hot and humid region. HDC use both thermal energy and electric energy with moderate thermal consumption and small electric power consumption. According to recent tri-generation systems propose, the hybrid desiccant cooling system could be effective cooling system for high efficiency and waste heat saving system.

ACKNOWLEDGMENT

This work was supported by the Korea Institute of Energy Research (KIER) granted financial resource from the Ministry of Science and ICT of Korea (No. 2018M1A2A2040670).

REFERENCES

- [1] International Energy Agency (IEA), The Future of Cooling: Opportunities for energy-efficient air conditioning (2018)
- [2] International Energy Agency (IEA), Transition of Sustainable buildings: Strategies and Opportunities to 2050 (2013)
- [3] International Energy Agency (IEA), Energy Technology Perspectives 2015: Mobilising Innovation to Accelerate Climate Action (2015)
- [4] A. Heidari, H. Rostamzadeh and A. Avami, A novel hybrid desiccant-based ejector cooling system for energy and carbon saving in hot and humid climates, International Journal of Refrigeration 101 (2019) 196–210
- [5] “National Centers for Environmental Information” last modified Feb. 17, 2019, accessed Feb. 17, 2019, <https://www.ncdc.noaa.gov/cdoweb/datasets/LCD/stations/WBAN:23111/detail>
- [6] “weatherbase, Middle East, Iran & Asia, Thailand” last modified Mar. 22, 2016, accessed Feb. 17, 2019, <https://www.weatherbase.com/weather/weatherhourly.php?3?s=11804>

HIGH ELECTRICAL EFFICIENT SOFC GENERATOR FOR PURE HYDROGEN WITH A MULTI-STAGE SOFC AND REGENERATION SYSTEM

○S. Akabane*, T. Nakajima*, K. Nakamura*, M. Shirai*,
T. Dohkoh*, Y. Kawabata*, T. Ide* and T. Hatae*
* Tokyo Gas Co., LTD., Suehiro-Cho 1-7-7, Tsurumi-Ku,
Yokohama, Kanagawa, 230-0045 (Japan)

Abstract – Solid Oxide fuel cell has possibility to increase electrical efficiency using pure hydrogen by improving fuel utilization ratio (Uf). To improve Uf, we focused on multi-stage SOFC and fuel regeneration system in our previous studies. In this system, two SOFC stacks were connected in series and regenerator was connected between the two stacks and removed H₂O and CO₂ from the anode off-gas of first stack.

In this study, we designed the system and demonstrated power generation test using pure hydrogen as fuel to our system which was developed for steam reforming gas.

Index Terms – Solid oxide fuel cell, Fuel utilization ratio, pure hydrogen, High electrical efficiency.

I. INTRODUCTION

Fuel cell is one of the green energy systems because it can generate power and heat without CO₂ emission when pure hydrogen is used as fuel. Some systems using pure hydrogen have been already released. Most of the systems were polymer electrolyte fuel cell (PEFC). It is said that solid oxide fuel cell (SOFC) is not suitable for using pure hydrogen as fuel compared with methane because of lower efficiency than PEFC. We aim to improve the electrical efficiency of SOFC using pure hydrogen with our original method [1].

There are some approaches to improve the efficiency. We focused on the fuel utilization ratio (Uf). Generally, the Uf of SOFC has limitation that is around 70%-80% to protect the anode from nickel oxidation caused by decrease of fuel concentration.

We have demonstrated that the system using multi-stage SOFC and fuel regeneration can be improve the each Uf of SOFC stack in our previous studies [1]. In this system, two SOFC stacks were connected in series and regenerator was connected between the two stacks to remove H₂O and CO₂

from the anode off-gas of first stack. Second stack could generate power by using regenerated gas as fuel. Hence, this system enabled to reach the total Uf value of 91.0%-96.0% under not high Uf conditions for each SOFC stack. We have demonstrated that our system could realize the DC efficiency value of 73%LHV with methane (the AC efficiency was 65%LHV assuming an inverter loss of 5% and an auxiliary devices loss of 6%)[2].

In this study, we designed the stack ratio (=first stack/second stack) and calculated the efficiency of the system for pure hydrogen as fuel.

We calculated the suitable stack ratio to reach highest total Uf of pure hydrogen based on the fuel concentration at the outlet of SOFC stack. As a result, the maximum total Uf could be realized when the stack ratio is 6.91 [3].

First SOFC stack could be operated under Uf value of 85.4%. Second stack also could be operated under Uf value of 85.0% by removing H₂O at fuel regeneration, which resulted in the maximum of total Uf value of around 97.8% [3]. Furthermore, this system has possibility to achieve the DC efficiency value of 73%LHV.

To make sure of this calculation, we demonstrated power generation test using pure hydrogen as fuel to our system which was developed for steam reforming gas.

II. EXPERIMENT

A. Schematic illustration of system flow of the hot module

Figure 1 shows the schematic illustration of system flow of the hot module. This system includes vaporizer and reformer because it was made for the system using methane as fuel. The vaporizer and reformer work as heat exchanger because of no vaporization and no reforming

reaction.



Fig.1. The schematic illustration of system flow of the hot module.

B. Power generation test

We demonstrated power generation test by controlling the current of first stack and second stack separately to be stack ratio as 6.91. Steam condenser removed 96.9% of H₂O in the anode off-gas of first stack.

C. Calculation of optimized system

By using the result of power generation test, we calculated the performance of optimized system.

III. RESULTS

The results of power generation test were shown in Fig. 2 and 3. Stable performance was obtained for over 2.5 hours with DC power value of 2.21 kW, DC efficiency value of 68.1%LHV, AC efficiency value of 60.8%LHV (assuming an inverter loss of 5% and an auxiliary devices loss of 6%), Total_Uf value of 96.8%, Voltage per cell value of 887 mV, stack temperature value of 615 °C, Combustor temperature value of 610 °C and Exhausted gas temperature value of 235 °C. These results indicate our system can improve Uf and efficiency using pure hydrogen as fuel for SOFC.

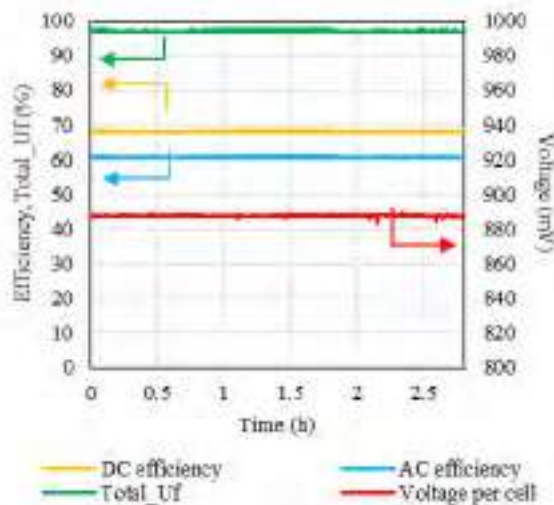


Fig.2. Power generation performance of our system.

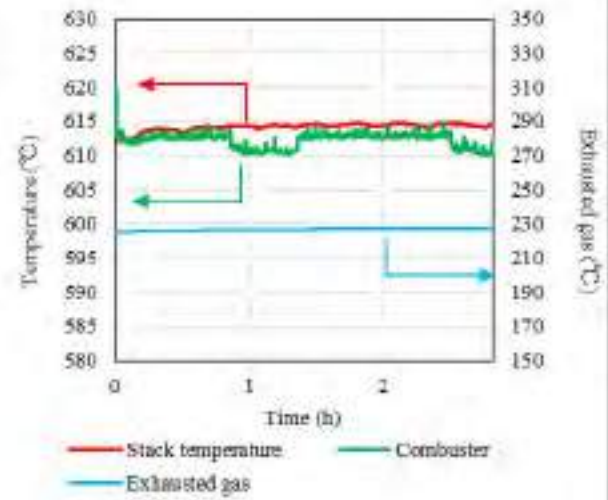


Fig.3. Temperature behavior during power generation.

However, we demonstrated power generation test by using non-optimized system for pure hydrogen. When we use optimized system, the system performance is shown in TABLE I by calculation.

TABLE I
THE OPTIMIZED SYSTEM PERFORMANCE

Stack ratio	6.91
Voltage per cell (mV)	847
Stack temperature (°C)	680
DC power (kW)	5.73
Total_Uf (%)	97.8
DC efficiency (%LHV)	64.5
AC efficiency (%LHV) assuming an inverter loss of 5% and an auxiliary devices loss of 6%	59.4

IV. CONCLUSION

We demonstrated good stability with 96.8 % of Uf in power generation test, which indicates our original system has potential to achieve high AC electrical efficiency value of over 60%LHV using pure hydrogen as fuel for SOFC. Furthermore, optimized system for using pure hydrogen can remove vaporizer and reformer and become smaller system than demonstrated system.

REFERENCES

- [1] K. Nakamura, et al., Development of a highly Efficient SOFC Module Using Two-stage Stacks and a Fuel Regeneration Process, FUEL CELLS 17, No.4, 2017, page 535-540.
- [2] K. Nakamura, et al., Proceedings of 13th European SOFC & SOE Forum, Switzerland, 2018, A1205.
- [3] S. Akabane, et al., Proceedings of the 27th Symposium on Solid Oxide Fuel Cells, Japan, 2018, 159C.

EVALUATING BAUXITE TAILINGS FOR POTENTIAL SOFC APPLICATIONS

Kishore Kumar Mayuranathan* and Ranjit Bauri*

*Energy Materials Laboratory, Department of Metallurgical and
Materials Engineering, New Academic Complex, IIT Madras,
Chennai (India)

Abstract - In this work, bauxite tailings (red mud) has been evaluated for its application in solid oxide fuel cells. Dilatometer was used to calculate the coefficient of thermal expansion, in order to study the compatibility with electrode and interconnect materials. The ionic conductivity was measured using electrochemical impedance spectroscopy and was found to be $\sim 10^{-2}$ S/cm at 800 °C. The phase formation after sintering has been studied using X-Ray diffraction.

Index Terms - Bauxite Residue, Red Mud, Solid Oxide Fuel Cells.

I. INTRODUCTION

The ever increasing global consumption of energy and resources has created a desperate need for clean energy and frugal use of the strategic materials leaving minimal environmental footprint. Depleting fossil fuels and their harmful environmental effects has led to the development of clean energy technologies like fuel cells and batteries. Among these, Solid Oxide Fuel Cells (SOFCs) are attractive because of their fuel flexibility and ability to be integrated with the currently existing energy technologies like gas turbines [1]. Conventional SOFC materials include yttria stabilized zirconia (YSZ), doped ceria, rare earth gallates, stabilized bismuth oxides, barium and bismuth based compounds etc. Most of these materials are scarce. Thus there is a need to develop easily available materials for such clean energy technologies [2, 3].

Red mud is the by-product of alumina refineries. For every ton of alumina, 0.7 to 1.5 tons of red mud is produced [4]. Because of this huge global inventory, it is generally stored in a dam or dried and stacked. Red mud consists of oxides of Fe, Na, Si, Al, Ti, K, P and trace amount of rare earth oxides. Because of its composition, red mud has been explored as a catalyst for several chemical processes, adsorbent to purify

water, construction materials etc [4]. In this work, red mud was evaluated for its suitability for application in SOFCs.

II. MATERIALS AND METHODS

The red mud was received from Hindalco Ltd, Belgavi, India. The chemical composition of red mud has been found using X-Ray fluorescence (XRF) spectrometer (Table 1). The red mud, in as received condition, was ground into fine powders and compacted into cylindrical pellets of 20 mm diameter under a uni-axial load of 300 MPa. The pellets were sintered at 1050 °C and 1200 °C. The phases formed after sintering were studied using X-ray diffraction analysis. The coefficient of thermal expansion was measured using a dilatometer. The sample for dilatometer was a pellet of square cross section sintered at 1000 °C. The ionic conductivity was measured using electrochemical impedance spectroscopy in a PARSTAT 4000A electrochemical workstation, with conductive silver ink applied on both sides of the sintered pellet.

Partial electronic conductivities were measured using a platinum micro-contact as the working electrode at the top of the pellet and a porous Pt layer on the opposite side of the pellet as the counter electrode. The micro-contact was sealed from the atmosphere using Ceramabond seal (AREMCO Products). The partial pressure of oxygen (pO_2) was varied by applying DC voltages in the range of 0.1V to -0.4V to the working electrode. The complete methodology used for the calculation has been described in [5].

III. RESULTS AND DISCUSSION

The composition of the red mud determined using XRF is given in Table I. In addition to the elements listed in the table, less than 1 mass % of MgO, K₂O, P₂O₅, NiO and MnO were also present.

TABLE I
COMPOSITION OF RED MUD FROM X-RAY FLUORESCENCE SPECTROMETER

Compound	Al ₂ O ₃	Fe ₂ O ₃	TiO ₂	CaO	SiO ₂	Na ₂ O
Mass %	22.22	32.57	7.80	2.28	24.32	9.71

The X-ray diffraction pattern of the sample sintered at 1200°C is shown in the Figure 1. There are several phases including Fe₂O₃, the spinels of Fe, Al and Ti and TiFe₂O₅ that have oxygen ion conductivity. However, role of the other phases is not clear.

The coefficient of thermal expansion was calculated to be $10 \times 10^{-6} \text{ K}^{-1}$ at 800 °C, which is close to that of the typical SOFC materials.

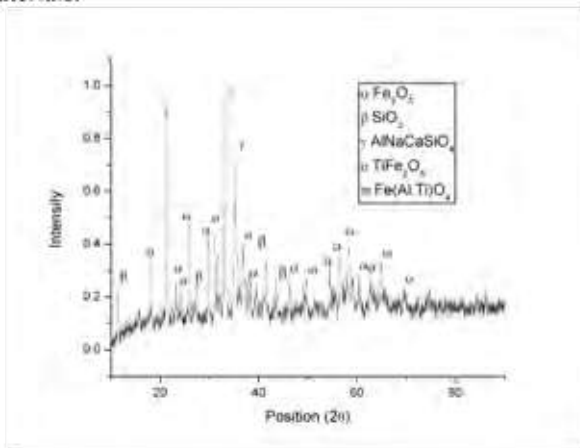


Fig. 1: XRD pattern of red mud sintered at 1200 °C

The total conductivity at 800 °C measured from the Nyquist plots was approximately 10^{-2} S/cm and 28.57×10^{-3} for the sample sintered at 1050 °C (Figure 2(a)) and 1200 °C (Figures 2(b) and 2(c)) respectively.

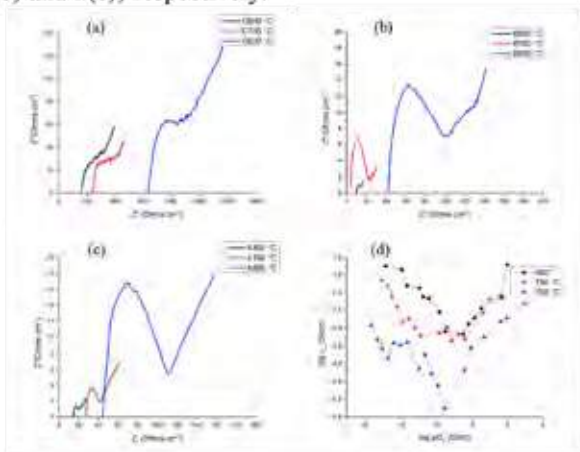


Fig. 2: (a) Nyquist plot of RM sintered at 1050 °C; (b) Nyquist plot of RM sintered at 1200 °C; (c) Nyquist plot of RM sintered at 1200 °C with different electrode size; (d) log-log plot of partial electronic conductivity vs pO₂

The partial electronic conductivity values exhibit 'n' type and 'p' type conductivities at low and high pO₂ regions respectively. Few more iterations of the polarization cycles are necessary to check for the presence of any hysteresis and thereby to quantify the partial electronic conductivity.

IV. CONCLUSION

In this work, the electrical conductivity of red mud has been measured using impedance spectroscopy. Partial electronic conductivities of the red mud are currently being measured to determine the transference number and to determine the suitability of red mud in SOFC applications. Employing red mud in such applications will lead to better utilization of the constituents of the red mud. Additionally, most of the applications using red mud, involve a modification treatment. This work employs the red mud is as received condition, which is highly beneficial. Also, material cost contributes a significant share to the overall cost of SOFCs. Developing SOFCs based on easily available materials like red mud could bring down the cost of SOFCs.

ACKNOWLEDGMENT

The authors are grateful to Hindalco Ltd, Belgavi plant, for providing the red mud used in this work.

REFERENCES

- [1] Roy, D., Samanta, S., Ghosh, S., Techno-economic and environmental analyses of a biomass based system employing solid oxide fuel cell, externally fired gas turbine and organic Rankine cycle, *Journal of Cleaner Production*, Volume 225, 2019, Pages 36-57.
- [2] da Silva, F.S., de Souza, T.M., Novel materials for solid oxide fuel cell technologies: A literature review, *International Journal of Hydrogen Energy*, Volume 42(41), 2017, Pages 26020-26036.
- [3] Nuss, P., Eckelman, M.J., Life Cycle Assessment of Metals: A Scientific Synthesis, *PLoS One*, Volume 9(7), 2014, Pages e101298.
- [4] Klauber, C., Grafe, M., Power, G, Bauxite residue issues: II. options for residue utilization, *Hydrometallurgy*, Volume 108, 2011, Pages 11-32.
- [5] Maheshwari, A., Wiemhöfer, H.D., Sr²⁺-Gd³⁺ co-doped CeO₂: A cost-effective variant for IT-SOFC electrolytes, *Ceramics International*, Volume 41, 2015, Pages 9122-9130.

DEVELOPMENT OF A COMPACT μ DMFC MODULE WITH INTEGRATED GAS-LIQUID SEPARATION

V. Lukassek*, J. Wartmann*, A. Heinzel* K. M. Dyrda**, P. Münzer**,
R. Dittmeyer**, T.-M. John***

*ZBT GmbH, Carl-Benz-Str. 201, 47057 Duisburg (Germany)

** KIT, Hermann-von-Helmholtz-Platz 1, 76344 Eggenstein-Leopoldshafen (Germany)

***PT&B Silicor GmbH, Steinfeldstraße 3, 39179 Barleben (Germany)

Abstract - Due to growing energy demand of small electronic appliances, micro fuel cells are seen as a possible replacement or supplement to conventional accumulators. The possibility to use liquid fuel and the resulting simplification of storage considers the direct methanol fuel cell (DMFC) having especially great potential in the field of portable micro fuel cell systems [1]. The system must yield adequate power output while at the same time maintaining criteria such as a small volume and lightweight packaging. Furthermore the robustness of the systems with regard to mass production is also an important aspect to consider. In this work, a DMFC stack with coated metal based bipolar plates of a performance category of 3 Watt consisting of five cells was set up including a downstream gas-liquid separator to remove gas from the anode product stream to allow its recirculation. The use of a membrane-based micro contactor has been studied as a separation unit.

Index Terms – Coating, Direct Methanol Fuel Cell (DMFC), gas-liquid separation, metallic bipolar plates

I. INTRODUCTION

Portable power systems up to 100 Watt (e.g. chargers for outdoor applications) have to meet stringent requirements regarding volumetric and gravimetric power densities. Bipolar plates constitute the main share of the total stack weight, volume and costs and have also to fulfil a number of material requirements such as high compressive strength, sufficient electrical and thermal conductivity, good electrochemical stability but also proper machinability. Although metallic based materials meet all necessary requirements, the main weak point of such materials is their susceptibility to corrosion in an acid environment, which is the case during the operation of the fuel cell. Therefore, a suitable coating for protection of the metallic bipolar plate material against the exposure to corrosive environment while preserving excellent electrical conductivity

has been successfully developed.

The cell environment of a DMFC places high demands on the material of the bipolar plate, in particular on the coating material. The high anodic potential and the low pH of 3 at the boundary layer of the membrane electrode assembly (MEA) present an increased risk of corrosion for the cell material itself. Coatings are required to reduce corrosion of the bipolar plate. Due to their high hardness, good wear resistance, as well as excellent corrosion and high-temperature oxidation resistance, chromium nitrides (CrN) are regarded as excellently suitable for use as coating materials, which have already been intensively investigated [2]. CrN coatings were applied to stainless steel substrate (1.4404) using physical vapor deposition (PVD) to increase the corrosion resistance [3]. Nevertheless, pitting-holes within such layers could lead to a reduction in the corrosion resistance. One way to overcome this problem is to fabricate multi-layer coatings with intermediate layers of a different material in order to cover surface defects of the CrN-layer. By alternating CrN-layers and thin intermediate layers a coating with excellent compactness, uniformity and corrosion resistance is realized. Amorphous Carbon (aC) is an interesting candidate for the use as thin intermediate layer because of its high corrosive resistance.

The use of a membrane-based micro contactor has been studied as a separation unit. Investigations regarding the separation efficiency have been dynamically performed with multiple DMFC-stacks. For this reason, both the behavior of two-phase flow inside the micro contactor as well as the gas production of the fuel cell have been looked into beforehand. Finally, after an evaluation of the gathered results from the individual experiments a general recommendation regarding the

design of an integrated separation unit for the fuel cell was given (fig. 1).

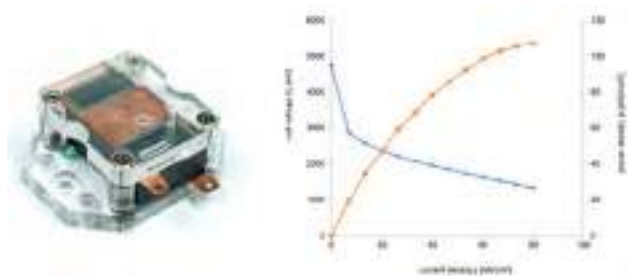


Fig. 1. stack consisting of 5 cells (left), polarisation curve (right)

II. EXPERIMENTS AND RESULTS

The coating was applied with and without prior plasma polishing of the substrate. The total thickness of the deposited coating was 1000 nm. Figure 2 shows an ICR measurement of CrN/aC samples re-presenting a change in contact resistance with and without prior plasma polishing. The contact resistance of the sample with prior plasma polishing and the CrN/C coating is in the range of the target values for bipolar plates defined by the DOE (lower than $10 \text{ m}\Omega\text{-cm}^2$ at 140 N/cm^2 compaction pressure) [3].

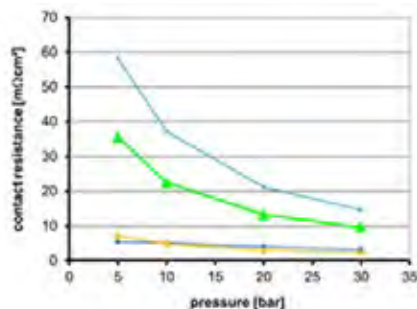


Fig. 2. ICR measurements of the sample

In the investigation of the separation efficiency of the micro contactor it could be shown that in the operating range of the cell stack it was possible to consistently achieve degrees of separation greater than 0.95. Complete separation of the gas was achieved at 120 mA/cm^2 , 140 mA/cm^2 and 160 mA/cm^2 at transmembrane pressures of 60 mbar, 80 mbar and 100 mbar (fig. 4). The overall performance of a DMFC is strongly dependent on the gas/liquid phase separation at the anode side, especially if the DMFC is operated transiently with a recovery system for unused fuel. The use of membrane technology enables the separation of the two-phase flow into liquid and gas in a compact and flat device. In general, this is achievable by using a polymeric membrane based micro contactor installed downstream of the DMFC. However, polymeric membranes are not methanol resistant in long-term use and have a high transport resistance. In contrast, metallic or ceramic microsieves have a high thermal and chemical stability in methanol as well as a low transport resistance due to their small uniform pore

diameters and length. Thus higher separation performance, tailored selectivity and low system energy consumption are possible. In this work, a metallic microsieve based micro contactor for the position-independent gas/liquid phase separation is developed. As a separation layer a nickel microsieve was used with a total thickness of $10 \mu\text{m}$. The suitability of the contact module for dynamic use for gas separation in a DMFC could thus be clearly confirmed.

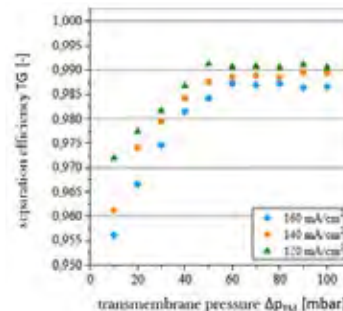


Fig. 3. separation efficiency at different trans-membrane pressures

III. CONCLUSION

In this work, a DMFC stack consisting of five cells was set up including a downstream gas-liquid separator to remove the gas from the anode product to allow an anode recirculation. It could be shown that in the operating range of the cell stack, it was possible to consistently achieve degrees of separation greater than 0.95. The suitability of the contact module for dynamic use for gas separation could thus be clearly confirmed. A new corrosion-resistant and conductive coating for stainless steel bipolar plates has been successfully developed. The corrosion resistance has been improved significantly by the CrN/aC coating and plasma polishing. However, further tests are necessary to investigate the long-term stability of the coated material.

ACKNOWLEDGMENT

This work has been carried out with the financial support of the German Federation of Industrial Research Associations (AiF) within the frame of the research projects entitled “Development of a compact μ DMFC module with integrated gas-liquid separation” (No. 18741N).

REFERENCES

- [1] Kamarudin S.K et al., Overview on the application of direct methanol fuel cell (DMFC) for portable electronic devices. International Journal of Hydrogen Energy, 34(16), 6902–6916, 2009
- [2] Yang C et al., Electrochemical behaviour of surface treated metal bipolar plates used in passive direct methanol fuel cell. International Journal of Hydrogen Energy, 37(1), 867–872, 2012
- [3] Antunes R., Corrosion of metal bipolar plates for PEM fuel cells: A review, International Journal of Hydrogen Energy, 35(8), 3632–3647, 2010

N-DOPING MODULATION BY PLASMA TREATMENT IN POLYACRYLONITRILE DERIVED CARBON-BASED NANOFIBERS FOR THE OXYGEN REDUCTION REACTION

G. Massaglia^{a,b*}, S. Bianco^{a,b}, M. Castellino^a, A. Chiodoni^b, F. Frascella^a, A. Sacco^b, F.C. Pirri^{a,b}, M. Quaglio^{a**}

^a Department of Applied Science and Technology, Politecnico di Torino, 10129 Torino (Italy)

^b Center for Sustainable Future Technologies@ POLITO, Istituto Italiano Di Tecnologia, 10129, Torino (Italy)

Abstract - This work aims to provide a simple and effective method for achieving highly active in situ catalysts for oxygen reduction reaction (ORR). This key challenge is required to substitute platinum, and related materials: even if they are the best option to catalyze the ORR with low over-potential and high current density, they suffer of problems which hinder the development to the market level of clean energy technologies as fuel cells. Key issues are the scarcity, high cost and limited durability of Pt-based catalysts. The main aim of this work is the optimization and improvement of nitrogen content into carbon-nanofibers, intrinsically doped with nitrogen (N-CNFs). To reach this goal, plasma treatments are employed, optimizing them in order to modify the distribution of the N-doping sites, tuning defects content to improve the ORR catalytic activity of the material.

Index Terms – Single chamber microbial fuel cell, Oxygen reduction reaction, Electrospinning, N-doped Carbon Nanofibers, Plasma treatment.

I. INTRODUCTION

Effective strategies to reduce human dependence on fossil fuels are the key steps towards climate change mitigation. To this purpose, the implementation of high performing renewable low-carbon technologies are mandatory [1]. Among all energy conversion and storage devices, fuel cell technologies (FCs) shine as the leading option toward sustainability, and among them Microbial Fuel Cells (MFCs) play a crucial role as the sole example of FCs able to harvest environmentally available chemical energy. MFCs require further improvements to increase their performance and efficiency. The key challenge is the oxygen reduction reaction (ORR) occurring at cathode. [2] Since the ORR is an energetically un-favored electrochemical heterogeneous reaction, the employment of new electrocatalysts with higher catalytic activity, longer durability and cost effective, are designed. To this purpose, metal-free nanomaterials play a crucial role, becoming the key enabling technology for further development in catalysis area. As demonstrated in our previous work [3], carbon-based nanomaterials, intrinsically doped with heteroatoms like nitrogen, have established as the most promising substitutes to platinum (Pt). The main aim of this work is the optimization of carbon nanofibers doped with nitrogen (N-CNFs), especially in terms of their content of graphitic, pyrrolic and pyridinic nitrogen

defects, as well as their high surface area. N-CNFs have been prepared by electrospinning, as discussed in our previous work [3], and thermally treated up to 900°C under inert atmosphere. Raman spectroscopy confirmed the partial graphitization of N-CNFs, and X-ray photoelectron spectroscopy (XPS) gave evidence of good content of graphitic and pyridinic nitrogen defects in CNFs. Two different plasma treatments are compared: the first one was an N₂-plasma and the second one was based on a mixture of O₂ and N₂ (78% N₂ and 22% O₂), named atmosphere based-plasma. It is commonly accepted that N₂-plasma ensures the increase of nitrogen content into carbon materials [4], while O₂-plasma is normally used for etching and surface cleaning [5]. In the present work, all obtained results demonstrate that atmosphere based-plasma allows an improvement of total nitrogen content, especially promoting the increase of pyridinic-N. The atmosphere based-plasma induced 2 concurrent effects: *i*) removal of surface atoms or clusters of atoms induced by etching reactions employed by O₂ and *ii*) further reactions between reactive sites and the reactant N₂ species in the plasma, tuning thus the N-doping active sites, as demonstrated by XPS. The electrochemical properties of all nanostructured materials were characterized by Rotating Ring Disk Electrode (RRDE), demonstrating an electron transfer number of 3.9 after plasma treatments.

II. EXPERIMENTAL SECTIONS

A. Materials and Methods

As reported in our previous work [3], CNFs are obtained by electrospinning technique starting from a polymeric solution, containing 12 wt% of PAN (average molecular weight Mw=150,000kDa) dissolved into DMF (assay 99.8%), purchased from Sigma Aldrich. Samples. A NANON 01A electrospinning apparatus (MECC., LTD) was used. Each nanofiber mat was obtained by applying a voltage value of 15kV for 2 hours. As spun nanofibers are subsequently thermally treated until 900°C into inert atmosphere for 1h (Carbolite, VST 12/300/3216/) [3]. Two plasma treatments (Diener) were performed, one based on N₂ only, at 50 W for 5 min, and a second one using a gaseous mixture of N₂ and O₂ with an atmospheric-based ratio, at 50 W for 5 min. The tuning

of the distribution of the N-Doping sites was demonstrated by XPS (PHI 5000 Versaprobe scanning X-ray photoelectron spectrometer) and Raman (Renishaw InVia Reflex spectrometer, $\lambda_{\text{ex}}=514.5$ nm) spectroscopies. In particular, two different plasma treatments were carried out: the first one is N₂-plasma, the second one is atmosphere-plasma. The morphology of the samples was analyzed with Field Effect Scanning Electron Microscope (FESEM, ZEISS Merlin, operating between 5 and 10 kV). RRDE technique were carried out by means of a CHI instrument 760D electrochemical workstation and an ALS RRDE-3A rotating ring disk electrode apparatus.

III. RESULTS AND DISCUSSION

As demonstrated in our previous work [3], the nitrogen defects play a crucial role for the optimization of catalytic features of these nanostructures toward ORR. In order to deeply demonstrate how the plasma treatments play a crucial role to tune the nitrogen defects content in N-CNFs two different treatments are differently employed: N₂-plasma and atmosphere-plasma. As reported in Fig.1b) and c), XPS leads to demonstrate an increasing of atomic percentage of nitrogen, occurred when atmosphere based-plasma s applied, comparing with the one obtained in N₂-plasma. Fig.1c) confirmed that N-CNFs treated with plasma in atmosphere based-plasmas how a high content of pyridinic nitrogen, close to 45.75 at%, together with a great content of graphitic-center nitrogen equal to 18.36 at%.

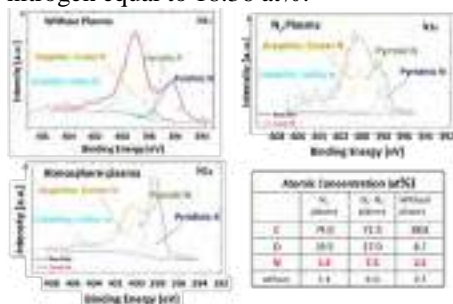


Fig1. High-resolution N1s spectra for N-CNFs obtained by implementing two different plasma treatments a) N₂ plasma treatments and b) atmosphere based-plasmatreatments.

The preservation of the nanostructures also after atmosphere based-plasma was confirmed by FESEM images, as sketched in Fig 2 a), confirming that the presence of O₂ in this treatment doesn't induce a detriment of the nanostructures. Raman spectroscopy (Fig. 2b) was performed to establish the defect level of all nanofibers mats, demonstrating how the defect level increases when the plasma treatments was carried out. Higher is the ratio between D-band and G-band, higher is the defect level of CNFs. Fig 2c) underlines an higher electrical conductivity, close to 18 S cm⁻¹, reached by CNFs treated with the atmosphere-plasma, than the one achieved by CNFs treated with the N₂-plasma. The RRDE technique allows validating the catalytic pathways of all nanomaterials by using 4-electrodes measurements.

In order to compare the electro-catalytic properties of N-CNFs and both of CNFs obtained after plasma treatments, it is possible to notice that nanofibers obtained after atmosphere based-plasma ensure a high number of electron transfer, close to the ideal values of 4, reached reached by Platinum (Pt), as shown in Fig. 2d).

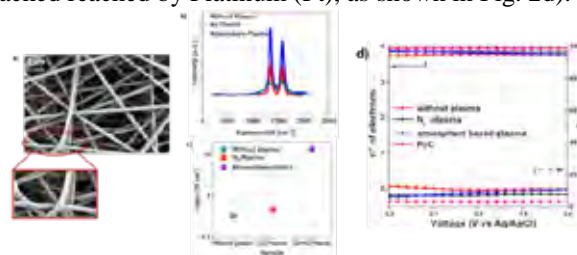


Fig2. a) FESEM images conducted after atmosphere based-plasma treatment, b) Raman Spectroscopy and c) electrical conductivity conducted on all nanofiber mats. d) Comparison of electron transfer number (left axis) and H₂O% (right axis) evaluated from RRDE measurements of N-CNFs (red line) compared with CNFs treated in N₂-plasma (black line), CNFs treated in atmosphere based-plasma (blue line) and the commercial catalyst based on Pt/C (pink line)

IV. CONCLUSION

In the present work, the crucial role achieved by plasma to tune the nitrogen defects content in CNFs was demonstrated. In particular, it was possible to confirm two effects induced by the presence of O₂ into the atmosphere-plasma: i) removal of surface atoms or clusters of atoms induced by etching reactions employed by O₂ and ii) further reactions between reactive sites and the reactant N₂ species in the plasma, tuning thus the N-doping active sites. This hypothesis was confirmed by XPS that underline a higher content of nitrogen, close to 7.5 at%, respect to the one achieved in CNFs treated with N₂ plasma (equal to 3.4 at%). Since the electrochemical properties of sample are optimized when the samples employ/achieve high electrical conductivity and high content of heteroatoms, all these latter results confirm how the atmosphere based-plasma is able to design an improved catalyst layer for direct ORR, granting also the preservation of the nanostructures. All these results confirmed the optimization of metal-free catalyst that can be applied as cathode electrode in air-cathode Microbial Fuel Cell (MFC), improving thus its overall performance.

REFERENCES

- [1] A roadmap for moving to a competitive low carbon economy in 2050, 2011, <http://ec.europa.eu/clima/policies/strategies/2050>
- [2] B.C.H. Steele et al. Materials for fuel-cell technologies, Nature, 414 (2001) 345–352
- [3] G. Massaglia et al. N-doped carbon nanofibers as catalyst layer at cathode in single chamber Microbial Fuel Cells. JHE;2018;44: 4533-42
- [4] S.Hussah, et al. Nitrogen plasma functionalization of carbonnanotubes for supercapacitor applications J. Mater. Sci; 2013; 48:7620–7628
- [5] J.P. Boudou et al. Oxygen plasma modification of pitch-based isotropic carbon fibres. Carbon;2003;41:41-56

APPLICATION OF HTFC POWERED BY LNG ON A CRUISE SHIP: A CASE STUDY

L. Micoli, T. Coppola and M. Turco

University of Naples Federico II, p.le Tecchio 80 - 80125 Naples, (Italy)

Abstract - The work is a case study of a cruise ship supplied by LNG and equipped with a solid oxide fuel cell. It is considered that 5x200 kW SOFC systems integrated with gas turbines are installed onboard assisting a dual fuel diesel/LNG engine to generate 10 MW during the stay in port time. The cruise ship spends almost 12 hour per day in ports thus contributing significantly to the local environmental pollution. Results indicate that the use of SOFC system allows both to save about 6.75% of LNG, in comparison to the dual fuel engine, and to reduce emissions of SO_x, CO, NO_x, PM by about 10% and CO₂ by 5.3%.

Index Terms – Cruise ships, Emissions, GNL, SOFC.

I. INTRODUCTION

Marine sector contributes to the global emissions of greenhouse gases (GHGs) and other hazardous air pollutants approximately for an amount of 5% [1]. It is subordinated to the current stringent international environmental standards as well, forcing to search alternative fuels and new technologies with lower environmental impact.

There are several fuels or energy carriers that can be used in shipping among which Liquefied Natural Gas (LNG) is one of the most commonly considered today. The use of LNG allows to reduce both 25% of carbon dioxide and a remarkably amount of sulfur oxides emissions (SO_x) in comparison to traditional marine Diesel oil fuel [2].

Nevertheless, using the traditional endothermic engines with LNG could not satisfy the environmental requirements, therefore alternative technologies are being sought. Among these, the use of Fuel Cell technology (FC) seems to be very promising [3].

Considering a vessel supplied by LNG, the use of High Temperature FCs (HTFCs) is more suitable than low temperature FCs since they can be powered directly by LNG, with no complex fuel treatment system and allowing higher efficiencies if used in cogenerative configurations [4].

Nowadays, it possible to find several commercial Solid

Oxide FCs (SOFCs) products offering attractive potentials for electrical generation in centralized and distributed applications. The SOFC is the simplest and most rugged among all FCs covering wide power ranges (up to few MW) and with very long lifetimes (up to 60000 h) [5].

According to this, the present study considers a case of a cruise ship supplied by LNG and equipped with SOFC modules integrated with gas turbines (GT), assisting the dual fuel diesel/LNG (DF) engine to generate electricity on board during the stay in port of the ship. The aim is to predict the CO₂, CO, SO_x, NO_x and particulate matter (PM) emissions of the SOFC system in the harbors compared to the DF engine. The fuel consumption has been estimated and compared as well.

II. METHODS

A. General layout of the cruise ship

Main characteristics of the cruise ship are summarized in Table I.

TABLE I
Main cruise ship characteristics

Passengers	6600 + 2035 crew members
Main dimension (m)	Length: 350-360; Breadth: 40-45; Height: 50-60
Design draught (m)	7.74
Decks	18
Cruise speed (kn)	19 (maximum: 21)
Autonomy	10 days
Propulsion	Double propeller with gas engines
Fueling	A complete fuel gas handling system for LNG fueled ships.
Maximum power (MW)	62.2

The propulsion power and the electrical power production are provided by four Wartsila Dual fuel diesel/LNG engines (model: 18V50DF) with a nominal power of 17.55 MW at 60 Hz.

Emission factors of such engine are estimated from data reported in recent literature [6], considering average values. It must be noted that we considered only the data of DF engines with emissions that respect the IMO tier II regulations [7].

B. Solid Oxide Fuel Cell

Technical data and emission factors are taken from some commercial SOFC-GT products sold by worldwide companies, such as Mitsubishi Hitachi Power Systems (Japan), BloomEnergy (USA), Convion (Finland), SunFire GmbH, (Germany), Elcogen (Estonia), etc., and considered in average values.

It is assumed that the SOFC is integrated with a GT in order to generate more electric energy allowing an increase of the efficiency from 57% to 85%.

C. Case Study

The cruise ship stays in port 12 hours per day requiring about 10 MW. Generally, the primary engines supply this power demand. In this case study we assumed that 9 MW are provided by a single DF engine, working with an efficiency of roughly estimated at 20%, and 1 MW by five SOFC-GT modules of 200 kW fueled by GNL.

III. RESULT

Emissions factors both for the DF and SOFC-GT have been evaluated and reported in Table II.

TABLE II
Dual fuel Diesel/LNG engine (DF) and SOFC-GT emission factors

Emissions	Unit	Value	
		DF	SOFC-GT
SO _x	mg/kWh	32 ± 17	negligible
NO _x	mg/kWh	7000 ± 2100	4.8 ± 0.2
CO	mg/kWh	15000 ± 4230	2.1 ± 0.1
PM	mg/kWh	175 ± 108	negligible
CO ₂	g/kWh	725 ± 234	343 ± 37

As expected, it resulted that the DF engine has NO_x, CO emissions significantly higher than SOFC-GT system. Any appreciable emissions of SO_x and PM are found for the SOFC-GT. CO₂ emission of SOFC-GT is lower than DF due to the higher efficiency of the SOFC.

Emissions in port of SOFC-GT system have been calculated and compared to those of DF. As expected, it results that the SOFC-GT emissions are lower and this allows to reduce the global emission of the cruise ship in port by the values reported in Table III.

LNG consumption of the SOFC-GT system, during the stay in port of the cruise ship, is estimated to 8 L/day. At the same time, the DF engine consumes about 94 L/day of LNG to generate a power of 9 MW for 12 hours. It means that in this case it is possible to save about 6.75 % producing 10 MW with such hybrid configuration.

TABLE III
Emissions reduction by using a SOFC-GT system

Emissions	Reduction, %
SO _x	10
NO _x	9.99
CO	10
PM	10
CO ₂	5.27

IV. CONCLUSION

It has been presented a case study of a cruise ship supplied by LNG working with a hybrid configuration made by a SOFC-GT system and a DF engine during the stay in port of the ship. A preliminary evaluation of the emissions and fuel consumptions in the port have been carried out both for the SOFC-GT and DF. It resulted that such a configuration allows to reduce the CO, SO_x, NO_x and PM emission by 10% and CO₂ by 5.27 %. In addition, about 6.75 % (8 L/day) of LNG is saved.

Favoring the introduction of high temperature fuel cell technology (SOFC) in cruising sector can contribute to respect the more and more stringent environmental regulations.

REFERENCES

- [1] [http://www.imo.org/en/About/Conventions/ListOfConventions/Pages/International-Convention-for-the-Safety-of-Life-at-Sea-\(SOLAS\)-1974.aspx](http://www.imo.org/en/About/Conventions/ListOfConventions/Pages/International-Convention-for-the-Safety-of-Life-at-Sea-(SOLAS)-1974.aspx). Accessed October 2019.
- [2] DNV GL. 2015. In Focus - LNG as a ship fuel. DNV GL Maritime Communications.
- [3] <http://www.emsa.europa.eu/implementation-tasks/environment.html>. Accessed October 2019.
- [4] Williams, M. C., Buckley, P. J., Fuel Cells for Cogeneration, Cogeneration and Distributed Generation Journal, 2009, pp. 6-24.
- [5] McPhail, S. J., Kiviaho, J., Conti, B., International Status of SOFC deployment 2017, VTT Technical Research Centre of Finland Ltd, 2017.
- [6] Micoli, L., Coppola, T., Turco, M., Application of High Temperature Fuel Cell powered by LNG on a ferry boat: a case study, Proceeding of International Congress of the International Maritime Association of the Mediterranean, 2019
- [7] <https://www.dieselnet.com/standards/inter/imo.php>. Accessed October 2019.

TRACE-METAL DISSOLUTION FROM COATED METALLIC BIPOLAR PLATES IN PROTON EXCHANGE MEMBRANE FUEL CELLS

Timon Novalin*, Björn Eriksson*, Sebastian Proch**, Mikael Stenström**, Ulf Bexell**,
Carina Lagergren*, Göran Lindbergh*, Rakel Wreland Lindström*

* Applied Electrochemistry, School of Engineering Sciences in Chemistry, Biotechnology and Health,
KTH Royal Institute of Technology, SE-100 44 Stockholm, Sweden

** Sandvik Materials Technology, SE-811 81 Sandviken, Sweden

Abstract – Metallic bipolar plates (BPPs) show promise as an alternative to plates made from graphite. However, dissolution of metals in fuel cell conditions may be responsible for losses in performance. Therefore, metallic BBPs are coated with a protective carbon layer. The aim of this study was to investigate the behaviour of such plates under automotive PEMFC conditions. The test shows no increase in contact resistance, but a higher voltage degradation in the presence of coated metallic BBPs. SEM/EDX analysis found the carbon layers to be intact, however, iron dissolution from metallic stains on top of the carbon layer was detected. The origin of those stains lies in unsuitable laser drilling used for the manufacture of the BPPs. This suggests that carbon coatings provide good protection for metallic BBPs but also that a systemic approach is needed and plate manufacturing has to be taken into account when analysing single-cell test results.

Index Terms – Bipolar plates, drive cycle, metal dissolution, proton exchange membrane fuel cell (PEMFC)

I. INTRODUCTION

To realize voltages of up to 200 V, required for electrical devices and automotive applications, single fuel cells are connected in series via bipolar plates to form a stack. BPPs, moreover, separate gases of adjacent cathodes and anodes and provide electrical conductivity.

Desired properties of bipolar plates are low interfacial contact resistance (ICR), low ohmic resistance, high chemical stability and good heat conductivity. Graphite as BBP material matches these criteria. It is, however, brittle and large scale manufacturing is costly. In comparison, metallic bipolar plates are cheap, have excellent forming and mechanical properties and can be made very thin. Their main disadvantage is the lack of chemical stability in the PEMFC environment. Anodic (oxide) film formation on metallic BPPs can increase their ICR [1]. Additionally, released metal ions can increase proton resistance as they replace protons in the membrane/ionomer phase [2]. Furthermore, Fenton-active

metal ions (e.g., Fe^{2+}) can cause continuous radical formation which, in turn, leads to membrane and ionomer degradation [3].

II. EXPERIMENTAL

A. Fuel cell hardware and testing parameters

All measurements were performed using an in-house cell with a PEEK body and two movable cylindrical current collectors (CC) made of graphite with an active area and flow field of 7 cm^2 . Gases were heated and humidified, to 66 % relative humidity (RH) at a cell temperature of $80 \text{ }^\circ\text{C}$. The clamping pressure applied to the cell was 8.2 bar. Gas flow rates were adapted continuously to the current profile to provide stoichiometric flows of 1.3 at the anode and 1.5 at the cathode. Gas pressures in the cell were 1 bar. For the membrane electrode assembly, a commercial GORE MEA (thickness $25 \text{ }\mu\text{m}$, anode loading $0.45 \text{ mg/cm}^2 \text{ PtRu}$, cathode loading $0.4 \text{ mg/cm}^2 \text{ Pt}$) was used. Sigracet 25 BC gas diffusion layers (GDL) were used on both electrodes. The BPPs used were carbon coated stainless steel plates with a spiral flow field where the total land area was 3.86 cm^2 . To measure the contact resistance probes were placed at the edge of the GDL and the back of the BPP plate.

B. Testing regime

Stability testing was based on the New European Driving Cycle [4]. Each cycle was made up of a current profile, simulating the changing demands during real-life driving. A total number of 700 cycles, corresponding to a driving time of six months, was chosen.

III. RESULTS

The results of a full experiment are shown in **Fig 1**. As can be seen the performance of the MEA was reduced and the transients in regions with higher current densities increased in intensity with progressing cycling.

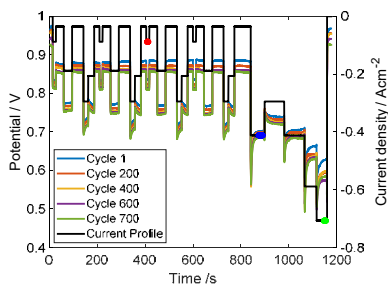


Fig 1. NEDC measurements of a 7 cm² commercial MEA with a carbon coated BPP at anode and cathode side.

Three regions from Fig 1. were chosen to evaluate degradation. A low (red marker at 410 s), a medium (blue marker at 880 s), and a high (green marker at 1150 s) current density region. The decay for each region, in the absence and presence of a carbon coated metallic BPP are shown in Fig 2a.

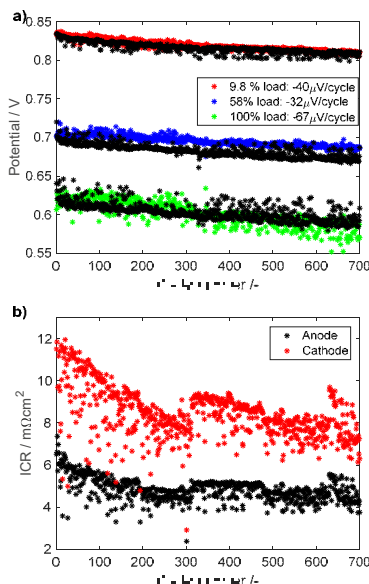


Fig 2. a) Voltage degradation in the low (red), medium (blue), and high (green) load regions in the presence of carbon-coated stainless steel BPPs and in their absence (graphite current collectors, black). The values in the legend indicate the performance loss per cycle. b) Temporal evolution of ICR on anode (black) and cathode (red).

An almost linear decay of performance was observed for the metallic BPPs and the graphite CCs, corresponding to a total of approximately 3 % loss in performance. In the high load region, the BPP sample showed a higher loss, most likely due to the presence of metal ions in the MEA [3].

The ICR evolution with progressive cycling (Fig 2b) exhibits a decrease, suggesting stable conductivity of the carbon layer. The initial ICR decrease is attributed to pressure-equilibration inside the cell. Stable carbon coatings were confirmed by SEM/EDX, where neither morphological nor compositional changes were detected

(orange area in Fig. 3). The presence of metal contaminations was found to be due to unsuitable laser drilling of the gas inlets, which caused stains to form on the coating (blue area in Fig 3).



Fig 3. a) Picture of carbon-coated stainless-steel BPP. The blue square shows the position of the gas inlet. b) SEM analysis of the gas inlet of the carbon-coated, laser-drilled, stainless-steel BPP. The scale bar is 2 µm.

It is important to note that this is a manufacturing error caused by the unique shape of the bipolar plates used in this setup. Nevertheless, the presence of even small amounts of iron negatively impacted the fuel cell performance.

IV. CONCLUSION

Single-cell test in the absence and presence of metallic BPPs were carried out and show stable carbon coatings during fuel cell operation. Performance losses are attributed to metallic stains on top of the coatings caused by specialized manufacturing steps required for the experimental set-up. The results show that even small amounts of bare metals can affect fuel cell performance and that manufacturing techniques must be considered in the interpretation of single-cell test results.

ACKNOWLEDGMENT

We acknowledge funding from Strategic Vehicle Research and Innovation (FFI) and the Swedish Vehicle Research and Innovation program (SSF), Sweden.

REFERENCES

- [1] H. Wang, M.A. Sweikart, J.A. Turner, Stainless steel as bipolar plate material for polymer electrolyte membrane fuel cells, *J. Power Sources*. 115 (2003) 243–251. doi:10.1016/S0378-7753(03)00023-5.
- [2] M. Sulek, J. Adams, S. Kaberline, M. Ricketts, J.R. Waldecker, In situ metal ion contamination and the effects on proton exchange membrane fuel cell performance, *J. Power Sources*. 196 (2011) 8967–8972. doi:10.1016/j.jpowsour.2011.01.086.
- [3] A. Pozio, R.F. Silva, M. De Francesco, L. Giorgi, Nafion degradation in PEMFCs from end plate iron contamination, *Electrochim. Acta*. 48 (2003) 1543–1549. doi:10.1016/S0013-4686(03)00026-4.
- [4] Tsotridis G, Pilenga A, Marco G De, Malkow T. EU Harmonised Test Protocols for PEMFC MEA Testing in Single Cell Configuration for Automotive Applications; JRC Science for Policy report. 2015. doi:10.2790/546.

COMPARISON OF HUMIDIFICATION SYSTEMS FOR FLEXIBLE STATIONARY PEMFC POWER SYSTEMS THROUGH A DYNAMIC SIMULATION

E. Crespi*, G. Guandalini*, S. Campanari*

*Politecnico di Milano, Department of Energy - Via Lambruschini 4A, 20156 Milano, (Italy)

Abstract - Following the increasing penetration of non-programmable Renewable Energy Sources, flexible resources are gaining importance to guarantee the reliability of the power grid. MW-scale Fuel Cell Power Plant based on low temperature PEMFC, with very fast ramp rates and excellent load following capabilities, are seen as a possible source of flexibility. Anyway, to ensure high performance and limit the degradation rate of PEMFCs, water management plays a crucial role. This work aims at comparing two different systems for air humidification: (I) packed bed humidifiers and (II) membranes humidifiers. A dynamic model of these humidification systems is built to analyse their behaviour during start-up and variable load operation. Results show that system II guarantee a better control of the air relative humidity, allowing to obtain the desired relative humidity over the entire load range and to reach the humidity set point faster after load changes and start up.

Index Terms - Dynamic modelling, Flexibility, Fuel cell, Humidification.

I. NOMENCLATURE

FCPP	Fuel Cell Power Plant
PEMFC	Polymeric Electrolyte Membrane Fuel Cell
RH	Relative Humidity

II. INTRODUCTION

In the last years, the need of flexible resources in power generation is raising due to the increasing penetration of non-programmable Renewable Energy Sources, that may hinder the grid stability and reliability. In this framework, MW-scale FCPP based on low temperature PEMFC, characterized by very fast ramp rates and excellent load following capabilities, are considered a possible source of flexibility. Aiming to demonstrate their ability to provide grid services, the project GRASSHOPPER [1] will set up a 100 kW_{el} PEM FCPP, flexible in power output and designed to provide grid support. Since performances and degradation rate of PEMFCs are strongly influenced by membrane humidity, this type of plant requires the implementation of an appropriate water

management system [2]. This work aims at comparing two different systems for air humidification in the flexible FCPP. The analyzed systems are (I) packed bed humidifiers and (II) membranes humidifiers.

III. SYSTEMS LAYOUT AND SIMULATION ASSUMPTIONS

The layouts of the analyzed systems are shown in Fig. 1.

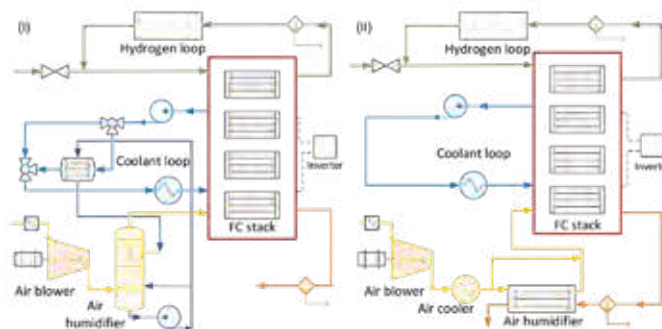


Fig. 1 PEMFC Power Plant layouts with (I) packed bed humidifier and (II) membrane humidifier

In both systems, the hydrogen flow rate is controlled to have a ratio to stoichiometry equal to 1.5, recirculating the excess hydrogen back to the stack. The presence of a system able to perfectly control the hydrogen flow conditions at the inlet of the FC stack is assumed; hydrogen is therefore always supplied to the stack at 55°C in saturated conditions. The air supply system includes the air compressor (controlled to have an oxygen ratio to stoichiometry equal to 2 with a stack backpressure of 1.6 bar) and the humidification system under investigation. Systems (I) comprises the packed bed humidifier, a pump for water recirculation and a heat exchanger. The packed bed humidifier is sized to guarantee that the outlet air is always in saturated conditions. The heat exchanger system allows to recover heat from the coolant circuit to heat up the saturated air leaving the humidifier, thus increasing its water content when further humidification is needed. System (II) adopts a membrane

humidifier in which the intake air is humidified by recovering water from the exhaust moist air; a heat exchanger before the humidifier allows to cool down to 55°C the air that leaves the compressor above 100°C. The humidity of the air stream at stack inlet is controlled with a bypass that regulates the fraction of air flowing through the humidifier. In both systems, the target FC average relative humidity (RH) is 100%. A coolant circuit is available to control the FC temperature. The coolant flow, entering the stack at maximum 60°C, is regulated to obtain the desired average FC temperature of 65°C.

For both configurations, a dynamic model is developed with the software Simulink by building models of each plant component and combining them together. The models are able to solve mass and energy balances; water transfer through the membrane humidifier is based on [3] while FC performances are calculated through semi-empirical polarization curve as explained in [4].

IV. DYNAMIC SIMULATION RESULTS

Simulations are firstly run to determine the system behavior during cold start up. It is assumed that the plant is off and all the plant components, as well as the coolant fluid, are at ambient temperature (20°C). The FC stack is then suddenly required to provide the minimum load (20 kW) for an hour. Then, according to a hypothetic fluctuation of load required to provide balancing services, simulations are performed changing the load every 15 minutes, starting from the stationary operating point reached at the end of the first simulation period. The entire range of operation (from 20 kW to 100 kW) is analyzed.

Fig. 2 shows how, immediately after plant start up, the temperature of the air at humidifier outlet, the average FC temperature and the average FC RH vary over time. Both systems allow to reach the desired average RH over the stack in less than 10 minutes. However, system I takes more than 30 minutes to reach the nominal FC average temperature, much more than system II that requires nearly 5 minutes.

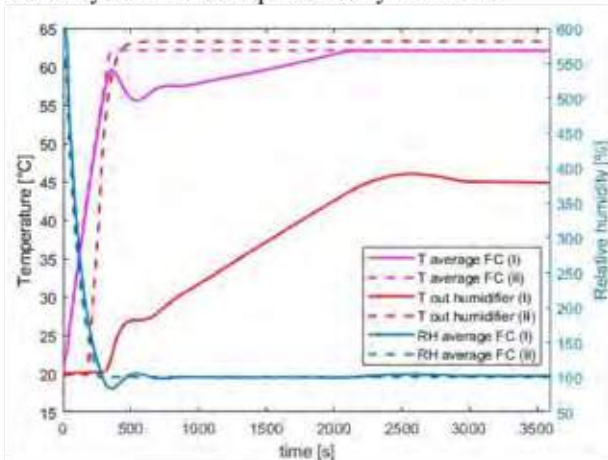


Fig. 2 Temperature and humidity profiles over time when operating at minimum load after cold start up, for system I (packed bed humidifier) and system II (membrane humidifier)

Furthermore, system II allows to minimize the temperature difference between the humidifier outlet air and the FC stack, thus reducing the air temperature rise over the stack. Fig. 3 shows that system II has a faster dynamic: the desired RH is reached almost immediately after changing the load. Finally, system II allows to reach the desired RH at any load while this is not possible for system I when operating at 20 kW.

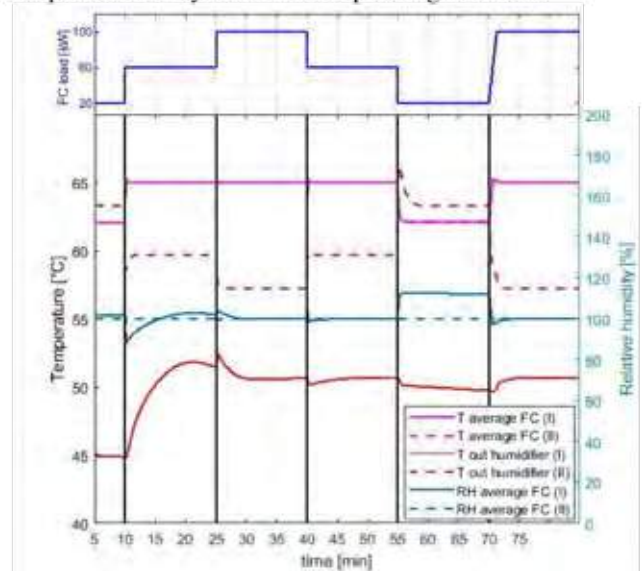


Fig. 3 Temperature and humidity profiles over time varying the FC load (represented on top) every 15 minutes, for system I (packed bed humidifier) and system II (membrane humidifier)

CONCLUSIONS

The analysis shows how a membrane humidifier can guarantee a faster and better control of the air relative humidity with respect to a packed-bed humidifier, allowing to obtain the desired relative humidity over the entire load range and to reach the humidity set point faster after start up and load changes. It has therefore to be preferred by the point of view of plant flexibility. However, a packed-bed unit may result more robust and provide air impurity cleaning (thanks to the scrubbing effect of the water sprayed in the system) which can make this solution preferable in some specific cases.

ACKNOWLEDGMENT

This work was developed within the project GRASSHOPPER, which has received funding from the Fuel Cells and Hydrogen 2 Joint Undertaking under grant agreement No 779430. This Joint Undertaking receives support from the European Union's Horizon 2020 research and innovation programme, Hydrogen Europe and Hydrogen Europe research.

REFERENCES

- [1] "GRASSHOPPER Project Official Website", <http://www.grasshopperproject.eu/>. Accessed Sep. 26, 2019.
- [2] Y. Chang, Y. Qin, Y. Yin, J. Zhang, X. Li, "Humidification strategy for polymer electrolyte membrane fuel cells – A review", *Applied Energy*, 2018.
- [3] D. Chen, H. Peng, "A Thermodynamic Model of Membrane Humidifiers for PEM Fuel Cell Humidification Control", *Journal of Dynamic Systems, Measurement and Control*, doi 10.1115/1.1978910, 2005.
- [4] S. Campanari, G. Guandalini, J. Coolegem, J. ten Have, P. Hayes, A. H. Pichel "Modeling, development and testing of a 2 MW PEM fuel cell plant fueled with hydrogen from a chlor-alkali industry", *Journal of Electrochemical Energy Conversion and Storage (JEECS)*, doi 10.1115/1.4042923, 2019.

THE USE OF MICROBIAL FUEL CELLS FOR SOIL REMEDIATION: A PRELIMINARY STUDY ON DDE

Aimola G.¹, Gagliardi G.G.², Barra Caracciolo A.³, Ancona V.¹,
Grenni P.³, Bagnuolo G.¹, Rolando L.³, Garbini G.L., Uricchio V.F.¹ and Borello D.²

¹National Research Council, Water Research Institute - Bari, (Italy)

²Department of Mechanical and Aerospace Engineering, University of Rome La Sapienza – Rome, (Italy)

³National Research Council, Water Research Institute, Monterotondo - Rome, (Italy)

Abstract - DDE is a very persistent and bioaccumulative polychlorinated compound from DDT transformation. Microbial Fuel Cells (MFCs) are environmentally friendly tools that convert the chemical energy of organic compounds present in the soil into electricity. The aim of this work was to test if MFCs can promote DDE degradation. MFCs containing contaminated soil were used under open circuit voltage (OCV) and closed-circuit voltage (CCV) conditions. The voltage was measured daily for the OCV condition. Power generation was calculated in the case of the CCV condition.

Chemical analysis for measuring the DDE concentration and microbiological analyses for evaluating the bacterial community abundance and activity were performed at 0, 60 and 180 days. The results show that MFCs were able to promote DDE degradation.

Index Terms - Microbial Fuel Cell, DDE, Bioremediation, Exoelectrogen microorganism, Green Technology.

I. NOMENCLATURE

DDD=Dichlorodiphenyldichloroethane
DDE=2,2-bis (p-chlorophenyl)-1,1-dichloroethylene
DDT=dichlorodiphenyltrichloroethane

II. INTRODUCTION

Although DDT production is no longer legal in most of the world countries, large quantities of DDT and its toxic polychlorinated metabolites (DDD and DDE) persist in soils [1][2]. Recently, the Microbial Fuel Cell (MFC) has been used as a Bioremediation Technology to restore contaminated soils. MFCs transform energy stored in the chemical bonds of organic compounds (as fuel) into electrical energy thanks to exoelectrogen microorganisms naturally present in the soil, catalyzing oxidation and reduction reactions in the area between two graphite electrodes [3]. The anode is used as an electron acceptor in anaerobic conditions and promotes bacterial biofilm growth around it. Electrons flow from the anode to the cathode through an external circuit, while protons flow through the soil directly to the cathode: here, in aerobic

conditions, electrons and protons react with oxygen to produce water. In this work, the MFC performance with and without contamination as well as the effectiveness of MFCs for DDE degradation were tested in presence or absence of compost. Two different conditions were performed: open and closed circuits (OCV and CCV). The pesticide degradation, the microbial activity and the electrical output were evaluated over the experimental time.

III. EXPERIMENT

A. Materials

The soil was sampled from an agricultural area (0-30 cm depth) in the Montelibretti area (Rome, Italy). Compost was supplied by Progeva s.r.l. (Taranto, Italy). DDE was purchased from Sigma-Aldrich.

B. Preparation of the fuel cells and experimental setup

MFCs were composed of two graphite electrodes, anode and cathode. The anode (at the bottom of the cell) was totally submerged in soil (moisture: 30%, mud consistency) to allow a proper functioning of the MFC. The cathode was placed on the top of the soil. The electrodes were connected by an external circuit for the electron movement.

Four experimental conditions (Soil, Soil+Compost, Soil+DDE, Soil+Compost+DDE) were set up in both MFCs and glass batches which were used as controls. MFCs containing soil treated with DDE [1 mg/kg] were tested using both open and close circuits (OCV and CCV) equipped with a resistance of 1500 Ohm. This value was obtained from a previous test in which a characteristic curve was performed in order to obtain the resistance corresponded to the maximum electrical power value. Destructive samplings were performed at 6, 60 and 180 days. The voltage was measured once per day using a multimeter tester for all the MFCs. In the case of closed-circuit

condition, the current was also measured. The power was calculated as the product of voltage and current. Microbiological (abundance by DAPI counts, viability by live/dead method and dehydrogenase activity, [3,4,5]) and chemical analysis (DDE concentration analyzed with a GC-MS Thermo Polaris Q) were carried out to assess the bacterial community and the DDE degradation in the various experimental conditions.

IV. RESULTS AND DISCUSSION

The MFCs where only DDE was present, showed a higher durability and a voltage value of 300 mV registered over more than 100 days, after an initial development stage lasting about 60 days (Fig.1). In the other cases the voltage varied substantially over the experimental time.

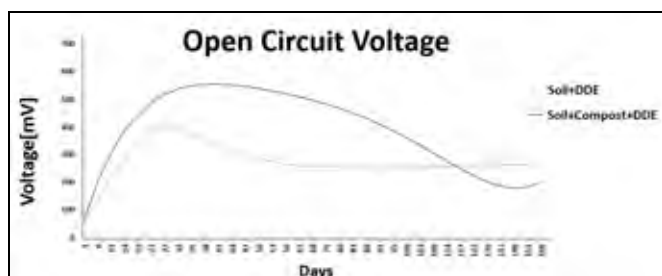


Fig. 1. Voltage in Soil+DDE and Soil+compost+DDE MFCs.

Adding compost with DDE reduced power generation especially in the first 60 days where the MFCs produced more than in the following period (Fig.2). After 60 days a reduction in the total amount of DDE was found in each pesticide-treated MFC: 40% in Soil+DDE and 25-30% in Soil+Compost+DDE, respectively. The higher power the MFC produced, the higher DDE degradation was obtained. However, at 180 days only “soil+DDE CCV” and “soil+compost+DDE OCV” showed a further decrease in DDE (6% and 30% respectively). Power output was very low during this period. Interestingly, no reduction in DDE concentration was observed in all batch conditions (controls). Table 1 summarises the overall chemical and microbial analyses.

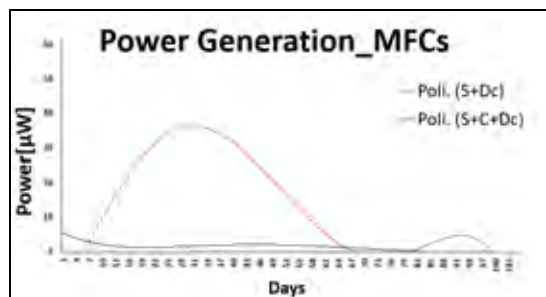


Fig. 2. Power generation in MFCs

The overall microbial activity (DHA) tends to decrease in all

treated conditions (from 6 d to 180 d).

Tab. 1. DDE decrease (%) Microbial abundance, Cell viability and Microbial activity at 6, 60 and 180 days.

	Time (days)	DDE Decrease (%)	Microbial Abundance (N. cells g/dry soil)	Cell Viability (%live cells/(live+dead))	Microbial Activity (µg TPF/g dry soil)
Soil+DDE Batch	6	0	4.6x10 ⁷	45.6	209.3
	60	0	8.8x10 ⁷	46.2	145.3
	180	0	1.4x10 ⁸	67.2	16.9
Soil+DDE OCV MFC	6	0	4.6x10 ⁷	45.6	209.3
	60	39	7.4x10 ⁷	51.3	364.4
	180	0	2.1x10 ⁸	72.1	23.0
Soil+DDE CCV MFC	6	0	4.6x10 ⁷	45.6	209.3
	60	38	8.8x10 ⁷	61.4	103.4
	180	6	2.2x10 ⁸	72.5	92.3
Soil+compost+DDE batch	6	0	1.4x10 ⁸	74.7	89.2
	60	0	1.4x10 ⁸	54.3	207.0
	180	0	4.7x10 ⁸	53.8	133.3
Soil+compost+DDE OCV MFC	6	0	1.4x10 ⁸	74.7	89.2
	60	26	1.2x10 ⁸	71.8	116.0
	180	30	8.1x10 ⁷	53.2	48.2
Soil+compost+DDE CCV MFC	6	0	1.4x10 ⁸	74.7	89.2
	60	31	1.3x10 ⁸	25.1	123.9
	180	0	1.8x10 ⁸	55.8	15.0

V. CONCLUSION

The results show DDE degradation in the MFCs up to 2 months. The voltage trend at 180 days was attributable to lower DDE degradation. MFCs were more effective in DDE degradation in absence of compost. This result agrees with a higher voltage value in the Soil+DDE OCV and CCV conditions. Presence of compost presumably stimulated bacterial populations not necessarily involved in DDE degradation. Further samplings are in progress to evaluate DDE degradation after 12 months. Microbial molecular investigations will be performed to phylogenetically characterize the bacterial populations in the various experimental conditions.

REFERENCES

- [1] J. M. Aislabie, et al., Microbial degradation of DDT and its residues - A review, New Zealand. J. of Agricultural Research 40, 1997, pp. 269-282.
- [2] Agency for Toxic Substances & Disease Registry (ATSDR) 2002, Toxicological profile for DDT, DDE, DDD. Atlanta, GA: U.S. Department of Health and Human Services, Public Health Service.
- [3] J.M. Pisciotta and J.J. Dolceamore Jr, Bioelectrochemical and conventional bioremediation of environmental pollutants, J. of Micr. & Biochem. Techn., 8, 2016, pp. 4
- [4] A. Barra Caracciolo, et al. Changes in microbial community structure and functioning of a semiarid soil due to the use of anaerobic digestate derived composts and rosemary plants, Geoderma 245-246, 2015, pp. 89-97
- [5] P. Grenni, et al., Effects of wood-amendments on the degradation of therbuthylazine and on soil microbial community activity in a clay loam soil, Water, Air & Soil Pollution, Volume 223, 2012, pp. 5401-5412.

INTEGRATION OF PORTABLE SEDIMENTARY MICROBIAL FUEL CELLS IN AUTONOMOUS UNDERWATER VEHICLES

M. Quaglio*, G. Massaglia***, A. Sacco**, A. Piscitelli*, A. Favetto**,
L. Scaltrito*, S. Ferrero*, R. Mo*, and C.F. Pirri***

* Department of Applied Science and Technology, Politecnico di Torino, 10129 Torino (Italy)

** Center for Sustainable Future Technologies@ POLITO, Istituto Italiano Di Tecnologia, 10129, Torino (Italy)

Abstract - Sedimentary microbial fuel cells (s-MFC) have been proposed as effective tools to power remote sensors in different aquatic environments, thanks to their ability to continuously and autonomously produce renewable and sustainable energy. In the present work, we propose s-MFC as a compact and cost-effective system suitable to be integrated as a payload in an Autonomous Underwater Vehicle (AUV). A new AUV payload, named MFC-payload, is designed to host the cylindrical s-MFC and a data acquisition system to collect and store information on the voltage produced by the cell.

This investigation permits to demonstrate power production by s-MFC during operation of the AUV in seawater, and analyzes the effective influence of environmental conditions on the output power. All the obtained results confirm a high stability of the cylindrical s-MFC integrated in the MFC-payload.

Index Terms - Microbial Fuel Cells; Sedimentary MFC; Floating MFC; Autonomous Underwater Vehicles; MFC-payload.

I. INTRODUCTION

Sedimentary microbial fuel cells (s-MFC) and floating microbial fuel cells (f-MFC) have been proposed for sensing applications in different aquatic environments, thanks to their ability to continuously and autonomously produce renewable and sustainable energy. In a previous work, we already demonstrated that this specific ability of f-MFCs can be preserved even designing portable, small-scale systems that we tested in the Mediterranean Sea.[1] In the present work, we analyze s-MFC with the aim to design a compact and cost-effective system suitable to be integrated as a payload in an Autonomous Underwater Vehicle (AUV). The goal of this investigation was to demonstrate and analyze power production by s-MFC during operation of the AUV in seawater, understating the possible influence of environmental conditions on the power output. To this purpose, we optimized a cylindrical architecture made of an inner-chamber, adapted to work as anodic chamber, and an outer-shell, working as cathode. A new AUV payload, named MFC-payload, was designed to host the cylindrical s-MFC and a data acquisition system to collect and store information on the voltage produced by the cell. After development in the

lab, a preliminary analysis of the performance of the cylindrical s-MFCs was evaluated during a measurement campaign carried out in the Mediterranean Sea in a static condition, meaning not yet integrated in the AUV. The overall performance of the cylindrical s-MFC integrated in the MFC-payload was then analyzed during two measurement campaigns: the first one to test the behavior at a maximum depth of 3 m, and the second one to test the performance of the new MFC-payload up to 9 m of depth. The results demonstrate a high stability of the cylindrical s-MFC integrated in the MFC-payload. The ability of the devices to continuously produce electricity during different AUV operation modes (i.e., depth and speed) and while changing environmental conditions (i.e., pressure, temperature and oxygen content) demonstrates that cylindrical s-MFC devices are robust system that can be successfully used in underwater applications.

II. EXPERIMENTAL

The newly designed MFC-payload is represented in Fig. 1a): it has been conceived to be integrated into a Fologa AUV-glider system by GraalTech srl, Italy. In Fig. 1b) the payload is sketched in its open position, which put in evidence the presence of the sedimentary, bottle-based MFC with a cylindrical shape. The inner-chamber was filled with sediment, acting as fuel-source and with low Oxygen content, and with the anode buried into the sediment. The cathode was placed outside, fixed by tie-wraps to the cylindrical structure and in contact with seawater. Both the electrodes were made of carbon felt purchased by Sigratherm (GFA5, SGL Carbon). Titanium wires were used as electron collectors. We implemented the in-situ biofilm formation method optimized in our previous work [1]. Before testing the s-MFCs in the real environment, the architecture was tested and optimized in lab experiments, carried out using water from the sea only. The electronic unit for data acquisition described in [1] was placed in a protected, water-free room of the payload. The payload was designed in order to allow continuous contact to water contact during operation. In Fig. 1c) a picture of the complete AUV-glider system is proposed, with the MFC-payload mounted on



Fig.1. a) 3D-render of the MFC-payload, b) the open payload, with pictures showing the s-MFC assembly, c) the final AUV-Glider system with the newly MFC-payload, d) a picture taken during tests in seawater.

In Fig. 1d) a picture is reported showing the AUV-Glider during an experiment in seawater.

III. RESULTS AND DISCUSSION

The first part of the experimental analysis was carried out in the lab, testing s-MFCs in fourfold. The results we obtained are shown in Fig. 2. The s-MFCs were quite stable during test. Given their better behavior, s-MFC_1 and s-MFC_2 were selected to be mounted in the MFC-payload for the experiments in seawater.

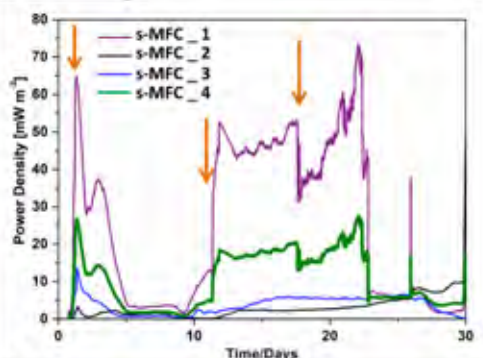


Fig.2. Power density generated during the 1-month lasting lab experiment by the 4 cylindrical s-MFCs. Orange arrows show seawater turnover.

The results of the two measurement campaigns are presented in Fig.3. The first set of results, exploring a maximum depth of 3 m, is shown in Fig.3 a), while the second one in which 9 m of depth were reached is reported in Fig. 3b). The results demonstrate a high stability of the cylindrical s-MFC integrated in the MFC-payload. The s-MFCs produce electricity continuously during the AUV-glider operation, without any break during AUV-glider movement. Fig. 3, both a) and b) dependence of the output parameters with depth. The reason for this behavior can be explained considering that changes of depth are actually associated to variations of environmental parameters, as pressure and temperature, being the last one a critical parameter for speeding up or reducing microbial metabolism.

Table I summarizes the value of voltage, current and power as a function of the analyzed depth. It is very important to observe that during all the tests performed in seawater, no dependence of the output parameters has been observed with the navigation conditions.

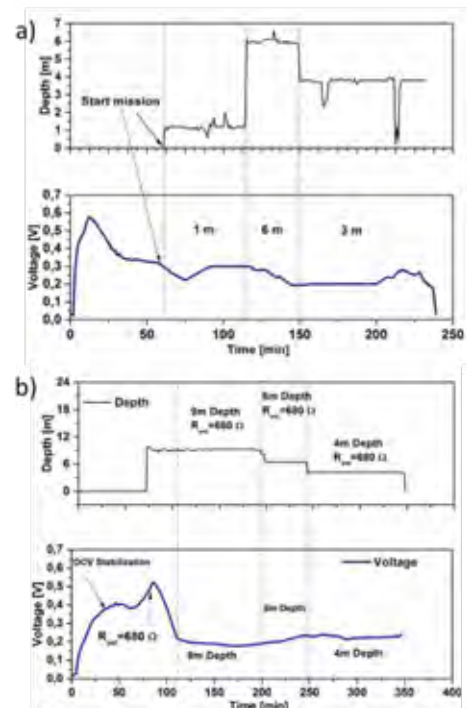


Fig.3. Results of the two measurement campaigns: a) shows results for a maximum depth of 3 m, b) reports the behavior of the MFC-payload up to 9 m.

This is an important finding, since it demonstrates that energy production by s-MFCs integrated in AUV systems is decoupled by the navigation of the autonomous vehicle itself, showing the effectiveness of the application of MFC-based technology in advanced systems for environmental analysis.

TABLE I
VOLTAGE, CURRENT AND POWER GENERATED BY THE MFC-PAYLOAD DURING THE TWO MEASUREMENT CAMPAIGNS AS A FUNCTION OF DEPTH.

Depth (m)	Voltage (mV)	Current (mA)	Power (mW)
0	440	0.647	0.285
1	290	0.426	0.124
3	210	0.309	0.065
4	220	0.324	0.071
6	190	0.279	0.053
9	192	0.282	0.054

IV. CONCLUSION

The results demonstrate a high stability of the cylindrical s-MFC integrated in the MFC-payload and continuous production of electricity during different AUV navigation. Interestingly changes in depth are directly reflected in changes of the output parameters, confirming the intrinsic sensitivity of the MFCs to environmental conditions, temperature first of all. Nevertheless cylindrical s-MFC devices behaved as robust system that can be successfully used in underwater applications.

REFERENCES

- [1] Massaglia G., Margaria V., Sacco A., Tommasi T., Pentassuglia S., Ahmed D., Mo R., Pirri C.F., Quaglio M., In situ continuous current production from marine floating microbial fuel cells, Applied Energy, 230, 2018, 78–85

CO-ASSISTED ELECTROLYSIS OF H₂O IN QUASI-SYMMETRICAL NI-YSZ CELL.

Michał Wierzbicki*,**2, Marek Skrzyplikiewicz* , Yevgeniy Naumovich* , Stanisław Jagielski**, Jakub Kupecki**,**

* Department of High Temperature Electrochemical Processes (HiTEP),
Institute of Power Engineering, Augustowka 36, 02-981 Warsaw, Poland

** Institute of Heat Engineering, Warsaw University of Technology,
Nowowiejska 21/25, 00-665 Warsaw, Poland

Abstract - Custom solid electrolyte cell for fuel-assisted electrolysis was produced using AS-SOFC half-cell as support for Ni-YSZ electrode. Cell was tested in fuel-assisted electrolysis of the steam using hydrogen or carbon monoxide as depolarizers. It was demonstrated that electrolysis may be conducted at 0.5 V (contrary to 1.3-1.5 V in regular SOECs), however usage of the carbon-containing depolarizer leads to fast degradation of the Ni-YSZ anode.

Index Terms – Fuel-assisted electrolysis, SOFEC, SOEC, depolarization.

I. INTRODUCTION

Fuel-assisted high temperature electrolysis (SOFEC) is a promising technology for the conversion of renewable energy and waste reductant-containing gases to high-quality fuel (H₂) and with possibility to segregate CO₂ [1]. Usage of reductant gas as depolarizer allows to drop electrolysis voltage, but requires elaboration of the dedicated anode, different from ones used in SOECs. In present work Ni-YSZ cermet was tested as SOFEC anode.

II. EXPERIMENTAL

In order to test fuel-assisted electrolysis special cells were fabricated using standard anode support with electrolyte from SOFC, prepared by CEREL [2]. SOFEC anode was screen-printed directly on the electrolyte using the same YSZ-NiO composite paste, which was used for SOFC anode. Electrochemical measurements were conducted using ZAHNER PP240 IM6ex galvanostat. U-I curves were measured in potentiostatic mode with voltage rate of 10mV/s, impedance spectroscopy studies were conducted at current density of 30 mA/cm² using frequency range 0.05 Hz -50 kHz. Electrochemical data was analyzed in self-made software, based on finite-element approach for DRT [3].

III. RESULTS AND DISCUSSION

State of the cell before and after measurements presented on Fig. 1. One can note imprints of the gold current collectors on both electrodes, but there were no observable delamination of the Ni-YSZ electrode from electrolyte, only some gluing to gold surface. Effective area of the cell was considered as 16 cm², which corresponds to the size of the anode.

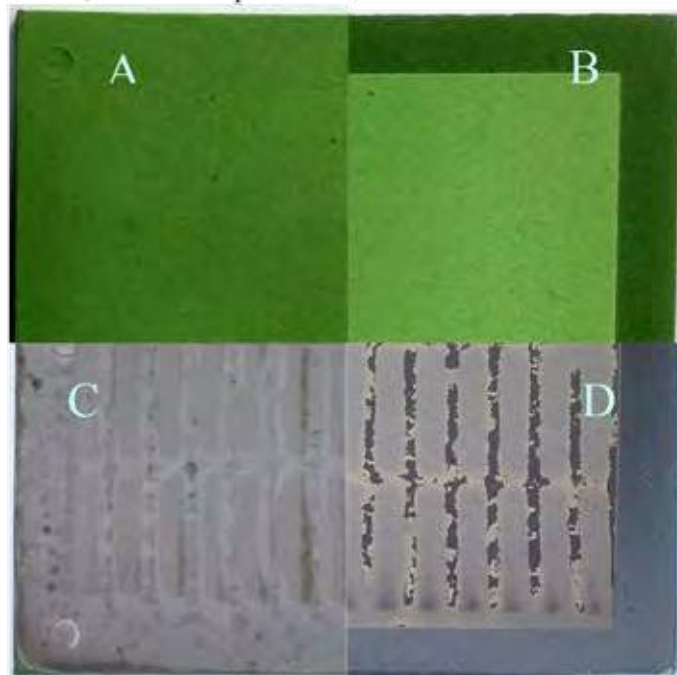


Fig. 2. Cell before and after electrochemical measurements. A- cathode before, B - anode before, C- cathode after, D- anode after.

Preliminary studies demonstrated that DC polarization should be constrained by 0.5 V to avoid oxidation of the Ni in anode. DRT analysis demonstrates, that usage of the CO/CO₂

mixture as depolarizer lead to observable evolution of the spectra even in relatively mild conditions (Fig. 2). One can note high-frequency shift and grows of the peaks, corresponding to increase of the integral polarization resistance up to 17%. Impact of the degradation includes also sufficient rise of the DC (~30%). In general, this behavior fits to pattern of the Ni coarsening mechanism, known for SOFC anodes [4], however revelation of the details for this process would require additional experimental studies.

Comparison of the DRT spectra of the hydrogen- and carbon monoxide depolarization (Fig. 3) confirms that CO oxidation leads to observable changes in electrochemical activity of anode: some low-frequency peaks were depressed up to total elimination while high-frequency peaks became significantly more prominent. DRT of CO oxidation is clearly different from H₂. Necessary to note that initial integral polarization for cell fed with CO/CO₂ depolarizer was very close to one measured for H₂/H₂O (3.14 Ω·cm² vs. 3.04 Ω·cm²) and all degradation should be addressed to overnight operation under carbon monoxide depolarization. This effect was also observed on DC polarization curves (Fig. 4).

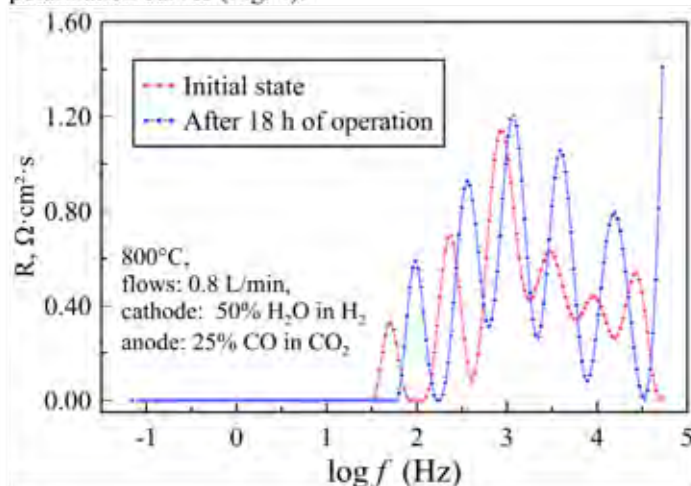


Fig. 2. Evolution of the DRT spectra during depolarization of the anode with CO/CO₂ mixture.

IV. CONCLUSION

Ni-YSZ SOFEC anode can operate up to 0.5 V of cell overpotential and 0.4 A/cm² current density, however its fast degradation in carbon-containing depolarizer may constrain possibility of its practical applications. Replacement of the Ni with more oxidation-stable and carbon-neutral metals (copper or transient metal alloys) might allow extended I-U operation domain and suppress degradation.

ACKNOWLEDGMENT

This work was financially supported by the National Science Centre, Poland, Grants No. 2017/01/X/ST8/00210, 2018/30/M/ST8/00675 and young scientist statutory grant CPE/093/STAT-MN/19.

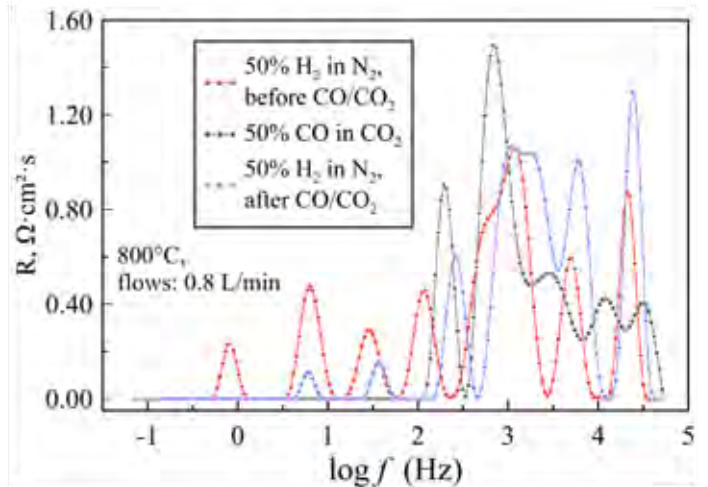


Fig. 3. Impact of the CO/CO₂ depolarization on DRT spectra.

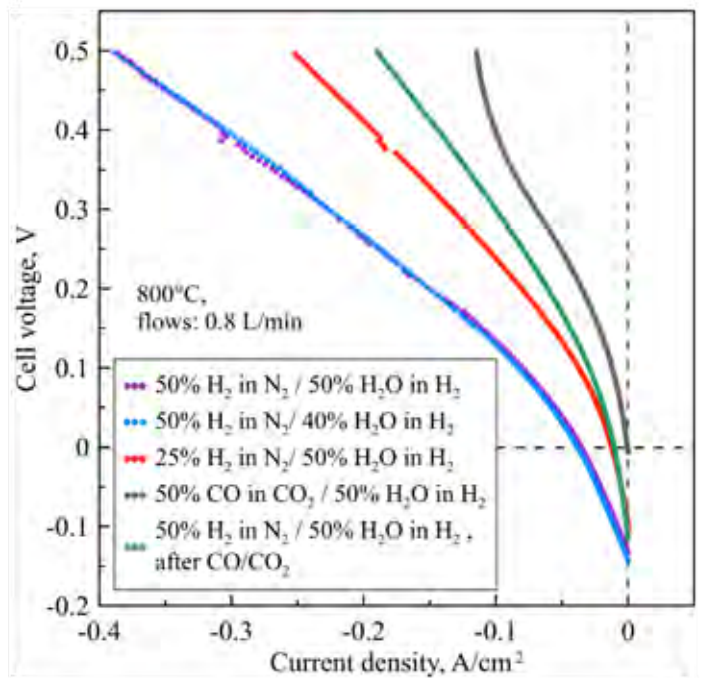


Fig. 4. DC polarization of the SOFEC..

REFERENCES

- [1] T. Kato *et al*, Development of low caloric gas assisted solid oxide electrolysis cells, ECS Transactions, 5 (2007) 627-635.
- [2] M. Kawalec, R.Kluczowski, M.Krauz, Manufacturing technology of AS-SOFC prepared with different commercially available precursors, doi: 10.1051/e3sconf/20161000033.
- [3] M. Saccoccio *et al*, Optimal Regularization in Distribution of Relaxation Times applied to Electrochemical Impedance Spectroscopy: Ridge and Lasso Regression Methods –A Theoretical and Experimental Study, Electrochimica Acta 147 (2014) 470–482.
- [4] OM Pecho *et al*, 3D Microstructure Effects in Ni-YSZ Anodes: Influence of TPB Lengths on the Electrochemical Performance. Materials 8 (2015), 7129-7144

IMPACT OF POROSITY GRADIENTS WITHIN CATALYST LAYER AND MPL OF A PEM FUEL CELL ON THE WATER MANAGEMENT AND PERFORMANCE: A NEUTRON RADIOGRAPHY INVESTIGATION

D. Kartouzian*, A. Mohseninia*, H. Markötter**, P. Langner*, J. Scholta*, and I. Manke**

* Zentrum für Sonnenenergie- und Wasserstoff-Forschung, Helmholtz Straße 8, Ulm
(Germany)

** Helmholtz-Zentrum Berlin, Hahn-Meitner Platz 1, Berlin (Germany)

Abstract – The porosity of the cathode microporous layer (MPL) and electrodes was modified using monodisperse polymer particles, which were then either evaporated or washed away during the preparation process, resulting in spherical pores. Three cathode MPL configurations were prepared, one without pore formers, one with one layer containing 10 vol.% 30 µm pore formers, and one double layer MPL of 10 vol.% 30 µm and 1.5 µm pore formers. Also, three configurations of the catalyst layer were prepared, one without pore formers, one with 5 wt.% pore formers, and one with 10 wt.% pore formers. These layers were assembled in 5 different configurations, in an 8 cm² fuel cell. Neutron radiography was used to investigate the water inventory of these cells, and polarization curves were recorded during the radiography images. The experiments showed, that modification of catalyst layers (CL) pushes the mass transport region to higher current densities, and in combination with the double layer MPL, the highest increase in cell performance was observed despite higher water content measured in the cell.

Index Terms – Microporous Layer, Neutron Radiography, Porosity, Water Management

I. INTRODUCTION

A better understanding of water management in a proton exchange membrane fuel cells (PEMFCs) is an important issue [1]. The conductivity of the membrane depends on its hydration, where, at the same time, the accumulation of the excess water inside the cell components can result in flooding inside the fuel cell, leading to a performance drop [2].

In this study, we aimed for a higher cell performance through modification of the porosity of cathode MPL, using monodisperse polymer particles and modification of porosity of CL using monodisperse PS particles. An individual cell design has been used to investigate the in-operando water management

of modified cells through neutron radiography. Cell performance has been measured for these cells.

II. EXPERIMENTAL

A. Catalyst Layer and MPL Preparation

A 20 wt.% Pt, based on carbon support commercial catalyst, was mixed with Nafion™ solution and deionized water. For porosity modification, monodispersed polystyrene (PS) particles with 0.5 µm diameter were added to the ink. The PS particles were washed out of the Catalyst Coated Membrane (CCM) with ethyl acetate at room temperature. Cathode and anode CL had a similar platinum loading of 0.3 mg/cm².

To prepare the cathode MPL ink, deionized water, carbon black, methylcellulose, Triton x-100, and PTFE were mixed together. For porosity preparation, monodispersed polymer particles with either 1.5 µm diameters (MX150, Chemisnow®) or 30 µm diameters (MX3000, Chemisnow®) were added to the inks. In this study, three types of cathode MPL, a reference MPL without pore formers, one with 10 vol. % MX3000 particles and a double layer MPL with 10 vol. % MX3000 added to the first layer and 10 vol. % MX150 added to the second layer were prepared.

Tested fuel cell configurations incorporating these CCM and MPLs are listed in TABLE I.

B. Neutron Radiography

The measurements were conducted at the CONRAD II Imaging beamline at the BER II research reactor of the HZB in Berlin, Germany.

For the presented measurements, a field of view of 26 x 26 mm and a pixel size of 12.9 µm was chosen. The transmitted water depth could be quantified using the attenuation coefficient and images of the dry cell as the reference.

TABLE I
Fuel Cell Compositions

	Anode GDL	Cathode MPL*	CCL
Cell 1	SGL 29BC	Reference **	Reference***
Cell 2	SGL 29 BC	10 vol.% MX3000	10 wt.% PS
Cell 3	SGL 29BC	10 vol.% MX3000	5 wt.% PS
Cell 4	SGL 29BC	Reference	5 wt.% PS
Cell 5	SGL 29BC	Layer 1 10 vol.% MX3000 Layer 2 10 vol.% MX150	5 wt.% PS

* GDL substrate: SGL 29 BA

** Reference self-made MPL contains 20 wt.% PTFE in the coating and no extra pores are introduced in the coating

*** Reference self-made CCL contains no PS as pore former

III. RESULTS

For the radiographic measurements, the fuel cell is operated in a galvanostatic mode increasing the current in a ramp, up to 1 A/cm². A quantitative evaluation of the water accumulation within both cathode and anode GDLs and the CCM is shown in Figure 2.

Water content is increased for all cells at lower current density values only slowly, continued with a steep slope at 0.25 A/cm² up to a steady-state plateau after 1500 s at 0.5 A/cm². Reference cell 1 reaches a lower water content at the plateau level. By increasing the porosity of the CL in cell 4, an increase in the water content can also be observed. Implementing a high porous cathode MPL in cell 3 does also not reduce the water content. Cell 5, with the double layer cathode MPL, shows the highest water content of all cells.

In the water plateau region, cells 2, 3, 4, and 5 show several semi periodic water peaks. Cell 1, with reference CCM and reference cathode GDL, shown in the red line in Figure 2, does not show any water peaks. As discussed in our previous study [3], these water peaks show a sudden water accumulation inside the anode side of the cells.

Separation of water accumulation under land and channel region of cell 5 can also be seen in Figure 2. As expected, higher water content can be observed under the land region of the cell.

Figure 3 shows the performances obtained during the measurement. The average potential value in each current step is plotted. Reference cell 1, which contains a low water content, shows a higher potential in the activation and ohmic loss area, but faces a significant voltage drop at higher current density.

Although cell 5 contained the highest water content within all cells, this cell shows a higher performance at high current densities.

Comparing cells with 5 wt.% PS added to the electrode ink, cell 4 with a reference MPL shows a worse performance compared to cell 3 with highly porous cathode MPL although a similar overall water content was observed for these cells. Both

cells appear to have a better performance process in mass transport limiting region.

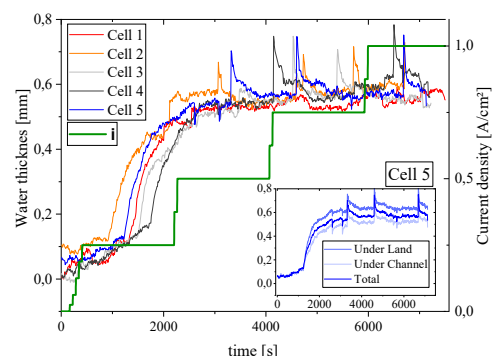


Fig. 2. Water thickness measured inside GDLs and CCM through radiography for cell 1*, cell 2*, cell 3*, cell 4* and cell 5* by increasing current density (green line). Water distribution under land and channel regions of Cell 5 are depicted in the right diagram

* Cell descriptions in TABLE I

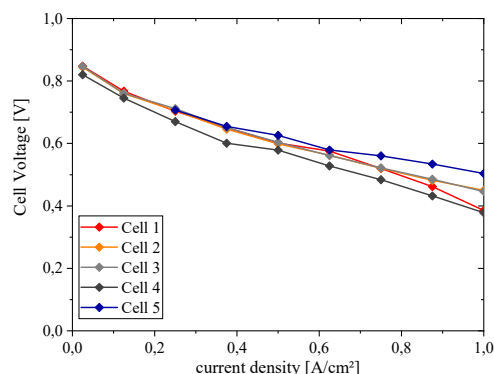


Fig. 3. Polarization curves acquired during radiography (Cell descriptions in TABLE I)

ACKNOWLEDGMENT

The financial support from NOW in the framework of the AutoStack-Industrie project is gratefully acknowledged [03B10103A / 031310103A2]. We are also grateful of HZB and especially Dr. Henning Markötter providing us beam time support and processing the radiography images.

REFERENCES

- [1] J. P. Owejan, J. E. Owejan, W. Gu, T. A. Trabold, T. W. Tighe, and M. F. Mathias, "Water Transport Mechanisms in PEMFC Gas Diffusion Layers," *J. Electrochem. Soc.*, vol. 157, no. 10, pp. B1456–B1464, Oct. 2010.
- [2] U. Pasaogullari, C.-Y. Wang, and K. S. Chen, "Two-Phase Transport in Polymer Electrolyte Fuel Cells with Bilayer Cathode Gas Diffusion Media," *J. Electrochem. Soc.*, vol. 152, no. 8, p. A1574, Aug. 2005.
- [3] A. Mohseninia, D. Kartouzian, H. Markötter, U. U. Ince, I. Manke, and J. Scholta, "Neutron Radiographic Investigations on the Effect of Hydrophobicity Gradients within MPL and MEA on Liquid Water Distribution and Transport in PEMFCs," *ECS Trans.*, vol. 85, no. 13, pp. 1013–1021, Jun. 2018.

PROJECT CLEAN-DRONHY: A HYDROGEN POWERED DRONE AT HIGH PERFORMANCES

J. Barale*, P. Rizzi*, C. Luetto**, S. Staulo*** and M. Baricco*

* Department of Chemistry and Inter-departmental Center Nanostructured Interfaces and Surfaces (NIS), University of Turin, Via P. Giuria 7, 10125 Torino, (Italy)

** Tecnodelta S.r.l., Via Francesco Parigi 5H, 10034 Chivasso (To), (Italy)

*** Stones sas, Via Sacra di S. Michele 21/b, 10093, Collegno (To), (Italy)

Abstract – A drone for high flight times is under construction, using hydrogen to supply a fuel cell. It will be charged by a hydrogen refueling station, using a metal hydride compressor.

Index Terms – fuel cell drone, hydrogen, solid state compressor

I. INTRODUCTION

Nowadays, drones are used in a wide range of applications, from civil to military. It is therefore of interest to develop systems with increasing performances, in terms of energy efficiency and running time. In this regard, the use of Fuel Cell (FC) is a possible solution, since hydrogen (H₂) has a higher energy density compared to batteries [1].

In this work, we show preliminary results obtained for the Clean-DronHy project, supported by Regione Piemonte (Italy). The aim is to design and to realize a demonstrative drone, which uses compressed hydrogen to supply a FC. The goal is to reach 2 h of continuous flight, showing the feasibility of a FC drones. The drone will be linked with a hydrogen refueling station (H₂RS). Hydrogen will be produced by an electrolyzer, driven by renewable energy. Afterwards, it will be compressed by a metal hydride compressor (MH-C) and finally stored as compressed gas to supply the drone. A schematic representation of the integrated system is reported in Figure 1.

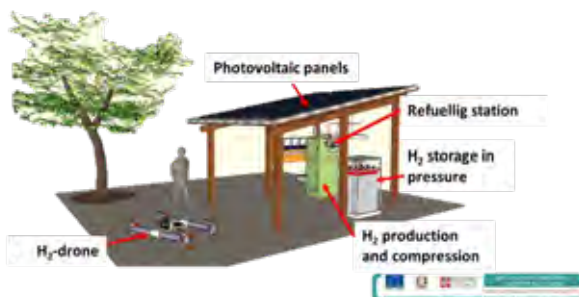


Fig. 1: representation of the integrated system: drone and H₂RS

II. HYDROGEN REFUELING STATION

The refueling station is sized for the delivery of the daily amount of hydrogen necessary to cover two flights of the drone per day. Table 1 reports main parameters considered for the system.

Table 1: Parameters for the drone flight

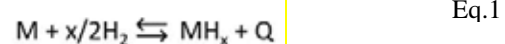
N° of tank on the drone	2
H ₂ pressure in tank	300 bar
Time of flight	2 h
N° of flight per day	2
Volume of tanks	1.5 l
H ₂ daily amount	166 g

A. Hydrogen production

H₂ will be produced in sufficient amount by an Enapter EL-250 electrolyzer. It produces high flows of H₂ (250 NI/h) at 30 bar, at room temperature. Then, H₂ will be compressed and stored in the gas phase. A fraction of the gas will be used to supply the drone and the other will be stored. The photovoltaic plant, consisting of 10 panels of 300 W, was sized starting from the power necessary to supply the electrolyzer.

B. Hydrogen compression and storage

Compared to conventional mechanical compressors, the compression of H₂ by MH is an innovative technology, which does not use electricity. Moreover, it is not noisy and does not require significant maintenance [2]. On the other hand, it needs a thermal fluid for running. At the basis of the use of MH for H₂ compression, there is a reversible reaction between H₂ and a metal hydride former (M) to produce heat (Q) and MH (Equation 1):



The thermodynamics of the equilibrium is characterized by H₂ pressure (p), concentration (c) in the solid phase and temperature (T), which are described in a p-c-T-diagram [2]. Based on the thermodynamics of the equilibrium, compression

occurs since M can absorb H_2 at low pressures and low temperatures (T_{low}), forming MH. Then, MH is heated up at T_{high} and H_2 is released at a significantly higher pressure. In the H_2RS , a two stage MH-C is planned, which will use commercial alloys $La_{0.9}Ce_{0.1}Ni_5$, as 1st stage, and the Hydralloy-C5 (TiMn₂-based alloy), as 2nd stage. H_2 will be compressed between room temperature (T_{low}) and 150 °C (T_{high}). Thermodynamics of alloys were studied acquiring pcT-diagrams (Fig. 2) for $La_{0.9}Ce_{0.1}Ni_5$ at 25°-42°-65°-87 °C (Fig. 2-a) and for Hydralloy at 32°-56°-79 °C (Fig. 2-b). From pcT-diagrams, enthalpy, ΔH , and entropy, ΔS , of absorption and desorption were obtained. They are necessary to simulate the H_2 compression behavior. It was obtained that, in the working temperature of T_{low} and T_{high} , H_2 can be compressed between 20 bar and 200 bar.

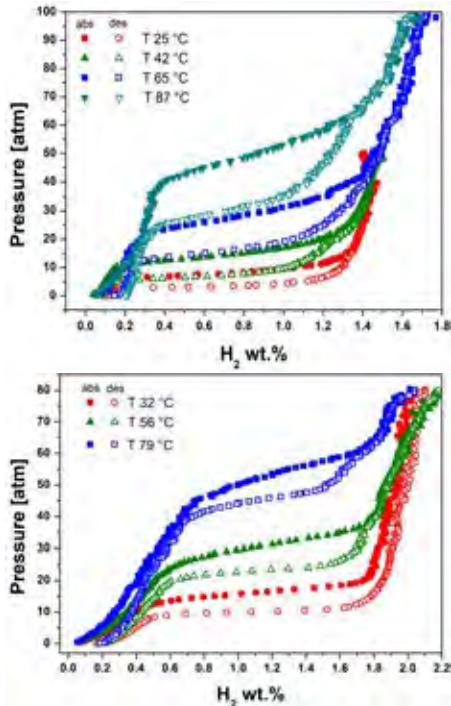


Fig. 2 pcT-diagram a) $La_{0.9}Ce_{0.1}Ni_5$ and b) Hydralloy

Powders were tested in a laboratory scale compressor (Fig. 3).

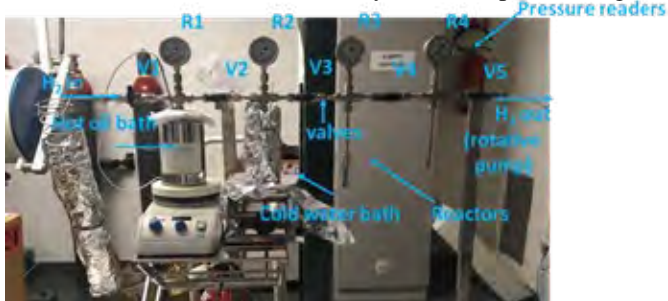


Fig. 3: Lab-scale compressor setup

From this test, a fast kinetics has been observed, since one cycle of compression (i.e. from the absorption in the 1st stage to

the desorption in the 2nd stage) occurs in only 40 min. Starting from the results of preliminary test, a scale-up of the H_2RS compressor is planned. In the real plant, 4 g of H_2 will be compressed up to 200 bar per cycle. Afterwards, H_2 will be further compressed by a commercial booster and stored at 400 bar. Finally, the compressed H_2 will be used to refill two tanks located in the drone. The hydrogen flow from the tank will be spontaneous, exploiting the difference of pressure between steps, avoiding the use of pumps.

III. DRONE SET-UP

The drone will use two FC power modules of 650 W each, supported by a battery, to reach a total power of 1.3 kW. A maximum peak power of 1000 W will be available from the FC-battery hybrid system. FCs are composed by 6 cells connected in series with bipolar plates, with a total voltage of 22/24 V. They are designed for 1000 hours of working time. The FCs consumption is 8 NI/h and, in order to supply them, two tanks of compressed hydrogen (300 bar) of 1.5 L each are located on the drone. With this system, the drone will be able to fly continuously for about 2 h.

IV. CONCLUSION

An integrated system is going to be created to show the feasibility of the use of H_2 for a drone flight. A small plant will be realized, in which hydrogen will be produced and used. The plant will work with renewable energy, limiting the consumption of electricity of the grid. The drone will fly for about 2 h, displaying the potentiality of the use of hydrogen compared to batteries [1]. Finally, an economic and environmental study (Life Cycle Assessment - LCA) will be considered to estimate the commercial potentiality of this solution.

ACKNOWLEDGMENT

We acknowledge Regione Piemonte for the financial support.

REFERENCES

- [1] N. Belmonte, S. Staulo, S. Fiorot, C. Luetto, P. Rizzi, M. Baricco, *Appl. Energy*. 215 (2018) 556–565. doi:10.1016/j.apenergy.2018.02.072.
- [2] M. V. Lototskyy, V.A. Yartys, B.G. Pollet, R.C. Bowman, *Int. J. Hydrogen Energy*. 39 (2014) 5818–5851. doi:10.1016/j.ijhydene.2014.01.158.

SUPPLY OF SOLAR ELECTRICITY TO UNINTERRUPTIBLE LOADS VIA SEASONAL STORAGE WITH POWER-TO-POWER SYSTEMS

E. Crespi*, P. Colbataldo*, G. Guandalini*, S. Campanari*

*Politecnico di Milano, Department of Energy - Via Lambruschini 4A, 20156 Milano, (Italy)

Abstract - In the framework of power sector decarbonization, this work aims at designing a Power-to-Power (P2P) system that allows to supply a given fraction of self-generated electricity from a solar photovoltaic (PV) plant to an uninterruptible 1-MW constant load. A model is set up to size the system components optimizing the annual operation, with the goal of minimizing through a MILP approach the annual average cost of supplying electricity to the load. Results show that, with the present cost of grid electricity and the present investment cost of the P2P system components, the installation of a P2P system able to supply 100% of the demand is not advantageous and the best solution in terms of average electricity cost is obtained by self-generating nearly 30% of the load annually with a simple PV plant. At any rate, to reach high share of self-generation the P2P system becomes mandatory to decouple generation and consumption on both daily and seasonal scale.

Index Terms – Energy storage, Hydrogen, Power-to-Power.

I. NOMENCLATURE

EE	Electric Energy
EL	Electrolyzer
FC	Fuel Cell
P2P	Power to Power
PV	Photovoltaics

II. INTRODUCTION

The decarbonization of the power sector plays a crucial role in the reduction of greenhouse gas emissions, mainly achieved by use of renewable sources. In this framework, this work aims at designing a system that allows to power an uninterruptible 1 MW constant load with electricity from a solar PV plant. Since PV power generation occurs only during daytime and is higher during summer, a Power-to-Power (P2P) system able to decouple demand and supply on both a daily and seasonal scale is considered.

III. SYSTEM CONCEPT AND LAYOUT

The P2P system includes a PV plant, an electrolyzer,

pressurized hydrogen tanks and a fuel cell. The system components as well as the energy and hydrogen flows are schematized in Fig. 1. The electricity demand of the uninterruptible 1 MW load is satisfied partially by the PV plant (directly or through the P2P system) and partially with power taken from the grid. The instantaneous share of these two contributions varies at each time step and influences the annual share of self-generated renewable energy on the total demand.

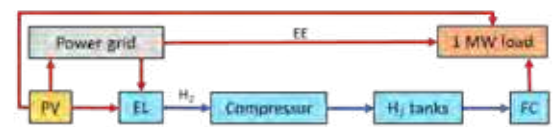


Fig. 1. Schematic of the system components and energy flows.

Given the specific generation of the PV plant, a model is set up that sizes the system components by optimizing the annual operation, with the goal of minimum average cost of the electricity annually consumed by the load. The problem is solved as a mixed-integer linear programming (MILP) optimization problem. Investment cost assumptions take into account recent cost evaluations of the main components [1]: 1000 €/kW_{el} for PV, 1000 €/kW_{el} for EL, 400 €/kW_{el} for H₂ compressor, 600 €/kg for H₂ tanks, 4000 €/kW_{el} for FC. A 10 %_{year} capital recovery factor is considered. Electricity is bought from the grid at a price that varies from 175 to 187 €/MWh_{el}, depending on the hour of the day and the day of the week. Electricity generated by the PV field and not supplied to the load or to the EL is sold to the grid at 60 €/MWh_{el}.

IV. RESULTS

Assuming that the P2P system is located in northern Italy (Milan), the average annual cost of electricity provision to the load is firstly optimized considering the share of self-generation as a variable, obtaining the 'best' case solution: installed PV capacity equals to 2.81 MW_p and no P2P or other components are present, resulting in a self-generation of 29% on an annual

basis. Thus, installing a PV plant is proved economically preferable to simply buying all the required electricity from the grid (reference case).

A sensitivity analysis is then performed, increasing the minimum annual share of self-generation that the system must guarantee. Up to 38% self-generation, the P2P system is not installed since increasing the size of the PV field (that reaches 8.56 MW_p at 38%) results less expensive. Above 38% self-generation share, the P2P system becomes necessary to decouple generation and consumption. Fig. 2 shows that in the range 40%-80% the electricity flows from PV to P2P and from the P2P system to the load increase at a nearly constant rate. On the contrary, the PV-generated electricity sold to the grid remains approximately constant, because the additional PV is installed only to supply the load. These trends change above 80% self-generation, where the FC installed capacity reaches its maximum. In this range, a steeper increase in the size of the PV field is observed (see Table I) and above 90% also the total size of the hydrogen tanks increases faster (tripling its value when moving from 90% to 100%), highlighting the need of a very large storage capacity for a full seasonal energy shift.

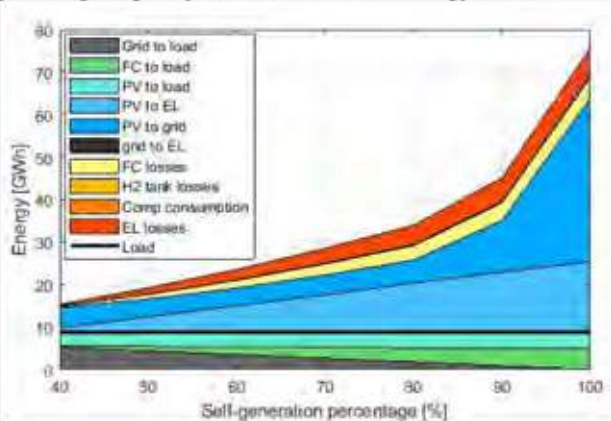


Fig. 2. Energy flows for increasing annual self-generation share in northern Italy.

TABLE I

INSTALLED CAPACITIES OF P2P SYSTEM COMPONENTS IN NORTHERN ITALY

Self-generation percentage		50%	60%	70%	80%	90%	100%
PV	P _{nom} [MW _p]	8.67	10.82	13.26	16.05	23.40	46.00
	Land footprint [ha]	4.3	5.4	6.6	8.0	11.7	23.0
	Energy capacity [MWh]	11.1	18.2	29.5	44.2	69.6	215.4
H ₂ tank	Volume capacity [m ³]	24.4	36.6	60.9	85.3	134.1	402.2
	Land footprint [m ²]	60	90	150	210	330	990
EL	P _{nom} [MW _{el}]	1.05	1.75	2.58	3.44	4.91	7.42
FC	P _{nom} [MW _{el}]	0.29	0.53	0.77	1.00	1.00	1.00

In terms of average annual cost of electricity provision, the results of the sensitivity analysis are shown in Fig. 3, compared with the costs obtained locating the same system in southern Italy (Ragusa). Indeed, the latitude affects the results because of the different solar radiation, leading to smaller annual hydrogen

storage need in southern areas. Therefore, for any imposed self-generation share the total average cost is lower in southern Italy, where the 'best' case self-generation increases to 38% (vs. 29% in northern Italy). In both locations, due to seasonal H₂ storage need, the cost increases faster when approaching 100% self-generation. However, electricity costs are quite different: while in the northern Italy case the price triples with respect to the reference case, in the southern case it only doubles.

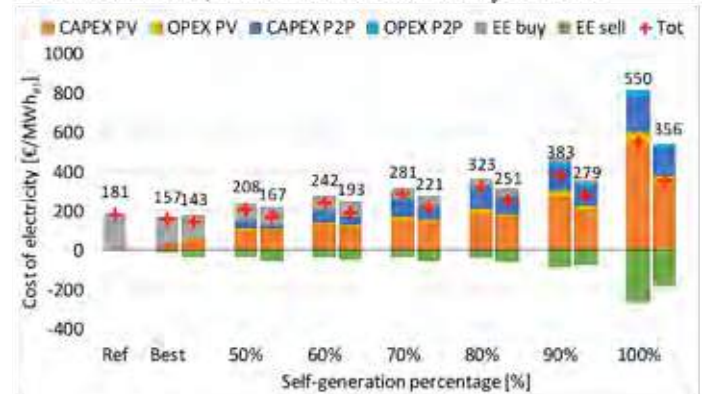


Fig. 3. Annual average cost of the electricity to the 1-MW load, in north Italy (left bars) or south Italy (right bars). Ref = only consumption from grid.

A further sensitivity analysis shows how the 'best' case solution for the plant in northern Italy conceptually varies with the cost of grid electricity. Increasing this cost up to very high (and unrealistic) prices, at 400 €/MWh_{el} more PV is installed, reaching 35% self-generation, but installing a P2P system becomes favorable only if this cost is increased further; only when the grid electricity price equals 800 €/MWh_{el}, the optimal solution (P2P included, 87% self-generation) almost halves the electricity provision cost with respect to buying all the electricity from the grid. A further increase in the cost would be needed, at present component costs, to make the 100% self-generation competitive.

V. CONCLUSIONS

With the present cost of grid electricity and today's investment cost of P2P components, the economic viability of installing a P2P system strongly depends upon the available solar radiation. Anyway, a storage system is necessary when a high share of self-generation is desired and P2P allows to comply with the seasonal storage needs. Results show that up to 50-60% of annual demand coverage the PV+P2P system may guarantee a final cost of electricity below 170-240 €/MWh, depending on the location, while at higher shares the system would require further reductions in component costs to become competitive.

REFERENCES

- [1] Multi-Annual Work Plan 2014-2020, Fuel Cells and Hydrogen Joint Undertaking (FCH JU)

OPTIMIZATION OF OPERATING PARAMETERS ON THE DIRECT METHANOL FUEL CELL USING NAFION-GRAPHENE OXIDE MULTILAYER MEMBRANE

Gabriele G. Gagliardi*, Ahmad El-Kharouf **, Franco Rispoli* and Domenico Borello*

*Department of Mechanical and Aerospace Engineering, University of Rome La Sapienza (Rome, Italy)

**School of Chemical Engineering, University of Birmingham (Birmingham, UK)

Abstract - We analyse and optimize the operating parameters of direct methanol fuel cells (DMFCs) using a Nafion/graphene oxide (GO) multilayer membrane. Several multilayer membranes with different GO loading were manufactured using casting method. Polarization and power curves of the DMFC were analyzed. The DMFC performance was enhanced by increasing the temperature and the flow rate. Increasing the molarity up to 1M, the power peak and the operational range increase when using GO membranes if compared with Nafion 117. However, further increase of the molarity leads to a rapid derating of the DMFC. The performance increases as the cathode flow rate increases. The best conditions are obtained for an anode flow rate of 800 microliter/min. Moreover, the methanol crossover was decreased.

Index Terms - DMFC, Graphene oxide, Multilayer membranes, Nafion modified, Solution casting.

I. NOMENCLATURE

C = Carbon; D.I. = Deionized; DMFC = Direct methanol fuel cell; GDL = Gas diffusion layer; GO = Graphene oxide; I = Current density; P = Power; V = Voltage

II. INTRODUCTION

The DMFC is an electrochemical system that produces energy by oxidizing the liquid fuel (a mixture of water and methanol) without auxiliary devices. The use of DMFC has several advantages: easy fuel storage, low cost of methanol, operation at low temperature and pressure, high efficiency, small system size and low weight [1]. However, several issues hinder the spreading of this technology. Firstly, we must consider that the fuel cell membrane is generally composed by Nafion, a perfluorosulfonic polymer, that is prone to allow the methanol cross-over, that strongly reduce DMFC performance. Furthermore, high cost and limited operating temperature range represent a strong limit to the commercialization of that technology. Research activities are focused on developing new polymer electrolyte membrane (PEM) materials aiming at reducing crossover. Among several types of material, graphene oxide (GO) has been considered as an exceptional element that offers excellent results in terms of water uptake and proton conductivity. Several authors [2-3] have reported that GO

contributes to reduce methanol permeability because it acts as a barrier, due to its higher tortuosity, while proton conductivity shows an opposite trend. In addition, it is well known that temperature [4], methanol concentration [5] as well as flow rate affect proton conductivity and methanol crossover and, consequently, DMFC performance. The aim of this study is to optimize the operating parameters of a direct methanol fuel cell using a Nafion/GO multilayer membrane, comparing its performance with the baseline Nafion.

III. MATERIALS AND METHOD

A. Materials

Materials and precursor were obtained from several companies: GO sheets and hydrogen peroxide (34%) from Sigma Aldrich; sulfuric acid (98%) from Alfa Aesar; Nafion dispersion, GDL and catalysts, Pt-Ru at the anode, PtC at the cathode, from Fuel cell store.

B. Preparation of multilayer membranes

The process of casting a membrane consists of solvent evaporation [6]. Then, the polymer forms a film on the flat surface. Here, three-layer membranes were prepared: Nafion/GO/Nafion. We considered three GO loading: 0.5, 1 and 1.5%. For membrane preparation the following procedure is adopted: a) pour Nafion solution in a flat petri dish; b) dry for 2 hours at 100°C; c) dry for half an hour at 50°C; d) pour the solution of GO in water over the 1st layer in the petri dish and dry it in the oven at 100°C for 2 hours; e) dry for half an hour at 50°C; f) pour Nafion solution over the 2nd layer and dry it in the oven with annealing (100°C for 2 hours and 120°C for 1 hour). Afterwards, the membranes were treated at 80 °C by immersion in the following sequence (each procedure lasted 1 h): in water, in 3% H₂O₂, in water, in 0.5 M H₂SO₄ and in water. Then, the membranes were immersed in water overnight.

C. Characterization

The microstructure of GO composite membranes was observed by using a scanning electron microscope. Fourier transform

infrared (FTIR) spectra of the GO composite membranes were obtained using a FTIR (model).

D. Fuel cell tests

The catalyst ink was prepared by mixing a predetermined amount of the catalyst into a solution of 10wt% Nafion ionomer solution, D.I. water, ethanol. The procedure was performed in an ultrasonicator for at least 15 minutes. Then, the catalyst slurries were brushed on the GDL. The anode contained 3 mg/cm² of Pt-Ru and the cathode contained 3 mg/cm² of PtC. The MEA was obtained by hot pressing the multilayer membrane sandwiched between the electrodes. The electrochemical performance (cell voltage and electrical current) of the fuel cell were measured by using the Scribner 885 potentiostat. The power density was calculated as the product of cell voltage and current density. The power density was plotted against the current density (P-I curve) to determine the peak power density (Pmax) at each tested operating condition. Here, the cell temperature ranges between 40°C and 70°C by 10°C intervals; the anode flow rate between 800 to 1500 µl/min; the cathode flow rate between 1 and 3 l/min at the cathode flow. The methanol concentration varied from 0.5 to 2M. The membrane tested was made of 1% of GO. Tests on multilayer membranes with 0.5% and 1.5% of GO are ongoing.

IV. RESULTS AND DISCUSSION

Chemical characterization is currently ongoing. Table 1 lists the maximum power output, obtained varying operating conditions: temperature, anode flow (AF), cathode flow (CF) using a GO membrane with 1% GO content. The anode was fed with 2M of methanol solution.

TABLE I DMFC OPERATION CONDITIONS GO MEMBRANE 1% AT 2M

		Power output [mW/cm ²]				
		Temperature	40°C	50°C	60°C	70°C
Operating condition	400AF 1CF		2.5	2.82	3.08	3.49
	400 AF 2CF		3.225	3.55	4.22	4.72
	400 AF 3CF		3.675	4.21	4.92	5.78
	800AF 1CF		3.36	2.57	3.07	3.6
	800 AF 2CF		3.625	3.28	4.39	4.4
	800 AF 3CF		3.9	3.99	5.02	5.86
	1500AF 1CF		2.3	2.97	2.9	3.37
	1500 AF 2CF		2.95	3.98	4.04	4.76
	1500 AF 3CF		3.35	4.71	4.79	5.44

It was observed that the increase in the cell temperature, as well as in the cathode flow, enhanced DMFC performance. This trend is in agreement with other experimental works [7]. The maximum performance is obtained for an anode flow rate of 800 microliters/min. Reducing methanol concentration from 2 to 1M and 0.5 M enhanced the maximum peak power: 5.86, 13.4 and 14.34 mW/cm² respectively. The best I-V characteristics obtained from single cell tests for the multilayer membrane was compared with the performance of commercial

Nafion using the same operating conditions (Fig.1).

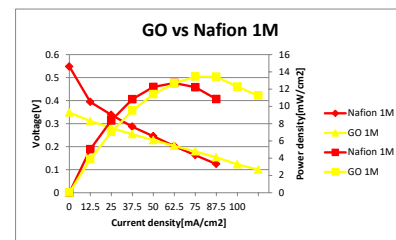


Fig. 1. Characteristic curves of Nafion 117 and GO membrane at 1M

The performance of bare Nafion was higher at low methanol concentration, the power output was 30% more than the multilayer membrane. The addition of a graphene oxide layer reduced methanol crossover at higher methanol solutions (1M) as the performance increases of 30% and the operating range is increased. In fact, the methanol crossover was decreased by 25% while the peak power of the multilayer membrane was slightly higher than the Nafion one.

V. CONCLUSION

In this study, the optimization of operating parameters on a direct methanol fuel cell, using a three layers Nafion/GO membrane, was carried out. The best performance was obtained at 70°C, 0.5M, 800 microliter/min of anode flow and 3 liter/min of cathode flow. The performance of the multilayer membrane with a GO loading of 1% is marginally better to that of Nafion membrane: this is principally due to the reduced methanol crossover.

REFERENCES

- [1] Shah R, Introduction to fuel cells, in recent trends in fuel cell Science and Technology. Springer, (2007) pp 1–9.
- [2] B. Choi *et al.*, Enhanced transport properties in polymer electrolyte composite membranes with graphene oxide sheets, Carbon, Volume 50, Issue 15, 2012, pp. 5395-5402
- [3] H. Chien, L. *et al.*, Sulfonated graphene oxide/Nafion composite membranes for high-performance direct methanol fuel cells, International Journal of Hydrogen Energy, Volume 38, Issue 31, 2013, pp. 13792
- [4] J.Han, H. Liu, Real time measurements of methanol crossover in a DMFC, Journal of Power sources, Volume 164, 2007, pp. 166-173
- [5] M. Ahmed, I. Dincer, A review on methanol crossover in direct methanol fuel cells: challenges and achievements, International Journal of energy research, Volume 35, 2011, pp. 1213-1228
- [6] J. Ma, D. Ping and X. Dong, Recent developments of Graphene oxide-based membranes: A review, Membranes, Volume 7, Numero 3, 2017,
- [7] S. H. Seo, C. S. Lee, Effect of operating parameters on the direct methanol fuel cell using air or oxygen as an oxidant gas, Energy & Fuels, Volume 22, 2008, pp. 1212–1219

OXYGEN REDUCTION REACTION ON NOVEL CARBON SUPPORTED Pt-Ir AND Pt-Pd ELECTROCATALYSTS

A. Seretis, A. Brouzgou and P. Tsiakaras

Laboratory of Alternative Energy Conversion Systems, Department of Mechanical Engineering,
University of Thessaly, Pedion Areos, Volos, (Greece)
tsiak@uth.gr

Abstract - In the present work, a series of carbon supported (20wt%M/Vulcan XC72 where M=Pt, Pd, Ir, Pt_xIr_y and Pt_xPd_y with x:y atomic ratios of 3:1, 1:1, 1:3) bimetallic electrocatalysts is thoroughly investigated for its durability in oxygen reduction reaction (ORR) in acidic medium (0.1M HClO₄). It is found that PtIr/C and PtPd/C exhibit outstanding durability even after 5000 accelerated durability test (ADT) cycles. However, the highest mass activities, which are 6 and 5 times higher than the one observed over the pure Pt/C, are presented by Pt₃Pd₁ and PtPd, respectively. This proves that performance does not always keep up with durability; factor that needs further investigation.

Index Terms -oxygen reduction reaction, Pt-Pd electrocatalysts, Pt-Ir electrocatalysts, synergistic effect

I. INTRODUCTION

It is established [1] that platinum-based materials are the most effective electrocatalysts for the sluggish oxygen reduction reaction (ORR). Significant studies have been devoted on alloying the precious metal Pt with another metal to increase its mass activity. Moreover, researchers [2] have focused on controlling the size and the shape of Pt-alloy nanostructures that could improve the electrocatalytic activity and stability. It has been found that the high surface area, accessible pore structure, the size and dispersion of Pt-based nanoparticles in electrocatalysts and the well-controlled electronic properties of Pt strongly influence their ORR performance [2]. While most researches has turned into the investigation of improving electrocatalytic performance in alkaline environment; today the insufficient durability of the electrocatalysts that present high activity in acidic media, still restrains them from practical application in proton exchange membrane fuel cells. In the present work, the ORR activity in acidic medium and the durability of a series of Pt-based bimetallic electrocatalysts is investigated thoroughly.

II. EXPERIMENTAL PART

The electrocatalysts were prepared via the microwave-assisted polyol method [3]. The catalysts were physicochemically and electrochemically characterized. XRD measurements were carried out with the aid of a D/Max-III A (Rigaku Co., Japan) employing Cu K α ($\lambda = 0.15406$ nm) as the radiation source at 40 kV and 40 mA. Catalysts were investigated by TEM using a Philips CM12 microscope (resolution 0.2 nm), provided with high resolution camera, at an accelerating voltage of 120 kV. All the electrochemical measurements were performed with an electrochemical workstation (AMEL 7050), in a three-electrode model cell with a glassy carbon as working electrode (d=3.0 mm), a saturated calomel electrode (SCE) and a platinum wire as the reference and counter electrodes, respectively. The ADT tests took place by applying a potential of 0.6 to 1V at a scan rate of 100 mV/sec in 0.1 M HClO₄ at 1600 rpm.

III. RESULTS AND DISCUSSION

A. Electrochemical characterization

Among the examined electrocatalysts the Pt₃Pd₁/C catalyst is better with mass specific activity $I_m=488.5$ mA/mg_{met} and $E_{1/2}=0.93$ V (Table I).

TABLE I ELECTROCHEMICAL CHARACTERISTICS OF THE PT-PD-BASED ELECTROCATALYSTS

Catalyst (20wt% metal loading)	ECSA (m ² /g _{met})	I_m (mA/mg _{met}) (0.85V)	I_k (mA/cm ² _{met}) (0.85V)	$E_{1/2}$ (V)
Pt/C	13.67	284	2.07	0.89
PtPd/C	52.3	479.5	0.91	0.9
Pt ₃ Pd ₁ /C	58	488.5	0.84	0.93
Pt ₁ Pd ₃ /C	43.3	396.6	0.91	0.88
Pd/C	28.3	117.2	0.41	0.83

However, the PtPd catalyst has lower Tafel slope and higher charge transfer coefficient and if we count in that this catalyst

has lower platinum content, it is concluded that PtPd presents higher kinetic current per mass of platinum $I_m=410 \text{ mA/mg}_{Pt}$ than Pt_3Pd_1 catalyst 339.4 mA/mg_{Pt} at $E=0.85 \text{ V}$. Also, the Tafel slopes of Pt-Pd-based catalysts were calculated 75, 65.5, 73, 68 and 164 mV/dec .

TABLE II ELECTROCHEMICAL CHARACTERISTICS OF THE Pt-IR-BASED ELECTROCATALYSTS

Catalyst (20wt% metal loading)	ECSA ($\text{m}^2/\text{g}_{\text{net}}$)	I_m ($\text{mA}/\text{mg}_{\text{net}}$) (0.85V)	I_s ($\text{mA}/\text{cm}^2_{\text{net}}$) (0.85V)	$E_{1/2}$ (V)
PtIr/C	33.34	522.45	1.56	0.91
Pt_3Ir_1/C	35.25	375.58	1.06	0.9
Pt_3Pd_1/C	11.43	9.07	0.079	0.73
Ir/C	7.33	1.15	0.015	0.55

The Tafel slopes for each respective catalyst as being reported in Table II were calculated 65, 74, 126 and 180.5 mV/dec , respectively. Concerning the durability tests, as shown in Fig. 1 the $E_{1/2}$ of both PtIr and PtPd catalysts exhibit a small negative shift of 20 and 30 mV respectively which is significantly smaller than that at Pt catalyst (140 mV negative shift) after 5000 cycles.

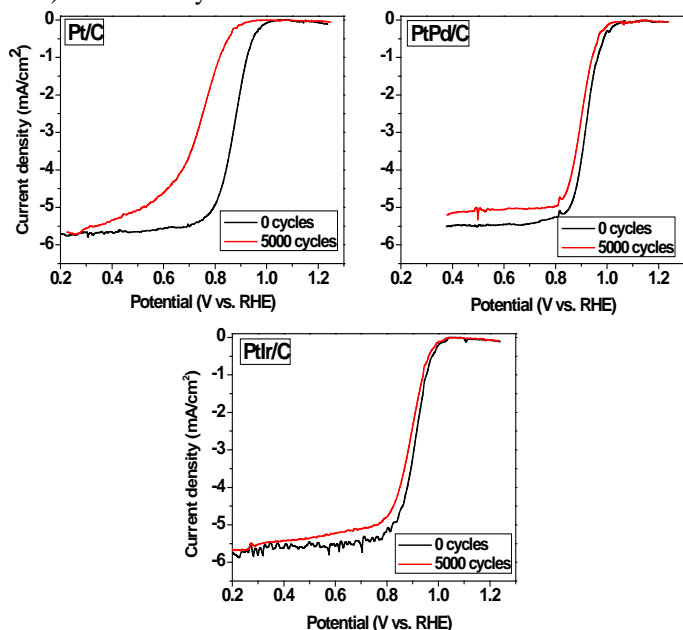


Fig.1. ORR polarization curves of Pt, PtIr and PtPd catalysts in O_2 saturated 0.1 M HClO_4 aqueous solution, anodic scan rate 20 mV/sec , 1600 rpm before and after 5000 cycles

The PtIr mainly and PtPd catalysts exhibit outstanding durability even after 5000 accelerated durability test (ADT) cycles confirming the synergistic effect of metal alloying [4].

B. Physicochemical characterization

In Fig. 2 the TEM images are given for the Pt_3Pd_1/C , PdPt/C and PtIr/C. The distribution is homogenous for both electrocatalysts, however the last one seems to have lower nanoparticles diameter; around 2-4 nm.

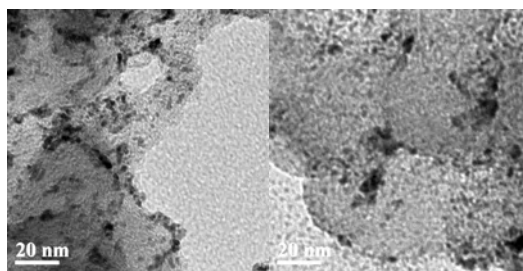


Fig.2. TEM images for PtIr/C (left) and PdPt/C (right)

In Fig.3 the XRD patterns are depicted. The diffraction peaks are the same for the two electrocatalysts indicating the formation of alloy. The diffraction peaks are appeared to the (111), (200), (220) and (311) $2\theta^\circ$ which are attributed to face centered cubic structure.

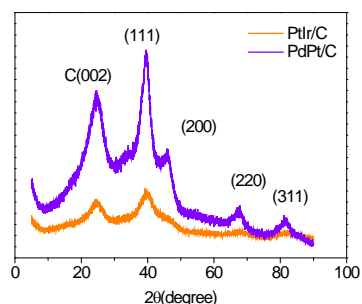


Fig.3. XRD images for Pt_3Pd_1/C , PdPt/C and Pt_1Ir_1/C

IV. CONCLUSION

Herein it is proved that the activity ORR results do not always agree with durability results. Despite the fact that Pd₃Pt/C exhibits the highest ORR activity, does not present the highest durability. However, in the case of PtIr the activity and durability are consistent.

ACKNOWLEDGMENT

The authors thankfully acknowledge co-financing by European Union & Greek national funds through the Operational Program Competitiveness, Entrepreneurship and Innovation, under the call RESEARCH – CREATE – INNOVATE (Project code: T1EDK-02442).



REFERENCES

- [1] Brouzgou, A., Song S.Q., Tsiakaras P., Low and non-platinum electrocatalysts for PEMFCs: Current status, challenges and prospects, Applied Catalysis B: Environmental, volume 127, 2012, pages 371-88.
- [2] Lu, J., Luo L., Yin S., Hasan S.W., Tsiakaras P., Oxygen Reduction Reaction over PtFeM (M= Mo, V, W) Alloy Electrocatalysts: Role of the Compressive Strain Effect on Pt, ACS Sustainable Chemistry & Engineering, volume 2019, pages
- [3] Brouzgou, A., Song S., Tsiakaras P., Carbon-supported PdSn and Pd₃Sn₂ anodes for glucose electrooxidation in alkaline media, Applied Catalysis B: Environmental, volume 158-159, 2014, pages 209-16.
- [4] Bertin, E., Muenzer A., Reichenberger S., Streubel R., Vinnay T., Wiggers H., et al., Durability study of platinum nanoparticles supported on gas-phase synthesized graphene in oxygen reduction reaction conditions, Applied Surface Science, volume 467, 2019, pages 1181-6.

EVALUATING THIN-FILM MODEL ELECTRODES FOR AEMFC

Eva Marra*, Björn Eriksson*, Timon Novalin*, Nikola Nikolić*, Gerard Monserrat Sisó**, Rosemary Brown**, Björn Wickman**, Rakel Wreland Lindström*, Göran Lindbergh*, Carina Lagergren*

* Department of Chemical Engineering, KTH Royal Institute of Technology, SE-100 44 Stockholm, (Sweden)

** Department of Physics, Chalmers University of Technology, SE-41296 Gothenburg (Sweden)

Abstract –AEMFCs open new possibilities for less expensive catalyst materials. Thin film model electrodes have previously been used in PEMFC and it was shown that Pt alloys achieved higher specific activities than Pt/C.

In this study, the thin film electrodes are for the first time used in AEMFC. The aim is to understand the electrochemical behavior of thin-film model electrodes in alkaline media. The first step is to establish optimal operating conditions, and for this purpose experiments with double MEA have been performed. This configuration allows a more accurate analysis of low current density regions. Results indicate that the double MEA configuration is an improved design, suitable for CO stripping voltammetry and superior electrochemical performance compared with the single MEA configuration.

Index Terms – Anion Exchange Membrane Fuel Cells (AEMFCs), Double MEA configuration, Pt alloys, Thin film model electrodes.

I. INTRODUCTION

Overcoming the sluggish kinetics of the oxygen reduction reaction (ORR) at the cathode and maintaining a durable high performance at a lower cost, are two of the main challenges for low temperature fuel cells. Anion exchange membrane fuel cells (AEMFCs) can potentially overcome these issues, by allowing for lower cost catalysts to be utilized. In previous studies, in proton exchange membrane fuel cell (PEMFC), thin film electrodes allowed the electrochemical evaluation of Pt and Pt₃Y [1]. Similar methodology, should also allow for evaluation of new catalysts for AEMFCs.

Thin film electrodes enable more accurate measurements of catalyst activity than the more conventional porous electrodes. This is due to the flat nature of the produced electrodes, minimizing the effects of current distribution. Using model electrodes direct in a fuel cell will also allow for the evaluation of these catalyst materials under more realistic conditions than typical rotating disk electrode measurements in aqueous solution.

However, during electrochemical measurements in a fuel cell, hydrogen crossover from the anode to the cathode can lower the measured activity. Hydrogen crossover causes a mixed potential at the cathode, influencing the kinetic evaluation of the ORR activity in the low current density region. It has been proven in PEMFCs that the use of a double MEA configuration can solve this issue. By introducing an additional Pt/C-membrane layer, between the membrane and the anode, the hydrogen crossing from this electrode reacts with permeating oxygen from the cathode and thus minimizes its influence on the ORR [2].

II. EXPERIMENTAL

A. MEA Assembly

Two FAA3-50 rectangular shaped membranes were sprayed with an ink composed of Pt/C, an ionomer solution (Fumion ionomer in methanol) and iso-propanol. The ratio between Pt/C and ionomer was 3:1 and the solid content of the ionomer solution was 25% w/w. The loading of the electrodes was 0.4 mg_{Pt}/cm². Before mounting the membranes were immersed in KOH 1M for 24 h (STP) to become anion exchanged from Br⁻ to HO⁻ form. They were then rinsed with Milli-Q water during 12 h (STP).



Fig. 1. Schematic view of single MEA (left) and double MEA (right) configurations.

The cell assembly followed these steps: 20 nm Pt thin film cathode electrodes, deposited onto a Carbel CL GDL, were shaped to get a GDE of 0.95 cm² circular geometrical area. To complete the single configuration, a one sided Pt MEA and Sigracet 25BC GDL were used as anode. The double MEA configuration was composed similarly, but with an additional sprayed electrode layer, as can be seen

in Fig 1. Every MEA configuration was mounted in a cell house (Fuel Cell Technologies Inc.) using graphite current collectors with customized spiral gas flow channels of 5.9 cm and clamped using screws with 5 Nm torque.

B. AEMFC Measurements

All measurements were performed with a cell temperature of 30 °C and at 100 %RH. Prior to electrochemical evaluation the cells were activated, in 5 % H₂ in Ar and O₂, by potential hold at 0.1 V for 3 h. The electrochemical activity of the thin film electrodes were evaluated by sweeping the potential between 0.9 and 0.3 V at a sweep rate of 20 mVs⁻¹.

After the activity measurement, the cathode gas was switched to N₂ (100 %RH) overnight, and the following day CO-stripping was performed to determine the electrochemically active surface area (ECSA).

III. RESULTS

Fig. 2 shows the CO-stripping for the two tested systems. As can be seen the single MEA configuration does not exhibit a clear CO adsorption peak for calculating the corresponding ECSA.

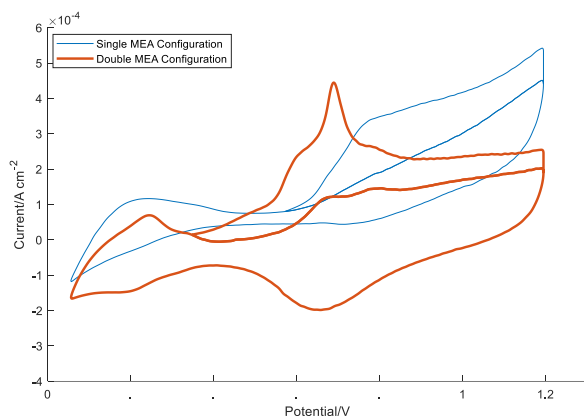


Fig. 2. CO-stripping cyclic voltammetry for single and double MEA configuration. Measurements done at 30 °C, 100 %RH using 5 % H₂ in Ar and N₂, and a sweep rate of 200 mVs⁻¹.

The double MEA configuration instead gives a clear CO adsorption. The resulting ECSA of this improved configuration is equal to 0.87 cm², which represents 92 % of the original electrode area. This is lower than the approximately 5 cm² obtained in PEMFC [1], suggesting that the FAA 3-50 membrane has lost contact, possibly due to lowered water content, during the gas switching time.

The polarization curves, presented in Fig. 3, show that the performance of the double MEA configuration is remarkably superior, reaching similar values as PEMFC [1]. The increase in performance is attributed to reduced influence of gas crossover.

The properties of the polymeric membrane, such as swelling and conductivity, are strongly related to water content (humidity). The double MEA configuration could improve to the complex water management, needed for preventing dry conditions at the cathode and flooding at the anode [3].

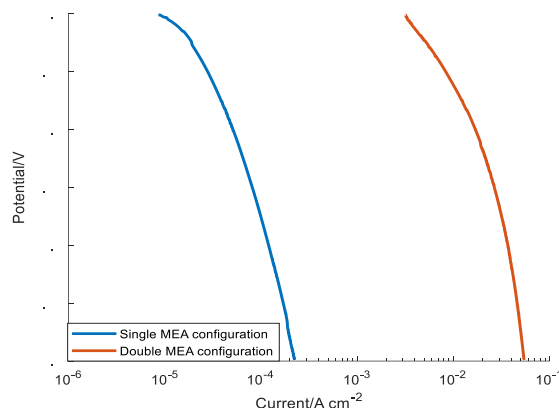


Fig. 3. Polarization curves of the single and double MEA configuration. Measurements done at 30 °C, 100 %RH using 5 % H₂ in Ar and O₂, and a sweep rate of 20 mVs⁻¹.

IV. CONCLUSION

In this study, thin film electrodes of Pt have been tested in AEMFC for the first time. The results show that the use of a double MEA setup is required to produce accurate results. With a double MEA configuration, similar current densities as in PEMFC, at 0.9 V, can be achieved.

ACKNOWLEDGMENT

We acknowledge funding from Strategic Vehicle Research and Innovation (FFI), the Swedish Foundation for Strategic Research (SSF), and the governmental initiative StandUp for Energy.

REFERENCES

- [1] Lindahl, N., Eriksson B., Grönbeck H., Lindström R., Lindbergh G., Lagergren C., and Wickman B. Fuel cell measurements with cathode catalysts of sputtered Pt₃Y thin films. *ChemSusChem*. 2018;11(9):1394–1394.
- [2] Ekström H. Evaluating Cathode Catalysts in the Polymer Electrolyte Fuel Cell [Internet] [PhD Dissertation]. [Stockholm]: KTH; 2007 [Trita-CHE- Report]. Available from: <http://urn.kb.se/resolve?urn=urn:nbn:se:kth:diva-4413>
- [3] Eriksson B., Grimler H., Carlson A., Ekström H., Wreland Lindström R., Lindbergh G., et al. Quantifying water transport in anion exchange membrane fuel cells. *International Journal of Hydrogen Energy*. 2019;44(10):4930–9.

ENHANCEMENT OF DURABILITY OF MICROPOROUS LAYERS FOR PEM FUEL CELLS BASED ON GRAPHENE NANOPATELETS

Marco Mariani*, Saverio Latorrata*, Stefano Patrignani*,
Paola Gallo Stampino*, Giovanni Dotelli*

*Department of Chemistry, Material and Chemical Engineering "G. Natta", Politecnico di Milano, Piazza Leonardo da Vinci 32, 20133
Milano (Italy)

Abstract - Issues as water management and components durability are still hindering the development of Polymer Electrolyte Membrane Fuel Cells (PEMFCs). These problems particularly affect the microporous layers (MPLs), which are usually obtained by coating the gas diffusion layers with a carbon black-based coating.

In this work, different graphene-based particles have been employed in partial or total substitution of carbon black with the aim to improve the electrical conductivity, the mechanical strength and the water management of the MPL. The samples have been characterized from an electrical, microstructural and morphological standpoint. Single fuel cell testing has been performed under different temperature and relative humidity conditions to determine the performance dependence on the cell humidity. Finally, the durability of the MPLs produced has been assessed through electrical repeatability tests with multiple cell flooding events and via mechanical accelerated stress tests performed in a dummy cell.

Index Terms – Durability, Graphene, Microporous Layer, Water Management.

I. NOMENCLATURE

CB	Carbon Black
EG	Exfoliated Graphite
FEP	Fluorinated Ethylene Propylene
GDL	Gas Diffusion Layer
GDM	Gas Diffusion Medium
GNP-L	Graphene Nanoplatelets – Large size
GNP-M	Graphene Nanoplatelets – Medium size
GNP-S	Graphene Nanoplatelets – Small size
MPL	Microporous Layer
PEMFC	Polymer Electrolyte Membrane Fuel Cell

II. INTRODUCTION

To overcome the limitations of carbon black (CB)-based microporous layers (MPLs), the employment of different carbonaceous phases has been considered a possible solution. In particular, the attention has been focused on graphene-based nanoparticles, which feature outstanding properties that are fundamental to the proper functioning of the fuel cell, as exceptional electrical and thermal conductivity and high mechanical strength. Recent studies have demonstrated the feasibility of this substitution [1-3]. In this work, the graphene nanoplatelets employed are distinguished mainly from their size and morphology. Multiple analyses have been performed to assess the effects of these features on the final properties of the MPLs and the cell performances. Possible synergic effects between the two carbonaceous phases have been studied by producing multi-components samples, too.

III. MPLS PREPARATION

All the samples were produced by deposition of a carbonaceous ink via doctor blade-coating technique on a previously hydrophobized gas diffusion layer (GDL). All the inks featured: deionized water as solvent, isopropyl alcohol as dispersing agent, fluorinated ethylene propylene (FEP) as hydrophobizing agent, a main carbonaceous phase (only CB/only graphene-based particles/50-50 wt.% CB-graphene) and a 10 wt.% carbon nanotubes addition. After deposition, the gas diffusion mediums (GDMs) were heat treated at 270 °C and re-hydrophobized with a 12 wt.% FEP suspension.

IV. EXPERIMENTAL RESULTS

A. Morphological Characterization

SEM images have shown that the MPLs have different surface aspects. Smaller particles, in particular CB but also GNP-S, tend to agglomerate due to Van der Waals interactions, forming smaller pores and macrocracks. Instead, larger graphene nanoplatelets (EG, GNP-L, GNP-M) stack on top of the GDL surface, forming a continuous network of particles with pores and voids in between them.

Mercury intrusion porosimetry has confirmed the observations made on the samples porosity: CB produces a bimodal pore distribution, while graphene produces unimodal distributions with pore radius increasing with the particle size.

The surface integrity and porosity affect the through-plane water permeability of the MPLs, which is larger for CB and bigger graphene particles (EG and GNP-L). The permeability does not seem to depend on the samples wettability that almost exceeds the superhydrophobic limit (static contact angle $> 150^\circ$) in all cases; instead, it seems to be related to the presence of large cracks and voids, which act as direct paths for the water flowing through the GDM.

B. Electrical Characterization

As expected, graphene-based particles positively affect the electrical conductivities of the MPLs along both the planar and the transverse direction, despite the strong reduction of the particles intrinsic conductivity with respect to single-layer graphene. The co-presence of CB and graphene is beneficial for the through-plane conductivity because CB fills the voids in between graphene particles, improving the continuity of the electrical paths inside the coatings.

C. Single Fuel Cell Testing

CB provides overall better performances, in particular at low temperature. Most of graphene particles features issues in terms of mass transfer with early flooding of the fuel cell, likely due to their low water permeability. The only exceptions are represented by GNP-L and GNP-M at 80 °C. The first allows to keep low ohmic and mass transfer resistances under dry conditions (high T, low RH), thus maintaining the ionomer hydration at medium current density and removing the excess water at high current density (Figure 1). This behavior is fundamental for the reduction of the fuel cell dependence on the external saturators and the exploitation of high T PEMFC. Therefore, GNP-L have been selected for the durability analyses.

Multicomponent samples feature improved mass transfer but larger ohmic resistance with respect to monocomponent graphene-samples.

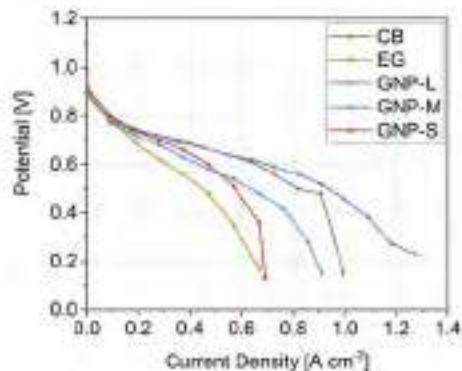


Fig. 1 Polarization curves obtained with the monocomponent MPLs at 80 °C and RH = 60 %.

D. Reliability and Durability Assessment

MPLs reliability has been tested by performing 10 single fuel cell testing sessions from open circuit voltage to flooding. GNP-L has revealed to be exceptional when compared to CB, with maximum peak power variations equal to 0.009 W cm⁻² and 0.055 W cm⁻² for GNP-L and CB respectively.

Mechanical accelerated stress tests have produced similar results. The loss of performance experienced by CB is much larger due to the intrinsic weakness of the MPL, which is easily deteriorated along the pre-existing cracks by the gas and water flows.

V. CONCLUSION

The analyses performed have shown that possible improvements can be achieved by substituting carbon black with other carbonaceous phases in the MPL. However, specific features must be present in the particles employed and it is of great importance determining how they assemble.

Large graphene nanoparticles stacking has produced optimal MPLs in terms of porosity and through-plane water permeability, which has guaranteed excellent cell performances also under dry conditions. In addition, they have provided an outstanding mechanical stability, due to the absence of macrocracks that has no equal with carbon black-based materials.

Future developments should consider the possibility of employing different or multiple graphene-based particles to utterly improve the water management and the mechanical resistance of the MPLs under critical conditions.

REFERENCES

- [1] S. Shahgaldi, A. Ozden, X. Li, F. Hamdullahpur, *Electrochimica Acta* 2019, 299, 809-819.
- [2] A. Ozden, S. Shahgaldi, X. G. Li, F. Hamdullahpur, *Renew Energ* 2018, 126, 485-494.
- [3] M. J. Leeuwner, A. Patra, D. P. Wilkinson, E. L. Gyenge, *J Power Sources* 2019, 423, 192-202.

HYSA SYSTEMS FUEL CELL PROTOTYPE DEVELOPMENT AND DEMONSTRATION FOR STATIONARY AND MOBILE APPLICATIONS IN SOUTH AFRICA

V. Linkov, M. Lototsky, A. Parsons, S. Pasupathi

HySA Systems Competence Centre, SAIAMC, University of the
Western Cape, Robert Sobukwe Road, Bellville 7530, South Africa

Abstract - HySA Systems is a Center of Competence for Technology Validation and Systems Integration on hydrogen and fuel cell technology (HFCT), located at the South African Institute for Advanced Materials Chemistry (SAIAMC), University of the Western Cape (UWC). HySA Systems is part of a long-term (15-year) Hydrogen and Fuel Cell Technologies (HFCT) Research, Development, and Innovation (RDI) strategy, which officially was launched in September 2008 by the Department of Science and Technology (DST) in South Africa. The main objective with HySA Systems is to (i) develop hydrogen and fuel cell systems, prototypes and products, (ii) perform technology validation and system integration and (iii) focus on system oriented material research in two key HySA-programmes: (1) Hydrogen Fuelled Vehicles (HFV) and (2) Metal hydride based technologies relevant to hydrogen economy. One of the principal objectives for HySA Systems is to establish long-term collaborations with industrial partners, including technology development, engineering and manufacturing companies in South Africa and the rest of the world involved in Hydrogen and Fuel Cell Technologies. HySA Systems has developed several prototype fuel cell systems, including a 1kW fuel cell combined heat and power (FC-CHP) system, a 2.5 kW backup power system, a 3 tonne fuel cell forklift containing hybrid metal hydride hydrogen storage, a 3.2 kW FC system for installation in a rural school, a hydrogen fuel cell scooter, to name a few. Currently HySA Systems is integrating an advanced local power module which is a fit in solution for forklifts together with an industry partner, HFC range extender scooter for South African Post Office etc. The results from the prototype systems will be presented and discussed.

Index Terms - Local Power Module, Hydrogen Fuelled Vehicles, Prototypes, Stationary systems.

I. INTRODUCTION

HySA Systems is one of three National Competence Centres which makes up HySA (Hydrogen South Africa). Initiated by the Department of Science and Technology (DST) and

approved by the Cabinet in May 2007, HySA is a long-term (15-year) programme within their Research, Development, and Innovation (RDI) strategy, officially launched in September 2008. This National Flagship Programme is aimed at developing South African intellectual property, knowledge, human resources, products, components and processes to support the South African participation in the nascent but rapidly developing international platforms in Hydrogen and Fuel Cell Technologies. The programme strives towards a knowledge-driven economy meaning that innovation will form the basis of South Africa's economy; this includes an aggressive capacity-development programme's approach. HySA also focusses on (i) the "Use and Displacement of Strategic Minerals", (ii) ways of harnessing South Africa's mineral endowments to promote both the hydrogen economy and renewable energy use, and (iii) seeking the most cost-effective and sustainable ways of incorporating PGM-based components in hydrogen fuel cell and other technologies, in turns resulting in commercialisation ventures and a viable industry around mineral beneficiation.

HySA Systems has integrated, validated and demonstrated various fuel cell powered systems [1]. This presentation will discuss the results from some of these prototypes.

II. RESULTS AND DISCUSSION

A. Locally developed fuel cell power module for electric forklift with integrated metal hydride hydrogen storage system

In 2017–2019, HySA Systems has developed a prototype fuel cell power module for 3-tonne electric forklift further integrated by Hot Platinum (Pty) Ltd, South Africa. The module based on 14.5 kW Ballard closed cathode PEMFC stack is characterised by average output power of 15 kW (30 kW in

peak) at bus voltage of 80 VDC. Main BoP components include deep cycle lead-acid battery, supercapacitors, as well as 20 Nm³ H₂ metal hydride hydrogen (MH) storage tank integrated with cooling system of the fuel cell stack. The power module provided stable operation of STILL-RX60-30L forklift during 60 complete cycles under VDI2198/VDI60 standard protocol.



Figure 1. Left: frame of the power module with installed MH tank (bottom) and gas buffer (top left). Middle: installation of the assembled power module into forklift compartment. Right: VDI2198/VDI60 tests of the forklift with the power module

B. Hydrogen refuelling station with integrated metal hydride compressor

In 2012–2015, HySA Systems developed a novel prototype hydrogen refuelling station with integrated MH hydrogen compressor which uses low-grade heat available at the site of industrial customer (steam at T~130°C) for the heating of the MH material to provide H₂ desorption at P≥200 bar. The station (dispensing pressure up to 185 bar) is intended for the refuelling of hydrogen fuel cell forklifts with “hybrid” MH and compressed hydrogen gas (CGH₂) on-board storage tanks. Since September 2015 the refuelling station is in 24/7 uninterrupted operation at Impala Platinum refineries in Springs, South Africa [2].



Figure 2. Refuelling of the fuel cell forklift with “hybrid” MH + CGH₂ hydrogen storage at Impala Platinum refineries

C. Metal hydride hydrogen storage tank for light fuel cell vehicle

The metal hydride hydrogen storage tank for light vehicle (electric scooter with fuel cell range extender) was developed in 2018 by HySA Systems, in collaboration with TF Design (Pty) Ltd, South Africa [3]. The tank (~1 Nm³ H₂) uses multi-

component AB₂-type hydrogen storage alloy manufactured by HySA Systems and comprises of two cylindrical aluminium canisters filled with MH powder and equipped with both internal and external fins for augmentation of heat supply and removal, which is provided from the outside using flow of ambient air. Two MH tanks installed on-board the scooter supply H₂ fuel to 1 kW open cathode fuel cell stack thus providing driving range extension from 70 km (original battery version) to 200 km (FC range extender with MH H₂ storage)



Figure 3. Fuel cell scooter (top) with MH hydrogen storage tank (bottom).

III. CONCLUSION

HySA Systems have successfully developed and demonstrated several hydrogen fuel cell prototypes, some in real-world environments. Some results from these developments are presented here

ACKNOWLEDGMENT

The authors would like to thank the Department of Science and Technology in South Africa (DST) for financial support under the Hydrogen and Fuel Cell Technologies RDI Programme (HySA).

REFERENCES

1. B.G. Pollet, S. Pasupathi, G. Swart, M. Lototskyy, M. Williams, P. Bujlo, S. Ji, V. Linkov, B.J. Bladergroen. *Platinum Met. Rev.* 58 (2014) 68-81
2. M. Lototskyy, M.W. Davids, D. Swanepoel, G. Louw, Y. Klochko, F. Smith, F. Haji, I. Tolj, S. Chidziva, S. Pasupathi, V. Linkov, *Int. J. Hydrogen Energy* (2019) DOI: 10.1016/j.ijhydene.2019.05.133
3. M.W. Davids, M. Lototskyy, M. Malinowski, D. van Schalkwyk, A. Parsons, S. Pasupathi, D. Swanepoel, T. van Niekerk, *Int. J. Hydrogen Energy* 44 (2019) 29263-29272

HIGH PERFORMANCE PEM ELECTROLYSER FOR POWER-TO-GAS APPLICATIONS - HPEM2GAS

Antonino Salvatore Arico'
CNR-ITAE, Via Salita S. Lucia, 5 - 98126 - Messina, (Italy)

Abstract – Advanced water electrolysers should provide proper dynamic behaviour to support grid-balancing services and thus address the rapid increase of intermittent renewable power sources interfaced to the grid. The HPEM2GAS project has developed an advanced 180 kW PEM electrolyser optimised for grid balancing service. The electrolyser is based on an improved stack design and components including Aquivion® membranes and core-shell/solid solution electrocatalysts. Several strategies have been applied to lower the overall cost. These specifically regard a three-fold increase in current density whilst maintaining high efficiency, a material use minimisation approach in terms of reduced membrane thickness whilst keeping the gas cross-over low, and reducing the precious metal loading. Utilizing a nanosized Ir-Ru oxide solid solution anode catalyst and a supported Pt/C cathode catalyst, in combination with the Aquivion® membrane, gave excellent electrolysis performances exceeding 3 A cm^{-2} at 1.8 V terminal cell voltage (~80 % efficiency) at 80 °C in the presence of a noble metal loading of 1.2 mg cm^{-2} and degradation rate $<5\text{-}10 \mu\text{V/h}$.

Keywords – Water Electrolysis, Hydrogen production, Polymer Electrolyte Membrane, Electrocatalysis.

I. INTRODUCTION

Hydrogen produced from water electrolysis can play a significant role as energy storage medium [1, 2]. Electrolysis can support the electricity grid in terms of power quality, frequency and voltage control, peak shaving, load shifting and demand response. In this regard, electrolysers should be designed to follow the variable energy generation profile of renewable power sources locally available and to adapt to the intermittent profile of electricity supply.

The overall objective of the HPM2GAS project was to develop, validate and demonstrate robust, flexible and rapid-response self-pressurising PEM electrolyser technology based on advanced cost-effective components with dynamic properties for interfacing to the grid.

The project addressed both stack and balance of plant

innovations and culminated in an advanced 180 kW PEM electrolyser demonstrated in Emden (Germany). In particular, the electrolyser developed consisted of an advanced BoP and improved stack design and components (e.g. bipolar plates, membranes, electrocatalysts).

Several strategies have been applied to lower the overall cost to enable widespread utilisation of the technology. These primarily deal with a three-fold increase in current density (resulting in the proportional decrease in capital costs) whilst maintaining cutting edge efficiency and applying a material use minimisation approach in terms of reduced membrane thickness whilst keeping the gas cross-over low, and reducing the precious metal loading. Further, improving the stack lifetime and reducing system complexity without compromising safety or operability have been addressed.

II. RESULTS AND DISCUSSION

Advanced catalysts and membranes were developed in the HPEM2GAS project by CNR-ITAE and Solvay, respectively. Short-side chain (SSC) perfluorosulfonic acid (PFSA) Aquivion® membranes and ionomers were developed and scaled up for this application.

Utilizing a nanosized $\text{Ir}_{0.7}\text{Ru}_{0.3}\text{Ox}$ solid solution anode catalyst and a supported Pt/C cathode catalyst, in combination with the Aquivion® membrane, gave excellent electrolysis performances exceeding 3 A cm^{-2} at 1.8 V terminal cell voltage (~80% efficiency vs. HHV at cell level) at 90 °C.

Low degradation rate at 3 A cm^{-2} at 80 °C was recorded at cell level. A scaling up of the selected formulations and optimisation of the manufacturing procedure of the catalyst inks and membrane-electrode assemblies was carried out.

Stack development activities at ITM produced an efficient and compact design. To eliminate expensive machining costs, traditional bipolar plates have been replaced for lower-cost components and injection-moulded parts.

The ITM stack design developed in HPEM2GAS was operated at high differential pressure operation, with hydrogen at working pressure and oxygen at ambient pressure.

An advanced ITM 75 cells stack, equipped with 415 cm² active area MEAs produced by IRD, was assembled and tested.

Cells containing coated components typically displayed a relatively stable voltage, indicating that the coating used was able to provide adequate protection. Stack tests with coated components showed an average voltage degradation rate for the stacks ≤ 5 $\mu\text{V}/\text{h}/\text{cell}$ when operated at 3 A cm⁻², 50–55°C.

Short periods of increased current density from 3 A cm⁻² to 4.5 A cm⁻² appeared to have had little effect on the voltage.

Stack and electrolyser assessment was carried out by ITM showing efficiency of 81% vs. HHV of H₂ at 3 A cm⁻² at stack level at 75°C with a loading of 0.3 mg PGM catalyst/W (Fig.1).

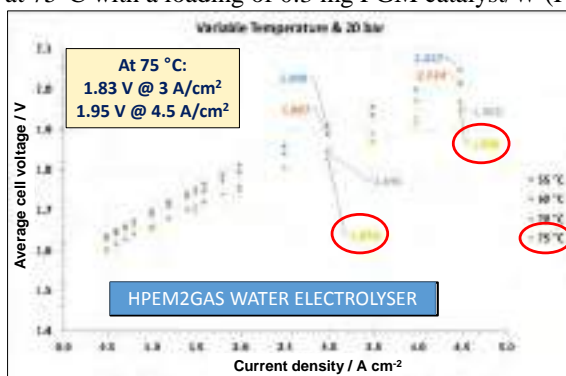


Fig. 1. HPEM2GAS Water electrolysis stack polarisation curves at 20 bar

System efficiency of 72 % vs HHV H₂ was achieved at 3 A cm⁻², at an operating temperature of 55°C.

Differential pressure operation was demonstrated for the novel stack geometry at 20-30 bar across a wide range of the load curve. Operation at 50 bar differential pressure, at the nominal current density of 3 A cm⁻², was also assessed. According to a cost analysis, the system cost is estimated in 1000 €/kW CAPEX with 20% stack contribution to the total cost.

Regarding field testing activities, interfaces to local construction ground in Emden (Germany) was finalized by SWE and test scenarios were defined by SWE and HS EL. The electrolysis system was operated at 20 bar at the field testing site. The pressure was reduced to 10 bar before being injected into the gas grid operating at 8.5 bar.



Fig. 1. HPEM2GAS Water electrolysis plant installed in Emden (Germany)

III. CONCLUSION

The HPEM2GAS project was addressing research and development in the field of PEM water electrolysis. Membrane-electrode assemblies (MEAs) designed for polymer electrolyte membrane (PEM) water electrolysis, based on Aquivion®, perfluorosulfonic acid (PFSA) membrane, with various cathode and anode noble metal loadings, were investigated in terms of both performance and durability. Utilizing a nanosized Ir-Ru oxide solid solution anode catalyst and a supported Pt/C cathode catalyst, in combination with the Aquivion® membrane, gave excellent electrolysis performances exceeding 3 A cm⁻² at 1.8 V terminal cell voltage (~80 % efficiency) at 80 °C in the presence of a noble metal loading of 1.2 mg cm⁻². A very small loss of efficiency, corresponding to 30 mV voltage increase, was recorded at 3 A cm⁻² using a total noble metal catalyst loading of less than 0.5 mg·cm⁻². Steady-state durability tests, carried out for >1000 h at 3 A cm⁻², showed excellent stability for the MEA with low noble metal catalyst loading (cell voltage increase ~5-10 $\mu\text{V}/\text{h}$). Therefore, operation at very high current densities is possible in the presence of low catalyst loading and a reduction of capital costs may be achieved without compromising significantly the stack durability.

ACKNOWLEDGMENT

HPEM2GAS project has received funding from Fuel Cells and Hydrogen 2 Joint Undertaking under grant agreement No 700008. This Joint Undertaking receives support from the European Union's Horizon 2020 research and innovation programme and Hydrogen Europe and Hydrogen Europe Research. The HPEM2GAS project partners: ITM POWER, SOLVAY SPECIALTY POLYMERS, IRD FUEL CELLS A/S, STADTWERKE EMDEN, HOCHSCHULE EMDEN/LEER, UNIRESEARCH BV are strongly acknowledged.

REFERENCES

- Briguglio, N., Siracusano, S., Bonura, G., Sebastián, D., Aricò, A.S. Flammability reduction in a pressurised water electrolyser based on a thin polymer electrolyte membrane through a Pt-alloy catalytic approach (2019) Applied Catalysis B: Environmental, 246, pp. 254-265.
- [1] Siracusano, S., Oldani, C., Navarra, M.A., Tonella, S., Mazzapioda, L., Briguglio, N., Aricò, A.S. Chemically stabilised extruded and recast short side chain Aquivion® proton exchange membranes for high current density operation in water electrolysis (2019) Journal of Membrane Science, 578, pp. 136-148.
- [2] Siracusano, S., Hodnik, N., Jovanovic, P., Ruiz-Zepeda, F., Šala, M., Baglio, V., Aricò, A.S. New insights into the stability of a high performance nanostructured catalyst for sustainable water electrolysis. (2017) Nano Energy, 40, pp. 618-632.

EFFECTS OF CATALYST SUPPORT MATERIALS AND IONOMER AMOUNTS IN THE CATHODE CATALYST LAYERS ON MEMBRANE ELECTRODE ASSEMBLY PERFORMANCES AT HIGH CURRENT LOADS

P. K. Mohanta*, M. S. Ripa, D. Yazili, F. Regnet and L. Jörissen

Department of fuel cell fundamentals (ECG), Zentrum für
Sonnenenergie-und Wasserstoff-Forschung Baden-Württemberg,
Helmholtzstrasse 8, 89081 Ulm, Germany

Abstract – We have compared the MEA performances of 30 wt% Pt containing homemade and commercial catalysts while changing the cathode catalyst layers in terms of supports and ionomer contents. The MEA prepared with the catalyst supported on low BET surface areas carbon black (CB) showed the highest performance at high current load, compared to the MEA prepared with catalysts supported on medium and high BET surface area CB, although the former catalysts showed lower ECSA as well as lower ORR activities. This indicates, the MEA performance not only depends on the intrinsic properties of the catalysts but also on the catalyst layer compositions and morphologies. We have also found a correlation between the ionomer content on the catalyst layers and the MEA performance in this work. The catalyst supported on the highest BET surface areas CB, the highest amount of ionomer is needed and vice versa to achieve the highest MEA performance.

Index Terms – MEA, PEMFC, Catalyst supports, Catalyst layers

I. INTRODUCTION

Membrane electrode assembly (MEA) performance of a low temperature PEMFC is highly dependent on the catalyst types, catalyst layers morphologies, membrane types and operating conditions. Due to the contribution of over-potentials (activation, ohmic and mass transport), the achievable voltages of MEAs are always lower than the theoretical voltages. In this work we designed the cathode catalyst layers with high to low BET surface areas CB supported 30 wt % Pt containing catalysts to investigate the MEA performance at high current loads (>1 A/cm²). A high and a medium BET surface area CB supported commercial Pt electrocatalysts were taken as references. In addition, same Pt containing electrocatalysts supported on very low to medium BET surface areas CB were prepared by using an already developed polyol process [1].

II. EXPERIMENTAL

A Carbon Black (Vulcan XC72, Cabot), a Timcal super C 65 (Imerys) and a stable carbon (SC1) support materials were

chosen for the investigation. Both Timcal and SC1 materials were oxidized in an air oven at 550°C for 1 hour in order to increase the wettability of the support materials. CB material was used as received. BET surface areas of the support materials were measured via N₂ adsorption by using a Sorptomatic 1990 device.

30 wt.% Pt containing catalysts were prepared by using our already developed modified polyol process. A high BET surface area CB (700 m²/g) and a medium surface area CB (250 m²/g) supported Pt electrocatalysts from the company Tanaka (TEC10E30E and TEC10V30E respectively) were taken as reference catalysts for comparison.

Homemade catalysts were annealed at 250°C in H₂/Ar atmosphere and then characterized by measuring Pt content (via ICP-OES), Pt particle sizes (via XRD) and oxygen reduction reaction activities (via RDE).

MEA performance tests of the catalysts were performed in a Fuel Cell Technology single cell of 25 cm² active surface areas with a triple serpentine flow field and in a greenlight innovation test station (G20). Catalyst coated membrane were prepared with Gore select (15 μm) membrane using an airbrush techniques. Keeping anode catalyst layer constant (Tanaka, TEC10V30E), we only varied the cathode catalyst layers with the investigated catalysts. Pt loadings of the MEAs were also kept constant; 0.1 and 0.25 mg/cm² for the anode and the cathode respectively. Pure hydrogen and air were used as fuels. After completion of each single cell performance tests, CVs and electrochemical impedance spectra's (EIS) of the MEAs were also measured.

III. RESULTS AND DISCUSSION

Table1 shows the list of support materials and catalysts that were used for the investigation, and their characterization results. Pt content of the homemade catalysts shows unique as desired, however, Pt particle size of the catalysts are increased as the BET surface areas of the support materials are decreased. Since Pt particles stayed closer at low BET surface area supported

catalysts, resulting agglomeration during synthesis and/or during annealing process. As expected, unlike reference catalysts, homemade catalysts with smaller Pt particles are showing higher ECSA as well as ORR activities in 0.1M HClO₄ electrolyte in RDE setup.

TABLE I
LIST OF CATALYSTS AND THEIR CHARACTERIZATION RESULTS

Supports	Supports BET [m ² /g]	Catalysts	Pt content [wt%]	Pt particle [nm]	ECSA [m ² /g-Pt]	Mass activities @ 0.9V vs RHE [A/g-Pt]
Vulcan XC72	192	Pt/CB	28.2	2.9	102	468
Timcal super C65	62	Pt/C65	29.1	3.3	78	294
Stable Carbon 1	32	Pt/SC1	28.9	5.6	47	229
Vulcan XC72	250	TEC10V30E (TKV)	28.9	<2	113	597
Carbon black	700	TEC10E30E (TKE)	28.2	<2	120	584

It was found necessary to optimize the ionomer to carbon ratio (I/C) for each catalyst in order to increase the so-called triple phase boundaries and to reduce the oxygen transport resistances [2-3], which is found highly dependent on the BET surface areas of the support materials, the catalyst supported on the highest BET surface area, the highest amount of I/C is needed and vice versa to achieve highest MEA performance (Table 2). Table 2 is also showing the cathode catalysts ECSA while using MEA test which are lower than the liquid electrolyte, nevertheless they are comparable.

TABLE 2
OPTIMUM I/C AND MEASURED ECSA OF THE CATHODE CATALYSTS (MEA)

Supports	Supports BET [m ² /g]	Catalysts	I/C	ECSA [m ² /g-Pt]
Vulcan XC72	192	Pt/CB	0.72	70
Timcal super C65	62	Pt/C65	0.5	64
Stable Carbon 1	32	Pt/SC1	0.37	43
Vulcan XC72	250	TKV	0.72	94
Carbon black	700	TKE	0.74	89

Figure 1 is showing the I-V characteristics of the MEAs prepared with the investigated catalysts with optimized I/C ratio on the catalyst layers (see table 2). The MEA prepared with the Pt/C65 catalyst shows the highest performance at high current densities (>1A/cm²), followed by TKV, Pt/CB, TKE and Pt/SC1. However, at low current densities (<0.5 A/cm²), the MEA performance are highly dependent on the Pt particle size, ECSA, ORR activities or more specifically intrinsic properties of the catalysts.

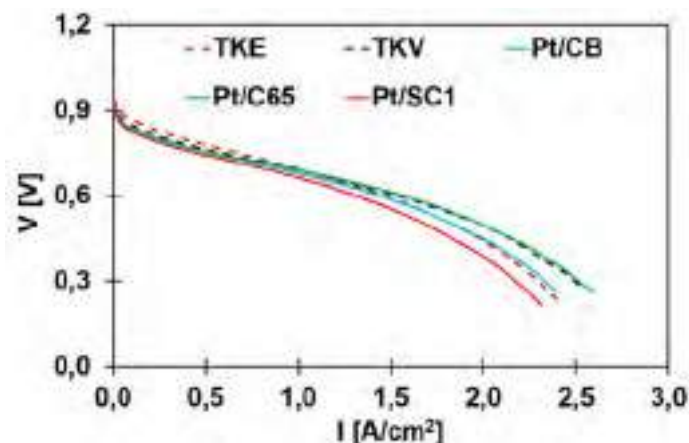


Fig. 1. I-V curves of the MEAs, Operating Conditions: T cell =80°C, A. dp=C.dp=80°C A.stoi=1.3, C.stoi = 3,150kPa, Pt loading: 0.1 mg/cm² (Anode) and 0.25 mg/cm² (cathode), Gore select membrane (15µm)

IV. CONCLUSION

Homemade Pt/C65 catalyst has been found excellent MEA performance as TKV reference catalyst, although it shows lower ECSA and ORR activities compared to the traditional CB supported catalysts. In this work we have established a correlation of MEA performance with the ionomer content on the catalyst layers and BET surface areas of the supports. At high current load, mass transport effect are found more prominent than the initial catalytic activities. The type of carbon support material has also a significant influence on the high current density part of the performance curve. Overall, catalyst, catalyst supports, electrode compositions and membrane are interacting in a complex manner which needs further understanding.

ACKNOWLEDGMENT

Funding of the project ASI (03B10103A/03B10103A2) by the Federal Ministry of Education and Research (BMBF) is gratefully acknowledged.

REFERENCES

- [1] Paritosh Kumar Mohanta, Fabian Regnet and Ludwig Jörissen, *Materials* 2018, 11, 907
- [2] A. Kongkanand, M.F. Mathias, *J. Phys. Chem. Lett.*, 2016, 7 (7), pp 1127–1137
- [3] A. Orfanidi, P. Madkikar, H. A. El-Sayed, G. S. Harzer, T. Kratky, and H. A. Gasteiger, *Journal of The Electrochemical Society*, 164 (4) F418-F426 (2017)

CHEMICAL CONVERSION COATING TECHNIQUE IN THE PREPARATION OF STRUCTURED CATALYSTS FOR THE CO-WATER GAS SHIFT REACTION

V. Palma, C. Ruocco, M. Martino

University of Salerno, Department of Industrial Engineering,
via Giovanni Paolo II 132, 84084, Fisciano, Italy

Abstract – In this study chemical conversion coating has been investigated as preparative technique for structured catalysts, based on aluminum structured carriers. The structured catalysts have been prepared by ceria coating of open cell aluminum foams through a surface protective technique. The resulting coated carriers were impregnated with a platinum salt precursor solution, and the resulting catalyst was tested in water gas shift reaction. The activity tests showed that the textural proprieties of the structured carriers play a crucial role in the performance of the catalysts.

Index Terms – Chemical conversion coating, structured catalysts, water gas shift reaction, nanocoating.

I. INTRODUCTION

Hydrogen is by far the most abundant element in the solar system and is the feedstock in several industrial processes, moreover it has a high energy density and low environmental impact. For these reasons it is considered the best candidate as the energy vector in the future. Hydrogen can be produced from fossil and renewable sources, however actually the most is obtained from fossil sources. Many processes are involved in the production of hydrogen, the syngas obtained from reforming stages is reacted in two stages of water gas shift, moreover to obtain high purity hydrogen a further stage of methanation or preferential oxidation, or the use of pemselective membranes is needed. The overall process is therefore effective but very inefficient, particularly when distributed hydrogen production is required. In this case the use of small compact reactors is indeed desirable. Among the processes involved, the water gas shift stage is certainly the most critical. Water gas shift reaction is an exothermic reversible reaction therefore, in adiabatic conditions, the heat of the reaction induces a thermal gradient on the catalytic bed. The

universally used strategy to overcome these limitations, is the multi-stage process, with intermediate cooling. Once again this configuration is effective but inefficient. Our group focused the attention on the use of structured catalysts with the intention of intensifying the water gas shift process. In particular the use of conductive carrier allows for a redistribution of the heat of the reaction, on the catalytic bed, with kinetic and thermodynamic improvements [1]. Structured catalysts are generally prepared by washcoating, that provides the formation of a layer of alumina or silica on the surface of the carrier. This layer makes compatible the surface with the active components and provides high specific surface area to the final catalyst, but unfortunately it presents many disadvantages, such as low thermal and mechanical resistance and is not catalytically inert. In this paper we show the results of a study on the use of chemical conversion coating as technique to prepare structured catalysts based on metallic carriers. Chemical conversion coating is used in corrosion, because it allows to realize a protective layer of oxide on the metallic surface [2].

II. EXPERIMENTAL

A. Catalysts preparation

Three open cell aluminum foams (Table I), with different porosity (Fn, n=5,10,40 PPI), were shaped to obtain a cylinder of 13 mm of diameter and 103 mm of length.

TABLE I
TEXTURAL PROPERTIES OF THE FOAMS

Sample	Porosity [PPI]	Relative density [%]	Surface area [in ² /in ³]
F40	40	10	49
F10	10	10	22
F5	5	10	10

The foams were firstly degreased with acetone and with a sodium hydroxide solution (5 wt %) for 1 minute, finally etched with nitric acid solution (35 wt %) for 1 minute. After each treatment the aluminum structure was washed with distilled water and, at the end of the pre-treatments, it was immersed in the chemical bath. The bath was composed by $\text{CeCl}_3 \cdot 7\text{H}_2\text{O}$, H_2O_2 35 wt % and water, in a weight ratio 1/3/75, and acidified with HCl (pH=3). The treatment was carried out at 50°C and repeated 4 times for 2 hours, and the resulting structure was dried at 120°C for 2 hours. The resulting coated foam was then loaded with platinum by impregnation with a solution of tetrammineplatinum (II)nitrate, dried at 120°C for 2 hours and calcined at 450°C for 3 hours [2].

B. Characterization techniques

The B.E.T. specific surface areas were measured with a Costech Sorptometer 1040 (Costech International). The mechanical resistance of the coating was evaluated by means of the ultrasound adherence test with an ultrasonic bath CP104 (EIA S.p.A.); the catalysts were dipped in ethanol at ambient temperature and submitted to the ultrasound for 30 minutes. The XRD diffractograms were obtained by means of a Bruker D8 Advance, with a Cu K α radiation source (35 kV; 40 mA) in the 2θ range 20-80°, (Stp= 737; Stp size=0.0814; t/Stp 0.5 s). The crystallite dimensions were calculated by applying the Scherrer equation to the peaks of the corresponding diffractograms. The chemical composition was evaluated by means of ARL QUANT'X ED-XRF spectrometer (Thermo Scientific).

C. Activity tests

The catalysts were reduced with a stream of 500 Ncc/min containing 5 vol% of H_2 in N_2 , in the temperature range of 20-450°C, with an heating rate of 10°C/min. The activity tests were carried out at atmospheric pressure, in the temperature range of 300-400°C, with a reaction mixture of 5 % CO , 15 % H_2O and 80 % N_2 , in a stainless steel tubular reactor with an internal diameter of 22 mm and 400 mm long, at a WHSV of 2.4 $\text{g}_{\text{CO}}/\text{g}_{\text{Pt/CeO}_2} \cdot \text{h}^{-1}$. The product composition was monitored, on dry basis, by means of an ABB system equipped with the non-dispersive infrared analyser Uras 14 for CO , CO_2 and CH_4 and a thermal conductivity detector Caldos 17 for H_2 .

III. RESULTS AND DISCUSSION

The surface area measurements highlighted a progressive increasing of the surface area of the structured catalysts with the increase of the PPI of the foam. This results were attributed to the selected coating technology: chemical conversion coating give rise to the formation of a protective layer on metallic surfaces, so the maximum loadable amount depends on

the surface area of the metal foam, that increase with the increase of the porosity. The ultrasound adherence tests showed no weight loss of the coating, highlighting the strength of the coating. The XRD diffractograms showed the presence of cubic ceria and metallic platinum on the surface of the catalysts. The XRF analysis were in agreement with the B.E.T. surface area results, to the increase of the porosity and of the surface area, the loading of the active components increases.

The activity tests were performed at the same weight hourly space velocity, calculated with respect the lonely active components loaded on the foam, to highlight the effect of the structured carrier. The activity tests showed the CO conversion dependence from the porosity of the parent foam; the highest conversion was obtained with the catalyst prepared with the 40 PPI foam, on the contrary the worst performance was obtained with the catalyst prepared with the 5 PPI foam, at the same temperature. The time on stream tests, carried out on 40 PPI derivate catalyst, showed that these catalysts are extremely stable; in the first five hours there happened a lowering of the CO conversion of less than 10% followed by a stable conversion in the following 30 hours. With all the catalysts no methanation occurred, highlighting a high hydrogen selectivity. As previously stressed the activity tests were carried out at the same space velocity, therefore no dependence on the amount of active components is expected. The dependence of the activity from the porosity of the parent foam was explained as the results of diffusion phenomena. In our tests two phenomena are in competition, the reaction and the diffusion: for the catalysts obtained with low porosity foams, such as 5 and 10 PPI, the diffusion is prevailing with respect the reaction, on the contrary for the catalyst obtained with 40 PPI, the reaction is prevailing with respect the diffusion.

IV. CONCLUSION

In this work we have shown that is possible to use chemical conversion coating as a preparation technique for structured catalysts, on metal carriers. Activity tests have shown a direct dependence between the performance of the catalyst and the porosity of the parent carrier, highlighting the occurrence of diffusion phenomena for low porosity foams.

REFERENCES

- [1] Palma, V., Pisano, D., Martino, M., Structured noble metal-based catalysts for the WGS process intensification, International Journal of Hydrogen Energy, Volume 43, 2018, Pages 11745-11754.
- [2] Palma, V., Martino, M., Truda, I., Nano- CeO_2 Coating on Aluminum Foam Carriers for Structured Catalysts Preparation, Chemical Engineering Transactions Volume 73, 2019, Pages 127-132.

EFFICIENT CATALYSTS FOR HYDROGEN PRODUCTION VIA ETHANOL REFORMING IN A FLUIDIZED BED REACTOR

V. Palma, C. Ruocco, and M. Martino

Department of Industrial Engineering, University of Salerno, Via
Giovanni Paolo II 132, 84084 Fisciano (SA), Italy

Abstract – In this study, oxidative steam reforming of ethanol has been investigated over bimetallic Pt-Ni as well as Ru-Ni catalysts supported on a CeO₂-SiO₂ mixed oxide. The samples have been prepared by wet impregnation by selecting different noble metals loading (0-3 wt%) and their stability was studied in a fluidized bed reactor at 500°C, steam to ethanol ratio of 4 and oxygen to ethanol ratio of 0.5 under a very low contact time (50 ms). The Pt series displayed the highest hydrogen yield and very low carbon formation rates during 25 hours of time-on-stream, with the monometallic Ni/CeO₂-SiO₂ catalyst performing better than the Ru-based samples.

Index Terms – fluidized bed, hydrogen, reforming, stability.

I. INTRODUCTION

Electrical energy generation in fuel cells devices is receiving increasing attention compared to the conventional combustion engines, due to the higher energy conversion efficiency and the lower pollutants generation. However, in order to propose a reliable solution to the envisaged environmental problems, the hydrogen production from widely available renewables is required. For example, bioethanol and biodiesel are already in the distribution grid for automotive purposes in many countries. In this regard, it seems highly realistic to apply the mature technology of reforming for renewable substrates [1]. In this work, different Ni-based catalysts supported on CeO₂-SiO₂, prepared at different noble metal (Platinum or Ruthenium) loading (0-3 wt%) were employed for oxidative steam reforming of ethanol in a fluidized bed reactor. In a previous work [2], it was highlighted that low noble metal loadings are sufficient to assure high activity for the investigated reaction in the interval 300-600°C, even at very low contact time (50 ms). However, the stability performance of the bimetallic catalysts can be itself affected by the Pt or Ru content in the sample. In this regard, the proper selection of

noble metal loading is crucial, due to its heavy effect on catalyst final price.

II. EXPERIMENTAL

A series of bimetallic Pt-Ni and Ru-Ni supported on CeO₂-SiO₂ was prepared by wet impregnation. The silica support was impregnated with a cerium acetylacetonate solution to yield 30wt% CeO₂ on SiO₂. Thereafter, drying overnight at 120°C and calcination at 600°C for 3 h occurred. Ni (10wt%) and Pt or Ru (0-3wt%) were sequentially impregnated on the support starting from the corresponding salt precursors (nickel nitrate, Platinum chloride, Ruthenium chloride).

The specific surface areas (SSA, m²·g⁻¹) of fresh and spent samples were measured through the Costech Sorptometer 1040 by applying the BET method; the carbonaceous deposits on the catalysts after stability test were measured in a TA Instrument Q600 (heating rate from 25 to 1000°C: 10°C·min⁻¹; total air flow-rate: 50 Ncm³·min⁻¹). The last data were shown in terms of carbon formation rate (CFR), defined as reported in [3].

Catalytic performances for oxidative steam reforming reaction were evaluated in a fluidized bed reactor under atmospheric pressure at 500°C. The liquid mixture, stored in a tank under N₂ pressure, was sent to a boiler for vaporization; Argon was used as diluent while oxygen was directly fed to the reactor in order to assure a final composition of 10% C₂H₅OH, 40% H₂O, 5% O₂, 45% Ar. The analysis of gas composition exiting the reactor was performed through a Mass Spectrometer provided by Hiden. Durability tests were performed for 25 h under a quite low contact time [3] (weight hourly space velocity WHSV was fixed to 62 h⁻¹), selected to eventually accelerate catalyst deactivation. The results were compared in terms of hydrogen yield (Y, Eq. 1)

$$Y_{H_2} = \frac{mol_{H_2,out}}{6 \cdot mol_{C_2H_5OH,in}} \quad \text{Eq. 1}$$

III. RESULTS AND DISCUSSION

The results of stability tests performed over the bimetallic catalysts prepared at different noble metals loadings are shown in Fig. 1 in terms of hydrogen yield as a function of time-on-stream. At the beginning of the test, only few samples displayed high H₂ production rates, close to the values predicted by thermodynamic equilibrium. On the other hand, all the prepared samples, whatever the noble metal loading, were characterized by a decreasing trend in hydrogen yield, ascribable to catalyst deactivation phenomena occurring during the stability test.

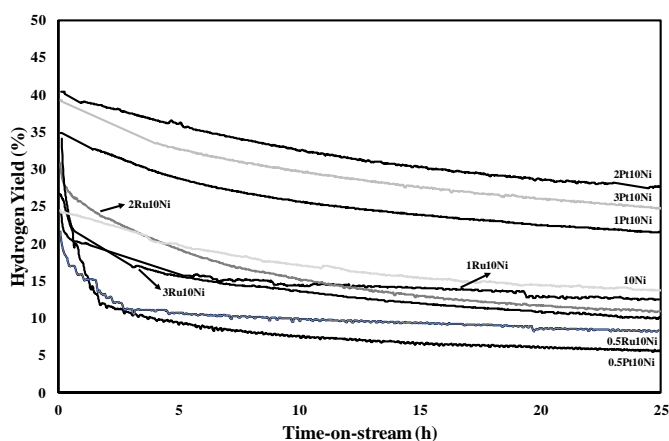


Fig. 1. Hydrogen yield as a function of time-on-stream during oxidative steam reforming of ethanol in a fluidized bed reactor; 10% C₂H₅OH, 40% H₂O, 5% O₂, 45% Ar, 500°C, 1 atm, 62 h⁻¹.

However, the experimental results revealed that Pt choice instead of Ru as well as the deposition of different metal contents on the Ni/CeO₂-SiO₂ sample results in a markedly different product selectivity. The best results in terms of hydrogen yield (Fig. 1) were recorded over the Pt-series: for the 2Pt10Ni sample, the hydrogen production rate was slightly lower than 30% after 25 hours of test. Interestingly, the monometallic catalyst containing only Nickel displayed a higher H₂ yield compared to the 0.5Pt10Ni catalyst, which, together with the 0.5Ru10Ni sample, reached the worse performances under the investigated operative conditions (Y lower than 10% at the end of the test). In particular, the addition of Ru to the 10Ni/CeO₂-SiO₂ catalyst had no positive effect on hydrogen production and Y profiles as a function of time-on-stream for those bimetallic catalysts were lower than that measured for the Pt-series. Looking at Ru-based samples, the highest performances in terms of hydrogen production were observed over the 1Ru10Ni catalyst while, for the Pt series, the 2Pt10Ni sample displayed the most promising results in terms of hydrogen production rates.

Table I shows the results of characterization measurements, in terms of specific area of fresh and spent catalysts as well as carbon formation rates evaluation. All the fresh samples

displayed high specific surface areas, ascribable to the mixed oxide CeO₂-SiO₂ [3]. However, a surface area reduction was observed as a consequence of stability tests, which was ascribed to the formation of carbonaceous deposits on catalyst surface, as attested by the trend of CFR values. In fact, higher carbon formation rates corresponded to more pronounced SSA variations. The most active sample (2Pt10Ni), for example, was subjected to an area reduction of only 15% coupled to a CFR of $1.5 \cdot 10^{-6} \text{ g}_{\text{coke}} \cdot \text{g}_{\text{catalyst}}^{-1} \cdot \text{g}_{\text{carbon, fed}}^{-1} \cdot \text{h}^{-1}$. Conversely, for the catalysts reaching the worst performances (0.5Ru10Ni and 0.5Pt10Ni), CFR was almost five times higher and the SSA variation was more marked (>30%).

TABLE I
RESULTS OF BET ANALYSIS AND CARBON CONTENT MEASUREMENTS.

Sample	SSA fresh (m ² ·g ⁻¹)	SSA spent (m ² ·g ⁻¹)	CFR ($\text{g}_{\text{coke}} \cdot \text{g}_{\text{catalyst}}^{-1} \cdot \text{g}_{\text{carbon, fed}}^{-1} \cdot \text{h}^{-1}$)
10Ni	230	182	$3.9 \cdot 10^{-6}$
0.5Pt10Ni	213	145	$8.4 \cdot 10^{-6}$
1Pt10Ni	214	179	$2.4 \cdot 10^{-6}$
2Pt10Ni	226	191	$1.5 \cdot 10^{-6}$
3Pt10Ni	227	186	$2 \cdot 10^{-6}$
0.5Ru10Ni	212	142	$7.9 \cdot 10^{-6}$
1Ru10Ni	208	143	$5.1 \cdot 10^{-6}$
2Ru10Ni	210	145	$5.8 \cdot 10^{-6}$
3Ru10Ni	218	149	$6.3 \cdot 10^{-6}$

IV. CONCLUSION

In this work, oxidative steam reforming of ethanol has been studied in a fluidized bed reactor at 500°C at very low contact time over a series of Pt and Ru based catalysts, supported on Ni/CeO₂-SiO₂ systems. The catalysts containing Pt (1-3 wt%) displayed the highest hydrogen yield (>25% after 25 hours of time-on-stream). Conversely, the bimetallic catalyst containing only Ni performed better than the Ru-based series, with the worst results recorded over the 0.5Ru10Ni and 0.5Pt10Ni catalysts. Spent catalyst characterization confirmed a different coke formation tendency of the catalysts: the 2Pt10Ni sample displayed a CFR almost 5 times lower than the catalysts containing 0.5 wt% of noble metals.

REFERENCES

- [1] Ramirez de la Piscina, P., Homs, N., Use of biofuels to produce hydrogen (reformation processes), Chemical Society Reviews, Volume 37, 2008, Pages 2459-2467.
- [2] Ruocco C., Palma V., Ricca A., Kinetics of Oxidative Steam Reforming of Ethanol Over Bimetallic Catalysts Supported on CeO₂-SiO₂: A Comparative Study, Topics in Catalysis, Volume 62, 2019, Pages 467-478.
- [3] Ruocco C., Palma V., Ricca A., Hydrogen production by oxidative reforming of ethanol in a fluidized bed reactor using a Pt-Ni/CeO₂-SiO₂ catalyst, International Journal of Hydrogen Energy, Volume 44, 2019, Pages 12661-12670.

DEGRADATION FACTORS OF CATHODE DURING OPERATION OF SOLID OXIDE FUEL CELLS

Koichi Eguchi, Toshiaki Matsui, and Hiroki Muroyama

Department of Energy and Hydrocarbon Chemistry,
Graduate School of Engineering, Kyoto University
Nishikyo-ku, Kyoto 615-8510, (Japan)

Microstructure change of perovskite-type oxides of $(\text{La,Sr})(\text{Co,Fe})\text{O}_{3-\delta}$ (LSCF) and $(\text{La,Sr})\text{MnO}_{3+\delta}$ (LSM) have been investigated as cathode for solid oxide fuel cells. The focused ion beam-scanning electron microscopy (FIB-SEM) provides essential information to understand the quantitative relationship among the microstructure, performance, and stability. In this study, the microstructural change of the perovskite oxide cathode with an elapsed time of discharge was quantitatively analyzed by the FIB-SEM technique. With initial current passage on the activation process of LSM cathode interface with yttria-stabilized zirconia (YSZ) has been significantly roughened. Microstructure of LSCF did not change significantly. The secondary phase of SrZrO_3 was formed with the current passage.

Solid Oxide fuel cell, SOFC, air electrode, microstructure

1. Introduction

Solid oxide fuel cells (SOFCs) are one of attractive power generation systems. Presently, this system is in an advanced stage of development for household application and gas turbine combined systems. Durability and reliability of SOFCs are urgent requirement for commercialization. Strontium-doped lanthanum manganite, $\text{La}_{1-x}\text{Sr}_x\text{MnO}_3$ (LSM), and strontium-doped lanthanum cobaltite-ferrite, $\text{La}_{1-x}\text{Sr}_x\text{Co}_{1-y}\text{Fe}_y\text{O}_3$ (LSCF), are the popular air electrode (cathode) materials for the YSZ electrolyte. On the perovskite oxide catalyst, gaseous oxygen is reduced to oxide ions. The LSCF cathode is more active for oxygen reduction than LSM, but less stable at elevated temperatures. Therefore, LSM has been used for high temperature application at ca. 900°C , while the LSCF electrode has been employed in the intermediate temperature region of $650\text{--}800^\circ\text{C}$. The electrochemically-active sites for the oxygen reduction reaction are restricted at the triple phase boundary (TPB) of electrode/YSZ/gas phase.

As mentioned above, the microstructures of the electrodes significantly contribute to the performance and stability of SOFCs. Recently the direct observation of electrode in a three dimensional (3D) space by using the focused ion beam-scanning electron microscopy (FIB-SEM) has attracted much attention as a powerful technique for microstructure analysis. This technique provides essential information to understand the quantitative relationship among the microstructure, performance, and long-term stability. In this study, the microstructural change in cell components with an elapsed time was quantified by the FIB-SEM technique to elucidate the degradation of the fuel electrode in various operating conditions and atmospheres. The impact of current passage on the activation process and microstructure of the perovskite-based air electrode were investigated during the course of

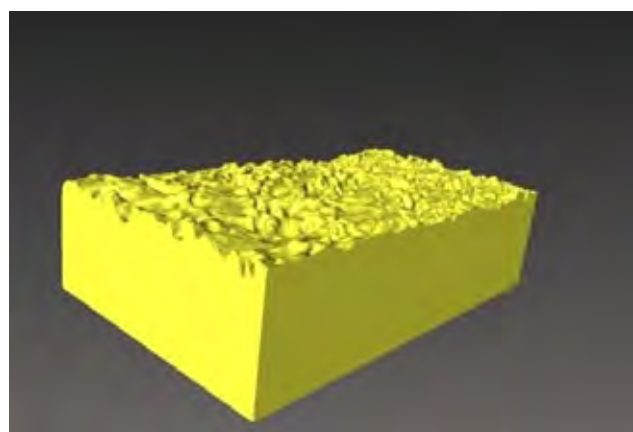


Fig. 1. Surface microstructure of YSZ at the interface with LSM electrode after discharge.

power generation.

2. Microstructure change of cathode with current passage

Perovskite-type oxides of $(\text{La,Sr})(\text{Co,Fe})\text{O}_{3-\delta}$ (LSCF) and $(\text{La,Sr})\text{MnO}_{3+\delta}$ (LSM) have been popularly employed as cathode for solid oxide fuel cells. The interface was roughened and micropores are formed in the vicinity of the interface [1]. This microstructural change gave rise to initial enhancement of the cell performance, whereas this may cause long term instability. The microstructural change at the interface between the LSM air electrode and YSZ electrolyte upon discharge was quantitatively evaluated from the 3D-reconstructed images after operation at 1000°C . The cell performance was enhanced during the initial current passage up to 5 h due to the reduction in polarization resistance at the air electrode. In response to this electrochemical behavior, the interfacial microstructure between LSM and YSZ changed significantly depending on the duration of discharge. Numbers of small pores were formed during discharge at the interface between YSZ and LSM. The roughness of YSZ surface measured from the 3D FIB-SEM images increased significantly with time as shown in Fig. 1. The pore formation rate depended significantly with the A site/B site metal ratio and Sr-substitution. The TPB in this case could be classified into active TPB facing to open pores and inactive TPB facing to closed pores. These results revealed that the increase in TPB-length is one of the factors affecting the activation of LSM air electrode during discharge but other factors, especially the influence of chemical stoichiometry of the perovskite oxide have to be considered for the understanding of the air electrode performance. Contact of LSM and YSZ and resulting microstructural change can be avoided by inserting interlayer of cation-doped ceria. The morphological change could be insignificant for the LSM/ceria/YSZ interface; thus ceria layer contribute to the stabilization of interface.

It is well known that the microstructural change of cell components proceeds with long term operation of the cell with LSCF cathode, resulting in the performance deterioration. Various factors have been proposed for this degradation behavior, such as the formation of resistive SrZrO_3 (SZO) phase and the sintering of LSCF cathode. It is noted for the LSCF/ceria / YSZ interface that the secondary phase of SZO was formed as island-like morphology to fill the pores in the interlayer of ceria (Fig. 2). The formation of SZO promoted by discharge with an elapse of time [2]. The influence of the ceria-zirconia solid solutions on the performance has not been studied quantitatively, with applying the results of dissection analysis of the cells operated; ceria-zirconia solid solutions are formed at the doped ceria interlayer/zirconia-based electrolyte interface. In this study, the ionic conductivity of these solid solutions formed in the LSCF/ $\text{Sm}_2\text{O}_3\text{-CeO}_2$ (SDC)/ $\text{Y}_2\text{O}_3\text{-ZrO}_2$ system was studied in detail. The dissolution of Sm^{3+} into the $\text{Y}_2\text{O}_3\text{-ZrO}_2$ phase resulted in the appreciable reduction in ionic

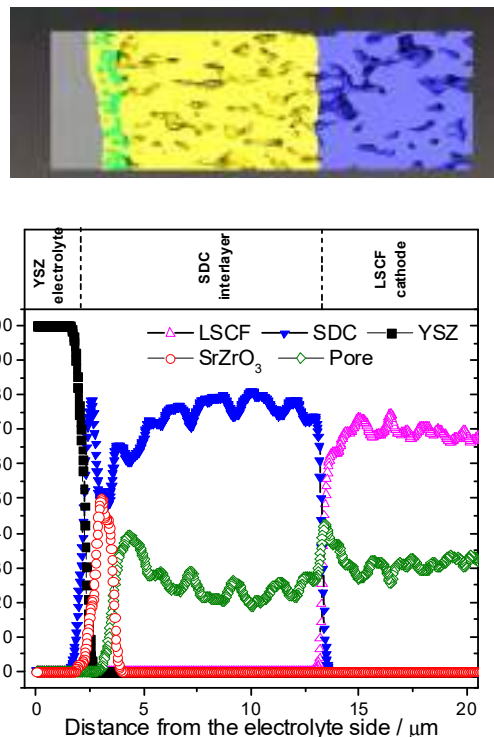


Fig. 2. Distribution profiles of each phase along the electrode thickness direction after discharge for 400 h.

conductivity [3]. Furthermore, the influence of dopant species in the doped ceria interlayer, Sm^{3+} and Gd^{3+} , on the ionic conductivity of solid solutions was investigated.

Acknowledgment

This work was partially supported by the New Energy and Industrial Technology Development Organization (NEDO), Japan (Development of System and Elemental Technology on Solid Oxide Fuel Cell Project).

References

- [1]. T. Matsui, Y. Mikami, H. Muroyama, K. Eguchi, J. Power Sources, 242, 790-796 (2013)
- [2]. T. Matsui, M. Komoto, H. Muroyama, K. Kishida, H. Inui, K. Eguchi, J. Power Sources, 312, 80-85 (2016)
- [3]. T. Matsui, S.Q. Li, H. Muroyama, K. Kishida, H. Inui, K. Eguchi, Solid State Ionics, 300, 135-139 (2017)

SOLID OXIDE CELLS OPERATING WITH C-CONTAINING FUELS: OVERCOMING THE NI BASED LIMITATION

A. Giralдин^a, S. Tomadini^a, E. Squizzato^a, G. Carollo^a,
A. Glisenti^a

^aUniversità degli Studi di Padova, Dipartimento di Scienze
Chimiche, Padova, 35131 (Italy)

Abstract - In this research, the use of an alternative anode for Solid Oxide Fuel Cells (SOFCs) has been investigated. The cermet Ni-YSZ is the state-of-the-art material. It possesses several detrimental characteristics as particle sintering, Sulfur and C-poisoning with C-containing gas mixtures and re-oxidation. Researches are focused on its replacement with perovskite-based electrodes. $\text{La}_{0.75}\text{Sr}_{0.25}\text{Cr}_{0.5}\text{Mn}_{0.5}\text{O}_{3-\delta}$ (LSCM) was proposed as an alternative anode. Inspired by previous works, LSCM is here fully characterized and its electrochemical performance has been analyzed utilizing both CH_4 and H_2 as fuel. The aim of this study is the improvement of LSCM characteristics by the impregnation of a metal like Ni. Moreover, this work wants to verify if a low quantity of impregnated nickel can enhance the electrocatalytic properties of LSCM electrode without the detrimental effects that nickel demonstrates in Ni-YSZ cermet. LSCM and Ni impregnated LSCM (Ni/LSCM) powders characteristics are compared to understand which properties are modified by nickel presence. Moreover, electrocatalytic tests permit to understand performance dependence by impregnation.

Index Terms – Electrode, Mixed Ionic and Electronic Conductor, Perovskite, Solid Oxide Fuel Cell

I. INTRODUCTION

In last decades, fuel cells have attracted attention because are highly efficient devices that directly transform chemical energy of fuels into electrical energy, with low or no pollutant emission. A cermet of Ni-YSZ is the state-of-the-art anodic material for Solid Oxide Fuel Cells (SOFCs). Even if it is a low cost and high stable material in reducing atmosphere, it presents several disadvantages. In particular, Ni can sinterize and suffers of Sulfur and C-poisoning when using hydrocarbons as fuel.[1] LSCM perovskite has been proposed as an alternative anodic material.[2] It is a Mixed Ionic and Electronic Conductor (MIEC) and works in different atmospheres, also using C-containing fuels without Ni-based anode disadvantages. In this work, LSCM is fully characterized and both H_2 and CH_4 are used as fuel. Moreover, a composite anode, Ni/LSCM, was prepared by impregnation of 5wt% of Ni on LSCM. The aim is the improvement of LSCM properties utilizing the impregnation

of a low amount of nickel. In this way, it has been tried to stabilize Ni by highly dispersing it on the perovskite surface, lowering carbon formation in methane atmosphere. In addition, Ni presence can permit higher electrocatalytic performance to LSCM electrode.

II. MATERIALS AND SYNTHESIS

A. LSCM

LSCM powder is synthesized by Marcellis method, starting from precursors as lanthanum oxide, La_2O_3 , strontium carbonate, SrCO_3 , manganese acetate tetrahydrate, $\text{Mn}(\text{CH}_3\text{CO}_2)_2 \cdot 4\text{H}_2\text{O}$, chromium nitrate nonahydrate, $\text{Cr}(\text{NO}_3)_3 \cdot 9\text{H}_2\text{O}$. [3] They are dissolved in water and/or nitric acid. Citric acid is then dissolved in water and added to the metallic solutions. Citric acid is a complexing agent, its third dissociation constant is reached in basic solutions. To change solution's pH from 1 to 7-8 and achieve the complexation of the metallic cations, ammonium hydroxide is used. The solution is then heated since the formation of a wet gel. At 400°C , there is a spontaneous combustion of the gel. The powder is formed, and it is treated at $6^\circ\text{C}/\text{min}$ since 700°C for 6 hours in air.

B. Ni impregnation

Impregnation of 5wt% of Ni is tempted to achieve higher catalytic activity and electronic conductivity. The nickel precursor, $\text{Ni}(\text{NO}_3)_2 \cdot 6\text{H}_2\text{O}$ is dissolved in water and added to a solution containing citric acid. LSCM powder is then added, and the basification permits to obtain the cations containing network formation. The solution is heated, until the formation of a gel and the spontaneous combustion. The powder is then treated at $6^\circ\text{C}/\text{min}$ since 850°C for 2 hours. From XRD pattern, it is evident that the perovskite phase of interest is formed. Ni is not a substitutional element inside the perovskite phase. In fact, peaks position is not modified by its presence. The low amount of Ni that is impregnated on LSCM powder makes not possible its quantitative determination by XRD, see Fig.1.

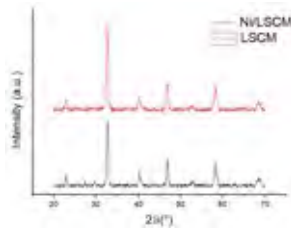


Fig. 1. XRD pattern of LSCM (red line) and Ni/LSCM (black line) taken by a Bruker D8 Advance diffractometer.

C. Cell Preparation

Inks have been made starting from LSCM and Ni/LSCM powders. A compatibility test, performed at 1400°C, demonstrates that Ytria-Stabilized Zirconia (YSZ) is a potential electrolyte because the formation of other species has not been observed. Each ink has been deposited, by tape-casting, over the center of a YSZ pellets which has a diameter of 20mm and a width of 2mm. After several tests, the ink optimal composition has been found. An elevated adhesion is achieved if an ink composed by 75wt% of the electrode powder mixed and by 25wt% of YSZ is chosen as first layer directly deposited on YSZ pellets. Next, a superficial layer of pure electrode ink is tape-casted on the composite layer. The cell is thermal treated at 1300°C. The final ink microstructure is granular, with high dispersed particles, as revealed by SEM. The width of each ink layer is in the order of 100µm. The electron collector that has been chosen is a commercial gold paste deposited using a brush.

III. CHARACTERIZATION

A. Temperature Programmed Reduction

To understand catalytic properties of the powders a temperature programmed reduction has been made. The temperature is raised from 40°C to 900°C under a constant flow of 5% H₂ in Ar. If LSCM sample is analyzed, it can be noted a single gaussian peak centered at 403°C. It is correlated to Mn reduction (Mn⁴⁺→Mn³⁺), see Fig.2a. Mn formed the redox couple that is fundamental in a MIEC for fuel cell application. In the case of Ni impregnated sample, it can be noted a single peak composed by two gaussian peaks. From deconvolution, a peak at 482°C related to Ni reduction (Ni²⁺→Ni⁰) and a peak at 456°C related to Mn reduction can be found, see Fig.2b. If Ni is added there is a stabilization of Mn(IV) correlated to Mn(IV)/Mn(III) reduction at higher temperatures.

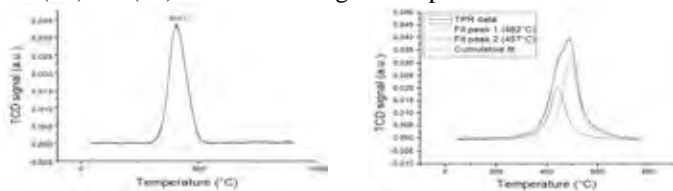


Fig.2 (a) LSCM H₂-TPR reduction peak (b) Ni/LSCM H₂-TPR reduction peak and deconvolution

B. Electrochemical characterization

Electrochemical characterization can be made using the EIS (Electrochemical Impedance Spectroscopy) technique. EIS

characterizations were performed using a PGSTAT 302 Autolab Frequency Response Analyser. Measurements have been taken at steady state in the frequency range between 10⁻³-10⁶ Hz and with signal amplitude of 50mV. A symmetrical cell is analyzed in a single chamber system using both H₂ and CH₄ as fuel at different temperatures. By impedance spectra and ASR values, it can be noted that the presence of Ni enhances the performance using H₂ as fuel and at high temperature in CH₄ atmosphere. Only when CH₄ is chosen as fuel below 750°C, higher ASR values are determined using Ni/LSCM as electrode instead of LSCM. The EIS spectra are presented in Fig.3.

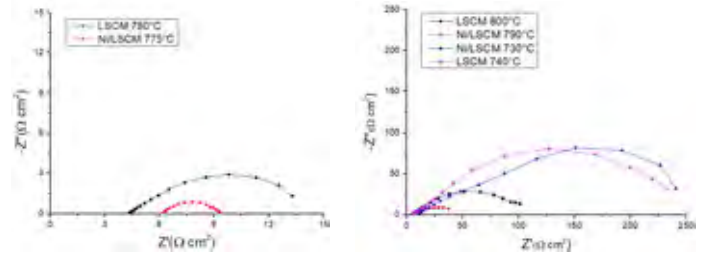


Fig.3 (a) LSCM (black) and Ni/LSCM (red) impedance curve at 780°C and 775°C, 10% H₂ in Ar (b) LSCM (black) and Ni/LSCM (red) impedance curve at 800°C and 790°C, 10% CH₄ in Ar, LSCM (green) and Ni/LSCM (blue) at 740°C and 730°C, 10% CH₄ in Ar.

IV. CONCLUSION

In this work, two anode materials, LSCM and a Ni-impregnated LSCM sample have been synthesized and characterized. The deposition of Ni at 5wt% by wet impregnation has been used to enhance the catalytic activity and electronic conductivity of LSCM sample. TPR demonstrated that the presence of Ni stabilized Mn(IV) species. The synergy between Mn and Ni permits an enhancement of electrochemical properties of the impregnated sample especially using H₂ as fuel. When electrochemical tests have been done using CH₄ as fuel, below 750°C there is a lowering of performance for the Ni-impregnated sample in relation to the pure LSCM electrode. This is due to the fact that Ni even if impregnated in a low amount is poisoned by a C-containing fuel, especially at lower working temperatures. A future step is the infiltration or exsolution of Ni to enhance its dispersion on LSCM sample reducing the C-poisoning effect.

REFERENCES

- [1] Zhou, F., Wang, X., Kang, J., Lin, B., Ling, Y., Budiman, R.A., Wei, K. Progress in Ni-Based Anode Materials for Direct Hydrocarbon Solid Oxide, Journal of Material Science, Volume 53, 2018, Pages 8747-8765.
- [2] Tao, S., Irvine, J. T. S. Synthesis and Characterization of (La_{0.75}Sr_{0.25}Cr_{0.5}Mn_{0.5}O_{3-δ}, a Redox-Stable, Efficient Perovskite Anode for SOFCs. Journal of Electrochemical Society, Volume 151, 2004, 151 (2), A252-A259.
- [3] Marcilly, C., Courty, P., Delmon, B. Preparation of Highly Dispersed Mixed Oxides and Oxide Solid Solutions by Pyrolysis of Amorphous Organic Precursors, Journal of American Ceramic Society, Volume 53, 1970, Pages 56-60.

SIMULATION OF MOLTEN CARBONATE FUEL CELLS UNDER DUAL-ANION WORKING CONDITIONS IN CARBON CAPTURE APPLICATIONS

D. Bove*, B. Bosio*, E. Audasso*, T. Barckholtz**, G. Kiss** and J. Rosen**

* PERT, DICCA, University of Genova, Via Opera Pia 15, 16145, Genova, (Italy)

** ExxonMobil Research and Engineering, 1545 Route 22 East, NJ 08801, Annandale, (United States)

Abstract - A Molten Carbonate Fuel Cell (MCFC) process model using a “dual-anion mechanism” has been coded into an in-house Fortran code and subsequently integrated in the Aspen Plus software. This integration allows the coupling of the advantages of the two simulation approaches: the calculation speed and flexibility of Fortran and the ability of Aspen Plus to connect the simulated MCFC to other operation units for system analysis.

In the present work, this new simulation tool and its application insensitivity analyses for optimizing the kinetic model is presented.

Index Terms - Carbon capture, molten carbonate fuel cell, process model, multi-scale simulation.

I. INTRODUCTION

Molten Carbonate Fuel Cells (MCFCs) are a commercial technology used for energy production. In the last few years we have been testing the use of MCFCs for CO₂ capture. We found that MCFCs do afford an energy efficient capture of CO₂ (on the cathode side) even from CO₂-poor streams and transport it to the CO₂-richer anode stream from which pure CO₂ can be easily separated. Compared to sorption-based CCS technologies, MCFCs can be effectively retrofitted into existing plants without onerous changes to the system [1,2].

Numerous models have been set-up to simulate and study MCFC behavior, optimize their design, and predict their performance [3-5]. However, these models could not adequately predict MCFC performance in carbon capture applications in which the gas to be treated has low CO₂ concentration, like in flue gases of natural gas fired power plants. Our recently developed kinetic model is better able to fit the behavior of MCFC. It is built on a “dual-anion mechanism” to predict the performance of MCFCs working with wet and CO₂-poor cathode feeds [6,7].

Generally, a high number of kinetic parameters is required to rigorously describe the processes operational in MCFCs. However, such complex models require a very extensive experimental database to fit their parameters. Also, the high complexity of such models may not yield commensurate improvements in their predictive power and accuracy [8]. Simpler models would be more practical and desirable.

Therefore, the main aim of this work is to identify, through sensitivity analyses, the parameters that are less significant under typical working conditions and therefore can be neglected.

II. MODEL

Our model has a distributed parameter structure that considers two parallel electrochemical pathways that involve two different anions, carbonate and hydroxide. Although the carbonate path is sufficient at high CO₂ cathode concentrations, the hydroxide path cannot be neglected with cathode feeds of low CO₂ contents.

This new reaction path was observed in our experiments showing that in presence of water in the cathode feed, current densities were higher than the values calculated from CO₂ fluxes [6].

The cell unit of the kinetic model, which is the core of our investigation, is written in Fortran language to ensure high calculation speed whilst at the same time maintain the flexibility of our in-house developed code that commercial software codes lack. It is a numerical 2-D deterministic model and is able to calculate the local mass balances based on the electrochemical and water gas shift reactions. The electrochemical model is built on the dual anion mechanism

[6,7].

The core of the model was integrated into the Aspen Plus software that otherwise lacks modules to describe fuel cells. The main advantages of using Aspen Plus for this work are the possibility to connect other operation units in the framework of a system analysis and to perform sensitivity analyses by varying the operating conditions systematically.

In particular, the model is able to calculate the main performance parameters on the 2D plane of both a single cell or stacks of fuel cells when the system geometry as well as the feeding flow rates, compositions, temperature, pressure and current density (galvanostatic mode) or voltage (potentiostatic mode) are provided as input data in Aspen Plus.

III. SENSITIVITY ANALYSES

In the Aspen model, different types of sensitivity analysis have been performed to better understand the behavior of the fuel cells and to identify the dominating parameters most influencing the results. These results were used to simplify the kinetic model and optimize parameter identification:

- operation conditions, such as the molar fraction of the i^{th} component and the ratio between reactant flow rates;
- functional parameters, such as l_{eff} , that is the effective length of diffusion of the gas in the cathode pores;
- physical parameters, such as diffusivity coefficients, tortuosity and porosity;
- kinetic parameters, that are semi-empirical coefficients used in the electrochemical kinetic formulation.

Figure 1 shows an example of a sensitivity analysis used to study the effect of the l_{eff} in terms of voltage. For this instance, two fuel cells with different cathode current collectors were considered. The gray and yellow lines represent the simulation results for the cell with a current collector that leaves 90% open area at the cathode surface (cell A), while the blue and orange lines show the simulation results for a current collector that leaves 35% (cell B).

IV. CONCLUSION

Our sensitivity analyses allowed the identification of the main parameters affecting the MCFC performance and consequently it was possible to simplify the kinetic model thus making model development and simulations more efficient.

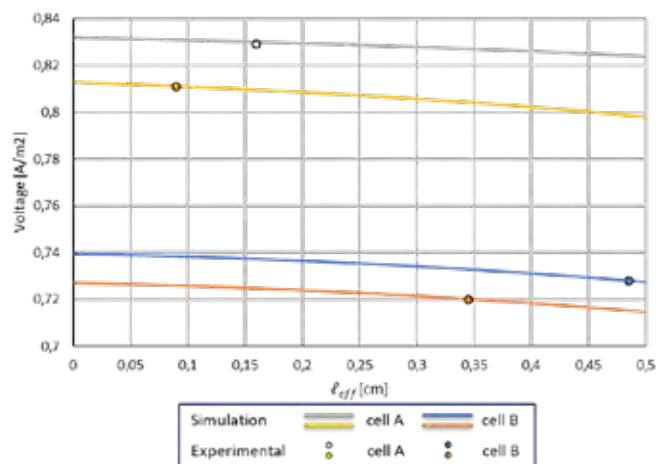


Fig. 1. Sensitivity analysis at different operation conditions

REFERENCES

- [1] Audasso E, Campbell P, Della Pietra M, Ferrari MC, Bosio B, Arato E. Molten carbonate fuel cells in integrated systems for the exploitation of poor fuels and the segregation of CO₂. *Bulg Chem Commun* 2018;50:99–107.
- [2] Campanari S, Chiesa P, Manzolini G, Bedogni S. Economic analysis of CO₂ capture from natural gas combined cycles using Molten Carbonate Fuel Cells. *Appl Energy* 2014; 130:562–73.
- [3] Audasso E, Barelli L, Bidini G, Bosio B, Discepoli G. Molten Carbonate Fuel Cell performance analysis varying cathode operating conditions for carbon capture applications. *J Power Sources* 2017;348:118–29.
- [4] Liu A, Weng Y. Modeling of molten carbonate fuel cell based on the volume-resistance characteristics and experimental analysis. *J Power Sources* 2010;195:1872–9.
- [5] Brouwer J, Jabbari F, Leal EM, Orr T. Analysis of a molten carbonate fuel cell: Numerical modeling and experimental validation. *J Power Sources* 2006;158:213–24.
- [6] G. Kiss, T. Barckholtz, L. Han, J. Rosen, T. Geary, H. Ghezel-Ayagh, A. Hilmi, C. William, C.Y. Yuh, Improved Understanding of Molten Carbonate Fuel Cell Electrolyte Behavior at Carbon Capture Conditions. 11th International symposium on Molten Salts, May 19-23 2019, Orleans (France).
- [7] E. Audasso, B. Bosio, D. Bove, E. Arato, T. Barckholtz, G. Kiss, J. Rosen, L. Han, T. Geary, C. Willman, A. Hilmi, C.Y. Yuh, H. Ghezel-Ayagh, The double-anion mechanism in Molten Carbonate Fuel Cells working with wet and CO₂-poor feeding at the cathode. 11th International symposium on Molten Salts, May 19-23 2019, Orleans (France).
- [8] Subramanian N, Haran BS, White RE, Popov BN. Full Cell Mathematical Model of a MCFC. *J Electrochem Soc* 2003;150:A1360–7.

HYDROGEN STORAGE & ΔH TEST LAB

S. Stelitano*, A. Rullo*, L. Piredda*, E. Mecozzi*, R. Agostino**, G. Conte** and A. Policicchio**

*Rina Consulting-Centro Sviluppo Materiali, Via Di Castel Romano 100 - 00128 ROMA, (Italy)

**Università della Calabria, via Pietro Bucci - 87036 Arcavacata di Rende, Cs, (Italy)

Abstract - The challenging decarbonization European target strongly pushes towards the use of renewable energy sources. In this scenario H₂, that can be stored from the surplus of renewable power energy, is the energy vector that can be the missing link in the transformation of the global energy system. To study the effect of H₂ on material properties and the performances of components in H₂ environment, a new facility, ΔH lab, has been built with a cooperation between Rina Consulting – CSM SpA and University of Calabria. The lab allows to study: materials and components in H₂ environment at pressure up to 100 MPa and temperature from 283 to 423K; solid materials at pressure up to 30 MPa and temperature from 77 to 473K. This paper reports a H₂ storage review, together with a description of the laboratory and preliminary results obtained.

Index Terms – Hydrogen Economy, Hydrogen Embrittlement, Hydrogen Storage, Hydrogen sorption

I. INTRODUCTION

The 2018/2001/EC Directive of the European Parliament [1] sets the objective of reaching at least 32% of the EU's final energy consumption through renewable energy sources (RES) by 2030. The RES drawback is their intermittence that has to be balanced for electric grid stability purposes through long term and large capacity storage. An alternative to batteries storage systems is the transformation of RES energy into H₂ that has highest energy density per unit mass of any fuel, but being the lightest and lower density element, it's hardly stored requiring more volume for given amount of energy. [2] Current H₂ storage methods are: gas compression (cGH₂), liquefaction (lH₂), cryo-compressed (CcH₂) and solid state materials (SSMs), which involve the H₂ interaction with the overall material (Chemisorption - Chem) or the material surface (Physisorption - Phys). [2,3,4] The storage solution must be carefully designed and selected to address specific applications depending on geometry, space and weight. In this scenario, materials for H₂ components and infrastructures are a crucial point to guarantee reliability and safety. To address this point, a new facility, ΔH lab, has been built in the South of Italy, by

Rina Consulting-CSM SpA and University of Calabria collaboration. The lab will be described in the paper together with preliminary results achieved and a synthetic review of the main H₂ storage techniques.

II. HYDROGEN STORAGE SYSTEMS

At the state of the art, H₂ can be stored in cGH₂, lH₂, CcH₂ and SSMs, as reported in Table I, where pros and cons of each storage method are listed.

TABLE I - HYDROGEN STORAGE SYSTEMS COMPARISON

Storage method	ρ_M [wt%] [4]	ρ_V [kgH ₂ /m ³] [3]	T [K]	P [MPa]	Pros	Cons
CGH ₂	6	< 40	RT	70	High efficiency, mature technology	Expensive cylinder, immature technology of fast filling.
lH ₂	8	70	20	0.1	High liquid density and storage efficiency	Energetically expensive, low temperature, boil-off
CcH ₂	-5	-40	20	30	Low boil-off	High costs
SSMs - Phys	2	20	77	10	Highly porous, high uptake, fully reversible	Very low storage temperature
SSMs - Chem	15	150	RT	2	High safety, good reversible	Absorbing impurities

Important parameters for a storage system are gravimetric (ρ_M : H₂ amount adsorbed per unit mass) and volumetric density (ρ_V : H₂ amount adsorbed per unit volume), pressure and temperature. [3] ρ_M and ρ_V influence the vessel weight and volume, while pressure and temperature determine the operative conditions influencing, besides the vessel geometry, costs and safety of the full system. CGH₂ at 70 MPa, the vehicles industrial standard solution, requires expensive tanks, as result of materials, geometry and mechanical properties considerations, and energy expenditure for compression and

fast filling. [5] IH₂ stores more H₂ than cGH₂, but requires a higher energetic expenditure for cooling and the vessel insulation, due to the H₂ boil-off with a lost energy content estimated as 40% in contrast to 10% of cGH₂. [3] The CcH₂ combines the properties of cGH₂ and IH₂ systems. SSMs have been considered as a long-term solution for their good storage capacities, [6] but present low temperature for Phys, high desorption temperature for Chem, complex kinetics and thermodynamics of the processes.

III. ΔH TEST LAB

A. Lab Description

The ΔH lab, built in the frame of the “EOMAT” project (PON03PE_00092_1), funded within of Italian National Operational Programme 'Research and Competitiveness' 2014-2017, presents the next test capabilities:

- Small scale tests (tensile, toughness, and fatigue) on materials in H₂ environment, in a pressure range (ΔP) of 0÷100MPa and temperature range (ΔT) of 283÷423K by a servo-hydraulic machine equipped with an autoclave;
- Full scale tests on components in a ΔP of 0÷100MPa, carried out inside an inert security chamber of 2500 l;
- Tests on SSMs in a ΔP of 0÷30MPa and ΔT of 77÷473K, by a High-Pressure-Concentration-Temperature prototype able to evaluate the material sorption/desorption capacity.

B. Experimental conditions

Slow strain rate tests (SSRT) have been carried out on AISI 4145 steel (according to NACE TM198) in a H₂ and N₂ environment at 80 MPa with a strain rate of 10⁻⁶ s⁻¹, to assess the effect of H₂ on the material ductility. A full scale cycling fatigue test has been performed in H₂ on AISI 4145 cylinder containing an intentionally machined defect at ΔP of 5÷45MPa.

C. Results and discussions

The SSR curves (Fig.1) show that the maximum strain before failure in the H₂ test is about half the strain of the sample in N₂ test and the advanced fracture surfaces analyses (shown in the inset) confirmed the presence of a brittle fracture and secondary cracks.

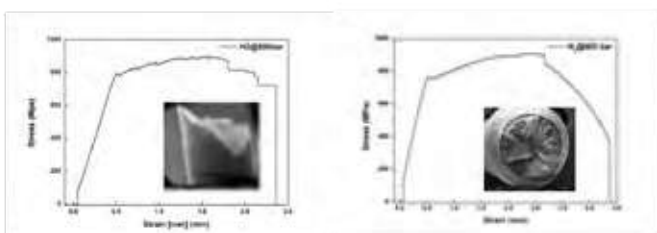


Figure 1: Left) Sample tested in H₂; Right) Sample tested in N₂

The full scale test results did not highlight any crack propagation at the end of the test (Fig. 2).

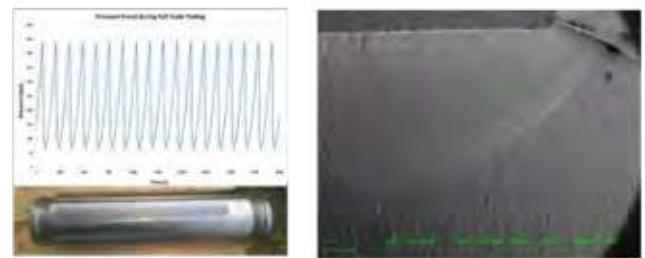


Figure 2: Left) Pressure vs. time in the full scale test and vessel photo, Right) SEM image

IV. CONCLUSION

The SSRTs highlight an evident H₂ effect on elongation and surface fracture of the material, while full scale fatigue test gave confirmation of the good performance of AISI 4145 at lower ΔP. The critical points for the H₂ economy development are the selection of the suitable storage method and the materials compatibility with gas. ΔH lab represents one of the few realities able to providing all the tools necessary for the development and optimization of H₂ storage methods and materials.

REFERENCES

- [1] Directive (EU) 2018/2001 of the European Parliament and of the Council of 11 December 2018 on the promotion of the use of energy from renewable sources.
- [2] Staffell, I., Scamman, D., Abad, A.V., Balcombe, P., Dodds, P.E., Ekins, P., Shahd, N., Warda, K. R., The role of hydrogen and fuel cells in the global energy system, *Energy Environ. Sci.*, Volume 12, 2019, pp. 463-491.
- [3] Zuttel, A., *Hydrogen storage methods*, *Naturwissenschaften*, Volume 91, 2004, pp. 157-72.
- [4] E. Rivard, M. Trudeau, K. Zaghbi, *Hydrogen Storage for Mobility: A Review*, *Materials*, Volume 12, 2019, pp. 1973.
- [5] Li, M., Bai, Y., Zhang, C., Song, Y., Jiang, S., Grouset, D., Zhang, M., *Review on the research of hydrogen storage system fast refueling in fuel cell vehicle*. *Int. J. Hydrog. Energy*, Volume 44, 2019, pp.10677-10693.
- [6] J., Musyoka, N.M., Langmi, H.W., Mathe, M., Liao, Sh., *Current research trends and perspectives on materials-based hydrogen storage solutions: A critical review*, *Int. J. Hydrog. Energy*, Volume 42, 2017, 289-311.

ENERGY ANALYSIS OF HYDROGEN GREEN PRODUCTION AND STORAGE FOR THREE CALABRIAN SITES (ITALY)

P. Fragiacommo, M. Genovese

Department of Mechanical, Energy and Management Engineering,
University of Calabria,
Arcavacata di Rende, 87036 Cosenza (Italy)

Abstract - Hydrogen is proposed as energy vector and as an alternative fuel. In this paper three renewable energy sources have been investigated and considered from which producing electricity to be used in the process of water electrolysis: primary wind source, primary solar source and geothermal energy. Three Calabrian sites have been studied, chosen by way of example and of which the meteorological and geophysical data were possessed: Capo Suvero for wind energy, Cosenza for solar energy and Civita for geothermal energy. The sizing of these renewable energy plants was based on an annual energy estimate. The performance of each system has been investigated, from an energy point of view. The overall efficiency of the system has been calculated.

Index Terms - Hydrogen Production, Hydrogen Infrastructure, Renewable Energy, Water Electrolysis

I. INTRODUCTION

Hydrogen is proposed as energy vector and as an alternative fuel [1]. Among several possibilities, the production of hydrogen from natural resources coupled with renewable energy is realized in the process of water electrolysis [2]. A possible method to mitigate the costs of electrolysis can be obtained through the cooperation of renewable energies systems: part of their energy can be used for hydrogen production [3]. This hydrogen will further create advantage for energy producers who concern about energy production stabilization and transients limitations. Several authors investigated and proposed a mathematical modeling of a hydrogen production system. Omdahl [4] included in his model an electrolysis unit for hydrogen onsite production, with the goal to investigate a further utilization of heat wasted from the thermal cooling management system. Dagdougui et al. [5] focused their investigation on the population density and the renewable supply as the crucial parameters affecting the performance of a green hydrogen station network.

Different aspects relating to hydrogen infrastructure have previously been analyzed, but there are still few overall investigations on a technical economic analysis for a potential business case. Calabria Region, in South Italy, has very suitable

sites or already equipped with renewable energy plants. In this train of thought, the proposed research activity wants to give a contribution to the international scientific community proposing a mathematical model to size the production of hydrogen through water electrolysis from renewable sources (wind, solar, geothermal) in three Calabrian sites, from an energy point of view.

II. NUMERICAL MODEL AND RESULTS

As mentioned above, three Calabrian sites have been studied, chosen by way of example and of which the meteorological and geophysical data were possessed: Capo Suvero for wind energy, Cosenza for solar energy and Civita for geothermal energy.

Capo Suvero is the site whose data have been used in this paper, normalised at 10 m of elevation. All the quantities were calculated as yearly mean value over an entire number of years (3 years). The annual energy produced by a DeWind D8 wind turbine at Capo Suvero is around 6 GWh. In the hypothesis of continuously dividing it at daily level, the daily energy produced by the turbine corresponds to about 17 MWh.

The site selected for the hydrogen production facility from photovoltaic system (PV) has been identified at the University placed in Cosenza (Italy). Calculation of the average monthly daily radiation on an inclined surface was made by referring to the Liu & Jordan model, with a peak of production in August (about 210 kWh/m²), and the lowest value on January (about 110 kWh/m²). The PV power plant will be realized by using mono-crystalline PV modules with a fixed both azimuthal angle and tilt angle.

The Calabrian territory does not possess high enthalpy geothermal resources, as can be seen from the data extrapolated from the site of the Ministry of Economic Development, A binary cycle plant was analyzed to allow the exploitation of the low-entrenched Calabrian resource for the production of electricity. In particular, the Civita site was analyzed, which presents, among the Calabrian locations, the highest

temperatures at 3000 m depth. These temperatures settle on average around 90 °C. The model used data from the CoolProp database, a cross-platform and open-source. The annual production in the Calabrian territory is about 0.2 GWhe, about 30 times lower than that estimated from wind. However, given the growing global demand for energy, it would in fact be desirable to make these technologies more widely used, since geothermal energy, among renewable energies, is able to provide a constant level of production throughout the year, without being heavily affected by external factors.

The authors have already proposed a mathematical model for a hydrogen production facility [6]. The model is based on a mass balance (fluid-dynamic analysis) and an energy conservation balance. The modeling concerned the following sub-models, related to different physical phenomena:

- Fluid-dynamic model, which represents mass flows in the electrolysis system;
- Thermodynamic model, which represents the pressure at cathode and anode;
- Electrochemical models, which allow to describe the electrical behavior of the electrolytic stack;
- Thermal models, to determine the transient thermal behavior of the stack.

The performance of each system has been investigated, with the operative parameters listed in Table 1.

Table 1 – Simulation Parameters

Parameter	Model
DI Water Requirement [l/h]	9.0
Delivery Pressure [bar]	30
Operating Temperature [K]	353
Operating Current [A]	135
Membrane Cross Section Area [cm ²]	100
Anode Working Pressure [bar]	2.00
Cathode Working Pressure [bar]	13.44
Anodic Chamber Volume [m ³]	0.001
Cathodic Chamber Volume [m ³]	0.001
Simulation Time [h]	24

The polymer electrolyte membrane (PEM) electrolyzer resulted to have a specific power consumption of 58 kWh/kg. Adding 1.24 kWh/kg for the compression system, the system overall electric efficiency achieves a value of 0.57. The water demand needed to meet the station size and produce the required hydrogen is 0.59 Nm³/h per kg of produced hydrogen. Table 2 below shows the hydrogen production for each site.

Table 2 – Hydrogen Production

PARAMETER	CAPO SUVER O	COSEN ZA	CIVITA
Average Daily Hydrogen Production [kg/day]	287	180	9.0
Electrolyzer Installed Power [kW]	674	423	21
Daily Energy Demand [MWh]	17	10.66	0.55

In order to promote a potential business case, an economic analysis will be integrated and performed, forecasting hydrogen further utilization in fuel cell electric vehicles and injection in natural gas grids. The analysis will adopt the COBRA tool [7] in order to take into account carbon footprint of these applications and their health and quality of life benefits.

III. CONCLUSION

By means of a mathematical model, the present paper sized the production of hydrogen through PEM water electrolysis from renewable sources (wind, solar, geothermal) in three Calabrian sites, from an energy point of view. The polymer electrolyte membrane (PEM) electrolyzer showed a specific power consumption of 58 kWh/kg, with a water consumption of 0.59 Nm³/h per kg of produced hydrogen. The overall system showed an electric efficiency of 57 %.

REFERENCES

- [1] Chapman A, Itaoka K, Hirose K, Davidson FT, Nagasawa K, Lloyd AC, et al. A review of four case studies assessing the potential for hydrogen penetration of the future energy system. *Int J Hydrogen Energy* 2019. doi:10.1016/j.ijhydene.2019.01.168.
- [2] Parra D, Valverde L, Pino FJ, Patel MK. A review on the role, cost and value of hydrogen energy systems for deep decarbonisation. *Renew Sustain Energy Rev* 2019. doi:10.1016/j.rser.2018.11.010.
- [3] Nikolaidis P, Poullikkas A. A comparative overview of hydrogen production processes. *Renew Sustain Energy Rev* 2017;67:597–611. doi:10.1016/j.rser.2016.09.044.
- [4] Omdahl N. Modelling of a hydrogen refueling station. Trondheim: Norwegian University of Science and Technology, 2014.
- [5] Dagdougui H, Ouammi A, Sacile R. Modelling and control of hydrogen and energy flows in a network of green hydrogen refuelling stations powered by mixed renewable energy systems. *Int J Hydrogen Energy* 2012;37:5360–71. doi:10.1016/j.ijhydene.2011.07.096.
- [6] Fragiaco P, Genovese M. Modeling and Energy Demand Analysis of a Scalable Green Hydrogen. *Int J Hydrog Energy* 2019 .
- [7] U.S. EPA. CO-Benefits Risk Assessment (COBRA) Health Impacts Screening and Mapping Tool 2018.

DETAILED MODELLING OF INTERNAL REFORMING FUEL CELLS FOR PROCESS ANALYSIS AND OPTIMISATION

E. Audasso*, F.R. Bianchi*, D. Bove*, and B. Bosio*

*PERT, DICCA, University of Genova, Via Opera Pia 15, 16145, Genova, Italy

Abstract – Solid Oxide and Molten Carbonate Fuel Cells are technologies commercially applied mainly for energy production. Because of their working conditions at high temperature ($>500^{\circ}\text{C}$) reforming reactions of hydrocarbon can take place, thus allowing the direct use of light hydrocarbon such as CH_4 instead of H_2 . Internal reforming fuel cells allow a simplification of the plant system but increase the complexity of the cells stack design and of the thermal balance of each cell. The possibility of having an internal reforming simplify the overall plant system reducing the necessary equipment. Indeed, the reforming reaction is an endothermic reaction that can cause relevant temperature drops in some point of the cell plane. The stiff thermal gradient can induce the degradation of the cell materials. For this reason, a proper simulation is fundamental to guarantee safe operating conditions, avoid underestimating or overestimating the required or generated heat and reducing maintenance cost.

In this work, the authors present a study about the modelling of the CH_4 internal reforming applied to high temperature fuel cells. The obtained reforming model will be integrated into the SIMFC code, an in-house developed Fortran constructed to simulate fuel cells performance. The simulation results will be compared to experimental and literature data to confirm their validity.

Index Terms - CH_4 reforming, high temperature fuel cells system, modelling, simulation

I. INTRODUCTION

Solid Oxide (SOFC) and Molten Carbonate (MCFC) Fuel Cells are well-known technology whose main commercial application is energy production.

Thanks to their high operating temperature ($>500^{\circ}\text{C}$) compared to other kind of fuel cells (usually $<200^{\circ}\text{C}$), they allow the use of non-precious metal catalyst decreasing the production material costs, the recycle of high temperature vapor fluxes for different purpose inside the plants, and a high fuel flexibility [1,2]. This last feature is extremely important

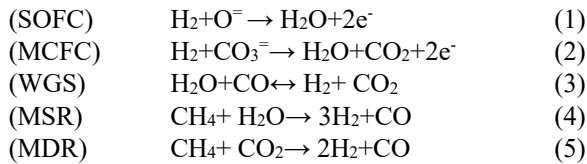
because it allows the direct use of light hydrocarbons (such as CH_4 or ethane) instead of H_2 . Thanks to the high operating temperature, provided a catalyst, the reforming reaction can effectively take place thus converting these light hydrocarbons to the H_2 needed by the electrochemical reactions directly into the cell apparatus. This feature can decrease the overall operating costs of the cells and allow them to be directly connected to, for example, natural gas networks.

Although this is a known features of high temperatures fuel cells, most of the current models that see their integration in complex system usually simplify the analysis including an external reformer unit [3]. Even though this simplification does not sensitively affect the overall performances, it neglects the local effects that the reforming reactions may have on the cells. As a result, not optimal conditions may be considered for cell operation.

In this work the authors are going to present a model to simulate fuel cells with internal reforming reactions. Different solutions to describe the reforming reaction will be investigated. The obtained model will be encoded into the SIMFC code, an in-house developed Fortran code. The SIMFC allows the simulation of fuel cells performance on the basis of local mass, energy, charge and momentum balances [4]. The SIMFC code can be easily integrated in system analysis software such as Aspen Plus, thus providing with more accurate and safe simulations.

II. CH_4 REFORMING

The main reactions that take place at the anode side of a fuel cell are H_2 oxidation to water (1 for SOFC and 2 for MCFC), water gas shift reaction (WGS, 3) and steam (MSR, 4) and dry (MDR, 5) reforming reaction.



The oxidation of H_2 is driven by the electricity produced by the fuel cell, while the WGS reaction has a fast kinetics and can be assumed to be an equilibrium reaction. The reforming reactions can be analyzed as both equilibrium governed or kinetic governed. For this reason, in our work we decided to analyze both possible solutions.

A. Equilibrium driven reforming

To evaluate the equilibrium constant K_p we decided to recur to its formal definition using the Gibbs free energy of reaction rather than empirical formula that can be found in literature.

As it can be easily deduced from the set of reactions 3-5, they are interdependent, thus the equilibrium of only two of them can be considered. However, we had to introduce both dry and steam reforming reactions, because, if the feed to be reformed is poor or does not contain water or CO_2 , mathematical convergence problems arise if one of the two possible reactants with CH_4 is not included.

Moreover, to fit different kind of catalysts we assumed a temperature approach, by considering a different reacting temperature for different hypothetical catalysts.

B. Kinetic driven reforming

To consider the kinetics of the reforming reactions, we decided to use kinetic formulations that can be found in literature, in particular the one used in [5].

It is important to notice that, although they are interdependent, both reforming reactions must be considered because they are affected by their own kinetics.

In addition to the presented reactions (1-5), other possible parasite reactions should be included to improve the mode reliability. These can include different reforming reaction stoichiometry and carbon deposition. However, as initial analysis, we decided to neglect them.

III. INTEGRATION INTO A FUEL CELL SIMULATION TOOL

Finally, both the equilibrium driven and the kinetic driven formulations were added to the SIMFC code.

It is worth noticing that the equilibrium driven simulation will give not satisfactory results because almost all the CH_4 will reform at the anode inlet of the cell. Thus, although it can be effectively used to simulate the performance, it will miss the

scope of obtaining local information.

On the other hand, the kinetic driven formulation provides with a more accurate simulation of the process. Thanks to its own structure, the code can also give the local map of current, gas molar fraction and most importantly temperature. Indeed, the exothermicity of the WGS and the endothermicity of the reforming reactions may balance each other or may need local study to find the best operating condition. This feature allows more precision in the cell and stack design. Indeed, it can put in evidence operating conditions apparently good, but locally unstable and harmful to the cell.

IV. CONCLUSION

In the work the authors developed a formulation to simulate high temperature fuel cells with internal reforming.

This was implemented into an in-house made code named SIMFC capable to simulate fuel cells performance with positive results. The SIMFC code can be easily integrated in system analysis tools such as Aspen Plus. In this way, it is possible to simulate complex solutions with internal reforming without the uncertainty of not knowing the local effects that it can have on the behavior of the stack of cells.

REFERENCES

- [1] Liu, Z., Shi, W., Han, M., Electrochemical characteristics and carbon tolerance of solid oxide fuel cells with direct internal dry reforming of methane, *Applied Energy*, Volume 228, 2018, pp. 556-557.
- [2] Cigolotti, V., Massi, E., Moreno, A., Poletini, A., Reale, F., Biofuels as opportunity for MCFC niche market application, *International Journal of Hydrogen Energy*, Volume 33, 2008, pp. 2999-3003.
- [3] Carapellucci, R., Di Battista, D., Cipollone, R., The retrofitting of a coal-fired subcritical steam power plant for carbon dioxide capture: A comparison between MCFC-based active systems and conventional MEA, *Energy Conversion and Management*, Volume 194, 2019, pp. 124-139.
- [4] Audasso, E., Bosio, B., Nam, S., Extension of an effective MCFC kinetic model to a wider range of operating conditions, *International Journal of Hydrogen Energy*, Volume 41, 2016, pp. 5571-5581.
- [5] Jun, H., Park, M., Baek, S., Bae, J., Ha, K., Jun, K., Kinetics modeling for the mixed reforming of methane over Ni-CeO₂/MgAl₂O₄ catalyst, *Journal of Natural Gas Chemistry*, Volume 20, 2011, pp. 9-17.

A DUAL-ANION MECHANISM IN MOLTEN CARBONATE FUEL CELLS FOR A DUAL-CHALLENGE: ENERGY PRODUCTION AND CARBON CAPTURE

E. Audasso*, B. Bosio*, D. Bove*, E. Arato*, T. Barckholtz**, G. Kiss**, J. Rosen**, L. Han**, T. Geary***, R. Blanco Gutierrez, H. Elsen, C. Willman***, K.Hilmi*** and H. Ghezal-Ayagh***

*PERT, DICCA, University of Genova, Via Opera Pia 15, 16145, Genova, Italy

**ExxonMobil Research and Engineering, 1545 Route 22 East, Annandale, NJ 08801

*** FuelCell Energy, 3 Great Pasture Road, Danbury, CT 06810

Abstract - Molten Carbonate Fuel Cells (MCFCs) are a well-known technology whose main applications are in energy production and Carbon Capture and Storage (CCS) applications.

A recent experimental campaign showed that, in presence of H₂O in the cathode feed, MCFC performance results higher than in otherwise similar conditions. This phenomenon was ascribed to the appearance of a secondary reaction path driven by the formation of hydroxide ions at the cathode side that can behave as the carbonate ions in normal MCFCs conditions.

In this work the authors will present a theoretical study to approach this newly observed dual-anion reaction mechanisms in order to derive a set of kinetic equations to describe the cell behaviour in these conditions. The derived kinetic core will be integrated in an in-house developed code to simulate high temperature fuel cell performance and its validity tested through comparison with experimental data.

Index Terms – Electro-chemical model, MCFC dual-anion kinetics, MCFC for Carbon Capture applications, Parallel electrochemical reactions.

I. NOMENCLATURE

E_m : equilibrium potential of the m-ion driven path, [V]

J_m : current density of the m-ion driven path, [$A\ cm^{-2}$]

J_{TOT} : cell total current density, [$A\ cm^{-2}$]

$R_{External}$: sum of the specific area resistances that are common to both ion paths, [$\Omega\ cm^2$]

R_i : specific area polarization resistance of the i-th reactant gas, [$\Omega\ cm^2$]

R_Ω : specific area ohmic resistance, [$\Omega\ cm^2$]

V: cell measured voltage, [V]

II. INTRODUCTION

Molten Carbonate Fuel Cells (MCFCs) are a developed technology whose main applications are in the field of energy production and Carbon Capture and Storage (CCS). For this latter purpose, MCFCs have been the focus of great research interest because they allow the production of additional energy while capturing CO₂ and compared to other technologies which reduce power output in natural gas combined cycle retrofits.

Past experimental campaign [1-4] have shown that, using wet cathode feed fuel cell performance is higher than with dry cathode conditions. Moreover, current densities corresponding to utilization of CO₂ sensibly higher than the theoretical ones were observed (even >100%) This was found to be the result of a mechanism with water as a possible intermediate for the reaction between CO₂ and O₂ which decreases the polarization due to the CO₂ diffusion. However, more recent tests performed at low CO₂ concentrations [5] showed the emergence of a second electrochemical reaction path involving hydroxide ions, parallel to the one provided by the reactions of the carbonate ions.

III. APPROACH TO THE DUAL-ANIONS PATH

The first step of the analysis consisted in the identification of an equivalent electrochemical circuit that can be used to describe the reactions occurring inside the cell.

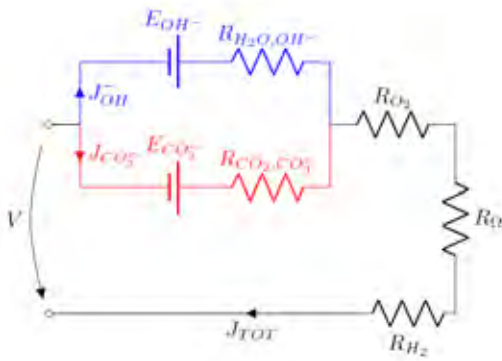


Fig. 1. Electrochemical equivalent circuit to describe an MCFC working with dual-anion mechanism.

Based on this analysis, the circuit presented in Fig. 1 was proposed. The phenomenon can be described by two parallel reaction paths that are represented by the two parallel branches of the circuit (red for the carbonate and blue for the hydroxide). Each parallel branch of the circuit is characterized by its own generator (the equilibrium potential of each path) and the resistance of the reactant gas that provides with the reacting ions. The ohmic resistances and the polarization resistances of H₂ and O₂ were situated in the common branch since the experimental data did not show preference for any of the two paths when varied.

Thus, to identify the cell performance, it is necessary to solve the following equations system that can be derived by the circuit analysis:

$$\begin{cases} V = E_{CO_3^-} - J_{CO_3^-} R_{CO_2} - J_{TOT} R_{External} \\ V = E_{OH^-} - J_{OH^-} R_{H_2O} - J_{TOT} R_{External} \\ J_{TOT} = J_{CO_3^-} + J_{OH^-} \end{cases}$$

To express the polarization resistances, starting from the Butler-Volmer equations different expressions were derived as described in previous works by the authors [3].

IV. INTEGRATION INTO THE SIMFC CODE

The system of equations and the resistances equations that describe this dual-anion model were implemented into the SIMFC (Simulation of Fuel Cells) code.

SIMFC is a Fortran code developed by the authors [3] that on the basis of local mass, energy, charge and momentum balances allows to model the performance of high temperature fuel cells (namely MCFCs and Solid Oxide Fuel Cells). Because of this, it can be used to acquire not only average cell information, such as the cell voltage or the total current density, but also to evaluate local variables, such as local compositions, polarisations, current density and reactant utilization factors. This feature is critical for both theoretical and feasibility studies: local cell data are essential to understand the phenomena that take place in the cells as well as to avoid critical points in optimising operating conditions. Nevertheless, many of these cannot be measured, but only calculated by an adequately detailed modelling.

Moreover, SIMFC can be implemented in more complex simulators such as Aspen Plus or other commercial software.

The results of the simulation are reported in Fig. 2 where the voltage obtained using the SIMFC code simulation (Simulated Voltage) is reported versus the Experimental Voltage.

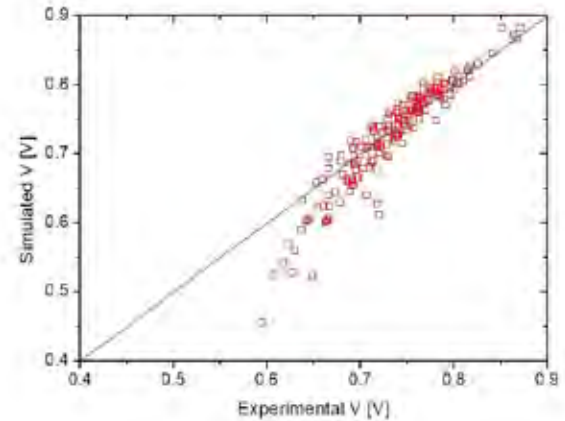


Fig. 2. Simulated Voltage vs. Experimental Voltage.

The average percentage errors on the Voltage fitting is of about 3%, with the % error for each point evaluated as:

$$\% \text{ error} = \frac{|V_{Experimental} - V_{Simulated}|}{V_{Experimental}} \cdot 100$$

V. CONCLUSION

In this work, the authors presented the theoretical analysis of MCFCs working with a dual-anion reaction mechanism. The authors developed a kinetic formulation capable to describe the performance of MCFC in these newly observed conditions. The average percentage error obtained by the fitting of the experimental data is of about 3% on the cell Voltage.

REFERENCES

- [1] Sugiura, K., Takei, K., Tanimoto, K., Miyazaki, Y., The carbon dioxide concentrator by using MCFC Journal of Power Sources, Volume 118, 2003, Pages 218–227.
- [2] Nishina, T., Ohuchi, S., Yamada, K., Uchida, I., Water effect on oxygen reduction in molten (Li + K)CO₃ eutectic, Journal of Electroanalytical Chemistry, Volume 408, 1996, Pages 181–187.
- [3] Arato, E., Audasso, E., Barelli, L., Bosio, B., Discepoli, G., Kinetic modelling of molten carbonate fuel cells: Effects of cathode water and electrode materials, Journal of Power Sources, Volume 336, 2016, Pages 18–27.
- [4] Audasso, E., Barelli, L., Bidini, G., Bosio, B., Discepoli, G., Molten Carbonate Fuel Cell performance analysis varying cathode operating conditions for carbon capture applications, Journal of Power Sources, Volume 348, 2017, Pages 118–29.
- [5] Kiss, G., Barckholtz, T., Han, L., Rosen, J., Geary, T., Ghezal-Ayagh, H., Hilmi, A., William, C., Yuh, C.-Y., Improved Understanding of Molten Carbonate Fuel Cell Electrolyte Behavior at Carbon Capture Conditions, 11th International symposium on Molten Salts, May 19-23 2019, Orleans (France).

FCHgo – FUEL CELLS HYDROGEN EDUCATIONAL MODEL FOR SCHOOLS

T. Altiero¹, M. Cesari¹, A. Contini¹, A. Landini¹, M. Romagnoli², F. Corni³, E. Dumont⁴, H. U. Fuchs⁴, and G. C. Karwasz⁵

¹Department of Education and Humanities, University of Modena & Reggio Emilia, Reggio Emilia (Italy)

²Department of Engineering 'Enzo Ferrari', University of Modena & Reggio Emilia, Modena, (Italy)

³Faculty of Education, Free University of Bozen, Brixen – Bressanone (Italy)

⁴Institute of Applied Mathematics and Physics, Zurich University of Applied Sciences, Winterthur (Switzerland)

⁵Nicolaus Copernicus University, Department of Physics Education, Torun (Poland)

Abstract - In this paper we present the development of our Horizon 2020 project FCHgo (Fuel Cell HydroGen educatiOnal model for schools, Call H2020-JTI-FCH-2018-1, GA n. 826246). This project is directed to children and adolescents between 8 and 18 years old. Its goal is to raise awareness for renewable energy sources, in particular hydrogen driven fuel cell technology. We will develop and disseminate a toolkit for teachers and pupils, based on a narrative approach to science and technology. We believe the narrative approach to be best suited for this project, because it enables us to take account of the cognitive tools of pupils at various stages of development.

Index Terms - Fuel Cell Hydrogen, Educational material, Science education, Sustainable energy.

I. NOMENCLATURE

FCHgo – Fuel Cell Hydrogen Educational model for schools.

EPDM – Educational Programme Delivery Model.

II. EXTENDED ABSTRACT

The EU project FCHgo (Fuel Cell HydroGen educatiOnal model for schools, Call H2020-JTI-FCH-2018-1, GA n. 826246), which is coordinated by the University of Modena and Reggio Emilia (Italy), involves other six partners from all over the Europe: Italy, Germany, Switzerland, Poland and Denmark. In addition, third parties from Turkey and Germany, and stakeholders from industry and schools are involved too. In Figure 1 the artistic logo.

The purpose of the project is to encourage a culture of ecological awareness and to develop behaviors based upon sound knowledge of key technologies by the coming

generations. It aims at creating and disseminating educational material for young learners and their teachers to be used in primary and secondary schools about science and technology of hydrogen fuel cells. Presently contacted number of schools exceeds the estimated number of 38 schools/ classes fixed in the Proposal.



Fig. 1. FCHgo logo

The partners involved in the project are nine, from six different countries. To achieve its specific objectives the project activities are divided into five Work-Packages (WPs): WP1 – Management (UNIMORE); WP2 - Educational program delivery model (EPDM) co-production; WP3 – Test and experimentation of the EPDM; WP4 – FCHgo European award; WP5 – Dissemination, communication and exploitation plan.

We will address a number of challenges faced by citizens in industrialized countries. Among these are a lack of basic understanding of the role of energy and energy carriers in physical and biological systems; lack of specific knowledge of fuel cell technology (such as the functioning of chemical batteries and fuel cells, the role of hydrogen as an energy

carrier); a lack of understanding of the interaction of technological, environmental, economic, and social systems. Better understanding of such challenges by a larger number of people, from pupils to their families and acquaintances will be central for technological, economic, and social progress that is to guide and help us through the transformation of society toward sustainable energy systems.

From a scientific and engineering viewpoint, we make use of modern developments in physics, chemistry, and systems engineering, and integrate it with the best knowledge available regarding FCH technologies. But young children cannot be expected to understand such complex systems derived from a top-down approach originating in formal science and engineering. Therefore, we will develop a narrative approach to FCH technologies, suitable to young children and consistent with a formal path without any loss of stringency.

Narrative has received much attention in recent investigations into science education; it has become clear that there is a wide range of forms and uses of narrative in science. We concentrate upon a meaning of narrative that is closely tied to conceptual structure and understanding of science.

The human mind creates images of the working of forces of nature that can be rendered in stories [1,2,3] or in animations using visual metaphors. Similarly to the simple animation about the exchanges of energy occurring in an imaginary perpetual motion machine developed by M. Deichmann [4], a video about fuel cells is in preparation.

Visual metaphors telling the story of the interaction of forces of nature in energy systems can also be cast in the form of plays. We shall produce such energy plays where students act as energy carriers in systems that create chains of processes (such as sun to solar cell to electrolysis of water to producing an electric output by a fuel cell to driving an engine or lighting a lamp).

While empowering the imagination and imaginative rationality with the help of stories and play of forces of nature (such as sunlight, hydrogen, electricity, heat) is in the foreground for young children (8-12 years of age), making use of imaginative rationality in the creation of mental and computer models from stories told and re-told, forms the core of a methodology for older students (12-18 years of age). Moreover, stories provide a repository, for adolescents, of much detailed knowledge about a subject that is more properly conveyed narratively than, say, in printed tables or long expositions.

Stories of forces of nature interacting in energy chains have been converted into graphical representations [5] using the same metaphors as those that structure stories and play in general. Process-diagrammatic techniques provide us with didactic means for older learners where story-worlds (models) are created in a form that is intermediate between story or play and formal computer models. Among educational materials, instructions how to use simple physical objects that allow students to assemble process diagrams for a large range of concrete systems will be tested and validated in a total of about 50 European pilot schools/classes, before to be disseminate all over the Europe.

III. CONCLUSION

This project aims at creating and disseminating educational material for young learners (primary and secondary schools) and their teachers to be used in primary and secondary schools about science and technology of hydrogen fuel cells. Our methodology is centered on narratives (stories and plays for the youngest) and provides direct physical as well as mental involvement for pupils. Students and teachers will be involved in telling and creating stories or narratives, experiencing the assembly and the functioning of simple toys or devices. They will discuss forces of nature acting in the toys and devices, design and play how forces of nature act and involve energy, construct process diagrams with more or less formalized iconographic materials, reflect upon FCH technology, applications, and job opportunities. The EPDM will provide didactic materials and teacher guides for the network of schools and stakeholders that will make use of this project.

ACKNOWLEDGMENT

The project FCHgo has received funding from the Fuel Cells and Hydrogen 2 Joint Undertaking under grant agreement No 826246. This Joint Undertaking receives support from the European Union's Horizon 2020 research and innovation programme.

REFERENCES

- [1] Hans U. Fuchs, Annamaria Contini, Elisabeth Dumont, Alessandra Landini, and Federico Corni (2018), "How metaphor and narrative interact in stories of forces of nature". In: Michael Hanne and Anna A. Kaal (Ed.), *Narrative and metaphor in education: Look both ways*. Abingdon, UK and New York, NY: Routledge, pp. 91-104.
- [2] Fuchs, H. U. (2013a). *Il significato in natura*. In Corni F. (ed.) (2013): *Le scienze nella prima educazione. Un approccio narrativo a un curriculum interdisciplinare*, Erickson, Trento, Italy. English version: *Meaning in Nature—From Schematic to Narrative Structures of Science*. Retrieved from www.hansfuchs.org/LITERATURE/Literature.html.
- [3] Fuchs, H. U. (2013b): *Costruire e utilizzare storie sulle forze della natura per la comprensione primaria della scienza*. In Corni F. (ed.) (2013): *Le scienze nella prima educazione. Un approccio narrativo a un curriculum interdisciplinare*, Erickson, Trento, Italy. English version: *Designing and using stories of forces of nature for primary understanding in science*. Retrieved from www.hansfuchs.org/LITERATURE/Literature.html.
- [4] Deichmann, M. (2014). *Im übertragenen Sinne. Metaphern und Bildvergleiche in der Wissenschaft* (Bachelor thesis). Zürcher Hochschule der Künste, Zurich. Movie to be found at <http://vimeo.com/98311515>
- [5] Fuchs, H. U. (2010): *The Dynamics of Heat*. Second Edition. Graduate Texts in Physics. Springer, New York. (First Edition: Springer, New York, 1996.)

DEGRADATION BEHAVIOR OF STATE OF THE ART PtCO CATALYST: AN EX- AND IN – SITU ANALYSIS

David Bernhard*, Thomas Kadyk**, Ulrike Krewer**, Sebastian Kirsch*
* Volkswagen Aktiengesellschaft, Brieffach 011/17775, 38436 Wolfsburg, Germany
** Institute of Energy and Process Systems Engineering at the TU Braunschweig,
Franz-Liszt-Straße 35, 38106 Braunschweig, Germany

Abstract - In this work, accelerated stress test aged PEMFC cathodes are analyzed with an advanced diagnostic procedure, designed to study the influence of platinum oxides on performance losses. It is found that ignoring losses from platinum oxide leads to a miss-interpretation of voltage losses – indeed, the so-far unassigned voltage losses are much more relevant than widely believed.

Index Terms – PEMFC, Degradation, Loss-Breakdown, Platinum oxides (PtOx),

I. INTRODUCTION

The proton exchange membrane fuel cell is a promising energy conversion device for automotive applications [1]. State of the art cathode materials – like the PtCo catalyst or the carbon support – are prone to lifetime limiting degradation under a wide range of relevant operation conditions [1,2]. This ageing must be reduced in order to be competitive with conventional combustion engines [2,3]. Car manufacturers must gain detailed understanding of degradation under relevant driving conditions. Only with this insight hybridization strategies can be developed in order to reach the necessary lifetime targets while using the minimum amount of precious metal.

High-loaded cathodes containing no Pt-alloys (but only Pt) suffer majorly from a loss of electrochemical surface area (ECSA), which is linked to the cell voltage losses via the Tafel-relation [4,5]. However, low-loaded cathodes containing Pt-alloys can suffer from additional mechanisms, such as an increased oxygen transport resistance (R_{O_2}), specific activity (SA) loss and reduced protonic conductivity in the ionomer (R_{H^+}) [3,6].

Although, examples like [3,6] show that many researchers are aware of the different cathode loss mechanisms and related properties, one loss mechanism that is always neglected when analyzing cathode degradation is the formation of surface oxides on the catalyst. Surface oxides are formed by the oxidation of physisorbed H_2O which impact the ORR by “poisoning” part of the active sites [3,7]. Such PtOx-losses grow logarithmically in time [8,9] and can be as high as ~100mV, depending on the potential and the hold time with which it is grown. In this work, a new diagnostic procedure is implemented to assign voltage losses in polarization curves to PtOx, high frequency resistance (HFR), R_{O_2} , ECSA, SA and R_{H^+} . Consequently, this procedure is used to study voltage losses during cathode degradation, whereby the focus

in this contribution lies on analyzing the PtOx-losses.

II. EXPERIMENTAL

Experimental data was gathered using a 5cm² MEA-design based on the studies of Baker and Caulk [10]. Prior to the ageing experiments, the MEAs (cathode: PtCo; 0.25mg_{Pt}/cm²) were activated with an in-house procedure, containing a current ramp to 1A/cm² and consecutive air starves. The cell was considered “conditioned” when the voltage benefit between air starves was lower than 2mV.

For the accelerated stress tests (AST) a square wave profile with an upper potential limit (UPL) of 1.0V and a lower potential limit (LPL) of 0.6V was used. The hold time at UPL and LPL was varied from 2.5s to 20s in the course of this study. The other operation conditions of the AST were 90°C, 100% relative humidity at the cell-inlet, 200kPa cell-inlet pressure and constant flows of 5.0nlm H₂ (anode) and air (cathode).

The cell performance and the related cell properties were determined with a new diagnostic procedure. Apart from cyclic voltammetry to derive ECSA, the procedure comprises individual holds at current densities between 2.0 and 0.0A/cm². Figure 1a shows one exemplary load point (3) with its conditioning steps (1-2). The outcome of the procedure applied to a BoL-sample can be seen in Fig. 1b.

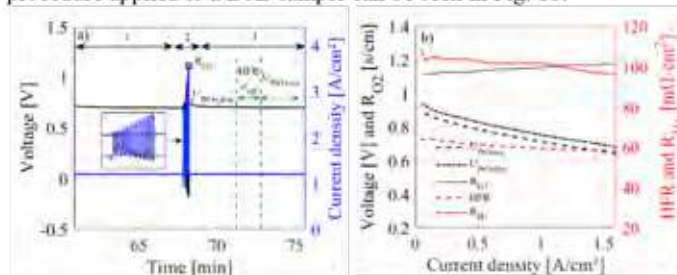


Fig. 1: a) Measurement procedure of the routine at an exemplary load point. In the diagnostic phase, other operation conditions are 80°C, 5nlm (air and H₂), 100%rH_{in} and 20bar_{in}. b) exemplary dataset obtained with the LBD-routine.

In the 1st step (Fig. 1) the cell is conditioned at the desired current density to set up the right liquid water profiles in the MEA. Under many operation conditions no liquid water is expected in the MEA – nevertheless, the 7min–hold is generally used as a standard scheme.

In the 2nd step ten quick jumps (1s each, see insert in Fig. 1a) to voltages lower than 0.2V are carried out. The aim of this sequence is two-fold. On the one hand, at these low voltages PtOx is completely reduced. On the other hand, from this sequence the true R_{O_2} can be estimated: In the first jump, the current density at 0.2V is gathered and this current density is increased in the next jumps by adding each time 5%. From averaging voltage and current density during these ten jumps the real limiting current (and therefore the real R_{O_2}) for the load point of interest can be estimated – namely the current density at the reversal point. This procedure to determine R_{O_2} for the conditioned load point is legitimate because the time constants of all processes but the adaption of the liquid water profiles are smaller than 20ms [11], whereby the liquid water adaption requires at least 10s. Oppositely, any stationary method (e.g. [6,10]), where hold times of minutes are applied, would measure R_{O_2} at saturation profiles different from those in the polarization curves and are therefore not suited to derive oxygen transport related voltage losses.

In the 3rd step the current density of interest is held for 7mins. Thereby, a voltage loss is seen that is attributed to the formation of PtOx. The maximal voltage in this transient (~1s after the start of step 3) is considered to be PtOx-free¹. The average of the last two minutes is referenced as PtOx-equi voltage. EIS-Spectra between 50Hz and 30kHz are recorded from minute 3 to minute 4.5 and fitted with the help of a transmission line model to derive HFR and R_{H^+} [12].

Additionally, the specific activity (SA) is derived from an estimation of the PtOx-equi voltage at 0.9V divided by ECSA.

III. RESULTS

The different contributors to the performance change due to degradation are summarized in equation (1). Importantly, the explicit calculation of the first six terms at rhs and the explicit measurement at lhs allows the quantification of so-far unassigned voltage losses ΔU_7 (discussed for example in [6])

$$\Delta U_{\text{loss}} = \Delta U_{\text{ECSA}} + \Delta U_{\text{SA}} + \Delta U_{\text{O}_2} + \Delta U_{\text{H}} + \Delta U_{\text{PtOx}} + \Delta U_{\text{H}^+} + \Delta U_7 \quad (1)$$

Figure 2a compares a representative begin of life (BoL) “PtOx-equi” polarization curve with end of test (EoT) curves for ASTs of different hold times. In Fig. 2b-d, the voltage differences between BoL and EoT is analyzed by means of equation (1), parametrized with the diagnostic information described above.

In the most cases, it was found that R_{O_2} and HFR experience very little change – therefore especially ΔU_{H} is negligible and the $\Delta U_{R_{O_2}}$ is not that significant although carbon corrosion can be detected with SEM measurements.

For the measured R_{H^+} values no discernible trend is observable for the different samples and therefore the cell performance can even be improved by an increased EoT proton conductivity.

Considerable voltage losses are arising from a drop in activity (ΔU_{ECSA} and ΔU_{SA}). Oppositely, voltage gains arise from PtOx. That does not mean that PtOx enhances activity at EoT but represents the fact that PtOx causes less voltage losses at EoT compared to BoL. The measured “PtOx free” polarization curves show differences up to 40 mV between the BoL and EoT samples. This finding is intuitive as PtOx formation is enhanced at higher half-cell voltages [7] and at EoT this voltage is lower compared to BoL.

¹ Clearly, the term “PtOx-free” is somewhat misleading as in the first second of the hold time some surface adsorbates will have formed. However, as losses from PtOx-formation develop logarithmic in time more PtOx-losses are to

IV. CONCLUSION

Performance losses after cathode degradation testing caused by PtOx formation are reduced at EoT. In this work, this reduction is quantified for the first time. With this work, we want to raise the awareness, that PtOx should be addressed (at best quantified) during cathode degradation testing. Otherwise, wrong conclusions about the other voltage losses at EoT would be drawn – especially the relevance of the unassigned voltage losses would be under-estimated.

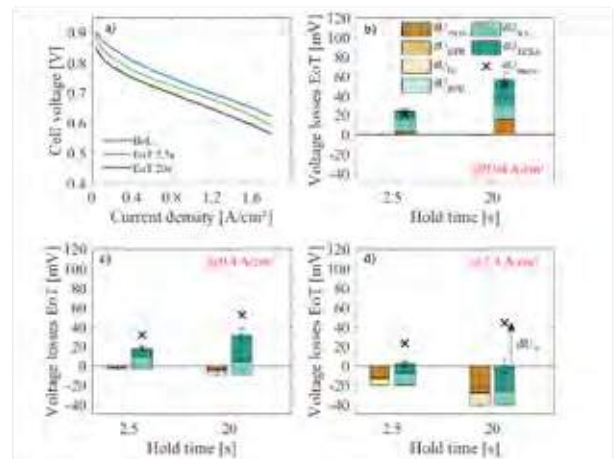


Fig. 2: (exemplary presentation) a) Polarization curves at the begin of test (BOT) and at the end of different ASTs (EOT) b) comparison of the calculated voltage losses or gains obtained from the LBD procedure and the measured voltage losses between BOT and EOT @ 0.04, 0.4 and 1.4 A/cm².

REFERENCES

- [1] S. Rasouli, R.A. Ortiz Godoy, Z. Yang, M. Gummalla, S.C. Ball, D. Myers, P.J. Ferreira *Journal of Power Sources* 343 (2017) 571–579.
- [2] Y. Cai, J.M. Ziegelbauer, A.M. Baker, W. Gu, R.S. Kukreja, A. Kongkanand, M.F. Mathias, R. Mukundan, R.L. Borup, *J. Electrochem. Soc.* 165 (6) (2018) F3132-F3138.
- [3] D.D. Papadias, R.K. Ahluwalia, N. Kariuki, D. Myers, K.L. More, D.A. Cullen, B.T. Sneed, K.C. Neyerlin, R. Mukundan, R.L. Borup, *J. Electrochem. Soc.* 165 (6) (2018) F3166-F3177.
- [4] P. Zihrl, I. Hartung, S. Kirsch, G. Huebner, F. Hasché, H.A. Gasteiger, *J. Electrochem. Soc.* 163 (6) (2016) F492-F498.
- [5] P. Schneider, C. Sadeler, A.-C. Scherzer, N. Zamel, D. Gerteisen, Fast and Reliable State-of-Health Model of a PEM Cathode Catalyst Layer, *J. Electrochem. Soc.* 166 (4) (2019) F322-F333.
- [6] G.S. Harzer, J.N. Schwämmlein, A.M. Damjanović, S. Ghosh, H.A. Gasteiger, *J. Electrochem. Soc.* 165 (6) (2018) F3118-F3131.
- [7] N.P. Subramanian, T.A. Gresler, J. ZHANG, W. Gu, R. Makharia, *J. Electrochem. Soc.* 159 (5) (2012) B531-B540.
- [8] B.E. Conway, B. Bamett, H. Angerstein-Kozłowska, B.V. Tilak, *J. Chem. Phys.* 93 (11) (1990) 8361–8373.
- [9] M. Alsabet, M. Grden, G. Jerkiewicz, *Journal of Electroanalytical Chemistry* 589 (1) (2006) 120–127.
- [10] D.R. Baker, D.A. Caulk, K.C. Neyerlin, M.W. Murphy, *J. Electrochem. Soc.* 156 (9) (2009) B991.
- [11] M. Göbel, S. Kirsch, L. Schwarze, L. Schmidt, H. Scholz, J. Haubmann, M. Klages, J. Scholta, H. Markötter, S. Alrwashdeh, I. Manke, B.R. Müller, *Journal of Power Sources* 402 (2018) 237–245.
- [12] R. Makharia, M.F. Mathias, D.R. Baker, *J. Electrochem. Soc.* 152 (5) (2005) A970.

come in the following minutes and the voltage after 1s is also a somewhat optimal voltage (at the conditioned liquid water profiles) from the perspective of a fuel cell under operation.

EXPERIMENTAL STUDY OF THE PERFORMANCE OF THE ANODE SUPPORTED SOLID OXIDE FUEL CELLS (SOFC) FED WITH AEROSOL CONTAMINATED FUEL

M. Skrzyplikiewicz*, M. Wierzbicki***, K. Motylinski***
and S. Jagielski***

*Department of High Temperature Electrochemical Processes
(HiTEP), Institute of Power Engineering, Augustowka 36, 02-981
Warsaw, (Poland)

**Institute of Heat Engineering, Warsaw University of Technology,
Nowowiejska 21/25, 00-665 Warsaw, (Poland)

Abstract - Various solid oxide fuel cells (SOFC) manufacturers and literature sources [1] state that SOFC does not tolerate the presence of solid particles in the delivered fuel (e.g. fly ash from gasification process). However, the issues related to feeding SOFCs with particulate matter suspended in the fuel have not been comprehensively investigated in the literature.

Within this study, a standard 5 cm x 5 cm anode-supported SOFC was fueled by an aerosol of solid inert powder (grain sizes and concentration equivalent to gasifier fly ash) suspended in a reference hydrogen - nitrogen mixture as well as with a dust-free reference gas.

Maximum power density of SOFC equaled 717 mW/cm² (850°C, reference fuel). Feeding aerosol-fuel caused no rapid change on power density value. Moderate drop of performance was observed throughout twin independent experiments. Post-mortem analysis revealed contamination on walls of gas channels, but no evidence of alumina was found within the anode.

Index Terms – degradation, dust, particulate matter, SOFC.

I. INTRODUCTION

The presence of particulate matter in a gas from the thermochemical conversion of coal, biomass, waste or other solid fuels is obvious (e.g. fly ash, condensed tars, char, etc.). The physical and chemical structure of particulates suspended in the gas depend on the gasified raw material (solid fuel) and the method for carrying out the thermochemical conversion process.

Similarly to Din and Zainal [1], back in 2016, the authors could not find any published results of experimental or theoretical works regarding the effect of particulates presence in the gaseous fuels on processes occurring in the SOFC anodic part. However, there are some publications in the literature with

investigations of the particulate size distribution and their chemical composition in the producer gas from gasification units [2]. Results from these analyses point on ranges of size distributions (1 ÷ 10 µm) and concentrations (600 ÷ 1000 mg/Nm³) of particles present in the producer gas. These values were used as a starting point for the design of experiment within this work.

The current study is focused on the possibility of precipitation of solid particles in the fuel channels, and inside the porous SOFC anode structure during its operation.

II. EXPERIMENTAL

A. Powder preparation

An alumina powder HVA (Cerel, Poland) was ball-milled overnight and a bimodal distribution fine powder was obtained. Then, the powder was sieved on a 32 µm sieve. As a result, an inert ceramic powder of grain size distribution between 1 and 10 µm was prepared. The powder was dried in a laboratory drier prior to test with the aerosol generator.

B. SOFC description and experimental setup

The cells with external dimensions of 5 cm x 5 cm and the thickness about 1 mm were manufactured in the Ceramic Department (CEREL) of the Institute of Power Engineering (IEn) consist of the following layers: Ni-YSZ(anode support)|YSZ|GDC|LSCF, and were described elsewhere [3].

The test stand has been designed basing on a standard IEn SOFC test-bench scheme, which was described elsewhere [4]. It has been additionally equipped with an in-house developed

solid aerosol generator installed on the anode gas supply line, just before entering the SOFC housing. The system allows to obtain aerosols of the powder of ca. $3500 \div 5000 \text{ mg/Nm}^3$ concentration. During the performed experiment, the generated aerosol was diluted to concentration ca. 1000 mg/Nm^3 .

C. Experimental procedure

After reaching the sealing temperature of 885°C (heat-up ramp 50°C/h , anode flow 200 Nml/min N_2 , cathode flow 500 Nml/min of air), the setup was kept at this temperature for 15 minutes, and cooled down to operational temperature of 850°C . After that, cell reduction occurred by the increase of hydrogen flow from 0 to 800 Nml/min in 4 equal steps within ca. 1h. Parallely air flow was increased to 2000 Nml/min .

Cell stabilization under 0.375 A/cm^2 was conducted for ca. 24 h (initial voltage 0.85 V). After preliminary characterization, the aerosol generator has been turned on and stabilized for 2 h, emitting aerosol to a water bubbler (nitrogen flow 200 Nml/min) and later connected to the fuel supply line. After that, the cell was operated on anodic aerosol ($800 \text{ Nml/min H}_2 + 200 \text{ Nml/min N}_2 + 1000 \text{ mg/Nm}^3$ alumina micro-powder) in constant current mode (0.375 A/cm^2) for 184 hours.

D. Experimental results

The voltage of the cell was recorded throughout the realized experiment. Cells polarization curves were measured before contamination and after ca. 140 h of operation on aerosol fuel.

In the initial phase of experiment, EIS spectrum was measured. Similar EIS scan has been recorded after applying the dust-contaminated fuel to the anode (Fig. 1) but with lower number of measurement points to avoid disturbances caused by predicted degradation of the cell over time.

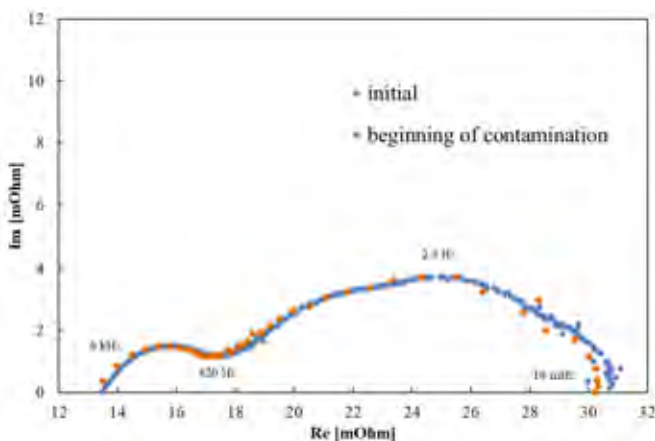


Fig. 1. EIS spectra measured initially (blue) and just after applying contamination (orange) at constant current 0.375 A/cm^2 (AS-SOFC $5 \text{ cm} \times 5 \text{ cm}$, temperature 850°C , anode flow: $800 \text{ Nml/min H}_2 + 200 \text{ Nml/min N}_2 + 1000 \text{ mg/Nm}^3$ alumina micro-powder).

The whole test has been repeated thereafter on a new cell, on

which a slightly lower power density was observed, not affecting any of the conclusions.

E. Post-mortem analysis

The post mortem analysis have been performed with SEM/EDX methods. The walls of gas channels were strongly contaminated with the white dust, but the cross-section of the pipes and channels remained open. No evidence of alumina was detected on the anode surface and pores with SEM/EDX.

III. CONCLUSION

A setup for investigation of SOFCs has been equipped with in-house developed aerosol generator. The system has been verified experimentally allowing repeatable cell performances.

Two independent tests have been performed to investigate the influence of micro-powder aerosol on SOFC performance. The influence of solid particles in the fuel flow on the performance of the cells is negligible in short term operation.

In extended operation (i.e. $> 100 \text{ h}$), significant amount of powder precipitated in inlet and outlet piping of the experimental setup. No dust inside the anode pores nor sticking to electrode surface has been observed. The cell performance was not influenced by chemically inert solid powder.

Operation in vertical arrangement could have had a positive influence on the anode state after the experiment.

Future work will address carbon-containing aerosol feed.

ACKNOWLEDGMENT

The work has been performed under NCN Preludium grant no. 2016/21/N/ST8/02349.

REFERENCES

- [1] Ud Din, Z. Zainal. Z.A., Biomass integrated gasification SOFC systems: Technology overview, *Renew. Sust. Energ. Rev.* 53, 2016, pp. 1356–1376.
- [2] Hofmann, P., Panopoulos, K.D., Fryda, L.E., Schweiger, A., Ouweltjes, J.P., Karl, J., Integrating biomass gasification with solid oxide fuel cells: effect of realproduct gas tars, fluctuations and particulates on Ni–GDC anode, *Int J HydrogEnergy* 2008;33:2834–44.
- [3] Kupecki J., Motylinski K., Skrzypekiewicz M., Wierzbicki M., Naumovich Y., Preliminary electrochemical characterization of anode supported solid oxide cell (AS-SOC) produced in the Institute of Power Engineering operated in electrolysis mode (SOEC), *Arch. Thermodyn.* 2017;38(4):53-63.
- [4] Skrzypekiewicz M., Wierzbicki M., Motylinski K., Jagielski S., Kozinski G., A test-bench for investigation of SOFC fuelled with gases containing solid particles, *Book of Abstracts, Konferencja Energetyka i Paliwa*, Kraków 19-21.09.2018, ISBN 978-83-948318-2-0.

Synthesis and Characterization of Ni-doped Double Perovskite $\text{Sr}_2\text{FeNi}_{0.4}\text{Mo}_{0.6}\text{O}_{6-\delta}$ as electrode for Symmetrical Solid Oxide Cell

A. Felli*, E. Squizzato**, G. Carollo**, M. Boaro*, and A. Glisenti**

* Università degli Studi di Udine, Dipartimento di Chimica, Fisica e Ambiente, Udine, 33100, Italy

** Università degli Studi di Padova, Dipartimento di Scienze Chimiche, Padova, 35131, Italy

Abstract - In this study, double perovskite $\text{Sr}_2\text{FeNi}_{0.4}\text{Mo}_{0.6}\text{O}_{6-\delta}$ was synthesized via citrate sol-gel method and characterized in order to investigate its structural and electrochemical properties as electrodes in a Symmetrical Solid Oxide Fuel Cell. XRD data revealed the formation of the double perovskite cubic phase. XPS analysis showed an enhanced presence of redox couples of both iron and molybdenum compared to non-doped $\text{Sr}_2\text{Fe}_{1.5}\text{Mo}_{0.5}\text{O}_{6-\delta}$. This implies the increase of electronic conductivity due to Ni^{2+} presence in the structure. $\text{Sr}_2\text{FeNi}_{0.4}\text{Mo}_{0.6}\text{O}_{6-\delta}$ was characterized as electrode in a symmetrical button fuel cell by EIS analysis. A carbon containing nanocomposite electrode was created by inducing a controlled hydrocarbon cracking. The electrochemical characterization was carried out using hydrogen and propane as fuels at 750 °C. The total polarization resistance of the cell was 1.414 $\Omega \text{ cm}^2$ in H_2 and 0.880 $\Omega \text{ cm}^2$ in propane at 750 °C, obtaining a maximum power density of 250 mW/cm^2 and 170 mW/cm^2 , respectively.

Index Terms - Double Perovskites, MIEC conductors, Molibdates, Redox Stability, Symmetrical and Reversible Solid Oxide Fuel Cells.

I. NOMENCLATURE

SFM: $\text{Sr}_2\text{Fe}_{1.5}\text{Mo}_{0.5}\text{O}_{6-\delta}$

SFNM: $\text{Sr}_2\text{FeNi}_{0.4}\text{Mo}_{0.6}\text{O}_{6-\delta}$

II. INTRODUCTION

The creation of a Symmetrical Solid Oxide Fuel Cell (SSOFC) is a way to reduce the fabrication costs and to improve reliability of SOFC, as well as the first step to realize Reversible Solid Oxide Cells (RSOC) [1]. Double perovskite $\text{Sr}_2\text{Fe}_{1.5}\text{Mo}_{0.5}\text{O}_{6-\delta}$ (SFM) have recently shown interesting properties as electrodes for SSOFC, such as its high stability in oxidizing and reducing atmospheres, and its good ionic and electronic conductivities in both the environments [2]. In order to increase the electronic conductivity of this material and enhance its catalytic activity with hydrocarbon fuels, we decided to study $\text{Sr}_2\text{FeNi}_{0.4}\text{Mo}_{0.6}\text{O}_{6-\delta}$ (SFNM), a Ni-doped variant of SFM. Our aim is in stabilizing Ni in the structure; we expect that this contributes to the capability to work as anode and cathode. Moreover, we will demonstrate the possibility to tune, through Ni presence, the formation of highly dispersed carbon by cracking of hydrocarbon fuel and to create a highly conductive electrode system.

III. EXPERIMENTAL AND RESULTS

A. Synthesis

SFNM powders were prepared by an auto-combustion based citrate procedure. The precursors we used were $\text{Sr}(\text{NO}_3)_2$, metallic Fe, $(\text{NH}_4)_6\text{Mo}_7\text{O}_{24} \cdot 4\text{H}_2\text{O}$, and $\text{Ni}(\text{NO}_3)_2 \cdot 6\text{H}_2\text{O}$. We prepared a solution by dissolving metallic Fe in HNO_3 (65%) and the other salts in distilled water. Citric acid was added to the solution as complexing agent in a 2:1 citric acid : cations molar ratio. The pH solution was adjusted at 8 using ammonia. The solution was then dried at 80 °C for 10 hours. The obtained gel was burned at 350 °C by auto-ignition and then calcinated at 1100 °C for 10 hours.

B. Characterization

XRD analysis showed a single pure cubic phase. The double perovskite was successfully obtained, without any secondary phase formation. Semi-quantitative XPS analysis (see Table I) showed that the ratios of iron cations and molybdenum cations are closer to 1, revealing that both the number of iron and molybdenum redox pairs increased in SFNM with respect to which is reported for the SFM in the literature [3].

TABLE I
 $\text{Fe}^{2+}/\text{Fe}^{3+}$ AND $\text{Mo}^{6+}/(\text{Mo}^{5+}+\text{Mo}^{4+})$ COUPLE RATIOS FOR SFM AND SFNM

	$\text{Fe}^{2+}/\text{Fe}^{3+}$	$\text{Mo}^{6+}/(\text{Mo}^{5+}+\text{Mo}^{4+})$
SFM	1,5	1,7
SFNM	0,8	0,9

This would be an evidence that the electron conductivity of SFNM is increased due to Ni^{2+} presence [3].

The chemical composition of SFNM, which is really similar to nominal values, is confirmed by EDX and XPS. It is, therefore, inferred that surface segregations are negligible.

C. EIS (Electrochemical Impedance Spectroscopy)

SFNM was characterized as electrode in an electrolyte-supported button cell using GDC (Gadolinium-Doped Ceria) as electrolyte. A SFNM ink was prepared and deposited as both anode and cathode by screen printing.

The cells were tested using hydrogen and propane as fuels. The Nyquist plots were fitted using Z-view software on basis of the equivalent circuit shown in Fig.1. The best results were obtained at 750 °C, as shown in Fig. 1. The R_1 contribution in the circuit is associated with the ohmic resistance of the cell.

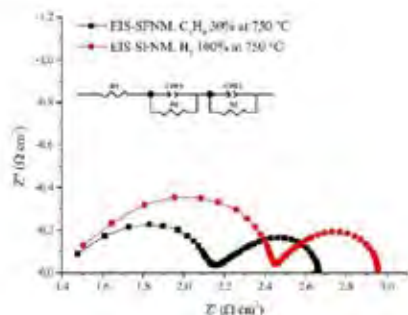


Fig. 1: EIS characterization of SFNM as electrode in a S-SOFC at 750 °C in hydrogen (red) and propane (black).

Impedance characterization has shown two main processes. The high frequency arc (R_2) was attributed to anode and cathode reaction processes (the hydrogen/propane oxidation reaction at the anode and the oxygen reduction reaction at the cathode). The difference of the values of R_2 between hydrogen (red) and propane (black) should be related to an improvement of the anodic process in presence of propane. The electronic conductivity of the electrode may have been increased as consequence of deposit of carbon from propane cracking reaction. The low frequency arc (R_3) was attributed to mass transfer limitations. The polarization R_3 has shown a constant value in different fuel flow rates and at different temperatures, so it should be related to the high density of the gold paste collectors, which hindered the access of fuel gaseous reactants to the active surface [4]. SEM images of gold collectors had confirmed this assumption. The total polarization of cell was 1.414 Ωcm^2 in H_2 and 0.880 Ωcm^2 in propane at 750 °C. By eliminating the second contribution, it would be possible to reach a total resistance of 0.960 Ωcm^2 in H_2 (which is higher than non-doped SFM [2]) and 0.440 Ωcm^2 in propane at 750 °C, respectively. SFNM was also characterized as a cathode by EIS, obtaining low ASR (Area Specific Resistance) value (0.206 Ωcm^2), which suggests that this is a better cathode material than non-doped SFM (0.240 Ωcm^2) [2].

D. Fuel Cell performance and stability

The performances of a single cell with symmetrical electrodes of SFNM were investigated. The starting OCV (Open Circuit Voltage) of the cell was 0.865 V. The maximum power density (P_{max}) reached at 750 °C were 250 mW/cm^2 in hydrogen and 170 mW/cm^2 in propane, respectively. The electrodes exhibited no degradation when tested in 10% of H_2 at 700 °C for 24 hours, and carbon formation on their surface during several hours in propane. A successive test in hydrogen have demonstrated how a controlled deposition of carbon on the surface of the electrodes (due to cracking reactions of propane) had a beneficial effect, increasing their electronic conductivity and performances. The

P_{max} using 5% of hydrogen at 750 °C was 115 mW/cm^2 before propane supply, and 129 mW/cm^2 after several hours of operation in propane.

IV. CONCLUSION

In this contribution we successfully demonstrated the possibility to stabilize Ni in a double perovskite $\text{Sr}_2\text{FeNi}_{0.4}\text{Mo}_{0.6}\text{O}_{6-\delta}$. We expected to be able to create i) a conductive nanocomposite electrode by inducing the formation of carbon by hydrocarbon fuel cracking, ii) an electrode working reversibly. The perovskite was properly synthesized via an auto-combustion based citrate procedure, as confirmed by XRD (single cubic phase) and XPS analysis. A larger number of redox couples than the non-doped SFM are generated by Ni-doping. EIS characterization has shown two different resistive processes, and the total polarization values of the electrodes were 1.414 Ωcm^2 in H_2 and 0.880 Ωcm^2 in propane at 750 °C, respectively. Impedance characterization in air has also showed that SFNM is a better cathode material than SFM, with an ASR of 0.206 Ωcm^2 . For the first time, we have also demonstrated that SFNM shows good performance in propane with a high resistance to carbon deposition. A controlled carbon deposition has been obtained and observed to have a positive effect on conductivity of the material, and to increase the cell power density. Stability tests proved that SFNM is stable in both oxidizing and reducing atmospheres and the electrochemical performance are good in both the electrodes.

Concluding, double perovskite $\text{Sr}_2\text{FeNi}_{0.4}\text{Mo}_{0.6}\text{O}_{6-\delta}$ can be considered a promising electrode in SSOFCs realization; moreover, when Ni dispersion and amount are highly controlled the formation of highly dispersed carbon can be obtained with significant increment of the electrochemical performance.

V. ACKNOWLEDGEMENT

Thanks to PRIN 2017 - *Direct Biopower* project to funding this work.

REFERENCES

- [1] J. C. Ruiz-Morales, D. Marrero-López, J. Canales-Vázquez, and J. T. S. Irvine, Symmetric and reversible solid oxide fuel cells, *RSC Advances*, Volume 1, 2011, no. 8, pp. 1403–1414.
- [2] Q. Liu, C. Yang, X. Dong, and F. Chen, Perovskite $\text{Sr}_2\text{Fe}_{1.5}\text{Mo}_{0.5}\text{O}_{6-\delta}$ as electrode materials for symmetrical solid oxide electrolysis cells, *International Journal of Hydrogen Energy*, Volume 35, 2010, no. 19, pp. 10039–10044.
- [3] N. Dai, J. Feng, Z. Wang, T. Jiang, W. Sun, J. Qiao and K. Sun, Synthesis and characterization of B-site Ni-doped perovskites $\text{Sr}_2\text{Fe}_{1.5-x}\text{Ni}_x\text{Mo}_{0.5}\text{O}_{6-\delta}$ ($x = 0, 0.05, 0.1, 0.2, 0.4$) as cathodes for SOFCs, *Journal of Materials Chemistry A*, Volume 1, 2013, no. 45, p. 14147.
- [4] S. B. Adler, Factors Governing Oxygen Reduction in Solid Oxide Fuel Cell Cathodes, *Chemical Reviews*, Volume 104, 2004, no. 10, pp. 4791–4844.

SIZING OF INTEGRATED SOLAR PHOTOVOLTAIC AND ELECTROLYSIS SYSTEMS FOR CLEAN HYDROGEN PRODUCTION

P. Colbertaldo*, G. Guandalini*, G. Lozza*, S. Campanari*

*Department of Energy, Politecnico di Milano, Via Lambruschini 4A, 20156 Milano (Italy)

Abstract - This work presents a method to design an optimised system that combines electrolysers and solar photovoltaic panels for sustainable hydrogen production. Given the daily and seasonal variations of the electricity output vs. a stable hydrogen demand, power exchange to/from the electric grid and hydrogen storage systems are considered. The aim is to determine the optimal size of the PV field, the electrolyser, and the storage, for a given hydrogen demand, by minimising the cost of the hydrogen produced.

Index Terms - Electrolysis; Hydrogen; Integration; Solar PV.

I. NOMENCLATURE

EL	Electrolyser
PV	Photovoltaic

II. INTRODUCTION

Hydrogen is a key enabling element of the energy transition. As a flexible carbon-free energy vector, it offers a strong sector coupling potential thanks to the multiplicity of end uses (e.g., industry, mobility, natural gas admixture). When produced from renewable sources, it also enables a fully sustainable energy supply chain, increasingly attractive thanks to recent improvements in electrolyser performance.

A number of applications is likely to introduce stable, if not constant, hydrogen demands along the year, e.g., industrial facilities aiming at a zero-carbon supply chain ('green chemistry') or hydrogen vehicle refuelling stations that are increasingly required to offer 'green hydrogen'.

This work presents a sizing method to design a system that combines electrolysers and solar photovoltaic (PV) panels for a sustainable hydrogen production, focusing on the small scale.

III. SYSTEM CONFIGURATION AND OPERATION

The study integrates an intermittent power generation technology (solar PV) with a flexible hydrogen production device (electrolyser, EL) and a hydrogen storage system.

The analysis considers a year-long hourly electricity generation profile of the solar PV plant and simulates the electrolyser operation with the aim of guaranteeing the required

demand. The annual hydrogen demand drives the required PV and electrolysis capacities, whereas the hydrogen delivery to the consumer is critical for storage sizing.

A. Hydrogen production from solar PV

Given the electricity generation time series, the amount of energy that can be transformed into hydrogen varies when the ratio of EL and PV nominal capacities ($P_{nom,EL}/P_{nom,PV}$) changes. Fig. 1 illustrates the interaction between the plants, with a nominal capacity ratio equal to 0.25, in two typical days with high and low irradiance. When the PV power output is comprised between the minimum load and the nominal capacity of the electrolyser, the latter absorbs the entire generation. When the PV output is larger than the electrolyser capacity, the surplus is directed to the power grid. The same happens when PV generation is below the electrolyser minimum load.

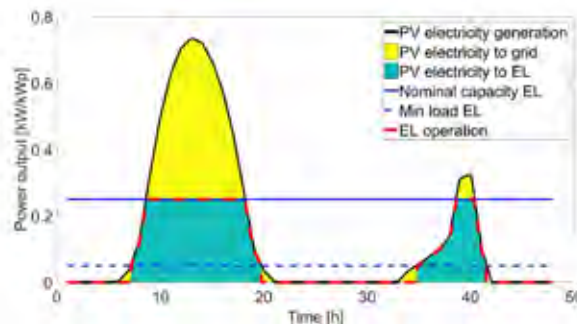


Fig. 1. Example of integration between PV generation and EL operation.

If the system is not required to provide 100% hydrogen production from PV, the electrolyser can absorb electricity from the grid at any time to satisfy the production needs (except for moments of PV-driven nominal operation and by respecting the minimum load constraint).

Year-long time series of PV power generation are taken from the European PV-GIS database [1] for the selected location, considering state-of-the-art PV panels. The system sizing assumes perfect scaling of electricity generation with the installed capacity.

B. Hydrogen storage for annual management

The electrolyser and the PV field are sized to comply with the cumulative annual demand. However, the fluctuations of solar energy during the year determine an unbalanced hydrogen production during summer and winter which imposes the need for hydrogen storage. Hydrogen storage is assumed in the form of conventional high-pressure metallic tanks (200 bar).

IV. CALCULATIONS AND RESULTS

Calculations are performed for the case of a hydrogen demand of 100 kg_{H2}/d (36.5 ton_{H2}/y), considering a location in northern Italy. Economic assumptions reflect short-term projections: 700 €/kW_p for PV, 900 €/kW_{el} for EL, 500 €/kg_{H2} for storage tanks [2].

As long as only PV panels and electrolysers are considered (without storage), the possibility to guarantee the cumulated production on annual basis depends on their installed capacities and on the solar radiation profile. At small installed capacities, only a limited fraction of hydrogen comes from PV electricity. This is shown by the black contour lines in Fig. 2 and Fig. 3, which represent the fraction of electricity coming from PV with respect to the total amount needed. The investment cost increases linearly with the installed capacities of PV and EL. The lowest-capital-cost configuration for 100% cumulated renewable H₂ has an investment cost of 2.2 M€ and features nearly 1.0 MW_{el} of EL and 1.8 MW_p of PV.

When considering the annual operation and requiring the plant to deliver the same quantity of hydrogen each day of the year, inter-seasonal storage becomes mandatory. Fig. 2 shows the required H₂ storage capacity (colour scale) as a function of electrolyser capacity and PV rated power. The storage capacity increases massively when the PV fraction is high and the oversizing is limited (i.e., cases close to the black line '1'). The minimum assumed storage size is 700 kg_{H2} (1-week demand).

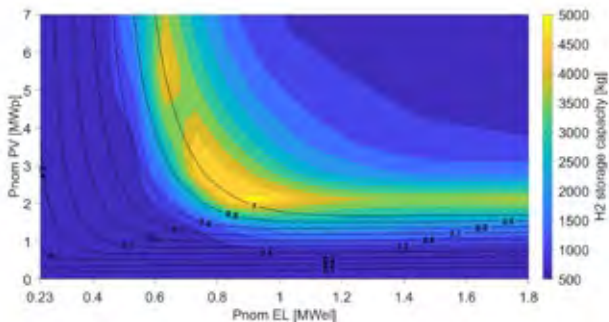


Fig. 2. Contour plot of hydrogen storage capacity, as function of electrolyser and PV rated power. The black lines represent the fraction of electricity generated by the PV field.

Consequently, the investment cost of the complete system shows a different and more complex structure, as depicted in Fig. 3. Due to its high specific cost, the large storage capacity required near the black line '1' increases the total system costs, while the optimal configuration is shifted to an oversized system where ~1.3 MW_{el} of EL are coupled to ~2.8 MW_p of PV

and ~2 ton_{H2} of storage (black dot), for a total investment cost of about 4.2 M€. Hence, the presence of the storage almost doubles the cost from the optimal PV+EL configuration.

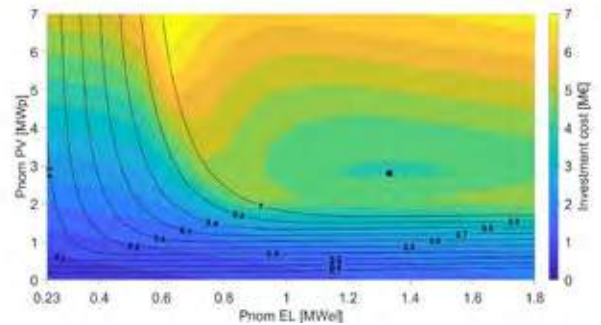


Fig. 3. Contour plot of total investment cost (PV+EL+storage), as function of electrolyser and PV rated power. The black lines represent the fraction of electricity generated by the PV field.

Based on the investment cost and on the annual energy balances of the system (PV generation, electrolyser operation, exchange with the grid), it is possible to determine the hydrogen specific cost. OPEXs are assumed as 1-2%/y of CAPEX, depending on the technology; the discount rate is set to 6%. Table I reports the system sizing that results from the optimisation with a 'minimum H₂ cost' objective. The injection of surplus electricity into the electric grid is calculated with a baseline selling price of 60 €/MWh_{el} (today's Italian average) and compared with a 20% reduction (48 €/MWh_{el}), which is likely to occur in the medium term, when more and more new solar plants will all aim to sell electricity in the central hours of the day. The lowest hydrogen cost is predicted at higher electricity value with a system featuring a large PV capacity, where the revenues are sustained by electricity sales rather than by hydrogen production (note that 7 MW_p is the assumed upper boundary of PV capacity for the solver).

TABLE I
SYSTEM CONFIGURATION AND H₂ COST AT VARIOUS CONDITIONS

Sold electricity value	PV [MW _p]	EL [MW _{el}]	Storage [kg _{H2}]	Investment cost [M€]	H ₂ cost [€/kg _{H2}]	PV coverage fraction
60 €/MWh _{el}	7.0	0.4	700	5.6	5.84	75%
	7.0	0.9	1104	6.3	6.29	100%
48 €/MWh _{el}	2.8	0.5	738	2.8	8.08	76%
	4.9	1.1	1137	5.0	9.46	100%

V. CONCLUSIONS

The analysis shows that hydrogen can be generated at costs in the range of 5.8 to 9.5 €/kg_{H2} depending on electricity cost assumptions and PV coverage fractions, influencing also the required storage size. Additional work will investigate effects of adopting different electrolysis and storage technologies.

REFERENCES

- [1] JRC, PV-GIS, https://re.jrc.europa.eu/pvg_tools/en/tools.html.
- [2] FCH2JU, Addendum to the Multi-Annual Work Plan 2014-2020, 2018.

MAMA-MEA, MASS MANUFACTURE OF MEAS USING HIGH SPEED DEPOSITION PROCESSES

M. Romagnoli* and P.E. Santangelo*

*DIEF - Università di Modena e Reggio Emilia, via Vivarelli, 10,
41125 Modena (I),

Abstract - The scope of MAMA-MEA is to develop an innovative additive-layer deposition process that integrates all the main CCM (Catalyst Coated Membrane) components within a single, continuous roll-to-roll production line. This project is focused on PEMFC (Polymer Electrolyte Membrane Fuel Cell) industry. Its mission is to foster an increase of the manufacturing rate up to 10 times faster than that currently achieved by state-of-the-art processes. The current manufacturing methods will not be able to meet CCM demand over the next 10 years, therefore, new strategies needs be sought, explored and translated into high-volume production lines to augment the capacity and follow the expected trend. The whole effort also has the potential to improve material utilisation and manufacturing costs.

Preliminary one-off prototypes have already established the feasibility of the proposed approach and patent applications have been filed. The engineering design of an ALM sealed CCM production line will be provided.

Index Terms - innovative additive-layer deposition process, PEMFC (Polymer Electrolyte Membrane Fuel Cell), CCM (Catalyst Coated Membrane).

I. INTRODUCTION

According with the Fuel Cell Industry Review 2018 [1], from 2014 to 2017, the market has seen a constant growth. The forecast for the 2018 is expected to follow this trend also in the 2019. North America and Asia are the world areas with the higher number of shipped megawatts. Europe follows quite far, but with a similar increasing trend. In particular, the PEMFC market is expected to grow by 10s GW per annum from 2025. The current manufacturing methods will not be able to meet CCM demand over the next 10 years, therefore, new strategies needs be sought, explored and translated into high-volume production lines to augment the capacity and follow the expected trend. The whole effort also has the potential to improve material utilisation and manufacturing costs.

The aim of MAMA-MEA (acronym for MAss MAnufacture of MEAs) [2], project starts in 2018, is to develop an innovative

layer deposition process that integrates all the main CCM components (membrane, catalyst layers, sealing) in a single continuous roll-to-roll manufacturing process for the PEM fuel cell industry. In Figure 1 the artistic logo.



Fig. 1. MAMA-MEA logo

A key project objective is an increase in the manufacturing rate of over 10 times compared to the state-of-the-art process, whilst also increasing material utilisation to 99%, and the product quality, and thus yield, to over 95%.

The project harnesses advanced deposition techniques from the coating and printing industry. To achieve this a consortium encompassing academia, SMEs and industry, will take the concept of additive layer deposition, already at MRL3, to deliver and demonstrate an MRL6 level process design utilising a verified EU supply chain and consistent with the MAWP.

II. CONSORTIUM COMPOSITION

The project is carried out by a consortium with extensive knowledge and expertise in both fuel-cell technology and manufacturing; as for the latter, the background in digital coating and printed electronics is used to develop the highly innovative concept of an Additive Layer Manufacturing (ALM) process for CCM. The key CCM components will be deposited with high precision and speed, one layer on top of one another, only onto the functional CCM surface. The components of the consortium and their roles are reported in tab.I. They have their headquarters in five different countries of the European community.

TABLE I
COMPOSITION OF MAMA-MEA CONSORTIUM AND ROLE OF EACH PARTNER

Name	Nationality	Role in the project	Organisation type
Technische Universität Chemnitz	Saxony, Germany	<ul style="list-style-type: none"> Project coordinator Literature review of suitable test protocols (optionally also ASTs) Technical and scientific coordination Dissemination and exploitation 	Public university
Unimore – Università degli studi di Modena e Reggio Emilia	Emilia-Romagna Italy	<ul style="list-style-type: none"> Literature review of suitable test protocols Formulation and optimisation of inks for deposition techniques Dissemination and exploitation LCA WP leader 	Public university
Fraunhofer Institute for Electronic Nano Systems ENAS	Saxony, Germany	<ul style="list-style-type: none"> Literature review of suitable test protocols technology identification layer characterisation, proving of printability concepts 	Public research institute
Johnson Matthey Fuel Cells Ltd	Swindon, UK	<ul style="list-style-type: none"> Literature review of suitable test protocols Technical and scientific management of project. Leader on CCM manufacturing development and integration. Testing of CCMs Leader on component layer specification. WP leader 	Private company
System Ceramics s.p.a.	Emilia-Romagna Italy	<ul style="list-style-type: none"> Literature review of suitable test protocols Test of inkjet technique applicability Leader in inkjet printing technology on contribution to ink formulation. Deposition process optimisation. Task leader 	Private company
INEA – Informatics Energy Automation	Ljubljana, Slovenia	<ul style="list-style-type: none"> Increased productivity Improved quality and repeatability levels Reduced costs Improved time to market High standard solution and documentation Automate where practical 	Private company
Nedstack Fuel Cell Technology B.V.	Ed Arnhem The Netherlands	<ul style="list-style-type: none"> Leader for testing and validation of the manufactured MEAs in stack configuration confirming performance, reproducibility and lifetime. Coordinating, recording and reporting exploitation activities. 	Private company

The MAMA-MEA project is implemented in seven work packages (WP), the interrelations of which are shown in Figure 2.

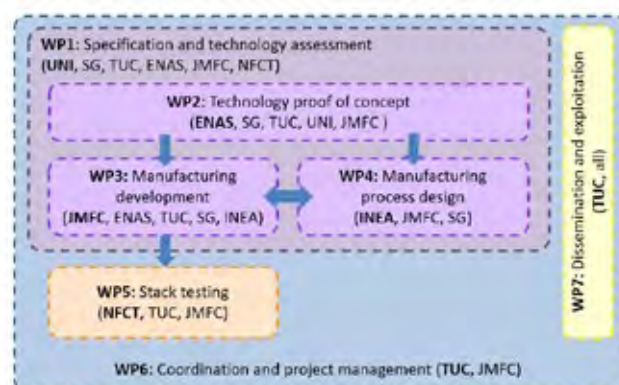


Fig. 2. MAMA-MEA project work package interrelations.

The project has been presented on several occasions around the world: in Germany, Italy, in the Czech Republic, in Japan at the World Smart Energy Week 2019 / FC Expo 2019 in Tokyo.

CONCLUSION

At the halfway mark, the project has identified the best technologies for the application of the different layers that form the MEA. In the next half, the inks will be optimized, applied according to the selected technologies and the produced MEA will be tested.

ACKNOWLEDGMENT

Mama-Mea project has received funding from the FCH JU and European Union's Horizon2020 research and innovation programme under Gran Agreement no.779591

SUBMISSION OF THE EXTENDED ABSTRACT

REFERENCES

List only one reference per reference number according to the following examples:

- [1] Fuel Cell Industry Review 2018, E4tech, www.FuelCellIndustryReview.com
- [2] www.mama-mea.eu

ELECTROCHEMICAL MODELLING OF SOLID OXIDE FUEL CELLS

F.R. Bianchi*, D. Bove*, E. Audasso*, B. Bosio*, A. Baldinelli**, L. Barelli**, G. Bidini**,
F. Nobili*** and A. Staffolani***

*PERT-DICCA, University of Genoa, Via Opera Pia 15, 16145 Genoa (Italy)

**Department of Engineering, University of Perugia, Via Duranti 93, 06125 Perugia (Italy)

***School of Science and Technology, Chemistry Division, Via S. Agostino 1, I-62032 Camerino (Italy)

Abstract - Solid Oxide Fuel Cell (SOFC) stands out as successful tool for energy production in medium-large size power plants. Indeed high working temperature allows both electricity and heat generation. For industrial applications, SOFC behaviour prediction is a fundamental point for process optimization and control during plant design and operation. For this purpose, the present work proposes a specific SOFC model, written in Fortran and then implemented in AspenPlus, to have a useful quick tool as baseline for future complete power plant simulation. It considers the electrochemical kinetic, basing on macroscale balances and a semi-empirical approach, in which theoretical equations and experimental data are used. Thanks to sensitivity analysis, system parameters are changed to study their influence on SOFC performance and so the best operative configuration is detected.

Index Terms – AspenPlus, Electrochemical modeling, Process optimization, SOFC

I. INTRODUCTION

Fuel cells are promising devices for energy production as alternatives to traditional power plants, since they do not have dangerous GreenHouse Gas (GHG) emissions in atmosphere. Indeed, these tools are based on direct H₂ electrochemical oxidation to H₂O. High temperature guarantees good charge conductivity and fast kinetic without noble metal use. Yet, before their spread on market, material and operative condition optimization is requested to reduce system cost and obtain a competitive technology. In this contest, system simulation plays the main role favouring a quick cell behaviour prediction. Many commercial software tools for standard process unit simulation are available, but there are not consolidated specific commercial blocks for SOFC simulation. So the implementation of an own code in AspenPlus permitted to overcome this limit. A detailed electrochemical kinetic was considered without

losing the utilization simplicity of the general process simulation software. Model building required the comparison with experimental data for both tuning and validation. The Design of Experiment (DoE) was carefully set: every operating parameter was changed once at time to underline its influence on the cell performance.

II. ELECTROCHEMICAL MODELING AND ASPENPLUS

The model consists of a macro stationary simulation, which describes cell performance solving both material and thermal balances for the anodic and cathodic sides. A specific SOFC electrochemical kinetic is considered: it is based on semi-empirical formulation, where some parameters derive from a theoretical approach, while others are detected fitting experimental data. Each polarization contribute is estimated evaluating temperature and gas composition influence. Ohmic overpotential is formulated assuming a thermal activated process by an Arrhenius type equation [1]. In agreement with literature, activation term is expressed in hyperbolic sine form to guarantee a wider validity range [2]. A microscale material balance is solved along electrode thickness to estimate concentration contributes [3]. Moreover, Nernst resistances are taken into account considering an average between gas inlet and outlet composition [4]. Thanks to these assumptions, a “pseudo 0-D model”, written in Fortran, is developed, in which macroscale approach is paired with local equations to consider the real system extension.

This model is successfully implemented in AspenPlus, where a sensitivity analysis is performed to detect more influencing parameters on cell behaviour.

III. CELL PERFORMANCE OPTIMIZATION

SOFC performance is evaluated through characteristic curves. After model validation by comparing experimental and simulated data (Figure 1), optimum system conditions are detected varying process and material parameters. From the experimental side, operating variables, like temperature, gas composition and feed flow rate, are modified to underline how cell performance changes; then the same influences are underlined by the simulation, which also presents single polarization contribute variations. Still a wider parameter range can be studied thanks to AspenPlus sensitivity analysis. In view of new system projects, the model also permits to evaluate requested features of cell materials to reduce voltage loss: for instance electrode porosity, thickness of layers and system conductivity. Moreover, the kinetic parameters are studied as well, to underline how the model is influenced by different polarization terms. Through this analysis, the desired characteristics for a good electrocatalyst are detected.

IV. CONCLUSION

Process modeling is a very useful tool for cell operation design; still the identification of optimum system parameters requests a specific system kinetic knowledge. For this purpose, the present study proposes a semi-empirical model of SOFC performances, written in Fortran and then implemented in AspenPlus, to have a particular simulation device for electrochemical cells. Single parameter influence is evaluated by sensitivity analysis to project focused optimization actions. As experimental tests show and model confirms, temperature and gas compositions have the main influences on cell behavior.

Yet their value is correlated to specific requested operative situation, so some performance improves can be achieved optimizing cell material. For instance, electrode porosity changes obtained voltage at high current density. The kinetic parameters influence above all curve shape: depending on electrocatalytic activity, the profile can have a more or less steep drop increasing the load.

REFERENCES

- [1] Conti, B., Bosio, B., McPhail, S.J., Santoni, F., Pumiglia, D., Arato, E., A 2-D model for intermediate temperature solid oxide fuel cell preliminarily validated on local values, *Catalysts*, Volume 9(1), 2019, pp. 36.
- [2] Noren, D.A., Hoffman, M.A., Clarifying the Butler-Volmer equation and related approximation for calculating activation losses in solid oxide fuel cell models, *Journal of Power Sources*, Volume 152, 2005, pp. 175-181.
- [3] Chan, S.H., Khor, K.A., Xia, Z.T., A complete polarization model of a solid oxide fuel cell and its sensitivity to the change of cell component thickness, *Journal of power Sources*, Volume 93, 2001, pp. 130-140.
- [4] Bove, R., Lunghi, P., Sammes, N.M., SOFC mathematical model for systems simulation. Part one: from a micro-detailed to macro-black-box model, *International Journal of Hydrogen Energy*, Volume 30, 2005, pp. 181-187.

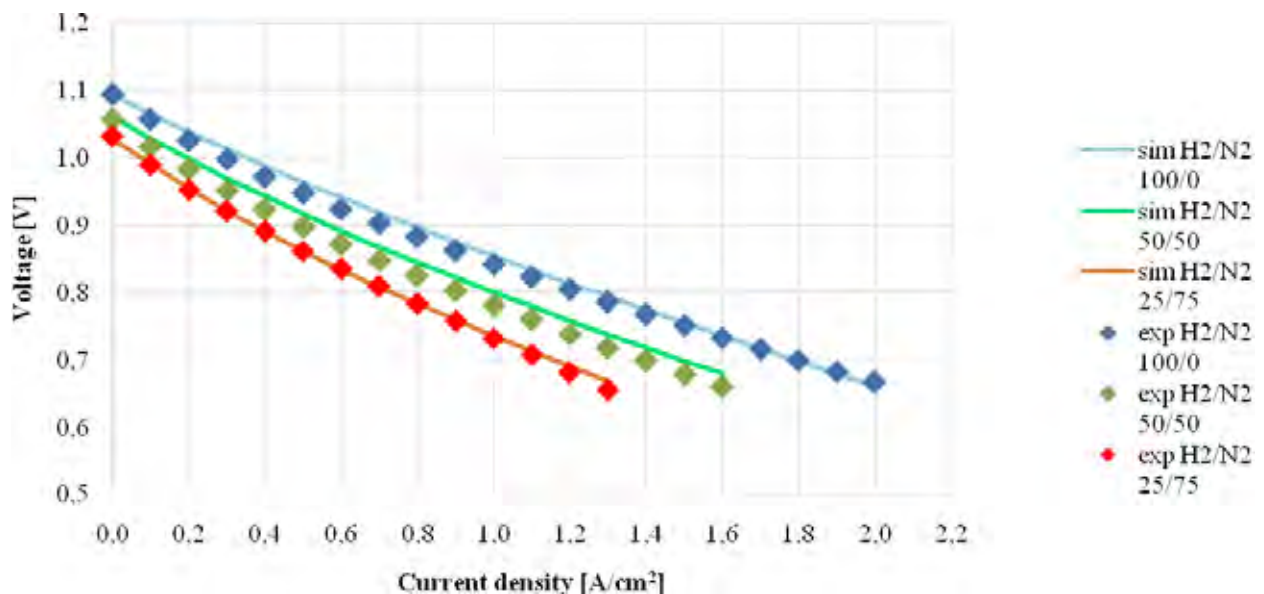


Fig. 1. Comparison experimental and simulated V-I curves at 800°C and different fuel composition

IN SITU MONITORING OF DISSOLVED OXYGEN IN WATER WITH A HYBRID PHOTOSYNTHETIC/SOIL MICROBIAL FUEL CELL BIOSENSOR

L.G.Olias** and M. Di Lorenzo*

*Centre for Biosensors, Bioelectronics and Biodevices (C3Bio) and Department of Chemical Engineering, Claverton Down, Bath, University of Bath, BA2 7AY (UK)

**Water Institute Research Centre (WIRC), University of Bath, BA2 7AY (UK)

Abstract – Continuous, *in situ* monitoring of water quality is required to prevent and control contamination events. With this aim, we here propose a hybrid photosynthetic/soil microbial fuel cell as a real time and on site biosensor. In particular, a soil anode is integrated with an algae-assisted cathode that acts as a dissolved oxygen (DO) probe. After 10 days of operation, the current generated by the hybrid fuel cell followed the day/night photosynthetic cycle, reaching the maximum power of 2.84 ± 0.99 μ W. Under steady conditions, the current increased during the day along with the increase in the catholyte DO, with a peak value of 158 ± 50 μ A, corresponding to 8.2 mg L⁻¹ of DO in the catholyte. Remarkably, the hybrid fuel cell operated without any addition of nutrients or organic matter in the soil.

Index Terms – Biosensor, Dissolved oxygen, Photosynthetic biocathode, Soil microbial fuel cell, Water quality.

I. INTRODUCTION

Electrochemical whole-cell biosensors are a promising technology for real time water quality monitoring. Particularly attractive are algae-based biosensors, since these microorganisms are ubiquitous, highly sensitive and yet resilient to adverse conditions [1]. In this context, biosensors based on the photosynthetic Microbial Fuel Cell (MFC) technology, combine the sensitivity of algae with great features, such as long-term stability, continuous monitoring, cost-effectiveness and self-powered applications. A MFC-based biosensor is characterized by an extremely simple design, since no transducer is needed, with benefits on portability. Successful implementations of MFC-based sensors have been demonstrated for either COD or BOD monitoring or the detection of bioactive compounds. Usually, in these sensors the anodic biofilm is the sensing element. Recently, a photosynthetic biofilm at the cathode has been instead suggested as the biorecognition element [2]. The advantage is a more stable sensor, since the cathodic biofilm would be less sensitive to changes of pH, T and conductivity that confound the

signal. Practical applications also demand for low cost materials. In this regard, ceramics has been widely investigated as a suitable material for MFCs, as it provides structural support while separating the two electrodes [3]. Finally, the sensor should require minimum maintenance to facilitate in-field applications, especially in remote areas. In this context, in this work we propose a low-cost hybrid photosynthetic/soil MFC as a DO sensor in water.

II. MATERIALS AND METHODS

The hybrid microbial fuel cells consisted of terracotta pots (3.5 x 4 x 2.7 x 0.3 cm), having the function of providing structural support while acting as electrodes separator, and Graphite Felt (GF, Online Furnace Services Ltd.) electrodes. For the case of the anode, GF (7 x 2 x 0.35 cm) was acid treated as previously described [4]. The electrode was buried inside 15 g of wet soil collected from the University of Bath campus and covered with parafilm. The cathode (11 x 2 x 0.35 cm) electrode was instead wrapped around the pot and immersed in a photosynthetic mixed culture sampled from a pond at the University of Bath. The culture was grown in 1 L of Bold's Basal Medium solution, for one month at 25 C and under a 12h/12h light (5 lm m⁻¹) regime before use. During the operation the catholyte ($Ab_{S750\text{ nm}} = 0.2$) was open to air. Light was provided with 60 W adjustable blue and red LEDs, on a 12 h on/off cycle in a black box (light intensity of 40 mW cm⁻¹). Tap water was added every day to account for evaporation losses. Ti wire (25 mm, Advent Research Materials, Oxford, UK) was used to connect the electrodes to an external resistance (R_{ext}) of 1 k Ω during enrichment and 10 k Ω after two weeks. The voltage output (V) was recorded with a Picolog (Pico Technology, UK) every minute. The current (I) was calculated according to Ohm's law ($I = V / R_{\text{ext}}$) and power (P) was calculated as $P = I \times V$.

III. RESULTS

The startup period (Fig. 1A) shows a slow enrichment process where the day/night cycle starts developing after 10 days of operation. The polarization sweep (Fig. 1B) shows a maximum power output of $0.17 \mu\text{W}$ at an external resistance of $10 \text{ k}\Omega$. After two months, however, the power output increased to $2.84 \pm 0.99 \mu\text{W}$. The slow improvement rate in performance has been reported for other ceramic based MFC, and is attributed to the decreased diffusion of oxygen through the terracotta towards the anode over time as a result of fouling [5]. Indeed, the internal resistance decreased a 40% in two months, from $10 \text{ k}\Omega$ to $6 \text{ k}\Omega$.

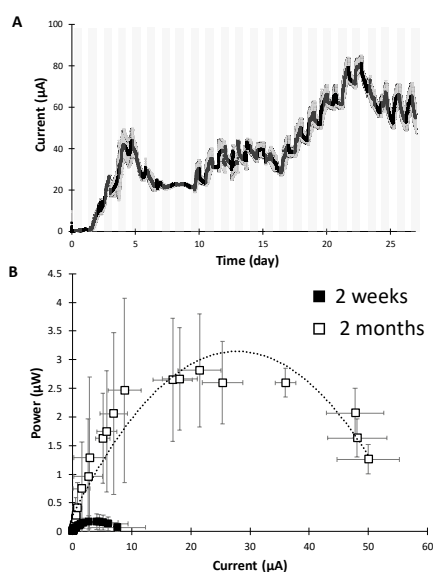


Fig. 1. Startup period (A) and power curves (B) after 2 weeks (black) and 2 months (white) of operation. Data is the average of three replicates. Shadowed areas represent the dark cycle.

The aim of this study was to investigate the ability of the hybrid MFC to detect in real time DO changes in the catholyte. In this way, the system becomes a tool to detect the presence of any disturbance in the water that would affect the metabolic activity of the algae at the cathode and, therefore, the photosynthetic generation of oxygen. For this application to be possible, the cathodic reduction should be the limiting step of the overall electrochemical reaction, so that the signal output would directly correlate with the DO in water [2]. As shown in Figure 2A, the DO increases steadily from 2 to 16 mg L^{-1} during the light cycle. This current increases up to a DO value of 8.2 mg L^{-1} with a sensitivity of $8.4 \mu\text{A L mg}^{-1}$ ($R^2=0.9$) but decreases a 17% afterwards (Figure 2B). A possible reason for the trend reversal could be the diffusion of oxygen from the catholyte into the anode chamber [3]. Mixed potentials arising from the direct reduction of oxygen at the anode will confound the signal and decrease the sensitivity of the sensor. Anodic anaerobic conditions should be therefore ensured by increasing the distance between electrodes.

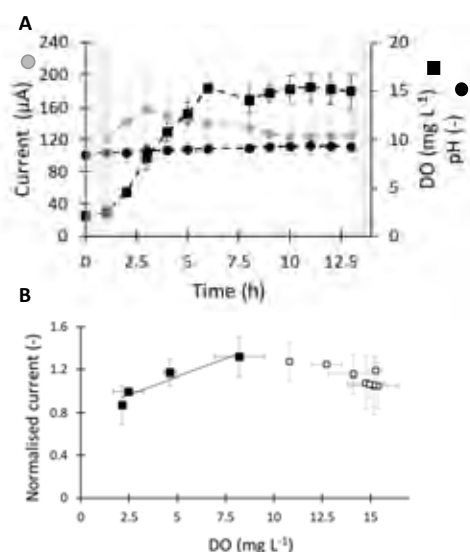


Fig. 2. (A) Evolution of DO (black squares), current (grey circles) and pH (black circle) over the 12 hours of the light cycle. Shadowed areas represent the end and beginning of the dark period. Data is the average of three replicates. (B) Correlation of current with DO during the time period shown in A (squares). Current is normalised by the value at the start of the light cycle. Black squares and black line indicate the linear range of correlation of the current with DO.

IV. CONCLUSIONS

An innovative hybrid photosynthetic/soil MFC was developed as a self-powered biosensor for DO in water. The sensor's output showed a positive linear correlation with the oxygen within the range $2 - 8.2 \text{ mg L}^{-1}$ with a sensitivity of $8.4 \mu\text{A L mg}^{-1}$. At higher DO levels, however, the trend reversed, probably due to diffusion of oxygen into the anodic chamber. Over the two months of operation, the hybrid MFC did not need any nutrients addition, thus showing the potential of this design for remote sensing applications.

ACKNOWLEDGMENTS

Thanks to the Water Informatics, Science and Engineering Centre for Doctoral Training, funded by the UK Engineering and Physical Sciences Research Council (EP/L016214/1).

REFERENCES

- [1] J. Livage, "Micro-algal biosensors," *Anal. Bioanal. Chem.*, 2011, vol. 401, no. October, pp. 581–579.
- [2] L. G. Olias et al., "Effect of electrode properties on the performance of a photosynthetic microbial fuel cell for atrazine detection", *Front. Energy Res.*, 2019, vol. 7, no. 105, pp.1-11.
- [3] J. Winfield et al., "A review into the use of ceramics in microbial fuel cells," *Biores. Tech.*, 2016, vol. 215, pp. 298-303.
- [4] S. M. Martinez and M. Di Lorenzo, "Electricity generation from untreated fresh digestate with a cost-effective array of floating microbial fuel cells," *Chem. Eng. Sci.*, 2019, vol. 198, pp. 108–116.
- [5] J. Winfield, et al. "Comparing terracotta and earthenware for multiple functionalities in microbial fuel cells," *Bioprocess Biosyst. Eng.*, 2013, vol. 36, no. 12, pp. 1913–1921.

STUDY OF THE EFFECT OF RU PRECURSOR IN RU-NI/CEO₂-ZRO₂ CATALYSTS FOR CO₂ METHANATION

S. Renda, A. Ricca, and V. Palma

Università degli Studi di Salerno, *Department of Industrial Engineering, Via Giovanni Paolo II 132,
84084 Fisciano (SA), (Italy)*

Abstract - The intermittency in power generation that characterizes renewable energy sources requires a way to convert the energy surplus. Among all the possibilities, the conversion of power in hydrogen via water electrolysis and then into methane via CO₂ methanation represents a competitive storage system. In this work, several Ru-Ni/CeO₂-ZrO₂ were prepared and compared with Ni/CeO₂-ZrO₂, in order to evaluate the effect of Ru loading and Ru precursor salt. The results showed that the presence of Ru in the formulation enhances the catalyst activity; in particular, the use of the Ru acetylacetonate, for the deposition of the noble metal on support, remarkably reduces the catalyst onset temperature. The effect is due to the templating effect of the precursor molecule, that allows a better dispersion of the active compounds.

Index Terms - Catalyst, Methanation, Power-to-Gas, Ruthenium

I. NOMENCLATURE

PtG: Power-to-Gas
AcAc: acetylacetonate
SSA: Specific Surface Area
XRD: X-Ray Diffraction
TPR: Temperature Programmed Reduction

II. INTRODUCTION

The growing interest towards renewable energy highlights issues related to the intermittency of power generation. Power-to-Gas processes are a promising option for the storage of the exceeding electrical energy as they allow the integration of renewable sources into the network. In the PtG process chain, power is converted into chemical energy by means of water electrolysis, that produces hydrogen; this is subsequently converted into methane, that is more suitable for a large

variety of processes. The conversion of hydrogen into methane is realized through CO₂ methanation. Methanation is a highly exothermic reaction, thermodynamically promoted by low temperatures; in adiabatic conditions, the heat of the reaction induces a thermal increase in the catalytic bed, limiting the CO₂ conversion. To mitigate the limitations related to such thermodynamic constrains, it could be advantageous to have low-temperature active catalysts, so that the overall temperature range of the process can be not-so-high. However, low temperatures are characterized by strong kinetic limitations. In this perspective, the studies of a low onset temperature catalytic formulation are matter of interest.

III. EXPERIMENTAL STUDY

Nickel is the most widely studied active component for CO₂ methanations catalysts: this is due to its inexpensiveness and also to its good activity and selectivity towards the reaction. However, ruthenium has been recognized as the most active specie for the Sabatier reaction [1]. In order to obtain a catalyst that could merge the Nickel inexpensiveness and Ruthenium activity, several mono- and bimetallic formulations were prepared and tested.

A. Catalysts preparation

In this work, fifteen Ru and Ni based catalysts were compared. For all the formulations, CeO₂ has been chosen as support, because of its ability in decreasing the onset temperature for methanation reaction [2]. All the tested formulations are listed in Table I.

All the catalysts were prepared via impregnation methods, choosing two different precursor salts for ruthenium impregnation. The bimetallic formulations were prepared by

Nickel impregnation at first, and a subsequent impregnation of Ruthenium, according to common methodologies described elsewhere [2].

TABLE I
SUMMARY OF THE PREPARED CATALYSTS AND MAIN RESULTS

	Sample	Ru [wt%]		Ni [wt%]	Maximum CH ₄ yield
		RuCl ₃	AcAc		
1	10Ni/CeZr	-	-	10	61%
2	0.5Ru-10Ni/CeZr (Cl)	0.5	-	10	73%
3	1Ru-10Ni/CeZr (Cl)	1	-	10	69%
4	2Ru-10Ni/CeZr (Cl)	2	-	10	58%
5	3Ru-10Ni/CeZr (Cl)	3	-	10	64%
6	2Ru/CeZr (Cl)	2	-	-	39%
7	3Ru/CeZr (Cl)	3	-	-	57%
8	0.5Ru/CeZr (AcAc)	-	0.5	-	15%
9	1Ru/CeZr (AcAc)	-	1	-	74%
10	2Ru/CeZr (AcAc)	-	2	-	74%
11	3Ru/CeZr (AcAc)	-	3	-	77%
12	0.5Ru-10Ni/CeZr (AcAc)	-	0.5	10	78%
13	1Ru-10Ni/CeZr (AcAc)	-	1	10	79%
14	2Ru-10Ni/CeZr (AcAc)	-	2	10	82%
15	3Ru-10Ni/CeZr (AcAc)	-	3	10	80%

B. Characterization

All the samples have been characterized via specific surface area analysis (B.E.T. calculation method), XRD and TPR.

SSA analysis showed that mono- and bi-metallic formulation prepared by acetylacetonate presents a higher surface area, resulting in a better ruthenium dispersion onto the surface. The XRD spectra and crystallites dimension calculation confirmed this hypothesis, as the nickel and ruthenium particles dimension resulted smaller when the catalyst was obtained by acetylacetonate. According to this result, the TPR profile highlighted a lower reduction temperature for the sample prepared by AcAc for both mono- and bi-metallic formulations. Moreover, for the AcAc based samples, the reduction takes place in a wider temperature range. All bi-metallic catalysts showed the presence of spillover phenomenon during the reduction, but this is more evident for the samples with a low ruthenium amount.

C. Experimental results

All the samples were tested with the following conditions: dilution ratio (Ar:CO₂) set to 5; stoichiometric feed ratio (H₂:CO₂ = 4) and WHSV = 60 NL/(h * g_{cat}).

The maximum CH₄ yield achieved in each test is reported in

Table 1.

The effect of ruthenium loading in the mono-metallic samples was the same for both the precursor salt employed: the increase of the metal percentage in the formulation leads to an increasing activity, resulting in lower onset temperature and higher values for CO₂ conversion and methane yield.

For the bi-metallic samples obtained by chloride, the increase of ruthenium amount in the formulation led to worsen catalytic performances in the whole temperature range. This aspect highlighted that the addition of ruthenium (chloride) to a Ni/CeZrO₄ in low percentages can promote the catalytic activity (max CH₄ yield increased from 61% up to 73%), but higher loading will inhibit the catalyst.

On the contrary, all the samples obtained by AcAc showed comparable results both in terms of yield and conversion: an optimum was found for the 1%-2% ruthenium loading with no sensible difference in the performances among the two samples. A comparison of these results with the monometallic Ni/CeZrO₄ formulation showed that, in this case, the addition of ruthenium always promotes the catalytic performances. Moreover, all the tests performed with AcAc based samples (samples 12 to 15) showed better performances than any of the chloride-based catalyst (2 to 5).

IV. CONCLUSION

Nickel and ruthenium are both high active species for the CO₂ methanation reaction. In mono-metallic formulation, an increase in the metal loading makes the catalyst reach higher values of yield and conversion. A different behavior is found increasing ruthenium loading in the bimetallic formulations: both in the case of chloride and the AcAc precursor salts is possible to individuate an optimum condition in Ru loading. This condition was found to be different with respect to the ruthenium precursor: when Ru was impregnated via chloride, a minimum amount of metal allowed the enhance of the activity. On the other hand, when Ru is impregnated via AcAc an optimum in Ru loading was found between 1 and 2%wt. Ruthenium dispersion onto the catalyst surface is a determining aspect for the catalytic activity: ruthenium acetylacetonate allows a better dispersion of metallic particles thanks to its templating effect and for this reason a higher loading is able to enhance the catalytic activity.

REFERENCES

- [1] M. A. Vannice, The Catalytic Synthesis of Hydrocarbons from Carbon Monoxide and Hydrogen, Catalysis Reviews, Volume 14, 1976, pp. 153-191.
- [2] A. Ricca, L. Truda, V. Palma, Study of the role of chemical support and structured carrier on CO₂ methanation reaction, Chemical Engineering Journal, in press.

SIMULATION, ANALYSIS AND CONTROL OF FUEL CELL ELECTRIC VEHICLE

A. Grimaldi*, T. Garancini*, M. Montauti*, E. Crespi*, A. Baricci*, and A. Casalegno*

*Department of Energy, Politecnico di Milano, Via Lambruschini 4, 21056 Milan, (Italy)

Abstract - A mathematical and physical model of fuel cell electric vehicle (FCEV) components is provided with great insight given into the modelling of the PEMFC stack and of the air supply system.

The FC model (consisting in a 1D + 1D model, including water and thermal management) has been calibrated and validated using several experimental data obtained from tests on a single cell both in stationary and dynamical operation and under several operating conditions. The stack is integrated into a simple vehicle platform, based on the architecture of recent FCEVs.

The governing equation are implemented into MATLAB Simulink environment. Two pressure regulation strategies have been compared to better understand water management and system efficiency response, comparing also the results with Toyota Mirai data.

Index Terms - FCEV, dynamic model, Simulink

I. INTRODUCTION

Proton exchange membrane fuel cells (PEMFCs) are on the edge of a significant commercialization as an alternative power source for the automotive sector, as demonstrated by Toyota, Hyundai and Honda [1]. Barriers are still present to market penetration, mainly related to cost and durability. Indeed, effective water management inside the stack as well as optimization of the fuel cell system, considering also the option of hybridization with a battery, are needed to tackle the present issues. Thus, a detailed analysis of the entire system is needed, that would allow to further enhance its performance and lifetime.

II. MODEL FORMULATION

A. PEMFC stack

PEMFC stack is supposed to be composed of 370 cells, operating under the same conditions. Each cell domain is composed of six layers, i.e. cathode channel, cathode GDL, cathode CL, polymer electrolyte membrane, anode CL and anode channel. Channel and GDL subdomains are divided into eight and seven control volumes respectively, where conservation

equations have been integrated spatially assuming a lumped behaviour. Both CLs are considered as superficial layer and liquid water transport is not resolved, supposing that water produced by Oxygen Reduction Reaction (ORR) is in vapour phase. Mass conservation equations (both global and for the single species) are solved in each control volume, along the channel direction as well as across the porous media, for the cathode and the anode side. In membrane, water transport occurs by means of two mechanisms, electro-osmotic drag and back diffusion, determining the hydration state of the membrane. Membrane conductivity, affecting ohmic losses, is dependent on membrane water content, according to [2]. Thermal performance of the fuel cell stack is based on assuming a lumped thermal mass of the single fuel cell that exchanges energy with the coolant.

B. Balance of Plant (BoP)

The BoP accounts for all components connected to the stack, mainly focusing on the ones related to air feeding, as shown in Fig. 1. Air is delivered by a compressor, coupled with an electric motor, to a humidifying system, before entering the stack. Dynamic model of compressor and supply manifold are based on the work presented in Pukrushpan et al. [3]. A plate-and-frame membrane humidifier has been used, with 35 channels per plate and 90 plates. It has been modelled as a domain composed of

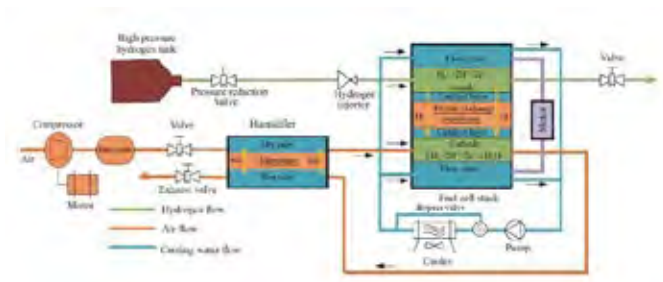


Fig. 1 Schematics of the balance of plant and PEMFC stack simulated.

five regions, representing the wet gas channel, wet micro-porous layer (MPL), ionomer, dry MPL and dry gas channel. Heat and mass transfer take place thanks to gas phase diffusion through porous media, according to [4].

C. Numerical Implementation and Model Validation

All the governing equations have been implemented into the MATLAB Simulink modelling environment.

The GDL oxygen diffusion $D_{O_2,GDL}$, the ORR kinetic constant K_T and the charge transfer coefficient α_{ORR} have been fitted so to reproduce experimental polarization curves, obtained from a single cell, with an active area of 25 cm^2 , for different inlet cathode RH, operating temperatures and pressures.

III. RESULTS AND DISCUSSION

A. System analysis

Simulation of the vehicle model under New European Driving Cycle (NEDC) has been performed in order to investigate fuel cell system and overall powertrain performance. In this case, a pure fuel-cell powered light duty vehicle is considered, by assuming that the stack is capable by itself, without a battery, to face power transients, thanks to NEDC regularity.

Two control strategies have been considered: in the first one, a constant stack pressure equal to 2 bar has been set by controlling the opening fraction of the back-pressure valve, while in the second one pressure varies according to a constant opening area of the valve, whose value is chosen such that the stack pressure would be equal for the two strategies when generating the maximum power during NEDC. This last control strategy is typically adopted in FCEV, as in Toyota Mirai [1].

As shown in Fig. 2, variable pressure regulation could lead to lower cathode inlet RH and, thus, to a lower hydration state of membrane that could affect membrane durability. Moreover, as shown in Fig. 3, the stack efficiency is higher for constant pressure regulation, with respect to variable pressure one.

However, in the low-load region, system efficiency is lower for the first case because of the higher power demand of the

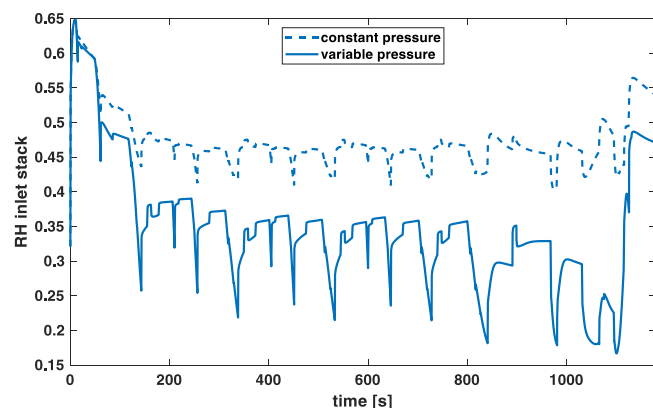


Fig. 2 Evolution of RH at cathode channel inlet, during NEDC simulation, for the two control strategies.

compressor, that represents a significant share of the total power generated. In the high-load region, system efficiencies obtained from the two control strategies become comparable since pressure, and thus compressor power, starts rising also in the second case. By comparing results of the second case with data obtained from Toyota Mirai experimental tests, the model is able to reproduce the same trend, even if experimental system efficiencies are higher. Cycle efficiency for NEDC simulation has been evaluated as well, obtaining 55.1% for variable pressure method, against 48.3% for constant pressure method.

IV. CONCLUSION

A dynamic PEMFC system model, focused on the air loop and capable of capturing significant transient phenomena, has been obtained. Through the simulation of NEDC, system response has been evaluated when two different strategies are adopted for pressure control: a constant pressure regulation and a variable pressure one, as typically used in FCEVs.

It has been demonstrated that the variable pressure regulation is globally better than the constant pressure one, by looking at the system efficiency and cycle efficiency, because of lower power demand of auxiliaries. However, results have also shown that cell membrane could suffer of stronger dehydration in the second case. This suggests a key role of system control strategies in obtaining an optimal water management of the stack, that would allow to enhance durability, together with performance.

REFERENCES

- [1] Lohse-Busch, H., Stutenberg, K., Duoba, M., & Iliev, S. (2018). Technology Assessment Of A Fuel Cell Vehicle: 2017 Toyota Mirai (No. ANL/ESD-18/12). Argonne National Lab.(ANL), Argonne, IL (United States).
- [2] Springer, T. E. et al. (1991) *Journal of the electrochemical society*, 138(8), 2334-2342.
- [3] Pukrushpan, J. T., Stefanopoulou, A. G., & Peng, H. (2004). *Control of fuel cell power systems: principles, modeling, analysis and feedback design*. Springer Science & Business Media.
- [4] Ahluwalia, R. K., et al. (2015) *Journal of Power Sources*, 291, 225-238.

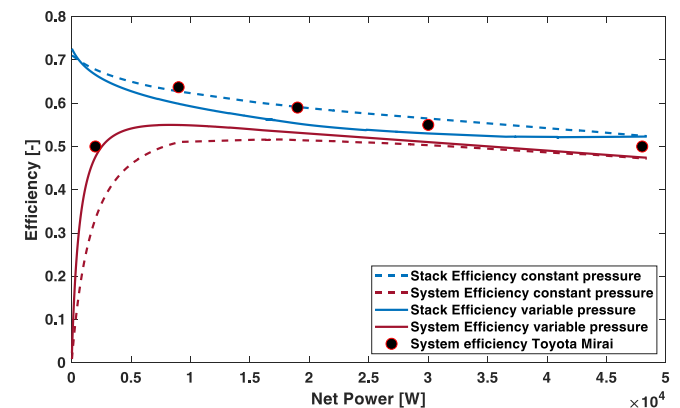


Fig. 3 Stack and system efficiencies, obtained by simulating the two control strategies. Black dots indicate system efficiency of Toyota Mirai [1].

SOLID OXIDE FUEL CELLS AS BEST PRACTICE FOR COMBINED HEAT AND POWER GENERATION FROM BIOGAS

M. Aciri*, S. Biollaz**, A. Calbry-Muzyka**, M. Gandiglio***, P. Gislou****, T. Hakala*****, A. Hawkes*****,
A. Lanzini***, S. McPhail****, M. Rautanen*****, M. Santarelli***, F. Santoni****, J. Van Herle*****

* SMAT s.p.a. Società Metropolitana Acque Torino, C.so XI Febbraio 14, Torino, (IT)

** Energy and Environment Research Division, Paul Scherrer Institut (PSI), Villigen, (CH)

*** Department of Energy, Politecnico di Torino, C.so Duca degli Abruzzi 24, Torino (IT)

**** ENEA C.R. Casaccia Via Anguillarese 301, 00123 Rome (IT)

***** Convion Oy, Tekniikantie 12, Espoo (FI)

***** Imperial College of London, South Kensington Campus, London (UK)

***** VTT Technical Research Centre of Finland, P.O. Box 1000, (FI)

***** Group of Energy Materials, Faculty of Engineering, Ecole Polytechnique Fédérale de Lausanne, 1950 Sion, EPFL Valais-Wallis, (CH)

Abstract - The use of high-efficiency fuel cell cogeneration systems (Solid Oxide Fuel Cell, SOFC) could play an important role for the overall improvement of the energy efficiency of small to medium size biogas plants. The presented work will analyze the goals and the preliminary results of two EU projects, to show the potential benefits of coupling biogas with SOFCs. By coupling real site experience on SOFC modules and an optimized biogas pre-treatment, which can reach the targets without affecting the costs too much, a final goal of a sustainable, high-efficiency and zero-emissions system for biogas exploitation could be reached.

Index Terms – biogas, SOFC, cleaning, fuel cell

I. INTRODUCTION

Biogas is a biofuel, which can be produced from different waste streams including the WWT sector (sewage sludge), municipal solid waste treatment (organic fraction, OFMSW), food industry (residuals from food processing plants) and agriculture (residuals from the livestock and farming activities). Biogas is usually exploited in internal combustion engines, gas turbines or upgraded to bio-methane for grid injection. Replacing a traditional cogeneration system with a high temperature solid oxide fuel cell (SOFC) can offer three key advantages: 1) High electrical efficiency (50-60% vs. 30-43%); 2) Zero emissions to the atmosphere in terms of NO_x, SO_x, PM and VOC; 3) Modularity: the concept could also be applied to small size plants where cogeneration is currently not feasible. In Italy, according to GSE 2017 data [1], 2'116 biogas plants were operating: 1'629 based on agricultural products (farms) and 487 using other biomasses.

II. THE DEMOSOFC PROJECT

The EU-funded DEMOSOFC project [2] demonstrates the technical and economic feasibility of operating a 150 kW SOFC system in a real WWTP. The integrated biogas-SOFC

plant includes a biogas clean-up and compression section, three SOFC power modules, and a heat recovery loop.



Fig. 1. Waste-to-energy circular approach with high temperature fuel cell-based cogeneration systems.

RESULTS

Results from the first two modules operation at the DEMOSOFC site confirmed the expected high level performance of the fuel cell system [2]–[5]. More than 7,000 hours of operation have been cumulated onsite. Measured SOFC efficiency from compressed biogas to AC power has always been close to 50%, with peaks at 56% at partial power (40%). Results are shown in Table I, where electricity and heat productions from SOFC module 1 and 2 are represented, together with efficiencies. Figure I indeed shows the monthly behavior of the power production at the plant site from January 2018. Both electrical and thermal power are self-consumed within the plant, thus reducing consumption of external fossil sources and generating a saving in the electricity and natural gas bills, as shown in the table.

A dedicated emissions measurements campaign has been performed in December 2017 by the Finnish research center VTT. Results show NO_x < 20 mg/m³, SO₂ < 8 mg/m³ and particulate lower than ambient air values (< 0.01 mg/m³).

TABLE I. DEMOSOFC PLANT PERFORMANCE RESULTS.

	SOFC 1	SOFC 2
Operating hours on site (h)	>3900	>5000
Plant capacity factor (%)	46.64	60.27
Electrical energy produced (kWh)	170'319	210'130
Thermal energy produced (kWh)	95'768	138'180
Average electrical efficiency (%)	52.34	50.18
Electrical energy saving (€)	>50'000€	
Thermal energy saving (€)	>15'000€	



TABLE I. DEMOSOFC PLANT ELECTRICAL PRODUCTION.

The technical performance of the system should be then linked with the economic aspects, essential for the development of market-ready concept. Table II shows the site preparation costs incurred during the projects, which include all the end-user costs (except the fuel cell system): mechanical works (piping, valves, pumps, etc.), electrical works (wires, cables, and control system), civil works (control room, electrical cabinet room, conditioning, platform, etc.), cleaning system and auxiliary works (cylinder gases, etc.).

A deep analysis has been performed, together with the plant owner SMAT s.p.a., to understand the potential reduction of costs of a second replication, thanks to the lesson-learned from the demonstration site. A total potential reduction of costs of 56% is achieved.

TABLE II. DEMOSOFC PLANT PREPARATION COSTS ANALYSIS.

	Actual Cost [€]	Optimized Cost [€]	
Mechanical Works	174'562	65'502	-63%
Electrical Works	173'913	100'819	-42%
Civil Works	191'920	23'758	-88%
Clean-up system	221'087	132'652	-40%
Auxiliary works	91'677	54'597	-40%
TOTAL	853'159	377'328	-56%

III. THE WASTE2WATT PROJECT

The DEMOSOFC concept could then be replicated in other biogas sectors and could become a best practice for CHP at small and medium size plants where competitive technologies are less efficient and costlier. As well-known from literature [6], SOFC tolerance to biogas impurities (sulphur, siloxanes, etc.) is extremely low and the gas should be cleaned at a deeper level than for traditional systems. WWTP biogas, as the one in the DEMOSOFC project, is one the cleanest biogas in terms of

inlet sulphur and other species. When moving to agricultural or OFMSW biogas, impurities level is increasing and the cleaning system need to be optimized in terms of performance and costs. This is the goal of the Waste2Watt EU project.

RESULTS

The aim of the project is to develop two cleaning solutions: the first one for a small size agricultural farm (Swiss-Austrian model) based on a lab-based defined matrix of commercial or innovative sorbents. The second one for a medium-large size plant producing biogas from the organic fraction of municipal solid waste based on an innovative cryogenic solution for sulphur and siloxanes removal.

The project is still in the design phase and the two cleaning solution are under investigation for what concerning sorbents testing at lab-scale, modeling and economic evaluations.

IV. PERSPECTIVES AND CONCLUSION

The concept demonstrated in the DEMOSOFC project, together with the cleaning upgrades from the Waste2Watts project, could then be replicated not only in biogas plants but also in the wider field of distributed generation, fed by natural gas from the grid, to performance services for the grid network in the view of future micro-grid energy systems

ACKNOWLEDGMENT

This project has received funding from the Fuel Cells and Hydrogen 2 Joint Undertaking under grant agreement No 826234 (Waste2Watts) and 671470 (DEMOSOFC). This Joint Undertaking receives support from the European Union's Horizon 2020 research and innovation programme, Hydrogen Europe and Hydrogen Europe research.

REFERENCES

- [1] "GSE - Gestore Servizi Energetici." [Online]. Available: <https://www.gse.it/>. [Accessed: 01-Oct-2019].
- [2] M. Gandiglio, A. Lanzini, M. Santarelli, M. Acri, T. Hakala, and M. Rautanen, "Results from an industrial size biogas-fed SOFC plant (the DEMOSOFC project)," *Int. J. Hydrogen Energy*, Sep. 2019.
- [3] M. Gandiglio, A. Lanzini, A. Soto, P. Leone, and M. Santarelli, "Enhancing the energy efficiency of wastewater treatment plants through co-digestion and fuel cell systems," *Front. Environ. Sci.*, vol. 5, p. 70, 2017.
- [4] M. Gandiglio, A. Lanzini, and M. Santarelli, "Large Stationary Solid Oxide Fuel Cell (SOFC) Power Plants," Springer, Cham, 2018, pp. 233–261.
- [5] M. Gandiglio, F. De Sario, A. Lanzini, S. Bobba, M. Santarelli, and G. A. Blengini, "Life Cycle Assessment of a Biogas-Fed Solid Oxide Fuel Cell (SOFC) Integrated in a Wastewater Treatment Plant," *Energies*, vol. 12, no. 9, p. 1611, Apr. 2019.
- [6] D. Papurello, M. Gandiglio, and A. Lanzini, "Experimental Analysis and Model Validation on the Performance of Impregnated Activated Carbons for the Removal of Hydrogen Sulfide (H₂S) from Sewage Biogas," *Processes*, vol. 7, no. 9, p. 548, Aug. 2019.

EXPERIMENTAL AND NUMERICAL STUDY OF PERFORMANCE HETEROGENEITIES IN A VANADIUM REDOX FLOW BATTERY

Mirko MESSAGGI, Andrea CASALEGNO, Matteo ZAGO
Politecnico di Milano, Department of Energy, Milan (Italy)

Abstract – An experimental investigation of global and local polarization curves and impedance spectra of a 25 cm² segmented vanadium redox flow battery is carried out, in order to have an insight on electrode-distributor interplay and on operation heterogeneity and the causes thereof.

From the analysis of local polarization curves and impedance spectra of the positive electrode, it is found that the serpentine suffers of mass transport issues in the area near the outlet, while the interdigitated shows those issues in the central area of the electrode. Instead, the negative electrode shows a higher homogeneity of operation, since it is characterized by a kinetic dominated regime and poorly influenced by mass transport.

The experimental campaign is supported by a 3D numerical model that couples fluid dynamics and electrochemistry, fitted on experimental data and then validated extensively, also locally, in different operative conditions, with different flow fields and different electrolytes configurations.

Index Terms – heterogeneity, impedance spectroscopy, segmented cell, VRFB.

I. NOMENCLATURE

EIS: electrochemical impedance spectroscopy;
SOC: state of charge;
VRFB: vanadium redox flow battery.

II. INTRODUCTION

With the growth of the electric production from renewable sources, the need of an efficient and durable on-grid and off-grid energy storage technology raised in the last years. Very promising candidates are vanadium redox flow batteries (VRFB) thanks to the possibility of decoupling power and stored energy, their high efficiency and high charge/discharge cycle life.

One of the key factors hindering the performance of vanadium redox flow batteries is the electrolyte distribution over the porous electrode, which is the result of a complex interaction among flow field geometry, electrode morphology and electrolyte properties. In the present work an experimental analysis is carried out with the aid of an innovative segmented cell hardware which allows a local resolution of polarization curves and impedance spectra, in order to have an insight on operation heterogeneity and the causes thereof. The experimental characterization is supported by the development of a 3D numerical model, that couples fluid dynamics and electrochemistry, fitted on experimental data and then validated

extensively, also locally, in different operative conditions, with different flow fields and different electrolytes configurations.

III. EXPERIMENTAL

An innovative 10 segments macro-segmented cell has been used for the characterization of the battery, in order to obtain a local resolution of performance and impedance. Not only all-vanadium configuration, but also positive symmetric and negative symmetric configurations have been investigated in order to study separately each side of the battery, at a SOC of 50% and 1M electrolyte concentration. Polarization curves have been performed at different flow rates, in potentiostatic mode inside a voltage range chosen to avoid undesired side reactions; EIS have been performed, only in the symmetric configuration to assure a constant SOC, in the same operative conditions of polarization curves at current values of 0.05 and 0.1 A cm⁻², with an oscillation semi-amplitude of 5 and 10 mA cm⁻² respectively. The frequency range has been selected between 10 kHz and 0.01 Hz, in order to catch both the kinetics-related and mass transport-related phenomena.

IV. EXPERIMENTAL RESULTS

The comparison of local polarization curves recorded for positive (a,b) and negative (c,d) electrolytes with serpentine (a,c) and interdigitated (b,d) flow fields is reported in Figure 1. It can be noticed how the positive electrolyte has a typical mass transport dominated behavior, while the negative one is characterized by a kinetic limited regime, which hinders the performance of this configuration. Moreover the serpentine outperforms the interdigitated distributor.

The local performance of the serpentine follows the depletion of reactants from the inlet to the outlet, while the interdigitated distributor shows a reduction of performance in the middle area of the electrode. In order to study the heterogeneities, a heterogeneity index (ξ) is defined as the coefficient of variation of the local currents corresponding to a selected value of global current. This index reveals greater heterogeneities for the positive electrolyte if compared with the negative one, due to the highly kinetics-limited behavior of the latter, which reduces the influence of mass transport and reactants consumption along the channel; moreover, an higher inhomogeneity is obtained for the interdigitated flow field with respect to the serpentine, because

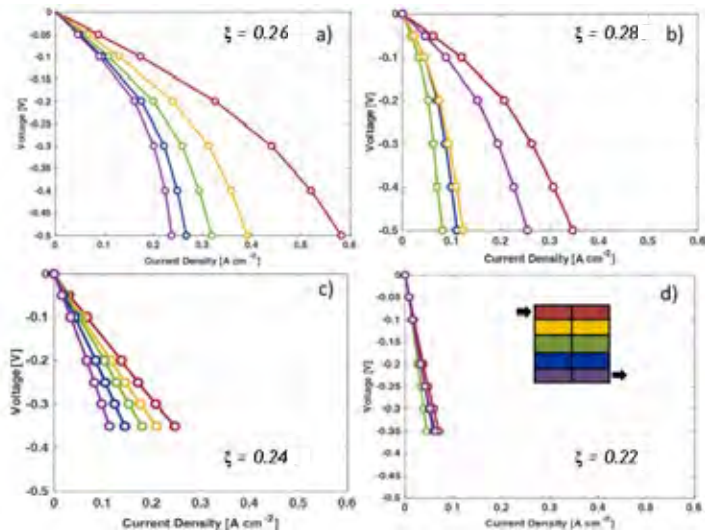


Figure 1: Local polarization curves for positive (a,b) and negative (c,d) electrolytes with serpentine (a,c) and interdigitated (b,d) flow fields. Heterogeneity index is evaluated at 0.05 A cm^{-2} .

of the reduced velocity of the flow in the porous electrode in the middle zone of the electrode, responsible for less intense and inhomogeneous under-the-rib fluxes. It is worth saying that, if the comparison is carried out at a fixed pressure drop, the interdigitated results less heterogenous than the serpentine.

Also the investigation of the local impedance is carried out to enlighten the local phenomena determining the performance: it can be observed that the positive electrolyte shows a large feature related to mass transport which overlaps the feature related to kinetics, that is not the limiting factor for performance with this electrolyte. Instead, the negative electrolyte, which is characterized by a kinetics limited regime and reduced mass transport issues, reveals clearly distinguished features and higher impedance values.

The spatial distribution of local spectra is consistent with the one observed for polarization curves, with growing impedance along the channel path for the serpentine, and a higher impedance of the middle segments for the interdigitated geometry.

V. MODEL FITTING AND VALIDATION

The 3D model has three fitting parameters: electrode active area, electrode permeability and negative electrolyte kinetic constant.

These parameters are fitted on global and local experimental data

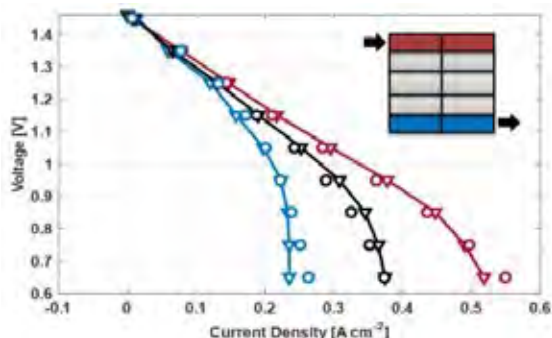


Figure 2: Results of fitting procedure on discharge of the all-vanadium configuration with serpentine flow field.

of positive and negative symmetric configuration at a flow rate of 20 ml min^{-1} , with both serpentine and interdigitated distributors. The obtained set of parameters is then validated at different flow rates and SOC values, showing a good agreement with experimental results (Figure 2).

VI. MODEL RESULTS

Analyzing the profile of velocity magnitude inside the electrode in three location and the contour of the reaction rate, it is visible a lower value of velocity in the middle zone of the interdigitated distributor, responsible for the lower reaction rate and then the lower performance of the middle segments observed during the experimental campaign, since the mass transport resistance in the proximity of the carbon fibers of the electrode is determined by a convective mechanism [1].

The model helps also to explain the overperformance of the serpentine with respect to the interdigitated distributor at fixed flow rate: the mean value of velocity inside the porous electrode for the former geometry is nearly 20 times higher than the latter.

The capability of the model to correlate the velocity field and the reactants distribution determined by the flow field pattern, with the global and local performance, allows not only to interpret and analyze the experimental data, but also to design optimized geometries of the distributor with the aim to achieve a better performance and reduced heterogeneity, topic that is investigated in a currently undergoing work.

VII. CONCLUSION

The main conclusions of the work are:

- The serpentine outperforms the interdigitated with both electrolytes. The reason of this behavior is found in the greater value of velocity of the electrolyte in the electrode, which enhances the reaction rate in serpentine;
- The local distribution of current density follows the pattern of reactants depletion along the channels, but performance shows a reduction in the middle zone of the interdigitated. The reason is found in the lower local value of the electrolyte velocity in the porous electrode;
- The positive electrode, characterized by a mass transport limited behavior, shows generally higher heterogeneity if compared with the negative one, characterized instead by a kinetic limited regime;
- The serpentine reveals lower heterogeneities than the interdigitated when coupled with the positive electrolyte, but its heterogeneity overcomes the interdigitated when the negative electrolyte is considered.

REFERENCES

- [1] M. Messaggi, P. Canzi, R. Mereu, A. Baricci, F. Inzoli, A. Casalegno, M. Zago, Analysis of flow field design on vanadium redox flow battery performance: Development of 3D computational fluid dynamic model and experimental validation, *Appl. Energy.* 228 (2018) 1057–1070. doi:10.1016/j.apenergy.2018.06.148

THE ECONOMICS OF HYDROGEN FOR RESIDENTIAL HEATING: AN ASSESSMENT OF HOW HYDROGEN FUEL CELL HEATING SYSTEMS COMPARE TO OTHER LOW-CARBON OPTIONS IN GERMANY AND THE UK

Steven Ashurst*, Robert Bloom*, and Jeremy Harrison*

* Delta Energy and Environment, Floor F, Argyle House, 3 Lady Lawson Street, Edinburgh, EH3 9DR, (UK)

Hydrogen (H₂) is being considered as a future low carbon energy source for heating. If widespread H₂ distribution becomes a reality, hydrogen boilers, hybrid heat pumps (HHP) and fuel cell micro combined heat and power systems (FC m-CHP) could be used to provide low carbon heat to homes. This paper models and compares the predicted end-user heating bills in 2030 using the above technologies, plus electric air-source heat pumps (ASHP), in Germany and the UK. Under “reference” conditions (expected product and energy costs), FC m-CHP offers the lowest heating costs in Germany; typically by €100s per year. In the UK FC m-CHP would require additional support to stimulate strong market activity; even under “optimistic” conditions, FC m-CHP delivers higher running costs than ASHPs and H₂ boilers.

Index Terms – Economics, Fuel cell micro combined heat and power (FC m-CHP), Hydrogen (H₂), heating.

I. NOMENCLATURE

Air-source heat pump (ASHP), condensing boiler (CB), Fuel cell micro combined heat and power system (FC m-CHP), hybrid heat pump (HHP), hydrogen (H₂), kilowatt hour (kWh), fully-installed cost (FIC).

II. INTRODUCTION

Hydrogen (H₂), when produced via low carbon methods, could reduce emissions from domestic heating. Countries with extensive gas grids (that could be repurposed to supply H₂), like Germany and the UK, have much potential for H₂-based heating.

Several heating technologies could use H₂, and the option of electric heating via air-source heat pumps (ASHP) must also be considered. The relative end-user heating costs in homes using different options must therefore be understood in detail.

However, heating technologies (especially FC m-CHP) are at various stages of commercial maturity, and there is no retail market for piped H₂ at present. Given this, two scenarios were modelled based on the future cost estimates of FC m-CHP

considering increasing production volumes and the reduction in product complexity from a switch from natural gas to H₂.

The “reference” scenario uses a conservative estimate for the fully-installed cost (FIC) of £/€12,000 for the FC m-CHP (currently ~£/€19,500). The “optimistic” scenario uses £/€8,000.

III. KEY ASSUMPTIONS AND CALCULATIONS

Key product specifications per country are shown in Table I. The FC m-CHP includes an integrated supplementary condensing boiler (CB). Inputs are derived from Delta-EE’s own databases and insights gathered via conversations with industry contacts. Differences in maintenance costs between products and the total maintenance cost over the product lifetime were considered negligible.

TABLE I: KEY PRODUCT ASSUMPTIONS

	H ₂ boiler	H ₂ HHP	ASHP	FC m-CHP
Fully-installed cost	£3,000 €7,000	£6,500 €10,000	£7,500 €12,000	£8,000-12,000 ^a €8,000-12,000 ^a
Thermal efficiency	90%	90% (CB) 300% (HP)	300% (HP)	90% (CB) 33% [1] (FC)
Electrical efficiency	-	-	-	57% [1] (FC)
Share of heat load provided	100%	80% (HP) 20% (CB)	100%	25-80% (FC) 75-20% (CB)
Product life	15 years	15 years	15 years	15 years

^a FIC of the FC m-CHP assumes no stack replacement is required when lifetime run hours are less than 80,000 kWh.

Energy price assumptions are given in Table II. An average of projections and targets for low carbon H₂ costs in Europe in 2030 was used, with supply chain costs (transportation, retail and tax) added to this as they are applied to natural gas supply today.

TABLE II: ENERGY PRICE ASSUMPTIONS

Year	Fuel cost	UK (per kWh)	DE (per kWh)
2019	Natural gas retail cost	£0.040 [2]	€0.061 [2]
	Electricity retail cost	£0.162 [3]	€0.299 [3]
2030	H ₂ retail cost	£0.083	€0.099

Electricity retail cost	£0.199	€0.300
-------------------------	--------	--------

Heating bills were calculated using the equations below:

$$\text{Amortized product cost} \left(\frac{\text{€}}{\text{kWh}} \right) = \frac{\text{fully installed product cost}(\text{€})}{\text{annual heat supplied} \left(\frac{\text{kWh}}{\text{yr}} \right) \times \text{product lifetime} (\text{yrs})}$$

Where amortized product cost is the cost to install and run the appliance over the lifetime run hours of the equipment.

$$\text{Product heat cost} \left(\frac{\text{€}}{\text{kWh}} \right) = \text{amortized product cost} \left(\frac{\text{€}}{\text{kWh}} \right) + \left(\frac{\text{energy cost} \left(\frac{\text{€}}{\text{kWh}} \right)}{\text{product thermal efficiency} (\%)} \right)$$

$$\text{Annual heating cost} = \frac{\text{Product heat cost} \left(\frac{\text{€}}{\text{kWh}} \right) \times \text{annual heat demand} (\text{kWh})}{\text{value of electricity generated} \left(\frac{\text{€}}{\text{kWh}} \right)}$$

IV. RESULTS

In the “reference” scenario for the UK, FC m-CHP is the most expensive technology in all properties. Annual heating bills are

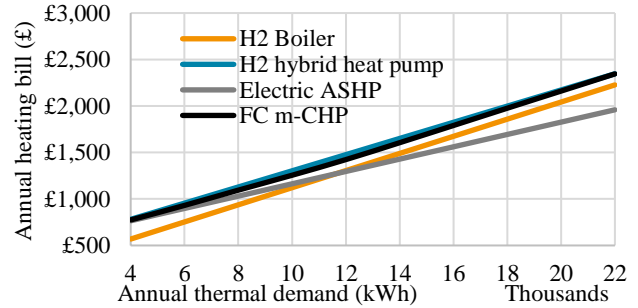
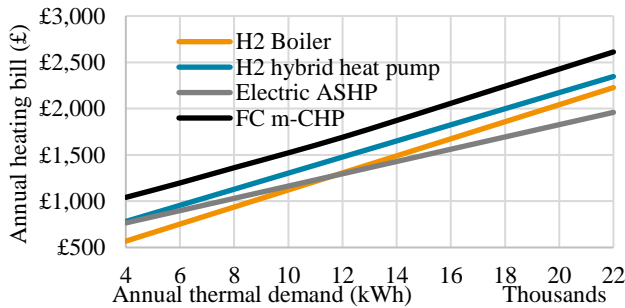


Fig. 1. Comparison of annual UK heating bill for satisfying annual thermal demands ranging from 4,000 kWh to 22,000 kWh with a H₂ boiler, H₂ HHP, ASHP and FC m-CHP in 2030 for the “reference” scenario (left) and “optimistic” scenario (right).

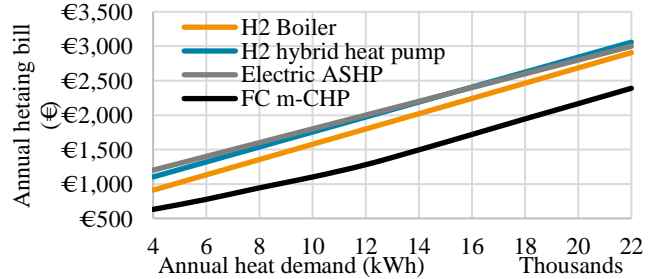
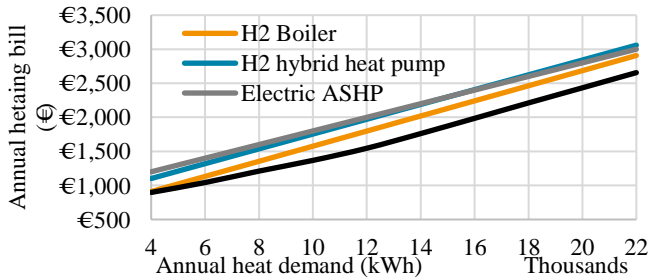


Fig. 2. Comparison of annual German heating bill for satisfying annual thermal demands ranging from 4,000 kWh to 22,000 kWh with a H₂ boiler, H₂ HHP, ASHP and FC m-CHP in 2030 for the “reference” scenario (left) and “optimistic” scenario (right).

V. CONCLUSIONS

If H₂ becomes viable as a heating fuel by 2030, Germany will be a very attractive market for FC m-CHP. FC m-CHP would still be highly competitive versus alternate low carbon heating options even if FIC was reduced to only €15,000 and the cost of H₂ is slightly higher than assumed at €0.11/kWh.

The UK market will only be attractive for FC m-CHP at around €6,000 FIC, or if the retail cost of hydrogen falls to £0.06/kWh. As such, the UK is unlikely to lead in the roll-out of FC m-CHP systems running on hydrogen.

REFERENCES

- [1] Panasonic, Panasonic to Commercialize Hydrogen Fuel Cell Generator [online] 2018, accessed 05/08/19, available from: <https://news.panasonic.com/global/press/data/2018/11/en181101-6/en181101-6.html>
- [2] Eurostat, Gas prices for household consumers (database), [online] 2019, accessed 01/05/2019, Available from: https://appsso.eurostat.ec.europa.eu/nui/show.do?dataset=nr_g_pc_203&lang=en
- [3] Eurostat, Elec. prices for household consumers (database), [online] 2019, accessed 01/05/2019, Available from: https://appsso.eurostat.ec.europa.eu/nui/show.do?dataset=nr_g_pc_204&lang=en

FUEL CELL MICRO-CHP: EUROPEAN MARKET STATUS AND FUTURE OUTLOOK

Steven Ashurst*, Robert Bloom*, and Cate Lyon*

*Delta Energy and Environment, Floor F, Argyle House, 3 Lady
Lawson Street, Edinburgh, EH3 9DR, (UK)

European micro-CHP (m-CHP) sales totaled 4,800 units in 2018 (products rated 5.5 kilowatts [kWe] and below). Combined sales of fuel cell product types contributed almost 3,400 units – or 70% of the market. This was a significant milestone; the first time fuel cell systems held the majority market share. Fuel cell micro-CHP (FC m-CHP) products have been aided by subsidies and favorable spark spreads in key markets, and this is expected to remain a driver as they come to dominate the European m-CHP market by 2025. The main barriers will be product costs remaining relatively high plus uncertainty around the long-term role for gas heating appliances.

Future sales will concentrate on single- or two-family homes. There is significant potential for overall market growth above the forecast 43,700 units, although there is little evidence the market is on the cusp of a transition to a ‘high’ growth scenario.

Index Terms - Fuel cell micro-CHP (FC m-CHP).

I. NOMENCLATURE

Proton exchange membrane fuel cell (PEMFC), micro-CHP (m-CHP), microturbine (MT), Stirling engine (SE), solid oxide fuel cell (SOFC).

II. INTRODUCTION

Throughout mid-2019 Delta-EE conducted research with the key companies that are selling or developing micro-CHP (m-CHP) products with a power output equal to or less than 5.5 kilowatts (kWe), as part of a yearly exercise to understand market trends and how global m-CHP sales will develop in future. Results are published in our members-only ‘Micro-CHP Annual Roundup and Market Outlook’ report [1].

This paper summarizes the highlights from the report with a specific focus on market activity and developments around fuel cell micro-CHP (FC m-CHP) products across Europe to 2025.

III. FINDINGS

A. State-of-play in the European m-CHP market

In 2018 the total number of European m-CHP product sales was 4,800 units. Volumes remain very small (combined sales of all heating devices are ~8 million per year), although this total did represent 8% growth from the previous year.

Major negative developments included BDR Thermea withdrawing its Stirling engine (SE) systems, and Vaillant removing its internal combustion engine (ICE) product line. Successes from some other brands did counterbalance the loss of sales, and both SOLIDpower and Viessmann grew sales relatively strongly – each company had a record sales year for their FC m-CHP offerings. This is clearly reflected in the sales trend by technology, highlighted in Fig. 1 below.

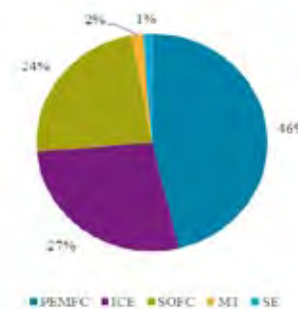


Fig. 1. European micro-CHP sales by technology, 2018.

Combined, the sales of all FC m-CHP products made up 70% of the total market – the first time fuel cells have had a majority share, and a significant milestone in the development of the European market. As per the historic trend, Germany accounted for the most significant amount of activity, with Belgium emerging as a market of growing importance.

The success of FC m-CHP brands was strongly aided by the availability of some significant investment subsidies at both

a European, national, and regional/state level. A typical 0.75kWe fuel cell unit targeted at the residential sector in Germany, for example, qualified for a base level federal subsidy of €9,300 (before the addition of any further local or performance-based grants). And in Belgium the European PACE subsidy provided by the European Commission, combined with an electricity-to-gas price ratio of up to 5:1 in some areas, brought about the rapid rise in interest witnessed there. Across the rest of Europe, sales remained at typical introductory level volumes – several tens of units per country.

B. Market development and key drivers in future

Looking forward, Fig. 2 below presents a market forecast for how sales of all m-CHP technologies are expected to develop under current, 'reference' conditions, and shows how important FC m-CHP technologies are to become in Europe where annual sales volumes have risen to more than 43,000 units.

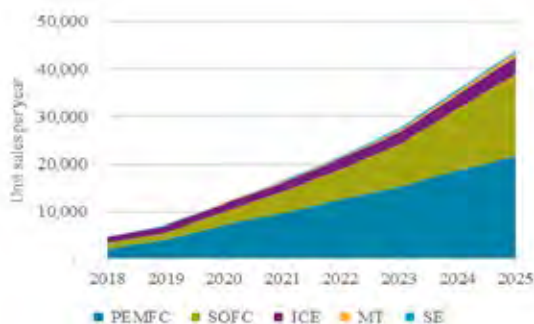


Fig. 2. European micro-CHP reference scenario market forecast to 2025.

By 2025, FC m-CHP products are forecast to share 90% of the market, with both proton exchange membrane fuel cell (PEMFC) and solid oxide fuel cell (SOFC) each increasing volumes to between 15,000-20,000 units per year. Other technologies will remain on the market but witness considerably lower volumes, as customers come to favor products with higher electrical efficiencies.

The most important drivers underpinning the future growth in FC m-CHP sales include increased market competitiveness as new products launch from major heating brands, at the same time as early movers release new products with improved specifications and lower costs via increasing production volumes. To 2025 the availability of subsidies will remain crucial. It is expected that products in Germany will continue to receive an upfront grant (through the federal subsidy programme until around 2023/24 at least) and incentives on the electricity produced (through the CHP Law) will apply to new installations likely to 2025, and potentially to 2030. Therefore as it is today, the most significant amount of activity is expected to occur in Germany. Although from the early 2020s newer markets will begin to open up as brands look to gain from their experience in Germany in other markets with similar characteristics, such as an attractive spark spread.

Some substantial barriers will also persist and serve to limit the growth potential; ultimately leading to m-CHP remaining a

relatively niche heating technology overall. Among them, comparatively high product costs, changes in the incentive regime (e.g. a general move away from feed-in tariffs and net metering), and political uncertainty around the long-term use of even high-efficiency gas heating technologies will have the largest impact on the rate of growth of m-CHP in Europe.

Overall, from a sales perspective, the residential market (products sized around 1.5kWe or less) will become the key focus of most m-CHP suppliers as is highlighted by Fig. 3 below.

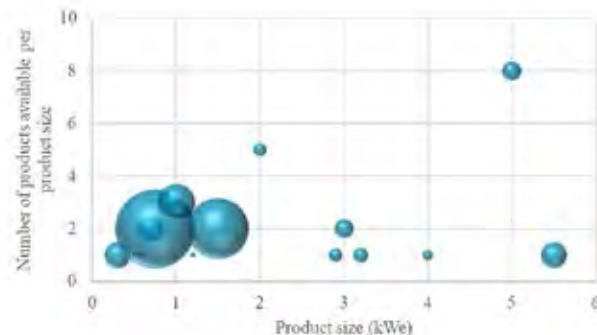


Fig. 3. Product availability across the entire EU m-CHP market in 2025.

The mid-point of each bubble on the x axis indicates product size, the mid-point on the y axis shows how many products in that size should be available, and the size of the bubble highlights our estimation for how many sales per product size will occur in 2025 i.e. the eight products sized 5kWe will contribute a relatively low volume of sales.

IV. CONCLUSION

The European micro-CHP market is on a positive, albeit a relatively limited growth trajectory. Based on a renewed focus on fuel cells by major heating brands, help from subsidies and spark spreads, and the benefit of cost reductions from increased production volumes, FC m-CHP will come to dominate the market in the years ahead. In spite of several challenging barriers, here remains much potential for volumes to be significantly higher than expected. However, at this stage there is not enough evidence to suggest that such a wildcard – for example in the form of the emergence of an incredibly low-cost product, or the carefully targeted interjection from a major utility company launching a very strong product offering for the mass market – is coming which would tip the market into a 'high' growth scenario.

ACKNOWLEDGMENT

The authors wish to acknowledge our appreciation for the contributions from our network of micro-CHP contacts.

REFERENCES

- [1] Delta-EE Gas Heating Service (2019) 'Micro-CHP Annual Roundup 2018 and Market Outlook', accessed 15-10-19, available from: <https://www.delta-ee.com/member-content/gas-heating-service.html>.

AUTOMOTIVE DERIVATIVE ENERGY SYSTEM: MODELLING DRIVEN PEMFC CHP PROTOTYPE DEVELOPMENT

G. Loreti*, A.L. Facci*, and S. Ubertini*

*DEIM Department of Economics, Engineering, Society and
Business Administration, University of Tuscia, 01100 Viterbo, Italy

Abstract – We present the key role of modelling in the development of the AutoRE project power plant prototype concept. Starting from the baseline power plant modelling we identify the most promising alternative configurations. Such configurations are further analyzed to gain fundamental insights on the design of energy systems based on hydrogen technologies and fuel cells.

Index Terms - PEMFC, CHP, power plant modelling.

I. INTRODUCTION

The AUTomotive deRivative Energy system (AutoRE) project (FCH-JU FCH-02.5-2014 call) has laid the foundations for the commercial diffusion of 50-100 kW PEMFC CHP systems for residential and commercial users. Leveraging on the mass production of the automotive sector the project has met the following goals: i) develop system components with reduced costs, increased durability and efficiency, ii) build and validate the 50 kW PEMFC CHP prototype, and iii) create the required value chain from automotive manufacturers to stationary energy end-users.

II. PEMFC CHP MODELLING ACHIEVEMENTS

The AutoRE CHP system encompasses an automotive derivative PEM fuel cell and a fuel processor that produces highly pure hydrogen from grid natural gas. The fuel processor is composed of a syngas production section and a syngas purification section (Figure 1).

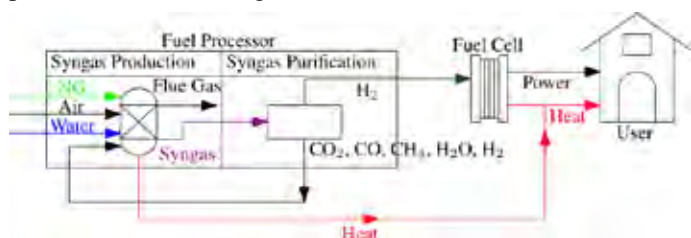


Figure 1: Schematic of the AutoRE cogenerative PEM fuel cell system.

The modelling is performed by mean of: i) a steady-state and lumped parameter thermo-chemical approach to estimate the performance, and ii) the assessment of the effective performance of the power plant within real energy management scenarios, considering an optimized control strategy.

A. Baseline Power Plant

The baseline power plant features a fuel processor based on steam reforming, water gas shift, and PSA purification unit. The model shows that the maximum electrical efficiency of the CHP plant is 38.9% and decreases to 32.7% at maximum power output [1]. Such an electrical efficiency is below the FCH-JU target [42%-55%] [2]. However, the fuel cell efficiency [46.9%-53.5%] suggests that the system efficiency can be improved, especially in the purification section of the fuel processor.

The assessment of the baseline CHP plant within real energy management scenarios, composed of five buildings types and six climatic conditions, shows that the payback period is as low as 3 years and the primary energy consumption reduction is as high as 40% [3], even though the electrical efficiency of the CHP is lower than the FCH-JU target. However, the results also highlight the need to study a technological solution to exploit the heat recovery in hot seasons and in hot climates.

B. Improved Efficiency Power Plant

The improvement of the FC efficiency raises the maximum plant electrical efficiency up to 41% [1]. However, the efficiency gain is marginal with respect to the increased cost of the fuel cell. Therefore, this configuration has been explored to prove that improving the efficiency of the most downstream element in the power plant is not a cost-effective strategy. In fact, the loss in efficiency from all the upstream elements cannot be recovered.

The enhanced thermal integration consists in recovering heat from the fuel processor and improves the maximum plant

electrical efficiency up to 40% (Figure 2, case B) without adding significant costs [4]. Therefore, we identify the thermal integration as a key feature for commercial PEMFC CHP system development.

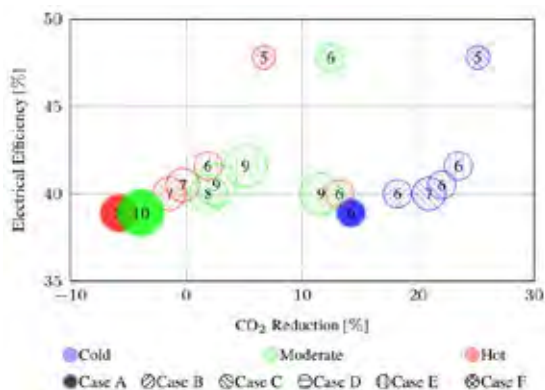


Figure 2: Electrical efficiency, CO₂ Reduction, and PBP for the power plants evaluated within real energy management scenarios for residential buildings in different climates and mean European energy context. The coordinates of the center of the circles represents the Electrical Efficiency and the CO₂ Reduction.

The size of the circles is proportional to the PBP. The value of the pay-back period is also reported in the center of the circles. The cost and CO₂ percentage reduction are calculated with respect to a reference scenario (electricity from the grid and heating by natural gas boiler). Case A, B, C, D, E, and F represent respectively: a) the baseline power plant, b) the enhanced thermal integration, c) the CHCP, d) the membrane separator, e) the water gas shift membrane reactor, and f) the steam reforming membrane reactor power plants.

We investigate three levels of selective membranes integration in the fuel processor: i) direct substitution of the PSA, ii) water gas shift membrane reactor, and iii) steam reforming membrane reactor. In these three cases the maximum electrical efficiency is 40.5%, 41.6%, and 47.8% respectively [4] (Figure 2, cases D, E, and F). Therefore, selective membranes as standalone purification unit do not significantly improve the overall CHP performance because placed in the most downstream element of the fuel processor. Instead, selective membranes integrated in reactors allow significant efficiency improvements and plant complexity reduction. However, the membrane stability at typical steam reforming temperature (700 °C-800 °C) is a critical aspect. Anyway, the fuel processor efficiency decreases for less than 4% by reducing the operating temperature to 600 °C of a steam reforming membrane reactor.

C. AutoRE CHCP

The AutoRE PEMFC CHP plant produces thermal power at a temperature between 73 °C and 77 °C. Moreover, half effect absorption chillers can be fed with thermal power at a temperature lower than 80 °C [5]. Therefore, we study the coupling of the AutoRE CHP, with a half-effect absorption chiller to establish the AutoRE Combined Heat, Cooling, and Power (CHCP) system.

The coefficient of performance of the half effect absorption chiller varies between 43% and 47% with respect to the set-point, as evidenced from the thermo-chemical model results [6]. However, the assessment of the AutoRE CHCP plant within real energy management scenarios shows that the usage

of the absorption chiller: i) reduces the carbon dioxide emissions of 8.33% on average, ii) increases the payback period of 1 year, but also increases the annual savings; and iii) extends the AutoRE plant profitability towards chilling based and hot climates [6] (Figure 2, case C).

III. CONCLUSIONS

The study of the AutoRE baseline power plant evidences that: i) the nominal efficiency is not always representative of the effective performance in real energy management scenarios, ii) the efficiency of the overall system can be increased, especially focusing on the fuel processor, and iii) the thermal power exploitation has to be increased to broaden the profitability of the CHP system towards hot climates.

Moreover, the study of the improved efficiency configurations shows that the most relevant results can be achieved by avoiding energy losses as upstream as possible in the power plant. In this sense, improved thermal integration and membrane based reactors are the most promising solutions to implement.

ACKNOWLEDGMENT

This project has received funding from the Fuel Cells and Hydrogen Joint Undertaking under grant agreement N° 671396. This Joint Undertaking receives support from the European Union's Horizon 2020 research and innovation programme and United Kingdom, Germany, Greece, Croatia, Italy, Switzerland, Norway. Swiss partners are funded by the State Secretariat for Education, Research and Innovation of the Swiss Confederation.

REFERENCES

- [1] Facci, A. L., Loreti, G., Ubertini, S., Barbir, F., Chalkidis, T., Eßling, R. P., ... & Bove, R. (2017). Numerical assessment of an automotive derivative CHP fuel cell system. *Energy Procedia*, 105, 1564-1569.
- [2] Fuel cells and hydrogen joint undertaking (FCH JU) multi-annual work plan 2014-2020.
- [3] Facci, A. L., & Ubertini, S. (2018). Analysis of a fuel cell combined heat and power plant under realistic smart management scenarios. *Applied energy*, 216, 60-72.
- [4] Loreti, G., Facci, A. L., Peters, T., & Ubertini, S. (2019). Numerical modeling of an automotive derivative polymer electrolyte membrane fuel cell cogeneration system with selective membranes. *International Journal of Hydrogen Energy*, 44(9), 4508-4523.
- [5] Deng, J., Wang, R. Z., & Han, G. Y. (2011). A review of thermally activated cooling technologies for combined cooling, heating and power systems. *Progress in Energy and Combustion Science*, 37(2), 172-203.
- [6] Loreti, G., Facci, A. L., Baffo, I., & Ubertini, S. (2019). Combined heat, cooling, and power systems based on half effect absorption chillers and polymer electrolyte membrane fuel cells. *Applied energy*, 235, 747-760.

GRASSHOPPER PROJECT: GRID ASSISTING MODULAR HYDROGEN PEM POWER PLANT

E. Crespi*, G. Guandalini*, J. Coolegem**, M. Martin^{3*}, S. Göbbling^{4*}, P. Beckhaus^{4*},
J. Petkovšek^{5*}, S. Buche^{6*}, S. Campanari*

*Politecnico di Milano, Via Lambruschini 4A, 20156 Milano, (Italy)

**Nedstack Fuel Cell Technology B.V., 6827 AV Arnhem, (The Netherlands)

^{3*} Abengoa Innovación, 41014 Sevilla, (Spain)

^{4*} ZBT GmbH, D-47057 Duisburg, (Germany)

^{5*} INEA d.o.o., SI-1000 Ljubljana, (Slovenija)

^{6*} Johnson Matthey Fuel Cell, RG4 9NH Sonning Common, Reading, (United Kingdom)

Abstract

The GRASSHOPPER FCH-JU2 European project aims to create a next-generation MW-size Fuel Cell Power Plant unit (FCPP), which is more cost-effective and flexible in power output, accomplishing an estimated CAPEX below 1500 €/kW_e. The power plant will be demonstrated in the field as a 100 kW_e sub-module pilot plant, implementing newly developed stacks with improved MEAs and BoP system components, combining benefits of coherent design integration. With respect to previously developed large-scale FCPP, the dynamic operating capability is a new feature necessary for economic participation in renewable-based energy markets. The plant optimization for ancillary services supply and the integration into the market are object of specific activities of the project. The stationary operation of the plant has been simulated to support the design of the plant and to choose the reference operating conditions.

Index Terms – ancillary services, fuel cell, MW-scale, plant integration

I. NOMENCLATURE

FCPP	Fuel Cell Power Plant
RES	Renewable energy sources

II. INTRODUCTION

The increasing share of electricity production from RES, necessary to meet the renewable energy target specified in the EU directives for climate change [1], causes demand-supply imbalances, more frequent occurrence of grid congestion,

volatility and increase in the wholesale electricity price. To overcome these issues, the Clean Energy for All European package [2] has introduced new electricity market structures. In this evolved framework, subjects able to provide margins of flexibility to the grid exploiting stored renewable energy are required. The large scale FCPPs can act as flexibility enablers for prosumers through the hydrogen-based dispatchable and distributed electricity production.

The technical feasibility of large MW-size PEM Fuel Cell Power Plant (FCPP) has been well demonstrated, for example in the DEMCOPEM-2MW project (FCH-JU 2015) [3]. However, a major step in the reduction of fuel cell stacks and system costs is still needed, together with the introduction of dynamic operation capability for providing ancillary services to the electrical grid. The GRASSHOPPER project (36 months, started in January 2018, [4]) aims at realizing a major step change in the cost structure of existing FCPP, realizing the next-generation modular FCPP unit targeting stationary application in the MW scale (such as > 2 MW) grid stabilization. The FCPP will be more cost-effective and flexible in power output, accomplishing an estimated CAPEX below 1500 €/kW_e (at a yearly production rate of 25 MW_e), as required to enter the markets as a competitive player.

III. GRASSHOPPER PROJECT

The project aims at a design optimization, coherently improving MEA, stack and system together, to realize a next-generation modular unit that does achieve the cost target when produced at full-scale. The MW-size FCPP unit will be based

on the learnings from a 100 kW sub-module pilot plant, that will be demonstrated in the field. The parallel development of components and system optimization will be followed by the integration in the complete pilot plant and the scale-up, as summarized in Fig. 1.

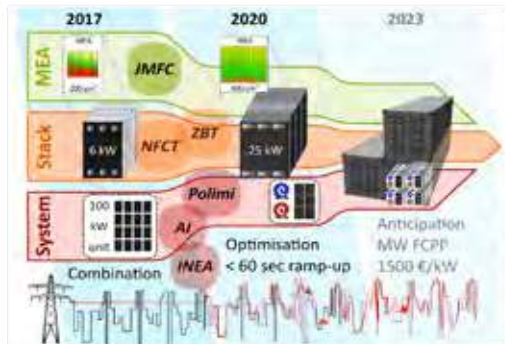


Fig. 1. Concept and project delimitations of the grid assisting modular hydrogen PEM power plant.

In the first step, the stack power output will be increased from 6 to 25 kW_e to reduce system complexity and the operating pressures will be increased to improve the dynamic load range and flexibility. The 100 kW_e plant is large enough to implement cost savings and validate operation flexibility fast response, performing a first major step to approximate 2000 €/kW_e. The feature of flexibility and grid support functionality will be introduced by using a smart grid integration. A Demand Side Management (DSM) interface developed by a partner of the project will be tested, integrating the plant in the industrial site in Delfzijl, the Netherlands. The operation strategy is defined by a prototype software interface used as a tool for aggregating and trading flexibility, offering services to the grid. The flexible demand driven operation will be demonstrated with a gross power set point range between 20 kW_e and 100 kW_e and a ramp-up rate delivering 50 kW within 20 seconds and 100 kW within 60 seconds.

The consortium has the leading experience with building, operating and maintaining FCPP and hence a good understanding of what is needed to meet efficiency, performance and lifetime expectations. The step change in stack design by NFCT is supported by know-how, measurements and detailed multi-physics modelling work from ZBT. JMFC focuses on the MEA cost reduction maintaining performance and durability. POLIMI and AI focus on cost reduction of the FCPP BoP, improving dynamic performance by accurate design and modeling. INEA will take care of the interface with the grid and trading optimization.

IV. THE FLEXIBLE 100 kW_e PILOT PLANT

The general concept of the 100 kW_e pilot power plant is depicted in Fig. 2. Pressurized hydrogen and air are humidified in a cross-flow packed-bed and fed to the PEM fuel cell. The

required heat is provided by the cooling water of the cells, assuring in all the operating conditions the correct humidity in the MEA. The residual heat is dissipated to the environment.

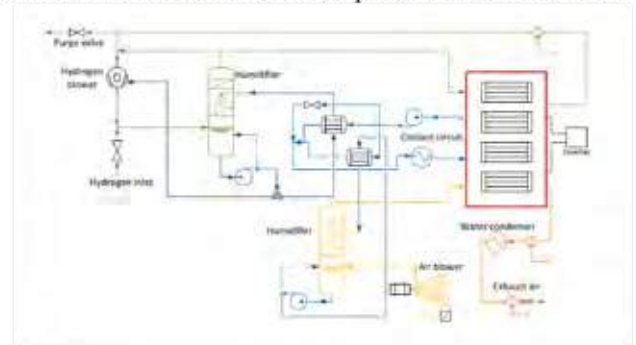


Fig. 2. 100 kW_e pilot PEM power plant configuration.

From the preliminary modelling activities, a slightly pressurized solution (0.6 bar_g) gives the best performance, given that an air expander could be included in the full-scale plant. Exhaust hydrogen flow is recirculated and mixed with fresh feedstock. An optimized operation strategy will be validated in the demo plant to take advantage of combined effects of current density and pressure on the polarization curve. The nominal current density of 1 A/cm² allows to increase the power density of the stacks.

V. CONCLUSIONS

GRASSHOPPER project will develop a FCPP characterized by operation flexibility and grid stabilization capability. It will represent an example of the hydrogen-based electrical power generator with ability to participate in the automated flexibility trading market and to receive remuneration for providing ancillary services. The design and optimization phase is concluded and the pilot unit will be constructed and operated continuously for 8 months in industrially-relevant environment in Delfzijl, the Netherlands.

ACKNOWLEDGMENT

This project has received funding from the Fuel Cells and Hydrogen 2 Joint Undertaking under grant agreement No 779430. This Joint Undertaking receives support from the European Union's Horizon 2020 research and innovation programme, Hydrogen Europe and Hydrogen Europe research.

REFERENCES

- [1] European Parliament, Directive (EU) 2018/2001 on the promotion of the use of energy from renewable sources. Official Journal of the European Union. December 2018.
- [2] European Commission, Clean Energy for All Europeans. 2016
- [3] S. Campanari, G. Guandalini, J. Coolegem, J. ten Have, P. Hayes, A. H. Pichel "Modeling, development and testing of a 2 MW PEM fuel cell plant fueled with hydrogen from a chlor-alkali industry", Journal of Electrochemical Energy Conversion and Storage (JEECS), doi 10.1115/1.4042923, 2019.
- [4] GRASSHOPPER project, 2019, www.grasshopper.eu

EXPLOITING THROUGH-PLATE REFERENCE HYDROGEN ELECTRODE TO STUDY CROSS-CONTAMINATION AND PERFORMANCE IN VANADIUM REDOX FLOW BATTERY

M. Cecchetti*, C. Oldani**, A. Casalegno* and M. Zago*

*Politecnico di Milano, Department of Energy, Via Lambruschini 4, 20156 Milano (Italy)

**Solvay Specialty Polymers, Viale Lombardia 20, 20021 Bollate (Italy)

Abstract – In this work a system of reference hydrogen electrode is applied at the inlet and outlet of both sides of a Vanadium Redox Flow Battery to measure how performance varies with different component such as membranes of different thickness and equivalent weight and electrodes of different morphology. The reference electrode set-up permits to distinguish between losses affecting the two electrodes at local level and is also able to monitor electrolytes potentials. The trends of open circuit potentials measured by the reference electrodes during cycling are associated to variation of the state of charge of the electrolyte solutions, which allows to evaluate the self-discharge of the battery and the imbalance of the electrolyte solutions. Furthermore, losses at positive and negative electrode are analysed from the measured overpotentials and associated with the characteristics of the electrodes.

Index Terms – Cross-contamination, Overpotentials evaluation, Reference Electrodes, VRFB.

I. INTRODUCTION

Vanadium Redox Flow Battery (VRFB) is a promising technology for energy storage due to its free energy power ratio high efficiency and long cycle life. However, its competitiveness is still hindered by low energy and power density [1]. The latter is limited by increased reaction overpotentials and ohmic losses through the membrane. Generally, VRFBs employ thick membranes to mitigate the self-discharge and capacity fade of the battery due to vanadium cross-over.

Therefore, measuring overpotentials and self-discharge of the battery is fundamental to develop improvements for the technology. For this purpose, in this work a system of through-plate reference hydrogen electrodes (RHE) was applied to a VRFB. This typology of RHE was firstly introduced in fuel cells by Brightman and Hinds [2], while the authors of this work proposed it in VRFB [3]. It consists in salt bridges

passing through the end-plates of the battery, creating a ionic contact between the electrode and a RHE placed outside the cell. Therefore, it enables the measure of the local potential of the electrodes, allowing the decoupling of positive and negative electrode contribution to the losses. In this way the evaluation of overpotentials of the two reactions is possible. Moreover, measuring the open circuit potential (OCP) of the single electrolyte solutions allows to estimate their State of Charge (SoC) and thus to evaluate the self-discharge of the battery due to cross-contamination during the operation.

II. EXPERIMENTAL

The performance of five membranes (*Nafion*[®] 212 and 115, *Aquivion*[®] E87-12S, E87-05S and E98-15S) in terms of ohmic losses and self-discharge were tested with Electrochemical Impedance Spectroscopy (EIS) and cycles of charge and discharge at fixed exchange capacity. The cell hardware was a “single-cell” VRFB of 25 cm² active area with two *Sigracet* 39AA as electrodes and electrolyte solutions of 100 ml made of 1 M of vanadium in 5 M sulphuric acid flowing at 40 ml min⁻¹. EIS were performed between 100 kHz and 1 Hz in Open Circuit Voltage (OCV) with a current oscillation of 4 mA cm⁻². Cycles of charge and discharge were performed by imposing the same capacity exchanged (1042 mAh) in charge and discharge to ensure that the self-discharge of the battery during cycling is due only to cross-contamination. Current density during charge was 40 mA cm⁻², while during discharge was 100 mA cm⁻² for the first 25 cycles and 50 mA cm⁻² for the following ones.

The performance of the battery at SoC 50% with three different electrodes (*Sigracet* 39AA, ELAT and AvCarb P50) were tested in galvanostatic polarization curves of current density steps of 50 mA cm⁻². The morphology, i.e. the surface area and the size of the pores, is reported in [4]. For

polarization curves the membrane used in the cell was Nafion 115.

III. RESULTS AND DISCUSSION

Table 1 shows the results from EIS and the cycles of charge and discharge of the tested membranes. The values of the resistance of the membranes, estimated with the High Frequency Resistance (HFR) of the EIS, are coherent with the thickness and the equivalent weight (EW) of the samples. Indeed, E98-15S has the largest HFR being the thickest, while the lowest values were observed in the membranes of thickness about 50 μm . Fixing the thickness, a lower EW reduces the resistance of the membrane [5] as the case of E87-05S and N212.

TABLE 1 PARAMETERS OF THE TESTED MEMBRANES AND THEIR SELF-DISCHARGE RATE OF THE ELECTROLYTES DURING CYCLES RELATIVE TO FIG.1

Parameter	N115	N212	E87-05S	E87-12S	E98-15S
Thickness [μm]	127	50	55	117	157
EW	1100	1100	865	865	946
HFR [$\text{m}\Omega \text{cm}^2$]	463	253	220	343	485
Positive SDR [% cycle ⁻¹]	0.85	2.31	1.51	0.84	0.35
Negative SDR [% cycle ⁻¹]	0.91	2.69	1.58	0.89	0.34

The self-discharge of the battery with the different membranes depicted in Fig. 1 is coherent with their thickness: E98-15S had the lowest self-discharge rates, whilst N212, the thinnest membrane tested, showed the fastest SoC decay. Moreover, although N212 has a similar thickness of E87-05S, it is lower selective to vanadium ions permeation due to the higher EW [5]. Accordingly, E87-12S, despite a lower thickness, had a similar self-discharge of N115.

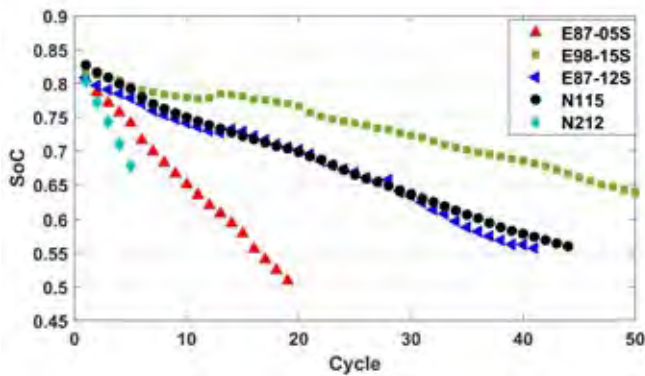


Fig. 1 SoC at the end of each charge for the tested membranes.

Fig. 2 shows overpotentials of the two reactions during discharge polarization curves. For all materials overpotentials are larger for the negative reaction and thus it is the limiting reaction for the operation of the battery. P50 has very small pores [4] which limits the permeation of the electrolytes into

both electrodes, resulting in large mass transport losses and a very low limiting current density. ELAT has a small surface area [4] and thus, considering that the negative reaction is kinetically limited [3], presents large negative overpotentials with an activation loss of 140 mV at 50 mA cm^{-2} . Instead, 39AA has a larger surface area [4] which guarantees lower negative overpotentials. However, 39AA has larger positive overpotentials than ELAT because its porous volume is mainly related to pores of high radius which increase the overall mass transport resistance.

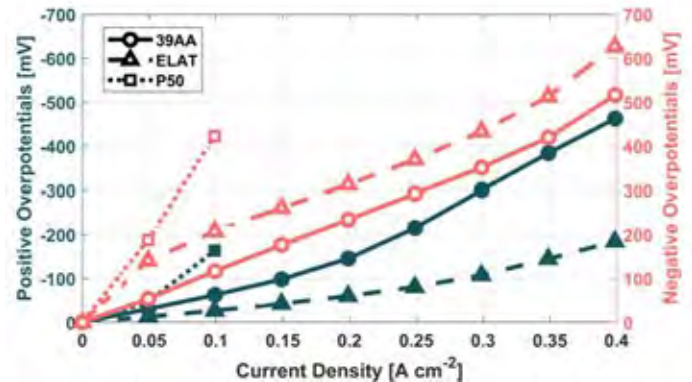


Fig. 2 Positive (full marker) and negative (empty marker) overpotentials during polarization curves in discharge at 40 ml min^{-1} .

IV. CONCLUSION

This work presented how through-plate reference hydrogen electrodes by separating the contribution of positive and negative electrode can provide more insights on the self-discharge of the electrolytes due to cross-contamination. Furthermore, the influence of morphological properties of electrodes on the performance of the single reactions can be analysed by evaluating the overpotentials, enabled by the reference electrodes. Negative reaction, which is the limiting one, requires a large surface area to reduce losses, whilst the positive reaction is favoured by a proper pore distribution that can guarantee permeation in the electrode, but without increasing the mass transport resistance.

REFERENCES

- [1] Weber A. Z. et al., Journal of Applied Electrochemistry 41.10 (2011): 1137.
- [2] Hinds G., and E. Brightman., Electrochemistry Communications 17 (2012): 26-29.
- [3] Cecchetti, M., et al., Journal of Power Sources 400 (2018): 218-224.
- [4] Cecchetti M. et al., "A combined morphological and electrochemical characterization of carbon electrodes in vanadium redox flow batteries: insights into positive and negative electrode performance." Electrochimica Acta, Under Review
- [5] Tang Z. et al., ECS Transactions 41.23 (2012): 25-34.

EFFICIENT THERMAL MANAGEMENT STRATEGIES FOR COLD START OF AUTOMOTIVE PEMFC SYSTEMS

G. Montaner Ríos*, J. Schirmer**, F. Becker*, S. Bleeck*,
C. Gentner*, M. Schröder*, I. Sokolov*, M. Zimmermann* and J. Kallo**

German Aerospace Center (DLR)
Institute of Engineering Thermodynamics
* Hein-Saß-Weg 22, 21129, Hamburg, (Germany)
** Pfaffenwaldring 38-40, 70569, Stuttgart, (Germany)
Tel.: +49-711-6862-670 Gema.MontanerRios@dlr.de

Abstract - The aim of this experimental work is to study different thermal management strategies for cold start of a PEMFC system for automotive applications. The obtained experimental results with a 4 kW commercial PEMFC at different startup temperatures will be presented in the conference. Moreover, the correlation between the startup temperature, the cold startup time and the energy requirement will be discussed. And finally, the most energy efficient system and fastest thermal management strategy for each start temperature from 0°C to -30°C will be shown.

Index Terms – cold start, startup time, system energy efficiency, thermal management strategy.

I. INTRODUCTION

A fast, reliable and harmless cold start of proton exchange membrane fuel cell systems is essential for mobile applications, especially in winter scenarios. Extensive research has already been carried out on this topic and several thermal management strategies have been developed for such a cold start. However, an energy efficient and rapid cold start as well as cold starts from temperatures below -20°C, are still challenging for automotive PEMFC systems.

II. EXTENDED ABSTRACT

A. Cold Start and Thermal Management Strategies

A successful cold start requires the cell to warm up above the freezing point before all the cathode catalyst

layer pores are plugged with ice. To achieve that, there are several thermal management strategies which can be classified into two main groups: a) passive (using heat generated within the stack), and b) active (using external heat) [1, 2].

B. Experimental

This experimental study was carried out with a 4 kW PEMFC (40 cells, 200 cm² electrochemical active surface area, graphite bipolar plates) and to conduct the active cold starts a 5 kW commercial heater for electric vehicles was used. The procedure followed to carry out each test consisted of four main steps: conditioning, purging upon shutdown, freezing to start test temperature, and cold start. The cold startup was operated with synthetic air and the purge method used was: dry gases (air in the cathode and H₂ in the anode). During the cold starts the standard coolant loop was switched to a small one with much lower thermal mass.

C. Results and Discussion

This section presents an example of the results obtained within this experimental study. But before discussing these results, it is necessary to note that in this work cold start is used as the time that the stack needs to produce 50 % of its electrical rated power by starting at freezing temperatures. The startup temperature strongly affects cold start, the startup time increases if the temperature is lower, as can be observed in Fig. 1 [1, 3].

Fig. 1 shows the evolution of the stack performance depending on the startup temperature using a passive cold start strategy run by potentiostatic mode. This strategy allows a self-cold start at very low temperatures without extra energy consumption, thus increasing the system's energy efficiency. Nevertheless, the cold startup time at extremely low temperatures (for instance -30°C) is too long. Moreover, at those temperatures a long ice formation phase (which can damage the cells) takes place, and once the cells reach above the freezing point a long flooding phase follows as well. Thereby, according to the DOE 2020 target for transportation applications, this specific passive cold start strategy is considered adequate at temperatures up to -15°C [4].

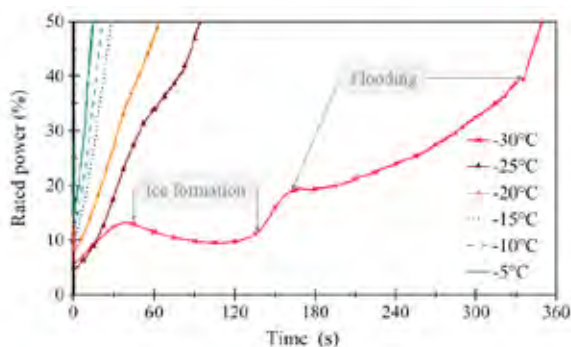


Fig. 1. Passive cold start performance at different startup temperatures

The 5 kW heater used during the active cold start strategies was able to warm up the coolant in 0.5 K/s. Thus considering that a passive start at 0°C took about 8 s, it can be concluded that the strategy (active heating the stack until 0°C and then self-start) is faster than a passive one at cold start temperatures below -15°C . Fig. 2 compares some thermal management strategies for cold start at -25°C . In this figure, once again can be noticed that the active strategies at startup temperatures below -15°C are faster than the passive one (brown lines).

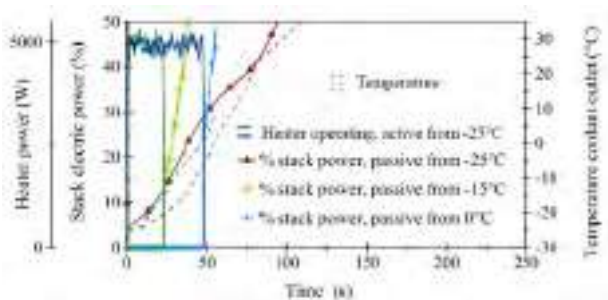


Fig. 2. Cold start performance and temperature, starting at -25°C with different thermal management strategies

Nevertheless, the fastest strategy is that one which the heater is operating only until -15°C (green lines) instead of until the freezing point (blue lines). Moreover, as can be seen in Table I, this fast strategy improves the system energy efficiency considerably.

TABLE I
STARTUP TIME AND EXTRA ENERGY REQUIREMENT FOR DIFFERENT COLD START STRATEGIES AT -25°C

Thermal management strategy	Startup time (s)	Extra energy requirement (J)
Passive	94	No
Active until 0°C \rightarrow passive	56	238
Active until -15°C \rightarrow passive	38	112

III. CONCLUSION

An experimental study of different thermal management strategies was performed in a 4kW PEMFC system. It was proved that regardless of the thermal management strategy used, the startup temperature has a profound influence on the cold startup time. Although the studied passive strategy already allows a self-start even at -30°C without extra energy consumption; it was found that at temperatures below -15°C the active strategies reduce the startup time. The relation between the startup temperature, the cold startup time and the energy consumption was briefly presented. Results showed that heating the stack just until -15°C by starting at very low temperatures not only increase the energy efficiency but also shorten the startup time. The remaining results of this study will be presented and discussed during the conferences, as well as the next steps to achieve a fast, energy efficient, reliable and harmless startup of a fuel cell powered vehicle until -40°C .

ACKNOWLEDGMENT

This work is part of the research project INNOvative Cost Improvements for BALANCE of Plant Components of Automotive PEMFC Systems funding from the Fuel Cells and Hydrogen 2 Joint Undertaking under grant agreement No 735969. This Joint Undertaking receives support from the European Union's Horizon 2020 research and innovation programme and Hydrogen Europe and N.ERGHY.

REFERENCES

- [1] Montaner Ríos, G., Schirmer, J., Kallo, J., Operation strategies for cold start of PEMFC systems, European Fuel Cell Technology & Applications Conference, Poster, Naples, Italy, December 2017.
- [2] Amamou, A., Boulon, L., Kelouwani, S., Agbossou, K., Sicard, P., Thermal Management Strategies for Cold Start of Automotive PEMFC, IEEE Vehicle Power and Propulsion Conference, Montreal, Canada, October 2015, pp. 1-6.
- [3] Montaner Ríos, G., Becker, F., Bleeck, S., Gentner, C., Sokolov, I., Schirmer, J., Kallo, J., Cold Start Improvement of a Polymer Electrolyte Fuel Cell System by Oxygen Enrichment, European Fuel Cell Forum, Poster, Lucerne, Switzerland, July 2019.
- [4] DOE 2020 Technical Targets for Fuel Cell Systems and Stacks for Transportation Applications. <https://www.energy.gov/eere/fuelcells/doe-technical-targets-fuel-cell-systems-andstacks-transportation-applications>.

FAULT DIAGNOSIS USING RESIDUALS FOR THERMAL MANAGEMENT SYSTEM OF A RESIDENTIAL FUEL CELL SYSTEM

H. Oh*, W. Lee*, M. Kim*, J. Won*, Y. Choi*, Y. Sohn*, S. Kim*, T. Yang*, S. Park*

*Korea Institute of Energy Research, Fuel Cell Laboratory, 152, Gajeong-ro, Yuseong-gu, Daejeon, 34129 (Republic of Korea)

Abstract – As the fuel cell supply increases, fault diagnosis and maintenance become more essential. In this paper, the faults on the thermal management system (TMS), that is a main sub-system of a residential fuel cell system, are diagnosed. Residuals are calculated in real time to detect faults from certain residuals exceeding acceptable threshold values. Then, the causes of faults are classified and diagnosed by checking the pattern change of the three residuals. Since the residual pattern is different for each fault, it is possible to clearly identify the cause of the fault. Furthermore, as the residual pattern is constant regardless of the different loads or the fault magnitudes, this method can be applicable under various operating conditions.

Index Terms – Fault Diagnosis, Residual, Regression, Thermal Management System (TMS)

I. NOMENCLATURE

I: Current (A)
 M: Mass flow (L/min.)
 T: Temperature (K)
 UA: heat transfer coefficient (W/K)
 U: control signal (-)
 V: Voltage (V)
 hex: heat exchanger
 re: reservoir
 st: stack

II. INTRODUCTION

The worldwide supply of fuel cell systems is steadily increasing with considering environment-friendly issues [1]. In Japan, residential fuel cell systems have already been commercialized [2], represented by Ene-farm. Korea is spurring the development and supply of the fuel cell system [3]. The more the supply, the more maintenance is needed. For a residential fuel cell system, the thermal management system (TMS) is especially important because the system utilizes the waste heat for a household while it produces electricity. In this study, a diagnostic method is suggested to identify various faults that can occur in the TMS of the residential fuel cell system.

III. CONFIGURATION AND CONTROL OF THERMAL MANAGEMENT SYSTEM

The TMS is divided into the stack cooling line, the heat exchanger, and the reservoir line. (Fig.1) The generated heat from the stack is transferred from the stack cooling line to the reservoir line through the heat exchanger. And the heated water on reservoir is supplied to a household boiler. As PID controllers, the pump-1 maintains the stack out temperature while the pump-2 maintains the stack in temperature. The temperature and level of the reservoir water are regulated by the fan's on-off control and by water discharge and supply through water external lines.

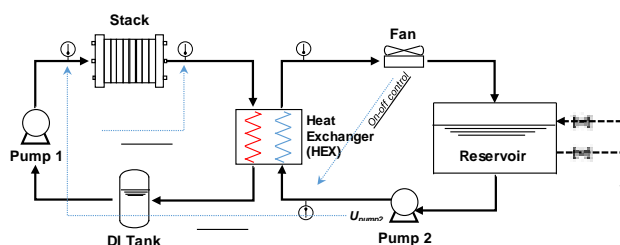


Fig. 1. Thermal Management System of a Residential Fuel Cell System

IV. FAULT DIAGNOSIS FOR THERMAL MANAGEMENT SYSTEM

A. Model-based method using residuals

A model-based method is used to detect and diagnose the faults by using residuals [4]. Nominal models are developed from generalized linear regression models in MATLAB using normal data set so that the models can predict analytical redundancies. The coolant flow rate at stack cooling line, the heat exchanger heat transfer coefficient, and the coolant flow rate at reservoir line are used as analytical redundancies. (Table I) Three residuals are generated from the differences between the predicted analytical redundancies and the measured actual values. If a residual is over the threshold, that is a fault detection. Then, from the residuals pattern, the faults can be classified and diagnosed. (Fig. 2)

TABLE I.
ANALYTIC REDUNDANCIES FOR THERMAL MANAGEMENT SYSTEM (TMS)

Number	Output	Input
1	M_{st}	$T_{st.in}, T_{st.out}, V, I$ (for measured) U_{pump1} (for predicted)
2	M_{re}	$T_{hex.in}, T_{hex.out}, V, I$ (for measured) U_{pump2} (for predicted)
3	UA_{hex}	$T_{st.in}, T_{st.out}, T_{hex.in}, T_{hex.out}, V, I$ (for measured) U_{pump1}, U_{pump2} (for predicted)

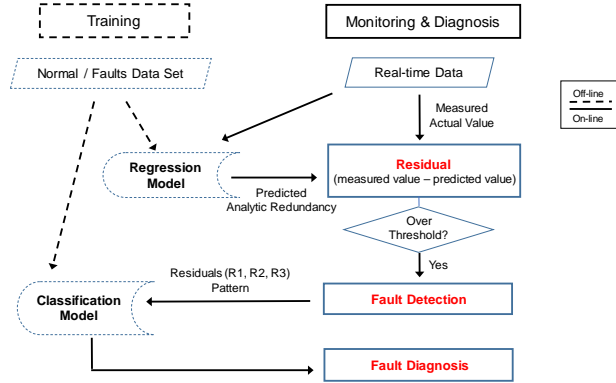


Fig. 2. Fault Detection and Diagnosis Process

B. Description of Thermal Management System faults

The faults that occurs in TMS are listed in Table II.

TABLE II. DESCRIPTIONS AND SIMULATING METHODS OF TMS FAULTS

TMS Faults	Description	Simulating Method
Pump degradation	Decreased mass flow at the same power consumption of pump	Decreased indicated control signal on monitor
Thermocouple offset	Lower offset	Decreased indicated temperature value on monitor
Heat exchanger fouling	Decreased heat coefficient of heat exchanger	Bypassed coolant
Fan failure	Not operable	Turned off
Leak	Coolant leakage out of line	Loosen joint

C. Classification model learned from residual patterns

To train the classification model, the residual patterns are used for the inputs while the pattern for artificial neural network (ANN) for the outputs, as shown in Table III. The residual patterns were obtained from the comparison of faults data set with normal data set during off-line training.

TABLE III. RESIDUAL AND OUTPUT PATTERNS TO TRAIN ARTIFICIAL NEURAL NETWORK CLASSIFIERS FOR TMS

		R1	R2	R3	ANN Output Pattern	Label
Normal					1 0 0 0 0 0 0 0	N
Stack Coolant Line	DI Pump	-1	0	-1	0 1 0 0 0 0 0 0	F1
	T.C._Stack In	-1	0	0	0 0 1 0 0 0 0 0	F2
	T.C._Stack Out	+1	0	+1	0 0 0 1 0 0 0 0	F3
Heat Exchanger	Fouling	0	0	-1	0 0 0 0 1 0 0 0	F4
Reservoir Coolant Line	Water Pump	0	-1	0	0 0 0 0 0 1 0 0	F5
	T.C._HEX In	0	0	+1	0 0 0 0 0 0 1 0	F6
	T.C._HEX Out	0	+1	-1	0 0 0 0 0 0 0 1	F7

D. Diagnosis result in real-time

An example of real-time diagnosis is shown in Fig. 3. The residuals are obtained in real-time using the input data and the regression models. With the patterns of residual 1, 2, 3 and the classification model learned, the diagnostic result can be shown also in real-time.

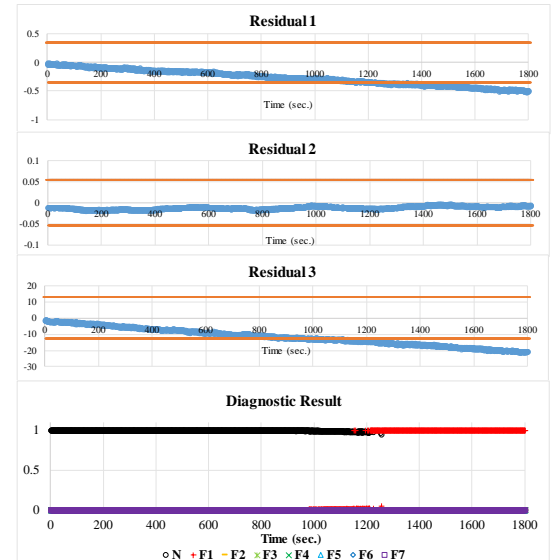


Fig. 3. An Example of Real-time Diagnosis (DI Pump Fault, F1)

V. CONCLUSION

This paper proposes a model-based method to diagnose the faults of TMS by using residuals. The residual patterns are the same regardless of the load conditions and fault magnitudes. And the pattern of each fault in TMS is separable. Thus, this method is versatile and effective to diagnose the fault of TMS even including the sensor fault.

ACKNOWLEDGMENT

This work was supported by the New & Renewable Energy Program of the Korea Institute of Energy Technology Evaluation and Planning (KETEP) grant funded by the Korean Government Ministry of Knowledge Economy (No. 20173010032150).

REFERENCES

- [1] E4tech, The Fuel Cell Industry Review, 2018.
- [2] Motomichi KATO, New product Development and Dissemination Strategy of Ene-farm in Panasonic, FC EXPO Technical Conference, FC-4, 2019.
- [3] Korean Government (MOTIE, MSIT, MOLIT), Korean Hydrogen Road Map, 2019.
- [4] R. Petrone, Z. Zheng, D. Hissel, M.C. Péra, C. Pianese, M. Sorrentino, M. Becherif, N. Yousofi-Steiner, A review on model-based diagnosis methodologies for PEMFCs, International Journal of Hydrogen Energy, Volume 38, 2013, pp. 7077-7091.

RENEWABLE HYDROGEN PRODUCTION THROUGH THE INTEGRATION OF AN SOE STACK WITH A SOLAR PARABOLIC COLLECTOR

P. Fragiaco*, G. De Lorenzo and O. Corigliano

Department of Mechanical, Energy and
Management Engineering, University of Calabria,
Via P. Bucci, 87036 Arcavacata di Rende, Cosenza, Italy.

* Corresponding author: phone: +39 0984 494615, e-mail: petronilla.fragiaco@unical.it

Abstract - Hydrogen is mainly produced through processes that employ fossil energy sources. These processes are economical, but cause the emission of polluting and greenhouse gases into the atmosphere and only 4% of the world production of hydrogen is conducted through water electrolysis. This last process can take place inside Solid Oxide Electrolyzer (SOE) fed by water with no environmental impact and a lower consumption of electrical energy produced from renewable sources.

The thermal energy necessary to the SOE for the hydrogen production can be supplied by a solar parabolic collector.

In the present work an energy analysis for the integration of an SOE short stack with a solar parabolic collector is presented.

The SOE short stack operates at the Intermediate Temperature (IT) equal to 750°C and is fed by water and electric energy. A simulation model of the IT-SOE system (stack and solar parabolic collector) is formulated ad hoc and implemented in Matlab environment.

Through the simulation model the best IT-SOE system thermal equilibrium current, in terms of the IT-SOE system efficiency and the H₂ mixture degree of purity, are evaluated. Furthermore, the hydrogen production is evaluated in a reference summer day.

Index Terms - H₂ production, Intermediate Temperature SOE, SOE modeling, performance analysis.

I. INTRODUCTION

There are four main sources for the commercial production of hydrogen: natural gas, oil, coal and water electrolysis, which account for 48%, 30%, 18% and 4% of the world's hydrogen production respectively [1].

Electrolysis consists of using electric energy to split water into hydrogen and oxygen. This process can take place inside Solid Oxide Electrolyzer (SOE) fed by water with no environmental impact and a lower consumption of electrical energy produced from renewable sources. The thermal energy necessary to the SOE for the hydrogen production can be supplied by a solar parabolic collector.

In the literature there are not many articles about fuel production through SOE, that represents a new, emerging and promising research field. In some of them [2-6] SOE fed by steam and steam/CO₂ mixtures were numerically modeled and experimentally tested.

The authors [7] conducted an experimental and theoretical activity on SOE short stack fed by steam and steam/CO₂ mixtures operating in electrolysis and co-electrolysis modes.

There are few articles about integration of SOE with solar parabolic collector. In one of them [8] Mohammadi et al. made a techno-economic analysis of SOE-solar parabolic collector system for hydrogen production inside a more complex plant, but only an indirect integration of SOE and solar parabolic collector through a thermo-vector fluid is considered.

In the present work an energy analysis for the direct integration of an SOE short stack with a solar parabolic collector is presented. The SOE short stack operates at the Intermediate Temperature (IT) equal to 750°C and is fed by water and electric energy. A simulation model of the IT-SOE system (stack and solar parabolic collector) is formulated ad hoc and implemented in Matlab environment. Through the simulation model the best thermal equilibrium current of IT-SOE system, in terms of the system efficiency and the H₂ mixture degree of purity, are evaluated. Furthermore, the hydrogen production is evaluated in a reference summer day.

II. SOE STACK - SOLAR PARABOLIC COLLECTOR SYSTEM

The integrated system is mainly composed of a SOE short stack, a water tank, a steam generator and a solar parabolic collector, dish shaped and equipped with an automatic sun tracking system. The solar parabolic collector directly supplies the thermal energy necessary to heat the SOE short stack up to its operative temperature, to superheat the water into the steam generator and to thermally sustain the SOE short stack during the hydrogen production.

The stack consists of six cells. Each cell is cathode supported and is designed to work at intermediate temperature. The SOE short stack was numerically modeled and experimentally tested in [7].

A. Math and Equations

During the start-up of the SOE system the useful thermal power absorbed for its pre-heating, $P_{th,abs,s}$, is instantly equal to the product of direct incident solar power on the concentrator aperture, $P_{sol,c}$, and the concentrator thermal efficiency, η_c . During the steam production phase the parabolic solar collector supplies the auxiliary thermal power necessary to steam generator, $P_{th,aux,sg}$.

If the SOE system is in thermal equilibrium, in hydrogen production phase the operating condition (1) must be verified:

$$P_{th,tot,sys} = P_{th,heat,gas,s} - P_{th,s} - P_{th,aux,H_2prod} = 0 \quad (1)$$

$P_{th,s}$, P_{th,aux,H_2prod} and $P_{th,heat,gas,s}$ are respectively the thermal power produced by stack, the auxiliary thermal power produced by solar parabolic collector during the hydrogen production phase and the thermal power required to heat the feeding gases at the stack inlet.

This condition expresses the equality of the thermal powers ($P_{th,s} + P_{th,aux,H_2prod}$), and the thermal power $P_{th,heat,gas,s}$ and in this condition SOE stack absorbs the thermal equilibrium current, $I_{th,eq}$.

The net production efficiency of the SOE system is calculated through equation (2):

$$\eta_{net,sys} = \frac{\dot{m}_{H_2} \cdot LHV_{H_2}}{P_{el,PS} + ((P_{th,tot,sys} > 0) + P_{th,aux,H_2prod} + P_{th,aux,sg}) \frac{\eta_{el,ref}}{\eta_{th,ref}}} \quad (2)$$

\dot{m}_{H_2} and LHV_{H_2} are respectively the mass flow and low heating value of hydrogen produced by SOE system;

$P_{el,PS}$, is the electric power required by the SOE stack power supply;

$P_{th,tot,sys}$ is the total additional thermal power (> 0) required by the SOE system;

$P_{th,aux,sg}$ is the thermal power required to produce the steam at the stack inlet starting from water at a temperature equal to 25 °C at the SOE system inlet;

$\eta_{el,ref}/\eta_{th,ref}$ is the ratio between the electrical and thermal reference efficiencies, which is used to convert the thermal power $((P_{th,tot,sys} > 0) + P_{th,aux,H_2prod} + P_{th,aux,sg})$ in equivalent electrical power.

III. PRELIMINARY RESULTS

Figure 1 shows the trends of $P_{th,tot,sys}$, $P_{th,aux,sg}$, P_{th,aux,H_2prod} and $\eta_{net,sys}$ for the stack fed by an equimolar steam-H₂ mixture and by air at varying the stack current. The stack reaches the maximum production efficiency at $I_{th,eq}$ that is about 0.60. The thermal equilibrium condition at the current, $I_{th,eq}$, of about 27 A.

IV. CONCLUSION

Through the simulation model the best IT-SOE system thermal equilibrium current of 27 A, in terms of the IT-SOE system efficiency of about 60 % and the H₂ mixture degree of purity of about 85 %, were evaluated.

Furthermore, through the hydrogen production was evaluated in a reference summer day, centered in July.

In the next future the calculation tool will be able to extend the evaluation period to all year.

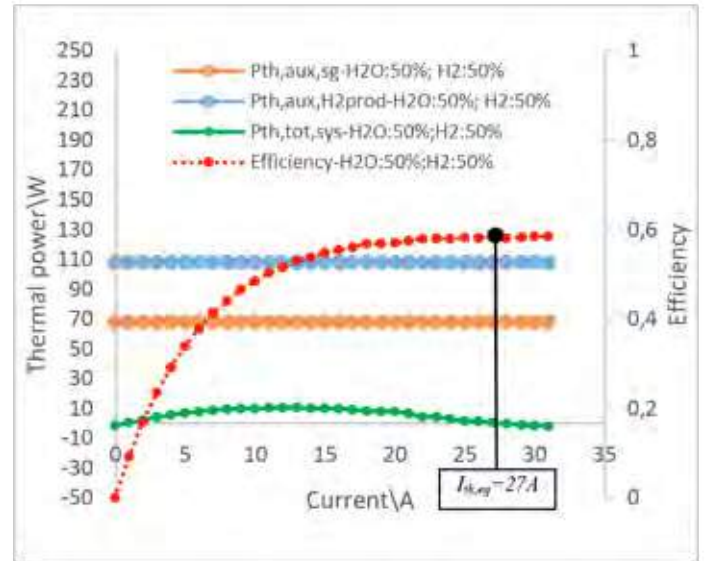


Fig. 1. Trends of $P_{th,tot,sys}$, $P_{th,aux,sg}$, P_{th,aux,H_2prod} and $\eta_{net,sys}$ for the SOE stack fed by an equimolar steam/H₂ mixture (H₂O: 50% and H₂: 50%) and by air at varying the stack current.

REFERENCES

- [1] Press, R. J., Santhanam, K. S. V., Miri, M. J., Bailey, A.V., Takacs, G. A. Introduction to hydrogen Technology, John Wiley & Sons, 2008, ISBN 978-0-471-77985-8.
- [2] Mougín, J., Mansuy, A., Chatroux, A., Gousseau, G., Petitjean, M., Reytier, M., Mauvy, F. Enhanced Performance and Durability of a High Temperature Steam Electrolysis Stack. Fuel Cells, 2013, Volume 13, pp. 623–630.
- [3] Camprubi, M.C., Izquierdo, S., Fueyo, N. Challenges in the electrochemical modelling of solid oxide fuel and electrolyser cells. Renew. Sustain. Energy Rev. 2014, 33, 701–718.
- [4] Cinti, G., Bidini, G., Hemmes, K. An experimental investigation of fuel assisted electrolysis as a function of fuel and reactant utilization. Int. J. Hydrogen Energy, 2016, Volume 41, pp. 11857–11867.
- [5] Kotisaari, M., Thomann, O., Montinaro, D., Kiviahho, J. Evaluation of a SOE Stack for Hydrogen and Syngas Production: A Performance and Durability Analysis. Fuel Cells, 2017, Volume 17, pp. 571–580.
- [6] AlZahrani, A.A., Dincer, I. Thermodynamic and electrochemical analyses of a solid oxide electrolyzer for hydrogen production. Int. J. Hydrogen Energy, 2017, Volume 42, pp. 21404–21413.
- [7] P. Fragiaco, G. De Lorenzo, O. Corigliano. Performance Analysis of an Intermediate Temperature Solid Oxide Electrolyzer Test Bench under a CO₂-H₂O Feed Stream. Energies, 2018, Volume 11, 2276.
- [8] Mohammadi, A., Mehrpooya, M. Techno-economic analysis of hydrogen production by solid oxide electrolyzer coupled with dish collector. Energy Conversion and Management, 2018, Volume 173, pp. 167-178.

Development of chitosan membrane modified with 2-aminoethanesulfonic acid and silica nano-fillers for fuel cell applications

Nondumiso Zungu and PO Osifo

Chemical Engineering Department, Vaal University of Technology, Vanderbijl Park, South Africa
Email: petero@vut.ac.za

ABSTRACT

In this study, sulfonated chitosan membranes were developed using the solution casting method. Chitosan was blended with the silica an inorganic nano-filler, amide plasticizers and 2-aminoethanesulfonic acid. The electrostatic interactions of 2-aminoethanesulfonic acid with the chitosan matrix was confirmed via FTIR. The SEM-EDS analysis showed a homogenous dispersion of silica particles on the surface of the membrane synthesised with 2-aminoethanesulfonic acid as compared to the control with 2.6 weight % of silica observed on the surface of the membrane. The findings elucidated the ability of 2-aminoethanesulfonic acid to prevent migration of silica nano-filler to the surface of the membrane. The X-RD patterns showed the absence of the crystalline characteristic peak which confirmed the synergistic effect of the amide plasticizers and the incorporated modifying agents in breaking the intermolecular hydrogen bonding between the acetamido groups and hydroxyl groups of the chitosan chain.

INTRODUCTION

In the quest for alternative sources of energy to meet the socio-economical demands, pollution remains a global threat hammering the current energy conversion technologies. The simplified infrastructure and high-power densities of direct methanol fuel cells (DMFs) have made these cells favourable as the alternative energy source to power electric vehicles and other portable appliances compared to hydrogen fuel cells [1,2]. The fabrication process of polymer electrolyte membranes with desired properties for use in solid polymer fuel cell applications have been a trial and error attempt for decades, the developed membranes were lagging below the design specification of the power density of 1 kW/m^2 until the development of a perfluorinated-sulfonic acid membrane called nafion 117 by Du Pont [3, 4]. However, slow oxidation kinetics of methanol at the anode and the depolarization at the cathode due to high methanol permeability across nafion 117 reduces the overall performance of direct methanol fuel cells, and the general high cost of nafion 117 surpass its advantages [2, 4, 5]. The shortfalls of nafion 117 has prompted enormous research interest on the low-cost biodegradable chitosan polymer. To produce a better flexible and a more conducting membrane, chitosan was blended with silica as a nanofiller, functionalized with 2-aminoethanesulfonic acid (taurine) to incorporate the sulfonic acid groups to improve its proton exchange channels, N, N-dimethylformamide was added to chitosan solution to increase flexibility of the produced membranes.

EXPERIMENTAL

Chitosan (30 g) and silica (1.5 g) were dissolved in 1000 ml of acetic acid solution (10 v/v %). 500 ml of the resulting chitosan-silica solution was mixed with 50 ml of N, N-

dimethylformamide. The solution was stirred for 30 min under the atmospheric condition and was termed Cs-M-DMF owing to the presence of silica (denoted as M) and dimethylformamide (DMF). In one beaker, 20 ml of 2-aminoethanesulfonic acid solution (0.06g/ml) was added to 200 ml of the Cs-M-DMF solution and stirred for 10 min. A standard solution was prepared substituting 20 ml of 2-aminoethane sulfonic acid (taurine) with 20 ml of distilled water. The prepared chitosan solutions were casted on glass plate each at a thickness of 250 μm and were left to dry for 5 hours in an oven heated at 50°C. The resulting films were cross-linked with 500 ml of the sulphuric acid solution (5 v/v %) for 24 hours, followed by the neutralisation of the membranes with 0.1 M NaOH solution for 2 minutes, followed by rinsing in distilled water. The chitosan membranes and powder were characterised using TGA, XRD, SEM and FTIR to determine thermal properties, X-Ray diffraction patterns, the morphology and functional groups resulting from the modification, respectively.

RESULTS AND DISCUSSIONS

Fig. 1 shows the FTIR spectra of two chitosan-based membranes for Cs-M-DMF-H and Cs-M-DMF-T. The stretching vibration ascribed to the sp^3 hybridised C-H groups around 2800 cm^{-1} is strongly absorbed in the Cs-M-DMF-T membrane due to the C-H₂ groups of 2-aminoethane sulfonic acid (taurine) and this is contrary to the control membrane prepared using distilled water. Furthermore, the stretching vibrations observed at 1152 cm^{-1} confirmed the incorporation of the S=O groups from the sulfonic acid groups of taurine, notably, this peak at 1152 cm^{-1} was absent on the control membrane, this confirmed the absorbance was not due to the C-O stretching vibrations of chitosan molecule. The stretching vibration observed at 894 cm^{-1} was ascribed to the -S-O^- ions resulting from the electrostatic interaction of 2-aminoethane with chitosan in the synthesised membrane. The broad band observed around $3700\text{-}2400\text{ cm}^{-1}$ was attributed to the O-H stretching vibrations of silica, this confirmed the incorporation of the nano-filler on both synthesised chitosan-based polymeric membranes. Furthermore, stretching vibrations at around 2130 cm^{-1} and 1998 cm^{-1} were observed for Cs-M-DMF-T membrane, these may be due to formation of imine derivatives N=C=S and C=C=N , respectively. The formation of imine is attributed to the reaction between the carbonyl group (C=O) of dimethylformamide acting as a plasticizer and the amino groups of chitosan (-NH_2), the reaction involves the splitting of the water molecule. The stretching observed around 565 cm^{-1} on the Cs-M-DMF-T membrane was attributed to the formation of a tetrahedral structure of silica (SiO_4).

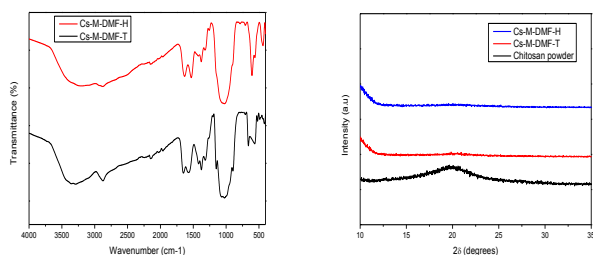


Fig. 1: FTIR spectra of Cs-M-DMF-T and Cs-M-DMF-H (left) and XRD pattern of chitosan powder, Cs-M-DMF-T and Cs-M-DMF-H (right)

The X-RD patterns of the chitosan powder and the two synthesised flexible Cs-M-DMF-T and Cs-M-DMF-H chitosan-based membranes is shown in Fig 1 (left). The characteristic peak at around 20° is attributed to the crystalline nature of chitosan. The peak at 20° was observed to be flattened on the X-RD patterns of both Cs-M-DMF-T and Cs-M-DMF-H chitosan-membranes. The modification disrupted the crystalline structures of chitosan chains through the disruption of the repeatable molecular arrangements by introducing side chains and breaking intra/intermolecular hydrogen bonding between the acetamido groups and hydroxyl groups of chitosan.

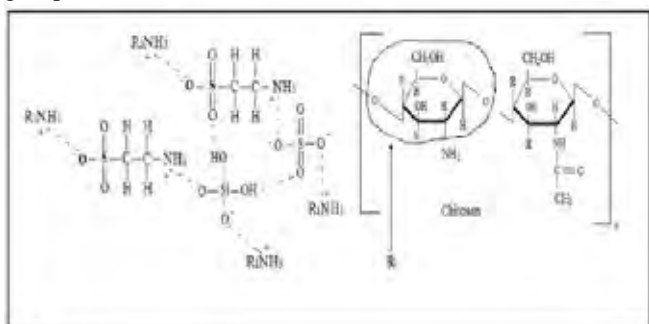


Fig. 2: Proposed interaction mechanism of 2-aminoethanesulfonic acid.

Table 1 presents the elemental results from the SEM-EDS analysis performed on the surface of the control membrane prepared without 2-aminoethanesulfonic acid. The agglomeration observed from the SEM image was attributed to the migration of the unmodified silica nanoparticles to the surface due to the absence of 2-aminoethanesulfonic acid.

TABLE 1: Elementary results of modified membrane:

Element	Cs-M-DMF-T (weight %)	Cs-M-DMF-H (weight %)
C	51.64	0
O	47.59	80.44
Si	0.77	2.57
S	0	16.99
Total	100	100

The absence of sulphur on the elementary analysis of the Cs-M-DMF-T membrane surface elucidated the formation of electrostatic interaction between the protonated amino groups ($-NH_2$) of 2-aminoethanesulfonic acid and the anion of the sulphate anion ($-SO_4^{2-}$) during crosslinking sulphuric acid.

Fig. 2 shows a proposed reaction mechanism formulated in this study to explain the interactions of 2-aminoethanesulfonic acid with the nano-filler silica, sulphate anion, and chitosan polymer. Interestingly, the incorporation of 2-amino acid as elucidated on the SEM images (Fig. 3) and elementary analysis, favours a uniform dispersion of the nanofiller, which enhance not only the proton conductivity of the polymeric membranes but also the thermal and mechanical properties when incorporated within the loading limit.



Fig. 3: SEM image of Cs-M-DMF-T membrane (left) and Cs-M-DMF-H membrane (right).

TGA results for Cs-M-DMF-T gave the first weight loss of about 7% occurred around $30^\circ\text{C} - 230^\circ\text{C}$ and was attributed to the evaporation of water molecules and other light components, at $\sim 230^\circ\text{C} - 380^\circ\text{C}$ was attributed to the loss of oxygen containing functional groups, and last phase was associated with the degradation of the main polymer backbone

CONCLUSION

Sulfonated chitosan membranes were developed by the solution casting method using 2-aminoethanesulfonic acid, silica nanofiller and amide plasticizers (N, N-dimethylformamide). The chemical interactions between chitosan and the incorporated components were confirmed using the FTIR. The developed membranes were all flexible and showed absence of the crystalline characteristic peak of chitosan at 2θ (20°). The SEM-EDS analysis elucidated the ability of 2-aminoethanesulfonic acid to inhibit the migration of silica and the sulfate anion to the surface of the membrane.

REFERENCES

- [1] P. Geng, Q. Tan, C. Zhang, L. Wei, X. He, E. Cao, *et al.*, *Science of the Total Environment*, vol. 572, pp. 467-475, 2016.
- [2] F. A. Zakil, S. K. Kamarudin, and S. Basri. *Renewable and Sustainable Energy Reviews*, vol. 65, pp. 841-852, 2016.
- [3] B. Smitha, S. Sridhar, and A. Khan. *Journal of membrane science*, vol. 259, pp. 10-26, 2005.
- [4] J. Mališ, M. Paidar, T. Bystron, L. Brožová, A. Zhigunov, and K. Bouzek. *Electrochimica Acta*, vol. 262, pp. 264-275, 2018.
- [5] P. Mukoma, B. Jooste, and H. Vosloo. *Journal of Membrane Science*, vol. 243, pp. 293-299, 2004.

STRATEGIES FOR HEALTH MONITORING AND DIAGNOSTICS OF COMMERCIAL SOLID OXIDE FUEL CELL SYSTEMS BASED ON REAL-TIME MODELLING

P. Wachel*, R. Thandi*, and H. Versteeg*

*Loughborough University, Loughborough, Leicestershire, (United Kingdom)

Abstract - This paper illustrates a novel, physics-based approach to monitor the health of a SOFC system. The system is composed of a steam-fuel mixing component, pre-reformer, reformer and a fuel cell stack. These system components are modelled using a one-dimensional fluid network along with chemical and electrochemical reactions to make predictions of the fuel cell stack voltage. Voltage of the fuel cell stack can be used to detect gas leakages, as the stack voltage is dependent on the fuel composition on the anode cell interface. Comparison of measured stack voltages with the output of a real-time computational model provides health indications of the system.

Index Terms – SOFC, health monitoring, diagnostics, fault detection, real-time model, industrial system

I. INTRODUCTION

Fuel cell systems developed for commercial demonstrations may have a higher probability of system failure as previous testing is conducted at low technology readiness levels before subsystems are integrated. When undetected these defects can cause a stack to break which increases cost and reduces system availability. The solution to this problem is a system that can detect these faults early and prevent damage to components. The current challenge with developing health monitoring algorithms for fuel cell systems are that most methods require a high number of reliable sensors that increase the cost of the system. Also, most techniques are dependent on high quality data sets with well understood failures signatures for methods such as machine learning. SOFC systems operate at high temperature and therefore can develop leakage paths due to thermal stresses. Not all leakages can be detected prior to the system being integrated and the ability to identify these issues early are critical for asset protection. The technique proposed in this paper was developed to integrate a physics-based real-time model using inputs from product level instrumentation that are transferable to different systems and stack configurations.

II. SYSTEM DEFINITION

The proposed health monitoring technique was developed for a system designed for a commercial application. The fuel cell system can be simplified to three gas streams; fuel, air and exhaust. The air is used to optimise the stack operating temperature and provides the oxidant for the cell reaction. The

natural gas in the fuel stream is reformed into hydrogen and carbon monoxide, the former is utilised in the stack reaction and converted into steam. The steam in the off-gas is recycled to reform the incoming fuel. The remaining fuel (off-gas) and air (off-air) is then combusted in the exhaust stream to reduce the system emissions and to increase system efficiency through heat recovery. The focus of the health monitoring system is the anode loop shown in Fig. 1. The anode loop takes Natural Gas (NG) mass flow through the NG inlet. The instruments used in the anode loop are represented by (T) temperature, (A) current, (V) voltage.

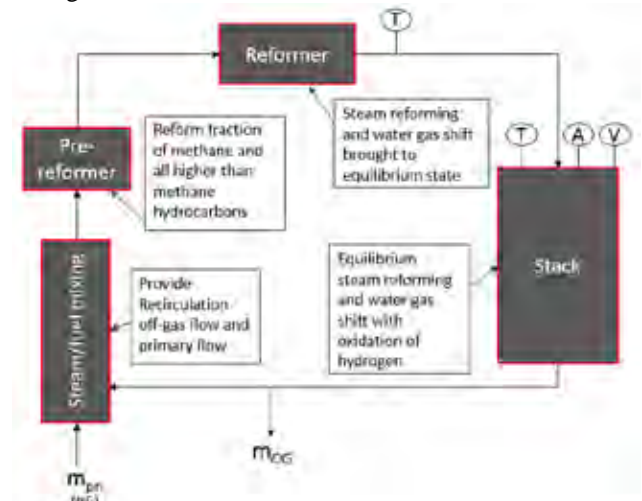


Fig. 1. Anode gas stream of a generic NG subsystem

III. REAL TIME MODEL

Stack voltage was chosen as the key parameter for health monitoring of the stack condition. The aim of this technique was to compare the predicted model and measured voltage. If the measured stack voltage was lower than predicted at a given stack current demand then this could indicate possible fuel leakage in the system. To model the stack voltage it was necessary to model the gas composition in the stack in order to calculate the Nernst voltage (1).

$$V_{Nernst} = V_o + \frac{R_u * T_{stack}}{2 * F} \ln \left(\frac{p_{H2} * p_{O2}^{0.5}}{p_{H2O}} \right) \quad (1)$$

Where the V_o is reference voltage, T_{stack} is measured average

stack temperature, F is Faraday constant, p are partial pressures of specified gas species. The gas composition was mostly impacted by the reformer outlet composition which was designed to reach equilibrium and validated by independent testing (2) using equilibrium constant calculations [2].

$$K_r = \frac{p_{H_2}^3 p_{CO}}{p_{CH_4} p_{H_2O}} \quad (2)$$

The key aspect of this modelling was to estimate the Area-specific resistance (ASR) of the stack as the focus of the monitoring was stack under load. A high fidelity mathematical model based on fundamental equations [1] was developed to predict each component of the ASR and the operating voltage V for a given measured current density (J) given in (3), which is the main output of the model.

$$V = V_{Nernst} - J * ASR_{cell} \quad (3)$$

A health monitoring system based on this resulting model was coded in Python and implemented on a fuel cell system. The voltage is predicted in real time and compared every 3 seconds with the measured voltage to indicate whether the correct amount of fuel is being delivered to the cells in the stack.

IV. MODEL VALIDATION

The model was validated against historical data from tests on healthy systems. The error was found to be within 1% of the operating voltage as shown in Fig. 2.

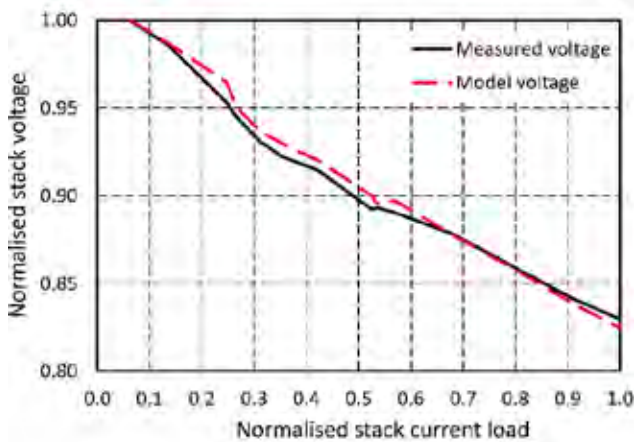


Fig. 2. Model validation against real system data

Further model runs were carried out to investigate the sensitivity of operating voltage to fuel leakage by inserting a leakage path at the stack inlet. Increased recirculation of steam/fuel mixing component due to the leakage was also considered. Fig. 3 shows the predicted relationship between the normalised stack voltage and stack current load. The data has been normalised with respective to the maximum test voltage and current for confidential purposes. The predictions show that the stack voltage at a given stack current load decreases rapidly as leakage

increases from 0% to 20% other leakage cases. At 30% stack load the difference between 0% and 20% fuel leakage is around 10% which can be easily detected and the signal can be used to prevent any damage to the stack that would result from further increase of loading as this would lead to fuel starvation.

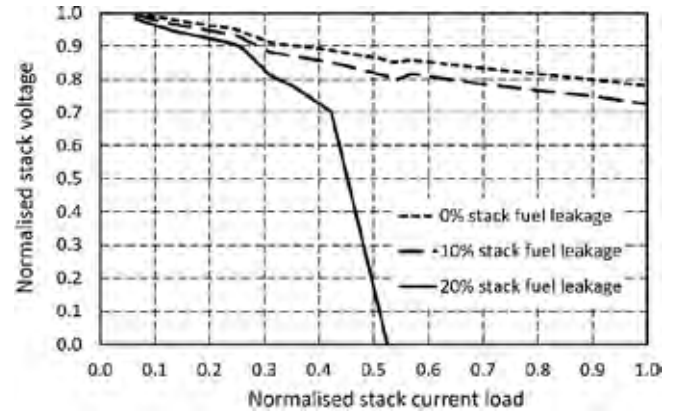


Fig. 3. Model fuel leakage sensitivity study

V. DISCUSSION

The initial results of the model showed potential, therefore a dashboard system was introduced to guide operators during the fuel cell system operation. During testing of a new stack configuration a leakage path occurred and was detected successfully in real-time. The model also demonstrated the ability to detect electrical faults in real-time during the early stages of system commissioning.

VI. CONCLUSION

The methods in this paper have successfully been applied to field trial units with the limitations of signals from a representative commercial system. However, it should be noted that the method relies on the availability of ASR calibration data. Polarisation performance curves from stack pass-off tests for a given assembly architecture and cell chemistry can be used to characterize the ASR. The real-time model has been validated on a commercial system. Further work to decrease the reliance on instrumentation is to model the heat exchange in the system and therefore reduce the number of sensors required in the system.

ACKNOWLEDGMENT

This work has been supported by Loughborough University.

REFERENCES

- [1] Costamagna, P. et al., Electrochemical model of the integrated planar solid oxide fuel cell (IP-SOFC), Chemical Engineering Journal, Volume 102, 2004, Pages 61–69.
- [2] Haberman, B. A. and Young, J. B., Three-dimensional simulation of chemically reacting gas flows in the porous support structure of an integrated-planar solid oxide fuel cell, International Journal of Heat and Mass Transfer, Volume 47, 2004, Pages 3617–3629.

THE EFFECTS OF PLATINUM OXIDE SPECIES ON PERFORMANCE DEGRADATION IN POLYMER ELECTROLYTE FUEL CELLS

Andrea Bisello², Elena Colombo, Amedeo Grimaldi, Andrea Baricci, Andrea Casalegno
Politecnico di Milano, Dipartimento di Energia, Via Lambruschini 4, Milan (Italy)

Abstract - The role of platinum oxides (PtOx) in PEMFC have been investigated through a dedicated experimental protocol. Regarding oxide growth, two main oxide species (α -oxide and β -oxide) have been observed. It has been demonstrated that PtOx coverage plays a major role in temporary degradation during potential holding test. As PtOx coverage increases, ORR activity decreases (reduced number of free active sites), causing performance decay in time. β -oxide have a greater effect on current density decay than α (4-6 times as effective), suggesting a larger number of blocked active sites. A unique and consistent correlation to separate the effect of α and β -oxide is proposed. Finally, a dedicated Accelerated Stress Test (AST) is performed and compared to AST from DOE protocol. It provides a stable oxide coverage during the ageing process, resulting in a reduced active area loss. Thus, different platinum oxides are believed to have a different protective role during operation.

Index Terms – Cyclic Voltammetry – Platinum Oxides – ORR activity – AST

I. INTRODUCTION

Temporary degradation is a decay in performance experienced during standard PEMFC operation. Huang et al.[1] correlated the reduction of ORR activity (current decay in time) with the increase in oxide coverage and related blocked active sites. Despite, Pt oxides have been widely investigated in the literature[2,3], there is still lack of a comprehensive understanding of their formation and effect on ORR activity. The reason is mainly due to the complexity of the topic, the unknown variables are: type of oxides, number of active sites occupied, degree of place exchange, number of oxide layers formed, without being exhaustive. In this work, an application-oriented approach is used, based on *in-situ* cyclic voltammetries on Membrane Electrode Assembly (MEA). Two major oxide families have been distinguished, according to literature[4], and the effect of these families have been investigated on both ORR activity (thus investigating

temporary performance loss due to Pt oxide formation) and Pt dissolution (by adopting properly defined AST protocols)

II. EXPERIMENTAL

Potential cycling and holding tests have been performed under inert atmosphere (anode H₂ /cathode N₂, RH 100/100 %) following protocol in Ref[4]. Three main tests are performed in inert conditions (as depicted in **Figure 1**):

- Holding test: a constant potential (850mV) is held for variable time (from 6s up to a few hours);
- Cycling test: Potential is linearly swept between lower potential limit (LPL) and Upper potential limit (UPL), base cases are 700mV and 850mV;
- Cycling+Holding test: A fixed number of cycles is performed, then a fixed potential (850mV) is held for a variable time (from 6s up to 1 h).

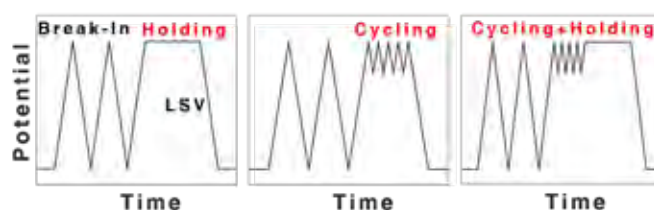


Figure 1 – Protocols representation: (left) Holding test; (middle) Cycling test; (right) Cycling+Holding test.

To elucidate the role of different oxides on performance in-operando tests are investigated. First, previous protocols in inert atmosphere are repeated but air is fed to the cathode during potential holding and subsequently platinum reduction charge is recorded. Then, *Cycling+Holding* test have been repeated and current density was recorded during all the tests.

III. RESULTS AND DISCUSSION

Results of potential cycling and holding tests were depicted in **Figure 2**.

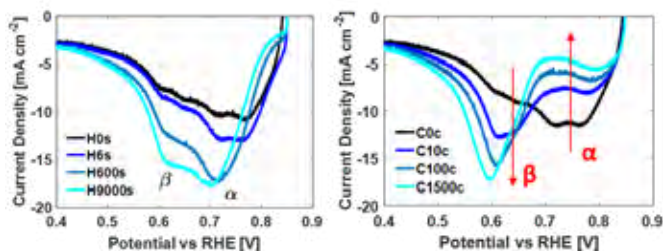


Figure 2 - LSV recorded after: (left) Holding protocol; (right) Cycling protocol.

The first test is performed applying a constant reference potential (850 mV) for a variable time (from seconds to hours), observing the increasing reduction peaks as holding time increases. In particular, two dominant peaks highlight the presence of two dominant oxide species. α -oxide peak is above 700 mV, hence a second test in inert conditions based on this finding is proposed. Cycling test applies a variable number of potential cycles (700mV-850mV, sweep rate 50mV/s), leading to the formation of β -oxide and reduction of α -oxide as the number of applied cycles increases. The third test is hybrid solution between the previous two measurements: a fixed number of cycles (100) is applied, followed by a variable holding time. In this way, α -oxide formation (during holding) is separated from β -oxide formation (during cycling).

The potential profiles applied in inert conditions prove that it is possible to selectively form a single oxide family.

The second part of the experimental protocol investigates the link between oxides formation and ORR activity. The same potential profiles applied before are considered, adding a relevant feature: cathode feed is switched from nitrogen to air just before the beginning of potential holding at 850mV. Current density output is measured during a standard 600s holding test, allowing to estimate PEMFC performance. At the end of the holding time, operation is switched back to nitrogen, measuring oxide reduction peaks during final LSV.

Comparison among final Linear Sweep Voltammetry in different operating conditions (nitrogen, air or pure oxygen fed to the cathode) highlights no significant difference in reduction peaks if the same potential profile is applied, as visible in **Figure 3-left**. Hence, there is a strong correlation between in-operando and inert tests, since there is no remarkable difference in terms of oxides formation. Oxides are likely formed from water, not from oxygen.

In **Figure 3-right**, a typical current decay recorded in a holding test is shown. The *Cycling+Holding* protocol reported is repeated under oxygen atmosphere to measure the impact of each oxide family on ORR activity, which is feasible thanks to the definition of holding and cycling tests.

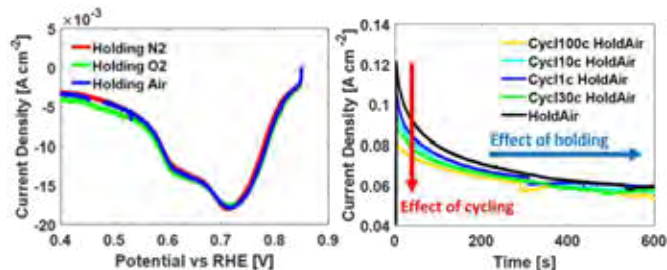


Figure 3 - (left) LSV recorded after holding operation in: Nitrogen, Air, Oxygen; (right) Current recording at 850 mV under air, ambient pressure, 80°C RH100 after different Cycling protocol

It is concluded that β -oxide coverage strongly affects the ORR activity (approximately 4-6 times more than α -oxide). A unique and consistent correlation to separate the effect of α and β -oxide is proposed. These results have been performed for fresh and aged samples, concluding a general consistency in the results, even though a lower coverage of β -oxides is formed after ageing.

Finally, a dedicated Accelerated Stress Test is performed and compared to Electrolyst AST defined by U.S. DoE. While standard AST adopts a triangular potential sweep between 0.6 and 1.0 V, the new AST has been proposed with a triangular sweep between 0.7 and 1.0 V, in order to guarantee a stable β -oxide coverage during the test. A lower loss of active area is reported in the dedicated AST test, suggesting a protective nature of β -oxide or a link between dissolution and oxides reduction.

IV. CONCLUSION

An experimental protocol, based on cyclic voltammetries, has been developed to distinguish two different families of oxides during MEA operation: α (0.7-0.75V vs RHE) and β (ca. 0.610 V vs RHE). Specific holding tests have allowed to conclude that platinum oxides are formed in consequence of the interaction between catalyst surface and the electrolyte, not from oxygen. Furthermore, the contribution of different oxides on ORR activity has been quantified: α is reported to occupy 0.5 active sites on Pt-O basis; β is reported to occupy 3 active sites on Pt-O basis. The effect of α and β -oxide, on platinum dissolution, has been finally investigated: a reduction of β -oxide seems to accelerate platinum degradation or it could protect catalyst from dissolution.

REFERENCES

- [1] Y. Huang, et al. - J. Electrochem. Soc. 161 (2014) 10–15. doi:10.1149/2.018401jes.
- [2] J. Huang, et al. - Curr. Opin. Electrochem. 13 (2019) 157–165. doi:10.1016/j.coelec.2019.01.004.
- [3] B. Jayasankar, et al. - Electrochim. Acta. 273 (2018) 367–378. doi:10.1016/j.electacta.2018.03.191.
- [4] T. Nagai, et al. - ECS Trans., 2010: pp. 125–130. doi:10.1149/1.3484509.

LOCAL DEGRADATION STUDY OF PEMFC DURING START-UP AND SHUT-DOWN CYCLING

Elena Colombo*, Andrea Bisello*, Amedeo Grimaldi*, Andrea Baricci*, Andrea Casalegno*

*Politecnico di Milano, Department of Energy
Via Lambruschini 4, 20156 Milano/Italy
Tel.: +39-02-2399-3840

In this study, a four-segmented hardware is used to evaluate the material degradation due to a repeated series of start-ups and shut-downs, both unmitigated and partially mitigated, in accordance with the strategies applied today. Indeed, while the high potentials during shut-downs could be avoided, start-up is still detrimental when rebooting after a long stop. The setup exploited in this work ensures a spatial characterization of the performance and of the electrochemical active surface area, evidencing the heterogeneity of the ageing mechanism. As also confirmed by the ex situ analysis, start-up impacts more on the cathode region at the anode outlet: only half of the cell is significantly degraded, while the other half tends to compensate in terms of performances.

Index Terms – Start-up and shut-down, Degradation mechanisms, PEM fuel cell, Catalyst durability

I. INTRODUCTION

Durability is one of the central issues for automotive PEMFC, mainly because of the dynamic nature of their functioning. The start-up and shut-down (SU/SD) processes have been recognized as ones of the most detrimental for the fuel cell longevity. During such events the presence of both air and hydrogen at the anode catalyst layer causes a rise of the local potentials to values as high as 1.5/1.6 V[1], that could lead to a severe carbon support corrosion, as studied in the literature[2]. Anyway, several mitigations are today applied in the stacks. Comprehensive shut-down strategies are implemented[3] while start-up is only partially mitigated, since air could not be avoided at the anode after a long stop. It's thus necessary to assess the impact of the partial mitigation on the lifetime of the components and to evidence how the performance evolves with the ageing. In this work, parameters close to the real operations are taken into account since the operating conditions are known to strongly impact on the start/stop transients [4],[5].

II. EXPERIMENTAL

A. Tools and MEA characterization

A single and a segmented triple-serpentine hardware of 25 cm² active area are operated in a counter-flow configuration. The hardware is structured with four macro-graphite segments[6], both at anode and cathode side. The segments are numbered from one to four in accordance with the cathode flow direction, such that the first segment includes the anode outlet. To investigate the alterations induced by the studied processes, electrochemical characterization methods are used: performance

i-*V* curves, electrochemical impedance spectroscopy and cyclic voltammetry. In addition, aged samples are examined by microscopic ex-situ techniques. Additional tools have been eventually implemented to clarify the start/stop mechanism, like the Reference Hydrogen Electrodes (RHEs)[7] for tracking the local potentials and the use of a 2D model in Comsol Multiphysics® for representing the main electrochemical reactions and the species transport during the transient.

B. Tested MEAs and protocols

A first type of MEA (by Ion Power Inc., assembled with Sigracet® 29BC GDL) was degraded using a single cell setup: an unmitigated SU/SD procedure was tested and the results compared to the carbon support AST DoE protocol. Five SU/SD were reproduced in a row: this procedure consists in applying a constant air flow (200 ml min⁻¹) to the cathode and fluxing alternatively (every 60 s) a hydrogen and an air flow of 50 ml min⁻¹ to the anode. Temperature and relative humidity are set equivalent to DoE AST parameters, at values of 80 °C and 100% respectively. Between one set of test and the next, current is fixed at 0.4 A cm⁻² for 10 min. A second MEA designed for automotive application (Pt/C based Johnson Matthey CCM on Freudenberg GDL), was subjected to a procedure designed to simulate a real strategy: after H₂/air OCV, nitrogen is fluxed into the cathode (5 min), in order to reproduce the complete consumption of oxygen that ensures the shut-down mitigation. However, in real stacks air leaks in after a long stop. In the developed procedure, air is thus fluxed firstly to the anode (120 s) and then into the cathode (120 s) to reach the air/air stop condition. Finally, an equivalent 1 A cm⁻² H₂ flow is introduced to mimic the start-up and the entire cycle is then repeated. Since a long time before stack rebooting is simulated, all the experimental steps are carried out at a temperature close to ambient (30 °C), while RH = 100%.

III. RESULTS AND DISCUSSION

The DoE carbon support AST exploits a potential range similar to which would occur in an unmitigated system start-up or shut-down, as verified in this work by the use of RHEs. Results of the real unmitigated transients at high temperature and the DoE AST really agree (in terms of polarization curves both in air and oxygen, Platinum active area and mass transport resistances). In these tests, the strong reduction of the limiting

currents suggests the collapse of the support structure. A clear quantitative correlation is found: an almost 10 ratio (9.6) exists between AST cycles and SU/SD series, while AST accelerates the ageing in time by a 10.3 factor. The absence of any mitigation for both start and stop makes the impact probably quite homogenous, such that the overall MEA indexes are very well described by the uniform ageing due to the support AST.

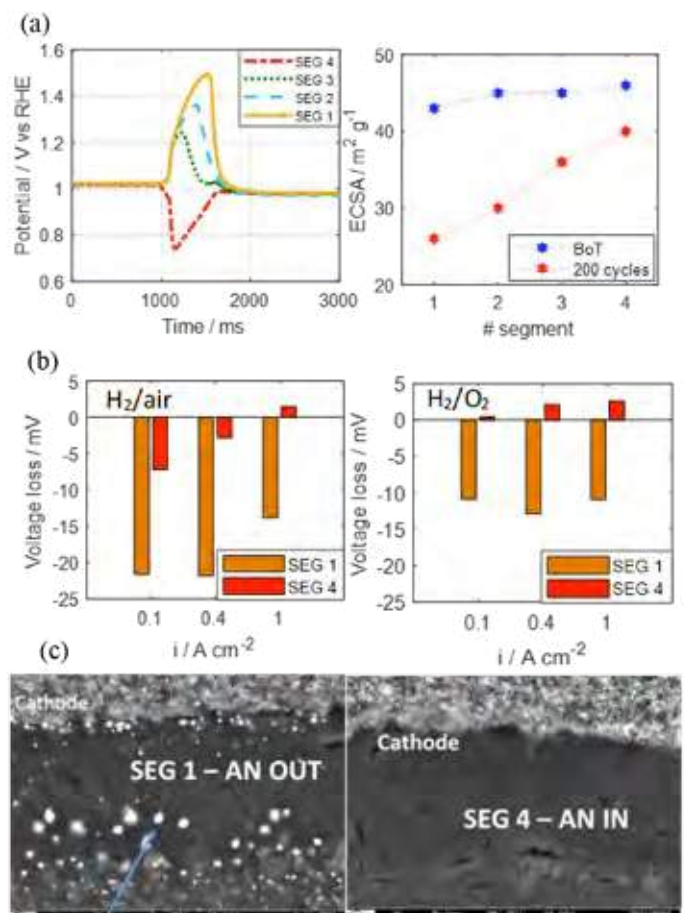
The adoption instead of the partially mitigated strategy results in an inhomogeneous degradation, as confirmed by other authors[8]. Segments 1 and 2 (anode outlet region) face a large ECSA loss (39% and 33% at 200 cycles), while the other half of the MEA is signed by an average 17% reduction. The decrease of Pt active area boosts the kinetic losses, causing a drop of performance visible both in H₂/O₂ and H₂/air polarization curves; the result is mainly a vertical translation of global *i-V* curves by 7 mV and 12 mV respectively, a loss that is almost doubled for the first segment (with a maximum of 13 mV and 22 mV respectively). The overall limiting current is unchanged: segments 1 and 2 undergo a slight reduction that is even compensated by segments 3 and 4. The slight changes in the mass transport resistances should be attributed to the variations of the roughness factor. All the results do not suggest an evident carbon corrosion: this is confirmed by the ex-situ analysis that does not highlight any cathode thinning, but reveals depleted Pt particles in the middle of the membrane. Such loss is greatly visible at the cathode inlet (anode outlet) as opposed to the cathode outlet (anode inlet), where no Pt band is evidenced.

IV. CONCLUSIONS

The results suggest that the DoE carbon support AST well reproduces the unmitigated start/stop at high temperature: they both significantly impact on performances and oxygen mass transport, suggesting a severe carbon corrosion. A proper mitigation strategy that limits the high potentials start-up to few long stops during the components' lifetime is effective in reducing the degradation: at 30 cycles, performance changes and ECSA decay are minor, within 5 mV and 10% variation respectively. At 200 cycles, which is a quite high number for a real stack, a strong heterogeneity is revealed: the ECSA loss is relevant for the half of the cell close to anode outlet (-39%) and the reduction of MEA performance is mainly led by this critical region. At the opposite, the portion of the cell close to the anode inlet even partially compensate the loss. Limiting current measurements do not highlight notable alterations of O₂ mass transport as well as SEM analysis revealed Pt deposition in the middle of the membrane but no cathode thinning. All these results do not indicate a significant support corrosion, but a localized electrocatalyst depletion.

ACKNOWLEDGMENT

The work received funding under grant agreement No 779565 (FCH-JU Project ID-FAST). This Joint Undertaking receives support from the EU Horizon 2020 program. Ex-Situ analysis were performed in cooperation with CEA and DLR.



Results for partially mitigated strategy on JM cell: a) left: Potential profiles of RHEs at cathode side during a start-up transient; right: ECSA loss measured from CV at $T = 35\text{ }^{\circ}\text{C}$, $\text{RH} = 1/1$ (H₂/N₂), flow = 60/60 ml min⁻¹ (H₂/N₂), scan rate = 50 mV s⁻¹, b) polarization curves at $T = 80\text{ }^{\circ}\text{C}$, $\text{RH} = 1/1$, air: $\lambda_a/\lambda_c = 2/4$, O₂: $\lambda_a/\lambda_c = 2/10$, $P_{an,in}/P_{cat,in} = 2.3/2.5$ bar, minimum flux: 0.5 A cm⁻² equivalent c) SEM analysis at 200 cycles: cathode in (anode out) reveals Pt depleted in the membrane, not present at cathode out (anode in).

REFERENCES

- [1] Reiser, C. A. et al. A Reverse-Current Decay Mechanism for Fuel Cells. *Electrochem. Solid-State Lett.* 8, A273 (2005).
- [2] Gu, W., Carter, R. N., Yu, P. T. & Gasteiger, H. A. Start/Stop and Local H₂ Starvation Mechanisms of Carbon Corrosion: Model vs. Experiment. *ECS Trans.* 11, 963–973 (2007).
- [3] Oyaree, A. et al. Comparing shut-down strategies for proton exchange membrane fuel cells. *J. Power Sources* 254, 232–240 (2014).
- [4] Mittermeier, T. et al. Fuel Cell Start-up/Shut-down Losses vs Temperature for Non-Graphitized and Graphitized Cathode Carbon Supports. *J. Electrochem. Soc.* 164, F127–F137 (2017).
- [5] Dillet, J. et al. Impact of flow rates and electrode specifications on degradations during repeated startups and shutdowns in polymer-electrolyte membrane fuel cells. *J. Power Sources* 250, 68–79 (2014).
- [6] Rabissi, C. et al. A locally resolved investigation on direct methanol fuel cell uneven components fading: Local cathode catalyst layer tuning for homogeneous operation and reduced degradation rate. *J. Power Sources* 404, 135–148 (2018).
- [7] Hinds, G. & Brightman, E. In situ mapping of electrode potential in a PEM fuel cell. *Electrochem. commun.* 17, 26–29 (2012).
- [8] Komini Babu, S. et al. Spatially resolved degradation during startup and shutdown in polymer electrolyte membrane fuel cell operation. *Appl. Energy* 254, 113659 (2019)

CHARACTERIZATION OF PEM WATER ELECTROLYSIS CELL WITH ELECTROCHEMICAL IMPEDANCE SPECTROSCOPY

A. Z. Tomić^{1,2}, I. Pivac^{1,2}, and F. Barbir^{1,2}

¹FESB University of Split, R. Boskovicica 32, 21000 Split, (Croatia)

²Center of Excellence STIM, University of Split, Poljicka cesta 35, 21000 Split, (Croatia)

Abstract – The paper deals with the diagnosis of the various operating conditions impact on the performance of a proton exchange membrane (PEM) water electrolysis cell. A 45 cm² single cell with Nafion N117 membrane, Ir-Ru oxide as anode catalyst and Pt black as cathode catalyst, is analyzed by means of electrochemical impedance spectroscopy (EIS) measurements at different cell temperatures and cathode backpressures via test station for PEM electrolyzers custom-made by Sustainable Innovations. Furthermore, a widely used equivalent circuit model was utilized to support the impedance analysis, in order to find common links between the relevant electrochemical processes within the electrolyzer, together with the PEM fuel cells findings. Based on these established approaches and obtained results, degradation diagnostics of the PEM electrolyzers will be further explored, also as the additional model upgrades.

Index Terms – electrochemical impedance spectroscopy, equivalent circuit model, PEM electrolyzer, proton exchange membrane

I. EXPERIMENTAL

Electrochemical impedance spectroscopy (EIS) is a non-destructive *in situ* technique capable of characterizing the behavior of electrochemical systems. In order to systematically determine the influence of the various operating conditions on the impedance spectrum of proton exchange membrane (PEM) water electrolysis cell, the EIS measurements were performed at different electrolyzer cell temperatures (50 °C, 65 °C, 85 °C), cathode backpressures (1.0 bar, 3.1 bar, 6.2 bar), and operating points (1 A, 5 A, 10 A). Reference values were 1 A, 50 °C and 1.0 bar. BioLogic SP-150 potentiostat in galvanostatic mode, with the associated VMP3B-10 signal booster, was used to measure impedance spectra. The measurements were performed in the frequency range of 5 kHz to 10 mHz, with 5 points per decade, measurement of each point was repeated 15 times. At all operating points, the AC perturbation current was 10% of the direct current driving the electrolysis.

II. EQUIVALENT CIRCUIT MODEL DESCRIPTION

The obtained data of measuring impedance spectra varying operating parameters were fitted with an equivalent electrical circuit model, shown in Fig. 1, to determine the effect of temperature and cathode backpressure on the model elements. The equivalent circuit is already well known and often used in the PEM electrolyzer and fuel cell literature, which was numerically fitted with the Z fit tool from EC-Lab[®] software.

In general, the applied equivalent circuit models the ohmic resistance of the membrane (R1), and the charge transfer resistances of the electrodes (R2 for the anode and R3 for the cathode, respectively) with the associated electrode capacitances. Moreover, PEM electrolyzer electrodes are porous structures that exhibit pseudo-capacitive behavior, therefore the capacitance of the anode and cathode were described here as the constant-phase elements (CPE2 and CPE3, respectively). However, the analysis and physical interpretation of the constant-phase element parameters is very complex and controversial; therefore, it was beyond the scope in this paper.

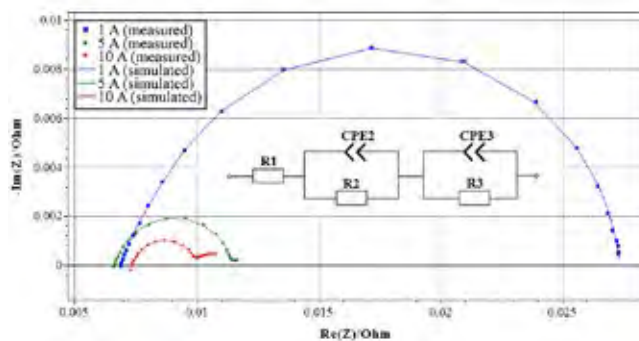


Fig. 1. Comparison of measured and simulated impedance spectra of the PEM electrolyzer at 50 °C, 1 bar and different currents (1 A, 5 A and 10 A), with the applied equivalent electrical circuit model.

III. RESULTS AND DISCUSSION

As the Fig. 1 shows, the operating point (i.e. current) has the greatest impact on the impedance spectrum, which also corresponds to the characteristic feature in the Nyquist diagram. The so-called activation region (1 A) corresponds to the largest arc in the Fig. 1, and with increasing current the impedance response decreases and changes shape continuously. The so-called ohmic region (10 A) is characterized by an arc and a tail formed at low frequencies corresponding to the raised diffusion processes, which is only slightly visible at 5 A. The same trends could also be found in PEM fuel cells research [1].

Fig. 2 shows the values obtained from the equivalent circuit model fitting. The membrane resistance (R1) is almost constant, while the anode charge transfer resistance (R2) is much higher than cathode resistance (R3) due to slower anode oxygen evolution. However, they both increase with increasing current.

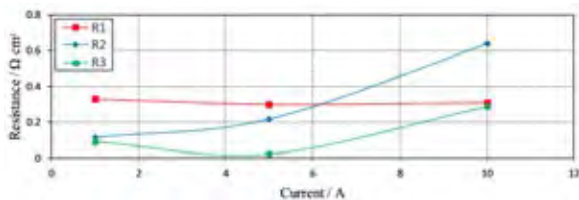


Fig. 2. Effect of operating point on model resistors.

Furthermore, as the Fig. 3 shows, electrolyzer temperature increase translates the complete impedance spectrum to the lower impedance values. Therefore, the membrane resistance R1 rapidly decreases with temperature, also as cathode R3, while the anode R2 remains constant (Fig. 4). Similar trend was present at all measured operating points, and it is significantly different from the findings in PEM fuel cells research [1].

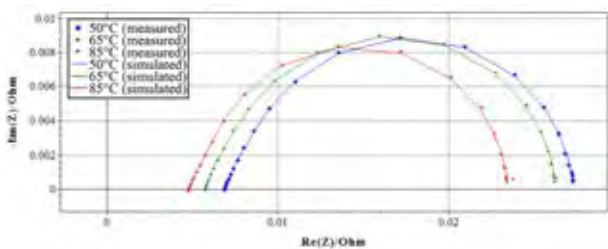


Fig. 3. Comparison of measured and simulated impedance spectra at 1 A, 1 bar and different electrolyzer cell temperatures (50 °C, 65 °C and 85 °C).

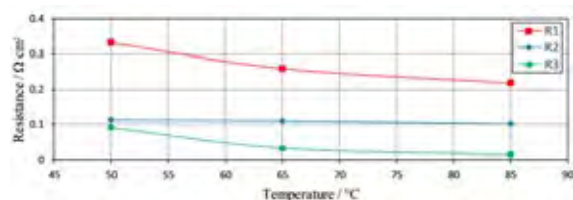


Fig. 4. Effect of electrolyzer cell temperature on model resistors.

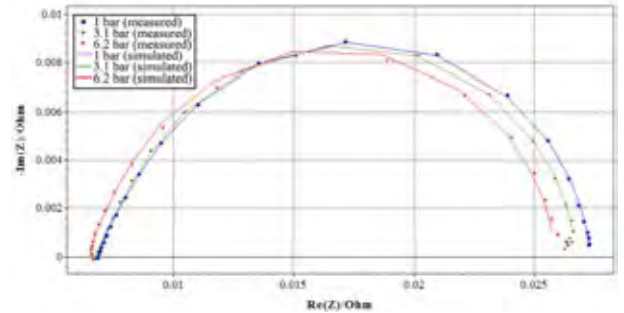


Fig. 5. Comparison of measured and simulated impedance spectra at 1 A, 50 °C and different cathode backpressures (1 bar, 3.1 bar and 6.2 bar).

As the Fig. 5 shows, the high-frequency intersection on the real axis at all cathode backpressures is almost the same point. An increase in pressure primarily corresponds to a decrease in the diameter of the semicircles, i.e. decrease of electrode resistances (Fig. 6), which is also in accordance with PEM fuel cells findings [1]. However, of all the variables considered, the influence of pressure on the impedance spectrum is the smallest, but a relatively small range of backpressures was considered here, because of the test equipment limitations.

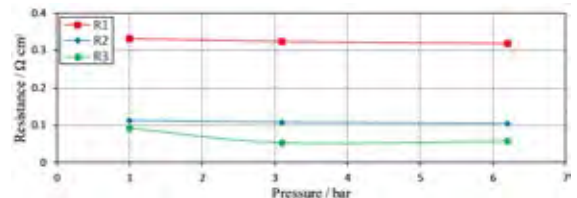


Fig. 6. Effect of cathode backpressure on model resistors.

IV. CONCLUSIONS

There is an obvious and consistent influence of the operating parameters on the impedance spectrum of the PEM electrolyzer tested. The operating point has the greatest influence on the impedance, and different operating points give qualitatively different curve features. Temperature has an impact on the impedance spectrum by translating the response along the real axis, while the basic curve shape remains defined by operating point. By increasing the temperature, the value of the high-frequency intersection with the real axis decreases, which primarily corresponds to the decrease in the membrane resistance. The effect of pressure is less visible in the impedance spectrum than temperature, and the effect is reduced by increasing the temperature. Pressure primarily influences the semicircle diameters, which decrease with rising pressure.

ACKNOWLEDGMENT

The research was supported under the project STIM – REI (KK.01.1.1.01.0003), a project funded by the EU through the ERDF - OPKK. Andrej Z. Tomić acknowledges the support from the Croatian Science Foundation (DOK-2018-01-7027).

REFERENCES

- [1] Pivac, I., Šimić, B., Barbir, F., Journal of Power Sources Volume 365, 2017, pp. 240-248.

3D PRINTING OF FUNCTIONAL CERAMICS FOR THE INDUSTRIAL FABRICATION OF SOLID OXIDE FUEL CELLS (SOFC)

A. Hornés*, A. Pesce*, M. Nuñez*, M. Torrell*, A. Morata*,
A. Tarancón**

*Catalonia Institute for Energy Research (IREC), Jardins de les
Dones de Negre 1, 08930 – Sant Adrià de Besòs, (Spain)

**ICREA, Passeig Lluís Companys 23, 08010 – Barcelona, (Spain)

Abstract - Fabrication of Solid Oxide Fuel Cells (SOFCs) by additive manufacturing technologies promises an increase of efficiency, reproducibility and customizability while the manufacturing cost is reduced, enhancing the deployment of this environmentally friendly technologies to the mass market. Within Cell3Ditor EU project this challenge is tackled. By using an innovative multi-material 3D printer for ceramics developed within the project, electrolyte-supported fuel cells have been fully printed for the first time. Structural, morphological and electrochemical characterization of the electrolyte reveals similar behavior than electrolytes produced by conventional technologies. On the other hand, characterization of the printed electrodes in symmetrical cell configuration evidences critical aspects affecting the electrochemical behavior which can be overcome by modification of the slurries. Finally, a fully printed SOFC has been achieved.

Index Terms – 3D printing, Solid oxide fuel cells, SOFC stack.

I. INTRODUCTION

SOFCs are very attractive devices from environmental, energetic and economic point of view. They have been proved to be one of the most efficient technologies to generate power from a gas fuel, showing a theoretical efficiency up to 75%. Moreover, the same device working in electrolysis mode allows the conversion of the chemical energy stored in a fuel into electrical energy. As a side effect, the deployment of this technology will make hydrogen an appealing solution to generate power or store the overproduction of energy from renewable resources during the high production/low demand hours, enabling hydrogen economy adoption.

The materials used for fabricating the SOFCs are characterized by showing high ionic/electronic conductivity at high temperature (above 700°C) and mechanical, thermal and chemical stability under operating conditions. On the other

hand, these materials show high stiffness and low machinability, which increase the cost and time required for manufacturing, constraining the possible cell geometries into planar or tubular. In addition, the final device consists of a stacking of single-repetition units (SRUs) to obtain an output power suitable for the designed application with gas connection and contact plates. The realization of such devices includes more than one hundred fabrication steps and involves intensive manual labor, impacting severely their commercialization due to the high cost of the devices, low reproducibility, long time-to-market and low flexibility of the process.

The Cell3Ditor project presents a disruptive manufacturing concept based on the utilization of 3D printing technologies for the fabrication of SOFCs. This radically innovative idea which follows the work of Ruiz-Morales et al. [1] takes advantage of every benefit provided by additive manufacturing technologies i.e. reduced material utilization, automation, customizability, etc., for the fabrication of SOFC stacks in a single-step. Moreover, a single co-sinterization process of the fully printed SOFC stack has been proposed. The entire automatization of the manufacturing process in only three steps: design, printing and sintering, will reduce the time and the wastes and, consequentially, decrease the cost, enhancing the penetration of this technology into the energy market.

II. EXPERIMENTAL

To reach this goal a dual multi-material 3D printer for ceramics where you can print by stereolithography (SLA) and robocasting has been developed, enabling to print up to five different materials which are necessary in a SOFC device: electrolyte, anode, cathode, interconnector and a sacrificial

material to generate embedded channels. In particular, SLA was chosen for building the scaffold and the electrolyte due to its ability for generating high aspect ratio structures and good resolution while robocasting was chosen for printing the rest of components. In Figure 1 the multi-material capabilities are shown.

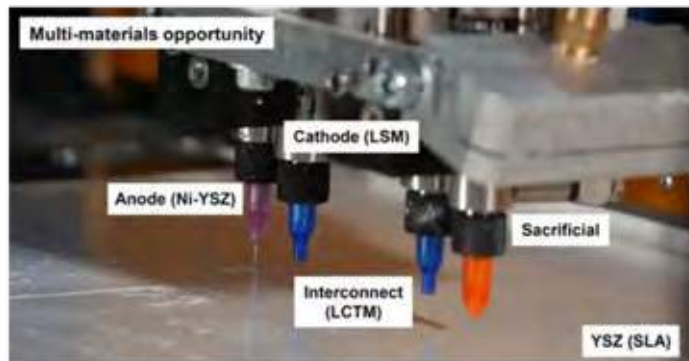


Fig. 1. Robocasting robotic arm with 4 delivery ports over YSZ layer printed by SLA.

The materials are supplied to the machine in the form of high viscosity slurries made of a ceramic material and an organic phase. Under UV irradiation the polymerization of the organic phase occurs following the desired design. Once the slurry is cured, a new layer is printed and cured on top of the previous one, enabling to build 3D structures. After printing, the so-called “green” pieces are treated at high temperature to remove the organic part and to sinter the ceramic particles in order to get the final mechanical properties.

In this work, initially printing of yttria-stabilized zirconia (YSZ) electrolytes has been achieved. Then, anodic and cathodic symmetrical cells have been produced and characterized. Moreover, entire SOFC cells were produced in a single step, while the co-sintering of the different layers in a single thermal treatment is under development. Printed cells show ca. 1.5 cm² projected area.

Structural, morphological and compositional characterization is carried out by XRD, Raman and SEM-EDS. Electrochemical properties of the materials are being analyzed by EIS while the performance of the printed full cells is being tested by polarization curves.

III. RESULTS

A. 3D printed electrolyte

YSZ electrolytes have been printed, debinded, sintered and characterized. Printed electrolytes present tetragonal crystalline structure and high density packaging and as-expected electrochemical behavior.

B. 3D printed symmetrical cells

Symmetrical cells of NiO-YSZ and LSM-YSZ were carried out in order to analyze the properties of the printed electrodes

separately. Bilayer and symmetrical cells were printed and their co-sinterization behavior studied. The effect of the heat treatment on the microstructure was evaluated by EIS, showing that temperatures higher than 1250°C generated gas diffusion issues in the electrode.

C. 3D printed stack

As a proof-of-concept of the capabilities of the printer a 3D printed stack prototype has been built. In the figure below a monolithic SOFC prototype is shown.



Fig. 2. SOFC stack prototype 3D printed. Onset: Model of the prototype.

D. 3D printed SOFC

A first fully 3D printed SOFC cell has been carried out and its electrochemical behavior has been tested, obtaining a maximum output power of around 75mW/cm² at 900°C.

IV. CONCLUSION

Implementation of 3D printing manufacturing technologies to the fabrication of SOFCs is a promising solution for improving their commercialization. Fabrication of the different fuel cell components has been achieved providing significant insights on their behavior. A fully 3D printed SOFC cell has been fabricated for the first time showing the feasibility of the technology for attaining the proposed goal.

ACKNOWLEDGMENT

The research leading to these results has received funding from the European Union’s Horizon 2020 Innovation Framework Program (H2020) for the Fuel Cells and Hydrogen Joint Technology Initiative under grant agreement no. 700266 (Cell3Ditor project).

REFERENCES

- [1] Ruiz-Morales, JC., Tarancón, A., et al., Three dimensional printing of components and functional devices for energy and environmental applications, Energy and Environmental Science, Volume 10, 2017, Pages 846-859.

NON-INVASIVE GLUCOSE/OXYGEN FUEL CELL FOR CONTINUOUS MONITORING OF GLUCOSE

C. Gonzalez-Solino, N. Parkar, E. Bernalte and M. Di Lorenzo

Department of Chemical Engineering, University of Bath, Claverton Down, Bath BA2 7AY, (UK)

Abstract - Diabetes affects more than 422 million people worldwide, causing more than 1.6 million deaths per year, and costing billions of pounds in primary healthcare. Therefore, there is an urgent need to develop new and affordable point-of-care technologies for the rapid and continuous monitoring of glucose levels in the body. In this regard, glucose fuel cells (GFCs) emerged as a very powerful tool due to their intrinsic self-powered nature, rapid response and simplicity. Highly porous gold films have shown great potential for the development of effective GFCs, given their large surface area. In this context, we investigate and compare two different methods for the development of such porous films according to their electroactive surface area and analytical sensitivity towards glucose.

Index Terms – Glucose fuel cell; Highly porous gold; Printed circuit boards.

I. INTRODUCTION

Glucose fuel cells have emerged as an attractive alternative to power small scale electronic devices for healthcare applications and for the self-powered detection of glucose. Nanostructured materials play an important role in the development of high-power density fuel cells, due to their superior catalytic activity and high surface area. Among them, nano and highly porous gold structures offer great compatibility and low overpotential for the oxidation of glucose in physiological conditions. Several techniques have been proposed for the development of nanostructured gold films, such as dealloying, dynamic hydrogen bubbling template or galvanic replacement. Dynamic hydrogen bubbling template (DBHT) allows the formation of highly porous structures without the need of organic or inorganic templates. DBHT also avoids the use of acids and high temperatures as well as reduces the deposition time to less than a minute [1]. Our group has previously reported the successful generation of hPG structures in both platinum wires and glass. Moreover, those developed hPG electrodes not only showed catalytic activity towards

glucose but they could also be used as a scaffold for the further immobilization of enzymes [2, 3]. In this study, for the first time we adapt the methodology for the development of hPG films to gold-plated electrodes on a printed circuit board (PCB). In this way, PCBs became an attractive platform for the development of miniaturized glucose fuel cells.

II. MATERIALS AND METHODS

A. Electrodes

Gold-plated electrodes on PCB were modified with highly porous gold (hPG) using the DBHT technique (Fig.1). Briefly, the electrodes were covered with a solution of 1 M NH_4Cl (Sigma Aldrich, UK) and 0.1 M HAuCl_4 (Fisher, UK). The DBHT technique was performed in potentiostatic mode (M1) as previously described by our team [2] and in galvanostatic mode (M2). With the first method (M1), the voltage applied was stepped down from -0.7 V to -4.0 V vs Ag/AgCl. With the second method (M2), the current was kept constant at -20 mA for 15 seconds.

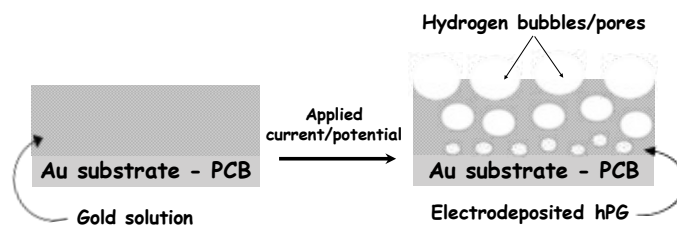


Fig. 1. Schematic of the highly porous gold (hPG) deposition on gold-plated electrodes on a Printed Circuit Board (PCB).

B. Characterization of the Electrodes

The morphology of the electrodes was characterized by scanning electron microscopy (SEM) using a JEOL JSM-6480LV. The electrodes were electrochemically characterized to determine the electrochemical surface area (ESA) and their

analytical sensitivity towards glucose. Thus, the ESA was calculated from the reduction peak of the gold oxide, after cycling the potential in 50 mM H₂SO₄ for 2 cycles at a scan rate of 50 mV s⁻¹ [4]. Additionally, the sensitivity of hPG electrodes towards glucose was determined at a potential of +0.22 V vs Ag/AgCl at increasing glucose concentrations from 50 μM to 100 mM in 0.1 M phosphate buffer pH 7.4. LOD was calculated according to IUPAC definition. All the electrochemical experiments were performed in a three-electrode cell, using Ag/AgCl as reference and Pt wire as counter electrodes, respectively. A potentiostat PGSTAT302N (Metrohm, UK) was used to perform the experimental work.

III. RESULTS

The DHBT relies on the formation of H₂ bubbles as a template for the formation of porous films. NH₄Cl is therefore added as a hydrogen source. SEM images (Fig. 2) of the hPG electrodes were compared for both methods tested. The electrodes obtained with M1 showed a rough rather than highly porous structure (Fig. 2a and 2b), with an ESA of 0.59 ± 0.14 cm². M2 led to a highly porous and homogeneous structure that better resemble the hPG structures previously reported by our team [2], as shown in Fig. 2c and 2d. In this case, the ESA was of 1.96 ± 0.15 cm², which is 30% higher than M1.

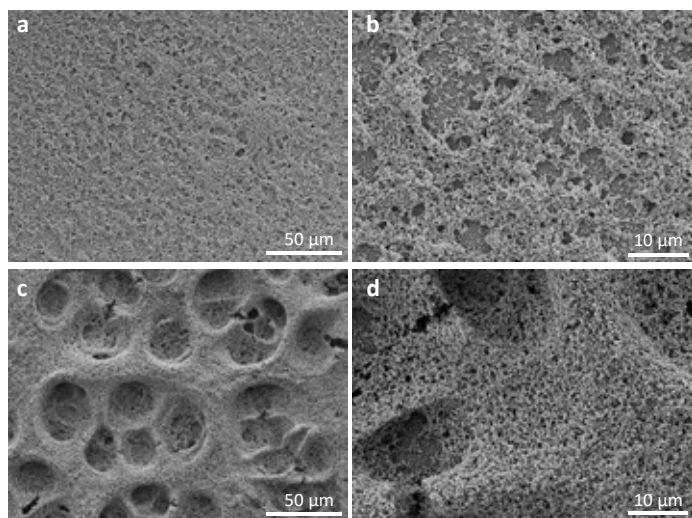


Fig. 2. SEM images of hPG electrodes prepared with (a, b) M1 and (c, d) M2.

The hPG electrodes also showed different sensitivities towards glucose depending on the deposition method employed (Fig.3). The electrodes hPG-M2 showed higher sensitivity, within the same linear range, than hPG-M1. Table 1 compares the analytical performance of both electrodes. Results suggest that the size of the pores and the ESA of the electrodes play an important role in the sensitivity of hPG electrodes. Moreover, the electrodes obtained with M2 showed a more homogenous response to glucose, with lower RSD (11.2%) compared to the electrodes obtained with M1 (57.2%). The differences between

both methods could be attributed to the mechanism of deposition. In galvanostatic mode, M2, the current and, therefore, the deposition rate is controlled. Consequently, more uniform and reproducible films are obtained.

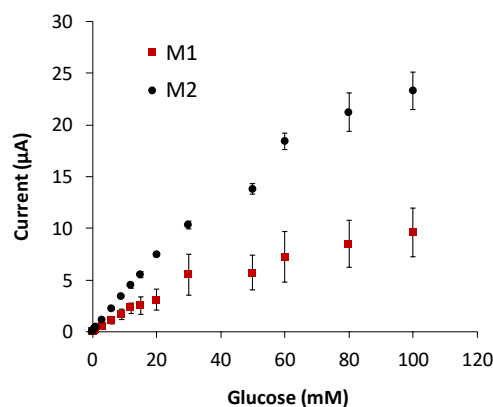


Fig. 3. Calibration curves for the hPG electrodes obtained with M1 and M2.

TABLE I
ANALYTICAL PERFORMANCE OF THE DEVELOPED ELECTRODES

	Sensitivity (μA mM ⁻¹ cm ²)	LOD (mM)	Linear range (mM)
M1	22.0	0.02	0 – 30
M2	44.3	0.06	0 – 30

IV. CONCLUSION

We explored DBHT technique for the development of hPG electrodes on novel PCBs substrates. Two methods were tested, based on chronoamperometry (M1) and chronopotentiometry (M2) respectively. M2 showed a better performance providing electrodes with a more homogeneous porous surface and increased surface area. M2 electrodes also showed improved catalytic activity, with a sensitivity to glucose two times higher.

ACKNOWLEDGMENT

C.Gonzalez-Solino thanks the University of Bath for funding her PhD. The authors thank Dr. P. Fletcher, from the Material and Chemical Characterization facilities (MC²) at the University of Bath, for assistance with the SEM and Dr D. Moschou from Electronic and Electrical Engineering for designing the PCBs. E. Bernalte acknowledges the Engineering and Physical Sciences Research Council (EPSRC) for funding (EP/R022534/1).

REFERENCES

- [1] B.J. Plowman, L.A. Jones, S.K. Bhargava, *Chemical Communications*, 51 (2015) 4331-4346.
- [2] H. du Toit, M. Di Lorenzo, *Sensors and Actuators B: Chemical*, 192 (2014) 725-729.
- [3] F.T.C. Moreira, M.G.F. Sale, M. Di Lorenzo, *Biosensors and Bioelectronics*, 87 (2017) 607-614.
- [4] G. Sanz , I. Taurino, R. Antiochia, L. Gorton, G. Favero, F. Mazzei, G. De Micheli, S. Carrara, *Bioelectrochemistry*, 112 (2016) 125-131.

EVALUATION AND SELECTION OF STABLE METALLIC MATERIALS FOR ELECTROLYSIS PROCESSES IN MOLTEN SALTS

C. Paoletti, L. Della Seta, and S. Frangini
ENEA CR Casaccia, DTE-PCU-SPCT, 00123 Rome (Italy)

Abstract – Low-Temperature Molten Carbonate Electrolysis (LT-MCE) at $T < 600^\circ\text{C}$ is a novel research area with emerging opportunities for sustainable synthetic fuel gas production and for CO_2 capture and exploitation. Melt corrosiveness in typical LT-MCE gas environments is a major obstacle for further technology development requiring selection of appropriate construction materials, both for structural and functional applications (as electrodes). In this work, the suitability of several metallic alloys to serve as inert anodes or as structural material has been investigated by Cyclic Voltammetry in the ternary eutectic $\text{Li}_2\text{CO}_3\text{-Na}_2\text{CO}_3\text{-K}_2\text{CO}_3$ carbonate at 500°C , under CO_2 gas atmosphere. Inconel 600 alloy showed the best anode electrocatalytic activity, yet with a non-optimal anode corrosion stability. Titanium with its exceptional corrosion resistance under wide electrochemical window appears ideal for realizing stable structural components for LT-MCE systems.

Index Terms – Electrolysis, molten carbonate, metallic alloys, Cyclic Voltammetry

I. INTRODUCTION

There is a growing interest in the development of electrolysis processes in molten salts, and especially in molten carbonates, for environment and conversion/energy storage applications at moderate/intermediate temperatures ($< 600^\circ\text{C}$). In particular, several recent studies have highlighted the potential key role of Low-Temperature Molten Carbonate Electrolysis (LT-MCE) processes for the development of sustainable and versatile systems for the production of synthetic fuels, as well as for the capture and exploitation of CO_2 [1,2].

Since LT-MCE processes use CO_2 or mixed $\text{CO}_2/\text{H}_2\text{O}$ gas mixtures as main feedstock, this causes the salt, usually the low-melting ternary Li-Na-K eutectic carbonate, to become strongly acidic and thus much more corrosive than under oxidizing or fuel cell gas environments.

Use of metallic alloys in LT-MCE processes appears in general a much more convenient approach than exotic ceramic materials due to cost and availability, although selection of

corrosion-resistant alloys may be a difficult task to accomplish due to scarcity of available information. In this context, Ni and Ni alloys are the most interesting anode candidates due to their high electrocatalytic activity. However, some recent studies [2,3] report a serious corrosion of Ni (and also of Fe) anodes in K-rich electrolytes at $T < 600^\circ\text{C}$, whereas apart noble metals like Pt or Ir, a better stable anode behavior was shown by copper and SnO_2 , at least in short-term experiments at 500°C [2]. On the other hand, a very recent study reports an excellent corrosion resistance of Titanium in LT-MCE environments at 500°C due to formation of a stable passive film, suggesting thus the possibility of using titanium for LT-MCE structural applications [4].

In the present work, therefore, the stability of several alloys for potential use as structural or anode material has been investigated by cyclic voltammetry in a ternary $\text{Li}_2\text{CO}_3\text{-Na}_2\text{CO}_3\text{-K}_2\text{CO}_3$ eutectic molten carbonate at 500°C , under a pure CO_2 gas atmosphere. Only commercially available alloys or metals have been taken into consideration for this screening activity. Due to scarcity of information, the study has included common alloys such as stainless steel, bronze, brass, german silver, nickel, Inconel 600 and titanium. Platinum has been used for benchmarking.

II. EXPERIMENTAL

The ternary eutectic $\text{Li}_2\text{CO}_3\text{-Na}_2\text{CO}_3\text{-K}_2\text{CO}_3$ (43.5-31.5-25.0 mol %) carbonate was prepared by thorough mixing pre-dried powders of the three constituents. Electrochemical experiments were conducted at 500°C under bubbling CO_2 atmosphere using a cell setup described elsewhere. Working electrodes consisted of 1 mm dia. wires with an active 0.5 cm^2 surface area. A graphite counter electrode with a tenfold larger area (5 cm^2) and a gold thin wire used as pseudo-reference electrode completed the electrode setup.

Slow-scan Cyclic Voltammetry (CV) was used in this work. CV experiments were started after the working electrode reached a stable equilibrium potential (Open Circuit Potential, OCP). CV curves were recorded at a 5 mV/s scan rate starting from OCP and with variable cathodic and anodic switching limits depending on the electrode material. Potential cycling was repeated until a stable CV profile was obtained.

III. RESULTS AND DISCUSSION

Fig.1 reports the steady-state CV profiles of 316L stainless steel, Ni metal, Inconel 600 and Pt after OCP stabilization, which was typically obtained after a few hour immersion.

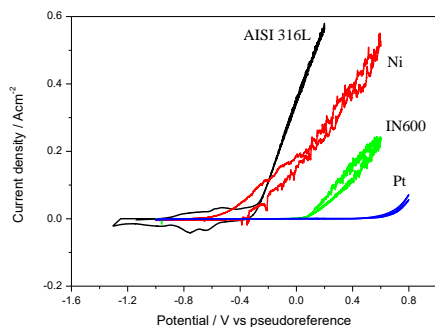


Fig. 1. CV behavior of AISI 316L, Ni, Inconel 600 and Pt electrodes in the eutectic ternary carbonate at 500°C and CO₂ gas atmosphere.

Anodic current sharply increase during the positive scan direction in all the electrode materials, although the potential at which the anodic current raises is different for each material. Theoretical standard potential for CO₂/O₂ gas evolution is about 0 Volt, which means that the high anodic currents of 316L steel and Ni are mostly due to corrosion rather than to gas evolution, as confirmed by post-test electrode examination. Much lesser corrosion was found on Inconel 600 electrodes showing also the best anodic electrocatalytic activity. Although less active, Pt electrode was found to be completely immune to corrosion.

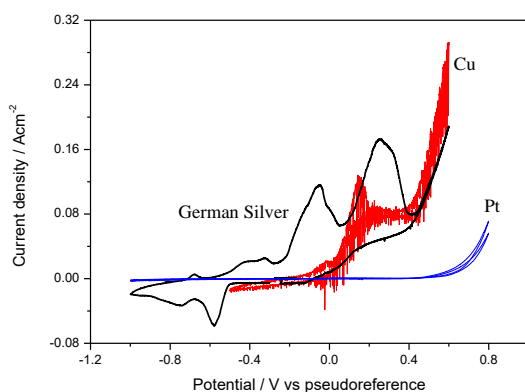


Fig. 2. CV behavior of German Silver and Cu metal in comparison to Pt electrode in the eutectic ternary carbonate at 500°C and CO₂ gas atmosphere.

The Fig.2 shows a weak corrosion resistance of German Silver under anodic polarization conditions, possibly due to lack

of a passive film. Cu electrodes provide some better anodic behavior, although clear traces of soluble corrosion products were found in the molten salt after test.

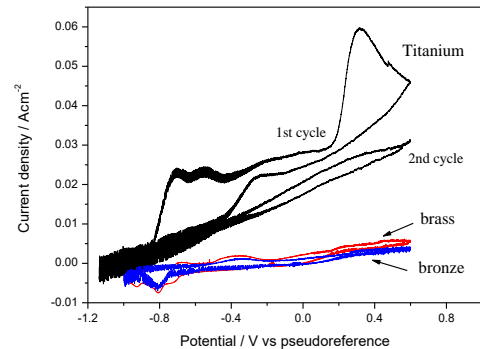


Fig. 3. CV behavior of brass, bronze and Ti metal electrodes in the eutectic ternary carbonate at 500°C and CO₂ gas atmosphere.

The results illustrated in Fig.3 indicates that alloys such brass, bronze and Ti metal cannot be used as anode electrodes due to their stable passive behavior resulting in very low anodic currents even under deep anodic polarization. However, these alloys could be useful for realizing corrosion-resistant structural components of LT-MCE systems. In particular, lack of CV peaks within a wide electrochemical window and no appreciable release of corrosion products into the molten salt were clear indications of the highest corrosion resistance of Ti in molten carbonates at 500°C.

IV. CONCLUSION

CV polarization experiments were conducted in eutectic ternary carbonate at 500°C under a CO₂ atmosphere on several metallic alloys for investigation as possible inert anodes or structural materials. Most promising results have been obtained with Inconel 600 electrodes, although their good anode electrocatalytic activity is challenged by some anode corrosion. On the other hand, due to its exceptional passive corrosion resistance, Ti appears an ideal material for structural components of LT-MCE electrolysis reactors.

REFERENCES

- [1] S. Frangini, C. Felice, P. Tarquini, A novel process for solar H₂ production based on water electrolysis in alkali molten carbonates, *ECS Trans.*, 61 (22), 2014, pp. 13-25.
- [2] H. Yin et al., Capture and electrochemical conversion of CO₂ to value-added carbon and oxygen by molten salt electrolysis, *Energy Environ. Sci.*, 6, 2013, pp. 1538-1545.
- [3] X. Wang, X. Liu, S. Licht, Exploration of alkali cation variation on the synthesis of carbon nanotubes by electrolysis of CO₂ in molten carbonates, *J. CO₂ utilization*, 34, 2019, pp.303-312
- [4] K. Du, et al, Durability of platinum coating anode in molten carbonate electrolysis cell, *Corros. Sci.*, 153, 2019, pp. 12-18.

DEFINITION OF EFFICIENT AND EXTENDED-LIFETIME-ORIENTED POWER MANAGEMENT FOR TRANSPORTATION FUEL CELL AUXILIARY POWER UNIT

L. Barelli*, G. Bidini*, D.A. Ciupăgeanu*, C. Pianese**, P. Polverino**, M. Sorrentino**

*Department of Engineering, University of Perugia, via G. Duranti 93, 06100 Perugia, (Italy)

**Department of Industrial Engineering, University of Salerno, Via Giovanni Paolo II 132, 84084 Fisciano (SA), (Italy)

Abstract - This paper reports on the model-based development of an advanced control strategy for hybrid auxiliary power units (APU), developed for heavy duty truck applications. The power sharing, among the SOFC and the lead-acid battery constituting the APU, is based on the Simultaneous Perturbation Stochastic Approximation algorithm, aiming at a smooth SOFC power profile. The SPSA strategy is implemented in the dynamic model of the hybrid APU, including the balance-of-plant (BoP). Typical auxiliary power demand profiles are simulated. Results in managing the storage devices are compared in terms of power profiles with the ones obtained by implementing a conventional power split control.

Index Terms – Hybrid Auxiliary Power Unit, SOFC, Lead-Acid Battery, SPSA algorithm.

I. INTRODUCTION

With reference to the transport sector, the supply of auxiliary loads is largely investigated to drastically reduce related emissions of CO₂, pollutants and noise. This paper addresses an innovative power management strategy for a hybrid APU, made of a SOFC stack and a lead-acid battery, to supply auxiliary electric loads in a heavy duty vehicle during truck stop. Power real time management strategy relies on the application of the Simultaneous Perturbation Stochastic Approximation (SPSA) principle, aiming at smoothing the SOFC power profile, to mitigate thermal stresses, with a consequent optimized exploitation of both devices. To the best of authors' knowledge, scientific literature does not present the SPSA implementation for similar applications. This highlights the novelty of this study and the relevance of the obtained outcomes.

II. HYBRID APU MODEL

The model-based analysis depicted in this paper is based on a SAE standard power request profile for the auxiliary services of a transport application in cabin conditions. Cabin loads

characterizing the off-driving power demand (i.e., hotel phase) of a long-haul heavy duty truck are considered. A hybrid APU (see Fig. 1) is implemented in the truck power supply system to satisfy the power demand, avoiding the use of the primary engine in cabin conditions.

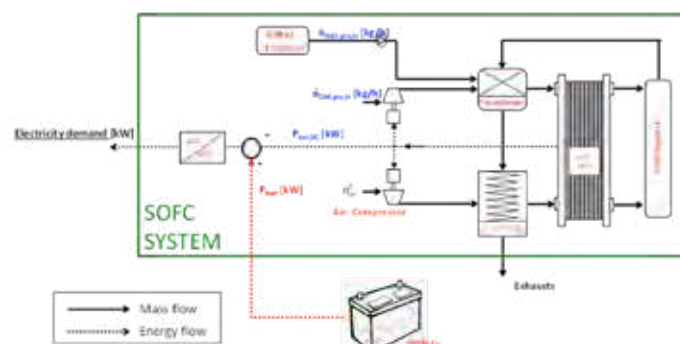


Fig. 1. Schematic representation of the hybrid SOFC-based APU under study.

It consists of a 5 kW SOFC stack, composed by 150 modules of 33.62 W each, and a 25.5 kW lead-acid battery with a storage capacity of 4.5 kWh. The battery is composed by 15 modules in series, each characterized by 25 Ah capacity and 12 V. The sizing process, as detailed in [1], accounts for cold-start impact on the SOFC system. Also a dynamic model of the hybrid APU was developed [1]. Details about modelling assumptions (including operating parameters as 700 °C SOFC operating temperature and 0.7 fuel utilization) and the main constitutive equations of the model can be found in [1][2].

III. POWER MANAGEMENT STRATEGY

The SPSA algorithm was first introduced by J. Spall in 1992 as a fast convergent alternative for the global optimization problem of an unknown functional form of systems performance, i.e. the loss function $L(\theta)$ [3]. Starting from an

initial estimation of the parameters vector ($\hat{\theta}$), the optimal solution is iteratively searched, simultaneously perturbing all parameters within the current estimate. For each iteration, algorithm parameters are updated according to equations (1). The values of the parameters $A(10)$, $a(0.0423)$, $c(2)$, $\alpha(0.602)$ and $\gamma(0.101)$ are set as to ensure calculation convergence [3][4]:

$$a_k = \frac{a}{(A+k+1)^a}; c_k = \frac{c}{(k+1)^c} \quad (1)$$

Two estimates of the parameters vector are determined, perturbing the current estimation according to eq. (2), where the perturbation vector (Δ_k) elements have to follow a Bernoulli distribution.

$$\hat{\theta}_k^* = \hat{\theta} \pm c_k \Delta_k \quad (2)$$

The solution of the optimization problem corresponds to a vector of parameters (q_{batt} and q_{SOFC} for the specific problem formulation) which ideally brings to zero the gradient of the loss function, calculated according to equation (3). The target is imposed in terms of a convergence threshold for the loss function $L(\theta)$.

$$g_k(\hat{\theta}_k) = \frac{\partial L}{\partial \theta} = \frac{y(\theta_k^*) - y(\theta_k)}{2c_k} \begin{bmatrix} \Delta_{k1}^{-1} \\ \dots \\ \Delta_{ki}^{-1} \end{bmatrix} \quad (3)$$

The current estimate is updated according to eq. (4) and the loss function is reevaluated. The iterative process stops when the convergence condition is satisfied or the limit number of iterations imposed is achieved.

$$\hat{\theta}_{k+1} = \hat{\theta}_k - a_k g_k(\hat{\theta}) \quad (4)$$

The SPSA algorithm is applied forward to determine the optimal q_{batt} and q_{SOFC} shares of the storage devices in managing the instantaneous load request P_{req} , so that the SOFC charge/discharge profile is smoothed, being the objective of the optimization problem according to equation (5).

$$y_i^l(\theta) = \left(\frac{q_{SOFC} \cdot P_{req}}{P_{SOFC}^{r-1}} \right)^2 \quad (5)$$

IV. RESULTS AND DISCUSSION

Simulations are performed over a single operation cycle (2 h interval), with a 1 second time step. Initial conditions are set likewise ($SoC_{t=0}=0.75$). The obtained results are compared to the ones exhibited by the reference power split control strategy, through a fuzzy controller based on the current SoC of the battery and the instantaneous power demand [5]. Comparing simulation time, it is emphasized that the scenario based on SPSA reaches the optimal solution in a time interval (1.74 s) 80% shorter than the reference one (18.84 s). Fig. 2 depicts the power share among the two APU integrated devices, alongside

with the power request profile (in red). In the reference scenario, SOFC power is increased mainly in correspondence of battery charging during the cycle; peaks are in the range 3-4 kW. This aims to maintain the battery operation at high SoC values (the SoC at the end of the cycle is restored to the initial value). Moreover the battery has to provide power peaks when the load request increases (up to 3.5 kW and over).

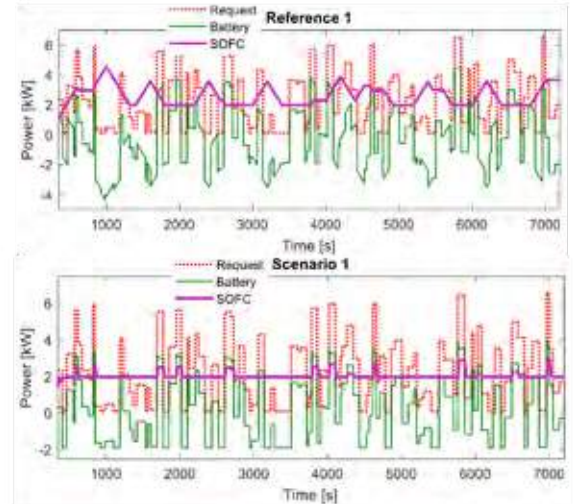


Fig. 2. Battery (green) and SOFC (purple) power profiles.

In the case the SPSA algorithm is implemented (Scenario 1 in Fig. 2), instead, according to defined performance function the SOFC delivers a more constant power profile (peaks are reduced down to 2.5-2.9 kW), since it is negatively affected by fluctuating operation conditions. Power peaks provided by the battery are in the 3-3.5 kW range; moreover the battery is charged only in correspondence of null or low load conditions and under a charging power limited to 2 kW.

V. CONCLUSION

It is highlighted that, according to the object of the optimization problem implemented in the SPSA algorithm, the SOFC supplies a more constant power with a reduction of power peaks of about 20%. Also battery operation is improved with specific reference to the charging phase; peak power during such process is halved.

REFERENCES

- [1] J. Fuel Cell Sci. Technol. 2009, 6 (4): 041011. doi: 10.1115/1.3081475.
- [2] Proceedings of 4th Int. ASME Conf. Fuel Cell Sci., Eng. and Tech., 411-422, 2006. doi: 10.1115/FUELCCELL2006-97237
- [3] R. C. Dorf and R. H. Bishop, Modern Control Systems Solution Manual, 2008.
- [4] Econ. Energy Environ. Policy, vol. 1, no. 2, pp. 3-18, 2012. doi: 10.5547/2160-5890.1.2.1.
- [5] I. Arsic et al., Proceedings of the 6th Biennial Conf. on Eng. Syst. Des. Anal., ESDA2002/AMP-121, 2002.

POISON-TOLERANT Pd ON NITROGEN-DOPED 3D HIERARCHICAL ORDERED MESOPOROUS ELECTROCATALYST FOR THE SIMULTANEOUS DETECTION OF ASCORBIC ACID, DOPAMINE AND GLUCOSE

A. Brouzgou¹, E. Gorbova², Y. Wang³, Song³, S. Jing⁴, Z. Liang⁵,
S. Freni⁶, S. Cavallaro⁷ and P. Tsiakaras¹

¹Department of Mechanical Engineers, University of Thessaly, Pedion Areos, Volos, (Greece)

²Institute of High Temperature Electrochemistry, Yekaterinburg, (Russia)

³School of Chemical Engineering and Technology, Sun Yat-sen University, (P.R.China)

⁴School of Information and Control Engineering, China University of Mining and Technology, Xuzhou, (P.R.China)

⁵School of Chemistry and Chemical Engineering, South China University of Technology, Guangzhou, (P.R.China)

⁶Department of Industrial Chemistry and Materials Engineering, University of Messina, Salita Sperone 31, (Italy)

⁷Institute for Advanced Energy Technologies "Nicola Giordano", CNR-Consiglio Nazionale Ricerche, Messina (Italy)

Abstract - In the present work, nitrogen-doped three dimensional hierarchical ordered mesoporous supported palladium (Pd 20 wt%/N-3D) electrocatalyst was successfully synthesized with the nanocasting method. The as-prepared electrocatalyst exhibits an hierarchical porous structure with interconnected walls, which permits the exposure of more active sites to the respective reactant. Due to its special structure the electrocatalyst: i) is highly poisonous-tolerant to the intermediates of glucose electrooxidation reaction, ii) presents high activity to the ascorbic acid electrooxidation, and iii) exhibits a moderate activity to dopamine electrooxidation reaction. Its sensitivity range is reported to be 0.990 $\mu\text{A } \mu\text{M}^{-1} \text{cm}^{-2}$, 0.38 $\mu\text{A } \mu\text{M}^{-1} \text{cm}^{-2}$ and 0.09 $\mu\text{A } \mu\text{M}^{-1} \text{cm}^{-2}$ for ascorbic acid, dopamine and glucose, respectively.

Index Terms— ascorbic acid, dopamine, glucose electrooxidation hierarchical ordered mesoporous, sensors

I. INTRODUCTION

In literature [1; 2], 3D nitrogen-doped hierarchical porous carbon materials are reported to provide high mass transfer and higher efficiency utilization of the active sites. More precisely, the nitrogen can alter the active sites, the hierarchical structure can provide better dispersion of active sites over various scales of pores, larger surface areas, while the three-dimensional geometrical structure can facilitate the mass transfer through the formed channels, allowing the diffusion of the reactant to the whole catalyst surface. Nsabimama *et al.* [2] studied three-dimensional (3D) N-doped hierarchically porous carbon for the simultaneous detection of ascorbic acid, dopamine and uric acid. According to the authors the as-prepared electrocatalyst showed a wide linear range of detection high sensitivity, good reproducibility and stability. Nguyen *et al.* [3]

reported long-term stability and excellent anti-interference ability of 3D Zn-doped hierarchical nanosheets for glucose detection. The hierarchical architecture of the electrocatalyst offered enhanced charge conductivity. In the present work we report a Pd/nitrogen-doped 3D hierarchical meso/macroporous carbon (Pd/N-3D) electrocatalyst that is poisonous tolerant towards glucose electrooxidation reaction and with a very good response for ascorbic acid, then for dopamine and finally for glucose.

II. ELECTROCATALYSTS PREPARATION AND CHARACTERIZATION

For the electrocatalysts preparation, 4.0 g tri-block copolymer EO20PO70EO20 (Pluronic P123, BASF) were dissolved in 20 mL HCl (AR, 37 wt%, Sinopharm Chemical Reagent Co., Ltd) solution and 126 mL deionized (DI) water. Then, the addition of 9.2 mL tetraethylorthosilicate (AR, TEOS, Sinopharm Chemical Reagent Co., Ltd) and were stirred for 20 h at 35 °C. The as-formed slurry was hydrothermally treated at 100 °C for 24 h. The final powders were collected and led to a microwave-digestion in order the organic template to be removed. For the N-doped carbon synthesis the nanocasting method was used. For the deposition of Pd on the as-prepared support, the appropriate amount of the carbon support was added in deionized water and was stirring until it was dissolved. Then PdCl₂ precursor was added to the solution and was stirring at 30°C for 1h. Then, sodium borohydride was drop by drop added to the as-prepared solution while the mixture was stirred with the aid of a magenta stirrer. Then the mixture was stirred for 4 h. After the mixture was filtered and washed with hot deionized water. The obtained 'mud' was dried in a furnace under vacuum at 75°C for 24h. The electrochemical behaviour of the as-prepared electrocatalysts was

investigated in a three-electrode half-cell with the aid of AMEL 7050 electrochemical station. An Ag/AgCl (3M KOH) and a needle type Pt electrode (AMEL) was used as reference and counter electrode, respectively. The working electrode was glassy carbon of 0.07cm² area.

III. PHYSICO-CHEMICAL CHARACTERIZATION

It is shown that the structure of the as-prepared electrocatalyst consists of interconnected short 'columns'. The N-3D specific area is calculated equal to 746 m²g⁻¹ and the elemental composition is of 88.75C, 3.88 N, 7.37 O and N:C is 0.044.

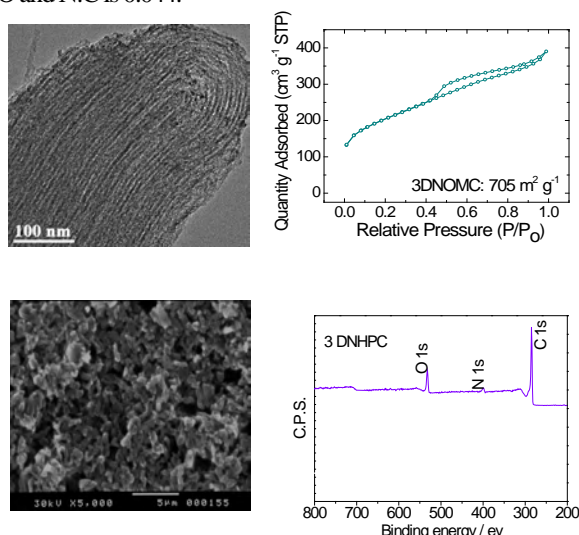


Fig.1. TEM images of the 3D carbon (top-left); N-isotherm (top-right); SEM Pd/N-3D (bottom-left) and XPS (bottom-right)

IV. ELECTROCHEMICAL CHARACTERIZATION

In the investigation of glucose electrooxidation reaction with CV method, the oxidation I_p is 1.8 mA cm⁻² (@-0.05V) (or 0.025 mAμg⁻¹) and 2.5 mA cm⁻² (@0.06V) (or 0.035 mAμg⁻¹) for 3.5 mM and 10 mM glucose, respectively.

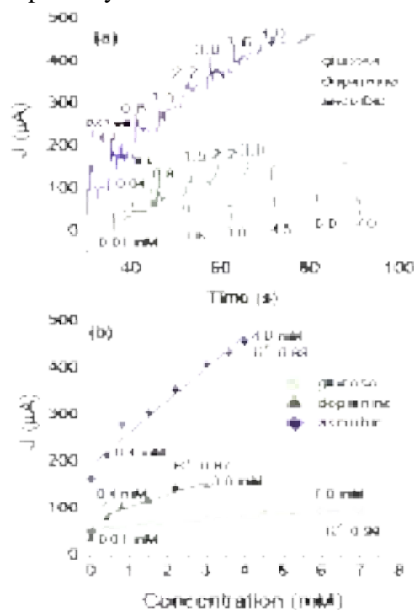


Fig.2. Amperometric response of Pd/3D at -0.14V (vs Ag/AgCl) in 0.1M KOH, at 36.6°C, 1600rpm (a) and the linear relationship of current response with time (b)

In the backward scanning, an oxidation peak current (I_b), appears at -0.33 and -0.25 V vs Ag/AgCl in 3.5 mM and 10 mM glucose, respectively. This is attributed to the further oxidation of intermediate products of glucose electrooxidation, highlighting the tolerance of the as-examined electrocatalyst to poisonous effect of the intermediates. The appearance of the two oxidation peaks can be ascribed to the formation of the oxidized glucose intermediates in the anodic sweep and its further oxidation to gluconic acid, during the cathodic sweep [4]. The amperometric responses of the as-prepared electrocatalyst in the case of glucose, dopamine and ascorbic acid are illustrated in Fig. 2. The appropriate amount of each substance was added in the solution until no current response was observed. It is obvious that electrocatalyst amperometric response is highest in the case of ascorbic acid, giving current ca 450 μA for 4 mM of ascorbic acid. Then dopamine follows with the current magnitude of 150 μA for 3 mM dopamine, and finally glucose records 80 μA for 7 mM glucose.

The linear range for glucose sensing is from 0.01 mM to 7.0 mM, for ascorbic acid sensing is from 0.4 to 4.0 mM, and for dopamine is from 0.4 to 3.0 mM.

V. CONCLUSION

The high current response of Pd/N-3D is ascribed to the interconnected bars that are indicated into its structure. Their wall-like structure offers a higher specific area than N-2D to the reactant, which facilitate the further oxidation of glucose intermediates. The detection ranges are from 0.01 to 7.0 mM for glucose, from 0.4 to 4.0 mM for ascorbic acid, and 0.4 to 3.0 mM for dopamine. Its sensitivity range is estimated 0.990 μA μM⁻¹ cm⁻², 0.38 μA μM⁻¹ cm⁻² and 0.09 μA μM⁻¹ cm⁻² for ascorbic acid, dopamine and glucose, respectively.

ACKNOWLEDGMENT

Dr. Angeliki Brouzougou thankfully acknowledges the post-doc program: «Strengthening Postdoctoral Researchers», co-funded by the Greek State Scholarships Foundation, the «Human Resource Development, Education and Lifelong Learning» with Priority Axes 6,8,9, by the European Commission Social Fund-ECB and the Greek government»

REFERENCES

- [1] Liang, J.-Y., Wang C.-C., Lu S.-Y., Glucose-derived nitrogen-doped hierarchical hollow nest-like carbon nanostructures from a novel template-free method as an outstanding electrode material for supercapacitors, *Journal of Materials Chemistry A*, volume 3, 2015, pages 24453-62.
- [2] Nsabimana, A., Lai J., Li S., Hui P., Liu Z., Xu G., Surfactant-free synthesis of three-dimensional nitrogen-doped hierarchically porous carbon and its application as an electrode modification material for simultaneous sensing of ascorbic acid, dopamine and uric acid, *Analyst*, volume 142, 2017, pages 478-84.
- [3] Nguyen, D.M., Bach L.G., Bui Q.B., Hierarchical nanosheets based on zinc-doped nickel hydroxide attached 3D framework as free-standing nonenzymatic sensor for sensitive glucose detection, *Journal of Electroanalytical Chemistry*, volume 837, 2019, pages 86-94.
- [4] Brouzougou, A., Song S., Tsiakaras P., Carbon-supported PdSn and Pd₃Sn₂ anodes for glucose electrooxidation in alkaline media, *Applied Catalysis B: Environmental*, volume 158, 2014, pages 209-16.

Pd₁₀Co₁ SUPPORTED ON KETJEN BLACK FOR THE SIMULTANEOUS DETECTION OF DOPAMINE, URIC ACID, ASCORBIC ACID IN PRESENCE OF GLUCOSE

A. Brouzgou*, C.Lo Vecchio**, V. Baglio**, A.S. Aricò**,
Z-X Liang***, A. Demin****, and P. Tsiakaras*

*Laboratory of Alternative Energy Conversion Systems, Department of Mechanical Engineering,
University of Thessaly, Pedion Areos, Volos, (Greece)

**Institute for Advanced Energy Technologies "Nicola Giordano", CNR-Consiglio Nazionale delle
Ricerche, Via Salita Santa Lucia sopra Contesse, 5, Messina, (Italy)

***School of Chemistry and Chemical Engineering, South China University of Technology,
Guangzhou, (China)

****Laboratory of Electrochemical Devices based on Solid Oxide Proton Electrolytes, Institute of
High Temperature Electrochemistry, Yekaterinburg, (Russia)

Abstract - In the present work palladium-cobalt supported on ketjen black (PCKB) electrocatalyst was synthesized and tested for the simultaneous detection of ascorbic acid, dopamine, uric acid and glucose substances. Cyclic voltammetry and potentiometric tests were conducted for its electrochemical evaluation as amperometric sensor electrode. It is found that the as-prepared electrocatalyst has the ability to promote the oxidation of each of one substances at the same time and at different peak potentials without appearing overlapping oxidation current peaks. Its electrochemical response at 0.67V for 3.5 mM glucose is 76 μ A, while for 0.1 mM ascorbic acid, dopamine and uric acid it is higher than 100 μ A. The sensitivity values are calculated to be 816, 1534, 1457, 1150 μ A mM⁻¹ cm² for glucose, ascorbic acid, dopamine and uric acid, respectively.

Index Terms -amperometric electrochemical sensors, co-detection, dopamine electrooxidation, glucose electrooxidation, uric acid electrooxidation

I. INTRODUCTION

According to our knowledge, up-to-date only a few number of investigations devoted to the co-detection of dopamine and uric acid, in the presence of glucose, are appeared in international literature [1]. Hassan *et al.* [2] investigated the co-detection of glucose, ascorbic and uric acid over polymer-modified nickel-based electrodes. They found that the oxidation of the three bio-molecules took place at the same potential value. Thus, in order to achieve separate peak oxidation potentials, they treated the working electrode surface with a liquid polymer. Ye *et al.* [3] investigated Pd nanocubes for the simultaneous detection of glucose, uric acid and ascorbic acid in NaOH solution. They found that the catalyst was more selective to glucose biomolecule rather than to the other two substances. The main challenge they faced was the overlapping of the bio-molecules oxidation peaks. It is characteristic the

majority of the works in order to overcome the overlap problem make use of the differential pulse voltammetry technique [4]. Herein we synthesized Pd₁₀Co₁/carbon ketjenblack electrocatalyst for the electrooxidation and the simultaneous detection of dopamine, uric acid and glucose without any previous treatment of the catalytic surface area. As far as we know, up-to-date, has not been investigated the same electrocatalyst for this purpose.

II. MATERIALS AND METHODS

A. Synthesis of PdCo supported on KB catalyst

The 30% Pd₁₀Co₁ on a high surface area ketjenblack (KB) carbon support (Pd₁₀Co₁/KB) was prepared as following: a Pd sulphite precursor was mixed in appropriate amount with the carbon source and then decomposed by H₂O₂ in order to obtain PdO_x/KB. The Co precursor was then mixed with the carbon-supported metal oxide dispersion and the impregnated product was carbothermally reduced at 500 °C in Ar atmosphere. Lastly, an acid washing was implemented with the aim to remove the unstable species in the final 30% Pd₁₀Co₁/KB electrocatalyst. The Pd(30wt%)/KB electrocatalyst was synthesized likewise the Pd₁₀Co₁/KB, while the commercial Pd(30 wt%)/Vulcan was supplied from Sigma-Aldrich.

B. Physicochemical analysis

X-ray diffraction (XRD) patterns for powder catalysts were recorded using an X'Pert 3710 X-Ray diffractometer (Philips), employing a CuK α source operating at 40 kV and 20 mA. X-ray photoelectron spectroscopy (XPS) measurements were carried out by using a Physical Electronics (PHI) 5800-01 spectrometer. XPS data were interpreted by using the online library of oxidation states implemented in the PHI

MULTIPAK 6.1 software and the PHI Handbook of X-ray photoelectron spectroscopy. Transmission electron microscopy (TEM) analysis was performed with the aid of a CM12 microscope (Philips). Energy dispersive X-ray (EDX) spectroscopy at 25 kV with an XL30 SFEQ scanning electron microscope (FEI) also took place.

C. Electrochemical analysis

For the electrochemical measurements an AMEL7050 electrochemical station was used, a platinum tip, a Ag/AgCl (3.0M KOH) and a glassy carbon ($d = 3\text{ mm}$) as the counter, reference and working electrode, respectively. The catalytic ink was prepared by mixing 5.0 mg of catalyst with 1.8 mL of ethanol and 0.2 mL of Nafion solution (5 wt%).

III. RESULTS AND DISCUSSION

Fig. 1a shows the survey spectra of the 30% Pd₁₀Co₁/KB. The atomic ratio between Pd and Co from the energy dispersive X-ray (EDX) analysis, more representative of the bulk composition, this ratio was 10:1. Fig. 1b shows the deconvolution spectra for Pd3d line before Ar⁺ sputtering. In Fig. 1c, the Co2p spectra for the alloyed catalyst are displayed. Metallic Co, found at 778.5 eV, represents 29%; this percentage increases up to 85% in the inner zone, as shown in Fig. 1d. Moreover, the XRD profiles indicated that alloy was formed. From TEM images is proved that the nanoparticles are almost homogeneously distributed on the ketjenblack surface; and the nanoparticles size is distributed between 2-4nm.

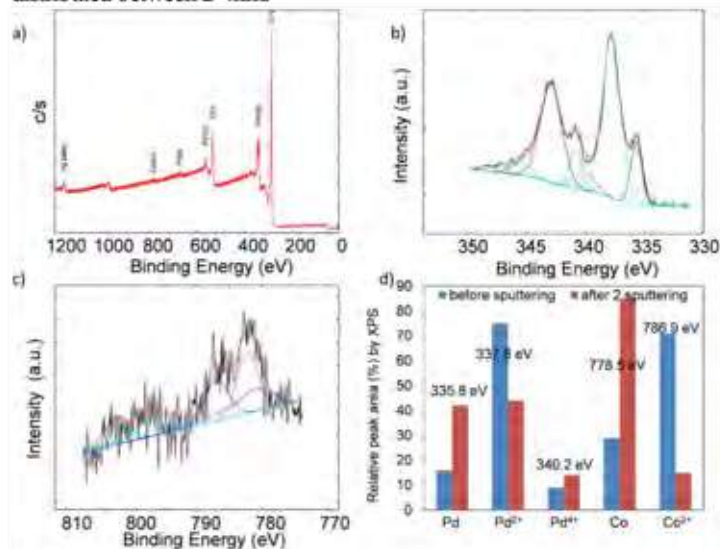


Fig.1 XPS measurements describing the survey spectra of 30% Pd₁₀Co₁/KB (a), the deconvolution spectra for the Pd3d line (b), the deconvolution spectra for Co2p line (c) and the relative percentage of the metals at different oxidation states (d)

The amperometric test was carried out with potentiostatic measurement, via the aid of RDE. The respective measurements were conducted at 0.67 V (vs. Ag/AgCl), in 3.5 mM glucose, 0.1 mM uric acid and dopamine (human body's concentration values) in 0.15M saline aqueous solution, at 36.6 °C.

When glucose is injected into the solution the response signal increases to ca 150 μA but stabilizes at 82 μA . After almost twenty seconds the appropriate amount of dopamine is added and the

response signal increase at 200 μA , but stabilizes at 150 μA , giving 68 μA amperometric response.

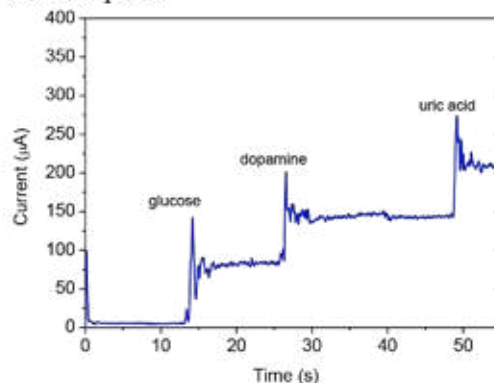


Fig. 2. Amperometric response of 3.5 mM glucose, 0.1 mM dopamine and 0.1 mM uric acid, at 0.67 V (vs. Ag/AgCl) in 0.15 M saline, at T=36.6 °C, 1600 rpm

The insertion of uric acid gives 268 μA current response which then stabilizes at 208 μA thus giving a net current response of 58 μA (Fig. 2). When a compound is added the as-prepared electrocatalyst responses instantly, within some seconds, indicating the quick response of the material.

IV. CONCLUSION

The as synthesized Pd₁₀Co₁ (30 wt %)/KB electrocatalyst shows very good electrocatalytic activity towards GOR. This activity is enhanced i) as glucose concentration increases up to 1.5 mM (while at higher concentration values it decreases) and ii) as the temperature increases from 18 to 42 °C. The addition of Co into Pd facilitates desorption of the intermediate products formed during the oxidation process, also offering a bi-functional ability toward the electrooxidation of glucose, dopamine and uric acid and consequently an ability of their co-detection.

ACKNOWLEDGMENT

Dr Angeliki Brouzgou thankfully acknowledges the post-doc program: «Strengthening Postdoctoral Researchers», co-funded by the Greek State Scholarships Foundation, the «Human Resource Development, Education and Lifelong Learning» with Priority Axes 6,8,9, by the European Commission Social Fund-ECB and the Greek government».

REFERENCES

- [1] Brouzgou, A., Gorbova E., Wang Y., Jing S., Seretis A., Liang Z., et al., Nitrogen-doped 3D hierarchical ordered mesoporous carbon supported palladium electrocatalyst for the simultaneous detection of ascorbic acid, dopamine, and glucose, Ionics, volume 2019, pages
- [2] Hassan, K.M., Elhaddad G.M., Abdel Azzem M., Simultaneous determination of ascorbic acid, uric acid and glucose using glassy carbon electrode modified by nickel nanoparticles at poly 1, 8-diaminonaphthalene in basic medium, Journal of Electroanalytical Chemistry, volume 728, 2014, pages 123-9.
- [3] Ye, J.-S., Chen C.-W., Lee C.-L., Pd nanocube as non-enzymatic glucose sensor, Sensors and Actuators B: Chemical, volume 208, 2015, pages 569-74.
- [4] Zhu, Q., Bao J., Huo D., Yang M., Hou C., Guo J., et al., 3D Graphene hydrogel-gold nanoparticles nanocomposite modified glassy carbon electrode for the simultaneous determination of ascorbic acid, dopamine and uric acid, Sensors and Actuators B: Chemical, volume 238, 2017, pages 1316-23.

THE DESIGN OF A SOLID-STATE HYDROGEN STORAGE SYSTEM

M. S. Chung*, Y. H. Jeon**, and H. Y. Lim**

* Hydrogen Energy R&D Center, KIER, 152 Gajeong-ro, Yuseong-gu,
Daejeon, (Republic of Korea)

**Hanon System, 95 Sinilseo-ro, Daedeok-gu, Daejeon, (Republic of Korea)

Abstract - Hydrogen storage is one of the key obstacles to the commercialization as well as market acceptance of hydrogen fueled vehicle. Besides the efficiency of power system, it is an extremely challenging technology to store sufficient hydrogen on the vehicle without compromising consumer requirement such as safety, space, driving range, and fuel cost. There are three main hydrogen storage methods including compression, liquefaction and hydrogen storage materials. Among the technologies currently under development, the hydrogen storage as a highly pressurized gas is the most prominent candidate for the hydrogen powered vehicle now. The advanced automobile industries have already demonstrated the highly pressurized hydrogen system on fuel cell vehicles for past several years. The hydrogen storage materials in solid state have some advantages such as high volumetric storage capacity, little energy loss, longer storage time and highest safety. Various carbonaceous and non-carbonaceous hydrogen storage materials have been studied over the past few decades. In this presentation, we would like to introduce our new developing hydrogen storage system including a heat exchanger for FCV based on a NaAlH_4 . See reference [1, 2, 3].

Index Terms – Hydrogen storage. Solid-state materials, Heat exchanger, Thermal conductivity

I. INTRODUCTION

Hydrogen storage is one of the key obstacles to the commercialization as well as market acceptance of hydrogen fueled vehicle. Besides the efficiency of power system, it is an extremely challenging technology to store sufficient hydrogen on the vehicle without compromising consumer requirement such as safety, space, driving range, and fuel cost.

The hydrogen storage materials in solid state have some advantages such as high volumetric storage capacity, little energy loss, longer storage time and highest safety. Various hydrogen storage materials have been studied over the past few decades [1]. However, they still have low specific storage capacity (weight & volume density) and poor cyclic properties.

Moreover, they need efficient heat exchangers for hydrogenation and dehydrogenation.

II. HYDROGEN STORAGE MATERIAL

The purpose of this research is to develop solid state hydrogen storage materials and storage system for fuel cell vehicle (FCV). In this work, we have tried to develop a process to prepare complex hydrides with more than 4.6wt% ($>40 \text{ kg H}_2/\text{m}^3$, $\sim 120^\circ\text{C}$, between 1 ~ 100 bar) for material itself [2] as shown in Fig. 1.

We should add and remove heat from the material about 40KJ/mol H_2 when dehydrogenation and hydrogenation processes, respectively. Therefore, we have to adopt an interior heat exchanger to achieve required speeds for hydrogenation and dehydrogenation in the storage system.

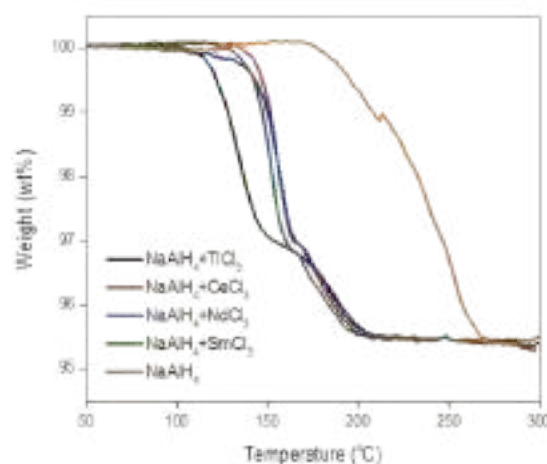


Fig. 1 Hydrogen storage capacity of NaAlH_4 with various catalysts[3].

III. HYDROGEN STORAGE SYSTEM

Our aim is to design and manufacture a hydrogen storage system using an efficient heat exchanger for heat transfer to and from the storage material as shown in Fig. 2, 3 & 4.

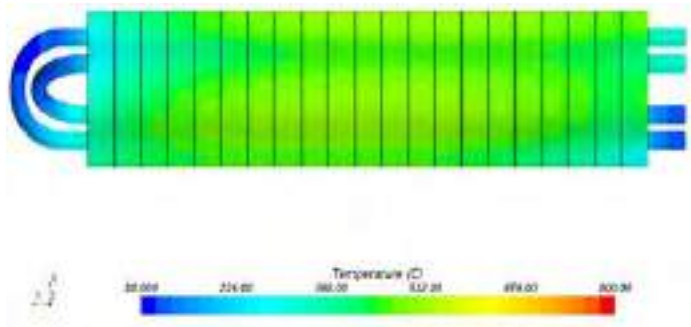


Fig. 2 Configuration of hydrogen storage system with interior heat exchanger for NaAlH₄.



Fig. 3 Coolant channels with cooling fins.



Fig. 4 Graphic image of hydrogen storage system for 200g-H₂.

The measured values of the thermal conductivities of the composites composed of the reference materials with ENG (Extended Natural Graphite) are about 6 W/m K. The error between the measured value of the thermal conductivity of the

reference material and their literature value was found to be within approximately 5%.

IV. CONCLUSION

In order to make the hydrogen storage system safe and compact, we designed the hydrogen storage vessel considered with an interior heat exchanger including cooling fins and disc type pellets of compressed NaAlH₄. To enhance the heat transfer coefficient, we fabricated the compressed NaAlH₄ powder with density about 1.18 mixing with 5wt% ENG. And then we measured the effective thermal conductivity of the sample pellets and its change of dimension or shape in the hydrogenation and dehydrogenation process as well.

ACKNOWLEDGMENT

This research is funded by MOTIE of Korea Government.

REFERENCES

- [1] Chung, M.-S., et al., "Current issues of hydrogen storage technology in Korea". *Proc. of European Fuel Cell Technology & Application conference* (2015).
- [2] Cho, Y.-W., et al., "Dehydrogenation and cycle studies of LiBH₄-CaH₂ composite", *International journal of hydrogen energy*, vol. 35, pp 6578-6582, (2010).
- [3] Lee, G.-J., et al., "Improvement in desorption kinetics of NaAlH₄ catalyzed with TiO₂ nano powder", *International journal of hydrogen energy*, vol. 33, pp 3748-3753, (2008)

A NEW PARALLEL FLOW FIELD SINGLE PEM FUEL CELL TESTING HARDWARE FOR HIGH POWER DENSITIES EXAMINATION

T. Bednarek, G. Tsotridis

European Commission, Joint Research Centre (JRC), Directorate
Energy, Transport and Climate (*The Netherlands*)

Abstract - The design and testing results of a new single cell testing hardware (JRC ZEROVCELL) are presented. Its objective is to enable testing the MEA under as much as possible uniform working conditions across the active area by employing a parallel pattern flow field. In this way the gradients of temperature, pressure and concentration of the reactants are minimised across the active area. The JRC ZEROVCELL hardware has been experimentally validated in terms of polarisation curve. The results show, that JRC ZEROVCELL is able to expose the tested material to the very high power densities up to 2.0 Wcm^{-2} and at the same time to respect rigorous criteria of operative conditions uniformity across the active area. The ohmic-constant slope region covers a broad range from ~ 1.0 to $\sim 3.2 \text{ Acm}^{-2}$. The JRC ZEROVCELL provides robust and reproducible experimental results and is well suited for performance testing of MEAs for automotive and stationary applications.

I. INTRODUCTION

The present requirements for increased current and power density of PEMFC (Proton Exchange Membrane Fuel Cell) commercial stacks drives the development of new and better Membrane Electrode Assembly (MEA) components, such as polymer membranes, catalysts and gas diffusion media. It also implies the need for improvement and optimisation of fuel cell testing hardware. For MEA characterisation, usually single cell tests are performed using hardware where the reactants are distributed by gas channels inside bi-polar plates.

However, none of the single cell testing hardware developed so far can guarantee uniform exposure of the MEA to the desired operating conditions. In addition, each single cell setup has its own unique flow field affecting testing results, hence comparison of results among different laboratories is a very challenging task.

This paper summarises the design of a single cell testing hardware (JRC ZEROVCELL) for the assessment of performance or durability tests. The new hardware aims at

exposing the MEA to as much as possible uniform conditions in terms of temperature, pressure and concentration of the reactant gases, as well minimising as much as possible the effects of flow field and liquid water accumulation. Hardware validation results are also reported.

II. DESIGN CRITERIA

To ensure that the JRC ZEROVCELL provides useful and comparable assessment results, the local working conditions across the whole active area should be as close as possible to the desired operating conditions. In particular, the effects of flow fields, liquid water removal, temperature gradient and compression on MEA performance/durability need to be minimised. The JRC ZEROVCELL does not aim designing advanced flow fields and improving the performance of a single cell. Instead, it has been designed to allow for a quantitative and reliable inter-comparison of test results between different MEA developing centres. These features were achieved by employing a flow field with straight parallel channels at both anode and cathode compartments.

The JRC ZEROVCELL was designed respecting the following requirements:

- active area 10 cm^2 ($20 \times 50 \text{ mm}$ in length),
- possibility for counter-flow and co-flow operation modes,
- pneumatic MEA compression,
- separate liquid-cooling possibilities for anode and cathode compartments,
- temperature, pressure and humidity sensors at the inlet and outlet gas manifolds,
- temperature distribution monitoring at anode and cathode by 5 thermocouples respectively,
- maximum allowable gas pressure drop of 10 kPa ,



Fig. 1 JRC ZEROVCELL installed on the testing station.

- maximum concentration gradient of 10% of reactants species,
- temperature variation across the active area of $\pm 1.0^{\circ}\text{C}$ at the current density of 4.0 Acm^{-2} .

III. EXPERIMENTAL RESULTS

The experiment was performed using the JRC ZEROVCELL connected to a GreenLight G11-620 test bench, shown in Fig 1. The following operating conditions were applied:

- operating temperature 80°C ,
- gas pressure (anode/cathode) 250/230 kPa abs,
- fully humidified fuel and oxidant gasses,
- operation stoichiometry (anode/cathode) 8.0/10.0.

The experiment is performed according to the protocols [1,2] in galvanostatic mode. Results are shown in Fig. 2, which shows the IV polarisation and the power density curves. To assess stability of the experiment, voltage development over 180s at current density 4.0 Acm^{-2} is presented.

Fig. 2 confirms that JRC ZEROVCELL allows to expose the MEA to very high current densities, up to 5.0 Acm^{-2} at 0.25V , hence investigation of relatively high power densities up to $\sim 2 \text{ Wcm}^{-2}$ electric power was possible. The IV curve shows three main regions of fuel cell operation, namely: 1) the region I where electro-chemical kinetics dominate, 2) the ohmic region II characterised by constant slope, where electric resistance of the MEA is the main reason of overpotential and 3) the mass transport limitation region III, where insufficient delivery of reactants to the catalyst layers dominates over the other overpotentials.

In the ohmic losses region II, the cell meets the most stable working conditions and approaches its highest power density. In this region reaction kinetic losses are relatively constant while mass transport losses are not yet dominant. It results in linear decay of cell voltage with increasing current density. For

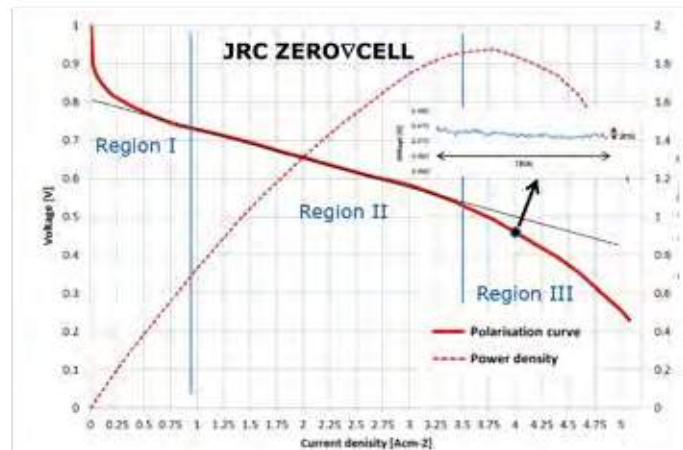


Fig. 2 Polarisation curve and power density plots obtained using JRC ZEROVCELL.

the JRC ZEROVCELL this region is observed in a broad range from $\sim 1.0 \text{ Acm}^{-2}$ up to $\sim 3.2 \text{ Acm}^{-2}$. This range fully covers the operation range of most commercial stacks. The JRC ZEROVCELL allows the assessment of MEA performances without visible mass transport limitation effects at the target current density of a commercial stack.

IV. CONCLUSIONS

The new single cell testing hardware JRC ZEROVCELL presented in this paper is able to minimise the temperature, pressure and concentration gradients, aiming at stability of the operative parameters under a broad range of conditions. Its polarisation curve shows linear ohmic behaviour up to $\sim 3.2 \text{ Acm}^{-2}$. Maximum electric power density reaches the value of $\sim 1.9 \text{ W cm}^{-2}$, while maximum current density goes up to 5.0 Acm^{-2} at $\sim 0.25\text{V}$ showing that hardware allows exposing the tested MEA to very high current densities. Very low voltage fluctuations demonstrate that liquid water effects are minimised.

The JRC ZEROVCELL, due to its stable operation, demonstrated ability to provide reproducible and robust experiment data. Because of robustness and small fluctuations of the provided data, JRC ZEROVCELL shows the potential to be the reference testing hardware for MEA performance quantification.

REFERENCES

- [1] G. Tsotridis et al. EU Harmonised Test Protocols for PEMFC MEA Testing in Single Cell Configuration for Automotive Applications, JRC Scientific Reports, 2015.
- [2] T. Malkow et al., Testing the voltage and power as function of current density JRC Scientific Reports, 2010.

DUAL ATMOSPHERE CORROSION OF COATED AND UNCOATED AISI 441 AND CROFER 22 APU FERRITIC STAINLESS STEELS UNDER SOLID OXIDE ELECTROLYSIS CONDITIONS

S. Frangini*, C. Paoletti*, D. Pumiglia*, M. Della Pietra*, L. Della Seta*, S. J. McPhail*, B. Talic**, B. R. Sudireddy**, and K. Couturier***

*ENEA CR Casaccia, DTE-PCU-SPCT, 00123 Rome (Italy),

**Dept. of Energy Conversion and Storage, Technical University of Denmark, 4000-Roskilde, (Denmark)

***Univ. Grenoble Alpes, CEA, LITEN, F38000, Grenoble (France)

Abstract – Coating effects on the oxidation behavior of two ferritic steels (441 and Crofer 22 APU) were investigated at 750°C in SOEC dual atmosphere conditions for 1500 h. Results indicate that the a SOEC dual exposure may promote accelerated outward Fe diffusion and consequent Fe oxide nodule attack similarly to dual SOFC tests. However, the oxidation resistance of the two uncoated steels was found to be markedly different since only the 441 steel was susceptible to evident Fe nodule attack. Further, no Fe poisoning was found in 441 steel samples protected with MCO spinels, whereas a few Fe oxide nodules were found on Ce/Co coatings. In comparison, uncoated and coated Crofer 22 APU steel samples were found to be immune to localized nodule attack, at least under the chosen SOEC dual test conditions.

Index Terms – Dual atmosphere, Solid Oxide, Stainless Steel, Coatings.

I. INTRODUCTION

High temperature electrolysis based on Solid Oxide Electrolysis Cell (SOEC) technology is today largely investigated for a wide range of renewable energy applications, such as hydrogen and syngas production, CO₂ valorization, fuel processing and storage of electrical energy. The SOEC systems generally use commercially available materials developed for Solid Oxide Fuel Cells (SOFC), although materials with an optimized performance and stability are required in the more demanding SOEC environments.

Interconnects are key stack components that must remain stable in an oxidizing atmosphere on one side and in a reducing atmosphere on the opposite side (dual-atmosphere exposure, DA). The state-of-the-art SOFC interconnect technology based on ferritic stainless steels (FSS) is also widely employed in SOEC stacks. In order to minimize Cr evaporation and growth of resistive oxide scales, metallic or ceramic functional layers

are generally applied for stable interconnect performance. Many studies on FSS materials indicate that a DA exposure can lead to anomalous air-side oxidation as a result of H₂ diffusion-related effects from the anode-side. Much less information is available about the DA effects in SOEC cells, namely in atmospheres characterized by high PO₂ at the O₂ side and high PH₂O/PH₂ ratio at the fuel side (1). Further, the oxidation behavior of coated FSS interconnects in SOEC atmospheres has been scarcely investigated (2).

In order to fill all these knowledge gaps, a campaign has been recently concluded within H2020 BALANCE Project aimed to qualify the DA oxidation of various coating materials (Ce/Co, Mn/Co spinel oxide, Y₂O₃) under SOEC exposure. Unlike the other two, Y₂O₃ has been deposited on the interconnect fuel side as potential H₂ diffusion barrier. Two widely employed ferritic stainless steels (AISI 441 and Crofer 22 APU steels) have been used in the DA experiments.

II. EXPERIMENTAL

Thin steel sheets were used to prepare the samples. Electrophoresis and electrolytic deposition were used for Mn/Co (MCO, about 20 μm thick) and Y₂O₃ coatings (about 0.3 μm thick), respectively. Before the DA exposure tests, the coatings were consolidated by proper heat treatments. A two-step sintering (red-ox sintering) first at 1000°C and then 800°C was applied to the MCO coatings, whereas the Y₂O₃ coatings were simply treated in air at 400°C. The Ce/Co coated samples were obtained from pre-coated PVD sheets provided by Sandvik Materials Technology. The resulting in-situ oxidized coating is much thinner than MCO coating (about 2 μm thick).

The DA setup used in this work is very similar to that described in (3). The tests were conducted at 750°C for 1500 h in a 50O₂/50Ar vol % gas mixture as the oxidizing atmosphere

and in a 50Ar/45H₂O/5H₂ vol % gas mixture as fuel atmosphere.

Post-test characterization was conducted with SEM/EDX and X-Ray Diffraction (XRD) analysis.

III. PRELIMINARY RESULTS AND DISCUSSION

Only the most important XRD results will be shown here due to space restriction. Fig. 1 reports the XRD spectra of the uncoated steel samples exposed to the O₂-Ar side under single and dual atmosphere testing conditions.

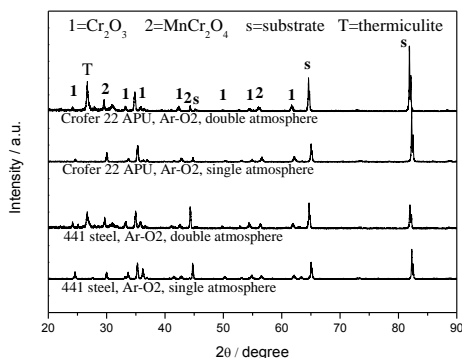


Fig. 1. XRD spectra for uncoated 441 and Crofer 22 APU steels after 1500 h at 750°C in 50Ar-50O₂ vol % single or dual atmosphere.

XRD spectra show only the presence of a protective Cr oxide film composed of Cr₂O₃ and MnCr₂O₄ spinel phases under both single and dual testing. However, SEM/EDX analysis showed incipient Fe oxide nodule growth, although the localized attack was found only on the 441 steel surface.

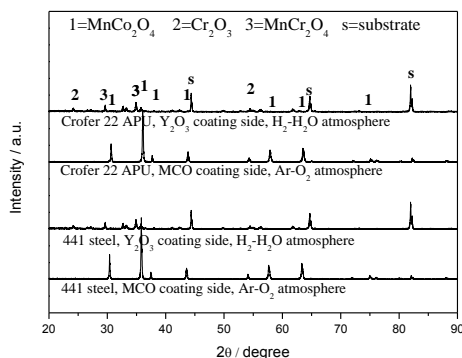


Fig. 2. XRD spectra for the MCO/Y₂O₃ coated 441 and Crofer 22 APU steels exposed to dual atmosphere for 1500 h at 750°C.

Fig. 2 indicates high stability of the MCO coating surfaces. Presence of both protective Cr₂O₃ and MnCr₂O₄ phases at the fuel side indicates protective oxide formation at the fuel side. Signs of the fuel-side thin-film Y₂O₃ coatings were not detected. SEM/EDX analysis confirmed absence of Fe oxide nodule growth, whereas Y was found yet in very small amounts (< 1 wt%). XRD data of Fig.3 indicate the presence of the only protective Co₃O₄, Cr₂O₃ and MnCr₂O₄ phases on the O₂ side of the Ce/Co coated surfaces.

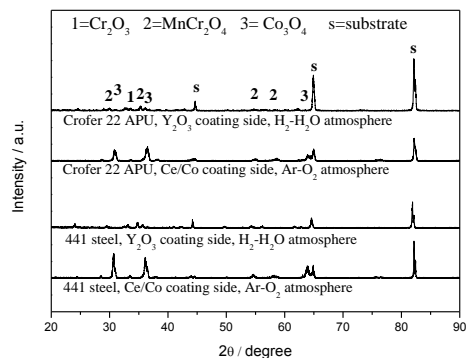


Fig. 3. XRD spectra for the Ce/Co/Y₂O₃ coated 441 and Crofer 22 APU steels exposed to dual atmosphere for 1500 h at 750°C.

However, SEM/EDX analysis allowed to detect incipient Fe oxide nodule growth on the coated 441 surface, however to a smaller extent compared to uncoated 441 sample. The tenfold higher coating thickness could most likely explain the absence of Fe poisoning on MCO coatings. Conversely, no Fe poisoning could be observed on the Ce/Co coated Crofer surface. Y detection was possible only with SEM/EDX analysis. Its presence is small (<1 wt %).

IV. CONCLUSION

Coated and uncoated 441 and Crofer 22 APU steels were subjected to long-term dual SOEC oxidation tests. XRD analysis showed only presence of protective oxide phases on the O₂-side steel surfaces, although SEM/EDX analysis revealed incipient Fe nodule attack on uncoated and, to a lesser extent, on the Ce/Co coated 441 steel, but not on MCO spinel coatings. No Fe poisoning was detected on the surface of uncoated and coated Crofer 22 APU samples. More experiments including a detailed micro-structural analysis appear necessary to clarify morphology of the fuel-side thin-film Y₂O₃ coatings and their role as H₂ diffusion barrier.

ACKNOWLEDGMENT

Balance Project has received funding from the EU Horizon 2020 research and innovation programme (grant No 731224).

REFERENCES

- [1] Ardigo M.R., et al., Dual atmosphere study of the K41X stainless steel for interconnect application in high temperature water vapour electrolysis, *Int J Hydrogen Energ*, Vol 40, 2015, pp. 5305-5312.
- [2] Ardigo M.R., et al., Effect of coatings on long term behavior of a commercial stainless steel for solid oxide electrolyser cell interconnect application in H₂/H₂O atmosphere, *Int J Hydrogen Energ*, Vol 39, 2014, pp. 21673-21677.
- [3] Alnegren, P., et al., Severe dual atmosphere effect at 600°C for stainless steel 441, *J. Power Sources*, 301 (2016), pp. 170-178.

PROTOMEM PROJECT: ACHIEVEMENTS AND CHALLENGES ON THE WAY TO INDUSTRIALLY RELEVANT PLANAR CELL DESIGN

M. E. Ivanova^{1*}, W. Deibert¹, Y. Huang², R. Merkle², D. Zhou², R. Yekani², W. Sigle², K. Ran³, J. Mayer³, W. A. Meulenberg¹, P. A. van Aken², J. Maier², O. Guillon¹

¹ Forschungszentrum Jülich GmbH, Institute of Energy and Climate Research (IEK-1), Jülich (Germany)

² Max Planck Institute for Solid State Research, Stuttgart (Germany)

³ Central Facility for Electron Microscopy GFE, RWTH Aachen University, Aachen (Germany); Ernst Ruska-Centre for Microscopy and Spectroscopy with Electrons ER-C, Forschungszentrum Jülich GmbH, Jülich (Germany)

*ProtOMem coordination, Corresponding author:
m.ivanova@fz-juelich.de

Abstract

Index Terms – Proton conducting ceramic cells, PCFC, H₂ separation ceramic membranes, BZYC, LWO

The global challenges to high efficiency and CO₂-neutral energy supply require innovative enabling technologies. The electrical surplus from renewables can be used to produce chemicals (e.g. H₂ being electrochemically generated by steam electrolysis) and vice versa to convert chemical energy into electricity in an efficient and a clean way (e.g. the energy stored in H₂ can be converted into electricity by means of a fuel cell). The combination of energy conversion and membrane technology extends the possible scenarios even more, e.g. synthesizing chemicals and fuels from CO₂ emitted by numerous industries in a chemical reaction with the renewably generated H₂. High-performance ceramic materials are the key to developing complex devices such as solid oxide fuel/electrolysis cells and gas separation membranes. The operation conditions (intermediate to high temperatures of 600-800 °C and specific gas environments) set numerous challenges towards the components and the system as a whole. Due to the unique combination of functional properties, like mechanical strength and durability, thermal and chemical stability, specific

electrical properties and catalytic activity, ceramic materials are a viable choice for these technological applications.

The R&D core of the three-year-project ProtOMem funded by the German Federal Ministry of Education and Research (BMBF) under the program Materials for Energy Transition has been focused at two classes of ceramic materials with high relevancy to the topic: BaZr_{1-x}(Ce,Y)_xO_{3-δ} as proton conducting electrolytes for intermediate temperature proton ceramic fuel cells (PCFC) and the mixed protonic-electronic conductor La_{6-x}W_{1-y}(Mo)_yO_{12-δ} as hydrogen permeation membranes for high-temperature water-gas shift reactors. Both types of devices require a gas-tight solid electrolyte/membrane exhibiting selective transport, hence their performance depends critically on the intrinsic properties of the functional materials, but also on their micro-structuring and scalability. These three aspects have been thoroughly explored in ProtOMem and as an outcome, planar design cells of up to 100 cm² - a size close to the final application geometry for fuel cells stacks and membrane reactors - could be successfully realized at an acceptable cost. This talk will highlight the project scientific achievements and perspective beyond ProtOMem on the challenging road to established proton conducting ceramic devices as competitive energy solutions.

ACKNOWLEDGMENT

Funding from BMBF, Germany (Grant Nr.: 03SF0537A) is gratefully acknowledged. Mrs. Astrid Lewalter, PtJ, Jülich is specially acknowledged for her engagement and guidance throughout the three years of the project. Finally, industrial partners Kerafol-Keramische Folien GmbH & Co. KG, Eschenbach, Germany and Morgan Advanced Materials Haldenwanger GmbH, Waldkraiburg, Germany are acknowledged for their engagement and trust in the ProtOMem Consortium.

ULTRA-LOW LOADING CATALYST LAYER DEVELOPMENT FOR ANODE ELECTRODE IN PEM WATER ELECTROLYZER (PEMWE) CELLS

A. P. Shirvanyan*, I. Garcia*, and F. van Berkel*

*ECN part of TNO, 1755 LE Petten, PO Box 15, The Netherlands

Abstract – In this work, we propose a system of auxiliary network of conductive nano-particles to achieve ultra-low loading of Ir in Proton Exchange Membrane Water Electrolyzer (PEMWE) while attaining superior catalyst utilization. Antimony-doped Tin Oxide (ATO) nano-particles of nominally 30 nm in diameter was used in conjunction with Ir-black conventional catalyst to form anode catalyst layers of 6-8 μm thick on Nafion 117 membranes. The preliminary results based on ex-situ rotating disk electrode (RDE) and electrolyzer cell-level tests indicate the advantage of this approach in enhancing catalyst utilization.

Index Terms – Iridium/Antimony-doped Tin Oxide (Ir/ATO) catalyst, PEM Water Electrolyzer (PEMWE), Low loading catalyst

I. INTRODUCTION

Current energy regulations require expedited replacement of fossil-based energy carriers by carbon-neutral ones such as hydrogen. Splitting water using Proton Exchange Membrane Water Electrolyzers (PEMWE's) powered by renewable electricity has been identified as a promising route to generate hydrogen (and oxygen). Rarity and high price of the commonly used Iridium-based (Ir) materials to catalyze the inherently sluggish oxygen evolution reaction (OER) will be a major impediment to widespread adoption and commercialization of PEMWE technology. In this work, we propose a system of auxiliary networks of electrically conductive nano-particles to achieve ultra-low loading of Ir in PEMWE's in an effort to attain superior catalyst utilization. Antimony-doped Tin Oxide (ATO) nano-particles of nominally 30 nm in diameter has been used to improve the in-plate conductivity of the anode's catalyst layer while opening up the venue for utilizing catalyst-support interactions. In this work, we utilized Rotating Disk Electrode (RDE) along with cell level testing to demonstrate an ultra-low loading Ir of 0.07 mg/cm² for anode.

II. EXPERIMENTAL

A. Materials and General Methods

ATO nano-powders were purchase from US Research Nanomaterials, Inc. Iridium black, 99.8% from Alfa-Aesar. Merck's Sulfuric acid 96% Suprapur was used to prepare 0.1

Molar electrolyte for RDE testing. Nafion ionomer (5 wt%) and membrane N117 were from Sigma-Aldrich. Titanium-based Porous Transport Layers (PTL) were provided by Bekaert Inc. Gas Diffusion Electrodes (GDE's) with 0.5 mg/cm² Pt on carbon-cloth from FuelCellsEtc. was used as cathode electrode. Ultrapure Water (Milli-Q) with a resistivity of 18.2 M Ω .cm was used throughout.

B. Electrochemical Measurements

The OER activity of the prepared materials was evaluated in a standard single-compartment three-electrode cell using a rotating disk electrode (RDE) setup (BioLogic RRDE-3A) with 3 mm gold tip and an Ivium Potentiostat Vertex.1A following the thin-film RDE approach [1]. Catalyst ink suspensions were prepared using 10 mg of Ir/ATO (~15 wt%) catalyst, 7.6 mL of Milli-Q water, 2.4 mL of IPA, and 20 μL of 5 wt% ionomer solution. The inks were sonicated for 30 min and coated on polished gold-disk electrodes (ϕ 3mm, 0.07 cm²) to achieve a loading of 17.5 μg cat./cm². Hydroflex Reference Hydrogen Electrode (RHE) from Gaskatel and a gold counter electrode from BioLogic was used for RDE tests.

With the ratio of ionomer to total weight of ionomer plus catalyst fixed at 10%, Membrane Electrode Assemblies (MEA's) were prepared by spraying catalyst ink directly on N117 using an Airbrush gun (Conrad, HP-200) to achieve the desired loading. In-house cell and test-station were used for further analysis.

III. RESULTS AND DISCUSSIONS

Figure 1 shows the iR-compensated polarization curve obtained from pure Ir catalyst (Fig.1a) and Ir (15 wt%)/ATO (Fig. 1b) with a linear sweep voltammetry 1.25 \rightarrow 1.65 V vs. RHE with 20 mV/s sweep rate while RDE tip rotated at 2500 rpm and the electrolyte was sparged with ultra-pure Argon gas to avoid interference with dissolved oxygen. The magnitude of current at 1.55 V is commonly normalized by the weight of the catalyst and reported as mass activity (MA). Based on these data, Pure Ir has a MA~0.166 A/mg of Ir, while Ir/ATO: MA~0.31 A/mg of Ir which indicates an improvement of 87%. Initial RDE results indicate the utility of using an auxiliary/support material in order to reduce the loading of Ir catalyst.

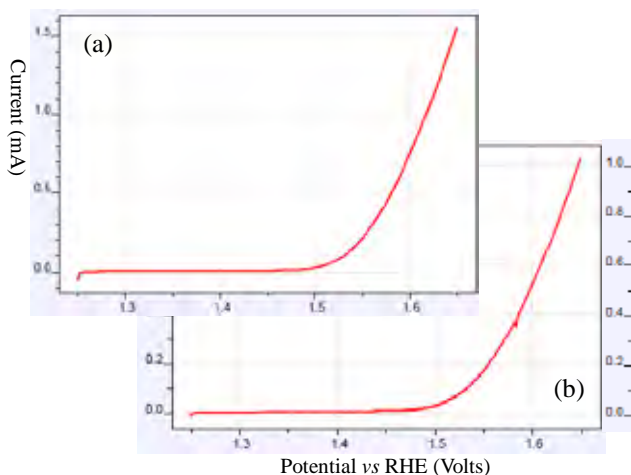


Fig 1. Polarization curves generated using RDE

We therefore decided to proceed with cell-level testing to evaluate the performance in an actual electrolyzer working environment. CCM's were prepared using Ir/ATO powder with Ir loading as low as 0.07 mg/cm^2 . The cell was conditioned at 80 C at 1.65 V potential hold for 12 hours prior to acquiring the polarization curve, as shown in Figure 2 along with a reference cell data.

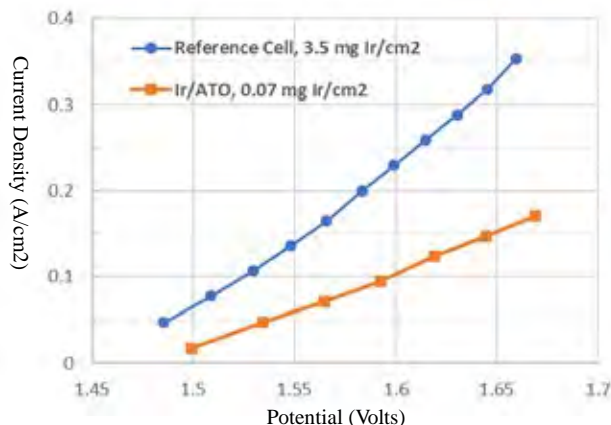


Figure 2. Cell-level polarization curves

The reference cell had the same membrane and cathode material but with Ir loading of 3.5 mg/cm^2 which is 50 times higher than the cell with Ir/ATO. Upon evaluation of MA's, we obtained 0.84 A/mg and 0.05 A/mg for Ir/ATO and reference cell, respectively. Figure 3 shows post-mortem SEM analysis on Ir/ATO-based MEA's cross section (Fig.3a) and anode surface (Fig.3b) as obtained using cryofracture method. The figure shows an almost continuous catalyst layer of $6\text{-}8 \text{ }\mu\text{m}$ covering the membrane. The catalyst layer is clearly seen to carry the impression of the PTL fibers that was separated from the anode prior to SEM analysis. Some spots are seen to be devoid of catalyst that could have been caused by removing the PTL.

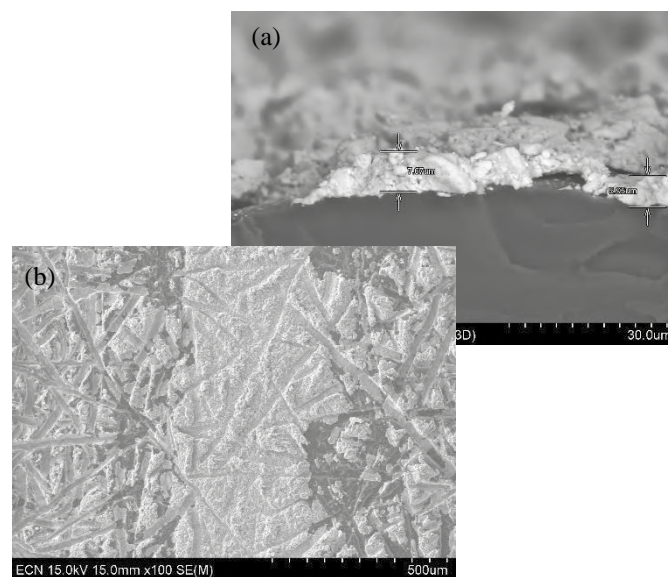


Figure 3. SEM micrograph for Ir/ATO-based MEA

While extensive tests along with stability and durability tests with detailed materials characterizations are needed to fully interpret the results, we hypothesis that the improvement in the catalyst utilization in Ir/ATO system is due to: (a) enhanced in-plane conductivity of catalyst layer at very low Ir-loading [2] (b) catalyst-support interactions. Further work is in progress to quantify the effects of auxiliary powders on PEMWE's performance and durability.

IV. CONCLUSION

Initial improvements in Iridium catalyst utilization in PEMWE cells have been indicated using ATO nano-powders as auxiliary/support materials. Using Ir/ATO combination, an ultra-low loading of 0.07 mg/cm^2 Ir was achieved. Further analysis is needed to better understand and quantify the role of auxiliary/support materials and their interactions with Ir catalyst.

ACKNOWLEDGMENT

Support from ECN part of TNO is acknowledge as part of KIP 2019 PEMWE Development project.

REFERENCES

- [1] Alia SM, Rasimick B, Ngo C, et al. Activity and Durability of Iridium Nanoparticles in the Oxygen Evolution Reaction. *J. Electrochem. Soc.* 2016, 163: F3105–F3112.
- [2] Bernt M, Siebel A, Gasteiger HA. Analysis of Voltage Losses in PEM Water Electrolyzers with Low Platinum Group Metal Loadings. *J. Electrochem. Soc.* 2018; 165: F305–F314.

ENZYMATIC CROSS-LINKED CHITOSAN-BASED ANION EXCHANGE MEMBRANES

Mojca Božič^{1,2}, Barbara Kaker¹, Silvo Hribernik^{1,2},
Tamilselvan Mohan¹, Rupert Kargl^{1,2}, Karin Stana
Kleinschek^{1,2}, Egon Pavlica³, Shingjiang Jessie Lue⁴

¹Laboratory for Characterization and Processing of Polymers,
Faculty of Mechanical Engineering, University of Maribor,
Smetanova 17, 2000 Maribor, Slovenia (mojca.bozic@um.si)

²Institute of automation, Faculty of Electrical Engineering and
Computer Science, University of Maribor, Koroška cesta 46, 2000
Maribor, Slovenia

³Laboratory of Organic Matter Physics, University of Nova Gorica,
Vipavska 13, 5000 Nova Gorica, Slovenia

⁴Chang Gung University, Department of Chemical and Materials
Engineering, Kweishan, Taoyuan 33302, Taiwan

Abstract - Present work describes a novel polymer based nanocomposite anionic exchange membranes (AEMs) with improved features for direct alkaline fuel cell applications. AEMs based on chitosan (CS), magnesium hydroxide (Mg(OH)₂) and graphene oxide (GO) with benzyltrimethylammonium hydroxide (BTMAC), as the hydroxide conductor, were fabricated by a solvent casting method. To impart better mechanical properties and suppressed swelling, the enzymatic cross-linking with dodecyl 3,4,5 - trihydroxybenzoate (DTHB) having C-10 alkyl chain was employed. Structure and surface morphology, KOH uptake and swelling ratio, ethanol permeability, mechanical property, ionic conductivity, cell performance and stability of AEMs were investigated.

Index Terms - Alkaline ethanol fuel cell, anionic exchange membrane, chitosan, graphene oxide.

I. INTRODUCTION

Search for technical advances and optimal solutions in the field of energy, ranging from designing new power sources to securing its financial viability and environmental conformability, has been at the forefront of scientific and applied endeavors for several of years now. To a large extent, this has been driven by an increased demand for energy in

combination with concerns over the environmental status of existing solutions. Anion exchange membrane fuel cells (AEMFCs) have recently received increasing attention since in principle they enable a reduced fuel crossover, improved water management, and the use of a wide range of fuels. The demand for cost effective and eco-friendly polymer electrolyte-based membrane from renewable sources are being rapidly promoted and becoming a promising substitute for synthetic polymers. In this work, chitosan CS-Mg(OH)₂ nanocomposite membranes that act as a solid electrolyte for direct ethanol alkaline fuel cells (DEAFCs) were investigated. To improve membranes' properties, graphene oxide and benzyltrimethylammonium hydroxide were dispersed in a CS-Mg(OH)₂ matrix, and thin films were prepared using a solution-casting method. In the end, membranes were cross-linked with dodecyl 3,4,5 - trihydroxybenzoate using laccase *Trametes Versicolor* as catalyst.

II. RESULTS AND DISCUSSION

IR spectroscopy was used as a bulk technique in order to characterize the reaction mechanisms of oxidized DTHB and to

distinguish chemical bonds present in all of the membrane samples. For CS+Mg membrane and all others, absorption peaks observed between 3000 and 3700 cm^{-1} are ascribed to the stretching vibration of O-H and N-H groups primary from CS and also from GO, BTMAC and DTHB (Fig. 1).

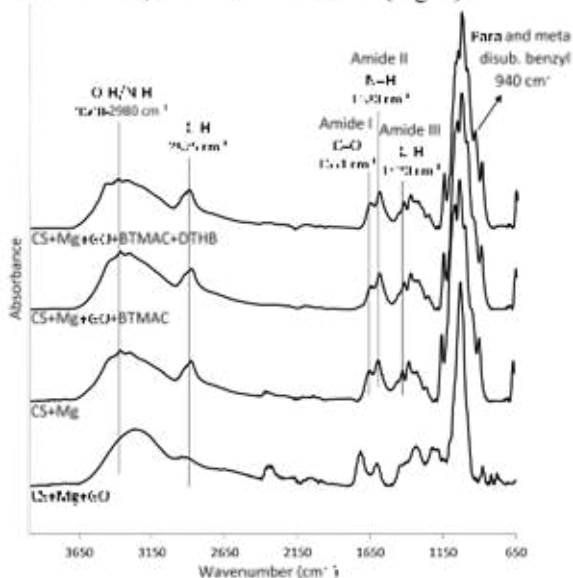


Fig. 1. ATR-FTIR spectra of chitosan (1 wt.%) membranes loaded with 12.6 mM $\text{Mg}(\text{OH})_2$, GO (0.01 wt.%), BTMAC (0.01 wt.%) and cross-linked membrane with DTHB (6 wt.%).

The spectrum of CS+Mg+GO+BTMAC after the cross-linking with oxidized DTHB has a new triplet splitting at wavenumbers of 1081, 1075 and 1057 cm^{-1} , which is compatible with the new C-O stretching vibration, indicating the polymerization between DTHB molecules, and the formation of new phenolic C-C linkages between DTHB and BTMAC.

Uptake of KOH and associated swelling degree, as reflected in resulting dimensional changes of the membranes, were determined as shown in Fig. 2. The highest swelling degree was found for CS+Mg+GO+BTMAC membrane, which can be attributed to the BTMAC presence. After the cross-linking with DTHB, membrane swelling decreased, being expected due to the consumption of the -OH and - NH_2 groups.

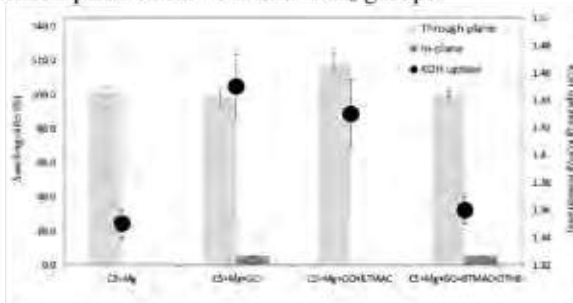


Fig. 2. KOH uptake and swelling ratios of CS (1 wt.%) membranes loaded with 12.6 mM $\text{Mg}(\text{OH})_2$, GO (0.01 wt.%), BTMAC (0.01 wt.%) and cross-linked membrane with DTHB (6 wt.%).

Permeability of fuel is one of the critical issues to consider when designing efficient membranes. High ethanol permeability does not only result in a decrease in power density and diminished fuel utilization in DEAFs, but also reduces electrocatalytic activity of the cathode catalysts due to the compromising of the catalysts performance. The ethanol permeability at 25°C with 2 M ethanol in 6 M KOH solution of the different prepared CS+Mg based membranes are shown in Table I. All membranes permeability values are lower compared to the well-known synthetic Nafion® 117 membranes, ranging from $4.5 \times 10^{-6} \text{ cm}^2 \text{ s}^{-1}$ to $9.2 \times 10^{-6} \text{ cm}^2 \text{ s}^{-1}$, and therefore, suitable for DEAFs application.

TABLE I
ETHANOL PERMEABILITY

Membrane sample	Ethanol permeability ($\text{cm}^2 \text{ s}^{-1}$)
CS+Mg	$4.74 \times 10^{-7} \pm 1.19 \times 10^{-7}$
CS+Mg+GO	$2.51 \times 10^{-7} \pm 3.39 \times 10^{-8}$
CS+Mg+GO+BTMAC	$6.17 \times 10^{-7} \pm 1.17 \times 10^{-7}$
CS+Mg+GO+BTMAC+DTHB	$4.52 \times 10^{-7} \pm 5.47 \times 10^{-8}$

The average peak power density data using the membranes are summarized in Table II. The CS+Mg sample resulted in the highest peak power density value of 72.7 mW cm^{-2} (at 209 mA cm^{-2}) at 80 °C. This is the highest reported power density value for chitosan based membranes. The CS+Mg+GO+BTMAC sample generated peak power densities of 71.3 mW cm^{-2} at 80 °C, similar to the CS+Mg values. The CS+Mg+GO+BTMAC+DTHB generated the lowest power.

TABLE II
DEAFC PEAK POWER DENSITIES (P_{MAX}) AT 80 °C USING CHITOSAN BASED MEMBRANES (OPERATED FOR 60 HOURS)

Membrane sample	P_{max} (mW cm^{-2}) at 80 °C
CS+Mg	69.4 ± 4.7
CS+Mg+GO	57.6 ± 3.7
CS+Mg+GO+BTMAC	68.6 ± 3.9
CS+Mg+GO+BTMAC+DTHB	51.3 ± 1.4

III. CONCLUSION

In conclusion, this study demonstrates that the developed novel CS+Mg membrane systems meet the benchmark of contemporarily applied membrane technology.

ACKNOWLEDGMENT

The authors would like to acknowledge the financial support received in the frame of M-era.NET program (NanoEIEem - Designing new renewable nano-structured electrode and membrane materials for direct alkaline ethanol fuel cell - <http://nanoelmem.fs.um.si/>, grant number C3330-17-500098).

ARTIFICIAL NEURAL NETWORKS FOR AUTOMATIC DETECTION AND CLASSIFICATION OF FUNCTIONAL DEFECTS IN MULTILAYERED SOLID OXIDE MEMBRANES

A. Litke and R. Höpener

HaikuTech Europe BV, Spoorweglaan 16
6221BS, Maastricht, The Netherlands

Abstract – A novel Automatic Optical Inspection systems was developed for real-time quality control of solid oxide half-cells. The system utilizes custom Artificial Neural Network for detection and classification of surface and subsurface features present on solid oxide cells in green or fired state. The developed system provides a comprehensive overview of detected (non)functional defects, their type, size, and location present on high-resolution digital images. The system is designed for quality control at all stages of product development including research, prototyping, upscaling, and mass production of solid oxide (half-)cells or other flat ceramic, polymeric, or composite cells or membranes.

Index Terms – artificial intelligence, multilayer ceramics, optical inspection, quality control

I. NOMENCLATURE

Artificial Intelligence (AI), artificial neural networks (ANN), automatic optical inspection (AOI), central processing unit (CPU), floating point operations per second (FLOPS, 1 TFLOPS is 1 billion FLOPS), graphical processing unit (GPU), megapixel (MP), Quality Control (QC), Quality Assurance (QA).

II. INTRODUCTION

High cost per kW power of solid oxide cell (SOC) stacks hinders their implementation for large scale energy conversion and storage. Production of SOCs makes up a significant part of the final price of SOFC or SOEC installation. These costs can be substantially reduced through automation of the main production steps and quality control routines. Optical inspection is widely used for QC of ceramic (half-)products to eliminate items with functional defects, which can compromise efficiency and stability of the SOC systems, from the production cycle. This tedious work is often performed by

human operators who rely on their experience to distinguish various functional defects from each other. However, it is practically impossible to programmatically describe all small differences, which humans use to tell apart individual features of interest. This results in relatively low detection accuracy and large number of false-positives for AOI systems based on standard image processing libraries.

The situation started changing only with the recent advancements of AANs for image classification and object detection. An ANN can learn to detect very complex objects in digital images through supervised deep learning. The resulting trained ANN has a human-like perception of high-level visual features and can reliably detect and localize multiple objects with super-human speed and high reproducibility.

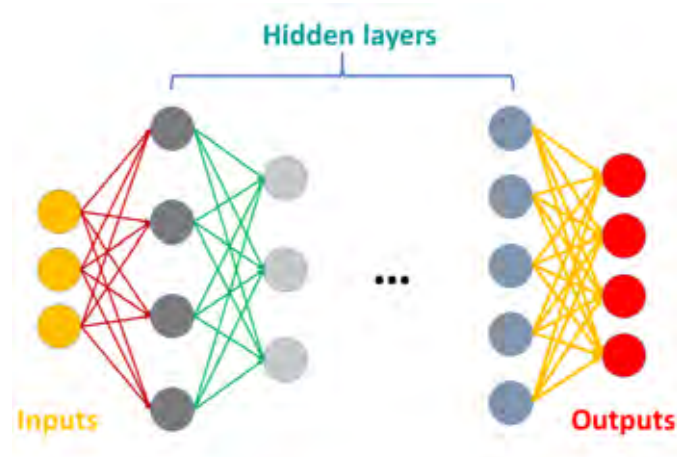


Fig. 1. An illustration of an artificial neural network. Left to right: data inputs, hidden layers, data outputs, and data outputs (object class in the case of an image classifier)

III. AI FOR CERAMIC CELL INSPECTION

Stability and reliability of SOC installation depends on performance of every individual cell. QA of mass-produced ceramic cells requires 100% inspection of every product within a short machine cycle. AOI systems, which are commonly deployed for this task, have optical resolution of 15-20 μm per pixel which renders objects smaller than 50-80 μm undetectable. Even this relatively low resolution generates large amounts of data per sample which can be rather challenging for CPU-bound algorithms to process during a short machine cycle. Unlike CPU, hardware accelerators (such as GPUs) are much better suited for parallel processing of large amount of visual data. Such accelerators can be used to deploy trained ANNs for feature extraction and object classification in high resolution digital images in real time. Detection speed and accuracy of such an ANN-based system substantially surpasses those of CPU-bound traditional image processing libraries.

HaikuTech has developed a novel AI-based AOI system for real-time detection and classification of surface and subsurface defects in fired solid oxide half-cells. The system utilizes high-speed line-scan cameras with the resolution of 3.5 μm per pixel. This enables detection of high-contrast features down to 12-20 μm in size. The system is equipped with a custom high-power illumination system which provides very stable and uniform illumination pattern even at high acquisition rates.

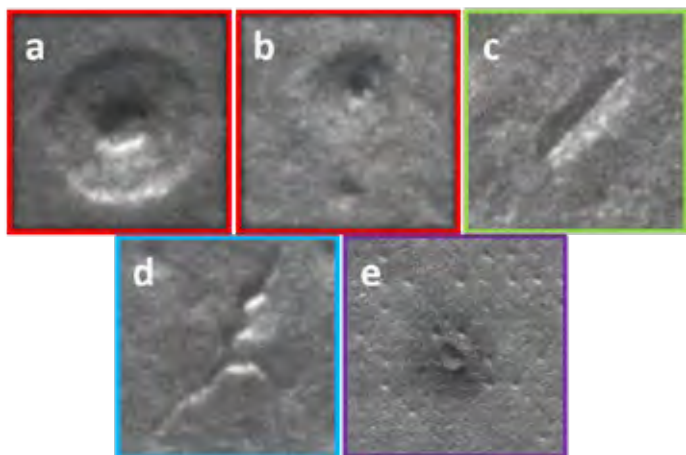


Fig 2. Examples of surface features present in the electrolyte layer of fired SOCs. Functional defects: pinholes (a) holes (b), fiber (c), crack (d), contamination (e). Tiles (a) – (d) have total size of 350 μm ; tile (e) – 1.2 mm.

The AI-based AOI system was designed to recognize and classify 5 types of surface features (Fig. 2) which compromise efficiency and stability of SOCs: pinholes ($\leq 50 \mu\text{m}$), holes ($> 50 \mu\text{m}$), fibers, cracks, and dark spots (contamination). A sufficient number of fired half-cells, containing the aforementioned function defects, were scanned under controlled conditions. The features of interest were labeled on the resulting digital images to yield a training data set.

Some features occur inherently less frequently than the others which can lead to a class imbalance in the training data set. Such an imbalance can result in an ANN which is over-trained for some objects but underperforms with other defects. We have developed a set of data augmentation tools in order to mitigate class imbalance and minimize its impact on the detection accuracy.

The trained ANNs were deployed in a processing unit with ca. 100 TFLOPS of compute power which was incorporated in a standalone AOI system. This prototype system achieved 10.5 s cycle time (excluding sample handling) with 140x140 mm² large samples yielding 1600 MP of visual data per complete scan. Detection accuracy across all categories was found to exceed 83% and up to 93% for some types of defects. Both the accuracy and detection speed can be further improved through hardware and software optimization. An example of the detection results is shown in Fig. 3.

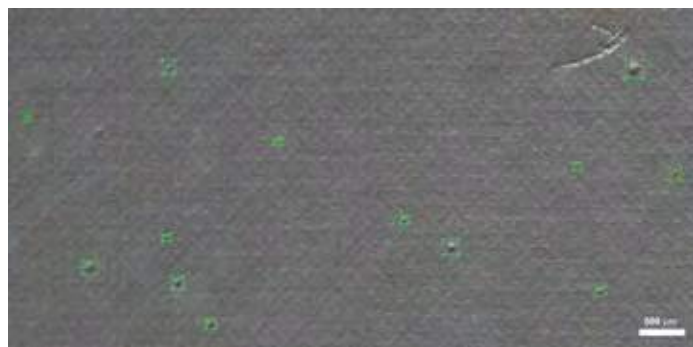


Fig. 3. Example of the detection results returned by a custom ANN after completed training.

IV. CONCLUSION

The results of this work demonstrate that custom ANNs are a robust tool for accurate real-time optical inspection of ceramic layers of fired solid oxide cells. ANNs can learn to extract very complicated high-level features from the images in the course of supervised deep learning. The resulting trained ANNs can be implemented for reliable categorization of features present on inspected material. Moreover, ANNs can discriminate between defects and features which do not have adverse effect on performance of the system which drastically reduces false-positives. Scalability of ANN-based AOI-systems makes them suitable for mass manufacturing where short operation cycles and reliability of detection are a must.

ACKNOWLEDGMENT

We thank our partners at Elcogen A.S. for their support and assistance. This project has received funding from the Fuel Cells and Hydrogen Joint Undertaking under **Grant Agreement No 735160**. This Joint Undertaking receives support from the European Union's Horizon 2020 research and innovation programme and Hydrogen Europe.

SANDVIK SURFACE TECHNOLOGY: MASS MANUFACTURING OF COATED METAL COILS FOR THE RAPID DEVELOPMENT OF FUEL CELLS, ELECTROLYZERS AND BATTERIES.

C. Bernuy-Lopez, S. Proch, U. Bexell, J. Westlinder
 Surface Research, Strategic Research, AB Sandvik Materials
 Technology, 81181 Sandviken, (Sweden)

Abstract – A pre-coated material solution has been developed by Sandvik Materials Technology (SMT) to facilitate fast market development of electrochemical energy conversion, i.e. fuel cells, electrolyzers, and batteries. Our process allows to mass produce essential components of those devices in a very cost-efficient manner. Various metal substrates can be combined with (multi)-(non)metal coatings to an unprecedented range of large volume materials in a coil-to-coil fashion. The Surface Research group at SMT Strategic Research addresses scientific questions like the formation of stable and protective, nonetheless, conductive oxide layers for more than 10,000 h of operation and the development of coatings and substrate compositions for fuel cells, electrolyzers, and batteries alike.

Index Terms – Mass manufacturing, PVD, SOFC, PEM

I. INTRODUCTION

Sandvik Surface Technology is a production unit within AB Sandvik Materials Technology (SMT). The business area SMT belongs to the Sandvik group and is a world-leading manufacturer of advanced stainless steels and special alloys for the most demanding applications.

Sandvik Surface Technology offers a portfolio of cost-effective coated metal strip materials for applications such as batteries, fuel cells, and electrolyzers.

II. PRE-COATED MATERIAL SOLUTION FOR MASS PRODUCTION OF ELECTROCHEMICAL DEVICES

Our roll-to-roll coating lines for mass production present an opportunity for cost-effective large-scale production of coated metal components. Pre-coating reduces the number of production steps compared to (post)-batch coating. Figure 1 shows a schematic of the coating line(s) available in Sandviken (Sweden).

PRE-COATED MATERIAL SOLUTION FROM SANDVIK NANOTECHNOLOGY READY FOR MASS PRODUCTION

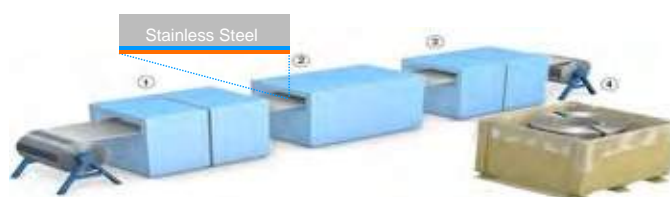


Figure 1. Schematics of the roll-to-roll coating line developed by Sandvik Surface Technology: In-line plasma cleaning/etching (1). Continuous PVD coating process (2). X-ray inspection system (3). Testing, slitting and packaging processes according to customer specifications (4).

A large portfolio of coated materials (Figure 2) can be produced for applications like Solid Oxide Fuel Cells (Sandvik Sanergy™ HT 441), PEM Fuel Cells (Sandvik Sanergy™ LT), and Batteries (Sandvik Santronic™). In addition, tailor-made products with customer-specific substrate and coating combinations are available upon request.

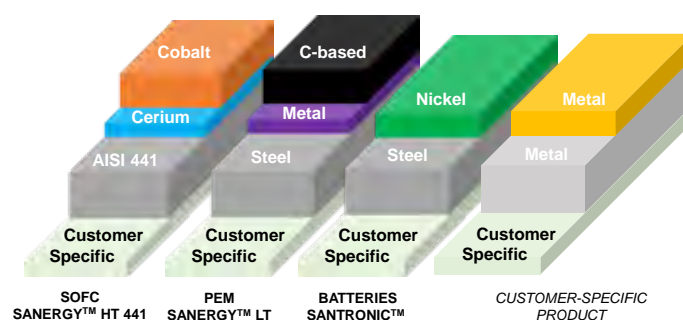


Figure 2. Portfolio of pre-coated materials

Our coatings can be applied to either one or both sides of the substrate whereby the specifications on the two sides can be selected independently, see Figure 3.

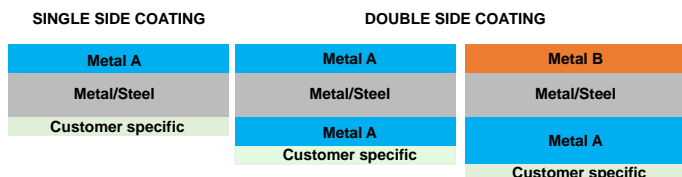


Figure 3. “Endless” Pre-coating Possibilities.

III. SURFACE RESEARCH AT SMT

Our SOFC product, Sandvik Sanergy™ HT 441, is coated with Ce/Co and has been investigated extensively within the past decade. At high temperatures (i.e., above 800 °C) it forms a stable and protective (Co, Mn)₃O₄ spinel by diffusion of Mn from the steel substrate into the coating [1]. However, the current demand in the SOFC market requires operation at temperatures below 650 °C, in this range diffusion of Mn from the steel substrate into the Co coating is much slower and, therefore, the formation of the (Co, Mn)₃O₄ spinel phase does not take place.

In a recent work [2], we have produced a new Ce/Co-Mn coating for temperatures below 650 °C and compared it with the standard Sandvik Sanergy™ HT 441 (Ce/Co coating). When exposed to air at 650°C, both materials form homogenous and dense oxides (Fig. 4), however, with different compositions: Mn_{1.5}Co_{1.5}O₄ spinel for the Ce/Co-Mn coating and Co₃O₄ spinel for our standard coating. In addition, a thin Cr₂O₃ scale is observed in both samples leading to equal performance in terms of area-specific resistance (ASR). Therefore, the addition of Mn to the coating does not seem to be necessary to obtain good Cr retention in the steel and for overall performance.

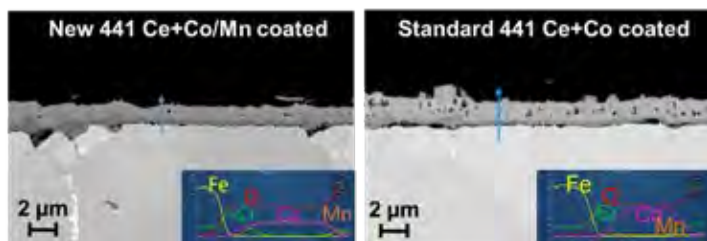


Figure 4. SEM images of cross sections BIB samples and the corresponding EDX lines scans (blue arrow) of the Ce/Co-Mn and the Ce/Co coated material on AISI 441 steel grade after 13,000 h of exposure in air at 650 °C. From [2].

Metallic bipolar plates (BPPs), especially stainless steel, present a cost-efficient solution for low temperature ($T < 100^{\circ}\text{C}$) fuel cells, such as the proton-exchange membrane fuel cell (PEMFC) and the anion-exchange membrane fuel cell

(AEMFC). However, anodic film formation at high positive potentials (approx. +1.5 V vs. RHE) on uncoated metals/stainless steels leads to high interfacial contact resistance (ICR) of the BPP once exposed to such a potential. A potential of +1.5 V vs. RHE is commonly reached under local and global hydrogen starvation, which rules out the use of uncoated metals in low temperature fuel cells.

Recently [3], we investigated the interfacial contact resistance (ICR) change and oxide film formation of several stainless steel grades and Ni-based alloys under simulated AEMFC operating conditions. We found that suppression of anodic (oxide) film formation and, in turn, low ICRs can be achieved by depositing a thin carbon coating. Since carbon is kinetically stable and survives high anodic potentials much longer, unchanged ICR has been recorded even after exposure to aqueous NaOH at high potentials.

REFERENCES

- [1] J. Froitzheim, S. Canovic, M. Nikumaa, R. Sachitanand, L.G. Johansson and J. E. Svensson, Long term study of Cr evaporation and high temperature corrosion behaviour of Co coated ferritic steel for solid oxide fuel cell interconnects. *Journal of Power Sources*, Volume 220, 2012, Page 217.
- [2] Bernuy-Lopez, C., Berger, R., Westlinder, J., Long term stability of a Mn-rich precoated AISI 441 for Solid Oxide Fuel Cell Interconnects at 650 °C in air. *Proceedings of 13th European SOFC & SOE Forum 2018*. B1313. Page 164.
- [3] Proch, S., Stenström, M., Eriksson, L., Andersson, J., Sjöblom, G., Jansson, A., Westlinder, J., Coated stainless steel as bipolar plate material for anion exchange membrane fuel cells (AEMFCs). *International Journal of Hydrogen Energy*. 2019. In Press.

INVESTIGATION OF OPERANDO ACCELERATED STRESS TEST FOR MEA COMPONENTS OF PEM FUEL CELLS

P. Aßmann^a, S. Hoffmann^a, J. Costa de Sousa^a, P. Gazdzicki^a, K.A. Friedrich^{a,b}

^a German Aerospace Center (DLR), 70569 Stuttgart, Germany

^b University of Stuttgart, 70569 Stuttgart, Germany

Accelerated Stress Tests (ASTs) were developed to quantify and investigate the influence of stressors on the different components of the polymer electrolyte membrane fuel cell (PEMFC) using operando and ex-situ methods. Since previous activities have addressed in-situ AST for catalyst layers and membranes [1] our study is focused on the aging of gas diffusion layer (GDL). The results show that under the applied stressors most degradation can be attributed to the CCM. Nevertheless, it was found that the cathode GDL also contributes to degradation under certain conditions. However, aging of GDL seems to be significantly slower than of the CCM. Moreover, there is indication of coupling effects between aged CCM and GDL components; i.e. behavior of aged GDL is sensitive whether it is assembled into an MEA using new or aged CCM.

Index Terms – Accelerated stress test, Degradation mechanisms, Durability, PEM fuel cell

I. INTRODUCTION

PEMFC gain significant momentum in terms of their application in the transport sector. Various properties of PEMFC systems have been successfully improved during the last years such as efficiency, power density, specific power and cold start properties [2]. However, cost and durability requirements have not yet been achieved and become even more challenging when going to very low Pt loadings of the MEA [3]. The required durability of PEMFC for automotive and heavy duty transport applications is 6,000 h and 20,000 h, respectively [4]. Hence, it is obvious that development of new materials and components for PEMFC under normal operation conditions are time consuming and costly. Therefore, the evaluation of PEMFC components needs to be carried out by accelerated testing to significantly reduce cost and time during development of new components.

II. EXPERIMENTAL

A. Characterization Methods

In this work, a study on development and evaluation of the impact of different operando AST protocols on aging of MEA components is presented. The tests are carried out in lab scale cells with 25 cm² and 12 cm² active areas. The investigated stressors are high water flux, high cathode potential, mechanical stress, and excess temperature.

To investigate the performance losses due to degradation, electrochemical characterization methods such as performance curves, electrochemical impedance spectroscopy, and cyclic voltammetry are applied. To discriminate the aging of different components after the ASTs, aged components are electrochemically evaluated in combination with pristine components. Eventually, aged samples are investigated by microscopic and spectroscopic ex-situ techniques.

B. Accelerated Stress Tests

Table I provides various investigated stressors. The stressors are listed in the first column. The second column shows the possible effects that using these stressors has on the PEMFC components. The third column entries explain the possible in-situ tests.

TABLE I
TESTED STRESSORS AS CANDIDATES FOR SPECIFIC ASTs

Stressor	Impact on GDL	Possible In-situ Test
High water flux	Particle erosion loss of carbon / polymer	High load (high water production)
Mechanical stress	Cracks / fiber damage	Temperature and humidity cycling
High electrode potential	Carbon corrosion	OCV or low load
High temperature	Sintering / damaging of polymer	Heating

In this abstract the focus is on high temperature AST and a possible coupling effect of aged components. During this test the cell was kept at 95°C for 219 h at a current density of 1 Acm⁻². The fed gases were humidified at 100% RH; the H₂ and Air stoichiometry were 1.5. The pressure at anode and cathode outlets was kept at 250 kPa_{abs} and 230 kPa_{abs}, respectively. The used MEA was composed of a commercial Pt/C based CCM from Johnson Matthey and a GDL from Freudenberg.

III. RESULTS AND DISCUSSION

The results of the High temperature test are provided here. Figure 1 a) shows an example of the polarization curves measured in the test bench. The blue line represents the polarization curve at the beginning of test (BoT), i.e. with new CCM and new GDL components. Before recording the red end of test (EoT) curve, the cell was refreshed by a shut-down procedure to eliminate reversible degradation effects [5]. After the EoT characterization, the cell was disassembled and the aged GDL and aged CCM were combined with new CCM and new GDL, respectively, to evaluate the impact of the stressor on these individual components. The corresponding polarization curves are provided in Figure 1 a) as well. In this case the black polarization curve represents a new CCM combined with an aged cathode GDL and a new anode GDL. The green line is a combination of an aged CCM and new anode and cathode GDL.

In Figure 1 b) the voltage losses are determined for the different material combinations (see legend). Apparently, combining aged GDL with new CCM leads to only minor voltage loss of -7 mV at 1.6 Acm⁻². This observation suggests that GDL aging is only minor during this test. Combining the aged CCM with a new GDL, on the other hand, leads to a significant voltage loss of -55 mV. Consequently, the data suggest that CCM aging under the high RH conditions occurs faster than GDL aging. However, the sum of the voltage losses due to aged GDL and aged CCM evaluated separately is at -62 mV and therefore clearly lower than the voltage loss observed at EoT (aged CCM and aged GDLs evaluated together). This strongly indicates a coupling effect of CCM and GDL degradation. This means, that the performance of an aged component A (e.g. CCM) is highly sensitive to the state of the other component B (e.g. GDL).

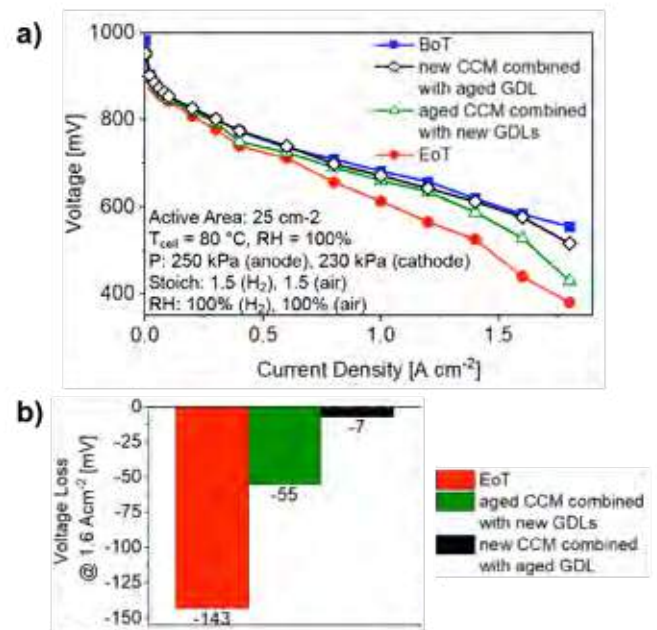


Fig. 1: a) Polarization curves of the high temperature AST under high humidified conditions. b) Voltages losses determined at 1.6 Acm⁻² for aged CCM combined with aged GDL (red) as well as aged CCM combined with new GDL (green) and new CCM combined with aged GDL (black).

IV. CONCLUSION

Generally, our results suggest that the catalyst layer is the major component affected by the applied stressors and most voltage losses can be recovered after replacing the aged CCM by a new one. Nevertheless, it is suggested that high temperature operation leads to GDL aging which, however, is much slower and with lower impact than CCM aging. Moreover, the results indicate a strong coupling effect between aged components.

ACKNOWLEDGMENT

This project has received funding from the Fuel Cells and Hydrogen 2 Joint Undertaking under grant agreement No 779565 (ID-Fast). This Joint Undertaking receives support from the European Union's Horizon 2020 research and innovation program.

REFERENCES

- [1] R. Petrone, D. Hissel, M. C. Péra, D. Chamagne, R. Gouriveau, (2015), Accelerated stress test procedures for PEM fuel cells under actual load constraints: State-of-art and proposals. *International Journal of Hydrogen Energy*, 40 (36), 12489–12505.
- [2] <https://www.energy.gov/eere/fuelcells/doe-technical-targets-polymer-electrolyte-membrane-fuel-cell-components>, 27/09/2019.
- [3] P. Gazdzicki, J. Mitzel, A. M. Dreizler, M. Schulze, K. A. Friedrich, (2018), Impact of Platinum Loading on Performance and Degradation of Polymer Electrolyte Fuel Cell Electrodes Studied in a Rainbow Stack, *Fuel Cells*, 18: 270-278.
- [4] <https://www.fch.europa.eu/page/multi-annual-work-plan>, 27/09/2019.
- [5] P. Gazdzicki, J. Mitzel, D. Garcia Sanchez, M. Schulze, K. A. Friedrich, (2016), Evaluation of reversible and irreversible degradation rates of polymer electrolyte membrane fuel cells tested in automotive conditions, *Journal of Power Sources*, Volume 327, 2016, Pages 86-95.

Electrodes for Reversible and Symmetrical solid oxide fuel cells based on Ruddlesden-Popper perovskites

S. Tomadini*, A. Giraladin*, E. Squizzato*, G. Carollo*, and
A. Glisenti*. **

*Università degli Studi di Padova, Dipartimento di Scienze
Chimiche, Padova, 35131, (Italy)

** CNR-ICMATE, INSTM

Reversible solid oxide fuel cells can be part of the solution to the constant increase of pollution derived from the more and more pressing energy consumption. In the SOFC technology the perovskites are established as good materials both for the electrolyte and for the electrodes. In this work two newly designed Ruddlesden-Popper materials are proposed as cheap alternatives to the state-of-the-art compounds: $\text{La}_{1.2}\text{Sr}_{0.8}\text{Fe}_{0.6}\text{Mn}_{0.4}\text{O}_4$ and $\text{LaSr}_2\text{CrMnO}_7$. The synthesis process was carried out through the Marcilly route; the effect upon the materials of three different calcination atmospheres has been analysed. The characterization has been carried out using different techniques as XRD, H_2 -TPR, XPS, EDX and SEM to evaluate the stability and phase purity of the samples. Lastly, the materials have been analyzed electrochemically using EIS to evaluate their suitability as SOFC electrodes using $\text{La}_{1.2}\text{Sr}_{0.8}\text{Fe}_{0.6}\text{Mn}_{0.4}\text{O}_4$ as the electrolyte.

Green and Sustainable energy, Low Cost new Materials, Reversible SOFC, Ruddlesden-Popper perovskites.

I. INTRODUCTION

Nowadays, the energy consumption and the emission of pollutants are continuously increasing with the fast development of the global economy. Until now, only few steps have been made to push the energy conversion and storage toward a green direction. Fuel cells can be part of the solution to these problems. These electrochemical devices convert chemical energy into electrical power with much greater efficiency and lower emission of greenhouse gases than well-established technologies based on traditional fossil fuel combustion. Moreover, water is the only by-product when hydrogen is the fuel.

A way to reduce costs and to increase the reliability and life span of a SOFC is the creation of a Reversible SOFC in which delamination or poisoning can be minimized.

As an alternative to the most used perovskites-based material

such as Sr doped LaMnO_3 (LSM), in this work two new Ruddlesden-Popper phase materials will be presented. These materials are characterized by blocks of perovskite alternated by layers of rock salt phase and their formula can be written as $\text{A}_{n+1}\text{B}_n\text{O}_{3n+1}$. Over the standard perovskites this new phase possesses a better ionic conductivity and mobility, making it suitable for SOFC applications. Therefore, this work will be focused on the study of two new low cost and good performing electrode materials for a reversible and symmetrical solid oxide cell, using Ruddlesden-Popper (RP) perovskites.

II. EXPERIMENT PROCEDURE

A. Synthesis

$\text{La}_{1.2}\text{Sr}_{0.8}\text{Fe}_{0.6}\text{Mn}_{0.4}\text{O}_4$ and $\text{LaSr}_2\text{CrMnO}_7$ powders were synthesized by citrate route.^[1] Stoichiometric quantities of La_2O_3 , SrCO_3 , $\text{C}_4\text{H}_6\text{MnO}_4 \cdot 4\text{H}_2\text{O}$ and Fe (or $\text{CrN}_3\text{O}_9 \cdot 9\text{H}_2\text{O}$, to obtain the second material) were dissolved in deionized water with nitric acid. Citric acid ($\text{C}_6\text{H}_8\text{O}_7$ Sigma-Aldrich $\geq 99.0\%$) is added as complexing agent under stirring and then the solution is lead to neutral pH by dropwise addition of ammonia hydroxide. At pH 7 the stirring was stopped, and the solution was heated to eliminate water and to induce the formation of a gel phase. The gel was heated to 400°C , to obtain the powders that were subsequently calcinated at 1150°C for 6 hours. The calcination has been carried out in three atmospheres (hydrogen, argon and air) to test the behavior of the materials under different synthesis conditions.

B. Material Chemical and Physical characterization:

XRD diffractograms confirmed that the target phase was achieved for both the materials in all the used calcination atmospheres. However, the phase purity was higher when hydrogen was supplied. The comparison between different

batches showed a good reproducibility of the synthesis method. The TPR analysis has highlighted the presence, beside Mn(III)/Mn(IV), of some interesting impurities in the RP-LSFM sample such as a γ -FeMnO₃ sub-phase. Moreover, for the RP-LSCM the presence of Cr⁶⁺ was detected, possibly due to the exposure to air of the calcined sample. In fact, the relative amount of Cr(VI)/Cr(IV) does not depend on the calcination atmosphere. For both the materials, the oxidizing atmosphere led to lots of impurities. The XPS semi-quantitative analysis showed the segregation of La and Cr in the RP-LSCM sample. The Cr segregation is particularly interesting due to the fact that it is dependent on the atmosphere of calcination: in H₂ and Ar environments, there is a modest and comparable quantity of Cr, both in the form of Cr⁴⁺ and Cr⁶⁺. In air, however, this quantity arises, possibly due to segregation effects. In the RP-LSFM the elements that segregate on the surface are La and Mn.

EDX analysis of RP-LSCM suggests that the quantity of lanthanum is higher than expectations while chromium and manganese's value is lower than the nominal. This behaviour is independent on atmosphere suggesting that surface segregation phenomena are not relevant. Instead, it is possible that structural defects may contribute: they can be related to some intrusions of agglomerates inside the rock-salt layers, typically the less stable and most stress-accumulated parts of the structure. For what concerns the RP-LSFM, instead, the compositions are in good agreement with the expected values apart from the sample calcined in air.

For both the materials SEM images have shown a flake-like morphology with a good porosity, confirmed by BET analysis.

The determined surface area is in good correspondence with typical perovskite values in literature. (RP-LSCM_{H₂}: 2.1 ± 0.1 m²·g⁻¹, RP-LSFM_{H₂}: 8.9 ± 0.1 m²·g⁻¹)

C. Electrochemical characterization results:

RP-LSFM/LSGM/RP-LSFM: to verify the electrochemical behavior of RP-LSFM, a study under anode conditions has been performed (Fig.1). The measurements were carried out at steady state condition (zero DC current) in the frequency range of 10⁻² - 10⁶ Hz and with signal amplitude of 20 mV. At 800°C, with a wet hydrogen flux (10% H₂ in Ar) the impedance spectra show two semicircles. Their frequencies and capacitances allowed to identify the processes involved: a charge transfer reaction (1·10⁴ Hz) and a polarization due to the hydrogen oxidation reaction (2.5 Hz). The same measurements were done with a dry flux, to study if the different atmosphere could led to other processes. The results highlighted the born of a new process at 0.04 Hz, that was related to a reduction of the material (driven by the reducing atmosphere), that induce the oxygen ions diffusion from the bulk to the surface of the material.^[2]

RP-LSCM/LSGM/RP-LSCM: the behavior of RP-LSCM has been analyzed using different hydrogen percentage. The impedance spectra showed the presence of two processes linked with adsorption of the hydrogen on the electrode surface active sites, at high frequencies (kHz) and to the polarization due to

the hydrogen oxidation reaction at low frequencies (at around 0.7 Hz). The results highlighted a worsening of the first process suggesting a change in the chemical equilibrium between the surface and its surrounding: in principle a reductive atmosphere is expected to decrease the number of sites active for hydrogen adsorption, with consequent worsening of the process. The second process instead, benefits from the change in the hydrogen amount, due to the higher amount of reagents provided.

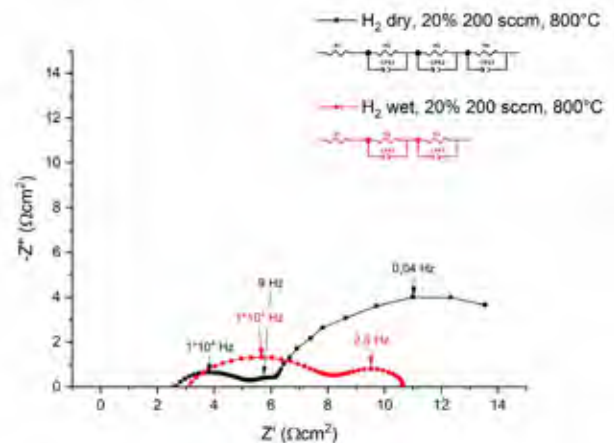


Fig. 1. Nyquist plots obtained with wet and dry hydrogen fluxes using RP-LSFM as the electrode material. The process that arises in the dry flux has been related to a reduction process of the electrode material.

III. CONCLUSION

In this work, two low cost Ruddlesden-Popper perovskites (La_{1.2}Sr_{0.8}Fe_{0.6}Mn_{0.4}O₄ and LaSr₂CrMnO₇) were synthesized and studied to understand their properties and performances as implied in R-SOFCs. These novel materials have been properly stabilized and a successful synthesis route is proposed.

EIS analysis have been performed, leading to an understanding on the processes involved for both the materials. The preliminary results for the RP-LSFM are very promising, even if the performances recorded are lower than the more costly state of the art materials.

All steps of device realization have been investigated and improved to increase adhesion and reduce electrode resistance (ink composition, thermal treatment, etc.). Further work is underway to optimize the performance of both materials.

REFERENCES

- [1] C. Marcilly, P. Courty, and B. Delmon, "Preparation of highly dispersed mixed oxides and oxide solid solutions," *J. Am. Ceram. Soc.*, vol. 53, no. 1, p. 56, 1970.
- [2] B. Mirfakhraei, S. Paulson, V. Thangadurai, and V. Birss, "Enhanced hydrogen oxidation activity and H₂S tolerance of Ni-infiltrated ceria solid oxide fuel cell anodes," vol. 243, pp. 95–101, 2013.

TOWARDS STABLE AND LOW-PGM FUEL CELL CATHODE WITH HIERARCHICAL NANOSTRUCTURED THIN FILM AS NON-CARBON SUPPORT

G. Rossetti^{a,b}, A. Perego^{a,b}, D. Iadicicco^a, A. Casalegno^b and F. Di Fonzo^a

^a Center for Nano Science and Technology @PoliMi, Istituto Italiano di Tecnologia, via G.Pascoli 70/3, 20133 Milano (IT)

^b Energy department, Politecnico di Milano, via Lambruschini 4, 20133 Milano (IT)

Abstract – In this dissertation, the recent progresses on the manufacturing of highly durable ($\approx 10\%$ ECSA loss after 5k support accelerated stress tests^[1]) titanium nitride (TiN), as non-carbon cathodic support, are presented. This new material deposited by pulsed laser deposition (PLD), showed high nitrogen content (45,5%) and increased crystallite size (18,8 nm). Furthermore, preliminary studies on a modified atomic layer deposition process, to reduce the platinum loading are o presented.

Index Terms – durability, low PGM, non-carbon support, PEM FC.

I. INTRODUCTION

Fuel Cell technology, especially for automotive applications, is on the brink of large-scale commercialization. However, some challenges still need to be solved. First, the price needs to be reduced in order to compete with traditional internal combustion engines. The research is focusing on reducing the loading of platinum catalyst or replacing platinum group metals (PGM) catalysts with earth abundant materials. Second, the durability of these devices needs to be increased. Here the main research fields are non-carbon support, increase of the durability of carbon or decrease the conditions where carbon corrosion happens. Perego et al^[1], demonstrated the high durability of a NSTF of titanium nitride (TiN, Fig 1), as cathodic support for platinum. During support accelerated stress test (AST: cycling between 1-1,5 V at a scan rate of 0,5 V/s), it showed less than 10% decrease of electrochemical active surface area (ECSA) after 5000 cycles, where the American Department of Energy (DOE) set the target of an ECSA decrease $<40\%$ for 2020. Furthermore, the support showed less than 15% ECSA decrease even after 15000 cycles. However, the MEA performances, showed poor performances with two main problems in the activation drop and in the electrical resistivity. While the activation drop can be attributed to the non-complete and non-uniform coverage of the whole structure by platinum; the high resistance can be attributed to the low content of nitrogen and low crystallinity^[2,3].

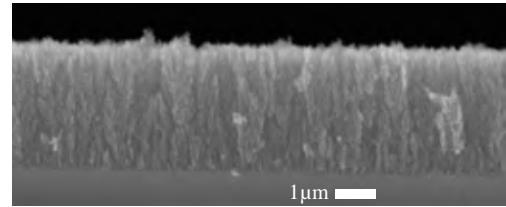


Fig. 1. SEM image of a porous NSTF of TiN .

II. MATERIALS

A. Titanium nitride support

The NSTF is deposited by pulsed laser deposition (PLD). This technique is a physical vapor deposition method. The choice of target and operational gas is based on the necessity to have a porous film with high nitrogen content. Different studies are present where the decrease in nitrogen amount and crystallinity is related to the increase in structure porosity^[4,5]. Furthermore, a porous film leads to a relaxation of the structure, leading to a higher adsorption of oxygen and formation of low conducting TiO_xN_y . For these reasons a pure TiN target and an operational gas with a reducing agent are chosen to increase the N content. Firstly, hydrogen was used as reducing agent for the oxygen in the reacting chamber. However, the resulting material showed still sub stoichiometric nitrogen content and low crystallinity. Therefore, hydrogen is replaced by NH_3 . Ammonia is widely used as nitration agent and for these reasons it should be able to both reduce the oxygen amount in the reacting plume and increase the nitrogen. The gas used for this work is a 5% mixture of ammonia in nitrogen at a pressure of 35 Pa to achieve a porous structure.

The evaluation of the progresses in composition and structure is done by Raman spectroscopy and X-Ray diffractometry.

B. Low platinum loading catalyst

Platinum is well-known to be the best catalyst for ORR. However, in order to decrease the loading while increasing the activity the thinnest possible Pt layer should be deposited onto

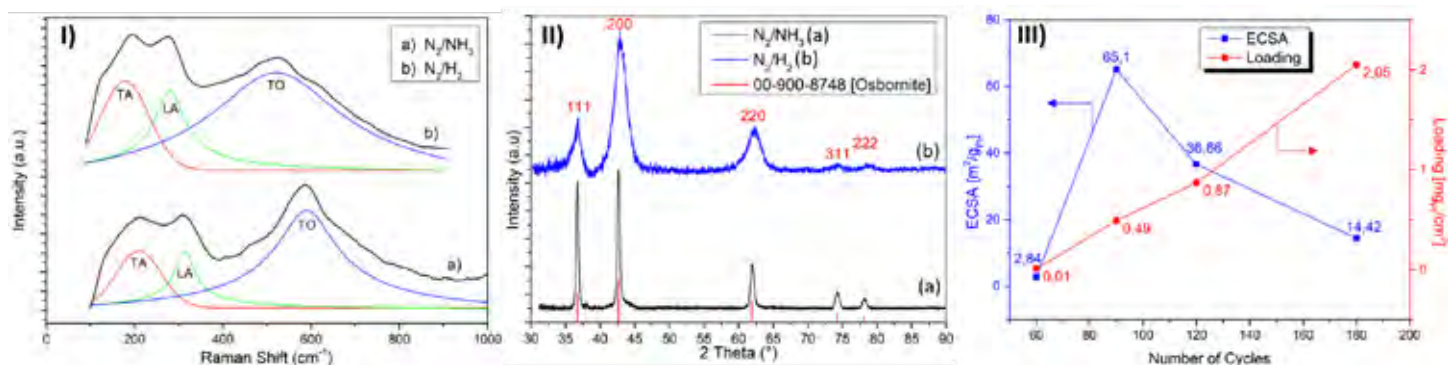


Fig. 2: I. Comparison of the Raman spectra; II. Comparison of the XRD spectra; III. Characterization of the ALD platinum films, by surface area and loading.

the whole structure. Electrochemical deposition, magnetron sputtering, and continuous flow atomic layer deposition (ALD) were able to cover only 2 of the 5 microns of the TiN NSTF [1]. For these reasons a custom stop flow thermal ALD is used.

Since the final goal is to deposit a single and continuous layer of Pt, a preliminary study is done to detect the minimum number of cycles needed to have a uniform nucleation.

(Trimethyl)methyl-cyclopentadienyl-platinum (IV), is widely used as platinum precursor in thermal ALD. However, as second precursor, O₂ is preferred to more active O₃ or O- considering the tendency of TiN to adsorb/react with active oxygen species.

The deposited films are electrochemically characterized by a three-electrodes setup, to detect the ECSA and by XRD to detect the structure and composition of the film.

III. CHARACTERIZATION

A. Titanium nitride support

TiN is well known to be a material with many defects in its structure, reason why it adsorbs oxygen from the atmosphere. Therefore, Raman spectroscopy can detect the change in defects due to a sub stoichiometric TiN [6]. In Fig. 2-I, there is an overall decrease in the first order acoustic peaks (TA-LA). These peaks arise from the vibration of Ti atom in presence of N vacancies. Therefore, a decrease in intensity can be attributed to a lower amount of N-vacancies. Moreover, the transverse optical (TO) vibration is related to Ti-N and so its increase in intensity can be ascribed to the higher amount of nitrogen.

These observations are confirmed by XRD analysis. The first thing that can be observed is a greater sharpness of all the peaks and a better agreement with reference osbornite. A general increase in crystallite size is also calculated by Scherrer's equation from 8 to **18,8 nm** (± 4). Furthermore, the difference between the calculated lattice parameter ($a=0,423$ nm) and that of a stoichiometric reference, is related to the increase or decrease in nitrogen content [8]. Therefore, by combining Bragg's law, d-spacing equation for a cubic structure and the empirical equation in literature, it is possible to confirm the increase of nitrogen content, also noted in Raman analysis, from 35,4 to **45,5 %** (± 1).

B. Low platinum loading catalyst

As already said, the main goal of this preliminary section is to discover the exact number of cycles where the formation of a continuous layer is achieved. In figure 2-III the number of cycles is plotted against the loading and the ECSA. Before 60 cycles no relevant deposition has been noted both electrochemically and by XRD, where no Pt peak was detected. This initial delay is characteristic of oxygen-based processes. Afterwards, the nucleation starts randomly onto the substrate and increasing the number of cycles, the dimension of these nanometric nuclei increases until they merge into a uniform coating. At 60 cycles an ultra-low loading is achieved with low ECSA as well. By XRD, no platinum was detected. The reason is that there is the formation of nanoclusters, that can be hardly detected electrochemically. If the number of cycles is increased to 90, there is a huge increase in loading, grain size (2,31 nm) and ECSA, meaning that we achieved a uniform layer of platinum or more. Then, as expected, increasing even more the cycles there is an increase in loading and grain size (5,12 nm) with a decrease in ECSA, meaning that there is a general smoothing of the support surface area.

IV. CONCLUSION

In this study, structure and composition of a highly durable TiN NSTF support for the PEM FC cathode [1], are improved. By changing the reducing gas to NH₃ in the PLD process, it was possible to achieve 45,5 % of nitrogen content (+10%) and great crystallite size (18,8 nm). Furthermore, a thermal ALD process showed the potential to completely cover the porous structure. Further studies are required to optimize the deposition of an ultra-low loading Pt film with high ECSA.

REFERENCES

- [1] Perego et al, ACS Appl. Energy Mater. 2019, 2, 1911–1922
- [2] N.K. Ponom et al, Thin Solid Films 578 (2015) 31–37
- [3] R. Chowdhury et al, J. Mater. Res., Vol. 11, No. 6, Jun 1996
- [4] Alessio Perrone 2002 Jpn. J. Appl. Phys. 41 2163
- [5] Bulletin of Alloy Phase Diagrams Vol. 8 No. 4 1987
- [6] J. Mater. Res., Vol. 11, No. 6, Jun 1996
- [7] Bulletin of Alloy Phase Diagrams Vol. 8 No. 4 1987

INFLUENCE OF SPINEL PROTECTIVE COATING ON CROFER INTERCONNECTS CONDUCTIVITY

P. Coquoz, D. Correia, F. Morand and R. Ihringer
Fiaxell Sàrl, EPFL Innovation Park, PSE A, 1015 Lausanne,
(Switzerland)

Abstract - Conductivity of interconnects has been measured in function of different parameters. Two ferritic stainless steel grades were used, Crofer 22H and 22APU. Two different spinel compositions were deposited, CuMn_2O_4 and $\text{Cu}_{1.35}\text{Mn}_{1.65}\text{O}_4$. Their thicknesses were varied from 4 to 16 μm to observe the influence on conductivity and its evolution over time. Measurements were done with direct contact between spinel coatings or by interposing an electrode material. For this purpose, LSC ($\text{La}_{0.5}\text{Sr}_{0.5}\text{CoO}_3$) or LSCF ($\text{La}_{0.6}\text{Sr}_{0.4}\text{Co}_{0.2}\text{Fe}_{0.8}\text{O}_3$) were directly screen printed on the spinel layer. All these different layers ($\text{Cu}_x\text{Mn}_y\text{O}_4$, LSC, LSCF) were deposited on small Crofer coupons (40x20x0.3 mm) and M_grid™. Experiments were performed under oxidizing atmosphere at 800°C under air flow during hundreds of hours. Several thermal cycles were done to assess the stability of the coatings.

Index Terms – Coating, Crofer, Interconnect, Spinel

I. INTRODUCTION

In the SOFC/SOEC industry, interconnects and their protective layer are a critical factor in the long term stack performances. The use of conductive and robust material is a necessity for stack performance and durability, which brought the development of alloys such as Crofer 22 APU and 22H. However due these alloys composition, chromium poisoning of the cathode causes a significant decrease of the cells performances. A coating is then essential to prevent chromium evaporation on the air electrode of the cells. In this article copper-manganese spinel coatings were studied, the influence on the conductivity of parameters such as layer thickness, temperature and contact material were investigated.

II. DESIGN OF EXPERIEMENTS

Two ferritic stainless steel grades were used, Crofer 22H and 22APU. The copper-manganese coatings were tested on small coupons (4x2 cm, 0.3 or 2 mm thickness), on the new

generation of 22APU M_Grid™ (Figure 1) and on Cell-Connex™, used for stack interconnects. Two different spinel compositions were tested, CuMn_2O_4 and $\text{Cu}_{1.35}\text{Mn}_{1.65}\text{O}_4$ in regards of the studied literature [1]. The thickness of the coating, measured with optical microscope varied from 4 to 16 μm .

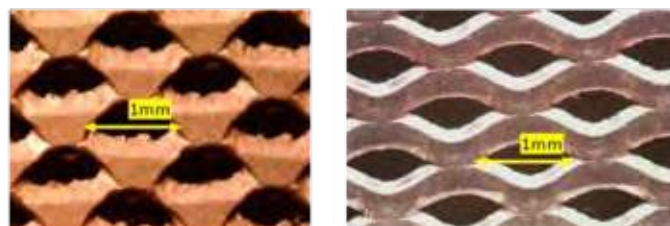


Fig. 1. Left: First generation of Crofer 22H M_Grid™ with CuMn_2O_4 coating (25% of contact surface area). Right: New generation of Crofer 22APU M_Grid™, more flexible and with up to 44 % of contact surface area.

The coatings were deposited on the samples by spraying, the former were then heat treated at 850°C for 3 hours under air. Some of the samples were treated under reducing atmosphere (92% N_2 , 8% H_2) at 900 °C for 4 hours, as treatment under reducing atmosphere has shown to achieve higher coating density than under air [1]. These are noted N_2/H_2 on the graphs.

Measurements were done with direct contact between coated coupon (or 22APU M_Grid™) in a stack. For additional contact layers testing, LSC ($\text{La}_{0.5}\text{Sr}_{0.5}\text{CoO}_3$) or LSCF ($\text{La}_{0.6}\text{Sr}_{0.4}\text{Co}_{0.2}\text{Fe}_{0.8}\text{O}_3$) were directly screen printed (~20 μm thickness) on the Cu-Mn-O_4 coated coupon.

Few other ways of measurements have been investigated with gold sheet or $\text{La}_{0.6}\text{Sr}_{0.4}\text{MnO}_3$ dense pellet and are described in the methods of testing section.

Tested samples and current collector were stacked and

mounted in the Open Flanges Set-Up™ with a defined mechanical pressure (5 kg/cm²) to ensure homogeneous experimental conditions and optimal electrical contact. Experiments were performed under oxidizing atmosphere at 800°C under air flow. Several thermal cycles were done to assess the stability of the coatings. All tests were performed in the range of 1000 hours.

III. RESULTS AND DISCUSSION

A. Preliminary experiments

Different methods of testing were first performed in order to determine which method would be the most reliable for recording the area specific resistance (ASR) of CuMn₂O₄ coatings. Gold sheets were first tested as current collector, but showed unusual behavior (no initial decrease of resistance) that could come from insufficient electrical contact. Testing with coated M_Grid™ and LSM pellet showed erratic behavior. Therefore testing the coatings with small coupons was the preferred method.

Comparative measurements were performed between Crofer 22APU (2 mm thick) and 22H (0.3 mm thick), with the same coating (15 μm, CuMn₂O₄), under current (0.5 A/cm²) and under air flow (200 ml/min). At the beginning both alloys started at similar ASR (about 5 mOhm.cm²), with a downward trend. However after 200 hours the Crofer 22H stops this trend and starts to increase. The coated Crofer 22 APU area specific resistance keeps decreasing up to 600 hours and appears to be stable, at about 1.2 mOhm.cm², until the end of the experiment (1100 hours). The 22APU also showed no increase of resistance under thermal cycling. 22APU coupons were then chosen for the following experiments.

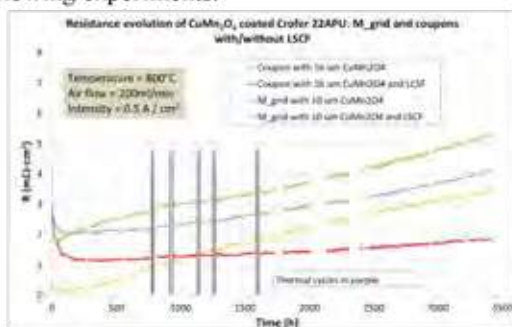


Fig. 2. Figure 10. Evolution of electric resistance over 1000 hours of 22APU coupons (0.3 mm) and 22APU M_Grid™ (0.24 mm) coated with CuMn₂O₄. The thicknesses of coatings are 10 μm for the M_Grid™ and 16 μm for the coupon.

B. Influence of parameters

The parameters studied were the coating thickness (4 to 16 μm), atmosphere for heat treatment (oxidizing or reducing), stoichiometry (Cu_{1.35}Mn_{1.65}O₄ or CuMn₂O₄) and contact material (LSC or LSCF). The 16 μm CuMn₂O₄ coatings prepared under oxidizing atmosphere presented the lowest resistance and were stable after thousands of hours. The

coatings with LSCF contact material were the most stable (fig. 3).

C. 22APU_M_Grid

Figure 2 shows the comparative results of coupons and M_grid (both 22APU). It show coherent behavior as the coupon, at 900 hours ratio of the resistance corresponds to the ratio of the contact surface area (ratio = 1/0.44=2.27). No significant impact of thermal cycles is observed.

IV. CONCLUSION

In this work the area specific resistances of copper-manganese oxide coatings on Crofer steel were studied. Most tested coated coupon and M_Grid™ (both in 22APU) presented a low and stable electrical resistance after 900 hours (and up to 1600 hours for some experiments) to be used with SOFC systems. Figure 3 presents some of the results obtained with additional contact layer of LSCF in order to simulate real interaction of material that are used in SOFC stacks. In this graph (fig. 3), all ASR are below 4 mOhm*cm² and the resistance increase is below 0.5 mΩ*cm²/1000*hours for all the coupon and below 1.2 mΩ*cm²/1000*hours for the 22APU M_Grid™. The 22H coupon and the Cu_{1.35}Mn_{1.65}O₄ coating showed however a significantly higher ASR (4 to 6 times the ASR with 22APU and CuMn₂O₄). A thicker coating (up to 16 μm) showed less resistance and more stability, with some contradictory behavior on test N°5 that will be investigated at the end of the test. LSC additional layer as a contact material presented less stability than LSCF, though only one coating with LSC was tested. Thermo-cycles have been imposed to all tested material and did not show any significant influence on the behavior of the resistance. Further testing will be performed on coupons, M_Grid™ and interconnect pattern, the Cell-Connex™, proposed by Fiaxell.

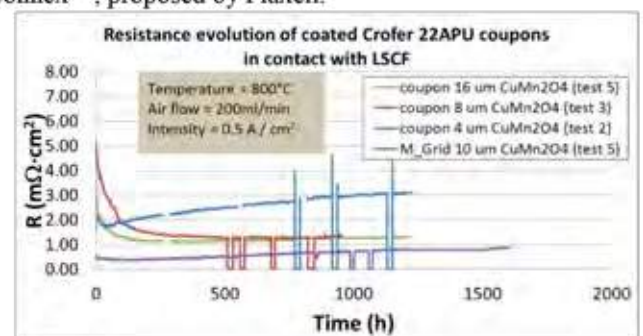


Fig. 3. Evolution of electric resistance over 1000 hours of coated 22APU coupons (0.3 mm) and 22APU M_Grid™ (0.24 mm) in contact with LSCF paste.

REFERENCES

- [1] R. Wang, Z. Sun, Y. Liu, U. B. Pal, S. N. Basu, and S. Gopalan, ECS Trans., 78(1), 1665 (2017).

HIGH TEMPERATURE SYNTHESIS OF TiO₂ NANOPARTICLES AS A CATALYST FOR PHOTOCHEMICAL HYDROGEN GENERATION USING PREMIXED FLAME BURNERS

S. S. HWANG*, and H. Y. LEE*

* Division of Mechanical System Engineering, Incheon National
University, Academy-Ro 119 Songdo-dong, Yeonsu-Gu, Incheon,
22012, (Korea)

Abstract - To produce hydrogen using the photoelectrolysis characteristic of TiO₂ nanoparticles, many previous researches have conducted to generate superiority nanoparticle with flame synthesis method. In this study, we performed experiments to investigate the synthesis characteristics of TiO₂ nanoparticles using the premixed burners. The effects of uniform temperature distribution and the concentration of oxidant in the reaction region on the growth and aggregation of particles were analyzed.

Index Terms – Photoelectrolysis, Hydrogen generation, TiO₂ nanoparticle, Premixed flame synthesis

I. INTRODUCTION

Recently, in order to deal with limitations of fossil fuels, researches on the production of hydrogen as an alternative fuel have been carried out widely. Especially, the production of H₂ by photoelectrolysis from water has been considered as the promising technology in many studies. In 1972, Fujishima and Honda found out the production of hydrogen with the photoelectrochemical decomposition of water under irradiation light using TiO₂ electrode[1]. And Anatase phase is metastable but it especially has the greater photocatalytic activity rather than other phases[2]. Among the synthesis methods of TiO₂ as such photocatalyst, high temperature flame synthesis has been considered effective for mass production of TiO₂ nanoparticles.

In this study, premixed burners were applied for the formation of the uniformly high-temperature zone which can synthesize the high purity TiO₂ nanoparticle. The morphology of captured TiO₂ was analyzed by TEM image, and the crystal structure was analyzed by XRD.

II. EXPERIMENTAL METHOD

The flat surface premixed burner was applied to investigate of the characteristics of the TiO₂ nanoparticles under different

flame conditions. And the inward premixed burner was employed as a prototype which has uniform temperature distribution of the reaction zone for mass production of the TiO₂. As a precursor for the synthesis of TiO₂, TTIP (Titanium IV isopropoxide) was delivered into the premixed flame in a vapor phase. In order to synthesize high-quality TiO₂ nanoparticles, it is necessary to investigate the temperature distribution and oxidant levels in the reaction zone through the combustion experiments.

A. Flat premixed flame

The flat premixed flame stability was compared when the heating value is from 1.5 to 2.5kW and the equivalence ratio is from 0.65 to 1.0. Stable ranges of the surface flame were in the widest equivalence ratio region (0.75 ~ 0.95) at the condition of heating value 1.5 kW. The temperature difference of the reaction zone at 1.5 between 2.5kW is about 60 degrees (°C) and the temperature distribution shows a similar trend at the different positions (burner above height: 10, 30, 50mm).

B. Inward premixed flame

Compared to the flat type, the inward premixed burner has the advantages which are maintaining of uniform temperature distribution and oxidant concentration in the nanoparticle synthesis reaction zone. In the case of inward premixed flame, the heating value and the equivalence ratio are coupled due to the AGM (Air- Gas Mixer) system. It uses the turbo-fan as the air supply therefore it is not available to control the equivalence ratio. So the temperature and the exhaust gas were measured at the stable state. The temperature distribution in the reaction zone formed a similar trend at both heating value 6.0 and 8.0 kW, and the temperature difference is about 50 degrees (°C). The temperature characteristic is not much different from the

flat premixed flame. However, the heating value increases, the equivalent ratio increases with decreasing of excess O_2 .

III. TiO_2 NANO PARTICLE SYNTHESIS

A. Effect of equivalence ratio with flat premixed burner

In Fig. 1 (a), as the equivalence ratio of the flat premixed burner decreases, the length of the synthesis flame length increases and the width narrows.

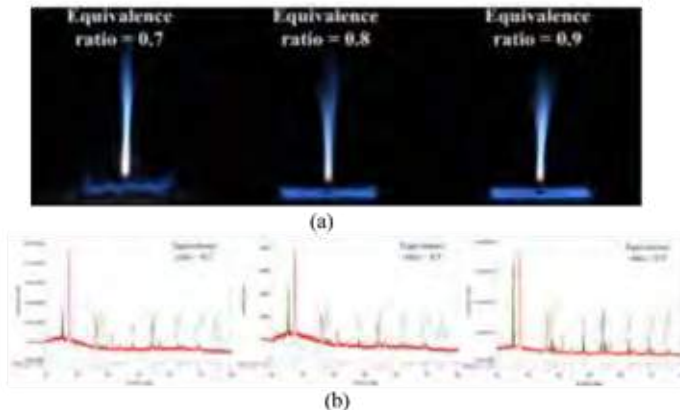


Fig. 1 The synthesis flame(a) and diffraction patterns(b) at the different equivalence ratio.

In the high-equivalent ratio region where the level of oxidant in the reaction zone is lower, the consist ratio of the anatase phase is become higher, as shown in Fig. 1 (b).

B. Synthesis characteristics of inward premixed burner

It is Similar with the flat premixed burner, the shape of the synthesis flame became wider when the equivalent ratio decrease while the heating value increase from 6.0 to 8.0kW. In addition, the flame is brighter than 8.0 kW. However, even though the oxygen concentrations are different in the reaction region, the diffraction patterns are similar and the component ratio of the anatase phase is significantly dominant.

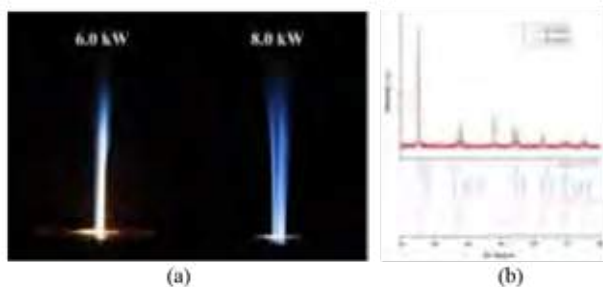


Fig. 2 Images of the inward synthesis flame(a) and XRD data(b)

C. Morphology of the TiO_2 nanoparticle

As shown in Fig. 3, the premixed flame synthesis has an intensive effect of aggregation as the equivalence ratio decreases. And the shape of the primary particles is closer to the sphere and became larger.

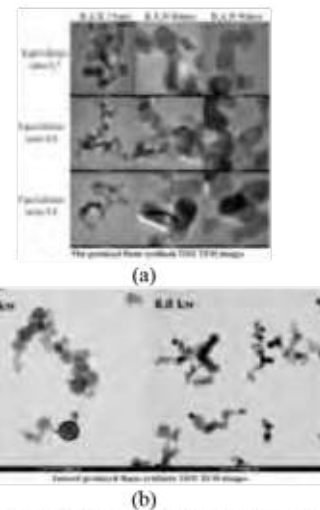


Fig. 8 TEM images at the different equivalence ratio and heating value.

IV. CONCLUSION

In this study, we investigated the effects on the formation of the crystal structure using the premixed burner which can easily control the condition of the synthesis reaction region. It seems that the crystal structure tends to become more the anatase than the rutile phase when the oxygen concentration in the high-temperature oxidation region is lower, through the diffraction patterns of the flat premixed case. It is also found that the size of the primary nanoparticles becomes larger and the morphology tends to be formed in a spherical shape as the equivalence ratio decreases from TEM data. And the morphology of TiO_2 tends to be more aggregative according to the equivalence ratio decreases. In the case of the inward premixed flame, the morphology of the primary particles becomes larger and more spherical since the oxidant level increases with the heating value decreases. And it seems that though the heating value and equivalence ratio are different, the crystal structure of TiO_2 form the anatase phase, as seen the XRD data.

ACKNOWLEDGMENT

This work 2016R1A2B4014853 was supported by Mid-career Researcher Program through NRF grant funded by the MEST.

REFERENCES

- [1] Fujishima, A., Honda, K., Electrochemical Photolysis of Water at a Semiconductor Electrode, Nature, Volume 238, 1972, pages 37-38
- [2] Valencia, S., Marin, J.M., Restrepo, G., Study of the Bandgap of Synthesized Titanium Dioxide Nanoparticles Using the Sol-Gel Method and a Hydrothermal Treatment, The Open Materials Science Journal, Volume 4, 2010, pages 9-14

COMBUSTION SYNTHESIS OF BINARY TiO₂-SiO₂ NANOPARTICLES AS PHOTOCHEMICAL CATALYST FOR HYDROGEN PRODUCTION

S. S. HWANG*, and H. Y. LEE*

* Division of Mechanical System Engineering, Incheon National University, Academy-Ro 119 Songdo-dong, Yeonsu-Gu, Incheon, 22012, (Korea)

Abstract - For producing the hydrogen as a fuel in an environment-friendly way, many researches of the water splitting have been studied with electrolysis, recent years. In particular, Fujishima found out the photocatalytic properties of TiO₂ nanoparticles to generate the H₂ using electrolysis in 1972. In this study, we conducted the experiment of the binary synthesis with the combustion method to improve the poor photocatalytic property of TiO₂, with a SiO₂ nanoparticle. To synthesize the TiO₂-SiO₂ nanoparticle, we applied the inward-type premixed burner and supplied the vaporized precursor mixture to the high-temperature reaction region.

Index Terms – Nanoparticle binary synthesis, Photocatalysis, Inward type premixed flame, Water splitting

I. INTRODUCTION

The hydrogen fuel cells that use hydrogen as fuel can produce electricity by electrochemical reaction and thus have excellent energy conversion and storage properties. The conventional method of producing hydrogen as a fuel has been reforming the common fossil fuel, but recently, it has been shifted to a method of generating H₂ by electrolysis or photocatalysis of water present in nature. The previous studies were conducted to improve the poor photocatalytic property of TiO₂, which is widely known as a key catalyst in the process of hydrogen production by photocatalytic method, using the binary composition with a semiconductor [1,2].

For the formation of nanoparticles, the chemical methods are generally used, and the chemical methods can be divided into a method of wet chemistry and dry processes such as sol-gel and an aerosol flame method. Especially, the aerosol flame synthesis is more beneficial for the mass production of superiority nanoparticles rather than the wet chemistry process. Therefore, many research groups have been studied the aerosol

flame methods for decades.

In this study, we performed the experiment with the flame aerosol method to synthesize binary nanoparticles of TiO₂ and SiO₂. And the effects on the binary nanoparticles using the flame synthesis by the heating value, equivalence ratio of the inward premixed combustor and the mixing ratio of the precursor were investigated.

II. EXPERIMENTAL METHOD

For the formation of TiO₂ nanoparticle as the photocatalyst, TTIP (Titanium IV isopropoxide) was applied as the precursor, and the precursor vaporized by the bubbler. And the gas-phase TTIP was supplied to the reaction region of the premixed burner to synthesize the nanoparticles through the high-temperature oxidation reaction. For the binary synthesis, the vaporized precursor HMDSO (Hexamethyldisiloxane) and TTIP were supplied with mixing simultaneously, as shown Fig. 1,2.

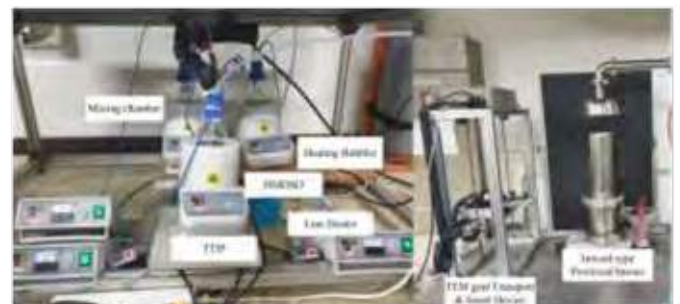


Fig. 1. The experimental equipment for binary synthesis.

In Fig. 1, the inward-type surface premixed burners applied to prepare for a high-temperature condition which has

advantages of the premixed combustion such as an easily control the temperature and the oxidant concentration in the reaction zone. And it is possible to make the reaction region has uniform temperature distribution.

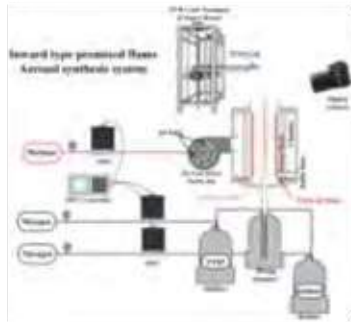


Fig. 2. Schematics of experimental system for binary synthesis.

The binary nanoparticles which were generated by the combustion synthesis method have analyzed some material properties by XRD (X-Ray Diffraction) method and the binding pattern of TiO_2 and SiO_2 through TEM (Transmission Electron Microscopy) image analysis.

III. TiO_2 - SiO_2 BINARY SYNTHESIS

A. Flame characteristics of the binary synthesis

In Fig. 3, the binary synthesis flame tends to be shorter as the composition of the TTIP inside the supplied precursor increases. And the flame turns yellow to blue. It can be seen as the natural trend of the changing from SiO_2 flame to TiO_2 flame.



Fig. 3. Images of the synthesis flame at the different components in precursor.

B. Morphology of the binary synthesis

The TEM image obtained by performing binary synthesis while changing the composition of the precursor is shown in Fig. 4.

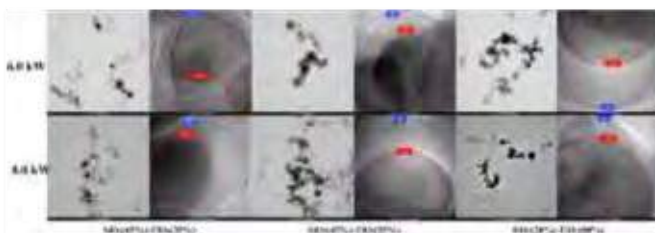


Fig. 4. TEM image at the different conditions.

It is found that SiO_2 nanoparticle surrounds the TiO_2 under all conditions, regardless of the composition ratio inside the precursor.

C. Characteristics of the crystal structure

Through the XRD analysis in Fig. 5, the diffraction patterns tend to shift the crystal structure from rutile to anatase under conditions of increased calorific value.

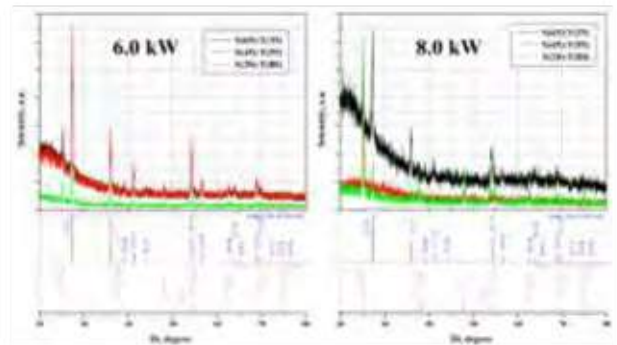


Fig. 5 The diffraction patterns of binary synthesis nanoparticles.

IV. CONCLUSION

It was found that the crystal structure of binary nanoparticles tends to feature more anatase than rutile phase as the heating value is increased and the equivalence ratio of the premixed burners decreased. And, at the higher ratio of TTIP in the precursor mixture, the amorphous structure turned to the crystal structure, and the rutile phase ratio was higher at the heating value of 6 kW and the anatase phase was more dominant at the high heating value of 8 kW.

From this study, combustion synthesis of binary TiO_2 - SiO_2 which has an advantage of mass production and less harmful process compared to sol-gel method can be verified by parametric analysis.

ACKNOWLEDGMENT

This work 2016R1A2B4014853 was supported by Mid-career Researcher Program through NRF grant funded by the MEST.

REFERENCES

- [1] Seiichiro, N., Fujishima, A., Honda, K., Experimental evidence for the hydrogen evolution site in photocatalytic process on Pt/TiO_2 , *Chemical Physics Letters*, Volume 102, 1983, Pages 464-465.
- [2] Kazuya, N., Fujishima, A., TiO_2 photocatalysis: Design and applications, *Journal of Photochemistry and Photobiology C: Photochemistry Reviews*, Volume 13, 2012, Pages 169-189.

Enhancement of Direct Methanol Fuel Cell Performance by Adding SBA-3 Silica Material to Nafion Membrane

Nihat Ozer Ucar*, İlay Gizem Ozbas* Gülce Cakman*, Berker Ficcilar*

*Ondokuz Mayıs University, Department of Chemical Engineering, Kurupelit Campus, Atakum, 55139, Samsun

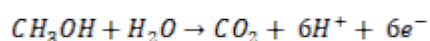
Abstract - Large surface area and pore volume of porous structures increase the importance of these materials day by day. The using of these materials in fuel cells such as Direct Methanol Fuel Cells (DMFC) provides an advantage in enhancing its electrochemical characteristics. DMFC becomes prominent because it does not cause environmental pollution. Otherwise, DMFC has advantage with using liquid fuel and providing portable system like laptop battery.

Increasing the reaction kinetics of DMFC will enable the fuel cell to operate more efficiently. The biggest parameter in increasing this kinetics can be said as temperature. In summary; theoretically, performance and efficiency of the fuel cell will increase at the same time. In this project, SBA-3 silica material will be synthesized under acidic conditions and examined the cell performance by adding 1% and 5% SBA-3 silica material into the perfluorosulfonic acid (Nafion), which is the electrolyte of the DMFC by using dropcasting method. Physical characterisations of silica materials such as SEM, XRD, BET will be performed. At the end of the research, the performance of the fuel cell will be measured by using DC electronic load and compared with pure Nafion electrolyte.

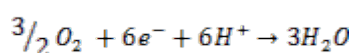
Keywords: Direct Methanol Fuel Cell, SBA-3, Nafion Membrane

I. INTRODUCTION

Methanol has a relatively high volumetric theoretical energy density compared to other systems such as conventional batteries. Thanks to this, it can be used in small portable applications. A direct methanol fuel cell (DMFC) consists of two electrodes are separated by a proton exchange membrane via an external circuit[1]. The direct methanol fuel cell (DMFC) consists of an anode electrode at which methanol is electro-oxidised to CO₂ through the reaction:



and a cathode at which oxygen is reduced to water or steam[2]:



Dupont's Nafion is the polymer electrolyte membrane material most frequently used for this type of application. However the nafion membranes also have several disadvantages such as a decrease in the ionic conductivity and low humidity at high temperatures[3]. Hereby, porous material is good candidate for the polymer membranes because it helps to maintain a suitable hydration of the membrane under fuel cell operating conditions and the mechanical properties are improved.

In this project, SBA-3 silica material investigated in the DMFC by adding 1% and 5% into the Nafion membrane. Fuel cell test performed by using DC electronic load and compared with pure Nafion electrolyte.

II. EXPERIMENTAL

A. Production of SBA-3

SBA-3 was prepared using cetyltrimethylammonium bromide(CTMABr) as a template and TEOS as a Silica source. An aqueous solution of HCl(37%) was added in order to control the pH of the system. 1g of CTMABr, 25mL of water and 10ml of HCl added in 250mL of a beaker. Acidic solution was mixed with vigorous stirring at 30°C for 15 min. 2,5mL of TEOS was added dropping to the acidic solution. After 2 h, the white precipitate was aged at room temperature for 12h. The sample was filtered and dried overnight. After drying it, SBA-3 was calcined at 550°C in air for 5h. The heating rate was 2°C/min.

B. Preparation of SBA-3/Nafion Nanocomposite

A 5% (w/w) Nafion solution was selected to manufacture the film. The original solution was dried at 50°C until obtaining a dry residue, successively diluted in dimethylacetamide as a solvent (10%, w/w, solution). Two different amount of SBA-3 powder (1%, w/w and 5%, w/w) was added and dispersed in an ultrasonic bath. After the casting, the membrane was dried on a hot plate at 80°C, then thermally treated at 155°C. A chemical treatment in 7M HNO₃, 5%(w/w) H₂O₂, 1M H₂SO₄ was carried out to purify the membrane. A membrane with a thickness of 60µm was obtained[4].

III. RESULTS

SBA-3 porous material characterised physically by XRD, TGA, BET and SEM. Also, electrochemical performance of the fuel cell will be discussed below.

A. SEM

SEM analysis of SBA-3 (show below in Fig.1.) has spherical morphology(pore size of 1.8 nm).

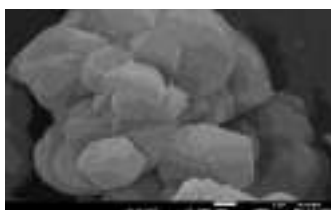


Fig.1. SEM analysis of SBA-3

B. Fuel Cell Test

Voltage-current values acquired by applying 1M methanol at 7 ml/min speed to the anode side under atmospheric pressure and oxygen at 1L/min to the cathode side under 2.5 bar pressure of composite nafion membrane with 1% SBA-3 added for the Direct Methanol Fuel Cell test, were given in the table below in order.

Table 3. Fuel Cell Performance of 1% SBA-3 included composite Nafion Membrane

Voltage (V)	Current (A)	Current Density (A/cm ²)	Power Density (W/cm ²)
0.382	0.283	0.056	0.021
0.349	0.467	0.093	0.032
0.321	0.539	0.108	0.034
0.293	0.551	0.110	0.032
0.264	0.587	0.117	0.031

0.235	0.659	0.132	0.031
0.207	0.707	0.141	0.029
0.179	0.767	0.153	0.027
0.150	0.863	0.173	0.026

A by pass system was installed for this system that runs at 80°C and pure nitrogen was circulated through at first. The advantages of this setup are; meeting of 1M methanol only in the fuel cell on anode side under fuel cell working conditions, purification of the fuel cell from contamination under inert atmosphere and the prevention of damage on MEA structure from pressure differences caused by liquid feed from anode side and gas feed from cathode side in the system. Also, the entry of oxygen under high pressure from cathode side into the fuel cell is another reason that can increase this damage.

Composite added membrane has given a better result and the study has reached its purpose. Because, increasing the temperature in the fuel cell would decrease the proton permeability of the membrane and would cause lower performance. The rate of material addition is an important parameter for the fuel cell. With the study in mind, even though 1% composite membrane was beneficial, proton permeability and membrane elasticity was lost with 5% membrane.

Physical characterisations will be performed.

REFERENCES

- [1] Kimberly M. McGrath, G. K. Surya Prakash, George. A. Olah, Direct Methanol Fuel Cells, J. Ind. Eng. Chem. , Vol 10, 2004, Pages 1063-1080
- [2] A. Hamnett, Mechanism and Electrocatalysis in the direct methanol fuel cell, Catalysis Today 38, 1997, Pages 445-457
- [3] Yilser Devrim, Ayhan Albostan , Enhancement of PEM fuel cell performance at higher temperatures and lower humidities by high performance membrane electrode assembly based on Nafion/zeolite membrane, International Journal of Hydrogen Energy 40, 2016, Pages 11328-15335
- [4] Jung-Hyun Nam, Yoon-Young Jang, Young-Uk Kwon, Jae-Do Nam, Direct methanol fuel cell Pt-carbon catalysts by using SBA-15 nanoporous templates, Electrochemistry Communications 6, 2004, Page 737-741

EFC 19131

Design and Optimization of Carbon Nanofiber Production by Carbondioxide Electrolysis

Nihat Ozer Ucar*, Berker Ficicilar*

*Ondokuz Mayıs University, Department of Chemical Engineering, Kurupelit Campus, Atakum, 55139, Samsun

Abstract - The energy demand, emerged due to the continuous increase in the population growth rate, has also increased and adherence to fossil fuels for generating energy has become a problem. Due to increasing emissions, it is estimated that the CO₂ concentration in the atmosphere was less than 300 ppm before the industrial revolution and is 400 ppm today and it will exceed 500 ppm this century. Commonly studied strategies are; Reducing the amount of CO₂ produced, capturing, electrolysis and storage of CO₂, and converting it into organic products. In this study, electrolysis of CO₂ in molten carbonate will be performed. Lithium carbonate (Li₂O₃) are used as molten carbonate. In this process, O₂ is produced in the anode and carbon nanofiber (CNF) is produced in the cathode.

Productivity comparisons will be made with the parameters studied; the effect of the amount of CO₂ entering the system on the productivity, the electrophoretic separation of carbon accumulated in the cathode electrode and the studies in the literature. In addition, physical characterizations of CNF such as SEM, XRD, XRF, BET and electrochemical characterizations will be performed.

Keywords: Carbon dioxide, Carbon Nanofiber, Electrolysis, Molten Carbonate

INTRODUCTION

The environment gets the biggest hit, when it comes to energy needs. Energy is needed for the maintenance and development of life. However, pollution occurring as a result of the commonly used energy production methods today adversely affects the environment. Greenhouse gases are the most important factors here.

As a result of the emission of greenhouse gases into the atmosphere, some of the heat emitted from the earth is transferred back to the earth and this process causes the earth to warm up to 32°C. Carbon dioxide has the largest share with 82% in the formation of greenhouse gases [1].

In this study, electrolysis of CO₂ in molten carbonate will be performed. Lithium carbonate (Li₂O₃) will be used as molten carbonate. Electrochemical reduction of CO₂ to CO and C in molten carbonates is a common reaction. With that being said, the temperature required for carbon production is lower than that required for CO. According to the study conducted by Stuart Licht et al., 900°C refers to the limit temperature herein [2].

Within the scope of this project, carbon nanofibers (CNF) will be synthesized in cathode electrode by performing electrolysis of molten alkali carbonate (Li₂CO₃) with CO₂, and the appropriate process will be designed and optimized. The melting point of Li₂CO₃ is 723 ° C and since high temperatures are involved here, more economical ways will be sought in the process and the "feasibility" of this design will be discussed.

I. EXPERIMENTAL

Li₂CO₃ was first dried in a drying oven at 140°C for 14 hours. Then, 20 grams of Li₂CO₃ was added to the alumina crucible. The ceramic paper was put over the opening of the crucible to serve as a gasket, then the anode and cathode electrodes made of nickel wire were placed on top of it. The part of the cathode electrode sinking into the carbonate solution was

helically formed to increase the surface area of the wire to be reacted. Furthermore, a mixture of CO₂ and N₂ gas was placed on this crucible with a steel tube and finally, a steel tube, the other end of which was immersed in water, was installed to allow the gas to be released. Lastly, this mechanism was placed in the middle of the gas oven, which was positioned vertically with a wire chamber, and electrolysis was performed for 1 hours at 800°C. Synthesized carbon with electrolysis is shown in Fig.1a and electrolysis process is shown in Fig.1b.



Fig.1a Electrolysed carbon, Fig.1.b Electrolysis process

II. RESULTS

Electrolysed carbon material characterised physically by XRD, TGA, BET and SEM. Also electrochemical characterisations will be discussed. Parameters such as CO₂ rate, structure of carbon, electrode selection and effect of O₂.

A. SEM-EDX

SEM analysis of electrolysed carbon show below in Fig.2. and observed quasi-spherical particles. Also EDX analyses revealed high carbon content in the sample %99,5 by weight.

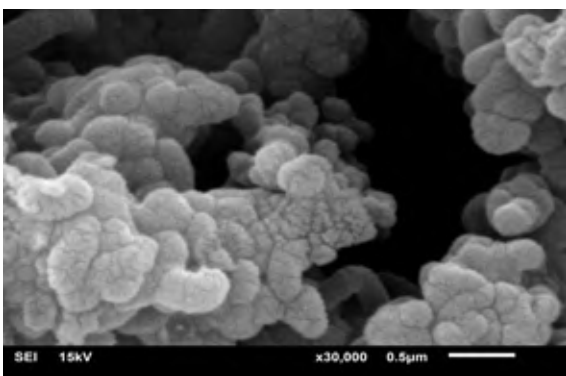


Fig. 2. SEM Analysis of Electrolysed Carbon

B. XRD

XRD analysis of carbon is shown below in Fig.3

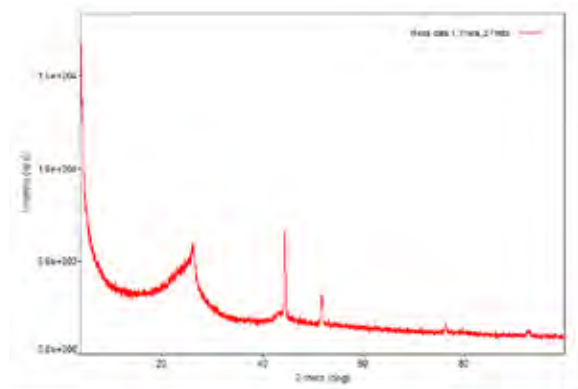


Fig.3. XRD Analysis of Electrolysed Carbon

The characteristic peak at $2\theta = 23^\circ$ and 42° can be attributed to the existence of amorphous phases. Happiness et al in 2014 reported that XRD results for typical electrolysed carbon with molten carbonate and XRD analysis in Fig.3, resemble with their report[3].

Other physical characterisations will be performed.

REFERENCES

- [1]: F. Murena, M. V. Prati, Catalytic Conversion of CO₂ to CH₄ with a Ru Catalyst; Application at Vehicle Exhaust, 2017
- [2]: Stuart Licht, Baohui Wang, Susanta Ghosh, A New Solar Carbon Capture Process: Solar Thermal Electrochemical Photo (STEP) Carbon Capture, 2010
- [3]: Happiness V. Ijije, Chenggong Sun, Indirect electrochemical reduction of carbon dioxide to carbon nanopowders in molten alkali carbonates: Process variables and product properties, 2014

MATHEMATICAL MODEL OF STEAM REFORMING IN ANODE CHANNEL OF MOLTEN CARBONATE FUEL CELL

L. Szablowski, A. Szczesniak, O. Dybinski, and J. Milewski
Institute of Heat Engineering, Faculty of Power and Aeronautical
Engineering, Warsaw University of Technology, Poland

Abstract - The paper presents a mathematical model of a molten carbonate fuel cell with a catalyst in anode channel. The fuel fed the modeled system was methane. The described system includes a model of the steam reforming process occurring in the anode channel of the MCFC fuel cell and the model of the cell itself. The calculations of the reforming were done in Aspen HYSYS software. Four values of the steam to carbon ratio (2.0, 2.5, 3.0, and 3.5) were used to analyze the performance of the reforming process. In the first phase, the reaction kinetics model was based on data from the literature

Index Terms - MCFC, molten carbonate fuel cell, steam reforming

I. INTRODUCTION

The authors of the article already have work related to modeling the reforming process. Mathematical model of a compact plate fin heat exchanger with catalytic coating was presented in [1]. Four values of the steam-to-carbon ratio (2.0, 2.5, 3.0 and 3.5) were used to analyze the performance of the heat exchanger, which was investigated in a temperature range of 500 to 750°C. It was found that the relative prediction error of the simulator does not exceed 3.5%.

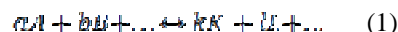
The next step is to build reformer more integrated with the fuel cell. In the proposed solution, the reformer is placed inside the anode channel.

II. THEORY

A. Reforming model

The speed of reaction depends on many factors, such as governing reaction, temperature, presence of a catalyst, etc.

A generic chemical reaction can be written in the following form:



where: a, b, ..., k, l, ... mean the number of moles of individual substances A, B, ..., K, L, ... involved in chemical reactions and are called stoichiometric coefficients.

In the general chemical reaction described by (1), subscripts a, b, k, and l represent stoichiometric coefficients while the products and reagent are identified with K and L, and A and B, respectively. The chemical reaction rate r in a closed, fixed volume system s can therefore be written according to (2).

$$r = \frac{1}{a} \frac{d[A]}{dt} = \frac{1}{b} \frac{d[B]}{dt} = \frac{1}{k} \frac{d[K]}{dt} = \frac{1}{l} \frac{d[L]}{dt} \quad (2)$$

Where: [i] denotes the concentration of component i.

$$r = \frac{d[A]}{dt} \quad (3)$$

The degree of reaction together with the partial pressure of reactants and fixed parameters can be correlated. The rate equation can be found by combining the reaction rate with the mass balance for the considered system. The simplest form of the equation for the degree of occurrence in the reaction for components A and B is described by (4) [2].

$$r = k \cdot [A]^x \cdot [B]^y \cdot [X]^z \quad (4)$$

where: k – coefficient of reaction rate, [] – concentrations of reactants, [X] – the influence of a catalyst; b, c, x – coefficients (orders of reaction) that take into account the type of catalyst and the type of reaction and reaction mechanism.

The influence of temperature on the rate of reaction k is determined by the Arrhenius equation (5).

$$k = A \cdot e^{-\frac{E_a}{RT}} \quad (5)$$

where E_a is the activation energy, and A is the pre-exponential coefficient. The values of A and E_a are different for individual reactions.

B. Fuel cell model

The electrochemical operation of MCFC is described by reduced order model approach [3] that is based on a combination of electric laws, gas flow relationships, solid materials properties, and electrochemical correlations. This approach for fuel cell operation is characterized by applying only physically explained parameters (with the minimum possible number of required factors) and takes into account all important thermal flow as well as architecture parameters. It makes this approach commonly used for cell modeling [4-6].

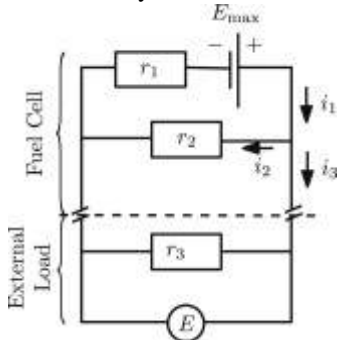


Fig. 1. Equivalent electric circuit of a Molten Carbonate Fuel Cell.

The adopted approach for MCFC modelling assumes that the main processes occurring during MCFC operation can be described by adequate flows of ions and electrons, which gives an adequate equivalent electric circuit of the fuel cell (Fig 1). On the basis of this electric scheme of MCFC, Ohm's law and Kirchoff's law, the equation for fuel cell voltage has been derived:

$$E_{MCFC} = \frac{E_{max} - \eta_f \cdot i_{max} \cdot r_1}{\frac{r_1}{r_2} \cdot (1 - \eta_f) + 1}$$

where: E_{max} – maximum fuel cell voltage, η_f – fuel utilization factor, i_{max} – maximum current density, r_1 – specific ionic resistance, r_2 – specific electric resistance.

III. RESULTS AND DISCUSSION

Fig. 2 shows current-voltage curves for MCFC fed by methane for S/C=2, 2.5, 3 and 3.5. Calculations were carried out for two pressures: 1 and 2 bar.

It can be seen that the cell's performance depends very much on its operating temperature. The relationship between performance and the S/C ratio is less visible, because 3 NI / h of methane is quite a large stream for a 4.5x4.5 cm cell. The reforming reaction works better at higher pressures, however, this increases the CO₂ concentration in anode gases, which leads to a voltage drop.

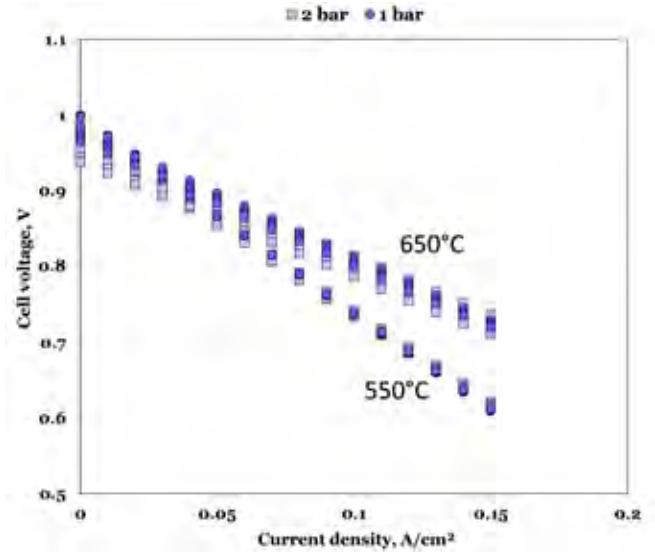


Fig. 3. Polarization curves for MCFC fed by methane for S/C=2, 2.5, 3, 3.5.

IV. CONCLUSION

A mathematical model of the MCFC cell and methane reformer inside the MCFC anode channel was built. The next step will be validation and calibration of the model based on data from future experiments.

ACKNOWLEDGMENT

This work was supported by the grant of the Dean of the Faculty of Power and Aeronautical Engineering of Warsaw University of Technology for 2019.

REFERENCES

- [1] Szablowski, L., Kupecki, J., Milewski, J., & Motylinski, K. (2019). Kinetic model of a plate fin heat exchanger with catalytic coating as a steam reformer of methane, biogas, and dimethyl ether. *International Journal of Energy Research*, 43(7), 2930-2939.
- [2] Young D.C., *Computational chemistry: a practical guide for applying techniques to real world problems*. New York: Wiley; 2001.
- [3] Milewski, Jarosław, et al. "A reduced order model of molten carbonate fuel cell: A proposal." *International Journal of Hydrogen Energy* 38.26 (2013): 11565-11575.
- [4] Kupecki, Jakub, et al. "Dynamic numerical analysis of cross-, co-, and counter-current flow configuration of a 1 kw-class solid oxide fuel cell stack." *International Journal of Hydrogen Energy* 40.45 (2015): 15834-15844.
- [5] Milewski, Jarosław, et al. *Advanced methods of solid oxide fuel cell modeling*. Springer Science & Business Media, 2011.
- [6] Milewski, Jarosław, Gabriele Discepoli, and Umberto Desideri. "Modeling the performance of MCFC for various fuel and oxidant compositions." *International Journal of Hydrogen Energy* 39.22 (2014): 11713-11721.

HIGH-PRESSURE WATER ELECTROLYSIS AND CORRESPONDING SAFETY ISSUES: THE ROLE OF PLATINUM-BASED RECOMBINATION CATALYST

F. Pantò, S. Siracusano, N. Briguglio and A. S. Aricò
CNR ITAE Institute of Advanced Energy Technologies,
Salita S. Lucia sopra Contesse 5, 98126 Messina, (Italy)

Abstract – A Platinum-based recombination catalyst (PtCo unsupported) was synthesized and investigated for recombining hydrogen and oxygen back into water. The catalyst allowed to decrease significantly the concentration of H₂ in the oxygen stream in the overall range of current density and especially at low partial load electrolysis operation. This produced an enhancement of the safety characteristics for the overall electrolysis system. The addition of ~~the~~ recombination catalyst to the anode also improved the electrolysis performance allowing to achieve a cell voltage as low as 1.958 V at 3 A cm⁻² current density with an efficiency better than 80%.

Keywords - Hydrogen production, High-pressure water electrolysis, Thin polymer electrolyte membrane, PtCo based recombination catalyst.

I. INTRODUCTION

Current high-pressure polymer electrolyte membrane (PEM) electrolyzers hold safety issues regarding the flammability limit in relation to the concentration of hydrogen in the anodic oxygen stream under high differential pressure. The flammability limit is 4% vol.; however, for the electrolysis system, safety considerations suggest to avoid exceeding 2-3%. This contribution deals with the integration in the anode side of a catalyst for the hydrogen oxidation reaction. The aim of this approach is to lower the hydrogen concentration well below the safety limits in a wide range of current densities and pressures in the presence of thin (50 and 90 μm) membranes.

II. EXPERIMENTAL

In this study, an unsupported platinum-based alloy catalyst was studied for recombining hydrogen and oxygen back into water. PtCo (75:25 at.) was synthesised by the sulphite complex

route and successively reduced in diluted hydrogen (10% vol. H₂ in argon at 300 °C) to form unsupported catalyst, carbon support was avoided at the high operating potential window because of the oxidation of carbon to CO₂. A pre-leaching process was finally employed using a solution of 0.1 M perchloric acid at 80 °C in order to remove both impurities and unalloyed atoms from the surface of the alloy.

The physico-chemical properties of the catalyst were examined by energy dispersive X-ray analysis (EDAX), scanning electron microscopy (SEM), transmission electron microscopy (TEM), and X-ray diffraction (XRD).

The catalyst was thus integrated in the anode side (metal loading 0.1 mg PtCo cm⁻²) of the membrane-electrode assembly (MEA) of a PEM cell operating up to 4 A·cm⁻² current density.

For the single cell, Solvay Aquivion® membrane with different thickness (respectively 50 and 90 μm for E98-05S and E98-09S) were used in combination with IrRuOx catalyst (70:30 at.) at the anode and 30% Pt/C catalyst (Ketjenblack® carbon) at the cathode of the PEM electrolyser.

In this work, very low precious metal loadings (PGM) were used in order to decrease the costs of the electrolysis system. The PGM loadings were 0.3 mg Ir + Ru cm⁻² for the IrRuOx catalyst at the anode and 0.2 mg Pt cm⁻² at the cathode, with considerable reduction compared to the state of the art (2-3 mg cm⁻² Ir at the anode and 0.5 mg cm⁻² Pt at the cathode).

The preparation of MEAs was carried out according to a catalyst-coated membrane (CCM) approach by spray-deposition of the catalyst-ionomer inks onto the membrane as reported previously. The catalyst - ionomer ink consisted of 25% wt. Aquivion® ionomer (D98-06AS) and 75% wt. Pt/C catalyst at the cathode, and 15% wt. Aquivion® ionomer and 85% wt. IrRuOx catalyst at the anode. A pressurised cell set-up was

combined with a micro gas chromatograph (Varian Micro GC) in order to assess hydrogen permeation at different current densities. The electrolysis cell operated in the differential pressure mode (pressurised hydrogen and non-pressurised oxygen). Polarization curves in the galvanostatic mode and Electrochemical impedance analysis in the potentiostatic mode at 1.5 V and 1.8 V were carried out to evaluate the performance of MEAs.

III. RESULTS AND DISCUSSION

A face-centered cubic phase (JCPDS card no. 40802) was observed for the catalyst; the peak shift with respect to the platinum diffraction used as reference was due to the formation of the solid solution. The structural and morphological analyses highlighted a sponge-like structure for the unsupported PtCo catalyst characterised by fine nanoparticles of 6.9 nm (Fig. 1).

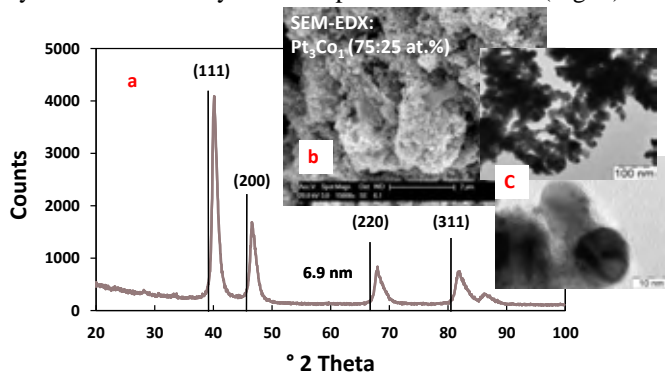


Fig. 1 a) X-ray diffraction pattern, b) scanning and c) transmission electron micrographs of the PtCo recombination catalyst.

Hydrogen concentration in the oxygen stream decreased significantly at high pressure conditions e.g. 20 bar, even at lower currents in the presence of recombination catalyst.

Fig. 2 a) shows that the use of the PtCo alloy at the anode did not affect negatively the performance of the oxygen evolution reaction instead produced a slight decrease of the cell voltage with a corresponding enhancement of efficiency. In particular, the implementation of the recombination catalyst at the anode compartment improved the electrolysis performance allowing to achieve a cell voltage as low as 1.8–95 V at 3 A cm⁻² current density with an efficiency better than 80%. Interestingly, the hydrogen concentration in oxygen was as low as 3% at very low partial load of 5% (150 mA cm⁻²) with significant extension of the safety limits for the electrolysis operation (Fig. 2 b)).

The depolarisation phenomena, observed in the presence of the PtCo catalyst would suggest the occurrence of an electrochemical oxidation mechanism for the permeated H₂, in parallel to the chemical recombination with oxygen into water. This can be in part due to the fact that the PtCo layer is coated directly on the membrane; thus, it is only partially exposed to the oxygen evolved at the IrRuOx layer that preferentially diffuses towards the titanium mesh backing layer. The present

approach can allow for the use of thinner membranes in electrolysis.

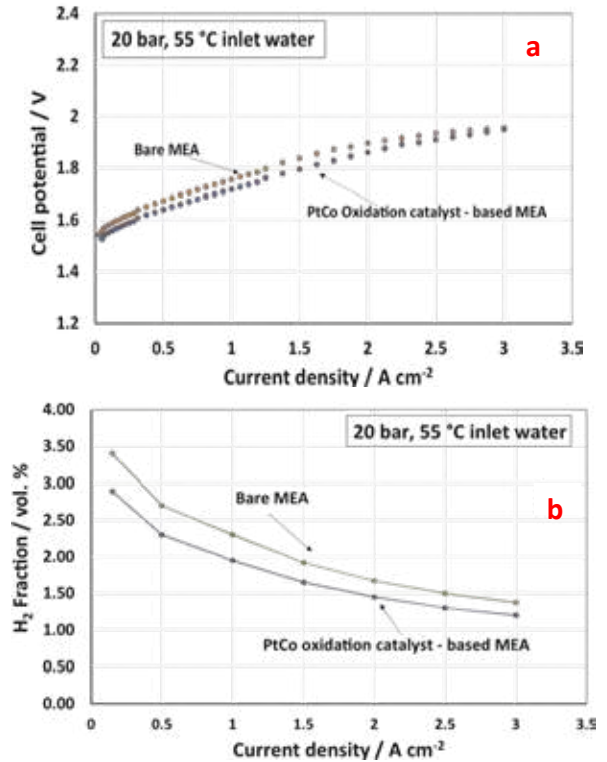


Fig. 2 Polarization curves a) and hydrogen fraction in the outlet anode stream b) for the bare MEA and the MEA containing the PtCo recombination catalyst at 20 bar differential pressure, at a constant water inlet temperature of 55 °C.

IV. CONCLUSION

The PtCo recombination catalyst allows keeping the electrolysis system below the safety limits also at 5% partial load operation. This result represents a significant progress beyond the state of the art (20%). This permits a better flexibility in the integration with intermittent renewable energy sources.

ACKNOWLEDGMENT

CNR-ITAE authors acknowledge the financial support from the NEPTUNE project. This project has received funding from Fuel Cells and Hydrogen 2 Joint Undertaking under grant agreement No 779540. This Joint Undertaking receives support from the European Union's Horizon 2020 research and innovation programme and Hydrogen Europe and Hydrogen Europe Research.

REFERENCES

- [1] Briguglio, N., Siracusano, S., Bonura, G., Sebastián, D., Aricò, A. S., Flammability reduction in a pressurised water electrolyser based on a thin polymer electrolyte membrane

MODEL-BASED INVESTIGATION OF BIOMASS GASIFICATION IN A FLUIDIZED BED REACTOR

F. Cipiti, G. Urbani, S. Maisano, V. Chiodo
Institute CNR-ITAE, Via S. Lucia sopra Contesse n. 5, 98126
Messina, (Italy)

Abstract - The present work concerns with Computational Fluid-dynamics modelling of biomass gasification in a fluidized bed reactor, where a dispersed phase, consisting of solid particles, is fluidized by air (fluid phase) and transported upwards through a vertical riser. The main aims of the mathematical model were to optimize the reactor geometrical key parameters (diameter and length of bed, diameter and shape of the dispersed phase, etc.) by parametric analysis, investigating the impact of gasifier temperature and air supply in order to identify the best fluidized bed configuration for the conversion of a typical lignocellulosic biomass into hydrogen rich syngas.

Index Terms - Biomass Gasification, Fluidized bed reactor, Computational fluid-dynamics, Momentum Transport Phenomena

I. INTRODUCTION

Gasification process, that converts carbonaceous materials with assistance of a gasifying agent (such as air, oxygen, steam CO_2 or a mixture of these oxidant species), is one of the most flexibility technologies to produce secondary biofuels (syngas), due to its suppleness to use a wide range of feedstocks (biomass, coal, waste, etc.) [1]. In this way the design of a fluidized bed reactor is a key aspect for the performance and efficiency of a biomass gasifier: the reactor should be able to work under steady state, weight and volume should be minimized and the heat management system optimized for different operating conditions. Based upon the above considerations, a mathematical model, based on momentum balances, has been developed, investigating the impact of gasifier temperature and air supply in order to identify the best-fluidized configuration for the conversion of a typical lignocellulosic biomass into hydrogen rich syngas. The mathematical simulations were achieved through the description of transport phenomena by Partial Differential Equations (PDEs), numerically solved through the Finite Element Methods (FEM), using a commercial software package Comsol Multiphysics. In particular, the paper presents a two-

dimensional model using a disperse method that does not explicitly track the position of the interface between the two fluids, but instead tracks the volume fraction of each phase, thus lowering the computational load. The model simulates the flow of two continuous and fully interpenetrating incompressible phases. This model requires the resolution of two sets of Navier-Stokes equations, one for each phase, in order to calculate the velocity field for each phase.

II. MODEL DEFINITION

The main advantage of the finite-element approach used is the possibility to easily adapt the model to different reactor geometry, allowing an accurate design, regardless by physical-chemical properties (mainly in terms of C, H, N, S, O contents) of the biomass to be converted.

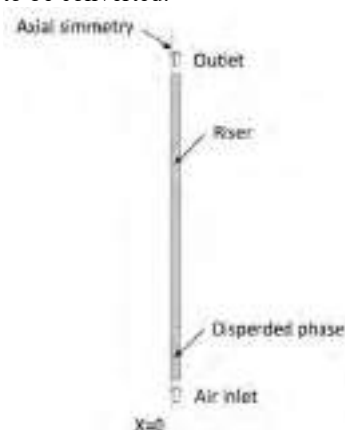


Fig. 1. Geometrical model in the mathematical simulations.

Fig. 1 shows the geometry of the fluidized bed, and schematically describes its means of operation. The fluid phase, consisting of air is injected at the bottom of the bed. The dispersed phase, particles with a diameter of 0.5 mm are

fluidized by the gas flow and transported upwards. The reactor is rotationally symmetric, which implies that we need to model a rotational cross section of it. Table 1 summarizes the bed geometries and the properties of the phases.

TABLE I
Fluidized bed properties

Property	Value
Particle diameter	0.5 mm
Particle density	1540 kg·m ⁻³
Gas density (air)	1.2 kg·m ⁻³
Gas dynamic viscosity (air)	1.8 · 10 ⁻⁵ kg·m ⁻³
Gas inlet velocity	0.03638 m·s ⁻¹
Reactor diameter	0.027 m
Bed height	0.475 m
Initial dispersed phase column height	0.0817 m

Both phases are modeled as inter penetrating continua governed by a separate set of Navier-Stokes equations. The model includes a transport equation for the dispersed-phase volume fraction. The viscosity of the dispersed phase is defined as [2]:

$$(1) \mu_d = 0.5 \phi_d$$

where ϕ_d is the dispersed-phase volume fraction.

Assume the momentum transfer to be dominated by the drag force and the drag acting on each phase is given by a drag coefficient β in the manner of

$$(2) F_{\text{drag,c}} = -F_{\text{drag,d}} = \beta u_{\text{slip}}$$

Here, the subscripts “d” and “c” indicate properties of dispersed continuous phase, respectively, and the slip velocity is defined as

$$(3) u_{\text{slip}} = u_d - u_c$$

To model the drag coefficient, the Gidaspow drag model has been used [3]:

$$(4) \beta = \frac{3\phi_c\phi_d\rho_c C_{\text{drag}}}{4d_d} |\mathbf{u}_{\text{slip}}| \phi_c^{-2.65}$$

for $\phi_c > 0.8$, and

$$(5) \beta = 150 \frac{\mu_c \phi_d^2}{\phi_c d_d^2} + 1.75 \frac{\phi_d \rho_c}{d_d} |\mathbf{u}_{\text{slip}}|$$

for $\phi_c < 0.8$.

Initially all dispersed particles are positioned in a packed bed section at the bottom, of the column.

The inlet velocity is gradually ramp up as a function of time at the start of the simulation in order to avoid discontinuity with the initial velocity, using a smoothly varying rectangle function

to define the packed bed column. To fluidize the bed, air is injected at the bottom: in order to assure that the initial dispersed volume fraction around the inlet matches the inlet dispersed fraction, the dispersed phase volume fraction at the inlet is set to zero. Moreover, to avoid large transient effects at the start of the simulation, the gravity is ramp up as a function of the time. In order to avoid that some particles settle towards the bottom of the reactor, a continuous phase through the inlet has been introduced and no-slip condition has been set for the dispersed phase. In this way, the dispersed phase can settle on the bottom without conflicting with the inlet condition.

For both phases, a pressure normal low condition has been used. Along the solid bed walls, a no-slip condition has been applied for the continuous phase and a slip condition for the dispersed phase. The volume fraction of the dispersed phase is tracked with an additional transport equation.

III. PRELIMINARY RESULTS

Fig. 2 shows a snapshot of the dispersed phase volume fraction during the start-up at the beginning of the simulation. The packed bed section is pushed upwards by the air, primarily in the center of the bed.

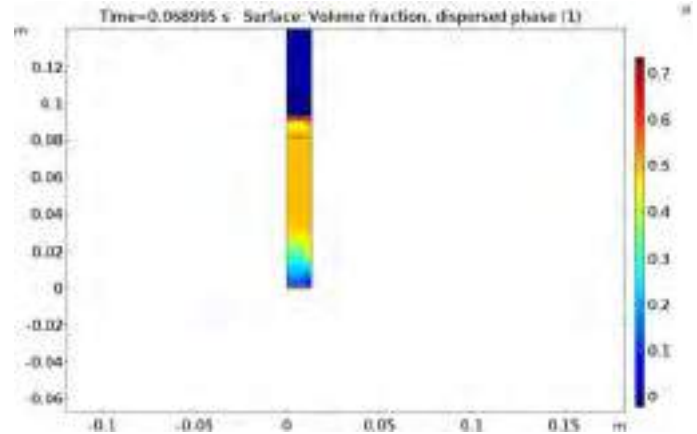


Fig. 2. A snapshot of the dispersed phase volume fraction at the beginning of the simulation

IV. CONCLUSIONS

A simulation model based on Computational Fluid-dynamics, in order to investigate biomass gasification in a fluidized bed reactor has been successfully developed. A comprehensive sensitivity analysis is on-going.

REFERENCES

- [1] Y. Torriero, I. Ortiz, G. Molina, M. Morono, V. Perez, J.M. Murillo, et al. Fuel vol. 225, pp. 71-79, 2018.
- [2] N. Yang, W. Wang, W. Ge, and J. Li, “CFD simulation of concurrent-up gas-solid flow in circulating beds with structure-dependent drag coefficient”, Chemical Engineering Journal, vol. 96, pp. 71-80, 2003.
- [3] D. Gidaspow, Multiphases Flow and Fluidization, Academic Press, San Diego, 1994.

PERFORMANCE ASSESSMENT OF MFC UNITS FED WITH DIGESTATE

A. Tremouli*, T. Kamperidis*, P.K. Pandis*, K.
Papadopoulou*, G.M. Lytras*, Christos Argirusis* and G.
Lyberatos**

*School of Chemical Engineering, National Technical University of
Athens, Heron Polytechniou 9, 15780, Zografou Athens, (Greece)

**Institute of Chemical Engineering Sciences (ICE-HT), Stadiou
Str., Platani, 26504, Patras, (Greece)

Abstract –

This study reports on the investigation of the digestate treatment from fermentable household food waste (FORBI) using the microbial fuel cell (MFC) technology. The effluents from a thermophilic and a mesophilic anaerobic digester were characterized and used as the feed in four air-cathode MFC units. The chemical oxygen demand (COD) removal ranged from 80 – 90% in all cases. The ammonium removal for the thermophilic digestate ranged from 85 to 99 % while for the mesophilic digestate ranged from 46% to 79%. The electrochemical characterization of the cells showed low internal resistances (10-50 Ω) of the units for both inlets. The work demonstrated the potential of using MFC technology to further treat and exploit anaerobic digestates which are produced from FORBI.

Index Terms – anaerobic digestion, FORBI, digestate, MFC

I. INTRODUCTION

Globally the Food and Agriculture Organization of the United Nations (FAO) has estimated that one third of food produced for human consumption is lost or wasted globally, equals to about 1.3 billion tons per year [1]. The anaerobic digestion (AD) of the Fermentable Household Waste (FHW) achieves both environmental and economic benefits. Although AD technology is used extensively for industrial applications a major issue is the potential use and treatment of its major by-products, the anaerobic digestate. The most common treatment for digestate is aerobic process in order to be used as a bio-fertilizer.

This study presents an alternative exploitation of digestate using the Microbial Fuel Cell (MFC) technology. In particular, four MFC units were evaluated when fed with digestate which originated from anaerobic digesters fed with FORBI. The

results indicated that digestate was successfully treated with simultaneous electricity production.

II. MATERIALS AND METHODS

A. Anaerobic Digestate

In the present study, anaerobic digestate was directly collected from a thermophilic 500 L and a mesophilic 4000 L CSTR anaerobic digesters fed with FORBI as a suspension. FORBI was produced by drying and shredding the pre-sorted fermentable fraction of household food waste collected door-to-door in the Municipality of Halandri, Athens, Greece [2]. Table 1 presents the characteristics of the digestate after solid-liquid separation (5 μ m filter sludge bag) which was used as feedstock for the MFC units. The total COD ranged greatly, due to the continuous operation and the alteration of the feed's organic load.

TABLE 1 Digestate characteristics

Average values \ Bioreactors	Thermophilic	Mesophilic
pH	7	7.04
Conductivity / mS/cm	3.64	2.41
gCOD / L ^{range}	6.12 – 9.97	3.67 – 11.1
Total Suspended Solids (TSS) / g/L	4.61	5.77
Volatile Suspended Solids (VSS) / g/L	2.53	3.44
NH ₄ ⁺ (g/L)	0.13	0.03
Volatile Fatty Acids VFAs (ppm)	2049	319

B. MFC set-up and operation

The experiments were conducted using four identical, membrane-less single chamber, four air-cathode MFCs. Each cell consists of a single cubical compartment and four plexiglas tubes run through it (120 ml volume). The manufacturing

process is presented in detail by [3]. Each cell was filled with graphite granules ($\text{\O}1.5\text{-}5$ mm, type 00514, Le Carbone, Belgium). The cathode tubes are open to the atmosphere and no special aeration is employed. GORE-TEX[®] cloth is used as a separator and as a catalyst (MnO_2) support of the cathode electrocatalyst, which was MnO_2 .

All units were operated in batch mode under a fixed external load of $100\ \Omega$ for each cell. In order to test the reproducibility of the results each feeding was tested in duplicate (Cells 1, 2: mesophilic digestate, Cells 3, 4 thermophilic digestate). EIS measurements were carried out for the entire cell in the frequency range of 100kHz to 1mHz at several applied cell voltages. Linear Sweep Voltammetry (LSV) curves were obtained through a Biologic SP-150 Potentiostat/Galvanostat.

III. RESULTS AND DISCUSSION

Voltage output of the Cells is shown in Figs. 1 and 2. Cell 1 obtained higher values of voltage output when compared with the Cell 3. Each batch cycle lasted 10 days on the average, depending on the cell and the digestate. The COD removal ranged from 80 – 90% and was achieved within the first 24 to 48 hours of each cycle operation. Although after the first 24 - 48 hour period, the COD value remained constant, electricity was still produced for more than 190 h. This result can probably be attributed to the relatively fast uptake and storage of the soluble COD in the biofilm of the anode electrode. Then, organic matter could be slowly used as substrate from the electroactive bacteria generating electricity. The pH was not changed during operation (pH 7). VFAs were completely consumed by the biomass throughout each cycle while the TSS and VSS were reduced by 83 and 86 % respectively, on the average in each batch.

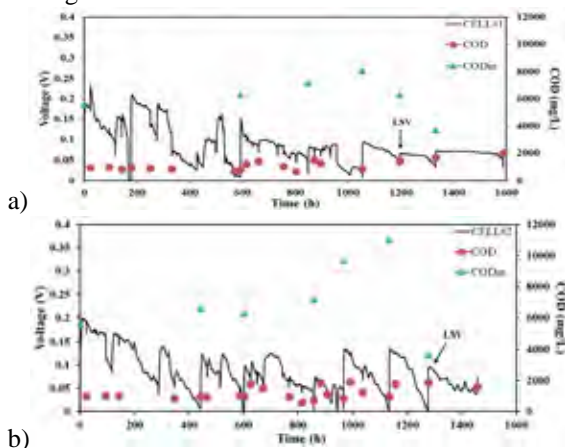


Fig. 1. Voltage behaviour of the (a) Cell 1 and (b) Cell 2 fed with mesophilic digestate versus time.

The ammonium removal which was achieved from the mesophilic fed MFCs was in the range of 46%-79%, whereas for the thermophilic fed MFCs was in the range of 85% - 95%. In order to determine the electrochemical behavior of the cells,

polarization experiments were conducted when the batch cycles reached the maximum voltage output. The maximum power output P_{max} which was achieved was in the range of 0.36 to 0.45 mW for both digestates. However, when the organic content of the mesophilic reactor increased from 3.7 g COD/L to 6.3 g COD/L P_{max} was also increased from 0.39 to 0.80mW, respectively. This fact is totally in correlation with the double COD feeding of the cell. Moreover, EIS experiments showed relatively minimum internal resistances for the MFCs in the range of $10\text{-}50\ \Omega$ for both inlets.

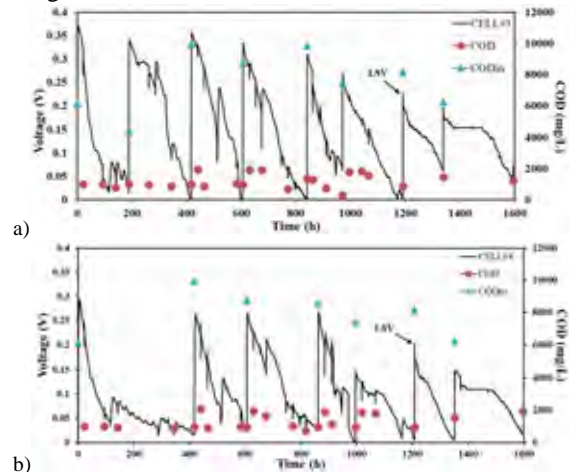


Fig. 2. Voltage behaviour of the (a) Cell 3 and (b) Cell 4 fed with thermophilic digestate versus time.

IV. CONCLUSION

The work demonstrated that digestate from fermentable household food waste (FORBI) can be successfully treated using the microbial fuel cell (MFC) technology. In particular, the easily biodegradable organic matter was removed by 80 – 90 % within the first 24 – 48 h, while power production was obtained for more than 190 h in almost all cycles.

ACKNOWLEDGMENT

This project has received funding from the Hellenic Foundation for Research and Innovation (HFRI) and the General Secretariat for Research and Technology (GSRT), under grant agreement No [862].

REFERENCES

- [1] Food and Agriculture Organization (FAO), <http://www.fao.org/about/en/>
- [2] Waste4Think: Moving towards Life cycle thinking by integrating Advanced Waste Management Systems, 2015. GA 688995.
- [3] Tremouli, A., Karydogiannis, I., Pandis, P. K., Papadopoulou, K., Argiris, C., Stathopoulos, V. N., Lyberatos, G., Bioelectricity production from fermentable household waste extract using a single chamber microbial fuel cell, Energy Procedia, Volume 161 2019, pp 2-9.

INTEGRATION OF METAL HYDRIDE HYDROGEN COMPRESSORS IN HYDROGEN REFUELING STATIONS: BENCH-MARKING & MARKET DEPLOYMENT ASPECTS

E. Stamatakis^{1,2}, E. Zoulias², C. Christodoulou², G. Karagiorgis²
and A. Stubos^{1,2}

¹National Centre for Scientific Research DEMOKRITOS, Athens, (Greece)

²CYRUS P.C., LEFKIPPOS Attica Technology Park, Athens, (Greece)

Abstract - Hydrogen compressors account for over 50% of the total capital cost of a hydrogen refueling station (HRS) for vehicles. Moreover, they are a critical component for stationary power applications as well, therefore they will play a significant role towards "Hydrogen Economy". More specifically, in the transport sector, it is estimated by the European Commission that the potential market share of hydrogen vehicles will be in the order of 0.3 – 0.4% of the total vehicle stock. In addition, it is expected that around 840 hydrogen refueling station will operate in Europe. Metal Hydride Compressors (MHC) without moving parts demonstrate significant advantages over conventional mechanical compressors, such as: slightly lower capital cost, significantly lower operation and maintenance cost, higher availability and reliability and almost zero noise. The scope of this paper is to present the results of the development phase of an MHC with a flow capacity of 10 Nm³/h of hydrogen, achieving pressure over 300 bar, using only water as the cooling / heating medium. The main concept of the MHC lies in the selection of appropriate alloys, which work in different inlet and outlet pressures and allow pressure increase in stages. The work deals also the next steps towards MHC introduction to the HRS market, the identification of the existing barriers and the methods to overcome these.

Index Terms – Metal hydrides, Hydrogen Compressors, Hydrogen Refueling Stations.

I. NOMENCLATURE

MHC	Metal Hydride Hydrogen Compressor
HRS	Hydrogen Refueling Station

II. INTRODUCTION

Compression is one of the most critical issues that associate with almost all storage methods for hydrogen and its subsequent usage. Hydrogen compression is only part of the so-called "Hydrogen Value Chain", but it is crucial for overcoming the entry barriers for a "Hydrogen Economy". It is widely accepted that there is a strong need for significant improvements in efficiency, durability and reliability of hydrogen compressors as well as for cost reductions, especially if the end-use is to be in vehicles or fueling stations and is accompanied by request for high hydrogen purity in transportation and other industrial

applications [1], [2].

This need for efficient, safe, and low-cost hydrogen compressors has begun to emerge. Hydrogen compression based on the reversible hydrogenation / dehydrogenation ability of metal hydrides (MH) has been proposed and investigated as a reliable process to compress hydrogen to high pressure without contamination and with relatively low energy costs. The method utilizes a reversible heat-driven interaction of a hydride-forming metal or alloy or intermetallic compound with hydrogen to form MH and offers an attractive alternative to conventional (mechanical) and other newly developed (electrochemical, ionic liquid pistons) concepts for hydrogen compression [3], [4]. The advantages of MH compression include simplicity in design and operation, absence of moving parts, compactness, safety and reliability, and the possibility to utilize waste industrial heat and/or excess renewable energy (e.g. solar thermal) for the required heating of the MH tanks. This latter possibility (exploitation of waste industrial and/or excess renewable heat) constitutes a major argument in favour of MH based compression as it may lead to very significant operational cost reductions.

III. CURRENT DEVELOPMENTS OF MHC

CYRUS PC has developed and manufactured a prototype Metal Hydride Compressor, composed of 5 stages each utilizing a specific specialized metal hydride. It is capable of raising hydrogen gas pressure from <5 bar to more than 350 bar, utilizing water as heat exchange fluid and achieving a stable hydrogen flow of about 10 Nm³/h. At each stage, specialized bleed valves can provide hydrogen at intermediate pressures, if required. Large scale refueling (e.g. for hydrogen passenger cars, bus and truck fleets, rail transport as well as maritime applications) is expected in the coming years to require HRS at pressure levels of 350 bar or 700 bar [5].

Moreover, the potential to exploit different heat sources (such as solar heating, geothermal energy and other waste heat sources) constitutes a significant competitive advantage over traditional mechanical hydrogen compressors.

The proposed compressor technology is benchmarked here against the mechanical compressor technology commercially available today in order to prove its merits (among others, higher reliability, with the potential of lower maintenance cost and less down time of compressor systems). In general, the MHC can serve a number of markets such as traditional industry, renewable energy, emergency power, hydrogen fuel infrastructure as explained further below.

IV. IDENTIFICATION OF TARGET MARKETS

MH Compressors can serve a number of markets such as traditional industry, renewable energy, emergency power and hydrogen fuel infrastructure. While some of these emerging markets are still small, hydrogen can be readily used in a number of industrial processes already today [6]. As a first step, the authors have identified the following key business cases where MHC can be directly introduced (early markets):

i. **Chemical industry**, by utilisation of waste industrial heat; many industrial chemical processes generate large amounts of waste heat that can be fed back to a MH compressor. Thus, we observe a good match between traditional industry and thermally driven MH hydrogen compressors. The advantages are especially pronounced in case of utilising waste industrial heat.

ii. **Hydrogen Refueling Stations (HRS)**; Hydrogen refueling infrastructure takes a significant part of the capital investments for the introduction of fuel cell powered vehicles. The most expensive H₂ refueling components originate from: (i) on-site hydrogen production and (ii) hydrogen compression (with a contribution of about 50% to the total cost of an HRS). Cost performance optimisation of the H₂ refuelling infrastructure can be achieved by the improvement of hydrogen compression technology (e.g. application of thermally-driven metal hydride hydrogen compressors) [7].

iii. **RES storage in compressed hydrogen**; It appears to be very promising to use MH compressors for large-scale hydrogen production from renewable energy sources for dynamic storage needs, including autonomous systems for isolated / remote communities like off-grid islands. Energy storage concepts enabling the maximum recovery of curtailed renewable electricity in a cost-effective way are needed. MH Compressors combined with electrolysers can use curtailed electricity and efficiently store it in the form of hydrogen generating additional profit to the electricity suppliers as well as to potential hydrogen off takers.

V. CONCLUSION

In summary, non-mechanical hydrogen compressors have several advantages over their mechanical counterparts, including smaller size, lower noise, lower operating and maintenance costs. MH compressors are thermally powered systems that use the ability of reversible metal hydrides to

compress hydrogen without any contamination. They also provide the ability to connect them to the outlet of electrolysers. Moreover, using available heat wastes or excess renewable energy to feed the chemical compressor enhances significantly the overall efficiency of the system [8].

CYRUS PC has developed and manufactured a noise free hydrogen compression system based on metal hydrides using only water as the cooling / heating medium achieving hydrogen pressures > 350 bar.

Hydrogen compressors can be considered as a growing market that is expected to pick-up pace in the near future when their most promising application, the hydrogen refueling infrastructure, will be expanded.

ACKNOWLEDGMENT

Mr. E. Stamatakis acknowledges partial support by the Industrial Research Fellowship Program funded by the S. Niarchos Foundation at NCSR "Demokritos" (SHESAM project).

Mr. A. Stubos & Mr. E. Zoulias acknowledge partial support by the National Operational Program Competitiveness, Entrepreneurship and Innovation, under the call RESEARCH – CREATE-INNOVATE (project code: T1EDK-05294)

REFERENCES

- [1] E.I. Gkanas, D.M. Grant, A.D. Stuart, C.N. Eastwick, D. Book, S. Nayeboassadri, L. Pickering, G.S. Walker, "Numerical study on a two-stage Metal Hydride Hydrogen Compression system", *Journal of Alloys and Compounds* 645, S18–S22, 2015.
- [2] A. Witkowski, A. Rusin, M. Majkut, K. Stolecka, "Comprehensive analysis of hydrogen compression and pipeline transportation from thermodynamics and safety aspects", *Energy*, Volume 141, , pp. 2508-2518, December 2017.
- [3] Volodymyr A. Yartys et al., "Metal hydride hydrogen compression: recent advances and future prospects", *Appl. Phys. A*, 122:415, 2016.
- [4] M.V. Lototsky et al., "Metal hydride hydrogen compressors: A review", *International Journal of Hydrogen Energy*, Volume 39, Issue 11, no. 4, pp. 5818–5851, April 2014.
- [5] FCHJU 2018 Annual Work Plan and Budget, <http://www.fch.europa.eu>
- [6] V.A. Yartys, M. Lototsky, V. Linkov, D. Grant, A. Stuart, J. Eriksen, R. Denys, R.C. Bowman Jr, "Metal hydride hydrogen compression: recent advances and future prospects", *Appl. Phys.*, 122:415, 2016.
- [7] Weinert JX, Shaojun L, Ogden JM, Jianxin M., "Hydrogen refueling station costs in Shanghai", *Int J Hydrogen Energy*, 32:4089-100, 2007.
- [8] A. Léon (ed.), *Hydrogen Technology*, Springer-Verlag, Heidelberg, Berlin, 2008.

COMPARATIVE ANALYSIS OF BEVs AND FCEVs FOR THE FUTURE DEVELOPMENT OF THE SUSTAINABLE MOBILITY IN ITALY

M. Minutillo*, E. Janelli*, P. Di Trolio*, S. D'Apolito*, M. Pulcrano*, V. Cigolotti**, A. Pianese*

*University of Naples "Parthenope", Via Amm. F. Acton 38, Napoli (Italy)

**E.N.E.A. – Portici Research Center

Abstract - Currently, almost 95% of vehicles worldwide are powered by internal combustion engines (ICE) fed by fossil fuels, but there is a growing interest in transitioning to more environmentally friendly vehicles. The candidates with a great potential in the replacing of ICE are the battery electric vehicles (BEV) and the fuel cell electric vehicles (FCEV).

This study presents the comparison between BEV, FCEV and ICE in terms of Total Cost of Ownership (TCO).

This economic analysis is based on costs that are assumed variable in the time according to market prevision trends.

Finally, the strengths, weaknesses, opportunities and threats of BEVs and FCEVs are discussed through a SWOT analysis in order to evaluate the best option for the development of the sustainable mobility in Italy.

Index Terms –Sustainable mobility, electric vehicles, hydrogen, batteries

I. NOMENCLATURE

BEV: Battery Electric Vehicle; FCEV: Fuel Cell Electric Vehicle; ICE: Internal Combustion Engines; TCO: Total Cost of Ownership; SWOT: Strengths, Weakness, Opportunity, Threats.

II. INTRODUCTION

Today a significant share of global anthropogenic emissions of CO₂ is due to road transport. In order to contain polluting emissions and energy consumption in this sector, the European Union urges Member States to promote common policies and financial supports for more efficient, safe and clean mobility [1]. The aim of this work is to identify, through an economic analysis, the best solution between BEV and FCEV, in terms of total cost of ownership (TCO). Moreover, by applying the SWOT analysis, the technical and market benefits/limits related these technologies are presented.

III. COST ANALYSIS

The economic analysis in terms of TCO refers to three years: 2010, 2020 and 2030. Moreover, an average vehicle lifetime of ten years is assumed for a common final user. The TCO analysis is based on the evaluation of CAPEX (a typical vehicle retail price) and OPEX (it includes the fuel/electricity

price calculated by considering an average range mileage of 10.000 km per year, while the maintenance cost is neglected).

In Fig. 1 the CAPEXs of BEV, FCEV and ICE are illustrated. It is worth noting that a decreasing trend is attended for BEV and FCEV, thanks to the technological maturity reachable in the time. BEV's retail price decreases from 40.000,00 to 20.200,00 € [2] at 2030; the FCEV's retail price from 75.000,00 € to 43.000,00 € at 2030 [1]; the ICE's price results to be quite constant in the time (about 26.000,00 €) [2]. According to these data, it results that the FCEV is always the most expensive vehicle.

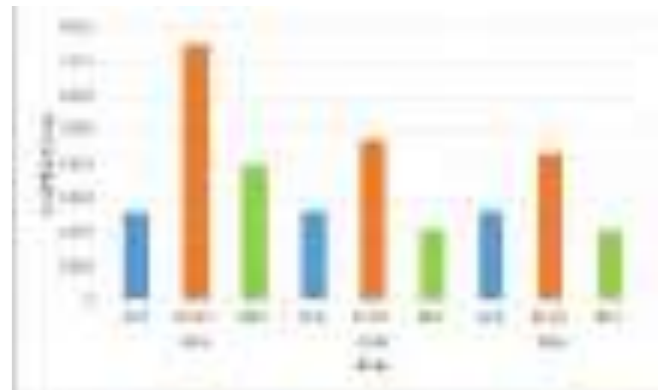


Fig.1. CAPEX (€/year) of ICE^[1,2], FCEV^[1] and BEV^[2] considering a vehicle life time of ten years

The Figure 2 shows OPEX (based on fuel and electricity) of these vehicles. These data have been calculated by considering the same travelled kilometers (10.000 km/year) and energy consumptions of 4.450, 2.700 and 1.400 kWh per ICE, FCEV and BEV respectively. As it is shown in ref. [3], the hydrogen price (o cost to the pump) decreases from 10.29 €/kg at 2020 to 5.00 €/kg at 2030 (hydrogen production from renewable electrolysis). The price of oil is conditioned by several factors, thus a growing trend has been calculated by analyzing the historical prices series of the last twenty years [4]: the oil price increases from 1.60 €/l in 2020 to about 2.00 €/l in 2030. With respect to the electricity, in Italy the current vehicles charging cost is 0.4 €/kWh [5]; this cost decreases to 0.20 €/kWh [3] at

2030 (the European average price), by assuming a better integration of the renewable energy and the better distribution of charging stations. Thus, the TCO for each vehicle, calculated as sum of CAPEX and OPEX, is shown in Figure 3.

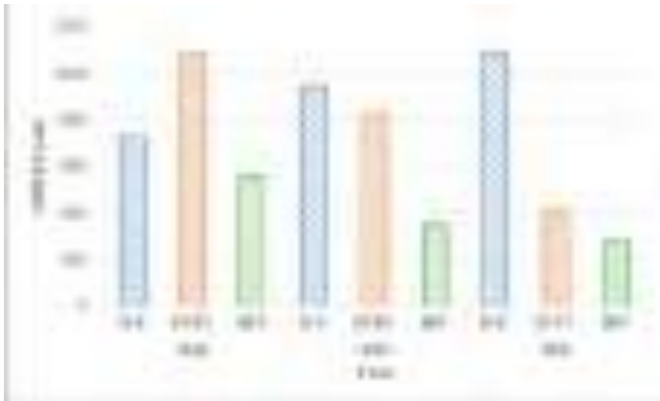


Fig.2. OPEX (€/year) of ICE^[4], FCEV^[3] and BEV^[3]

It can be noted that BEV will be the most economically competitive solution both at 2020 (TCO equal to 2.427 €/year) and 2030 (it is due to the reduction in the cost of battery packs and to the greater incidence of the oil cost). The FCEV remains the most expensive option, although its TCO will decrease approximately to 4.700 €/year in 2030 (45%), thanks to the reduction of the hydrogen cost and above all of the powertrain cost.

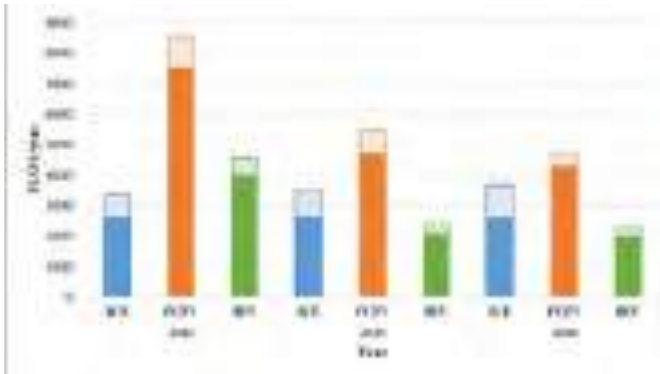


Fig.3. TCO of ICE, FCEV and BEV

IV. SWOT ANALYSIS

The present Italian economic-productive context has been examined to identify strengths and weaknesses, opportunities and threats in relation to the spread of BEVs and FCEVs, reported in the SWOT matrices below [6].

V. CONCLUSION

Most energy policy incentives call for drastic reductions in CO₂ emissions, which will increase the need of alternative to conventional fuels in transport, such as hydrogen or electricity. Basing on the results of the economic analysis, BEVs will be the most competitive and viable option for the final consumer from 2020, thanks to the low cost of electricity compared to oil and to reduction of battery pack price. Finally,

on the basis of SWOT analysis, the common limits to the spread of BEVs and FCEVs, are related especially to the lack of infrastructure and the high present vehicle purchase price, which does not encourage consumers to change their own mobility habits.

Tab.2. SWOT matrix for BEVs

Strengths	Weakness
<ul style="list-style-type: none"> • Reduction of environmental impact • Higher energy efficiency of vehicles • Cost of recharging less than cost of purchasing fuels • More using of electric vehicles through the Sharing Mobility • Possibility of charging at home 	<ul style="list-style-type: none"> • Lack of charging infrastructure • High vehicle purchase cost • Negative effects on battery lifetime • Battery disposal • Limited autonomy • Long charging times
Opportunity	Threats
<ul style="list-style-type: none"> • Development of more performing technologies • Public funding for RS&I • New business models • Expanding product portfolio • Creation of specialized jobs • Greater collaboration between OEMs and public administrations 	<ul style="list-style-type: none"> • Skepticism of consumers and reluctance to abandon their "unshared" mobility habits • Request for fast recharge • Risk of oversizing the charging infrastructure • Introduction of new foreign competitors specialized in green technological solutions

Tab.3. SWOT matrix for FCEVs

Strengths	Weakness
<ul style="list-style-type: none"> • Reduction of environmental impact • Higher energy efficiency of vehicles • Smarter and safer urban transport • Autonomy comparable to ICE • No change in the refueling process • Strategic options for hydrogen storage • Flexibility for the integration of renewable energy 	<ul style="list-style-type: none"> • Lack of refueling infrastructure • Higher FCEV investment costs • Higher hydrogen purchasing • Production of upstream energy not totally renewable • Lower efficiency of the hydrogen supply chain compared to BEVs • Limited market availability
Opportunity	Threats
<ul style="list-style-type: none"> • Development of more performing technologies • Public funding for RS&I • Best collaboration and risk sharing between suppliers and OEMs • Expanding product portfolio • Creation of specialized jobs • Best collaboration between OEMs and public administrations 	<ul style="list-style-type: none"> • Skepticism of consumers and reluctance to abandon their "unshared" mobility habits • Introduction of new foreign competitors specialized in green technological solutions • Probable unavailability of key component suppliers

ACKNOWLEDGMENT

Research supported by Campania Region for the project "Consultazione per la revisione e il consolidamento delle linee strategiche di Ricerca e Innovazione nell'ambito di sviluppo "Automotive"" (2018).

REFERENCES

- [1] G.J. Offer, D. Howey, M. Contestabile, R. Clague, N.P. Brandon, Comparative analysis of battery electric, hydrogen fuel cell and hybrid vehicles in a future sustainable road transport system, *Energy Policy*, Vol. 38, 2010, pp. 24–29.
- [2] Juhani Laurikko, Present and near-future outlook on hybrid, electric and hydrogen-fuelled vehicles, VTT-CR-04638-16, 2016
- [3] Global EV Outlook 2019, IEA, May 2019
- [4] www.mise.gov.it
- [5] www.enelx.com
- [6] M. Robinius, J. Linßen, T. Grube, M. Reuß, P. Stenzel, K. Syranidis, Patrick K. and D. Stolten; Comparative Analysis of Infrastructures: Hydrogen Fueling and Electric Charging of Vehicle, *Energy & Umwelt/Energy & Environment*, Vol. 408, 2018.

DIFFERENT TYPES OF REAL HOUSEHOLD GREYWATER AND URINE USED IN MICROBIAL FUEL CELLS: POWER GENERATION AND TREATMENT EFFICIENCY

J. You, J. Greenman, and I. Ieropoulos

Bristol BioEnergy Centre (BBiC), University of the West of
England, Bristol, BS16 1QY (UK)

Abstract – Various types of domestic greywater and wastewater from five different sources (bathroom, kitchen sink, dishwasher, laundry washing machine and urinal) were tested in otherwise identical MFCs. In terms of power output, urine outperformed other feedstock types by producing a maximum power of 3.9 mW. When urine was diluted with either bathwater or tap water, results showed that MFC power output decreased with increasing dilutions. Interestingly, when consumer products such as bleach or toilet cleaner were added in full concentration, the level of instantaneous power dropped, but power output recovered to the previous levels within 48 hours in all cases after this was replaced with fresh urine. This suggests that the MFC systems are fairly robust and can be resistant to domestic chemical exposure. These novel findings provide a stepping-stone to more sustainable future buildings and cities with the MFC technology fully integrated.

Index Terms - feedstock, greywater, microbial fuel cell (MFC), urine

I. INTRODUCTION

The transition towards more sustainable buildings and dwellings in terms of waste/wastewater production and treatment as well as energy generation and use, is a global phenomenon that cannot be overlooked. “Living Architecture” is a research project that looked into how future homes and cities could be developed with a ‘living technology’ such as microbial fuel cell (MFC). This project suggested that our future habits should harmonise with other living organisms, which can be used for on-site wastewater treatment, energy generation and resource recovery [1].

In this study, different types of real household greywater as well as human urine were tested as feedstock in MFCs in order to assess feasibility and investigate where MFCs can be integrated within residential buildings in the future. In addition to the exemplars of household effluent, harsh chemicals that are

commonly used in domestic dwellings or offices were tested in order to assess the resilience and limitations of MFC systems within the domestic environment.

II. MATERIALS AND METHODS

A. Household Greywater and Urine

Various types of real domestic greywater and wastewater from five different sources (bathroom, kitchen sink, dishwasher, washing machine and urinal) were tested as MFC feedstock. Greywater was collected anonymously from two households with no dietary restrictions. Neat human urine was donated from consenting adults and pooled before testing.

B. Microbial Fuel Cell Design, Inoculation and Operation

Anode electrodes were made from plain carbon fibre veil (PRF Composite Materials Poole, Dorset, UK) with a macro surface area of 270 cm². A hot-pressed activated carbon cathode with a total surface area of 40 cm² was wrapped outside of the ceramic separator; this cathode was open to air. A 7 cm-long ceramic cylinder (internal diameter 17 mm, thickness 2 mm) was used both as a membrane and as an anode chamber, with a displacement volume of 10 mL.

Activated sludge from a local wastewater treatment plant (Wessex Water, Saltford, UK) was used to inoculate the MFCs. Following the inoculation, MFCs were fed continuously with the subject feedstock at a flow rate of 0.35 L/day.

C. Household Cleaning Products

For this line of work, two commonly used house cleaning products, namely bleach and toilet cleaner (made in the UK products, available from mainstream supermarkets) were chosen. The chemicals were added in full concentration

according to the manufacturers' instructions for use. Exposure time to the chemicals was 18 hours and 7 hours for bleach and toilet cleaner respectively (specific product information can be provided upon request).

III. RESULTS AND DISCUSSION

A. Household Wastewater in MFCs

The highest power of 3.91 ± 0.27 mW per unit was produced when urine was fed, followed by 0.47 ± 0.12 mW from dishwasher effluent fed MFCs. The organic loading, measured as chemical oxygen demand (COD) of the feedstock did not directly correspond to power output, which suggests electricity generation of the anode biofilm is not directly linked to the availability of carbon in the feedstock. Given that tested domestic wastewater was generated as a result of normal daily life, each feedstock varied significantly in terms of composition and concentration, which inevitably resulted in large differences in levels of power output between batches and may also partly explain why the COD reduction is not proportional to the electrical power.

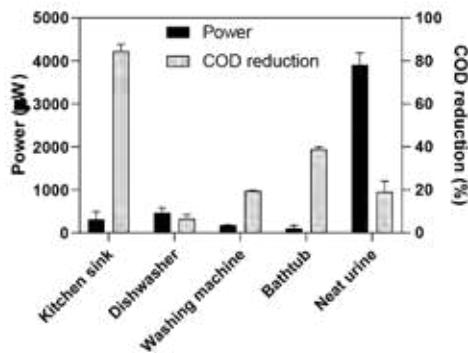


Fig. 1. Power output and treatment efficiency with different types of household wastewater

B. Dilution of Urine

Urine was diluted with either bathtub water or tap water, as a realistic representation of flush water mixed with urine. Results showed that MFC power output decreased with increasing dilutions (2.80 ± 0.31 mW from neat urine down to 0.13-0.20 mW from 15 x diluted urine), whereas COD reduction rate increased (data not shown).

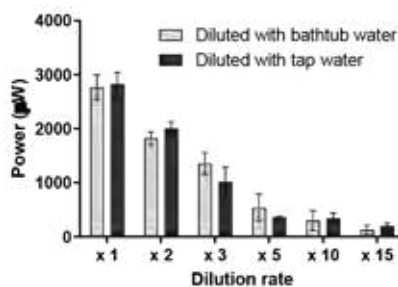


Fig. 2. Power output change with diluted urine as a feedstock

C. Resilience of MFC Biofilms to Household Cleaning Products

Interestingly, when consumer products were added to the systems, the level of instantaneous power dropped, but only in some cases. When the cleaning product was replaced with fresh urine, power output recovered to the previous levels within 48 hours in all cases. This demonstrates that the MFC systems is robust and can be resistant to domestic cleaning products exposure.

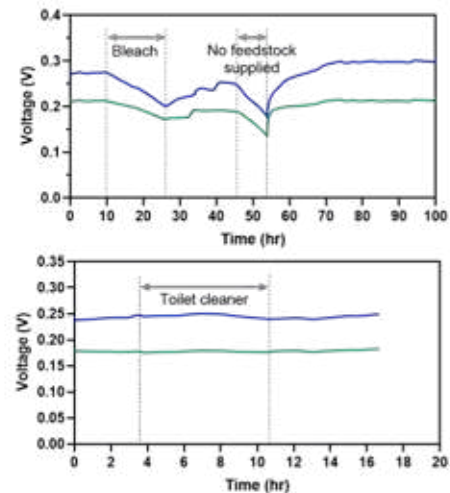


Fig. 3. MFC behaviour during and after experiencing harsh chemicals; bleach (top) and toilet cleaner (bottom)

IV. CONCLUSIONS

Household greywater and wastewater vary between batches in terms of composition and concentration, which leads to variance in the MFC performance. Some waste streams such as bathwater or washing machine effluent that have low organic content thus low MFC power output, could be used for toilet flushing which would be mixed with the favourable MFC substrate, urine. Although dilution of urine reduces the level of electricity generation, a trade-off should be possible. Lastly, MFC systems in a domestic context seem robust enough with short-term exposure to harsh chemicals. These novel findings provide a stepping-stone to more sustainable future buildings and cities with the MFC technology fully integrated.

ACKNOWLEDGMENT

This research was funded by the European Commission Horizon 2020 FET-OPEN Living Architecture Project (grant no. 686585).

REFERENCES

- [1] Living Architecture – transform out habitats from inert spaces into programmable sites, <https://livingarchitecture-h2020.eu/>.

ENERGY AND ENVIRONMENTAL PERFORMANCES ASSESSMENT OF MICROBIAL FUEL CELLS APPLIED TO ANIMAL-WASTE SLURRY TREATMENT

S. D'Apolito*, M. Pulcrano*, V. Sassi**, L. Barelli**, G. Bidini**, E. Sisani**, A. Di Michele*** and M. Minutillo*

*University of Naples "Parthenope", Via Amm. F. Acton 38, Napoli (Italy)

**Department of Engineering, University of Perugia, Via G. Duranti 93, Perugia (Italy)

***Department of Physics and Geology, University of Perugia, Via Pascoli, Perugia (Italy)

Abstract - Microbial fuel cells (MFCs) represent a potential alternative method for treating animal-waste slurry and simultaneously producing electricity. In this work, a MFC that uses the wastewater of a pig breeding company as substrate is tested to evaluate its performance in terms of Nitrogen removal capacity, as well as energy production. It is remarked as the work is focused on Nitrogen abatement, since it represents a pollutant regulated with respect to both discharge into surface water and land spreading; moreover, it is not removed by digestion processes. The obtained experimental results after a period of 42 h are: i) maximum power density of 73 mWm^{-2} at a resistance of 1000Ω and a current density of $324 \text{ mA}\cdot\text{m}^{-2}$, corresponding to an electric energy production of 0.046 Wh , and, mainly, ii) Nitrogen content reduction of 46%, proving the potential impact of applying MFCs to treating technologies for animal sewage.

Index Terms - Animal-waste treatment, Microbial fuel cells, Nitrogen abatement, Renewable energy production.

I. NOMENCLATURE

COD: chemical oxygen demand; MFC: microbial fuel cell; OCV: open circuit voltage; PLA: polylactic acid; PTFE: polytetrafluoroethylene.

II. INTRODUCTION

Microbial fuel cells are bioelectrochemical devices that work as traditional fuel cells and directly convert the chemical energy stored in the organic matter into electrical energy, exploiting the metabolism of exoelectrogenic bacteria. These microorganisms, if forced to work in anaerobic conditions, are able to transfer the electrons, produced during substrate oxidation, outside their cell membrane, thus donating them to a conductive electrode (anode) [1]. Beside COD reduction, MFCs can also operate Nitrogen abatement: specifically, ammonia can be oxidized into nitrites and nitrates (cathodic side), which are

then degraded via denitrification processes (anodic side) in presence of sufficient organic carbon sources [2]. In this case, a single chamber air-breathing cathode configuration is required, since both electrodes have to be in contact with the substrate. Therefore, MFCs exploit a renewable source for power generation and, at the same time, perform the degradation and stabilization of the organic matter. Further advantages are the operation at neutral pH and at nearly ambient temperature.

In this work, a pig-sewage slurry is used as organic substrate: the aims are the evaluation of Nitrogen removal capacity, in order to follow environmental constraints, and the estimation of the produced electrical power.

III. MATERIALS AND METHODS

A. Materials

The MFC reactor is realized according to a single chamber air-breathing cathode configuration. It has a volume of 28 ml for substrate containment and is realized in PLA material by 3D printing. The anode is a carbon fiber brush, while the cathode (active area 7 cm^2) is formed by three-layers, namely, starting from the inner part of the cell: a Nickel mesh for electrons collection, a carbon paper and a PTFE layer for oxygen diffusion. The electrodes are placed orthogonally each other: this configuration allows a better cathodic covering by the anode and, consequently, a higher performance in terms of energy production [3]. The anode biofilm used for the experiments comes from fresh compost taken from an anaerobic digestion plant and it is obtained by applying an appropriate acclimatization and bacterial growth procedure.

B. Sample Collection and Testing Procedure

A sample of pig-waste slurry is collected at the breeding company from a storage tank after the separation of the solid

fraction. The sample is sterilized in autoclave using a standard procedure (1 atm, 121°C, 20 minutes) and then frozen at -20°C. With regards to the MFC test, 10 ml of sample is initially diluted with 20 ml of NaCl (9%) obtaining a solution with pH 9. During the experimental activities, NaCl (9%) is added to maintain the anode covered when the solution level decreases. The cell is maintained at the constant temperature of 30°C for 24 h in OCV mode (acclimation period). At the end of the acclimation period, the cell has reached an OCV equal to 0.62 V. The spent sample, collected after MFC operation, is analyzed in terms of Nitrogen content, comparing the results with the fresh sample ones.

IV. RESULTS AND DISCUSSION

Results are presented in terms of polarization curve and power density (power and current densities are calculated with respect to the cathodic active area). The polarization curve, as shown in Fig.1, is measured by applying the batch-mode method (the resistance is varied in the range 10,000-220 Ω and, at each step, the resistance is maintained constant for 5 min) [3]. The maximum power density (Fig.1) is 73.3 mWm⁻² (at a current density of 323.6 mA m⁻²). It is achieved at 1000 Ω.

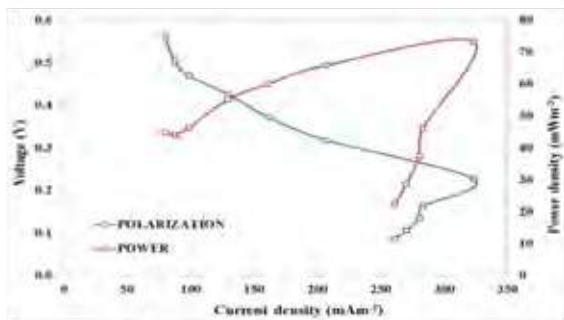


Fig. 1. First polarization curve ($R = 10,000-220 \Omega$)

Moreover, by analyzing the polarization curve, it can be noticed that, in the field of high current densities (or low resistances), the phenomenon of power overshoot occurs; in this case, both the voltage and the current density decrease, because the bacteria are not able to produce electricity at low external resistances. Finally, in order to evaluate the cell operation in terms of energy production, the resistance (1000 Ω), at which the maximum power density is reached, is applied for a period of 23 h. The power density production trend is shown in Fig.2. It is worth noting that the maximum power density (75.2 mWm⁻²) is reached after 8 hours; then, it decreases as the substrate is consuming (the substrate was not replenished during this experimentation). The energy production has been 1.22 Whm⁻²

By applying the same experimental procedure, the MFC is further tested. In this last test, the measured OCV is 0.53 V and the maximum power density of 39.6 mWm⁻² (at a current density of 237.9 mA m⁻²) is reached at 1000 Ω.

Moreover, the operation at constant load is monitored for additional 20 h. In this case the energy production has been 0.4 Whm⁻².

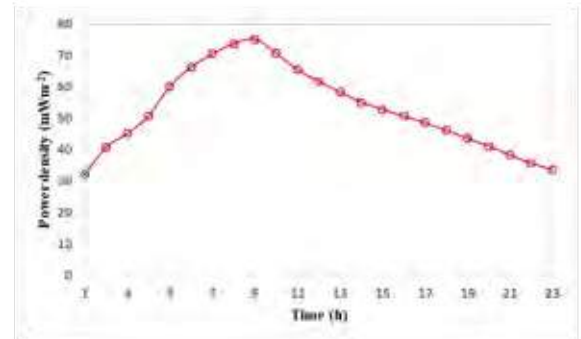


Fig. 2. MFC operation at constant load ($R = 1000 \Omega$)

The biochemical analysis of the substrate, before and after the cell operation, is performed. Results (Table I) illustrate a significant reduction of both ammoniacal (-66%) and total (-46%) Nitrogen contents.

TABLE I
AMMONIACAL AND TOTAL NITROGEN REDUCTION DURING MFC OPERATION

	SAMPLE IN (mg l ⁻¹)	SAMPLE OUT (mg l ⁻¹)	REDUCTION (%)
N-NH ₄ ⁺	1690	583	66
N _{tot}	1700	914	46

V. CONCLUSION

The investigated MFC exhibited Nitrogen abatement from a pig-waste slurry, obtaining an ammoniacal and total Nitrogen removal capacity of 66% and 46% respectively, during about 43 h of operation. Basing on these results, it is possible to affirm that the MFC could be coupled to traditional technologies to operate the degradation and stabilization of the organic matter, producing a final waste that follows environmental constraints. Moreover, instead of highly energy demanding purification systems, the MFC is also able to directly produce small amounts of electrical energy, which can be used for some auxiliary devices in the treatment plant.

ACKNOWLEDGMENT

This research activity was partially granted by the Basic Research Funds supplied by the Department of Engineering of the University of Perugia.

REFERENCES

- [1] M.H. Osman, A.A. Shah, F.C. Walsh; *Biosensors and Bioelectronics*, Vol. 26, 2010, pp. 953-963.
- [2] N. Yang, G. Zhan, D. Li, X. Wang, X. He, H. Liu; *Chemical Engineering Journal*, Vol. 356, 2019, pp. 506-515.
- [3] V. Lanas, B. E. Logan; *Bioresource Technology*, Vol. 148, 2013, pp. 379-385.

A TECHNO -ECONOMIC ANALYSIS OF ON-GRID SOLAR HYDROGEN PRODUCTION BY ELECTROLYSIS IN THE NORTH OF CHILE AND THE CASE OF EXPORTATION FROM ATACAMA DESERT TO JAPAN

Gallardo, Felipe Ignacio ¹; Monforti Ferrario, Andrea ^{2,3,*}; Lamagna, Mario ¹; Bocci, Enrico ²; Astiaso Garcia, Davide ⁴ and Bacza-Jeria, Tomas E. ⁵

¹ Department of Astronautics, Electric and Energy Engineering. Sapienza University of Rome, Via Eudossiana 18, (Italy)

² Faculty of Applied Sciences and Technology. USGM, Via Plinio 44, Rome (Italy)

³ Centro Interuniversitario di Ricerca Per lo Sviluppo Sostenibile "CIRPS", Piazza U. Pillozzi, Valmontone (Italy)

⁴ Department of Planning, Design, and Technology of Architecture. Sapienza University of Rome, Via Flaminia 72, Rome (Italy)

⁵ Chilean Solar and Energy Innovation Committee, Agustinas 640, Santiago (Chile)

*corresponding author: email a.monforti@lab.unimarconi.it

Abstract - H₂ production from solar electricity in the region of the Atacama Desert – Chile – has been investigated for 2018 and projected to scenarios up to 2025. The multi-year hourly electrical profiles data have been provided from real operating PV and CSP power plants as well as reported commercial electricity PPA prices in the Chilean electricity market. The Levelized Cost of Hydrogen "LCOH" of each production pathway is calculated by a case-sensitive techno-economic MATLAB/Simulink model for scales from 1 MW_e to 50 MW_e for alkaline and PEM electrolyser technologies coupled with real power plants. Successively, storage and transportation are evaluated based on the 2030 Japanese case study according to the capacity of currently available transport ships. Transport in the form of liquefied hydrogen (LH₂) and via ammonia (NH₃) carrier is compared from the port of Antofagasta, CL to the port of Osaka, JP.

Keywords – Solar hydrogen, Techno-economic analysis.

I. INTRODUCTION

Techno-economic feasibility of green hydrogen production from renewable energy is highly dependent from country specific resources and energy market characteristics which play a key role in determining cost competitiveness. Also, demand volume relevantly affects the feasibility of H₂ production and can foster one supply-chain configuration respect to others. In this context, this paper aims to investigate techno-economic feasibility of various supply chain configurations of hydrogen production by on-grid solar driven electrolysis in Chile and transportation to Osaka, Japan [1].

II. SOLAR H₂ PRODUCTION

The production of solar-H₂ is studied in 4 different scenarios:

1. Electrolysis by PEM electrolyzer supplied by an on-grid CSP+TES. PPA with flat profile (24/7).
2. Electrolysis by PEM electrolyzer supplied by an on-grid PV. PPA with solar profile (8:00 – 18:00).

3. Electrolysis by Alkaline electrolyzer supplied by an on-grid CSP+TES. PPA with flat profile (24/7).
4. Electrolysis by Alkaline electrolyzer supplied by an on-grid PV. PPA with solar profile (8:00 – 18:00).

This choice is made based on the well-known market maturity and dominance of PV during solar hours and CSP+TES for 24/7 schemes [2,3]. Solar PV with batteries and CSP without TES are therefore excluded.

A. Input data

The average seasonal electrical profile of solar PV plants was obtained from the operational data of several installed plants in the Atacama Desert region – Chile (Figure 1). CSP+TES data was simulated using NREL System Advisor Model in hourly resolution and adapted TMY historical meteorological data. The two profiles mainly differ in the capacity factor, ranging from around 37% for solar PV against 92.5% for CSP with TES plants due to seasonal variations.

The bilateral Power Purchase Agreements "PPA" reported in the Chilean energy market are summarized in Table I.

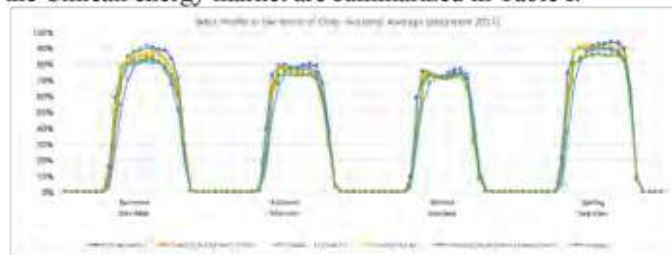


Fig. 1. Input Solar Profiles. Source CEN Chile (ISO)

TABLE I
PPA PUBLIC PRICES: LICITACIONES ELECTRICAS 2017 - MINISTRY OF ENERGY

Technology	PPA price (US\$/MWh)
Solar PV	20-25
Solar CSP+TES	50-55

B. On-grid electrolysis

On-grid Alkaline and PEM electrolyzers can be sized from the energy performance parameters reported in Table II. Via a scale-sensitive (1-50 MW_e) techno-economic model, developed in MATLAB/Simulink, the electrolyser black-box operation can be simulated throughout the year with hourly resolution.

TABLE II
ELECTROLYSER PARAMETERS [4]

Electrolyser performance parameters		Alkaline	PEM
System specific consumption (20% auxiliaries)	kWh _{AC} /kg	54 (2018) 49 (2025)	60 (2018) 52 (2025)
Stack lifetime	Operating hours (h)	80.000	60.000
Load threshold	% P _{nominal}	80%	160%
Specific cost	MUS\$/MW (utility-small scale)	0.75-1.2 (2018) 0.48-0.9 (2025)	1-1,5 (2018) 0.6-1 (2025)

III. STORAGE AND TRANSPORT

The Japanese Ministry of Economy, Trade and Industry (METI) reported a projected hydrogen demand in 2030 of 300 kTons/year, which sets the demand for the analysis. The supply is limited by the current capacity per transport ship which can complete a return trip from Antofagasta, CL to Osaka, JP in approximately 60 days. The analysed transport configurations are the following (parameters in Table III):

1. Liquified Hydrogen "LH₂" by Claude cycle
2. Liquified Hydrogen by compressed hydrogen buffer.
3. Liquid Ammonia carrier by Haber-Bosch process

Table III
Transport and storage parameters [5]

Type	Pressure (bar)	Specific Work (kWh/kg)	Capacity per ship	Specific investment cost
Buffer compression	30-80	1-2	2.8 Ton _{H₂} (daily)	800 US\$/kW compressor 250-500 US\$/kg stored
Liquefaction and blow-off	30-50	9-12	170 Ton _{H₂}	55 US\$/kg/h liquefaction 75 US\$/kg stored (boil-off)
Ammonia (existing plant)	30	6,14 (NG)	4000 Ton _{H₂}	700 US\$/Ton _{NG} 1400 US\$/Ton bulk H ₂

IV. RESULTS AND DISCUSSION

According to the capacity factors, 20 MW solar PV is required compared to 7 MW for the CSP case to produce the set amount of H₂ per ship. Despite the larger size, the solar PV configuration coupled to Alkaline electrolysis is more cost competitive as the reduced PV energy cost compensates the oversized CAPEX: LCOH is as low as 1.69 US\$/kg_{H₂} in the utility 2030 scenario (Figure 2). The sensitivity analysis confirms greater dependence from the electricity respect to CAPEX.

The LH₂ LCOH oscillates between 5.72-6.86 US\$/kg_{H₂} (Figure 3 - Utility scale) according to the configuration. The NH₃ LCOH is 5.99 US\$/kg_{H₂}. The larger OPEX contribution is

balanced with a reduced travel cost. However, the system is relevantly under-sized respect to standards.



Fig. 2. LCOH in Chile from solar technologies (2025) repartitioned by scale and consistency (%) respect to 2018

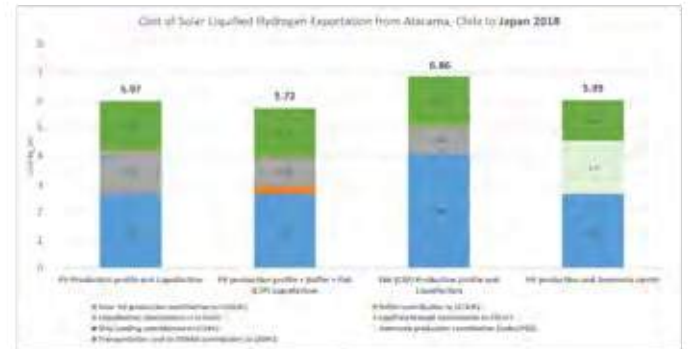


Figure 3. LCOH for exportation case study at Osaka, Japan

V. CONCLUSION

In the Chilean electricity market, it is more competitive to oversize an alkaline electrolyser supplied by PV system (25 USD/MWh – capacity factor around 35%), with respect to a CSP system (55 US\$/MWh – flat profile) due to the high electricity intensity of the H₂ production process counterbalancing the increase in CAPEX of the electrolysers.

For the exportation case an opposite tendency is verified: the most competitive configuration is to produce with a PV profile and liquefy H₂ with a 24/7 profile supplied by CSP with a daily buffer of compressed H₂ due to the higher specific cost of the liquefaction system. The NH₃ carrier can be advantageous for larger capacities but for the selected one it suffers relevant capacity mismatch obtaining only comparable results.

ACKNOWLEDGMENT

Hans Kulenkampff from H2chile is kindly acknowledged for providing feedback regarding electrolyser parameters. Ana Maria Ruz Frias from Comit  Solar is kindly acknowledged to provide guidance for this work.

REFERENCES

- [1] Chilean Solar Committee - Tractebel, Opportunities for the development of hydrogen industry in the region of Antofagasta and Atacama, 2018.
- [2] Photovoltaics Report – Fraunhofer 2019.
- [3] DOE USA 2019. Solar-Plus-Storage 101
- [4] Tractebel Engineering and Hincio, Study on Early Business Cases for H₂ in Energy Storage, FCH-JU, 2017.
- [5] ACIL. Allen Consulting, Opportunities for Australia from Hydrogen Exports, 2018.

Abstract Number: EFC19141

LSCF/GDC CO-ELECTROSPUN NANOFIBER CATHODES FOR APPLICATION IN IT-SOFCs

Caterina Sanna^a, Wenjing Zhang^b, Paola Costamagna^a, Peter Holtappels^b

^a Department of Chemistry and Industrial Chemistry, University of Genoa,
Via Dodecaneso 31, I-16146 Genoa, Italy

^b Department of Energy Conversion and Storage, Technical University of Denmark,
Frederiksborgvej 399, DK-4000 Roskilde, Denmark

Abstract - Preparation and electrochemical testing of cathodes formed by a mixture of $\text{La}_{0.6}\text{Sr}_{0.4}\text{Co}_{0.2}\text{Fe}_{0.8}\text{O}_{3-\delta}$ (LSCF) and $\text{Ce}_{0.9}\text{Gd}_{0.1}\text{O}_{1.95}$ (GDC) fibers is reported. The electrodes are obtained by simultaneous electrospinning of the two precursors solutions, using an apparatus equipped with two spinnerets working in parallel. Results of electrochemical testing carried out through electrochemical impedance spectroscopy (EIS) are presented and discussed. The results suggest that the electrochemical reaction takes place in an electrode thickness close to the electrode/current collector interface, and that the oxygen ions then flow along the ionic conducting path of the GDC fibers. At 650°C, the polarization resistance is $R_p = 5.6 \Omega \text{ cm}^2$, in line with literature values reported for other IT-SOFC cathodes.

Index Terms – Electrochemical impedance spectroscopy (EIS), Electrospinning, Nanofiber, Percolation.

I. INTRODUCTION

Intermediate temperature-solid oxide fuel cells (IT-SOFCs) are under development for operation in the temperature range 600-800°C. Reduction in working temperature is expected to mitigate degradation, reduce sealing problems, enable the use of inexpensive materials and improve response to rapid start-up. However, lowering the operating temperature also lowers the fuel cell performance. For this reason, high performance electrolytes and electrodes are currently under development, often based on mixed ionic electronic conductors (MIECs). In parallel, also the technique of electrode manufacturing is being refined. Electrospun 1-D materials like nanotubes, nanowires, nanorods and nanofibers have gained significance mainly due to their high surface area and mechanical properties.

In this framework, the present work is focused on the preparation and electrochemical testing of cathodes formed by a mixture of $\text{La}_{0.6}\text{Sr}_{0.4}\text{Co}_{0.2}\text{Fe}_{0.8}\text{O}_{3-\delta}$ (LSCF) and $\text{Ce}_{0.9}\text{Gd}_{0.1}\text{O}_{1.95}$ (GDC) fibers electrospun simultaneously through an electrospinning apparatus equipped with two spinnerets.

II. EXPERIMENTAL

A. Sample preparation

LSCF/GDC nanofiber electrodes are prepared through a sol-gel assisted electrospinning method to synthesize ceramic nanofibers. The LSCF precursors are $\text{La}(\text{NO}_3)_3 \cdot 6\text{H}_2\text{O}$, $\text{Sr}(\text{NO}_3)_2$, $\text{Co}(\text{NO}_3)_2 \cdot 6\text{H}_2\text{O}$ and $\text{Fe}(\text{NO}_3)_3 \cdot 9\text{H}_2\text{O}$, which are dissolved in de-ionized water. Polyvinylpyrrolidone (PVP) is used as carrier polymer, with a weight ratio of PVP in solution 0.1. Further details are reported in [1]. The GDC precursors are $\text{Gd}(\text{NO}_3)_3 \cdot 6\text{H}_2\text{O}$, $\text{Ce}(\text{NO}_3)_3 \cdot 6\text{H}_2\text{O}$ dissolved in a solution 50%-50% vol of water and ethanol; PVP is dissolved in another solution 50%-50% vol of water and ethanol. The final GDC solution is obtained by mixing 50%-50% vol of the previous solutions. The electrospinning laboratory equipment is RT Advanced by Linari Engineering. During electrospinning, the applied electrical potential is 40 kV; the injection rate is 0.5 mL/h for the LSCF solution and 1 mL/h for the GDC solution. After drying, circular electrodes are cut from the nanofiber tissue, which are then heat treated at 800 °C. To prepare the symmetrical cells, the electrodes are applied on both sides of a GDC electrolyte disk.

B. Morphological characterization and electrochemical tests

Scanning electron microscopy (SEM) is carried out through Zeiss Ultra 55 microscope. Energy Dispersive X-ray (EDX) analyses are carried out through a Bruker SCU instrument.

For the characterization, the cells are mounted in a four sample set-up in which each cell is fixed between two gold meshes, which also act as current collectors. The set-up is placed in a furnace, sealed and attached to the gas supply system. First of all, the symmetrical cells are fired in situ in the electrochemical testing equipment, at 950°C for 3 h. Then, EIS spectra are recorded using a Gamry Reference 600 potentiostat.

III. RESULTS AND DISCUSSION

Fig. 1 reports a top view of the LSCF-GDC electrode after heat treatment. The structure of the fibers is well maintained. The EDX analyses make it possible to ascertain that the LSCF fibers are significantly thicker than the GDC fibers.

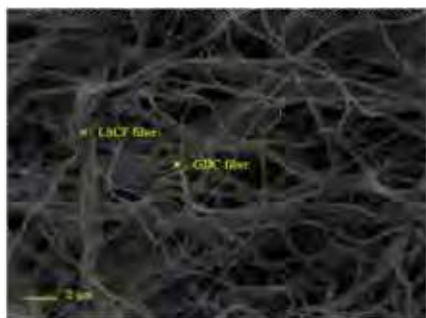


Fig. 1. SEM picture of LSCF-GDC electrode after heat treatment at 800°C.

Experimental EIS tests are carried out at open circuit voltage and with 20% oxygen in argon atmosphere. The results are reported in Fig. 2, displaying typical Gerischer behavior in the high frequency part while another process is indicated at low frequencies. From a qualitative point of view, the experimental data are similar to those found with LSCF electrospun nanofiber electrodes [1,2]. From a quantitative point of view, at 650°C, an R_p of 5.6 $\Omega \text{ cm}^2$ is obtained from LSCF/GDC electrodes, whereas for LSCF electrospun electrodes, an R_p of 1 $\Omega \text{ cm}^2$ has been reported in previous works [1,2]. Considering the intercept of the EIS arcs with the real axis, usually denominated R_s , it is found that R_s is 2.8 ohm cm^2 for the Nyquist arc in Fig. 2. This value is significantly larger than with pure LSCF electrospun nanofiber electrodes [1,2]. Further analyses, not reported here, demonstrate that this value is consistent with that obtained by summing up the electrolyte resistance, the contact resistance and the ionic resistance of the GDC fibers in the electrodes. This suggests that the electrochemical reaction occurs in a part of the electrode close to the electrode/current collector interface; then the oxygen ions follow the GDC path to the electrolyte. At 650°C, in principle, the lowest resistance path through the electrode should be the

electronic conducting path along the LSCF fibers. This is in contrast with the findings reported above, that the electrical charges flow along the electrode under the form of oxygen ions. This contradiction can be explained considering that the LSCF nanofibers do not percolate through the electrode. This can be justified in the case where LSCF fibers have higher concentration close to the electrode/current collector, and GDC fibers have higher concentration close to the electrode/electrolyte interface. Another explanation could be based on the consideration that, despite the volume of LSCF and GDC deposited through the electrospinning process is practically the same, nevertheless, as already pointed out, the dimension of the LSCF nanofibers is larger than the dimension of the GDC nanofibers (Fig. 1). Consequently, LSCF percolation is hindered.

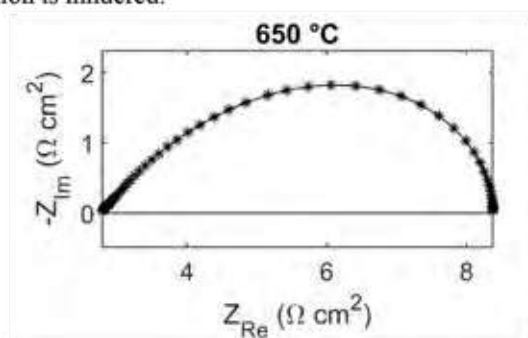


Fig. 2. Nyquist plot of EIS experimental spectrum at 650°C.

IV. CONCLUSION

In this work, 5-6 times higher electrode resistances are obtained for composite LSCF/GDC fibers compared to electrospun LSCF fibers. This is attributed to the fact that the LSCF fibers do not form a percolated network, and thus the electrochemical reaction takes place in the outer part of the electrode, close to the current collector. Thus, percolation issues affect not only bimodal granular electrodes, but also bimodal nanofiber electrodes. Percolation may be very different with fibers laying in plane or randomly distributed in 3-D (for example, nanorods).

REFERENCES

- [1] Enrico A., Zhang, W., Lund Traulsen, M., Sala, E.M., Costamagna, P., Holtappels, P., $\text{La}_{0.6}\text{Sr}_{0.4}\text{Co}_{0.2}\text{Fe}_{0.8}\text{O}_{3-\delta}$ nanofiber cathode for intermediate temperature–solid oxide fuel cells by water-based sol-gel electrospinning: Synthesis and electrochemical behavior, *Journal of the European Ceramic Society*, Volume 38, 2018, pp. 2677–2686.
- [2] Costamagna, P., Sala, E.M., Zhang, W., Lund Traulsen, M., Holtappels, P., Electrochemical impedance spectroscopy of $\text{La}_{0.6}\text{Sr}_{0.4}\text{Co}_{0.2}\text{Fe}_{0.8}\text{O}_{3-\delta}$ nanofiber cathodes for intermediate temperature–solid oxide fuel cell applications: A case study for the ‘depressed’ or ‘fractal’ Gerischer element, *Electrochimica Acta*, Volume 319, 2019, pp. 657–671.

FROM BIOGAS TO BIO-HYDROGEN FOR REFUELING STATIONS: ANALYSIS ON THE PLANT AVAILABILITY AND ECONOMIC EVALUATIONS

M. Minutillo*, A. Perna**, S. Di Micco*, P. Di Trolio*, A. Forcina*,

*University of Naples "Parthenope", Centro Direzionale, Is C4, (Naples, Italy)

** University of Cassino and Southern Lazio, Via G. Di Biasio 43, (Cassino, Italy)

Abstract - In this study the economic analysis of a biogas based-hydrogen refueling station is carried out, by considering the plant availability. A hydrogen rich gas stream, that is generated by a biogas processing unit based on the autothermal reforming process, is purified by means of a Pd-Ag membrane separation unit and is compressed up to 820 bars by using an ionic compressor system. An SOFC power unit fed with part of the syngas exiting the autothermal reactor supplies the electric power required from the hydrogen separation and storage section. In order to evaluate the variation of hydrogen cost, a sensitivity analysis, based on reliability performance and real operating conditions of the plant, has been performed.

Index Terms - Availability, Hydrogen, Ionic Compressor, LCOH, O&M.

INTRODUCTION

The growing interest in the development of the hydrogen mobility emphasizes the need for novel refueling stations that start to be developed and deployed in many countries. In the present research the economic assessment of a biogas-based hydrogen refueling station is carried out taking into account two aspects: the plant availability and the operating costs variation.

BIO-HYDROGEN REFUELING STATION: PLANT DESCRIPTION

The proposed plant has been designed taking into account that the hydrogen is produced by biogas (60%CH₄ and 40% CO₂) from anaerobic digestion [1]. The electric energy required for the plant operation is supplied by a SOFC power unit. Fig.1 shows a simplified scheme of the plant configuration.

Biogas, water and air fed the Syngas Production Unit, consisting of an autothermal reactor and a water gas shift reactor working at atmospheric pressure.

Thus, the hydrogen rich gas stream (25.8 H₂, 28.5 N₂, 24.5 H₂O, 11.4 CO₂, 9.8 CO) exiting the ATR is split into two fluxes: the first one feeds the SOFC power unit (36 kW AC),

while the second one is sent to the hydrogen purification unit (consisting of a water gas shift reactor and a Pd-Ag membrane separation unit) and compression (ionic compression) unit.

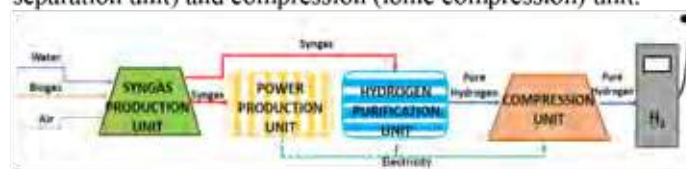


Fig.1. Layout of the biogas based-hydrogen refueling station

The plant designed and sized for producing 100 kg/day of hydrogen at 820 bar, has been simulated by using thermo-electrochemical models developed in Aspen Plus environment [2].

LCOH EVALUATION: O&M COSTS AND PLANT AVAILABILITY

The levelized cost of hydrogen (LCOH) has been assessed as [3]:

$$LCOH = \frac{\text{Total Costs}}{\text{Annual Production}} = \frac{C_{inv,a} + C_{O\&M} + C_{rep,a}}{MH_{2,a}} \quad (1)$$

The annual capital repayment ($C_{inv,a}$), calculated by considering the total plant capital investment costs (C_{inv}), the economic lifetime of the plant of 20 years (n) and the nominal discount rate (i) of 6.4%, is defined as:

$$C_{inv,a} = \frac{i \cdot (1+i)^n}{(1+i)^n - 1} \cdot C_{inv} \quad (2)$$

Table 1 summarized the capital investment costs of the main components of the plant.

TABLE 1 - Capital investment costs

COMPONENTS	CAPITAL INVESTMENT COST	k€
SYNGAS PRODUCTION UNIT		150.0
POWER PRODUCTION UNIT		315.5
HYDROGEN MEMBRANE SEPARATION UNIT		51.5
COMPRESSION UNIT		1200.0
AUXILIARIES*		248.0
Total plant capital investment costs (C_{inv})		1965.0

* Heat Exchangers, Measurement and Control, Piping & BOP and Civil work.

The annualized replacement cost ($C_{rep,a}$), calculated by considering the replacement cost, the year of replacement (t) and the nominal discount rate (i), is calculated as:

$$C_{rep,a} = \frac{i \cdot (1+i)^n}{(1+i)^n - 1} \cdot \frac{C_{rep}}{(1+i)^t} \quad (3)$$

The replacement costs (every 5 years) refer to the SOFC stack replacement (46.5 k€) and to the catalysts replacement (27.0 k€) [2]. The $C_{inv,a}$ and the $C_{rep,a}$ result equal to 176.9 k€ and 11.0 k€, respectively.

A. Effect of O&M costs on LCOH

In this study the yearly operating time has been assumed equal to 8000 hours [4], which corresponds to a plant availability of 91%. In order to evaluate the impact of the O&M costs on the LCOH, three cases (Base Case, Case 1 and Case 2) have been defined. In the Base Case, that is the reference case, the O&M costs have been assumed equal to the 3% of the initial investment for each component of the plant as suggested in ref [4]. In the Case 1 and Case 2, the specific O&M cost of the SOFC unit, which represents the most critical component of the plant, has been given equal to 5.5% of the initial investment, according to [5], while, for the membrane separation unit, a value of 2.67% has been set [6]. With referring to the ionic compressor there is no reference in the scientific literature concerning its O&M costs, being this technology recently introduced on the market. Thus, in order to evaluate the impact of these costs on the LCOH, the 2% and 4% of the initial investment are assumed for the Case 1 and Case 2, respectively. Table 2 lists the assumptions for the O&M costs and the calculated values in the 3 cases analyzed.

TABLE 2. LCOH evaluation

Components	Base Case	Case 1	Case 2
SYNGAS PRODUCTION UNIT	3%	3%	3%
POWER PRODUCTION UNIT	3%	5.5% [5]	5.5% [5]
HYDROGEN PURIFICATION UNIT	3%	2.67% [6]*	2.67% [6]*
COMPRESSION UNIT	3%	2%	4%
AUXILIARIES*	3%	3%	3%
O&M	58.9 k€	54.7 k€	78.6 k€

* In [6] this value was 2.5% because it was referred to 7500h.

Fig.2 shows the individual cost items for the calculated LCOH. The ionic compressor O&M cost strongly affects the LCOH; as a matter of fact, by considering the hydrogen production rate (100 kg/day) and the calculated costs (eq. 3), the LCOH ranges from 7.28 €/kg (Case 1) to a value of 8.00 €/kg (Case 2).

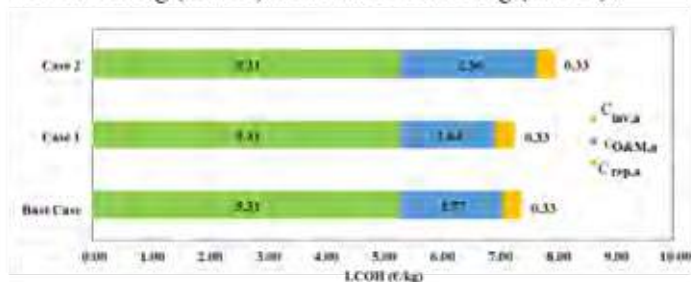


Fig. 2. Individual cost items calculate d for LCOH evaluation.

Table 3 summarizes the incidence of each component's cost on the LCOH value.

TABLE 3 - Incidence of each unit on LCOH

Unit	Base Case		Case 1		Case 2	
	€/kg	%	€/kg	%	€/kg	%
SYNGAS PRODUCTION UNIT	0.66	9	0.66	9	0.66	8
POWER PRODUCTION UNIT	1.34	18	1.58	22	1.58	20
HYDROGEN PURIFICATION UNIT	0.19	3	0.18	2	0.18	2
COMPRESSION UNIT	4.32	58	3.96	54	4.68	59
AUXILIARIES*	0.90	12	0.90	12	0.90	12
LCOH (€/kg)	7.41		7.28		8.00	

* Heat Exchangers, Measurement and Control, Piping & BOP and Civil

B. Effect of yearly operating time on LCOH

The analysis has been carried out by evaluating the hourly availability cost calculated as:

$$C_{AV,h} = \frac{C_{O\&M,a} + C_{rep,a}}{\text{Operating Time}} \quad (4)$$

By assuming 8000 h/year as the reference operating time and the yearly O&M costs of the Case 2, the $C_{AV,h}$ results to be 11.21 €/h. Thus, by assuming this value as the reference for this kind of plants, it is possible to calculate the LCOH for different operating times in the range 7500-8200 h, corresponding to a plant availability ranging from 80 to 95%. Results in terms of LCOH and hydrogen production are summarized in table 4.

TABLE 4. LCOH and hydrogen production vs. plant operating time

Plant operation time (h)	7500	7600	7700	7800	7900	8000	8100	8200
H2 production (10 ⁵ Nm ³)	3.47	3.52	3.56	3.61	3.66	3.70	3.75	3.80
LCOH (€/kg)	8.35	8.28	8.20	8.13	8.06	8.00	7.93	7.87

CONCLUSION

Results of this study can help to choice the best plant management strategy; in particular, it is possible to affirm that it is better to minimize the O&M costs (case 1) rather than maximize the availability of the plant (8200 h); as a matter of fact, by reducing the compressor O&M cost from 4% to 2% (8000 h), the LCOH decreases of 9%, while, increasing the operating time from 7500 to 8200 h, LCOH decreases of 6%.

REFERENCES

- [1] Minutillo M, Perna A, Sorce A. Combined Hydrogen, Heat and Electricity Generation via Biogas Reforming: Energy and Economic Assessments, Int. J Hydrogen Energy. 2019;44 (43):23880-23898.
- [2] Minutillo M, Perna A, Sorce A. Biofuel-based Polygeneration Energy System for Electricity, Heat and Mobility Demands: Plant Design and Energy Streams Management, Proceedings of 13th SDEWES, Palermo (Italy), September 30 - October 4, 2018.
- [3] Hinkley J, Hayward J. Cost assessment of hydrogen production from PV and electrolysis, CSIRO, (Australia,2016).
- [4] Giarola S., Forte O., Techno-economic assessment of biogas-fed solid oxide fuel cell combined heat and power system at industrial scale, Applied Energy. 2018;211:689-704.
- [5] Catalog of CHP technologies, Section 6. 2015.
- [6] Di Marcobernardino G.,Knijff J, Techno-Economic Assessment in a Fluidized Bed Membrane Reactor for Small-Scale H₂ Production: Effect of Membrane Thickness, Membranes. 2019;9:116

RECOVERY PROCEDURE FOR 30 KW PEM FUEL CELL STACKS

E. Gadducci*, T. Lamberti*, L. Magistri, A.F. Massardo*

*Università degli Studi di Genova, (Italy)

Abstract – The University of Genoa hosts the HI-SEA (Hydrogen Initiative for Sustainable Energy Applications) joint laboratory with Fincantieri, to study the best design of a 240 kW PEMFC system for shipping. It is made up of 8 stacks (by Nuvera Fuel Cells) with BoP that come from a previous national project; stacks were left inactive for more than 2 years before being installed in the HI-SEA container. Inactivity leads to severe issues linked to the membrane's water content, and for this reason during the study we focused on developing a performant recovery procedure for the stacks, based on thermal and humidity management. The implementation of the procedure will be described, showing its successful implementation. The 8 stacks were recovered, and their performance was restored, in comparison with polarization curves from factory tests and from the experimental campaign.

Index Terms – Hybridization, PEMFC, Recovery, System engineering

I. NOMENCLATURE

GHG	Green House Gases
RES	Renewable Energy Sources
SOA	State Of the Art
PEMFC	Polymeric Electrolyte Membrane Fuel Cell
BoP	Balance of Plant
CVM	Cell Voltage Monitoring
PLC	Programmable Logic Controller
FAT	Factory Test
FC	Fuel Cell

II. INTRODUCTION

The problem of reducing GHGs emission in shipping was first faced by IMO in 2018 [1]. The use of alternative fuels on-board can decrease navigation's environmental impact, hydrogen and fuel cells resulted one of the most interesting candidates, due to the the high potential of FC systems installation and to the possibility to combine them with RES excess production issues and increased efficiencies [2][3]. The technology SOA is nevertheless still poor due to the absence of prescriptions for installation nor of regulations on ships emissions [3]. TESEO Project [4] was carried out by the University of Genoa in collaboration with the Italian National Research Centre (CNR), Nuvera Fuel Cells and Fincantieri, to investigate the use of PEMFC for the development and demonstration of an electrical generator of 240 kW output power for shipping. The final goal

was to define the best design for a modular FC system to guarantee the maximum life spam of FC stacks without omitting performance. After the end of the project, the stacks – 30 kW each – were left inactive for almost 2 years before being employed in the HI-SEA laboratory, founded by the University of Genoa and Fincantieri, designed to study the behaviour of the PEMFC system in a grid with different sources of electrical and thermal power. The HI-SEA Lab is equipped with all the required FC system interface: hydrogen and air pipes and collectors, air compressor, cooling circuit, gaseous hydrogen storage in tanks and a modular resistive load. As inactivity is linked to many issues, mainly to membrane dehydration [5], stacks were at first in poor conditions and it was necessary to find out an effective recovery procedure.

III. EXPERIMENTS

Voltage is among the most important parameters to ensure the state of health when operating a PEMFC [6]. Stacks in the HI-SEA plant are provided with a Cell Voltage Monitoring (CVM) system that acquires, amplifies and digitalizes the signals from each one of the almost 200 cells per stack. Data are collected and elaborated by a Programmable Logic Controller (PLC) that saves, among others, values of the average (V_{avg}), maximum (V_{max}) and minimum (V_{min}) cell voltage. The data analysis linked to V_{min} was crucial at the beginning of the experimental campaign to hint issues linked to inactivity and dehydration, and at the end of it to suggest that recovery was effective. The acquired voltage was in fact compared with Factory Tests (FAT) performance and with the results of the stack voltage model developed on Matlab-Simulink [7].

Before recovery, stacks could reach half the nominal power, showing significantly low voltage values and strong instabilities. Increasing the air flow rate with respect to the original design settings gave the opportunity to reach higher voltages, in accordance with Nernst equation [8], and to explore the entire operative range of FC stacks. This condition highlighted the main problematics that were faced by the recovery procedure. This procedure is focused on thermal management, aiming to restore the original performance by establishing back a good membrane humidity level on the dehydrated polymers in accordance with other recovery procedures showed in [9].

IV. RESULTS

When the stack to be recovered is turned on, the operator should monitor the correct implementation of the startup procedure, and then should start imposing an increasing 1 kW-load through the modular resistive bank installed. The power load should be increased as long as oscillations in V_{\min} are verified: oscillations on cell's voltage prevent to increase the power load and could be related to dehydration problems. Therefore, the elaborated procedure prescribes to decrease of 1 kW the power load and maintain the stack in static operation at the attained current level for a given time. Changes in V_{\min} is then interpreted: if the oscillations are reduced, it is possible to increase the load again up to the next oscillation is encountered. If not, the stack inlet cooling temperature should be decreased by 3°C at first. This will allow an accumulation of water on the polymeric membranes, that would establish back a good relative humidity of a de-hydrated membrane. If the operation does not bring any benefit, the opposite operation should be conducted, by rising the cooling temperature instead, to assess the flooding condition of the membrane.

The peculiarity of the recovery procedure developed in the HI-SEA laboratory with respect to other previous procedures is the effectiveness at the stack level, while the SOA is generally referred to single cells.

The recovery procedure can be usefully adopted also in case of shorter inactivity time, before starting tests, to ensure a good relative humidity in the membranes.

V. CONCLUSION

Next figures show polarization curve of stack 6 (FCM6) denominated ORI-14-09, before (Fig.1) and after (Fig.2) recovery, where the blue dotted line represents FATs results, orange circles are the model's results and blue, green and red points are respectively V_{\max} , V_{avg} , V_{\min} . Values of voltage are hidden from the figures due to confidentiality issues with the FC stacks supplier, Nuvera Fuel Cells.

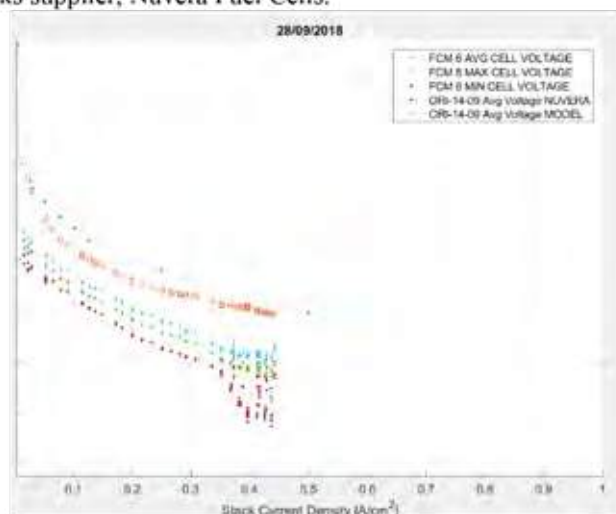


Fig. 1. Polarization curve of stack ORI-14-09 (FCM6) before recovery

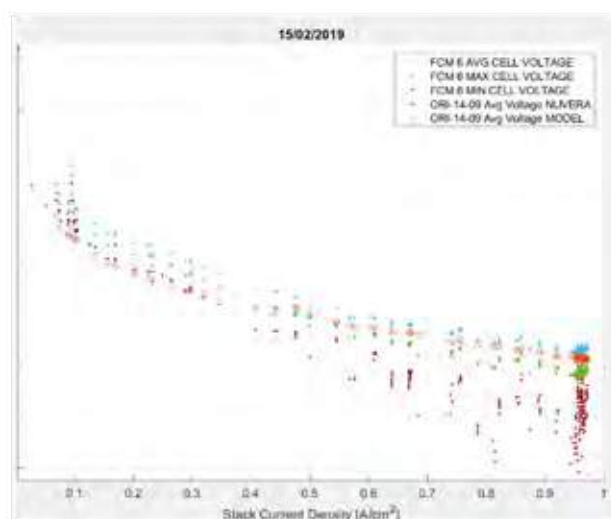


Fig. 2. Polarization curve of stack ORI-14-09 (FCM6) after recovery

Not only stacks can now be fully operated, but cell voltage results higher and shows lower oscillations, demonstrating the effectiveness of the recovery procedure for 30 kW stacks designed in the HI-SEA laboratory.

REFERENCES

- [1] ICCT, "the International Maritime Organization's Initial Greenhouse Gas Strategy," 2018.
- [2] A. Boudghene Stambouli and E. Traversa, "Fuel cells, an alternative to standard sources of energy," *Renew. Sustain. Energy Rev.*, vol. 6, no. 3, pp. 295–304, 2002.
- [3] V. Eyring, H. W. Köhler, A. Lauer, and B. Lemper, "Emissions from international shipping: 2. Impact of future technologies on scenarios until 2050," *J. Geophys. Res. D Atmos.*, vol. 110, no. 17, pp. 183–200, 2005.
- [4] T. Lamberti, "TESEO Project, High Efficiency Technologies For On-Board Energy And Environmental Sustainability, PON02_00153_2939517, 2012-2015."
- [5] L. Hao, H. Yu, J. Hou, W. Song, Z. Shao, and B. Yi, "Transient behavior of water generation in a proton exchange membrane fuel cell," *J. Power Sources*, vol. 177, no. 2, pp. 404–411, 2008.
- [6] W. Schmittinger and A. Vahidi, "A review of the main parameters influencing long-term performance and durability of PEM fuel cells," *J. Power Sources*, vol. 180, no. 1, pp. 1–14, 2008.
- [7] E. Gadducci, L. Magistri, and T. Lamberti, "Assessment of PEMFC system performance for marine application," in *EFCF 2019: Low-Temp. FUEL CELLS, ELECTROLYSERS & H2 Processing, Lucerne Switzerland*, 2019.
- [8] NETL, "Seventh Edition Fuel Cell Handbook," *Other Inf. PBD 1 Nov 2004*, no. November, p. Medium: ED; Size: vp., 2004.
- [9] Y. Zhan, Y. Guo, J. Zhu, and L. Li, "Natural degradation and stimulated recovery of a proton exchange membrane fuel cell," *Int. J. Hydrogen Energy*, vol. 39, no. 24, pp. 12849–12858, 2014.

HYDROGEN TO BOAT, FUEL CELL AND HYDROGEN APPLICATION FOR SAILBOATS

T. Lamberti*, P. Olivieri, A. Sorce*

*h2boat s.c.a.r.l., (Italy)

**Università degli Studi di Genova, (Italy)

Abstract – The present paper presents the innovative application of fuel cell and hydrogen technology in the marine sector, in particular for sailboats [1]. The system is designed as an energy storage, it exploits the high volumetric energy density and safety properties of Metal Hydrides to store large quantities of hydrogen in the keel of the sailboat without increasing the weight and volume of the original project. A PEM Fuel Cell is used to convert the hydrogen into DC current to supply power to traditional (12 Vdc equipment) consumers, but, more important, it gives the possibility to power new consumers also at 230 Vac at zero emissions, thanks to the large availability of energy. The presence of an Electrolyser gives the possibility to produce hydrogen onboard exploiting the renewable energy sources already available [2] as well as the shore connection, bypassing the logistic problem of hydrogen refueling. The solution results to be technically competitive and advantageous in terms of weight and volume against the most advanced Li-Ion battery solution, opening new market to the hydrogen technologies. The study demonstrates the feasibility in terms of weight and volume of the installation of a FC system on a sailboat, comparing the performance with batteries. Technical problems and proposed solutions are presented.

Index Terms – PEMFC, Marine, System engineering

I. NOMENCLATURE

AUX	Auxiliary Systems
BAT	Battery
EL	Electrolyser
FC	Fuel Cell
GHG	Green House Gases
ICE	Internal Combustion Engine
MH	Metal Hydride
PEMFC	Polymeric Electrolyte Membrane Fuel Cell
RES	Renewable Energy Sources
SOA	State Of the Art
ICE	Internal Combustion Engine

II. INTRODUCTION

The assessment focused on sailboats (10<Length OA<24m) applications of fuel cells and hydrogen technologies as a potential niche market favored by technical advantages given by both the technology and the application. The SOA of energy usage on-board sailboats is given by a combination of traditional technologies (12V dc circuit powered by lead acid batteries and

supported by alternators moved by the main propulsion ICE) and by reduced power and energy profiles (typically $P < 1$ kW for AUX only, $E < 4$ kWh on batteries). To increase the “zero emission” (without ICE turned on) operative profiles, different RES are harvested towards Photovoltaic Panels, Wind Turbines or Hydrokinetic Propellers, that are able to sustain $P < 1$ kWmax only when RES are present. Moreover, due to the low energy capacity of the batteries, more powerful RES systems cannot be exploited to store energy surplus.

Towards a correct sizing and disposition of the three key elements composing the h2boat Energy Pack (FC, EL, MH) it is possible to increase the performance of the zero emission sailboat power profile in terms of power and energy, exploit RES and give power to the propulsion. The comparison has been done by the assessment of two different operative profile (Weekend and Sailing).

III. ENERGY PACK

The Energy Pack for sailboats integrate thermally FC and MH, maximizing the whole system efficiency. Tests [3] demonstrated that the FC is able to produce 4-5 times more heat than what required from MH to release the hydrogen flow requested by the FC. The working temperatures (about 50°C for FC and 35°C for MH) are compatible as well as the sea water temperature (20-25°C) to cool down the MH during the charging phase.

The FC is integrated with a BAT towards a DC/DC converter. The BAT sizing is related to the hypothetical max power required for the propulsion. The FC+BAT control strategy is under development.

The MH hydrogen storage system is integrated inside the sailboat keel by means of a patented solution that enable to exploit the weight of MH as a ballast.

IV. RESULTS

A direct comparison between in terms of Specific Energy (SE) FC&Hydrogen technologies, BAT and traditional ICE is not feasible due to many technical differences. A general comparison could be made on Weight as reported in Table 1, while Table 2 report the also the volume comparison. The

advantage of the sailboat application is given by the installation of MH inside the keel that permit to integrate the MH weight in the keel, reducing 360 kg the complex weight.

Table 1. Weight SE comparison

P	10	kW	
E	30	kWh	
unit	l	kg	Note
FC+H2	187,3	411,5	PEM+MH
BAT Li-Ion	457,6	331,2	Energy based
ICE+Diesel	178,0	70,4	Diesel ICE 4T
BAT Pb	777,8	1368,2	AVG Bat

Table 2. Weight and Volume energy density comparison

Fuel		kWh/l	kWh/kg	-	Note
	H2	0,58	0,17	-	MH system
	BAT	0,07	0,09	-	Li-Ion
Diesel	10,55	10,99	-	MDO	
Gen		kW/l	kW/kg	η	Note
	Fuel Cell	0,12	0,19	50%	PEM
	BAT	0,20	0,27	99%	3C discharge
	ICE	0,06	0,17	25%	Diescl avg

V. CONCLUSION

In order to assess the advantage of the large energy storage availability on-board, two operative profile are presented.

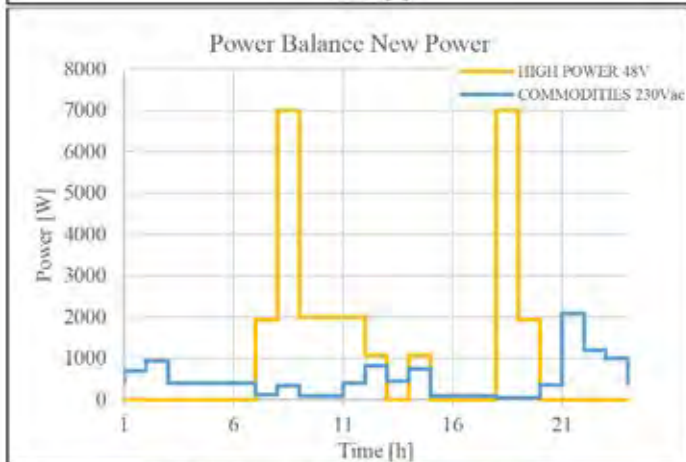
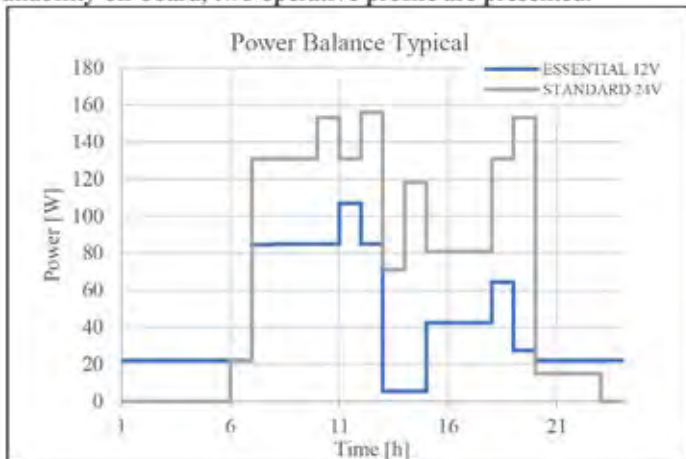


Figure 1. New power profiles with propulsion

Figure 1 shows the comparison between a traditional power profile dedicated only to AUX system and a new potential one that enable to have an electric propulsion at zero emission.

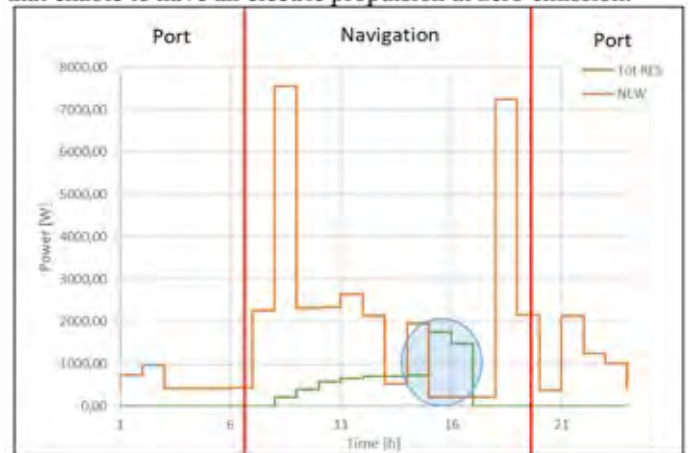


Figure 2. Weekend operative profile

A high operative profile like the one in (designed for a Weekend usage) gives 3 days of zero emission autonomy, but don't exploit RES. A less energy intensive operative profile like the one in Figure 3 gives 6 days of operativity at zero emission and enable RES exploitation.

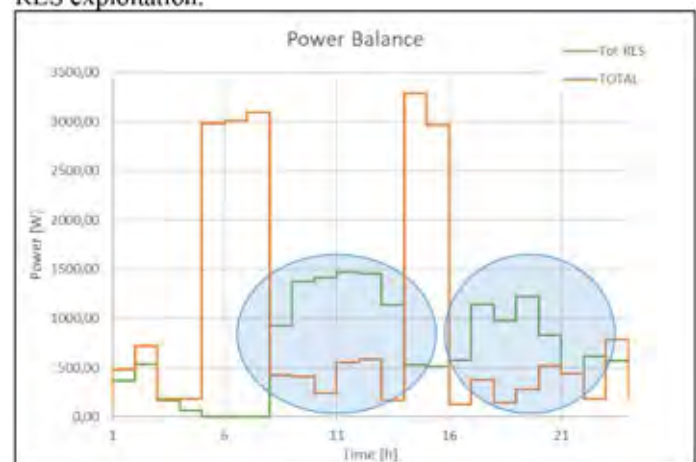


Figure 3. Sailing operative profile

In conclusion, FC&Hydrogen technologies if well integrated enable new operative profile for sailboats opening to new future market opportunity.

VI. REFERENCES

VII.

- [1] h. S.c.a.r.l., "www.h2boat.it," 2019. [Online].
- [2] T. Lamberti, A. Sorce, L. Difresco and S. Barberis, "H2Boat: a hydrogen energy pack for sailing boat application," in *10th October 2013, Nice, France, PlugBoat 2013 World Electric & Hybrid Boat Summit*.
- [3] M. D. Campo, T. Lamberti, A. Sorce and L. Magistri, "Dynamic model and experimental tests of a system coupling proton exchange membrane fuel cell and metal hydrides hydrogen storage" in *European Fuel Cell Technology & Applications Conference - Piero Lunghi Conference, Naples, Italy, December 12-15, 2017*.

EXPERIMENTAL ASSESSMENT OF FCS FOR MARINE APPLICATION

E. Gadducci *, T. Lamberti*, L. Magistri*, A.F. Massardo*

*Università degli Studi di Genova, (Italy)

Abstract – This paper presents an experimental assessment on the Fuel Cell System (FCS) performance tests conducted in the Hydrogen Initiative for Sustainable Energy Application (HI-SEA) Joint Laboratory of Fincantieri and University of Genova (UNIGE) [1]. The HI-SEA FCS plant is made up of 8 Fuel Cell (FC) stacks of 30 kW each for a total power of 240 kW_e, originally designed for automotive applications, installed in two equal branches of 4 stacks in series. The two branches can be connected in parallel by means of two DC/DC converters together with an AC/DC converter that is able to simulate the presence of a 60 kW battery (BAT). The goal of the experimental campaign is to assess the performance and real behavior of the FCS when connected in parallel with and without DC/DCs, with or without the battery to assess the optimum BoP setup and the most feasible and efficient configuration for a ship application. The tests are conducted using typical ship power profiles. The results show that the operative profile could influence the FC performances if the BoP setup is not well optimized [2]. Stationary and dynamic performance of the system are evaluated in single branch and parallel branches configuration, with and without DC/DCs.

The study conclusion gives important indications on how to assemble, setup and control an FCS powerplant for marine application.

Index Terms – PEMFC, Marine, System engineering

I. NOMENCLATURE

BAT	Battery
BoP	Balance of Plant
FC	Fuel Cell
GHG	Green House Gases
PEMFC	Polymeric Electrolyte Membrane Fuel Cell
SOA	State Of the Art

II. INTRODUCTION

THE SYSTEM

The original FCS was assembled in 2015 during the cofounded TESEO project. At the end of the project, the system was brought to Savona and integrated into the HI-SEA Joint Laboratory. The integration required a long period of refitting and modification conducted in 2017/2018 [1].

The long period of inactivity required a dedicated recovery phase in which one of the stacks was also repaired after a damage occurred during the TESEO project [3]. During the operation a dedicated recovery procedure was also developed.

The first tests demonstrated that the original load-following

control of the stacks (voltage control), conducted by means of two standalone DC/DCs on each branch, did not allow the work in parallel of the stacks and generated instabilities (due to voltage variabilities), resulting in the impossibility to reach a stable condition. A modification of the DC/DCs towards the installation of a control board that equalizes the output voltages of the branches improved the system performance. Eventually, the system was tested in stationary and dynamic condition as well as under marine operative profile.

Before the tests were conducted, a long tuning phase was required to tune the cooling system parameters, the cathode air flow parameters, the laboratory power load and to calibrate the sensors, demonstrating the system's sensibility to the BoP modifications, in particular regarding temperature management.

III. TESTS

Stationary load

Tests with stationary power load were conducted for each stack, for each branch and for the whole system (with the branches in parallel). Tests were repeated 3 times each, under 3 different power profiles, corresponding to 10, 20, 30 kW power for each stack.

Dynamic load

Tests with dynamic power load were conducted for singular stacks, singular branches and for parallel configurations. During the tests, power steps from 1 kW to the maximum achievable were conducted, starting from different initial power levels (1, 5, 10, 15, 20 kW), achieving a maximum of about 7kW/stack power step, demonstrating that the stacks are more performant (dynamically) at low current density and that the limiting parameter is given by the cathode air flow dynamics.

Operational profile

Eventually a marine power profile, defined together with Fincantieri technicians was tested on single branch and in parallel configuration.

All the tests where conducted with and without the DC/DC converter presence in order to assess the static and dynamic performance of the system in different configurations.

IV. RESULTS

Tests demonstrated that the FCS is able to respond to static, dynamic and operative loads. Many important information can

be derived from the results regarding the system operativity, control and optimization. Figure 1 shows the results of a long lasting 10 kW/stack test conducted on a single branch. It is possible to appreciate the voltage decreasing due to the membrane drying given by a not optimized temperature control as well as the long operation at 1/3 of the nominal stack power.

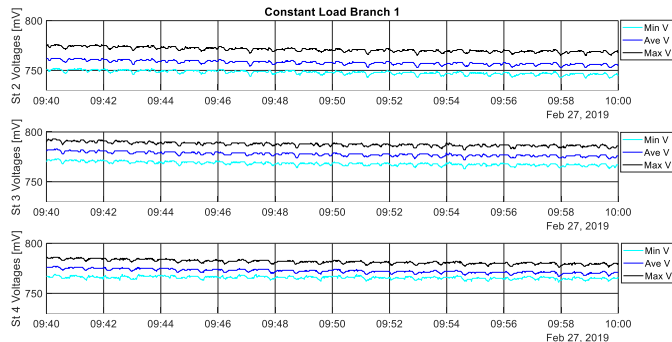


Figure 1. Effect of long-lasting power demand at low power load

Dynamic tests showed the sensibility of the stacks to the cathodic air flow. While for single stacks with dedicated blower this problem is directly related to the blower performance, a system integrating more stacks requires well designed BoP and, in any case, suffers from high dynamic power loads. Figure 2 shows the incidence of air flow surplus (with respect to the nominal value) on the branch performance.

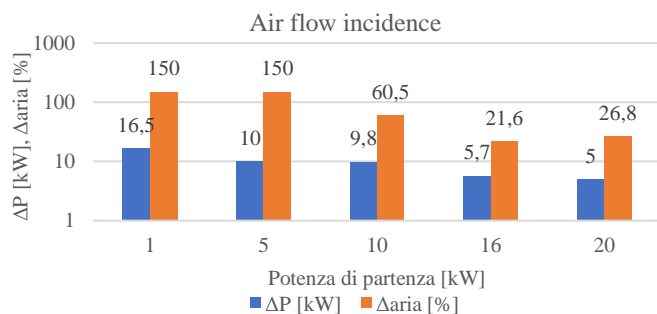


Figure 2. Air flow incidence on FCS dynamics

Figure 3 and Figure 4 show the results of tests conducted with the two branches in parallel with and without the DC/DC. It is interesting to note that at low dynamic power profiles, the branches are able to make up to voltage differences and to work in parallel without particular problems.

V. CONCLUSION

The test campaign on the HI-SEA FCS demonstrates that an FCS can satisfy typical marine power profiles. In order to scale up the system from kW to MW size, issues regarding the BoP and FCs integration require deeper analysis. DC/DC converter resulted in a higher control flexibility but for certain applications it is possible to operate FC branches in parallel without them.

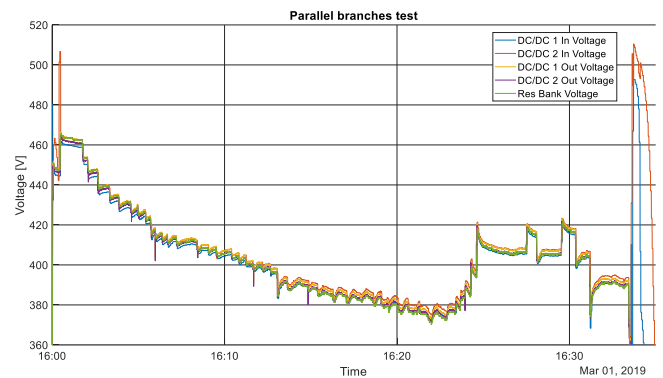


Figure 3. FCS performance without DC/DC

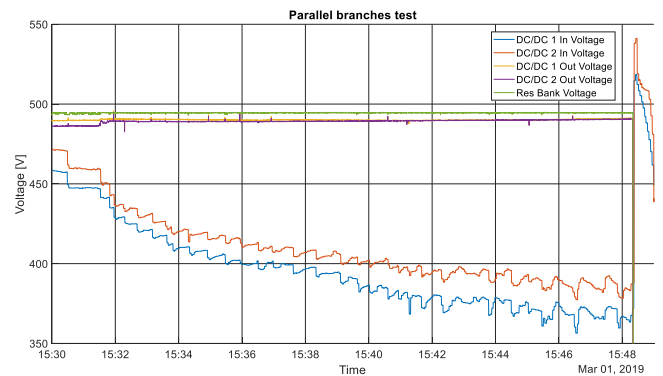


Figure 4. FCS performance with DC/DC

VI. REFERENCES

- [1] G. Borgogna, E. Speranza, A. Dellacasa, T. Lamberti, M. D. Campo, A. N. Traverso, L. Magistri and A. Massardo, "HI-SEA (Hydrogen Initiative for Sustainable Energy Application): Development Of A Joint Laboratory For Pem And H2 Marine Applications," in *European Fuel Cell Technology & Applications Conference - Piero Lunghi Conference*, Naples, Italy, December 12-15, 2017.
- [2] E. Gadducci, T. Lamberti and L. Magistri, "Assessment of PEMFC performance for marine application," in *EFCF 2019: Low-Temp. FUEL CELLS, ELECTROLYSERS & H2*, Lucerne Switzerland, 5 July 2019.
- [3] E. Gadducci, L. Magistri and T. Lamberti, "Analysis of consequences of cells rupture on PEMFC," in *EFCF 2019: Low-Temp. FUEL CELLS, ELECTROLYSERS & H2*, Lucerne Switzerland, 2 – 5 July 2019,.

ASSESSING THE BIOELECTRICITY PRODUCTION IN AIR-CATHODE MFCS USING DIFFERENT ORGANIC SUBSTRATES.

F. Flagiello^{1,2}, M. Minutillo², S. D'Apollito², M. Pulcrano², P. Di Trolio², D. Pant³, H. G. Arellano⁴ and C. Avignone Rossa²

1. University of Naples "Parthenope", Engineering department (Italy)

2. University of Surrey, Faculty of Health and Medical Sciences (England)

3. Separation & Conversion Technology, Flemish Institute for Technological Research, (VITO),
Boeretang 200, 2400 Mol (Belgium)

4. University of Surrey, Department of Chemical and Process Engineering, (England)

Abstract - In this study, the performances in terms of Power Density (PD), Current Density (CD) and Coulombic Efficiency (CE%) of three substrates were investigated using a 30 ml single chamber air-cathode microbial fuel cells (MFCs), coupled to a carbon brush anode. A mix of fruits and vegetables (fuelA) was the first substrate, Acetate 0.5 M (fuelB) was the sole carbon source of the second substrate tested, while the liquid fraction of a 300 °C hydrothermal treated banana peels, (fuelC) constituted the third substrate. All experiments were performed using compost bacteria recovered from a 100 days old compost, at room temperature and pH 7. In order to characterize the energy content of the different substrates and the biofilm growth, PD, CD and voltage were monitored every 5 minutes for 60 days using a digital multimeter. Results were for the fuelA: 53 mW/m² at 560 Ω, 422 mW/m² at 220 Ω for fuelB and 16.6 mW/m² for fuelC at 2200 Ω.

Index Terms – Compost bacteria, hydro-pyrolysis, Microbial Fuel Cell, organic waste

I. INTRODUCTION

Organic waste is considered by many researchers a good substrate for electrical energy conversion and good results have been achieved by biogas and pyrolysis plants, but the drawbacks related to the high costs of maintenance and reaction complexity are limiting factors for the further development of these plants. Compost is a cheap fertilizer and represents the final step in the circular treatment of organic waste. Bacteria coming from compost are typically "*Firmiculites*" able to perform different tasks including bioelectrogenesis. Many works in these last 10 years, has been focused on the use of MFC technology for wastewater and organic waste treatment because of its cost-effectiveness and eco-compatibility [1]. In MFC systems, the substrate can be considered a pivot parameter and the chemical composition can influence the

growth of bacterial communities and power performances. In this work we evaluated and compared, the performances in terms of Power Density (PD), Current Density (CD) and Coulombic efficiency (CE%) of three different organic substrates: fruits and vegetables coming from a typical municipal organic waste, 0.5M acetate and a 300 °C hydrothermal treated liquid banana peels compound, using compost bacteria coming from a 100 days old pile.

II. MATERIALS AND METHODS

Three different organic fuels were made for the experiment: fuelA, fuelB and fuelC. For the fuelA, 500 g of fruits and vegetables were chopped and mixed with 9% saline solution (ratio 1:3). For FuelB, sodium acetate 0.5M (1 g/L) were added to an electrolytic solution. For FuelC, 500 g of chopped and dried banana peels were hydro-pyrolyzed for 2 hours at 300 °C, then cooled to room temperature before testing. FuelA and FuelB were used as substrate in two reactors, each consisting of 30 ml single chamber cubic shape air cathode MFCs. The electrodes were a carbon fiber brushes as anode (2.5 cm of diameter, 5 cm of length), and an activated carbon layer provided of nickel mesh current collector and PTFE binder as cathode [2]. The fuelC was used as substrate in a double chamber reactor (20ml of total volume) with 6 cm² carbon fiber electrode tissue as electrodes. A Potassium ferricyanide (0.01M) was used as cathode electrolyte and a Cation Exchange Membrane (CEM) was used for separating the two chambers. Carbon fiber anodes were pretreated in 0.5 HCl liquid for 24 hours to remove unwanted elements and increase the performance [3]. Bacteria were collected from a biofilm (30 days old) coming from another MFC compost-based. Data regarding voltages, power and current densities, were collected

every 5 minutes for 60 days using a digital data-logger; in particular, the polarization curves were measured every week by varying the applied resistance in a range 10000 - 47 Ω . The CE% values were calculated by using the formula (1):

$$CE = \frac{\int_0^{i_b} 8FVan \, Idt}{FVan\Delta COD} \quad (1)$$

where I is the current, F is Faraday's constant ($96\,458\text{ C mol}^{-1}$) and Van is the volume of the anode chamber and COD is the chemical oxygen demand.

The pH was adjusted to 7 by using HCl 0.1 M or NaOH 0.5M. In fuelA and fuelB the anodic electrode is placed orthogonally to the cathodic electrode at 1.5 cm of distance from it. Fuels have been replaced every week, before to perform the polarization curves.

III. RESULTS

Three samples were tested using compost bacteria for 60 days, measuring power densities and polarization curves every week. Results are reported in the *Table 1*.

TABLE I
EXPERIMENT RESULTS

MFC	CD (mA/m^2)	R (Ω)	PD (mW/m^2)	CE (%)
fuelA	367.3	220	53	28.0
fuelB	1655.0	560	422	31.0
fuelC	166.1	2200	16.5	10.5

Figs 1-3 show the trend of PD vs. CD and the polarization curves for the three substrates.

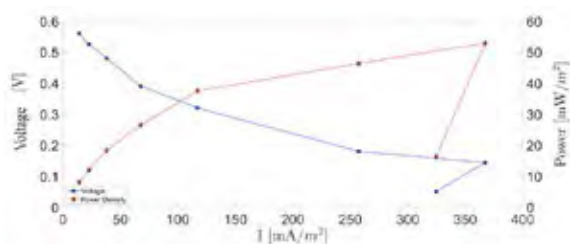


Fig.1 fuelA: Voltage and PD vs. CD

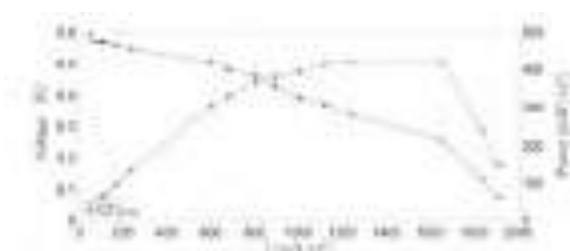


Fig.2. fuelB: Voltage and PD vs. CD



Fig.3: fuelC: Voltage and PD vs. CD

IV. CONCLUSION

The complexity of the organic matter, the molecular structure and the affinity with the compost bacteria are aspects that influence the MFCs performances. As a matter of fact, the internal resistance resulted a limiting factor for power production, but even when it's low as in fuelA, a good PD result is difficult to reach ($367.3\text{ mA}/\text{m}^2$). Hydro-pyrolyzed banana peels used in fuelC are probably not suitable for MFC systems, due to the quantity of produced inorganic carbon that limits the available organic substrate. As expected, acetate is the most efficient fuel for feeding a MFC [4] guarantying high power density. However, it is possible to affirm that the using of wastes in MFCs represents an interesting solution because the electricity production, even if is low, can be considered an additional benefit that comes from the treatment/disposal of wastes. Further improvements in performances are expected by improving engineering aspects (materials, configurations, etc.).

REFERENCES

- [1] Florio, C., Nastro, R. A., Flagiello, F., Minutillo, M., Pirozzi, D., Pasquale, V., Dumontet, S. (2019). Biohydrogen production from solid phase-microbial fuel cell spent substrate: A preliminary study. *Journal of Cleaner Production*, 227, 506-511.
- [2] Hiegemann, H., Littfinski, T., Krimmler, S., Lübken, M., Klein, D., Schmelz, K-G., Ooms, K., Pant, D., Wichern, M., Performance and inorganic fouling of a submergible 255 L prototype microbial fuel cell module during continuous long-term operation with real municipal wastewater under practical conditions, *Bioresource Technology* (2019), 294, 122227.
- [3] Yoshimura Y, Nakashima K, Kato M, Inoue K, Okazaki F, Soyama H, Kawasaki S. Electricity Generation from Rice Bran by a Microbial Fuel Cell and the Influence of Hydrodynamic Cavitation Pretreatment. *ACS Omega*. 2018 Nov 30;3(11):15267-15271
- [4] D. Pant, G. Van Bogaert, L. Diels, K. Vanbroekhoven, a review of the substrates used in microbial fuel cells for sustainable energy production, *Bioresource Technology*, (2010)101 (6), 1533-1543.

INFLUENCE OF ELECTRODE CONFIGURATION ON THE PERFORMANCES OF AIR-CATHODE MFCS.

M. Minutillo*, E. Jannelli*, P. Di Trolio*, F. Flagiello*, S. D'Apolito*, M. Pulcrano*, D. Pant**

*University of Naples "Parthenope", Via Amm. F. Acton 38, Naples (Italy)

**Separation & Conversion Technology, Flemish Institute for Technological Research (VITO), Boeretang
200, 2400 Mol (Belgium)

Abstract - In the last 10 years, the Microbial Fuel Cell (MFC) technology has captured the attention of the scientific community for the possibility of direct conversion of biomass into electrical energy, thanks to the ability of electrogenic bacteria to generate and transfer electrons to a solid electrode.

In this paper, the influence of the electrodes configuration, in terms of arrangement and dimension, on the performances of air-cathode MFCS has been evaluated. For the anodic electrode, its orthogonal or horizontal arrangement, with respect the cathode layout, has been considered; for the cathodic electrode, three different sizes (4 cm², 7 cm², 12 cm²), were chosen taking into account three different ratios between the anodic frontal surface and the cathodic surface (or anodic coverage of the cathode equal to 1:0.5, 1:1, 1:2) and then examined. Results showed that best performances can be reached realizing MFCS in which the anodic electrode is placed orthogonally with respect to the cathodic electrode and the anodic coverage of the cathode is 1:1.

Index Terms – Renewable energy production, Microbial fuel cells, Anode disposition, Cathode size.

I. NOMENCLATURE

PLA: polylactic acid; PTFE: polytetrafluoroethylene;
OFMSW: Organic Urban Solid Waste Fraction;

II. INTRODUCTION

Traditional biological processes allow the generation of the electrical energy indirectly, through the production of biogas and/or hydrogen. The MFCS are innovative technologies, able to directly convert biomass/waste into electrical energy and, simultaneously, to solve the problem of the treatment/disposal/use of organic wastes. The MFCS consist of anodic (anaerobic) and cathodic (aerobic) compartments, separated or not by proton exchange membranes.

In the anodic compartment the organic substrate (glucose, acetate, civil waste, zootechnical, or industrial, etc.) is oxidized by an electrogenic microbial consortium, generating electrons and protons. The electrons, transferred to the anodic electrode by the bacterial consortium, reach the cathode through an external electrical circuit; the protons arrive in the cathodic compartment through a membrane/separator, where they react with the electrons and the oxygen producing water [1]. In this paper the aspects concerning the electrodes configurations have been studied in order to evaluate the best configuration that allows to reach the best performance.

III. MATERIALS AND METHODS

A. Materials

The tested MFCS are single-chamber reactors with a cubic geometry; the internal volume is 28 ml. These reactors have been realized through a 3D printer by using a biocompatible material, such as polylactic acid (PLA). The anode is a carbon fiber brush 25 mm in diameter (surface area 7 cm²) and 20 mm in length, which, thanks to its overall high surface area and porosity, presents a structure conducive to the biofilm growth. The cathode is a multilayer material consisting of a nickel mesh (electron collector), a carbon cloth and a hydrophobic diffusive PTFE layer [2]. The choice of the type of carbon-based electrodes depends on the high conductivity, the large surface area, the high porosity, and the good biocompatibility that can be obtained [3]. The biofilm on the anodic electrode has been obtained from endogenous bacterial species of the compost by applying an opportune growing procedure. The data acquisition system consists of a DAQ, connected to sensors that record voltage and current for each set condition. The DAQ, with a sampling frequency of 0.1 Hz, is able to automatically switch (every 5 minutes) the resistance for obtaining the polarization curves according to the monocyclic method [4].

B. Experimental tests

Two experimental tests have been carried out in order to evaluate the influence of the anodic electrode arrangement (TEST1) and the optimal cathodic electrode size (TEST2).

In the TEST1 two MFCs configurations, with respect to the anode layout, have been analyzed: in the first one (MFC_a) the anodic electrode is placed horizontally to the cathodic electrode; in the second one (MFC_b) the anodic electrode is placed orthogonally to the cathodic electrode. The substrate, selected for experimental activities in this test, is a mixture containing 50 ml of acetate 1 M and a mineral solution [5].

In the TEST2 three MFCs configurations, with respect to the cathode size, have been analyzed; in this test the anode is placed orthogonally to the cathode. In the first cell (MFC_c) the cathode surface is equal to 4 cm² (the ratio between the area of anode facing the cathode and the cathode area is about equal to 1:0.5); in the second one (MFC_d) the cathode surface is equal to 7 cm² (the ratio between the area of anode facing the cathode and the cathode area is about equal to 1:1); in the last cell (MFC_e) the cathode surface is equal to 12 cm² (the ratio between the area of anode facing the cathode and the area of the cathode is about equal to 1:2). The substrate, selected for experimental activities in this test, is a mixture (slurry) of organic fraction of municipal solid waste (OFMSW) and physiological solution at 0.9% NaCl, with a volume ratio of 1: 3 (weight / volume); 200 mM of PBS (Phosphate buffered saline) is added to this mixture to bring the slurry to neutral pH conditions.

IV. RESULTS AND DISCUSSION

Results of TEST1, in terms of power density vs. current density, are shown Fig.1 (power and current densities are calculated with respect to the cathodic active area). As it can be noted the MFC_b, reaches a maximum power density of 422 mW/m² (the applied external resistance is 220 Ω) at a current density of 1656 mA/m², and the MFC_a shows a maximum power density of 390 mW/m² (at 390 Ω) at a current density of 1195 mA/m².

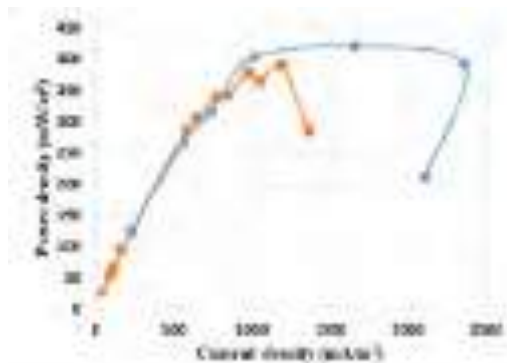


Figure 1. Power density curves for different anode disposition in the reactor.

Results of the TEST2 are shown Fig. 2. The best performance is recorded for the MFC_d: the maximum power density is 53 mW/m² (at 560 Ω) at a current density of 367 mA/m². The MFC_e has a power density of 44 mW/m² (at 1000 Ω) and the MFC_c produces 23 mW/m² (at 10000 Ω). As it can be noted, the greatest difference between the MFCs performances is related to the current densities (from 70.4 to 367 mA/m²); this means that the cathode size has a great influence on the range of the current densities. Thus, an anodic coverage of the

cathode equal to 1:1 (MFC-d) permits a good exchange of the electrons from the anode to the cathode (the brush should be placed to fully cover the cathode).

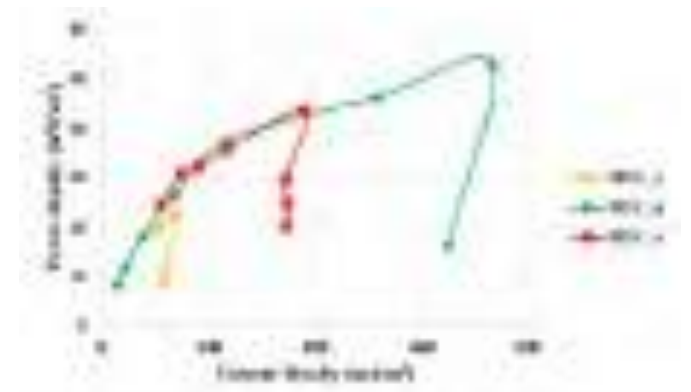


Figure 2. Power density curves in term of different size of catode.

V. CONCLUSION

In this paper the influence of the electrodes configuration on the MFC performance is evaluated.

Results have shown that best performance can be reached realizing MFCs in which:

- the anodic electrode is placed orthogonally with respect to the cathodic electrode (the maximum power density can be improved of 8 % with respect to the horizontal layout)
- the anodic coverage of the cathode is 1:1 (the maximum power density can be improved of 17% with respect to the ratio 1:2 and of 57% with respect to the ratio 1:0.5); thus the anodic brush should be placed to fully cover the cathode in order to improve the power production.

ACKNOWLEDGMENT

Research supported by University of Naples “Parthenope” for the project “Microbial fuel cell as new technology for bioelectricity generation: Design and Development” (2017).

REFERENCES

- [1] M.Minutillo, P.Di Trolio, S.D’Apolito, M. Pulcrano, Bioelectricity with microbial fuel cells: configurations and performance analysis, Termotecnica, pag.
- [2] R Rossi, D Jones, J Myung, Emily Zikmund, W Yang, Y Alvarez Gallego, D Pant, P J. Evans, Martin A. Page, Donald M. Cropek, Bruce E. Logan, Evaluating a multi-panel air cathode through electrochemical and biotic tests, Water Research, 2019;148: 51-59
- [3] P. Aelterman, S. Freguia, J. Keller, W. Verstraete, K. Rabaey, The anode potential regulates bacterial activity in microbial fuel cells, *Appl. Microbiol. Biotechnol.* 2008;8(3):409-418.
- [4] JV Watson, BE. Logan, Analysis of polarization methods for elimination of power overshoot in Microbial Fuel Cells. *Electrochemistry Communications.* 2011;13;54–56
- [5] H. Liu, R. Ramnarayanan, B. E. Logan, Production of electricity during wastewater treatment using a single chamber microbial fuel cell, *Environ. Sci. Technol.* 2004;38(7); 228

A PROPER AND EFFECTIVE CHOICE OF THE VOLTAGE OF A FUEL CELL STACK: A STUDY ON THE CORRELATION BETWEEN THE ELECTRICAL PARAMETERS AND GEOMETRICAL SHAPE.

O. Barbera*, G. Giacoppo*, N. Briguglio*, L. Andaloro* and V. Antonucci*

*CNR - ITAE, Consiglio Nazionale delle Ricerche, Istituto di Tecnologie Avanzate per l'Energia "N. Giordano",
Via Salita S. Lucia sopra Contesse n.5, 98126 MESSINA (Italy)

Abstract -

In this study, the authors have verified how, once the power and efficiency of a fuel cell stack has been set, the choice of voltage, number of cells and current is influenced by the geometry of the device.

The study demonstrates that there is a correlation between the electrical parameters of the stack and its shape, independently from electrochemical phenomena. As a further result, the behavior of the volume and mass of the fuel cell stack is non-linear with the stack voltage and it is possible to find a stack voltage, which minimizes its volume and / or mass.

Index Terms – Fuel cell stack, Design, Polymer Electrolyte Fuel Cell, PEM

I. INTRODUCTION

The phenomenon of increasing average air temperature near the Earth's surface (global warming), over the past one to two centuries, is considered by climate scientists to be responsible for social, economic and ecological damage [1]. A special report produced by Intergovernmental Panel on Climate Change (IPCC) in 2018 noted that human activities have been responsible for a worldwide average temperature increase since preindustrial times, and most of the warming observed over the second half of the 20th century [1, 2]. In this context, the hydrogen – fed fuel cell stacks, due to their ability to generate power for many applications (automotive, stationary, portable and so on) without injection of greenhouse gases in the environment, are an important element in the 'green' chain of energy production starting from renewable energy sources. For this reason, considering a future mass production of these devices, a standardization of the procedure for fuel stack design is needed. In this field, many authors used different approaches to define the geometry of the components of the fuel cells tack

starting from the requested power and efficiency [3, 4, 5, 6, 7, 8]. The most of the proposed approaches use numerical methods and mathematical algorithms to optimize the fuel cell stack in terms of mass and volumetrically power density. In this study, a simplified approach is used for a preliminary estimation of mass and volume of a fuel cell stack as a function of voltage and efficiency. In particular, starting from a parameterization of the geometry of the bipolar plate, for a "stacked" architecture, the power density and the volume of the fuel cell stack have been calculated by varying the voltage and the current at a fixed power and cell efficiency (that is related to the final application). As result, a non - linear behavior of the functions, which correlate the voltage with the mass, and volume of the stack has been observed. Moreover, a minimum value of the mass and volume of the fuel cell stack at a specific voltage can be found.

II. METHODOLOGY

As first, a multi cell unit with a "stacked" configuration has been chosen, and then the geometry of the bipolar plat has been parameterized. As fig.1 illustrates, a typical configuration of bipolar plate has been used.



Fig. 1. Bipolar plate configuration used for the parameterized model

Numerous parameters have been considered: gasket width, bipolar plate thickness, channel height of flow field for gases and coolant, thickness of clamping plates and current collector. Moreover, the density of the materials considered to use for manufacture the stack, the pressure drop of both follow – fields for gas and coolant (for manifold cross section design) and the operative conditions (for active area and cell number calculation) have been taken into account.

III. APPLICATION FOR STACK DESIGN

The methodology has been used to fix the voltage and design the components of a 3.5 kW fuel cell stack with a theoretical efficiency of 60%. As can be observed from Fig. 2, the number of cell and the active area increase linearly with the increasing of the stack voltage; whereas, the active area and the stack current decrease not – linearly with the increase of the stack voltage. As Fig.2 shows, it is clear that the matter is of an indeterminate nature, indeed, there are ten different fuel cell stack configuration (in terms of active area, cell number and stack current), with the same power and efficiency in the range of 24 – 60 V.

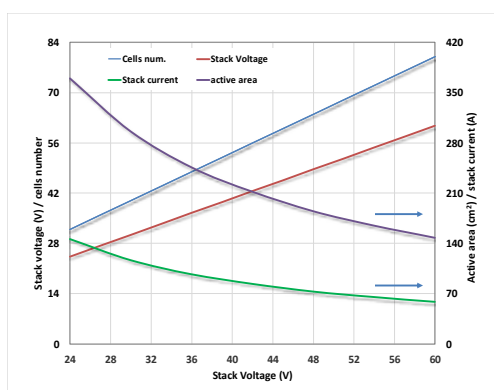


Fig. 2. Behavior of stack number of cells, stack voltage, stack current and active area as function of stack voltage, at constant power

To overcome this indetermination, the geometry of the fuel cell stack bipolar plate, as above illustrated, has been used to calculate the mass and the volumetric power density of the fuel cell stack. As a result, a fuel cell stack voltage of 36 V has been chosen as best compromise between mass and volumetric power density. This is clearly illustrated in Fig.3, where the maximum value of volumetric power density is visible at 36 V, whit an acceptable mass power density.

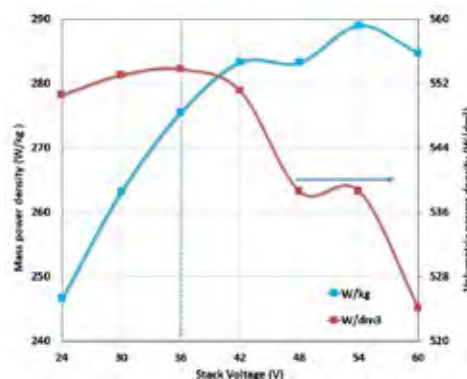


Fig. 3. Mass and volumetric power density of the fuel cell stack as a function of stack voltage.

IV. CONCLUSION

A parametric study for correlating stack voltage and geometry has been carried out. The study demonstrates that, once the stack power and efficiency are fixed, there is an indetermination for fuel cell stack voltage calculation. Consequently, only by taking into account the geometry of bipolar and clamping plates, the best voltage can be determined, as best compromise between mass and volumetric power density.

REFERENCES

- [1] <https://www.britannica.com/science/global-warming>
- [2] <https://www.ipcc.ch/sr15/download/>
- [3] Oscar Santiago O., Arandae Rosales M., Navarro E., Raso M.A. Leo J.T. , Automated design of direct methanol fuel cell stacks: A quick optimization, International Journal of Hydrogen Energy 44 (2019) 10933 -10950
- [4] Qina Y. G.Liua, Changa Qing Dua Y. , Modeling and design of PEM fuel cell stack based on a flow network method Applied Thermal Engineering 144 (2018) 411–423
- [5] Squadrito G., Barbera O., Giacoppo G., Urbani F., Passalacqua E. , Computer aided fuel cell design and scale up, comparison between model and experimental results, Journal of Applied Electrochemistry (2007) 37:87-93
- [6] Squadrito G., Giacoppo G., Barbera O., Urbani F., Passalacqua E., Borello L., Musso A., Rosso I. , Design and development of a 7kW polymer electrolyte membrane fuel cell stack for UPS application, International Journal of Hydrogen Energy 35 (2010) 9983 – 9989
- [7] Barbera O., Stassi A., Sebastian D., Bonde J.L., Giacoppo G., D'Urso C., Baglio V., Aricò A.S. , Simple and functional direct methanol fuel cell stack designs for application in portable and auxiliary power units, International Journal of Hydrogen Energy (2016) 12320-12329
- [8] Giacoppo G., Hovland S., Barbera, O. , 2 kW Modular PEM fuel cell stack for space applications: Development and test for operation under relevant conditions, Applied Energy (2019) 1683-1696.

(Put paper number here) EFC19151

REDUCING ELECTROLYTIC HYDROGEN COSTS BY OXYGEN CO-PRODUCTION

G. Squadrito, A. Nicita, A.P.F. Andaloro, G. Maggio
CNR - Istituto di Tecnologie Avanzate per l'Energia "Nicola
Giordano" (CNR-ITAE), Via Salita S. Lucia sopra Contesse 5,
98126 Messina (Italy).

Abstract – Production of hydrogen by electrolysis is considered the greener solution for reducing greenhouse gas emissions, especially if renewable energy is used.

At present, hydrogen is mainly produced from fossil fuels, and steam methane reforming (SMR) is the most widely used route for producing hydrogen from natural gas and none of the conventional methods used is GHG-free. By comparing the production price of electrolytic hydrogen with the production price of SMR-Hydrogen, the electrolytic hydrogen results too expensive if both environmental advantages and oxygen co-production are neglected.

In previous works, we demonstrated that in some markets, the commercialization of the 8 kg of oxygen produced for each kilogram of electrolytic hydrogen allows a significant hydrogen cost reduction.

In this paper, we present the results of a new analysis aimed at evaluating the possibility to apply RES based electrolytic hydrogen/oxygen co-production in niche appliance with large oxygen consumption.

Index Terms – Financial analysis, hydrogen, electrolysis, RES power.

I. NOMENCLATURE

CAPEX – Capital Expenditure
NPV – Net Present Value
OPEX – Operating Expense
RES – Renewable Energy Sources

II. INTRODUCTION

Electrolysis is often mentioned as a well-established and mature technology to produce hydrogen. This is an environmentally friendly process that requires water and electricity, best when this last is derived from renewable energy sources (RES). One of the main disadvantages of water electrolysis is the cost of the electrical energy, so also the hydrogen produced is more expensive than that obtained by methods based on fossil fuels,

such as the conventional steam methane reforming (SMR). It is mainly for this reason that electrolysis currently accounts for only 4% of global hydrogen production; while 96% of hydrogen comes from fossil fuels (48% from natural gas, 30% from oil, and 18% from coal) [1].

Based on our previous studies [2-3], an extra revenue could be obtained by considering the amount of oxygen produced as a by-product from electrolysis: 8 kg of oxygen are produced for each kilogram of hydrogen. In agreement with considerations recently reported by IEA [4], the by-product oxygen can be used at a smaller scale in the health care sector, or at a larger scale for industrial purposes (feedstock).

In this new contribution, we reverse the point of view, by considering a hypothetical enterprise or business activity (public or private) adopting an electrolysis plant to fulfil its needs of oxygen for a particular application, while the obtained hydrogen could be sold to external users to achieve additional revenues. The objective is to verify if the proposed approach is economically attractive, compared to the case when the same enterprise simply buys the oxygen from local gas distributors/resellers.

III. METHODS

The examined system consists of 1 MW photovoltaic plant and an alkaline electrolyser rated at 0.8 MW; compressor and storage units are also included in the analysis. This plant is assumed to be located in the Southern regions of Italy. The amount of gaseous oxygen produced is about 120,000 Nm³ per year, which is assumed as a target value for our hypothetical enterprise.

Based on the method proposed by Kuckshinrichs et al. [5], and adopted in our previous work [3], we perform an economic-financial analysis of the investigated solutions. In particular, the investment costs to realize the plant, operative and maintenance (O&M) costs and taxes have been evaluated, in order to

determine the corresponding net present value (NPV). The avoided costs related to the non-purchased oxygen are also considered, by assuming a purchase price varying between 1 and 7 €/kg of compressed oxygen @200 bar (standard bottles for technical gases) [6].

IV. RESULTS

By assuming the above-reported target production, if the market price of gaseous oxygen is above a certain value (about 4 €/kg), it is economically feasible to self-produce the oxygen by a proprietary PV-powered electrolysis plant. In fact, in such a case, the NPV of the proposed investment – calculated assuming a plant lifetime of 20 years – results to be positive, indicating a profit margin even when the co-produced hydrogen is not sold to third parties. Therefore, this would be an ideal solution for enterprises that could use the co-produced gaseous hydrogen for their requirements or applications, or even for the needs of the same industrial chain.

On the contrary, so far as the purchase price of gaseous oxygen is lower than the above-mentioned value, the NPV results to be negative, but it is possible to recover – at the end of the 20 years – at least 3/4 of the initial investment and about 40% of the global expenses (investment, O&M costs, and taxes). Besides, a balance between expenses and incomes (or avoided expenses), i.e. an NPV null, can be obtained by selling the co-produced hydrogen. As lower the purchase price of oxygen as higher the hydrogen price to get a null NPV.

V. CONCLUSION

In this work we carried out an economic analysis to evaluate the attractiveness, for an enterprise that needs gaseous oxygen for a specific purpose, to produce it by a proprietary plant based on water electrolysis and powered by a PV field. Preliminary results and evaluations indicate that the examined opportunity could be an interesting alternative to the use of oxygen purchased from the local gas market.

It should also be remarked that the use of a green (carbon-free) process to co-produce hydrogen and oxygen can represent a value-added for the enterprise, in terms of image and benefits (e.g., carbon credits).

REFERENCES

- [1] S. Banerjee, M.N. Musa, A.B. Jaafar. *Economic assessment and prospect of hydrogen generated by OTEC as future fuel*. International Journal of Hydrogen Energy 42 (1), 26-37, 2017.
- [2] G. Maggio, A. Nicita, G. Squadrito. *How the hydrogen production from RES could change energy and fuel markets: A review of recent literature*, International Journal of Hydrogen Energy 44 (23), 11371-11384, 2019.
- [3] A. Nicita, G. Squadrito, A.P.F. Andaloro, G. Maggio. *The green hydrogen as a feedstock: a techno-economic analysis of a photovoltaic-powered electrolysis plant*, Proceedings of the 42nd International Association for Energy Economics International Conference (IAEE 2019) – “Local Energy, Global Markets”, Montréal, Canada, May 29 – June 1, 2019.
- [4] IEA, *The Future of Hydrogen: Seizing Today's Opportunities*, Report prepared by the IEA for the G20 meeting in Tokyo, Japan, June 2019.
- [5] W. Kuckshinrichs, T. Ketelaer, J.C. Koj. *Economic analysis of improved alkaline water electrolysis*. Frontiers in Energy Research 5, art. no. 1, 2017.
- [6] M. Hurskainen. *Industrial oxygen demand in Finland*. Research Report VTT-R-06563-17, VTT Technical Research Centre of Finland, December 20th, 2017.

DIAGNOSIS OF ELECTROCATALYST DEGRADATION IN POLYMER ELECTROLYTE FUEL CELLS UNDER AUTOMOTIVE CONDITIONS

D. Low*, L.M.Jackson*, and S.J.Dunnett*

*Department of Aeronautical and Automotive Engineering,
Loughborough University, Loughborough, (United Kingdom)

Abstract – This paper presents a fuzzy inference system approach for diagnosis of electrocatalyst degradation in polymer electrolyte fuel cells (PEFC's) under automotive conditions. The fuzzy inference system enables diagnosis of electrocatalyst degradation based on fuel cell operating conditions. The method incorporates classification of selected input parameters on a scale of membership to fuzzy sets or categories and provides connection to any consequential degradation through a database of diagnostic rules. Experimental procedures involved drive cycle durability testing including the world harmonized light-duty vehicle test procedure (WLTP) and start/stop cycling. The observed results support the validation of the proposed membership functions within the fuzzy inference system and the database of diagnostic rules. This approach can provide a fast and effective diagnosis of electrocatalyst degradation in PEFC's and enable proactive decision support for planning operation and maintenance strategies for improved fuel cell reliability, availability and durability.

Index Terms – Diagnosis, electrocatalyst degradation, polymer electrolyte fuel cells, transportation application.

I. INTRODUCTION

With the transport sector transitioning to low carbon technologies to reduce emissions and environmental impact, the application of fuel cells has become increasingly important. However, for commercialisation and consumer adoption to grow, attaining lifetime targets of up to 5,000hrs for automotive applications is required [1][2]. In order to achieve this, the reliability and durability aspects of fuel cells needs to be improved. Diagnosing the impact of operating conditions on fuel cell performance and lifetime is crucial to the advancement. An effective, low complexity diagnostic approach can provide the necessary improvement in health management and decision support for fuel cells in transport applications. This paper presents a diagnostic fuzzy inference system approach for electrocatalyst degradation in polymer electrolyte fuel cells (PEFC's) operated under automotive conditions. Automotive conditions for fuel cells include

start/stop cycles and load cycling. It was estimated that the proportion of fuel cell degradation caused by these dynamic operating modes was 44% and 28% respectively [3]. Therefore, these operating modes were selected as input parameters for the diagnostic fuzzy inference system (FIS). Electrocatalyst degradation was identified to significantly impact the performance and lifetime of fuel cells and is known to be strongly influenced by automotive conditions [1][2]. Hence, this approach provides an effective diagnosis of electrocatalyst degradation for fuel cells under automotive conditions.

II. METHODOLOGY

The diagnostic fuzzy inference system approach incorporates fuzzification of selected indicators, a database of diagnostic rules, and defuzzification. The fuzzification process classifies the input data into broad categories based on severity. The classification is then compared to the database of diagnostic rules to identify the occurrence of any subsequent degradation. Defuzzification converts the broad classification into a numeric output for interpretation. The fuzzification of the input parameters and database of diagnostic rules were developed from a literature review and validated through experimental testing. Table 1 outlines the diagnostic rules for electrocatalyst degradation.

Table 1 Diagnostic rules for electrocatalyst degradation.

Rule	If	Then	References
1	Start/stop cycle number is high AND cell voltage cycle number is high	Electrocatalyst degradation is certain	[1][2][4][5]
2	Start/stop cycle number is high OR cell voltage cycle number is high	Electrocatalyst degradation is evidenced	[1][6][7] [8][9][10]
3	Start/stop cycle number is low OR cell voltage cycle number is moderate	Electrocatalyst degradation is none	[1][2]

III. EXPERIMENTAL

Experimental testing involved 145hrs of start/stop cycles and 145hrs of WLTP drive cycles on a 5cm² cell and 25cm² cell respectively. MEA's consisted of a 50-micron membrane and integrated carbon cloth GDL, with a 0.5mg/cm² platinum loading anode and cathode (an/ca). Start/stop cycles included 30mins operation at steady state and 30 mins off (with nitrogen purge). Steady state conditions included 0.6V, 70°C, 80% RH (an/ca), 1.5 and 2.0 stoichiometries (an/ca), 1e⁻⁶ and 3e⁻⁶ m³/s flow rates (an/ca), 1 bar pressure.

IV. RESULTS

Polarisation curves (IV curves) were used to analyse fuel cell performance and compare OCV differences which indicate electrocatalyst degradation. Figure 1 shows the beginning of life (BoL) and post test IV curves for start/stop cycle testing.

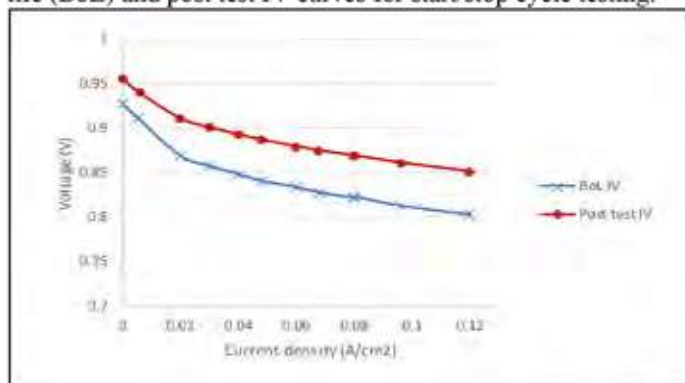


Fig. 1. Polarisation change curve after start/stop cycle testing

In Figure 1, the post test OCV increased by 28mV and overall performance improved. This confirms electrocatalyst degradation does not occur if start/stop cycles are low validating rule 3 outlined in table 1. Figure 2 shows the IV curves before and after WLTP drive cycle testing.

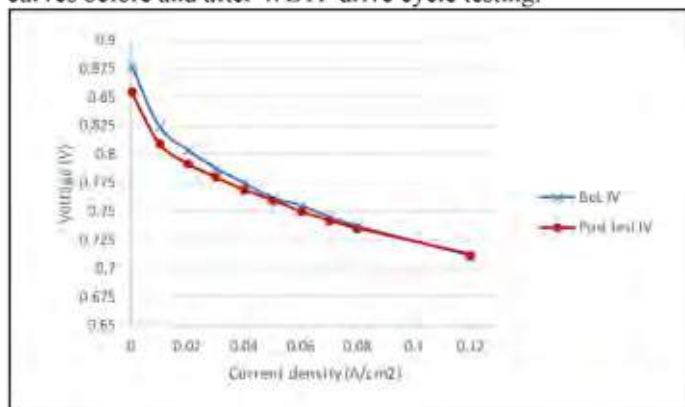


Fig. 2. Results from WLTP drive cycle testing

In Figure 2, the post test OCV decreased by 25mV confirming that if the voltage cycle number is high then electrocatalyst degradation is evident. Results show that start/stop cycles and voltage cycles can be effective indicators and support the diagnostic rules for electrocatalyst degradation.

V. CONCLUSION

Electrocatalyst degradation was not evident after the start/stop cycle test as OCV increased. The OCV decreased after the WLTP drive cycle test indicating that electrocatalyst degradation was evident. These results validate the diagnostic rules developed and show the diagnostic FIS can be utilised as an effective method for diagnosing electrocatalyst degradation in PEFC's under automotive conditions. Further work includes remaining useful life estimation based on degradation rates.

REFERENCES

- [1] Y. Yu, H. Li, H. Wang, X. Yuan, G. Wang, and M. Pan, "A review on performance degradation of proton exchange membrane fuel cells during startup and shutdown processes: Causes, consequences, and mitigation strategies," vol. 205, pp. 10–23, 2012.
- [2] M.M Mench; E.C Kumbar; T.N Veziroglu, *Polymer Electrolyte Fuel Cell Degradation*, 2012.
- [3] R. Shimoi, T. Aoyama, and A. Iiyama, "Development of Fuel Cell Stack Durability based on Actual Vehicle Test Data: Current Status and Future Work," *SAE Int. J. Engines*, vol. 2, no. 1, pp. 960–970, 2009.
- [4] J. H. Kim, E. A. Cho, J. H. Jang, H. J. Kim, T. H. Lim, I. H. Oh, J. J. Ko, and S. C. Oh, "Effects of cathode inlet relative humidity on PEMFC durability during startup-shutdown cycling: I. Electrochemical study," *J. Electrochem. Soc.*, vol. 157, no. 1, pp. 104–112, 2010.
- [5] J. H. Kim, Y. Yeon Jo, E. A. Cho, J. H. Jang, H. J. Kim, T. H. Lim, I. H. Oh, J. J. Ko, and I. J. Son, "Effects of cathode inlet relative humidity on PEMFC durability during startup-shutdown cycling: II. Diagnostic study," *J. Electrochem. Soc.*, vol. 157, no. 5, pp. 633–642, 2010.
- [6] R. L. Borup, J. R. Davey, F. H. Garzon, D. L. Wood, and M. A. Inbody, "PEM fuel cell electrocatalyst durability measurements," vol. 163, pp. 76–81, 2006.
- [7] V. Dam and F. de Bruijn, "The Stability of PEMFC Electrodes," pp. 494–499, 2007.
- [8] W. Bi, Q. Sun, Y. Deng, and T. F. Fuller, "The effect of humidity and oxygen partial pressure on degradation of Pt / C catalyst in PEM fuel cell," *Electrochim. Acta*, vol. 54, pp. 1826–1833, 2009.
- [9] S. J. Bae, S. J. Kim, J. I. Park, C. W. Park, J. H. Lee, I. Song, N. Lee, K. B. Kim, and J. Y. Park, "Lifetime prediction of a polymer electrolyte membrane fuel cell via an accelerated startup-shutdown cycle test," *Int. J. Hydrogen Energy*, vol. 37, no. 12, pp. 9775–9781, 2012.
- [10] Y. S. Suk Joo Bae, Seong-Joon Kim, Jin-Hwa Lee, Inscob Song, Nam-In Kim and J.-Y. P. Ki Buem Kim, Naesung Lee, "Degradation pattern prediction of a polymer electrolyte membrane fuel cell stack with series reliability structure via durability data of single cells," *Appl. Energy*, vol. 131, pp. 48–55, 2014.

OPTIMIZATION OF ENERGY MANAGEMENT IN A CITY BUS POWERED BY HYDROGEN FUEL CELLS

A. Malek*, R. Taccani**, D. Kasperek***, and J. Hunicz****

* University of Economics and Innovation, Projektowa 4, 20-209 Lublin (Poland)

** University of Trieste, Piazzale Europa, 1, 34127 Trieste (Italy)

*** Ursus Bus, Frezerów 7a, 20-209 Lublin (Poland)

**** Lublin University of Technology, Nadbystrzycka 36, 20-618 Lublin (Poland)

Abstract - The article describes the design and optimization of the operation of an electric bus powered by hydrogen fuel cells. At the beginning, an approach to the design of a 12-meter inter-city bus powered by hydrogen was presented. Examples of components for its construction are presented. Next, the problem of selecting the size of traction batteries and stacks of PEM hydrogen fuel cells was discussed. These are the key components affecting the price of the bus and should be subject to optimization. The results of optimization of the size of traction batteries and the fuel cell system for a bus traveling in inter-urban traffic are presented. The optimization was based on data from the literature, data from the monitoring system of actual hydrogen buses located on the Internet platform and simulation testing.

Index Terms – bus, fuel cells, traction batteries, total cost of ownership.

I. INTRODUCTION

In the 21st century, many components became available to build an electric bus drive system. The most important of them include: an electric motor and traction batteries, and in the case of hydrogen propulsion, a fuel cell stack and hydrogen tanks. The appropriate selection of each component determines the suitability of the bus for a specific application (urban, inter-city) and its price. In addition to the correct selection of components, it is also important to integrate them in order to obtain trouble-free operation with high efficiency [1].

II. RESEARCH AIM

A practical example of performance design and production cost optimization is the Ursus Demo Hydrogen Bus [4]. The vehicle uses two 30 kW LTPEM cell modules (total power 60 kW), compatible with a pack of NMC lithium-ion batteries [2] with an energy capacity of 70 kWh. More specifically, it is an electric bus with a hydrogen range extender. This is due to the

impossibility of the supplying the electric motor directly from the fuel cell system. The motors are powered by traction batteries and the hydrogen system recharges them constantly.

Hydrogen is stored on board in a compressed form under a pressure of 35 MPa, which is the European standard in this area. The vehicle range is approximately 450 km and is expected to increase. The service life assumed by the manufacturer is 20 000 working hours, which corresponds to a mileage of 700 000 km.

The drive system consists of electric motors located in the wheel hubs, roof-mounted traction batteries and 2 hydrogen fuel cell modules located at the back of the bus, as shown in the Figure 1.



Fig. 1. Arrangement of components in the bus

III. SIMULATION TESTING

Effective structural optimization in the scope of component selection and cost reduction in the area of the costs of constructing and operating electric-hydrogen buses cannot be based solely on a literature analysis. All issues subject to theoretical analysis should be validated under real conditions.

On the basis of real data from driving an electric-hydrogen bus, dynamic models of electricity and hydrogen consumption were constructed on board the bus [3]. Results of testing dynamic models were presented in Figure 2. After that, a representative inter-city route of 275 km was chosen, which the vehicle covered at an average speed of 38.6 km/h. This distance is too great for a conventional electric bus to travel, especially at such a high speed. 300 kWh of energy is required to complete the entire journey. It is therefore necessary to use an electric-hydrogen drive. The task of the simulation tests is to determine which components are capable of accumulating electricity (traction batteries) and generating energy (hydrogen fuel cells) on board the vehicle. Various fuel cell system and energy split control algorithms have been tested taking into account fuzzy logic/proportional and adaptive.

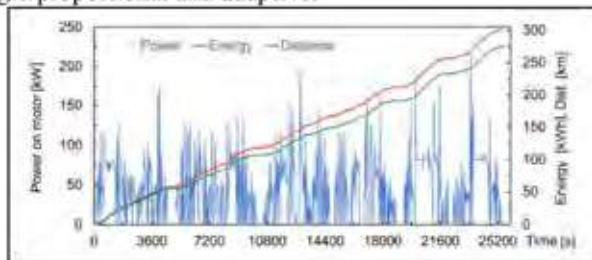


Fig. 2. Results of testing dynamic models

The following assumptions were used during the simulation tests:

- the price of a basic bus with 33 kg hydrogen tanks is 280,000 €
- the size of the lithium-ion battery packs is 33.33 kWh and is scalable to a maximum energy capacity of 233.33 kWh
- the power of the hydrogen fuel cell systems is 30 kW and it is scalable to a maximum power of 210 kW
- the prices of the lithium-ion battery packs are the average value of 3 offers received from various manufacturers in 2018 and amount to 27,906.98 €
- the prices of the hydrogen fuel cell systems are the average value of 3 offers received from various manufacturers in 2018 and amount to 58,139.53 €
- the hydrogen price is 6 € / kg
- the price of electricity is 0.2 € / kWh
- the vehicle starts its journey with 100% SOC
- the traction batteries are not charged from external sources
- the vehicle recovers energy during braking
- no hydrogen refuelling takes place while driving
- the vehicle travels along a representative route 340 days a year over a period of 8 years of operation
- the total cost of ownership (TCO) includes the cost of buying a bus in a given configuration and the cost of fuel (electricity and hydrogen)

As a result of simulation tests the following was determined:

- total cost of building an electric-hydrogen bus in various battery and fuel cell configurations
- the amount of electricity and hydrogen consumed

- fuel costs (electricity + hydrogen)
- TCO

The results of the simulation tests are shown in the Figure 3. Hypothetical cases are highlighted in various colours:

- insufficient energy capacity of traction batteries (pink)
- battery discharge current too high (yellow)
- excessive hydrogen consumption (blue)

Battery capacity [kWh]	Fuel cells power [kW]						
	30	60	90	120	150	180	210
33.33	685 639	899 935	1 078 821	1 173 836	1 340 669	1 586 296	1 872 226
66.66	696 677	896 666	1 071 924	1 160 443	1 309 752	1 539 429	1 787 939
100	708 227	894 957	1 051 423	1 156 733	1 295 389	1 500 821	1 726 161
133.33	724 437	895 502	1 052 019	1 151 802	1 277 641	1 465 263	1 667 999
166.66	742 438	902 689	1 045 848	1 152 396	1 268 434	1 446 621	1 634 001
200	753 763	896 373	1 027 418	1 131 253	1 238 222	1 391 260	1 544 793
233.3	770 089	899 276	1 024 505	1 132 183	1 233 531	1 374 912	1 512 005

Fig. 3. TCOs for different bus configurations

IV. CONCLUSION

The construction of a structurally and cost-optimized electric-hydrogen bus is not straightforward, but it is feasible. A scientific approach should be used. Firstly, a review of the current state of the relevant science and technology in selected areas is required. These areas are associated with the relevant components needed to construct such a bus. An analysis of the state of the art would enable the selection of the most common and reliable components. This would allow for cost optimization. For TCO, there is an optimum - minimum (gold colour in Figure 3) that corresponds to a bus configuration consisting of a 60 kW fuel cell system and traction batteries with an energy capacity of 100 kWh. An analysis of the relevant research areas is even more important because it allows for the sourcing of innovative components that will deliver a competitive advantage.

REFERENCES

- [1] de Miranda P. E. V., Carreira E. S., Icardi, Nunes G. S., Brazilian hybrid electric-hydrogen fuel cell bus: Improved on-board energy manage U. A. ment system. International Journal of Hydrogen Energy, Volume 42, Issue 19, 11 May 2017, Pages 13949-13959
- [2] Jwa K., Lim O., Comparative life cycle assessment of lithium-ion battery electric bus and Diesel bus from well to wheel. Energy Procedia, Volume 145, July 2018, Pages 223-227
- [3] Vepsäläinen J., Otto K., Lajunen A., Tammi K., Computationally efficient model for energy demand prediction of electric city bus in varying operating conditions. Energy, Volume 169, 15 February 2019, Pages 433-443
- [4] Wielgus J., Kasperek D., Małek A., Lusiak T., Developed generations of electric buses produced by Ursus. AUTOBUSY – Technika, Eksploatacja, Systemy Transportowe 11/2017, Pages 20 – 25

OXYGEN REDUCTION REACTION ON FeM@PtFe/C (M=MO, V, W) CORE-SHELL ELECTROCATALYSTS: THE ROLE OF COMPRESSIVE STRAIN EFFECT OF FEM CORE ON PtFe SHELLS

J. Lu*, L. Luo*, S. Yin*, S. Waqar Hasan*, S. Kontou**, A. Brouzgou** and P. Tsiakaras**

*Collaborative Innovation Center of Sustainable Energy Materials, Guangxi Key Laboratory of Electrochemical Energy Materials, College of Chemistry and Chemical Engineering, State Key Laboratory of Processing for Non-Ferrous Metal and Featured Materials, Guangxi University, 100 Daxue Dong Road, Nanning, (China)

** Department of Mechanical Engineering, School of Engineering, University of Thessaly, 1 Sekeri Street, Pedion Arcos, Volos, (Greece)

Abstract - Ternary FeM@PtFe/C (M = Mo, V, W) core-shell electrocatalysts, with different compressive strain on shells were systematically synthesized by the impregnation reduction method, followed by post-treatment at high temperature. The physicochemical characterization displays that the FeM core is crucial toward inducing a compressive strain effect on the PtFe shells and enhancing the catalytic activity for oxygen reduction reaction (ORR). In all the as-prepared electrocatalysts, a remarkably ~19-fold enhancement in mass activity at 0.9 V, compared with commercial Pt/C, is witnessed on the Fe₅Mo₁@PtFe/C that possesses the moderately compressive strain effect on PtFe shells and the suitable electronic ligands. After 5k cycles between 0 V and 1.1 V, the Fe₅Mo₁@PtFe/C exhibits ~4-fold activity as compared with pristine Pt/C.

Index Terms - activity enhancement, compressive strain effect, core-shell structure, oxygen reduction reaction

I. INTRODUCTION

Low-platinum, non-platinum, or even nonmetal electrocatalysts thus have been widely studied in developing low cost electrocatalysts that possess good catalytic activity and stability [1]. To design electrocatalysts rationally for the ORR, the catalytic process is studied in detail. A typical reaction path is that O first becomes active by capturing an electron and a proton to produce the adsorbed OOH on the electrocatalyst surface and then the O-O band in the adsorbed OOH is broken to generate adsorbed O and OH as intermediate species. Eventually, these adsorbed species combine with electrons and protons to form H₂O, leaving the electrocatalyst surface. By analyzing the above process, the adsorption energy of the intermediate species on the electrocatalyst surface is proposed as a direct descriptor for the regulation of ORR activity [2]. Nørskov *et al.* [2] calculated the oxygen adsorption energy of some alloys through density functional theory and constructed a Sabatier volcano based on the experimental results of other reports. In addition, they synthesized the Pt₃Y and Pt₃Sc alloys, which exhibit enormously improved ORR activity over Pt in line with their theoretical predictions. Here, ternary PtFeM/C (M =

Mo, V, W) alloy electrocatalysts with different levels of compressive strain on Pt were systematically synthesized using the method of impregnation-reduction, post-treated at high temperatures. The electrocatalytic activity of all the investigated materials, in order to be applied as cathode materials to low temperature fuel cells, was evaluated in O₂-saturated 0.1 M HClO₄, employing a rotating ring-disk electrode.

II. EXPERIMENTAL PART

A. Synthesis of the Electrocatalysts

Ternary PtFeM (M = Mo, V, W) alloy electrocatalysts were prepared by reducing the Pt, Fe, and M precursors with NaBH₄, followed by calcination at high temperatures. In a typical synthesis of PtFeMo/C, known amounts of H₂PtCl₆·6H₂O, FeCl₃·6H₂O, (NH₄)₆Mo₇O₂₁·4H₂O, and Vulcan XC-72 were placed into deionized water with stirring and ultrasonication for 30 min, forming a homogeneous suspension. Later on, NaBH₄ was added. After 6 h, the above suspension was filtered, washed, and dried. The as-obtained product was then ground and subjected to multistep heating. First, it is heated to 350 °C at a rate of 10 °C min⁻¹ under the flowing 90% Ar-10% H₂ atmosphere. After maintaining this temperature for 30 min, the temperature was further increased up to 520 °C and then held at this value for 2 h in an NH₃ flow. These samples were denoted as Pt₆₀Fe₃₅Mo₅/C, Pt₃₅Fe₆₀Mo₅/C, and Pt₂₅Fe₇₀Mo₅/C. The synthetic procedure for PtFeV/C or PtFeW/C was similar to that of PtFeMo/C, whereas NH₄VO₃ and H₄₀N₁₀O₃₁W₁₂·XH₂O were, respectively, added instead of (NH₄)₆Mo₇O₂₁·4H₂O. In addition, the benchmark electrocatalyst is the commercial Pt/C, supplied from Johnson Matthey Company (HiSPEC 4000) with 38–41 wt % Pt, and the average size of Pt is smaller than 2.3 nm. The carbon support was provided from the Cabot Company (Vulcan XC-72R).

B. Materials characterization

X-ray powder diffraction (XRD; D8 ADVANCE, Bruker AXS, Germany) was adopted to evaluate the crystal information of the samples. Transmission electron microscopy (TEM; Titan ETEM G2 80-300, FEI Co, America) was used to characterize the morphology and composition of electrocatalyst nanoparticles. X-ray photoelectron spectroscopy (XPS) data were recorded by an ESCALAB-250i instrument (Thermo Fisher, USA). Composition information for all the electrocatalysts was characterized by an inductively coupled plasma (ICP) optical emission spectroscopy (Thermo Fisher iCAP 7400, USA). For the electrochemical characterizations a bipotentiostat (Pine, USA) with a standard three-electrode cell was used. The reference electrode was Ag/AgCl, Pt foil was employed as a counter electrode and a glassy carbon (0.2475 cm²) was employed as working electrode.

III. RESULTS AND DISCUSSION

The morphology, structure, and composition of as-prepared electrocatalysts were investigated by TEM and XPS. According to Fig.1 the nanoparticles are spherical, and their average diameters of Pt₂₅Fe₇₀Mo₅/C, Pt₂₅Fe₇₀V₅/C, and Pt₂₅Fe₇₀W₅/C are about 15.83, 12.26, and 18.66 nm, respectively.

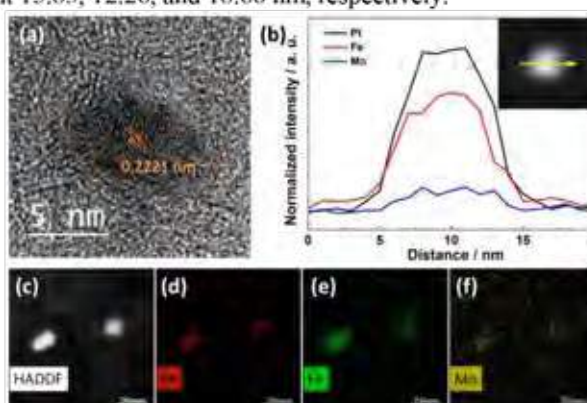


Fig. 1. (a) A representative high-resolution TEM image of Pt₂₅Fe₇₀Mo₅/C nanoparticles. (b) EDS line-scanning profile across a Pt₂₅Fe₇₀Mo₅/C nanoparticle. (c) HAADF-STEM images at high magnification of Pt₂₅Fe₇₀Mo₅/C. (d–f) distribution of Pt (red), Fe (green), and Mo (yellow) in EDS composition maps of Pt₂₅Fe₇₀Mo₅/C nanoparticles

Fig. 1a highlights the lattice spacing of 0.2221 nm for Pt(111) crystal facets of Pt₂₅Fe₇₀Mo₅/C. As the distance of crystal facets for Pt₂₅Fe₇₀Mo₅/C is smaller than that of the commercial Pt (0.22316 nm), it is indicative of the compressive strain effect on Pt. As displayed, in the high-angle annular dark-field scanning transmission electron microscopy (HAADF-STEM) image of Pt₂₅Fe₇₀Mo₅ nanoparticles in Fig. 1c and the corresponding EDS elemental mapping in Fig. 1d–f, the Pt and Fe atoms are uniformly distributed in nanoparticles, but Mo atoms are mainly concentrated in the center of nanoparticles.

Fig.2a–c depicts the polarization curves for the ORR and the inserted graphs are the corresponding mass activities (MA) curves. The ORR polarization curves demonstrate that the half-wave potentials ($E_{1/2}$) of the electrocatalysts are in the range between 0.91

and 0.96 V. The results indicate that all the electrocatalysts yield good oxygen reduction activity. Notably, the half-wave potential of Pt₂₅Fe₇₀Mo₅/C is the highest compared with all the other prepared electrocatalysts. Its $E_{1/2}$ is 36 mV more positive than one of Pt/C, and even 14 mV more positive than Pt₆₀Fe₃₅Mo₅/C that is the second highest $E_{1/2}$ in all the electrocatalysts.

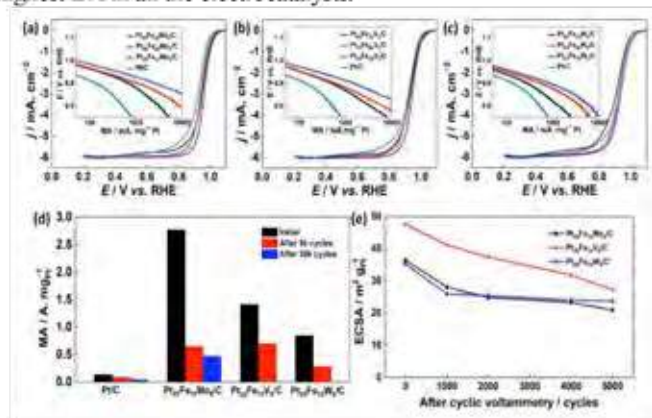


Fig. 2. (a–c) ORR polarization curves and MAs of all the investigated electrocatalysts in O₂-saturated 0.1 M of HClO₄ aqueous solution, 5 mV s⁻¹, and 1600 rpm. Inset: comparison of MA for the different electrocatalysts. (d) The MA for Pt/C, Pt₂₅Fe₇₀Mo₅/C, Pt₂₅Fe₇₀V₅/C, and Pt₂₅Fe₇₀W₅/C at 0.9 V before and after 5k or 30k cycles. (e) ECSAs of Pt₂₅Fe₇₀M₅/C (M = Mo, V, or W) electrocatalysts after different cyclic voltammetry cycles

IV. CONCLUSION

Ternary PtFeM/C (M = Mo, V, W) alloy electrocatalysts, with different degrees of compressive strain on Pt were prepared. The XRD, TEM, XPS, and ICP were adopted to study the composition and structure of the as prepared electrocatalysts. Subsequently, we discussed the relationships between the ORR activity and the compressive strain effect on Pt. The results show a volcano trend and Pt₂₅Fe₇₀Mo₅/C is at the apex.

ACKNOWLEDGMENT

This work was supported by the National Basic Research Program of China (2017YFB0103000), the Natural Science Foundation of China (21872040), the Natural Science Foundation of Guangxi (2016GXNSFCB380002), and the Nanning Science and Technology Project (AB16380030).

Prof. Tsiakaras and Dr Brouzgou thankfully acknowledge co-financing by the European Union & Greek national funds through the Operational Program Competitiveness, Entrepreneurship and Innovation, under the call RESEARCH – CREATE – INNOVATE (Project code:T1EDK-02442).



REFERENCES

- [1] Brouzgou, A., Song S.Q., Tsiakaras P., Low and non-platinum electrocatalysts for PEMFCs: Current status, challenges and prospects, Applied Catalysis B: Environmental, volume 127, 2012, pp 371-88.
- [2] Norskov, J.K., Rossmeisl J., Logadottir A., Lindqvist L., Kitchin J.R., Bligaard T., et al., Origin of the overpotential for oxygen reduction at a fuel-cell cathode, J. of Physical Chemistry B, volume 108, 2004, pp 17886-92.

HYCARE: HYDROGEN CARRIER FOR RENEWABLE ENERGY STORAGE

Matteo Testi^{a)}, Erika M. Dematteis,^{g)} Jussura Barale,^{b)} Paola Rizzi,^{b)} Luigi Crema,^{a)} Nils Bornemann,^{d)} Camel Makhloufi,^{c)} Quentin Nouvelot,^{c)} Bettina Neumann,^{d)} Carlo Luetto,^{e)} Holger Stühff,^{f)} Klaus Taube,^{h)} Giovanni Capurso,^{h)} Jose Bellosta Von Kolbe,^{h)} Bjorn Hauback,ⁱ⁾ Stefano Deledda,ⁱ⁾ Davide Damosso,^{l)} Sabina Fiorot,^{l)} Fermin Cuevas,^{g)} Michel Latroche,^{g)} Marcello Baricco^{b)}.

a) Fondazione Bruno Kessler, Povo (TN), Italy

b) Department of Chemistry and Inter-departmental Centre Nanostructured Interfaces and Surfaces (NIS), University of Turin, Torino, Italy

c) ENGIE Lab H2 – CRIGEN, Saint-Denis, France

d) GKN Sinter Metals Engineering GmbH, Germany

e) Tecnodelta srl, Chivasso Italy.

f) Stühff GmbH, Geesthacht, Germany

g) ICMPE (UMR7182), CNRS, UPEC, Thiais, France

h) Helmholtz-Zentrum Geesthacht Zentrum für Material- und Küstenforschung GmbH, Geesthacht, Germany

i) Institutt for Energiteknikk, Kjeller, Norway

l) Environment Park, Turin, Italy

Abstract - The intermittent production of energy from renewable source requires suitable storage systems for an efficient integration of green energy production into electrical grid. Hydrogen allows storing large amounts of energy with elevate energy density and with low environmental impact (>33 kWh/kg(H₂)). Hydrogen cycle includes production using renewable energies by electrolysis, storage and conversion into electrical energy by means of a fuel cell. However, hydrogen storage remains a challenge. The main objective of the HyCARE project is the development of a prototype hydrogen storage tank with use of a solid-state hydrogen carrier on large scale coupled with an innovative concept of thermal module based on PCM materials.

Index Terms - Hydrogen storage, Metal hydride, PCM

Nomenclature

PCM: Phase Change Material

HyCARE: Hydrogen CARRIER for Renewable Energy storage

I. INTRODUCTION

The introduction of large amount of renewable source requires suitable and feasible storage system for an efficient integration into electrical grid. Among different solutions proposed, hydrogen gas as energy carrier has been investigated for many

years, with several and mature technologies already in the market. Hydrogen cycle includes production using renewable energies by electrolysis, storage and conversion into electrical energy by means of a fuel cell. Hydrogen can be stored in different form: compressed gas, liquefied and chemically bonded to metal hydrides. Solid-state hydrogen storage ensures safe storage, reducing the volume required for storing large quantities of hydrogen. Hydrogen storage remains a challenge. The HyCARE project plans to address it at big scale, providing 50 kg of stored hydrogen, which will represent the highest quantity ever accumulated in Europe within solid state approach. The project involves the tailoring and optimization of a proper alloy composition and the production of 5 tons of selected material. Metal hydride material will fill optimized tanks for large-scale stationary hydrogen storage. Appropriate phase change materials (PCM) will be used to increase the overall efficiency of such ambitious hydrogen systems. The thermal management of the tanks will take place through an innovative approach, selecting a PCM with a phase transition temperature coherent with working temperature of metal hydride material. The consortium is led by the University of Turin, together with the Environment Park, and sees the presence of a large metallic powder producer (GKN Sinter Metals) and the French energy multinational company Engie, which will make its LAB CRIGEN site in Paris available for

the demonstration. The plant will be built by two small-medium enterprises, a German (Stühff) and an Italian (Tecnodelta) one. The research teams will support the project, with the Italian Bruno Kessler Foundation (FBK) of Trento for modelling activity and control development, the French CNRS for metal hydride selection and study, the Helmholtz Zentrum of Geesthacht (HZG) in Germany for modelling and characterization activity for the hydrogen storage tank and the Norwegian Institute for Energy (IFE) in charge of advanced material characterization on metal hydride material.

II. METHOD

The main objective of the HyCARE project is the development of a prototype hydrogen storage tank with use of a solid-state hydrogen carrier on large scale. Main concepts are reported in Figure 1 and Figure 2, for the hydrogen charging and discharging step, respectively. The developed tank will be joined with a PEM electrolyzer as hydrogen provider and a PEM fuel cell as hydrogen user. The following goals are planned in HyCARE:

- High quantity of stored hydrogen ≥ 50 kg
- Low pressure < 50 bar and low temperature $< 100^\circ\text{C}$
- Low footprint, comparable to liquid hydrogen storage Innovative design
- Hydrogen storage coupled with thermal energy storage Improved energy efficiency
- Integration with an electrolyser (EL) and a fuel cell (FC) Improved safety
- Demonstration in real application Improved safety
- Techno-economical evaluation of the innovative solution
- Analysis of the environmental impact via Life Cycle Analysis (LCA)
- Exploitation of possible industrial applications
- Dissemination of results at various levels
- Engagement of local people and institution in the demonstration site

III. CONCLUSION

HyCARE project is at the first year. Main activities during this time were focused on the definition of the metal hydride alloy composition and its characterization, in compliance with technical requirements of the project. Activities about hydrogen storage tank and heat management system are under progress and will provide first results at the beginning of 2020.

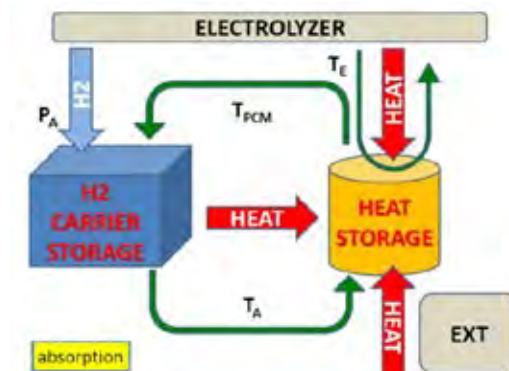


Figure 1 Scheme of concept: hydrogen charging into the tank by electrolyzer.

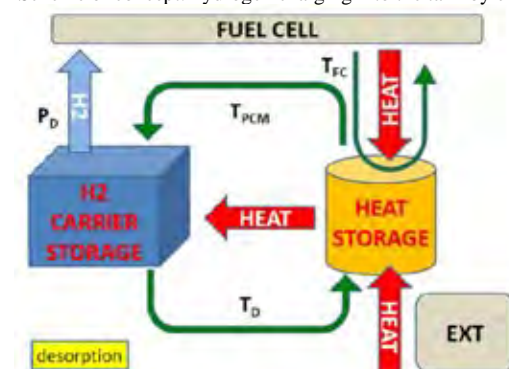


Figure 2 Scheme of concept: hydrogen discharging form storage tank and heat exchange.

Acknowledgments: this project has received funding from the Fuel Cells and Hydrogen 2 Joint Undertaking under grant agreement No 826352. This Joint Undertaking receives support from the European Union's Horizon 2020 research and innovation programme and Hydrogen Europe and Hydrogen Europe Research

REFERENCES

- [1] Møller, K. T.; Jensen, T. R.; Akiba, E.; Li, H.-W. Hydrogen - A Sustainable Energy Carrier. *Prog. Nat. Sci. Mater. Int.* 2017, 27 (1), 34–40. <https://doi.org/10.1016/j.pnsc.2016.12.014>.
- [2] Jensen, C.; Akiba, E.; Li, H.-W. Hydrides: Fundamentals and Applications. *Energies* 2016, 9 (4), 308. <https://doi.org/10.3390/en9040308>.
- [3] Belmonte, N.; Girgenti, V.; Florian, P.; Peano, C.; Luetto, C.; Rizzi, P.; Baricco, M. A Comparison of Energy Storage from Renewable Sources through Batteries and Fuel Cells: A Case Study in Turin, Italy. *Int. J. Hydrogen Energy* 2016, 41 (46), 21427–21438. <https://doi.org/10.1016/j.ijhydene.2016.07.260>.

FIRST RESULTS OF THE H2020-LC-SC3-RES-11 BLAZE PROJECT: BIOMASS LOW COST ADVANCED ZERO EMISSION SMALL-TO-MEDIUM SCALE INTEGRATED GASIFIER FUEL CELL COMBINED HEAT AND POWER PLAN

Enrico Bocci¹; Luca Del Zotto¹, Andrea Monforti Ferrario¹, Vera Marcantonio², Andrea Di Carlo³; Alessandro Di Giuliano³; Elisa Savuto⁴, Donatella Barisano⁵; Stephen Mac Phail⁶; Massimiliano Della Pietra⁶, Davide Pumiglia⁶, Maurizio Cocchi⁷; Jan Pieter Ouweltjes⁸; Ligang Wang⁹, Jan Van Herle⁹

¹ Nuclear and Radiation Physics Department, Marconi University, Via Plinio 44, 00193 Rome, Italy

² Tuscia University, Via San Camillo de Lellis, snc 01100 Viterbo, Italy

³ University of L'Aquila, Via Campo di Pile, L'Aquila, Italy

⁴ University of Teramo, Via R. Balzarini 1, 64100 Teramo, Italy

⁵ Enea Trisaia Research Centre, SS Jonica 106 - km 419 + 500, 75026 Rotondella (Mt), Italy

⁶ Enea Casaccia Research Centre, Via Anguillarese, 00123 Rome, Italy

⁷ European Biomass Industry Association, Scotland House, Rond-Point Schuman 6, 1040 Brussels, Belgium

⁸ SOLIDpower S.A., Avenue des Sports 26, CH-1400 Yverdon-les-Bains, Switzerland

⁹ Group of Energy Materials, Institute of Mechanical Engineering, EPFL, CH-1951 Sion, Switzerland

*corresponding author: email e.bocci@unimarconi.it

Abstract - BLAZE aims at developing Low cost, Advanced and Zero Emission first-of-a-kind small-to-medium Biomass CHP. This aim is reached by developing bubbling fluidised bed technology integrating a high temperature gas cleaning & conditioning system and integration of Solid Oxide Fuel Cells. The technology is characterised by the widest solid fuel spectrum applicable, high efficiencies (50% electrical versus the actual 20%), low investment (< 4 k€/kWe) and operational (≈ 0.05 €/kWh) costs, as well as almost zero gaseous and PM emissions, projecting electricity production costs below 0.10 €/kWh. The paper shows the first project activities: the preliminary economic analysis, the choice of 10 samples and 5 mixtures of representative biomass wastes to be tested in the gasification labs and the bio-syngas representative tar and contaminants to be tested in the SOFC lab scale facilities.

Keywords – Biomass, Gasification, SOFC, CHP.

I. INTRODUCTION

At present, installed electricity generation capacity by Combined heat and power (CHP) in the EU-28 is about 120 GWe (ST 62 GWe, CC 30 GWe, ICE 15 GWe, GT 12 GWe), which generates approximately 11% of the EU electricity demand (362 TWh, i.e. on average ≈ 3000 annual equivalent hours) [1]. The CHP heating capacity is about 300 GWth with a heat production of 775 TWh, i.e. an average of ≈ 2.5 thermal/electrical power ratio and 2500 annual equivalent hours. Renewables, mainly biomass and in particular low-cost biomass or biomass waste, are becoming increasingly important having attained 20% of the market. The bioenergy contribution for heating and cooling has currently the largest share (88%) of all RES used for heat and cooling with 76 Mtoe, not far from the 2020 Member States plan of 90 Mtoe [2]. CHP systems have significant penetration in the EU industry, producing approximately 16% of final industrial heat demand [3]. It is worth noting that cogeneration (CHP) plants account for about 60% of EU-28's bioenergy production from

solid biomass [4]. The total EU28 energy demand for Heating and Cooling (H/C) equals 51% of the total final energy demand; the majority of the demand for H/C is due to space heating (52%), followed by process heating (30%) and water heating (10%) with ambitious policy objectives which include, for instance, that all new buildings must be Nearly Zero Energy Buildings (NZEB) from 31st December 2020. The European bioenergy potential derived from residues is 314 Mtoe; the currently consumed share is less than half of this value [5]. Major limitations of the bioenergy potential relate to the facts that S-o-A small-medium solid biomass power plants currently have annual operating time 4000 h, electrical efficiency 25%, high local and environmental impacts and a capital cost 5.000 €/kWe. They cannot compete with the liquid or gaseous fossil fuels CHP where, even if the fuel cost is higher, the CAPEX is lower, the annual operating time higher and local emissions lower [6].

II. BLAZE

The project aims at the development of a compact bubbling fluidised-bed gasifier integrating primary sorbents and ceramic candle filters with Ni catalyst (IBFBG), a high temperature fixed bed sorbents reactor and an integrated solid oxide fuel cell (SOFC) including first-of-a-kind heat-driven gas recirculation. The technology is developed for a CHP capacity range from 25-100 kWe (small scale) to 0.1-5 MWe (medium scale) and is characterised by the widest fuel spectrum applicable (forest, agricultural and industrial waste also with high moisture contents, organic fractions of municipal waste, digestate), high net electric (50%) and overall (90%) efficiencies as well as almost zero gaseous and PM emissions. Such targets can be achieved by the technology development undertaken in this project that allows to convert with high efficiency low cost fuel,

BIOMASS CHP COST PER kWh_e

	BLAZE		ICE		ORC	
	3000	2500	3000	2500	3000	2500
Equivalent annual hours	3000	2500	3000	2500	3000	2500
OPEX €/kWh	0.06	0.03	0.16	0.04	0.20	0.04
CAPEX €/kWh	0.08	0.03	0.11	0.02	0.13	0.02
Tot CAPEX+OPEX €/kWh	0.14	0.06	0.27	0.06	0.33	0.06
Equivalent annual hours	7500	7500	7500	7500	7500	7500
OPEX €/kWh	0.04	0.02	0.12	0.03	0.14	0.03
CAPEX €/kWh	0.06	0.02	0.07	0.01	0.06	0.01
Tot CAPEX+OPEX €/kWh	0.10	0.04	0.19	0.04	0.20	0.04

The table shows that BLAZE is the only system that, in case of lower annual equivalent hours, has a competitive electricity generation cost, and that BLAZE, in case of high annual equivalent hours, can have electricity generation cost of 0.05 €/kWh.

IV. GASIFICATION AND SOFC LAB SCALE SETUP

The project started the first of March 2019. In the first 6 months the consortium:

- undertake a preliminary cost analysis, showed in the section before,
- chose 10 samples and 5 mixtures of representative biomass wastes to be tested in the gasification labs,
- chose bio-syngas representative tar and contaminants to be tested in the SOFC lab scale facilities,
- set up the experimental gasification, conditioning and SOFC labs that will undertake a comprehensive lab activities in the next 12 months

Regarding the bio-syngas representative tar and contaminants to be tested in the SOFC lab scale facilities the project done an open access literature overview (www.blazeproject.eu/resources) analyzing 83 papers (mostly experimental). It has been decided to focus on 1 representative syngas composition (owing to the decision to focus only on the steam gasification tested at pilot scale, on wet basis: 45% H₂, 24% CO, 11% CO₂, 2% CH₄, 18% H₂O) and 2 organic (toluene and naphthalene) and 3 inorganic (H₂S, KCl; HCl) representative contaminants levels. In particular, Naphthalene has been selected to represent so-called slow tars, i.e. tars with slow conversion kinetics. In order to make meaningful tests, the investigated contaminant levels will be aligned with those reported in literature regarding experimental work on SOFCs, i.e. 25 mg/Nm³ (5 ppm) and 75 mg/Nm³ (15 ppm) naphthalene. Toluene has been selected to represent so-called fast tars, i.e. tars with relatively fast conversion kinetics. Tolerable toluene levels are less clear than for naphthalene, and thus will be aligned with those expected from BFB steam gasifiers with

catalytic filters, i.e. 250 mg/Nm³ (to be expected from clean biomass such as almond shells) and 750 mg/Nm³ (feedstock emitting high toluene concentrations). H₂S has been selected to represent sulfur compounds. In order to make meaningful tests, the investigated contaminant levels will be aligned with those reported in literature regarding experimental work on SOFCs, i.e. 1 ppm and 3 ppm H₂S. KCl has been selected to represent both halogens and alkalis. Although it is unclear whether KCl will actually reach the SOFC in this form, other compounds like HCl and alkali hydroxides might reach the SOFC, and therefore investigating the impact of halogens and alkalis is relevant. Thus, KCl is considered a suitable representative to simultaneously assess the impact of halogens and alkali metals. Investigated contaminant levels are 50 ppm and 200 ppm KCl. The following photos show gasification and SOFCs lab scale facilities fitted for the experimental activities.



Fig. 2. UNITE gasification and UNIVAQ catalyst and sorbent test rig

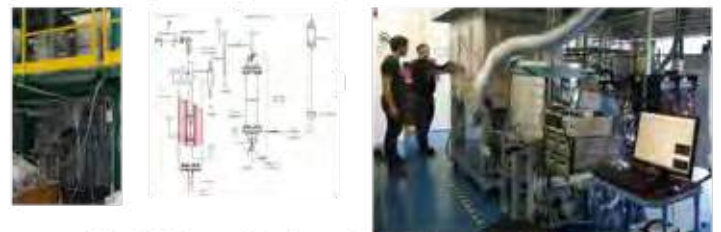


Fig. 3. ENEA gasification and EPFL/SP stack SOFC test rig

ACKNOWLEDGMENT

This research has been supported from the European Union's Horizon 2020 research and innovation program under grant agreement No 815284, project "BLAZE".

REFERENCES

- [1] Eurostat. CHPdata2005-2017. Bruxelles: 2019.
- [2] Commission E. SET - Plan – Issues Paper. 2016.
- [3] Commission E. Green Public Procurement-Electricity Green Public Procurement Electricity Technical Background Report. 2011.
- [4] EurObserver. The State of Renewable Energies in Europe 2011;33:4-7.
- [5] EurObserver. Solid biomass barometer. 2012,2013,2014 2018.
- [6] Agency USEP, Heat C, Partnership P. CHP project development handbook [electronic resource]. Comb Heat Power Proj Dev Handb 2008.

MOLYBDENUM-MODIFIED AND VERTEX-REINFORCED QUATERNARY HEXAPOD NANO-SKELETONS AS EFFICIENT ELECTROCATALYSTS FOR METHANOL OXIDATION AND OXYGEN REDUCTION REACTION

L. Huang*, M. Wei*, N. Hu*, A. Brouzgou**, Peikang Shen*, P. Tsiakaras**

*Collaborative Innovation Center of Sustainable Energy Materials, Guangxi Key Laboratory of Electrochemical Energy Materials, State Key Laboratory of Processing for Non-ferrous Metal and Featured Materials, Guangxi University, Nanning, 530004, (PR China)

**Laboratory of Alternative Energy Conversion Systems, Department of Mechanical Engineering, University of Thessaly, Pedion Arcos, (Greece)

Abstract - Noble metal binary and ternary catalysts have become a new class of fuel cell electrocatalysts due to their high catalytic activity. However, improvement is still necessary to reduce the consumption of Pt and obtain the quaternary Pt-based catalyst by Mo modification. Through the introduction of $\text{Mo}(\text{CO})_6$, quaternary hexapod nano-skeletons with high-index facets are obtained here, which are composed of core, first-layer feet and second-layer feet. Compared with PtCoNi nanoparticles, the vertex-reinforced PtCoNiMo hexapod nano-skeletons due to abundant tip areas can facilitate electron transfer and mass exchange. It is found that the as prepared PtCoNiMo nano-skeletons catalyst exhibits enhanced mass activity, stability and anti-poisoning ability towards the methanol oxidation reaction (MOR) and oxygen reduction reaction, compared to commercial Pt/C catalyst and PtCoNi nanoparticles.

Index Terms -high-index facets; vertex-reinforced, methanol oxidation reaction, oxygen reduction reaction

I. INTRODUCTION

The high-efficiency catalysts are mainly hollow spheres, nanoframes and nano-skeletons [1]. For this type of catalytic material, they exhibit a highly open structure and efficient atomic utilization. Electron transfer and mass exchange are accelerated in electrochemical tests, which is very beneficial for improving catalytic performance. It is well known that carbonyl compounds ($\text{Mx}(\text{CO})_y$, $\text{M}=\text{Fe}$, Co , W , Mo , etc.) [2] as surfactants and reducing agents play an important role in the preparation of many nanomaterials, such as the synthesis of nanowire, concave cube, nanorod, etc. Carbonyl compounds are popular in the synthesis of nanomaterials due to the presence of carbonyl groups in its organic composition. In addition, carbonyl compounds are safe and convenient compared to CO gas, which is good for controlling the synthesis and growth of nanocrystals [2]. Herein, we report vertex-reinforced quaternary PtCoNiMo hexapod nano-skeletons (NSs), achieved by introduction of $\text{Mo}(\text{CO})_6$, for efficient oxygen reduction and methanol oxidation catalysis.

II. MATERIALS AND METHODS

The synthesis procedure is as follows: in a typical synthesis, 10.0 mg of $\text{Pt}(\text{acac})_2$, 9.0 mg of $\text{Co}(\text{acac})_3$ and 6.5 mg of $\text{Ni}(\text{acac})_2$ were dissolved in a glass bottle containing 5 ml of oleylamine, followed by the addition of 60 mg of glucose and 5 mg of $\text{Mo}(\text{CO})_6$. After stirring for 10 min, it was sonicated until the solution was evenly mixed. It was then transferred to an oil bath at 120 °C for 5 h, and the as obtained product was collected by centrifugation. For the physicochemical characterizations, X-ray powder diffraction (XRD) patterns were performed at 40 kV and 30 mA using a SmartLab3 X-ray diffractometer (Rigaku, Japan) with $\text{Cu K}\alpha$ radiation ($\lambda = 1.5405 \text{ \AA}$). Transmission electron microscopy (TEM), High-resolution TEM (HRTEM) and high-angle annular dark field scanning TEM (HAADF-STEM) images were obtained at 300 kV using a TITAN G2 microscope (FEI, American) equipped with an energy dispersive X-ray spectroscopy (EDS) detector. Moreover, the EDS mapping images were collected using a 60-300 electron microscope (300 kV). For the electrochemical characterization, as working electrode was used a glassy carbon electrode (0.196 cm^2), a saturated calomel electrode, or a reversible hydrogen electrode as reference electrode, and graphite rod as counter electrode.

III. RESULTS AND DISCUSSION

As can be distinguished from the high-magnification TEM images (1g-1i), the first image shows 4 feet (Fig. 1g), the second image shows 5 feet (Fig. 1h), and the third image shows 6 feet (Fig. 1i). The fast fourier transform images, insets in the TEM images, indicate that PtCoNiMo hexapod NSs have good crystallinity. Moreover, the EDS mapping images show that the Pt, Co, Ni, Mo are evenly distributed and the Mo element is less relative to other metal elements (Figs. 2j).

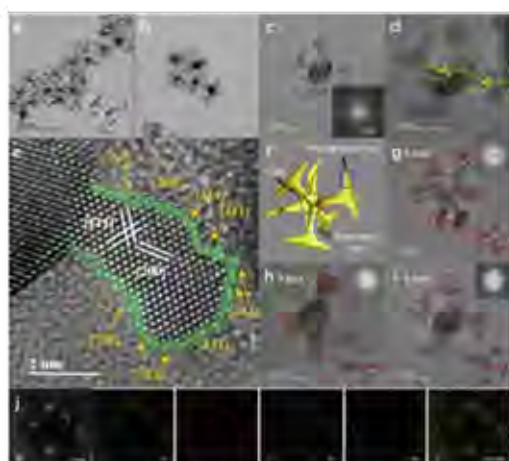


Fig.1 (a, b) Low-magnification TEM image, (c, d) high-magnification TEM image, (e) atomic-scale HRTEM image, (f) the model and structure, (g, h, i) high-magnification TEM images, corresponding models and FFT images at different angles. (j) EDS mapping images of PtCoNiMo hexapod NSs

Concerning electrochemical activity, the results indicate that compared to Pt/C and PtCoNi NPs, the PtCoNiMo exhibits enhanced anti-poisoning ability to the presence of MOR (Fig. 2d).

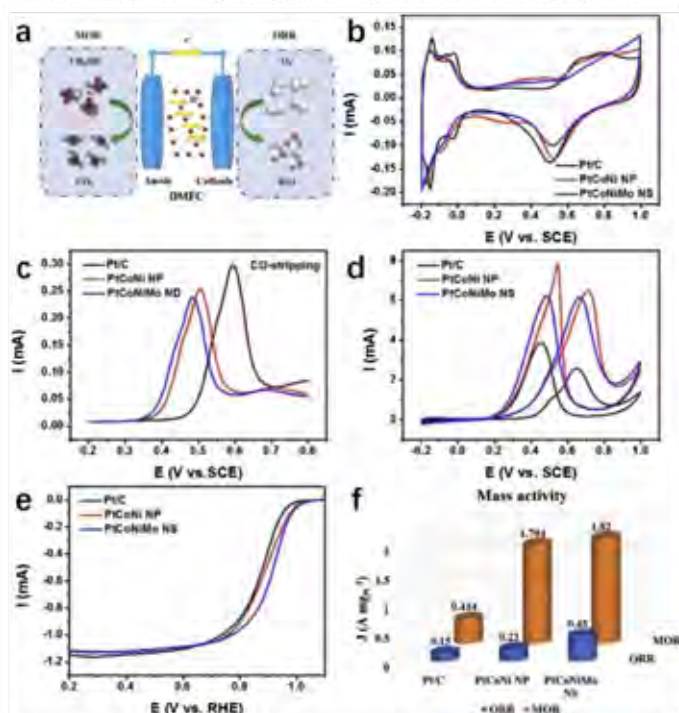


Fig. 2 (a) Schematic diagram of methanol oxidation reaction and oxygen reduction reaction processes. Electrochemical measurements of the PtCoNiMo NSs, PtCoNi NPs and Pt/C catalysts. (b) CV curves recorded in 0.5 M H₂SO₄ solution, (c) CO-stripping curves, (d) MOR curves recorded in 0.5 M H₂SO₄ + 1.0 M CH₃OH solution, (e) ORR polarization curves in 0.1 M HClO₄ solution, (f) mass activity towards MOR and ORR

Based on the oxidation peak intensity and Pt loadings for PtCoNiMo NSs (6.15 mA, 17.4 μg_{Pt} cm⁻²), PtCoNi NPs (6.44 mA, 19.4 μg_{Pt} cm⁻²) and Pt/C catalysts (2.59 mA, 30.6 μg_{Pt} cm⁻²), the PtCoNiMo NSs displayed for MOR a better mass activity (1.82 A mg_{Pt}⁻¹); which was 4.2 times greater than that of commercial Pt/C (0.43 A mg_{Pt}⁻¹) (Fig. 2f).

In Fig. 3 the results indicate that the PtCoNiMo NSs catalyst has an efficient mass activity, and the mass activity of PtCoNiMo NSs catalyst can still reach 1.51 A mg_{Pt}⁻¹, which was 5.2 times higher than that of commercial Pt/C catalyst (mass activity of 0.29 A mg_{Pt}⁻¹). In addition, the stability of PtCoNiMo NSs catalyst for ORR was investigated by using ADTs for 10,000 cycles (Fig. 3).

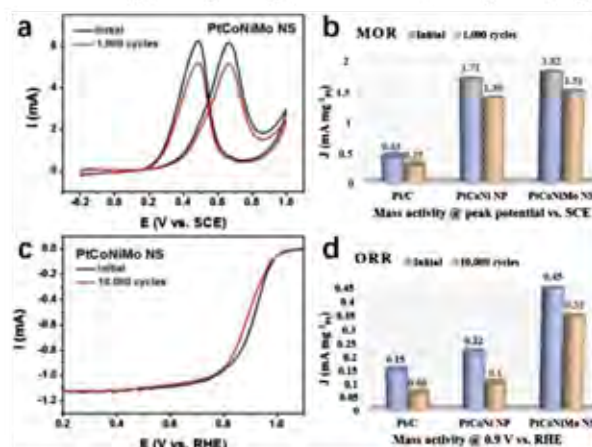


Fig.3 (a) MOR curves, (b) mass activity at the peak potential vs. SCE before and after 1000 cycles. (c) ORR polarization curves, (d) mass activity at 0.9 V vs. RHE before and after 10,000 cycles

IV. CONCLUSION

The quaternary PtCoNiMo hexapod NSs possess a series of tip areas with high-index facets, which can facilitate electron transfer, mass exchange and performance improvement. Compared with commercial Pt/C catalyst and PtCoNi NPs, quaternary PtCoNiMo hexapod NSs exhibit efficient mass activity, stability and anti-poisoning ability for MOR and ORR.

ACKNOWLEDGMENT

This work was supported by the Guangxi Science and Technology Project (AA17204083, AB16380030), National Basic Research Program of China (2015CB932304), the Natural Science Foundation of Guangdong Province (2015A030312007), the link project of the National Natural Science Foundation of China and Fujian Province (U1705252) and the Danish project of Initiative toward Non-precious Metal Polymer Fuel Cells (4106-000012B). Prof. Tsiakaras and Dr Brouzgou thankfully acknowledge co-financing by European Union & Greek national funds through the Operational Program Competitiveness, Entrepreneurship and Innovation, under the call RESEARCH – CREATE – INNOVATE (Project code: T1EDK-02442).



REFERENCES

- [1] Hou, Y.-N., Zhao Z., Zhang H., Zhao C., Liu X., Tang Y., et al., Designed synthesis of cobalt nanoparticles embedded carbon nanocages as bifunctional electrocatalysts for oxygen evolution and reduction, Carbon, volume 144, 2019, pages 492-9.
- [2] Xiao, Q., Cai M., Balogh M.P., Tessema M.M., Lu Y., Symmetric growth of Pt ultrathin nanowires from dumbbell nuclei for use as oxygen reduction catalysts, Nano Research, volume 5, 2012, pages 145-51.

DESIGN OF BIO-BASED CARBONACEOUS FIBROUS STRUCTURES AS CATALYSTS IN FUEL CELLS

Silvo Hribernik^{1,2}, Mojca Božič^{1,2}, Selestina Gorgieva^{1,2} and David DeVallance³

¹ University of Maribor, Faculty of Electrical Engineering and Computer Science, Koroška cesta 46, 2000 Maribor (Slovenia)

² University of Maribor, Faculty of Mechanical Engineering, Smetanova ulica 17, 2000 Maribor (Slovenia)

³ InnoRenew COE, Livade 6, 6310 Izola (Slovenia)

Abstract - Morphology of nanofibrillar cellulose, with its well defined structure and resulting high Young modulus, can crucially improve the mechanical properties of catalyst component, ensuring a much longer life cycle. Presentation will focus on (i) development of functionalization processes for cellulosic fibrillar building blocks with an emphasis of heteroatom and metal particles introduction, (ii) construction of porous 3D matrices from functionalized lignocellulosic building blocks and (iii) carbonization processes for transformation of cellulose into carbonaceous matrices. Design of cellulose-based carbonaceous porous structures will be assessed through their potential to meet membrane fuel cell catalyst requirements, such as: high electrical conductivity, high specific surface area and high porosity, uniform distribution of catalyst particles on the support, high interaction between catalyst particles and support surface, high mass transport.

Index Terms – cellulose-based porous matrices, fuel-cell catalysts, metal doping

I. INTRODUCTION

Cellulose, ranking among the most abundant materials available, possesses superior mechanical properties, which, combined with the multitude of available structural forms, can efficiently contribute towards achieving aerogel structure and subsequently serve as a building blocks for porous products [1]. Development of new energy devices for transportation (more efficient batteries and fuel cells) is a research field that on one hand tackles increasingly serious concerns regarding CO₂ emissions from fuel engines by offering clean energy solutions, but on the other has to struggle with its own dependence on oil-based materials to construct these advanced products. Harnessing and engineering renewable wood-derived resources

as materials for future generation energy devices holds a great potential to fabricate technologically advanced products on a large scale, which, even more importantly, will be able to compete with the existing, oil-based products [2]. Present study deals with the development of cellulose-based carbon materials as catalyst support, aimed for oxygen reduction reactions (ORR) in proton-exchange membrane fuel cells (PEMFC). While a majority of state-of-the-art catalysts exhibit good performance in terms of activity for ORR, they are fatally hindered by their poor stability during prolonged operation of PEMFC. Pre-determined morphology of nanofibrillar cellulose, with its well defined structure and resulting high Young modulus, can crucially improve the mechanical properties of catalyst component, ensuring a much longer life cycle. Emphasis will be placed on design and elaboration of construction of porous cellulose fibril-based aerogels, which hold a great potential as a material for catalyst supports.

II. METHODS AND PROCEDURES

Nanofibrillar cellulose (NFC) from University of Maine (USA) was employed as the building block for the construction of aerogels; these porous matrices were prepared using freeze-drying method, where aqueous-based NFC slurries of different concentrations and with and without the addition of water soluble cellulose derivatives (methylcellulose) were frozen, followed by a sublimation of ice, effectively avoiding the transition through liquid phase. Hetero-atom introduction into cellulose fibres prior carbonization was achieved by metal complexation of iron salts with charged groups on cellulose

backbone and Schiff base reaction with hydroxylamine to introduce nitrogen. Carl Zeiss FE-SEM SUPRA 35 VP field-emission electron microscope was used for observation of the morphology of NFC aerogels, enabling us to study in detail the templating effect of ice crystals during freezing of hydrogel casting and the addition of polymer solution into fibrous slurry. SEM images were used to elucidate the influence of process parameters on the size, orientation and shape of formed pores. In order to conduct SEM analysis, samples were attached by means of carbon conductive tape onto brass specimen holders and sputtered with a thin layer of palladium. The images were recorded with an acceleration voltage of 1 kV at a working distance of 4,5 mm.

III. RESULTS

In Figures 1 and 2, scanning electron microscope (SEM) images of porous cellulose aerogels are presented.

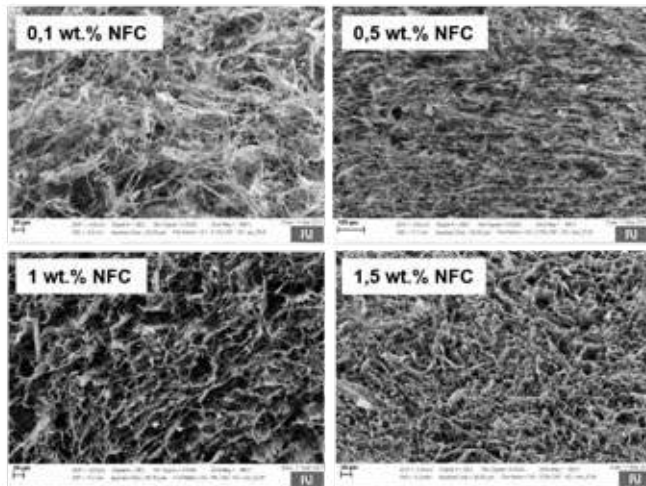


Fig. 1. Scanning electron microscope images of aerogels' porous structure; influence of NFC concentration

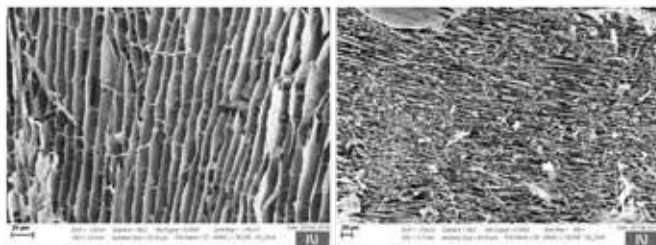


Fig. 2. Scanning electron microscope images of aerogels' porous structure; influence of methylcellulose

In aerogel fabrication, we have paid a particular attention to materials processing and shaping routes with an aim to prepare highly porous materials; to this end, we have relied on freeze drying to ensure efficient water removal that will not cause

collapsing of the pores during drying. Growth of ice crystals during freezing of colloids or, in present case fibre suspensions, acts as porosity templating tool. Foregoing removal of the water in its liquid state, which would inevitably result in densely packed, non-porous structure (common occurrence during conventional drying) and instead sublimate water in its solid state directly into water vapour enables retention of structure where air occupies the spaces formerly filled with ice crystals. SEM images in Figures 1 and 2 clearly confirm above statements, since the resultant aerogels exhibit a highly porous structure, with pore dimensions dependent on the concentration of nanofibrillar cellulose used. Figure 2 further showcases the influence of an addition of water-soluble polymer, i.e. methylcellulose into the fibrous slurry; an evident, large-scale structuring of the aerogel is achieved, where somewhat random pore ordering of the CNF slurries alone is rendered into gallery-like sheets.

IV. CONCLUSION

A variety of aerogels morphologies has been constructed by implementing different freezing protocols when processing nanofibrillar cellulose slurries of varying constitutions; we were able to retain and exert control over the porosity of the fabricated materials. Carbonization process effectively rendered cellulose aerogels into carbon-rich porous matrices, which can be applied as catalyst supports for fuel cells, as well as catalysts themselves, in the case of hetero-atom doped carbonaceous materials.

ACKNOWLEDGMENT

The authors would like to acknowledge European Commission for funding the project InnoRenew CoE (#Grant Agreement 739574) under the Horizon 2020 Widespread-Teaming program and bilateral project between Austria (FWF Der Wissenschaftsfonds) and Slovenia (ARRS Slovenia research Agency) no. N2-0087 (GO DEFC - Graphene oxide based membrane electrode assemblies for direct ethanol fuel cells).

REFERENCES

- [1] Long, L.-Y., Weng, Y.-X., Wang, Y.-Z., Cellulose Aerogels: Synthesis, Applications, and Prospects, *Polymers*, Volume 10, 2018, pp. 623-650.
- [2] Zhu, H., Luo, W., Ciesielski, P. N., Fang, Z., Zhu, J. Y., Henriksson, G., Himmel, M. E., Hu, L., Wood-Derived Materials for Green Electronics, Biological Devices, and Energy Applications, *Chemical Reviews*, Volume 116, 2016, pp. 9305-9374.

Bioelectrochemical TiN|FDH Catalyst for CO₂ Reduction to HCOOH

F. Arena ^{a,b,‡}, G. Giuffredi ^{a,b,‡}, S. Donini ^a, E. Stancanelli ^c, C. Cosentino ^c, E. Parisini ^a, F. Di Fonzo ^a

^a Center for Nano Science and Technology - Istituto Italiano di Tecnologia (IIT) Via Pascoli, 70/3 Milano, Italy

^b Politecnico di Milano - Department of Energy, Via Lambruschini, 4 – Milano, Italy

^c Ronzoni Institute for Chemical and Biochemical Research, Via Colombo 81 – Milano, Italy

[‡] These authors contributed equally

Abstract - In this work, we present a BES where the FDH from *Thiobacillus* sp. KNK65MA is deposited on a TiN nanostructured realized by PLD. We realize an electrode with tree-like morphology that maximizes the available surface area for catalyst absorption and enhances the bio-interface. We quantify the amount of immobilized enzyme on the nanostructure through enzymatic assays, demonstrating that the nanostructuring of the TiN increases the surface area available for enzyme immobilization, achieving a maximum enzyme adsorption of 59 $\mu\text{g}/\text{cm}^2$. The electro-synthesis of HCOOH from CO₂ is investigated by chronoamperometry at different applied potentials, showing a productivity for formic acid that ranges from 1.5 to 3.7 $\text{mmol}/\text{mg}_{\text{enzyme}}\text{h}$ according to the applied overpotentials. Unparalleled in previous studies, this performance achieved thanks to the high reducing activity of *Ts*FDH and the high contact area offered by the TiN support and demonstrates the feasibility and as well as the potential for a biotechnological device.

Index Terms - bioelectrochemical system (BES), CO₂ reduction, hybrid electrode, formate dehydrogenase (FDH); nanostructured Titanium Nitride (TiN).

I. INTRODUCTION

Electrochemical CO₂-reduction is an approach that holds potential for exploiting the cyclic reduction and oxidation of carbon-based fuels. As of today, high efficiency in these systems can only be achieved by employing precious metals, which suffer from both low natural availability and high costs [1] as well as unsatisfactory energy efficiencies and lack of conversion product specificity [2].

Recently, the development of a novel hybrid technology based on the combined use of biological organisms or molecules and nanomaterials has created great opportunities to produce renewable fuels and chemicals from the reduction of CO₂ with a minimal overpotential [3]. According to this, the enzymatic electro-synthesis (EES) exploits pure enzymes to catalyze reactions with higher transformation efficiency, higher activity under controlled experimental conditions and higher selectivity towards both specific substrates and products [4].

The first step of CO₂ reduction enzymatic process consists of the production of formic acid using the catalytic properties of the enzyme formate dehydrogenase (FDH) (EC 1.2.1.2.). This enzyme reversibly catalyzes the transformation of CO₂ to formate as the only product of the reaction. In this

contest, we used the NAD-dependent FDH from the aerobic bacterium *Thiobacillus* sp. KNK65MA (*Ts*FDH). Its superior CO₂-reducing activity ($K_{\text{cat}} = 0.318 \text{ s}^{-1}$), compared to the currently used FDH from *C. bovidinii* (*Cb*FDH) ($K_{\text{cat}} = 0.015 \text{ s}^{-1}$) [5], makes it the most suitable FDH enzyme known to date for EES development. Surface chemistry and surface morphology play a key role in the interaction between the enzyme and the electrode. The atomic composition of the material and its structure affect enzyme immobilization, which in turn influences the electrochemical performance of the EES. In this context, titanium nitride (TiN) can be used as a scaffold for enzyme immobilization by exploiting its surface-exposed Ti⁴⁺ atoms for the binding. As such, TiN has been described as a promising general catalyst support material with high electrical conductivity, good biocompatibility, as well as outstanding oxidation and acid corrosion resistance, together with a hybrid metallic/ceramic behaviour [6]. The aim of this work is to realize a nanostructured TiN scaffold featuring an increased available surface area to enhance the interface between the enzyme and the electrode. To this end, we developed a novel hybrid device where the FDH enzyme from *Thiobacillus* sp. KNK65MA (EC 1.2.1.2) is deposited on a nanostructured mesoporous support of TiN fabricated by Pulsed Laser Deposition (PLD) [7]. This deposition method allows the production of a nanostructured support with high surface area and a tree-like morphology. Its high porosity and high specific area maximize the contact with the enzyme, thus improving the efficiency of the EES for CO₂ reduction.

II. RESULTS AND DISCUSSION

A. Enzyme binding efficiency

In order to identify the most suitable film morphology, the immobilization process on TiN support with different porosity (TiN deposited at 30 Pa, 45 Pa and 60 Pa background gas pressures) was assessed by enzymatic assay after drop-casting (active area of 1 cm^2). The results show that there is an increase in the amount of *Ts*FDH that is bound to the TiN nanostructure (after the rinsing process) when the porosity, and therefore the surface area, of the nanostructure increases. For the more porous morphology (TiN 60 Pa) the percentage of adsorbed *Ts*FDH is 48%, corresponding to 1 μg of specifically adsorbed *Ts*FDH, which provides evidence that the more

porous TiN nanostructure is the most suitable surface for the development of a bioelectrochemical system.

After, a calibration curve was performed to determine the maximum binding capacity of the TiN 60 Pa support. The result shows that, by increasing the concentration of the drop-casted *Ts*FDH, the enzyme unit calculated on the TiN support after the rinsing process increases until a *Ts*FDH loading quantity of 1,14 mg is used, corresponding to 59 μg of immobilized protein.

B. CO_2 reduction performance of TiN/*Ts*FDH catalyst

The CO_2 conversion efficiency of TiN/*Ts*FDH catalyst is investigated at different applied potentials, $-0.15 V_{\text{RHE}}$, $-0.45 V_{\text{RHE}}$ and $-0.75 V_{\text{RHE}}$, for a total time of 3 hours. As expected, when $-0.15 V_{\text{RHE}}$ is applied, the observed current density is small with a registered value of $-25.9 \mu\text{A cm}^{-2}$, because in this condition the available overpotential for the reduction of CO_2 to HCOOH is quite limited and, consequently, the kinetics of the reaction is very low. When the applied potential is increased to more negative values of $-0.45 V_{\text{RHE}}$ and $-0.75 V_{\text{RHE}}$, the current density increases respectively to $-200 \pm 20.2 \mu\text{A cm}^{-2}$ and $-1.61 \pm 0.25 \text{ mA cm}^{-2}$ (Fig.1). The increase in current density and its stabilization to significantly higher values suggests that the CO_2 reduction reaction proceeds at a faster rate.

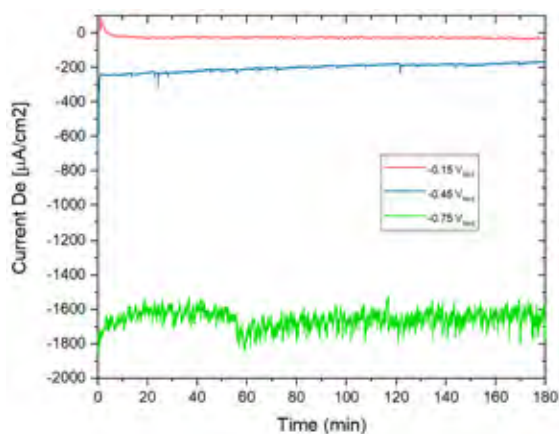


Fig.1: Comparative current profile for $-0.15 V_{\text{RHE}}$, $-0.45 V_{\text{RHE}}$ and $-0.75 V_{\text{RHE}}$ during 3 h period reaction in BES.

Formic acid produced through electrocatalytic CO_2 was analyzed by ^1H NMR spectroscopy. The electrolyte solution was examined before and after the chronoamperometry to have a pre-electrolysis reference NMR spectrum. A ^1H NMR peak is observed at 8.458 ppm for the spectra collected after 3-hour electrolysis at the three different applied potentials, demonstrating that formic acid is a product of the catalytic reaction performed by *Ts*FDH. As expected, the quantity of synthesized formic acid increases when more cathodic potentials are applied. The concentration of formic acid evolved at $-0.15 V_{\text{RHE}}$, calculated through the ^1H NMR spectrum is $6.5 \pm 0.5 \text{ mmol L}^{-1}$. For the applied potentials of $-0.45 V_{\text{RHE}}$ and $-0.75 V_{\text{RHE}}$, the formic acid concentration increases to 14.5 ± 0.4

mmol L^{-1} and $16.4 \pm 0.7 \text{ mmol L}^{-1}$ respectively. The average Faraday efficiency (*FE*) for the electrosynthesis of formic acid is then calculated considering the amount of product obtained during the chronoamperometries and the total charge passed through the TiN/*Ts*FDH electrode (Fig.2).

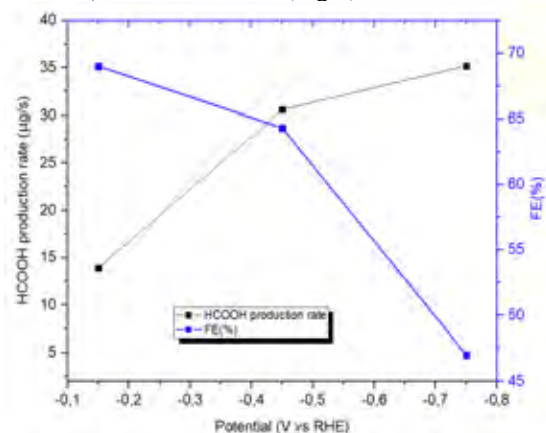


Fig. 2: Production rate of HCOOH and corresponding Faraday efficiency under different potential applied.

For the chronoamperometry at $-0.15 V_{\text{RHE}}$ an FE of 68% is obtained, which gradually decreased to 64% and to 47% with more negative potential applied ($-0.45 V_{\text{RHE}}$ and $-0.75 V_{\text{RHE}}$ respectively). Most likely, this decrease in efficiency was due to the competitive hydrogen evolution reaction (HER) occurring on the surface of the nanostructured support.

III. CONCLUSION

Unparalleled in previous studies, the TiN/*Ts*FDH catalyst shows the best CO_2 reduction performance. These results are the best for inorganic support-immobilized enzymes of the FDH family, achieved thanks to the high CO_2 reducing activity of *Ts*FDH and the high surface area of nanostructured TiN support that allows an increase in the enzyme adsorption.

In this work, we demonstrate the feasibility and potential for a biotechnological hybrid device in terms of product specificity, stability and sustainability for the development and the optimization of an alternative CO_2 -conversion technology.

REFERENCES

- [1] I. Ganesh, Renewable and Sustainable Energy Reviews, 2016, vol. 59, 1269-1297.
- [2] Toru Hatsukade et al., Phys. Chem. Chem. Phys., 2014, vol.16, 13814-13819
- [3] Ahmed ElMekawy et al., Bioresource Technology, 2016, vol.216 357-370
- [4] T. W. Woolerton et al., Energy. Environ. Sci., 2012, vol.5, 7470-7490.
- [5] H. Choe et al., PLOS ONE, 2014, vol. 7, 14-16.
- [6] Bharat Avasarala et al., Electrochimica Acta, 2010, vol. 55, 9024-9034.
- [7] Peregó et al, ACS Appl. Energy Mater. 2019, 2,1911–1922.

COMPARISON OF DIFFERENT PLANT LAYOUTS AND ENGINEERING SOLUTIONS FOR FUEL CELLS UTILIZATION ON A SMALL FERRY

R. Taccani, C. Dall'Armi, N. Zuliani, D. Micheli
University of Trieste, Via A. Valerio 10, 34127 Trieste – Italy

Abstract – In the present study, a process simulation model is implemented to compare different plant layouts to be installed on board of a ferry. Liquid Natural Gas (LNG), hydrogen (H₂) and ammonia (NH₃) have been considered as alternative fuels for power generation plants based on Internal Combustion Engines (ICE) and Polymer Electrolyte Membrane (PEM) fuel cells. Results show overall system efficiency, emissions and fuel volume in comparison with a traditional Internal Combustion Engine (ICE) fuelled by Marine Diesel Oil (MDO) with Selective Catalytic reduction (SCR).

Index Terms – fuel cells, LNG, marine propulsion, ship emissions.

I. INTRODUCTION

International Maritime Organization (IMO) and other bodies are making growing efforts to impose severe limits on shipping pollution especially for vessels, whose routes are concentrated in coastal areas [1]. For this reason, ship-owners are looking for different technologies to be used on ships in order to reduce emissions. It has already been demonstrated [2] that the use of different fuels such as Liquefied Natural Gas (LNG) is an interesting alternative to expansive and bulky exhaust gases after-treatment equipment or fuels with low sulphur content. Among the possible alternative energy systems, fuel cells are currently considered one of the promising solutions for power generation on board of vessels [3], even though the lack of specific certification on their application on board is still the main issue for a large-scale application on a large scale.

In the present study, a process simulation model is utilized to evaluate, at a preliminary stage, different power generation systems on board of a ferry in terms of conversion efficiency, pollutant and greenhouse gases emissions and tank size variation due to different fuels considered.

II. METHODOLOGY

The ferry considered in the simulations is a typical car and passenger ferry with an installed power of 1.5 MW that operates about 30 travels per day. Auxiliary power is considered 75 kW. The ship operating profile is implemented in the built up

simulation model through the definition of three different operating conditions:

- Harbour phase: 60 % of time; power demand of 75 kW (auxiliary power);
- Manoeuvring phase: 12% of time; power demand of 1350 kW (propulsion and auxiliary power);
- Cruise phase: 28 % of the time; power demand of 765 kW (propulsion and auxiliary power).

Different power generation systems have been evaluated to cover both propulsion and auxiliary power demand during the day. A traditional Marine Diesel Oil Internal Combustion Engine (MDO-ICE) generation plant with Selective Catalytic Reduction (SCR) is taken as reference plant for comparative analysis with alternative fuels and power generation systems. The maximum efficiency for traditional MDO-ICE is considered 39 % [4]. Other generation systems included in the calculations are based on Polymer Electrolyte Membrane fuel cells (PEMFC) and Internal Combustion Engines (ICE). Logistic fuels considered for PEMFC are LNG, ammonia (NH₃), and hydrogen (H₂). Both compressed hydrogen (CH₂) and liquid hydrogen (LH₂) storage solutions are evaluated. ICE plants solutions are considered fuelled by LNG and ammonia-hydrogen mixture with 5% content of H₂ in mass [5]. Efficiencies of the considered ICE and PEMFC at different load conditions are based on commercial products datasheet[6][7]. If PEMFC utilizes a logistic fuel different from hydrogen, a fuel-processing unit is needed to produce H₂. If LNG is the hydrogen carrier, an efficiency of 78 % is considered for the LNG reformer [8]. If NH₃ is considered, an efficiency of 76 % is set for the cracking unit [9]. Systems overall conversion efficiency, emissions and required fuel volume are calculated.

III. RESULTS

As shown in Fig.1, overall system conversion efficiency appears to be the highest for PEM fuel cells generation systems ran by hydrogen, due to the better response of fuel cell systems at partial load operation. When LNG or ammonia feed fuel cells, the fuel-processing units

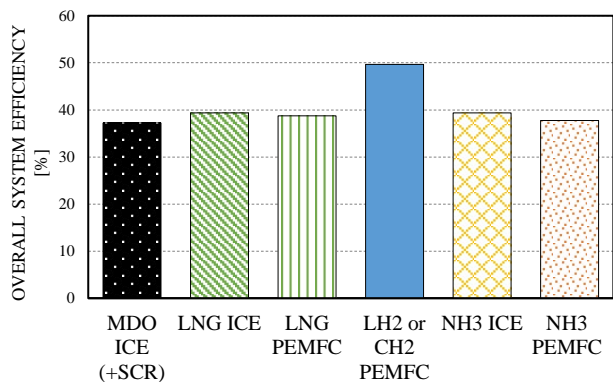


Fig. 1. Comparison of overall conversion efficiencies of different generation systems.

(reformer for LNG or cracker for ammonia) are responsible for significant decrease in overall efficiency. Local pollutant and greenhouse gases emissions are zero for fuel cells systems fed by hydrogen and ammonia, and therefore are not reported in Fig. 2. If PEMFC are fed by LNG there are carbon dioxide (CO_2) emissions due to the reforming process. ICE fuelled by ammonia-hydrogen mixture and LNG presents lower CO_2 , sulphur oxides (SO_x) and particulate matter (PM) emissions than the MDO case, however an emission abatement system (for example SCR) should be applied to decrease nitrogen oxide emissions (NO_x).

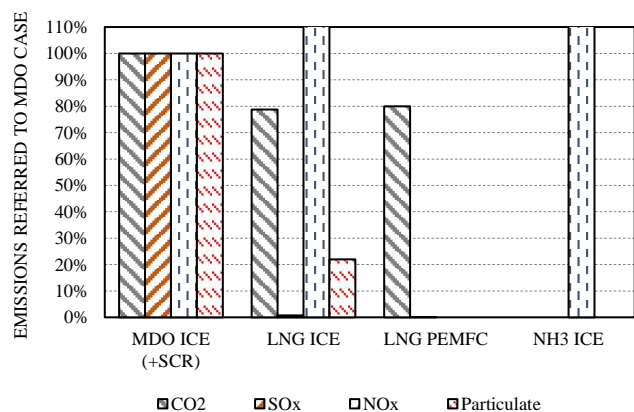


Fig. 2. Comparison of pollutant emissions and carbon dioxide emissions from different generation systems, with reference to emission factors in [5] [10].

Fig. 3 shows alternative fuels volume requirements with reference to MDO case. Compressed hydrogen storage is the most critical, requiring approximately 14 times the space needed by MDO.

IV. CONCLUSIONS

The use of fuel cells based generation systems on ferries has the potential to reduce emissions and to improve the average system efficiency, especially for ships where engines often operate in

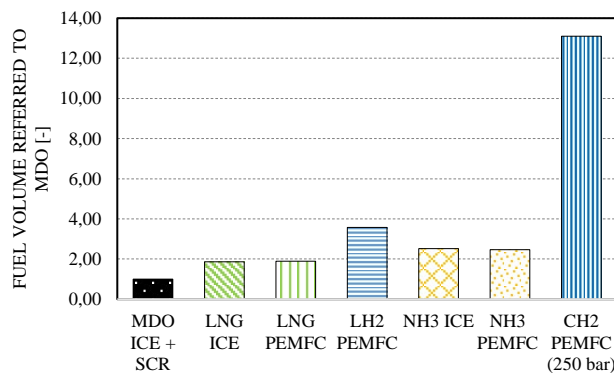


Fig. 3. Volume required by the fuel for different generation systems under consideration.

transient conditions and at part loads. A downside of alternative fuels is the fuel volume, especially for hydrogen. However, this aspect needs further investigations to determine the effective useful cargo volume reduction by taking into account the overall power generation system volume. Ammonia could represent an interesting solution, even though the low technology maturity and the ammonia toxicity limit its implementation in the near future.

The research will continue taking into account different alternative fuels and hydrogen carriers, such as Liquid Organic Hydrogen Carriers (LOHC) and Methanol. Other aspects, like safety, thermal optimization and optimization of fuel volume as function of the specific ferry route are also essential to complete the present study.

REFERENCES

- [1] Prevention of Air Pollution from Ships, IMO website, <http://www.imo.org/en/OurWork/environment/pollution-prevention/airpollution/pages/air-pollution.aspx>, (accessed on October 2019).
- [2] F. Burel, R. Taccani, N. Zuliani, Improving sustainability of maritime transport through utilization of liquefied natural gas (LNG) for propulsion, *Energy* 57 (2013) 412-420.
- [3] Van Biert, L., Godjevac, M., Visser, K., & Aravind, P. V. A review of fuel cell systems for maritime applications. *Journal of Power Sources*, 327 (2016), 345-364.
- [4] https://www.cat.com/en_US/products/new/power-systems/marine-power-systems.html, (accessed on October 2019).
- [5] S. Frigo, R. Gentili, Analysis of the behavior of a 4-stroke Si engine fuelled with ammonia and hydrogen, *International Journal of Hydrogen Energy* 38 (2013) 1607-1615.
- [6] <https://www.hydrogenics.com/>, (accessed on October 2019).
- [7] <https://www.wartsila.com/marine/build/engines-and-generating-sets/dual-fuel-engines>, (accessed on October 2019).
- [8] WSFloX Reformer, "Compact C1, technical datasheet", WS Reformer GmbH, Dornierstraße 14, D-71272 Renningen, Germany (2008).
- [9] S. Giddey, S.P.S. Badwal, C. Munnings, M. Dolan, Ammonia as a renewable energy transportation media, *ACS Sustainable Chemistry & Engineering* (2017) 5(11), 10231-10239.
- [10] Third IMO GHG study 2014 – Executive summary and final report, *International Maritime Organization* (2015).

DESIGN AND IMPLEMENTATION OF A NEW CONCEPT OF PHOTOELECTROCHEMICAL CELL FOR SOLAR WATER SPLITTING

G. Giacoppo*, O. Barbera*, S. Trocino*, C. Lo Vecchio*, E. Baglio*, M. I. Diaz**, R. Gomez** and A. S. Aricò*

*National Research Council, Advanced Energy Technology Institute, CNR-ITAE, Salita S. Lucia sopra Contesse 5, 98126 Messina, Italy

**Departament de Química Física i Institut Universitari d'Electroquímica, Universitat d'Alacant, Apartat 99, E-03080 Alicante, Spain

Abstract – Photo electrochemical water splitting from sun is a potential solution to the growing energy crisis because this method can directly convert solar energy into chemical energy. Although this technology is attractive, up to now it presents a series of scientific challenges. In this work a new design of photoelectrochemical zero gap tandem cell is proposed. The designed cell is based on cheap photoactive materials at both anode and cathode and follows the idea to simplify as much as possible the fluid paths as well as the separation of gaseous hydrogen from water. This work will cover the concept phase, the fabrication of components manufacturing the assembly phase and the test phase. First results are encouraging enough to implement this concept at a panel level even though some issue need to be addressed.

Index Terms – Photo-electrochemical water splitting, PEC cell design.

I. INTRODUCTION

Rational use of renewable energy sources can play an important role in the reduction of CO₂ emissions and particularly, solar energy can cover a substantial share of our energy need. Therefore, intermittency of sunlight must be alleviated through energy dense storage [1]. Hydrogen from solar sun is an option. The most common way to produce hydrogen from sun is through an electrolyzer (EZ) powered by Photovoltaics (PV). Photo-Electro-Chemical (PEC) cells represent an alternative to PV-EZ combination by integrating photo-absorption and photocatalysis in a single device. Merits and disadvantages of both technologies have been widely discussed in the literature. [2-4].

A PEC cell is a device that achieves water splitting and production of a solar commodity or fuel, e.g. hydrogen, with sunlight as the only energy source. The electrode assembly is the heart of the PEC cell. It consists of photoactive materials such as semiconductors or photosensitizers that absorb light and produce charge carriers. These are separated and consumed in redox reactions at the surface of the photocatalyst or the (electro)catalysts attached to the photoactive material. Several concept of PEC cells have been demonstrated [5, 6] and they can be categorized as: i) single compartment, ii) dual

compartment, iii) wired cells, iv) wireless cells. The present work presents results of an innovative PEC cell design based on a solid alkaline membrane and quasi zero liquid electrolyte zero-gap concept. Considering the research activity was carried out in the framework of the European project FotoH2

II. THE ZERO GAP PEC CONCEPT

As depicted in Fig. 1 the zero gap PEC concept, consists of a tandem photo-electrolysis cell architecture having an anion conducting membrane separating the photoanode and photocathode and enabling the use of low-cost metal-oxide electrodes such as Fe₂O₃ and CuO, and Ni/Fe based co-catalysts. The cell is composed by a photoanode deposited on a Fluorine Tin Oxide Glass (FTO) where the photoanode is deposited, an alkaline membrane is used as ionic conductor media and a photocathode deposited on a porous backing.



Fig. 1. Picture of the FotoH2 concept cell.

A. From materials test cell to 25cm² scaled-up cell

A deep material screening has been carried out to find out the most promising formulation of both photoanode and photocathode. A 0.25cm² was developed to demonstrate the zero-gap concept and provide the test cell for the photoelectrodes material screening. The cell is composed of a FTO coated with Fe₂O₃ photoanode, a solid membrane (Fumatech FAA3-50) and a Gas Diffusion Layer (GDL Sigracet 35BC) coated with CuO photocathode. Before the cell assembly, the alkaline membrane was immersed in a 1M KOH solution to fully hydrate the membrane and improve the ionic transport properties at the photoelectrode interfaces. By stacking the components, the cell was clamped by two paperclips and tested under simulated condition of 1.5AM sun

HYDROGEN REFUELING STATIONS BASED ON DIFFERENT RENEWABLE TECHNOLOGIES: ENERGY AND ECONOMIC ASSESSMENTS

A. Perna*, M. Minutillo**, V. Cigolotti***, E.Jannelli**, S. Di Micco**, A. Forcina**

*University of Cassino and Southern Lazio, Via G. Di Biasio 43, (Cassino, Italy)

**University of Naples "Parthenope", Centro Direzionale, Is C4, (Naples, Italy)

***E.N.E.A. – Portici Research Center (Portici, Italy)

Abstract - In this paper two hydrogen production systems for the development of small size refueling stations are studied. The hydrogen is produced by renewable energy and the systems are sized for self-sustaining the electric power requirements. In the first one the hydrogen is produced by the steam reforming of biogas generated in an anaerobic digester and the electric power for the plant operation is supplied by a PEMFC power module. In the second one, the hydrogen production is performed by using an electrolyzer and the electric power for its operation and for all plant auxiliaries is generated by a PV power plant. The systems performances have been compared from energy and economic points of view. The hydrogen production efficiency and the levelized cost of the hydrogen (LCOH) have been considered as comparison parameters.

Index Terms – Refueling, Hydrogen, biogas, solar, LCOH

INTRODUCTION

Hydrogen produced from renewable energy could play a key role in automotive sector as alternative fuel to gasoline and diesel. In this paper two hydrogen production systems based on renewable sources for the development of small size refueling stations (the annual hydrogen production is 33.3 tons, 1.1GWh) are studied. The systems performances have been compared from energy and economic points of view. The hydrogen production efficiency and the levelized cost of the hydrogen (LCOH) have been considered as comparison parameters.

BIOGAS TO HYDROGEN REFUELING STATION

Figure 1 shows the layout of the biogas to hydrogen (B2H) refueling station. In the B2H plant the hydrogen is generated by means of a biogas steam reforming unit and purified by using a membrane separation unit. The electric power for the plant operation and for the hydrogen compression unit is provided by a PEMFC power module. The biogas (60% CH₄, 40% CO₂; 49.4 kg/h) produced from an anaerobic digester is compressed up to the operating pressure (8 bar) of the fuel processing unit

(Steam Reformer and Shifter) and of the membrane separation unit; then it is mixed with steam (S/C molar ratio 1.7) and sent to the steam reforming reactor (750°C). In order to increase the H₂ content prior to enter the Pd-Ag membrane, the reformat is sent to the Shifter (400°C). The pure hydrogen from the multi-tubes membrane separation unit (7 module with 16 tubes/module, the hydrogen recovery factor is 0.8 and the calculated area is 4.4 m²) is cooled down to 65°C (heat Q1=8 kW eventually available for cogeneration purpose) and it is then split into two streams feeding the H₂ compression unit (an ionic compressor consisting of five stage with a pressure ratio of 2.7 [1]) and the PEMFC power module, respectively.

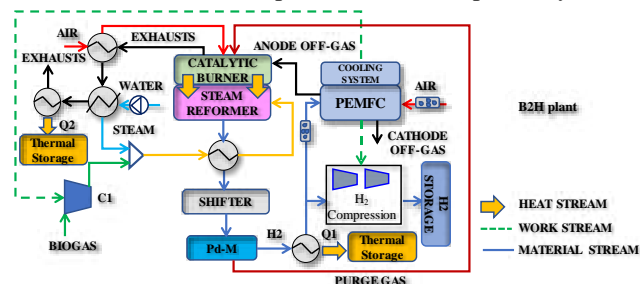


FIG. 1 – B2H plant lay-out

The PEMFC power unit (4 module with 4 stacks for each, 50 cells/stack, 0.682V@40A, fuel utilization factor 0.88) is sized for satisfying the electric demand of the plant (Biogas and H₂ compression and auxiliaries). The thermal demand for the steam reforming process and the steam production is supplied from a catalytic burner fed by the retentate gas (purge gas) and the anode off-gas. The heat recovery from the exhaust is completed by heating (up to 350°C) the combustion air and by making available heat for cogeneration (Q₂=7 kW). Table 1 reports the main data and performance of the B2H plant (the operating time is 8000 hours per year).

TABLE 1. B2H plant performance and data

Annual Biogas chemical energy (MWh _{LHV})	2043
Annual Biogas Compressor consumption (MWh)	34
Annual PEMFC energy production DC/AC (MWh)	174/167
Annual H2 Compression unit consumption (MWh)	120
Annual auxiliaries consumption, 8% of DC PEMFC power (MWh)	14
H2 chemical power (MWh _{LHV})	1117
H2 efficiency (LHV)	0,55

POWER TO HYDROGEN REFUELING STATION

Figure 2 shows the layout of the power to hydrogen (P2H) refueling station. In the P2H plant the hydrogen production is performed by means of an alkaline electrolysis (AEL) unit where the required electric power is supplied from a PV power unit.



FIG. 2 –P2H plant lay-out

The PV unit consists of mono-crystalline PV modules (Model 1Soletech 1STH-240-WH, Anodized Aluminum Alloy), with a fixed both azimuthal angle and tilt angle (157.5°, 33°). The PV unit is sized (2 MW_p) by taking into account that it has to supply electricity for the AEL unit (its efficiency is assumed constant in all operating conditions and equal to an average value of 60%), the hydrogen compression unit and the plant auxiliaries. The size of the AEL (1.27 MW) has been chosen according to the maximum electricity produced by the PV plant. Table 2 reports the main data and performance of the P2H plant (the operating time is 2190 hours per year).

TABLE 2. P2H plant performance and data

Annual PV electric power production (AC) (MWh)	2340*
Annual AEL electric power consumption (MWh)	1850
Annual H2 Compression unit and auxiliaries consumption (MWh)	490
H2 efficiency (LHV)	0,47

* Inverter efficiency 0.92

EVALUATION OF THE LCOH INDEX

The levelized cost of hydrogen (LCOH) is:

$$LCOH = \frac{Total\ Costs}{H_2\ Annual\ Production} = \frac{C_{inv,a} + C_{rep,a} + C_{O\&M}}{M_{H_2}} \quad (1)$$

The annual capital repayment ($C_{inv,a}$), calculated by considering the total plant capital investment costs (C_{inv}), the plant economic lifetime (n) and the nominal discount rate (i), is:

$$C_{inv,a} = \frac{i \cdot (1 + i)^n}{(1 + i)^n - 1} \cdot C_{inv} \quad (2)$$

The annualized replacement cost ($C_{rep,a}$) is defined as:

$$C_{rep,a} = \frac{i \cdot (1 + i)^n}{(1 + i)^n - 1} \cdot \frac{C_{rep}}{(1 + i)^t} \quad (3)$$

where C_{rep} is the replacement cost, t is the year of replacement. For the B2H plant the replacement costs regard the PEMFC stacks, (stack lifetime is 40000 h, corresponding to 5 years) and the reactors catalysts (the lifetime is 5 years), which correspond to 31.3 and 27 k€, respectively [1,2]. For the P2H plant, the AEL stacks lifetime is assumed equal to 60,000 hours [3] like for continuous operation. At 25% of plant utilization, 60,000

hours correspond to 27.4 years of the plant operational time, so that the stack replacement is not needed. The O&M (OPEX) costs are calculated as percentage of the capital investment cost of each component. Tables 3 and 4 summarize the capital investment costs (CAPEX) and the OPEX for the B2H and P2H plants.

TABLE 3. CAPEX and OPEX for B2H plant.

	CAPEX k€	OPEX (% of CAPEX) k€
BIOGAS PROCESSING UNIT	150.0 [1]	4.5 (3%)
PEMFC POWER UNIT	197.8*[4]	9.89 (5% [4])
HYDROGEN SEPARATION UNIT	34.8 [1]	0.93 (2.67%[5]**)
HYDROGEN COMPRESSION UNIT	1200.0 [1]	24 (2%)
AUXILIARIES (Heat Exchangers, piping, etc.)	248.0 [1]	7.4 (3%)

* It is calculated by considering the PEMFC stack specific cost equal to 8248 €/kW [4].

** In [5] this value was 2.5% because it was referred to 7500h.

TABLE 4. CAPEX and OPEX for P2H plant

	CAPEX k€	OPEX (% of CAPEX) k€
PV POWER UNIT	1900.0*	30.0 (1.58 % [6])
ALKALINE ELECTROLYSYS UNIT	1404.6**	70.2 (5% [3])
HYDROGEN COMPRESSION UNIT	1200.0	24 (2%)

*It is calculated by considering the PV power unit specific cost equal to 950.0 €/kW [2].

**It is calculated by considering the AEL unit specific cost equal to 1100.0 €/kW [3].

The LCOH calculated for B2H and P2H, is reported in Table 5.

TABLE 5. LCOH for B2H and P2H plant

	B2H	P2H
Economic Lifetime (years), n	20	20
Nominal Discount Rate (%), i	6.4%	6.4%
Annual Capital Repayment ($C_{inv,a}$) (k€)	164.82	405.6
Annualized replacement cost ($C_{rep,a}$) (k€)	8.7	-
Annual O&M costs ($C_{O\&M}$) (k€)	46.8	124.2
Annual H ₂ Production (tons)	33.33	33.33
LCOH (€/kg)/(€/kWh)	6.6/0.21	15.9/0.48

CONCLUSION

The aim of this work was to compare two hydrogen production and distribution plants from an energy and economic point of view. The analysis has highlighted that the performances of the B2H plant are better than those of the P2H plant: the H2 efficiency is 0.55 vs. 0.47 and the LCOH is lower of 58% (6.6 €/kg vs. 15.9 €/kg).

REFERENCES

- [1] Minutillo M, Perna A, Sorce A. Combined hydrogen, heat and electricity generation via biogas reforming: Energy and economic assessments. International Journal of Hydrogen Energy 2019;44(43), 23880-98.
- [2] Staffell I, Green R. The cost of domestic fuel cell micro-CHP systems. International Journal of hydrogen energy, 2013; 38(2): 1088-102.
- [3] Schmidt O, Gambhir A. Future cost and performance of water electrolysis: An expert elicitation study, International Journal of Hydrogen Energy, 2017;42(52):30470-92.
- [4] R. Napoli, M.Gandiglio, A.Lanzini, M.Santarelli, Techno-economic analysis of PEMFC and SOFC micro-CHP fuel cell systems for the residential sector,Energy and Buildings,2015;103:131-46.
- [5] Di Marcobernardino G.,Knijff J, Techno-Economic Assessment in a Fluidized Bed Membrane Reactor for Small-Scale H2 Production: Effect of Membrane Thickness, Membranes. 2019; 9(9):116.
- [6] K. Wang, M. Herrando, Techno-economic assessments of hybrid photovoltaic-thermal vs. conventional solar-energy systems: Case studies in heat and power provision to sports centres, Applied Energy. 2019;254:113657.

VIABILITY ANALYSIS OF TRAINS HYDROGEN REFUELING STATIONS USING ELECTROLYZERS

C. Fúnez Guerra^a, L. Reyes-Bozo^b, E. Vyhmeister^c.

^a National Hydrogen Centre (CNH2), Prolongación Fernando el Santo s/n, 13500 Puertollano (Ciudad Real), Spain.

^b Facultad de Ingeniería, Universidad Autónoma de Chile, Av. Pedro de Valdivia 425, Santiago, Chile.

^c Insight Research Centre for Data Analytics, University College Cork, Cork, Ireland.

Abstract - Hydrogen has the potential to be a powerful enabler for this application because it offers a clean, sustainable, and flexible option.

Hydrogen trains, using compressed hydrogen as fuel to generate electricity using hybrid system (fuel cell and batteries) to power traction motors and auxiliaries. This hydrogen train are fueled with hydrogen at the central train depot, like diesel locomotives.

The main goal to this paper is to develop technical-economic analysis for 20 hydrogen trains captive fleet and a hydrogen refueling stations using on-site production from PEM electrolyser technology and to carry out a sensitivity analysis of the main parameters that we need know in order to take the decision to implement this solution like electricity cost, hydrogen price, number of operation hours and trains captive fleet size.

The use of hydrogen as an alternative fuel in trains is a good solution from an economic, environmental and security of supply point of view.

It is necessary to have an electricity price lower than 50 €/MWh, hydrogen sales price more than 4.5 €/kg, facility operation hours more than 4,700 hours, a trains captive fleet more than 8 trains in order to obtain a positive Net Present Value. Also, the heat utilization, oxygen by-product, CO₂ emission reduction, can allow obtain a higher Net Present Value.

Index Terms – Hydrogen refueling station, hydrogen trains, PEM electrolyser, technical and economical viability.

I. INTRODUCTION

The need for an energy transition is widely understood and shared.

Unlike other forms of transportation, the railroad industry is already fairly familiar with electric power. But the infrastructure demands of electric trains are considerable, limiting where it is practical to deploy them.

Hydrogen has the potential to be a powerful enabler for this application because it offers a clean, sustainable, and flexible option.

Hydrogen trains, using compressed hydrogen as fuel to generate electricity using hybrid system (fuel cell and batteries) to power traction motors and auxiliaries. This hydrogen train are fueled with hydrogen at the central train depot, like diesel locomotives.

II. MOTIVATION

Zero tailpipe emissions of pollutants (esp. NO_x) and greenhouse gases (esp. CO₂).

Lower noise pollution (depending on speed and track conditions reduction of overall noise emissions).

Increased passenger comfort through reduced noise and vibration, fewer adverse impact on neighbouring communities.

Public health benefits (esp. urban areas near tracks/station), reduced social security expenses, higher standard of living.

Avoiding cost of future electrification of several million € investment per km (i.e. power generation, transformers and transmission lines as well as service disruption caused by overhead wire installation).

Flexibility to move into service areas not covered by electrification (for industry-stakeholders involved).

III. OBJECTIVES AND TECHNICAL PROPOSAL.

The main objective to this study is to develop technical-economic analysis for 20 hydrogen trains captive fleet and a hydrogen refuelling stations using on-site production from PEM electrolyser technology.



Figure 1. Trains Hydrogen Refueling Station.

Another goal is to carry out a sensitivity analysis of the main parameters that we need know in order to take the decision to implement this solution:

- Electricity cost.
- Hydrogen price.
- Number of operation hours.
- Trains captive fleet size.

IV. TECHNICAL AND ECONOMICAL VIABILITY.

The main considerations for the technical and economical viability are the following:

- Operation rate: 7,200 hours/year.
- Electrolyzer efficiency: 76.5 – 70%. Stack degradation $2\mu V/hour$.
- Stack replacement: 10% stack degradation.
- No oxygen and heat valorization.
- 30% of capital own resources. 70% of capital French loan. 10 years.
- CAPEX and OPEX:
Electrolyzer: 800 €/kW and 1,5% investment cost each year. Stack replacement: 30% CAPEX.
Compressor: 863 €/Nm³ and 7% investment cost each year.
LP Hydrogen Storage: 280 €/kg H₂ and 1% investment cost each year.
HP Hydrogen Storage: 850 €/kg H₂ and 1% investment cost each year.
Dispensers: 4 units at 150,000 €/unit and 3% investment cost each year.
Other facilities cost: 20% main equipment's.
Total hydrogen facility investment: 17.965.714 €
- Electricity cost: 40 €/MWh.
- Water cost: 2.5 €/m³.
- Personal cost: 250,000 €/year.
- Site rental cost: 200,000 €/year.
- Sales Hydrogen price: 5.3 €/kg.
- WACC: 8%.
- Inflation rate: 1.5%.
- Study period: 25 years.

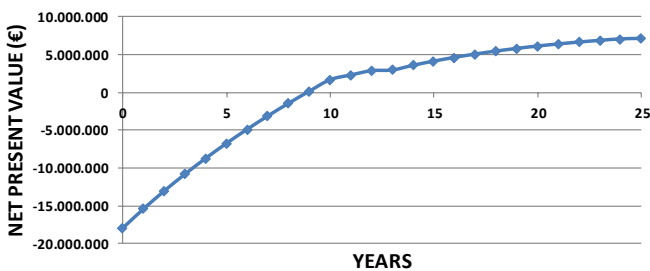


Figure 2. Net Present Value VS Years.

The main results regarding technical and economical viability are the following:

- NPV: 7,115,391 €

- Pay-Back: 9.90 years.
- Internal Rate Return: 15%.

V. SENSITIVITY ANALYSIS.

It is needed make some sensitivity analysis of the main parameters that we need know in order to take the decision to implement this hydrogen refuelling station. The main parameters are electricity cost, hydrogen price, number of operation hours and trains captive fleet size.

The main results for all the sensitivity analysis are the following:

- It is necessary to have an electricity price lower than 50 €/MWh in order to obtain a positive Net Present Value.
- It is necessary to have hydrogen sales price more than 4.5 €/kg in order to obtain a positive Net Present Value.
- It is necessary to have facility operation hours more than 4,700 hours in order to obtain a positive Net Present Value.
- It is necessary to have a trains captive fleet more than 8 trains in order to obtain a positive Net Present Value.
- Heat utilization, oxygen by-product, CO₂ emission reduction, can allow obtain a higher Net Present Value.

VI. CONCLUSIONS.

The use of hydrogen as an alternative fuel in trains is a good solution from an economic, environmental and security of supply point of view.

It is necessary to have an electricity price lower than 50 €/MWh, hydrogen sales price more than 4.5 €/kg, facility operation hours more than 4,700 hours, a trains captive fleet more than 8 trains in order to obtain a positive Net Present Value. Also, the heat utilization, oxygen by-product, CO₂ emission reduction, can allow obtain a higher Net Present Value.

REFERENCES

- [1] Karasawa H. Cost Evaluation for centralized hydrogen production. *Prog Nucl Energy* 2005;47:512e8.
- [2] Barbir F. PEM electrolysis for production of hydrogen from renewable energy sources. *Sol Energy* 2005;78:661e9.
- [3] Bhandari R, Trudewind CA, Zapp P. Life cycle assessment of hydrogen production via electrolysis e a review. *J Clean Prod* 2014;85:151e63.
- [4] Holladay JD, Hu J, King DL, Wang Y. An overview of hydrogen production technologies. *Catal Today* 2009;139:244e60.
- [5] Agll AAA, Hamad TA, Hamad YM, Bapat SG, Sheffield JW. Development of design a drop-in hydrogen fueling station to support the early market buildout of hydrogen infrastructure. *Int J Hydrogen Energy* 2016;41:5284e95.
- [6] Remer DS, Nieto AP. A compendium and comparison of 25 project evaluation techniques. Part 1: net present value and rate of return methods. *Int J Prod Econ* 1995;42:79e96.
- [7] Bartoov V, Majerk P, Hrakov D. Taking risk into account in the evaluation of economic efficiency of investment projects: traditional methods. *Proc Econ Finance* 2015;24:68e75.

VIABILITY ANALYSIS OF GREEN METHANOL PRODUCTION PLANT IN CHILE AND SUBSEQUENTLY TRANSPORT TO JAPAN.

C. Fúnez Guerra^a, G. Alcalde Ranz^a, L. Reyes-Bozo^b and E. Vyhmeister^c.

^a National Hydrogen Centre (CNH2), Prolongación Fernando el Santo s/n, 13500 Puertollano (Ciudad Real), Spain.

^b Facultad de Ingeniería, Universidad Autónoma de Chile, Av. Pedro de Valdivia 425, Santiago, Chile.

^c Insight Research Centre for Data Analytics, University College Cork, Cork, Ireland.

Abstract - As one of the world's most flexible compounds, methanol is the basis of hundreds of chemicals and thousands of products that touch our daily lives. It is also the second product in the world in amount shipped and transported around the globe.

Most methanol is produced from natural gas and coal, but renewable or green methanol does exist in form of biogas or biomass gasification. Through a power to gas process based on renewable hydrogen and carbon dioxide synthesis, it is possible to balance the energy mix and fix carbon emissions from industrial production.

The main objective is to develop technical-economic analysis for methanol production using renewable hydrogen by electrolysis (using solar, wind and hydraulic renewable energy).

The green methanol will be produced in Chile and will be transported to Japan using a chemical ship and to carry out a sensitivity analysis of the main parameters that we need know in order to take the decision to implement this solution like electricity cost, methanol price, number of operation hours and facility size.

Hydrogen production in Chile and transportation up to Japan using methanol as an energy carrier is a profitable solution.

It is necessary to have an electricity price lower than 35 €/MWh, a methanol sales price more than 380 €/t, more than 5.200 operation hours per year, a green methanol facility bigger than more than 85 MW of electrolyser power in order to obtain a positive Net Present Value.

Index Terms – methanol production facility, Fischer-Tropsch, PEM electrolyser, technical and economical viability.

I. NOMENCLATURE

CAPEX: Capital Expenditure.

OPEX: Operational Expenditure.

CCS: Carbon Capture and Storage.

WACC: Weighted Average Cost of Capital.

NPV: Net Present Value.

II. INTRODUCTION

As one of the world's most flexible compounds, methanol is the basis of hundreds of chemicals and thousands of products that touch

our daily lives. It is also the second product in the world in amount shipped and transported around the globe every year.

Methanol is a truly global commodity and a key component of modern life and it is constantly being applied in new and innovative ways. Additionally, methanol is an excellent energy carrier and is much easier to storage than hydrogen and much cleaner than fossil fuels. Being a liquid fuel, it is much easier to handle and store than hydrogen and can be handled by the existing distribution system.

Methanol is readily available and is used in major quantities around the world as a mass-produced commodity. In cost-per-unit-of-energy terms, methanol compares favourably with gasoline and diesel.

Besides being favourable in terms of cost-per-unit-of-energy and being a mass-produced commodity, methanol is safer than gasoline, being less prone to ignite and burns clearer than gasoline.

The methanol industry spans the entire globe, with production in Asia, North and South America, Europe, Africa and the Middle East. On a global scale, over 100 methanol plants have a combined production capacity of about 100 million metric tons (125 billion litres).

Every day more than 180.000 tons of methanol is used as a chemical feedstock or as a transportation fuel (225 million litres). The methanol industry creates over 100.000 jobs around the globe.

Most methanol is produced from natural gas and coal, but renewable methanol (green methanol) does exist in form of biogas or biomass gasification. Through a power to gas process based on renewable hydrogen and carbon dioxide synthesis, it is possible to balance the energy mix and fix carbon emissions from related industrial production.

III. OBJECTIVES AND TECHNICAL PROPOSAL.

The main objective is to develop technical-economic analysis for methanol production using renewable hydrogen by electrolysis (using solar, wind and hydraulic renewable energy).

The green methanol will be produced in Chile and will be transported to Japan using a chemical ship.

Another goal is to carry out a sensitivity analysis of the main parameters:

- Electricity cost.

- Methanol sales price.
- Operation hours.
- Facility size.



Figure 1. Technical proposal.

IV. TECHNICAL AND ECONOMICAL VIABILITY.

The main considerations for the technical and economical viability are the following:

- Operation rate: 8,000 hours/year.
- Electrolyzer efficiency: 76.5 – 70%.
- Stack degradation $2\mu V/hour$.
- Stack replacement: 10% stack degradation.
- Not considering heat valorisation. It is considering CO_2 saved and O_2 valorisation.
- 30% capital of own resources. 70% capital by a French loan. 10 years.
- CAPEX and OPEX:
 - Electrolyzer system: 450 €/kW and 1.5% investment cost each year. Stack replacement: 30% CAPEX.
 - Fischer-Tropsch and methanol storage: 600 €/kW and 5% investment cost each year.
 - Other costs. 10% main equipment.
 - Total methanol production plant investment: 173.250.000 €
- Electricity cost: 28 €/MWh.
- Water cost: 2.5 €/m³.
- CCS cost: 50 €/t.
- Personnel cost: 800 k€/year.
- Site rental cost: 200 k€/year.
- Methanol sales price: 460 €/t.
- Methanol transportation price: 50 €/t.
- Oxygen sales price: 0.2 €/Nm³.
- CO_2 avoided income: 30 €/t.
- WACC: 8%. Inflation rate: 1.5%.
- Study period: 25 years.

The main results regarding technical and economical viability are the following:

- CH_3OH production: 109,000 t/y.
- CO_2 emissions avoided: 149,100 t/y.
- NPV: 77,727,302 €
- Pay-Back: 8.68 years.
- Internal Rate of Return: 15%.

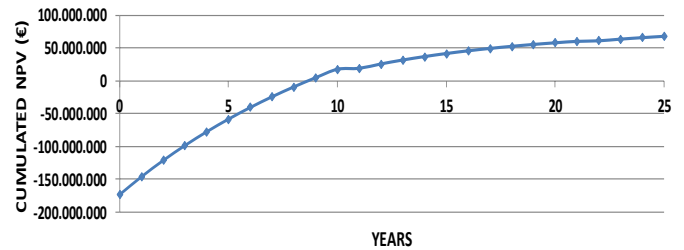


Figure 2. Net Present Value (NPV) VS Years.

V. SENSITIVITY ANALYSIS.

It is needed make some sensitivity analysis of the main parameters that we need know in order to take the decision to implement this methanol production facility. The main parameters are electricity cost, methanol sales price, operation hours and facility size.

The main results for all the sensitivity analysis are the following:

- Electricity prices over 35 €/MWh are required in order to obtain positive NPV.
- Methanol prices over 380 €/t are required in order to obtain positive NPV.
- Operation hours over 5.200 hours per year are required in order to obtain positive NPV.
- Green methanol facility size over 85 MW are required in order to obtain positive NPV.
- Heat utilization can allow green methanol price to be cheaper.

VI. CONCLUSIONS.

Hydrogen production in Chile and transportation up to Japan using methanol as an energy carrier is a profitable solution.

It is necessary to have an electricity price lower than 35 €/MWh, a methanol sales price more than 380 €/t, more than 5.200 operation hours per year, a green methanol facility bigger than more than 85 MW of electrolyser power in order to obtain a positive NPV.

Also, heat utilization can allow green methanol price to be cheaper.

REFERENCES

- [1] Bhandari R, Trudewind CA, Zapp P. Life cycle assessment of hydrogen production via electrolysis e a review. *J Clean Prod* 2014;85:151e63.
- [2] Holladay JD, Hu J, King DL, Wang Y. An overview of hydrogen production technologies. *Catal Today* 2009;139:244e60.
- [3] Remer DS, Nieto AP. A compendium and comparison of 25 project evaluation techniques. Part 1: net present value and rate of return methods. *Int J Prod Econ* 1995;42:79e96.
- [4] Bartoov V, Majerk P, Hrakov D. Taking risk into account in the evaluation of economic efficiency of investment projects: traditional methods. *Proc Econ Finance* 2015;24:68e75.

LCA ANALYSIS OF A SOFC-BASED COGENERATION SYSTEM WITH THERMAL ENERGY STORAGE

G. Di Florio[†], M. Testi[§], E. Macchi[§], N. Destro[§], L. Crema[§], M. Caliano[#], V. Cigolotti[#], L. Mongibello[#],
R. Basosi[†], M. C. Baratto[†], E. Busi[†]

[†] *Dipartimento di Biotecnologie, Chimica e Farmacia, Dipartimento di Eccellenza, Università degli Studi di Siena, via Aldo Moro 2, 53100 Siena, Italy*

[§] *Fondazione Bruno Kessler, Unit ARES, Via Sommarive 18, 38123 Trento (TN) Italy*

[#] *ENEA – Italian National Agency for New Technologies, Energy and Sustainable Economic Development – Portici Research Center, P.le E. Fermi 1, 80055 Portici (NA), Italy*

Abstract - An environmental analysis on a SOFC-based cogeneration system integrated with a hot water storage tank was carried out. The methodology applied was Life Cycle Assessment, which allows to quantify ecological indicators of a process or product. The advantages of implementing a reversible fuel cell have been highlighted and the comparison among different thermal storage systems addressed. Results point out the significant reduction in fossil fuel consumption, as consequence of optimization of the system. Furthermore, the analysis shows that a wise choice of the materials could affect the total impact of the cogeneration system.

Index Terms – Cogeneration, Life Cycle Assessment, Reversible Solid Oxide Fuel Cell, Thermal Energy Storage

I. INTRODUCTION

Solid Oxide Fuel Cell (SOFC) systems represent an innovative technology, that could substitute conventional power generation systems and reduce their environmental impact. Advantages of this class of fuel cells include high combined heat and power efficiency, long-term stability, fuel flexibility and zero or low emissions. Fuel cells generate electricity and heat; such heat can be supplied to a thermal storage system for sanitary domestic hot water.

In this study, environmental analysis is applied to a cogeneration system based on a reversible SOFC (rSOFC) that produces and consumes hydrogen, provided with a thermal energy storage system, in order to quantify its environmental advantages and identify any eventual critical issue.

II. METHODS

The environmental analysis is performed via Life Cycle

Assessment (LCA) of the system. LCA model and calculations are carried out with SimaPro® v.9, using the commercial database Ecoinvent® v.3.5 [1].

The environmental characterization of the analysed systems was performed with the following Life Cycle Impact Assessment (LCIA) methods: CED (Cumulative Energy Demand) and ReCiPe. Specifically, ReCiPe method allows the study at an impact (mid-point) or damage (end-point) category level. The environmental analysis is performed with the ReCiPe 2016 Midpoint level approach, associated with a hierarchic perspective.

A. Goal & Scope and Functional Unit

The goal & scope of this LCA analysis is to investigate the environmental performance of an innovative cogeneration system, based on a reversible SOFC technology in combination with a domestic hot water thermal energy storage.

The functional unit is the amount of hot water needed in a day for a family of three persons. A cradle-to-gate analysis was performed.

B. System Boundaries

The system boundaries include the cogeneration system (rSOFC stack, blowers, heat exchangers, etc.), the hydrogen storage system, control units and a thermally insulated hot water tank (Fig. 1).

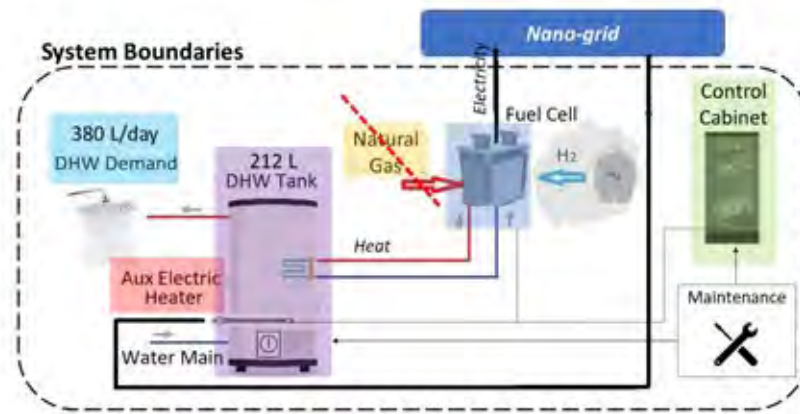


Fig. 1: System Boundaries of SOFC-Cogeneration for thermal storage

C. Life Cycle Inventory (LCI)

Inventory analysis is carried out following attributional modeling approach. The main source of primary data comes from the research project on community energy storage ComESto, focused on the integration of energy storage technologies in a nanogrid. In particular, data on SOFC module and related components are provided by FBK and thermal energy storage data by ENEA. Background data are taken from Ecoinvent® database, version 3.5. Whenever possible, primary data is used for modeling foreground processes; the rest is provided as secondary data [2]. For background processes, secondary data is always used.

D. Results and Discussion

The ecological earnings were evaluated by comparing results of the production and the use phase of the rSOFC-based cogeneration system with different cogeneration systems.

The detailed assessment of each step of the process is analysed by decomposition of the system into all sub-processes to reconstruct the pathway of all impacts related to their primitive flows. In particular, our attention has been focused on 1) the advantages of using a reversible fuel cell and 2) comparing different thermal storage tanks.

In consideration of the functional unit, the use of a reversible SOFC instead of gas boiler or standard SOFC fueled by natural gas, reduces drastically the emissions of CO₂, due to the environmental burden of the natural gas streamline.

The same result is obtained when a Cumulative Energy Demand (CED) analysis is applied.

An important part of the analysis dealt with the choice of the most sustainable system for the storage of hot water for domestic use. A comparison between a storage tank, made out of enameled unalloyed steel, and a stainless steel tank was performed. The analysis evidenced that in production phase the stainless steel has a higher environmental burden. Of course, the

higher performances of stainless steel could increase the lifetime of the storage system and, consequently, reduce its impact along all the life cycle.

Finally, we found out that particular attention has to be devoted to the optimization of all the electronic components. Indeed, the use of metals and precious metals in the circuitry carries a high pollution potential along with their extraction, processing and dismission.

III. CONCLUSION

Life Cycle Assessment demonstrated that the implementation of a reversible SOFC has a beneficial effect in comparison with other cogeneration systems, when the use phase is considered. Regarding the thermal storage, a balance between employed materials and life duration of the systems has to be always determined.

ACKNOWLEDGMENT

The work was supported by the ComESto PON project (Community Energy Storage, aggregated management of energy storage systems in Power Cloud) proj. number ARS01_01259, funded by MIUR and European Union.

MIUR for the “*Dipartimento di Eccellenza 2018-2022*” grant.

REFERENCES

- [1] Moreno Ruiz, E., Valsasina, L., Brunner, F., Symeonidis, A., FitzGerald, D., Treyer, K., Bourgault, G., Wernet, G., Documentation of changes implemented in ecoinvent database v3.5. Ecoinvent, Zürich, Switzerland, 2018.
- [2] Smith, L., et al. Applied Energy 235, 2019, pp. 1300-1313

PERFORMANCE ANALYSIS OF SOFC STACKS UNDER SEVERE OPERATING CONDITIONS

Y. Mugikura^{1*}, A. Ido^{1*}, K. Asano^{1*}, H. Morita^{1*}, and T. Yamamoto^{1*}

^{1*}Central Research Institute of Electric Power Industry, 2-6-1 Nagasaka
Yokosuka-shi Kanagawa-ken Japan 240-0196, (Japan)

Abstract -Central Research Institute of Electric power Industry (CRIEPI) has operated four types of SOFC cell stacks, which are developed by KYOCERA, NGK INSULATORS (NGK), NGK SPARK PLUG (NTK), and DENSO under NEDO's project on high efficiency and toughness of cell stacks from 2018 to 2019. For the estimation of toughness of cell stacks, load variation tests that involve applying periodic current variation for 0.02-20 sec to cell stacks as a severe operating condition have been carried out to evaluate the possibility of SOFC system toward dynamic operation for load variation.

Index Terms - Cell stack, Durability, Load variation test, SOFC

I. INTRODUCTION

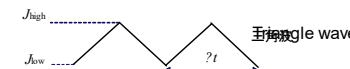
SOFCs are generally operated at the rated power. Recently, demand adjustment in electric power systems when large amounts of variable renewable energy are introduced, is very important. SOFCs should be required for responding to high-speed load variations that can respond to variations within 10 seconds. To investigate the applicability of SOFCs to load variation, severe tests such as high-speed load variations are conducted to verify the effect on cell stack performance.

II. EXPERIMENTAL

To evaluate the high-speed load variation response of SOFC, the fuel flow rate is fixed at the set fuel utilization (U_f) for severe test parameters such as load waveform (triangular wave), variation period (milliseconds to several tens of seconds), U_f . A severe test protocol was established for the load variation of the current control that becomes $\pm 15\%$ of the set U_f as the load variation test (Table 1). Since only the current applied to cell stack is changed, the relationship between the current and the fuel utilization is proportional. Further, when $U_f = 80\%$, it is a severe test in which $U_f = 95\%$ instantaneously. At first, short-term load variation test was performed with the variation period

changed from 0.02 to 20 seconds with the setting $U_f = 80\%$. To evaluate the long term durability, the variation period was set to 10 seconds and the continuous load variation test was conducted for 2,000 hours. In addition, a constant load test of over 5,000 hours was also observed as a comparison. Performance change before and after the load variation tests and constant load tests, was analyzed.

TABLE I. TEST PROTOCOL OF SEVERE OPERATION FOR LOAD VARIATION

Stack	Flattened Tubular (Kyocera)	Segment-in-series flattened tubular (NGK)	Planar (NTK)	Planar (DENSO)
Pressure	0.101MPa			
Temperature	750°C	750°C	700°C	700°C
Fuel Composition Oxidant gas composition	$H_2/CO_2 = 80/20\% + H_2O = 20\%$ Air			
Fuel Utilization U_f Low/High $U_{f, low}/U_{f, high}$	$U_f = 80\% : 65/95\%$			$U_f = 75\% : 60/90\%$
Current density J Low/High J_{low} / J_{high}	0.36 A/cm ² 0.29/0.43 A/cm ²	0.20 A/cm ² 0.16/0.24 A/cm ²	0.52 A/cm ² 0.42/0.62 A/cm ²	0.53 A/cm ² 0.42/0.64 A/cm ²
Interval time Δt	0.02, 0.2, 2, 10, 20sec			0.02, 0.2, 2sec
Wave				

Fuel flow rate to supply a SOFC cell-stack is constant. Current applied on a SOFC cell-stack is changed. Therefore, fuel utilization is changing with applied current.

III. RESULTS AND DISCUSSION

Load variation test was performed under the condition of $U_f = 95\%$ exceeding the operation limit instantaneously from around $U_f = 80\%$ to understand problems for high-speed load responsiveness of SOFCs. The load variation tests with short-term (60 minutes) and long-term (2,000 hours) were performed to understand the response characteristics of the cell stack and the performance degradation factors.

Shapes of power waves were not changed for 60 minutes testing as shown in Fig. 1. Powers by cell stacks followed set power waves. Average powers by cell stacks satisfied within $\pm 15\%$ of set powers.

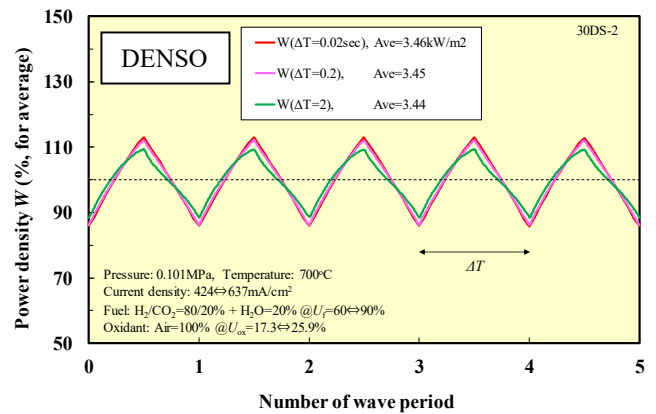
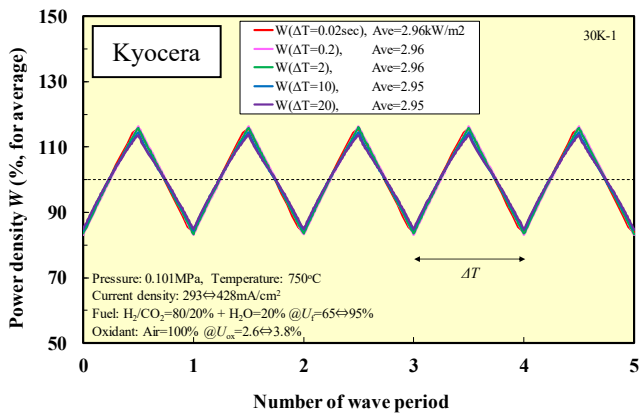
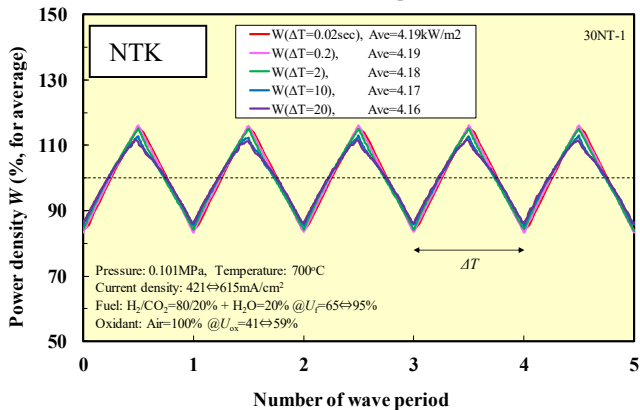
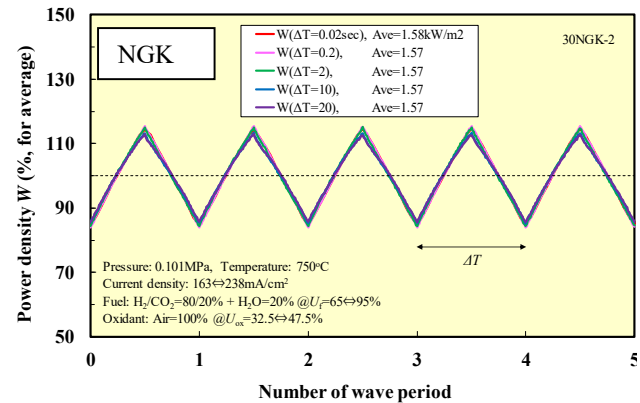


Fig. 1. Characteristics of relative power density with load variation.



Durability of cell stack for load variation test was different among SOFCs (Table II). According to evaluating the performance degradation factor analysis before and after the load variation tests, deterioration of the electrolyte and the cathode, rather than the anode after load variation test, was the main performance degradation factor.

ACKNOWLEDGMENT

This work has been carried out under a contract research with the SOFC developing project of the New Energy and Industrial Technology Development Organization (NEDO), Japan. We would like to express our gratitude to NEDO, Kyocera, NGK, NTK and DENSO, as well as to the National Institute of Advanced Industrial Science and Technology (AIST).

REFERENCES

- [1] T. Yamamoto et al., Proceeding of 13th European SOFC & SOEC Forum 2018, Abstract B1314 (2018).
- [2] Y. Mugikura, Yasumoto, H. Morita, T. Yamamoto, M. Yoshikawa, "Degradation analysis of SOFC Performance (4)", Fuel Cell Seminar & Energy Exposition, (2017)

TABLE II. RESULTS OF SEVERE OPERATION TESTS

Stack(Manufacturer)	Flattened tubular (Kyocera)	Segment-in-series tubular (NGK)	Planar (NTK)	Planar (DENSO)
Periods of load variation test ($U_f=80\%$ base $\pm 15\%$, $\Delta t=10$ seconds)	2,014hrs	1,558hrs	2,016hrs	863hrs *1
Average cell voltage drop rate	-0.28%/1kh	-2.10%/1kh	-0.61%/1kh	-2.49%/1kh
Rate difference by load variation test *2	-0.02%/1kh (-0.26%/1kh)*3	-1.23%/1kh (-0.87%/1kh)*3	-0.16%/1kh (-0.45%/1kh)*3	-1.55%/1kh (-0.94%/1kh)*3
Performance factors related to load variation	No	IR drop, Cathode overvoltage	No	IR drop
Cell type	2018 model	2018 model	2014 model adv.2	2018 model

*1 : In case of planar (DENSO), load variation condition was $U_f=75\%$ base $\pm 15\%$, $\Delta t=2$ seconds.

*2 : Rate difference by load variation test = (average cell voltage drop rate during load variation test) - (average cell voltage drop rate during constant load test)

*3 : In (), it is average cell voltage drop rate during constant load test period as same as load variation test period.

ROBUST VOLTAGE CONTROL FOR DC-DC BOOST CONVERTER IN PROTON EXCHANGE MEMBRANE FUEL CELL POWER SYSTEM

Hai-Bo Yuan*, Young-Bae Kim*

*School of Mechanical Engineering, Chonnam National University,
77 Yongbong-ro, bukgu, Gwangju, Korea

Abstract - In the present paper, a PEMFC-fed DC-DC boost converter power supply control-oriented model based on the equivalent electrical circuit is constructed to investigate the system characteristics, where design, output voltage control and performance analysis of DC-DC boost converter are developed. Continuous conduction mode (CCM) of DC-DC boost converter is concerned, and each component has been designed and selected for circuit assembly. Small-signal AC model based on pulse-width modulated DC-DC boost converter is constructed as well as the analysis of system's nonlinearity. Several control algorithms such as proportional-integral (PI) control, deadbeat control, and active disturbance rejection control (ADRC) are put forward to suppress the disturbances and uncertainties in order to regulate the stable converter output when faced with immeasurable input and load disturbance, mismatched model dynamics, and parameter perturbations. The treatment here emphasizes the objective steering the output voltage to its reference value with fast response, little overshoot and response ripples. The disturbance rejection and tracking performance have been tested and compared, indicating that the proposed control method has the best rejection effect on above-mentioned system disturbances, which improves the boost converter stability. Simulation model in MATLAB/Simulink and LabVIEW-based field programmable gate array (FPGA) experimental rig are constructed for the verification of DC-DC boost converter performance with the developed control theories.

Index Terms - ADRC, DC-DC boost converter, LabVIEW-based FPGA experimental rig, MATLAB/Simulink, PI control, small-signal AC model.

I. INTRODUCTION

With increasing visibility of the environmental pollution, proton exchange membrane fuel cell (PEMFC) using chemical reaction between hydrogen and oxygen to generate electricity efficiently with no combustion and zero emission attracts much consideration in power supply system recently [1]. As one of electrical balance of plants (EBOPs), DC-DC boost converter plays an important part in PEMFC power system to regulate the

output voltage of PEMFC system against the conditions of varied power demands and different kinds of disturbances. Also, it has the ability to distribute the fuel cell and battery powers in the fuel cell-battery hybrid system.

In general, output voltage feedback control is widely used for voltage regulation of DC-DC boost converter. Due to the low cost and easy design, proportional-integral-derivative (PID) controllers is usually the first choice. But for large disturbance and various load conditions, PID controller should be tuned again to guarantee the system stability. To deal with system uncertainties and disturbances, researchers have studied robust control algorithms, such as, sliding mode control (SMC), fuzzy control, time-delay control (TDC), and so on to optimize the control performance. Active disturbance rejection control (ADRC), as a new observer-based control theory is introduced in presented paper to steer the output voltage of the converter.

The paper is comprised of four parts. After introduction part, mathematical model and control theory design is depicted in Section II. In Section III, experimental results and discussion are introduced. Finally, the conclusion of this research is drawn in Section IV.

II. MATHEMATICAL MODEL AND CONTROLLER DESIGN

A. Mathematical Model

In the present paper, continuous conduction mode (CCM) of DC-DC boost converter is concerned for the research, and the small-signal ac DC-DC boost converter model is described as Equation (1). In addition, the desired output power of converter is 120 W with regulated output voltage of 24 V. And a 30 kHz pulse-width modulation (PWM) control signal is generated for the control input of MOSFET switch. The interpretation of each component and their nominal values of a boost converter are listed in Table I.

$$\begin{cases} \begin{bmatrix} \hat{i}_L \\ \hat{v}_C \end{bmatrix} = \begin{bmatrix} -\frac{1}{L}(R_L + \frac{(1-D)RR_C}{R+R_C}) & -\frac{(1-D)R}{L(R+R_C)} \\ \frac{R}{C(R+R_C)} & -\frac{1}{C(R+R_C)} \end{bmatrix} \begin{bmatrix} \hat{i}_L \\ \hat{v}_C \end{bmatrix} + \begin{bmatrix} 1 \\ 0 \end{bmatrix} \hat{v}_{in} + \begin{bmatrix} \frac{1}{L(R+R_C)}(R_C R_L + R V_C) \\ -\frac{R}{C(R+R_C)} V_C \end{bmatrix} \hat{d} \\ \hat{v}_o = (1-D) \frac{RR_C}{R+R_C} \frac{R}{R+R_C} \begin{bmatrix} \hat{i}_L \\ \hat{v}_C \end{bmatrix} - \frac{RR_C}{R+R_C} I_L \hat{d} \end{cases} \quad (1)$$

TABLE I
NOMINAL VALUES AND CIRCUIT PARAMETERS OF BOOST CONVERTER

Parameter	Description	units	value
V_{in}	Normal input voltage	v	16
D	Normal duty cycle	-	0.4
C	Filter capacitance	μF	820
L	Filter inductance	μH	250
R_C	ESR of capacitor	Ω	0.083
R_L	ESR of inductor	Ω	0.027
R	Load resistance	Ω	4.8

B. Controller Design

To regulate the output voltage of DC-DC boost converter, proportional-integral (PI) control, deadbeat control, and active disturbance rejection control (ADRC) are developed in this paper. Due to the space limitation, only ADRC is described in detail here to illustrate the control behavior.

For ADRC design, setting $x_1 = \hat{v}_o(t)$, $x_2 = \dot{\hat{v}}_o(t)$, a dynamic DC-DC boost converter model can be written as follows:

$$\begin{cases} \dot{x}_1(t) = x_2(t) \\ \dot{x}_2(t) = -\beta_0 x_1(t) - \alpha_0 x_2(t) + \gamma_0 \hat{d}(t) + f(t, \hat{v}_o(t), \dot{\hat{v}}_o(t), \hat{d}(t), \dot{\hat{d}}(t), \hat{v}_{in}(t), \dot{\hat{v}}_{in}(t), \omega(t)) \\ y(t) = x_1(t) \end{cases} \quad (2)$$

Let $x_3 = f$, and the derivative of f is defined as h , then the state-space equation of the augmented system is constructed.

$$\begin{cases} \dot{x}(t) = Ax(t) + Bu(t) + Eh(t) \\ y(t) = Fx(t) \end{cases} \quad (3)$$

Disturbance is estimated through conventional bandwidth-based parameterization technique, which is described as

$$\begin{cases} \dot{z} = Az + Bu + L(y - \hat{y}) \\ \hat{y} = Fz \end{cases} \quad (4)$$

where $A = \begin{bmatrix} 0 & 1 & 0 \\ -\beta_0 & -\alpha_0 & 1 \\ 0 & 0 & 0 \end{bmatrix}$, $B = \begin{bmatrix} 0 \\ \gamma_0 \\ 0 \end{bmatrix}$, $C = [1 \ 0 \ 0]$,

$E = \begin{bmatrix} 0 \\ 0 \\ 1 \end{bmatrix}$, $F = [1 \ 0 \ 0]$, and $L = [\vartheta_1 \ \vartheta_2 \ \vartheta_3]^T$ being the

observer gain matrix. And $z = [z_1 \ z_2 \ z_3]^T$ is the estimated state of $x = [x_1 \ x_2 \ x_3]^T$, and $\vartheta_1, \vartheta_2, \vartheta_3$ are defined as observer bandwidth, which are presented simply by observer bandwidth ω_0 as follows:

$$\vartheta_1 = 3\omega_0, \vartheta_2 = 3\omega_0^2, \vartheta_3 = \omega_0^3 \quad (8)$$

Finally, the related control law can be obtained as (5) and PD controller is designed for optimization with (6), where k_p and k_d are the proportional and derivative gains, respectively, which are indicated as the function of the bandwidth of closed-loop control system ω_c as Equation (7).

$$u = \frac{-f + u_0}{\gamma_0} \quad (5)$$

$$u_0 = k_p(V_r - z_1) - k_d z_2 \quad (6)$$

$$k_p = \omega_c^2, k_d = 2\omega_c \quad (7)$$

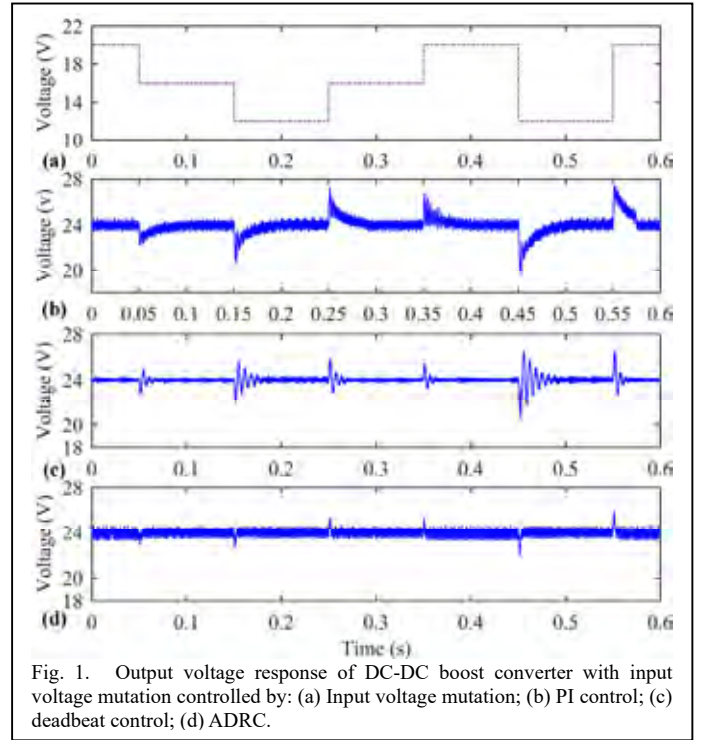


Fig. 1. Output voltage response of DC-DC boost converter with input voltage mutation controlled by: (a) Input voltage mutation; (b) PI control; (c) deadbeat control; (d) ADRC.

III. RESULTS AND DISCUSSION

Under the condition of input voltage mutation, experimental output voltage responses of DC-DC boost converter with the control of proportional-integral (PI) controller, deadbeat controller, and ADRC are presented by Fig. 1, which indicates that ADRC gives a fast-dynamic response with small overshoot.

IV. CONCLUSION

1. In this study, a DC-DC boost converter system is analyzed and mathematical model with parasitic resistance of the inductor and the capacitor is derived for controller design.
2. Proportional-Integral (PI) controller, deadbeat control, and active disturbance rejection control (ADRC) are designed to regulate the output voltage, and the ADRC provides better dynamical performance than the first two, providing a stable performance.

ACKNOWLEDGMENT

This work was supported in part by the National Research Foundation of Korea (2018R1D1A1B07044005 and 15R1A4A1041746).

REFERENCES

- [1] Wang, Y. X., Ou, K., & Kim, Y. B., Modeling and experimental validation of hybrid proton exchange membrane fuel cell/battery system for power management control, International Journal of Hydrogen Energy, Volume 40(35), 2015, pp. 11713-11721.

FUEL CELLS AND HYDROGEN TECHNOLOGIES: CRITICAL MATERIALS AND SUPPLY CHAIN

D. Blagoeva*,

*European Commission, Joint Research Centre, Westerduinweg 3,
(Netherlands)

Abstract - Fuel cells and hydrogen (FCH) technologies is one of the options for large scale electricity storage capacity for better integration of renewable energy sources as well as a promising low carbon transport solution. The EU transition to more sustainable low carbon energy and transport sectors however go along with high demand for certain raw materials flagged as critical materials for the EU economy. Reliable and unhindered access to raw materials is a growing concern within the EU and across the globe. While the EU energy dependency is more than 50%, our reliability on raw materials is even higher, often reaching 100% for some critical materials. The transition to low carbon energy and transport will also imply a shift from fuel dependency to materials dependency along with the associated geopolitical shift. Our dependency on Russia, Norway, Colombia, USA and Algeria and others for the supply of natural gas, crude oil and coal will be smoothly shifted to reliance on countries like China, Brazil and South Africa for the supply of key raw materials required in central low carbon technologies such as wind energy, photovoltaic (PV) energy and Lithium ion batteries being key components in electric cars as well as required for stationary storage for the better integration of renewable energy sources.

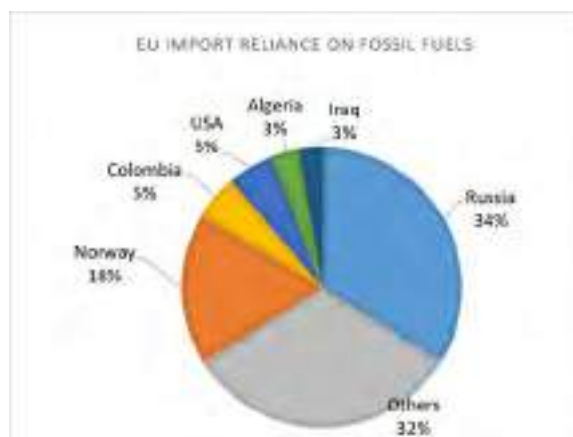


Fig. 1. EU import reliance of natural gas, crude oil and coal: aggregated 2017 data

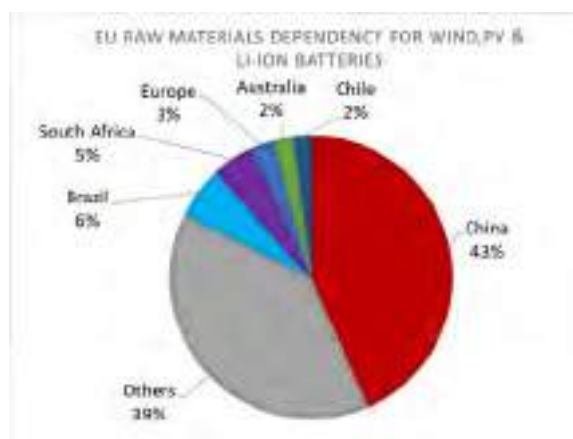


Fig. 2. EU raw materials dependency on the supply of raw materials required in wind, PV energy and Li-ion batteries

Index Terms – Fuel cells, critical raw materials, supply chain

I. INTRODUCTION

The EU import reliance on fossil fuels is around 50%. Russia, Norway, Colombia and USA are the four major suppliers of fossil fuels for the EU (Fig. 1) [1]. The major suppliers of raw materials for low carbon technologies such as wind energy, photovoltaic (PV) energy and Li-ion batteries are China (having more than 40% share), Brazil and South Africa. Europe delivers only 3% of the raw materials required in these key low carbon technologies (Fig. 2). The raw materials supply data are taken from an official EC study [2].

In addition, fuel cells and hydrogen represent also a promising low carbon transport solution as well as attractive option for large-scale electricity storage capacity for better integration of renewable energy.

II FUEL CELL SUPPLY CHAIN DEPENDENCY

Due to the promising role, which fuel cells and hydrogen (FCH) might play in future, further attention is given hereafter on the supply chain dependency of Europe for this technology. The global supply chain for fuel cell is discussed and evaluated considering the whole supply chain from raw materials down to fuel cell stacks. Quantitative evaluation is carried out allowing for proposals on the way forward towards higher degrees of security of supply.

The key players along the supply chain are shown in Fig 3.

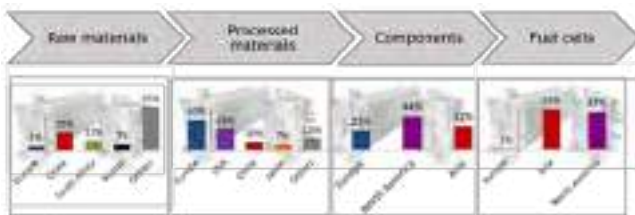


Fig. 3. Fuel cells: key players along the supply chain

China is the major supplier of raw materials for Fuel cells (22%), followed by South Africa (11%) and Russia (7%). Europe produces only 5% of the raw materials but it is the largest producer of processed materials with about 40% production share. The largest manufacturers and suppliers of fuel cell components (including hydrogen vessels) and fuel cells are Asia (mainly Japan) and North America (USA and Canada). There are many European companies involved in fuel cell integration but this step of the supply chain is not considered here [3].

In Fig. 4, an overview is given of the raw materials, processed materials and components required in FC technology and considered in the analysis. The country (regions) shares shown in Fig. 3 are estimated correspondingly [3].

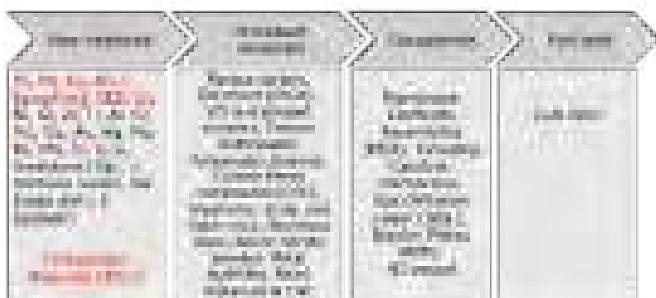


Fig. 4. Fuel cells: an overview of raw materials, processed materials and components considered in the analysis

The risk of supply of critical raw materials for fuel cells is even higher. Eleven materials, namely Pt, Pd, Co, Rh, REE, C (natural graphite), Ru, Si, Mg, B and V are flagged as critical for the EU economy in the 2017 Critical Raw Materials list [2]. China delivers more than 1/3 of the critical materials, followed

by South Africa (17%) and Russia (13%) (Fig. 5).



Fig. 5. Supply of CRM for Fuel cells: key players

In particular, indispensable materials used in fuel cells and electrolysers such as Platinum, Palladium, Ruthenium, Iridium, Niobium, Cobalt, Lanthanum and Yttrium among others are assessed by the European Commission as critical materials for the EU, meaning that high risk is associated with their supply. Again, these materials have highly concentrated supply, delivered predominantly by very few countries; e.g. Platinum (71% South Africa), Niobium (95% Brazil), Lanthanum and Yttrium (95% China), Ruthenium (50% Russia) etc.

In addition to supply risk shortages, the end of life input recycling rates for these materials are relatively low ranging between <1% and 11%. The substitution of these materials is also challenging or not feasible at all without sacrificing the performance level.

II CONCLUSIONS

The high risk of supply shortages, limited recycling and substitution potential for certain materials could hinder the smooth deployment of fuel cells and hydrogen technologies in Europe in future. All these are critical aspects that need further attention. Securing reliable, adequate and continuous supply of such materials together with substitution and recycling can underpin the successful deployment of FCH technologies in the EU.

REFERENCES

- [1] Eurostat, 2019a. Energy production and imports, Statistics Explained, <https://ec.europa.eu/eurostat/statistics-explained/pdfscache/1216.pdf>
- [2] EC, 2017. European Commission, 2017, Study on the review of the list of critical raw materials – Final report, Publications Office of the European Union, Luxembourg, 2017, ISBN 978-92-79-47937-3, doi 10.2873/876644.
- [3] Blagoeva, D. et al., 'Materials dependencies for dual-use technologies relevant for Europe's defence sector'; JRC Science for Policy report – to be published soon.

NANOSTRUCTURES OF NAFION ULTRATHIN FILM ON THE PLATINUM AND CARBON SURFACES IN PEMFC CATALYST LAYER: MOLECULAR DYNAMICS SIMULATION APPROACHES

Haisu Kang and Seung Geol Lee*

* Department of Organic Material Science and Engineering, Pusan National University, 2, Busandaehak-ro 63beon-gil, Geumjeong-gu, Busan 46241 (Republic of Korea)

Abstract - We performed full atomistic MD simulations in order to understand nanostructures of the hydrated Nafion ultrathin film on the surfaces of PEMFC catalyst layer (CL), which are catalyst surface (platinum) and support surface (carbon sheet), at 353.15K under different water contents. We found that water molecules, hydronium ions and sulfonic acid groups dominate at the nearest region on Pt surface, while carbon surface, Nafion PTFE backbones dominate as lying on the surface. We concluded that they have different phase segregated structure on each surface. Thus, we analyzed hydrophilic and hydrophobic domain separately and found that hydrophilic domain is more concentrated with lower volume and Nafion backbone in the hydrophobic domain is aggregated more on Pt surface.

Index Terms - Fuel cell catalyst layer, molecular dynamics (MD), Nafion thin film, perfluorosulfonic acid (PFSA) membrane,

I. INTRODUCTION

Polymer electrolyte membrane fuel cells (PEMFCs) are promising power sources for various application. A typical PEMFC consists of a membrane electrode assembly (MEA), which mainly includes a polymer membrane (PEM) and a catalyst layer (CL). Particularly, since multicomponent transport phenomena take place in a catalyst layer (CL) regions, to design highly performing CL is crucial for fuel cell performance. When the PEMFCs operate, water generated by electrochemical reaction. By this process, water swells into PEM and perfluorosulfonic acid (PFSA) polymer forms segregated structure with hydrophilic and hydrophobic domains due to its inhomogeneous structure. Efforts to understand nano-phase segregated structure of the hydrated ionomer ultrathin film were conducted in recent years. Nevertheless, due to their complexity, questions are still remained from the interactions between the surface and Nafion ultrathin film, to the induced

correlations between the components of Nafion ultrathin film especially on cell operation temperature.

In this study, we performed full atomistic molecular dynamics (MD) simulations in order to reveal nano-phase structure of the hydrated ionomer ultrathin film on the surfaces consisting CL, catalyst surface (platinum) and support surface (carbon sheet), especially under different water contents when the PEMFCs operated at 353.15K. The structural properties are analyzed by number distribution of atoms and radial distribution functions (RDFs). For the macroscopic inspection, the hydrophilic domains were analyzed by their volumes, since the effective volumes of water molecules in hydrophilic domains are crucial for the transport properties in Nafion film. On the other hand, hydrophobic domains were comprised of Nafion backbone chains, which crystallinity causes phase segregation of the Nafion thin film. Thus, we conducted solvent volumes analysis and radius of gyration (R_g) analysis of the equilibrated systems and compared their swelling by film thickness.

II. COMPUTATIONAL DETAIL

All MD simulations were performed using full atomistic models. Nafion ionomer with molecular weight 9969.83 g/mol was used. A modified DREIDING force field was used to describe the inter- and intramolecular interaction in the system. However, we applied van der Waals (vdW) parameters reported by Brunello et al. for the off-diagonal interactions between Pt molecule and nonmetals. Canonical ensemble (NVT) MD simulation was performed for equilibrium at 353.15K.

III. RESULT AND DISCUSSION

A. Structural Analysis

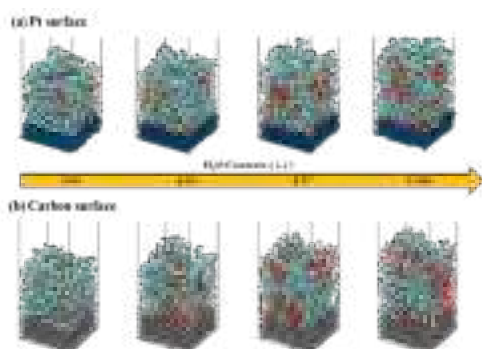


Fig. 1 Snapshots of equilibrated Nafion ultrathin film on (a) Pt surface and (b) carbon surface under different hydration level (λ) of 2.91, 6.15, 9.77, 13.84. Color code: white, gray, red, cyan, and yellow are hydrogen, carbon, oxygen, fluorine, and sulfur, respectively.

The snapshots of the equilibrated structures in Fig. 1. showed that Nafion film on both Pt and carbon surface gradually segregated into hydrophilic and hydrophobic region with the increase of hydration level. However, they show different interface structure on Pt and carbon surface. The interface snapshots are described in Fig. 2. Nafion backbones lying flat on the surface are shown on both Pt and carbon surface at low hydration level ($\lambda = 2.91$). However, when the hydration level increases, water molecules, hydronium ions and sulfonic acid groups are counted more on the Pt surface than carbon surface due to relatively higher hydrophilic interaction on Pt surface. Whereas on carbon surface, they do not show clear differences by hydration level but Nafion backbone stays lying flat on the surface in all cases due to hydrophobic interactions between Nafion backbone and carbon surface. When we analyzed the number distribution of atoms, they show correspondent results on each surface. Meanwhile, by analyzing Radial Distribution functions (RDFs) between molecules, we found that the distribution of hydronium ions is highly dependent on that of sulfonic acid group regardless of the surface condition.

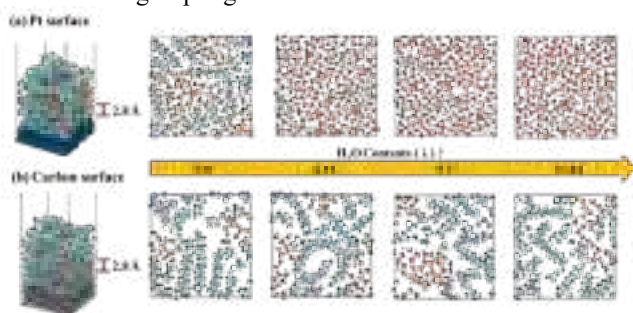


Fig. 2 Top-view snapshots of equilibrated Nafion ultrathin film at the distance of 2.8 Å from (a) Pt surface and (b) carbon surface under different hydration level (λ).

B. Solvent Volume Analysis

We analyzed the hydrophilic domains with its volume occupied with solvent (water in this paper). We found that the average volume occupied with solvent is higher on carbon surface than Pt surface under hydration level, which means that the hydrophilic domain is concentrated on Pt surface than carbon surface at the same amount of water.

C. Radius of gyration

We calculated ionomer radii of gyration (R_g) to quantitatively analyze morphology of Nafion ionomer backbone in the hydrophobic domains on Pt and carbon surface. As the hydration level increases, R_g increases on both surface. However, it has higher value on carbon surface than Pt surface. This result indicates that backbone of Nafion ionomer on Pt surface is more aggregated. Whereas on carbon surface, backbone of Nafion ionomer has reduced aggregation, which gets more extended as hydration level increases. Thus, we found that hydrophobic regions on Pt surface are shown to be highly compacted with PTFE backbones. Consequently, we found that Nafion film is $\sim 13\%$ thinner on Pt surface.

IV. CONCLUSION

Visual inspection shows that water molecules, hydronium ions and sulfonic acid groups dominate as a monolayer on the nearest Pt surface, while Nafion PTFE backbones dominate the nearest carbon surface also as a monolayer. Structural analyses confirm that inhomogeneous distribution of molecules leads to different hydrophilic regions on Pt and carbon surface, when they segregate to hydrophilic-hydrophobic domains. Compared to carbon surface, those segregated hydrophilic and hydrophobic regions on Pt surface show higher concentration of their composition with lower solvent volume and more aggregated chain morphology. Considering the distinctly layered hydrophilic-hydrophobic domains in Nafion ultrathin film from our results, possible transport mechanisms depending on surface hydrophilicity will be narrowed to certain respect. We expect that this investigation will shed light to the further researches to design highly performing PEMFC.

ACKNOWLEDGMENT

This research was supported by the National Research Foundation of Korea (NRF) funded by the Ministry of Science, ICT & Future Planning (Nos. NRF-2016M1A2A2937151 and NRF-2015M1A2A2057129) and Global Frontier Program through the Global Frontier Hybrid Interface Materials (GFHIM) of the National Research Foundation of Korea (NRF) funded by the Ministry of Science, ICT and Future Planning (No. 2013M3A6B1078882).

ELECTRONIC PROPERTIES OF NITROGEN AND SULFUR DOPED GRAPHENE: DENSITY FUNCTIONAL THEORY APPROACH

J. H. Lee*, and S. G. Lee*

* *Department of Organic Material Science and Engineering, Pusan National University, 2, Busandaehak-ro 63beon gil, Geumjeong-gu, Busan 46241, Republic of Korea*

Abstract - In this work, we investigated the adsorption behavior of Li atom on N, S co-doped graphene using density functional theory (DFT). We found that the adsorption energy of Li atom on N, S co-doped graphene was dramatically enhanced by tailoring the electrochemical activity of graphene with mono-vacancy defect, and N and/or S dopant atoms. The calculated results indicated the following order in the adsorption energies from the least to the most strongly bound: N₃G (-4.971 eV) < S₃G (-4.818 eV) < N₁S₂G (-4.274 eV) < N₂S₁G (-3.455 eV). In addition, the Mulliken charge distribution analysis and charge density plots showed that the electron-deficient system of N, S co-doped graphene give rise to remarkable charge transfers from a Li atom to the graphene, which are -0.562e in N₃G, -0.598e in N₂S₁G, -0.631e in N₁S₂G and -0.553e in S₃G, confirming that the strong adsorption of Li atom is caused by the Columbic interaction. Consequently, our study provides in-depth theoretical insights into the potentially enhanced electrochemical activity of N, S co-doped graphene systems, thereby offering high capacity of Li storage for lithium ion batteries (LIBs) and supercapacitors.

Index Terms - co-doping, mono-vacancy, graphene, electrode material, lithium storage, density functional theory

I. INTRODUCTION

Over the last two decades, lithium-ion batteries (LIBs) have rapidly dominated the commercial rechargeable battery market for portable electronic devices owing to their high energy density and long cycling life. However, the state-of-the-art LIBs in large-scale electric energy storage applications require further developments in energy density, rate capability and electrode durability. Until now, graphite is the most widely used anode material in commercially available LIBs because of its high Columbic efficiency and better cycle performance. Unfortunately, the limited specific capacity of graphite (372 mA h g⁻¹) and poor rate performance induced by its low lithium diffusion coefficient (10⁻⁷ ~ 10⁻¹⁰ cm² s⁻¹) restrict the

improvement of next-generation LIBs. Consequently, it is imperative to design and synthesize novel carbonaceous anode materials with enhanced electrochemical performances for Li storage by taking advantage of their high theoretical capacities and excellent rate and cycling stability. Various carbonaceous materials such as carbon nanotubes, graphene and porous carbons are attracted attention as anode for LIBs. Moreover, unlike the graphite, in which the Li ions are reversibly stored by intercalation/deintercalation, these carbonaceous materials with high surface areas can store additional Li ions depending on the structure and morphology, thus resulting in high specific capacity of > 1500 mA h g⁻¹ with long cycling span. Significant efforts have been made to design novel carbonaceous anode materials with various nanostructures. Recently, it has been found that N-doped graphene showed better electron-transfer ability and increased electro-catalytic activity, thus exhibiting great Li storage capability. Additionally, doping with S atom can further attracted increasing attention in current carbonaceous material research. Since S doping can change the charge state of the neighboring C atoms, it leads to enhance the adsorption ability between graphene and Li ions, which exhibits competitive chemical reactivity, catalytic activity and storage capacity compared with N-doped graphene. However, single heteroatom doping inevitably encounters a limitation for enhancing the specific capacity. More recently, when two different heteroatoms (B, N, P and S) are simultaneously doped into the graphene, synergetic effect can be induced owing to the more powerful active sites. To date, only a few studies have been focused on the influence of N and S co-doping into graphene materials. In addition, information on the the role and influence of N and S co-doping on structural and electrochemical characteristics are scarce despite the fact that the N and S co-doping is believed to be a key factor in

imposing explosive electrochemical activity and high Li storage capacity. Therefore, there is an emerging need for a better understanding on electrochemical structure and properties of N, S co-doped graphene. Aiming at revealing the cause about synergetic effect on N, S co-doping and investigating the storage mechanism of Li ion onto N, S co-doped graphene, we have performed density function theory (DFT) calculations using various N and S doping levels focusing on its adsorption characteristics.

II. RESULTS

The results show that the adsorption energies between Li atom and graphene can be tuned with the help of N and S co-doping of mono-vacancy defect, thereby leading to greater Li uptake capacity of N and S co-doped graphene. The adsorption energies of Li atom were in the order of N3G (-4.971 eV) < S3G (-4.818 eV) < N1S2G (-4.274 eV) < N2S1G (-3.455 eV) (Fig. 1). Through Mulliken charge distribution analysis and charge difference plots, it has been observed that the co-doped graphene becomes an electron deficient system by the presence of N and S dopant atoms and mono-vacancy defect. Upon adsorption, the charge of Li atom transferred to the N and/or S co-doped graphene, as evidenced by the yellow region representing the charge accumulation. From a Li atom, the doped graphene gained the electronic charge of -0.562e in N3G, -0.598e in N2S1G, -0.631e in N1S2G and -0.553e in S3G, respectively.

III. CONCLUSION

By performing density functional theory (DFT) calculations, in this paper we simulated the adsorption process of Li atom on several N, S co-doped graphene, and calculated the adsorption energies and corresponding charge distribution analysis in order to analyze the mechanism of Li storage on the N, S co-doped graphene and verify the applicability of N, S co-doped graphene as anode materials for LIBs. Accordingly, a significant amount of electrons was accumulated around the N and/or S decorated mono-vacancy region, demonstrating the strong electrostatic interaction between the doped graphene and Li atom. Thus, these interesting results provide that the possibility of tailoring the electronic properties and improving a Li storage capacity and its application in anode materials for LIBs.

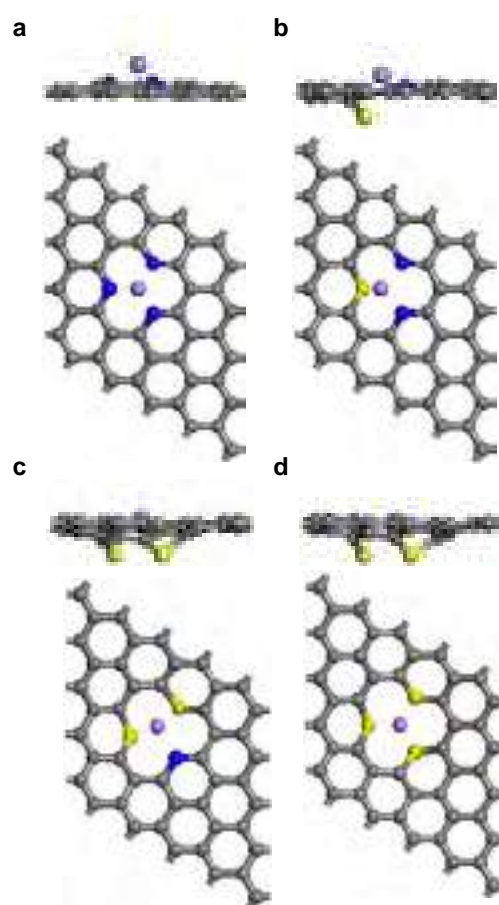


Fig. 1. The top and side views of the optimized structures for Li adsorption configurations on (a) N₃G system; (b) N₂S₁G system; (c) N₁S₂G system; and (d) S₃G system. The purple, gray, blue, and yellow colors denote lithium, carbon, nitrogen, and sulfur, respectively.

ACKNOWLEDGMENTS

This research was supported by the National Research Foundation of Korea (NRF) funded by the Ministry of Science, ICT & Future Planning (Nos. NRF-2016M1A2A2937151 and NRF-2015M1A2A2057129). This research was supported by the Global Frontier Program through the Global Frontier Hybrid Interface Materials (GFHIM) of the NRF of Korea funded by the Ministry of Science, ICT, and Future Planning (No. 2013M3A6B1078882). This work was supported by the BB21+ Project in 2018.

NANO-FABRICATION OF A HIGH-PERFORMANCE L_{NiO}₃ CATHODE FOR SOLID OXIDE FUEL CELLS VIA AN ELECTROCHEMICAL ROUTE

S. Lee^{*,***}, S. Rehman^{*}, R. Song^{*,***}, J. Hong^{*} and S. Park^{*,***}

^{*}Fuel Cell Laboratory, Korea Institute of Energy Research, 152 Gajeong-ro, Yuseong-gu, Daejeon 34129, (Republic of Korea)

^{**} Department of Advanced Energy Technology, University of Science and Technology, 217 Gajeong-ro, Yuseong-gu, Daejeon 34113, (Republic of Korea)

Abstract - Chemically assisted electrodeposition (CAED), a new means of fabricating nanostructured SOFC cathodes in a single loading step, provides the advantage of the simultaneous deposition of multiple cations while using dilute aqueous solutions of readily available salts. In this study, CAED is demonstrated by fabricating a cobalt-free LaNiO₃/GDC composite cathode. The LaNiO₃/GDC composite cathode prepared by CAED exhibits superior electrochemical properties compared to LaNiO₃/GDC composite cathodes fabricated by sintering or self-assembly (a recently introduced low-temperature SOFC cathode fabrication method) approaches. An anode-supported SOFC with a LaNiO₃/GDC composite cathode fabricated by CAED shows a high power density of 974 mW cm⁻² at an intermediate operating temperature of 750 °C. Low-temperature nano-fabrication by CAED, producing a cathode with a high surface area while avoiding the formation of insulating phases, is believed to play an important role in achieving better SOFC performance.

KEYWORDS: SOFC, cobalt free cathode, low-temperature nano-fabrication, chemically assisted electrodeposition

I. INTRODUCTION

Solid oxide fuel cells (SOFCs) are one of the most efficient energy conversion devices whose performance is not affected by the fuel combustion efficiency limitations, i.e., the Carnot cycle. SOFC energy conversion systems can achieve the efficiencies of 70 – 90 % when power and high-quality waste heat are combined. As they provide the unique advantages of high-temperature operation, all solid-state construction, scalability, high fuel flexibility and a benign effect on the environment, SOFCs are very attractive in the era of the global energy crisis and climate change.

Here we report the low-temperature nano-fabrication of LNO as a SOFC cathode by CAED into a backbone of the GDC ion conducting phase. Anode-supported SOFCs with LNO/GDC composite cathodes fabricated by CAED as well as sintering and self-assembly methods are tested and compared in terms of their electrochemical performance with hydrogen as a fuel source.

II. EXPERIMENTAL

Anode-supported SOFCs were fabricated for electrochemical performance measurements of various LNO/GDC composite cathodes. For the fabrication of anode-supported SOFCs, NiO (Kojungdo, Japan), YSZ (LTC, South Korea) and activated carbon (YP-50F) powders were mixed by ball milling using zirconia balls and ethanol. After drying and sieving, the mixed powder was uniaxially pressed into circular green disks which were then pre-sintered at 1100 °C for 5 h to form the anode supports. A NiO/ScCeSZ (60:40) anode functional layer (AFL) and ScCeSZ electrolyte layer slurries were prepared for dip coating using appropriate amounts of a solvent (isopropanol alcohol, toluene), a binder (polyvinyl butyral), a plasticizer (dibutyl phthalate), a dispersant (fish oil) and a surfactant (Triton X-100). The pre-sintered anode supports were dip-coated with AFL and electrolyte layers successively, after which the anode-supported half-cell was sintered at 1400 °C for 5 h.

LNO cathodes were fabricated by CAED and by screen printing onto anode-supported SOFCs. For the fabrication of the LNO cathodes by CAED. Compartment 1 contained the mixed metal nitrate solution for the CAED of LNO, in which the CNT-modified GDC scaffolds were used as working

electrodes. The button cells were masked before the CAED step using polymer paint so that only the GDC scaffolds were exposed to the CAED electrolyte. Compartment 2 contained a KNO_3 solution at the same concentration used for the mixed metal nitrate solution, with a Pt mesh used as a counter electrode. CAED was performed galvanostatically by cathodically polarizing the working electrode.

III. RESULTS AND DISCUSSION

Cross-sectional SEM images after each step during the fabrication of the LNO/GDC composite cathode (near surface region) by the CAED method are shown in Fig. 1. The pristine GDC scaffold shows a well-defined porous structure. Sintering at 1250 °C produces a good attachment of GDC scaffold with ScCeSZ electrolyte and there is no delamination detected. Infiltration of cobalt nitrate into GDC scaffold produces uniformly distributed cobalt nanoparticles with an average particles size of ~40 nm. CNTs are grown onto cobalt nanoparticles by high-temperature CCVD at 800 °C using ethylene as a carbon source. The CNTs are grown into an interconnected network, and the CNT-modified GDC scaffolds are found to have enough electrical conductivity for the CAED step. CAED clearly produces La-Ni-OH agglomerates onto the CNT-modified GDC scaffolds, as shown by the increased thickness and roughness of the CNTs after the CAED step. A heat treatment at 800 °C removes the CNTs and forms the LNO perovskite phase. CAED produces a uniform deposition of LNO throughout the body of the GDC scaffold, as shown in the cross-sectional SEM images of the LNO/GDC composite cathode fabricated at the cathode/electrolyte interface region.

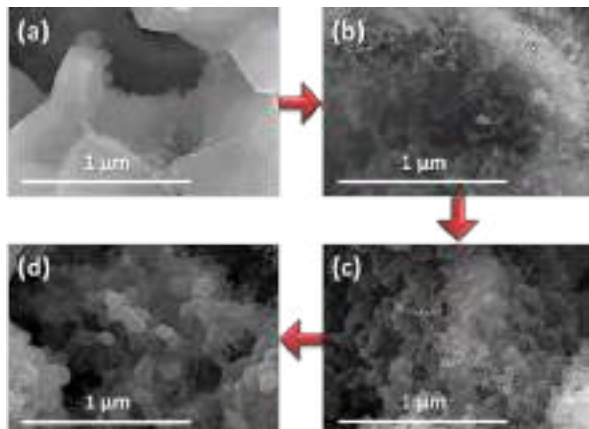


Fig. 1. SEM images of the GDC scaffold (near the surface) after (a) Co infiltration, (b) CNT modification, (c) CAED of La-Ni-OH, and (d) a heat treatment at 800°C

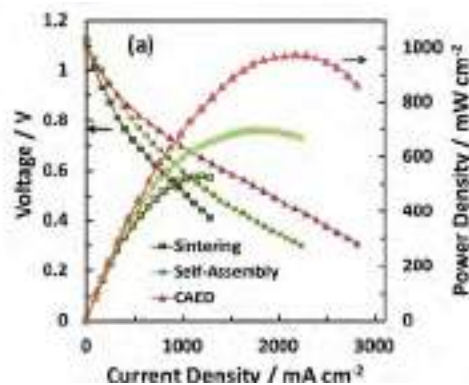


Fig. 2. I-V curves of SOFCs at 750 °C prepared by various methods

LNO/GDC composite cathodes are fabricated by CAED, self-assembly and sintering methods onto the dense ScCeSZ electrolyte of anode-supported SOFCs having identical anodes (SOFCs belonging to the same batch). Before the measurement of the electrochemical performance, all button cells are preloaded with a constant current density of 500 mA cm^{-2} for a time period of 20 h. Fig. 2 shows the polarization curves of the SOFCs consisting of the LNO/GDC composite cathodes fabricated by the CAED, self-assembly and sintering methods measured at 750 °C. It is evident that the SOFC with the LNO/GDC composite cathode fabricated by CAED possesses superior performance (974 mW cm^{-2}) as compared to the performance outcomes of 697 and 528 mW cm^{-2} for the SOFCs with the LNO/GDC composite cathodes fabricated by the self-assembly and sintering techniques, respectively.

IV. CONCLUSION

The SOFC consisting of a nanostructured LNO/GDC composite cathode fabricated by CAED exhibited superior performance in terms of the power density due to its high electrocatalytic activity for the ORR as compared to SOFCs consisting of LNO/GDC composite cathodes fabricated by sintering or self-assembly methods.

ACKNOWLEDGMENT

This work was supported by the Technology Development Program to Solve Climate Change in the form of a grant from the National Research Foundation (NRF) funded by the Korean government (Ministry of Science and ICT).

REFERENCES

- [1] S. Rehman, A. Shaur, R.-H. Song, T.-H. Lim, J.-E. Hong, S.-J. Park, S.-B. Lee, *Journal of Power Sources*, Volume 429, 2019, pp. 97-104.

CH2P: COGENERATION OF HYDROGEN AND POWER USING SOLID OXIDE-BASED SYSTEM FED BY METHANE RICH GAS

L. Crema*¹, M. Testi*, J. Van Herle**, S. Diethelm**, M. Pérez-Fortes**,
S. Santhanam***, E. Varkaraki****, I. Fadanelli****, G. Prosperi****, R. Makkus*****,
I. Mirabelli*****, R. Schoon*****

* Fondazione Bruno Kessler, 38050 Povo (Trento), Italy ** École Polytechnique Fédérale de Lausanne, 1015 Lausanne, Switzerland
*** German Aerospace Center, 70569 Stuttgart, Germany
**** SOLIDpower Spa Mezzolombardo, Italy/SOLIDpower SA, 1400 Yverdon, Switzerland
***** Hygear, 6802 EG Arnhem, The Netherlands
***** Shell Global Solutions International B.V., 1031 HW Amsterdam, the Netherlands

Abstract - The CH2P project aims at building an innovative system prototype for hydrogen refueling stations (HRS) that can support early transport infrastructure deployment for the uptake of Fuel Cell Electric Vehicles (FCEV).

The CH2P system cogenerates hydrogen, heat and power using Solid Oxide Cell technology fueled by methane-rich gases. The CH2P technology reduces the carbon footprint by achieving an extremely high overall system efficiency.

By providing a transition technology to support the deployment of HRS, CH2P contributes to shift the EU towards Hydrogen Mobility. The use of hydrogen in the transport sector will improve the air quality while mitigating the effect of mobility on climate change. At the same time, the transition to hydrogen have the potential of providing a competitive advantage of the EU that can lead to significant impact in terms of economic value generated, new business opportunities, new job creation and improved R&D in Europe.

Index Terms – Cogeneration of hydrogen and power, Hydrogen Refueling Stations, Solid Oxide Fuel Cells.

I. INTRODUCTION

CH2P project [1] aims to realize an innovative energy system for the cogeneration of hydrogen (H₂), heat and power using a solid oxide fuel cell (SOFC) fueled by methane rich gases or mixtures. The system generates both hydrogen and electricity, more efficiently and with a reduced environmental

impact compared to conventional technologies. The CH2P system operates in the following modes:

1. production of different fractions of hydrogen and electricity at the HRS. It can reach 100% hydrogen and power capacity, or a partial load of both;
2. the system can operate in a net electricity consumption mode and produce hydrogen-only, using the reforming reaction;
3. in some of the working modes, the system can generate hydrogen without the need to add water in regions where water is not abundant. The system layout configures an off-grid solution.

II. CH2P TECHNOLOGY

The cogenerating SOFC technology is under development, having indeed progressed to the design of the solution, engineering of most of the components, qualified and validated at the laboratory scale. The main elements constituting the technology and its application are described here below.

A. Use cases

Considering data on refueling stations, in particular power consumption, at the detail of single components, and hydrogen utilization, a usage scenario has been elaborated to account for

¹ Main author: Tel.: +39-0461-314922. crema@fbk.eu

the technology dynamic behavior. To sum up, different usage scenarios have been considered for a CH2P. These cases can be fulfilled by considering 6 operations points that are illustrated in **Error! Reference source not found.** Tests follow the scheme.



Fig. 1. CH2P operation points with laboratory testing scheme

B. Technology Scheme

Alongside design and engineering, a overall P&ID scheme for the technology has been designed as illustrated in the following figure 2.

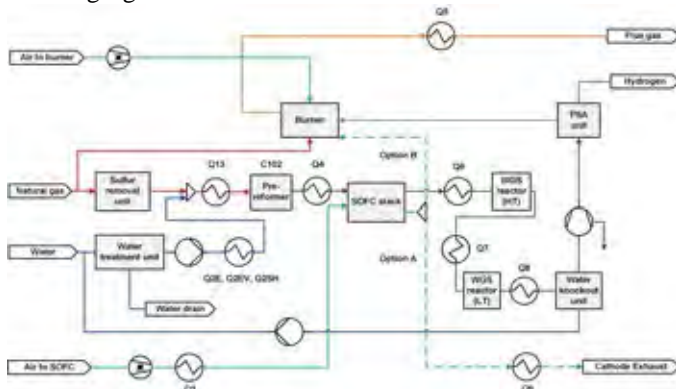


Fig. 2. CH2P final PFD after multi objective optimization

The CH2P plant is the result of a complex integration of different sub-components: natural gas sulfur removal, fuel pre-reforming reactor, steam generator with heat recovery system, SOFC stacks, water-gas shift- WGS reactor for full conversion of residual carbon monoxide to carbon dioxide, H₂ separation by water knock out system, compressor and a pressure swing adsorption – PSA unit. The high purity hydrogen flow produced complies with ISO 14687-3:2014. The CH2P system will support fuel demand in novel refueling stations, producing H₂ for vehicles and electricity for both the refueling station needs (self-consumption and recharging of vehicles) and for business applications (grid balancing, energy selling) with high

flexibility of cogeneration. Moreover, it will present an innovative cost model for hydrogen production. The CH2P system was designed based on a systematic and multi objective optimization approach. The overall system was initially analyzed in steady state using the results obtained in Aspen Plus™, where three main layout options were identified and evaluated through well-known key targets. Then, a multi-objective optimization tool was applied to define the best operating conditions and heat exchangers network of the system considering efficiency and feasibility aspects. The proposed PFD (Process Flow Diagram) was converted and completed in a P&ID taking in consideration a proper safety analysis (HAZOP). The development of control followed a similar pathway. By means of the dynamic model developed in Dymola platform using the modelica code, the whole CH2P system was simulated to define and optimize its control strategy and the implementation of the control logic over the hardware of the system. The results from numerical simulation show that the plant could reach a weighted efficiency (i.e. it considers the overall working hours per period per day) over 75%, considering all generated fractions.

III. CONCLUSION

In laboratory testing the main technology targets have been validated. This is including the single and large stacks behavior. The Large Stack Module has been qualified to produce 25 kW power and 20 kgH₂/day equivalent, with target efficiency.

Thermal losses have been accounted for 1,5 kW instead of 2,5 kW from the initial simulations. Efficiency is expected to be considerably higher than 80% modelled for main modes.

The prototype is entering in a pilot testing phase, with the target to test the fully integrated 20 kgH₂/d system within Q1 2020. There results from laboratory testing are promising for the validation of the overall technology. Advanced controls with Hazop analysis are almost finalized.

Based on the optimization results, a plant prototype of 20 kg H₂/d will be built (alpha version). A second system provided of higher readiness level (beta version) will be installed at Shell Technology Centre in Amsterdam (STCA), at a scale of 40 kg H₂/day. Both single and pilot systems will support the design of a full-scale solution for a refueling station with a capacity of 400 kg H₂/day.

ACKNOWLEDGMENT

CH2P project has received funding from the Fuel Cells and Hydrogen 2 Joint Undertaking under grant agreement No 735692. This Joint Undertaking receives support from the European Union's Horizon 2020 research and innovation program, from Hydrogen Europe and Hydrogen Europe Research.

REFERENCES

- [1] For more info www.ch2p.eu

DESIGN OPTIMISATION OF SOIL MICROBIAL FUEL CELLS FOR ENERGY HARVESTING IN REMOTE AREAS

J. Dziegielowski, N. Poyiatzi, and M. Di Lorenzo

Centre for Biosensors, Bioelectronics and Biodevices (C3Bio) and
Department of Chemical Engineering, University of Bath, Claverton Down,
BA2 7AY, (UK)

Abstract - Soil microbial fuel cells (SMFCs) are a specific type of microbial fuel cells, in which the soil acts as the electrolyte, and as the source of microorganisms and organic fuel. Given the great simplicity of the system design, SMFCs represent an interesting avenue for energy harvesting and sensing in remote areas. In this study, we investigate the influence that geometrical factors, such as the electrode spacing, have on the electrochemical performance of SMFCs. We also test the relevance that the hydrophilicity of both the anode and the cathode, has on performance. Finally, we investigate on the possibility of using urine to moisturize the soil. Our conclusions provide important guidelines for the design and operation of effective SMFCs.

Index Terms – Soil Microbial Fuel Cell; Bioenergy; Urine; Electrode spacing.

I. INTRODUCTION

The threat of climate change pushes the search for alternative energy sources that minimize carbon pollution. In this context, Microbial Fuel Cells (MFCs) hold great promises. This carbon-neutral, biomass-based technology takes advantages of the action of electroactive microorganisms to directly convert the chemical energy of organic compounds into electrical energy. Particularly interesting are soil microbial fuel cells (SMFCs). In these systems, the soil acts as the electrolyte and as the source of both microorganisms and fuel. SMFCs are characterized by an extremely simple and cost-effective design, with no need for pumping and/or electrolyte replacement. Minimum maintenance is required since the organic matter is naturally provided in the soil by plants, thus allowing long term operations in remote areas. With the aim of optimizing the design of a flat geometry SMFC previously developed by our team [1], we here investigate on the effect that the electrode acid pre-treatment, the electrode distance and the use of a metallic mesh at the cathode have on performance. We also investigate on the use of urine rather than water to moisturize the soil, to define operation conditions that are also suitable for areas characterized by scarce access to water. The SMFCs are compared in terms of electroactive biofilm enrichment and maximum power curves.

II. MATERIALS AND METHODS

A. Materials

All reagents used were purchased of analytical grade from Alfa Aesar and Sigma-Aldrich, unless otherwise specified, and used without further purification. The soil was collected from a maximum depth of 30 cm below the surface around the campus area of the University of Bath. Soil pH (6.44 ± 0.19) and conductivity ($\kappa = 195.2 \pm 23.3 \mu\text{S cm}^{-1}$) were measured by using a Thermo Scientific Orion Star A325 probe. The moisture content expressed as a percentage by mass, W_m (% m/m), calculated according to Eq 1, was 64.01 ± 0.79 %.

$$W_m = \frac{(m_w - m_D)}{(m_w - m_0)} \times 100 \quad (1)$$

where m_w (g) is the mass of the wet sample in the crucible; m_D (g) is the mass of the dried sample in the crucible; m_0 (g) is the mass of the empty crucible.

The organic matter content, 5.26 ± 0.92 % (expressed as a percentage by mass) was estimated with the Loss on Ignition analysis.

B. SMFC designs and operation

Six different SMFCs were tested. Each consisted of graphite felt electrodes (8.5 x 8.5 x 0.7 cm) held in place with nylon screws (Fig. 1). As summarized in Table I, the SMFCs differed for: electrode spacing; electrode acid pretreatment according to [2]; use of a stainless-steel mesh at the cathode; soil moisturizing fluid (synthetic urine and tap water from the lab). No catalyst was used at the cathode.

TABLE I. SMFCs TESTED IN THIS STUDY

SMFC	Electrode spacing cm	Electrode treatment	Mesh	Soil moisturizing electrolyte
SMFC-T	4	Both anode and cathode	No	Tap water
SMFC-A	4	Anode only	No	Tap water
SMFC-0	4	No	No	Tap water
SMFC-2	2	Anode only	No	Tap water
SMFC-U	4	Anode only	No	Urine
SMFC-M	4	Anode only	Yes	Tap water

The SMFCs were fit into PVC containers (20 x 15.5 x 8.5

cm) filled up with soil (Fig. 1E). The anode was buried inside the soil and the cathode was exposed to air. The soil was kept moisturized with either tap water or synthetic urine [3] as specified in Table I. The electrodes were connected to an external resistance of 500 Ω and to a data acquisition system (ADC-24 Pico data logger, Pico Technology, UK), by means of titanium wire (0.25 mm diameter), manually woven through the electrodes. Polarization tests were performed by connecting the SMFCs to a resistance box (Cropico RM6 Decade) and varying the applied resistance. Ohm's law ($I=E/R_{ext}$) was used to calculate the current (I) corresponding to each external resistance (R_{ext}).

During the enrichment stage, the output voltage, E , over time was interpolated with the modified Gompertz model [4]:

$$E = E_{max} \cdot \exp\left(-\exp\left(\frac{\mu_{max} \cdot e}{E_{max}}\right) \cdot (\lambda - t) + 1\right) \quad (2)$$

Where: E_{max} is the maximum cell voltage (V) achievable under close circuit conditions; λ is the lag phase duration (days); e is the Napier's constant (2.71828); μ_{max} is the maximum specific growth rate (d^{-1}).

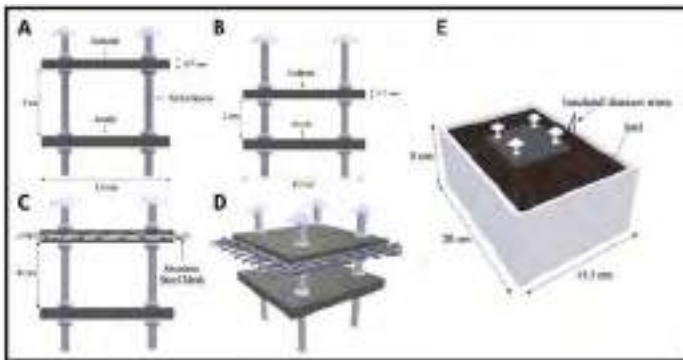


Fig. 1. Several electrode arrangements used in this study. A) large electrode spacing (4 cm); B) short electrode spacing (2 cm); C) and D) mesh configuration; E) experimental set-up.

III. RESULTS

The SMCs were characterized by different lag times, λ (Fig. 2). SMFC-U, SMFC-A and SMFC-2 showed lag times of approximately 4 - 5 days, with a minimum of 4.17 ± 0.58 days for SMFC-U. In all these designs only the anode underwent pre-treatment. SMFC-0 showed both the highest λ (8.25 ± 2.47 days) and the lowest μ_{max} , which was 1.5 times lower than SMFC-A. SMFC-T showed a higher λ than SMFC-A, SMFC-U and SMFC-2. This result suggests that the cathode pre-treatment may hinder the oxidation reduction reaction, due to the electrode soaking in the electrolyte (moisturized soil) that would limit oxygen diffusion. SMFC-0 showed significantly slower biofilm formation, thus reinforcing the importance of anode pre-treatment to increase the electrode surface area and promote bacterial attachment and electron transfer [2].

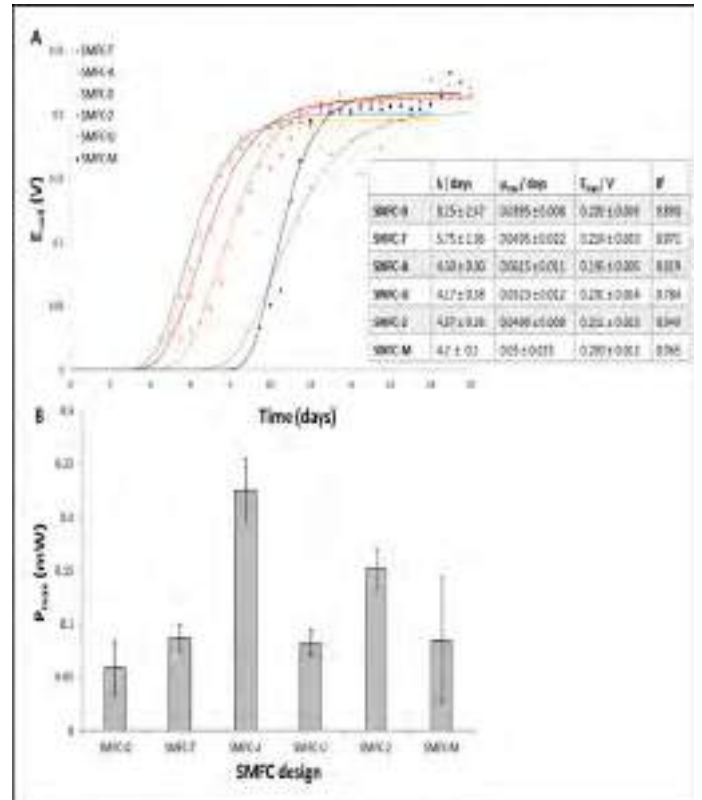


Fig. 2. A) Enrichment of the SMFCs. Data points refer to average experimental data (n=3). Lines and table refer to the interpolated values from the Gompertz model. B) Maximum power obtained from polarization tests (n=3).

In terms of maximum power generated, SMFC-A was the best-performing design, with a P_{max} of 0.203 ± 0.154 mW at a current peak of 0.420 ± 0.288 mA. SMFC-0 showed the worst performance, while the use of a mesh at the cathode posed issues on reproducibility.

IV. CONCLUSION

The different SMFCs tested in this work highlighted the importance of anode treatment to speed up the lag phase during the enrichment phase and reach steady-state conditions. A larger electrode spacing leads to a higher power output by minimizing oxygen diffusion to the anode. Finally, tap water is the preferred electrolyte for moisturizing the soil.

ACKNOWLEDGMENT

This project was funded by the UK Research England, under the Global Challenges Research Fund (GCFR).

REFERENCES

- [1] Castresana, P., et al., *Electrochim. Acta* 298, 2019, pp. 934-942
- [2] Monasterio, S., et al., *Chem. Eng. Sci.*, vol. 198, 2019, pp. 108-116
- [3] Chouler, J., et al., *Electrochim. Acta*, Vol. 192, 2016, pp. 89-98.
- [4] Mateo, S., et al., *Electrochim. Acta*, Vol. 297, 2019, pp. 297-306

INVESTIGATING THE USE OF SOIL MICROBIAL FUEL CELLS FOR SENSING

S. Rengaraj*, J. Wing Kam**, and M. Di Lorenzo*

*Centre for Biosensors, Bioelectronics and Biodevices (C3Bio) and
Department of Chemical Engineering, University of Bath, Bath, BS2 7AY, (UK)

**Aberystwyth University, Aberystwyth, SY23 3EB, (UK)

Abstract - Online monitoring of soil health can enhance land management and agricultural practices. Soil Microbial Fuel Cell (SMFC) is an interesting technological option for this purpose. The current generated by a SMFC is related to the metabolic activity of microorganisms naturally present in soil. This activity is influenced by key factors in the soil, including nutrients levels, pH, moisture and presence of any bioactive compounds. As such, SMFCs can provide real time and on-site feedback on soil quality. Moreover, the technology allows self-powered operations, which facilitate its use in remote areas. In this study, we report an innovative and low-cost SMFC design and test its ability to detect pesticides in soil. The encouraging results demonstrate the great potential of this technology for practical applications.

Index Terms –Biosensor, Endosulfan, Soil health, Soil Microbial Fuel Cells

I. INTRODUCTION

In the context of a growing population and climate change, effective and sustainable land management is key to enhance crop production and safeguard our environment. Soil health is tightly bonded to food security. This link demands for strategic and immediate actions to prevent soil degradation and alleviate food insecurity in the areas where it is most needed (FAO). As such, the development of diagnostic tools capable of monitoring soil health in real time and at site is of high interest to scientists and stakeholders. An interesting target is the redox status of a soil, since it provides information on moisture, nutrient availability, pollutant mobility and microbial diversity. [1] Traditional methods to measure this parameter are discrete and expensive. Microbial Fuel Cell (MFC) technology has been widely investigated for water quality monitoring. [2] The electrochemical processes in MFCs are a direct measure of the metabolic activity of microorganisms at the anode and/or cathode and can be related to the presence of bioactive compounds. [2] MFC biosensors offers several advantages over conventional analytical techniques, such as simplicity of operation, cost-effectiveness and self-powered operation.

In this study, we propose for the first time a cost-effective membrane-less soil microbial fuel cell system (SMFC) as self-powered tool for soil monitoring. We test the system in two different soils and investigate its response to endosulfan.

II. MATERIALS AND METHODS

A. Materials

All reagents were of analytical grade and used without further purification, and purchased from Alfa Aesar and Sigma-Aldrich, unless otherwise specified. The soil used in this work was collected from Aberystwyth Miscanthus Plantation (Institute of Biological, Environmental and Rural Sciences, Aberystwyth University). Two different collection areas for soil were considered, a flooded one and a dry one, here named as Type 1 and Type 2 soil samples respectively.

B. SMFC design

A catalyst-free membrane-less air-cathode SMFC design was used (Fig. 1). The system consists of two rectangular pieces of graphite felt (5 x 5 x 0.7 cm, Online Furnace Services Ltd), held in place with nylon screws (RS components) at a fixed distance of 5 cm. To increase the exposed area of the electrodes, nine holes of 4 mm diameter each, at a distance of ≈ 1 cm from each other, were pierced onto the graphite felt (Fig. 1B). The system was operated in a 500 mL beaker filled with soil for half of its length (Fig. 1C). The anode was depth into the soil, while the cathode was exposed to air. Titanium wire (0.25 mm dia., Alfa Aesar) was used for electrical contacts.

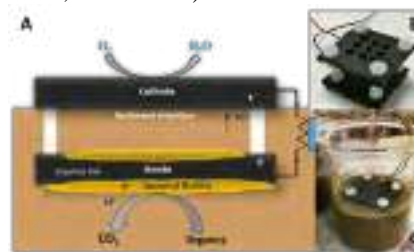


Fig. 1. A) Principle of operation of the Soil Microbial Fuel Cell used in this study. B) Electrode design. C) Experimental set-up.

C. SMFCs operation

During the operation, the anode and the cathode were connected through an external load of 10 k Ω and to a data acquisition system (ADC-24 Pico data logger, Pico technology, UK) to monitor the cell voltage over time. Tap water was added to the soil on a regular basis to keep it moisturized. Care was

taken not to flood the system. Polarisation tests were performed by *in situ* linear sweep voltammetry (LSV) measurements, scanning the cell potential from the open circuit voltage to zero at a scan rate of 5 mV s⁻¹, with a PGSTAT 302 potentiostat (Metrohm-Autolab, The Netherlands). Before the LSV test, the cells were left under open circuit for 2 h. Differential pulse voltammogram (DPV) tests were also performed. For the toxic test, 1mM of endosulfan in water, from a stock solution (25 mM in 10 % DMSO), was added to the soil. Three individual replicates were performed.

D. Microbial analyses

For the microbial analysis, 1 g of soil was dissolved in 10 mL of distilled water. Suspended particles were then allowed to settle, and the resulting supernatant was filtered with 100 µm filter paper. Bacterial colony forming units (CFU) of the resulting sample was assessed with the standard microbial colony plating method. Impedimetric measurements were also performed by using the biosensor recently developed by the team, under testing conditions previously reported. [3]

The soil microbiota was also analyzed via the Automated Phospholipid Fatty Acid (PLFA) Analysis using MIDI's Sherlock PLFA Analysis Software and the Agilent 6890N GC

III. RESULTS

The SMFCs showed a different electrode biofilm enrichment trend according to the type of soil (Fig. 2A). The exponential phase was much shorter (6 days) when the SMFCs were operated in Type 1 soil compared to Type 2 soil (25 days). In the case of Type 1 soil the steady-state voltage was 1.5 lower, 170 ± 10 mV for Type 1 compared to 250 ± 30 for Type 2. The different trend may be attributed to the type of nutrients and microbial population in the two soils. Type 1 soil has been collected in a flooded area. Soils saturated in water have reduced bacterial diversities. [4] Also, high levels of water induce anoxia in the soil, thus providing favourable conditions for fermentative bacterial, such as *Geobacter* sps, which are capable of extracellular electron transfer in MFCs. [5] Indeed, the much shorter exponential phase in the case of Type 1 soil, suggests greater levels of bacteria in the soil readily available to populate the electrode surface. PLFA analyses revealed a biomass content of 234 nmol g⁻¹ for Type 1 soil compared to 200 nmol g⁻¹ for Type 2. In addition to PLFA, both the samples underwent a rapid screening of bacterial concentration. Fig. 2a shows that the charge transfer resistance (R_{ct}) was higher for Type 1 soil, which is a result of more lectin-bacterial cell complex formation and, therefore, is an index of higher bacterial content in the soil sample. Type 1 soil resulted in higher microbial colony forming units of 2800 CFU mL⁻¹ compared to Type 2 (1300 CFU mL⁻¹).

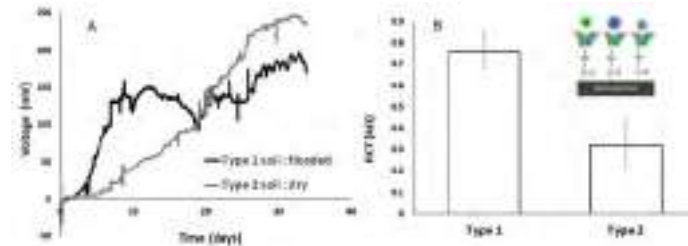


Fig. 2. A) SMFCs enrichment. Data is the average of three replicates with a 30% maximum variation. B) Microbial concentration analysis of the soil sample with an impedimetric biosensor (sensor schematic represented in the insert). Error bars refer to n=3

To investigate the ability of the system to detect pesticides, Type1 soil was spiked with endosufan (Fig 3). Endosulfan is a pesticide extremely toxic to both the aquatic biota and mammals, with a half-life in soil as high as 800 days. [6] The pesticide caused a 102 mV drop in the output voltage. After 3 days, however, the voltage was recovered, and a 13% increase from the initial baseline was observed (Fig 3A). This increase was confirmed by the presence of a redox peak at -0.35 V, that was absent during the voltage drop, which suggests full recovery in the microbial electrocatalytic activity (Fig 3B).

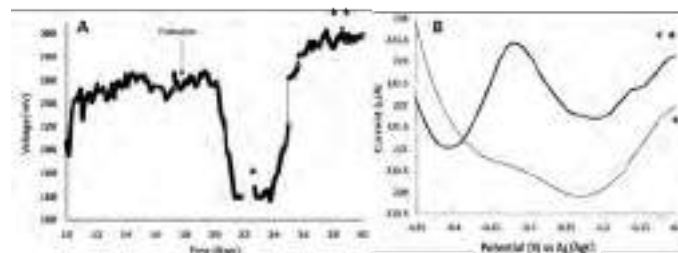


Fig. 3. A) SMFC response to endosulfan addition into the soil. B) DPV tests of the SMFC performed during the points * and ** shown in A.

IV. CONCLUSION

A cost-effective membrane-less SMFC system is reported and investigated as soil sensor. The shape of the exponential phase during enrichment is a function of the microbial content in the soil. The presence of endosulfan affected the output voltage, with a voltage baseline recovery after 3 days. Future work should assess the fate of the pesticide in the soil.

ACKNOWLEDGMENT

Thanks to the Engineering and Physical Sciences Research Council (EPSRC) for funding (EP/N005961/1).

REFERENCES

- [1] Husson, O., Plant Soil, vol. 362, 2013, pp. 389–417
- [2] Chouler, J., Di Lorenzo, M., Biosensors, 2015 vol. 5(3), 2015, pp 450-70
- [3] Rengaraj, S, et al., Sens. Actua.B: Chem., vol 265, 2018, pp. 50-58.
- [4] Randle-Boggis, R. J., et al., Microbiologyopen, vol. 7(1), 2018, e00548
- [5] Nevin, K. P. H., et al., Environ. Microbiol., vol. 10, 2008, pp. 2505-2514
- [6] Kumar, M., Philip, L., J. Hazardous Materials., vol. 136 (2), 2006, pp. 354-364.....

PRELIMINARY DESIGN OF INNOVATIVE LOW EMISSIONS SYSTEMS FOR DIFFERENT MARITIME APPLICATIONS

D. Rattazzi*, M. Rivarolo*, T. Lamberti** and L. Magistri*

*Thermochemical Power Group, University of Genoa, via Montallegro 1, 16145 Genoa, Italy

**H2Boat, Via Magnaghi 3/11, 16129 Genoa, Italy

Abstract - This paper describes a software tool aiming at the preliminary design of production and storage energy systems onboard for different kind of ships. The tool considers different fuels, storage systems and power units, including both traditional (i.e. diesel ICEs) and innovative ones (i.e. fuel cells): the different technologies are compared considering weights, volumes, costs and emissions as decision parameters. Different relevance is given to the parameters according to the application under analysis. In this paper two case studies are presented considering the specific peculiarities of each application, where the innovative solution with PEM Fuel Cells is compared with the state-of-the-art. The first case is a cargo ship that should be refueled replacing the container where the storage system is installed, avoiding the issues related to hydrogen refueling. the second one is a cruise ship operating in Norwegian fjords where zero emissions will be soon required. The best solutions are presented for each case, showing the impact of the relevance parameters on the choice.

Index Terms - PEM fuel cells, marine energy storage, energy systems management, pollutants mitigation

I. INTRODUCTION

A study performed by International Maritime Organization (IMO) reports that from 2007 to 2012 international shipping contributed on average 2.6% of global CO₂ emissions, furthermore a growth in global trades using seaborne transports is foreseen [1]. IMO sets for 2030 the goal of reducing CO₂ emissions from shipping by a minimum of 40% per cargo ton-mile, while for 2050 the reduction is 50% [2]. Therefore, the reduction of pollutant emissions throughout the use of innovative and sustainable technologies clashes with the compliance with safety regulatory requirements. In this context, the introduction of clean technologies for ship propulsion is the focus of the IMO research: PEM Fuel Cells, fueled by hydrogen, are one of the most promising solutions, as they are a zero-emission system [3]. On the other hand, the impact that volumes and weights have in maritime applications cannot be

neglected [4]: since its low energy density, H₂ presents some drawbacks, if compared with diesel oils that are traditionally employed for maritime applications at present day [5]. Finally, the economic impact of the different solutions must be considered as well. Therefore, it is useful to have, in a preliminary design phase, the chance to understand which can be the most suitable and performing solution for energy production onboard.

II. METHODOLOGY

A. Tool description

The authors have developed a tool, HELM, which allows users to choose the best technology, in terms of power and storage energy systems. Maps relating the ship features with input parameters (total power required by the vessel and hours of navigation without docking) have been developed through a detailed market investigation, employing the data provided by industrial partners of author's research group. The tool library includes different fuels (Hydrogen, LNG, Diesel Oil), storage technologies (liquid H₂, compressed H₂, metal hydrides, LNG vessels and diesel oil vessels) and power units (PEM Fuel Cells, micro Gas Turbines, ICEs). The choice of the best solution also depends on the different relevance of the single parameters (weights, volumes, costs, emissions), representing the priority for the kind of ship and the considered application. HELM gives in output the most suitable technology for the scenario considered. The evaluation is given in terms of score for each technology: the best technology obtains the highest score. The total score for each solution is the sum of single scores obtained for the four categories (weight, volumes, costs and emissions). For each category, the score is in a range 1 - 10: the technology with the lowest value (i.e. lowest cost) obtains the maximum score; the other technologies are compared with the best one by using a coefficient X, which is the ratio between the considered

solution and the best choice; a score is given depending on the range of the coefficient X. According to the specific application requirements, a different relevance can be considered for each of the four parameters mentioned above; therefore, the score for each technology is multiplied by the corresponding relevance (i.e. if cost relevance is 2, the maximum score for the cost parameter is 20 points).

B. Case studies

In this section, two case studies are analyzed using HELM. The first case study refers to a cargo ship operating in Baltic Sea. The idea is to develop a low emission ship in compliance with the current normative for onboard energy generation, avoiding the refueling process and its issues. To do that, the storages have to be placed inside standard containers in order to guarantee safe and easy operations during the substitution process. The empty storages will be re-filled in-land, respecting all the already existing normative, making them available for being used on the incoming ships. The considered ship for this application requires a power generation of 2 MW and an entire week period without docking. Considering the peculiarities of this application, the relevance parameters in the tool have been set in order to minimize costs and emissions, without neglecting the impact of volumes and weights. Table 1 reports the scores for the main solutions.

Table 1 Scores for main technologies, Case study 1

	PEMFC + LH2	mGT+LNG	ICE + LNG	ICE + FO
Volume	4	10	12	20
Weight	2	8	10	20
Cost	4	28	32	40
Emission	40	24	18	4
TOTAL	50	70	72	84

The state of the art (ICE+FO), is the best solution nowadays. Considering also the next future, with expected restrictions on pollutant emissions, it is worth to understand the potential of these technologies in this context. The scores detail shows that ICE+FO is the most compact and economic, while the PEMFC represents the most competitive solution from the environmental point of view. Focusing on the application of this case study, the use of 40 ft containers for energy storages (internal volume of 66 m³) will be considered. Table 2 shows the impact of this configuration on the system dimensions.

Table 2 Volume requirements analysis

	PEMFC + LH2	mGT+LNG	ICE + LNG	ICE + FO
Storage system [m ³]	1116	284	267	121
N° of Containers	17	5	5	2
Containers [m ³]	1122	330	330	132

The second case study refers to a medium size cruise ship operating in Norwegian fjords (7MW for 10 hours without docking) [7]. This area is already one of the most severe in terms of pollutant emissions, therefore the use of low or zero emission technologies is fundamental.

Considering these aspects, the main priority for this application is given to pollutant emission minimization,

followed by the volumes. Costs have lower impact because, in this development phase, a possible financial contribution by EU funds can be considered. Impact of weights is very low in this phase. The simulation with HELM of the described scenario gives as output the results showed in Table 3.

Table 3 Scores for the main solutions, Case study 2

	PEMFC + LH2	PEMFC + CH2	ICE + LNG	ICE + FO
Volume	15	3	21	30
Weight	6	5	8	10
Cost	12	12	18	20
Emissions	50	50	22.5	5
TOTAL	83	70	69.5	65

The scores show how the use of PEMFC coupled with hydrogen stored as liquid is the most promising solution. The state of the art solutions are strongly penalized by their pollutant emissions. The use of compressed hydrogen, even if guarantees a zero level if pollutant emissions leads to volumes, due to the low compactness of the storage system. The solutions with PEMFC+LH2 has a storage volume of 239 m³, while the total volume is 328 m³; the use of compressed H₂ leads to a storage system volume of 882 m³ and a total volume of 972 m³.

III. CONCLUSIONS

In this study, a tool developed by authors' research group, has been used to perform a preliminary design of energy systems on board for two different maritime application. The study shows how the peculiarities of each application affect significantly the results. Among all the innovative solutions considered for their low environmental impact, the use of PEMFC with LH₂ storage seems to be the most promising, even if lacks in the current regulation could make its application complicated. In the future, the authors are going to update the tool with more solutions (such as SOFC, methanol storages, etc..) also keeping it updated in accordance with the incoming new normative in terms of maritime pollutant emissions.

REFERENCES

- [1] IMO, Resolution MEPC.213(63), "2012 Guidelines for the development of a ship energy efficiency management plan (SEEMP)" IMO MEPC, Adopted on 2 March 2012.
- [2] "Setting the course to low carbon shipping", ABS, 2019
- [3] Özgü T., Yakaryılmaz A. C., Int.J. of Hydrogen Energy, 2018 (43), 18007-18013.
- [4] Rivarolo M, Rattazzi D, Magistri L, Int. J. of Hydrogen Energy, 43 (2018), 23500-23510.
- [5] Zhang F. et al., Int. J. of Hydrogen Energy, 2016, vol. 41, no 33, p. 14535-14552.
- [6] Rattazzi D., Rivarolo M., Lamberti T., Magistri L., E3S Web Conf. Vol 113, 2019 SUPEHR19, no 02005
- [7] <https://www.windstarcruises.com/yachts/star-pride/overview/>, accessed 30/08/2019.

SIMULATION OF A NOVEL ANODE SUPPORTED DOUBLE-SIDED SOFC

X. Zhang* ,**, M. Espinoza-Andaluz***, T. Li*, Y. Qi** and M. Andersson* ,**

* University of Electronic Science and Technology of China, Sichuan 611731 (China)

** Energy Sciences, Lund University, Lund 22100 (Sweden)

***Escuela Superior Politécnica del Litoral, Guayaquil 90112 (Ecuador)

Abstract – Solid Oxide Fuel Cells (SOFCs) are promising electricity producing devices, since it can convert chemistry energy into electricity directly without any combustion reactions. The traditional SOFC has its own intrinsic drawbacks, such as cracks and delamination due to mismatch of thermal expansion coefficient (TEC) between different components as well as gas leakage due to the sealing problems. Therefore, design a new type of SOFC is important and provide possibilities to solve the above problems.

A novel anode supported symmetrical double-sided cathode SOFC model was built through COMSOL Multiphysics based on the cell developed and tested at Ningbo Institute of Material Technology and Engineering (NIMTE) in China. The model consists of support anode, functional anode, electrolyte and functional cathode layers, which were pasted one by one on both side of support anode. The interconnects mounted on the outside as current collectors.

Index Terms - Solid Oxide Fuel Cells, Double-sided cathode, Electric properties, Thermal stresses

I. NOMENCLATURE

Interface of cathode and electrolyte	ICE
Interface of anode and electrolyte	IAE

II. INTRODUCTION

Solid oxide fuel cells (SOFCs) are promising electricity production devices for its high efficiency, environment friendly and sustainability [1-5]. The electrolyte supported SOFC has applied extensively, but its high operation temperature causing the limited material choices for cell components, besides its power density is lower than anode supported one. Therefore, many research works focused on anode supported SOFC in order to achieve higher power density, efficiency and longer life span.

Mechanical stability of electrode and a rigid sealing properties are closely related to the structure of SOFC. A novel anode supported symmetrical double-sided cathode SOFC model was built through COMSOL Multiphysics based on the cell developed and tested at Ningbo Institute of Material Technology and Engineering (NIMTE) in China [2]. The cell consists of hollow support anode, the active anode, electrolyte, GDC, active cathode, support cathode are pasted one by one on both side. In order to reduce the compute time, we have simplified the model as is show in Figure 1. For instance, the model is symmetrical across xy plane and xz plane, so only quarter of the cell was built. Meanwhile, there is only active cathode and single layer YSZ electrolyte to simplify the model, and this will not affect the research topic. The air is feed in air inlet and will distribute through air channel, which is separated through interconnect ribs as is show in Figure 1. The specific geometry size parameters are showed in Table 1. The materials properties are adapted from the literature. The model solved equations for ion, electron, momentum, gas species and heat transport simultaneously and are coupled to kinetics describing the electrochemical and internal reforming reactions within the electrodes.

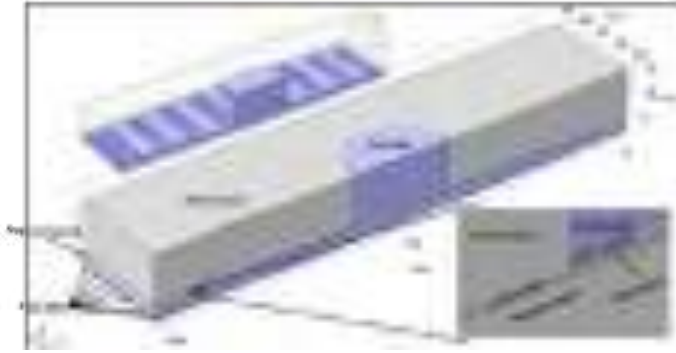


Fig. 1. Schematic diagram of the double-cathode model

TABLE I GEOMETRY SIZE AT DIFFERENT DIRECTION OF EACH LAYER

Components	X [mm]	Y [mm]	Z [mm]
Support anode	102	47	2.5
Active anode		44	0.02
YSZ	86	42	0.008
Active cathode			0.03

III. SIMULATION RESULTS

High electrical efficiencies is of great importance for SOFC, which is related to materials properties, gas feeding rate and mechanical stability. The electron and ionic current density are displayed in Figure 2 and 3. It is found that both current density are mainly distributed under the interconnect ribs away from the air inlet. Further simulation is needed to get the polarization, temperature and thermal stress distribution in the cell.

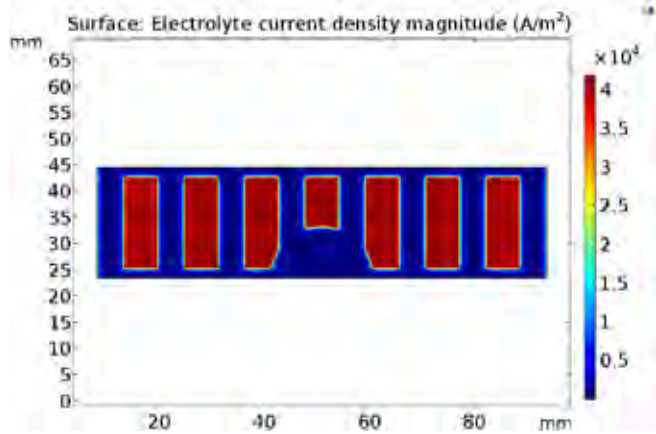


Fig. 3 Ionic current density at the interface of anode and electrolyte.

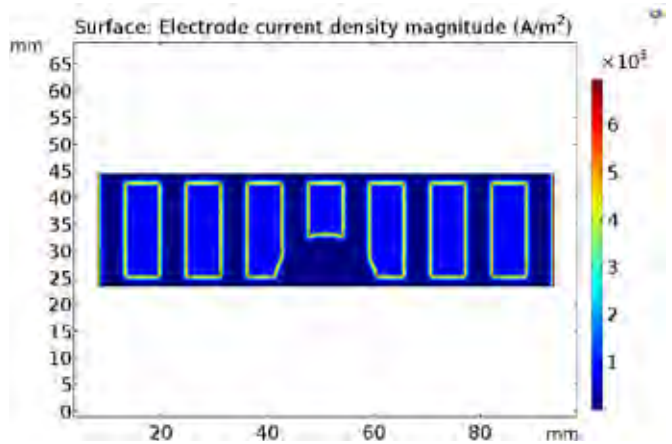


Fig. 2 Electric current density at the interface of cathode and electrolyte

ACKNOWLEDGMENT

The authors would like to acknowledge support from the Chinese Scholarship Council, grant number: 201906070189 and 201706080005 as well as from Åforsk project 17-331.

REFERENCES

- [1] Kendall K. Introduction to SOFCs. In: Kendall K, Kendall M, editors. High-temperature Solid Oxide Fuel Cells for the 21st Century Fundamentals, Design and Applications: Joe hayton; 2015. p. 1-2.
- [2] Liu W, Zou Z, Miao F, Li X, Wang J, Yang J, et al. Anode-Supported Planar Solid Oxide Fuel Cells Based on Double-sided Cathodes. *Energy Technology*. 2019;7:240-4.
- [3] X. Zhang, J. Parbey, G. Yu, T. Li, M. Andersson, *Thermal stress Analysis of Solid Oxide Fuel Cells with Chromium Poisoning Cathodes*, *J Electrochem. Soc.*, 165, F1224-F1231, 2018
- [4] S.B. Beale, U. Reimer, D. Froning, H. Jasak, M. Andersson, J.G. Pharoah, W. Lehnert, *Stability Issues for Fuel Cell Models in the Activation and Concentration Regimes*, *ASME Journal of Electrochemical Energy Conversion and Storage*, JEECS-17-1070,
- [5] H. Paradis, M. Andersson, J. Yuan, B. Sundén, *CFD modeling considering different kinetic models for internal reforming reactions in an anode-supported SOFC*, *J. Fuel Cell Science and Technology*, 8, 031014, 2011

CONJOINT EFFECTS OF CHEMICAL AND MECHANICAL DEGRADATION STRESSORS ON FUEL CELL PFSA MEMBRANES

Mylène Robert, Assma El Kaddouri, Jean-Christophe Perrin, Kévin Mozet,
Jérôme Dillet, Jean-Yves Morel, Stéphane André, Olivier Lottin

Université de Lorraine, CNRS, LEMTA, UMR 7563, Nancy, France

Abstract - To improve the lifetime of proton-exchange membrane (PEM) fuel cells, it is necessary to get a better understanding of the degradation mechanisms of their perfluorosulfonic acid (PFSA) electrolyte. In this work, an investigation on the effects of radical attacks (i.e. Fenton's reagents exposure) was carried out. The results confirmed that the chemical degradation of PFSA depends significantly on hydrogen peroxide (H_2O_2) and iron (Fe^{2+}) concentration and made it possible to optimize the degradation rate. Secondly, a specific custom-made device was developed to examine the impact of coupled chemical and mechanical degradations. The results showed that a cyclic mechanical stress leads to an accelerated chemical decomposition.

Index Terms – Degradation, Durability, PEM fuel cells, PFSA membranes

I. INTRODUCTION

The degradation of perfluorosulfonic acid (PFSA) electrolyte remains one of the main factors limiting proton-exchange membrane (PEM) fuel cells lifetime [1]. During fuel cell (FC) operation, PEM are subjected to aggressive chemical environment and mechanical fatigue. Chemical damages are mostly due to radical attacks leading to the scission of the polymer chains (backbone or/and side chains), while mechanical fatigue results mostly from repeated swelling/shrinkage cycles caused by the membrane water-uptake. To better understand the mechanisms of membrane degradation during fuel cell operation, it is important to discriminate between the effects of chemical and mechanical stresses. Indeed, a few studies have already shown that considered together, they increased the membrane degradation rate [2]–[4].

Fenton's reaction is by far the most common *ex-situ* method to study the chemical degradation of PFSA membranes. This reaction of H_2O_2 with Fe^{2+} forms hydroxyl ($HO\cdot$) and hydroperoxyl ($HOO\cdot$) radicals, also observed during FC operation [5]. This allows to reach a higher chemical degradation rate than in fuel cell, and thus a first – and quick – assessment of membranes durability. However, there is a need for *ex-situ* protocols considering also mechanical constraints. For this purpose, *Kusoglu et al.* developed a compression apparatus to study the effect of mechanical compression on chemical degradation of

Nafion[®] membranes [2] and showed that a static compression accelerates the chemical decomposition of the polymer chains. In our case, the membrane degradation was induced by exposing the membrane simultaneously to a free radical environment and to a cyclic compression. Cyclic compression was implemented to reproduce the mechanical fatigue resulting from the swelling/shrinkage of the membrane during transient FC operation. As a first step, we determined the concentration of Fenton's reagents leading to the maximum fluoride emissions – and thus membrane degradation – without extreme morphological changes such as delamination and/or bubbles formation, which are not observed during or after FC operation. This study was necessary because there was no consensus in the literature on this matter [2], [7]–[9].

II. RESULTS AND DISCUSSIONS

A. Effect of Fenton's reagent concentrations on PFSA membrane chemical degradation

A preliminary study, similar to the work of *Frensch et al.* [6] was performed to assess the effect of Fenton's solutions on Nafion[®] XL – a 27.5 μm thick reinforced membrane – and Nafion[®] NR-211 – 25.4 μm thick, unreinforced, but chemically stabilized membrane – [10].

Prior to each utilization, the membranes were pretreated according to a procedure close to that established by *Xu et al.* [11]. To expose uniformly the samples to the radicals, they were kept completely flat thanks to a (24 cm^2) polycarbonate frame and nylon screws. The chemical degradation was performed 24 hours at 80°C under magnetic stirring. Then, the samples were treated with EDTA- Na_2 to eliminate any residual cationic contaminant, re-acidified, washed, and dried. To evaluate their chemical degradation rate, the remaining Fenton's solutions were analyzed for fluorine concentration using an ion-selective electrode (DX219, Mettler Toledo) and a pH/millivolt meter (SevenCompact S220, Mettler Toledo).

The ferrous ions concentration was varied between 1 to 44 ppm and that of H_2O_2 between 0.2 and 20 %_{vol}. **Figure 1** summarizes the total amount of fluoride ions released with respect to the samples dry weight as functions of

hydrogen peroxide and iron concentrations for Nafion® XL – blue circles – and Nafion® NR-211 – orange circles –.

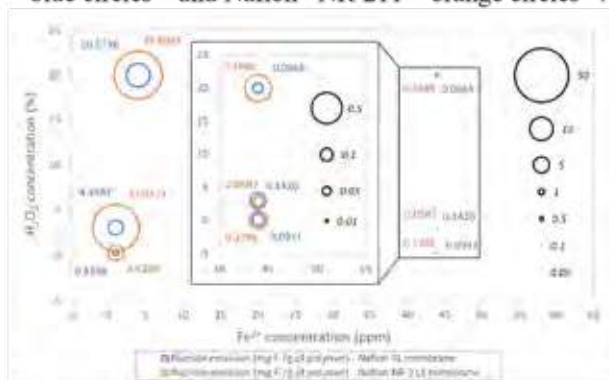


Fig. 1. Fluoride emissions from degraded membrane samples as a functions of Fenton's reagent concentrations. The inset in the middle of the figure shows a close-up on weak fluoride emissions obtained at high iron concentration.

As observed by *Frensch et al.*, low iron concentrations (1-4 ppm) led to much more significant fluoride emissions than high iron concentrations (44 ppm). Moreover, at low iron concentration, the degradation rate depends also significantly on the hydrogen peroxide concentration: up to 13 times higher in the case of Nafion® XL membrane when it was increased from 0.2 %_{vol} to 20 %_{vol}. Nafion® XL membranes were more stable than NR-211 with fluoride emissions 3 to 8 times lower. It must be noted that at high H₂O₂ (\approx 30 %_{vol}) many bubbles with a diameter varying from some micrometers to several millimeters appeared at the surface of both membranes [8]; such morphology evolutions cannot be considered as representative of degradation occurring during FC operation.

B. First results on the impact of coupled chemical and mechanical stresses on PFSA membranes

Coupled mechanical and chemical degradation tests were carried out using a custom-made device that mimics the operating conditions of the fuel cell. For this purpose, a continuous flow of solution was circulated with a flow rate of $0.0503 \text{ cm}^3 \cdot \text{s}^{-1}$ through two thermostated (80°C) half-cells on both sides of the membranes. As a first step, only water and 3 %_{vol} diluted hydrogen peroxide were used. The half-cells were inserted between the clamps of an electromechanical universal testing machine (MTS load frame model 312.21) and the mechanical stress consisted in a sinusoidal constraint between 0 and 5 MPa at 0.1 Hz. The degradation rate of the aged membranes was estimated from fluoride emissions in the circulating solutions, as in the case of chemical degradation. As expected, no – or negligible – fluoride emission was measured in pure water. However, fluoride emissions became much more significant when the diluted H₂O₂ solution was circulated. These results are summarized in **Figure 2**, along with those of purely chemical degradation protocols performed with a similar diluted H₂O₂ solution (3%_{vol}) and – for comparison – with a Fenton's solution.

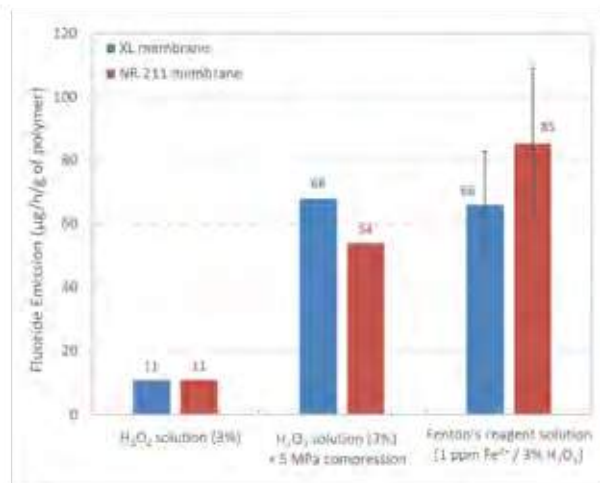


Fig. 2. Fluoride emissions rates for both XL & NR-211 Nafion® membranes under chemical or both chemical and mechanical stresses.

As expected [2], the application of a cyclic compression increased significantly the degradation rate (**Figure 2**): the fluoride emissions were 5 to 7 times higher than under chemical stress only. Indeed, Nafion® XL's degradation rate increases from $11 \text{ µg/h/g}_{\text{Nafion}}$ to $68 \text{ µg/h/g}_{\text{Nafion}}$ when mechanical stress was applied in addition to chemical stress. Likewise, the values increased from 11 to $54 \text{ µg/h/g}_{\text{Nafion}}$ with NR-211. Moreover, with the combination of cyclic compression and H₂O₂ solution exposure, the degradation rates approached the values obtained with a Fenton's reagents exposure.

III. CONCLUSION

An innovative custom-made device that mimics fuel cell operating conditions was developed to better understand the mechanisms of membrane degradation. Our first results show that the combination of chemical and mechanical stresses accelerates significantly the degradation rate. This method and this device constitute thus efficient tools to assess membrane durability.

REFERENCES

- [1] R. Borup *et al.*, *Chem. Rev.*, 107 (10), 3904–3951, 2007.
- [2] A. Kusoglu *et al.*, *ECS Electrochem. Lett.*, 3 (5), F33–F36, 2014.
- [3] S. velan Venkatesan *et al.*, *J. Electrochem. Soc.*, 163 (7), F637–F643, 2016.
- [4] V. M. Ehlinger *et al.*, 166 (7), F3255–F3267, 2019.
- [5] L. Lin *et al.*, *J. Power Sources*, 233 98–103, 2013.
- [6] S. H. Frensch *et al.*, *J. Power Sources*, 420, 54–62, 2019.
- [7] J. Healy *et al.*, *Fuel Cells*, 5 (2), 302–308, 2005.
- [8] S. Mu *et al.*, *J. Appl. Polym. Sci.*, 129 (3), 1586–1592, 2013.
- [9] T. Kinumoto *et al.*, *J. Power Sources*, 158 (2), 1222–1228, 2006.
- [10] W. G. Grot, *Macromolecular Symposia*, 82 (1), 161–172, 1994.
- [11] F. Xu *et al.*, *Fuel Cells*, 5 (3), 398–405, 2005.

PRESSURE GRADIENT METHOD TO RESOLVE WATER FLOODING IN PEMFC

Ajit Bhambure*, Mahesh Vaze **

* Department of Mechanical Engineering, Birla Institute of
Technology and Science, Pilani, Hyderabad Campus, (India)

** Indian Corporate Research Centre, ABB Ability Innovation Centre,
Bangalore, (India)

Abstract - PEMFCs are very popular for the transport and portable applications due to their several merits over other fuel cell configurations. Research in past years was focused on the flow field developments in PEMFC and still, it is open-ended choice for researcher to model the flow field. Water management in PEMFC is being the central issue of study for the researchers. Flow field development and water management need to be addressed for better performance of PEMFC. We developed a new approach for water management and water removal from the gas diffusion layer (GDL). The study is focused on creating a pressure gradient along the flow channel and GDL. The water from GDL is removed due to pressure difference. Flow analysis of developed flow field for water management in PEMFC. The transient simulation results showed promising results by removing 90% of the water from the flow channel and GDL within 3 minutes.

Keywords: PEMFC, water flooding, pressure gradient

I. INTRODUCTION

Proton Exchange Membrane Fuel Cell (PEMFC) uses hydrogen and oxygen to produce clean electricity and by-products like heat and water [1]. Working principle involves the flow of reactants to the catalysts through GDL, electrochemical reactions at catalysts, the flow of ions and electrons through the separate path, and finally the combination of electrons, ions, and oxygen that produces water at the cathode side. Water accumulates at the cathode side, leads to significant water concentration difference. This excess water results in the formation of water films or water patches at cathode catalyst and GDL. Cathode flooded with water and starts resisting air diffusion through GDL, which further decreases air (or O₂) mass diffusion rate for reaction to happen. The decrease in reaction rate results in a drastic fall in power output and fuel cell efficiency. This phenomenon generally observed at high current density.

II. PRESSURE GRADIENT APPROACH TO AVOID WATER FLOODING

Among the various methods to resolve water flooding issue, a pressure gradient is simplest. The effect of an obstacle placed in the flow channels causes the variation in pressure distribution in the channel [2]. They reported the effect of obstacle placed near the exit of channels. Their results showed the improvement in electrochemical reaction and high current densities are obtained at relatively higher cell voltage. Current density improvement was also reported by Ahmadi *et al.* [3]. The effect of inverted trapezoidal channel geometry was studied for different dimensions for optimization. Also, effect of convergent flow along the length of the channel was considered and current density improvement observed due to increased velocity of reactants.

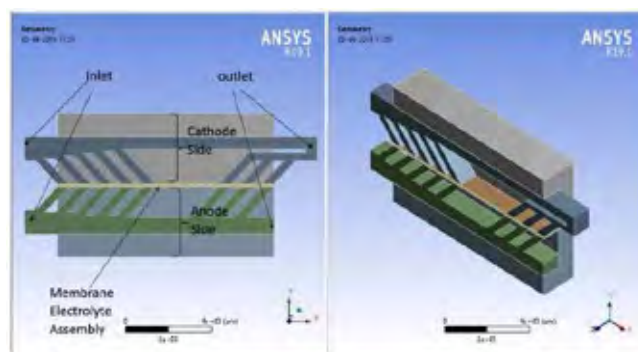


Figure 1 3D Model for pressure gradient flow field

The present study is focused on the design of the flow field to solve the water accumulation issues in GDL. The water flooding in cathode GDL can be avoided by creating a directional pressure gradient in GDL. This can be achieved by creating high-pressure reign near inlet and creating low pressure or suction pressure near the outlet, especially inside the gas diffusion layer.

Figure 1 shows an innovative design of flow channels. Subchannels connect the main channel to the membrane electrolyte assembly. Sub-channels at inlet reign divert flow from the main channel to gas diffusion layer at an angle. The flow pattern is designed in such a way that when air flows through the main channel, near the exit it creates negative pressure in returning subchannels which pulls the accumulated water from GDL.

III. MATHEMATICAL MODELLING

For the current study, only cathode channel, GDL and cathode side catalyst were considered as computational domain. Our model assumes (1) Flow is laminar, (2) Water and air mixture follow ideal gas laws, (3) To analyze the worst possible case, catalyst layer and GDLs were assumed to be flooded completely, and, (4) Porosity of GDL and catalyst layer was assumed to be isotropic. For this study transient simulation were modelled with the help of finite volume method. Mesh sensitivity analysis was carried considering the pressure drop as mesh independent parameter and further simulations were performed on this mesh.

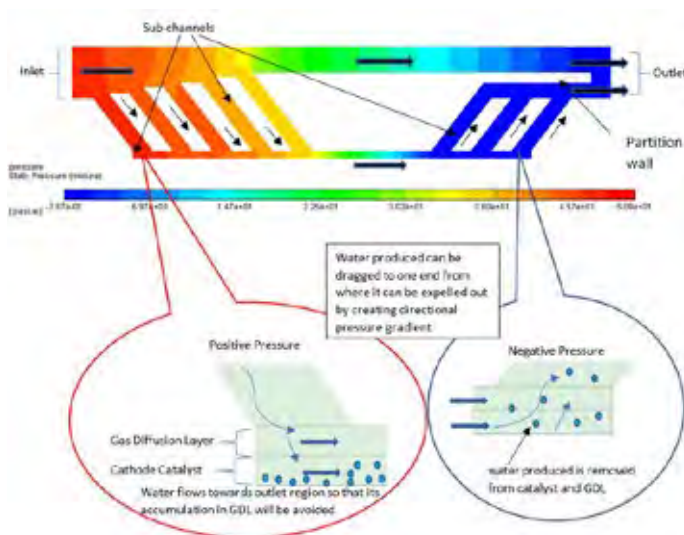


Figure 2 Physics of water removal from GDL on cathode side

IV. RESULTS AND DISCUSSIONS

Fuel cell modelling is a complex task and holistic modelling of it requires careful consideration of many parameters. In order to simplify the complex fuel cell modelling, we carried out the flow investigation assuming two-phase flows and the geometrical parameters.

Figure 2 shows the pressure distribution in the cathode side channel and gas diffusion layer. As the flow enters in, part of the flow is diverted to gas diffusion layer through subchannels and remaining part of the flow leaves channel through the outlet.

To check the performance for the worst condition, it was considered that GDL and catalyst are completely flooded with water. Figure 3 shows the water volume fractions with respect to

time. It is observed that water started to flow from GDL and catalyst towards the exit of the channel. The transient response of water removal in gas diffusion layer shows that accumulated water can be removed successfully within 2 to 3 minutes. Some water accumulation in outlet reign is observed because of high flow resistance in outlet reign.

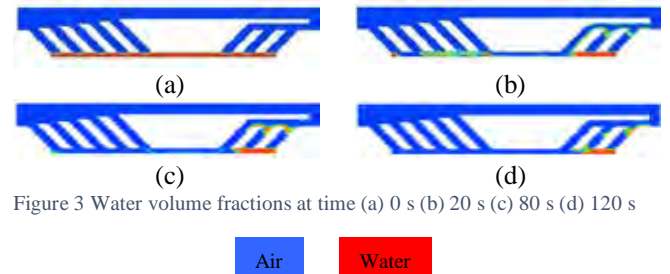


Figure 3 Water volume fractions at time (a) 0 s (b) 20 s (c) 80 s (d) 120 s

V. CONCLUSION

The flow analysis of pressure gradient method in PEMFCs for water management was successfully studied. The transient simulation results showed that within 3 minutes of the time 90% of the water is removed from GDL. Water accumulated in GDL near the channel inlet area is removed faster, while water near the outlet channel takes little more time. This is because reactants and water try to flow through minimum flow resistant area. Thus, some part of the accumulated water near the outlet remains accumulated and get removed slowly. Presented simulation work describes that the pressure gradient approach and the new design of the flow channel worked successfully and helped in removing the water from GDL. Further investigation with the full PEMFC model will be the future task.

REFERENCES

- [1] M. Vaze and M. Kajava, "The Fuel Cell: A Green Powerhouse," *ABB Review*, vol. Quarter 3, pp. 60-68, 2019.
- [2] M. Bilgili, M. Bosomoiu and G. Tsotridis, "Gas flow field with obstacles for PEM fuel cells at different operating conditions," *International Journal of Hydrogen Energy*, vol. 40, no. 5, pp. 2303-2311, 2015.
- [3] N. Ahmadi, S. Rezazadeh, A. Dadvand and I. Mirzaee, "Study of the Effect of Gas Channels Geometry on the Performance of Polymer Electrolyte Membrane Fuel Cell," *Periodica Polytechnica*, vol. 62, pp. 97-105, 2018.

PARAMETER SENSITIVITY ANALYSIS OF A THERMODYNAMICALLY CONSISTENT ELECTROCHEMICAL PEMFC MODEL FOR VIRTUAL OBSERVERS

A. Kravos*, D. Ritzberger**, G. Tavčar*, C. Hametner***, S. Jakubek** and T. Katrašnik*

* Faculty of Mechanical Engineering, University of Ljubljana, Aškerčeva 6, (Slovenia)

**Institute of Mechanics and Mechatronics, TU Wien, Getreidemarkt 9, (Austria)

***CD Laboratory for Innovative Control and Monitoring of Automotive Powertrain Systems, TU Wien, Getreidemarkt 9, (Austria)

Abstract - The reduction and prevention of degradation effects of proton exchange membrane fuel cells (PEMFC) calls for precise on-line monitoring and control tools such as coupled virtual observers. To present significant progress in the area of computationally fast electrochemical models used in observer applications, this contribution presents a zero-dimensional thermodynamically consistent electrochemical model for PEMFC performance modelling and control and its extension with a simplified one-dimensional model for the transport of gaseous species through the gas diffusion layer (GDL). Additionally, the presented contribution features the determination of an optimal set of calibration parameters and consequential model reductions, originating from mathematical and physical rationale, which is further supported by a parameter sensitivity analysis. Owing to the mechanistic basis of the model, the calibration parameters of an advanced observer model exhibit direct correlation with the state of health parameters of the PEMFC.

Index Terms - Electrochemical PEMFC performance model, Observers, Parameter sensitivity, Reduced dimensionality models.

I. INTRODUCTION

PEMFC are emerging as a feasible zero tank-to-wheel energy conversion technology for use in transport applications. Reduction and prevention of degradation effects of PEMFC and their influence on the remaining useful life, while retaining high performance of the PEMFC, are considered to be significant challenges towards their wider market adoption. Tackling these challenges under highly dynamic operations calls for precise on-line monitoring and control tools such as coupled virtual observers. Observer models are characterized by a low computational effort, good extrapolation capabilities and are easy to parametrize. As demand on low computational effort is obvious for on-line applications, good extrapolation capabilities significantly enhance applicability and accuracy of the observer model as they can be parametrized on small data sets, while still

yielding high fidelity outputs in a larger operating region of a PEMFC. To present significant progress in the addressed area of computationally fast electrochemical models used in observer applications, this contribution presents an innovative electrochemical model for PEMFC performance modelling and control originating from thermodynamically exact zero-dimensional derivation.

II. ELECTROCHEMICAL MODEL

The model is based on mathematical equivalent of a Butler-Volmer equation with the sinus hyperbolicus term, which results in an invertible expression valid for all current density regions, while enabling a thermodynamically consistent treatment of forward and backward reactions for both the anode and the cathode side. In addition, zero-dimensional thermodynamically consistent fuel cell (TC FC) electrochemical model is extended with a simplified one-dimensional approach of accommodating the diffusive transport of species in the GDL. For the sake of brevity only functional dependence of FC potential on model calibration parameters is given, which can be written as:

$$U = U_{OCV_c}(k_{oxc}, k_{rdc}, CD_c) + \eta_c(E0_c, CD_c) - IR - U_{OCV_a}(k_{oxa}, k_{rda}, CD_a) - \eta_a(E0_a, CD_a), \quad (1)$$

where U_{OCV_c} and U_{OCV_a} are terms describing open circuit voltage on the cathode and anode side, η_c and η_a overvoltage on cathode and anode side respectively and I net current of the FC. Set of 9 calibration parameters consists of $E0_c$ and $E0_a$ which describe activation energies on cathode and anode side, CD_c and CD_a are combined diffusivity parameters including geometric data of GDL and effective diffusivity, R is combined resistivity parameter, k_{oxc} , k_{rdc} and k_{oxa} , k_{rda} are cathodic and anodic reaction rates of oxidation and reduction.

III. PARAMETER SENSITIVITY ANALYSIS

A high level of accuracy, extrapolation capabilities and robustness of the model inherently arises from a balance between adequate modeling basis and identifiability as well as determination of model calibration parameters. Therefore, to analyze ease of parametrization, presented contribution features determination of an optimal set of calibration parameters originating from mathematical and physical rationale, which is further supported with a parameter sensitivity analysis. The latter was performed via analysis of the calibration parameter values obtained in a Monte Carlo like simulation procedure that included a genetic algorithm. To test this aspect of the model, a genetic optimization algorithm (Matlab - *ga*) was run for single and multiple polarization curves 500 times with 1000 generations each with a population size of 200 and InitialPopulationRange determined as 0.20. The initial vector θ consisted of an already optimized set of parameters obtained from a calibration procedure on the TC FC electrochemical model with the initial 9 calibration parameters. In this kind of analysis, each individual parameter has a certain amount of spread based on which probability distribution can be obtained as shown in Fig. 1.

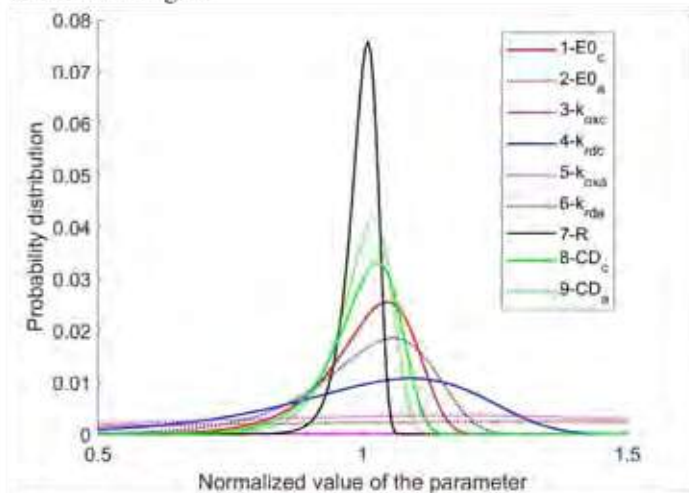


Fig. 1. Probability distribution of the normalized value of calibration parameters of TC FC electrochemical model on the interval [0.5, 1.5] for original set of 9 calibration parameters.

Theoretically speaking, a lower variance of individual parameter distribution is directly correlated with the possibility of its unique determination on the used data set. From Fig. 1 it can be seen that $E0_c, k_{rdc}, R, CD_c, CD_a$ can be uniquely determined with high probability, whereas probability of unique determination is much lower in the case of $E0_a, k_{oxc}, k_{rda}, k_{oxa}$, which exhibit a much higher variance.

In addition, it is important to assess capability of unique determination of calibration parameters. Based on the mathematical assessment of dependencies of calibration parameters with Fisher information matrix analysis, two pairs of dependent calibration parameters are obtained (k_{oxc}, k_{rdc} and k_{oxa}, k_{rda}). To successfully reduce the set of calibration parameters and enhance their identifiability replacements of k_{oxc}

and k_{rdc} with a lumped parameter K_c and k_{oxa} and k_{rda} with a lumped parameter K_a are performed. Consequentially, functional dependency of FC potential with 7 parameters can be written as

$$U = U_{ocv_c}(K_c, CD_c) + \eta_c(E0_c, CD_c) - IR - U_{ocv_a}(K_a, CD_a) - \eta_a(E0_a, CD_a), \quad (2)$$

Results of parameters sensitivity analysis for reduced set of calibration parameters is presented in Fig. 2.

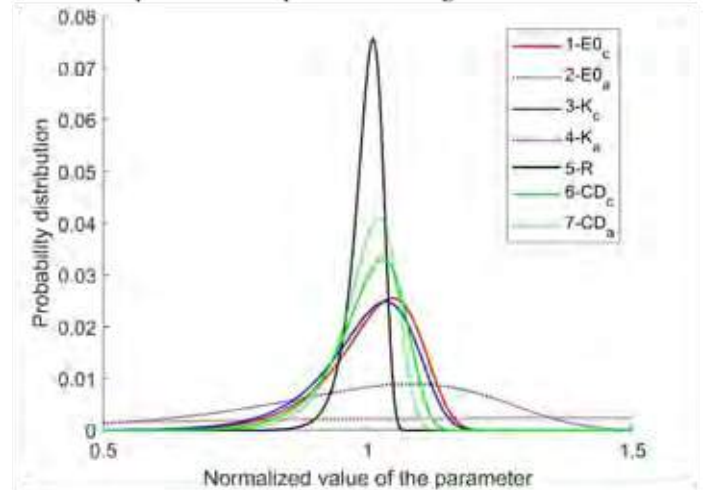


Fig. 2. Probability distribution of the normalized value of calibration parameters of TC FC electrochemical model on the interval [0.5, 1.5] for reduced set of 7 calibration parameters.

It can be seen that probability distributions of lumped calibration parameters K_c and K_a have much lower covariance, which inherently means, that they can be uniquely determined with high probability, thus confirming reasonableness of the proposed reduction. Due to the smaller set of calibration parameters the reduced model is easier to parametrize and less computationally demanding.

IV. CONCLUSION

Newly devised framework enables determining an optimal set of calibration parameters of a TC FC electrochemical model for virtual observers. Application of this approach enables enhanced identifiability of calibration parameters leading to improved robustness of the TC FC electrochemical model. In addition, it allows for parametrization of a model on a small calibration data set within shorter computational times, while retaining high generalization and extrapolation capabilities when modeling operational points outside the calibrated variation space of parameters. Newly devised framework for determining an optimal set of calibration parameters positions the proposed modelling framework as a beyond state-of-the-art model for virtual observers.

ACKNOWLEDGMENT

The research is partially funded by the Slovenian Research Agency (research core funding No. P2-0401), by the CD Laboratory for Innovative Control and Monitoring of Automotive Powertrain Systems and by the Austrian Research Promotion Agency (research project no. 854867: SoH4PEM).

LIFE CYCLE ASSESSMENT OF SYNTHETIC NATURAL GAS PRODUCTION FROM DIFFERENT CO₂ SOURCES: A CRADLE-TO-GATE STUDY

E. Bargiacchi* and U. Desideri*

*University of Pisa, Department of Energy, Systems, Territory and Constructions Engineering (DESTeC),
Largo Lucio Lazzarino 1, 56122, Pisa (Italy)

Abstract - Fuel production from hydrogen and carbon dioxide looks an attractive solution as a long-term storage of electric energy and as a temporary storage of carbon dioxide. A large variety of CO₂ sources are suitable for Carbon Capture Utilization (CCU), and the process energy intensity depends on the separation technology and, ultimately, on the CO₂ concentration in the flue gas. Since the carbon capture process emits more CO₂ than the expected demand for CO₂ utilization, the most sustainable CO₂ sources must be selected. This work aims at modeling a Power-to-Gas (PtG) plant and assessing the most suitable carbon sources from a Life Cycle Assessment (LCA) perspective. The PtG plant is supplied by electricity from a 2030 scenario for Italian electricity generation. The plant impacts are assessed using data from the Ecoinvent database version 3.5, for different CO₂ sources (e.g., air, cement, iron and steel plants).

Index Terms - Carbon Capture Utilization, Energy Storage, Life Cycle Assessment, Power-to-Gas.

I. NOMENCLATURE

AEL=Alkaline Electrolysis; CCU=Carbon Capture Utilization; DAC=Direct Air Capture; LCA=Life Cycle Assessment; PEMEL=Proton Exchange Membrane Electrolysis; PtH=Power to Hydrogen; PtG=Power to Gas; SNG=Synthetic Natural Gas.

II. INTRODUCTION

The increasing penetration of renewable energy in the energy mix demands new technologies for energy storage. For long-term storage (weekly to seasonal), PtG is regarded as one of the most promising technologies for its potential of storing large amounts of energy into an easily transportable chemical vector. In order to verify the sustainability of the proposed solution, it is crucial to assess its impacts on broad boundaries, under several impact categories and different inputs and system architecture (e.g., electricity generation mix, carbon separation technology). In this context, Assen et al. [1] identified and ranked several carbon sources which could serve as CO₂ utilization in Europe on the basis of the marginal CO₂ emissions. In the framework of LCA, Zhang et al. [2] compared

different PtH and PtG technologies using the current Swiss energy mix and for a few CCU technologies. On the wake of these studies, the paper aims at assessing PtG impacts from an LCA perspective for a broad spectrum of CCU technologies and for a 2030 electricity generation mix (the Italian 2030 electricity mix was chosen as a case study). Both CO₂ point sources and DAC were included in the study.

III. METHODOLOGY

In this work, an LCA methodology was applied, according to the ISO 14040 and ISO 14044 guidelines [3,4]. SimaPro version 8.5.2.0 was used as software with Ecoinvent version 3.5 database coupled with literature data, as described below.

A. Assumptions and study boundaries

The system boundaries include all the steps for SNG production from water and a point source (or air), as visualized in Fig. 1. All conversion processes (electrolyzer, CCU plant, methanator and compression steps) are covered. The SNG end-use scenario is out of the scope of the present work.

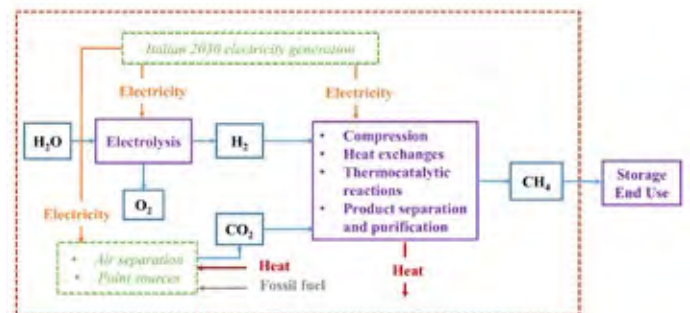


Fig. 1. Study boundaries

B. Power-to-Gas plant layout

The methanation plant was developed in Aspen Plus® environment [5]. Methanation is carried out in a fixed-bed reactor at 300°C and 60 bar to achieve a high purity SNG.

C. Life Cycle Inventory (LCI) inputs

The data used in the present study included both data from

Ecoinvent version 3.5 database and data from literature and assumptions based on engineering practice for electricity generation, electrolysis and concerning carbon dioxide sources.

- **Electricity generation**

Besides supplying the electrolyzer, electricity is used to power the feed gases compressors and the carbon capture plant. In the present study the supply electricity was assumed from the Italian generation mix in the 2030 scenario [6] (see Fig. 2). Where only aggregated data were provided, the single technology installed power was calculated keeping the same current proportions.

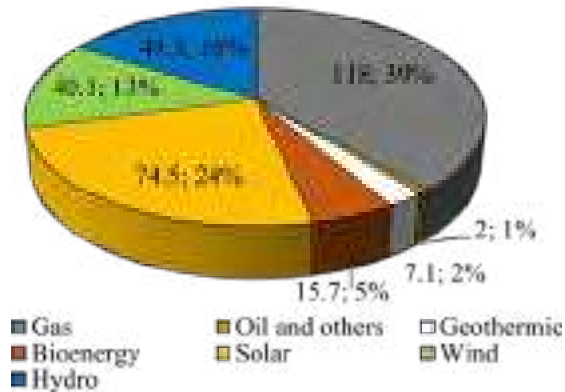


Fig. 2. Italian energy mix for electricity generation (scenario 2030) in TWh (adapted from [6])

- **Electrolysis**

Electrolysis electric consumption was assumed 4.5 kWh/Nm³, a typical value for AEL and PEMEL [7].

- **Carbon Dioxide Sources**

CO₂ emissions data were taken from Assen et. al [1], who built a database for CO₂ emissions of individual facilities in Europe, including average consumptions for DAC.

IV. RESULTS AND DISCUSSION

The impacts of synthetic natural gas production from different CO₂ sources were calculated (see Fig. 3). The plants with the CO₂ captured from hydrogen production plants and integrated pulp and paper mills result the most sustainable solutions in terms of all the indicators. Separating CO₂ from cement plant is the most pollutant process for global warming, ozone formation, fine particulate matter formation, terrestrial acidification, freshwater and marine ecotoxicity, human toxicity. The high impacts are due to the use of coal. Under the current assumptions for DAC technologies, separating CO₂ from air results the most pollutant in terms of stratospheric ozone depletion, mineral resource scarcity and fossil resource scarcity due to the elevated amount of natural gas required by the current technologies employed for air separation. CO₂ separation from refineries and steam cracker, instead, reports the highest impacts on terrestrial ecotoxicity and land use due to the high amount of heat required by the process; these impacts can be mainly attributed to light fuel and heavy oil and to wood chips utilization for heat production, namely. To

improve the graph readability, only some of the aforementioned indicators are reported in Fig.3.

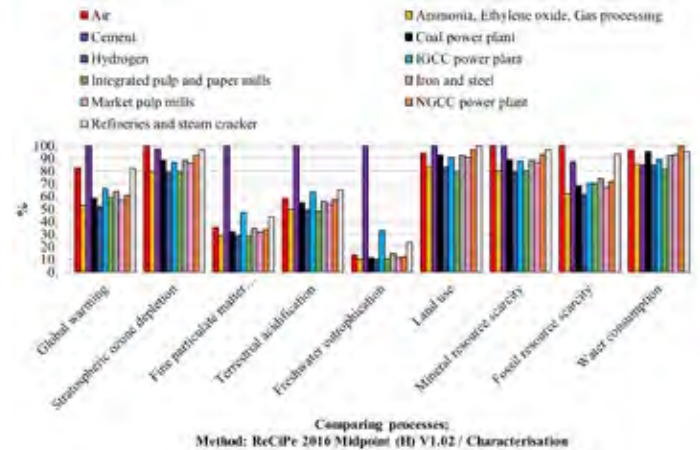


Fig. 3. Impact assessment for a PtG plant with different CO₂ technologies

V. CONCLUSIONS

In this work the impacts of a PtG plant in a future scenario for electricity generation with different CO₂ separation technologies from point sources as well as from DAC were assessed. The most sustainable CO₂ sources are hydrogen production plants and integrated pulp and paper mills, while CO₂ separation from DAC and cement plants proved to be critical for their heavy use of natural gas and coal.

REFERENCES

- [1] Assen N., Muller L. J., Steingrube A., Voll P. and Bardow A., Selecting CO₂ Sources for CO₂ Utilization by Environmental-Merit-Order Curves, Environmental Science and Technology, Volume 50 Issue 3, 2016, Pages 1093-1101.
- [2] Zhang X., Bauer C., Mutel C. L., Volkart K., Life Cycle Assessment of Power-to-Gas: Approaches, system variations and their environmental implications, Applied Energy, Volume 190, 2017, Pages 326-338.
- [3] ISO. 14040 Environmental management - Life cycle assessment - Principles and framework. 2nd ed. Switzerland 2006.
- [4] ISO. 14044 Environmental Management - Life Cycle Assessment - Requirements and Guidelines; 2006.
- [5] Bargiacchi E., Antonelli M., Desideri U., A comparative assessment of Power-to-Fuel production pathways, Energy, Volume 183, 2019, Pages 1253-1265.
- [6] Italian Ministry of Economic Development, Proposta di Piano Nazionale Integrato per l'Energia e il Clima (2018) 238. URL https://www.mise.gov.it/images/stories/documenti/Proposta_a_di_Piano_Nazionale_Integrato_per_Energia_e_il_Clima_Italiano.pdf. Last accessed: 04/09/2018
- [7] Bhandari R., Trudewind C. A., Zapp P. Life cycle assessment of hydrogen production via electrolysis – a review, Journal of Cleaner Production, Volume 85, 2014, Pages 151-163.

INVESTIGATION OF MOLDING PARAMETERS ON GRAPHITE/EPOXY COMPOSITE-BASED BIPOLAR PLATES

F. Roncaglia,^a A. Di Bona,^b R. Biagi,^c M. Romagnoli,^d
D. DeGrandis,^e and A. Mucci^a

^a Dip. di Scienze Chimiche e Geologiche, UniMORE, Via Campi 103, 41125 Modena (Italy)

^b CNR - Istituto Nanoscienze - Centro S3, via Campi 213/A, 41125 Modena (Italy)

^c Dip. di Scienze Fisiche, Informatiche e Matematiche, UniMORE, via Campi 213/A, 41125 Modena (Italy)

^d Dip. di Ingegneria "Enzo Ferrari", UniMORE, via Vivarelli 10, 41125 Modena (Italy)

^e Graf S.p.A., via Galilei 32/36, 41015 Nonantola (MO) (Italy)

Abstract - In order to obtain a material suitable for manufacturing bipolar plates for PEM Fuel Cells the effect of molding parameters (pressure, temperature and time), relative to a graphite/epoxy composite of fixed composition, were studied and modeled by means of a two-level full factorial Design Of Experiment approach. In-plane conductivity and mechanical strength were the dependent variables.

Index Terms – Bipolar plates, graphite/epoxy composites, PEM Fuel Cells, conductivity.

I. INTRODUCTION

Bipolar plates (BP) are important parts of PEMFCs which account for ~ 30% of the stack cost [1]. They are commonly composed of pure graphite, metals or metal alloys but recently, in order to reduce weight and/or manufacturing costs, composite materials based on graphite powder and polymeric resins are emerging as a main technology.

To work as BP, the composite must display high mechanical strength, high thermal and electrical conductivities, corrosion resistance, low gas permeability and density. Such characteristics may be obtained with a proper choice of starting materials and forming conditions. Recently we developed a simple yet promising graphite/epoxy composite featuring 90 wt% of commercial graphite, able to meet the electrical characteristics required by US Department of Energy (> 100 S/cm).

In this work, the effect of moulding parameters (pressure, temperature and time) measured using a custom-made pressing machine (Fig. 1) were studied by means of a two-level full factorial Design Of Experiment (DOE) approach.

II. MATERIALS AND METHODS

A. Wet mixing

The components (graphite, secondary modifiers, epoxy resin and polyamine hardener) were suspended in acetone and mixed using a magnetic stirrer. The mixture was vacuum dried and the wet powder so obtained was directly poured inside the pressing-machine's mould.



Fig. 1. Pressing machine (Graf S.p.A.)

B. Molding

Mould temperature (r.t. - 150 °C), applied force (up to 96 kN) and time were managed and recorded by a software via an interfaced PC.

C. Electrical and mechanical characterizations

In-plane conductivity was measured by a four-point probe connected with a Keithley 2400 digital source meter. The mechanical strength was evaluated measuring the Flexural modulus in a 3-point test.

D. Design Of Experiment (DOE)

The data were statistically analyzed using the software Design Expert 7.1.6.

III. RESULTS

The independent variables studied were: forming pressure, forming time and temperature. In-plane conductivity and mechanical strength were the dependent variables. Pressure and temperature were the ones used in the mould, the time is the residence time of the material in the mould under the set pressure and temperature. In Table I the factors and runs for the DOE are shown (mean value of each sample, prepared in double). Statistical data analysis provide a mathematical model for each dependent variable.

TABLE I
TWO LEVEL FULL-FACTORIAL DESIGN USED IN THE EXPERIMENTATION

Sample no.	Pressure (MPa)	Temperature (°C)	Time (h)
1	3	60	1
2	3	80	2
3	30	80	2
4	30	60	2
5	30	60	1
6	30	80	1
7	15	80	2
8	15	80	1

The in-plane conductivity is influenced by all the three considered parameters. Less of the 10% of variability could be explained with other, not controlled, parameters. No interaction between the considered min variables was found out. The model (1) describes the effect of the three independent variables on in-plane conductivity (σ), where P is the pressure in MPa, T the Temperature in °C and t the time in hours. In Fig.2 the 3D plot.

$$\sigma = -157.91 + 1.08 P + 2.95 T + 23.30 t \quad (1)$$

In-plane conductivity is improved by high values of pressure, temperature and time. An absolute maximum is not observable in the analysed ranges, so it seems possible obtain higher σ values considering higher values of the independent variables.

The flexural modulus depends by the three main independent variables, but it is also influenced by synergistic interactions between the considered independent variables. In Fig.3 the 3D plot.

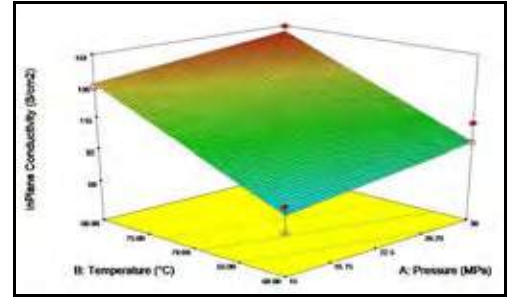


Fig. 2. 3D plot of the in-plane conductivity vs P, T with (t = 2 h)

A plateau is reached at the highest temperature, but at the lowest of pressure and time. Also for this model, less of the 10% of variability could be explained with other, not controlled, parameters.

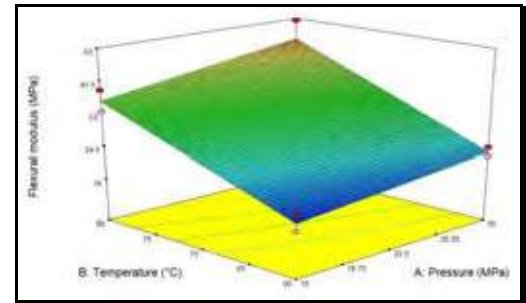


Fig. 3. 3D plot of the flexural modulus vs P, T with (t = 1 h)

IV. CONCLUSION

The best conductivity, 160 S/cm, was obtained with a temperature of 80 °C, a pressure of 30 MPa applied for 2h. The best flexural modulus, 49 MPa was got with a temperature of 80 °C, a pressure of 30 MPa applied for 1h. The in-plane conductivity is influenced only by the main parameters while the mechanical strength is determined also by synergistic interactions between the considered independent variables.

The best compromise, considering the conductivity as the most important parameter and the mechanical resistance always at high value, is the setting for the best conductivity.

ACKNOWLEDGMENT

The authors are thankful to Fondazione CRMO for funding the CARCOM project (grant LINEAFCRM2019FAR INTERDMUCCI).

REFERENCES

- [1] J. P. Kopasz, T. G. Benjamin, Argonne National Laboratory - 2017 Bipolar Plate Workshop Report, <https://publications.anl.gov/anlpubs/2017/11/137641.pdf>

EXPERIMENTAL CHARACTERIZATION OF POLYMER ELECTROLYTE MEMBRANE FUEL CELLS WITH LOW PLATINUM LOADING OPERATED UNDER DRY GAS FEED

A. Baricci*, H. Yu**, D. Croci***, A. Palmieri***, Z.
Zeng**, R. Ouymet**, G. Picciotti***, R. Maric** and A.
Casalegno*

*Politecnico di Milano Dipartimento di Energia, via Lambruschini 4
20156 Milano (Italy)

**Center for Clean Energy Engineering, University of Connecticut,
44 Weaver Road, Storrs, CT, 06269-5233 (U.S.A.)

***Eldor Corporation, via Don Paolo Berra, 18
22030 Orsenigo (Italy)

Abstract - Water management is a key feature for the efficient operation of polymer electrolyte membrane fuel cells (PEMFC) for automotive applications. Perfluorosulfonic acid (PFSA) polymer materials, which are used for electrolytes in the membrane and the catalyst layers, present in fact a drop in ionic conductivity when the dissolved water content in the ionomer becomes low. The amount of dissolved water in the polymer results from a complex balance of produced water by electrochemical reaction, relative humidity of the gas feed and water transport across the membrane, driven by gradient in water concentration and electroosmotic drag. In this work, the operation under low relative humidity of automotive materials produced by Reactive Spray Deposition technology (RSDT) was investigated with the aid of polarization curves and electrochemical impedance spectroscopy. The impact of low relative humidity was evaluated to separate the contributions of polymer membrane, anode and cathode catalyst layers. A loss of electrocatalyst active surface under low RH was observed consistently with the literature, and some improvements have been implemented by adapting platinum distribution, ionomer/carbon ratio in the catalyst layer and operating conditions.

Index Terms - polymer fuel cells; low platinum; water management; dehydration.

I. INTRODUCTION

Polymer electrolyte membrane fuel cells for transport applications are expected to cover a relevant share of future electro-mobility for passenger cars, heavy duty transport and trains thanks to the improvements achieved in recent years in the development of new materials and innovative system

strategies. For transport applications, a strict requirement is the operation under dry operating conditions, which must be fulfilled because of limitations in capability of air humidification and thermal management. In this work, the attention is focused on the operation under dry condition, which is realistic for real world stack operation under partial load. In this analysis, innovative materials manufactured by reactive spray deposition technology with low platinum catalyst loading are considered as future generation of fuel cell materials.

II. EXPERIMENTAL

A. Material preparation

Electrodes were deposited on commercial Nafion membranes (Nafion® XL) by reactive spray deposition technology, which is a flame-based process which allow for contemporary deposition of Pt catalyst nanoparticles, formed in the flame, over the catalyst support, which is provided after flame quenching with by a nozzle spraying a slurry containing carbon support (Ketjen black) and ionomer (Nafion®). The process which was described in previous publications [1,2]. A list of produced materials is reported in Table 1, in which the major properties are described. Additional ionomer in catalyst layer was added by spraying after RSDT manufacturing (samples 3-4) or during RSDT process (samples 5). CCM's with an active area of 25 cm² were assembled with GDL (Sigracet SGL29BC) under a compression ratio of approximately 80% that resulted optimal, as demonstrated from

experimental tests comparing different compression ratios in the range 95% - 70%. Single cell hardware with triple serpentine and co-flow gas configuration was adopted for the cell testing (Fuel Cell Technology).

B. Material characterization

Material characterization was performed by means of scanning electron microscopy (SEM) for thickness evaluation, and transmission electron microscopy (TEM), to better analyze nano particle size and triple phase boundary.

TABLE I
LIST OF TESTED SAMPLES

N	Description	I/C cath/an	Estimated Pt loading	Membrane
1	Uniform sample	1 / 0.5	0.15 / 0.07	Nafion XL
2	Gradient sample (Pt loading)	1 / 0.5	0.15 / 0.07	Nafion XL
3	High I/C at anode (spraying)	1 / 1	0.15 / 0.07	Nafion XL
4	High I/C at cathode (spraying)	2 / 0.5	0.15 / 0.07	Nafion XL
5	High I/C at anode (RSDT)	1 / 1	0.15 / 0.07	Nafion XL
7	Combination of improvements	1 / 1	0.15 / 0.07	Nafion XL

C. Single cell testing

Single cell tests were performed according to the procedures reported in previous works [1]. After cell assembly and leak test, 20 voltammetry scans from 0 to 1 V_{RHE} were performed at room and 60°C cell temperature, followed by a series of fully humidified polarization curves until performance resulted stable. A proprietary procedure was thus applied overnight to guarantee full activation of the catalyst layers and ionomer.

Polarization curves in operating conditions listed in Table II were recorded on all samples in order to evaluate the effect of low relative humidity. Electrochemical impedance spectroscopy was performed at three levels of current density 0.2, 0.8 and 1.2 A cm⁻².

TABLE II
LIST OF TESTED SAMPLES

Feeding		T (°C)	RH (A/C)	Stoich. (A/C)
H ₂ / Air		60	30/30	2/4
H ₂ / Air		60	100/100	2/4
H ₂ / O ₂		60	30/30	2/9.5
H ₂ / O ₂		60	100/100	2/9.5

III. RESULTS AND DISCUSSION

Polarization curves and electrochemical impedance spectra reported on the reference sample (uniform sample 1) are reported in Fig. 1. A performance loss is visible from polarization curve both under oxygen and air feed when low RH are applied. Analysis of EIS allows to ascribe the performance loss to severe membrane dehydration, loss of catalyst active surface (ECSA, as confirmed by cyclic voltammetry and literature [3]), ion transport limitations across

the active layer. Since loss is mitigated under 100% oxygen, it is concluded that a first action could consist in improving ion transport in cathode catalyst layer.

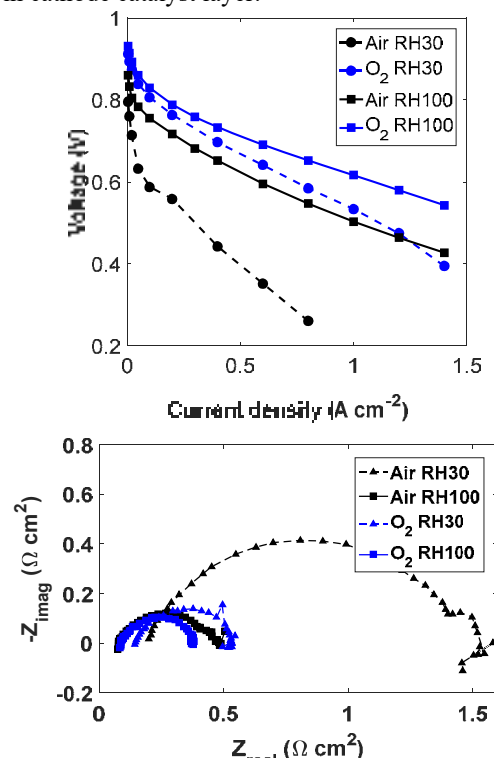


Fig. 1. Polarization curves (up) and impedance spectra (down) of the reference sample 1 (table I) under conditions in Table II.

IV. CONCLUSION

The improvements (not discussed here for space limitations) led to the following conclusions:

1. Increasing ionomer content in anode or cathode shows improvements mainly under fully humidified condition.
2. Additional ionomer at anode gives some benefits.
3. Adoption of a gradient catalyst layer with higher Pt loading next to the membrane is beneficial for low RH condition [2,4].
4. Combination of improvements resulted in a final design which mitigated the performance loss under low RH.

REFERENCES

- [1] A. Baricci, M. Bonanomi, H. Yu, L. Guetaz, R. Maric, A. Casalegno, J. Power Sources. 405 (2018) 89–100. doi:10.1016/j.jpowsour.2018.09.092.
- [2] A. Baricci, M. Bonanomi, H. Yu, L. Guetaz, R. Maric, A. Casalegno, J. Power Sources. 405 (2018) 89–100. doi:10.1016/j.jpowsour.2018.09.092.
- [3] K. Shinozaki, H. Yamada, Y. Morimoto, J. Electrochem. Soc. 158 (2011) B467. doi:10.1149/1.3556906.
- [4] A. Baricci, M. Zago, A. Casalegno, Electrochim. Acta. 222 (2016) 596–607. doi:10.1016/j.electacta.2016.11.014.

CHARACTERIZATION OF INTERCONNECTS OPERATED IN REAL STACKS UP TO 20K HOURS

P. Piccardo*, R. Spotorno*, V. Bongiorno*, G. Ghiara*, C. Geipel**

*DCCI, Università di Genova, Via Dodecaneso 31, 16146 Genoa, (Italy)

**SUNFIRE, Dresden, (Germany)

Abstract - Interconnects represent the main component of an SOFC stack in terms of weight and volume. They are typically made of ferritic stainless steel (FSS) as CROFER 22 APU, CROFER 22 H and AISI 441. At the stack service conditions, the interconnect is operating in a dual atmosphere: air at the cathode side; hydrogen-rich mixture at the anode side. The interconnect is coated at the air side with Co-Mn spinel while the fuel side is left uncoated.

The stacks taken into account for this study operated for 5000 h, 9000 h, 20000 h respectively. One interconnect has been studied for each stack, sampling areas connected to the FSS plate. The samples were characterized by SEM-EDS. The effect of the exposure atmosphere and the contact with the electrodes were investigated.

Index Terms - SOFC, interconnect, post-experiment characterization, operating conditions.

I. INTRODUCTION

Metallic interconnects (MIC) are the main component of a Solid Oxide Fuel Cell (SOFC) stack in terms of weight and volume. They are typically made of ferritic stainless steel (FSS) that have a suitable high temperature oxidation resistance and a coefficient of thermal expansion (CTE) matching with the one of the components of the fuel cells [1]. Their high Cr content promotes the growth of Cr-based spinels that are effective against further oxidation and ensure high electrical conductivity due to their semiconducting behavior [2]. CROFER 22 APU, CROFER 22 H and AISI 441 are grades commonly used as interconnects for these applications. At the stack service conditions, the interconnect is operating in a dual atmosphere: air at the cathode side; hydrogen-rich mixture at the anode side [3]. On the cathode side MIC is usually coated with a spinel protective layer of Co-Mn or Cu-Mn to avoid Cr evaporation

which lead to poisoning the cathode active sites [4]. The coated interconnect is usually contacted to the cathode with an electrically conductive perovskite, mainly LaSrCoFeO₃ (LSCF) or LaSrMnO₃ (LSM) [5, 6]. On the fuel side the interconnect is usually left uncoated and is in direct contact with Ni base contacting layer compliant with the MIC and the anode.

In this work we characterized the above-mentioned layers in stacks operating at 1123 K for 5000 h, 9000 h, 20000 h, respectively. The study was performed using Scanning Electron microscopy coupled with energy dispersive X-ray spectroscopy (SEM-EDS). Furthermore, image analysis was performed using the software ImageJ 1.49f to verify the evolution of the thickness of the oxides formed.

The aim of the study is to investigate how the dual atmosphere and the contact with different materials (namely air and perovskites at the cathode, hydrogen and Ni at the anode, respectively) significantly influenced the evolution of the interface layers on the MIC.

II. MATERIALS AND METHODS

MIC in the investigated stack consisted of CROFER 22APU suitably shaped (ribs and channels) to ensure electrical contact and gas flow at the electrodes. The protective coating consisted of Co-Mn spinel protective layer. MIC were disassembled from stacks and mounted in epoxy resin before cutting in order to avoid the loss of material during the sample preparation. Three sites of interest, namely gas inlet, middle and gas outlet were sampled in order to study changes related to the position in the cell (fig. 1). The cross sections were polished up to 0.25 μm to be characterized by SEM-EDS.

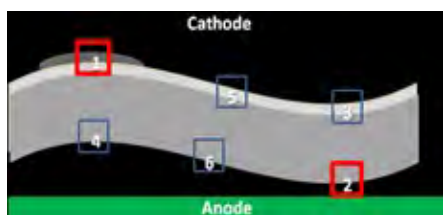


Fig. 1. Schematic representation of the investigates positions on the interconnect. In red those discussed in this paper

III. RESULTS

The two analyzed areas, as visible from fig. 1, are those closer to the related electrodes, namely cathode (1) and anode (2). Both sides exhibit a layer composed of Cr and Mn oxides, coherently with the oxidation of the metal substrate at such operating temperatures (1123 K). Fig. 2 (up) shows the trend of oxide growth together with the decrease in porosity of the Co-Mn coating connected to a densification process [4, 7]. The trend showed a decrease in scale growth rate over time possibly connected to the densification of the protective layer hindering the oxygen diffusion toward the metal substrate. The oxidation at the anode side (fig. 2, down) might be related to the presence of water vapor as a carrier of oxygen. This affects the oxide growth which is characterized by a trend visibly lower when compared to the air side. This phenomenon should be taken into account in long lasting operations since could affect the overall conductivity of the MIC. The evolution of the abovementioned parameters should be thoroughly considered when modelling the degradation processes and planning accelerated test campaigns.

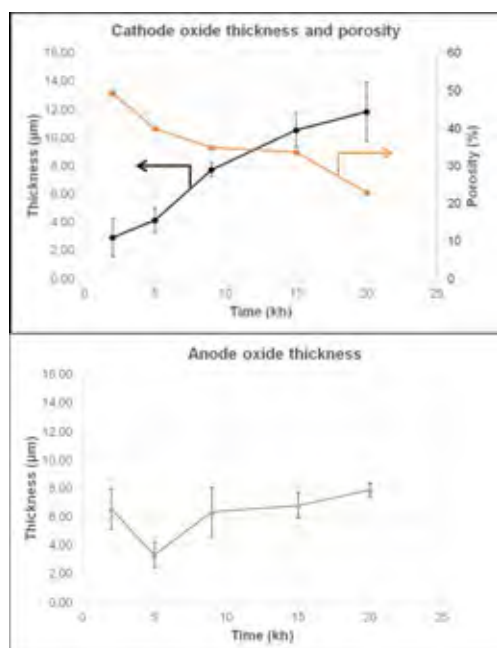


Fig. 2. Oxide thickness and coating porosity at air (cathode) and fuel (anode) side of the same interconnect vs. operating time

IV. CONCLUSION

The opportunity to investigate MIC coming from SOFC stacks operated up to 20000 h offered an important insight on the interaction between the interconnect with the coating, applied at the air side, and the working atmospheres. The cathode side exhibited an expected thermally grown oxide at the interface metal/coating. The oxide growth rate is closely related to the densification of the spinel coating. The anode side showed the formation of an oxide layer with limited growth rate, possibly depending on the presence of water vapor. Further experiments will be performed in order to better define the reactivity of the MIC in anodic conditions. The gathered information is relevant to the understanding of the long-lasting phenomena and the parameters affecting their evolution.

ACKNOWLEDGMENT

This project has received funding from the Fuel Cells and Hydrogen 2 Joint Undertaking under Grant Agreement No 825027. This Joint Undertaking receives support from the European Union's Horizon 2020 research and innovation programme and Hydrogen Europe.

REFERENCES

- [1] Wincewicz K.C., Cooper J.S., Taxonomies of SOFC material and manufacturing alternatives, *Journal of Power Sources*, Volume 140, Issue 2, 2005, Pages 280-296.
- [2] Wu J., Liu X., Recent Development of SOFC Metallic Interconnect, *Journal of Materials Science & Technology*, Volume 26, Issue 4, 2010, Pages 293-305.
- [3] Singhal S.C., Kendall K., *High Temperature and Solid Oxide Fuel Cells*, Elsevier, 2003.
- [4] Spotorno R., Piccardo P., Perrozzì F., Valente S., Viviani M., Ansar A., Microstructural and Electrical Characterization of Plasma Sprayed Cu-Mn Oxide Spinel as Coating on Metallic Interconnects for Stacking Solid Oxide Fuel Cells, *Fuel Cells*, Volume 15, Issue 5, 2015, Pages 728-734.
- [5] Spotorno R., Piccardo P., Schiller G., Effect of Cathode Contacting on Anode Supported Cell Performances, *Journal of The Electrochemical Society*, Volume 163, Issue 8, 2016, Pages F872-F876.
- [6] Spotorno R., Piccardo P., Perrozzì F., Interaction between Crofer 22 APU Current Collector and LSCF Cathode Contacting Layer under Cell Operation, *ECS Transactions*, Volume 68, Issue 1, 2015, Pages 1633-1640.
- [7] Talic B., Falk-Windisch H., Venkatachalam V., Hendriksen P.V., Wiik K., Lein H.L., Effect of coating density on oxidation resistance and Cr vaporization from solid oxide fuel cell interconnects, *Journal of Power Sources*, Volume 354 2017, Pages 57-67.

ASSESSMENT OF THE HYDROGEN RECEIVING POTENTIAL OF A DISTRIBUTION GAS NETWORK USING A MULTI COMPONENT AND TRANSIENT GAS NETWORK MODEL

M. Cavana* and P. Leone*

* Department of Energy, Politecnico di Torino
Corso Duca degli Abruzzi 24, 10129 Torino, (Italy)

Abstract – A transient and multi-component fluid-dynamic model of the gas network was applied to a real distribution network of a small municipality. The aim was to perform a series of investigations about the hydrogen injection practice. First, the evaluation of the hydrogen receiving potential of each point of the gas network was carried out under a defined percentage of hydrogen blending, following the seasonal and infra-day variation of the users' gas consumptions. Then, an example of distributed injection of solar-produced hydrogen is performed so to evaluate the impact of hydrogen blending according to a realistic curve of production. By crossing the results of the two simulations, it is possible to highlight and quantify opportunities and criticalities of the hydrogen blending practice at a local level as well as to draw preliminary considerations on the regulatory framework about hydrogen presence within the gas network.

Index Terms – Energy storage, Gas network model, Greening the natural gas, hydrogen injection.

I. INTRODUCTION

In the context of the energy transition, the role of the natural gas infrastructure is controversial. On the one hand, as indicated in the IPCC report [1], the decarbonization goals set long-term scenarios for which the fossil fuel shift towards natural gas will not be sufficient to achieve the mitigation results, with natural gas undergoing then a substantial reduction by the end of the century. On the other, it is considered as a fundamental enabler for the transition itself [2] as well as a power network stabilizer when higher share of fluctuating energy from renewables will be present in the system [3]. A possible solution to this dilemma may be given by the decarbonization of the gas network with the integration of the electricity and the gas systems through grid injection of hydrogen from power-to-gas path. Recent studies have estimated that the employment of renewable gases for the decarbonization of the energy system

may result a viable economic option, with annual savings ranging between 8 and 138 billion €/year [4].

However, while the distributed injection of biomethane and synthetic natural gas within the existing gas infrastructure is almost technically straightforward, the case of hydrogen blending is rather more complex. This practice would have a remarkable impact on the whole natural gas system, from the physical infrastructure to the management of the gas quality and to the final users' appliances. Several studies and reviews aimed at summarized technical evidences of both strengths and weakness of the gas infrastructure under unconventional gas distribution [5],[6].

In this work, the issues of gas quality management as well as the network receiving capacity have been addressed taking advantage of the feature of the transient and multicomponent fluid-dynamic model of the gas distribution network.

II. METHODOLOGY

In order to gain expertise in modelling and managing future, smart and complex gas grids, a fluid-dynamic model of the network was developed, with the following features:

- 1) transient fluid-dynamic: the time-dependent evolution of the network can be evaluated following the fluctuating consumptions patterns;
- 2) multi-component: the natural gas is modeled as a mixture of hydrocarbons and other gases (hydrogen among the others) whose composition may change throughout the network and along the simulation time frame. A more detailed description of the model is presented in [7]. The structure of the model allow its application to any network topology and to any gas mixture.

III. CASE STUDY DESCRIPTION

In this work, a gas distribution network of a small municipality was simulated under hydrogen blending scenarios.

The distribution network covers an area of 29 km² with a population of approximately 6,500 inhabitants. The modeled portion of the network is the higher pressure one, from the city-gate booth to the secondary reduction stations, with pressure set point at 3 bar_g at the city gate. The topological structure of the network is given in Fig. 1.

Starting from the annual gas consumption of the area, the hourly pattern consumption has been obtained following the procedure presented in [7].

A. Estimation of the nodal hydrogen receiving potential

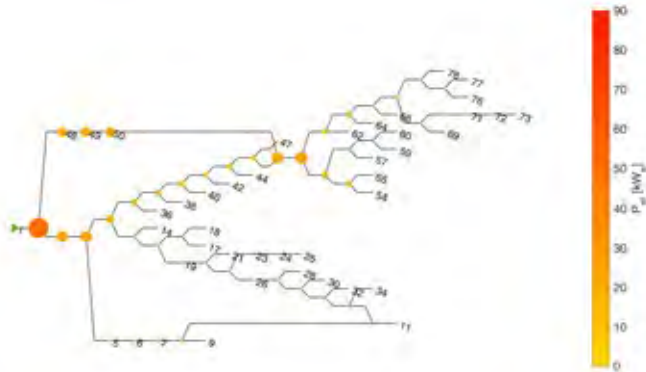


Fig. 1. Nodal potential map of the electrical storage via power-to-hydrogen pathway relative to the case of maximum H₂ blend equal to 7%_{mol} - values for 1:00 PM of mid-August day (minimum consumption rates)

The hydrogen receiving potential throughout the network varies according to the gas consumption rates and thus it depends on the gas flow rates that pass through each node. Furthermore, it depends on the blending limit constraint.

The showcase here presented was built on the assumption to limit the hydrogen molar fraction to 7%, in order to keep the blend within the national quality limits on relative density. In Fig. 1 a screenshot of the nodal hydrogen receiving potential of the whole network is given for a specific hour of the year. The power values refer to the amount of hydrogen that is possible to inject considering an electrolyzer efficiency of 65%_{HHV}.

B. Impact of distributed hydrogen injection from solar source.

This second case study is devoted to show the quality tracking capabilities of the gas network model. Two distributed hydrogen stream have been assumed, originated by two PV plants of 333 kW_p and 500 kW_p coupled with an electrolyzer system with 65%_{HHV} efficiency. The hydrogen is directly injected following the solar panel production curve. In Fig. 2, a screenshot of the gas network conditions for a specific summertime hour. It is a critical case because the network is at the minimum of gas consumption (and thus of the hydrogen receiving potential) and at the maximum of the PV panels production (and thus of the hydrogen production). As it can be observed, the hydrogen blending practice generates areas where the hydrogen percentage exceeds 40% and 90%.

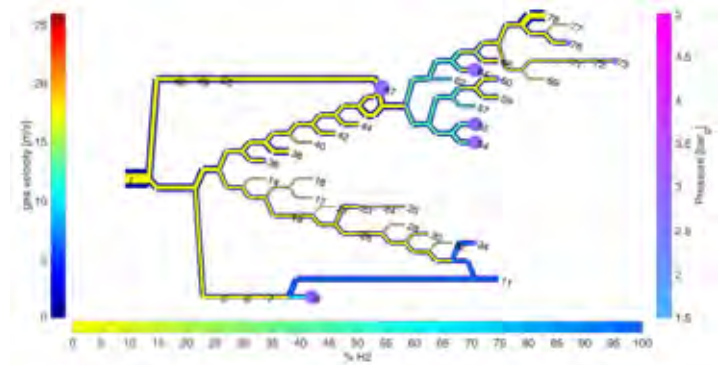


Fig. 2. Gas network topological map with indication of gas velocity along the branches, nodal pressures and consumptions (bullet size) and gas quality (hydrogen molar concentration) - values for 1:00 PM of mid-August day (minimum consumption rates)

IV. CONCLUSION

The simulation activities within this work aims at showing the non-trivial practice of the integration among power and gas sectors in order to obtain more flexibility for the overall energy system. In general, unbalances from the electrical side may affect the gas one. This is particularly critical at distribution level, where infrastructures are more constrained. Further studies with similar approach may bring to a finer estimation of the actual flexibility improvement from the sector integration process.

ACKNOWLEDGMENT

Part of the project “Heat in the Pipe” – bando “*Metti in Rete la tua Ricerca*” financed by *Compagnia di San Paolo*.

REFERENCES

- [1] IPCC, Climate Change 2014: Mitigation of Climate Change, Chap. 7: Energy systems, 5th assessment report (2014).
- [2] X. Zhang et al., Climate benefits of natural gas as a bridge fuel and potential delay of near-zero energy systems, *Appl. Energy*, 167 (2016).
- [3] M.A. Mac et al., The role of natural gas and its infrastructure in mitigating greenhouse gas emissions , improving regional air quality , and renewable resource integration, *Prog. Energy Combust. Sci.* 64 (2018).
- [4] Ecofys, Gas for Climate: How gas can help to achieve the Paris Agreement target in an affordable way (2018).
- [5] M.W. Melaina et al., Blending Hydrogen into Natural Gas Pipeline Networks : A Review of Key Issues (2013).
- [6] K. Altfeld et al., Admissible hydrogen concentrations in natural gas systems, *Gas Energy* (2013) 1–12.
- [7] M. Cavana et al., Towards Renewable Gases Distribution Networks: the Importance of a Transient and Multi-component Fluid-dynamic Gas Model, *Proc. 27th EUBCE* (2019).

QUALITY ASSURANCE OF BIPOLAR PLATES USING X-RAY TOMOGRAPHY

M. Sietmann*, H. Janßen*, M. Müller* and W. Lehnert***

*Forschungszentrum Jülich GmbH IEK-3, Electrochemical Process
Engineering, Jülich 52425, (Germany)

**Modelling in Electrochemical Process Engineering, RWTH
Aachen University, Aachen 52056, (Germany)

Abstract - High resolution X-Ray computer tomography (CT) can be used to investigate the morphology of graphite composite bipolar plates (BPP). We applied reversed engineering on the tomograms and simulated how voids and cracks have an impact on the electrical conductivity of graphite composite BPPs. This approach brings the result that only larger cracks or defects have a measurable impact on the electrical resistance of the BPP. In addition the position and orientation of the defects is important for their influence on the electrical properties of the BPP. With the Nano-CT images and conductivity simulation measuring methods like electrical potential measurements can be validated.

Index Terms – Bipolar plate, quality assurance, reverse engineering, X-Ray tomography

I. INTRODUCTION

Graphite composites are possible materials for BPPs in fuel cells. Compared to metallic BPPs those materials have a better corrosion resistance and chemical stability in the fuel cell. However higher manufacturing costs and lower electrical conductivity are some drawbacks of the graphite composite BPP [1].

Studies [2-4] have shown that the current through the graphite composite BPP is conducted via graphite particles or other conductive particles. Through voids, cracks, foreign non-conductive particles or the polymer binder material the graphite particles can lose contact and therefore the electrical resistance will be increased.

II. METHODOLOGY AND RESULTS

X-Ray tomography

The X-Ray tomography is a non-destructive measuring method to investigate the inner structure of materials and components [5]. For our investigation we used the high

resolution CT Xradia 410 Versa from Carl Zeiss AG. With this CT we have on the one hand the opportunity to investigate the whole flow field (4 cm x 4 cm) and scan a test BPP for larger imperfections. On the other hand we can zoom into the material and get a resolution below a micrometer making the morphology visible. Compared to scanning electron microscopy (SEM) the X-Ray CT has the advantage, that the sample needs no special preparation before measuring and that we can take 3D tomograms instead of 2D images. The CT generates a grey level tomogram. Strongly absorbing materials are shown in brighter colors and less absorbing materials are shown in darker colors.

Figure 1 shows a 2D section from the tomogram of a BPP material. Three vertical cracks can be seen inside the sample.

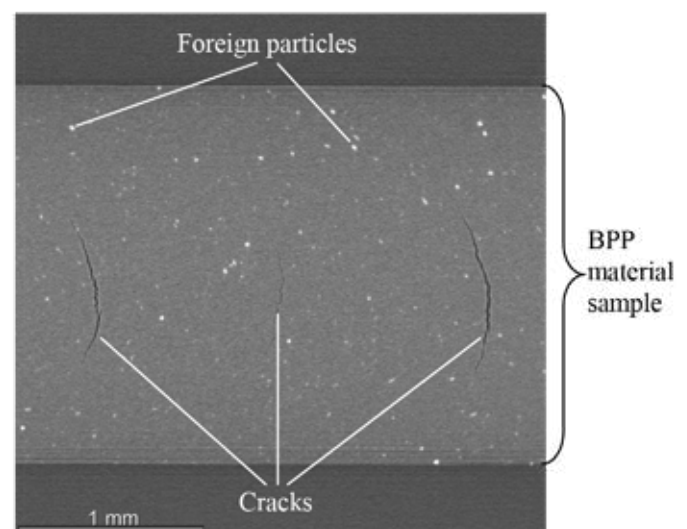


Fig. 1: 2D section from BPP tomogram with larger imperfections

Figure 2 shows a high resolution image of another BPP material with larger graphite particles. On the basis of the grey levels the different structures can be assigned to the graphite particles, the polymer binder, foreign material particles and voids or cracks.

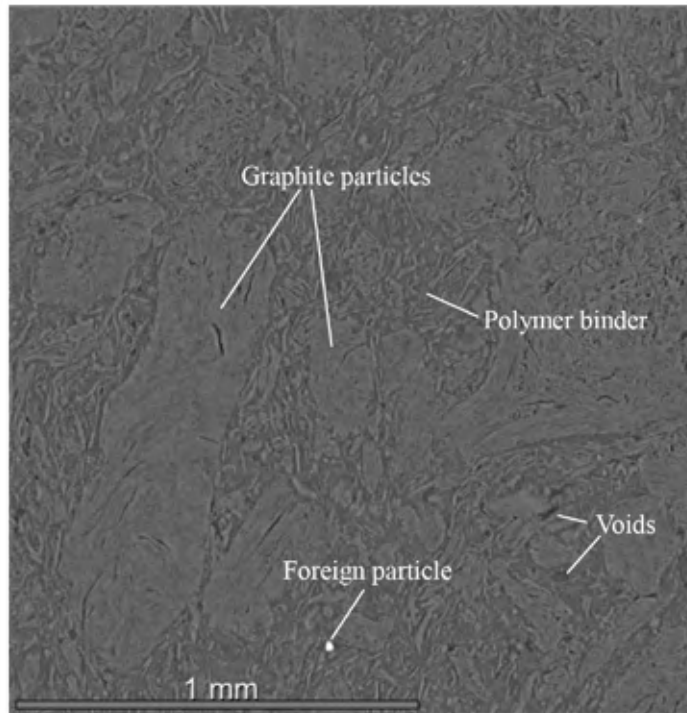


Fig. 2: High resolution image of graphite composite BPP material

Electrical simulation

A reverse engineering process was applied on the BPP samples. With the help of the Software Dragonfly by ORS the structures seen in Figure 2 as well as the overall structure of the BPP can be transferred into a mesh. We transferred the generated data to the FEM solver of ANSYS Mechanical and simulated the electrical conductivity of the scanned BPP. In the simulations we reduced the complexity of the model to reduce the computational time. We assumed that the BPP is made out of a homogeneous conductive material. Only cracks and voids can influence the electrical conductivity, small foreign particles are neglected for the simulation. This approach brings the result that only cracks or defects with a dimension larger than 100 μm have an impact on electrical resistivity and can be measured through electric potential measurements. In addition the position and orientation of the defects is important for their influence on the electrical properties of the BPP. Defects close to the surface influence the measurable electrical conductivity more than defects in the middle of the BPP. Therefore near surface measuring methods can be an option for BPP quality assurance. Simulating through plane conductivity cracks with an

expansion in the through plane direction have barely any impact on the electrical resistance. Cracks with an expansion in the in plane direction have an impact on the through plane resistivity.

III. CONCLUSION

X-Ray tomography can be used to show larger cracks or defects in graphite composite materials for bipolar plates. In addition X-Ray tomography can be used to investigate the morphology of those materials.

The conductivity simulation with ANSYS Mechanical shows the correlation between the inner structure of the graphite composite BPP and the electrical resistance of the BPP. Voids or cracks inside the BPP have an impact on the electrical resistance of the BPP depending on their size, position and orientation.

With the reverse engineering of the BPP through X-Ray tomography and conductivity simulation other measuring methods like electrical resistance measurement can be validated.

ACKNOWLEDGMENT

The authors would like to thank the German Federal Ministry Transport and Digital Infrastructure (BMVI) for supporting and funding the project BePPel (Grant No.: 03B11002D/03B11002D2) in which the results presented here have been gained. We would also like to thank the provider of the BPPs within the project.

REFERENCES

- [1] R. Taherian, A review of composite and metallic bipolar plates in proton exchange membrane fuel cell: Materials, fabrication, and material selection, *Journal of Power Sources*, vol. 265, 2014, pp. 370-390.
- [2] C. Kreuz, PEM-Brennstoffzellen mit spritzgegossenen Bipolarplatten aus hochgefülltem Graphit-Compound, *Dissertation, Universität Duisburg-Essen*, 2008.
- [3] B. K. Kakati, D. Sathiyamoorthy, and A. Verma, Semi-empirical modeling of electrical conductivity for composite bipolar plate with multiple reinforcements, *International Journal of Hydrogen Energy*, vol. 36, no. 22, 2011, pp. 14851-14857.
- [4] B. K. Kakati, V. K. Yamsani, K. S. Dhathathreyan, D. Sathiyamoorthy, and A. Verma, The electrical conductivity of a composite bipolar plate for fuel cell applications, *Carbon*, vol. 47, no. 10, 2009, pp. 2413-2418.
- [5] L. Salvo et al., X-ray micro-tomography an attractive characterisation technique in materials science, *Nuclear Instruments and Methods in Physics Research Section B: Beam Interactions with Materials and Atoms*, vol. 200, 2003, pp. 273-286.

THE EFFECT OF DIFFERENT ADDITIVES ON KOH/ XANTHAN HYDROGELS PROPOSED AS ELECTROLYTES FOR AL/AIR PRIMARY CELLS

M.F. Gaele, T. Di Palma, F. Migliardini, P. Corbo

Institute of Science and Technology for Energy and Sustainable
Mobility, National Research Council of Italy, Via Marconi, 4 –
Naples, Italy

Abstract - This paper presents the results of an experimental study aimed at preparing high conductivity solid electrolytes for Al-air primary cells, using alkaline gel based on a natural polysaccharide (xanthan) and different substance as additive to control the anode corrosion. Solid gel electrolytes have been prepared starting from a mixture of xanthan and KOH aqueous solutions at different solid/liquid ratios, and by using polygalacturonic acid sodium salt (PGASS), alginic acid sodium salt (AASS), methanol and KI as additives. We have found that the Xanthan/liquid ratio of 0.7 g/ml and the KOH concentration of 11 M give the best cell performance in terms of discharge profiles, while the anodic efficiency is positively affected by the presence of additives. The best efficiency (91% at 10 mA cm⁻² as discharge current) was obtained for a sample at 0.7 g/ml and 11 M KOH with addition of 10% of PGASS.

Index Terms – Al-air batteries, Xanthan, self-corrosion inhibition, anodic efficiency.

I. INTRODUCTION

Primary aluminium air batteries, also defined as Al semi-fuel cell, using alkaline aqueous electrolytes suffer from severe self-corrosion due to a parasitic reaction involving hydrogen evolution. This parasitic reaction limits the cell performance leading to low coulombic efficiency and short shelf life. Many materials, both organic and inorganic, show protective properties against corrosion of aluminium in aqueous alkaline solutions and may be used as additive in the preparation of electrolytes. Among them, alginates and pectates are natural polymers showing appreciable influence on the rate of aluminium dissolution in alkaline media [1,2]. Moreover, the presence of halide ions in alkaline solutions containing organic compounds has been found to stabilize the absorption of organic cations on the aluminium surface leading to an improved corrosion inhibition efficiency [3]. As water

molecules are involved in the parasitic reaction, a different strategy to control aluminium corrosion is based on the elimination of the water from the alkaline solution and its partial replacement with methanol [4]. This paper is aimed at verifying the effect of different additives as self-corrosion inhibitors in alkaline electrolytes based on xanthan hydrogels for Al-air primary cells.

II. EXPERIMENTAL

Xanthan gum (MW = 2 x 10⁶ g mol⁻¹) and KOH solutions were provided by Sigma-Aldrich. Aluminum anodes for Al/air cells were cut from a foil 0.5 mm thick (Puratronic, 99.998%) provided by Alfa Aesar. From these foils discs of 13 mm diameter were cut. Pt/C air cathodes were supported on carbon cloth (CC) samples provided by H2-Planet (0.35 mm thick, 116 g m⁻²), according to a procedure described elsewhere [5,6]. A hydrogel alkaline electrolyte was prepared starting from a KOH 11 M solution and Xanthan powder (sample KOH_GEL), by mixing and kneading solid and liquid phases at room temperature for 20 minutes (solid/liquid ratio = 0.7 g/ml) [6]. Polygalacturonic acid sodium salt (PGASS), alginic acid sodium salt (AASS), CH₃OH and KI were used as additives in order to obtain a concentration of 10 %wt with respect to the xanthan amount. Discharge test were performed at a discharge current density of 5 and 10 mA cm⁻², while anodic efficiency measurements were effected by weight loss technique in order to evaluate the influence of additives on the anode corrosion and the cell performance.

III. RESULTS AND DISCUSSION

The effect of different additives on discharge performance is shown in Figures 1 and 2. In Figure 1 the discharge profiles for

KOH_GEL without and with the addition of KI and PGASS at 5 mA cm^{-2} are reported.

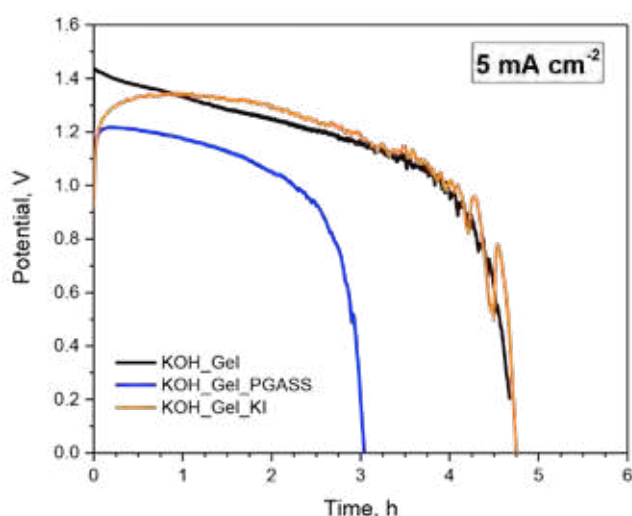


Fig. 1. Discharge tests of Al-air cells with KOH_GEL at 5 mA cm^{-2} with KI and PGASS additives.

Initial voltage for the sample KOH_GEL was about 1.4 V, that decreased to 0.2 V after about 4.5 h. The addition of KI did not substantially alter neither the discharge duration nor the initial voltage, but provided an anodic efficiency of 74%, to be compared with that of KOH_GEL at 5 mA cm^{-2} (65%). The addition of PGASS implied minor initial voltage (about 1.2 V) and discharge duration (the voltage decreased to 0.2 V after about 3h), without any improvement of anodic efficiency.

The discharge curves at 10 mA cm^{-2} are shown in Figure 2 for KOH_GEL without and with the addition of PGASS, AASS and CH_3OH .

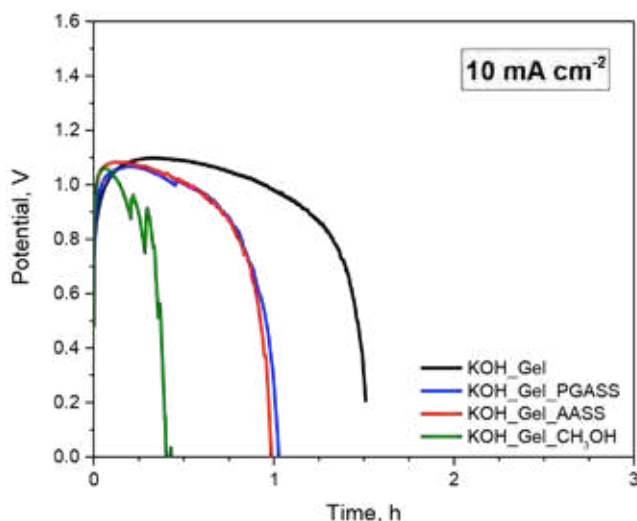


Fig. 2. Discharge tests of Al-air cells with KOH_GEL at 10 mA cm^{-2} with CH_3OH , PGASS, AASS additives.

The initial voltage of KOH_GEL was about 1.1 V, while the discharge duration was about 1.5 h. The addition of CH_3OH determined an evident lowering of both discharge duration and initial voltage, without a significant gain in anodic efficiency (81%, to be compared with 78% of KOH_GEL at 10 mA cm^{-2}). The addition of PGASS and AASS did not alter the initial voltage, but determined a 30% diminution of discharge duration. However, an appreciable improvement of anodic efficiency was observed, especially for PGASS additive (91%).

IV. CONCLUSION

We have found that the best cell performance in terms of discharge profiles can be obtained with a Xanthan/liquid ratio of 0.7 g/ml and a KOH concentration of 11 M, while the anodic efficiency increases due to the presence of some additives inside the electrolyte. In particular, the best efficiency was obtained for a sample at 0.7 g/ml and 11 M KOH with addition of 10% of PGASS. For this electrolyte an efficiency of 91% was detected at 10 mA cm^{-2} as discharge current.

REFERENCES

- [1] Zaafarany, I., Corrosion Inhibition of Aluminum in Aqueous Alkaline Solutions by Alginate and Pectate Water-Soluble Natural Polymer Anionic Polyelectrolytes, *Portugaliae Electrochimica Acta* Volume 30 (Issue 6), 2012, Pages 419-426.
- [2] Hassan, R., Zaafarany, I., Gobouri, A., Takagi, H., *International Journal of Corrosion*, Volume 2013, Article ID 508596.
- [3] Umoren, S.A., Synergistic Influence of Gum Arabic and Iodide Ion on the Corrosion Inhibition of Aluminium in Alkaline Medium, *Portugaliae Electrochimica Acta* Volume 27 (Issue 5), 2009, Pages 565-577.
- [4] Umoren, S.A., Eduok, U.M., Application of carbohydrate polymers as corrosion inhibitors for metal substrates in different media: A review, *Carbohydrate Polymers* Volume 140, 2016, Pages 314-341.
- [5] Di Palma, T.M., Migliardini, F., Caputo, D., Corbo, P., Xanthan and κ -carrageenan based alkaline hydrogels as electrolytes for Al/air batteries, *Carbohydrate Polymers* Volume 157, 2017, Pages 122-127.
- [6] Di Palma, T.M., Migliardini, F., Gaele, M.F., Corbo, P., Physically cross-linked xanthan hydrogels as solid electrolytes for Al/air batteries, *Ionics*, Volume 25 (Issue 9), 2019, Pages 4209-4217.

$Ce_{0.8}Ln_{0.2}O_{2-\delta}$ (Ln= Gd, Sm, La, Nd, Pr) COMPOUNDS APPLIED AS EFFECTIVE ANODE CATALYTIC LAYERS FOR BIOGAS FUELED SOFCs

A. Beata Bochentyn*, B. Patryk Błaszczak*, C. Araceli Fuente**, D. Maria Gazda*, E. Sea-Fue Wang*** and F. Piotr Jasiński****

* Faculty of Applied Physics and Mathematics, Gdansk University of Technology, 80-233 Gdańsk, ul. Narutowicza 11/12 (Poland)

** Energy Department, Centre for Energy, Environment and Technology(CIEMAT), Av. Complutense, 40, 28040 Madrid (Spain)

*** Depart. of Mat. and Mineral Resources Eng., National Taipei Univ.of Technol., 1, Sec. 3, Zhongxiao E. Rd., Taipei, 106 (Taiwan)

**** Faculty of Electronics, Telecomm. and Informatics, Gdansk Univ.of Technol., 80-233 Gdańsk, ul. Narutowicza 11/12, (Poland)

Abstract - The nanocrystalline, single-phase compounds of lanthanide-doped ceria $Ce_{0.8}Ln_{0.2}O_{2-\delta}$ (Ln=La, Pr, Nd, Sm, Gd) were fabricated by the Pechini method. The mixed valence state (3+/4+) of praseodymium was confirmed in ceria. All fabricated compounds were deposited in a form of layers on the surface of SOFC anode in aim to act as electrochemically active materials for biogas reforming process. It has been found that a reference (unmodified) cell degraded gradually with time mainly due to deposited carbon, whereas deposition of additional catalytic layer led to improved stability of fabricated fuel cell powered by biogas.

Index Terms – ceria, biogas, direct internal reforming, catalyst

I. INTRODUCTION

Cerium oxide is a catalyst of reactions of steam conversion and oxidation of carbohydrates [1]. It may increase the efficiency of a Solid Oxide Fuel Cell (SOFC) anode operation throughout the acceleration of the process of charge exchange in the triple-phase boundary (TPB). It was reported in the literature that Ni-YSZ anode modified by zirconium doped ceria decreases the amount of deposited carbon [2]. Cerium oxides have also been commonly used as sulfur-tolerant components in cermet anodes because of their good performance and low cost relative to those of the available alternatives. Kurokawa et al. have reported that a power density of a fuel cell with CeO_2 -infiltrated Ni-YSZ anode in H_2 fuel containing 40 ppm of H_2S was 3 orders of magnitude higher than that for the unmodified reference fuel cell. Moreover, the infiltrated fuel cell was able to operate for 500h, whereas the reference one degraded within 13 minutes [3].

II. EXPERIMENTAL

In this work various nanocrystalline compounds of lanthanide-doped ceria $Ce_{0.8}Ln_{0.2}O_{2-\delta}$ (Ln=La, Pr, Nd, Sm, Gd) were fabricated by the Pechini method. They were deposited in a form of layers on the surface of SOFC anode in aim to act as electrochemically active materials for biogas reforming process. The aim of modification was to increase a lifetime and efficiency of commercially available SOFC operating with biogas without the need of an external reformer.

The XRD, SEM, AFM, EDX and XPS methods were used to investigate structural properties and composition of these materials. Furthermore, the electrical properties of SOFCs with catalytic layers deposited on the Ni-YSZ anode site were examined by current density-time and current density-voltage dependence measurements in hydrogen (10h) and biogas (at least 24h). Simultaneously an analysis of the catalytic activity of specific anode materials towards internal biogas reforming based on the composition of outlet gases was performed. For this purpose, a method based on the Fourier Transform Infrared Spectroscopy as well as predestinated software for the in-situ, quantitative analysis of the outlet gases composition from SOFC was developed. From FTIR data conversion rates for both CH_4 and CO_2 were calculated as well as yields and selectivities of CO and H_2 . Moreover, a carbon balance was determined. To predict the direction of particular reforming reactions, a non-equilibrium analysis was performed. Namely, a thermodynamic probability of a solid carbon formation was obtained based on calculations of carbon activity coefficients.

III. RESULTS AND DISCUSSION

The comparison of XRD patterns of $Ce_{0.8}Ln_{0.2}O_{2-\delta}$ powders fabricated by the Pechini method is presented in Fig.1.

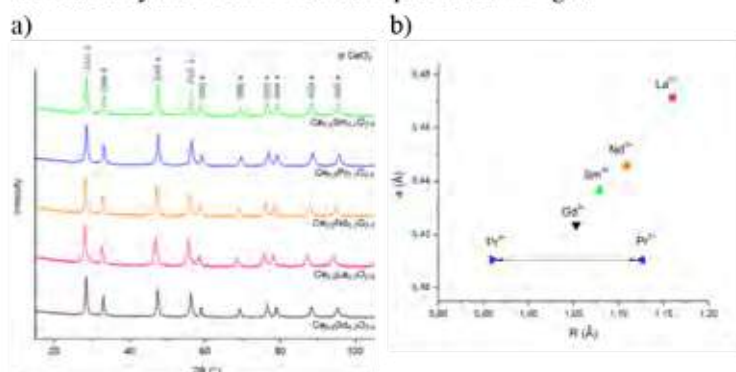


Fig.1. a) XRD plots of fabricated compounds; b) Dependence of unit cell parameters vs. ionic radius of particular dopants (for coordination number 8).

All diffraction peaks can be attributed to $CeO_{2-\delta}$, what indicates that all materials are single-phase. Therefore it can be stated that the amount of dopants applied in this work (20 mol%) is below their solubility limit in ceria. The sizes of crystallites calculated from the Scherrer equation are collected in Table 1 and confirm the nanocrystalline character of fabricated materials. These calculations are in agreement with an analysis of morphology of synthesized powders performed by the SEM and AFM microscopes.

TABLE I

UNIT CELL PARAMETERS (a), AVERAGE SIZE OF CRYSTALLITES (D) WITH UNCERTAINTY (ΔD) AND THE IONIC RADII FOR IONS WITH COORDINATION NUMBER EQUAL TO 8.

	a [Å]	$\alpha=\beta=\gamma$ [°]	R [Å] [57]	D [nm]	ΔD [nm]
$Ce_{0.8}La_{0.2}O_{2-\delta}$	5.471372	90	1.16 (La^{3+})	18.8	0.6
$Ce_{0.8}Nd_{0.2}O_{2-\delta}$	5.445779	90	1.109 (Nd^{3+})	28.0	1.3
$Ce_{0.8}Sm_{0.2}O_{2-\delta}$	5.436658	90	1.079 (Sm^{3+})	26.3	2.5
$Ce_{0.8}Gd_{0.2}O_{2-\delta}$	5.423596	90	1.053 (Gd^{3+})	30.1	1.0
$Ce_{0.8}Pr_{0.2}O_{2-\delta}$	5.410510	90	1.126 (Pr^{3+}) 0.96 (Pr^{4+})	23.1	2.3

The unit cell parameters of analyzed compounds calculated by Rietveld refinement are also shown in Table 1. The graphical dependence of unit cell parameters vs. ionic radius of particular dopants (for coordination number equal to 8) is shown in Fig.1b. For almost all investigated dopants the plot is linear. The only exception is praseodymium, which exists on mixed valence state 3+/4+. The intersection of the trend line with the straight line connecting the ionic radii of the Pr^{3+} and Pr^{4+} makes it possible to estimate that approx. 38% of all praseodymium ions occur at +3 oxidation state [4].

In next step the materials were examined as potential anode catalytic layers for direct internal reforming of biogas. The current density plots vs. time are shown in Fig.2 and indicate that in contradiction to a reference fuel cell (without a catalytic

layer) SOFCs with Nd, Sm and La-doped ceria do not degrade, but even improve their properties in time when they are fed with biogas. This is probably due to the ability of ceria materials to oxidize a deposited solid carbon and to efficiently remove it from the anode side.

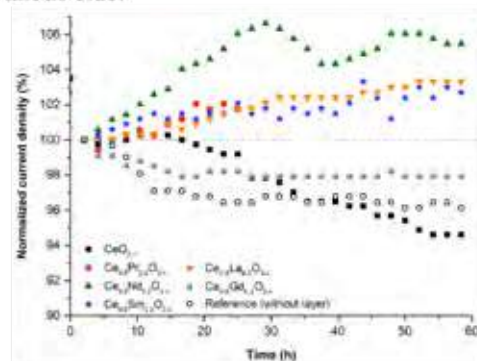


Fig.2. Normalized current density as a function of time for a reference cell and for fuel cells with the selected ceria-based catalytic layers.

In order to determine which of synthesized materials gives the best long-term stability in direct biogas feeding conditions the results of longer measurements (at least 85h) will be shown at the conference. Moreover, a deep analysis based on composition of outlet gases for particular SOFCs will be presented in order to calculate the conversion rates of fuel components and yields of products, to predict the direction of particular reforming reactions, as well as a thermodynamic probability of a solid carbon formation.

IV. CONCLUSION

The lanthanide-doped ceria materials were proved to be easy to fabricate in a nanocrystalline form which is desired due to a high surface area for catalytic reactions. When they are deposited as additional anode layers they improve the long-term stability of biogas-fed SOFC, mostly due to a higher resistance to carbon deposition, without a need to use an external reformer in a system.

ACKNOWLEDGMENT

This work was supported by the National Science Center under grant No. NCN 2017/26/D/ST8/00822.

REFERENCES

- [1]. Q. Fu, H. Saltsburg, M. Flytzani-Stephanopoulos, Science 301 (2003) 935–938.
- [2]. H. He, J.M. Hill, Applied Catalysis A: General 317 (2007) 284–292
- [3]. H. Kurokawa, T. Sholklafter, C. Jacobson, L. De Jonghe, S. Visco, Electrochem. Solid-State Lett. 10 (2007) B135–B138.
- [4]. Balaguer M., Solís C., Serra J. M., J. Phys. Chem. C, 116, 2012, s. 7975–7982.

A FEASIBILITY ASSESSMENT OF A RETROFIT MOLTEN CARBONATE FUEL CELL COAL-FIRED PLANT FOR FLUE GAS CO₂ SEGREGATION

R. Cooper*, D. Bove**, E. Audasso**, M.C. Ferrari*, and B. Bosio**

*School of Engineering, University of Edinburgh, Robert Stevenson Road EH9 3FB Edinburgh, (UK)

**PERT, DICCA, University of Genoa, Via Opera Pia 15, 16145, Genoa, (Italy)

Abstract - This work considers the use of a Molten Carbonate Fuel Cell (MCFC) system as a power generation and CO₂ concentrator unit downstream of the coal burner of an existing production plant. In this way, the capability of MCFCs for CO₂ segregation, which today is studied primarily in reference to large-scale plants, is applied to an intermediate-size plant providing interesting environmental developments.

A technical feasibility analysis was performed using an MCFC system-integrated model capable of determining steady-state performance across varying feed composition. The MCFC user model was implemented in Aspen Custom Modeler and integrated into the reference plant in Aspen Plus. The model considers electrochemical, thermal and mass balance effects to simulate cell electrical and CO₂ segregation performance. Model validation was carried out using data from an experimental MCFC unit showing good agreement with the results obtained.

Finally, a preliminary economic assessment was carried out for the proposed MCFC implementation.

Index Terms - Aspen Custom Modeler, carbon capture, fuel cell applications, MCFC process simulation.

I. INTRODUCTION

Fuel cell research and development is an area which has seen significant interest in recent years, especially for high temperature cells (Molten Carbonate Fuel Cells (MCFCs) and Solid Oxide Fuel Cells (SOFCs)). The interest in these technologies results from their ability to generate energy highly efficiently using readily available hydrocarbon fuel sources. The high temperature operating conditions mean the use of expensive electro-catalyst materials is not required increasing the range of usable fuel constituents compared to other cell types. Additionally, the high operating temperatures allow the introduction of a gas turbine system increasing process

efficiency via utilisation of cell exhaust heat. MCFCs, in particular, are of interest due to their potential for energy generation in combination with CO₂ segregation. This ability could allow the capture of CO₂ without the efficiency reduction associated with conventional capture methods. With the effects of climate change leading to ever-increasing environmental consciousness within society, the use of MCFCs is believed to be a key player in future industrial projects.

The capacity for MCFC CO₂ segregation comes from the transfer of carbonate ions from the cathode to the anode. This ion movement acts to concentrate the CO₂ in the anode exhaust stream simplifying CO₂ capture. There have been numerous studies proposing the use of MCFC units for CO₂ segregation. Examples of computational work include MCFC implementation in natural gas combined cycles^{[1][2][3]}, pulverised coal-fired plants^{[3][4]}, integrated gasification combined cycles^[5], cement production^[6], steel production^[7] and wastewater biogas processes^[8]. In these works, CO₂ capture rates of up to 90% can be achieved with plant efficiency maintained at near previous plant operation levels.

Although significant study has been carried out regarding implementation of MCFC, this largely has been in looking at its application in large plants. The advantage of fuel cell operation is that unlike conventional power generation methods, there is little dependence of efficiency on the scale of operation. Due to this, the potential for fuel cell use in smaller-scale applications is likely to pose a more economical prospect. For this reason, this study focuses on MCFC implementation in a mid-size plant. In particular, this study examines the retrofitting of an MCFC unit to a mid-size textile production plant.

II. METHOD

A. Modelling Software

This paper presents a simplified computational model which describes the cell electrochemical, thermal and mass balance effects to model cell electrical and CO₂ segregation performance. Consideration of the balance of plant necessary for MCFC implementation in the reference case is also presented. In most computational models, the equations that describe the unit operation are coded together with a solver in a programming language requiring significant knowledge of the numerical methods involved. In this study, the fuel cell user model was developed in Aspen Custom Modeler; this software was chosen due to its applicability for coding unit operations and its preprogrammed numerical methods. This, along with the Aspen property database, allows modelling of complex process systems with comparative ease. The ability to define a user unit and simulate this in combination with standard units in Aspen Plus provides the opportunity to study the MCFC directly integrated into the plant system.

B. MCFC modelling

The development of the MCFC mass and energy balances was based on the following general assumptions: (i) adiabatic fuel cell operation, (ii) feed temperature and velocity profiles were fully developed, (iii) rate of the electrochemical reaction was modelled considering appropriate kinetics, (iv) based on the high operating temperature and Nickel catalyst employed, the water gas shift reaction was assumed to reach equilibrium.

The assumed electrochemical kinetics will not be discussed in detail in this work as it is the subject of a previous paper^[9]. The kinetic model considers the impact of internal resistance, cathodic polarisation resistance as a function of O₂ and CO₂ partial pressure and anodic polarisation resistance as a function of H₂ partial pressure to simulate cell behaviour.

Testing of the model results was performed using literature experimental data^[9]. Model validation over multiple feed flowrates and compositions was carried out with the obtained results showing good replicability of the experimental data.

C. System modelling

System data were obtained from a reference textile production plant where water vapour is generated via a coal burner. This work considers the retrofitting of the MCFC unit downstream of the burner to segregate the flue gas CO₂. On the basis of plant data, simulation of the coal burner unit and necessary balance of plant was modelled in Aspen Plus. On user model integration, the effect of the MCFC unit could be directly assessed.

A preliminary economic assessment of MCFC implementation was carried out. The economic assessment was performed based on both current and proposed fuel cell prices, allowing an assessment of the current and future prospect of MCFC retrofitting in the reference plant.

III. CONCLUSION

The work presented in this paper allows the simulation of MCFC operation within a reference mid-size industrial plant. Upon validation, the fuel cell user model exhibited good agreement with experimental testing. As such, the user model allows the design of a user-friendly unit operation which can simulate MCFC performance across a wide range of feed conditions. Upon testing within the reference plant benefits can be observed in terms of specific emissions produced and overall plant power.

REFERENCES

- [1] Capellucci, R., Saia, R., Giordano, L., Study of Gas-steam Combined Cycle Power Plants Integrated with MCFC for Carbon Dioxide Capture, *Energy Procedia*, Volume 45, 2014, Pages 1155-1164.
- [2] Campanari, S., Chiesa, P., Manzolini, G., Bedogni, S., Economic analysis of CO₂ capture from natural gas combined cycles using Molten Carbonate Fuel Cells, *Applied Energy*, Volume 130, 2014, Pages 562-573.
- [3] Spinelli, M., Campanari, S., Consonni, S., Romano, M., Kreutz, T., Ghezal-Ayagh, H., Jolly, S., Molten Carbonate Fuel Cells for Retrofitting Postcombustion CO₂ Capture in Coal and Natural Gas Power Plants, *Journal of Electrochemical Energy Conversion and Storage*. Volume 15, Issue 3, 2018, 031001.
- [4] Campanari, S., Carbon dioxide separation from high temperature fuel cell power plants, *Journal of Power Sources*, Volume 112, Issue 1, 2002, Pages 273-289.
- [5] Spallina, V., Romano, M., Campanari, S., Lozza, G., Application of MCFC in Coal Gasification Plants for High Efficiency CO₂ Capture. *Journal of Engineering for Gas Turbines and Power*, Volume 134, Issue 1, 2011, 011701.
- [6] Spinelli, M., Romano, M., Consonni, S., Campanari, S., Marchi, M., Cinti, G, *Energy Procedia*, Volume 63, 2014, Pages 6517-6526.
- [7] Mastropasqua, L., Pierangelo, L., Spinelli, M., Romano, M., Campanari, S., Consonni, C., Molten Carbonate Fuel Cells retrofits for CO₂ capture and enhanced energy production in the steel industry, *International Journal of Greenhouse Gas Control*, Volume 88, 2019, Pages 195-208.
- [8] Chacartegui, R., Monje, B., Sanchez, D., Beccera, J., Campanari, S., *International Journal of Greenhouse Gas Control*, Volume 19, 2013, Pages 453-461.
- [9] Audasso, E., Bosio, B., Nam, S., Extension of an effective MCFC kinetic model to a wider range of operating conditions, *International Journal of Hydrogen Energy*, Volume 41, Issue 12, 2016, Pages 5571-5581.

OVERVIEW OF THE DEVELOPMENTS AND RESULTS OF THE DESIGN 2 SERVICE PROJECT

A. Linhart*, H. Bekebrok*, M. Zobel*, A. Dyck*, T. Optenhostert**, C. Spicker**, C. Spitta**,
D. Rasmussen***, L. Tognana****, S. Modena****, D. Laner****,
Y. De Vos*****, J.-P. Janssens*****, M. Francioni*****, and M. Galavotti*****

- * DLR Institute of Networked Energy Systems, Carl-von-Ossietzky-Str. 15, 26129 Oldenburg, Germany
- ** The hydrogen and fuel cell center ZBT GmbH, Carl-Benz-Str. 201, 47057 Duisburg, Germany
- *** BALLARD POWER SYSTEMS EUROPE, Majsmarken 1, DK-9500 Hobro, Denmark
- **** SOLIDpower SpA, viale Trento 115/117 - c/o BIC - Mod C/D, 38017 Mezzolombardo (TN), Italy
- ***** BOSAL EMISSION CONTROL SYSTEMS NV, 20 Dellestraat, 3560 Lummen, Belgium
- ***** Energy Partner SRL, Via Circonvallazione 11/A, 61048, Sant'Angelo in Vado (PU), Italy

Abstract – This contribution gives an overview of the major developments and results of the Design2Service (D2Service) project. The main objective of the project is the improvement of the serviceability of fuel cell-based micro-CHP and back-up power systems. The project seeks this goal by addressing various aspects of the serviceability of the systems; including improvement and standardisation of components, system layout, remote monitoring and diagnosis, service manuals. The improvements are verified in laboratory and field trials.

Index Terms – Back-up power, micro-CHP, PEMFC, SOFC

I. INTRODUCTION

The Design2Service project is a European Union Horizon 2020 project with the main objective of simplification of service procedures and reduction of service effort for fuel cell-based micro-CHP and back-up power systems. A consortium of six European companies and research institutes works jointly on these goals. The project started in August 2015 and ends in March 2020.

II. OVERVIEW OF DEVELOPMENTS AND IMPROVEMENTS

In the following, notable developments and improvements of the D2Service project are briefly described. More detailed information can be obtained from the project website [1].

A. SOFC micro-CHP

Various aspects of the serviceability of a 1.5 kW_{el} SOFC micro-CHP system has been improved by SOLIDpower (SP). The main improvements are listed in table I.

TABLE I
MAIN IMPROVEMENTS OF THE 1.5 kW SOFC MICRO-CHP

Objective	Starting point	Improvements
BOP accessibility	Difficult removal of heavy lateral panels.	Front panel light and easily removable with four cam locks.
Stack	Stack integrated in Hot BoP. Removal requires special tools; can only be performed at SP facilities.	Stack connected to Hot BoP by a flat manifold and integrated into BoP. Stack replacement only at SP facilities; whole BoP is replaced in case of stack failure.
Hot BoP	Hot BoP is part of frame and cannot be replaced outside SP facilities.	Hot BoP including stack can be easily replaced in the installation site with a dedicated tool by one single operator.
Cold BoP	Placed below Hot BoP; layout affected	Cold BoP is placed before Hot BoP;

	by Hot BoP complexity; difficult to reach certain components.	components easily replaceable. Hydraulic and electrical connections are fool proof.
Water treatment system	Simple mixed resin cartridge surrounded by many pipes; difficult to move. Fixed to frame with 4 screws.	Very complex but effective and reliable; contains also a pump to feed the process water and related control board. Easy to remove and mount without tools. Fool proof hydraulic and electrical connections.
Air Filter	Two air filters, one for blower, not easy to handle because surrounded by pipes and cables.	Air filter fixed by a wingnut can be removed and installed without interferences with other devices.
Desulphuriser	Consists of two cartridges; not easily reachable because of cabling and piping; difficult to tighten some connections.	One single cartridge, very easy to replace. Apart from gas connections, the cartridge is fixed with cable ties.

B. Life-time desulphurisation

Catalyst investigations and the following reactor qualification showed potential for retaining the sulphur load over long periods of time. It seems possible to achieve an operating time of 60,000 hours aimed for at the beginning of the project, significantly lowering the maintenance costs. Field tests over life time still have to confirm this.

C. Remote monitoring and diagnosis

A diagnostic tool to estimate the remaining of life of the fuel cell system in back-up power systems taking into account various stack measurements has been developed as well as an air starvation optimisation routine using the diagnostic results to increase the life time of the system and reduce stack replacement.

Remote monitoring systems for micro-CHP and back-up power systems have been improved to facilitate early failure detection and reduce travel and service time costs.

D. Manual Design Guidelines

Guidelines for creating easily understandable service manuals have been elaborated, aiming at enabling non-specialised, local technicians and companies to perform maintenance tasks smoothly (see Fig. 1). The manual design guidelines are available for download from the project website [2].

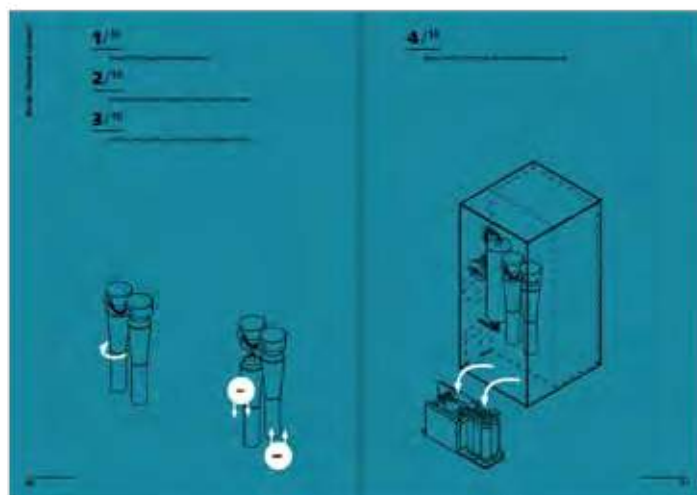


Fig. 1. Excerpt from the manual design guidelines.

E. Laboratory evaluation

Laboratory tests of several micro-CHP versions were performed to investigate system performance under benchmark conditions.

F. Field trial

A field trial with six units is currently being performed to evaluate the system performances as well as the improvements on the systems within the project. Installation configuration variants and the suitability of the technology in several use cases are tested as well.

G. Knowledge transfer

System design knowledge transfer to the development of a 6 kW_{el} micro-CHP based on the 1.5 kW_{el} micro-CHP is taking place within the project duration.

III. CONCLUSION

Within the project, substantial improvements of various aspects of the serviceability of fuel cell-based micro-CHP and back-up power units have been worked on. The verification of these improvements is the main objective of the currently ongoing field trial.

ACKNOWLEDGMENT

This project has received funding from the Fuel Cells and Hydrogen 2 Joint Undertaking under grant agreement No 671473. This Joint Undertaking receives support from the European Union's Horizon 2020 research and innovation programme, Hydrogen Europe and Hydrogen Europe research.

REFERENCES

- [1] D2Service project website, www.project-d2service.eu
- [2] Design Guidelines for easily understandable Service Manuals, <https://project-d2service.eu/documents/>

DEVELOPMENT OF CORE COMPONENTS FOR HIGH TEMPERATURE PEM FUEL CELLS

Maria K. Daletou*, Aikaterini K. Andreopoulou**,
Joannis K. Kallitsis**, Stylianos G. Neophytides*

*Foundation of Research and Technology-Hellas, Institute of Chemical
Engineering Sciences FORTH/ICE-HT, Patras 26504, Greece

**Department of Chemistry, University of Patras, 26504 Patras, Greece

Abstract – Acid doped polymer electrolyte membranes are optimally combined with low Pt loaded electrocatalysts on functionalized carbon nanostructured supports. Different polymeric structures have been used in order to examine the influence of the detailed chemical structure on the final membrane properties. The versatility of the polymerization conditions allows the creation of numerous polyelectrolytes. Combining polar pyridine with apolar or polar units as side or as main chain groups led to a vast library of polymers whose properties greatly depend on the precise chemical and topological architecture of the backbone and the pendant groups. Moreover, stabilization of selected polymeric structures by chemical crosslinking is the method of choice in order to enhance the robustness and integrity of the H₃PO₄ doped membranes. Complementing our work on polymer membranes, efforts to reduce Pt amount at the electrodes focus on the development of electrocatalysts supported on chemically modified supports. Surface chemistry can differentiate the crystal properties and the electrochemical interface. This approach constitutes a promising route for developing materials with innovative features aiming to increased catalyst activity and metal utilization and, ultimately, serious reduction in the Pt loads.

Index Terms – High Temperature Polymer Electrolyte Membrane Fuel Cells, Cross-linked Polymers Electrolytes, Ultra Low Pt Electrocatalysts.

I. INTRODUCTION

High power/high energy applications are expected to greatly benefit from Polymer Electrolyte Membrane Fuel Cells (PEMFCs). The high temperature PEMFCs offer significant flexibility when used as energy converters in stationary, mobile and portable power devices. The Membrane Electrode Assembly (MEA) is a key component of the systems and should have specific properties to withstand the strong conditions during the fuel cell operation. The state of the art MEA

technology is based on H₃PO₄ imbibed polymer electrolytes and Pt based catalysts.

The herein presented work is a combinatorial approach, in which the components of the MEAs, polymer electrolytes and electrocatalysts/electrodes are developed, evaluated and optimized so as to complement each other's properties and requirements.

II. EXTENDED ABSTRACT

A. Polymer Electrolytes

The most widely used and studied polymer electrolyte is polybenzimidazole and its derivatives imbibed with phosphoric acid.¹ Aside those, polymer electrolytes that have gained ground in recent years are pyridine based aromatic polyethers.²⁻⁷ More particularly, our efforts have long concentrated on the development of polymers bearing basic main chain pyridines to ensure interaction and complexation with the strong acid used as proton carrier. Through this route, a large number of functionalized copolymers having high molecular weights, increased solubility, high mechanical integrity and the ability to form complexes with acids has been created bearing in some cases side cross-linkable functionalities that led to stabilized doped membranes which in turn led to extended operation temperatures even up to 210°C.^{5,7,8}

Herein we present our ongoing efforts for the development of high molecular weight but still soluble, robust and at the same time processable, aromatic polyether sulfones that bear less rigid polymer backbones. The polymer electrolytes bear additionally high ratios of side double bonds allowing for their further stabilization via crosslinking.

B. Pt based electrocatalysts

Pt supported on carbon electrocatalysts are the most efficient and stable materials. The low abundance and high cost of Pt make urgent the need to reduce the amounts of Pt used, therefore increase catalyst utilization and/or catalyst's activity⁹. There are three approaches that can be followed separately or combined: (a) enhance the specific activity, (b) increase the specific surface area of the catalyst and (c) form stable and extended electrochemical interfaces, increasing Pt utilization.

Catalyst layers employing pyridine modified CNTs as Pt support were developed¹⁰. The amount of phosphoric acid on the electrodes plays a significant role in the formation of the electrochemical interface¹¹. In situ evaluation of the electrochemical active surface area and catalyst utilization, as well as performance degradation under specific conditions took place. Significant decrease in the Pt loading was achieved, while the stable electrochemical interface formed allows operation under conditions that were prohibitive with conventional catalysts (e.g. harsh reformat conditions at the anode¹²).

The performance and stability of the (electro)catalysts strongly depend on the physicochemical characteristics. Reducing the size of the metal in atoms or small groups of atoms can significantly increase both the active surface and the activity of the catalyst through diversification or strengthening of the metal-support interactions. Exploiting the differentiations induced to the metal by the surface chemistry of the support can result in customized properties and control its performance. In this work, we have developed Pt based electrocatalysts with different surface functionalities and loadings. The introduction of certain groups on the sidewalls of the carbon support resulted in differentiation of the properties, not only in terms of quantitative deposition and dispersion, but also with respect to metal-support interactions, platinum crystal properties and/or oxidative state¹³. Important is the interpretation of the relationship between the electrochemical activity and the structure/composition of the catalysts.

III. CONCLUSION

Towards a sustainable energy economy, this work presents promising routes for developing materials with innovative features aiming to increased performance and durability and decreased cost.

ACKNOWLEDGMENT

Financial support from (a) the Region of Western Greece and the European Regional Development Fund of the European Union in the framework of the Action "Strengthening research and development projects in RIS3", through the projects AdE14PEM ΔE1MΠI-0057 and DemoCHP ΔEP7-0019758, (b) the Fuel Cell and Hydrogen Joint Undertaking (FCH JU), program "Development of a Portable Internal Reforming

Methanol High Temperature PEM Fuel Cell System" IRMF-CFCH-JU-325358 is acknowledged.

REFERENCES

- [1] Li, Q.; Jensen, J.O.; Savinell, R.F.; Bjerrum, N.J.; High temperature proton exchange membranes based on polybenzimidazoles for fuel cells, *Prog. Polym. Sci.* 2009, 34, 449–477.
- [2] Gourdoupi, N.; Andreopoulou, A.K.; Deimede, V.; Kallitsis, J.K.; Novel Proton-Conducting Polyelectrolyte Composed of an Aromatic Polyether Containing Main-Chain Pyridine Units for Fuel Cell Applications. *Chemistry of Materials* 2003, 15 (26), 5044-5050.
- [3] Daletou, M.K.; Kallitsis, J.K.; Voyiatzis, G.; Neophytides, S.G.; The interaction of water vapors with H3PO4 imbibed electrolyte based on PBI/polysulfone copolymer blends. *Journal of Membrane Science* 2009, 326 (1), 76-83.
- [4] Geormezi, M.; Chocho, C.L.; Gourdoupi, N.; Neophytides, S.G.; Kallitsis, J.K.; High performance polymer electrolytes based on main and side chain pyridine aromatic polyethers for high and medium temperature proton exchange membrane fuel cells. *Journal of Power Sources* 2011, 196 (22), 9382-9390.
- [5] Morfopoulou, C.I.; Andreopoulou, A.K.; Daletou, M.K.; Neophytides, S.G.; Kallitsis, J.K.; Cross-linked high temperature polymer electrolytes through oxadiazole bond formation and their applications in HT PEM fuel cells. *Journal of Materials Chemistry A* 2013, 1 (5), 1613-1622.
- [6] Kalamaras, I.; Daletou, M.K.; Gregoriou, V.G.; Kallitsis, J.K.; Sulfonated Aromatic Polyethers Containing Pyridine Units as Electrolytes for High Temperature Fuel Cells. *Fuel Cells* 2011, 11 (6), 921-931.
- [7] Kalamaras, I.; Daletou, M. K.; Neophytides, S. G.; Kallitsis, J. K.; Thermal crosslinking of aromatic polyethers bearing pyridine groups for use as high temperature polymer electrolytes. *Journal of Membrane Science* 2012, 415-416, 42-50.
- [8] Papadimitriou, K. D.; Geormezi, M.; Neophytides, S. G.; Kallitsis, J. K.; Covalent cross-linking in phosphoric acid of pyridine based aromatic polyethers bearing side double bonds for use in high temperature polymer electrolyte membrane fuelcells. *Journal of Membrane Science* 2013, 433, 1-9.
- [9] Notter, D.; Kouravelou, K.; Karachalios, T.; Daletou, M.K.; Haberland, N.T.; Life cycle assessment of PEM FC applications: electric mobility and μ -CHP. *Energy Environ. Sci* 2015, 8, 1969-1985.
- [10] Orfanidi, A.; Daletou, M.K.; Neophytides, S.; Preparation and Characterization of Pt on Modified Multi-Wall Carbon Nanotubes to be used as Electrocatalysts for HT Fuel Cell Applications. *Appl Catal B: Environ* 2011, 106, 379-389.
- [11] Geormezi, M.; Paloukis, F.; Orfanidi A.; Shroti, N.; Daletou, M.K.; Neophytides, S.J.; The structure and stability of the anodic electrochemical interface in a high temperature polymer electrolyte membrane fuel cell under reformat feed. *Journal of Power Sources* 2015, 285, 499-509.
- [12] Orfanidi, A.; Daletou, M.K.; Neophytides, S.G.; Mitigation strategy towards stabilizing the Electrochemical Interface under high CO and H2O containing reformat gas feed. *Electrochim. Acta* 2017, 233, 218-228.
- [13] Zagoraoui, E.; Daletou, M.K.; Sygellou, L.; Ballomenou, S.; Neophytides, S.G.; Highly dispersed platinum supported catalysts - Effect of properties on the electrocatalytic activity. *Appl. Catal. B: Environ.* 2019, 259:art. no. 118050.

FABRICATION AND CHARACTERIZATION OF PLANAR SOFCs MADE BY TAPE CASTING AND SPRAYING TECHNIQUES

R. Campana *, A. Wain-Martin *, E. Nieto* and J. Gorauskis **

* Centro Nacional del Hidrógeno, Prolongación Fernando el Santo
s/n, 13500 Puertollano, (Spain)

**ARAID researcher in ICMA CSIC-UZ, C/ Pedro Cerbuna 12, 50009
Zaragoza, (Spain)

Abstract – The aim of this work is to study the manufacture of a solid oxide fuel cell (SOFC) with Anode/Electrolyte/Barrier/Cathode structure. The nickel-yttria stabilized zirconia cermet (Ni-YSZ) anode supports has been developed using a tape casting method, while the rest of the components were fabricated by wet powder spraying. As components, yttria stabilized zirconia (YSZ) have been used as electrolyte, $\text{Sm}_{0.2}\text{Ce}_{0.8}\text{O}_{1.9}$ (SDC) as diffusion barrier and $\text{La}_{0.6}\text{Sr}_{0.4}\text{FeO}_3$ (LSF) or $\text{La}_{0.8}\text{Sr}_{0.2}\text{MnO}_3$ (LSM) as cathodes. In addition, an interlayer composed by diffusion barrier and cathode have been added to improve mechanical properties and adherence between the cathode thin films. The cells were characterized using a Scanning Electron Microscope (SEM). An electrochemical characterization has been carried out in a button cell test rig (NorECs) measuring polarization curves with a multichannel Potentiostat/Galvanostat VMP3 (Biologic), feeding humidified H_2 at 3% as reactant gas in the anode compartment and air in the cathode one at 800 °C.

Index Terms – Processing, SOFC, Tape Casting, Wet Powder Spraying.

I. NOMENCLATURE

LSF	$\text{La}_{0.6}\text{Sr}_{0.4}\text{FeO}_3$
LSM	$\text{La}_{0.8}\text{Sr}_{0.2}\text{MnO}_3$
Ni-YSZ	Nickel-Yttria stabilized zirconia
SDC	$\text{Sm}_{0.2}\text{Ce}_{0.8}\text{O}_{1.9}$, Samarium doped ceria
SEM	Scanning electron microscopy
SOFC	Solid oxide fuel cell
TEC	Thermal expansion coefficient
YSZ	$(\text{ZrO}_2)_{0.8}(\text{Y}_2\text{O}_3)_{0.2}$ Yttrium stabilized zirconia
WPS	Wet powder deposition

II. INTRODUCTION

In recent years, solid oxide fuel cells (SOFC) technology has

attracted attention due to the advantages in terms of high efficiency, low noise and low emissions [1]. SOFCs systems operate between 600 and 1000°C and the main used configurations are tubular and planar. Tubular SOFCs present good thermal shock resistance and an easy sealing, separating efficiently anode and cathode sides. On the other hand, planar SOFCs exhibit the advantages of presenting higher power densities and simpler manufacturing processes than their tubular counterparts, but still face important challenges for their commercialization.

Manufacturing processes for planar SOFC supports are usually performed by tape casting, which is one of the most suitable ceramic processing technique to obtain large surface flat tapes. Additionally, fabrication of coatings is usually made by techniques such as dip coating, screen printing or chemical vapor deposition. Wet powder spraying (WPS) is considered an alternative processing route, suitable for different geometries and applicable in large-area ceramic layers controlling the morphologies, with the advantages of being a simple and low-cost technique.

Owing to its favorable mechanical and chemical properties in oxidizing and reducing atmospheres and high ionic conductivity, 8 mol% Y_2O_3 stabilized ZrO_2 (YSZ) is the most used electrolyte. Considering YSZ as electrolyte, Ni-YSZ cermet fulfills most of the requirements of an ideal anode, due to the high catalytic activity for hydrogen oxidation and the thermal expansion coefficient (TEC), close to YSZ TEC, it is important to have a good adherence. In cathodic side, perovskites such as $\text{La}_{0.6}\text{Sr}_{0.4}\text{FeO}_3$ (LSF) or $\text{La}_{0.8}\text{Sr}_{0.2}\text{MnO}_3$ (LSM) are suitable candidates to be used as SOFC cathodes, presenting good properties to be used as cathode, including a proper oxygen reduction reaction catalytic activity. In order to prevent the formation of poorly conducting secondary phases,

such as $\text{La}_2\text{Zr}_2\text{O}_7$ or SrZrO_3 , the use of protective barriers like samarium doped ceria (SDC), between the cathode and electrolyte is commonly used.

The current work describes the fabrication of SOFCs by tape casting and WPS deposition, performing the characterization of them, to later scale up the dimensions of the cells.

III. EXPERIMENTAL

Anode supported cells have been fabricated and characterized in this work. The cells consist of a porous anode made by Ni-YSZ, a dense electrolyte of YSZ, a diffusion barrier interlayer of SDC and a porous cathode (LSF or LSM). To overcome failures related with the thermal expansion coefficients, a composite layer has been added between the barrier and cathode, made from the mixture of the two components.

For the fabrication of the NiO-YSZ anode tapes, the amount of binder and surfactant were optimized in the slurry, and the doctor blade gap was adjusted in 180 μm thick, achieving 65 cm long and 11 cm wide tapes (Figure 1a)). For the production of the supports, 3 tapes were cut with a diameter of 26 mm and then assembled using hot pressing (40 bar and 125 $^\circ\text{C}$). Afterwards, the sinterization was performed at 1100 $^\circ\text{C}$, getting an homogeneous adherence between the tapes, with a suitable porosity and microstructure for the anodes. Later, the deposition of additional layers has been carried out at room temperature, using an Iwata Eclipse HP-BCS airbrush. For the preparation of the deposition inks, the starting powders were ground through ball milling for 24 h, using 2-propanol as solvent. Subsequently, all layers were sintered at 1050 $^\circ\text{C}$ for 2 h, except in the case of YSZ electrolyte, in which 1350 $^\circ\text{C}$ have been applied. The thermal treatment of YSZ layer has been optimized until a good planarity has been achieved for a posterior stacking, while the density is high enough to avoid gas leakage. In this way, cells with a thickness of 550 μm and 20 mm diameter have been achieved, with a cathode active area of 2.54 cm^2 (Figure 1b)).



Fig. 1. Photographs of (a) the top view of the green tape and (b) complete cells.

IV. RESULT AND DISCUSSION

A. Morphological characterization

Figure 2 presents the micrographs of cells cross sections after electrochemical characterization. As can be seen, the cells were composed of a thick Ni-YSZ anode support, a 15 μm YSZ electrolyte, 5 μm SDC barrier, 15 μm mixed composite

interlayer and 25 μm cathode (LSF or LSM). The SEM image confirms that the thin films homogeneity is adequate and that the components have a good adherence between them, without cracking and delamination.

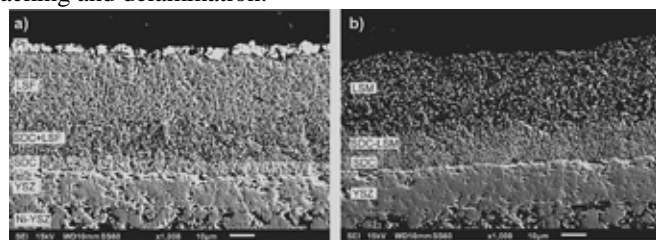


Fig. 2. Cross section of the cells using a) LSF and b) LSM as cathode, after measuring them.

B. Electrochemical characterization

Current-voltage and current density characteristics of both single cells at 800 $^\circ\text{C}$ are shown in Figure 3.



Fig. 3. I-V and I-P curves at 800 $^\circ\text{C}$ of the cells with a) LSF and b) LSM as cathode.

The maximum power densities at 400 $\text{mA}\cdot\text{cm}^{-2}$ current density and 800 $^\circ\text{C}$ are 223 $\text{mW}\cdot\text{cm}^{-2}$ and 211 $\text{mW}\cdot\text{cm}^{-2}$ for LSF and LSM cathode cells, respectively.

V. CONCLUSION

In this work cells with different cathodes have been processed and studied. The experimental study shows good electrochemical performances at 800 $^\circ\text{C}$, showing a slightly higher potential when LSF is used as cathode. In this way, a first attempt has been done before study the long term degradation and scale the size of the cells.

ACKNOWLEDGMENT

This research has been co-financed by the Junta de Comunidades de Castilla La Mancha and European Union under the European Regional Development Fund (FEDER) [ABPLY/17/180501/000550].

REFERENCES

- [1] Boudghene Stambouli A., Traversa E., Solid oxide fuel cells (SOFCs): a review of an environmentally clean and efficient source of energy, Renewable and Sustainable Energy Reviews, Volume 6, 2002, Pages 433-455.

DEVELOPMENT AND INVESTIGATION OF A TUBULAR HT-PEM-FUEL CELL WITH 3D-PRINTED ANODE GDL

María Catalina Bermúdez Agudelo*, and Manfred J. Hampe*

* Institute for Nano- and Microfluidics (NMF), Thermal Process Engineering Group (TVT), Technische Universität Darmstadt, Otto-Berndt-Str. 2, 64287 Darmstadt, (Germany)

Abstract - Tubular HT-PEM-fuel cells were developed using 3D-printed metallic porous elements fabricated *via* powder bed fusion using a laser beam (PBF-LB) process as anode gas diffusion layer (GDL). The morphology of the 3D-printed elements was examined by means of SEM micrographs. The manufactured fuel cells were electrochemically characterized in a commercial test station under atmospheric pressure, 160°C and H₂/air gas-feeding. Additionally, a short-term stability test at constant load (0.1A) for 45h was conducted. Initially, the effect of the fabrication material was evaluated using EN 1.4542 stainless steel and EN 1.4404 stainless steel. Subsequently, the influence of a post-treatment was assessed using the material that exhibited the best performance in the previous evaluation. A positive impact on overall performance was obtained with GDL manufactured using material EN 1.4404 stainless steel and without post-treatment. Results indicate that PBF-LB process is a promising technology for development of robust GDLs and alternative designs in future.

Index Terms - Additive Manufacturing, Gas Diffusion Layer, Fuel Cell Performance, Tubular HT-PEM-fuel cell.

I. INTRODUCTION

The planar geometry is the most used design for HT-PEM-fuel cells, both in research and market. However, alternative designs may have certain benefits with respect to fabrication costs, gravimetric and volumetric power density. Additionally, the tubular fuel cells design is a promising candidate for future developments of fuel cell stacks due to the absence of bipolar plates, the smaller sealing surfaces and the flexible disassemble/reassemble of individual defective cells. In the field of HT-PEM fuel cells, the tubular design is still under development and only few studies have published in this topic [1, 2].

In this work, tubular HT-PEM-fuel cells with these two fabrication materials and a post-fabrication treatment

for the 3D-printed anode GDL are investigated. The morphology of the anode GDLs are examined by SEM analysis and the fuel cell performance is evaluated by means of single cell electrochemical characterization and short-term stability test.

II. EXPERIMENTAL

A. Tubular HT-PEM-fuel cell preparation

The process PBF-LB is used to produce the 3D-printed anode gas diffusion layer (GDL). For the membrane electrode assembly (MEA) fabrication, two coating processes were applied in three subsequent steps. Catalyst inks are prepared dispersing homogeneously a commercial catalyst powder (HisPEC 3000) and a PTFE dispersion in an alcohol/water solution. A spray coating process is used to deposit both inks. After the 3D-printed anode GDL was coated with the anode catalyst ink, the sol-gel membrane was applied by a dip coating process. Once the gelation process took place, the second catalyst ink was sprayed (cathode side). Finally, a commercial carbon hose (KB-4002) was employed as cathode GDL and fixed with a tungsten wire using a lathe machine.

B. Single fuel cell testing

The produced tubular HT-PEM-fuel cells with an area of 4.78 cm² were tested with the fuel cell test station Evaluator C100 under atmospheric pressure, 160°C and H₂/air gas-feeding, with flow rates of 2.64 cm³ s⁻¹ and 52.86 cm³ s⁻¹, respectively. The polarization curve was recorded from open circuit voltage (OCV) to 0.25V with a holding time of 120s per point. The fuel cell resistances were measured by *in situ* EIS measurements at 0.1A. Besides a stability test was conducted for 45h interrupted by *in situ* measurements every 5h.

III. RESULTS AND DISCUSSION

SEM micrographs of the 3D-printed anode GDLs under investigation are presented in Fig. 1. In the one hand, materials EN 1.4542 stainless steel (GP1) and EN 1.4404 stainless steel (316L) show a similar surface morphology (cf., left and middle figures). On the other hand, the post-treated piece (right figure) exhibited an even surface, due to the fact that the small particles attached to the principal structure were removed through the treatment.

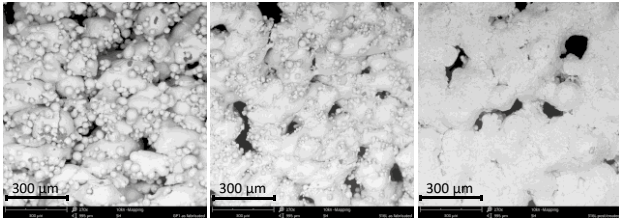


Fig. 1. Micrographs of the 3D-printed anode GDL with GP1 (right figure), 316L (middle figure) and 316L post-treated (left figure).

Fig. 2 shows performance of the evaluated fuel cells (upper) and presents the corresponding impedance spectra (down). This work involves two studies: in the first study two different anode GDL materials were assessed (orange color); then the material 316L was selected to conduct a second investigation. Two 3D-printed anode GDLs were compared: one as fabricated and one post-treated with a micro blasting process (black color). Different platinum loading was used for the studies. In the first case anode and cathode loading was 0.48 mg cm^{-2} and 0.46 mg cm^{-2} , respectively; while the second study used 0.74 mg cm^{-2} and 0.41 mg cm^{-2} .

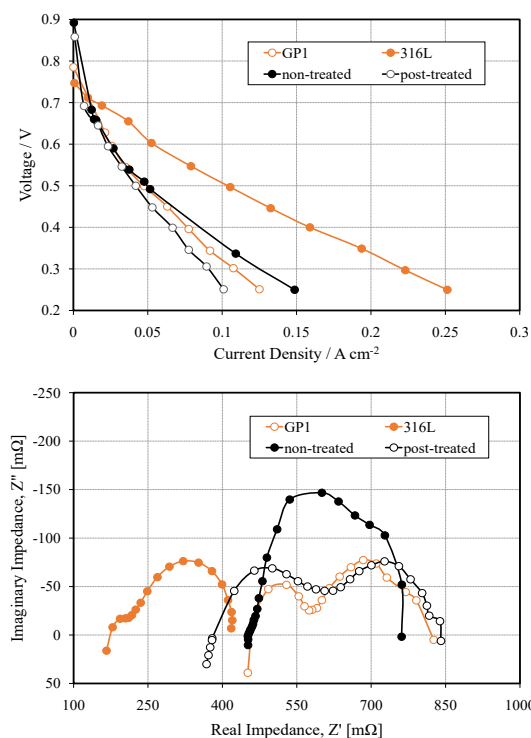


Fig. 2. Electrochemical characterization: polarization curve (upper figure) and Nyquist plots at 0.1 A (lower figure). Tubular HT-PEM-fuel cell with 3D-printed anode GDL using materials: GP1 (○), 316L (■), and non-treated (●), post-treated (◐) specimens.

The polarization curves in Fig. 2 (upper figure) show that 316L material has a positive effect on overall performance. Comparing to the material GP1, this result can be attributed to a possible higher corrosion resistance in fuel cell operation and the lower membrane and electrochemical resistances (lower figure). Also, it can be seen that the performance of the fuel cell constructed upon the blasted 3D-printed anode GDL is lower along the current density region, with higher influence as the current density increases, although the post-treated prototype displayed a lower membrane resistance. Additionally, all fuel cells experienced degradation along the short-stability test, however, the fuel cells with 316L material and without post-treatment exhibited a less strong decay compared with the GP1 material and the post-treated anode GDL.

IV. CONCLUSION

The present work provides an important progress regarding alternative fuel cell designs. In order to manufacture functional tubular HT-PEM-fuel cells, the PBF-LB process was used to fabricate the novel 3D-printed anode GDLs. This 3D-printing technique demonstrated not only its potential in the production of fuel cell components but also its feasibility in the incorporation of new geometrical designs in the fuel cell field. In two studies the material of the anode GDL was investigated. The results reported here from these studies indicate that tubular HT-PEM-fuel cells with 3D-printed anode GDL using 316L material and without post-treatment have higher fuel cell performance and stability over the short-term test period. The peak power density reached 0.068 W cm^{-2} and 0.037 W cm^{-2} for the first and the second study, respectively; which means an increment in performance by 108% and 36% was achieved compared with the GP1 material and the post-treated anode GDL.

ACKNOWLEDGMENT

This work was financially supported by the German Research Foundation (DFG) under the Project HA 1283/11-1. The authors thank the Institute of Production Management, Technology and Machine Tools (PTW), Technische Universität Darmstadt for its collaboration in the production of the 3D-printed elements.

REFERENCES

- [1] Abele, Eberhard, Stoffregen, Hanns, Lang, Sebastian, Hampe, Manfred Josef, Elektrode zum Betrieb einer Brennstoffzelle und Verfahren zur ihrer Herstellung, Technische Universität Darmstadt, EP 2744028 A1, 18.06.2017
- [2] Lang, Sebastian, Entwicklung tubularer Mitteltemperatur-Brennstoffzellen - Experimentelle Untersuchungen, Modellierung und numerische Simulation, München, Dr. Hut, 2016.

NEW Cu/Me_xO_y and Cu/SrTiO₃ CATALYTIC MATERIALS FOR DRY REFORMING AND SYNTHESIS OF METHANE.

A. Adrian Mizera*, B. Patryk Błaszczak**, C. Ewa Drożdż*,
D. Piotr Jasiński***, E. Beata Bochentyn**

* Faculty of Materials Science and Ceramics, AGH University of
Science and Technology, al. A. Mickiewicza 30,
30-059 Kraków, Poland

** Faculty of Applied Physics and Mathematics, Gdansk University
of Technology, 80-233 Gdańsk, ul. Narutowicza 11/12, Poland

*** Faculty of Electronics, Telecommunications and Informatics,
Gdansk University of Technology, 80-233 Gdańsk,
ul. Narutowicza 11/12, Poland

Abstract – Reforming and synthesis of methane are processes that can be involved into syngas preparation as well as energy storage. In order to provide high reaction efficiency new catalytic materials based on metal oxides Me_xO_y (Me=Zr, Ce, Al) or SrTiO₃ infiltrated with Cu were prepared. Influence on catalytic activity of microstructure, surface area, Cu loading and composition of as synthesized materials were examined using fixed-bed quartz reactor and in situ measurement of outlet gas composition. Bohemite containing 5 wt% of Cu metal revealed best catalytic properties towards methane dry reforming in short-term tests with 24 % maximum CO yield. Proper design of ceramic substrate allows to obtain stable and efficient catalysts.

Index Terms – catalyst, dry reforming of methane, impregnation, methanation.

I. INTRODUCTION

Increasing concentration of greenhouse gases (e.g., CH₄, CO₂) in atmosphere causes much effort being put into development of technologies, that allow the conversion of those into other, industrially useful products. For such purposes, dry reforming of methane (DRM) or methanation processes can be involved. DRM is the process, which enables the production of syngas using both methane and carbon dioxide ensuring elimination of harmful CO₂ from the atmosphere. Methanation process allows converting CO_x and hydrogen into methane that can be easily stored and further utilized if needed. Regardless of the considered process, the catalytic material must provide high catalytic activity as well as chemical stability and increase the efficiency of the reaction. In case of both processes, widely

used in industry catalyst, are based on nickel dispersed onto alumina support. Despite high catalytic activity and relatively low price [1,2], nickel susceptibility towards coking and its tendency to agglomerate, prompt to seek for alternative materials.

II. MATERIALS PREPARATION

All samples were prepared using incipient wetness impregnation to achieve 1 and 5 wt. % of Cu load in resultant materials. Proper copper (II) nitrate aqueous solutions were added to a catalyst supports, which were as follows: ZrO₂ prec. (obtained from precipitation method), ZrO₂ cit. (synthesized via citrate-combustion method), CeO₂ (Sigma-Aldrich, ≥99.0%), Al₂O₃ (TM-DAR 99.99%, Taimei Chemicals Co. Ltd.), bohemite and SrTiO₃ (from citrate-combustion synthesis). After impregnation, the materials were dried at 80 °C and calcined at 250 °C. Before catalytic tests, samples have undergone reduction in dry hydrogen at 600 °C for 2h.

III. EXPERIMENTAL

A. Methods

The XRD analyses were carried out by using Panalytical X'Pert Pro diffractometer. The microstructure of the prepared materials was observed using scanning electron microscope FEI Quanta 250 FEG. Catalytic tests were performed in fixed-bed quartz reactor within the temperature range from 500 to 800 °C

and 25 to 700 °C for DRM and methanation tests, respectively. FTIR spectroscope was used in order to determine the amounts of reactions products. Additionally, development of active surface area was investigated using BET isotherm.

B. Results

Selected catalytic tests of DRM process results for the materials are presented in Fig. 1. The highest methane conversion efficiency, up to 24 %, was demonstrated by sample containing 5 wt.% of Cu on the bohemite support (Fig. 1, red curve). Both infiltrated ZrO₂ samples obtained by precipitation method showed the lowest efficiency of ca. 2 %. In case of bohemite, the increase of Cu content in the material from 1 to 5 wt.%, resulted in doubled maximum amount of produced carbon monoxide during the process (from 12 to 24%). For SrTiO₃-based sample, the amount of CO also increases for higher Cu loads. From 6 to 18 % for 1 wt.% Cu and 5 wt.% Cu, respectively.

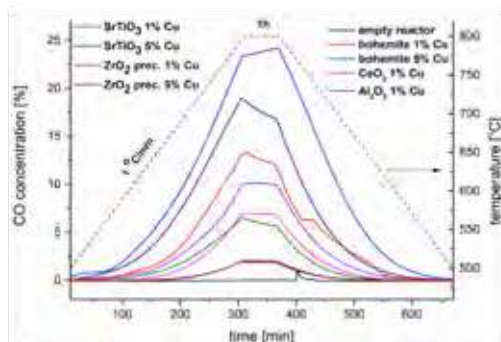


Fig. 1. CO concentration as a function of temperature for selected samples subjected to catalytic tests in the DRM reaction.

Figure 2. shows the change in concentrations of products (CO) and reagents (CH₄, CO₂) for a 5 wt.% Cu-impregnated bohemite. The arrows indicates the direction of heating/cooling cycle. In case of bohemite, the shape of the curves is similar during the heating and cooling of the system. Such behavior may indicate, that material has a high resistance towards coking and high chemical stability over testing time.

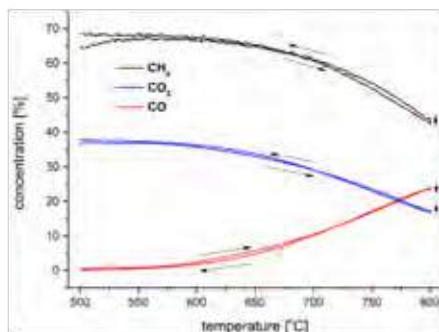


Fig. 2. Concentrations of the reagents during catalytic test of 5 wt. % of Cu on bohemite support.

In case of Cu dispersed onto SrTiO₃ surface (5 wt.% of Cu),

the discrepancy between heating and cooling curves is more pronounced (Fig. 3.). This behavior results from lowering catalytic activity of prepared catalyst in a short period of time, probably due to coking and microstructural changes.

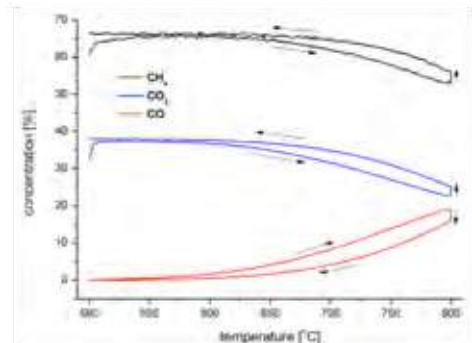


Fig. 3. Concentration of the products/reagents during catalytic tests of 5 wt.% of Cu on SrTiO₃ support.

IV. CONCLUSION

The influence of copper amount on catalytic activity of the materials and hence on carbon monoxide concentration is clearly visible in bohemite as well as SrTiO₃. Microstructure, composition and metal loading affects final CO yield. Those properties depends strictly on substrate's preparation route. Bohemite decorated with 5 wt.% of Cu revealed so far the best short-term efficiency towards dry reforming of methane.

ACKNOWLEDGMENT

This work was supported by the 5th Polish-Taiwanese/Taiwanese-Polish Joint Research Project PL-TW/V/4/2018 "Materials for Direct Power-to-Hydrocarbon Conversion" granted by the National Centre for Research and Development of Poland and Ministry of Science and Technology of Taiwan.

REFERENCES

- [1] Delmelle, R.; Duarte, R.B.; Franken, T.; Burnat, D.; Holzer, L.; Borgschulte, A. "Development of improved nickel catalysts for sorption enhanced CO₂ methanation." *International Journal of Hydrogen Energy* 41 (2015) 20185–20191
- [2] Therdtianwong, Supaporn, et al. "Synthesis gas production from dry reforming of methane over Ni/Al₂O₃ stabilized by ZrO₂." *International Journal of Hydrogen Energy* 33.3 (2008) 991-999.

INTERFACE REACTIVITY OF ORIENTED OR POLYCRYSTALLINE ALD-PROCESSED ULTRA THIN LAYERS FOR SINGLE OR HYBRID HIGH TEMPERATURE FUEL CELLS

M. Cassir, A. Grishin, D. Mendoza Muñiz, M-H. Chavanne, A. Ringuedé

PSL Research University, Chimie Paristech-CNRS, Institut de Recherche de
Chimie de Paris, 11 rue Pierre et Marie Curie, F-75231 Paris Cedex 05,
France ; michel.cassir@chimieparistech.psl.eu

Abstract – This work is dedicated to the processing of interfacial layers by Atomic Deposition Layers (ALD) either for SOFC & SOFC/MCFC or PCFC/SOFC devices. The feasibility of producing oriented or polycrystalline layers is analyzed. Properties and electrochemical behavior of either YDC or BCY are investigated showing what practical advantages may result, *i.e.* in the case of epitaxial YDC layers.

Index Terms: Thin layers, ALD, BCY, SOFC/PCFC.

I. INTRODUCTION

The role of ultrathin layers with respect to the performance of high temperature fuel cells has largely been developed in the literature concerning mainly solid oxide fuel cells (SOFC) but also proton conductor fuel cells (PCFC) and molten carbonate fuel cells (MCFC). We will focus on two kinds of electrolyte thin layers: yttria-doped ceria (YDC) and yttria-doped cerate (BCY). YDC has very interesting catalytic properties towards hydrogen oxidation (probably also towards direct oxidation of methane) in SOFC or hybrid SOFC/MCFC devices. We selected atomic layer deposition (ALD) to process homogeneous and dense polycrystalline and oriented ceria and YDC layers of different thicknesses. Structural, morphological and electrochemical approaches are used to analyze the role and properties of such layers [1]. BCY ($\text{BaCe}_{0.85}\text{Y}_{0.15}\text{O}_{2.925}$) has the property of conducting protons and oxide ions recombining them to form protons. This electrolyte has been proposed in a dual membrane fuel cell combining PCFC anode and SOFC cathode (so-called ideal cell [2]). The main purpose here is to evaluate the feasibility and efficiency of ultrathin conformable and dense layers of BCY15 by ALD as electrolyte catalysts [3].

II. YDC THIN LAYERS FOR SOFC AND SOFC/MCFC APPLICATIONS
Pure ceria and YDC films were obtained by a thermally activated ALD process within a SUNALETM R-200 ALD tool. Precursors and procedure were described elsewhere [4,5]. The temperature of substrate was fixed at 250 °C. In order to obtain epitaxial layers of pure and doped ceria, a YSZ substrate (9.5 mol.% Y_2O_3) oriented (100) was used. For polycrystalline layers, the compatible YSZ pellets were made of YSZ powder (8 mol.% Y_2O_3), annealed at 1350 °C for 4 hours and polished on both sides. The structure of 100-nm-thick YDC thin film (15 at. % for Y^{3+}) was demonstrated by XRD in the Bragg-Brentano configuration. Fig. 1 (left) shows XRD of the layer deposited on YSZ(100) and that of pristine substrate. Both phases are

indexed in the cubic space group system Fm3m (225). The most intense maxima are attributed to YSZ substrate (indexed by asterisks), the other phase is attributed to YDC doped layer. For YDC15 deposited on monocrystalline YSZ (100), we observed only 4 intense maxima, corresponding to (200) and (400) planes of YDC15. Two other maxima are assigned to single-crystal substrate YSZ (100). Presence of only 2 peaks tends to show an epitaxial growth of the layer in a preferential crystallographic direction [100] perpendicular to the surface. Epitaxy between YDC15 layer and YSZ (100) was evidenced by ϕ -scan (Fig. 1, right). Two Bragg angles were set at 47.68° (YDC layer) and 50.08° (YSZ (100)), then the scan was done in the range 0-360° by rotation of the sample. Reflections occur at the same angular values of the substrate with an offset of 90°. Therefore, an epitaxial relation can be defined as (100)YDC || (100)YSZ, or as [001]YDC || [001]YSZ, indicating growth of YDC15 layer in the direction perpendicular to surface [001].

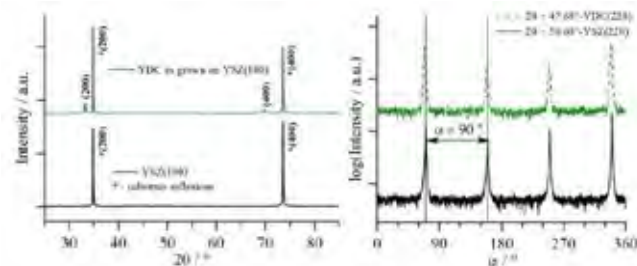


Fig. 1- XRD pattern of monocrystalline (100)-oriented YSZ substrate and 100-nm-thick YDC15 as grown on this (left). ϕ -scans at 47.68° corresponding to (220) plan of YDC15 100-nm-thick film and that at 50.08° corresponding to the same plan of YSZ(100) substrate.

Reactivity of epitaxial and polycrystalline YDC thin films in a hydrogen reducing atmosphere was analyzed by impedance spectroscopy in comparison with layers of pure ceria (epitaxial and polycrystalline) deposited also processed by ALD. The asymmetrical two electrodes set-up was already described by Marizy *et al.* [5]. Once the layers are exposed to H_2 , electronic conduction is favored by ceria reduction and the total resistance of the system (intersection of Nyquist diagrams with real axis) is registered as a function of the reduction time (Figs 2 and 3). Regarding the reactivity of pure ceria (Fig. 2), the epitaxial layer is more reactive with respect to hydrogen, compared to the polycrystalline one. The kinetics of the reduction process is the derivative of total resistance as a function of time. Clearly, epitaxy improves the properties of ionic transport within the crystallographic structure, accelerating the reduction.

Moreover, yttrium doping of CeO_2 stabilizes this structure, without a notable decrease in the reduction kinetics by H_2 . As shown in Fig. 3, the reduction rate of both (100)-oriented epitaxial CeO_2 and YDC layers remains the same. Nevertheless, when a stable resistance value is reached, we can consider the difference between these resultant values. This difference can be attributed to residual conductivity present in YDC layer compared to pure ceria (conduction by O^{2-} due to the introduction of Y^{3+}). Furthermore, we showed that depositing ceria layer between the anode and electrolyte in a hybrid SOFC/MCFC system increases the cell performance by 1.4.

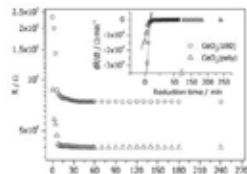


Fig. 2- Resistance evolution in systems YSZ substrate/ CeO_2 100-nm-thick films (epitaxial and polycrystalline) as a function of time (10 vol.% of H_2 at 430°C).

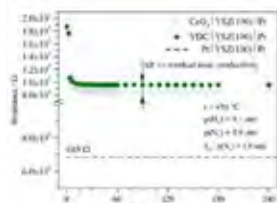


Fig. 3- Resistance evolution in systems YSZ(100) substrate/ CeO_2 (100) and YDC15(100) epitaxial 100-nm-thick films as a function of time. The 685 ohm resistance value, shown as reference, corresponds to the (100)-oriented YSZ substrate without films.

III. BCY THIN LAYERS FOR IMPROVING PCFC/SOFC DEVICES

The first goal was to stabilize and optimize the composition of the ternary BCY compound. Here again we used an ALD-Picosunale vertical reactor R200. The precursors were organometallic compounds: tetrakis (2,2,6,6-tetramethyl-3,5-heptanedionato) (tmhd) for cerium and yttrium, and (isopropylcyclopentadienyl) (iPr_3Cp) $_2$ for barium. The layers were processed on non-oriented Si wafer substrate or other substrates (BCY15 pellets, stainless steels...) within an optimal temperature range with respect to ALD cycles, related to the thickness of the layers [6-8]. Temperatures of $250\text{-}300^\circ\text{C}$ were explored, selecting finally $290\text{-}300^\circ\text{C}$ as the optimum temperature for stable film growth. The big difficulty was to avoid formation of BaCO_3 . The samples of 70 to 100 nm were analyzed by Grazing Incidence XRD, EDS analysis, SEM microscopy, ToF-SIMS and XPS. In some conditions we obtained in majority a BCY10 phase ($\text{BaCe}_{0.90}\text{Y}_{0.10}\text{O}_{2.95}$); in general, it coexisted with CeO_2 and/or YDC phases. Layers were homogeneous at the level of surface and thickness. However, distribution of elements, in particular Ba, was mostly non-homogeneous along the layer thickness. Ba was enriched at the extreme surface and at the interface between the layer and Si substrate. We succeeded in few cases to produce homogeneous distribution of Ba, Ce and Y, with two phases: $\text{BaCe}_{0.85}\text{Y}_{0.15}\text{O}_{2.95} + \text{YDC}$, as seen in Fig. 4.

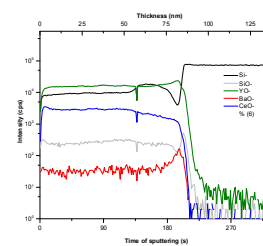


Fig. 4- ToF-SIMS depth profile of BCY deposited on Si wafer by ALD (300°C , 6:10:2 cycle). The measurement was carried out on a dual-beam ToF-SIMS V spectrometer, with Bi^+ as secondary ion producer and Cs^+ as the sputter of material.

Electrochemical impedance spectroscopy, EIS was developed to investigate the electrical/electrochemical properties of ALD-processed layers onto BCY15 substrates. Arrhenius plot in Fig. 5 shows the comparative behavior of the previously mentioned ALD-layer (Fig. 4) deposited on a BCY15 substrate with respect to pristine BCY15 pellet. It can be seen that from temperatures below 530°C , the added layer improves the conductivity of the electrolyte system; this is due to the nature of the layer BCY10 + YDC and homogeneity of the distribution of elements within it.

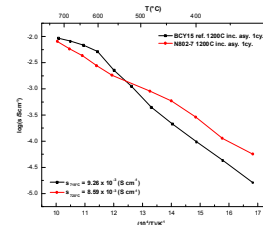


Fig. 4- Arrhenius plots at $320\text{-}720^\circ\text{C}$ from EIS measurements. BCY15% is the reference and N802-7 thin film is deposited on a BCY15 pellet (sintering at 1200°C). Flow 65 mL/min with 50% of H_2 and N_2 in a humidified system at 50°C .

Conclusion

Processing thin layers by ALD has a large scope of breakthrough applications. We proved the feasibility of depositing highly oriented epitaxial YDC deposits, with as major result the reduction of YDC under hydrogen, more intense and efficient for oriented YDC than for polycrystalline YDC. First tests show that depositing by ALD a ceria layer (between anode and electrolyte) in a hybrid SOFC/MCFC system provides better performance than polycrystalline YDC. As for BCY, although deposition of Ba-containing electrolyte is a difficult challenge, we succeeded in obtaining a compound with a stoichiometry close to BCY10, with some proportion of CeO_2 and/or YDC within the interfacial layer. We also analyzed systematically the electrochemical properties of the layers, showing in some cases their benefits on the performance.

- [1] A. Grishin, Ph.D. dissertation, University Paris 6 (2019).
- [2] A. Thorel, French Patent N° 0550696000 (2005).
- [3] Diego Mendoza, Ph.D., PSL-University, unpublished results.
- [4] T. Désaunay *et al.*, *J. Catal.* 297 (2013) 297, 193.
- [5] A. Marizy, P. Roussel, A. Ringuedé, M. Cassir, *J. Mater. Chem. A* 3, 503 (2015) 10498.
- [6] S. Acharya, *et al.*, *J. Mater. Chem. C*, 4 (2016) 1945.
- [7] J.H. Shim, *et al.*, *Chem. of Mater.*, 21 (2009) 3290.
- [8] J. An, Y.B. Kim, J.S. Park, J.H. Shim, T.M. Gur, F.B. Prinz, *J. Vacuum Sci. & Tech. A: Vacuum, Surfaces, and Films*, 30(2012) 01A161.

MODELLING LIQUID WATER EFFECT ON PROTON-EXCHANGE MEMBRANE FUEL CELLS

J. A. Aguilar*, A. Husar*

*Institut de Robòtica i Informàtica Industrial, Barcelona, (Spain)

Abstract - This work introduces our ongoing research in developing accurate models for predicting and analyzing Proton-Exchange Membrane Fuel Cells performance. An initial model, whose response is compared with experimental data is first implemented. The simulated (and theoretically expected) cell voltage deviates from real behavior when the operating conditions change. Then an improved model, aimed to better approximate instantaneous voltage response to changing operating conditions by including liquid water dynamics, is developed. The results show that the new model achieves a better approximation of the voltage profile. The model is validated through experiments on a real fuel cell test-bench.

Index Terms - ECSA, fuel cell modelling, liquid water dynamics, proton-exchange membrane fuel cells

I. NOMENCLATURE

V	Voltage
R	Universal gas constant
T	Temperature
T_{REF}	Reference temperature
α	Charge transfer coefficient
F	Faraday constant
P_c	Cathode gas pressure
P_{cREF}	Cathode gas reference pressure
i	Current
A	Catalyst layer geometric area
ΔG	Gibbs free energy change
J	Water flux

II. INTRODUCTION

Many variables affect the performance of a fuel cell, specifically, water, among them is an important and hard to model one. Liquid water is produced in the cathode catalyst layer during fuel cell operation and it is also removed through evaporation, diffusion and transport.

Electrical power generation in Proton-Exchange Fuel Cells (PMFC) is based on two electrochemical half reactions, that produce a potential difference between the anode and cathode electrodes, the main resultant specie is liquid water [1].

Starting with the Butler-Volmer equation, fuel cell voltage can be modeled as a function of operating conditions and cell parameters (1):

$$V = E_N - \frac{RT}{\alpha 2F} \ln\left(\frac{i}{i_0}\right) - \frac{RT}{\alpha 2F} \ln\left(\frac{P_c}{P_{cREF}}\right) \quad (1)$$

The cell output voltage is usually modeled as the result of subtracting three sources of voltage losses from an ideal Nernst potential (E_N).

The first subtracted term represents the so called activation voltage losses (2). These losses are a function of two operating conditions temperature (T) and load current (i) and an internal cell parameter, exchange current density (i_0).

$$V_{act} = \frac{RT}{\alpha 2F} \ln\left(\frac{i}{i_0}\right) \quad (2)$$

III. INITIAL MODEL

The initial model has been created in Simulink® following a modular architecture with differentiated parts for each of the main components of the fuel cell. As part of the INN-BALANCE project, a series of experiments have been carried out to characterize cell dynamic. Figure (1) shows the results of a stoichiometry sweep experiment: oxygen (cathode) stoichiometry is stepped down through time while all other operating conditions (including anode stoichiometry) are held constant.

It can be noted in the experimental curve that, when input oxygen stoichiometry changes to a lower level, the cell voltage decreases following that dynamic at first, however, after some time and even though every other cell input variable remains constant (temperature, current, pressure) the voltage recovers to a close value of the initial higher value in the step. This behavior is not accurately reproduced by the simulated curve, this one follows the decrease in oxygen flow and steps down to a lower voltage level remaining in it through the full step time.

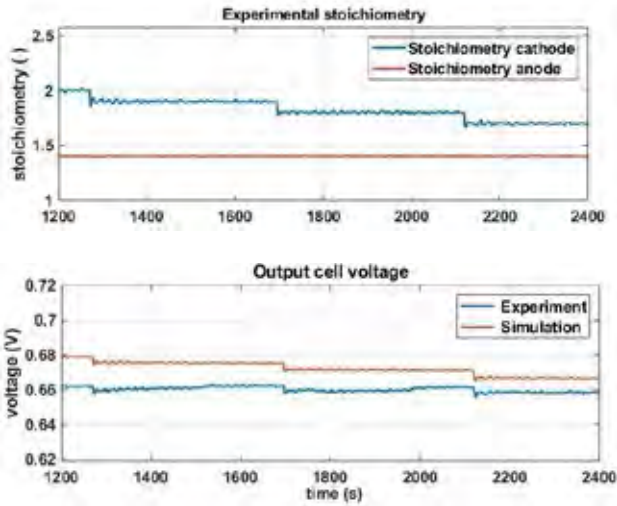


Fig. 1. Stoichiometry sweep experiment at cathode (anode constant) and comparison between real and simulated voltage

IV. IMPROVED MODEL

A. Liquid Water Dynamics

As stated before, activation losses depend on, among others, the exchange current density, furthermore, i_0 is related with the catalytic efficiency of the Cathode Catalyst Layer (CCL) [2]:

$$i_0 = i_{0RE} \frac{ECSA}{A} \left(\frac{P_c}{P_{cREF}} \right)^{0.5} e^{\left[\left(\frac{-\Delta G}{RT} \right) \left(1 - \frac{T}{T_{REF}} \right) \right]} \quad (3)$$

Electrochemical Active Surface Area (ECSA) defines the capacity of the cell catalyst to fulfill its function as an accelerator in the Oxygen Reduction Reaction (ORR), thus defining the efficiency in converting chemical energy into electrical energy. There is a relation between the water in the porous structure of the CCL and the instantaneous value of ECSA. The porous model of the CCL, proposed by Strahl et. al. establishes that removing larger amounts of water from the porous structure of the CCL, either by evaporation (changes in cell temperature) or by displacement (changes in the flow of oxygen), results in instantaneous variations of effective ECSA. Finding the optimal amount of water, the optimum effective ECSA (thus performance) could be achieved [3].

There is a relation to approximate ECSA as a function of fractional water contained in the CCL:

$$ECSA = ECSA_{REF} (e^{K_{act} s_{CCL}} - 1) \quad (4)$$

Where s_{CCL} is the fractional amount of liquid water in the catalyst layer. The mass flux balance in the CCL completes the required relations to model liquid water dynamic [4].

$$K \frac{ds_{CCL}}{dt} = J_{gen} - J_{evap} - J_{diff} \quad (5)$$

B. Validation

This liquid water dynamic is now included in the model.

The updated model now achieves to better approximate the behavior presented in the experimental data. When the stoichiometry levels of the inlet oxygen step down, the amount of water being displaced from the CCL porous structure decreases, favoring an optimal hydration of the CCL and therefore improving cell voltage response, which recovers to a near constant value, even though oxygen supply is diminishing, figure 2.

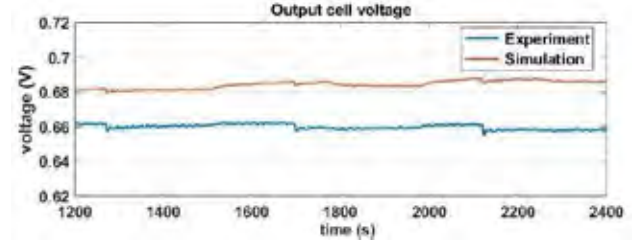


Fig. 2. Comparison between real and simulated voltage for the updated model.

V. CONCLUSION

We have developed, implemented and experimentally validated an accurate model of a Proton-Exchange Fuel Cell, in which the dynamic of liquid water in the catalyst layer has been successfully included. This model allows to better explain and predict the cell output voltage behavior. It is shown that variations in the fractional content of water located in the CCL has a relative immediate effect in the instantaneous output voltage profile of the fuel cell. Our on-going research effort is in applying accurate models for designing advanced high level model-based controllers to set optimal fuel cell operating conditions in order to improve performance and extend durability.

ACKNOWLEDGMENT

This work is supported by the Spanish State Research Agency through the María de Maeztu Seal of Excellence to IRI MDM-2016-0656 and by the European Union through the INN-BALANCE project of the Fuel Cells and Hydrogen 2 Joint Undertaking under grant 735969.

REFERENCES

- [1] Barbir, F., PEM fuel cells: theory and practice, Elsevier Academic Press, 2005.
- [2] Luna Pacho, J., Development of control systems and state observers for efficiency and durability improvement in PEM fuel cell based systems, PhD Thesis, Universitat Politècnica de Catalunya, January 2017.
- [3] Strahl, S., Husar, A., Franco, A. A. Electrode structure effects on the performance of open-cathode proton exchange membrane fuel cells: a multiscale modeling approach, International Journal of Hydrogen Energy, 39, pp. 9752–9767, 2014.
- [4] Strahl, S., Husar, A., Puleston, P., Riera, J., Performance improvement by temperature control of an open cathode PEM Fuel Cell system, Fuel Cells, vol. A247, pp. 529–551, March 2014.

PROMISING NI-CONTAINING CATALYSTS FOR EFFECTIVE CONVERSION OF CO₂ WITHIN CO-ELECTROLYSIS PROCESS IN SOEC

A. Patryk Błaszczak*, B. Emilia Kaczmarczyk**, C. Sea-Fue Wang***, D. Beata Bochentyn*, E. Piotr Jasiński**

* Faculty of Applied Physics and Mathematics, Gdansk University of Technology, 80-233 Gdańsk, ul. Narutowicza 11/12, Poland

** Faculty of Electronics, Telecommunications and Informatics, Gdansk University of Technology, 80-233 Gdańsk, ul. Narutowicza 11/12, Poland

*** Department of Material and Mineral Resources Engineering, National Taipei University of Technology, 1, Sec. 3, Zhongxiao E. Rd., Taipei, 106 Taiwan

Abstract – SOEC-based systems performing co-electrolysis and co-generation of methane can be involved into production of easily available fuels by consumption of excess electrical energy. Additionally, while ongoing process greenhouse gas CO₂ is being utilized and removed from atmosphere. Making this process to happen requires strong catalysts. In this study various composites of metal oxide support materials Y₂O₃, YSZ and GDC with different amounts of introduced Ni were examined. All materials' ability to improve methanation efficiency was tested in specially designed unit simulating conditions of operating SOEC. It was proved that Y₂O₃-, YSZ- and GDC-supported catalyst allowed to reach 55, 46 and 53 % of CH₄ in dry outlet stream, respectively. After performing short-term test for 24 h only GDC-based catalyst remained in its pristine composition.

Index Terms – catalyst, SOEC, co-electrolysis, methanation, FTIR

I. INTRODUCTION

As CO₂ is one of the main contributors to greenhouse effect and hence to climate change, there is a growing interest in its chemical conversion to easily transportable fuels or raw materials. CH₄ is suitable for this due to existence of highly developed infrastructure for transporting and storage of natural gas. Methanation reaction is a main route to produce methane of high purity using CO and H₂ as a starting materials. Unlike conventional routes both of required gases can be also obtained from high temperature co-electrolysis of CO₂ and H₂O in operating SOEC system. Produced CO and H₂ can be further transformed into methane using catalysts deposited onto anodic side of SOEC. As the methanation reaction needs to undergo

rapidly, it requires really strong catalyst, so many noble metals are being used [1]. Due to their high price Ni is more preferred these days. Microstructure, surface area and composition of substrate material have a major impact on final catalytic activity [2].

II. MATERIALS PREPARATION

All samples were prepared by mixing support ceramic powder 1:1 by wt. with nickel (II) nitrate hexahydrate (Sigma-Aldrich, 99,9%) dissolved in distilled water. Slurry was heated using hotplate with constant stirring until nearly dry. Samples were calcined at 700 °C for 2h and properly grinded. Supporting metal oxides were as follows: Al₂O₃, GDC (Ce_{0.8}Gd_{0.2}O_{2-δ}), CeO₂, YSZ and Y₂O₃ used as received.

III. EXPERIMENTAL

A. Methods

The XRD analyses were carried out by using Panalytical X'Pert Pro diffractometer. The microstructure of the prepared materials was observed using scanning electron microscope FEI Quanta 250 FEG. For all compositions, the ability to form methane from highly (25 % H₂O) humidified CO and H₂ mixture was examined. Those are normally formed as products of CO₂ and H₂O electrolysis process and can truly simulate conditions in real SOEC. Catalytic tests were performed in fixed-bed quartz reactor packed with 200 mg catalyst while heating and cooling cycle at temperature ranging from room up to 700 °C with 1 °C/min rate. Before each test catalysts underwent reduction in wet H₂ at 600 °C within 6h. FTIR

spectroscopy-based unit was used in order to determine the amounts of reaction products and reagents in exhaust stream and calculate catalytic parameters.

B. Results

The changes of CH₄, CO and CO₂ concentrations in outlet gas stream, during cooling within the catalytic performance measurements, for Ni/Y₂O₃, Ni/YSZ and Ni/GDC are presented in Fig.1-3., respectively. As it can be seen best results were obtained for Y₂O₃- and GDC-supported nickel particles resulting in over 50 % of methane concentration in dehumidified outlet gas stream.

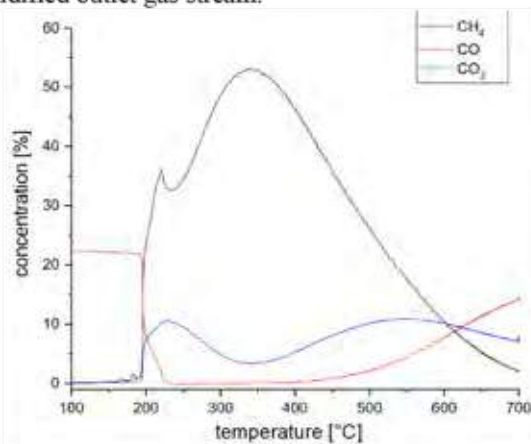


Fig. 1. Change of CH₄, CO and CO₂ concentrations while testing Ni/Y₂O₃ catalyst.

In case of YSZ-supported Ni catalyst concentration of CO₂ is significantly higher than for other two samples. It means that production of carbon dioxide is much more pronounced and at the same time it lowers CH₄ yield. Additionally, shift in temperature of maximum concentration is visible. It is due to slight decomposition of catalyst and agglomeration of nickel particles discovered thanks to *post mortem* XRD and SEM characterization.

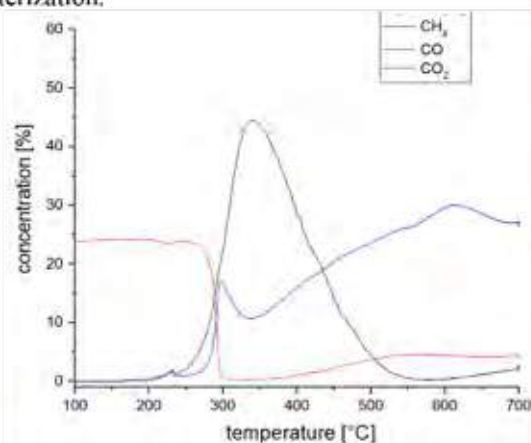


Fig.2. Change of CH₄, CO and CO₂ concentrations while testing Ni/YSZ catalyst.

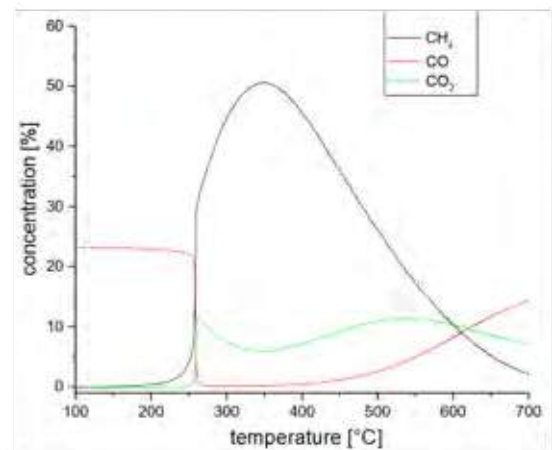


Fig.3. Change of CH₄, CO and CO₂ concentrations while testing Ni/GDC catalyst.

Examination of temperature dependence of methane yield revealed that catalysts containing GDC and Y₂O₃ are most promising for application in real SOEC cell as those can provide noticeable concentration of CH₄ at temperatures of operating electrolyzer exceeding 500 °C.

IV. CONCLUSION

Catalysts based on metal oxides mixed with Ni were prepared using water-soluble nickel salt. All of examined samples allowed to enlarge methane amount in exhaust stream. GDC- and YSZ-containing catalytic materials provided the highest methane yield of over 50 % in dry mixtures. The same samples remained in pristine form after catalytic test and no carbon deposition was observed. Materials can be applied in systems containing SOECs as those allow to still obtain reasonable amount of methane at higher temperatures.

ACKNOWLEDGMENT

This work was supported by the 5th Polish-Taiwanese/Taiwanese-Polish Joint Research Project PL-TW/V/4/2018 "Materials for Direct Power-to-Hydrocarbon Conversion" granted by the National Centre for Research and Development of Poland and Ministry of Science and Technology of Taiwan.

REFERENCES

- [1] Muroyama, Hiroki, et al. "Carbon dioxide methanation over Ni catalysts supported on various metal oxides." *Journal of catalysis* 343 (2016): 178-184.
- [2] Rönsch, Stefan, et al. "Review on methanation—from fundamentals to current projects." *Fuel* 166 (2016): 276-296

EFFECT OF IONOMER DISTRIBUTION UPON SURFACE FUNCTIONALIZATION OF THE CARBON SUPPORT IN THE CATALYST LAYER: MOLECULAR DYNAMICS SIMULATION APPROACH

J. H. Lee*, and S. G. Lee*

* Department of Organic Material Science and Engineering, Pusan
National University, 2, Busandaehak-ro 63beon gil, Geumjeong-gu,
Busan 46241, Republic of Korea

Abstract - The ability to control the ionomer distribution on the Pt/C catalyst is critical when designing high-performance polymer electrolyte membrane fuel cells (PEMFCs). Due to the complexity of the three-phase interface in a cathode catalyst layer (CL), controlling the ionomer distribution on the Pt/C catalyst is a challenge task. Here we used molecular dynamics (MD) simulations to provide molecular insight into the structural changes associated with the ionomer distribution on a carbon-support surface upon chemical functionalization. According to the interfacial binding energies, the introduction of functional groups onto the carbon support enhances molecular interactions between the ionomer solution and the carbon-support surface, with interaction energies that enhance in order: hydroxyl-functionalized (-2191 ± 37 KJ/mol) > epoxy-functionalized (-1994 ± 32 KJ/mol) > amino-functionalized (-1975 ± 28 KJ/mol) > pristine (-1904 ± 16 KJ/mol) carbon-support surface. We conclude that functionalization of the carbon support leads to a more uniform distribution of the ionomer over the surfaces of both the Pt catalyst and the carbon support by improving interactions between the carbon support and the Nafion ionomer solution.

Index Terms - Polymer electrolyte membrane fuel cell, Ionomer distribution, Nafion ionomer, Carbon support, Functionalization, Molecular dynamics

I. INTRODUCTION

Developing and optimizing the structural designs of membrane electrode assemblies (MEAs) that consist of polymer electrolyte membranes (PEMs), catalyst layers (CLs), microporous layers (MPLs), and gas diffusion layers (GDLs), are essential to reduce the cost for the large-scale commercial viability of PEMFCs.[1,2] In particular, the catalyst layers (CLs) are multiscale components; that is, they are micro-scale random porous media that consist of nanoscale materials, where electrochemical reactions and mass transport take place

simultaneously.[3] Therefore, studies that optimize CLs by lowering the Pt loading are important for achieving efficient pathways for electrons and protons (H^+), the H_2 and O_2 reactants, and the water product to reach the active sites. In this regard, uniform ionomer distribution on the surfaces of both the Pt catalyst and the carbon support is a key criterion for reducing the Pt loading used in these electrodes and establishing well-balanced paths for the transport of O_2 , protons, and water. Therefore, uniform and continuous ionomer coverage on the surfaces of the Pt catalyst and the carbon support through the control of ionomer distribution is strongly desired in order to achieve high-performance PEMFCs. Therefore, as a subsequent study, we introduce chemical functionality onto the carbon surface in order to improve ionomer coverage on the carbon support and suppress the formation of localized ionomer populations on the Pt catalyst, and, as a result, facilitate uniform ionomer distribution on the Pt/C catalyst. In this study, we investigated variations at the ionomer/carbon interface on the molecular scale using classical molecular dynamics (MD) simulations by introducing several functional groups, namely hydroxyl (-OH), epoxy (-O-), and amino (-NH₂), onto the carbon surface.

II. METHODOLOGY

Classical molecular dynamics (MD) simulations were performed using fully atomistic models. To examine the effect of chemical functionalization of the carbon surface on ionomer distribution, we simulated four different carbon-surface systems, including a pristine surface, and surfaces functionalized by hydroxyl (-OH), epoxy (-O-), and amino (-NH₂) groups. A modified DRIEDING force field [4] was employed to describe the inter- and intra-molecular interactions

in the Nafion solutions and the functionalized carbon-support surfaces. The flexible three-center (F3C) force field [5] was used to model the water molecule. All classical MD simulations were performed using the Large-scale Atomic/Molecular Massively Parallel Simulator (LAMMPS) [6] software package described by Plimpton (Sandia National Laboratories).

III. RESULTS

The equilibrium interfacial binding energy for the Nafion solution to the carbon support surface was found to enhance in the following order: hydroxyl-functionalized (-2191 ± 37 KJ/mol) > epoxy-functionalized (-1994 ± 32 KJ/mol) > amino-functionalized (-1975 ± 28 KJ/mol) > pristine (-1904 ± 16 KJ/mol) surface. All carbon support structures favor the Nafion solution and have negative interfacial binding energies. (Fig. 1) More negative binding energy indicated stronger molecular interactions between the Nafion solution and the carbon-support surface.

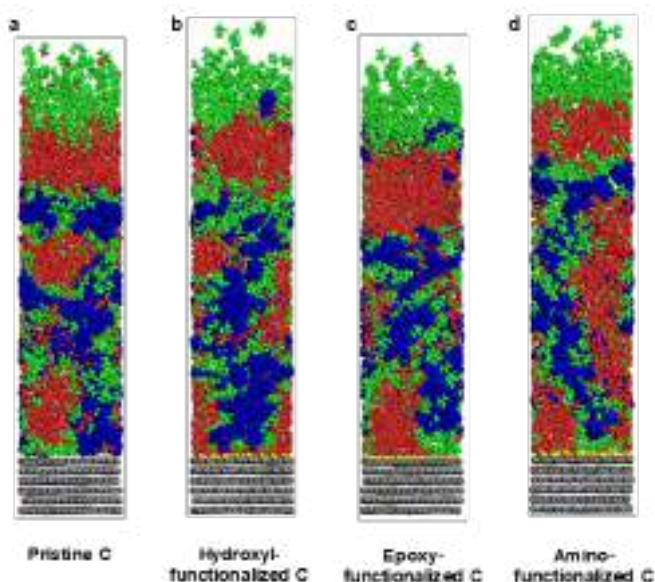


Fig. 1. Color-coded snapshots by component type for the four equilibrated models at the (a) pristine, (b) hydroxyl-functionalized, (c) epoxy-functionalized, and (d) amino-functionalized carbon support surfaces. Blue, red, green, yellow, and gray correspond to the Nafion ionomers, water molecules and hydronium ions, isopropyl alcohol (IPA) molecules, the functional groups, and the carbon-support surfaces, respectively.

IV. CONCLUSION

In order to understand the effect of carbon-support functionalization on ionomer-solution distribution, with the aim of eventually achieving uniform ionomer-solution coverage over the surfaces of both the Pt catalyst and carbon support in a PEMFC catalyst layer, we performed classical MD simulations on a variety of systems that contain a Nafion solution (Nafion ionomer dispersed in IPA/water) adsorbed onto four different

carbon-support surfaces (a pristine surface, and hydroxyl-, epoxy-, and amino-functionalized carbon surfaces). The calculated interfacial binding energies reveal that the introduction of functional groups onto the carbon support enhances molecular interactions between the Nafion solution and the carbon-support surface, with binding enhancing in the following order: hydroxyl-functionalized > epoxy-functionalized > amino-functionalized carbon-support surface. We therefore propose that functionalization of the carbon support can successfully alter the distribution of the Nafion solution and mitigate against the strong interactions between the Pt catalyst and Nafion ionomer, resulting in uniform coverage of the ionomer over the surfaces of both the Pt catalyst and the carbon support. This understanding provides guidance for the rational design of CLs for use in high-performance PEMFCs through control of ionomer coverage on the surfaces of both the Pt catalyst and carbon support.

ACKNOWLEDGMENTS

This research was supported by the National Research Foundation of Korea (NRF) funded by the Ministry of Science, ICT & Future Planning (Nos. NRF-2016M1A2A2937151 and NRF-2015M1A2A2057129).

REFERENCES

- [1] Carrette, L., Friedrich, K. A., Stimming, U., Fuel Cells - Fundamentals and Applications. Fuel Cells, Volume 1, 2001, Pages 5-39.
- [2] Sharaf, O. Z., Orhan, M. F., An overview of fuel cell technology: Fundamentals and applications. Renewable & Sustainable Energy Reviews, Volume 32, 2014, Pages 810-853.
- [3] Holdcroft, S., Fuel Cell Catalyst Layers: A Polymer Science Perspective, Chemistry of Materials, Volume 26, 2014, Pages 381-393.
- [4] Mayo, S. L., Olafson, B. D., Goddard, W. A., Dreiding - a Generic Force-Field for Molecular Simulations. Journal of Physical Chemistry, Volume 94, 1990, Pages 8897-8909.
- [5] Levitt, M., Hirshberg, M., Sharon, R., Laidig, K. E., Daggett, V., Calibration and testing of a water model for simulation of the molecular dynamics of proteins and nucleic acids in solution. Journal of Physical Chemistry B, Volume 101, 1997, Pages 5051-5061.
- [6] Plimpton, S., Fast Parallel Algorithms for Short-Range Molecular-Dynamics. Journal of Computational Physics, Volume 117, 1995, Pages 1-19.

(Put paper number here) EFC2019-01204

PUT PAPER TITLE HERE

A. Author1*, B. Author2**, and C. Author3*

*Affiliation, Address, (Country)

**Affiliation, Address, (Country)

Abstract - This template describes the guidelines for the preparation of an extended abstract for publication in EFC2019 conference proceedings. This document is itself an example of the desired layout (inclusive of this abstract) and can be used as a template if you are using Microsoft Word 97 or later. The abstract is limited to 150 words and cannot contain equations, figures, tables, or references. It should concisely state what was done, how it was done, principal results, and their significance

Index Terms - The authors will provide up to 4 keywords or phrases (in alphabetical order and separated by commas) to help identify the major topics of the paper.

I. NOMENCLATURE

A nomenclature list, if needed, should precede the Introduction.

II. INTRODUCTION

This document contains information regarding desktop publishing format, type sizes, and typefaces. Style rules are provided to explain how to handle equations, units, figures, tables, abbreviations, and acronyms. Sections are also devoted to acknowledgments and references.

III. EXTENDED ABSTRACT PREPARATION

The total paper length should not exceed TWO (2) pages. **Papers longer than 2 pages are not acceptable.**

A. *Format*

Prepare your extended abstract in single-spaced, double-column format, on A4 paper sheet (210×297 mm).

Set top and bottom margins to 25 mm, and left and right margins to 20 mm. The column width has to be 82 mm; the space between two columns is 6 mm. Paragraph indentation is 4 mm. Please use left and right justification of your columns.

Use one space-line between sections, and between text and tables or figures. Adjust the length of the columns on the last page.

B. *Type Sizes and Typefaces*

Please use “Times Roman” or “Times New Roman” typeface and embed all fonts (See your software’s “Help” section if you do not know how to embed fonts).

Table I provides samples of the appropriate type sizes and styles to use.

TABLE I
TIMES NEW ROMAN TYPE SIZES AND STYLES FOR EFC2017

Type size (pts)	Regular	Bold	Italic	Small caps
8	Figure captions, table text, figure text, footnotes, subscripts and superscripts			Table captions
9		Abstract title, abstract, keywords		
10	Body text, equations, Authors’ affiliation, references		Subheadings	Title of sections
11	Authors’ names			
12		Title of the paper		

C. *Section Headings*

A primary section heading is enumerated by a Roman numeral followed by a period and is centered above the text. A primary heading should be in small caps. The first letter of each important word is capitalized.

Do not number Appendix, Acknowledgment and References.

A secondary section heading is enumerated by a capital letter

followed by a period and is flush left above the section. The first letter of each important word is capitalized and the heading is italicized.

D. Figures and Tables

In labeling figure axes please use words rather than symbols. Put units in parentheses as in Fig. 1.

Large figures and tables may span both columns, but may not extend into the page margins. Figure captions have to be below the figures; table captions have to be above the tables.

Do not put captions in “text boxes” linked to the figures. Do not put borders around your figures.

All figures and tables must be placed just after they are first mentioned. Digitize your tables and figures. Use figures to adjust the length of the columns on each page of the manuscript.

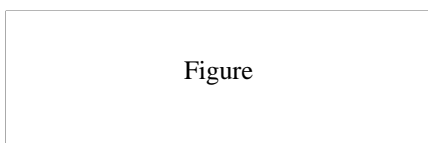


Fig. 1.

E. Numbering

Please do not number pages.

Number reference citations consecutively in square brackets [1].

All figures and tables must be numbered consecutively. Use Arabic numerals for figures and Roman numerals for tables.

F. Abbreviations and Acronyms

Define less common abbreviations and acronyms the first time they are used in the text, even after they have been defined in the abstract. Do not use abbreviations in the title unless they are unavoidable.

G. Math and Equations

Use either the Microsoft Equation Editor or the MathType commercial add-on for MS Word for all math objects in your paper.

Number equations consecutively with numbers in parentheses flush with the right margin (for example (1)).

IV. UNITS

Use International System of Units (SI) as primary units. British units could be used as secondary units in parentheses.

V. CONCLUSION

Conclusions are one the most important parts of a paper. Please give careful consideration to this section.

APPENDIX

Appendixes, if needed, have to appear before the Acknowledgment.

ACKNOWLEDGMENT

Please place an eventual Acknowledgment here, before the References.

SUBMISSION OF THE EXTENDED ABSTRACT

Your draft must be submitted both as DOC and PDF file with your abstract number in the filename (e.g. EFC17001.doc, EFC17001.pdf).

REFERENCES

List only one reference per reference number according to the following examples:

- [1] Li, X., Ogden, J., Yang, C , Analysis of the design and economics of molten carbonate fuel cell tri-generation systems providing heat and power for commercial buildings and H2 for FC vehicles, Journal of Power Sources, Volume 241, 2015, Pages 668-6791892, pp. 68-73.
- [2]
- [3]

HYDROGEN-BIKE EQUIPPED WITH HYBRID POWER UNIT: ENERGY PERFORMANCE ANALYSIS AND ELECTROMAGNETIC EMISSIONS TEST

A. Buono*, P. Di Trolio*, M. Minutillo*, M. Migliaccio*, E. Jannelli*, N. Massarotti*, F. Conventi*, C. Di Donato*, F. Nunziata*, L. Vanoli*, A. Gifuni*, and G. Grassini*

*Dipartimento di Ingegneria, Università degli Studi di Napoli Parthenope, Centro Direzionale isola C4, 80143, Napoli, (Italy)

Abstract – In the innovative context of smart cities, new mobility concepts are needed that combine high performance, eco-friendly energy and human safety. In this study, an experimental analysis is made on an electric bike prototype equipped with a new hybrid power unit. Numerical simulations and actual measurements demonstrate the remarkable performance of the hydrogen-bike in terms of energy consumption and the very limited electromagnetic emissions.

Index Terms – EMC, energy, hydrogen-bike mobility.

I. INTRODUCTION

In recent years, the urbanization growing posed several critical issues in actual urban mobility network, boosting the transition to electro-mobility concepts, including electric bikes, that became a key point to limit air pollution, to avoid traffic congestion and to exploit new and “clean” energy sources. It was estimated that, just in 2012, more than 31 million electric bikes were sold all around the world, and this trend is increasing faster and faster [1]. Actually, the most up-to-date electric bikes adopt a hybrid configuration where the engine exploits energy both from battery storage and fuel cell (FC) stack production. In this study, the energy performance and the electromagnetic emissions of a hybrid power unit-electric bike based on a FC stack fed by hydrogen are analyzed.

II. ENERGY PERFORMANCE ANALYSIS

The powertrain developed for the bicycle is based on a series connection between a FC stack (rated power 500 W) and the battery pack (36 V, 12 Ah). These are coupled thanks to a DC-DC (direct coupling) converter (Fig. 1) that manages the power of the system according to the control strategy developed in [2]. The design concept of the powertrain starts considering the

power needed to maintain a constant velocity, evaluated as the sum of the power due to air-drag, the slope and friction between wheel and ground [3]:

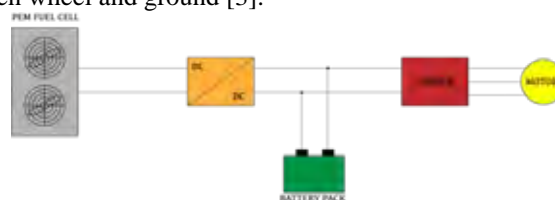


Fig. 1: Powertrain technical scheme.

$$P_{load} = \frac{1}{2} C_D \rho_{air} (v_g - v_w)^2 v_g + m_t v_g g \sin(\tan^{-1}(\theta)) + m_t v_g g \delta_{rolling} \quad (1)$$

Eq. (1) considered an average value present in literature for the drag coefficient (C_D), for a cyclist equal to 0.5, a 3% slope for the angle as average value, finally, the rolling friction parameter ($\delta_{rolling}$) was set equal to 0.015. The relative velocity of wind (v_w) was considered high (2 m/s) to show the significant performance of the concept. Moreover, the DC-DC introduced in the powertrain is able to control the energy fluxes that occurs during standard operation. The main idea is to maximize the range of the bicycle maintaining the fuel cell at high efficiency rate, due to that starting from the state of charge (SoC) of the battery pack 4 different operating conditions occurs: i) $SoC > 0.8$, the load is fully satisfied by the battery pack; ii) $0.4 < SoC < 0.8$, the fuel cell works at constant power to satisfy the load and to recharge the battery; iii) $SoC < 0.4$, the fuel cell starts to produce power to satisfy the load and to recharge the battery (if it is possible); iv) $SoC < 0.2$, the powertrain is switched off to prevent damages to the battery pack.

Since there are no official driving cycles for e-bikes, the ARTEMIS URBAN drive cycle was used as benchmark. The maximum velocity and total mass (bike + rider) are set to 25

km/h and 90 kg, respectively. Fig. 2 shows the results obtained from the simulations: starting with SoC > 80%, the FC does not work and the load is covered by the battery, but after about 400 s, the SoC drops < 80% results in a FC producing power at maximum efficiency, in a continuous way. Fig. 2 also shows the power sharing strategy when initial SoC is equal to 25%, when the FC covers the power and, when it is possible, recharges the battery (maximum charge rate C/4).

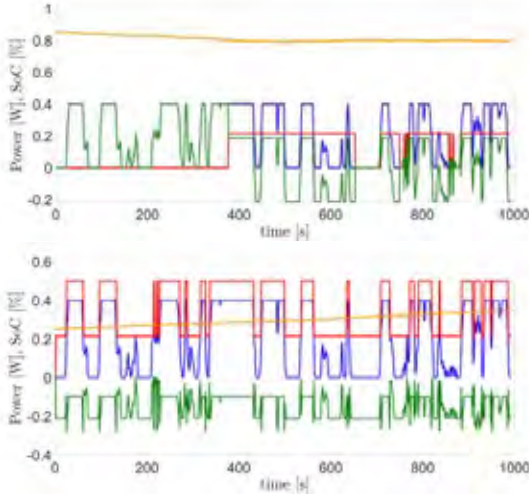


Fig. 2: Power Sharing Strategy under different SoC conditions. SoC is in orange, FC power is in red, battery power is in green and the load is in blue.

III. ELECTROMAGNETIC RADIATION TEST

Electromagnetic emission tests have been accomplished in the facilities of the Università degli Studi di Napoli Parthenope. They include a 5 m × 6 m × 4 m reverberating chamber (RC), i. e., a metallic chamber usually employed for electromagnetic compatibility, scattering measurements, etc., and a spectrum analyzer (SA) [4]. The radiation measurements are accomplished in the frequency range 250 MHz–1 GHz, by placing the hydrogen-bike in the RC where an isotropic and random electric field, uniform on average, is obtained by means of continuous-mode stirring achieved with two volume and three plane stirrers (see Fig. 3).



Fig. 3: Measurement setup.

The total power radiated by the operating hydrogen-bike is obtained according to the IEC 61000-4-21:2011 standard, as follows:

$$P_{rad} = \frac{P_{r,SA} \eta_R}{\eta_R \eta_T IL_c Att_c} = \frac{P_{r,SA}}{\eta_T IL_c Att_c} \quad (2)$$

where the numerator is the power received by receiver antenna in the RC and measured by the SA, while the denominator take into account the RC insertion loss (including mismatching), the attenuation introduced by the cable linking the receiver antenna and the SA, and the radiation effectiveness of the antennas.

Results relevant to a constant load are shown in Fig. 4, where the power is below -74 dBm in the considered frequency range, approaching the RC noise floor (about -100 dBm) for frequencies larger than 850 MHz.

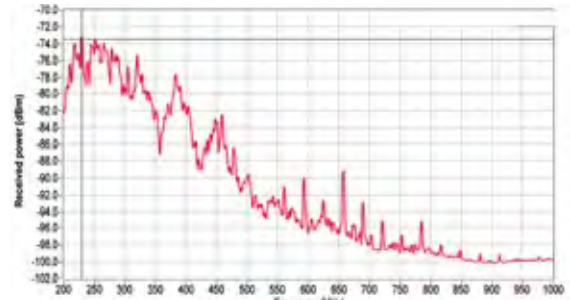


Fig. 4: Total power measured by SA when the hydrogen-bike is operating.

IV. CONCLUSION

Numerical simulations and actual measurements demonstrate the remarkable energy performance of the hydrogen-bike and its very limited level of electromagnetic emissions.

ACKNOWLEDGMENT

This study is supported by the Università degli Studi di Napoli Parthenope under the project “Ricerca Competitiva” - DING 202.

REFERENCES

- [1] Fishman, E., Cherry, C., E-bikes in the Mainstream: Reviewing a decade of research, *Transport Reviews*, Volume 36, 2016, pp. 72-19.
- [2] Di Giorgio, P., Di Trolio, P., Jannelli, E., Minutillo, M., Conte, F.V., Model based preliminary design and optimization of Internal Combustion Engine and Fuel Cell hybrid electric vehicle, *Energy Procedia*, Volume 148, 2018, pp. 1191-1198.
- [3] Muetze, A., Tan, Y.C., Electric Bicycles – A performance evaluation, *IEEE Industry Applications Magazine*, Volume 13, Issue 4, 2007, pp. 12-21.
- [4] Sorrentino, A., Ferrara, G., Migliaccio, M., Cappa, S., Measurements of backscattering from a dihedral corner in a reverberating chamber, *Newsletter of the Applied Computational Electromagnetic Society*, Volume 33, 2018, pp. 91-94.

USE OF HYDROGEN TRAINS ON NON-ELECTRIFIED RAILWAY LINES: ASSESSMENT OF COSTS AND EMISSIONS AND COMPARISON WITH ALTERNATIVES¹

G. Carcasi*, M. V. Migliarese Caputi**, L. Cedola** and D. Borello**

*RFI - Rete Ferroviaria Italiana, Rome (Italy)

**Department of Mechanical and Aerospace Engineering, University of Rome La Sapienza – Rome (Italy)

Abstract - In recent years, rail sector showed an increasing interest in powertrains based on PEM fuel cells employed as viable alternative to the diesel engines that are usually adopted for non-electrified railway sections.

Here we assess the total cost of ownership (TCO) and the emissions (also in economic terms) related to the operation of hydrogen trains on a non-electrified railway network of selected lines in Italy.

We compare the existing solution, operated with a diesel train, with a commercial hydrogen-powered fuel cell train; the results are compared also with the TCO for the electrification of the lines. We analyze the impact of producing hydrogen using different renewable sources such as wind and solar.

Costs and emissions of the investigated solutions are assessed.

Index Terms - Hydrogen Fuel Cells for trains, Total Costs of Ownership, Emissions

I. NOMENCLATURE

H₂ = Hydrogen; PEM= Proton exchange membrane; FCH = Hydrogen fuel cells; O&M = Operations and maintenance; RUs = Railway Undertakings; LCOE = Levelized cost of energy; IM = Infrastructure manager; ALK = alkaline;

II. INTRODUCTION

In recent years, rail sector showed an increasing interest in powertrains based on PEM fuel cells as viable and cost-competitive alternative to rolling stocks with diesel engines that are usually adopted for non-electrified railway sections. This interest is pushed by stringent emissions targets and diesel bans on one side and by the huge costs for the electrification of railway lines on the other one. An alternative solution, based on the use of H₂-fueled trains seems to be a convenient alternative, provided

that costs are affordable, that performance are comparable with existing rolling stocks and that a decisive improvement is obtained in terms of emissions reduction.

Here, we analyze the pro & cons of such alternative.

III. DESCRIPTION OF THE ANALYZED CONFIGURATION

The proposed study refers to some portions of the national railway network operated by the IM RFI for a total length of about 425 km of tracks in order to assess the potential implementation of FCH technology in the railway sector on a network level and to introduce appropriate economies of scale. These lines have been selected as potential candidates considering appropriate locations to produce hydrogen due to the availability of renewable wind and solar energy at competitive costs.

Presently, RUs produce over these lines over 52 weeks per year about 180 transport services on working days, about 145 on Saturdays and about 100 on Sundays and Holidays operated by using a mixture of Aln668 diesel trains, D445 locomotives with multiple cars, ALn668/663 trains, ATR365 and ALn501/502 trains. The resulting total daily journey is of about 11,400 tr*km and circa 3.86 million tr*km per year. Assuming an average fuel consumption of 1.50 km/l, then the daily diesel fuel consumption is of about 17,100 l and the estimated annual need of diesel fuel is assumed of 5.78 million liters.

The current railway configuration is compared with a possible alternative consisting of the adoption of the Alstom Coradia iLint trains fueled by hydrogen. Coradia trains are powered by a stack of hydrogen fuel cells (400 kW) and equipped with a battery pack for the management of the energy tips (making available additional 450 kW) and its recovery in braking. The traction power pack is equivalent in performance with the equivalent diesel train (the Coradia Lint54), therefore no operational

¹ The opinions expressed in this paper are those of the Authors and do not necessarily reflect the views of their respective Organizations

problems are expected with regards to slopes and maximum speeds, especially when considering technological developments expected in the incoming years. Indeed, FCH trains can already reach speeds up to 180 km/h and autonomies up to 800 km with a full load.

For such reason, analyzing the data released by Alstom, we assume a constant hydrogen consumption of 0.25 kg/km (with a safety factor of 20% in relation to the declared minimum specific consumption) and dimensioning the hydrogen production facility with an overcapacity of 15%. This leads to a daily requirement of 2,850 kg of hydrogen (on working days). With the same assumptions done before for the diesel train, we estimate an annual hydrogen consumption of about 964 tons.

IV. COST ANALYSIS

We perform now a comparison between the total cost of ownership of hydrogen trains ("hydrail" scenario), diesel trains ("diesel" scenario) and electric trains² ("electrification" scenario), by adding financial infrastructure costs (i.e. initial investment in technical fixed assets³, design expenses, overhead costs and contingencies, electricity costs, full O&M costs including extraordinary maintenance and personnel costs) and financial transport service costs (rolling stock acquisition, full O&M costs including extraordinary maintenance and personnel – both on board and off ground – costs, and track access charges) on a life cycle perspective. The individual costs are estimated over the technical life of the project, evaluated in 30 years of operations (assuming no residual value for the assets) and are discounted at a 4% financial rate.

The size of the rolling stock fleet in the *hydrail* scenario is designed respecting the current transport capacity offered by RUs in terms of passengers per hour and preserving the current operational working timetables of RUs, without altering their industrial and logistic organization including downtimes, stops for maintenance and refueling scheduled.

Specific infrastructure costs and full O&M costs in the different scenarios are estimated through a detailed process of market analysis, literature review and evaluation of technical data provided by leading companies in their respective sector.

Special clarification is needed for the cost for acquisition of hydrogen for FCH trains: since at this stage there is no definition about financing/supporting schemes for hydrogen infrastructures – including their ownership scheme and their business model – and about supporting mechanism for hydrogen production/acquisition, adopting a systemic perspective, it is assumed that the cost of H₂ is at least equal to the cost of the electricity consumed for its production (c.a. 150/160 €/MWh for off-peak/peak hours for the marginal cost of electricity absorbed by the national transmission grid in the railway sector, c.a. 60 €/MWh for the LCOE of electricity produced by wind or PV power plants).

Diesel costs is assumed c.a. 0.7 €/l (by considering the tax deduction) or c.a. 1.5 €/l (without tax deduction).

² Average specific electric consumption 12 kWh/km

³ Overhead lines and power transmission substations (including connecting lines) for the *electrification* scenario; ALK electrolyzes, compressors, storage tanks – considering strategic reserves for emergency conditions – and refueling stations for the *hydrail* scenario; no additional infrastructure for the *diesel* scenario.

V. EMISSIONS ANALYSIS

Emissions, assessed as "tank-to-wheels", of CO₂ and marginally of NO_x, SO_x, PM_x and COVNM derive from specific values emission provided by ISPRA (2019) for electricity consumed for hydrogen production and compression in the *hydrail* scenario (c.a. 13.5 MW installed and c.a. 52 GWh/year absorbed) and for electricity consumed directly for traction power in the *electrification* scenario (c.a. 47 GWh/year absorbed).

For diesel trains in the remaining scenario, a specific emission factor of 5.5 kgCO₂/tr*km is adopted along with publicly available emission factors typical of high duty vehicles for NO_x, SO_x, PM_x and COVNM.

The economic value of these externalities is evaluated according to price values outlined by DG-MOVE (2014) and are discounted again at a 4% rate.

TABLE I
DISCOUNTED TCO ANALYSIS

Unit	Diesel scenario		Hydrail scenario		Electrification scenario
	w/o tax	incl. tax	green H ₂	grey H ₂	
€/tr*km	6.9	7.6	7.7	8.4	9.9

TABLE II
EMISSIONS (ANNUAL VOLUMES AND DISCOUNTED SPECIFIC COST)

Unit	Diesel scenario		Hydrail scenario		Electrification scenario
	w/o tax	incl. tax	green H ₂	grey H ₂	
t/CO ₂ eq	21,400		0	15,700	14,200
€/tr*km	0.5		0	0.4	0.3

VI. CONCLUSION

Identified opportunities for implementation of FCH mobility in the railway sector must be the subject of specific regulatory, normative, technical and economic insights by all stakeholders in order to determine the actual opportunity to implement the hydrogen mobility and related ground infrastructure to the particular application context. Even though results derived from a specific context cannot be generalized directly to other territorial contexts, the comparisons between the three scenarios for the selected lines demonstrated that the FCH trains can be considered a viable, cost competitive and sustainable alternative to present alternative solutions, especially when considering the restrictions in emission limit expected in the next years. Specific efforts should be used to guarantee maximum integration of hydrogen production facilities with renewables in order to improve the economic and financial performance of the hydrail scenario and drastically improve the emissions profile and unlock full benefits deriving from the sector coupling also benefitting the power sector.

REFERENCES

- [1] "Study on the use of fuel cells & hydrogen in the railway environment", Roland Berger (2019).
- [2] "Update of the Handbook on External Costs of Transport - Final Report", DG MOVE (2014)
- [3] "Fattori di emissione atmosferica di gas a effetto serra nel settore elettrico nazionale e nei principali Paesi Europei", ISPRA (2019)

ENERGY TRANSITION BY MEANS OF “BOTTOM-UP” APPROACH: PYROSLUDG_EN FOR SUSTAINABILITY AND LOCAL DEVELOPMENT

Giuseppe Maria Perfetto¹, Massimo Di Nicola², Riccardo Lombardo³, Liborio L'Abbate⁴

¹ *P. Architect, Sustainability Manager, G_EN Engineering Srl, Moncalieri (TO), Italy*

² *P. Engineer, Innovation & Application Manager, G_EN Engineering Srl, Moncalieri (TO), Italy*

³ *Strategy & CSR Manager, G_EN Engineering Srl, Moncalieri (TO), Italy*

⁴ *CEO & Link Manager, G_EN Engineering Srl, Moncalieri (TO), Italy*

Corresponding mails: ¹ archis@genhub.eu - ² techman@genhub.eu

Energy Transition by means of “bottom-up” approach: PyrosludG_EN for Sustainability and Local Development

Abstract

The energy transition is a process of interaction between transnational and macroeconomic policies, which can be enriched by a small and "bottom-up" intervention; this document highlights the main objectives of the PyrosludG_EN project, a model of fully sustainable and "zero kilometer" local development, which can be easily replicated anywhere. It starts from the creation of a territorial HUB, based on the construction of a

pyrolysis plant treatment of "local" organic waste components to produce energy, in particular using sludge from civil wastewater treatment.

It transforms the ecological, and economic, problem of waste treatment into heat, electricity and water production, with particular attention to emissions and environmental impact, following the most restrictive standards.

Further winning factors are represented by the research to use the syngas produced in the process in fuel cells and the recovery of the organic residues transformed in fertilizer to rebalance the soil, as well as the creation of a local energy community.

Keywords: Sustainable Development, Energy Transition, Pyrolysis Plant, Energy from Waste,

I. WASTE TO ENERGY AS PARADIGM OF CIRCULAR ECONOMY

Sustainability has become a central focus in our economy. Energy from renewables, cogeneration from biomass, energy saving, extension the lifespan of the landfills, reuse, recycle, integrated management of the waste, emission reduction, smart grid, energy communities.....are only some of the new paradigm who preside over the energy transition from fossil sources as traditional way of production and consumption of energy to innovative models compatible with environmental sustainability, without penalizing the competitiveness of the systems and the economic and social development of the communities. We need to focus on the development of prototypes and innovative business models, exchange and sharing at local level and integrated resource management, not least waste. In light of the technology evolution become very relevant for the environment the reuse, as feedstock for cogeneration of power, of biomass with short renewal cycle like for instance sludge from biological civil wastewater treatment plants.

G_EN Energineering brings its contribution, entrepreneurial, scientific, technological and social in this scenario, proposing and creating a model that, in the most traditional sense of creativity, combines elements known in different ways:

- uses "ancient" and safe technologies to produce energy (pyrolysis),
- valorize feedstock waste with a very high rate of renewability (sludge, agro-food by-products, green waste, plastics ...),
- reduce the disposal in the landfill and disposing inert material,

Sludge from water treatment plants are composed mainly by water and organic matter. Today they end up in collection and storage plants and then to treatment, which separates the component that can be again assimilated to surface water from the biological residue, which is sent to the landfill after an inertization process using chemicals. At the time of the disposal, the biological residue or sludge still contains a water rate of approximately 75%. PyrosludG_EN is an industrial project focused in cogeneration in which the plant is fed by biological sludge coming from civil wastewater treatment plants, as well as biomass and agro-food by-product and micro-nano-plastics, treating the material using the process of pyrolysis a termochemical treatment in principle in absence of oxygen without any combustion. Besides the PyrosludG_EN is able to recover

material for recycling use, to produce an organic fertilizer useful for agriculture and as final result the volume reduction of the waste reducing up to 10 times the landfill use due to evaporation of the moisture.

The main values of the project are:

- Valorization of biological waste as a resource; the use of local biological matrix for the cogeneration of electrical and thermal energy through pyrolysis plants for energy production and the simultaneous realization of an Energy Community
- Environmental sustainability in the overall balance sheet which allows to obtain a model with approximately zero emissions;
- Repeatability on a local scale and in a widespread manner on a territorial scale also based on the availability and type of matrix can be used in the process.

II. A PROCESS

"ENVIRONMENTAL FRIENDLY"

The aim of PyrosludG_EN is to provide a technologically advanced solution which solves two critical elements of current industrial development namely: the management and disposal of organic waste, and the high demand for energy. Its innovative value is configured as the real new frontier of the circular economy. If until now the concept of "recycling" has been highlighted in the opportunity to obtain energy from sewage, here is another fundamental concept of a zero kilometer model, namely being the advanced point of a "circular economic model applied to the 'water'". Today, in Italy, waste water is considered as an element of possible health and environmental contamination, treated and, after separation, given to the landfill the organic solid component, with very high costs (it is paid to confer a matrix that weighs very much, due to the presence of water in the form of moisture and which has enormous volumes, again due to water, with over all very low times of saturation of the landfills and risks of contamination of groundwater). The PYROSLUDG_EN process develop an extraordinary perspective: waste water as a source of energy co-generation and not as a cost to be paid.

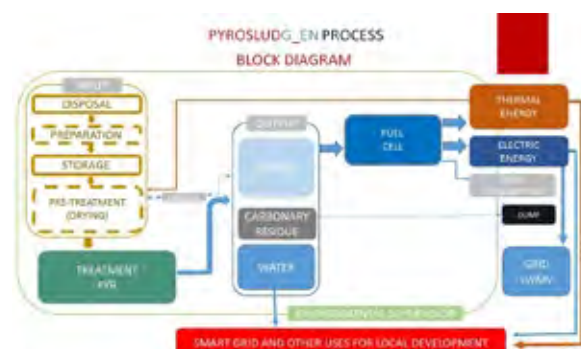


Fig. 1 PyroGEN Process: Block Diagram

With the process of molecular thermo-disintegration at low temperature, the organic substances contained in the waste water are used for the production of a gas (syngas) similar to methane, which feeds the co-generation units, facilitating the transformation from plants at high energy consumption (negative balance) to plants producing energy with positive energy balance.

As regards the modeling of the chemical part, the chemical reaction constants they are modeled according to Arrhenius and the accruals are calculated as shown in Tables 1 and Table 2. Table 2 also includes the values assumed for in the calculation of the constants of Arrhenius [1].

Reazione	R_i	E_i [J/K mol]	A_i [s ⁻¹]
Biomassa → Gas	$R_1 = k_1 C_{Biom}$	88600	14400
Biomassa → Tar	$R_2 = k_2 C_{Biom}$	112700	4130000
Biomassa → CHAR	$R_3 = k_3 C_{Biom}$	106500	738000
TAR → Gas	$R_4 = k_4 C_{Tar}$	107500	100000
TAR → CHAR	$R_5 = k_5 C_{Tar}$	107500	4280000

Tab. 1 Pyrolysis Process: Cynetic's Reaction

Reazione	R_i	E_i [J/mol]	A_i [s ⁻¹]
$C + O_2 \rightarrow CO + CO_2$	$R_6 = \alpha \frac{C_{O_2}}{\frac{1}{T_i k_1} + \frac{1}{k_2}}$	160	5.67×10^8
$C + CO_2 \rightarrow 2CO$	$R_7 = \alpha \frac{C_{CO_2}}{\frac{1}{T_i k_1} + \frac{1}{k_2}}$	218	7.92×10^8
$C + 2H_2 \rightarrow CH_4$	$R_8 = \alpha \frac{C_{H_2}}{\frac{1}{T_i k_1} + \frac{1}{k_2}}$	218	79.2
$C + H_2O \rightarrow CO + H_2$	$R_9 = \alpha \frac{C_{H_2O}}{\frac{1}{T_i k_1} + \frac{1}{k_2}}$	218	7.92×10^8
$2CO + O_2 \rightarrow 2CO_2$	$R_{10} = k_{10} T_i^2 (C_{CO})^2 C_{O_2}$	89	9.2×10^8
$2H_2 + O_2 \rightarrow 2H_2O$	$R_{11} = k_{11} C_{CO} (C_{O_2})^2 (C_{H_2O})^3$	166	10^{15}
$TAR + O_2 \rightarrow CO + H_2O$	$R_{12} = k_{12} C_{Tar} C_{O_2}$	42	1×10^{11}
$CO + H_2O \rightarrow CO_2 + H_2$	$R_{13} = k_{13} \left(C_{CO} C_{H_2O} - \frac{C_{CO_2} C_{H_2}}{K_{eq}} \right)$	12.6	2.78

Tab. 2 Pyrolysis Process: CONSTANTS USED FOR THE CALCULATION OF REACTION RATINGS [2]

The following Figure 2 shows the profiles of the concentrations of the components of the syngas along the reactor

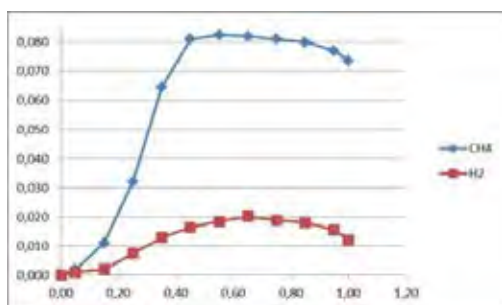


Fig.2 Pyrolysis Process: CONCENTRATION PROFILES OF CNG AND HYDROGEN [kg / Nm3]

III. INNOVATION AND RESEARCH FOR SUSTAINABLE DEVELOPMENT

The decisive element in the proposed model is research, a central and transversal asset to all phases, especially about the development of new solutions for the storage and use of energy and syngas produced in the process as a "poor" fuel for cells, the reuse of the carbon solid residual in agriculture as fertilizer, until the management of local communities of supplying energy for an "on-site" consumption. One of the developments with the greatest potential in fact is the "fuel cells". Today the research is oriented to the use of hydrogen or bio-fuel, components that require large amounts of energy to be produced and / or managed. In the PyrosludG_EN, the produced syngas will be used in a Fuel Cell battery for the production of electricity to be used for supplying the induction system and supporting the process.

IV. VIRTUOUS CYCLE AND BUSINESS MODEL

The proposed model combines sustainability, social responsibility and industrial profitability. It is a process that starts from biomass and organic components, apparently at the end of the cycle, to generate energy, recover water, reuse solid carbon based by-product as fertilizer, feed cold storage for the preservation of agricultural products, develop new "poor" fuel cells, use energy in smart grids, develop energy communities. The limited investment, about 1 million euros for a small-sized plant, and the very short payback time, in the order of three/four years, with excellent annual yields resulting from the value of the gate fee, make it scalable at a territorial and attractive level both for private and public investors.

V. CONCLUSION

The case presented, in the prototyping phase in a province of region Piemonte (Italy), by a B Corp oriented company, represents an interesting development in terms of "social design", of the creation of a green and circular economy model for local development that can be replicated in the territory with the objective of producing sustainable employment and territorial development, with particular emphasis on environmental and social impact.

REFERENCES

- [1] C. De Santis, "Development of a simulation model for gasification plants biomass", "Sapienza" University of Rome, PhD in Energetics XXV Cycle A.A. 2011/2012
- [2] Di Blasi, C., "Dynamic Behavior of Stratified Downdraft Gasifiers," Chem. Eng. Sci., 55, 2931 (2000).

RE-DIRECTING MICROBIAL METABOLISM: BIOELECTROCHEMICAL SYSTEMS IMPROVE CO₂ ASSIMILATION IN *Clostridium spp.* AND *Cupriavidus necator*.

R.A.Nastro¹, C.Avignone-Rosssa²

¹SUGGEST scarl, Via Breccia a Sant'Erasmo 112, 80146, Naples (Italy)

²Department of Microbial Sciences, University of Surrey, Guildford,
Surrey GU2 7XH, United Kingdom (United Kingdom)

Abstract - Bioelectrochemical systems (BESs) have shown their potential in different applications, including CO₂ capture and assimilation by means of electrofermentation. In this work, we tested the ability of *Clostridium spp.* and *Cupriavidus necator* to capture CO₂ in two-chamber Microbial Fuel Cells (MFCs), while applying different external potentials and operational conditions. A *Shewanella oneidensis* MR1 and *Pseudomonas aeruginosa* PA1430/CO1 consortium was used at the anode to sustain CO₂ capture operated by bacteria at the cathode.

While *C.necator* showed the highest CO₂ capture rate (95.6%) when a +1.5V was applied at the electrodes (-750 mV at the cathode and +750 mV at the anode), *Clostridium spp.* maximum CO₂ assimilation (78.6 %) was achieved when the MFCs were kept at maximum power (i.e. with no external potential applied). This last result gives evidence of the ability of the *Shewanella oneidensis* MR1 and *Pseudomonas aeruginosa* PA1430/CO1 consortium to sustain CO₂ capture by *Clostridium spp.*

Index Terms – CO₂ capture, electrofermentation, Microbial Fuel Cells.

I. INTRODUCTION

The assimilation of CO₂ can give bacteria some advantages as dissipating excess reducing equivalents produced by metabolic processes, accumulate organic molecules as energy and carbon storage (Shimidzu et al., 2015). Electro-fermentation represents one of the newest most promising application of Bioelectrochemical Systems (BESs), combining CO₂ capture and organic compounds synthesis in the so-called “microbial electrosynthesis”. Potential advantages of such process over other renewable sources of energy and chemicals include the 100-fold higher efficiency of photovoltaics in harvesting solar energy. Other advantages of electro-synthesis include the elimination of

the need for arable land and the direct production of desired products (Nevin et al., 2011). The interest about microbial electrosynthesis is increasing, and much more information on the microbiology of this process is required.

In a typical system, bacteria able to assimilate CO₂ are inoculated in the cathode of a two-chamber Microbial Fuel Cell, where a potential is generally provided by the use of a potentiostat. Nevertheless, it is possible to set-up a system in which the electrons necessary to reduce CO₂ at the cathode are provided by microorganisms inoculated in the anode. In this work we tested the utilization of *Cupriavidus necator* and *Clostridium spp.*, a bio-butanol producer, in CO₂ capture under different experimental conditions in double-chamber MFCs .

A. Microbial Fuel Cells set-up and operation

We used two-chamber MFCs (20 mL in volume), provided with cation exchange membranes, to test the efficiency of CO₂ capture and assimilation in *Clostridium spp* and *Cupriavidus necator* DSM-428. Specific Minimal Salt Media (with CO₂ as sole carbon source) were used at the cathode while a *Shewanella oneidensis* M1/*Pseudomonas aeruginosa* PA1430/CO1 consortium was inoculated in M9 medium (containing 0.4% glycerol) and used in the anode compartments. Gas mixtures containing 2% and 10% CO₂ were used in the assimilation test for *Clostridium spp* and *C.necator* respectively (Figure 1). CO₂ assimilation was tested by applying 3.0 V and 1.5 V external voltage, in MFCs working at maximum power; in MFCs kept in OCV; and in control cultures and abiotic controls after sparging the gas mix in the catholite overnight. An ElectroLab CO₂ -meter was used to assess CO₂ concentration in the cathode compartments. All MFCs and

controls were run in double replicas. Electric outputs were measured by an Arbin Fuel Cell Test Equipment (Arbin Instruments©, Peach Creek, USA).

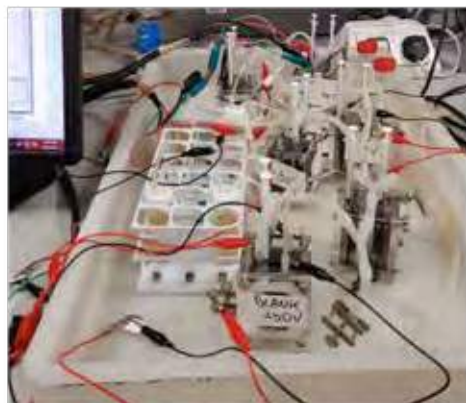


Figure 1: MFCs experimental set-up with control cultures (in the white rack), MFCs with different applied voltages.

Electrode biofilm preparation

Two carbon cloth electrodes (2.5 x 3.5 cm surface) were connected by a 100 Ohm resistor and placed in 100 mL Duran bottles inoculated with *Clostridium/Cupriavidus* pure cultures. Bottle lids with portholes for the carbon cloth electrodes wires and an air cathode made up by a graphite rod free of any wire connections. Control cultures were constructed without electrodes. The same scheme was adopted for both anode and cathode biofilm preparation. In order to obtain a progressive switch of *Clostridium* spp. biofilm microbial metabolism towards chemolithotrophic growth, initial cultures of Clostridial medium (Oxoid) were prepared and kept in anaerobiosis at 30°C for 48 h. The medium was switched to Tryptone-Soya Yeast Extract Medium (1/4 strength) without sucrose for further 48 h at 30 °C. Thereafter, bacteria were incubated in a modified Tryptone-Soya Yeast Extract Medium (1/4 strength) composed by yeast extract (2.5 g/l), (NH₄)₂SO₄ (0.5 g/l), FeSO₄ (0.025 g/l), NaHCO₃ (10 ml of a 5% solution in 990 ml of medium), pH 6.8±0.2. As for *C. necator*, we used Nutrient Broth (Oxoid) as first culture medium (48 h at 30°C), then we switched to the medium for chemolithotrophic growth (Medium 81, DSMZ) with NaHCO₃ as carbon source and incubated for further 96 h at 30°C (with medium changed every 48 h). As to the *Pseudomonas aeruginosa/Shewanella oneidensis* M1, the media used to develop the biofilm were: Tryptic Soy Broth (first 48 h at 30 C) followed by M9 added with sodium lactate (0.4%) and casaminoacids (0.2%) (for 96 hours at the same temperature with medium changed every 48h).

B. Results

Table 1 shows CO₂ concentration in *Clostridium* spp. MFCs, control cultures and abiotic controls. *Clostridium* spp. maximum CO₂ sequestration from the gas mix (78.6%) was

achieved when MFCs were kept at maximum power (i.e. with no external potential applied). This result suggests the ability of the *Shewanella oneidensis* MR1 and *Pseudomonas aeruginosa* PA1430/CO1 consortium to sustain CO₂ capture by *Clostridium* spp. *C. necator* showed the highest CO₂ capture rate (95.6%) when +1.5V was applied at the electrodes (-750 mV at the cathode and +750 mV at the anode). Very low decrease in CO₂ was observed in MFCs kept at maximum power (just 8.5% in comparison to the control culture).

Table 1: CO₂ removal in *Clostridium* spp. MFC_+3V: MFCs with +3V applied; MFC_+1.5V: MFCs with 1.5V applied; MFC_Load: MFC kept at maximum power; MFC (blank): MFC fed with sterile medium.

Operation conditions	% CO ₂ removal (vs abiotic controls)	% CO ₂ removal (vs control cultures)
MFC_+3 V	22.8	18
MFC_+1.5V	40	17
MFC_OCV	32	13
MFC_Load	78.6	67
MFC(blank)_+3V	0	1.6
MFC(blank)_+1.5V	14	-2*
MFC(blank)_Load	8	0
MFC(blank)_OCV	0	0
Control culture	2	//
Abiotic control	//	-3*

N.B.: * negative values stand for an increase in concentration.

C. Conclusions

MFCs have the potential to contribute to CO₂ capture from gas mixtures. The maximum CO₂ capture efficiencies were achieved in different conditions, possibly due to different metabolic routes active in target microorganisms (*Clostridium* spp and *C.necator* in our research). To the best of our knowledge, this is the first time that an anode microbial consortium is able to sustain CO₂ assimilation in MFCs.

ACKNOWLEDGE

This research was supported by a CINET BBSRC Proof of Concept Grant.

REFERENCES

- [1] Nevin K.P., Hensley S.A., Franks A.E., Summers Z.M., Ou J., Woodard T.L., Snoeyenbos-West L.O., Lovley D.R. 2011. Electrosynthesis of Organic Compounds from Carbon Dioxide Is Catalyzed by a Diversity of Acetogenic Microorganisms. *Applied and Environmental Microbiology*, 2882–2886.
- [2] Shimizu R., Dempo Y., Nakayama Y., Nakamura S., Bamba T. Fukusaki E, Fukui T. 2015. New Insight into the Role of the Calvin Cycle: Reutilization of CO₂ Emitted through Sugar Degradation. *Scientific Reports* 5:11617.

ENERGY HARVESTING FROM WASTEWATER BY IN-BACH FEEDING SYSTEMS

R.A. Nastro**, M. Di Giuseppe**, M. Toscanesi, M. Trifuoggi, M. de Pertis*, M. Minutillo*, R. Cioffi*

*Department of Engineering, University Parthenope of Naples Centro Direzionale Isola
C4, 80146 Naples (Italy)

**1SUDGEST scarl, Via Breccia a Sant'Erasmus 112, 80146, Naples (Italy)
Department of Chemical Sciences, University of Naples "Federico II", Complesso
Universitario di Monte Sant'Angelo, Via Cinthia 5, Naples (Italy)

Abstract - Microbial Fuel Cells (MFCs) represent an emerging technology for the direct conversion of organic molecules into electricity. Even though the effectiveness of this technology has been proved at small size scale, few examples of scaled-up MFCs are nowadays available. The main limitation to the development of larger-scale MFCs is the decrease of electric power with the cell size increase. In the present study carried out within the IDRICA research project, we report the first results about the performance of MFCs inoculated with bacteria from compost and municipal wastewater. MFCs were arranged in different configurations to investigate their performance in terms of power and current outputs as well as COD, phosphorous and nitrogen removal.

Index Terms –MFCs, wastewater treatment, scaling-up through plurality, compost.

I. INTRODUCTION

Scaling-up of Microbial Fuel Cells (MFCs) represents one of the major issues to the in-field application of MFCs to waste treatment. Mainly, two different approaches are being applied: the scaling-up through plurality i.e. the set-up of modules made up MFCs connected in parallel and/or in series and the set-up of multielectrodes systems (Santoro et al., 2017). Increasing the electrode size in SMFC will lead to drop in power density. As an alternative to the physical scale-up of SMFCs, construction and operation of mini SMFCs, by connecting them to an appropriate power management system, will be the best way to enhance the overall process efficiency (Chandrasekhar et al., 2017). New and cheap electrodes materials are being set-up and tested as well as inocula able to provide high power outputs while degrading the organic compounds, nitrogen and phosphorous compounds (Nastro et al., 2017; Frattini et al., 2016). In this paper we report the preliminary results about the utilization of compost as a source of electrogenic bacteria in MFCs fed with municipal wastewater. We also explored the

efficiency of MFCs arranged in parallel as units for a scale-up through plurality.

A. Materials and methods

Single chamber, air cathode cuboid Microbial Fuel Cells (MFCs) (5x5 cm) with a cilindric chamber of 3 cm in diameter and 4 cm in length were crafted by a 3-D printer using polylactic acid (PLA). Graphie brushes (2.5 cm in length) (Millrose ltd.) were previously incubated in a suspension composed by compost, PBS and acetate (0.2%) for 2 at 30°C before being used as anodes in MFCs. We provide each MFCs with polytetrafluoroethylene based multilayer material at the cathode. A LIFA ARDUINO MEGA was used to monitor the voltage and perform polarization experiments. We arranged the MFCs as both single cells and modules composed by two MFCs with parallel connection.

As a first step, all MFCs were fed with a GM Medium using sodium acetate as sole source of carbon (4% w/V) (<https://sites.psu.edu/microbialfuelcells/>).



Fig. 1. Experimental set-up.

The medium was replaced when at least one MFC/module voltage dropped below 40 mV when put at maximum power. Wastewater was sampled at the sewage treatment plant placed in Acerra (Naples, Italy) soon after the primary treatments (screen, sand grinder, oil removal and denitrification) and before entering the oxidation compartment. Besides single MFCs, we arranged modules of two cell with parallel connections (Figure 1). We performed polarization experiments (260 K Ω - 1 K Ω) every 48 hrs and MFCs were kept at maximum power. MFCs kept in OCV and controls without electrodes were prepared and monitored as well. Chemical Oxygen Demand (COD) of both GM medium and wastewater mixes (1:1, 3:1 and sole wastewater) were carried out before and after being used as fuel in MFCs according to Standard Methods. We report here the results obtained when the MFCs were fed with the 1:1 GM medium/ww mix.

B. Results

In Figure 2, we report the polarization and power curves obtained in MFCs using the 1:1 mix as feedstock for one week.

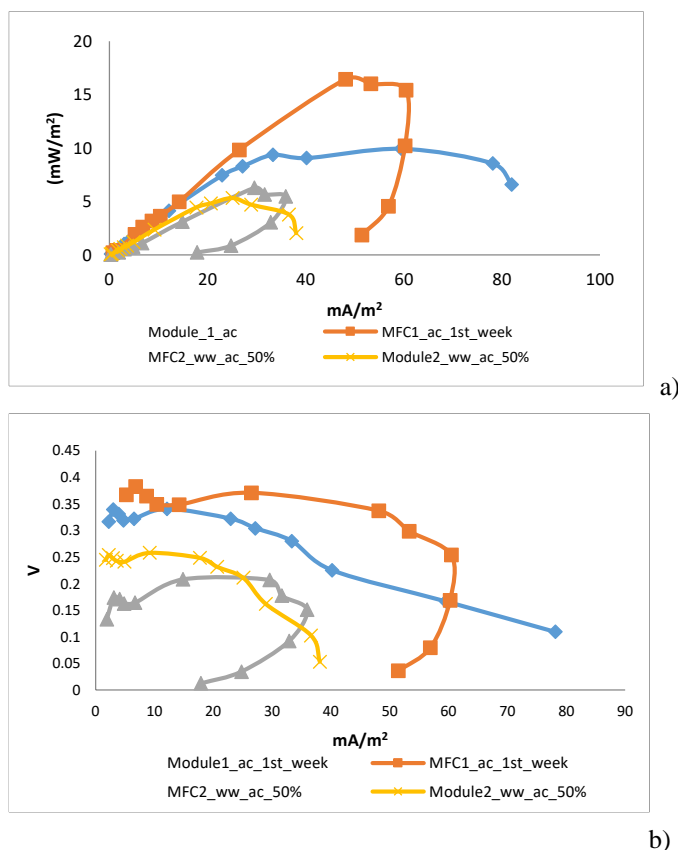


Fig.2: Power (a) and polarization (b) curves of MFCs and MFCs module with 1:1 mix.

The double MFCs units (modules) showed higher stability (absence of overhooks) and about the double current density, in accordance to Ohm's law. The maximum PD was obtained in

single MFCs fed with GM medium (15.6 mW/m²), while the highest CD was measured in Module 1 (81.2 mA/m²). The higher electric outputs find an explanation in the different availability of chemical energy in the feedstocks. Chemical analyses revealed a COD value of 2.14 and 0.887 g/l O₂ for the GM medium and the mix ww/GM medium (1:1) respectively. After three weeks of operation, the highest COD removal was observed in MFCs fed with the mix GM/ww, with a maximum of 52% in double-cell units. A coulombic efficiency calculation will be performed to evaluate single MFCs and double units efficiencies in converting chemical energy into electric power.

C. Conclusions

Bacteria from compost were able to produce electric power in single-chamber air cathode MFCs fed with wastewater mixed with GM medium containing acetate as sole source of carbon.

Furthermore, the results obtained showed a higher stability of double cells units and an increase in current production that makes modules of MFCs with parallel connections good candidates for a scaling-up through plurality for wastewater treatment. The design and set-up of a power management system represents an indispensable prerequisite for energy harvesting in MFCs applied to wastewater treatment, as already observed in the set-up of other bio-electrochemical systems.

ACKNOWLEDGMENT

This research was funded by the Italian Government, with the IDRICA project "Laboratorio integrato per il monitoraggio, controllo e gestione ottimale delle risorse idriche e ambientali".

REFERENCES

- [1] Santoro C., Arbizzani C., Erable B., Ieropoulos I. Microbial fuel cells: From fundamentals to applications. A review *Journal of Power Sources* 356 (2017) 225-244.
- [2] https://sites.psu.edu/microbialfuelcells/files/2019/09/Media_GM_092107.pdf
- [3] Chandrasekhar K., Kadier A., Kumar G., Nastro R.A., Jeevitha V., 2017. Challenges in microbial fuel cells and future scope. Published in "Microbial Fuel Cell: a bioelectrochemical system that convert waste into watts. Edited by M/S Capital/Publishing. Company, India and M/S Springer Switzerland.
- [4] Nastro R.A., Jannelli N., Minutillo M., Facci A.L., Guida M., Krastev V.K., Trifuoggi M. and Falcucci G. (2017). Performance evaluation of Microbial Fuel Cells fed by solid organic waste: parametric comparison between three generations. *Energy Procedia*; 105:1102-1108.
- [5] Frattini D., Falcucci G., Minutillo M., Ferone C., Cioffi R., Jannelli E. 2016. On the Effect of Different Configurations in Air-Cathode MFCs Fed by Composite Food Waste for Energy Harvesting. *Chemical Engineering Transactions*, 49, 85-90.

(EFC19210)

DEVELOPMENT OF A MODULARLY DESIGNED STANDARD TEST SYSTEM FOR HIGH-TEMPERATURE POLYMER ELECTROLYTE FUEL CELLS WITH HYDRAULIC SINGLE CELL COMPRESSION

Georg Siestrup*, Jeffrey Roth* **, Ulrich Rost* **, Cristian Mutascu* **,

Lester Engelhardt*, Eugen Hoppe***, Holger Janßen***,

Michael Brodmann*, Martin Müller***, Werner Lehnert*** ****

*Westfälische Hochschule University of Applied Sciences,
45877 Gelsenkirchen, Germany

** ProH+ GmbH,
45897 Gelsenkirchen, Germany

***Forschungszentrum Jülich GmbH, Institute of Energy and Climate Research,
IEK-3: Electrochemical Process Engineering, 52425 Jülich, Germany

**** RWTH Aachen University, Modeling Electrochemical Process Engineering,
52062 Aachen, Germany

Abstract - In this work a novel testing device for high temperature polymer electrolyte membrane fuel cells (HT-PEFC) based on a unique cell compression mechanism [1] is described. This approach eliminates common technical difficulties by homogeneous electrical contacting, pressure distribution and thermal management (temperature distribution on the cell and layer level). A significant further advantage of the new design is the quick and easy exchangeability of individual cells from the stack. In the presented modular test system, the individual cells are situated in separate flexible pockets. The compression of the pole plates with interposed membrane electrode assemblies is realized via a hydraulic medium, which applies an externally adjustable equal pressure to the pockets. The main advantage of this design [2] for the HT-PEFC application is that the hydraulic fluid will also be used as a heat transfer medium.

Index Terms - HT-PEFC, hydraulic compression, stack, testing

I. INTRODUCTION

Hydrogen energy systems are recently discussed to be a solution to overcome fossil fuels related economic and environmental issues. Due to elevated operation temperature of about 160 °C and robustness against fuel impurities high temperature polymer electrolyte membrane fuel cells (HT-PEFC) offer promising specifications for several mobile or stationary energy applications such as auxiliary power units or combined heat and electrical power generation. However, although massive research has been performed on this technology, HT-PEFC is still not commercially competitive in comparison to conventional technologies. Therefore, further

research on HT-PEFC components, especially on catalysts, membranes, pole plates to mention just few, is still necessary. Within the framework of an ongoing R&D project a novel testing device was developed for analysis of MEAs and pole plates with an active cell area of up to 50 cm². Based on a pocket-design the system can facilitate hydraulic cell compression and is able provide necessary test conditions for a homogeneous HT-PEFC operation.

II. EXPERIMENTAL SETUP

The testing system is designed to run one to five fuel cells under variable required conditions. While the five test cells are electrically connected in series, each test cell is connected to a manifold that provides necessary gases in parallel. The temperature can be adjusted in a range between 30 °C and 180 °C and a hydraulic pressure up to 10 bar can be applied to the installed single fuel cells. Graphitic pole plates with a flow field of up to 50 cm² are mounted to a clip and can be swapped with ease. Sensors measure the pressure and temperature of the hydraulic fluid and the processing gas. The single cell voltage is recorded for each individual slot and a combined stack potential and current signal are measured. The design as schematically seen in Fig. 1. consists of a pressure housing containing five pockets for HT-PEFC. The manifolds used to connect the hydraulic fluid and the process gases are mounted to the stack. To enhance the usability all wiring and piping is realized at the backside of the stack and the fuel cell clip is accessible from the

front side. All sealing is achieved by viton (FKM) o-rings.

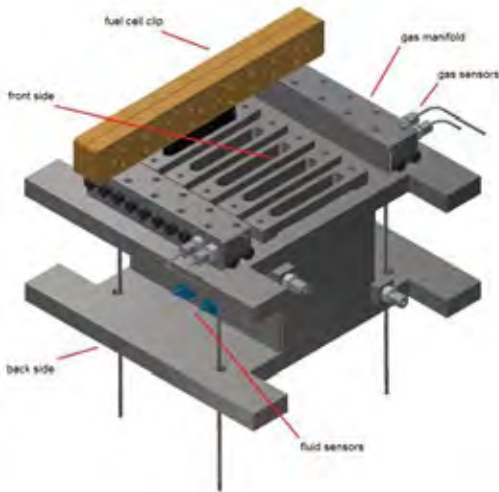


Figure 1 construction sketch of the test device

The system offers the ability to simultaneously test and compare several cells (e.g. MEAs, flow fields, pole plates ...).

III. RESULTS

As a major part of this work the testing device was characterized in different operating situations. To optimize the system, the temperature distribution was recorded as seen in Fig. 2.

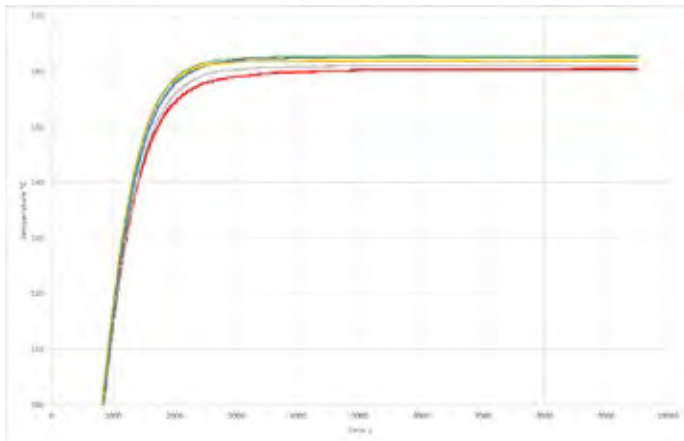


Figure 2 temperature distribution of all five pockets during a heat-up sequence

The temperature distributes fairly equal between all five pockets and has further been optimized by adjusting the flow of the high-temperature/pressure pump and adding a layer of thermal isolation. All five temperatures differ in a range of 2 °C.

Another useful parameter to be investigated was the pressure distribution on the pole plate which was visualized using pressure sensitive film (see Fig. 3).

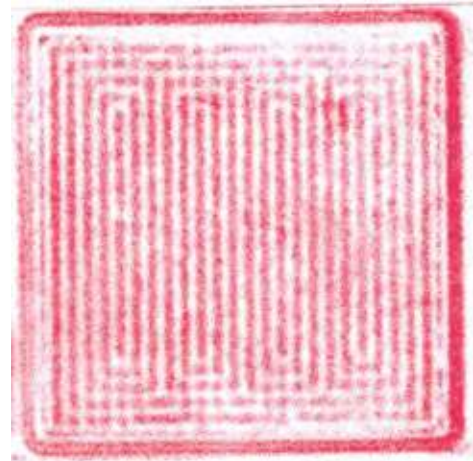


Figure 3 pressure distribution of hydraulically compressed test cell with active cell area of 70 mm x 70 mm (determined with pressure sensitive film)

The pressure sensitive film type Fujifilm Prescale LLLW (2 to 6 bar) shows marginal variations in the pressure distribution over the dimensions of a comparable flow field with an active cell area of 70 x 70 mm². The pressure pattern displays a homogeneous symmetric compression along the vertical symmetry axis of pole plate.

IV. CONCLUSIONS

The developed testing device is able to provide the required stable conditions regarding cell temperature and compression homogeneity to characterize HT-PEFCs. However, long-term testing is needed for the validation of all functions of the test stack.

ACKNOWLEDGMENT

This work has been financially supported by the EU and LeitmarktAgentur.NRW within the scope of the program Energie & Umweltwirtschaft.NRW. (funding number: EFRE-0800099).

REFERENCES

- [1] Ulrich Rost, Cristian Mutascu, Jeffrey Roth, Christoph Sagewka, Michael Brodmann, Proof of Concept of a Novel PEM Fuel Cell Stack Design with Hydraulic Compression. U Rost, C Mutascu, J Roth, C Sagewka, M Brodmann - Journal of Energy and Power Engineering, 2015, DOI: 10.17265/1934-8975/2015.09.003.
- [2] Ulrich Rost, Gabriela Marginean, Roxana Muntean, Pit Podleschny, Michael Brodmann, César Merino, Roberto Díez, A., cost-effective PEM fuel cell test system based on hydraulic compression with optimized platinum catalyst loading, 2016 International Energy and Sustainability Conference (IESC), 1-6, DOI: 10.1109/IESC.2016.7569500.

COMPARATIVE STUDY BY DESIGN OF EXPERIMENTS OF LINEAR AND NONLINEAR CONSTITUTIVE MODELS AND GEOMETRIC PARAMETERS EFFECTS ON PEMFC PERFORMANCE

C. Charbonné¹, M. L. Dhuitte¹, K. Bouziane^{1,2,3,4}, D. Chamoret⁵, D. Candusso^{2,4}, and Y. Meyer^{1,3}

¹Univ. Bourgogne Franche-Comté, UTBM, 90010 Belfort Cedex, France.

²Laboratoire SATIE (UMR 8029), ENS Paris Saclay, IFSTTAR, Université Paris Saclay, Université Paris-Sud. 25 allée des marronniers 78000 Versailles Satory, France.

³Sorbonne Universités, Université de Technologie de Compiègne, CNRS, UMR 7337 Roberval, centre de recherche Royallieu, CS 60 319, 60203 Compiègne cedex, France.

⁴FR FCLAB, Plateforme pile à combustible, UTBM bât. F, Rue Thierry Mieg, 90010 Belfort Cedex, France.

⁵ ICB UMR 6303, CNRS Univ. Bourgogne Franche-Comté, UTBM, Belfort, France

Email presenting author: chloe.charbonne@utbm.fr

Abstract - PEMFC appears to be a promising technology to address the challenges of energy transition. So, it seems necessary to optimize these systems. In our study, we have addressed the mechanical aspects and their impacts on the performance of a PEMFC. More specifically, the main objective of this work is to understand the influence of the mechanical properties of the fuel cell core on the electrical resistances of the system's internal contacts. Indeed, electrical contact resistances are one of the major sources of losses and therefore require special attention. To do this, a DoE associated with a Finite Element Model was used in order to obtain the influence of geometric and mechanical parameters on the performance of a PEMFC, where each layer thickness and the GDL constitutive law were examined.

Index Terms - PEMFC, Design of experiments, Numerical modeling, Gas diffusion layer, Nonlinear behavior.

I. NOMENCLATURE

BPP: Bipolar Plate; CPress: Contact Pressure; CR: Contact Resistance; DoE: Design of Experiments; EP: End Plate; GDL: Gas Diffusion Layers; FC: Fuel Cell; MEA: Membrane Electrode Assembly; PEMFC: Proton Exchange Membrane Fuel Cell.

II. INTRODUCTION

The performance of a PEMFC, subjected to external-internal mechanical excitations [1] and environmental conditions, is one of the significant factors influencing its industrialization. The constitutive law allows to specify a material and to approximate the reaction of the material to external forces with a relation between two physical quantities. The constitutive law can be linear (the stiffness is constant, or the strain is less than 10 % of that of the object) or non-linear (change in stiffness with strain or large strain). We are especially interested in the

influence of the GDL constitutive law - linear and non-linear constitutive law - and the thickness on the CPress, a fundamental quantity associated with the performance of PEMFC.

At each interface there will be a loss of current intensity, called electrical CR, due to insufficient surface-to-surface contact. Studies have found CPress can strongly affect CR [2,3] and discovered a relation between CR and CPress [5]. The most important electronic ohmic losses in FC are at the BPP and GDL interface with the electrical CR [1,3]. The aim is therefore to have the higher contact pressure between them in order to reduce the CR. The influence of component thicknesses causes stress variations and therefore affects the performance of a stack.

The purpose goes further by using a DoE with a Finite Element Model to study the effect of geometry and constitutive law of material, on the performance of a PEMFC stack. The next section presents our methodology. Our numerical approach is given in Section IV. The last section displays the results of the parameters effects on the overall performance.

III. METHODOLOGY

Finite Element Analysis allowed to extract the CPress and Von Mises stresses for each element for each contact interface by integrating the pressure on the surface. DoE provides an optimal simplified model to maximize the pressures for each interface and minimize the constraints.

IV. NUMERICAL SIMULATION AND TAGUCHI APPROACH

A. Model

A 2D plane strain Finite Element model has been developed with the commercial software ABAQUS. Due

to symmetry, only half of the single fuel cell is modelled. The model consists of EP, BPP, GDL and MEA as shown in Fig. 1.

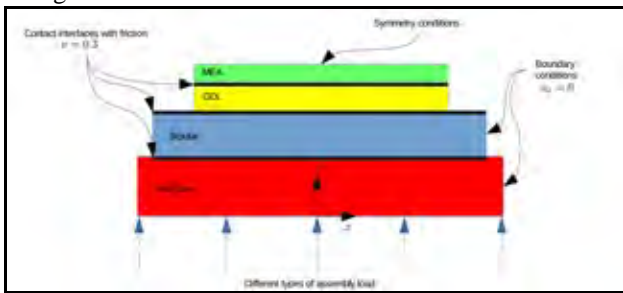


Fig. 1. 2D plane strain numerical model

The model was built with the following assumptions:

- ❖ Materials are homogeneous and isotropic solids.
- ❖ EP, BPP and MEA are linearly elastic. GDL is assumed to be a linear elastic or hyperelastic (Use of Marlow model extracted from experimental results [4]). Here the hyperelastic (non-linear) constitutive law more accurately represents the actual behavior of material.
- ❖ Assembly pressure is applied uniformly on the collector plate and boundary conditions applied on BPP and EP are $u_x=0$.

B. Design of Experiments [6]

A DoE is a series of tests organized in advance to observe with maximum precision the influence of multiple parameters in a minimum of tests. It avoids combining all the modalities of all the parameters. In addition, we have reduced the number of models to be run from 27 to 9 and we carry out geometric factors in effect analysis tables. To extend our analysis, 2 DoE models (L_9) were used with linear and non-linear behavior respectively.

V. RESULTS OF PARAMETER EFFECTS

A. Limitations

During the runtime, some of the models did not converge because the EP thickness must be strictly greater than 53% of the BPP. We believe that there is a minimal thickness ratio between the BPP and the EP, that makes it possible to operate.

B. Effect of the GDL constitutive law

The GDL constitutive law does not influence the characteristics of the best thicknesses which optimize the FC performance. On the contrary, the constitutive law affects the extremum of the DoE according the thickness ratio. So, the GDL constitutive law plays a role in the FC performance but has less impact than thickness variation.

The GDL has a highly nonlinear constitutive law. Therefore, using a linear constitutive law is an assumption to be carefully used.

C. Most influential components and best thicknesses

The EP thickness seems to control the behavior of stress and pressure in the other components. A thin EP

considerably increases the CPress and especially the stress. The best EP thickness seems to be in [7.5mm; 15mm]. According to our effect analysis table, the best thickness for the MEA was to choose the smallest, in our case 254 μm . For the GDL, the best choice is a thickness equal to 0.28 mm, and finally for the BPP a thickness equal to 3 mm.

D. Behavior of compression and stress at interfaces

For the EP-BPP interface, there is a general behavior with a minimal contact pressure on the edge, then a pressure drop leading to a non-homogeneous behavior on the surface. This suggests that there is a slip effect and shear at the EP-BPP interface.

On the interface BPP-GDL, the behavior is the opposite. The pressures reach their maximum at the border, almost five times more than the previous interface. For the last two layers, the same behavior is obtained. The pressures reach their maximum at the ends and drop sharply to 0 MPa. This creates a large variation in resistance throughout the structure.

E. Best set of parameters

Thanks to the effects table, we select the optimal solution. We have carried out the model with the optimal dimensions and we obtain the results given in Table I.

TABLE I: OPTIMAL RESULTS FROM THE DOE

Hyperelastic GDL			
Results	Contact type	Van Mises Stress MAX [MPa]	Contact Pressure MAX [MPa]
Optimal	Contact GDL-MEA	14.66	18.13
	Contact BPP-GDL	5.84	18.04
	Contact EP-BPP	28.6	13.23

VI. CONCLUSION

After reviewing the results, it appeared that the thickness ratio plays a major role in the conduction of electricity. Moreover, the choice of the GDL constitutive law has a weaker influence that is currently not yet understood.

REFERENCES

- [1] Y. Hou, X. Zhang, X. Lu, D. Hao, L. Ma, P. Li, AC impedance characteristics of a vehicle PEM fuel cell stack under strengthened road vibrating, *Int. J. Hydrog. Energy*, Vol.39:32, 2014.
- [2] E. Alizadeh, M. Ghadimi, M. Berzagui, M. Momenifar, S. Saadat, Development of contact pressure distribution of PEM fuel cell's MEA using novel clamping mechanism, *Energy*, Vol. 131, pp. 92-97, 2017.
- [3] E. Alizadeh, M. Barzegari, M. Momenifar, M. Ghadimi, S. Saadat, Investigation of contact pressure distribution over the active area of PEM fuel cell stack, *Int. J. Hydrog. Energy*, Vol. 41:4, pp. 3062-3071, 2016.
- [4] P.A. Gigos, Y. Faydi, Y. Meyer, Mechanical characterization and analytical modeling of gas diffusion layers under cyclic compression, *Int. J. Hydrog. Energy*, Vol. 40:17, pp. 5958-5965, 2015.
- [5] P. Zhou, C.W. Wu, G.J. Ma. Contact resistance prediction and structure optimization of bipolar plates. *J. Power Sources* 2006, 1115–1122.
- [6] A. Joneja, Design Principles, The Hong Kong University of Science and Technology, 2001.

AN ULTRA-LIGHT-WEIGHT POLYMER ELECTROLYTE FUEL CELL BASED ON 0.1 MM THICK CARBON FIBER BIPOLAR PLATE

Chi-Young Jung^{1*}, Hyunguk Choi^{*}, and Seo-Won Choi^{*}

^{*}Korea Institute of Energy Research, Jeollabuk-do, 56332,
(Republic of Korea)

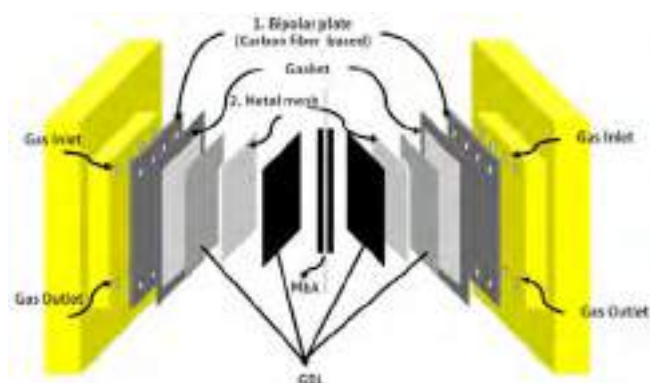
Abstract - The polymer electrolyte fuel cell consists of membrane electrode assembly, gas diffusion layer, bipolar plate, gasket, etc. Among them, the bipolar plate, i.e., the second largest cost component, is typically fabricated from graphite or metallic composite materials. While the graphite bipolar plate is over a few mm thick due to the poor mechanical strength, the metallic bipolar plate is prone to corrosive environment with O₂ with enlarged amount of weight. In this work, we present carbon fiber composite bipolar plate to realize the ultra-light-weight fuel cell and possibly stack. The woven-type carbon fiber plate filled with epoxy resin is first fabricated by hot-pressing, followed by polishing the epoxy resin-rich layer and coating carbon layer, which thus reduce bulk and interfacial electronic resistances, respectively. Consequently, the fuel cell short stack with the proposed carbon fiber bipolar plate exhibited as high as triple times the weight-specific power density when compared to the conventional graphite composite bipolar plate.

Index Terms - Polymer electrolyte fuel cell, Ultra-light weight bipolar plate, Carbon fiber, Epoxy resin

I. INTRODUCTION

The polymer electrolyte fuel cell consists of various components such as membrane electrode assembly, gas diffusion layer, bipolar plate, and gasket [1]. Among them, the bipolar plate, that is the second largest cost component, is typically fabricated from the graphite composites or metallic composite materials [2]. While the graphite bipolar plate is over a few mm thick due to the poor mechanical strength, the metallic bipolar plate is prone to corrosive environment with O₂ with enlarged amount of weight. In this work, we present carbon fiber composite bipolar plate to realize the ultra-light-weight fuel cell that is possibly usable to stack. The woven-type carbon fiber plate filled with epoxy resin is first fabricated by hot-pressing, followed by polishing the epoxy resin-rich layer and coating carbon layer, which thus reduce bulk and

interfacial electronic resistances, respectively. Subsequently, the resultant bipolar plate was further evaluated on the electric conductivity, mechanical strength and gas permeability that are vital for the employment in fuel cell stack. Finally, the fuel cell performance was measured after the use of new cell fixture with newly proposed carbon fiber bipolar plate (Scheme 1).



Scheme. 1. A unit cell structure based on the newly-proposed carbon fiber plate based bipolar plate

II. RESULTS AND DISCUSSION

A. Microstructure of the carbon fiber bipolar plate

Figs. 1 and 2 showed the SEM images on surface and cross-section of the carbon fiber bipolar plate with increasing polishing time. From Figs. 1A and 2A, the as-fabricated carbon fiber bipolar plate showed polymeric resin with an overall thickness of 300 μm while the physically polished ones revealed more portion of carbon fiber exposed on surface with the reduced thickness down to 190 μm .

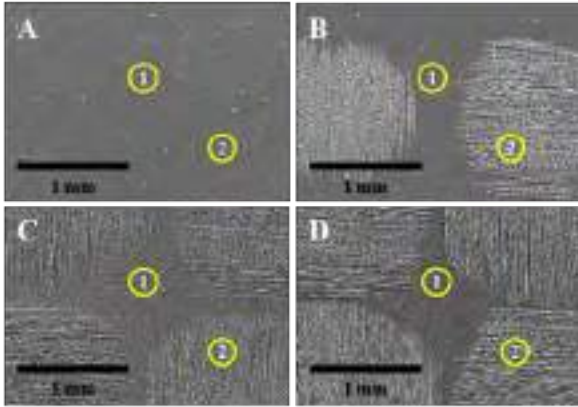


Fig. 1. SEM images on surface of the as-fabricated carbon fiber bipolar plate and carbon fiber bipolar plates after physical polishing – A: 0 min polishing (as-fabricated), B: 30 min polishing, C: 60 min polishing and D: 90 min polishing.

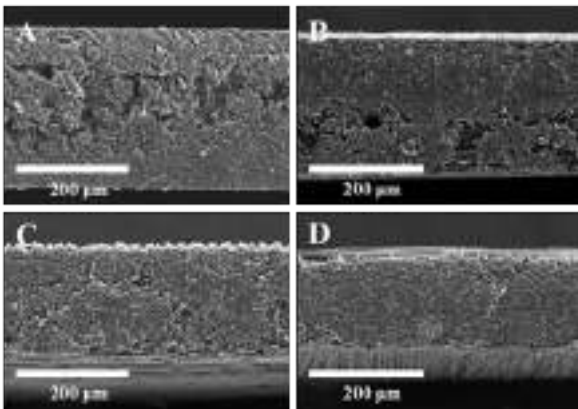


Fig. 2. SEM images on cross-section of the as-fabricated carbon fiber bipolar plate and carbon fiber bipolar plates after physical polishing – A: 0 min polishing (as-fabricated), B: 30 min polishing, C: 60 min polishing and D: 90 min polishing.

B. Physical characterization

After polishing, the electron conductivity can be enhanced due to the removal of epoxy resin layer, while the mechanical strength as well as gas permeation resistivity may be aggravated. As shown in Fig. 3, the 90 min polished carbon fiber bipolar plate resulted in quite acceptable electron conductivity up to 500 S cm^{-1} with 4-fold increased tensile strength and 2-fold increased gas permeation resistivity compared to the US DOE 2020 technical targets. These values indicate that the resultant carbon fiber bipolar plate can be an excellent candidate for replacement of the conventional graphitic or metallic bipolar plate.

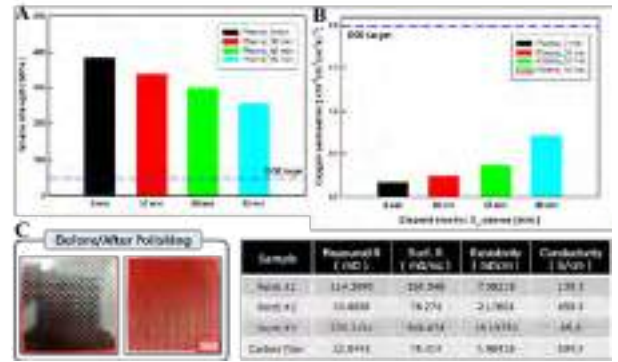


Fig. 3. Physical characterization of carbon fiber bipolar plates after physical polishing – A: tensile strength and B: gas permeability with increasing polishing time, and C: electric conductivity after 90 min polishing.

C. Fuel cell performance

Fig. 4 shows the i-V performance of the newly proposed carbon fiber bipolar plate based single cell when compared to the state-of-the-art one based on the graphite composite bipolar plate. The results show that an approximately 90% of cell performance can be achieved after the use of newly proposed carbon fiber bipolar plate where the 10% of the performance loss is coming from the increased iR loss.

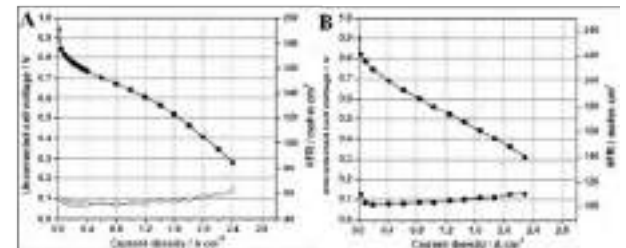


Fig. 4. Cell performance after the use of newly proposed carbon fiber bipolar plate – A: single cell with the conventional graphite composite bipolar plate and B: single cell with the 90 min polished carbon fiber bipolar plate.

III. CONCLUSION

Fuel cell with newly proposed carbon fiber bipolar plate exhibited 3-fold weight-specific power density compared to the conventional one with the graphite composite bipolar plate.

ACKNOWLEDGMENT

This work was conducted under framework of the R&D program of the Korea Institute of Energy Research (B9-2413).

REFERENCES

- [1] Staffell, I., Scamman, D., Abad, A.V., Balcombe, P., Dodds, P.E., Ekins, P., Shah, N., Ward, K.R., Energy Environ. Sci. 12, 2019, pp. 463-491.
- [2] Papageorgopoulos, D., US DOE Annual Merit Review, Crystal City, VA, 2019.

AMMONIA AS A FUEL IN SOFC: TECHNOLOGY STUDY AND SYSTEM DESIGN

G. Cinti*, L. Barelli*, F. Mondì* and G. Bidini*

*Università degli Studi di Perugia, Engineering Department, via
Duranti 93 – 06100 Perugia, (Italy)

Abstract – The development of renewable energies requires a suitable energy carrier that allows to store and reuse of the electricity produced. Hydrogen is proposed as a suitable candidate for energy storage both for power production and transport. Main drawback of hydrogen technology is related to low energy density. Ammonia, nowadays well known fertilizer, is also an high density and carbon free fuel. This study investigates the use of ammonia as a fuel when coupled with high temperature fuel cells. Advantages in terms of technology assessment and system design are studied both by means of experimental activity and system modelling.

Index Terms – ammonia, energy storage, experimental, fuel cell, SOFC.

I. NOMENCLATURE

SOFC: Solid Oxide Fuel Cell

Uf: Utilization of fuel

II. INTRODUCTION

The development of renewable energies strongly increased the request of a sustainable solution to store electrical energy. One of the feasible route is to transform energy into chemicals that can be easily stored or transported for any kind of energy application. Ammonia is one of the chemical products more synthesized worldwide. Ammonia is usually distributed as a fertilizer directly in the gaseous form or can be used as a base component for the production of solid urea. At the same time ammonia is also a fuel with a chemical energy that can be released when oxidized. Ammonia as a fuel has extremely interesting peculiarities since it is no toxic, not flammable and, in particular, is carbon free. When ammonia is used as a fuel no CO₂ is emitted. To evaluate the sustainability of ammonia it is necessary to consider the production process. Nowadays ammonia is produced from natural gas via the well known Haber Bosh process. It is possible to produce ammonia also from renewable energies. In particular, looking to renewable

electrical energy, it is possible to produce hydrogen from electrolysis and nitrogen from air separation and feed the two chemicals to the NH₃ synthesis loop. The use of ammonia in power systems has been deeply investigated in literature. One of the most promising application is the coupling of NH₃ with Solid Oxide Fuel Cells (SOFCs). SOFCs technology was strongly improved in the recent years and stacks in the range of 1-300 kW are available in the market. Such technology can achieve high efficiencies (60% natural gas based systems) and very low emissions. In fuel cells there is no direct mix of fuel and oxidants and typical emissions such as NO_x are not produced.

SOFC technology has important advantages when fed with ammonia: (i) thermodynamic conditions and anode catalyst enhance ammonia decomposition; (ii) no risk of carbon deposition occurs in the anode since ammonia is carbon free, (iii) ammonia decomposition is endothermic and the stack can be cooled directly in the anode reducing the air flow in the system. Literature research was mainly focused on the feasibility of using ammonia as a fuel in SOFCs [1]. One of the first issue investigated was the production of NO_x. In particular in [2] both experimental and theoretical study was presented demonstrating that nitrogen oxides can not be produced in the cell. Such evidence moved the study from H-SOFC to O-SOFC due to the more stage of developed of the latter. Following studies demonstrated as a two stage reaction occurs in the cell with a preliminary decomposition of ammonia and a subsequent electrochemical reaction of hydrogen. Additional issues, less investigated in literature, arise the risk of material degradation due to nitridation of nickel catalyst in the anode. Degradation mechanism are presented but with no complete study of operating conditions.

In this study three different aspects of the technology are investigated:

- 1) Study of SOFC cell degradation due to long term

- exposition to ammonia via experimental study;
- 2) Test of SOFC stack when fed with ammonia in real operating conditions;
 - 3) System design based on stack results;

III. DEGRADATION TEST

Degradation was studied at single cell level. Experimental studies were performed on a commercial single cell planar, anode supported with materials Ni/YSZ-YSZ-GDC-LSCF. Long term tests, 100 h, were performed operating the cell at 500 mA cm² and fuel utilization of 33%. Ammonia fed cell was performed with hydrogen equivalent results. Tests were performed at 700, 750 and 800°C. Results are reported in Table I. Comparing results at 750°C, same degradation was measured with hydrogen and ammonia. Post mortem analysis showed that there was no anode nitridation.

TABLE I
RESULTS OF THE DEGRADATION TEST

Gas	H ₂	NH ₃	NH ₃	NH ₃	
Temperature	745.4	744.5	797.4	693.3	°C
Gas Flow	10.24	6.85	6.85	6.85	NI/h
Voltage decay (mV)	11.7	12.5	14.2*	3.0	mV/100 h
Voltage decay (%)	1.4%	1.5%	1.6%*	0.4%	100 h

* Projection after 50 h

IV. STACK TEST

The stack test was performed on a six cells SOFC planar short stack. The stack was operated at different conditions varying utilization of fuel (Uf), temperature and current density. Fig. 1 reports results at 750°C. In particular, the graph reports measured efficiency for three different values of fuel utilization: 0.6, 0.7 and 0.8. Up to 60% of efficiency was achieved at 200 mA cm⁻² and Uf of 0.8. Off gasses measurements showed how at nominal current density, 500 mA cm⁻², 260 ppm on NH₃ were measured in the off gasses. Higher efficiencies and lower NH₃ concentration in the off gasses were obtained operating the stack at 800°C.

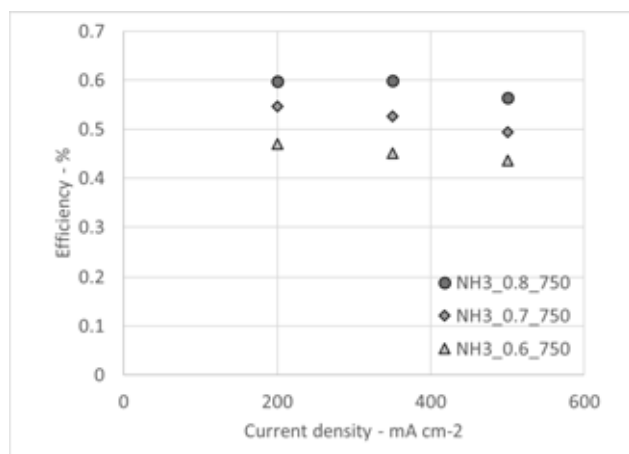


Fig. 1. Efficiency of stack test at 750°C and Uf of 0.6, 0.7 and 0.8

V. SYSTEM DESIGN

Experimental results in terms of voltage variation at different operating parameters were implemented in a zero dimensional model. System scheme is reported in Fig.2. Ammonia is directly decomposed in the stack and preheated in a heat exchanger. Air flow is heated in two heat exchangers up to stack temperature. The system was studied operating the cell at 750°C and utilization of fuel of 0.8. The model calculated an oxidant utilization of 0.17 and a DC efficiency of 0.57. Moreover, considering a heat exchanger efficiency of 0.9, it is possible to remove the after burner from the system and substitute it with a simple mixer (M in Fig.1). In the latter case, hydrogen is directly released to the atmosphere with a chemical energy loss of 22.8 %.

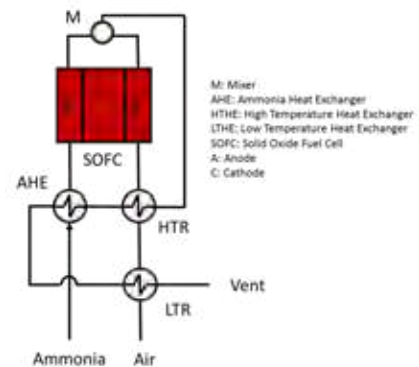


Fig. 2. Conceptual scheme of the ammonia system

VI. CONCLUSION

The use of ammonia as a fuel was investigated at single cell, short stack and system level. Single cell test demonstrated that no degradation due to anode nitrification occurs at operating temperatures. Short stack study showed efficiency up to 60% at 750°C. Finally, system design was studied so to obtain 57 % of system efficiency and a scheme solution without the after burner was presented.

ACKNOWLEDGMENT

The study was supported by ENVIU, PROTON VENTURES BV and C-JOB & PARTNERS BV, in the frame of a scientific collaboration.

REFERENCES

- [1] D. Cheddie, "Ammonia as a Hydrogen Source for Fuel Cells: A Review," in *Hydrogen Energy - Challenges and Perspectives*, vol. i, no. tourism, InTech, 2012, p. 13.
- [2] Q. Ma, R. Peng, L. Tian, and G. Meng, "Direct utilization of ammonia in intermediate-temperature solid oxide fuel cells," *Electrochem. commun.*, vol. 8, no. 11, pp. 1791–1795, Nov. 2006.

(Put paper number here) EFC19215

ADVANCED NEUTRON SCATTERING TO REVEAL STRUCTURE-DYNAMICS CORRELATION IN MEMBRANE TECHNOLOGY

F. Foglia*, B. Quentin**, J-M. Zanotti**, V. Garcia-Sakai***,
S. Lyonnard**, G. Gebel**, K. Smith****, T. Miller****, D.
Brett**** and P.F. McMillan *

*UCL, Chemistry Dept, London (UK)

**CEA, Grenoble (France)

*** ISIS, Rutherford Appleton Laboratories, Didcot (UK)

**** UCL, Chemical Engineering Dep, London (UK)

Abstract - Despite the widespread use (e.g. in healthcare, energy and water treatment applications) and the continued development of new materials and solutions for their implementation in advanced devices, improving membrane performance and durability remains a non trivial problem. In large part this is due to the lack of a detailed understanding of the dynamics of the permeant confined within the membrane structures, that are typically multi-scale in terms of correlation lengths and relaxation timescales for the different processes involved. It is therefore difficult to disentangle individual contributions to the various motions and their involvement in the membrane structure-dynamics correlation, especially *in situ* and under *operando* conditions. Here we present how using advanced neutron scattering (quasi-elastic neutron scattering: QENS and neutron reflectivity: NR) techniques can shed light on developing new understanding of the correlations between the structures and dynamics of composite membranes with the aim of optimising membrane technology and designing new materials with improved performance characteristics.

Index Terms – QENS, NR, Fuel Cell, AEM.

I. INTRODUCTION

Despite their already widespread use in healthcare, energy and water treatment applications, design and development of new membranes for selective water and electrolyte transport are required for improving performance and durability for efficient operation. The main challenges to achieve this goal stem from a lack of detailed understanding of the dynamics of the permeant confined within the membrane, particularly *in situ* and under *operando* conditions.

In the specific case of fuel cells (FCs), interest has mainly focused on polymer electrolyte membrane fuel cells (PEMFCs) because of their high power densities, quick start-up, lower cost and wider applications compared to other types of fuel cells. They can be classified into two categories, namely proton conducting cation exchange membranes (CEMs) and hydroxide conducting anion exchange membranes (AEMs). In the first case precious metal catalysts such as Pt are necessary to facilitate the electrochemical reactions [1], while AEMs offer the great advantage that the precious metal catalyst can be replaced by cheaper and more available transition metal alternatives [2]. The main challenge with AEMs is developing efficient membranes for use within these systems. Intensive efforts are under way to develop and improve the AEM membranes from a synthetic point of view, to optimize their chemical and thermal stability, mechanical processability and production costs. However, the AEMs to date display poor ionic conductivity. The mobility of the OH⁻ ions is mainly impacted by molecular architecture and nanoscale organization of the ionic channels [3]. Attempts have been made to “mimic” the morphology of the Nafion membranes that are considered as a reference [4], in order to improve ionic conductivities in AEMs [5]. However, very little is known to date on the molecular level mechanisms, in particular the relation between OH⁻ transport and water dynamics. Theoretical studies have predicted that hydroxide ion transport in AEMs results from a combination of Grotthuss-like mechanism (i.e., proton transfer

through the hydrogen bonded water molecules by solvation-shell fluctuations) and mass diffusion. Because the dynamics of the permeant confined within membrane are usually multi-scale in nature it is difficult to disentangle various contributions to the diffusive processes as well as correlations between the membrane structure and local to longer-range dynamics.

Neutron scattering is ideal for this type of study because it allows a unique view of structures of soft condensed matter systems. The nature of neutron-matter interaction provides a non-destructive approach, making it a perfect tool to investigate structurally delicate membrane structure-dynamics properties as well as biological systems. Cold neutrons, with wavelengths of a few Å and energies from μeV to several meV , allow investigations and correlations of structure on the Å- to nano-scale combined with molecular motions on a nano- to pico-second time regimes. Furthermore, because of the difference in neutron scattering cross section between H and D, isotopic contrast experiments can be used to highlight different spatial/dynamic regions under varied chemical and physical conditions.

In this presentation we describe examples from our recent work that illustrate how using advanced scattering (quasi-elastic neutron scattering: QENS and neutron reflectivity: NR) techniques can provide new information to correlate structure and dynamics of composite membrane materials with improved performance characteristics. Our examples are specifically applied to anion exchange fuel cells where depicting permeant dynamics in a benchmark membrane is crucial to help understand and improve the hydroxide ion conductivity to design and develop advanced AEMs for FC applications.

ACKNOWLEDGMENT

This project has received funding from the EU Graphene Flagship under Horizon 2020 Research and Innovation programme grant agreement No. 696656 – GrapheneCore2. We thank the Materials Research Hub for Energy Conversion, Capture, and Storage (M-RHEX) (EPSRC EP/P007775/1) for support, and Prof D. Brett, Dr T. Miller, Dr S. Lyonard, Dr J-M. Zanotti, Dr G. Gebel and Dr V. Garcia-Sakai for useful discussions and support during experiments and data analysis. We also thank Dr J. Copper and Dr M. Campana for support during reflectivity experiments. Finally we are grateful to the Institut Laue Langevin (Grenoble, France) and ISIS (Harwell, UK) for neutron beamtime.

REFERENCES

- [1] Y. Shao, G. Yin, Y. Gao, *J. Power Sources*, 2007, 171, 558.
- [2] J. R. Varcoe & R. C. T. Slade, *Fuel Cells*, 2005, 5, 187.
- [3] S. Maurya, S.-H. Shin, M.-K. Kim, S.-H. Yun, S.-H. Moon, *J. Membr. Sci.*, 2013, 443, 28.
- [4] K. D. Kreuer, *J. Membr. Sci.*, 2001, 185, 29.
- [5] M.-S. Kang, Y.-J. Choi, S.-H. Moon, *AIChE J.*, 2003, 49, 3213.

MICRO-CHP IN RURAL AREAS: MARKET OPPORTUNITIES FOR SOLID OXIDE FUEL CELLS

A. Baldinelli*, G. Cinti*, L. Barelli*, G. Bidini*

*Università degli Studi di Perugia, Department of Engineering, Via
Duranti 93 Perugia, (Italy)

Abstract - The project **TEZIO** (*Zero Emissions Energy Technology*) concerns power generation in micro-scale plants and targets at the pre-prototypal study of an advanced energy system based on fuel cells, for the efficient energy conversion of waste (i.e. agricultural scraps, animal waste, organic residues). The cornerstone of the project is the concept of energy and environmental sustainability in a circular supply chain. Moreover, looking at local synergies, the region Umbria is the perfect candidate to develop this concept, for the high awareness to environmental safeguard and the high number of small enterprises involved in agriculture and farming. Many of them, in particular, have been experiencing economic crisis and call for innovation to earn competitiveness and enlarge the impacts of their business.

Index Terms – SOFC, microCHP, biogas, circular economy.

I. NOMENCLATURE

ICE	Internal Combustion Engine
mCHP	Micro Combined Heat and Power generation
SOFC	Solid Oxide Fuel Cell
TEZIO	Tecnologia Enegetica a Zero Impatto

II. INTRODUCTION

The project TEZIO aims at investigating local opportunities for the demonstration of the SOFC technology in a real environment. This is expected to bring technological innovation in the region Umbria (central Italy), creating synergies between rural areas economy and research expertise. The market niche of biogas producers and SOFCs are rather complementary. For their operating conditions and typical power ranges, SOFC are the ideal CHP technology to fill this market segment (installed power c.a.10-100 kWe). Moreover, biogas is produced from organic waste. Hence, its efficient energy conversion is particularly appealing to the end of a circular economy vision.

This paper presents the project goals and current advancements. As summarized in Table I and discussed in the

following sections, TEZIO is organized according to three main threads. Results from each part will lead to the definition of specifications for a prototype system, to be tested in a real environment.

TABLE I
TEZIO RESEARCH THREADS: GOALS AND ADVANCEMENT STATUS.

Thread	Goals	Advancements
Market Analysis	Definition of local cases-study. Benchmarking of biogas energy chains. Local policies and subsidies.	Completed: focus on cattle/swine farms
System Analysis	Biogas pretreatment specifications Thermal integration and in-situ use of cogenerated heat.	Literature review. Basic system analysis.
Experimentation	Experimental characterization of single components (SOFC cells and stacks) a) degradation b) performance vs. fuel quality	Test on single cells

III. MARKET FRAMEWORK

The potential local market has been analyzed and all results are reported in [1]. From the survey about farms, it emerged that the most significant farms (potential users for the technology investigated) are: 100 head-sized cattle farms and 1000 head-sized swine farms. The same farm classes were spotted as relevant for similar purposes, scouting the European market [2]. Looking at the potential market existing in Umbria, the number of farms that are eligible as customers for micro-scale digestion and CHP, as well as their share of unexploited biogas potential, are summarized in Table 2. These results have been estimate from national census data (ISTAT and BDN).

As final indication for SOFC suppliers, the potential customers identified in the first stage of the project would require SOFC m-CHP systems under 30 kWe.

TABLE II
POTENTIAL USERS FOR SOFC M-CHP IN UMBRIA (CO-DIGESTION RATIO
MANURE-SILAGE 0.4)

Farm type	Feedstock and Process	Number of farms	Share of unexploited biogas potential
Cattle (beef, dairies, mixed) > 100 heads	Animal manure Anaerobic Digestion	100	38%
	Animal manure + silage Anaerobic Co-Digestion	240	56%
Swine >1000 heads	Animal manure Anaerobic Digestion	20	41%
	Animal manure + silage Anaerobic Co-Digestion	80	76%

IV. SYSTEM ANALYSIS

In order to facilitate the market success of the technology and downscale micro digestion and CHP systems, biogas pretreatment prior SOFC feeding plays a major role (especially on the economic feasibility). Direct feeding of biogas to SOFC, after removal of sulfur compounds [5], has risen much interest to this end [3]. Rather stable performances are obtained thanks to the addition of oxygenated gases (air, steam, CO₂), to have methane decomposition completed in the SOFC (via catalytic partial oxidation and hybrid steam/dry reforming). Beside the simplicity of implementation, air addition to biogas seems reasonable for at least 3 reasons: i) improved SOFC stability, thanks to coking suppression on the Nickel anodes [4]; ii) internal temperature management, balancing endothermic and exothermic reactions [5]; iii) nitrogen addition, enhancing the cell performance in low-current region, further contributing to the reduction of coking risk for kinetic reasons [6].

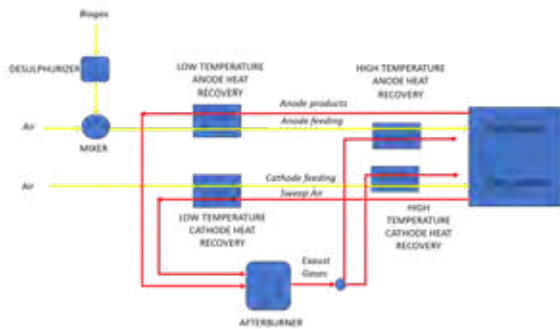


Fig. 1. Simplified system flowsheet.

According to the literature, the optimal dilution ratio is Air/Biogas = 0.4-1.5 – as found in [5] showing results of experiments performed on commercial cells at 800°C and in current density range 0-400 mA/cm². Rather high Air/Biogas ratio is applicable without large loss of electrical efficiency due to the reduction of overvoltage. The cell operation under electric load yields significant amount of water, initiating internal methane steam reforming reactions. This allows tuning the cell operating conditions on low Air/Biogas ratios.

Preliminary system simulations (Fig.1) highlighted a mild loss of efficiency (47% electric efficiency for the SOFC fed with air diluted biogas, vs. 53% obtained with biogas fed SOFC). Yet, durability is expected to be more favorable. This needs to be experimentally proved.

V. EXPERIMENTAL

The experimental activity begins from characterizing SOFC single cell performances in laboratory facilities, reproducing biogas with technical gases. 100-h tests on single cells proved the operability of SOFC with direct biogas and direct air-diluted biogas. Experimental results from this stage are used to validate the system model. Nonetheless, tests on SOFC stacks on longer durations are still to be performed (second part of the project).

VI. CONCLUSION

This paper resumes the current development of the project TEZIO. Small and micro biogas producers represent a niche market for SOFCs. In turns, SOFCs feature some advantages which allow the efficient valorization of an unexploited share of distributed renewable energy potential. A few farms in Umbria may be selected as real-life benches to test an innovative SOFC m-CHP prototype. Preliminary tests performed on laboratory scale, as well as system simulations, proved the consistency of the concept.

ACKNOWLEDGMENT

This research has been performed within the project TEZIO (*Tecnologia Energetica a Zero Impatto ambientale*), funded by Fondazione Cassa di Risparmio di Perugia.

REFERENCES

- [1] A. Baldinelli, et al. "Springboard applications for small cogeneration plants based on Solid Oxide Fuel Cells," in *14th SDEWES Digital proceedings*, 2019,
- [2] M. Scheftelowitz et al, "Unlocking the energy potential of manure-an assessment of the biogas production potential at the farm level in Germany," *Agric.*, vol. 6, no. 2, 2016.
- [3] A. Baldinelli et al. "SOFC direct fuelling with high-methane gases: Optimal strategies for fuel dilution and upgrade to avoid quick degradation," *Energy Convers. Manag.*, vol. 124, pp. 492–503, 2016.
- [4] M. Pillai et al "Stability and coking of direct-methane solid oxide fuel cells: Effect of CO₂ and air additions," *J. Power Sources*, vol. 195, no. 1, pp. 271–279, Jan. 2010.
- [5] Y. Takahashi et al. "Thermo-mechanical reliability and catalytic activity of Ni–Zirconia anode supports in internal reforming SOFC running on biogas," *Solid State Ionics*, vol. 225, pp. 113–117, Oct. 2012.
- [6] Z. Lyu et al. "Electrochemical characteristics and carbon tolerance of solid oxide fuel cells with direct internal dry reforming of methane," *Appl. Energy*, 2018.

ANALYSIS OF PERFORMANCE IMPROVEMENT OF HYDROGEN/BROMINE FLOW BATTERIES BY USING BROMATE ELECTROLYTE

Muhammad Faizan Chinannai, Afroz Alam, and Hyunchul Ju*

Department of Mechanical Engineering
Inha University

100 Inha-ro, Nam-Gu, Incheon 402-751, Republic of Korea

Abstract - A 3-D transient model of H₂/Br₂ redox flow battery is developed rigorously accounting for the redox reactions of H₂ and Br species. It has been validated experimentally against the discharge and charge voltage curves measured over the range of 1.4 A/cm² of Current density. The kinetic expression of bromate-bromide chemical reaction was derived in consideration of various reactions and coupled with the mass and energy transport equations in the previously developed 3-D H₂/Br₂ flow battery model. The model was then validated against the experimental discharge data which exhibit the voltage recovery period resulting from the bromate-bromide chemical reaction. The model predictions suitably agree with the experimental data. It also provides detailed analysis of performance enhancement in terms of activation, ohmic and concentration overpotentials. This study clarifies the advanced features of promising H₂/Br₂ flow battery system through extensive multidimensional contours of species concentration, temperature and current density.

Index Terms - Hydrogen bromine flow batteries; Bromate; Numerical simulation.

I. NOMENCLATURE

Nomenclature

C_{KC}	Kozeny-Carman constant
D	diffusion coefficient, m ² ·s ⁻¹
E_0	thermodynamic equilibrium potential, V
F	Faraday's constant, 96485 C·mol ⁻¹
K	permeability, m ²
M	molecular weight, kg·mol ⁻¹
nd	electro-osmotic drag coefficient
r_{PM}	pore radius in porous media, m
v_{fi}	volume fraction of species i
z	valence
α	transfer coefficient
ϵ	porosity
η	overpotential, V
κ	proton conductivity, S·m ⁻¹
μ	viscosity, kg·m ⁻¹ ·s ⁻¹
ρ	density, kg·m ⁻³
σ	electronic conductivity, S·m ⁻¹
τ	viscous shear stress, N·m ⁻² or tortuosity

b	bromine electrode side
e	electrolyte
h_{CL}	hydrogen catalyst layer
i	species i
s	solid (electronic)
u	momentum

II. INTRODUCTION

With growth of new and renewable energy market, demands on energy storage system (ESS) have been rapidly increasing in order for saving extra energy production. As compared to the peak power of all vanadium redox flow batteries, roughly 10 times higher power density of 1.46 W·cm⁻² were reported for 10–25 cm² lab-scale cells[1,2]. The H₂/Br₂ flow battery utilizes gaseous hydrogen for the negative electrode and aqueous Br₂/HBr solution for the positive electrode.

The objective of this paper is to analyze the performance improvement of H₂/Br₂ flow battery when the aqueous bromate electrolyte was employed as the catholyte instead of bromine/bromide solution. First, the kinetic expression of bromate-bromide chemical reaction was derived in consideration of various reaction steps and coupled with the mass and energy transport equations of the three-dimensional (3-D) H₂/Br₂ flow battery model developed in our previous studies [our previous papers related to H₂/Br₂ flow batteries]. The model was then validated against the experimental discharge data measured by Cho and Razaulla [3] that exhibit the voltage recovery period resulting from the bromate-bromide chemical reaction. This study elucidates the advanced features of promising hydrogen-bromate flow battery systems through extensive multidimensional contours of species concentration, temperature, and current density.

III. MODEL DESCRIPTION

The model is applied to all computational domain consisting of membrane, catalyst layer (CL), porous electrodes and flow field plates (FFPs)

Mass conservation:

$$\frac{\partial \varepsilon \rho}{\partial t} + \nabla \cdot (\rho u) = 0 \quad (1)$$

Momentum conservation:

$$\frac{1}{\varepsilon} \left[\frac{\partial \rho u}{\partial t} + \frac{1}{\varepsilon} \nabla \cdot (\rho u u) \right] = -\nabla P + \nabla \cdot \tau + \rho g - \frac{\mu}{K} u \quad (2)$$

$$\text{Species conservation: } \frac{\partial (\varepsilon C_i)}{\partial t} + \nabla \cdot N_i = S_i \quad (3)$$

$$\text{Charge conservation: } \nabla \cdot i_e = \nabla \cdot i_s = S_\phi \quad (4)$$

Ionic current density:

$$i_e = \sum_i i_i = -\kappa^{eff} \nabla \phi_e - F \sum_i z_i (D_i^{eff} \nabla C_i + C_i u) \quad (5)$$

$$\text{Electronic current density: } i_s = \sigma^{eff} \nabla \phi_s \quad (6)$$

From the species conservation equation in Eq. (3), the species flux, N_i , can be described in terms of diffusion, migration, convection and electro-osmosis as follows:

$$N_i = \underbrace{-D_i^{eff} \nabla C_i}_{\text{(Diffusion)}} + \underbrace{\frac{z_i F}{RT} D_i^{eff} C_i \nabla \phi_e}_{\text{(Migration)}} + \underbrace{C_i u}_{\text{(Convection)}} + \underbrace{\frac{n_{d,i}}{F} i_e}_{\text{(Electro-osmosis)}} \quad (7)$$

where the effective diffusion coefficient of species i , D_i^{eff} , in porous electrode can be modified from its intrinsic diffusivity based on Bruggeman correlation:

$$D_i^{eff} = \varepsilon^\tau D_i \quad (8)$$

The effective permeability, K , through the porous electrode in Br2 electrode can be determined by the Kozeny-Carman equation:

$$K = \frac{4r_{PM}^2}{C_{KC}} \frac{\varepsilon^3}{(1-\varepsilon)^2} \quad (9)$$

IV. RESULTS

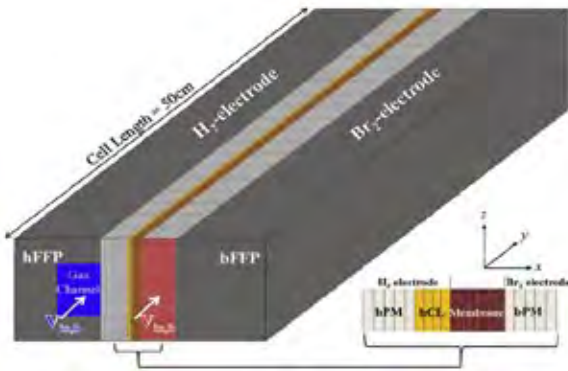


Fig.1 Computational domain and mesh configuration

The bromate electrolyte used at the Positive electrode ends up with chemical reaction leading to production of Br₂ for the reaction. This use of bromate as electrolyte boosts the performance of the cell by its characteristic of auto-catalytic reaction leading to no-limit in current density i.e., mass transfer

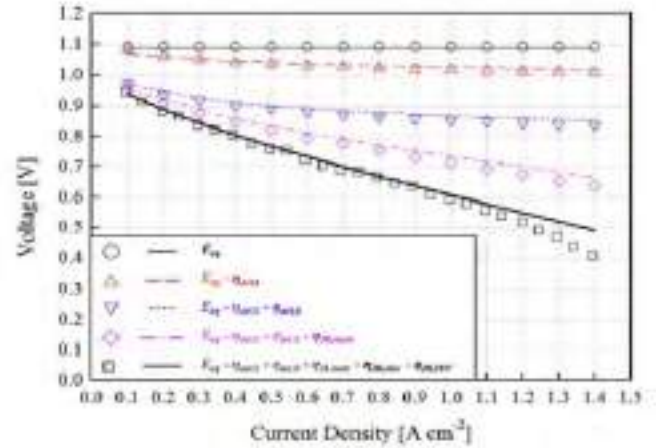


Fig. 2 Comparison of simulated and measured polarization curves during discharge

loss can be avoided. In addition, voltage recovery from the open circuit voltage is also achieved at high current condition.

V. CONCLUSION

A 3-D transient H₂/Br₂ model developed considering the crossover through membrane. A charge and discharge cycle were simulated and validated against the experimental discharge data which exhibit a good agreement. With the use of thin bPM superior performance at high current density was observed. With the innovative characteristics of bromate, good cell performance can be achieved. With transient condition simulated, shows the better response of the cell. Additional effects of convection and kinetic loss at high current conditions needs to be investigated to understand this promising technology.

ACKNOWLEDGMENT

Please place an eventual Acknowledgment here, before the References.

REFERENCES

- [1] Sun CN, Mench MM, Zawodzinski TA. High Performance Redox Flow Batteries: An Analysis of the Upper Performance Limits of Flow Batteries Using Non-aqueous Solvents. *Electrochim Acta* 2017. doi:10.1016/j.electacta.2017.03.132.
- [2] Cho KT, Albertus P, Battaglia V, Kojic A, Srinivasan V, Weber AZ. Optimization and Analysis of High-Power Hydrogen/Bromine-Flow Batteries for Grid-Scale Energy Storage. *Energy Technol* 2013;1:596–608. doi:10.1002/ente.201300108.
- [3] Cho KT, Razaulla T. Redox-Mediated Bromate Based Electrochemical Energy System. *J Electrochem Soc* 2019;166:A286–96. doi:10.1149/2.0841902jes.

MULTI-DIMENSIONAL STEADY STATE MODELING OF AN ALKALINE WATER ELECTROLYSIS CELL

Afroz. Alam, Muhammad Faizan Chinannai, Jaeseung Lee,
Kisung Lim, Nammin lee, Hyunchul JU*

* Eco-Smart Power Lab (ESPL), Department of Mechanical
Engineering, Inha University
100 Inha-Ro, Michuhol-Gu, Incheon 22212, Republic of Korea

Abstract - A multi-dimensional steady state model of the Alkaline water electrolyzer is newly developed accounting, the Butler-Volmer equation in terms of species concentrations in order to study the performance of a single electrolyzer cell. Even though there have been substantial efforts have been made theoretically to analyze water electrolyzer cells, but in our customary knowledge, numerical simulations in depth, based on concentration of the species are not found in literature. Emphasis is placed on analyzing the potential distribution and concentration variations with respect to the reduction and oxidation reactions at negative and positive electrode respectively. The model predictions compare well with the experimental data over the range of 0.1 to 2 A/cm² of current density to voltage characteristics.

Index Terms - Numerical Model, Overpotential, Concentration, voltage-current characteristics.

I. NOMENCLATURE

C_{KC}	Kozeny-Carman constant
D	diffusion coefficient, m ² ·s ⁻¹
E_0	thermodynamic equilibrium potential, V
F	Faraday's constant, 96485 C·mol ⁻¹
K	permeability, m ²
r_{PM}	pore radius in porous media, m

II. INTRODUCTION

Alkaline water electrolysis is the widely used and established electrolysis technology for the hydrogen production [1] Due to complexity of the electrolysis processes taking place simultaneously, numerical modelling will be the effective tool for understanding these complex phenomena going inside the AWE. In our current scenario many mathematical models have been proposed based on the Butler Volmer equation without concentration of species [2]. In this work we have developed a mathematical model considering the concentration of species. With this mathematical model multi-dimensional and simulation analysis of the AWE has been made. In specific, the electrode and electrolyte potential distribution in the AWE

components were not studied precisely in the previous literatures.

III. MODELLING

Essential part of the model has been represented for a single cell. The computational domain used for the simulation is exhibited in Fig 1.

The AWE model is governed by four principle of conservation: mass, momentum, species and charge conservation as follows.

1. Mass Conservation: $\nabla \cdot (\rho u) = 0$

2. Momentum conservation:

$$\frac{1}{\varepsilon} \left[\frac{1}{\varepsilon} \nabla \cdot (\rho \vec{u} \vec{u}) \right] = -\nabla P + \nabla \cdot \tau + \rho \vec{g} - \frac{\mu}{K} \vec{u}$$

3. Species conservation: $\nabla \cdot N_i = S_i$

4. Charge conservation: $\nabla \cdot i_e = \nabla \cdot i_s = S_\phi$

$$i_e = \sum_i i_i = -\kappa^{eff} \nabla \phi_e - F \sum_i z_i (D_i^{eff} \nabla C_i + C_i u)$$

$$i_s = \sigma^{eff} \nabla \phi_s$$

IV. RESULTS AND DISCUSSION

Figure 2 represents the solid/electrolyte phase potential distribution along the cell thickness. The electrolyte potential drop across the electrodes and separator is clearly visible (approximately 100mV/120mV and 0.80mV through the negative/positive electrodes and separator, respectively). The solid phase potential drop occurring in the current collectors and electrodes is relatively higher side because of the less electron conductivity. Figure 3 represents the overpotential distribution along the electrodes. The calculated overpotential values in the negative and positive electrodes vary from -0.30 V to -0.39V and 0.32V to 0.42V, respectively, almost equal to the ohmic voltage drop in the membrane. Figure 4 represents the concentration of species distribution along the flow channel.

Because of the redox reactions of the aqueous KOH solution in the negative and positive electrodes, the concentration of the water decreases and increases towards the downstream, respectively. Because of the redox reactions of the aqueous KOH solution in the negative and positive electrodes, the concentration of the anion increases and decreases towards the downstream. Figure 5 represents the validation of the model with V-I characteristics. Simulated voltage –current characteristics of Alkaline water electrolysis cell validated against the reference [3].

V. FIGURES

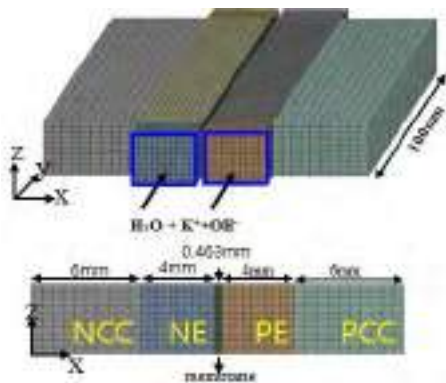


Fig.1 Computational domain

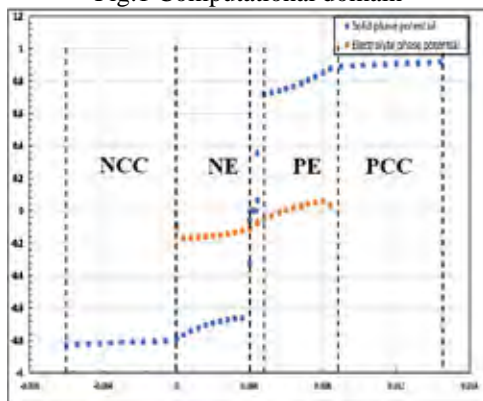


Fig 2 Phase Potentials distribution along the thickness of the Cell at 0.5 A/cm² and 1.723V

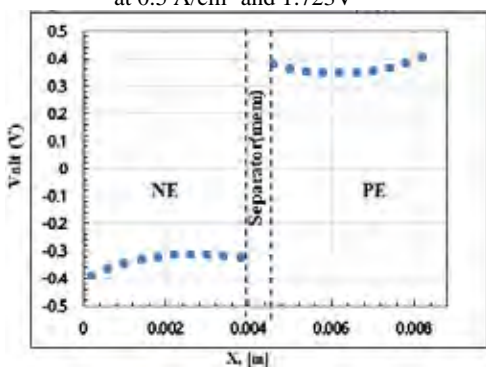


Fig 3. Overpotential distribution along the Cell thickness at 0.5 A/cm² and 1.7 V

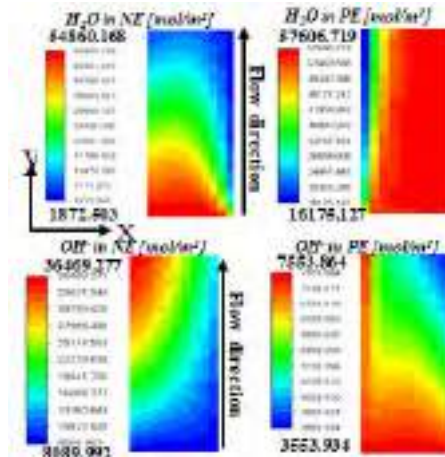


Fig 4 Concentration distribution in the electrodes along flow direction

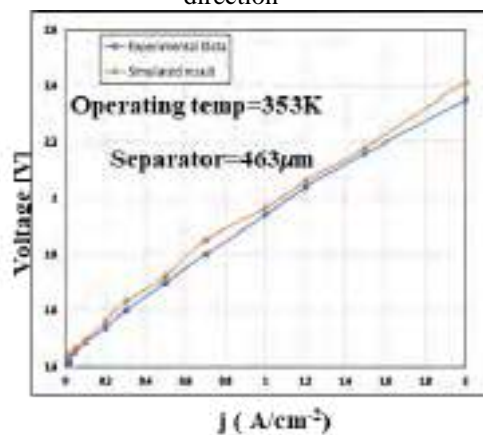


Fig 5 Voltage-current characteristics

VI. CONCLUSION

A three-dimensional steady state model of AWE has been developed in order to predict the electrode/electrolyte potential and overpotential distributions along the various AWE components at 0.5A/cm².As the charging process proceeds, the overpotentials in the negative and positive electrodes continuously increases.

VII. REFERENCES

- [1] L. An, T.s. Zhao, Z.H.Chai, P.Tan, L. Zeng, Mathematical Modelling of an anion -exchange membrane water electrolyzer for hydrogen production, International journal of Hydrogen energy, Volume 39, issue 35, 3 December 2014, pages 10869-19876.
- [2] Maximilian Schalenbach, et al. Acidic or Alkaline? Towards a New perspective on the efficiency of Water Electrolysis, Journal of Electrochemical society ,163(11) F3197-F3208(2016)

EFFECTS OF WATER TRANSPORT ON PERFORMANCE BEHAVIORS OF HYDROGEN BROMINE REDOX FLOW BATTERIE

Muhammad Faizan Chinannai, Afroz Alam, and Hyunchul Ju*

Department of Mechanical Engineering
Inha University

100 Inha-ro, Nam-Gu, Incheon 402-751, Republic of Korea

Abstract -This study presents the three-dimensional (3-D) H₂/Br₂ RFB model in which the effect of membrane dehydration was taken into account. The hydrogen electrode flooding, i.e. likely during high current charge processes, induces strongly two-phase flow in the hydrogen side, making the removal process of crossed-over HBr more difficult and complicated. The main purpose of this study is to expand upon the 3-D H₂/Br₂ RFB model by incorporating two-phase water transport equation and hence addressing the effects of flooding and dehydration. A detailed water uptake model for PFSA membranes under water and HBr solution is formulated by combining the experimental water uptake data of Nafion membrane and proton conductivity data measured under various HBr concentrations. This study clearly illustrates the profound effect of water management on dynamic behaviors of H₂/Br₂ cell during charge and discharge.

Index Terms - Numerical simulation; two-phase RFB; water transport model;

I. NOMENCLATURE

Nomenclature

C_{KC}	Kozeny-Carman constant
D	diffusion coefficient, m ² ·s ⁻¹
E_0	thermodynamic equilibrium potential, V
F	Faraday's constant, 96485 C·mol ⁻¹
K	permeability, m ²
M	molecular weight, kg·mol ⁻¹
nd	electro-osmotic drag coefficient
r_{PM}	pore radius in porous media, m
v_{fi}	volume fraction of species i
z	valence
α	transfer coefficient
ϵ	porosity
η	overpotential, V
κ	proton conductivity, S·m ⁻¹
μ	viscosity, kg·m ⁻¹ ·s ⁻¹
ρ	density, kg·m ⁻³
σ	electronic conductivity, S·m ⁻¹
τ	viscous shear stress, N·m ⁻² or tortuosity
b	bromine electrode side
e	electrolyte
h_{CL}	hydrogen catalyst layer

i	species i
s	solid (electronic)
u	momentum

II. INTRODUCTION

Several H₂/Br₂ models have been developed over the last decade, but few have accounted for the water transport and membrane dehydration phenomena inside a H₂/Br₂ cell. Recently, we presented the three-dimensional (3-D) H₂/Br₂ RFB model in which the effect of membrane dehydration was taken into account, using empirical proton conductivity expression as a function of the bromide concentration [1]. However, the limitation of the model comes from the facts that the water equation was not accounted and thus two key performance degradation mechanisms, i.e. the dehydration and flooding occurring in the electrodes and membrane, cannot be simulated. Furthermore, the hydrogen electrode flooding, i.e. likely during high current charge processes, induces strongly two-phase flow in the hydrogen side, making the removal process of crossed-over HBr more difficult and complicated. The two-phase situation exacerbates the degree of membrane dehydration via HBr and thus has a substantial influence on proton conduction and ohmic polarization. The main purpose of this study is to expand upon the 3-D H₂/Br₂ RFB model by incorporating two-phase water transport equation and hence addressing the effects of flooding and dehydration during charge and discharge and more accurately capturing the accumulation of HBr and resultant membrane dehydration level. A detailed water uptake model for PFSA membranes under water and HBr solution is formulated by combining the experimental water uptake data of Nafion membrane and proton conductivity data measured under various HBr concentrations. Fully 3-D numerical simulations for a single-straight channel H₂/Br₂ cell are performed along with a theoretical analysis. This study clearly illustrates the profound effect of water management on dynamic behaviors of H₂/Br₂ cell during charge and discharge.

III. MODEL DESCRIPTION

The model is applied to all computational domain. The general governing equations are as follows

Mass conservation:

$$\frac{\partial \varepsilon \rho}{\partial t} + \nabla \cdot (\rho u) = 0 \quad (1)$$

Momentum conservation:

$$\frac{1}{\varepsilon} \left[\frac{\partial \rho u}{\partial t} + \frac{1}{\varepsilon} \nabla \cdot (\rho u u) \right] = -\nabla P + \nabla \cdot \tau + \rho g - \frac{\mu}{K} u \quad (2)$$

$$\text{Species conservation: } \frac{\partial (\varepsilon C_i)}{\partial t} + \nabla \cdot N_i = S_i \quad (3)$$

$$\text{Charge conservation: } \nabla \cdot i_e = \nabla \cdot i_s = S_\phi \quad (4)$$

Ionic current density:

$$i_e = \sum_i i_i = -\kappa^{eff} \nabla \phi_e - F \sum_i z_i (D_i^{eff} \nabla C_i + C_i u) \quad (5)$$

$$\text{Electronic current density: } i_s = \sigma^{eff} \nabla \phi_s \quad (6)$$

The species conservation equation in Eq. (3), \vec{N}_i , is defined in terms of diffusion, migration, convection and electro-osmosis:

$$N_i = \underbrace{-D_i^{eff} \nabla C_i}_{\text{(Diffusion)}} + \underbrace{\frac{z_i F}{RT} D_i^{eff} C_i \nabla \phi_e}_{\text{(Migration)}} + \underbrace{C_i u}_{\text{(Convection)}} + \underbrace{\frac{n_{d,i}}{F} i_e}_{\text{(Electro-osmosis)}} \quad (7)$$

The membrane transport properties are mutually associated with its water content, λ , which is again a function of the water activity, a [2]:

$$\varepsilon = \frac{c_p \lambda M_w}{\rho_{dry}} \quad (8)$$

$$\lambda = \begin{cases} \lambda_p = 0.043 + 17.81a - 39.85a^2 + 36.0a^3 & \text{for } 0 < a \leq 1 \\ \lambda_l = 22 & \end{cases} \quad (9)$$

IV. RESULTS

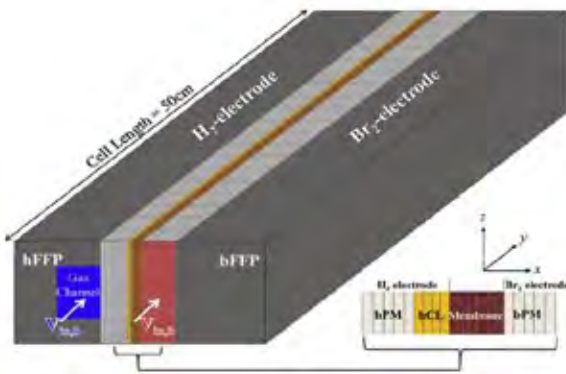


Fig.1 Computational domain and mesh configuration

The multidimensional transient H_2/Br_2 RFB model in this study was validated against the experimental data recorded by Cho et al.[3] at various charge and discharge current densities.

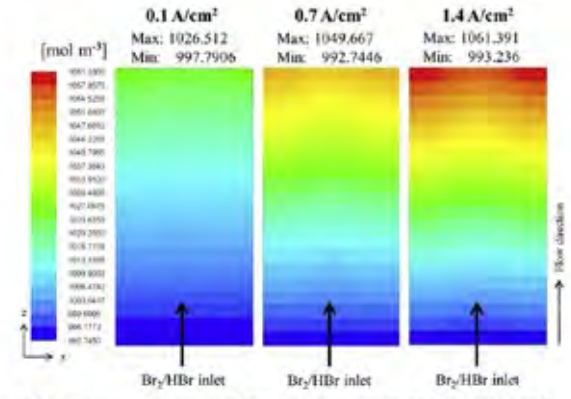


Fig. 2 H_2 Br concentration contours

V. CONCLUSION

A 3-D transient H_2/Br_2 model developed accounting the water uptake to analyze the dehydration and flooding behavior in the membrane. A complete discharge cycle was simulated to validate with the experimental data which has a good agreement. An extensive multi-dimensional contour of water and species concentration was reported to analyze the detailed mechanisms of flooding and dehydration. The simulation results was validated with experimental data at various current densities.

ACKNOWLEDGMENT

Please place an eventual Acknowledgment here, before the References.

REFERENCES

- [1] Oh K, Weber AZ, Ju H. Study of bromine species crossover in H_2/Br_2 redox flow batteries. Int J Hydrogen Energy 2017;1–14. doi:10.1016/j.ijhydene.2016.12.063.
- [2] Springer TE, Zawodzinski TA, Gottesfeld S. Polymer Electrolyte Fuel Cell Model. J Electrochem Soc Ceram Soc IEEE Trans Indust This J 1993. doi:10.1149/1.2085971.
- [3] Cho KT, Ridgway P, Weber a. Z, Haussener S, Battaglia V, Srinivasan V. High Performance Hydrogen/Bromine Redox Flow Battery for Grid-Scale Energy Storage. J Electrochem Soc 2012;159:A1806–15. doi:10.1149/2.018211jes.

A TRANSIENT, TWO-PHASE MODEL OF PEM FUEL CELL – PERFORMANCE ANALYSIS UNDER COOLANT FLOW VARIATION

Jaeseung Lee, Muhammad Faizan Chinannai, Nammin Lee,
Kisung Lim, Yoonseung Kang and Hyunchul Ju
Eco-Smart Power Lab (ESPL), Department of Mechanical
Engineering, Inha University, 100 Inha-ro Nam-Gu, Incheon 22212,
(Republic of Korea)

Abstract - In this study, a transient model of a 3D two phase multi-scale PEMFC is developed and analyzed the effects of the system performance under various malfunctions and defects by varying the coolant temperature. The common and important factors of defects such as the humidity, air stoichiometry, Catalyst layer degradation, and species crossovers accounts for the heat generation which tends to lower the performance of the cell. All the malfunction cases show similar performance degradation due to temperature rise. Hence, to control the operating temperature of the cell, the coolant flow rate needs to be varied accordingly. The study resulted with the variation of coolant flow rate with respect to time in order to control the cell operating temperature within the range. This study is believed to help in detection and isolations of the system malfunctioning by the variations in the coolant flow rate and hence can avoid failure of the PEMFC stack and system. For better understanding, extensive multi-dimensional contours are provided.

Index Terms - PEM fuel cell, Fuel cell modeling, Malfunction analysis, BOP components Nomenclature

I. INTRODUCTION

The present generation researchers are consistently bestowing their possible efforts on the development of an efficient renewable source of energy to the world. Polymer Electrolyte Fuel cells have come up as a highly favorable sustainable energy, especially in transport application. It is believed that the fuel cell poses a very high energy conversion efficiency more than 40-50% compared to other fossil fuel operative devices [1].

II. NUMERICAL MODEL

A three-dimensional (3-D), two-phase PEM fuel cell model developed in our previous study [2] was employed to analyze the malfunctioning modes of PEM fuel cell system. The computational domain for the 3-D PEM fuel cell model is shown in figure 1 consisting of Membrane Electrode Assembly (MEA),

Gas Channels (GCs), Bipolar Plates (BPs), and the Cooling Channels (CCs). The present model is combination of 3-D macro-scale PEFC model and the micro-scale CL model based on spherical coordinate system which accounts the effects of key micro and nano-structural parameters of catalyst layers (CL) such as Pt and carbon nanoparticle sizes, ionomer film thickness. The micro-scale CL model estimates the electrochemically active surface area (ECSA) as well as the local oxygen transport resistance through ionomer and/or water films in various CL designing and operating conditions

III. RESULT & DISCUSSIONS

To analyze the influences of coolant flow rate changes and MEA temperature rise under various PEM fuel cell malfunctions, the aforementioned 3-D multi-scale two-phase PEM fuel cell model was applied to a single straight channel fuel cell geometry with coolant channels shown in Fig. 1 with the relevant computational mesh configurations. In Fig. 2, the temperature rises in MEA and the coolant flow rate required to maintain the set-point temperature of 60°C at the coolant outlet were first investigated under normal fuel cell operations without any malfunctioning components. Despite nonlinear relationship of current density, cell voltage, and waste heat released, both the rate of coolant flow per unit MEA area ($\phi_{cool} = \dot{m}_{cool}/A_{MEA}$) and the maximum temperature rise in MEA relative to the coolant outlet temperature (i.e. denoted by $\Delta T_e = T_{max,MEA} - T_{cool,out}$) almost linearly increase with increasing average current density (I_{avg}) in a range of $I_{avg}=0.1-0.5 \text{ A}\cdot\text{cm}^{-2}$. The curve fitting of ϕ_{cool} vs I_{avg} and ΔT_e vs I_{avg} are also provided in Figs. 2a and 2b, respectively, which can be used as the reference data for the early detection of malfunctions in PEM fuel cell stack and system components.

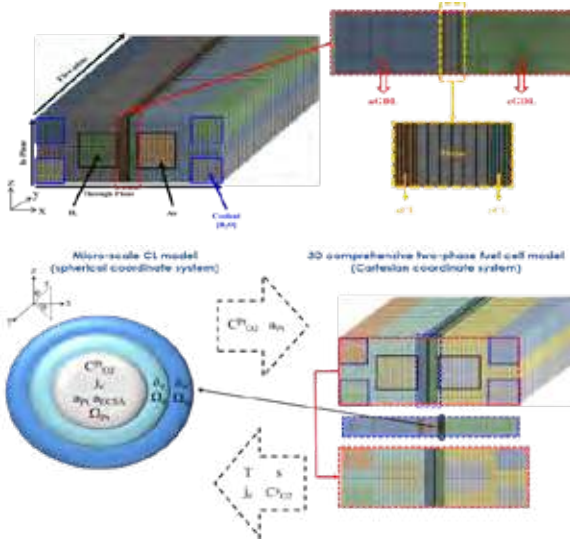


Fig. 1. Computational domain

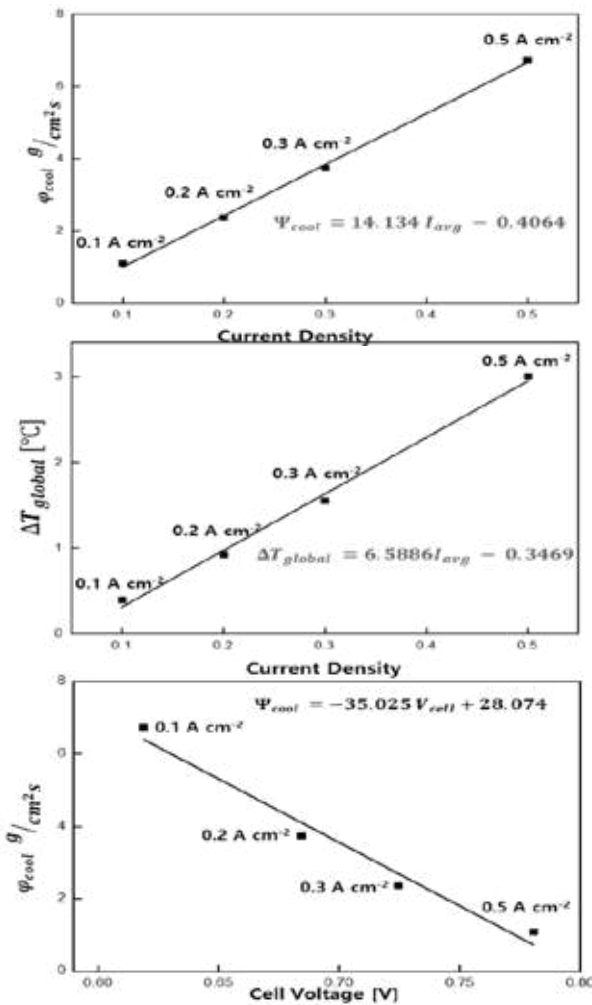


Fig. 2. (a) Coolant flow rate vs Current density (b) ΔT vs Current density (c) flow rate vs cell

IV. UNITS

C	Molar concentration of species, mol m ⁻³
D	Species diffusivity, m ² s ⁻¹
E	Activation energy, kJ mol ⁻¹
EW	Equivalent weight of a dry membrane, kg mol ⁻¹
F	Faraday's constant, 96,487 C mol ⁻¹
i ₀	Exchange current density, A cm ⁻²
I	Operating current density, A cm ⁻²
j	Transfer current density, A cm ⁻²
L _{Pt}	Amount of Pt loading, mg cm ⁻²
T	Temperature, K

V. CONCLUSION

The main focus of this study is to provide a basic understanding of PEM fuel cell operations under various malfunction modes that include malfunctioning of reactant gas humidifiers and cathode air blower, and component degradations such as the aggregation of Pt particles in the cathode CL and increase in reactant gas crossover through membrane pinholes due to the membrane degradation. These malfunction cases were simulated under the practical operating strategy of PEM fuel cell stack in which the coolant flow rate was controlled to maintain the pre-set temperature at the coolant outlet. The simulation results showed that the coolant flow rate increased in proportion to the degree of voltage degradation caused by fuel cell malfunction, clearly indicating that the change of coolant flow rate is a good indicator for early detection of malfunctioning PEM fuel cell stack and system components. However, the maximum temperature rise inside MEA relative to the coolant outlet temperature was not always proportional to the magnitude of voltage degradation due to malfunction but more directly influenced by local current density distributions. Showing that the coolant flow direction and configuration should be designed in consideration of local current density distribution to maximize the cooling efficiency, this study further indicated that PEM fuel cell malfunction could alter the local current density distribution, which decreases the overall cooling efficiency and accelerates the formation of local hotspots in MEAs. Therefore, early detection of malfunctioning components and proper precautions are so important to prevent more serious irreversible failures.

REFERENCES

- [1] Sopian, K., Daud W., Challenges and future developments in proton exchange membrane fuel cells, Renewable Energy, Volume 31, 2005, page 719-727,
- [2] Chinannai, M., Lee J., Ju H., Numerical study for diagnosing various malfunctioning modes in PEM fuel cell systems, International Journal of Hydrogen Energy, In press

A TRANSIENT PARAMETRIC STUDY FOR PASSIVE AIR-COOLED POLYMER ELECTROLYTE MEMBRANE (PEM) FUEL CELL

Jaeseung Lee, Muhammad Faizan Chinannai, Nammin Lee,
Kisung Lim, Yoonseung Kang and Hyunchul Ju
Eco-Smart Power Lab (ESPL), Department of Mechanical
Engineering, Inha University, 100 Inha-ro Nam-Gu, Incheon 22212,
(Republic of Korea)

Abstract - A passive air-cooled PEM fuel cell is considered a proficient technology for small scale portable applications. In passive air-cooled PEMFC system, air is drawn through a fan and is used for both fuel and coolant making it a significant challenge in terms of water and heat management. To understand key factor of water and heat transportation phenomena under extra dry air supply circumstances, a parametric study was carried out using three-dimensional multiscale transient condition, two phase fuel cell model. The focus is to design variables of membrane electrode assembly and cathode flow-field. The operating characteristics of air-cooled PEM fuel cell systems according to periodic changes are analyzed with respect to time. This study provides a vital contour of temperature profiles, water content, relative humidity, oxygen concentration to make a successful design and process a passive air-cooled PEM fuel cell.

Index Terms - Passive air-cooled fuel cell, Membrane electrode assembly, Membrane dehydration, Water transport, Heat removal

I. INTRODUCTION

The present work provides an extensive parametric study of passive air-cooled PEM fuel cell operations. The three-dimensional (3-D), multi-scale, two-phase PEM fuel cell model is employed to investigate the impacts of key design parameters of membrane electrode assembly (MEA) and the cathode flow-field under excess air supply conditions of passive air-cooled PEM fuel cell stack.

Because membrane dehydration with excess dry air supply tends to strongly limit cell performance, water uptake and subsequent water transport in the membrane are widely studied issues in PEM fuel cell research [1,2].

II. NUMERICAL MODEL

The three-dimensional (3-D), multi-scale, two-phase PEM fuel cell model is employed to investigate the impacts of key

design parameters of membrane electrode assembly (MEA) and the cathode flow-field under excess air supply conditions of passive air-cooled PEM fuel cell stack.

The basic model is shown in fig1.

In addition, according to the conditions, we divided into 12 cases and analyzed with ANSYS program that applied the governing equation.

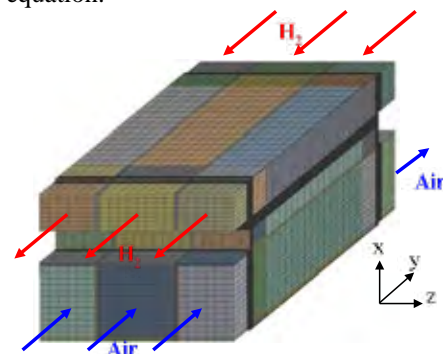


Fig. 1. Computational domain and cell dimensions

III. RESULT & DISCUSSIONS

The present numerical study is focused on investigating the effects of key design parameters of MEA and cathode flow-field on the degree of membrane hydration as well as the overall cell performance under excess air supply condition of passive air-cooled PEM fuel cell stack.

The various constituent overpotentials are calculated from the simulation results and plotted in Fig 2 for a comparison purpose.

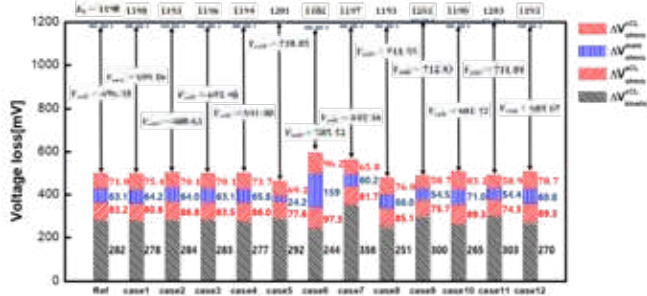


Fig. 2. Voltage loss of all cases

IV. UNITS

HOR	hydrogen oxidation reaction
ORR	oxygen reduction reaction
P	pressure, Pa
RH	relative humidification of the inlet
R_u	universal gas constant, $8.314 \text{ J mol}^{-1} \text{ K}^{-1}$
S	source term in the transport equation
T	temperature, K
UAV	unmanned aerial vehicle
U_o	thermodynamic equilibrium potential, V
V_{cell}	cell potential, V
W	width, m
δ	thickness
ε	volume fraction
μ	viscosity, $\text{kg m}^{-1} \text{ s}^{-1}$
h	enthalpy, J
ρ	density, kg m^{-3}
ν	kinematic viscosity, $\text{m}^2 \text{ s}^{-1}$
τ	viscous shear stress, N m^{-2}
ζ	stoichiometry flow ratio
avg	average value
c	cathode
CL	catalyst layer
CC	cooling channel
GC	gas channel
GDL	gas diffusion layer
i	species index
k	region index
O_2	oxygen

V. CONCLUSION

Using a 3-D, multi-scale, two-phase PEM fuel cell model, a parametric study has been conducted to develop a quantitative understanding of passive air-cooled PEM fuel cell operations in excess dry air conditions in which the cell performance is mainly determined by MEA dehydration and oxygen transport.

The use of thinner membrane and higher ionomer fraction of the cathode CL lead to less ionic resistance through the MEA, producing higher cell performance and smaller temperature rise.

In contract, the wider rib width of the cathode flow-field, the thicker MPL or MPL in a MEA slightly improve the water-retaining capability of the MEA under excessive dry air supply conditions but result in lower cell performances and non-uniform current distribution due to a combined result of the higher oxygen and thermal transport resistances through the MEA.

The model finds that the lower set-point temperature at the air outlet and lower ambient temperature are more advantageous in terms of MEA hydration, uniform current density distribution as well as overall cell performance. However, the lower set-point temperature requires the higher air flow rate drawn by fans and thus larger fan power consumption. Therefore, the set-point temperature should be optimized to provide the best overall efficiency of air-cooled fuel cell system.

REFERENCES

- [1] G. J. M. Janssen, M. L. J. Overvelde, "Water transport in the proton-exchange-membrane fuel cell: Measurements of the effective drag coefficient," *J. Power Sources*, vol. 101, no. 1, 2001, pp. 117–125.
- [2] T. A. Zawodzinski, "Water Uptake by and Transport Through Nafion® 117 Membranes," *J. Electrochem. Soc.*, vol. 140, no. 4, 2006, p. 1041.

MODELING AND ANALYSIS OF COMPLEX MULTI-HUB PAFC SYSTEM FOR HEAT, POWER AND HYDROGEN GENERATION

Yoonseung Kang, Jaeyoo Choi, Nammin Lee, Kisung Lim,
Muhammad Faizan Chinannai, Jaeseung Lee, Afroz Alam and
Hyunchul Ju

Eco-Smart Power Lab (ESPL), Department of Mechanical
Engineering, Inha University, 100 Inha-ro Nam-Gu, Incheon 22212,
(Republic of Korea)

Abstract - We present a complex multi-hub system model that accounts for fuel reforming, PAFC stack, Turbo Expander Generator (TEG) modules along with heat exchangers and balance of plant (BOP) components. The model is developed to analyze the reaction kinetics for the fuel reforming processes, considered to accurately capture exhaust gas compositions and reactor temperatures under various operating conditions. The PAFC stack model is simplified from the three-dimensional PAFC CFD models developed in our previous studies. An experimental fuel reforming reactor for a 440 kW PAFC system was tested to validate the fuel reforming sub model. The model predictions were found to be in good agreement with the experimental data in terms of exhaust gas compositions and bed temperatures. Additionally, the simulation revealed the impacts of the burner air-fuel ratio (AFR) and the steam-carbon ratio (SCR) in steam reforming reactor on the system performance and efficiency. It was done, principal results, and their significance

Index Terms - complex multi-hub system modeling, PAFC, TEG, Steam reforming, PSA

I. INTRODUCTION

A complex multi-hub system for heat, power and hydrogen generation consists of three major subsystems: a fuel processor, PAFC power system, and TEG system. These subsystems are connected to various auxiliary components such as BOP components and heat exchangers. Due to the complex configurations, systems integration and optimization are critical to improve the performance and efficiency of the PAFC system.

II. NUMERICAL MODEL

The main assumptions invoked in this model are as follows:

(1) The natural gas is composed of 100% methane (CH₄). Therefore, minor species and their effects on system

performance and durability are neglected. This assumption implies that the minor species in the incoming gas mixture are completely removed during the fuel pretreatment processes.

(2) Individual gases and their mixture obey Peng-Robinson's equation of state, i.e., highly accurate and relatively simple to analyze natural gas reacting systems.

(3) All reactors and the fuel cell stack in the PAFC system are operated under the steady-state condition.

(4) The catalyst deactivation within the SR reactor is neglected. The assumption is based on the fact that a desulfurization unit is included in the PAFC system and successfully alleviates sulfur poisoning of metal catalysts such as Ni or Rh catalyst within the SR reactor.

(5) The CO poisoning effect of the PAFC stack performance is neglected. It was reported experimentally and numerically that the CO poisoning effect was diminished at the operating temperature of 160°C for 2% CO in the anode feed stream [17,18]. Therefore, this assumption is reasonable at a higher operating temperature (>160°C) and/or lower CO content (<1%)

A fuel-reforming module

Fig. 1a illustrates a typical SR based fuel-reforming reactor that contains several sub-reactors such as an SR reactor, WGS reactors, and auxiliary catalytic burner. Initially, the process natural gas (PNG) and steam are supplied to the SR reactor while the burner is fed with the burner natural gas (BNG), air, and the anodic exhausts from the HT-PEMFC stack. Although there are more than ten chemical reactions involved in the SR process [16], the model simplifies the process by only accounting for the three major reactions, i.e.:

Methane steam reforming:



WGS



Direct steam reforming

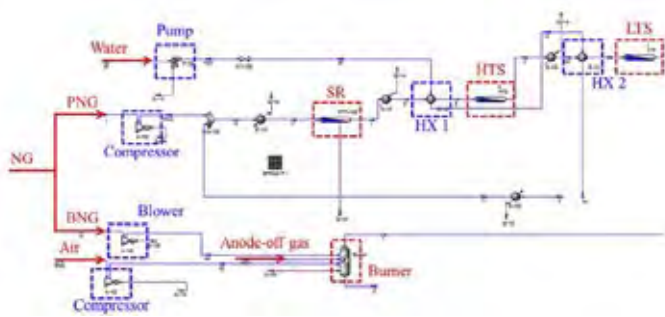
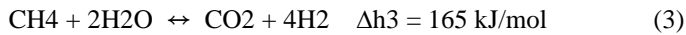


Fig. 1. relevant flowsheet generated by Aspen HYSYS®

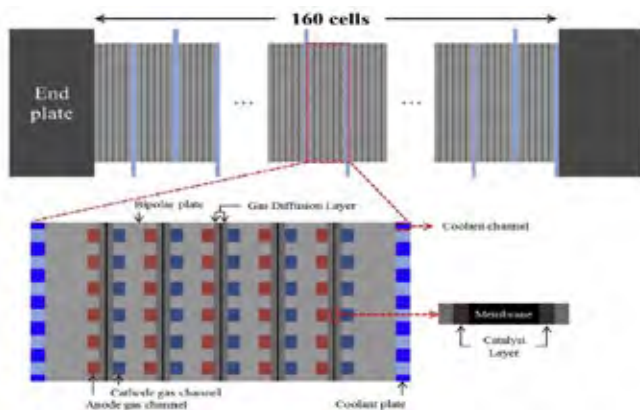


Fig. 1. Configuration of an HT-PEMFC stack with coolant channels and

III. UNITS

A	area, m ²
H	head, m
P	pressure, Pa
P	stack power, W
Q	total heat generation from a stack, W
n	number of cell

IV. CONCLUSION

In this study, we presented a complex multi-hub PAFC system model comprising three major modules, a fuel reformer, PAFC fuel cell system, and TEG system along with several BOP components and heat exchangers. Reforming processes of methane to hydrogen in the fuel reformer were modeled based

on the kinetics expressions of methane reforming and WGS reactions. The PAFC stack model was formulated via simplification of the 3-D PAFC model developed in our previous studies. The PAFC system model was implemented into a commercial flowsheet simulator, ASPEN HYSYS®, and then applied to the 440 kWe PAFC system. The model was first validated against the in-house test data wherein the model successfully reproduced exhaust gas compositions and reactor temperatures measured in the experiments. Using the validated model, we carried out the parametric study in terms of two major operating variables, i.e., the AFR for the burner and SCR for the SR reactor. The burner AFR controlled the rate of heat supply from the burner to SR reactor and hence, influenced both the hydrogen yield and system efficiencies. The optimal value of the burner AFR was near ER = 1 which maximized the burner heat supply, hydrogen yield, and system efficiencies. The highest electrical, thermal, and CHP efficiencies (i.e., 35.53, 42.42, and 77.95%, (respectively) were achieved with an ER=1.057. In contrast, the hydrogen yield and system efficiencies were almost invariant within a range of SCR change from 3.0 to 3.6 for the SR reactor. However, controlling the SCR was effective for reducing the level of CO content in the exhaust gases from 0.37% at SCR=3.0 to 0.23% at SCR = 3.6. The detailed simulation results highlighted that designing and operating a fuel reformer to keep an optimal temperature difference between the SR and WGS reactors is critical to improving the performance and efficiency of PAFC systems.

REFERENCES

- [1] Xu J, Froment GF. Methane steam reforming methanation and water-gas shift. I. Intrinsic Kinetics. *AIChE J* 1989;35(1):88e96.
- [2] Oh K, Ju H. Temperature dependence of CO poisoning in high-temperature proton exchange membrane fuel cells with phosphoric acid-doped polybenzimidazole membranes. *Int J Hydrogen Energy* 2015;40(24):7743e53.
- [3] Das SK, Reis A, Berry KJ. Experimental evaluation of CO poisoning on the performance of a high temperature proton exchange membrane fuel cell. *J Power Sources* 2009;193:691e8

FUEL CELL AND HYDROGEN TECHNOLOGIES AS AN EFFECTIVE SOLUTION FOR THE COMMUNITY ENERGY STORAGE: COMESTO PROJECT

Viviana Cigolotti^a, Giovanna Adinolfi^a, M. Testi^b, N. Destro^b, E. Macchi^b, M. Bolognese^b, Anna Pinnarelli^c, Daniele Menniti^c, Nicola Sorrentino^c, Raffaele Agostino^d, Giuseppe De Lorenzo^c, Orlando Corigliano^c, Petronilla Fragiacomò^c

a ENEA – Italian National Agency for New Technologies, Energy and Sustainable Economic Development – Portici Research Center, P.le E. Fermi 1, 80055 Portici (NA), Italy

b Fondazione Bruno Kessler, Unit ARES, Via Sommarive 18, 38123 Trento (TN) Italy

c Department of Mechanical, Energy and Management Engineering - University of Calabria

d Department of Physics - University of Calabria, Cubo 31c, Via P. Bucci, 87036 Rende (CS)

Abstract - ComESto project aims at addressing the integration of innovative solutions, based on PEM and SOFC technologies, in a nanogrid located in the university campus of Rende, Cosenza, Italy. The nanogrid is a hybrid power supply system of nominal power not exceeding 5kW able to integrate several different types of generation and storage systems and operating both in grid-connected and stand-alone configuration.

The prototype of energy storage device in the form of hydrogen is made up of a PEM electrolyzer, as hydrogen generator, a hydrogen storage tank with a hydrogen capacity of 1.6 Nm³ and a PEM fuel cell generator for the electric energy production of about 1 kW. The hydrogen production will deliver gas with an intermediate pressure allowing a comparative test between two different kind hydrogen storage systems: compressed gas and metal hydride reservoirs.

A highly efficient and reversible SOFC (rSOFC) technology will be developed to produce hydrogen or viceversa, generate back electric and thermic power. The target characteristics for the module will be a reference power of 1.5 kW and a storage capacity of about 5 kWh (in form of hydrogen gas, about 1.6 Nm³).

Index Terms – Hydrogen production, Polymer Electrolyte Membrane Fuel Cells, Polymer Electrolyte Membrane Electrolyzer, Smart Grids, Hydrogen Energy Storage System

I. INTRODUCTION

The growing need for decentralized power generation calls for small-scale systems that maximize electrical efficiency. Moreover, the intermittent production of energy from renewable

source requires suitable storage systems for an efficient integration of green energy production into electrical grid. Fuel cells and hydrogen technologies are the ideal candidates for fulfilling this demand. The electrochemical production of hydrogen has enormous potential for the profitable matching of large-scale renewable energy generation, the decarbonisation of our energy system and economic development of our society. Fuel Cell and Hydrogen technologies are able to deliver unique solutions to complex problems for the implementation of wider basis for renewables installation. As a matter of fact, these solutions can be applied to remote installations where any other alternatives are not feasible.

ComESto project aims at addressing the integration of innovative solutions, based on PEM and SOFC technologies, in a nanogrid located in the university campus of Rende, Cosenza, Italy. The nanogrid is a hybrid power supply system of nominal power not exceeding 5kW able to integrate several different types of generation and storage systems and operating both in grid-connected and stand-alone configuration.

II. PROJECT OVERVIEW

In the first phase of the project, the two solutions will be studied and tested in laboratory in order to assess the potential of the new technologies and define their optimal integration and management in the nanogrid.

The prototype of energy storage device in the form of

hydrogen is made up of a PEM electrolyzer, as hydrogen generator, a hydrogen storage tank with a hydrogen capacity of 1.6 Nm³ and a PEM fuel cell generator for the electric energy production of about 1 kW. The response time is of approximately 1 minute and the prototype includes integrated control and safety systems. The hydrogen production will deliver gas with an intermediate pressure allowing a comparative test between two different kind hydrogen storage systems: compressed gas and metal hydride reservoirs. The PEM system will be tested in Unical laboratories and several production and consumption trends, which are typical for a nanogrid in different load conditions, will be simulated.

FBK will develop an innovative energy-storage module integrating a highly efficient and reversible SOFC (rSOFC) technology. The energy system will be able to produce hydrogen or viceversa, generate back electric and thermic power. The target characteristics for the module will be a reference power of 1.5 kW, a storage capacity of about 5 kWh (in form of hydrogen gas, about 1.6 Nm³) and response time of less than 1h for the SOFC system, to reverse the operation mode. The system will include an integrated control and safety system. The rSOFC system will be tested in FBK H2 facility simulating and testing several production and consumption profiles typical for a nanogrid in different load conditions, also focusing on the cogeneration efficiency of system.

III. H₂ ENERGY STORAGE SYSTEM BASED ON PEM FUEL CELLS/ELECTROLYZER

The lay-out of the energy storage prototype in the form of hydrogen based on PEM Fuel Cells/Electrolyzer is shown in figure 1.

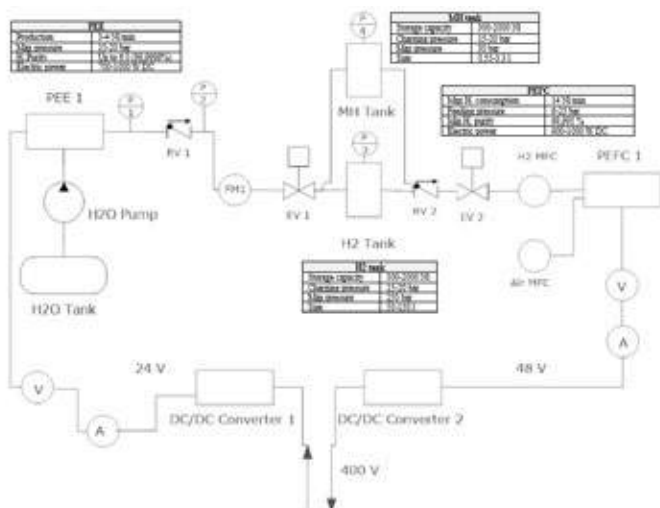


Figure 1 Lay-out of H₂ energy storage system based on PEM Fuel Cells/Electrolyzer

It is composed of a PEM Electrolyzer (PEE1), which is fed by the smart grid DC bus at 400 V through the DC/DC

converter 1 and produces hydrogen, which is stored in compressed gas (H₂ Tank) and metal hydride (MH Tank) reservoirs. By occurrence, the stored H₂ is sent to PEM fuel cell generator (PEFC), which converts it into electric energy. The electric energy is sent to smart grids DC bus at 400 V through DC/DC converter 2. The main characteristics of the main components are shown in the figure 1.

Four pressure meters (P1, P2, P3, P4), a flow meters (FM1), two mass flow controllers (H₂ and Air MFC), two not return valves (RV1 and RV2), two electro-valves (EV1 and EV2), four voltage and current meters (V and A) and a water pump (H₂O Pump) complete the lay-out.

ACKNOWLEDGMENT

The work was supported by the ComESTo PON project (Community Energy Storage, aggregated management of energy storage systems in Power Cloud) proj. number ARS01_01259, funded by MIUR and European Union.

MIUR for the “Dipartimento di Eccellenza 2018-2022” grant.

LOW-COST OXYGEN REDUCTION CATHODES FOR BIOELECTROCHEMICAL SYSTEMS: APPLICATION IN MICROBIAL DESALINATION CELLS

M.P. Bernícola*, P. Bosch-Jimenez*, M. Aliaguilla*, D. Molognoni*, M. D. Pirriera*, D. Morillo**, S. Martinez**, E. Borràs*

*LEITAT Technological Center, C/ de la Innovació 2, 08225 Terrassa (Spain)

** LEITAT Technological Center, C/ Pallars, 179-185, 08005 Barcelona (Spain)

Abstract – Microbial desalination cells represent an energy saving desalination technology. Their desalination efficiency depends, among other factors, on the catalyst used for the oxygen reduction reaction, taking place at the air-cathode. In this study, different electrochemical techniques were used to characterize a series of carbon-based electrodes doped with Pt-free catalysts. Selected materials were tested in a lab-scale MDC, to study the influence of the adopted cathode catalyst on desalination process.

Index Terms – desalination; microbial electrochemical technologies; platinum-free catalyst; oxygen reduction reaction.

I. INTRODUCTION

Bioelectrochemical systems (BES) use electroactive bacteria (EAB) to drive the conversion of chemical energy to electrical energy, or vice versa. The standard cell architecture comprises an anode, where organic matter is oxidized by EAB, and an air-cathode, where oxygen is abiotically reduced. The two electrodes are separated by one (or more) ionic exchange membranes, depending on application [1]. This “decoupled” redox reaction can be used to generate power, as in the case of microbial fuel cells (MFC), or to desalinate a saline stream, i.e. microbial desalination cells (MDC).

Air-cathode MDCs desalination performance is dependent on cathode material, among other factors. Indeed, oxygen reduction reaction (ORR), happening at the air-cathode, has a slow kinetics and must be catalyzed. A good ORR catalyst is the one allowing the highest current density at the lowest overpotential (E_{cat}) at BES operating conditions: while a material with high open circuit potential and low overpotential could be beneficial for power production in MFCs, high current densities (at high overpotential) are desired for MDCs,

where desalination is driven by current (Figure 1). The best material would be Pt, but cheaper air-cathodes are needed for practical application of MFC as desalination technology.

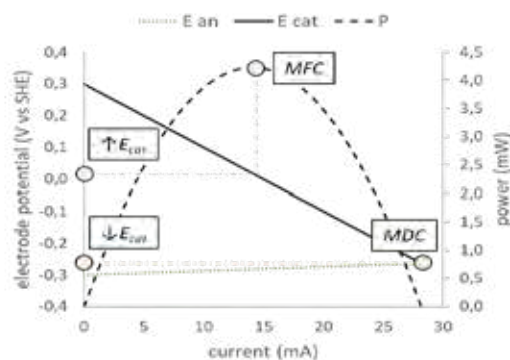


Fig. 1. Cathode potential (and ORR catalyst selection) depends on BES operating conditions: high power for MFCs, high current for MDCs.

II. MATERIALS AND METHODS

A Pt-free air-cathode was developed based on carbon nanofibers doped with iron nanoparticles (CNF-Fe), prepared by electrospinning technique: PAN (polyacrylonitrile) and PVP (polyvinylpyrrolidone) solutions with iron acetate (II) were electrospun and treated by pyrolysis. A second air-cathode was prepared adding 15% graphene oxide to carbon nanofibers for improving iron insertion (CNF-rGO15%). A MnO_2 carbon-based electrode (SGL, Germany) was used for benchmarking.

Electrochemical tests were performed to evaluate the ORR catalytic activity of the air-cathodes, by means of a three-electrode cell connected to a VMP3 potentiostat (BioLogic, France): open circuit voltage (OCV), cyclic voltammetry (CV) and chronoamperometry (CstV). The cell was composed by a

Pt-wire as counter electrode and an Ag/AgCl reference electrode. The working electrode was a sample (6mm diameter) of the cathode material under study, inserted in a stainless-steel frame acting as current collector. The electrolyte was a 100 mM PBS solution with pH of 7 and conductivity of 10 mS cm^{-1} . The solution was purged with N_2 and O_2 (each gas for 30 min), while measuring the OCV. Then, CV was performed at a scan-rate of 10 mV s^{-1} in a potential range from -0.6 V to 0.4 V vs Ag/AgCl, for 3 cycles. Finally, three CstV of 30 min duration were carried out at 0.1, -0.1 and -0.3 V vs Ag/AgCl, under convection regimen.

The air-cathodes were validated in a lab-scale MDC to test their desalination performance. A saline solution (6 g L^{-1} NaCl) was adopted for this purpose. The MDC was batch-operated for 72 h with an external resistance (R_{ext}) of 2.5Ω . The bioanode was made of carbon felt (SGL, Germany) and fed with synthetic wastewater. The MDC was monitored in terms of conductivity evolution in the saline chamber, cathode potential and generated current.

III. RESULTS AND DISCUSSION

The best ORR catalyst for an air-cathode is the one allowing the more positive half-wave and onset potential ($E_{1/2}$ and E_{onset} , respectively), i.e. the lower overpotential. Even though, the air-cathode must guarantee a high current density at MDC operating condition (low R_{ext} , near short-circuit condition). In this scenario, the cathode works at a very low potential, near -0.3 , -0.4 V vs Ag/AgCl, due to the lower internal resistance of the bioanode (vs air-cathode), generally occurring in BES [2].

Figure 2 shows that carbon nanofibers-based cathodes (CNF-Fe and CNF-rGO15%) were more catalytic than the reference one (GDL-MnO₂), because $E_{1/2}$ and E_{onset} were more positive. Nevertheless, CNF samples did not allow high current densities at low operating potentials, where MDCs typically work. This observation gets clearer when looking at CstV results (Figure 3). The GDL-MnO₂ cathode, which is not highly catalytic at high potentials, was the one reaching the highest current density at -0.3 V vs Ag/AgCl. On the other hand, CNF air-cathodes showed a good catalytic activity at low overpotential, where CNF-Fe performed better than CNF-rGO15%. These results agree with consulted literature [3].

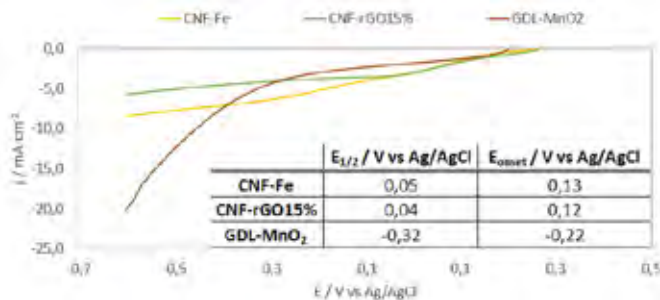


Fig. 2. Results of CV analysis (reduction semi-curve of the first cycle is shown).

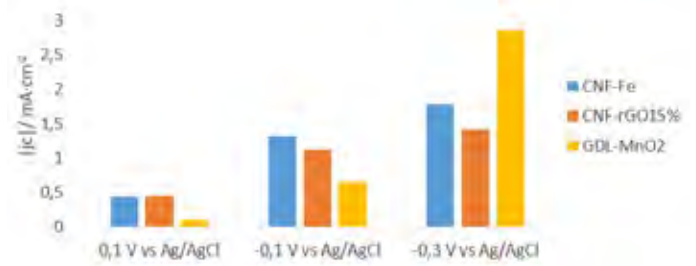


Fig. 3. Results of CstV at 0.1, -0.1 and -0.3 V vs Ag/AgCl (steady-state values).

The 3 air-cathodes were tested in a lab-scale MDC to evaluate the desalination performance depending on cathode material. Figure 4 shows desalination efficiency, cathode potential and current density generated by the different air-cathodes. The MDC equipped with GDL-MnO₂ cathode showed the highest current density and desalination efficiency (51% after 72 h), in agreement with previous electrochemical characterization (Figures 2-3). However, laboratory tests showed that the MDC could not work at a current density as high as in ORR experiments (0.4 mA cm^{-2} vs 2.9 mA cm^{-2}), due to scale-up effects. This aspect must be tackled for future technology development.

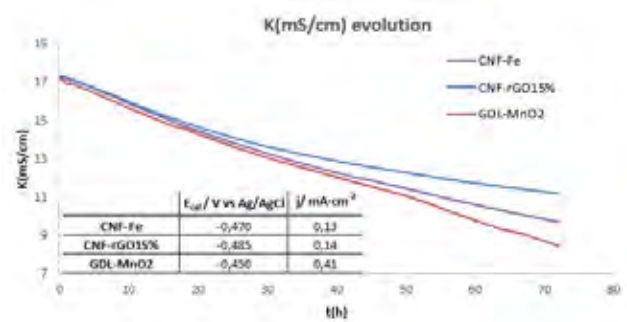


Fig. 4. MDC desalination performance with different air-cathodes.

IV. CONCLUSION

The selection of a proper air-cathode catalyst depends on the specific BES application. In the case of MDCs, a GDL-MnO₂ electrode showed a good ORR catalytic activity, allowing to reach the highest desalination efficiency, compared with metal-doped CNF samples.

ACKNOWLEDGMENT

This research received funding from EU-Horizon 2020 programme, Grant Agreement N°685793 (MIDES project).

REFERENCES

- [1] C. Santoro, et al., «Microbial fuel cells: From fundamentals to applications. A review», *Journal of Power Sources*, 2017.
- [2] D. Molognoni, et al., «Reducing start-up time and minimizing energy losses of Microbial Fuel Cells using Maximum Power Point Tracking strategy», *Journal of Power Sources*, 2014.
- [3] P. Bosch-Jimenez et al., «Non-precious metal doped carbon nanofiber air-cathode for Microbial Fuel Cells application: Oxygen reduction reaction characterization and long-term validation», *Electrochimica Acta*, 2017.

Enzymatic BIOelectrodes for BioSENSors and Biofuel CELLS – BIOSENSCELL

Laura García-Carmona*, Mireia Buaki-Sogó*, Jessica Calleja-Langa*, Pedro Llovera-Segovia**, Alfredo Quijano-López**

* Instituto Tecnológico de la Energía (ITE), Av. Juan de la Cierva, 24, 46980 Paterna Valencia (Spain)

** ITE, Universitat Politècnica de València, Camino de Vera s/n Edificio 6C 46022 Valencia (Spain)

Abstract - BioSensCell project develops enzymatic bioelectrodes for their application in biofuel cells and biosensors. It comes from the need of new energy sources for biomedicine related applications whereas biosensor development is of great interest in pharma, food, environmental and agricultural sectors. BioSensCell faces the challenge of developing new energy sources capable of supplying energy to next generation electronic devices, especially those involved in biomedicine (monitoring and diagnosis) and wellness. On the other hand, electrochemical biosensors are gaining interest due to their selectivity, sensitivity and the ease of use as well as the possibility to be integrated as a part of portable devices allowing thus, the performance of analysis *in situ* in a simple, fast and reliable manner. In both systems, biosensors and biofuel cells, the key step relies on enzymatic bioelectrodes development, main component and goal of BioSensCell project.

Keywords - Biofuel cells, biosensors, energy harvesting, enzyme immobilization.

I. INTRODUCTION

Enzymatic bioelectrode development is an emerging technology that constitutes a challenge for scientists focused on biofuel cells and biosensors development. Biofuel cells consist of bio-devices able to produce electric energy from the surroundings (Energy Harvesting), using the chemical energy stored in a biological compound. Energy thus obtained, could be used to power small electronic devices working with low power requirements or implantable devices in biomedicine [1]. On the other hand, biosensors are devices with the same capacity for energetic transformation as biofuel cells, but in this case, the transformation leads to an electric response that can be used in the monitoring and control of target analytes [2], [3].

Enzymatic bioelectrodes are a promising approach due to their selectivity towards a specific substrate, enzymes availability and the capacity to perform biological transformation under soft operation conditions; in addition, energy is obtained in a clean, safety and efficient manner. However, enzymatic bioelectrodes suffer from low operation stability and loss of activity and active research in overcoming these problems needs to be

conducted. To overcome the problems related with enzyme stability and loss of activity, the most common approach is the enzyme immobilization onto a suitable support [4].

II. PURPOSE OF THE STUDY

In BioSensCell project, the main objective relies on the development of flexible and biocompatible enzymatic bioelectrodes for their use in enzymatic biofuel cells and biosensors. Developments must be focused on the use of non-toxic and biocompatible materials, with flexibility and conductive capacity for efficient electron transfer reactions. In BioSensCell project novel materials for enzyme immobilization will be synthesized to be used as support and transducer surface; in addition, commercial supports will be evaluated and modified for the development of biosensors aimed to detect and analyse target compounds such as lactate with relevance in sports, health and food technology. Term for project execution will be 2 years starting from April 2019.

III. RESEARCH METHODS AND METHODOLOGY

ITE will make use of technologies that combined are expected to give satisfactory results for project progress and development. ITE is an international technological centre which offers high-added value services to companies and public entities focused on the energy, electrical and communications sectors.

ITE has a wide knowledge and background in polymeric membranes preparation and characterization [5]. This technology plays an important role in the industry due to its versatility, excellent reproducibility and simplicity [6]. In this sense, membrane technology will be useful to meet the requirements of enzymatic bioelectrodes for being implanted avoiding the appearance of protuberances, edges and enhancing the adaptability to skin morphology. Conductive capacity will be achieved by addition of carbon-based materials.

On the other hand, commercial screen-printed electrodes will be modified to optimize their performance for lactate monitoring

to achieve an enhanced selectivity and fast biosensor response. To accomplish this, redox mediators and carbon-based nanomaterials will be used for biosensor preparation and testing.

IV. RESULTS AND INNOVATION

During execution of BioSensCell project, an evaluation of the state of the art on conductive polymers for enzyme immobilization has been carried out to select the polymer with the best conductive capacity for enzyme immobilization. Conductive polymers found in literature are displayed in Table 1 together with conductivity values for these polymers, advantages and drawbacks detected.

TABLE I

CONDUCTIVE POLYMERS SCREENING FOR TRANSDUCING SUPPORTS FOR ENZYME IMMOBILIZATION

Conductive Polymer	Conductivity	Advantages	Drawbacks
Polyaniline (PANI)	up to 100 S/cm when doped	Sensitivity and selectivity Biocompatible	Inactivity at neutral pH
Polypyrrole (PPy)	up to 160 S/cm doped with I ₂	Biocompatible Composites	Brittle Synthesis with FeCl ₃ (toxic)
Polythiophene (PT)	0.001-10 S/cm when doped	Conductivity and optical properties	Low mechanical integrity Biocompatible if co-polymerized
Polyethylenedioxiide thiophene (PEDOT)	Up to 210 S/cm 10 S/cm When doped with PSS 0,0006 S/cm non-doped	Biocompatible Thermal stability	Low dispersability in water, needs to be mixed with PSS Swelling and collapse in aqueous solutions

PEDOT appears to be the best candidate due to its conductivity, film forming ability, and biocompatibility. However, films formed tend to swell and collapse in aqueous solutions; and this will be bioelectrodes working medium. A re-evaluation of state of the art showed that biopolymers could be good candidates for the development of flexible supports for enzyme immobilization since they have been used for multiple tasks in the development of bioelectrodes. Biopolymers are a class of polymers from natural origin divided in following families: proteins such as globulin; polysaccharides such as cellulose; and nucleic acids. Deep investigation on biopolymers is currently on-going in order to select the best biopolymer bearing in mind ability for forming composite films and for enzyme immobilization.

Besides, the response to lactate using lactate oxidase (LOx) has been evaluated using mediators to detect electrochemically its enzymatic product (H₂O₂). Thus, commercial carbon screen-printed electrodes modified with Co-Phtalocyanide, Prussian blue (PB) and Ferrocyanide have been evaluated. Firstly, the detection potential was evaluated in order to select the optimal in terms of sensitivity and selectivity. In this sense, -0.2V was selected for Ferrocyanide and PB and +0.4V in case of Co-Phtalocyanide (Figure 1A). This is because higher potential can

lead to interferences in the following real sample analysis. Then, lactate calibration was performed with each mediator-based electrode at the selected potential to select the best to be used together with LOx according to their sensitivity. In this sense, PB was selected as the best mediator due to its good sensitivity (2326.9 nA·mM⁻¹), which has been proved to be 9 times higher than others mediators studied in the linear range explored (0.1 – 2 mM). From these results, the following steps in BioSensCell project will involve the use of PB to improve the response of the bioelectrodes in terms of sensitivity and selectivity, due to the low potential required for the measurement.

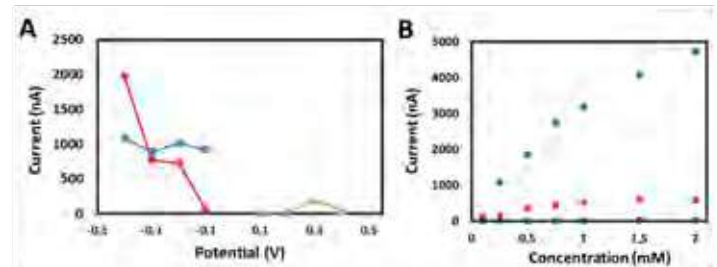


Fig.1. Mediators evaluation (A) Hydrodynamic voltammogram using different mediators Co-Phtalocyanide (green), Ferrocyanide (red) and PB (blue) modified with LOx. (B) Lactate calibration plot. Conditions: Lactate 0.5mM, PBS pH=7.

ACKNOWLEDGMENT

Instituto Valenciano de Competitividad Empresarial (IVACE) is gratefully acknowledged for funding.

REFERENCES

- [1] Buaki-Sogó, M; Zubizarreta, L; Gil-Agustí, M; García, M; Quijano, A. Biopilas: la energía sostenible en los seres vivos. Avances en Química 2018, volume 13, pp. 21-31
- [2] Zebda, A.; Cosnier, S.; Alcaraz, J.-P.; Holzinger, M.; Le Goff, A.; Gondran, C.; Boucher, F.; Giroud, F.; Gorgy, K.; Lamraoui, H.; Cinquin, P. Single Glucose Biofuel Cells Implanted in Rats Power Electronic Devices. Scientific Reports 2013, Article number: 1516
- [3] Bruen, D; Delaney, C; Florea, L; Diamond, D. Glucose Sensing for Diabetes Monitoring: Recent Developments. Sensors 2017, Volume 17, issue 8, pp. 1866.
- [4] Putzbach, W., Ronkainen, N. J. Immobilization Techniques in the Fabrication of Nanomaterial-Based Electrochemical Biosensors: A Review. Sensors, 2013, Volume 13, pp. 4811-4840.
- [5] Lithium polymeric membrane based on a semi-crystalline fluorinated polymeric matrix and a non-ionic surfactant. L. Zubizarreta Saenz De Zaitegui, M. Gil-Agusti, A. Quijano López, M. Garcia Pellicer. EP 2 860 790
- [6] B.S. Lalia, V. Kochkodan, R. Hashaiheh, N. Hilal. A review on membrane fabrication: Structure, properties and performance relationship. Desalination 2013, volume 326, pp. 77-95.

LOW ENERGY DESALINATION IN MICROBIAL DESALINATION CELLS USING NEW ION EXCHANGE MEMBRANES

M. Aliaguilla*, M.P. Bernícola*, P. Bosch-Jimenez*, D. Molognoni*, M. Meijlink**,
A. Alhadidi**, E. Borràs*

*LEITAT Technological Center, C/ de la Innovació 2, 08225 Terrassa (Spain)

** FUJIFILM Manufacturing Europe B.V. P.O. Box 90156, 5000 LJ Tilburg, The Netherlands

Current desalination technologies are energy intensive and microbial desalination cells (MDC) could represent a suitable alternative. The ion exchange membranes represent key components for proper MDC operation. Membranes biofouling can cause a loss of desalination performance due to decreased permselectivity or increased internal resistance. Different membranes have been studied through electrochemical characterization and desalination performance assessment.

Index Terms - Bioelectrochemical systems (BES), Desalination, Ion Exchange Membranes.

I. INTRODUCTION

Market available desalination technologies require high-energy input, being reverse osmosis (RO) the most-widely employed for seawater desalination, with an energy consumption between 3 and 6 kWh·m⁻³.

Microbial desalination cells (MDC) have emerged as a low energy consumption alternative. MDCs concept, relies on microorganism's electron transfer capacity to drive electrochemical processes. Like in a conventional air-cathode Microbial Fuel Cell (MFC), in the cathode the oxygen reduction reaction takes place while the bioanode oxidises organic matter contained in wastewater.

In a standard MDC, the electrochemical potential gradient between the electrodes is the driving force for ions removal from a saline stream through selective ion exchange membranes (IEMs), resulting in water desalination, as depicted in Figure 1. IEMs are key components for MDC proper operation. The most common parameters for their characterisation for MDC application are electrical resistance and permselectivity. Biofouling due to microbial population in the anodic chamber might have an impact on anionic exchange membranes (AEMs) performance over time. Thus, the present work is aimed at studying different AEMs for avoiding the loss of performance over time in MDC application.

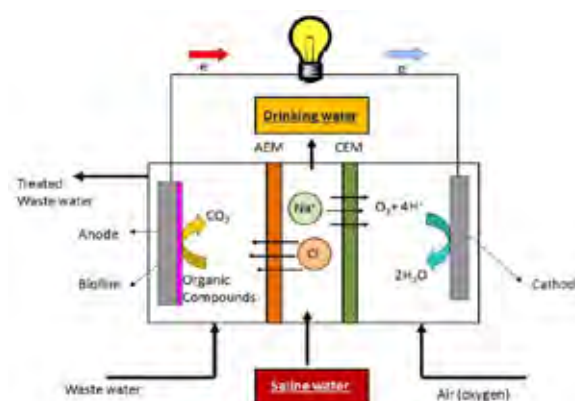


Fig. 1. Microbial desalination cell diagram (Source: Z. Borjas et al 2017) [1]

II. MATERIALS & METHODS

A. Electrochemical Characterization

Three commercial AEMs AMI-7001 were employed as standard AEMs (Membrane International Inc., USA), AMX-Neosepta (ASTOM, Japan) and Type10 (FUJIFILM, Japan) were employed as standard AEMs. Two Type 10 (FUJIFILM) modified IEMs with different antibiofouling properties (named #2 and #16), were also tested. Corresponding cationic exchange membranes (CEMs) from each supplier were employed in each MDC experiment. The electric resistance (in NaCl 0.5M) and permselectivity (towards Cl⁻ in 0.1-0.5M NaCl) of AEMs were determined in a six-compartment and two-compartment, respectively, electro dialysis cell specifically designed and constructed by Leitlat. The voltage drop generated across the AEM was measured using a VMP-3 potentiostat (BioLogic, France), at different values of electrical current. Two reference electrodes (Ag/AgCl) submerged in 3M KCl lugging capillaries were used for that measurements, one on each side of tested membrane.

B. Biofouling trend study

The biofouling trend in MDC was studied in one-week desalination cycles with FUJIFILM Type 10 IEMs (including the mentioned modified membranes, #2 and #16) by pre- and post- treatment electrochemical characterization. The best performing membrane was tested further (up to 10 weeks) with weekly electrochemical characterization.

C. Desalination performance

MDCs architecture was based on air-cathode, as described in M. Aliaguilla *et al.* 2018 [2]. Desalination performance of all previously mentioned membranes was studied by conductivity evolution in the saline chamber, with on-line readings (CDC40101 Hach-Lange) with synthetic brackish water ($10 \text{ g-NaCl}\cdot\text{L}^{-1}$) in batch mode (3 days duration). Anodic chamber was fed with acetate based medium at $0.227 \text{ kg-COD}\cdot\text{m}^{-3}\cdot\text{d}^{-1}$ of organic loading rate (OLR) and the catholyte was 100mM phosphate buffer solution. Anode and cathode were connected by an external load of 2.5Ω .

III. RESULTS

A. Membrane Characterization

Figure 2 shows that FUJIFILM type 10 has the highest permselectivity for Cl^- and the lowest electrical resistance being the most promising membrane for the MDC application. The anti-biofouling treatment of Type 10 modifications, #2 and #16, results in a significant loss of permselectivity (26 and 19% loss respectively) and a slight increase of electrical resistance.

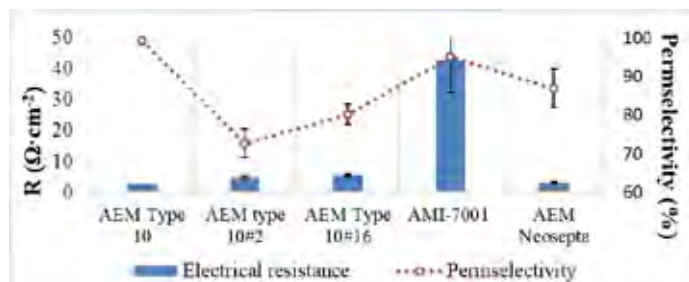


Fig. 2. AEM characterization: i) electrical resistance in NaCl 0.5M and ii) permselectivity in 0.1-0.5M NaCl. *(Permselectivity results for #2 and #16, unlike the other AEM results, are not corresponding with manufacturer data).

B. Biofouling

After one desalination cycle Type 10 membrane maintained the highest permselectivity, being the biofouling effect equal or minor than in #2 and #16.

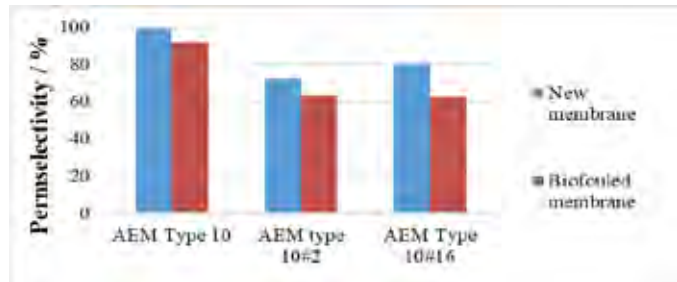


Fig. 3. AEMs electrical resistance (in NaCl 0.5M) evolution

Longer exposure time trials were carried out with Type 10 IEMs. Figure 4 shows a very low fluctuation in terms of electrical resistance over time. Thus, no clear trend has been identified in correlation with biofouling. On the other hand, permselectivity decreased from 99% to 80% after 3 weeks and then remained around that value until the 10th week. Desalination rate decreased accordingly over time, from $1.44 \text{ g}\cdot\text{m}^{-2}\cdot\text{h}^{-1}$ to $1.25 \text{ g}\cdot\text{m}^{-2}\cdot\text{h}^{-1}$ the 3rd week, and to $0.99 \text{ g}\cdot\text{m}^{-2}\cdot\text{h}^{-1}$ the 7th.

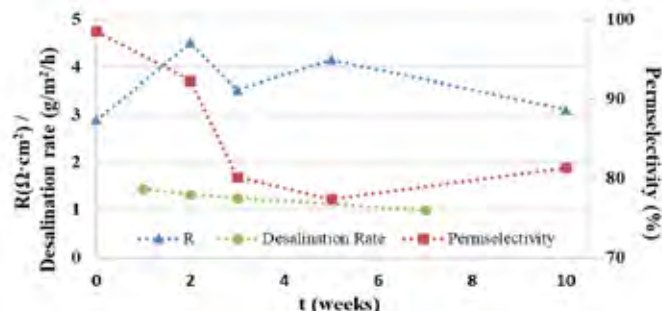


Figure 4. Biofouling effect on the electrical resistance, permselectivity and desalination rate for an AEM Type 10 over time.

C. Desalination

Figure 5 shows that in terms of desalination in air cathode MDC FUJIFILM IEMs perform in the range of Neosepta and outperform the results reached by Membrane international.

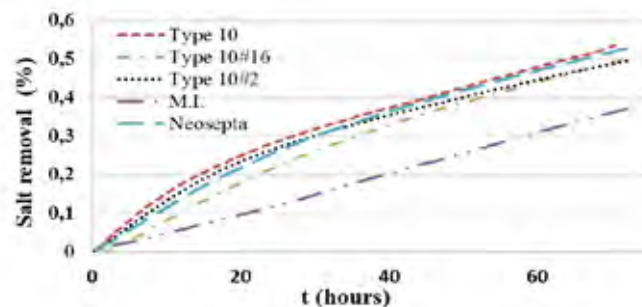


Figure 5. Desalination performance over time of the studied IEMs.

IV. CONCLUSIONS

FUJIFILM Type 10 IEMs are suitable membranes for desalination in air cathode MDC. Their electric properties and salt removal rates are matching and overcoming the reference results. Long MDC operation indicates that biofouling has direct effects on permselectivity and, also, on desalination performance, but results are unclear respect on electrical resistance.

REFERENCES

- [1] Z. Borjas, *et al.* Strategies for merging microbial fuel cell technologies in water desalination processes: start-up protocol and desalination efficiency assessment, *Journal of power sources* 356 (2017) 519-528.
- [2] M. Aliaguilla, *et al.*, Searching for air-cathode Microbial Desalination Cells optimal niche for production of drinking water. Joint conference 7th European Bioremediation Conference (EBC-VII) and 11th International Society for Environmental Biotechnology conference (ISEB 2018). ISBN: 978-618-81537-6-9

ADVANCED MODEL-BASED AGING ESTIMATION OF SOLID OXIDE FUEL CELL STACKS

Marco Gallo*, Pierpaolo Polverino* and Cesare Pianese*

* Department of Industrial Engineering, University of Salerno
Via Giovanni Paolo II, 132 - 84084, Fisciano (SA), ITALY.

Abstract - In this work, an online natural aging estimation algorithm is developed, coupled with an Electrochemical Impedance Spectroscopy (EIS) -based diagnostic algorithm, to refine diagnostic features extraction during Solid Oxide Fuel Cell stack operation and to predict its Remaining Useful Life (RUL). A combination of a lumped dynamic model along with features extracted from real-time EIS measurements is herein proposed for on-line applications. An Equivalent Circuit Model (ECM) is considered to identify parameters, such as ohmic and total resistances that are coupled with an Area Specific Resistance (ASR) approach within the lumped model. The information derived from the EIS spectrum allows to estimate the voltage degradation over time along with its nominal behavior. Indeed, the trend of the identified parameters is proportional to the aging of the cell, if any other abnormal condition does not occur. This guarantees an on-line RUL estimation and a more robust fault diagnostic outcome.

Index Terms – Dynamic Lumped Model, EIS-Based Diagnosis, Remaining Useful Life, SOFC Aging Estimation.

I. INTRODUCTION

Solid Oxide Fuel Cells (SOFCs) are one of the most suitable alternatives to conventional energy production systems for power production, cogeneration and Auxiliary Power Unit (APU) applications. Actually, high manufacturing costs and limited lifetime, particularly due to degradation processes, hinder the spread of the SOFC in the market [1]. Indeed, their durability is significantly affected by several degradation mechanisms, which reduce cell performance during time and can lead to stack failure.

Real-time lifetime estimation techniques, to directly observe degradation phenomena and predict Remaining Useful Life (RUL), are usually difficult to implement. Indirect State-of-Health (SoH) indicators, related to voltage decay over time, are adopted [2]. Aiming at extending the lifetime, a fast diagnostic algorithm might be fundamental to detect reversible incipient faults and anticipate stack failures. Therefore, a suitable diagnostic algorithm needs to satisfy a tradeoff between computational time, accuracy and reliability to be applied in real-time [3]. For diagnostic purposes, lumped modelling is a suitable option to simulate the nominal state of the system to have a real-time reference of the system characteristic

parameters. Electrochemical Impedance Spectroscopy (EIS) proved to be a suitable technique providing a wealth of information on electrochemical phenomena taking place inside the stack. EIS can be applied to extract useful metrics for stack modelling and fault diagnosis by means of an Equivalent Circuit Modelling (ECM) approach.

This work focuses on the coupling of the information derived from a lumped dynamic model and ECM-based features to updated operating parameters evaluation (i.e., voltage, temperature, etc.) under detrimental conditions. This allows reproducing the nominal behavior of the stack and its natural aging via real time EIS measurements.

II. ADVANCED MODEL-BASED AGING ESTIMATION

The concept behind the model herein presented consists in a lumped model which runs in parallel with the real system and the EIS measurement carried out at defined intervals. The features extraction performed through an ECM-based approach allows integrating the real-time information on the system state directly into the voltage estimation, modelled through an Area Specific Resistance (ASR) approach.

A. Dynamic lumped model

The stack dynamic model herein adopted is partially derived from a previous authors' work [4]. The energy conservation principle is applied, as shown in eq. (1), where K is the stack heat capacity, T is the stack outlet temperature, \dot{E}_{in} and \dot{E}_{out} are the inlet and outlet energy flows, P is the electrical power and Q is the heat exchanged in case of non-adiabatic conditions. More details on the approach can be found in [4].

$$K \frac{dT}{dt} = E_{in} - E_{out} - P + Q \quad (1)$$

The voltage is modelled through an ASR approach:

$$V_{Stack} = n_{cell} \cdot (V_{Nernst} - J \cdot ASR - V_{off}) \quad (2)$$

where the Nernst potential V_{Nernst} is computed over gas concentrations (i.e. partial pressures) average, calculated between stack inlet and outlet sections. The ASR is expressed in eq. (3), where ASR_0 , T_0 , E_a and V_{off} are lumped parameters identified against experimental data [4].

$$ASR = ASR_0 \cdot \exp \left[\frac{E_a}{R} \cdot \left(\frac{1}{T_{out}} - \frac{1}{T_0} \right) \right] \quad (3)$$

B. EIS-based metric extractions

In the literature, several approaches are exploited to extract specific features from EIS measurements. Among them, ECM correlates proper circuital components to the investigated physical phenomena. By doing so, suitable impedance contributors (i.e., ohmic resistance, charge-transfer resistance, etc.) can be identified by analyzing these parameters [5]. From their evaluation, it is possible to discern between nominal and faulty conditions. Obviously, the choice of the most effective ECM is crucial to group the occurring phenomena and to quantify their magnitude properly. The identification of the circuital model and the related parameters (e.g., resistances, capacitances, etc.) are performed through a minimization problem, speeded up by means of an authors' patented technique¹, which allows high generalizability and fast fitting performance. The result is a parameter extraction from the EIS spectrum in less than 5 seconds. Usually, a commonly used circuit is made of at least two complex elements and an ohmic resistance (R_0). Defined i as the number of these elements, the total resistance (R_{TOT}) is thus calculated as follows:

$$R_{TOT} = R_0 + \sum_i R_i \quad (4)$$

C. Aging model

The stack dynamic model simulates the nominal voltage of the system according to the input flows and the operating variables. The circuital model allows monitoring the changing in the magnitude of the parameters related to electrochemical phenomena via EIS measurements. Coupling these information, it is possible to estimate the nominal voltage along with the aging derived from the total resistance evaluated through ECM. The variation of the total resistance (ΔR_{TOT}) can be expressed as a further voltage loss in the ASR approach (eq. (3)), as a term (η_{deg}) related to the degradation, according to the follow equations:

$$\eta_{deg} = i \cdot \Delta R_{TOT} \quad (5)$$

$$V_{Stack} = n_{cell} \cdot (V_{Nernst} - J \cdot ASR - V_{off} - \eta_{deg}) \quad (6)$$

Literature survey proves that the total resistance measured via EIS during long term tests increases with time. According to the measurement performed in [6], the increase in the ohmic (R_0) and polarization (R_{pol}) resistances suggests a link with the degradation rate. Thus, improving the ASR approach with the evaluation of η_{deg} , it is possible to match the natural aging of the system and thus to perform a RUL estimation.

Moreover, the increase in the total resistance, without further changes in the other extracted features, suggests a deviation from nominal conditions different from any expected fault [7], thus identifying this latter as natural aging. The methodology

herein described has been applied to the data presented in [6] and the results are shown in Figure 1. They suggest the effectiveness of such methodology, particularly if applied on-line with real time EIS measurements.

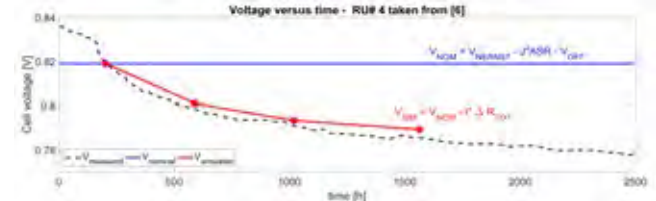


Fig. 1 - Voltage simulation coupling ASR approach and EIS features

III. CONCLUSION

This work focused on the development of an aging estimation algorithm for SOFCs coupling a fast lumped dynamic model and the features extracted from a EIS-based diagnostic algorithm. The nominal behavior of the stack is reproduced through an ASR approach while the natural aging is identified via real time EIS measurements, integrated as a further loss in the voltage estimation.

The methodology has been applied to literature data to prove its effectiveness. The interesting results suggest its usefulness into on-line applications to improve the reliability and robustness of the dynamic simulation with real-time updates of the stack State of Health via real-time EIS measurement. The overall methodology is under validation upon experimental dataset on a 6-cells short stack.

ACKNOWLEDGMENT

The research leading to these results received funding from the European Union's Horizon 2020 research and innovation programme for the FCH2-JU under grant agreement n.735918 (Project - INSIGHT).

REFERENCES

- [1] Tucker, D., et al. (2014). Journal of Fuel Cell Science and Technology, 11(5), 051008. Doi: 10.1115/1.4028158
- [2] Guida, M., et al. (2015). Reliability Engineering & System Safety, 140, 88-98. Doi: 10.1016/j.res.2015.03.036
- [3] Polverino, P., et al. (2017). Applied energy, 204, 1198-1214. Doi: 10.1016/j.apenergy.2017.05.069
- [4] Gallo, M., et al. (2018). Energy conversion and management, 171, 1514-1528. Doi: 10.1016/j.enconman.2018.06.062
- [5] Leonide, A., et al. (2009). ECS Transactions, 19(20), 81-109. Doi: 10.1149/1.3247567
- [6] Mosbæk, R. et al. (2013). Fuel Cells, 13(4), 605-611. Doi: 10.1002/face.201200175
- [7] Polverino, P., et al. (2015). Journal of Power Sources, 280, 320-338. Doi: 10.1016/j.jpowsour.2015.01.037

¹ Petrone R. et al. (2016). International Patent Number WO2016/071801.

DEVELOPMENT OF A MODEL-BASED ALGORITHM FOR ONLINE DEGRADATION ESTIMATION OF SOLID OXIDE FUEL CELLS

P. Polverino*, M. Gallo*, and C. Pianese*

*Department of Industrial Engineering, University of Salerno, via Giovanni Paolo II 132, 84084, Fisciano (SA), (Italy)

Abstract - The present work illustrates the development and application of a model-based algorithm capable of estimating in real time the performance decay of Solid Oxide Fuel Cells due to degradation phenomena. The main outcome of the algorithm consists in the estimation of the Remaining Useful Life (RUL) of the SOFC stack, function of its operating conditions. A multi-scale modelling approach is considered to couple information at different physical scales, to increase model accuracy and generalizability. A full SOFC stack model is accounted to identify representative key parameters sensitive to the considered degradation phenomena. Detailed degradation sub-models are developed according to information derived from the literature and are linked to the full stack model through the aforementioned parameters. The developed algorithm is tested in simulated environment, and a sensitivity analysis is performed to investigate the main parameters and operating conditions that influences the SOFC lifetime.

Index Terms - Degradation models, Prognostics, RUL estimation, SOFC.

I. INTRODUCTION

Researchers and industrial companies are currently committed on the investigation of several degradation phenomena affecting SOFCs, and many advancements have been achieved also thanks to Accelerated Stress Test (AST) techniques. Nevertheless, to proper design AST protocols, the knowledge on the effects of operating conditions on the Remaining Useful Life (RUL) of SOFCs is required.

The present paper illustrates a model-based algorithm that couples different scales to relate degradation phenomena and SOFC performance. Voltage degradation can be estimated under different operating conditions, to derive useful guidelines that can be used for AST protocols definition.

II. MODELLING FRAMEWORK

A multi-scale modelling approach is here followed, combining degradation sub-models to an overall SOFC performance model. In this way, the effects of the degradation phenomena can be evaluated in terms of degradation rate

change under different operating conditions.

As first step, the reference degradation phenomenon is selected, and a relevant model is designed from the literature [1]. Then, key microscopic parameters that are affected by degradation are identified and related to macroscopic variables of a comprehensive SOFC performance model, partially derived from [2].

A. Degradation sub-model

The degradation phenomenon accounted in this work refers to Ni agglomeration at the anode catalyst layer. This phenomenon mainly develops as surface diffusion, where two or more particles are in contact and the smaller ones are absorbed by the bigger ones [1]. The main effects at microstructural scale are related to the variation of the average Ni particles radius r_{Ni} , which can be expressed as [1]:

$$\frac{dr_{Ni}}{dt} = \frac{C}{r_{Ni}^4} \exp(-\gamma t) \quad (1)$$

where γ represents the time unit probability of a Ni particle that stops growing at a certain time, and C is a proportional coefficient depending on operating temperature, anode composition and Ni particles properties [1].

The main effect at mesoscale level can be identified in the change in the Triple Phase Boundary (TPB) length and Ni conductivity. The TPB length dependency on Ni particle radius can be defined as [3]:

$$\lambda_{TPB} = \zeta_{Ni,YSZ} n_{Ni} Z_{Ni,YSZ} \quad (2)$$

where λ_{TPB} is the TPB length for unit volume, $\zeta_{Ni,YSZ}$ is the contact perimeter between Ni and YSZ particles, n_{Ni} is the number of Ni particles for unit volume and $Z_{Ni,YSZ}$ is the coordination number between Ni and YSZ particles. They can be thus calculated as [3]:

$$\zeta_{Ni,YSZ} = 2\pi \sin(\vartheta) \cdot \min(r_{Ni}, r_{YSZ}) \quad (3)$$

$$n_{Ni} = 3(1-\varphi) \frac{\psi_{Ni}}{4\pi r_{Ni}^3} \quad (4)$$

$$Z_{Ni,YSZ} = \frac{1}{2} \hat{Z} \left(1 + \frac{r_{Ni}^2}{r_{YSZ}^2} \right) \left(\frac{\psi_{YSZ} \cdot r_{Ni}}{\psi_{YSZ} \cdot r_{Ni} + \psi_{Ni} \cdot r_{YSZ}} \right) \quad (5)$$

In the previous equations, ϑ is the particles contact angle, r_{YSZ} is the YSZ particle radius, φ is the composite-electrode porosity, ψ_{Ni} and ψ_{YSZ} are the Ni and YSZ volume fractions, respectively, and \hat{Z} is the average coordination number [3].

The dependency of Ni conductivity σ_{Ni} on Ni particle radius can be defined as [4]:

$$\sigma_{Ni} = \sigma_{Ni}^0 \left[(1-\varphi) \frac{(\psi_{Ni} - \psi'_{Ni})}{1 - (1-\varphi)\psi'_{Ni}} \right]^2 \quad (6)$$

where σ_{Ni}^0 is the dense solid Ni conductivity, which depends on the operating temperature, and ψ'_{Ni} is the threshold Ni volume fraction, computed as [4]:

$$\psi'_{Ni} = \frac{1.764 \cdot \psi_{YSZ}}{(\hat{Z} - 1.764) r_{YSZ}} r_{Ni} \quad (7)$$

B. SOFC performance model

The degradation sub-model describing Ni particle radius change is here related to the SOFC performance through the identified key mesoscale parameters. The reference SOFC model accounted in this work derives from a previous model already presented by the authors in [2]. The single cell voltage is modelled taking into account Nernst potential E_N as well as activation V_{Act} , ohmic V_{Ohm} and concentration V_{Con} losses:

$$V_C = E_N - V_{Act} - V_{Ohm} - V_{Con} \quad (8)$$

In accordance with the identified mesoscale parameters, the main polarization losses affected by Ni agglomeration are the activation [5] and ohmic losses [4]:

$$V_{Act} = \frac{RT_s}{F} \left[\sum_{i=a,c} \sinh^{-1} \left(\frac{J}{2J_{0,i}} \right) \right] \quad (9)$$

$$V_{Ohm} = \left(\frac{l_a}{\sigma_{Ni}} + \frac{l_e}{\sigma_{YSZ}} + \frac{l_c}{\sigma_{LSM}} \right) J \quad (10)$$

where the term R is the Universal Gas Constant (8.314 J/mol/K), F is the Faraday constant (96485 C/mol) and $J_{0,i}$ is the local exchange transfer at anode ($i = a$) and cathode ($i = c$) sides. Particularly, $J_{0,i}$ is expressed as [5]:

$$J_{0,i} = k_i \cdot \lambda_{TPB,i} \cdot \exp \left(-\frac{E_{Act,i}}{RT_s} \right) \prod_j \left(\frac{p_j}{p_{ref}} \right)^{\nu_j} \quad (11)$$

where k_i is a constant, $E_{Act,i}$ is the activation energy, p_{ref} is a reference pressure, p_j is the reactant/product partial pressure (H₂

and H₂O at anode side, O₂ at cathode side) and ν_j is an exponential coefficient (1 at anode side, 0.25 at cathode side).

III. RESULTS AND DISCUSSION

The results achieved with the presented model are reported in terms of voltage decay over time in Table I under different working conditions. It can be observed that the degradation increases with high temperature, low inlet pressure and high current density.

TABLE I
SOFC VOLTAGE DEGRADATION AT DIFFERENT OPERATING CONDITIONS

Current density of 0.5 A/cm ² and H ₂ partial pressure of 1 atm			
T _c [°C]	V(t=0 h) [V]	V(t=50'000 h) [V]	Degradation [%]
600	0.5024	0.5015	-0.18
700	0.7628	0.7554	-0.97
800	0.8958	0.8373	-6.53
Current density of 0.5 A/cm ² and temperature of 800°C			
p _{H₂} [atm]	V(t=0 h)	V(t=50'000 h)	Degradation [%]
1	0.8958	0.8373	-6.53
2	0.9441	0.8980	-4.82
3	0.9558	0.9125	-4.53
Current density of 0.5 A/cm ² and temperature of 800°C			
j [A/cm ²]	V(t=0 h)	V(t=50'000 h)	Degradation [%]
0.2	1.0088	0.9843	-2.43
0.5	0.8958	0.8373	-6.53
0.7	0.8314	0.7525	-9.49

IV. CONCLUSION

The developed algorithm couples micro-scale degradation models with macro-scale performance models to evaluate SOFC voltage degradation over time. The achieved results show that the degradation is mainly affected by high temperature and current density and low inlet reactant pressure. Such results can be used as guidelines to define AST protocols.

ACKNOWLEDGMENT

The research leading to these results has received funding from Fuel Cells and Hydrogen Joint Undertaking under Grant Agreement No. 825027 (AD ASTRA project). This Joint Undertaking receives support from the European Union's Horizon 2020 Research and Innovation Framework Programme and Hydrogen Europe.

REFERENCES

- [1] Gao et al., J. Pow. Sour. 255 (2014) 144-150. doi: 10.1016/j.jpowsour.2014.01.033.
- [2] Gallo et al., Energy Convers. Manag. 171 (2018) 1514-1528. doi: 10.1016/j.enconman.2018.06.062.
- [3] Chen et al., J. Pow. Sour. 191 (2009) 240-252. doi: 10.1016/j.jpowsour.2009.02.051.
- [4] Chen et al., J. Pow. Sour. 195 (2010) 6598-6610. doi: 10.1016/j.jpowsour.2010.04.065.
- [5] Ni et al., Energy Convers. Manag. 48 (2007) 1525-1535. doi: 10.1016/j.enconman.2006.11.016.

Impact of GDL modifications on the gas transport properties and PEMFC performances

F.Fouda-Onana*, J.Thery and J.Pauchet

* Univ. Grenoble Alpes F-3800 Grenoble, France

CEA, LITEN, DEHT, F-38054 Grenoble, France

Frederic.fouda-onana@cea.fr

Abstract – This work is reporting on the impact of MPL- and GDL-substrate modifications on PEMFC and it investigates routes for the detection of non-uniformities in GDL. MPL- and substrate were modified and tested in a small (2 cm²) fuel cell. MPL modifications were prepared by the removal of a controlled area of the microporous layer (MPL) while the subsurface non-uniformities were obtained by modifying the substrate before applying the MPL. It was found that the areas of removed MPL positively affect the cell performances at high current densities in wet conditions when the Gas diffusion layer (GDL) was placed on the cathode with a high stoichiometry ratio (25 for the anode and the cathode at 2 A/cm²). No influence was observed when the modified GDL was placed on the anode. Although modified GDL improved the cell performances in wet and mild-wet conditions, the hydrogen cross permeation was drastically increased and the performances in dry conditions were considerably reduced. In the follow-up of this work, substrate modifications will also be addressed and the importance of defects detection methodologies will be discussed.

Index Terms – GDL, defects, PEMFC, transport

I. INTRODUCTION

Proton Exchange Membrane Fuel Cells (PEMFC) are becoming an envisioned alternative for transportation and stationary applications. Unfortunately the wide development of this technology for mobility is presently circumscribed by a high fuel cell stack price (50 €/kW) and relatively low durability (3 500 h). In addition, the challenging compactness requirement for automotive applications leads fuel-cell makers to raise the power density. Consequently, the current power density has to be considerably increased (from 1 to 2 W/cm²) and such a high power demand requires high current densities. In such fuel cell operation conditions, it is well-known that the voltage drop is mainly caused by the mass transport limitation [1]. To overcome this problem, a lot of work has been done on the preparation of

the gas diffusion layer (GDL) [2-3]. This component which is composed by a macro porous substrate (MPS) and a micro porous layer (MPL), both hydrophobized, is supposed to supply the gas to the active layer, transport the electrons (until / out of) the active layer to the flow field, and drain the liquid water out of the active layer toward the flow fields. However, non-uniformities may appear on GDL during handling or production, such as an absence of MPL on the MPS surface or an inhomogeneous hydrophobic agent treatment. These defects, that can be detected visually, may affect the PEM Fuel cell performances and in this work, we propose to report on their influence on the performance of the PEM fuel cell. Additionally, non-uniformities that may be located in the core of the GDLs may also be detrimental to the performance. Flash IR thermography was applied to detect internal modifications and their influence on the FC performance will be discussed.

II. EXPERIMENTAL

GDL surface modifications were prepared in two ways, either by removal of the MPL by laser ablation or by using scotch tape. The substrate modifications were prepared by localized compression of the substrate before applying the MPL on the top of the substrate. Examples of defects GDL are shown in **Figure 1**. Selection of modified areas was done thanks to thermal diffusivity mapping. A flash excitation is applied to the GDLs backside, and the temperature profile evolution is recorded with a cam FLIR X6900. Thermal diffusivity is calculated from the resulting thermogram [4]

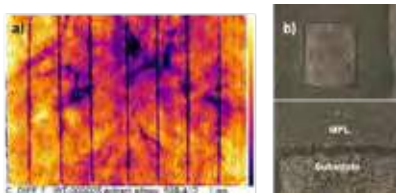


Figure 1 Modified GDL. a) Substrate modifications analyzed via thermal diffusimetry b) Surface modifications by MPL removal

Freudenberg GDL was used as the starting material in this study. A commercial GDL for the study of MPL modification and an experimental material grade for substrate modification. For the study of the impact of the modified GDL cathodes, we used a dedicated cell with a reduced active surface of 2 cm², for enhanced sensitivity to defects. A high stoichiometry ratio is applied in this case in order to be as homogenous as possible throughout the entire electrode surface (in order to avoid large oxygen concentration gradient between the inlet and the outlet of the channels).

In all the cases, the membrane electrode assembly (MEA) of the study was Gore PRIMEA^(R) (A510.1/M820.15/C510.4).

III. RESULTS AND DISCUSSION

Figure 2 shows IV curves in mild-wet conditions for cathode GDLs with variable MPL removal percentage. It is clear that the removal of MPL affects the performance, but positively at high current densities in these testing conditions. Such a trend was also observed at 100 % RH but, it is reversed order in dry conditions (20% RH).

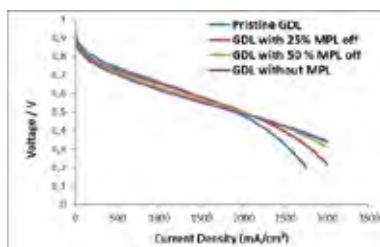


Figure 2. IV curves at 50% RH – 80°C -1.5 bar_g

It was already reported that modifications of the GDL helped the gas transport [5]. We also observed such a trend by analyzing the limiting current [6] of the various GDL in the different conditions. As shown on **Figure 3** the gas transport resistance is higher for the pristine GDL except in dry conditions. We assume that the dried ionomer of the catalyst layer could slow the gas transport, while in the other conditions the main limiting transport resistance takes place inside the GDL. Consequently, treated GDL positively affects the gas transport.

With respect to gas transport, the entire volume of GDLs is however involved. New strategies for non destructive control might hence help to better understand the performance of the fuel cell, and derive which non-uniformities should be classified as defects.

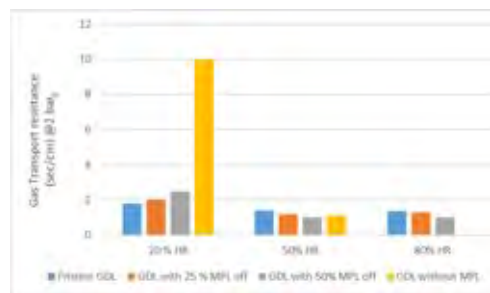


Figure 3. Oxygen transport resistance @ 2 bar_g

The IR flash method was applied to GDLs to verify that introduced modifications can be detected. The method will be discussed, and the influence of the thermal defects detected with respect to the performance will be presented.

IV. CONCLUSION

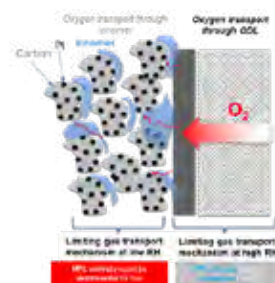


Figure 4. Sketch of gas transport dependence with RH.

Transport properties of the GDL has large influence on the PEM fuel cell performances. We have seen that depending on the humidity conditions, the gas transport could be limited by the diffusion through the ionomer in dry conditions or by the GDL properties in wet conditions.

In the latter case, the absence of the MPL improves the cell performance due to a lower diffusion path.

On the other hand, in dry conditions, the MPL helps to maintain the wetness of the active layer sufficiently to guarantee a better gas diffusion through the entire layer. This approach is summarized schematically on **Figure 4**.

The research leading to these results has received funding from the European Union's HORIZON 2020 program for the Fuel Cells and Hydrogen Joint Technology Initiative under Grant Agreement 736290 (DIGIMAN project).

References

- [1] Fuel Cell and Technology HandBook, Editors Gregor Hoogers, CRC Press, 2003 Chap 4.
- [2] S.Park *et al.* Journal of Power Sources 177 (2008) 457–463
- [3] S. Hirakata *et al.* Electrochimica Acta 120 (2014) 240–247
- [4] D.Mourand *et al.* Review of Scientific Instruments **69**, 1437 (1998)
- [5] J. Haußmann *et al.* Journal of Power Sources 239 (2013) 611–622
- [6] D. R. Baker *et al.* Journal of The Electrochemical Society, 156,9, (2009), B991-B100

Numerical Investigation of a Direct Ammonia Tubular Solid Oxide Fuel Cell in Comparison with Hydrogen using Different Supports

¹Mustafa Ilbas, Berre Kumuk, Molla Asmare Alemu,
Gazi University, Department of Energy Systems Engineering, Ankara, Turkey

Abstract- Nowadays, modern energy technologies are very essential to convert the available limited carbon-rich fuels and other green alternative energies into useful energy efficiently with an insignificant environmental impression. Amongst all kinds of power generation systems, SOFCs running with high temperatures are emerging as a frontrunner in chemical to electrical transformation efficiency, allows the engagement of all-embracing fuel varieties with negligible environmental impact. This study investigates the effect of ammonia usage in SOFC performance. Firstly, the use of ammonia and hydrogen in the electrolyte-supported SOFC (ES-SOFC) has been investigated. Then, the effects of using NH₃ in AS-SOFC, ES-SOFC and CS-SOFC on performance have been examined by using COMSOL software. As a result of the study performed, it is found that the NH₃ can be used in SOFC's and CS-SOFC shows better performance compared with ES-SOFC and the use of NH₃ as fuel for SOFCs is comparable to the use of H₂.

Keywords: Modeling, Tubular SOFC, Ammonia, Hydrogen

1. Introduction

In 1980 Vayenas and Co-workers have investigated the direct use of NH₃ in SOFC for nitric oxide and electricity production. NO is formed in platinum rhodium-based catalysts during ammonia decomposition due to the partial oxidation reaction. Yet, Wojcik[1] revealed that NO is not formed during NH₃ cracking when iron catalyst is employed at the anode side. Nowadays, numerous models of NH₃ powered SOFCs have been explored whereas more of them were concentrated on planar structures[2]–[9]. Yet, there are very few works on tubular SOFC using direct ammonia as a fuel[1], [8], [10]. Therefore, the central objective of this research is developing a numerical model for tubular SOFC fed with NH₃ as a green fuel in comparison with H₂.

2. Modeling

A 3D numerical model was developed to use NH₃ as the primary fuel in tubular SOFC using COMSOL 5.3a software according to the Batteries and Fuel Cells Module present in the program. The geometry used in the SOFC analysis is shown in Fig. 1 and the parameters are given in Table 1.



Fig.1. Schematic of the tubular SOFC model
Table1. Parameters used in SOFC structure

	Electrolyte-supported SOFC	Anode-supported SOFC	Cathode-supported SOFC
Dimension	Size	Size	Size
Anode thickness	50µm	100 µm	50 µm
Electrolyte thickness	100µm	50 µm	50 µm
Cathode thickness	50 µm	50 µm	100 µm
Inside diameter	2.1mm		
Cell length	30cm		

Table 2. Governing Equations

Continuity Equation	$\frac{\partial(\epsilon_{eff} \rho)}{\partial t} + \frac{\partial(\epsilon_{eff} \rho u_i)}{\partial x_i} = S_m$
Momentum Equation	$\frac{\partial(\rho_{eff} u_i)}{\partial t} + \frac{\partial(\rho_{eff} u_i u_j)}{\partial x_j} = -\frac{\partial P}{\partial x_i} + \frac{\partial}{\partial x_j} \left(\mu_{eff} \left(\frac{\partial u_i}{\partial x_j} + \frac{\partial u_j}{\partial x_i} \right) \right) + S_{\mu}$
Energy equation	$\frac{\partial(\rho C_p T)}{\partial t} + u_i \frac{\partial(\epsilon \rho C_p T)}{\partial x_i} = \frac{\partial}{\partial x_j} \left(k_{eff} \left(\frac{\partial T}{\partial x_j} + \frac{\partial T}{\partial x_i} \right) \right) + S_T$
Mass equation	$\frac{\partial(\rho C^k)}{\partial t} + \frac{\partial}{\partial x_i} (\gamma \rho u_i C^k) = \frac{\partial}{\partial x_i} \left[\rho D_{eff}^k \left(\frac{\partial C^k}{\partial x_j} + \frac{\partial C^k}{\partial x_i} \right) \right]$

3. Results and Discussions

This study presents the performance of tubular SOFC powered by ammonia in comparison with hydrogen. This model is validated with Wojcik[1] experimental results on tubular SOFC running with direct ammonia using Pt and Ag anode electrodes with and without iron bed packed catalyst at 800°C. As can be obviously seen from Fig.2, it revealed that the numerical polarization curve is agreeing with the experimental values. Therefore, the performance of NH₃ powered tubular SOFC provides an energetic opportunity to use NH₃ as an alternative green fuel for different applications using electrochemical devices soon. Different studies have been confirmed that CS NH₃ powered tubular SOFC has considerable performance over hydrogen under similar working environments. However, according to this study, AS-tubular SOFC powered with ammonia as the primary fuel is obtained as superior from ES- and has a comparable performance with CS- tubular SOFC.

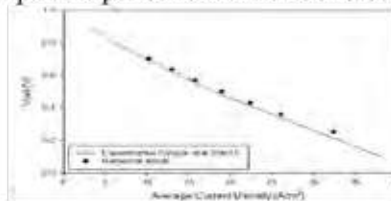


Fig.2. The polarization curve comparison between the numerical value and experimental results for model validation [1]

Fig. 3 (a) and (b) show the polarization curve and the power output as a function of voltage for ammonia as a direct fuel for electrolyte supported SOFC correspondingly. As can be seen from Fig.3, the ohmic losses are high and declining vertically when pure ammonia is fuelled at the anode and the air electrode is supplied with moist atmospheric air at 800°C which results in low power density. Therefore, to increase the power and current densities, either employed anode supported configuration with iron packed bed catalysts or cathode supported, increasing the active surface area of electrodes or working temperature, increasing the active surface area of electrodes or working temperature. This is because large surface areas encourage more reaction sites and the temperatures enhance the ion conductivity of the electrolyte, in turn, minimizes the ohmic loss. Moreover, depletion of oxygen is substantial compared with ammonia even if the mole fraction of ammonia is also decreased along the channel. Hence, the concentration of oxygen should be increased to enhance power generation.

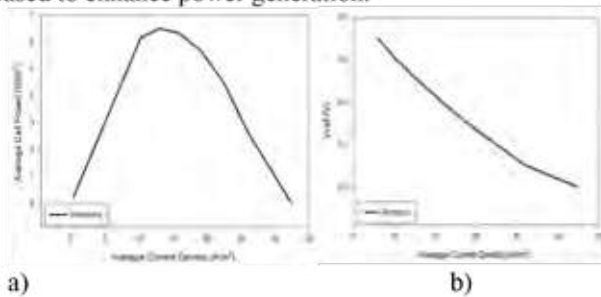


Fig. 3. The power output (a) and polarization curve (b) for fuelled ammonia. As well, Fig.4 proves the performance comparison between ammonia and hydrogen-fueled tubular SOFC in terms of polarization curve and power density working in similar conditions which confirms that ammonia has virtually the same performance that of hydrogen.

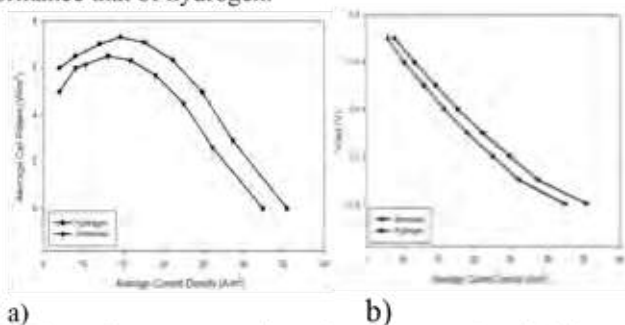


Fig. 4. The performance comparisons between ammonia and hydrogen-powered tubular electrolyte-supported SOFC. The performance of SOFC fuelled ammonia for different supported values is given in Fig. 5 (a) and the polarization curve is given in Fig. 5 (b).

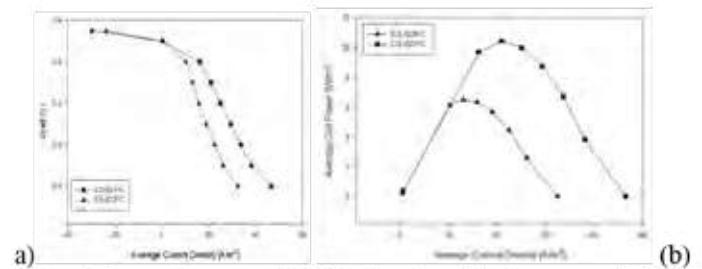


Fig. 5. The performance of SOFC (a) and polarization curve (b) fuelled ammonia for ES-SOFC, and CS-SOFC

4. Conclusions

According to this work, AS-tubular ammonia fuelled SOFC has high performance over ES- and has comparable performance with CS-tubular SOFC operating at similar conditions. This is because ohmic polarization is decreasing as electrolyte thickness becomes thinner. This is often thanks to tubular SOFCs powered with direct NH_3 has higher volumetric power density, mechanical stability, high thermal shocking resistance, and no sealing issue problems. Besides, the performance comparison between H_2 and NH_3 as fuel confirmed that NH_3 is a very promising alternative fuel for electrochemical devices. Among them, anode layer support is the most rampant solution due to mechanical stability, lower electrical losses over the CS- and ES cells. Besides, it is portable that can be worked everywhere when there is energy demand.

References

- [1] A. Wojcik, H. Middleton, I. Damopoulos, and J. Van Herle, "Ammonia as a fuel in solid oxide fuel cells," in *Journal of Power Sources*, 2003.
- [2] M. Ni, "Thermo-electrochemical modeling of ammonia-fueled solid oxide fuel cells considering ammonia thermal decomposition in the anode," *Int. J. Hydrogen Energy*, vol. 36, no. 4, pp. 3153–3166, 2011.
- [3] D. F. Cheddle, "Modelling of ammonia-fed solid oxide fuel cells," pp. 504–511, 2013.
- [4] M. Kishimoto, T. Kume, H. Iwai, and H. Yoshida, "Numerical Analysis of NH_3 -Fueled Planar SOFCs," *ECS Trans.*, 2017.
- [5] W. Y. Tan, "Numerical simulation on the performance of a solid oxide fuel cell with direct ammonia internal decomposition," *Energy Sources, Part A Recover. Util. Environ. Eff.*, vol. 36, no. 21, pp. 2410–2419, 2014.
- [6] W. C. Tan, H. Iwai, M. Kishimoto, G. Brus, J. S. Szymid, and H. Yoshida, "Numerical analysis on effect of aspect ratio of planar solid oxide fuel cell fueled with decomposed ammonia," *J. Power Sources*, 2018.
- [7] Q. A. Huang, R. Hui, B. Wang, and J. Zhang, "A review of AC impedance modeling and validation in SOFC diagnosis," *Electrochimica Acta*. 2007.
- [8] Z. Limin, C. You, Y. Weishen, and L. I. N. Liwu, "A Direct Ammonia Tubular Solid Oxide Fuel Cell," *Chinese J. Catal.*, vol. 28, no. 9, pp. 749–751, 2007.
- [9] S. Farhad and F. Hamdullahpur, "Conceptual design of a novel ammonia-fuelled portable solid oxide fuel cell system," *J. Power Sources*, vol. 195, no. 10, pp. 3084–3090, 2010.
- [10] S. A. Hajimolana and M. A. Hussain, "Dynamic modelling and sensitivity analysis of a tubular SOFC fuelled with NH_3 as a possible replacement for H_2 ," *Chem. Eng. Res. Des.*, vol. 90, no. 11, pp. 1871–1882, 2012.

SOLID OXIDE FUEL CELLS WITH NI-FREE ANODES FOR THE DIRECT UTILIZATION OF CARBONACEOUS FUELS AND SPECIAL BALANCE OF PLANT

B.J.M. Sarruf*, S.A. Venâncio*, A. Coralli*,
and P.E.V. de Miranda*

*The Hydrogen Laboratory – COPPE – Federal University of Rio de Janeiro, Rio de Janeiro, 21942-971, (Brazil)

Abstract – Solid oxide fuel cells, SOFC, as very efficient devices to perform the electrochemical conversion of hydrogen to electricity and heat may also admit the direct utilization of carbonaceous fuels such as hydrocarbons and alcohols, provided its catalyst be able to operate without carbon coking. This work presents our latest nickel-free anode developments for this purpose and its respective promising performances with lesser or none carbon formation, which was proved by scanning electron microscopy. In addition, a special configuration of balance of plant is also demonstrated.

Index Terms – Balance of plant, ethanol, nickel-free anodes, solid oxide fuel cells.

I. INTRODUCTION

The direct utilization of carbonaceous fuels in SOFCs is advantageous for eliminating the need for previous reforming and purification of the reformat gas, but cannot be attained with the use of Ni-based anodes and conventional balance of plants, due to the occurrence of coking and clogging with inactivation of the anode electrochemical activity and its mechanical failure, as well as the production and deposition of carbon within the piping of the fuel cell balance of plant, thereby interfering within the fuel stream. The purpose of the present study was to search for solutions to these problems, which involved the design and development of new Ni-free materials for SOFC anodes and to conceive new devices and their arrangement into a SOFC balance of plant for the direct utilization of carbonaceous fuels such as methane and ethanol.

The main challenges for the anode development consisted of attaining electrochemical activity for the fuel oxidation, while resisting to carbon coking under operational conditions with a material that should not contain nickel, and being able to keep mechanical compatibility with the other ceramic components of the fuel cell by possessing a similar coefficient of thermal expansion. This was accomplished by the development of two

sets of materials and their correspondent anodes, one based on ceria, alumina and YSZ to create a ceria-alumina-zirconium solid solution with the addition of copper for better electronic conductivity, and another one composed composed of ceria, Co_3O_4 and CuO . Their electrochemical performances and carbon resistance were explored in SOFC single cells, yielding satisfactory results for actual application.

The SOFC balance of plant was conceived to run on carbonaceous fuels under internal reforming regime. The components of the stand-alone system were purchased or specifically designed and fabricated. The stand-alone system was tested both with hydrogen and a fuel/water mixture, demonstrating the capability to start up, generate current and shut down to validate the choice of components.

It was concluded that the new materials, anodes and balance of plant were innovative and responded with adequate performance for the direct utilization of carbonaceous fuels in SOFC.

II. RESULTS

A. $\text{Cu}-(\text{Zr}_x\text{Ce}_{1-x}\text{Y}_{0.2}\text{O}_{2-\delta}-\text{Al}_2\text{O}_3)$ anode

Figure 1(a) and (b) presents, respectively, micrographs obtained by SEM with EDS mapping of the anode elements, and the potential and power density versus current density curves for SOFCs anode composed of the solid solution $\text{Zr}_{1-x}\text{Ce}_x\text{Y}_{0.2}\text{O}_{2-\delta}$. The SOFCs were operated with hydrogen or ethanol as fuels at 750, 800, 850, 900 and 950 °C. The cell has shown its best performance while operating with direct hydrogen, reaching a maximum power density of 455 mWcm^{-2} , compared to 261 mWcm^{-2} obtained when direct ethanol was the fuel stream. Previous evidence that mixing ceria-alumina based ceramic powder as SOFC anode precursors with 8YSZ was suitable for the direct use of ethanol with limited carbon coking was obtained [1].

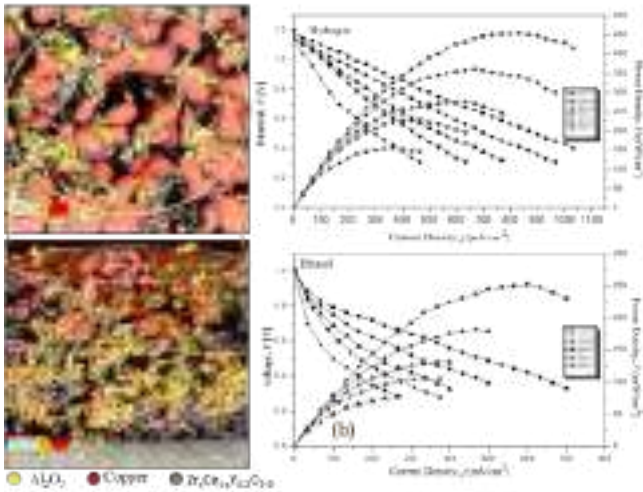


Fig. 1. (a) SEM micrographs, and (b) electrochemical performance of the Cu-(Zr_xCe_{1-x}Y_{0.2}O_{2-d}-Al₂O₃) anode.

B. CeO₂-Co-Cu anode

The ceria-based anode with cobalt and copper additions have shown promising electrochemical results as demonstrated in Figure 2a reaching power densities such as 550, 410 and 380 mWcm⁻² when hydrogen, methane and ethanol served as fuels directly to the anode cells, respectively. Details can be found elsewhere [2]. The anode was successfully sintered at low temperature (900°C) as seen in the micrograph of Figure 2b.

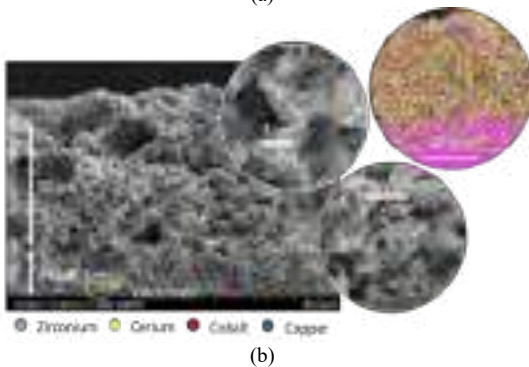
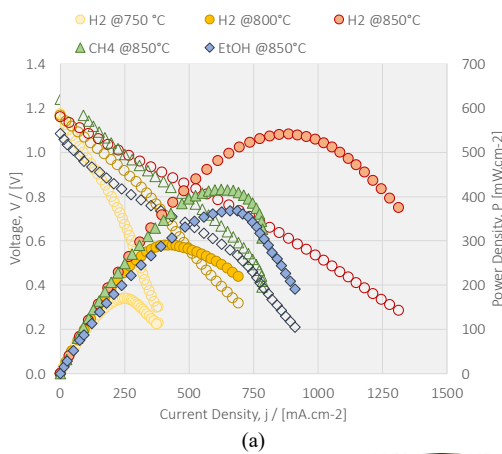


Fig. 2. (a) Electrochemical performance the CeO₂-Co-Cu anode, and (b) SEM micrographs with EDX mapping.

C. Stand-alone balance of plant for ethanol feeding

The balance of plant that was designed and fabricated was tested with both hydrogen and an ethanol/water mixture, demonstrating the ability to safely start-up, produce electrical power and shutdown while complying with the operating conditions required by the stack manufacturer [3]. The balance of plant efficiency was reasonable, both with H₂ (78.2 %) and with ethanol (73.5 %). Figure 3 shows the composition of the balance of plant power consumption.

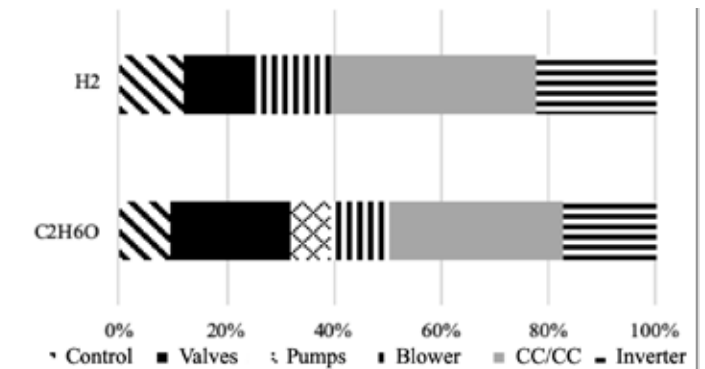


Fig. 3. Composition of Balance of Plant power consumption.

The components that show the higher potential for reducing the power consumption are the DC/DC converter, the solenoid valves and control system. Reducing the power consumption of the other BoP components appears rather difficult: in all cases, they are optimized, energy-efficient commercial devices, well suited for application in the stand-alone system.

III. CONCLUSIONS

The development of nickel-free anode for SOFCs has been demonstrated in our works since 2011 and currently we have been able to double the anode electrochemical performance while decreasing its operation temperature.

Remarkable improvements have been made ever since and the next steps will follow aiming at developing anode-supported cells and stacks to be integrated with the special balance of plant, composing an ethanol micro combined heat and power unit.

REFERENCES

- [1] S.A., Venâncio, P.E.V. de Miranda, Solid oxide fuel cell anode for the direct utilization of ethanol as a fuel. Scripta Materialia 2011; 65; 1065-1068.
- [2] B.J.M., Sarruf, J-E., Hong, R. Steinberger-Wilckens, Ceria-Co-Cu-based SOFC anode for direct utilisation of methane or ethanol as fuels, 2019 doi 10.1016/j.ijhydene.2019.04.075
- [3] A. Coralli, Balanço de planta para pilha a combustível de óxido sólido alimentada com etanol, PhD. thesis, COPPE/UFRJ, Rio de Janeiro, 2018.

INFLUENCE OF ENVIRONMENTAL FACTORS ON MFC-BASED SENSOR FOR WASTEWATER MONITORING

M. Tucci*, E. Barontini**, A. Schievano*, M. Papacchini***, A. Espinoza-Tofalos**, A. Franzetti**, P. Cristiani****.

* e-Bio Center, University of Milan, via Celoria 2, 20133 Milan, Italy

**University of Milan-Bicocca, Piazza della Scienza 1, 20126 Milan, Italy

***INAIL, Rome, Italy

****RSE – Ricerca sul Sistema Energetico S.p.A., via Rubattino, 54,
20100 Milano, Italy

Abstract - Microbial Fuel Cells (MFCs) are attracting increasing attention as multipurpose sensing devices, since the current generated by these devices is influenced by various environmental factors. Nevertheless, a better understanding of the separate contributions of such parameters is needed before implementation.

Herein, two different prototypes of MFCs have been built and tested in the denitrification tank of the wastewater treatment plant of Bresso-Niguarda (MI). Parameters such as light, temperature, organic and nitrate content have been continuously monitored and their impact on the current output has been evaluated. Moreover, the analysis of the microbial communities present on the electrodic biofilms underlined a strong influence of light and dissolved oxygen on the MFC performances.

Index Terms – Biosensor, MFC, BOD, wastewater

I. INTRODUCTION

As many recent studies show, the current produced by Microbial Fuel Cells (MFCs) can be employed as signal for wastewater monitoring. Indeed, several physical and chemical factors (e.g. BOD, dissolved oxygen, temperature etc.) have an influence on the microbial metabolism and thus on the cell output [1]. MFC-based sensors are particularly suitable for remote sites and diffuse environmental monitoring, as they do not require an external power source and need minimum maintenance. Nevertheless, real field studies are still scarce for this technology. An interesting setup used to this end consist in

floating MFCs that can be directly applied in the wastewater treatment plant. At the submerged anode occurs the oxidation of organic matter present in the wastewater, while oxygen is reduced on the surface of the air-cathode [2]. However, the understanding of the impact of environmental factors on the current output is essential to analyse the signal. For example, light variation can strongly influence the system output both directly and indirectly (e.g. temperature change, enhancement of photosynthetic organisms, etc.). The current fluctuations caused by the circadian cycle were recently reported for flat MFC of small geometry [3]. Moreover, the variability of the wastewater composition can strongly affect the MFCs performance, as the presence of recalcitrant organic compounds, dissolved oxygen, nitrates etc., can create disturbances in the current signal [4].

II. MATERIALS AND METHODS

Two prototypes of cells were built and tested directly in the denitrification tank of a wastewater treatment plant (Bresso-Niguarda, MI). The first type was made of a floating frame holding two identical carbon cloth electrodes 10 x 10 cm separated by a polypropylene felt. The anode was submerged in the wastewater while the cathode was facing air. In the second type, a terracotta cylinder served both as rigid structure and separator between the electrodes. The cylinder remained afloat perpendicularly to the wastewater surface by means of a floater. One end of the cylinder was sealed and the other was open to the atmospheric air. The anode consisted in a plain carbon cloth

electrode (5x15cm) fixed on the outer part of the tube, while the carbon cloth cathode (18x20cm) was placed inside the cylinder. A plastic lid on top of the tube protected the cathode from sunlight while allowing the passage of air. The voltage was continuously monitored across a resistance of 100 Ω and 500 Ω for the first and the second type respectively.

To continuously measure light irradiation and temperature, a pyranometer and a thermometer were installed by the MFCs. An automatic sampler was designed and built to collect wastewater sample from the denitrification tank. The samples were analysed in terms of soluble COD and nitrate using spectrophotometric techniques. Illumina sequencing of 16S gene was performed to analyse the bacterial communities present in the anodic and cathodic biofilms.

III. RESULTS AND DISCUSSION

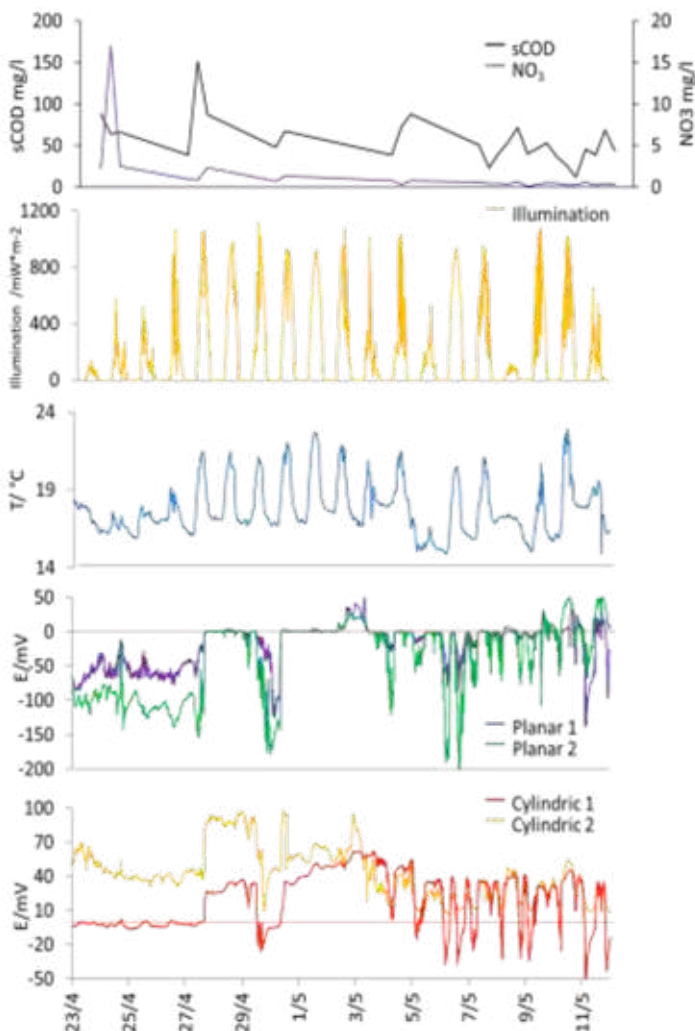


Fig. 1. Trends of light, temperature, cell potential, nitrate and sCOD content in the wastewater over 20 days between the months of April and May 2019. The voltage is obtained as average of three replicates.

Fig.1 shows the trends of light, temperature, cell potential, nitrate and sCOD content in the wastewater over 20 days. No clear correlation can be noted between the measured physical-chemical factors and voltage trends of the cells.

The voltage of the planar prototype is often below zero, meaning that the potential of the two electrodes becomes inverted: the electrode exposed to air works as anode and the submerged electrode behave as cathode. This phenomenon is probably linked to the presence of dissolved oxygen in the top first centimetres of wastewater. Indeed, the analysis of the microbial communities revealed the presence of aerobic strains on the anodes. Moreover, bacteria belonging to the family of *Geobacteraceae* were enriched on the cathodes. The cylindrical prototype was less affected by the inversion phenomenon, as their anodes were placed deeper in the wastewater. Overall the anodic biofilms were poorly differentiated from the bacterial pool found in the wastewater bulk, while the cathodes showed significant differences, with presence of photosynthetic strains on the air cathodes of the flat type.

IV. CONCLUSION

This study shows that understanding the impact of environmental factors on MFC-based sensors is crucial for real field applications. Further studies should focus on the methodology to discern between their different contributions in view of the implementation of MFC-based monitoring systems in wastewater treatment plants.

ACKNOWLEDGMENT

The authors acknowledge WeMake s.r.l. (MI), and Ing. Paolo Bonelli, for the construction of the automatic sampler, and Gruppo CAP Amiacque for the possibility to work in the wastewater treatment plant of Bresso-Niguarda.

REFERENCES

- [1] A. Larrosa-Guerrero, K. Scott, I.M. Head, F. Mateo, A. Ginesta, C. Godinez, Effect of temperature on the performance of microbial fuel cells, *Fuel*. 89 (2010) 3985–3994. doi:10.1016/j.fuel.2010.06.025.
- [2] M. Tucci, A. Goglio, A. Schievano, P. Cristiani, Floating mfc for BOD monitoring in real time: field test in a wastewater treatment plant, *Proc. 7th Eur. Fuel Cell Piero Lunghi Conf.* (2017).
- [3] E. Martinucci, F. Pizza, D. Perrino, A. Colombo, S.P. Trasatti, A. Lazzarini Barnabei, A. Liberale, P. Cristiani, Energy balance and microbial fuel cells experimentation at wastewater treatment plant Milano-Nosedo, *Int. J. Hydrogen Energy*. 40 (2015) 14683–14689. doi:10.1016/j.ijhydene.2015.08.100.
- [4] Y. Jiang, X. Yang, P. Liang, P. Liu, X. Huang, Microbial fuel cell sensors for water quality early warning systems: Fundamentals, signal resolution, optimization and future challenges, *Renew. Sustain. Energy Rev.* 81 (2018) 292–305. doi:10.1016/j.rser.2017.06.099.

DIFFERENT MODES OF THE HYDROGEN VALUE CHAIN – HOW FAR FROM LNG TO LIQUID H2?

G. Tchorck*, G. Roslonck**, W. Koziol*, S. Wójtowicz*
*University of Warsaw, Faculty of Management, Warsaw, Poland
**Polish Oil and Gas Company (PGNiG), Warsaw, Poland

Abstract – We try to find similarities and differences between two fuels value chain: liquid natural gas (LNG) and liquid hydrogen (LH2). While in some areas they are not comparable (e.g. different materials used in equipment as H₂ is more demanding because of its lower liquefaction temperature - 253 °C, and very high ability for permeation) we find important factor to claim that LNG can be seen as a transition fuel for hydrogen, mainly liquid. The two critical factors for the LH2 market development, in comparison to LNG, would be lowering H₂ production prices and increasing efficiency of the liquefaction process. When we divide the whole liquid H₂ stage into three parts, namely liquefaction, transport and regasification, the first one is the most energy consuming (currently about 10-kWh/kg and around 5kWh/kg in large scale plants in the future) and low (but improving) exergy efficiency. Transport and regasification consumes low share of the LH2 value unit.

Index Terms - LNG, liquefaction, hydrogen, value chain.

I. INTRODUCTION

Hydrogen seems to be an attractive alternative fuel which can make our planet more cleaner and energy systems more efficient. The reason is that H₂ can be obtained from many sources (also renewable energy), can be storage for a very long time and then can be transformed into electricity which is zero – emission process.

H₂, which the main drawbacks is very low energy density (in no pressure environment), can be stored and transported within a few value chains. The first one is compressed gaseous hydrogen with different pressure (about 200 bar for transportation, 350 or 700 bar for refueling vehicles). While compression process is energy consuming (up to 13-15% of the initial energy) it is easier and cheaper to store hydrogen with low pressure and at large scale, in salt cavern (used now for natural gas) after small infrastructure adjustment. The third form of hydrogen transport (medium ranges) and storage in gas pipelines with the share up to 10-20%, but it depends on local conditions. The fourth way is liquid organic hydrogen carrier (LOHC), which means that hydrogen is storage in chemically bound form like e.g. toluene or ammonia (see table 1). The fourth form is liquid hydrogen. Making hydrogen liquid

demands a lot of energy input (up to 20-35 % of the initial energy). While for the large scale and far distant H₂ delivery, ammonia would be cheaper, liquefaction process results in pure hydrogen, so include the costs of the purification processes.

TABLE I. HYDROGEN TRANSPORT METHODS AND COSTS

VEHICLE	STORAGE TYPE	INDICATIVE DISTANCES	DESCRIPTION/USE
Truck (Virtual pipelines)	Compression, liquefaction, ammonia	<1000km ¹⁰⁰	Transport of liquefied and compressed hydrogen as well as ammonia is available commercially. Ammonia is less likely as a hydrogen carrier here given the scale requirements and need to convert back to hydrogen for use. Higher pressures/liquefactions are typically used for trucking distances greater than 300km.
Rail	Compression, liquefaction, ammonia	>800-1100km ¹⁰⁰	As per trucks but for greater distances travelled
Pipeline	Compression	300-4000km	More likely to be used for (multi)regional distribution to multiple points/for intercity transmission
Ship	Ammonia, liquefaction	>4000km	Unlikely to use compression storage for shipping given cost of operation, distance and lower hydrogen density. Likely vehicle for export.
METHOD	COMPRESSION (\$/km H ₂) 430 bar	LIQUEFICATION (\$/km H ₂)	AMMONIA (\$/km NH ₃)
Truck	0.33	0.31	0.33
Rail	0.35	0.28	0.04
Shipping	0.52	0.09 ¹⁰⁰	0.03

Source: National Hydrogen Roadmap, www.cisro.au

Because of its high energy density in relation to mass unit, liquid hydrogen can be attractive form of energy storage and the way in which H₂ is transported. Literature confirms that LH₂ at 1 bar pressure contains about four times the energy per volume unit than does compressed H₂ at 250 bar and almost three times as much than for 350 bar. Thanks to those features, liquid H₂ can be transported on long distances and at large scale.

II. LNG AND LH2 VALUE CHAINS

While generally the structure of value chains for LNG and LH₂ should be roughly similar – see figure 1, cost of LNG will be still lower than hydrogen (especially green, within the next five to ten years). The second critical chain elements which will be more costly in the case of H₂ is liquefaction. When comparing hydrogen with methane, we have to keep in mind that nowadays the cheapest and the most common source of hydrogen which is steam reforming of methane from natural gas:



The stoichiometry of methane: hydrogen is a ratio of 1: 4 and we get four moles of hydrogen from one mole of methane and produce excess hydrogen.

	Production	Liquefaction	Transport	Regasificat.	Distribution	End-use
LNG	Steam gas reforming, autothermal gasification	LNG liquefaction	Large scale shipping	Small scale liquefaction	Large scale liquefaction	Highly heating energy demands
Liquid H ₂	H ₂ electrolysis, catalytic and gasification	H ₂ liquefaction	Large scale shipping	LNG liquefaction (reverse)	Large scale liquefaction	Highly heating energy demands
Similarities	H ₂ production mainly from natural gas	Energy intensive (LNG: ~10°C to 162°C, H ₂ : 0°C to -253°C) liquefaction processes	Large scale shipping	Small scale liquefaction and production	Large scale liquefaction (reverse)	Highly heating energy demands
Differences	Steam gas reforming, autothermal gasification, CO ₂ capture	H ₂ electrolysis, catalytic and gasification, CO ₂ capture	H ₂ liquefaction, shipping, storage, distribution	H ₂ liquefaction, shipping, storage, distribution	H ₂ liquefaction, shipping, storage, distribution	H ₂ liquefaction, shipping, storage, distribution

Fig.1. LNG and LH₂ value chain, Source: own compilation

In fact, the "clean" reaction of steam reforming applied in chemical industry is as follows:



The product a mixture of carbon monoxide and hydrogen in a stoichiometric ratio of 1: 3 is a typical syngas (synthesis gas used for syntheses - for this reason, Poland is one of the largest producers of hydrogen in the world, but it is hydrogen for synthesis and is not available in trade).

There is a very large mass difference between methane (16u) and hydrogen (2u). As a result of reaction (1), taking into account stoichiometry, to get 1kg of hydrogen we need to reform 2kg of methane, but unfortunately we release 5.5kg of carbon dioxide into the atmosphere. It is true that with 2 kg of methane we could get 2kg*50MJ/kg, i.e. about 100MJ, and burning 1kg of hydrogen, we can get 1kg*120MJ/kg or 120 MJ. So we benefit about 20% profit, but taking into account the cost of reforming, this method is difficult to defend, because CO₂ sequestration should be taken into account, which is difficult and expensive.

In chemistry, the best unit for comparison that does not introduce these disproportions in molecular weights is mole. We calculated how much energy would be needed to cool 1 mole of hydrogen at normal temperature (20°C) to the liquid state (-253 °C) and the process of changing the phase from gas to liquid and the same for 1mole of methane to cool to - 162°C (we took into account the heat of condensation of both gases). The calculations are for isochoric conditions, i.e. in constant volume. In industrial conditions, we do not change the volume of reactors, but the pressure of the reactants changes (depending on whether we take a constant volume or a constant pressure, we have different specific heat for gases, so-called C_p and C_v (we assumed constant volumes and took C_v into account).

Theoretically, in the case of liquefaction of a mole of hydrogen 8.6kJ of energy that must be delivered, while in the

case of liquefaction of a methane mole it is 17.0kJ. Indeed, for 1 mole of hydrogen it is twice less than for a mole of methane. But, stoichiometry is equal to 1: 4, that is, to liquefy hydrogen, which is formed from 1 mole of methane, unfortunately we must now provide twice as much energy. If we wanted to use these two fuels, here we will get the same hydrogen surplus about 20%, but in total we lose energy.

To use LH₂ and LNG as a fuel, it needs to be gasified and also demands energy. Evaporation energy is not taken into account because it is similar in mass (444kJ/kg for hydrogen and 577kJ/kg for methane) and the process is not very energy-consuming. What cannot be neglected, after evaporation the gas has a very low temperature and to transfer it further, e.g. through a gas meter, it must be heated. At this stage we will use more energy for hydrogen, because it is colder than for methane in liquid state.

Based on the above we would get the impression that LH₂ is in worse position comparing to LNG. It is true if we consider hydrogen from reforming, but, the world goes in different directions - i.e., technologies for producing hydrogen from other sources are developing and with large scale production plants the green hydrogen should compete with fossil fuels within the next 10-20 years. There are a few big projects aiming to produce liquid hydrogen from different sources like coal gasification with CCS (Australian-Japanese *Hystra* project) or Norwegian *Hyper* project based on renewables and fossil fuels.

III Conclusions

Analyzing differences and similarities, the LH₂ chain may appear to be "built" on the LNG chain. This is due to current technical and technological similarities primarily in the field of production and transport, but also gasification and regasification. Lower energy density forces the search for cost-effectiveness of using LH₂ in relation to LNG in the entire value chain. Currently widespread production methods of LH₂, their technical and economic effectiveness and already visible in the analysis of the value chain conditions of gasification and regasification and H₂ transport indicate that although this is a very promising source of energy in the future, today it will be difficult for it to compete with LNG. The conditions for the dissemination of LH₂ will be lowering the costs of H₂ due to wide scale production methods, related to the popularization of hydrogen energy storage and use. At the same time, technological changes in the scope of hydrogen transport costs will be significant, including the use of the superconducting effect of many materials at the temperature of liquid hydrogen. As a consequence, LNG turns out to be an interesting temporary alternative in the process of energy transformation. However, at present it is difficult to assess how long the transitional period with LNG will be.

REFERENCES

- [1] Berstad, D.O., Stang, J.H. and Nekså, P., 2009. Comparison criteria for large-scale hydrogen liquefaction processes. *International journal of hydrogen energy*, 34(3), pp.1560-1568
- [2] *National Hydrogen Roadmap*, www.cisro.au

HYSCHOOLS: HYDROGEN IN SCHOOLS

A Gaffar*, L J Currid *, G. Cinti**, F. Mondi**, C. Barchiesi***
*Manchester Metropolitan University, Faculty of Science and Engineering,
All Saints Campus, Oxford Road, Manchester (UK)
** Università degli Studi di Perugia, Engineering Department, via Duranti
93 – 06100 Perugia, (Italy)
*** Regione Abruzzo, piazza Vittorio Emanuele Secondo Pescara, (Italy)

Abstract – The HySchools project is an educational project financed under the Erasmus+ program by the European Union with the aim of introducing and increasing Hydrogen knowledge in secondary schools. Hydrogen based technology is, in fact, one of the major players in the desired transition from a carbon based society to a sustainable development and a pollution-free future. Spreading the knowledge of high-efficiency, low-emission technologies such as the ones based on hydrogen is of paramount importance and should be introduced to new generations in an educational environment as soon as possible. In this task, teachers are the most important and valuable players. As a first step, the project will propose a survey to secondary school teachers to ask them how much they know about hydrogen and hydrogen based technology and what they think about it. Then, in the second phase, teachers will receive educational material produced by universities to deepen their understanding about this topic. Based on this educational material, teachers will take part in events where, in collaboration with a facilitator and experts in the subject, they will structure the backbone of future lessons for their pupils, that will subsequently be inserted into future teaching programs.

Index Terms – Education, hydrogen, teacher, resources, schools

I. INTRODUCTION

The need for new energy options is no secret. Across the globe, movements towards sustainable energy production are preparing for a change of policy towards a greener economy and energy production. The big challenge for the 21st Century is how we can create a sustainable future for young people while meeting demand for energy. Hydrogen plays a major role in creating green and emission-free energy for the future and hydrogen fuel cells are a viable way of addressing the decarbonising strategies of countries across the world. To ensure the research and technical development continues to

make hydrogen fuel cells a preferred leader in future energy generation, a number of fundamental issues need to be resolved. This project focuses on what we believe to be the critical factor: skills shortage. To cover this gap school teachers were targeted since, compared to other groups such as policy makers, teachers are involved in school education and can engage students into hydrogen technologies.

HySchools is a consortium of eight partners led by the Fuel Cell Innovation Centre at Manchester Metropolitan University (UK), with the University of Lorraine (FR), Technifutur (BE), University of Franche Comte (FR), University of Perugia (IT), Patras Science Park (GR), Maramures Energy Agency (RO), University of Perugia/Abruzzo Region (IT). Together partners have already undertaken research to elicit the needs of teachers across Europe. The results from this research have informed the development of resources to address teachers' needs and build the confidence of teachers to bring this exciting and fundamental topic into the curriculum. From October 2019, pupils and staff from schools across Europe will test out the resources developed. The feedback from these demonstrations and testing events will prove invaluable to further adapt and tailor the resources to the needs of teachers.

The end of the project in February 2020 will see the resources rolled out across the partner countries for distribution to schools. The unique aspect of this project is that the resources created will be free to access worldwide, ensuring that everyone has access to high quality materials and resources to enhance knowledge and skills.

At its heart, the project aims to support stakeholders in engaging with the future workforce. The HySchools partners believe that this kind of cross-sector, interdisciplinary approach is essential to developing the future of hydrogen energy. The

THE ASSEMBLY OF THE ANODIC MICROBIAL COMMUNITY IN MICROBIAL FUEL CELLS IS CONTROLLED BY INCREMENTAL CHANGES IN THE EXTERNAL LOAD CONTROL

Douglas M. Hodgson ^{1*}, Sonal Dahale ¹, André Grüning ^{2†}
and Claudio Avignone Rossa ^{1‡}

¹ Department of Microbial Sciences, University of Surrey,
Guildford GU2 7XH, United Kingdom

² Department of Computer Sciences, University of Surrey,
Guildford GU2 7XH, United Kingdom

Abstract - We studied how incremental increases in external resistance across a wide load range affect the structure and metabolism of anodic microbial communities, and their bioelectrical performance. MFCs inoculated with a natural microbial community and fed with a complex medium were run at increasing external resistances (250 to 100 000 Ω). The maximum voltage and peak power increased with increasing loads in a non-linear relationship, suggesting a threshold at which the external load stops affecting the output. The highest and lowest peak power were $0.49\text{W}\cdot\text{m}^{-3}$ (at $40\text{k}\Omega$) and $0.23\text{W}\cdot\text{m}^{-3}$ (at 250Ω), respectively.

The effect of the load on the community was determined by 16S rRNA gene sequencing. Ten genera represented 96.5% of all genera identified, with 4 of them being 82% the total. The abundance of anaerobic respirators decreased with increasing resistances: 81.7% at 250Ω to 27.6% at $100\text{k}\Omega$, indicating that low resistances impart a selective advantage to electrogenic species over fermentative species.

The increase in diversity with the load suggests that higher resistances require the cooperation of multiple species to convert chemical energy into bioelectrical output. A low resistance is easier to use as a terminal electron acceptor, favouring a less diverse community of specialised exoelectrogens.

The correlation between anodic microbial consortia structure with resistance demonstrates that microbial community assembly can be controlled by manipulation of external load. This is of importance for optimization of MFCs and for the thermodynamic control of complex living systems.

Index Terms – Anodic biofilm, External load, Microbial Communities, Microbial Fuel Cells,

I. INTRODUCTION

In Microbial Fuel Cells (MFCs), microbial species oxidise organic feedstocks using the anode as terminal electron acceptor (TEA). Complex microbial communities show a strong correlation between their metabolic function and the electrical output. In general, communities consist of fermenters (F), anaerobic respirators (AR, able to oxidise fermentation products), and species with variable metabolism. ARs transfer electrons to the anode, which move through an external circuit to the cathode, generating an electrical current. Changes in external resistance affect the capability for electron transfer, causing changes in abundance and diversity of the community. This property can be used to control the performance of the community. We determined the effect of incremental increases in external resistance on the dynamics and bioelectrical performance of a natural microbial community inoculated in MFCs.

Materials And Methods. MFC design and operation. The design of the MFCs and the preparation of the DDGS medium and the inoculum were as previously described [1]. MFCs were fed with 10% DDGS medium at a flow rate of $6.35\text{ ml}\cdot\text{h}^{-1}$ (hydraulic retention time, HRT: 20 h). MFCs were acclimatized for 48h, and run at increasing external resistances (250 to 100 000 Ω) for 4 HRT at each load. **Electrochemical measurements.** Voltage was monitored continuously and the electrical current and electrical power calculated at each load. Polarisation curves were carried out for each MFC after at least 80h at the set external resistance. **Microbial community analysis.** DNA was extracted from the anode biofilm using FastDNA Spin Kit for Soil (MP Biomedicals, UK) and analysed as described elsewhere [1]. **Metabolite analysis.** Metabolic analysis of the supernatants was performed as described previously [1].

* Current address: BASF SE, Carl-Bosch-Strasse 38, 67056 Ludwigshafen am Rhein, Germany

† Current address: Faculty of Electrical Engineering and Computer Science, University of Applied Sciences Stralsund, 18435 Stralsund, Germany

‡ Corresponding author; e-mail: c.avignone-rossa@surrey.ac.uk

II. RESULTS

Effect of external resistance on MFC performance. Fig 1 shows that the maximum voltage and the peak power attained in the MFCs increased with increasing loads. The non-linear behavior indicates a level at which external load stops having a positive effect on output. The highest peak power ($0.49 \pm 0.02 \text{ W.m}^{-3}$) was achieved at an external resistance of $40 \text{ k}\Omega$, while the lowest peak power ($0.23 \pm 0.04 \text{ W.m}^{-3}$) was observed at 250Ω . A statistically significant relationship exists between peak power and open circuit voltage (Table 1).

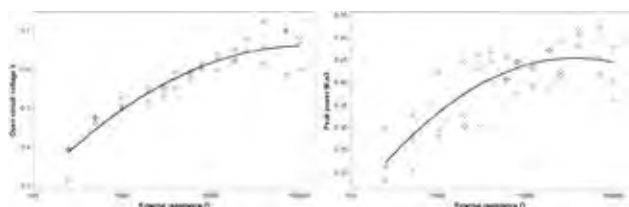


FIGURE 1. Maximum voltage and peak power observed in MFCs under different external loads.

Table 1. Regression analysis between external load and peak power and open circuit voltage.

x variable	y variable	n	R	R-squared %	P
Peak power	Log external resistance	42	-	66.59 - quadratic model	<0.001*
	Open circuit voltage	42	0.77	59.14 - linear model	<0.001*
Log resistance	Open circuit voltage	42	-	89.09 - quadratic model	<0.001*

Anodic biofilm composition. The impact of changing external load on the biofilm community was determined by 16S rRNA genes sequencing. Ten genera made up 96.5% of the community, and the top four made up 82% of all genera observed across the 14 external resistances (Table 1).

Table 2. The 10 most abundant genera in the anodic biofilms, and their assigned metabolism

Genus	Abundance	Class
<i>Citrobacter</i>	32.5%	AR
<i>Clostridium</i>	20.1%	F
<i>Stenotrophomonas</i>	15.9%	AR
<i>Pseudomonas</i>	13.4%	AR
<i>Lachnospiracea</i>	4.3%	F
<i>Eisenbergiella</i>	2.9%	F
<i>Achromobacter</i>	2.5%	AR
<i>Myroides</i>	1.8%	AR
<i>Anaerosporebacter</i>	1.6%	F
<i>Rhizobium</i>	1.6%	AR

Each genus was assigned a metabolic class with respect to terminal electron acceptors, according to their typical metabolism: Fermenters (F), which use intracellular metabolites as EAs, or anaerobic respirators (AR), able to fully oxidize fermentation products using a terminal EA other than O_2 . The dominant AR in the anodic biofilm (*Citrobacter*, *Stenotrophomonas* and *Pseudomonas*) are genera previously identified as exoelectrogenic [2] [3]. The relative abundance of AR in each biofilm decreased significantly with increasing external resistance (Figure 2, Table 2), from $81.7 \pm 2.3\%$ at 250Ω to $27.6 \pm 7.7\%$ at $100 \text{ k}\Omega$. Low external resistances cause

higher anode potentials, resulting in more free energy to the anodophilic community, thus imparting a selective advantage to electrogenic species. Increasing external resistances may caused a metabolic shift from respiratory to fermentative [4], and theoretical models suggest that higher external resistances favour strictly anaerobic species [5] [6].

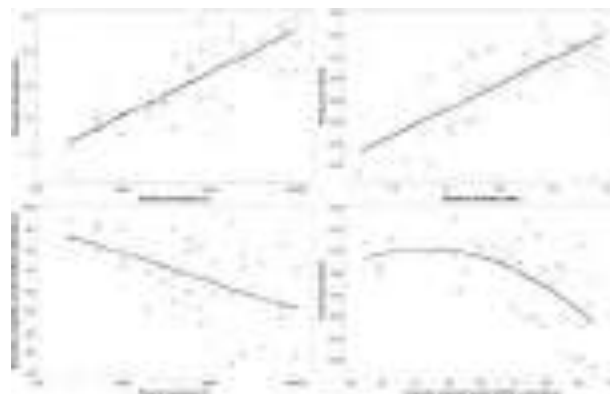


FIGURE 2. Effect of the external resistance on the relative abundance of anaerobic respirators in anodic biofilms.

Table 2. Regression analysis between electrochemical parameters and the diversity and abundance of the anodic biofilms under different external loads

variable	variable	n	R	R-squared %	P
Shannon diversity index	Peak power	40	0.80	64.12 - linear model	<0.001*
	Open circuit voltage	40	0.28	7.91 - linear model	0.079
	Log resistance	40	0.83	69.72 - linear model	<0.001*
Anaerobic respirator % abundance	Peak power	40	-	36.60 - quadratic model	<0.001*
	Open circuit voltage	40	-	23.94 - quadratic model	0.006*
	Log resistance	40	-0.55	30.34 - linear model	<0.001*

Peak power shows a significantly negative correlation with the relative abundance of AR. Previous work has demonstrated that electrogenic bacteria produce higher yields when oxidising the products of fermentative metabolism [7], indicating that the breakdown of complex substrates requires the cooperation of both F and AR [1]. Figure 2 and Table 2 show that diversity increases with increasing resistances.

III. CONCLUSION

This report demonstrates a relationship between external resistance and community diversity: Higher external resistances require the cooperation of multiple species to drive the conversion of chemical energy to bioelectrical output. Low external resistances are easier to use as terminal EA, so a less diverse community of specialised exoelectrogens can proliferate. Biofilm structure and composition can be controlled by adjusting external resistance, allowing optimal performance of complex systems.

ACKNOWLEDGMENT

DMH, SD and CAR were supported by grant BB/J01916X/1 from the Biotechnology and Biological Sciences Research Council (BBSRC, UK).

REFERENCES

- [1] Hodgson et al (2016). *Front. Microbiol.* **7**:699; [2] Xu and Liu (2011) *J Appl Microbiol* **111**, 1108 – 1115; [3] Venkidusamy and Megharaj (2016) *Front. Microbiol.* **7**:1965; [4] Rismani-Yazdi et al (2011) *Biores Technol* **102**, 278–283; [5] Picioreanu et al (2008) *Water Sci Technol* **57**, 965 – 971; [6] Picioreanu et al (2007) *Water Res* **41**, 2921–2940; [7] Kiely et al (2011) *Biores Technol* **102**, 388–394

TAILORED CATALYST LAYER AND MICRO-POROUS LAYER POROSITY AND THE EFFECT ON THE PERFORMANCE AND WATER CONTENT IN PEMFC.

A. Mohseninia*, D. Kartouzian *, H. Markötter**, F. Wilhelm*, J. Scholta* and I. Manke**

* Zentrum für Sonnenenergie- und Wasserstoff-Forschung Baden-Württemberg (ZSW), Helmholtzstraße 8, 89081 Ulm, Germany

** Helmholtz-Zentrum Berlin, Hahn-Meitner-Platz 1, 14109 Berlin, Germany

In this work, we present a study on the effect of the porosity of cathode microporous layer (MPL-C) and catalyst layers (CL) on the water distribution and performance of PEMFC. Pore former polymers are used to introduce macropores inside catalyst layers and cathode MPL. Internally-developed MEAs and MPLs with different degrees of porosity are implemented in a specially designed fuel cell with an active area of 8 cm² to perform high resolution neutron tomography measurements. Neutron tomography is used to investigate the water content and distribution inside the operating fuel cells under humid conditions. The evaluation of water density reveals that the cells containing more porous layers decreased the accumulation of water beneath channels while it increased the water content beneath the lands. A performance improvement is observed for the cells containing additional macropores at the mass transport region.

In Operando Neutron Tomography, Perforation, Polymer Electrolyte Membrane Fuel Cells (PEMFCs), Water Management.

I. INTRODUCTION

In polymer electrolyte membrane fuel cells (PEMFCs) water management plays a crucial role. From one hand, the membrane should be fully humidified to enable proton conductivity. On the other hand, excess water accumulation inside the catalyst layer, gas diffusion layers and the channels of the flow fields plates causes flooding which consequently reduces the power density. Numerous studies have investigated the effect of microstructure properties of catalyst layer and gas diffusion layers on water balance and performance of PEMFC. Neutron imaging has been proven to be a powerful tool to visualize liquid water inside the components of PEMFC. Neutron beam is highly sensitive to light atoms like hydrogen whereas metals and graphite plates show lower interactions with neutrons and therefore tend to be rather transparent to it.

II. EXPERIMENTAL

The neutron tomography is carried out at the neutron imaging

instrument Conrad (V7) at the research reactor BER II at the Helmholtz-Zentrum Berlin, Germany. With the optics used, an imaging field of view of (28×13; w×h) mm² with a pixel size of 13 μm is achieved. Membrane electrode assemblies (MEAs) and MPLs were internally-developed at Center for Solar Energy and Hydrogen Research Baden-Württemberg (ZSW). The detail procedure for preparation of reference catalyst layer and MPL-C is provided in Ref [1-2]. The porosity of electrodes are modified by utilization of polystyrene particles (PS) as pore former polymer (diameter of 500 nm) and then removing it by ethyl acetate to obtain the desired pores inside catalyst layers. The catalyst layers have a Platinum loading of 0.3 mg cm⁻² both on anode and cathode side and are coated on a Nafion™ membrane NR-212. The content of polystyrene particles is 5 and 10 wt.% with respect to dry ink. For preparing the perforated MPLs monodisperse poly methyl methacrylate (PMMA) particles with an average diameter of 30 μm are utilized as pore former. Cathode MPLs with 10 Vol.% PMMA are coated on Sigracet® 29BA. These particles are removed by thermal decomposition to create the macropores. Miniature single PEMFCs with an active area of 8 cm² are used to perform tomography measurements. The fuel cells are operated at RH=120%, T=50°C, P_c=60 kPa, P_a=70 kPa (representing a humid operating condition) prior to tomography imaging.

III. RESULTS

Prior to tomography imaging, the cells are operated for 30 minutes at the mentioned operating points to reach the steady-state conditions and then the gas flows and current are cut off. The cells are investigated with the neutron beam of a region centered in the middle of the vertical cell extension. The water thickness is calculated according to Lambert Beer's law within mm-scale. Water density distribution of the cells containing the perforated catalyst layers (reference, 5 and 10 wt.% PS) and

cathode MPL (reference and 10 Vol.% PMMA) beneath land and channel regions are depicted in Figure 1 a-b.

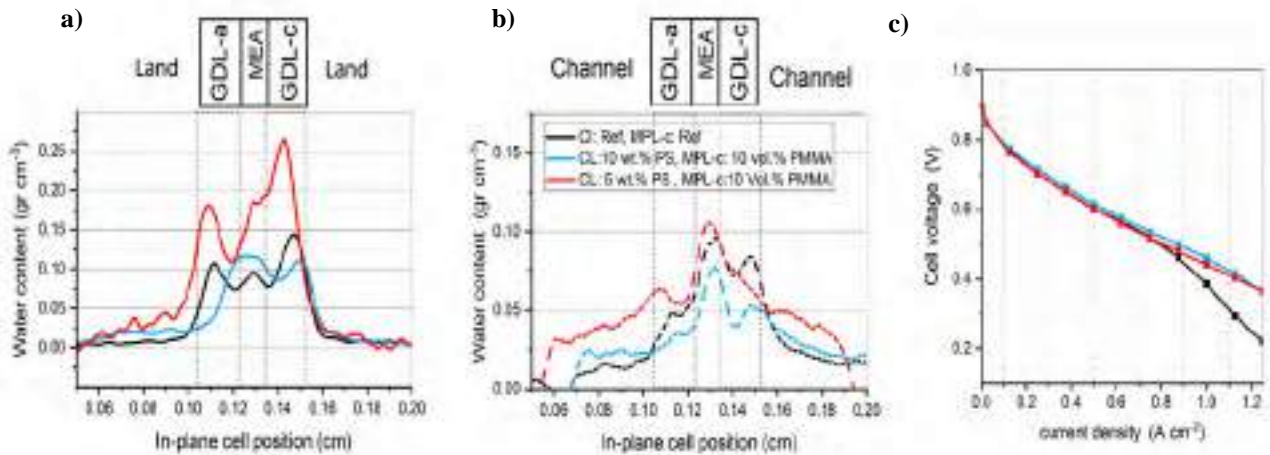


Fig. 1. Plots of water density distribution under lands (a) and channels (b) at current density=1 A/cm². The regions under Polarization curve at relative humidity = 120 % (c). The cells were operated at RH=120%, T=50°C, P_c=60 kPa, P_a=70 kPa

The Areas associated to the each specific component of the cell including MEA, anode and cathode gas diffusion layers (GDL-a and GDL-c), channel and land regions are separated by vertical lines in the in-plane direction. Under the land regions, the overall water content is higher than the channel regions. Beneath the channels, the cells with perforated layers decreased the water content especially in the cathodic gas diffusion region (GDL-C) compared to the reference (Ref) material. Moreover, the peak of water accumulation exist in the MEA region. Under the land regions, an increase of the water content is observed for the perforated layers. The peak of water is mainly located within the intersection of GDL and Land region. Polarization curves are obtained at relative humidity (RH) of 120% to represent humid conditions. Performance improvement in the mass transport region is observed for the cell containing the perforated layers (Fig1-c).

This observations can be explained by higher water filling degree of the introduced macropores within CL and MPL-C, as the capillary pressure decreases for bigger pores. On the other hand, the air flow in the channels regions hinders higher water saturation within the adjacent GDLs explaining lower water accumulation compared to the land regions. These results reveal that while the macropores are preferentially filled with liquid water, the small pores act as effective oxygen transport pathways.

IV. CONCLUSION

High-resolution neutron tomography is used to study the effect of catalyst layer and cathode MPL perforation on the liquid water content and distribution in PEM fuel cell. Pore former polymers are utilized to create macro pore inside catalyst layer and MPLs. The local water distribution under land and channel

regions are quantified. Higher water content is identified for the areas under lands than under the channels. With the presence of more porous materials, the amount of water accumulated beneath the land regions is increased. Performance increase at high current density regions is observed for the more porous layers at humid conditions (RH 120%).

We assign this to the improved mechanism of two-phase flow transport of oxygen and liquid water, where the oxygen transport occurs within the smaller pores and water is preferably transported via bigger pores.

ACKNOWLEDGMENT

Financial support by the German Federal Ministry of Transport and Digital Infrastructure (grant numbers 03B10103A / 031310103A2) is gratefully acknowledged.

REFERENCES

- [1] Mohseninia, A., Kartouzian, D., Markötter, H., Ince, U., Manke, I., Scholta, J., Neutron Radiographic Investigations on the Effect of Hydrophobicity Gradients within MPL and MEA on Liquid Water Distribution and Transport in PEMFCs, ECS Transactions, Volume 85 (13), 2018, PP.1013–1021
- [2] Simon, C., Kartouzian, D., Müller, D., Wilhelm, F., Gasteiger, H., Impact of Microporous Layer Pore Properties on Liquid Water Transport in PEM Fuel Cells: Carbon Black Type and Perforation, Journal of The Electrochemical Society, Volume 164 (14), 2017, Pages 668-679/1892, F1697–F1711.

COPPER-ADAPTED BIOFILMS FOR Cu^{2+} IONS MONITORING WITH MICROBIAL FUEL CELL BASED BIOSENSORS

Abdelghani GHANAM^{1,2}, Aziz AMINE², Hasna MOHAMMADI², François BURET¹ and Naoufel HADDOUR¹

¹ Laboratoire Ampère, École Centrale de Lyon 36 avenue Guy de Collongue 69134 Écully Cedex – France

² Laboratoire Génie des Procédés et Environnement, équipe analyse chimiques et biocapteurs, Faculté des Sciences et Techniques B.P. 146, Mohammedia, Université Hassan II de Casablanca – Maroc

Abstract - In this work, a new configuration of a single chamber cube biosensor based on Microbial fuel cell (MFC) has been developed for the real-time detection of Cu^{2+} ions in water. Preliminary results show the possibility of specific detection of Cu^{2+} ions using copper-adapted biofilms formed on flow-through anodes. MFC sensors based on copper-adapted and nonadapted biofilms, have been challenged with analytes containing a Cu^{2+} concentration selected according to WHO guideline value for copper in drinking water (2 mg.L^{-1}). Copper ions led to an increase of output current of MFCs based on copper-adapted biofilms, while a no response obtained on MFC based on nonadapted biofilms. Using pollutant-adapted biofilms could be a new approach to improve the specificity of MFC-based biosensors.

Keywords: Adapted-biofilms, Biosensor, Copper ions, Microbial fuel cell, Real-time detection.

I. INTRODUCTION

On-line monitoring of water quality plays a central role in providing safe drinking water and in the operation of wastewater treatment plants. Conventional physicochemical methods usually used for monitoring of water quality, have the significant limitation that the measured pollutant concentrations do not readily reflect their effects on biological organisms [1]. To address this issue, sensors based on physiological response of living organisms, have been developed to evaluate the toxicity associated with multiple contaminants. In this context, biosensors based on MFC platform have recently been received increasing attention from researchers to monitor water quality. Microbial fuel cells are bioelectrochemical systems that utilize microorganisms as catalysts to convert chemical energy to electrical energy. Biofilms composed of electroactive microorganisms, oxidize organic matter in the anodic compartment to produce protons and electrons. The resulting

electrons are captured at the anode and transferred to the cathode through an external circuit producing electricity. The current generated by MFCs depends on the metabolic activity of the electroactive bacteria at the anode [2]. The basic principle of MFC-based biosensors relies on a change in the current output for any disturbances on metabolism of the anodic biofilm that acts as the recognition component. MFC-based biosensors offer advantages of being self-powered and directly generate electrical signals without any need for a separated transducer, which is the case for most biosensor systems [3]. However, it is challenging to use MFC biosensors for toxicity monitoring when a high specificity is required. Indeed, MFC biosensors are sensitive for an overall toxicity and it is difficult to identify exactly the individual chemicals in water sample regarding whether two or more shocks happened simultaneously. A major challenge actually for the development of specific MFC based biosensors is the formation of electroactive biofilms that have the ability to distinguish among different analytes, in simple, as well as complex solutions.

In this study, biosensors based on flow-mode single-chamber microbial fuel cells, were investigated to further improve the MFC sensor's specificity. A differential sensing approach based on the difference in response of MFC biosensors based on copper-adapted and nonadapted biofilms was investigated to detect Cu^{2+} ions.

II. MATERIALS AND METHOD

A. Chemicals and reagents

All chemical and reagent used in this work were analytical grade and were used without any previous treatment.

B. MFC-based biosensor design

The flow-mode single-chamber MFC was constructed with three electrodes (Fig.1): carbon foam (1 cm³) as working electrode (anode), air cathode containing 10% (C/Pt) for oxygen reduction, and Ag/AgCl as reference electrode.

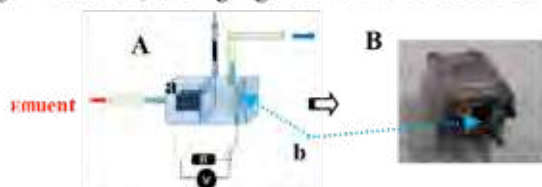


Fig. 1. (A) Schematic and (B) photo of a MFC-based biosensors equipped with a flow-through: a) anode (carbon foam) and b) an air-carbon-cathode.

C. Microbial Fuel cell set-up and biofilm formation

The MFCs were filled with primary effluent, 5 g.L⁻¹ dehydrated sludge from a Grand Lyon domestic wastewater treatment plant (Lyon, France) and fed with 1g.L⁻¹ of sodium acetate (Roth, Karlsruhe, Germany) as carbon source. All reactors were cultivated simultaneously at a stable ambient temperature. An external resistance of 330 Ω is connected to the electrodes during the biofilm formation in order to shuttle electrons from the anode to the cathode. Copper-adapted and nonadapted biofilms were formed with and without 2 mg.L⁻¹ of Cu²⁺ ions, respectively.

III. RESULTS AND DISCUSSION

A. Electrochemical behavior of biofilms growing with and without Cu²⁺

The electrochemical behavior of biofilms growing without and with Cu²⁺ was examined by cyclic voltammetry (CV) and polarization curves (Fig.2). After two weeks, CVs of anode biofilms formed with and without Cu²⁺ ions, exhibited faradaic peaks centered at around -370 mV vs. Ag/AgCl for copper-adapted biofilm and -200 mV vs. Ag/AgCl for nonadapted biofilms. This potential shift indicates two different modes of electron transfer used by both biofilms. Copper-adapted biofilms showed a lower electroactivity with small faradaic peaks compared to the response of nonadapted biofilms. These results were confirmed by the polarization curves that showed a significant decrease in the maximal power density and current output: 500 mW.cm⁻²; 2200 mA.cm⁻² for MFCs based on copper-adapted biofilms compared to those based on nonadapted biofilms 800 mW.cm⁻²; 5000 mA.cm⁻² (Fig.2B).

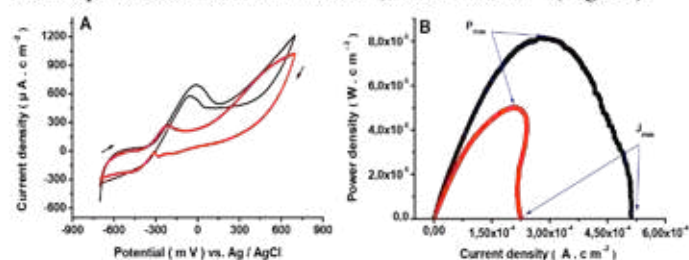


Fig. 2. (A) Cyclic voltammograms and (B) MFC polarization curves obtained with copper-adapted (red curves) and nonadapted (black curves) biofilms.

B. Analytical performance of MFC biosensor

Figure 3 shows the temporal changes in the MFC biosensors' output currents when they were operated in the external resistance mode under the optimal conditions. The current output of MFC biosensor based on nonadapted biofilm kept constant before and after the dosing of 2 and 4 mg.L⁻¹ of Cu²⁺ ions. Comparatively, current production obtained with in MFC biosensor based on copper-adapted biofilm increased in response to 2 mg.L⁻¹ of Cu²⁺ ions. An increased response of MFC sensors to copper was probably achieved by regulating the metal reduction pathway of electrogenic bacteria with a copper-sensitive promoter. However, a decrease in mean current output was observed at a higher concentration (4 mg.L⁻¹), which may be explained by the saturation of promoter activity in combination with the toxic effects of protein overexpression.

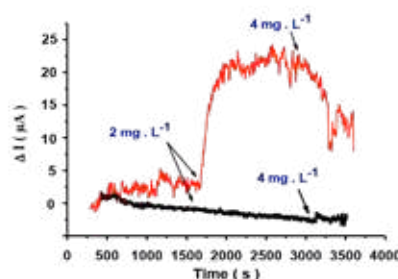


Fig. 3. Change in the output current of MFCs based on copper-adapted (red curves) and nonadapted (black curve) biofilms and challenged with 2 and 4 Cu²⁺ ions.

IV. CONCLUSION

The specificity of the MFC-based sensor towards Cu²⁺ ions was enhanced by using copper-adapted biofilms compared to the nonadapted biofilms. Although the electroactivity of copper-adapted biofilms is lower than that of nonadapted biofilms, the presence of Cu²⁺ ions at the concentration used for biofilm formation, improves metabolism of the anodic biofilm that increases the out current. The concept of bacteria adaptation to the pollutant can be exploited in a differential sensing approach for development of biosensors not only for monitoring an overall toxicity of environmental contaminants, but also for distinguishing different analytes in complex solutions.

ACKNOWLEDGMENT

The authors greatly acknowledge the PHC Maghreb 2019 project N°41382WC for its support to do this work.

REFERENCES

- [1] Adekunle, A., Raghavan, V., & Tartakovsky, B, On-line monitoring of heavy metals-related toxicity with a microbial fuel cell biosensor, *Biosensors and Bioelectronics*, Volume 132, 2019, Pages 382-390.
- [2] Rasmussen, M., & Minteer, S. D, Long-term arsenic monitoring with an *Enterobacter cloacae* microbial fuel cell, *Bioelectrochemistry*, Volume 106, 2015, Pages 207-212.
- [3] Grattieri, M., & Minteer, S. D, Self-powered biosensors, *ACS sensors*, Volume 3, 2017, no 1, Pages 44-53.

FUNCTIONAL CHARACTERISATION OF HYDROCARBON DEGRADING MICROBIAL COMMUNITIES IN BIOELECTROCHEMICAL SYSTEMS

A. Espinoza Tofalos*, M. Daglio*, E. Palma**, G. Bestetti*,
F. Aulenta**, A. Franzetti*

*Department of Earth and Environmental Sciences, University of
Milano-Bicocca, Piazza della Scienza 1, 20126 Milan (Italy)

**Water Research Institute (IRSA), National Research Council
(CNR), Via Salaria km 29,300, 00015 Monterotondo, RM, (Italy)

Abstract - In this study, the removal of hydrocarbons (phenol, toluene and a mixture of BTEX) was assessed in continuous-flow Bioelectrochemical Systems (BES) and the functional profiles of the anodic microbial communities and the inoculum was characterized by shotgun metagenome sequencing. The system operated with phenol was inoculated twice: first with a municipal activated sludge (inoculum 1) and after 33 days was re-inoculated with a refinery wastewater from a petrochemical plant (inoculum 2). Inoculum 1 was used to inoculate the runs with toluene and BTEX respectively. The genus *Geobacter* was highly enriched on the anodes of the three systems. *Geobacter* species have been related to BES, due to their capacity to degrade hydrocarbons in absence of oxygen and to use the anode as solid electron acceptor.

The genes coding for benzoate-CoA ligase and catechol 2,3-dioxygenase, selected as genetic markers for the anaerobic and aerobic degradation of aromatic compounds. The shotgun metagenomic approach provided useful insights into the ecology and complex functions within hydrocarbon degrading electrogenic biofilms.

Index Terms – Bioelectrochemical Systems, *Geobacter*, Shotgun metagenomics.

I. INTRODUCTION

Bioelectrochemical Systems (BESs) is an innovative technology that has been recently studied to stimulate the anaerobic degradation of hydrocarbons. Understanding the microbial community structure and genetic potential of anode biofilms is of great interest to interpret the degradation mechanisms that take place in BES.

In this study, the removal of hydrocarbons (phenol, toluene and a mixture of BTEX) was assessed in continuous-flow BES and the composition of the anodic microbial communities in the inoculum and in the anodic biofilm after the treatment was characterized shotgun metagenome sequencing approach, to obtain taxonomic and functional diversity patterns of the microbial communities.

II. METHODS

A. BES set-up

A continuous-flow BES were set up and operated with three separate water solutions containing phenol, toluene and a mixture of BTEX [1]. The system operated with phenol was inoculated twice first with a municipal activated sludge (inoculum 1 and after 33 days was reinoculated with a refinery wastewater from a petrochemical plant (inoculum 2). Inoculum 1 was used to inoculate the runs with toluene and BTEX.

B. Molecular microbiological analysis

A taxonomic and functional characterization of the microbial communities were carried out on Inoculum 1 and 2 and on the anodic biofilms developed after the BES treatments (Phenol, Toluene and BTEX).

Shotgun sequencing, read assembly, annotation and metagenome-assembled genomes (MAGs) were obtained as reported in [1].

III. RESULTS AND DISCUSSION

A. Enrichment of key functional genes

Benzoate-CoA ligase and benzyl succinate synthase were selected as marker genes for the anaerobic biodegradation of all aromatic hydrocarbons and toluene, respectively. Catechol 2,3-dioxygenase were selected as genetic markers for the aerobic of aromatic compounds, respectively. Benzoate-CoA ligase gene was abundant in the inoculum 2 and on the anode of the phenol-BES. Moreover, 24% 18% and 43% of the genes that encode for Benzoate-CoA ligase in the reactors with BTEX, phenol and toluene respectively, belongs to *Geobacter* spp..

Benzyl succinate synthase was undetectable in the inocula and in the anodic biofilm of the phenol-BES, whereas it was

enriched in the anodic community of the BES fed with toluene and BTEX. These results confirmed that the microbial communities are functionally selected at the anode as a response to the presence of the hydrocarbons. Anoxic condition in the BES favored the development of anaerobic metabolic metabolisms for the degradation of aromatic hydrocarbons.

Catechol 2,3-dioxygenase gene, the marker for aerobic degradation of BTEX and phenol, was very abundant in the inoculum 2 and detectable in the phenol-BES but almost absent on the anodes of the toluene and BTEX treatment. This result indicates that aerobic metabolism are negatively selected in the BES, despite they were abundantly present in the inoculum. BES-phenol maintained detectable amount of this gene, suggesting a role of aerobic degradation in phenol removal due to possible trace of oxygen in the anodic compartment.

B. Metagenome-assembled genomes

Among the 380 metagenome-assembled genomes reconstructed, the 7 most abundant MAGs in inocula and anodic biofilms are reported in table 1.

TABLE I
COVERAGE AND TAXONOMIC AFFILIATION OF MOST ABUNDANT MAGS

MAG ID	Completeness	Inoculum 1	Inoculum 2	BTEX	Phenol	Toluene	Taxonomy
2	65%			448	282	970	<i>Geobacter metallireducens</i>
4	84%			184		112	<i>Ignavibacterium album</i>
7	90%			84		255	<i>Geobacter pickerinii</i>
107	99%				242	129	<i>Geobacter sulfurreducens</i>
221	79%		233				<i>Desulfomicrobium baculatum</i>
227	90%	151					<i>Acidimicrobium ferroxidans</i>
289	97%		102				<i>Alkaliphilus metalliredigens</i>

As reported in table 1, four MAGs (2, 4, 7, 107) were representing abundant bacteria in the anodic biofilms, whereas the MAGs number 221, 227, 289 were representing bacteria dominating inoculum communities. Interestingly, three out of four anodic MAGs were affiliated to *Geobacter* genus. *Geobacter* spp. microorganisms have been extensively reported as dominating populations operating at the anode of BES due to their ability to use the electrodes as terminal electron acceptors [2].

The annotation of the genomes revealed that the MAGs affiliated to *Desulfomicrobium* sp. and *Acidimicrobium* sp. harbored the genes coding for the anaerobic biodegradation of aromatic compounds such as ethylbenzene, phenol and toluene. However, these bacteria, which were inoculated in the reactors,

were virtually absent in the developed biofilm after the BES operations, despite *Desulfomicrobium* sp. members are well known electrogenic bacteria [3].

Conversely, among the *Geobacter* MAGs dominating the electrogenic biofilm, only *G. sulfurreducens* MAG (107) harbored the gene for the anaerobic degradation of aerobic compounds (ethylbenzene, toluene, phenol). These results suggest that in the studied BES the presence of an anode with high electric potential act as a stringer selective driver of the taxonomy and the functions of the microbial community in respect to the presence of hydrocarbons.

IV. CONCLUSION

The results collected in this study provides important insights into the ecological processes assembling the microbial communities operating in BES. Anodic microbial communities in BES are highly selected both taxonomically and functionally, mainly due to the presence of the electrode as solo electron acceptor and due to the presence of specific carbon and energy sources.

ACKNOWLEDGMENT

The work was partially founded by CARIPLO FOUNDATION (Project BEVERAGE) and by INAIL (BRIC 2017).

REFERENCES

- [1] Franzetti A, Tagliaferri I, Gandolfi I, Bestetti G, Minora U, Azzoni RSS, et al. Light-dependent microbial metabolisms drive carbon fluxes on glacier surfaces. ISME J 2016; 10: 2984–2988.
- [2] Zhang T, Tremblay P-L, Chaurasia AK, Smith JA, Bain TS, Lovley DR. Anaerobic benzene oxidation via phenol in *Geobacter metallireducens*. Appl Environ Microbiol 2013; 79: 7800–6.
- [3] Jung SP, Yoon MH, Lee SM, Oh SE, Kang H, Yang JK. Power generation and anode bacterial community compositions of sediment fuel cells differing in anode materials and carbon sources. Int J Electrochem Sci 2014; 9: 315–326.

EFFECT OF PEDOT-PSS MODIFIED ANODES ON THE POWER OUTPUT BY URINE-FED MICROBIAL FUEL CELLS

M.J. Salar-Garcia*, A.B. Delgado-Egea**, I. Gajda*, F. Montilla**, I. Ieropoulos*

* Bristol BioEnergy Centre, Bristol Robotics Laboratory, University of the West of England, Coldharbour Lane, E-BS16 1QY, Bristol (United Kingdom)

**Institute of Materials, University of Alicante, Ap. 99, E-03080 Alicante (Spain)

Abstract –The need for improving the energy harvesting from Microbial Fuel Cells (MFCs) has boosted the design of new materials in order to increase the power performance of this technology and facilitate its practical application. According to this approach, in this work different poly(3,4-ethylenedioxythiophene)-polystyrenesulfonate (PEDOT-PSS) modified electrodes have been synthesised and evaluated as anodes in urine-fed MFCs. PEDOT-PSS was potentiodynamically electropolymerised onto the surface of carbon veil under two different conditions: A) potential range 0.1-2.4 V, scan rate $100 \text{ mV}\cdot\text{s}^{-1}$ and 28 potential cycles and B) potential range 0.1-2.4 V, scan rate $100 \text{ mV}\cdot\text{s}^{-1}$ and 14 potential cycles. The results show that an increase in the number of the potential cycles applied improves the electrochemical properties of the modified electrodes. Thus, the use of PEDOT-PSS modified anodes elaborated by using 28 potential cycles method allows MFCs to increase the power output up to 44.62 % compared to the unmodified anodes.

Index Terms – Bioenergy, Microbial Fuel Cells, PEDOT-PSS

I. INTRODUCTION

Microbial fuel cells (MFCs) are bioelectrochemical systems, which are able to generate electricity and treat organic wastes simultaneously without an external energy input [1]. Despite the potential of this technology, its large-scale implementation is still limited by the high cost of some materials and its moderate level of power output. So far, big efforts have been made in terms of architecture design, new materials and energy harvesting in order to improve the power performance and reduce the cost of the overall systems. These improvements will boost the real implementation of the technology in the near future [2][3]. Conducting polymers, as electrode modifiers, offer high versatility for several biotechnological applications

as enzyme immobilizers, DNA biosensors, electronic transducers or drug delivery systems. Concretely, poly(3,4-ethylenedioxythiophene) doped with poly-(styrenesulfonate) (PEDOT-PSS) is one of the most successful conducting polymers in terms of practical applications due to its good electrical conductivity, wide electroactive window and good stability and electrocatalytic properties. Specifically, PEDOT-PSS modified electrodes present a very high heterogeneous rate constant for electron transfer to the redox protein cytochrome c, constituting a promising modifier for the development of different biocatalytic devices [4].

In this context, this work focuses on synthesising PEDOT-PSS modified electrodes for being used as anodes in urine-fed ceramic-based MFCs. To the best author's knowledge, this is the first time that this type of anode modification has been tested in MFCs continuously fed with real waste.

II. MATERIALS AND METHODS

Acrylic air-breathing single-chamber MFCs were used to perform the experiments. Cathodes consisted of a blend of activated carbon and polytetrafluoroethylene (PTFE) pressed over a piece of stainless steel. Regarding the anodes, carbon veil (20 g m^{-2} , PRF composites, UK) was used as a control material and being then compared with carbon veil electrochemically modified. PEDOT-PSS was potentiodynamically electropolymerised onto the surface of carbon veil under the following conditions: A) potential range 0.1-2.4 V, scan rate $100 \text{ mV}\cdot\text{s}^{-1}$ and 28 potential cycles and B) potential range 0.1-2.4 V, scan rate $100 \text{ mV}\cdot\text{s}^{-1}$ and 14 potential cycles. Systems were matured during 4 days with a solution 1:1 v/v sludge and urine and then, continuously fed with neat urine

at a feed flow of $0.06 \text{ mL}\cdot\text{min}^{-1}$. MFC voltage was continuously monitored by using a multichannel Agilent recorder data logger (LXI 34972A data acquisition/Switch unit) and the experiments performed in duplicate.

The polarisation of MFCs working with the different anodes was performed using a potentiostat (AUTOLAB III/FRA2, Metrohm, The Netherlands) by linear sweep voltammetry (LSV) from open circuit voltage (OCV) to 0.02 mV at a scan rate of $0.25 \text{ mV}\cdot\text{s}^{-1}$. The MFCs were left in open circuit voltage (OCV) for at least two hours before performing the measurements to allow the stabilisation of the OCV. The polarisation were performed in a two-electrode configuration with the anode connected to the counter electrode, the cathode connected to the working electrode and reference channel short-circuited with the counter electrode channel. Polarisation curves were obtained by plotting the cell voltage versus current (V vs. I) whereas power curves were obtained by plotting power versus current (P vs. I).

III. RESULTS AND DISCUSSION

PEDOT-PSS films were prepared by potentiodynamic electropolymerisation from their monomer precursor. Figure 1 shows the electrochemical response of the polymers showing an increase of the capacitive current related with the increment of the electroactive area exposed to the solution. The polymer stays in its conducting (doped) state during the whole range of potentials scanned.

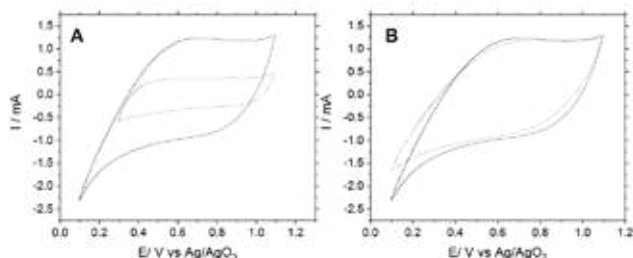


Figure 1. Overlapped voltammograms of bare carbon veil and PEDOT potentiodynamically electropolymerised during 28 potential cycles (A) and during 14 potential cycles (B). --- bare carbon veil; — PEDOT-modified electrode.

Figure 2 shows the average results of the polarisation (A) and power curves (B) of each MFC duplicate working with the different anodes synthesised. As can be observed, both modified anodes allow MFCs to reach higher values of power output than bare carbon veil electrode. Among them, the maximum power output by MFCs was obtained with anodes elaborated by using 28 potential cycles method ($385.77 \mu\text{W}$). In this case, the performance of the MFCs increases up to 44.62 % by using the PEDOT-PSS-modified anode compared with the unmodified anode made of carbon veil. These results might be due to the good biocompatibility and high conductivity of this polymer, which facilitate both the biofilm growth and the electron transfer mechanism in the anode [4].

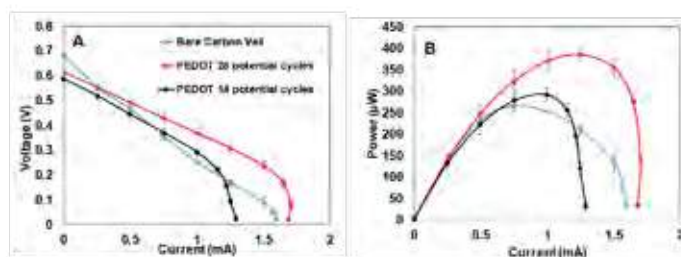


Figure 2. Average polarisation (A) and power curves of each MFC duplicate operated with different anodes synthesised.

IV. CONCLUSIONS

The high conductivity and biocompatibility of PEDOT-PSS make this organic polymer suitable for a wide variety of applications involving biological-electronic interfaces. Due to these properties, this polymer allows us to develop carbon-based modified anodes with improved electron transfer capacity. According to the results obtained, the presence of PEDOT-PSS in the anode increases the power performance of the urine-fed MFCs, probably because facilitates the biofilm growth and the electron transfer from the bacteria to the electrode. Among the different potentiodynamic techniques studied, it was observed that an increase in the number of potential cycles applied results in improving the performance of the modified-anodes and therefore, the overall system.

ACKNOWLEDGMENT

M.J. Salar-Garcia is supported by Fundacion Seneca (Ref: 20372/PD/17). I. Ieropoulos is grateful to the Gates Foundation (Ref: OPP1149065) for the financial support of parts of this work. A.B. Delgado-Egea and F. Montilla also thank the support of Generalitat Valenciana (Ref: PROMETEO/2018/087) and Ministerio de Ciencia, Innovación y Universidades (Ref: MAT2016-76595-R).

REFERENCES

- [1] J.L. Stirling, H.P. Bennetto, G.M. Delaney, J.R. Mason, S.D. Roller, K. Tanaka, C.F. Thurston, Microbial fuel cells., *Biochem. Soc. Trans.* 11 (1983) 451–453. doi:10.1042/bst0110451.
- [2] C. Santoro, C. Arbizzani, B. Erable, I. Ieropoulos, Microbial fuel cells: From fundamentals to applications. A review, *J. Power Sources.* 356 (2017) 225–244. doi:10.1016/j.jpowsour.2017.03.109.
- [3] I. Gajda, J. Greenman, I.A. Ieropoulos, Recent advancements in real-world microbial fuel cell applications, *Curr. Opin. Electrochem.* 11 (2018) 78–83. doi:10.1016/j.coelec.2018.09.006.
- [4] S. López-Bernabeu, F. Huerta, E. Morallón, F. Montilla, Direct Electron Transfer to Cytochrome c Induced by a Conducting Polymer, *J. Phys. Chem. C.* 121 (2017) 15870–15879. doi:10.1021/acs.jpcc.7b05204.

TESTING ELECTRO-STIMULATION OF THERMOTOGA NEAPOLITANA METABOLISM

Pierangela Cristiani¹, Giuliana D'Ippolito², Gaetano Squadrito³ Angelo Fontana²

¹Ricerca sul Sistema Energetico SpA, V. Rubattino 54, Milano, Italy
[pierangela.cristiani@rse-web.it]

²Institute of Biomolecular Chemistry (ICB), National Research Council (CNR), Via Campi Flegrei 34, 80078 Pozzuoli (Na) Italy

³Institute of Advanced Technologies for Energy (ITAE), National Research Council (CNR), Messina Italy

Abstract – The possibility of electrostimulate the production of lactic acid by *Thermotoga neapolitana* settled on electrodes is investigated in this work. Three days experiment was conducted supplying an alternated electric energy in polarized and unpolarized bioreactors fed with 30mM of glucose. The solution Optical density decrease and documentation produced by scanning electron microscopy micrographs showed a strong affinity of bacteria to form biofilm both on the polarized and unpolarized electrodes.

Evidence of the lactate/acetate ratio modification with respect the control bioreactors was achieved, both for polarized and unpolarized bioreactors.

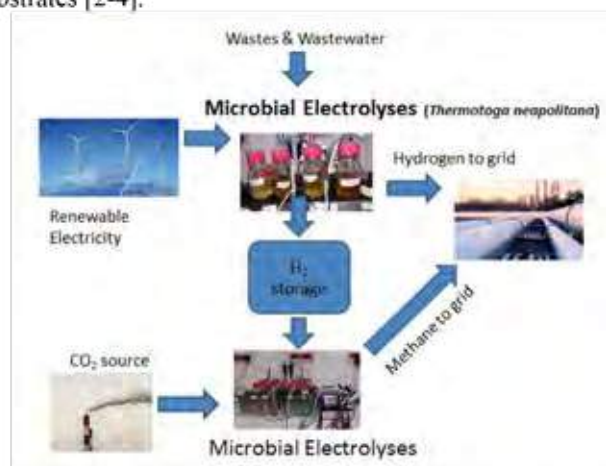
These results globally confirm the affinity of *T. neapolitana* to carbon cloth electrodes and the possibility of electrostimulate their metabolism, opening future perspectives on electro-fermentation with this hyperthermophilic strain.

Index Terms – *Thermotoga neapolitana*, Bio-Hydrogen, bioelectrostimulation.

I. INTRODUCTION

The environmental impact of unsustainable growth has led researchers to increasingly address the technologies able to supply clean energy and to minimize wastes. In this new vision, hydrogen (H₂) is considered a suitable energy vector for renewable energy sources (RES) since its utilization is carbon-free and produces only water as a by-product. Indeed, the generation of bio-hydrogen in a Power-to gas (P2G) concept (Figure 1) is a new frontier of research¹. Moreover, hydrogen is largely used in the chemical industry like in the production of ammonia-fertilizers, methanol and the production of polymers.

Not least, the increased attention to reduce waste and the electrical power consumption of conventional electrochemical hydrogen-producing technologies [1] induced increasing attention to the biological production of hydrogen. Research on biological hydrogen (Bio-H₂) has increased over the years leading to very promising results that can be achieved using different technologies and several selected bacteria strains applied to a wide variety of waste streams and energy crops as substrates [2-4].



Thermotoga neapolitana (DSM 4359, ATCC 49049), more than others Thermotogales is able to accumulate biohydrogen from waste organic matter, in a selective environment (>80°C). This bacterium is also able to use a peculiar anaerobic biochemical pathway named Capnophilic Lactic Fermentation (CLF) that accomplishes chain elongation of acetate with direct reduction

of CO₂, producing lactic acid [2]. This is a carbon fixation mechanism which, differently from autotrophism, leads to direct elimination of fixed carbon into excreted metabolites, such as lactic acid, instead of converting and accumulating it into biomass. *T. neapolitana* is therefore a promising microorganism for recovering added-value chemicals from organic wastes [3]. An electrostimulation of the lactic metabolism of *T. neapolitana* was successfully attempted in this work, operating with bioreactors equipped with carbon cloth electrodes.

II. METHODS

The experiments were carried out using *Thermotoga neapolitana* cf *capnolactica*, a recently described lab strain derived from *T. neapolitana* DSMZ 4359T. Anaerobic culture of *T. Neapolitana* was routinely maintained on medium Tn supplemented with 28mM (0.5% wt/v) glucose and 0.4% (wt/v) yeast extract/tryptone [4]. Cultures were sparged for 5 min with 30 ml min⁻¹ of pure CO₂ gas at the beginning of the fermentation process and after inoculation with the fresh cells. The pH was corrected to 7.5 for all the experiments.

An alternating polarization up to $\pm 1.2V$ was imposed between two identical electrodes of carbon cloth, immersed in the electrochemical bioreactors of 250mL. Bioreactor without applied polarization and without electrodes were also tested, as control. Glass reactors were operated at temperature of 80°C, with a culture media of *T. neapolitana* containing 5g/L (~30mM) of glucose, in triplicates. Three successive cycles of chemical measurements, every 24 hours, was carried out to estimate the glucose consume and the acetic/lactic acid production, as well the hydrogen yield in each tested bioreactor.

Gas (H₂ and CO₂) measurements were performed by gaschromatography. Acetic acid and lactic acid were quantified in culture media by 1H Nuclear Magnetic Resonance (NMR) on a 600MHz spectrometer (Bruker Avance 400). At the end of the tests, each electrode from each sample bottle was extracted, cut and stored for SEM analysis. SEM analysis was carried out with, using acceleration voltages in the range 5-15kV.

III. RESULTS

The decrease of the solution Optical Density and micrographs produced by scanning electrode microscopy showed a strong affinity of bacteria to form biofilm on electrodes.

Evidence of the lactate/acetate ratio modification with respect to the control bioreactors was achieved, especially under the higher polarization, but also in the bioreactors with unpolarized electrodes.

The presence of the electrodes induced a significant alteration of the hydrogen and lactic acid production, both in polarized and unpolarized bioreactors.

The bacteria colonizing the electrodes demonstrated repulsion for the electrode when a significant polarization of $\pm 1.2V$ is imposed. In particular, a bioreactor which the polarization of $\pm 1.2V$ was imposed the second day (cell 6 in

Figure 2) showed the highest ratio of lactic/acetic acid production. Nevertheless, the changes in chemical productions between polarized and un-polarised electrodes was not sufficiently evident between the replicates.

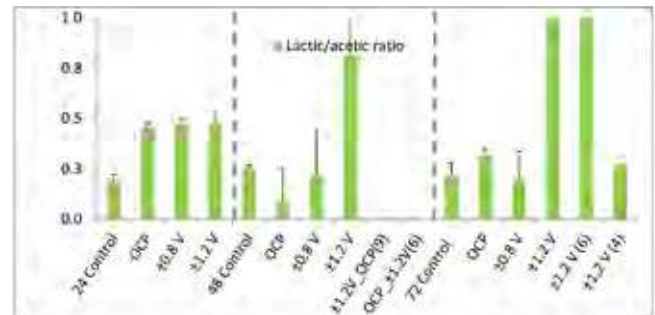


Figure 2: graphic of lactic acid production in un-polarised and polarised reactors measured during 72 hours test.

IV. Conclusion

In this work, we demonstrate that the introduction of conductive carbon based electrodes in a bioreactor of *T. neapolitana* culture and a light alternated polarization (up to $\pm 1.2V$) have an effect on the hydrogen production and on Lactate/acetate formation ratio. Moreover, an electrostimulation of $\pm 1.2V$ affects the bacteria settled on the electrodes and was also able to modify the lactate product balance. New experiments are necessary to quantify the effect of polarization and to investigate the possibility to drive the bacteria to the preferential production of hydrogen or lactic acid. Nevertheless, the achieved results, although preliminary, globally confirm the affinity of *T. neapolitana* to carbon cloth electrodes and the possibility of electrostimulate their metabolism, opening future perspectives on electro-fermentation with this hyperthermophilic strain.

V. Acknowledgment

This work was financed by the Italian Ministry of University and Research (MIUR) and by the Research Fund for the Italian Electrical System in compliance with the Decree of March, 19th 2009.

References

- [1] A. Schievano, A. Goglio, C. Erckert, S. Marzorati, L. Rago, P. Cristiani. *Detritus* / Volume 01 - 2018 / pages 57-63.
- [2] Pradhan N., Dipasquale L., et al. 2015, *Int. J. Mol. Sci.* 16, 12578-12600
- [3] Fontana EP EP14711847.5. EU patent application: EP14711847.5; Priority IT20130109 24/01/2013
- [4] d'Ippolito G, Dipasquale L, Vella FM, Romano I, Gambacorta A, Cutignano A, Fontana A. *Int J Hydrogen Energy* 2010;35:2290-5.

MFC RUNNING LOW-POWER APPLICATIONS WITHOUT ANY POWER-MANAGEMENT CIRCUITRY

X. A. Walter *, J. Greenman *, and I. A. Ieropoulos *

*University of the West of England, Bristol, United Kingdom

Abstract - Many studies have demonstrated that microbial fuel cells (MFCs) can serve as low-level power sources. However, to be employed as such, MFC systems rely on energy management circuitry that are mainly used to increase voltage levels, act as energy buffers, and thus deliver stable power outputs. The present study demonstrates for the first time that the MFC technology can directly and continuously act as low-level power source. The present study reports the direct powering of a microcomputer and its coloured screen (*GameBoy*, Nintendo®). Moreover, the results presented herewith show how to set a MFC-LED system to continuously provide lighting using urine as fuel. In conclusion, this study demonstrates how the MFC technology and the target application could be developed simultaneously for better and longer performance.

Index Terms - Membraneless microbial fuel cell, Urine, Energy source, Direct power.

I. INTRODUCTION

Individual MFC are low-power energy transducers with a working potential often between 300mV and 500mV. In addition, smaller MFCs are more power dense than larger ones [1]. One of the aims driving the development of the technology is to be able to employ MFCs as power sources. The common strategy pursued by researchers is to assemble a plurality of MFCs into stacks. This strategy allows to electrically connect the units either in series or in parallel to increase either the voltage or the current. However, in the case of serial connections, voltage reversal can be observed between MFCs [2]. Therefore, the most common approach to reach high voltages (e.g. >1.5 V) is to electrically connect all MFCs in parallel and employ electronic circuitry to boost the voltage. However, the cost of MFC systems has to be kept low for the technology to be deployed in society, and power management systems represent an additional cost that could limit the technology's implementation. Therefore, the objective here was to investigate how a MFC-stack could directly power applications without the need for a power management circuitry.

II. MATERIALS AND METHODS

A. Reactors

The stack assembled employed self-stratifying membraneless MFCs modules (S-MFCs) and was fuelled with human urine at different rates. In each module, a plurality of anodes (31 per modules) and cathodes (41 per modules) are inserted in a single container and share the same electrolyte (6.9L). The catalyst of the cathodes was an activated-carbon (AC) and polytetrafluoroethylene (PTFE) mixture (80% AC; 20% PTFE). The anodes were made from 3000 cm² of 10gsm carbon veil folded down to a projected surface area of 150 cm². The first stack employed a single cascade of 4 modules electrically connected in series. Further experiments were carried out with a cascade comprising either 4, 5 or 6 modules. The anodes of the first module and the cathodes of the cascade's last module served as the negative and positive terminals of the system, respectively. The stacks were directly connected to the positive and negative terminals of either a *GameBoy Color* (GBC) [3], or a purpose-built spotlight with different numbers of LEDs connected in parallel (Samsung LM561C, 4000K).

B. Data capture

The current produced by the cascade was measured by monitoring the voltage drop across a wire of a known resistance (0.00371 Ω). In addition, the voltage of the cascade and of each of its modules were also monitored. A polarisation experiment was performed by linear sweep voltammetry (LSV) under a two-electrode configuration and with a scan rate of 0.25 mV.s⁻¹.

III. RESULTS AND DISCUSSION

The GBC needed a minimum voltage of 1.832 V with a current of 70-75 mA to run. Early versions of S-MFC prototype of similar size could provide roughly 200 mA at 500 mV under optimal feeding conditions [4]. Hence, it was hypothesised that

a cascade of 4 modules electrically connected in series would deliver an electrical output matching the GBC needs.

The polarisation experiments showed that a cascade of 4 modules delivered 283 mA at 1.551 V under optimal feeding conditions. However, due to the limited availability of fuel, the cascade could only be sustainably fuelled with 2 L of fresh fuel every 6 hours. Under these conditions, the cascade could deliver a maximum of 174 mA at 1.751 V. The voltage monitoring of the individual modules during both polarisation experiments showed that a voltage reversal was occurring in the lower modules of the cascade. This indicates that the series connection within a single cascade was affected by the difference in feedstock quality between modules. Hence, to maximise the efficiency of the setup, the GBC was directly connected to the cascade and several feeding regimes were tested (Fig. 1).

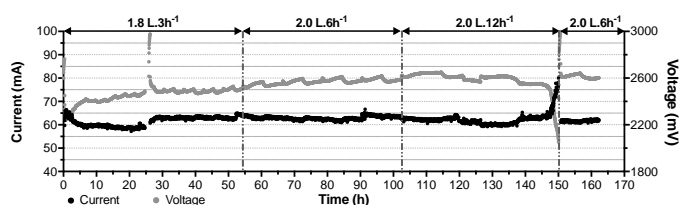


Fig. 1. Electrical output of the system comprising a single cascade of four S-MFC modules, electrically connected in series, and directly connected to a GBC. Current is drawn by the GBC and the voltage is from the cascade [3].

After being connected to the cascade, the GBC was turned ON and a video game was run. During this 160 h continuous run, the cascade was delivering an average current of 62.1 ± 1.5 mA at an average voltage of 2.542 ± 0.076 V. Compared to the results of the polarisation experiments, the electrical outputs were below the maximum capacity of the cascade. However, with a feeding rate of 2 L every 12 hours, the last module of the cascade displayed voltage reversal that caused the voltage output of the cascade to drop below the 1.832 V needed to power the GBC (Fig. 1). This result emphasises the importance of uniformity between MFC units for system stability. A different test was also run with a 3-module cascade and results showed that although sufficient power was produced (≈ 150 mW; ≈ 82 mA), the voltage was below the threshold level and the GBC switched OFF.

Following this experiment, the capacity of a MFC system to directly power LED lights was investigated. The same 4-module cascade was connected to an 8-LED spotlight. The 4-module cascade had an open circuit voltage of 2.901 V and once connected to the 8 LEDs, the electrical output was of ≈ 65 mA and ≈ 2.630 V (Fig. 2a). Although this output was stable, the produced light was insufficient (≈ 18 Lux @ 1m). Two more S-MFC modules were added to the same cascade to power 8 LEDs. Because the current consumption of an LED is proportional to the voltage provided, the 6-module cascade generated high voltage output, but the LED consumed too high a current (≈ 210 mA @ ≈ 2.740 V), which resulted in the last module displaying cell reversal after 10 min. Hence, the cascade was set with 5-

modules. While the voltage and current output of the cascade were more aligned with the 8 LEDs consumption (≈ 160 mA @ 2.711 V), the slightest voltage increase caused cell reversal of the module used as the positive terminal (module 5; Fig. 2b).

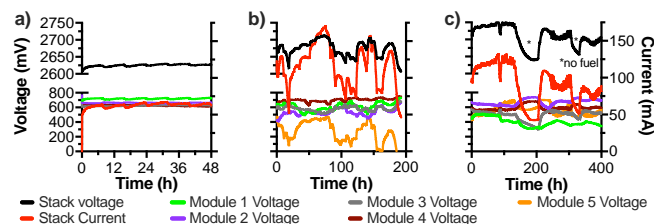


Fig. 2. Outputs of a cascade comprising different number of S-MFC modules and connected to different number of LEDs: (a) 4-module powering 8 LEDs, (b) 5-module powering 8 LEDs, (c) 5-module powering 4 LEDs.

Following a systematic approach, the configuration was changed by decreasing the number of LED. The 5-module cascade was therefore connected to 4 LEDs. Although the module used as the positive terminal (module 1; Fig. 2c) had a lower potential than the other 4, the system as a whole was stable over the 400 h of the experimental run (≈ 85 mA @ 2.700 V; ≈ 23 Lux @ 1m).

IV. CONCLUSIONS

To date, all systems reported powering applications with MFCs include power management circuitry. The results presented here demonstrate for the first time that a MFC system could directly and continuously power two types of applications without any energy management apparatus: a microcomputer and LEDs. With a systematic approach, the MFC stack has to be tailored to the needs of the application and the application has to be tailored to the capacity of the MFC stack.

ACKNOWLEDGMENTS

The work has been funded by the Bill & Melinda Gates Foundation for funding the work (grant no. OPP1149065).

REFERENCES

- [1] Ge, Z., Li, J., Xiao, L., Tong, Y.R., He, Z., Recovery of Electrical Energy in Microbial Fuel Cells, *Environmental Science & Technology Letters*, Volume 1, 2014, pp. 137-141.
- [2] Sugnaux, M., Savy, C., Cachelin, C.P., Hugenin, G. Fischer, F., Simulation and resolution of voltage reversal in microbial fuel cell stack, *Bioresources Technology*, Volume 238, 2017, pp. 519-527.
- [3] Walter, X.A., Greenman, J. Ieropoulos, I.A., Microbial fuel cells directly powering a microcomputer, *Journal of Power Sources*, Volume 446, 2020, N° 227328.
- [4] Walter, X.A., Merino-Jiménez, I., Greenman, J., Ieropoulos I., PEE POWER® urinal II – Urinal scale-up with microbial fuel cell scale-down for improved lighting, *Journal of Power Sources*, Volume 392, 2018, pp.150-158.

HIGH EFFICIENCY REVERSIBLE TECHNOLOGIES IN FULLY RENEWABLE MULTI-ENERGY SYSTEM

A. Sorce*, B. Bosio*, M. Romano**, S. Campanari**, P. Polverino***, M. Sorrentino***, S. Ubertini****, A. L. Facci****L. Barelli*****, G. Bidini*****, E. Jannelli*****, M. Minutillo*****

* University of Genova, Via Balbi 5, Genova (Italy)

** Polytechnic of Milano, Piazza Leonardo da Vinci, 32 – Milano (Italy)

*** University of Salerno, Via Giovanni Paolo II, 132 – Frisciano - Salerno, (Italy)

**** University of Tuscia, Via S.Maria in Gradi, 4 - Viterbo, (Italy)

***** University of Perugia, P.zza dell' Università, 1 - Perugia, (Italy)

***** University of Naples “Parthenope”, Centro Direzionale Isola C4 - Napoli (Italy)

Abstract – The HERMES project aims to design an advanced Multi-Energy System oriented towards the poly-generation of heat, power, chilled water, hydrogen and oxygen at purity level suitable for fuel cells and industrial applications. The core of the system is represented by the reversible solid oxide high-temperature cells (rSOC), which smartly integrate with up to 100% renewable energy power generators (e.g., PV panels, wind, etc.) and storage systems (i.e., fuel tanks, battery etc.).

The main project objective is to create a multi-energy system able of generating sustainable and secure energy at an affordable cost and capable of promoting the transition from a prevalence of fossil fuels to 100% renewables.

Index Terms – Multi-Energy System (MES), rSOC, poly-generation system, hydrogen, renewable energy.

I. INTRODUCTION

The needs to generate energy with zero harmful emissions, and of levelling the discontinuous production of energy from renewable sources, are leading to considerable interest in poly-generation systems in which renewable energy generators are combined with innovative energy production technologies [1]. The proposed project represents a step forward compared to the state of art as it integrates the rSOCs that allow the production not only of electric and thermal energy, but also of hydrogen, usable for the automotive sector. It is in line with the objectives of the European Union whose energy policy has targeted the reduction of 40% of the CO₂ towards 2030 and 80% before 2050. Such a transition path relies, among others, on the implementation of hydrogen-based technologies, that the Fuel Cell and Hydrogen Joint Undertaking (FCH-JU) has been supporting for more than a decade.

II. PROJECT DESCRIPTION AND METHODOLOGY

The project plans to design a Multi-Energy System (MES),

characterized by the combination of energy conversion technologies in a whole modular energy system, with the aim of decarbonizing electricity generation, heating and cooling as well as the transport sectors, while also taking into account the interactions with fuel and electricity grids and other infrastructures.

This system must be able to store and supply different energy sources guaranteeing an excellent technical, economical and environmental performance. Electricity can be either obtained by renewable energy sources and rSOC stacks working as fuel cells, while providing heat and chilled water, whereas clean fuels (H₂ and Synthetic Natural Gas - SNG) can be generated through electrolysis operation.

High efficiency, flexible and reliable technologies are needed to realize the MES. Fig.1 shows the major MES objectives.

The MES in its final configuration, must be able to: i) interact (by import or export) with the utilities, which are the electric, thermal and NG grids; ii) satisfy the thermal and electric loads; iii) produce fuels and electricity for mobility (hydrogen, SNG and electric vehicles); iv) store energy (electricity and heat) and valuable chemicals (demi water, H₂, O₂, SNG, CO₂).

Therefore, the MES must be able to generate and store energy through the rSOC, it must be able to operate both with natural gas and with hydrogen, or the combination of two.

Furthermore, the system must be able to produce heat and power, to provide secondary and primary frequency support to the grid and to produce hydrogen and oxygen.

The project activities span from the definition of future scenarios (RES penetration, utilities demands) and the selection of the most promising MES layout, to the experimental investigation of the rSOC and the multiphysics modelling and validation, ending with the development of the control system and the test of the concept in a cyber-physical system.



Fig. 1. MES general block diagram

III. FIRST RESULTS

A. Polygeneration from biogas

A biogas-based MES configuration has been analyzed through energy and exergy analyses [2]. The plant consists of: i) a fuel processing unit (Auto-thermal Reactor plus Water Gas Shift Reactor), ii) a power production unit based on the SOFC (Solid Oxide Fuel Cell) technology, iii) a hydrogen separation, compression and storage unit. The plant outputs are hydrogen, and heat. The produced electricity is completely used for sustaining the electric energy consumption of the plant. In table 1 the main streams and calculated performances for a power plant feeding a 100 kg/day hydrogen refueling station.

TABLE I
BIOGAS-BASED MES OPTIMIZED FOR HYDROGEN PRODUCTION

Flow	Mass Flow [kg/h]	Exergy [kW]	Performance	Energy Efficiency	Exergy Efficiency
Biogas	69.98	362.4	Hydrogen	40.7%	37.7%
Hydrogen	4.2	138	Heat	36.6%	15.4%
Heat	-	56.3	Overall	77.3%	53.1%

B. Experimental Activities on polygeneration with solid oxide technology

Since degradation phenomena in reversible operation of SOC are a relatively untapped subject, the project aims to characterize the degradation rate varying the main operating parameters relative to cycling operation [3]. A wide experimental study on rSOC technology will be performed by studying system behavior under real operation.

Meanwhile, preliminary tests were performed on an anode-supported NiYSZ/8YSZ/GDC-LSCF button cell to develop a performance simulation and a real time diagnosis tools that detect performance gaps with respect to new&clean conditions, identifying the degradation sources. Only the SOFC operating mode was considered so far. A semi-empirical model of the cell was developed for performance prediction. It is based on macroscale material balances, assuming a 0D system for the tested button cell, and solves the 1D local equations along the electrode thickness. Thus, it considers the electrochemical kinetics, which is influenced by gaseous reactant and product transport. The model was successfully validated on a different set of polarization curves with an error lower than 3% [5].

Experimental trials were used to build an equivalent circuit model suitable for real-time diagnosis based on DRT analysis of EIS measurement. For what concerns the anode, DRT deconvolution highlights five major processes, namely (as relaxation times becomes longer): charge transfer, charge transfer at the TPB, anodic diffusion, charge transfer at the cathode and cathodic diffusion. Control and real-time applicable energy management strategies will be developed mainly aiming at ensuring proper management (e.g., charge-sustaining) of energy storage devices, such as the hydrogen tank, while guaranteeing meeting load demands in the most efficient and clean (from the carbon footprint point of view) way. Preliminary analyses were conducted on sizing and controlling an rSOC-based renewable power plant, suitable for highly resilient and possibly islanded use [5].

The tuning of ECM lumped parameters has to be extended to a larger variation domain of operating parameters. Moreover, also the cathode side needs to be investigated.

IV. CONCLUSION

The HERMES project aims to design an advanced Multi-Energy System capable of promoting the transition from a prevalence of fossil fuels to 100% renewables.

The first research activities to analyzed a MES configuration based on the biogas utilization for the co-production of hydrogen, heat and electricity. Moreover, experimental studies on degradation phenomena occurring in the solid oxide fuel cell, that will be the core technology of all MES configurations, where carried out. The next research steps will evaluate different system configurations and estimate, through numerical and experimental activities, their expected performances and the economic issues.

ACKNOWLEDGMENT

This research is founded by Italian Government (PRIN project 2017, code 2017F4S2L3_005).

REFERENCES

- [1] M.L. Ferrari, A. Traverso, A.F. Massardo 2016 "Smart polygeneration grids: experimental performance curves of different prime movers", Applied Energy, Vol. 162, pp. 662-630
- [2] M.Minutillo, A.Perna, Alessandro Sorce, Exergy analysis of a biomass-based multi- energy system, E3S Web of Conferences **113**, 02017 (2019) *SUPEHR19 Volume 1*
- [3] L. Barelli, G. Bidini, G. Cinti, A. Ottaviano, Study of SOFC-SOE transition on a RSOFC stack, Int. J. of Hydrogen Energy, 42/41 (2017) 26037-26047
- [4] F.R. Bianchi, D. Bove, E. Audasso, B. Bosio, A. Baldinelli, L. Barelli, G. Bidini, F. Nobili and A. Staffolani, Electrochemical modelling of solid oxide fuel cells, European Fuel Cell Technology & Applications Conference, December 9-11, 2019, Naples, Italy.
- [5] M. Sorrentino, A. Adamo, G. Nappi, Self-Sufficient and Islanded-Oriented Design of a Reversible Solid Oxide Cell-Based Renewable Microgrid, Energies, 12/17 (2019) 3224.

LONG-TERM OPERATION OF A BIO ELECTRICAL SYSTEM TREATING AWAMORI DISTILLERY WASTEWATER

David Simpson*, Vyacheslav Fedorovich*, Michael Cohen**, Igor Goryanin*,***

*Okinawa Institute of Science and Technology, Okinawa (*Japan*)

**Sonoma State University, Rohnert Park, CA (*USA*)

***University of Edinburgh, Edinburgh (*UK*)

Abstract - One of the challenges in BES applied research is the scaling up of reactors. A number of MFCs have already been shown to simultaneously treat organic waste and generate electricity when fed with artificial wastewater or actual wastewater at a laboratory scale. However, a few reports have shown electricity generation and organic removal performances of scaled-up BES bioreactors fed on industrial wastewater, albeit with reduced initial organic concentrations. Since 2013, our unit has deployed three scaled-up (60 L) air-cathode MFC reactors at Mizuho Awamori distillery in Okinawa to treat rice wash and distillery wastewater. This was one of the first pilot-scale MFC reactors treating actual wastewater at the time. We monitored the system for 5 years, the longest on-site operation of an MFC, with consistent removal of Chemical Oxygen Demand (COD) and Biological Oxygen Demand (BOD) from the wastewater.

Index Terms – Bioelectrical systems (BES), Microbial fuel cells (MFC), wastewater treatment (WWT), long term operations.

I. INTRODUCTION

Conventional municipal, agricultural, and industrial wastewater treatment systems are based on energy-intensive aerobic biological processes. MFCs are bio-electrochemical reactors in which bacteria oxidize various organic compounds in their anaerobic anodic chambers and pass electrons to conductive materials that enable external electron transfer to a cathode, resulting in the production of electricity. “Fuel cell” implies electricity generation; however, our approach focuses mainly on bolstering their effectiveness in wastewater treatment. MFCs allow for reduction of oxygen external to the treated water; therefore, they use substantially less energy than aeration technologies [1,2,3] However, a few reports have shown electricity generation and organic removal performances of scaled-up BES bioreactors fed on industrial wastewater, albeit with reduced initial organic concentrations [4,5,6] One of

the challenges is the scaling up of reactors to develop scalable solution capable to treat >10m³ of waste water per day..

II. EXTENDED ABSTRACT

Three pilot-scale, tray-type BES bioreactors, each with a 60-L (Fig. 1) active volume, were constructed and operated in continuous-flow mode at the distillery using rice wash and distillery wastewater as the substrate. Anodic chambers were seeded with anaerobic microorganisms from an anaerobic digester and tested for BOD and COD removal as well as methane, and electrical current generation.



Under stable Organic Loading Rates (OLR) of 2 g/L, 5 g/L and 10 g/L, BOD removal performance was 99%, 98%, and 90%, respectively at a system Hydraulic Retention Time (HRT) of 34 hours. Biogas generation at 2 g/L BOD reached a maximum of 49.8 L/m³/day with a 50% methane concentration. The system was evaluated on power consumption, maintenance, space requirements, and robustness against currently available treatment methods for potential commercialization. The reactors ran for >3 years, followed by a low maintenance period of 2 years, which was the world first for length of testing of a BES reactor of this size.

We have specialized in developing demonstrations of the scale and longevity that this technology can achieve, with

experiments having been carried out continuously over the past 8 years and expanded from 1 L to the current prototype unit with a capacity of 1.7 m³ making it one of the largest BES reactors in the world. Our cooperation with the Mizuho distillery demonstrated the ability to treat waste *in situ* and to produce effluent suitable for legal release

This was one of the first pilot-scale MFC reactors treating actual wastewater at the time [7]. Power to pump wastewater into the reactor and to run monitoring equipment were the sole electricity draws, making the MFC system potentially more cost-effective than aeration-based treatment systems. The major components of air-cathode MFC are conductive electrodes, proton permeable membranes or cation exchange membranes, as separators and catalysts. To further scale-up competitive BES/MFC reactors, we developed and patented a cost-effective catalyst and separator (cation and anion exchange membranes), anodes, cathodes and scale-up units. These patented technologies are now used to construct lab-scale (~5L), pilot-scale (~50L) and large scale (~2m³) units, which allows to discharge directly into surface waters (river or sea).

- Anode electrode; Based on carbon fiber brushes with a special surface treatment. This material provides large contact area for bacterial biofilm formation and mass transfer.
- Cathode electrode; Considered the most limiting element (costs and performance) in MFC systems, we have developed effective low-cost materials for the two key parts of this electrode;
- Ion-selective anion and cation exchange membranes specifically designed for MFC and BES systems for use with wastewater treatment and performance equivalent to DuPont (Nafion).
- Catalyst, non-precious metal based to enhance oxygen reduction. Material is based on carbon and pyrolysis of nitrogen.
- Large scale scalable MFC design

In addition, our technology was successfully used for BOD biosensor development [8]

III. CONCLUSION

Pilot scale testing of a rapidly emerging biotechnology, Biological Electro-chemical Systems (BES) for on-site treatment of highly concentrated organic industrial wastewater over an extended period, and subsequent disposal of effluent into environmentally delicate waterways on the island of Okinawa is an important step toward commercializing the BES technology. Without an understanding of how real-world conditions can affect performance and stability of a reactor, improvements to electrode design and microbial conditioning cannot be adequately quantified. We have engaged local industry, science, local business and nongovernmental regulatory bodies (NGO).

This study was able to demonstrate that BES technology can

be operated across a realistic spectrum of operating conditions and can be considered for industrial adoption in Okinawa, and elsewhere.

ACKNOWLEDGMENT

We thank OIST subsidy and Proof Of Concept, Okinawa Prefecture and JST START grants for financial support.

REFERENCES

- [1] Huggins, T., Fallgren, P.H., J., Jin S. and Ren, Z. (2013) Energy and performance comparison of microbial fuel cell and conventional aeration treating of wastewater. *Journal of Microbial & Biochemical Technology* S6(002).
- [2] Liu, H., Ramnarayanan, R. and Logan, B. (2004) Production of electricity during wastewater treatment using a single chamber microbial fuel cell. *Environmental Science & Technology* 38(7), 2281-2285.
- [3] Tota-Maharaj, K. and Parneet, P. (2015) Performance of pilot-scale microbial fuel cells treating wastewater with associated bioenergy production in the Caribbean context. *International Journal of Energy and Environment Engineering* 6(3), 213-220
- [4] Cusick, R.D., Bryan, B., Parker, D.S., Merrill, M.D. and Logan, B.E. (2011) Performance of a pilot-scale continuous flow microbial electrolysis cell fed winery wastewater. *Appl Microbiol Biotechnol.* 89(6), 2053-2063.
- [5] Liang, P., Duan, R., Jiang, Y., Zhang, X., Qiu, Y. and Huang, X. (2018) One-year operation of 1000-L modularized microbial fuel cell for municipal wastewater treatment. *Water research* 141, 1-8.
- [6] Logan, B. (2010) Scaling up microbial fuel cells and other bioelectrochemical systems. *Applied microbiology and biotechnology* 85(6), 1665-1671
- [7] Kiseleva, L., Garushyants, S.K., Ma, H., Simpson, D.J.W., Fedorovich, V., Cohen, M. and Goryanin, I. (2015) Taxonomic and functional metagenomic analysis of anodic communities in two pilot-scale microbial fuel cells treating different industrial wastewaters. *Journal of Integrative Bioinformatics* 12(3), 273-288
- [8] B. Lóránt, M. Gyalai-Korpos, I. Goryanin, GM Tardy *Biotechnology Letters*, 41(4-5):555-563 DOI: 10.1007/s10529-019-02668-4G, 2019

A REDUCED ORDER MODEL OF PROTON CONDUCTING SOLID OXIDE FUEL CELL: A PROPOSAL

J. Milewski

Faculty of Power and Aeronautical Engineering, Warsaw University
 of Technology, Institute of Heat Engineering, 21/25 Nowowiejska
 Street, Warsaw (Poland)

Abstract - This paper presents a mathematical model of the Proton Conducting Solid Oxide Fuel Cell (H⁺SOFC), proposing a new approach for modeling the voltage of H⁺SOFC. Electrochemical, thermal, electrical and flow parameters are collected in an 0-D mathematical model. The aim is to combine all cell working conditions in as a low number of factors as possible and to have the factors relatively easy to determine. A validation process for various experimental data was carried out and the results are shown. The model was validated for various fuel mixtures across relatively wide ranges of parameters. A distinction is made between design-point and off-design operation.

Index Terms - Fuel cells; Proton-conducting SOFC; Numerical modeling.

I. INTRODUCTION

Mathematical modeling is now the basic method for analyzing fuel cells [1] and most often a zero-dimensional approach is used for modeling the H⁺SOFC. Generally speaking, H⁺SOFC working principles are based on partial hydrogen pressure differences between the anode and cathode side (see Fig. 1), which forces protons to pass from the anode side to the cathode. Hydrogen partial pressure on the cathode side must be very low (10⁻²⁰ MPa) to obtain practical voltage values with a single cell, which can be achieved through the oxidization of fuel on the cathode side.

The main processes occurring during H⁺SOFC operation and indicated in Fig. 1 can be described by adequate flows of ions and electrons, which gives an adequate equivalent electric circuit of the fuel cell see Fig. 2. The current i_t indicates total flow of electrons transported by solid electrolyte (H⁺), then the electrons are divided into two circuits, the electrons which pass through the electrolyte layer in the same direction as the protons (see Fig. 2) due to the presence of electronic conductivity. The detailed description about the used set of equations can be found in our

previous works [1, 2]. By solving them, an equation for cell voltage is obtained:

$$E_{H^+SOFC} = \frac{E_{\max} - \eta \cdot i_{\max} \cdot r_1}{\frac{r_1}{r_2} \cdot (1 - \eta) + 1} \quad (1)$$

The meaning of the used variables are also included in the other publications as well as the detailed explanation of them.

For proton conducting solid oxide fuel cells, the general form of Nernst's equation is used to estimate the maximum voltage of H⁺SOFC.

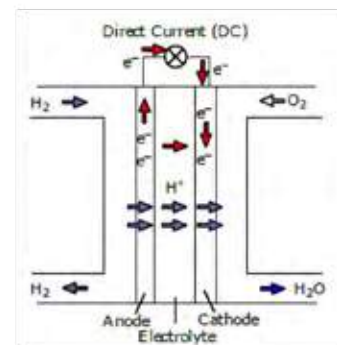


Figure 1: Working principles of Proton Conducting Solid Oxide Fuel Cell

The way to calculate the partial pressure especially at cathode is also explained in our works about oxygen conducting SOFCs. Based on the researchers' own calculations, which were based on data taken from [3] i_{\max} of 3.18 A/cm² was determined.

The generation of water vapor on the cathode side increases the hydrogen partial pressure. Therefore, overall system efficiency increases with respect to the classical SOFC. The main advantage of electrolyte made with proton-conducting material is the high ionic conductivity at an intermediate range

of temperatures (sufficient performances are reported in the literature at 600 .. 700°C [4]). The most popular type of material for solid state proton conductors are perovskite-type oxides structures which, in the presence of a wet atmosphere and elevated temperatures, exhibit high protonic conductivity [5]. Total protonic resistance of the cell is a function of many parameters. The H⁺SOFC consists of electrolyte sandwiched between anode and cathode layers. Those layers influence protonic conductivity as well (e.g., triple boundary phase processes). The material used, porosity and design of the electrodes affect fuel cell voltage significantly. Additionally, both electrolyte and electrodes can be built as multi-layers. Based on data gathered by the authors from [3], adequate factors were obtained, as shown in Fig. 3.

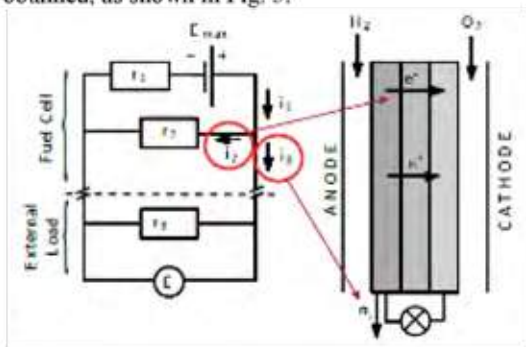


Figure 2: Equivalent electric circuit of a Proton Conducting Solid Oxide Fuel Cell

II. CONCLUSIONS

The present study shows the Reduced Order model of a proton conducting solid oxide fuel cell. Based on our experience of using this way of describing electrochemical devices, we built a model which rivals the classic way of modeling H⁺SOFC. Our model was validated based on two different sets of experimental data, giving acceptable coherence. The model is based on a combination of electric laws, gas flow relationships, solid materials properties and electrochemical correlations.

The paper describes clearly how the model was obtained and provides all details required to understand its validity. The model contains only physically explained parameters (with the minimum number of required factors possible) and takes into account all important thermal flow as well as architecture parameters.

The presented model is very stable and can be used for both simulations and H⁺SOFC system optimization procedures during which both material and thermal flow parameters are changed. The parameters can be changed across the whole, practically achieved range, which is in stark contrast to models based on the Butler Volmer and diffusion equations (they are very sensitive to input parameters and very often generate non physical results).

The proposed model was validated for various temperatures, fuel mixtures and oxidant mixtures across relatively wide ranges.

Based on the presented equations, a fuel cell model was created and compared against experimental data.

A separation is made between the design-point and o -design operation modes (by using the factor of maximum current density). The design point model can be used to select fuel cell size according to other system elements (gas turbine, heat exchangers, etc.). In those situations, a fuel/oxidant utilization factor is equivalent to current density and the cell characteristics can be drawn as a voltage fuel/oxidant utilization factor curve instead of a voltage current density curve (which is correlated to o -design operation). For instance, the parameter i_{max} for data taken from [6] is 4.88 A/cm² and regards the amount of oxygen delivered (hydrogen is not a limiting factor here). The same factor for data given by [3] is 2.75 A/cm² (also for oxidant electrode). Thus, the second fuel cell is not ten times worse, as can be read just from current density, but only partially due to the fact that less oxidant and fuel are delivered. In actual fact, the fuel cell used by [3] has a maximum efficiency of 3.32% whereas [6] is slightly better at 4.14%.

Not all of the model parameters are estimated in depth: further work is required and will be done (e.g., area specified internal electronic resistance, the influence of layer porosity, etc.).

It should be underlined that the proposed model is very light and serviceable for system level performance prediction, but may be less reliable for detailed H⁺SOFC prediction or cell optimization.

REFERENCES

- [1] J. Milewski, K. Świrski, M. Santarelli, P. Leone, *Advanced Methods of Solid Oxide Fuel Cell Modeling*, 1st Edition, Springer-Verlag London Ltd., 2011.
- [2] J. Milewski, M. Wołowicz, A. Miller, R. Bernat, A reduced order model of molten carbonate fuel cell: A proposal, *International Journal of Hydrogen Energy* 38 (26) (2013) 11565–11575.
- [3] G. Taillades, J. Dailly, M. Taillades-Jacquin, F. Mauvy, A. Essouhmi, M. Marrony, C. Lalanne, S. Fourcade, D. Jones, J.-C. Grenier, et al., Intermediate temperature anodesupported fuel cell based on BaCe0.9yO3 electrolyte with novel Pr2NiO4 cathode, *Fuel Cells* 10 (1) (2010) 166–173.
- [4] F. Lefebvre-Joud, G. Gauthier, J. Mougou, Current status of proton-conducting solid oxide fuel cells development, *J Appl Electrochem* 39 (2009) 535–543.
- [5] R. Hariharan, T. Prasanna, P. Gopalan, Novel perovskite based proton conductor for solid oxide fuel cells, *Scripta Materialia* 66 (2012) 658–661.
- [6] A. Zhu, G. Zhang, T. Wan, T. Shi, H. Wang, M. Wu, C. Wang, S. Huang, Y. Guo, H. Yu, et al., Evaluation of SrSc0.175Nb0.025Co0.8O3-δ perovskite as a cathode for proton conducting solid oxide fuel cells: The possibility of in situ creating protonic conductivity and electrochemical performance, *Electrochimica Acta* 259 (2018) 559–565.

MODELLING POLYMER ELECTROLYTE MEMBRANE DEGRADATION: FROM BIPOLAR PLATES TO MEMBRANE...

I.ELFERJANI^{a,b}, B.NORMAND^a, B.TER-OVANESSIAN^a and G.SERRE^b,

^aUniversité de Lyon, INSA-LYON, MATEIS UMR CNRS 5510, 69621 Villeurbanne, France

^bCEA, LITEN, DEHT, F-38054, Grenoble, France

Abstract: The work presented addresses the modelling of the Polymer Electrolyte Membrane fuel cell ageing process. We focus on the membrane degradation coupled with the bipolar plates (BPs) corrosion. That can lead to membrane failure. The BPs corrosion is an iron ions source. These latter catalyze the formation of radicals that damage the membrane and promote fluorides releasing. Thus, both mechanisms are strongly coupled. Our work is based on experimental and modeling approaches. The first modelling step is based on parametric corrosion study. Obtained results allow to determine the ions flux released by BPs corrosion using a look-up table. The second step is the modeling of iron ions effect on the membrane degradation in the Fenton mechanism. Our final coupled degradation model is implemented in a PEMFC simulator based on the Matlab Simulink platform used to predict and quantify the degradation for various operating conditions.

Key words: Bipolar plates, Corrosion modelling, Fenton mechanism, Membrane degradation modelling, Polymer electrolyte membrane fuel cell.

I. NOMENCLATURE

- I Current density / A/cm²
- E Electrical voltage/V

II. INTRODUCTION

The metallic BPs corrosion is a critical phenomenon for polymer electrolyte membrane fuel cells, since it does not only impact the cell performance by increasing the contact resistance (1) but also affects the membrane integrity (2). Once the membrane degradation occurs, the thinning process starts and therefore the gas cross over increases. Since the integrity BPs and the membrane affect the fuel cell lifetime, a lot work in the literature had described the BPs corrosion and the membrane degradation (3). However, the link between the two phenomenon is not fully understood. Our work based on an experimental and modeling approach is an opportunity to create this link. The first approach is experimental. A preliminary study defined the most representative operating simulation conditions for PEMFCs. These conditions defined the study of stainless steel corrosion and

membrane degradation. The second approach is the modeling, which offers the link between the consequences of the BPs corrosion and the chemical degradation model of the membrane based on the Fenton mechanism.

III. RESULTS AND DISCUSSIONS

A. Corrosion study and modelling:

The potentiodynamic measurements were carried out on a thermally controlled three electrodes device. The three electrodes are: a 316L stainless steel sample as working electrode, a saturated mercury sulfate as reference electrode and the counter electrode is graphite. The three electrodes are controlled by a Gamry ref 600 potentiostat. The electrochemical schedule starts with 12 hours Open-Circuit Potential (OCP) followed by a potentiodynamic measurement performed at a scanning rate of 0.1 mV/s. The polarization curve gives the variations of the current density in function of the potential. In order to simulate the PEMFC working environment, the measurements were carried out in cell at the temperature 60°C, 70°C and 80°C, with different chloride content 10⁻² M, 10⁻³ M and 10⁻⁴ M, (Chlorides are here substituted for fluorides released by membrane degradation.). Different pH values are considered (3.5, 4, 4.5 and 5). The objective of this work is to establish the current density relationship with different parameters and the identification of synergisms effects. Figure 1 gives an example of the obtained results. The 316L corrosion resistance decreases with the chloride content. In fact, high chloride concentration and anodic potential, promote pitting corrosion (black curve). The material is dissolved. All the data collected from this study are gathered in a look-up table in Matlab with various entries: temperature, potential, pH and Fluoride (chloride) concentration. This table can provide the current density at different PEMFC's operating conditions.

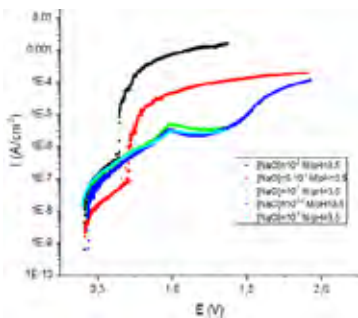


Fig. 1. 316L SS current density in function of potential (V/Vs DHE) at 80° C temperature, pH 3.5 and at different chloride concentrations

B. Membrane degradation model:

The degradation model is based on the Fenton mechanism, which is a complex multistep chemical mechanism presented in [4]. The 14 differential equations for the concentration species involved in the degradation process (oxygen, hydrogen, iron, and hydrogen peroxide, radicals and Nafion structure) are simulated using their kinetics [4] as function of temperature. The reaction rates and the concentrations of the different species are provided by the model, based on initial conditions, activation energies, PEMFC operating parameters and membrane characteristics. The set of equations have been implemented in the MePHYSTO code developed by CEA on the Matlab/Simulink platform. Ex-situ membrane degradation results provided by Frensch et al. [4] have been used to validate the model. The model developed on MePHYSTO by Frensch and us has been revisited to take into account the diffusion of species between the membrane and the solution, leading to a significant improvement of the simulations. The figure 2 is a comparison of fluoride concentration released by membrane degradation over time, between experimental and simulation results (Ex-Situ experiment conditions: Nafion 115 membrane, 80°C temperature, $[H_2O_2] = 3000$ (ppm) and $[Fe^{2+}] = 1$ ppm for 72 hours). At this condition the model seems to be in accord with the experiment.

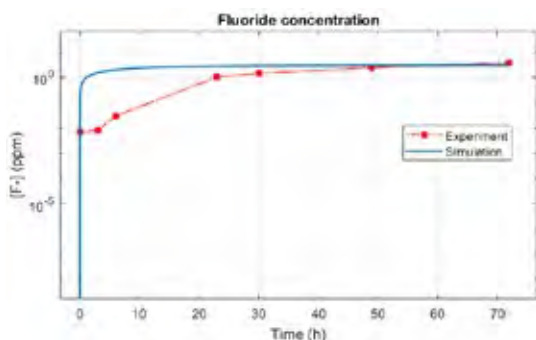


Fig.2. Fluoride concentration over time, simulation and experimental results comparison

C. Coupling model:

The CEA code is 1D through cell plane, 1D or 2D along the cell channels. It involves electrochemical reactions, fluid transport

and thermic transport [5]. The iron ions flux is calculated on the cathode channels, depending on the local conditions and based on the look-up table of corrosion. The Fenton equations are calculated in the membrane mesh using the local values of the involved parameters. Several simplified assumptions have been made: the pH is set at 4, the iron flux is deduced from the corrosion current (applying the Faraday law 80% of the emitted moles are supposed to be iron), iron and fluoride transport are also simplified. We assume an infinite diffusion coefficient through gas diffusion layer (GDL) and therefore we have a homogeneous fluorides and iron ions content in the channel and the GDL. The convection along channel is not considered and thus, we perform simulation using one mesh along the cell and five through cell (2 channels, 2 GDL and 1 membrane). With this coupling process we get the coupled effect between the corrosion mirrored by the iron ions release and membrane degradation mirrored by fluoride release.

IV. CONCLUSIONS

In one hand, the parametric corrosion study allowed to understand the 316L SS BPs behavior in PEMFC environment and to identify the BPs weak points. The corrosion data collected were used to generate an iron source term introduced in the model as a function of the operating conditions. On the other hand, the 14 equations Fenton model were validated with the ex-situ membrane degradation analysis which underline the catalytic effect of iron cations on the membrane degradation and fluoride releasing. The originality of this work remains in the tracking of two degradation mechanisms: - the corrosion of BPs and membrane degradation and - modeling the synergism effect.

REFERENCES

- [1] S. Kreitmeyer, A. Wokaun, F. N. Büchi, Polymer Electrolyte Membrane Durability - Local Degradation at Pinholes, ECS Transactions 50(2)927-933(2012).
- [2] PR.Tian, S.Junca, Corrosion resistance and interfacial contact resistance of TiN coated 316L bipolar plates for proton exchange membrane fuel cell, Int. J. Hydrog. Energy 36(11)(6788-6794).
- [3] G.A. Futter, A.Latz, T.Jahnke, Physical modeling of chemical membrane degradation in polymer electrolyte fuel cells: Influence of pressure, relative humidity and cell. J. Power. Sources 410-411(11).
- [4] S.H.Frensch, G.Serre, F.Fouda-Onana, H.C.Jensen, M.Y.Christensen, S.SAraya, S.K.Kær, Impact of iron and hydrogen peroxide on membrane degradation for polymer electrolyte membrane water electrolysis: Computational and experimental investigation on fluoride emission, J. Power. Sources 420 (2019) (54-62).
- [5] C.Robin, M.GERARD, J.D'Arbigny, P.Schott, L.Jabbour, Y.Blitel, Development and experimental validation of a PEM fuel cell 2D-model to study heterogeneities effects along large area surface. Int. J. Hydrog. Energy 40 (2015) 10211-10230

Developing Accelerated Stress Test Protocols for Solid Oxide Fuel Cells and Electrolysers: the European project AD ASTRA

S.J. McPhail^a, D. Pumiglia^a, J. Laurencin^b, A. Hagen^c, A. Leon^d, J. Van Herle^e, D. Vladikova^f, D. Montinaro^g, P. Piccardo^h, P. Polverinoⁱ, and K. Herbrig^j

^aENEA, Rome 00123, Italy

^bCEA, Grenoble 38054, France

^cDTU Energy, Roskilde 4000, Denmark

^dEIFER, Karlsruhe 76131, Germany

^eEPFL, Sion 1951, Switzerland

^fIEES, 1113 Sofia, Bulgaria

^gSolidPower, Mezzolombardo 38017, Italy

^hUniversity of Genoa, Genova 16145, Italy

ⁱDept. of Industrial Engineering, University of Salerno,
via Giovanni Paolo II 132, Fisciano 84084, Italy

^jSunfire, Dresden 01237, Germany

Abstract - In order to finally and systematically address the growing need for accelerated stress tests, given the longer lifetimes of solid oxide cells – both in fuel cell and electrolysis operation – the Fuel Cells and Hydrogen Joint Undertaking has launched an international initiative to overcome this epic challenge. These will build firstly on the analysis of numerous field-tested samples of SOC stacks provided by the industrial partners, followed by applying existing and developing improved testing and modelling methods based on ex-situ component ageing and aggravated stack testing.

Index Terms – Accelerated testing, solid oxide cells, power-to-x, combined heat and power

I. EXTENDED SOC LIFETIMES LEAD TO INCREASED NEED FOR ACCELERATED TESTING

Considering the useful lifetimes that are expected for commercial Solid Oxide Cell (SOC) stacks of up to 80000 hours (both for stationary CHP and energy storage applications), the current state-of-art durability is still a long way from meeting market requirements. As increasing service times are being achieved, further development of more robust SOCs therefore calls urgently for accelerated lifetime tests, which enable rapid analysis of realistic degradation rates, and

for degradation models that enable an extrapolation of realistic performance to system end of useful life.

Generally, a great number of operational parameters influence SOC degradation during lifetime, each contributing according to characteristic times and intensities, often in convoluted or even contrasting fashion. Aggravation of test input parameters (TIPs) can thus lead to non-representative accelerated degradation of a component where concurring effects are differently influenced, leading to a biased end state of the component investigated. For example, extensive studies on the effects on SOC positive electrodes of chromium evaporation from hot steel components have shown that aggravating different TIPs leads to diverging responses of the governing mechanisms (dissolution of Cr species in the perovskite phase, deposition and electrochemical volatilization of Cr species on active sites), see Figure 1 [1].

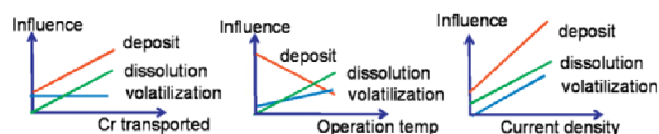


Fig. 1: Influence of operating conditions on processes dominating Cr-poisoning of SOFC cathodes [1]

From the trends depicted in Figure 1, only varying current density could generate a coherent variation of the mechanisms (though the slight divergence of influences would need to be taken into account). Furthermore, the closely knit processes in a working SOC often lead to domino-effects, whereby acute degradation occurring in one component or area can trigger or accelerate degradation elsewhere in the stack. Thus, it is crucial to identify the critical locations and dominant mechanisms that curtail SOC lifetime.

II. AD ASTRA: A WORLD-WIDE INITIATIVE TO HARNESS DEGRADATION MECHANISMS AND VALIDATE ACCELERATED TESTING PROTOCOLS

Whereas SOFC operation and possible accelerated ageing procedures have been extensively studied and attempted, respectively, capturing electrolysis degradation in short-term tests is radically innovative, since there are not even a significant number of stacks and systems in the field that have operated for more than 1 or 2 years consecutively.

The industrial partners in AD ASTRA (SOLIDPower and Sunfire) have among the most extensive records of SOC operation in the field, and world-class expertise on SOC manufacturing. This precious demonstration record and know-how – in both SOFC and SOEC operation – has led to the identification of three critical components limiting SOC stack lifetime:

- fuel (or negative) electrode
- oxygen (or positive) electrode
- interconnect

These critical areas were identified in the FCH JU project ENDURANCE [2], where a preliminary Failure Mode and Effects Analysis (FMEA) has been carried out, and by the SOC manufacturers through in-house FMEAs, all of which will serve as input to AD ASTRA. Furthermore, two types of applications will be considered that are most relevant for SOC systems:

- combined heat & power generators (CHP)
- electrical energy storage into chemical energy (P2X)

The failure modes are different in dynamic and in stationary operation, both for electrolysis (which is relevant for P2X) and power generation (CHP). However, defects in the above mentioned components occur in both applications, and have been cited as critical by both participating industries (SOLIDpower for CHP, Sunfire for P2X), who will supply sufficient samples of SOC stacks and components operated in the real world to the research partners for analysis of the degradation effects and for benchmarking stacks and components tested in the accelerated stress conditions defined in AD ASTRA.

III. HARNESSING DEGRADATION: APPROACH AND METHODOLOGY IN AD ASTRA

The testing approach will consist of a dual-focus campaign

targeting:

- macroscopic stack testing procedures, where short stacks will be operated in situ, in aggravated conditions with the objective of identifying test settings that will stress the stack in a representative way but minimizing testing time and resource expenditure
- specific component ageing tests, to reproduce (ex-situ) the degraded condition of critical stack components or interfaces in a faster time, based on analysis of the components extracted from stacks that have been field-tested.

Furthermore, a radical innovation will consist in the integration of these two methods: components specifically aged ex situ will be assembled into otherwise “new” stacks for in-situ testing, so that their effect on stack performance can be easily isolated from other components that in real-world conditions would also degrade. These tests allow to observe from the start ($t=0$) the end-of-service stack degradation, radically reducing in-situ testing time and providing powerful means to validate models simulating the long-term effects of component degradation in a stack.

IV. MODELLING OF DEGRADATION AND REMAINING USEFUL LIFE (RUL) PREDICTION

In AD ASTRA, a real attempt will be made towards integrating degradation and RUL prediction in performance models. In order to concretize the understanding of the physical degradation mechanisms, a multi-scale numerical tool will be adapted and optimized, combining two electrode-scale models with a macroscopic two-dimensional cell approach. To assist and simplify the physical modelling, the best grey-box dynamic modelling approaches (i.e. based on Ordinary Differential Equations) will be selected among, for example, first principle macro balances, lumped parameters or statistical models.

The main outcome will be a set of fast models describing the time evolution of parameters representing each selected degradation phenomenon as a function of operation as well [38], allowing to estimate the SOC performance and lifetime (RUL) as function of operation severity.

ACKNOWLEDGMENT

This project has received funding from the Fuel Cells and Hydrogen Joint Undertaking under Grant Agreement No 825027. This Joint Undertaking receives support from the European Union's Horizon 2020 research and innovation program and Hydrogen Europe.

REFERENCE

- [1] H. Yokokawa, T. Horita, K. Yamaji, H. Kishimoto, T. Yamamoto, M. Yoshikawa, Y. Mugikura, K. Tomida, *Fuel Cells*, **13** (2013)

DEVELOPMENT OF A 50M³/H HIGH PURITY HYDROGEN SYSTEM AND INTEGRATION WITH AN AUTOMOTIVE DERIVATIVE LOW TEMPERATURE PEM FUEL CELL

Thomas I. Chalkidis *, Andreas G. Kouroumlidis**

*HEL BIO SA, 10 Old National Rd Patras Athens, (Greece)

** HEL BIO SA, 10 Old National Rd Patras Athens, (Greece)

High purity hydrogen production has drawn substantial interest over the past years as the potential energy carrier for use either as a fuel in fuel cell vehicles or for power production via fuel cells. Within the Autore project (Automotive derivative energy system, EU project number: 671396) the aim was to create the foundations for commercializing an automotive derivative fuel cell system in the 50 to 100 kW range, for combined heat and power (CHP) applications in commercial and industrial buildings. The project's objectives were: to develop system components allowing reduced costs, increased durability and efficiency, to build and validate a first 50 kW PEM prototype CHP system and to create the required value chain from automotive manufacturers to stationary energy end-users. Mass-market production of fuel cells is a strong factor in reducing first costs. In this respect, joining the forces of two non-competing sectors (automotive and stationary) brings benefits to both namely to increase production volume and ultimately reduce costs to make fuel cells competitive. As a consequence, the project partners identified a PEM fuel cell-based CHP concept to address the stationary power market, primarily for commercial and industrial buildings requiring an installed capacity from about 50 kWe to some hundreds of kWe. The main components of the system have been validated to at least laboratory scale (TRL>4). A part of the AutoRE project was that the overall system had to be demonstrated and validated so as to increase the technology readiness level to TRL5. The project consortium reflected the full value chain of the fuel cell CHP system which would enhance significantly the route to market for the system/technology.

Index Terms – Hydrogen, PEMFC, process development.

I. NOMENCLATURE

PEMFC: Proton exchange membrane fuel cell.

CHP: Combined Heat and Power

P&ID Piping and instrumentation

II. INTRODUCTION

The present document covers the design and construction of a hydrogen generation unit (fuel processor) and the integration with the purification subsystem (PSA) so as to meet the specification for both quantity and quality of hydrogen set by

the fuel cell supplier (Daimler). Hydrogen was purified employing the pressure swing adsorption (PSA). Finally the fuel processor was integrated with a low temperature PEM fuel cell provided by Daimler.

III. TECHNIQUE, A STATE OF THE ART AND COMMERCIALY AVAILABLE TECHNOLOGY.

A. State of the art

Large scale hydrogen production, employing steam reformation of natural gas, is a well-established technology and accounts for 95% of the global hydrogen production. However, it has several drawbacks when used for lower hydrogen production capacities i.e. 20-500 Nm³/h. The conventional steam natural gas reformers are based on large expensive reactors consisting of long length (i.e >5m) tubes filled with the reforming catalyst. An elevated heat supply is necessary in order to achieve a high methane (natural gas) conversion. The heat supply normally comes from combustion (flame burners) of a part of the incoming fuel gas feedstock or from burning waste gas. The required reactor volumes are usually very large. Approximately 95% of the volume of a conventional reformer is empty due to operation limitation as a safety distance between the very hot burner flames (T>1200 °C) and the reformer tubes is necessary to prevent tube corrosion and destruction by overheating. To increase the efficiency, novel reactors have to be designed and constructed for fuel reforming with lower volumes. Small-scale reformers are commercially available from several traditional suppliers mainly in USA, Japan and Germany, who are often targeting the conventional industrial gas market [1]. Few of them are presently aiming at the hydrogen refueling station and almost none in the CHP market. Steam reforming is essentially the only technology used commercially for the small-scale production of hydrogen from hydrocarbons. Nearly all small-scale reformers available today are down-scaled versions of the well-established large-scale steam-reforming technology. Due to the relatively high cost the small-scale on-site generators fail

to penetrate massively the hydrogen gas market. Helbio's innovative natural gas flameless reformer (HIWAR concept,) shown in Fig.1, was used in the project, was designed with a catalytic burner, which increased efficiency, decreased size with an impressive factor of 40 relative to conventional designs, and as a result of the latter, is cheaper to produce than conventional ones. The heat required for the process is produced by catalytic combustion of a fraction of the primary fuel, eliminating open flames and reducing the reactor size.

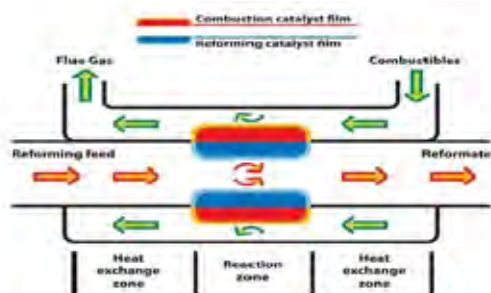


Fig. 1. Schematic presentation of the Heat Integrated Wall Reactor (HIWAR) concept

Contrary to conventional reformers, combustion takes place inside the tubes and reforming in the shell of the reactor/heat exchanger. The combustion takes place on a catalyst in the shape of a corrugated foil placed inside the tubes and in contact with the inner tube wall, while the reforming reaction on commercial catalyst is in pellets form. The flameless reactor exhibits improved efficiency compared with conventional ones (about 5% higher). In addition, lower combustion temperatures eliminate NOx emissions, a significant consideration in urban areas, and require lower cost material for the reactor tubes. Finally, the specific reformer can easily be transported in a container, thus allowing for factory manufacturing instead of on-site manufacturing, leading to higher quality, shorter building time, lower and more predictable cost.

B. Technical approach

i) The design targets set for the hydrogen production system were the high process efficiency balanced with the process's simplicity. Based on the above settings and after several iterations the derived process consisted from the following parts:

a) Reforming reactor, b) Water Gas Shift reactor, for CO minimization c) steam generator, where the steam required for the steam reforming reactions is produced, d) associated heat exchangers, which are placed between the various reactors to utilize the produced heat and e) Hydrogen purification system (PSA).

The mass and energy balances for the process were calculated assuming the reactor(s) are under thermodynamic equilibrium at pre-selected operating conditions (steam to carbon ratio, temperature, pressure etc.). The next step in the design of the fuel processor was to draw-up the Piping and Instrumentation

Diagram, (P&ID). By this process the various peripherals and instruments which are necessary for the safe operation of the system were identified and sized. A detailed HazOp analysis were also conducted upon completion of the P&ID. Next step was the construction of the hydrogen production system and integration with the PSA system. For the needs of the specific task, detailed drawings (2D and 3D) for each of the fuel processor sub-systems (reformer, WGS reactor, burner, steam generator, heat exchangers, reactants and air pre-heaters, condensers, etc), were conducted following the applicable safety standards. Construction was conducted in a major machine shop in Greece.

C. Integrated system realization

Integration of the supplied systems namely the fuel cell and the fuel processor were done in GE facilities in Rugby UK (Fig. 2). The system was connected with the necessary utilities e.g. water, natural gas. Special attention was given to fulfill all the safety parameters set in HazOp analysis.



Fig. 2. Installation of the complete system at GE's site in United Kingdom.

IV. CONCLUSION

The fuel processor system was designed and constructed so as to meet the specification set for the fuel cell supplier. The final systems namely the fuel processor and fuel cell were integrated and installed for testing in GE facilities in Rugby UK.

ACKNOWLEDGMENT

Automotive Derivative energy system (Autore,) project was founded from EU under the grant agreement 671396.

REFERENCES

- [1] Technology watch report: Small scale reforming systems for hydrogen refueling stations

H2PORTS - IMPLEMENTING FUEL CELLS AND HYDROGEN TECHNOLOGIES IN PORTS

Viviana Cigolotti^a, P. Di Giorgio^b, A. Pianese^b, M. Minutillo^b, E. Jannelli^b

a ENEA – Italian National Agency for New Technologies, Energy and Sustainable Economic Development – Portici Research Center, P.le E. Fermi 1, 80055 Portici (NA), Italy

b Department of Engineering, University of Naples “Parthenope”, Naples (Italy)

Abstract - Maritime transport and its logistic infrastructures (maritime ports, inland waterways, logistics platforms, etc.) are essential to keep the European Union (EU) in the leading position of world-developed areas. Promoting innovation on efficiency and sustainability of seaports is a fundamental issue, and Hydrogen is an energy carrier with great potential for clean, efficient power in transport applications.

I. PROJECT OVERVIEW

The H2Ports project, funded by FCH JU and starting in January 2019, tries to introduce hydrogen as an alternative fuel in the port industry, with the aim of providing efficient solutions to facilitate a fast evolution from a fossil fuel based industry towards a low carbon and zero-emission sector. The expected results of the project are to test and validate hydrogen-powered solutions in the port-maritime industry, with the aim of having applicable and real solutions without having repercussions on the port operations while producing zero local emissions. H2Ports is a highly ambitious project, aiming to deploy port equipment working with hydrogen as a fuel in the Port of Valencia (Spain) as a test and demonstration site.

H2Ports will perform the first experiences in the port sector concerning the integration of fuel cell technologies into heavy-duty vehicles, responsible of half of the emissions generated at ports. The project will evaluate fuel cell technology from multiple perspectives: prototype performance, adaptation to real life operation conditions, maintenance procedures, environmental benefits, hydrogen supply logistics, risks and safety aspects involved, etc. H2Ports will make available hydrogen Fuel Cell technology in heavy-duty port equipment for market adoption by 2020.

H2Ports will test under real life operations two prototypes equipped with hydrogen Fuel Cell technologies as “range extenders” of the electrical autonomy of each vehicle: Hydrogen Fuel Cell Reach Stacker and Hydrogen Fuel Cell Yard Terminal Tractor. These prototypes will substitute the fossil fuel generator by a hydrogen Fuel Cell, transforming both machines into a zero-emissions heavy-duty port equipment. Moreover, a third prototype will comprise a mobile Hydrogen supply station, with specific requirements from the terminal operators.

The H2Ports project would also have a transversal objective that consists on developing a sustainable hydrogen supply chain at the port, coordinating all actors involved: customers, hydrogen producers, suppliers, etc. The project will run the equipment on a daily basis during real operational activities and will analyse ways of improving the energy, performance and safety of operations with fuel cells port equipment.

The project is set up with a core group of partners, predominately end users (MSC Terminal Valencia, Grimaldi Group with Valencia Terminal Europe), fuel cell supplier (Ballard Power Systems), port equipment manufacturer (Hyster-Yale Group), research centres (Fundación Valenciaport, Spanish Hydrogen Centre and ATENA), authorities (Port Authority of Valencia) and a gas infrastructure company (Enagas).

With more than 800 ports in Europe, this project currently only represents only a small step in the right direction and represent an opportunity for fuel cell and hydrogen industry stakeholders and port communities in Europe to work together and prove on-field the capability of this solution.

ACKNOWLEDGMENT

This project has received funding from the Fuel Cells and Hydrogen 2 Joint Undertaking under grant agreement No 826339. This Joint Undertaking receives support from the European Union's Horizon 2020 research and innovation programme, Hydrogen Europe and Hydrogen Europe research

ADAPTIVE DYNAMIC CELL RECONFIGURATION OF MICROBIAL FUEL CELLS FOR POWER STABILITY

A. Mendis, J. You, J. Greenman and I. Ieropoulos
Bristol BioEnergy Centre (BBiC), University of the West of
England, Bristol, BS16 1QY (UK)

Abstract – A principal concern in Microbial Fuel Cell technology is obtaining maximum energy from fuel cell stacks whilst maintaining stability in performance. In this work, an adaptive dynamic cell reconfiguration mechanism is studied in order to overcome this problem. Using the illustrated mechanism, a peak power of 59mW was produced from an array of 15 microbial fuel cells for a dynamically variable load, in comparison to 23mW using a fixed topology.

Index Terms – dynamic reconfiguration, cell topology, microbial fuel cell (MFC), MFC performance recovery

I. INTRODUCTION

The Microbial fuel cell (MFC) technology is becoming widely accepted in electrical systems, robotics and renewable energy systems. The power demand of the load is met either by direct supply from source or by a power harvester-to-charger configuration. In the majority of applications, load requirements on the power system are dynamic and could significantly change over time. The current state of the technology requires multiple MFCs to be cascaded into stacks for useful applications.

In this work, we focus on two of the most prominent issues with regard to MFC stack operation. Firstly, the ability to draw maximum power, whilst running the cells simultaneously in a stack [1]. Secondly, the dynamic variation of load may cause the cells or the stack to underperform and degrade [2]. We propose an adaptive dynamic cell reconfiguration (ADCR) mechanism, in which the cells' electrical wiring topology is dynamically changed based on power demand and cell state. This is achieved through MFC state feedback. Observed variables are output power and MFC health.

II. MATERIALS AND METHODS

A stack containing 15 three-chambered (one anode and two

cathode chambers) MFCs working in continuous feeding mode were used to perform the tests. Anodes were made of plain carbon veil (20 g/m²) and cathodes consisted of carbon veil coated with activated carbon. Anodic and cathodic compartments were separated by ceramic membranes.

The 15 cells were dynamically configured using a custom-made electronic controller to the following four topologies: All in parallel (15P), all in series (15S), 5 cells in parallel with in 3 series segments (5P3S) and 3 cells in parallel with in 5 series segments (3P5S). Each fixed configuration was tested independently and within the following algorithms.

1. Fixed gain based on cell internal impedance; cells were cycled in the order {15P, 5P3S, 3P5S, 15S} and vice versa, based on the rate of change of power. Denoted: parallel-to-series (PtoS) and series-to-parallel (StoP).
2. Fixed gain (FG); based on observed gain and the rate of change of power.
3. Adaptive gain (AG); based on dynamic gain allocation and rate of change of power. A variant of adaptive gain with voltage clamping (AGC) is also tested.

A pseudo time varying non-linear voltage controlled current sink was used as a test load. Voltage range: 0.15~5V, max sink current: 70mA.

A constant feedstock flow rate of 0.32 ml/min was maintained throughout the tests. For studying long-term cell sustainability with the use of ADCR, the cells were subjected to two additional flow rates of 0.16 ml/min and 3.20 ml/min.

III. RESULTS AND DISCUSSION

A. Power Output

At a fixed flow rate of 0.32ml/min, the MFCs had a mean open circuit voltage (OCV) of 550mV. Fixed topologies gave a peak power of 23mW on 5P3S with degradation to 14mW over

a 12-hour period. Fixed topologies were able to provide an average power of 9mW on 15P configuration and maintained the cells without degradation at $1.68\mu\text{W}/\text{min}$ mean power gain over a period of 150 hours. ADCR algorithms AG provided a maximum average power of 59mW, AGC clamped between 350~450mV was able to provide a mean power of 48mW over a period in excess of 70 hours with a gain of $3.36\mu\text{W}/\text{min}$.

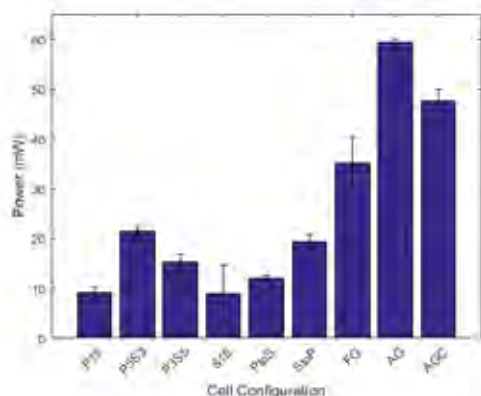


Fig. 1. Average power output based on controller configuration

B. Cell Sustainability

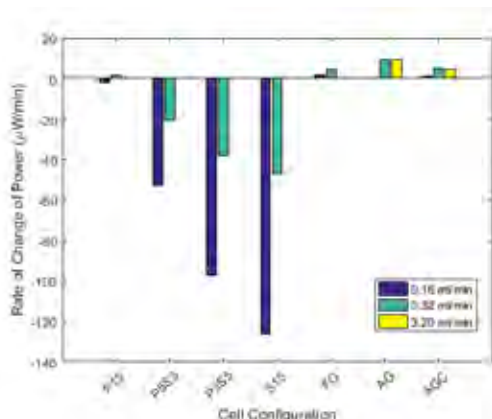


Fig. 2. Rate of change of output power based on flowrate for each configuration

Of the fixed topologies, 15P topology maintained a positive gradient of $1.7\mu\text{W}/\text{min}$ at $0.32\text{ml}/\text{min}$. This was used as the default configuration. Series-based topologies caused severe cell degeneration under low flow rates. In contrast, all ADCR configurations maintained a positive gradient on the rate of change of power even with a reduction in the flow rate to $0.16\text{ml}/\text{min}$. FG performs for over 200 hours with a $1.7\mu\text{W}/\text{min}$ positive gradient, and AGC performs for 60 hours, with a positive gradient of $0.9\mu\text{W}/\text{min}$.

C. Regulated Output

The voltage clamped AGC configuration maintained a set voltage level between 350~450mV and delivered 48mW of power over the changing flow rates of $0.32\text{ml}/\text{min}$ and $0.16\text{ml}/\text{min}$, over 90 hours for a time varying load.

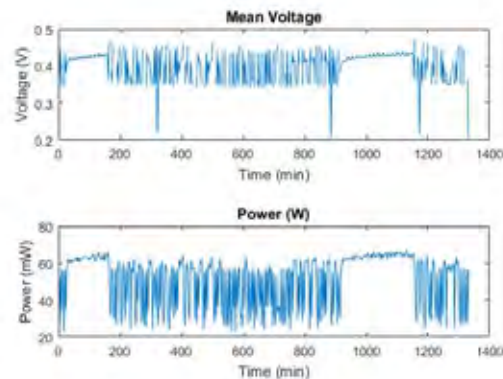


Fig. 3. Average power output based on controller configuration

IV. CONCLUSIONS

The study showed that the use of ADCR on the 15-cell stack achieved 6.5 times higher power generation compared to a fixed electrical configuration. ADCR method also maintained cells for a period of 90 hours at an optimal level for a dynamic load even at low flow rates. It can be concluded that the MFCs delivered different power output levels depending on the stress levels enforced by topology; MFC stress levels did not consistently correlate to output power. ADCR maintained the MFCs in both initial stages and mature steady state operation of the biofilm. ADCR was also able to provide regulated power within a specified voltage window.

ACKNOWLEDGMENT

This research was funded by the European Commission Horizon 2020 FET-OPEN Living Architecture Project (grant no. 686585).

REFERENCES

- [1] Menicucci, Joseph, Haluk Beyenal, Enrico Marsili, Raajaraajan Angathevar Veluchamy, Goksel Demir, and Zbigniew Lewandowski. "Procedure for determining maximum sustainable power generated by microbial fuel cells." *Environmental science & technology* 40, no. 3 (2006): 1062-1068.
- [2] Grondin, F., M. Perrier, and B. Tartakovsky. "Microbial fuel cell operation with intermittent connection of the electrical load." *Journal of Power Sources* 208 (2012): 18-23.

ENERGY ISLAND SYSTEM IN MARGINAL AREA

G.Santonocito*, M. Fanizzi**

*Idrogeno Biogas e Cogenerazione, (Italy)

**Ce.Eco Group, (Switzerland)

Abstract - The CE.ECO project we implemented, founded by the Mother Theresa of Calcutta Foundation, aims to create a system for energy production in remote areas, through the exploitation of renewable sources in a transportable unit, equipped with a system storage of the H₂ produced. The system will consist of no.1 electrolyzer with 9kW nominal power. The electrolyzer will be powered at 380 V by electricity coming from the photovoltaic system. Since the energy produced by the photovoltaic system is in direct current, the power supply will take place by means of an inverter that will transform the electricity from continuous into alternating current with an output voltage of 380 V. The electric energy generation section will be completed with units of general protection and control of the electrolyzer power supply line. The H₂ produced by the electrolyzer will be sent to a storage system after having undergone a pressure increase up to 100 bar, obtained by means of a compressor with a nominal power of 1 kW also supplied by the photovoltaic system. We are going to configurate an "island type" system. The storage consists of cylinders and will have a total capacity of 20 Nm³. Downstream of storage system a pressure accumulation reducing system will be set up from 100 bar to 2-6 bar, needed to guarantee the optimum operation of the fuel cell that will be placed downstream the hydrogen storage system. The H₂ powered fuel cell will produce electricity in CC that will be converted into AC current by means of an inverter to be located nearby the Fuel Cells. The AC current output will be connected by cable lines to the panel electrical production system to be placed inside the container. The general production framework will be accompanied by all necessary protections and energy measurement devices produced. From the general production framework, both the supplies will be provided with electric utilities installed in the settlement and plant control management area. In particular, the plant will power 50-60 led bulbs of 16W, one for each house unit, and a refrigeration unit common to the settlement. During the final design phase it will be possible to install inside the container both the refrigeration unit and a small cold room. Within the installation a drinking water system for civil use will be equipped.

The above options will be evaluated together with the customer in terms of site priorities.

TECHNICAL PLANT DESCRIPTION.

Hydrogen plant

The Electrolyzer

Hydrogen generation system is made of a single electrolyzer. The equipment will be installed over a skid having size 240 x 200 cm. See below main features of electrolytic plant

H ₂ Production	: 2 Nm ³ /h
Gen Pressure	: 4-6 barg
Power Consumption	: 9 kW
Electric energy supply	: 380V/50 Hz/3 Ph+N+Earth
Softened process water flow	1,8 l/h
Hydrogen Humidity	: DRY
Assembling on skid	: YES

Electric panel board which contains all switches and parts needed for plant operation.

Management device system which permits the remote control of electrolyzer operation with mode for working parameters resetting.

The electrolysis plant is suitable to be installed inside the container with overturned side-tipped mode (see picture on front page)

Compression System

The system is made of a single piston-compressor positioned on a separate skid inside the container by means of threaded or welded connections. Compressor and its components are installed inside the container away in an isolated area far from Fuel Cell unit and H₂ production area and cylinder storage compartment.. Compressor can be fitted in an iron structure inside the container as prescribed by 1st degree Safety Rules.

The electrical control board will be installed in a safe area and connected to plant auxiliary instrumentation.

Compressor will have the following features :

Gas to be compressed	: H ₂
Flow rate	: 2 Nm ³ /h
Inlet Pressure	: 6 barg
Working Pressure	: 100 barg
H ₂ inlet temperature	: 30°C
H ₂ output temperature	: 40°C

TECHNICAL DATA

Compressor Model	: Market
Compression	: Lubricated
Number of cylinder	: 2
Pistons ave speed	: 2,17 m/s
Compression stages	: 2
Revs	: 650 RPM
Shaft power	: 1 kW
Cooling water flow rate	: 3 m ³ /h ($\Delta T=10^{\circ}\text{C}$, $T_{in}=30^{\circ}\text{C}$)
Assembling on skid	: YES
Installation	: Indoor
Electric Site Classification	: Dangerous Area
Certifications	: ATEX-ASME-PED

H2 Storage Cylinders.

The main storage function is to accumulate compressed gas. The plant is designed for the installation of no.4 cylinders having geometric capacity of 50 liters that will be placed in a detached area as per 1st degree safety level

Cylinders will be in composite metallic alloy , cylinder shape, horizontal axis,built and tested according to current EU legislation for technical gas and pressurized equipments. Storage system will be supplied with proper instrumentation suitable to detect pressure and temperature besides all the safety devices required by the relevant technical standards.

TECHNICAL DATA

Gas	: H2
Pressure	: 100 barg
Cylinder Qt	: 4
Geom.Capacity	: 50 lt
H2 stored Qt	: 20 Nm ³

Fuel Cell

Fuel Cell electric generation system will consist of a machine capable of dispensing a nominal power of 2 kW. The Fuel Cell will be installed inside a standard 40 ' container in a properly delimited area designed to conform 1st degree safety features and environment conditions in order to assure an optimized working process of the machines installed inside the container itself.

TECHNICAL DATA

Nominal Power	: 2 kW
Voltage	: 36 VCC
H2 Inlet Pressure	: 2-6 bar

A piping distribution system will transfer H2 from electrolyzer to storage system and then to the Fuel Cell. All pipings are in stainless steel . Their size will allow a 2 Nm³/h Hydrogen flow rate in the section between electrolyzer and cylinders and 1,6 Nm³/h between storage system and Fuel Cell

The network can be subdivided in 3 tract according to working

pressures applied :

1st tract: electrolyzer-compressor , 2-6 bar

2nd tract : compressor-cylinder-100 bar pressure reducer system

3rd tract : Pressure reducer system - Fuel Cell 2-6 bar

I. CONCLUSIONS

PURITY 3.0 can be considered both from a functional point of view and its single components (electrolyzer, fuel cell, compressor...etc) as a recent technology product as market presence is concerned and therefore not yet introduced in final user distribution networks. This means that , lacking yet an economics of scale, the actual cost of the system may induce to evaluate as non-feasible the initial investment required. It is nevertheless evident however, that nowadays pressing need of an increased use of alternative energies, is orienting all green economy players and government institutions to start with new applications.

PURITY 3.0 is presenting its total virtuosity due to the absolute Zero Emission pattern, as well as the proven production entirely due to renewable sources such as water and sun. Moreover, Purity 3.0 is decreasing the **dispersion**, typical aspect of energy production and distribution , inherent on large scale national systems. In fact Purity 3.0 allows H2 storage and its subsequent transformation in electric energy that will be directly supplied to the site network , satisfying in this way the neighbor territorial needs.

We are allowed to think that, as it happened for Photovoltaic panels, the dissemination and further large scale production of Purity 3.0 , will result in a relevant cost decrease of the system, both in terms of finished plant and its components and parts .

Purity 3.0 is a self-regenerating system and even the water used for the initial process of H2 generation can be condensed and recycled as Fuel Cell working process residual is water steam.

Purity 3.0 is a Zero impact closed system

PURITY 3.0

- STORAGE**
 - HYDROGEN
 - 1 Electrolyzer 20kwh
 - Storage 20Nm³
 - Fuel Cell 0.2-3kW
- 20 KWH ENERGY**
 - Fu Modulo 20 kW
 - Modulo SunPower 220w
 - Energy Canale
- 3G HOT-SPOT**
 - Modulo Wi-Fi 3G -4G -5G
- WATER DEPURATION**
 - Water 1/10 M³/Day

Dr. GAETANO SANTONOCITO
IDROGENO BIOGAS E COGENERAZIONE

Dal sole, dal vento, dall'acqua
L'ENERGIA PULITA' idroenergia

TERRACOTTA AND BIOCHAR-DERIVED ELECTRODES FOR BIOELECTROCHEMICAL SYSTEMS

Pierangela Cristiani*, Stefania Marzorati**, Andrea Goglio**, Stefano Trasatti, Maksim Bogadish***, Andrea Schievano**

* Ricerca sul Sistema Energetico – RSE S.p.A., via Rubattino, 54, 20134 Milano, Italy

** e-Bio Center, University of Milan, Department of Environmental Science and Policy, via Celoria 2 - 20133 Milano (Italy)

***Politecnico di Milano, Department of Chemistry, Materials and Chemical Engineering, V. Mancinelli 7, 20131 Milano (Italy)

Abstract Research in the field of bioelectrochemical systems (BES) has been addressing the improvement of cost-effective electrodes materials and their manufacturing processes. An emerging class of biogenic materials for potential application in BES has been recently proposed, based on charcoal. In this work, new composite materials, produced by pyrolysis of raw biomass derived from *Arundo Donax L.* plant mixed with terracotta in different percentages, were produced and characterized. The conductivity, electrocatalytic properties and biocompatible characteristics of the new materials were determined aiming to their suitable application in BES for nutrient recovering from wastewater treatment, in a circular economy perspective.

Index Terms – nutrients recovery, BES, charcoal, wastewater

I. INTRODUCTION

In the last decades, research in the field of bioelectrochemical systems (BES) has been focusing on cost-effective electrodes materials and their manufacturing processes for applications such as environment pollution remediation [1]. Typically, electrodes for BES are fabricated using conductors based on graphite carbon-fibers or metals. However, their high economic and environmental costs impede their large-scale applications. Addressing the issues of cost and availability, an emerging class of biogenic materials for potential application in BES has been recently proposed, based on charcoal [1-3]. In continuity with those studies, new composite charcoal were experimented in this work, produced by a single step pyrolysis of residual biomass differently mixed with terracotta. These special and suitable charcoals can be largely available at relatively low

costs and impacts, therefore, it is a great candidate for BES systems. The conductivity, electrocatalytic properties and biocompatibility of the new composites from raw *A. donax L.* (arundo) were presented here, in comparison with identical ones produced from commercial biochar .

Different percentages (1%, 5%, and 10%) of *A. donax L.* plant residual biomass was mixed with terracotta and then pyrolyzed in a single heating step, with the target to create different levels of porosity in the composite inducing, consequently, a different potential water content and permeability. The pyrolysis of the raw material, indeed, makes it porous and at the same time conductive (generating graphite-like carbon crystals). Electrochemical measurements were previously performed on biochar based cathodes in single chamber air breathing Microbial fuel cell systems for wastewater treatment [2]. After the operation, air-exposed cathodes induced biofouling and deposition of salts on the electrode material. By these phenomena, organic carbon, nitrogen and other macro- and micronutrients, were recovered inside the carbon electrodic matrix. Since biochar is widely recognized to act as agricultural soil fertility promoter, the recovered nutrients-enriched electrodes might be re-used as soil conditioner, in a circular economy perspective.

II. MATERIALS AND METHODS

Samples of composites were built mixing terracotta and raw *A. donax L.* chippings or charcoal already produced from same vegetal.

All the prepared mixed (terracotta and carbon) materials were pyrolyzed at 900°C for one hour under Nitrogen atmosphere. Cylindric samples of the composites were produced with 3

different thickness (4mm, 8mm, 12mm), using the two carbon elements: raw arundo (arundo) and biochar with three percentages (1%, 5%, 10%). The following analysis were performed on the samples: material electrical resistivity by impedance analysis (Start = 0V Stop = 0.5V, Voltage slope = 0.01V s⁻¹), material water retention by water pressure measurements and air/water pressure resistance at 0.5, 1, and 1.5m of water column.

Each material was built and tested in triplicate.

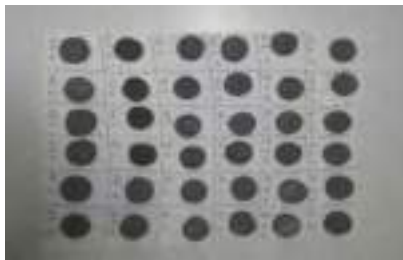


Figure 1. Image of samples characterized by different thickness (4, 8, 12 mm), carbon source (arundo or biochar) and its gravimetric percentage (1%, 5%, 10%, clay balance) .

III. RESULTS AND DISCUSSION

The resistivity of the biochar used to build the composites was 39 Ω cm ± 0.013, which resulted quite low, as not much different from the resistivity measured on carbon cloth (28 Ω cm ± 0.002).

After pyrolysis, the electrical resistivity of samples measured for each composite sample is reported in the Table 1. The results indicate a decrease of resistivity of more than two order of magnitude for 10% content in the case of arundo composites, which performed better than biochar composites. The water retention capability of the samples is reported in the Table 2. This parameter varied not so much among the samples.

The Air/water pressure resistances of arundo-composite samples at 0.5, 1, and 1.5m of water column are reported in the Table 3.

Table 1. Material electrical resistivity

	Arundo (MΩ cm)	Biochar (MΩ cm)
1% 4mm	45.5 ± 43.5	90.0 ± 18.0
1% 8mm	76.3 ± 54.0	95.3 ± 45.0
1% 12mm	76.3 ± 12.0	110 ± 84.0
5% 4mm	1.16 ± 0.02	10.9 ± 6.0
5% 8mm	7.06 ± 4.57	15.5 ± 14.1
5% 12mm	1.05 ± 1.4	21.2 ± 6.0
10% 4mm	2.89 ± 4.0	19.5 ± 10.3
10% 8mm	1.51 ± 2.01	5.96 ± 0.37
10% 12mm	0.45 ± 0.46	31.2 ± 31.5

This last parameter is always < 0.01 ml h⁻¹ for the biochar-

composite samples and increases of more than two order of magnitudes for 10% arundo samples.

Table 2. Water retention of materials samples

	Arundo (g kg ⁻¹)	Biochar (g kg ⁻¹)
1% 4mm	194 ± 0.3	181 ± 1.1
1% 8mm	185 ± 3.1	178 ± 1.6
1% 12mm	185 ± 4.8	172 ± 4.4
5% 4mm	283 ± 7.5	198 ± 3.2
5% 8mm	278 ± 0.3	202 ± 14
5% 12mm	281 ± 0.3	195 ± 3.2
10% 4mm	351 ± 8.0	226 ± 3.4
10% 8mm	350 ± 8.0	215 ± 7.9
10% 12mm	349 ± 4.0	212 ± 5.2

Table 3. Air/water pressure resistances of the Arundo composite samples at 0.5, 1, and 1.5m of water column.

	ml h ⁻¹ 0.5m	ml h ⁻¹ 1m	ml h ⁻¹ 1.5m
1% 4mm	0.03 ± 0.1	0.19 ± 0.1	0.47 ± 0.2
1% 8mm	0.02 ± 0.0	0.18 ± 0.2	0.41 ± 0.3
1% 12mm	0.00 ± 0.0	0.01 ± 0.0	0.14 ± 0.2
5% 4mm	0.88 ± 0.2	1.75 ± 0.2	2.08 ± 0.3
5% 8mm	1.36 ± 0.2	2.85 ± 0.1	2.95 ± 0.7
5% 12mm	2.32 ± 1.4	6.26 ± 3.9	8.35 ± 1.0
10% 4mm	5.43 ± 0.2	16.9 ± 4.1	25.1 ± 1.1
10% 8mm	6.90 ± 0.2	19.8 ± 3.3	26.2 ± 6.3
10% 12mm	4.70 ± 2.1	12.3 ± 3.6	22.6 ± 5.3

IV. CONCLUSION

The direct pyrolysis of raw biomass mixed with terracotta clay produces suitable composites for BES-system electrodes, which better perform than mixed biochar-clay in terms of conductivity and water absorption and detection. Increasing the percentage of biomass mixed with clay is possible to decrease the electrical resistivity of the materials, suitably improving the porous texture of it.

ACKNOWLEDGMENT

This work was financed by the SIR 2014 Grant (PROJECT RBSI14JKU3), Italian Ministry of University and Research (MIUR) and the Research Fund for the Italian Electrical System (Decree: MISE, April 16, 2018).

REFERENCES

- [1] A. Giudicianni et al. Pyrolysis for exploitation of biomasses selected for soil phytoremediation: Characterization of gaseous and solid products. *Waste Manag.* 2017, 61, 288–299.
- [2] S. Marzorati et al. Air-breathing bio-cathodes based on electro-active biochar from pyrolysis of Giant Cane stalks 2018 *International Journal of Hydrogen Energy*, 44 (2019) 4496e4507.
- [3] A. Goglio et al. Microbial recycling cells: First steps into a new type of microbial electrochemical technologies, aimed at recovering nutrients from wastewater, *Bioresource Technology* 277 (2019) 117–127.

HYBRID ENERGY STORAGE SYSTEM FOR A PLUG-IN FUEL CELL ELECTRIC SCOOTER

P. Di Giorgio*, F.V. Conte **, E. Jannelli*

*Università di Napoli Parthenope, (Italy)

**Hochschule Augsburg, (Germany)

Abstract – This paper concerns the development of prototype of a new hybrid storage system for a plug in hybrid fuel cell electric scooter. The hybrid storage system is composed of a lithium ion battery pack fully enclosed in a metal hydride tank. This configuration allows to store in a single device hydrogen and electric energy. Moreover, it is possible to exploit the endothermic hydrogen desorption from metal hydride to perform the thermal management of the battery pack during the vehicle operation. A FEM model of the whole system was developed in order to evaluate the performance of the integration of the proposed hybrid storage system in the scooter.

Index Terms: Plug-in Fuel Cell Electric Scooter, Hybrid storage system, Metal hydride,

I. NOMENCLATURE

PFCHEV: Plug in Fuel Cell Hybrid Electric Vehicle

WLTC: Worldwide Harmonized Light Vehicles Test Cycle

II. INTRODUCTION

The transport sector is one of the main contributor to the EU's greenhouse gas emission, accounting for 23% of the total as of 2016. PFCHEV are regarded as an interesting zero emission alternative to common internal combustion engines. Compared to conventional Fuel Cell vehicles, PFCHEVs are more fuel efficient due to the optimization of the fuel cell operation and the higher recovery of kinetic energy during braking. The relatively small battery pack needed (when compared to pure EVs) can be charged with no need of supercharger infrastructure and the short everyday drives, that account for the majority of a vehicle utilization, can be covered only using cheaper electric energy [1]. The Fuel Cell can ensure the required range and the compressed hydrogen tanks allow for a quick fueling solution. The battery thermal management in such vehicles can be quite difficult; in fact, the battery experiences more severe thermal stress than EV since it generally undergoes higher C-rates and it has lower

thermal capacity. The scope of this work is to evaluate a new concept for an energy storage system specifically designed for a Plug-in Fuel Cell electric scooter that is composed of a metal hydride tank fully integrated in a lithium-ion battery pack. This design allows performing the thermal management of the battery pack using the endothermic desorption of hydrogen from the metal hydride-forming alloy.

III. SCOOTER POWER UNIT AND HYBRID STORAGE SYSTEM INTEGRATION

The scooter power unit has to feed a 2kW electric motor and is composed of a 1kW fuel cell stack and a 48V 12Ah lithium-ion battery pack, and it is part of the hybrid storage system. A DC/DC converter adjusts the fuel cell voltage and regulates its power output. The main hydrogen storage system is composed of 5 metal hydride cartridges for a total of 150g of hydrogen and of the secondary metal hydride tank enclosed in the hybrid storage system that contains 40 additional grams.

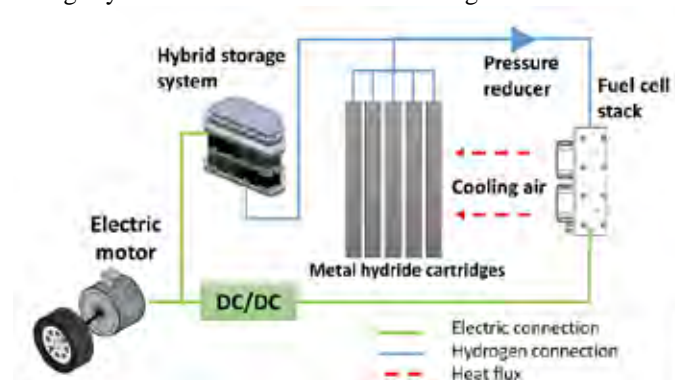


Fig. 1. Power unit configuration

The cartridges are positioned in front of the fuel cell fans, which act as air feeding and cooling system, in order to exploit the waste heat to promote the hydrogen desorption process.

The secondary metal hydride tank is directly connected to the cartridges, as shown in Figure 1. In this way, if the battery pack temperature rises, the hydrogen desorption is favored in the secondary metal hydride tank with respect to the cartridges, cooling the pack. On the contrary, when the temperature of the battery pack is low and does not need cooling, the cartridges will desorb more hydrogen. The FEM model developed aims to verify whether the integration of the hybrid energy storage device with the scooter power unit and the on-board hydrogen storage system as proposed, represents a feasible solution to be used in lightweight vehicles to improve the battery pack performance and the range.

IV. SYSTEM SIMULATION

A 2D COMSOL model of the system was developed. Only the model of one cartridge and of a quarter of hybrid storage system were realized. During the coupling of the two sub-models appropriate corrections were made for the hydrogen fluxes.

The power sharing strategy between the fuel cell and the battery pack was assumed from [2]. The power needed by the motor was estimated from a WLTC Class 1 for vehicles with power to weight ratio lower than 22 W/kg, as described in [2]. It was decided to repeat the cycle for 7 times, for a total simulation time of around 2 hours. The metal hydride alloy belongs to the TiMn family and it is produced by Gesellschaft für Elektrometallurgie (GfE). The model of the hydrogen desorption was developed and validated in [3].

Table 1 shows some of the simulation parameters.

TABLE I
TIMES NEW ROMAN TYPE SIZES AND STYLES FOR EFC2017

Parameter	Unit	Value
Convective heat exchange air- cartridge	W/m ²	25
Fuel cell air temperature	K	308
Plastic holder thermal conductivity	W/(mK)	0.6
Battery cell internal resistance	Ω	0.06
Initial temperature	K	293
Initial hydrogen concentration	%	1.5
Average fuel cell hydrogen request	mol/min	0.36
Average battery cell thermal power production	W	0.3

V. SIMULATION RESULTS

Figure 2 and 3 shows the temperature distribution in the hybrid storage system and in the metal hydride cartridge at the end of the simulation. The temperature of the battery cell is kept within an acceptable range by the hydrogen desorption in the metal hydride alloy. At the same time, the cartridges and the hybrid storage system are able to provide the hydrogen needed by the fuel cell stack.

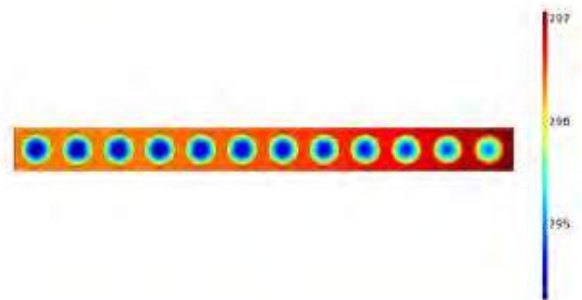


Fig. 2. Temperature distribution in the metal hydride cartridge at the end of simulation time

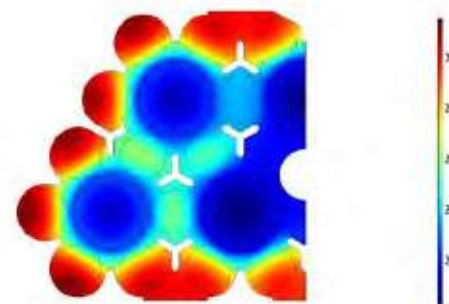


Fig. 3. Temperature distribution in the hybrid storage system at the end of the simulation time

VI. CONCLUSION

This work proposes and evaluates using a FEM model the integration of a hybrid energy storage system on a Plug-in Fuel cell electric scooter, during a typical operation cycle. The hybrid storage system is composed by a metal hydride tank in thermal contact with a lithium-ion battery pack, in order to exploit the endothermic hydrogen desorption process to control the temperature of the battery pack. The main hydrogen storage system on the scooter is composed by 5 metal hydride cartridges able to store around 150g of hydrogen, which is added 40g contained in the hybrid storage system. The simulation results show that through simple connection of the hybrid storage system to the cartridges it is possible to ensure a good operation of the system, since the temperature of the battery pack is kept into an acceptable range and the fuel cell hydrogen request is satisfied.

REFERENCES

- [1] B. Lane, B. Shaffer, G. S. Samuelsen, Plug-in fuel cell electric vehicles: A California case study, *International Journal of Hydrogen Energy*, Volume 42, 2017, pp. 14294-14300
- [2] P. Di Giorgio, P. Di Troilo, E. Jannelli, M.G. Minutillo, F.V. Conte, Model based preliminary design and optimization of Internal Combustion Engine and Fuel Cell hybrid electric vehicle, *Energy Procedia*, Volume 148, 2018, pp. 1191-1198
- [3] K. Herbrig, L. Rontzsch, C. Pohlmann, T. Weissgaerber, B. Kieback, Hydrogen storage systems based on hydride-graphite composites: Computer simulation and experimental validation, *International Journal of Hydrogen Energy*, Volume 38, 2013, pp. 7026-7036.

FULLY INTEGRATED POWER SYSTEM FOR LIGHTWEIGHT PLUG-IN FUEL CELL ELECTRIC VEHICLES

P. Di Trolio*, P. Di Giorgio*, E. Frasci*, M. Genovese**, S. Di Micco*, M.G. Minutillo*, E. Jannelli*

*Università Napoli Parthenope (Italy)

** Università della Calabria (Italy)

Abstract - The fuel cell-electric drive system is an attractive technology for a sustainable mobility with zero emissions. Hybrid fuel cell battery powertrain configurations in particular are gaining more and more attention thanks to the advantages they offer in terms of fuel cell downsizing. Such a solution usually implies the presence of several DC/DC converters to be able to perform the power sharing between fuel cell and battery pack. In this work, a fuel cell battery passive hybrid powertrain is proposed. This configuration eliminates the need for costly DC/DC converters. The power sharing is regulated directly coupling the voltages of the fuel cell and of the battery pack.

Index Terms - Plug-in Fuel Cell Electric Vehicles, Hybrid powertrain

I. NOMENCLATURE

FCEV- Fuel Cell Electric Vehicles
PFCEV- Plug-in Fuel Cell Electric Vehicles
LT-PEM Low Temperature Proton Exchange Membrane
WLTC- Worldwide harmonized Light-duty vehicles Test Cycles.
OCV- Open Circuit Voltage

II. INTRODUCTION

Fuel cell electric vehicles have been proposed as a fully sustainable solution for the mobility. Fast charging, lightweight vehicles and high range can be obtained from the adoption of fuel cell in powertrains. However, pure FCEV have a limited market penetration due to the lack of hydrogen refueling stations and high costs of the fuel cell system. PFCEVs have been proposed since they can reduce the cost of the system and increase the overall performance reducing the need for a widespread fueling infrastructure [1]. On the other hand, most of the solutions presented in literature uses expensive and complex power electronics to control the power sharing and to couple the battery pack and the fuel cell stack, decreasing the system overall efficiency and increasing cost and complexity. The authors here

present a plug-in fuel cell power unit architecture specifically designed for lightweight vehicles that avoids power converters and directly couples the battery pack and the fuel cell stack.

III. EXPERIMENTAL SETUP

The powertrain developed in this work is composed of:

- Five fuel cells connected in series, Horizon 500W LT-PEM.
- Two resistors (9 Ω each)
- 72V battery pack, LiFePO₄

The architecture is presented in Figure 1. Electrical coupling of the two subsystem of the powertrain was made possible through a system of resistors that reduce the voltage of the fuel cell stack to make it compatible with the battery pack one.

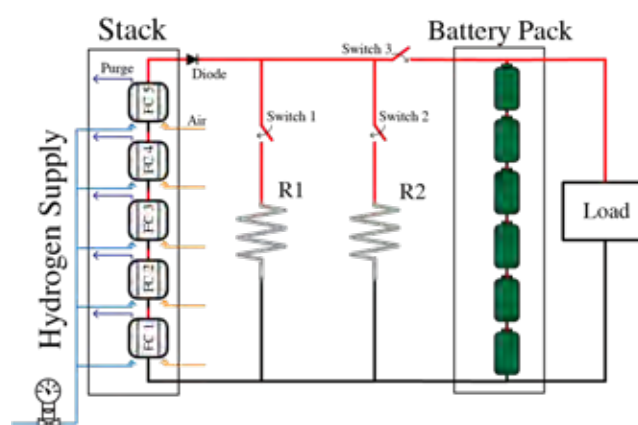


Fig. 1. Power unit schematics

To test the performance of the power unit a 2.6 kW electronic load was used to simulate the electric motor power request during an urban cycle (WLTC) for a lightweight electric vehicle, as showed in [2].

IV. EXPERIMENTAL RESULTS

A. Power Unit Start-Up

Figure 2 shows the voltage of the battery and of the fuel cell stack. Initially, at OCV, the fuel cell stack voltage is much higher than the battery pack one, and a direct connection would result in current spikes that could damage the battery pack and the fuel cells. For that reason, fuel cell stack is connected to two-resistance bench that brings the stack voltage closer to the battery pack one. At this point, the resistance benches are disconnected and the normal operation can begin.

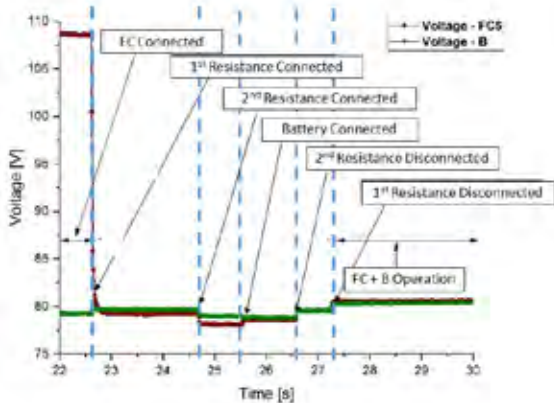


Fig. 2. Voltage profiles during the power unit start-up

B. Standard system operation

Once the start-up is completed the system evolves freely. The voltage at load node is the same for the battery pack and the fuel cell stack. The power sharing between the two components is a function of their polarization curves: the operative point is defined by the intersection between the two curves. Since the battery polarization curve depends on its SOC, at lower SOC will correspond a higher fuel cell stack current. In this way the power unit is able to self-regulate the power sharing increasing the fuel cell stack contribute when the battery charge is low.

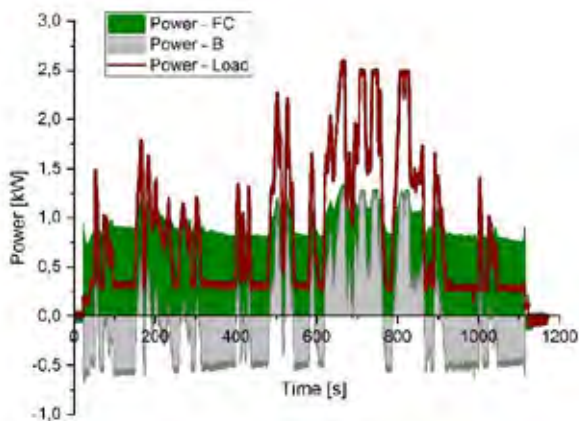


Fig. 3. Power sharing between battery pack and Fuel cell stack during the WLTC

C. Power Unit Shut-Down

Before shutting down the fuel cell stack, the same operations describer for start-up is performed, only in reverse order: at first the two resistance benches are connector, then the battery is disconnected, and finally the resistance benches are disconnected, and the fuel cell stack returns to OCV

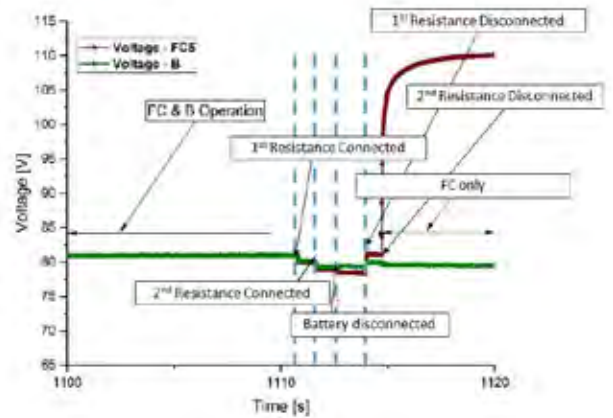


Fig. 4. Voltage profiles during the power unit shutdown phases

V. CONCLUSION

The presented power unit architecture allows to couple the battery pack and the fuel cell stack without power converter. The power sharing between the fuel cell and the battery pack is ensured by the characteristics of the two subsystems and .This solution is simple and cheap but at the same time capable of high overall efficiency. These features make it particularly suitable for application in lightweight vehicles.

ACKNOWLEDGMENT

This research was supported by the University of Naples "Parthenope", for the project "Sviluppo di sistemi di mobilità sostenibile con tecnologie smart capaci di utilizzare le risorse di Internet of Things (IoT)" (2016).

REFERENCES

- [1] B. Lane, B. Shaffer, G. S. Samuelsen, Plug-in fuel cell electric vehicles: A California case study, *International Journal of Hydrogen Energy*, Volume 42, 2017, pp. 14294-14300
- [2] P. Di Giorgio, P. Di Trolio, E. Jannelli, M.G. Minutillo, F.V. Conte, Model based preliminary design and optimization of Internal Combustion Engine and Fuel Cell hybrid electric vehicle, *Energy Procedia*, Volume 148, 2018, pp. 1191-1198



EUROPEAN FUEL CELL

CONFERENCE & EXHIBITION

NAPLES Hotel Royal Continental

9 > 11 December, 2019

Contents



ATENA
FUTURE TECHNOLOGY



Agente nazionale per le nuove tecnologie,
l'energia e lo sviluppo economico sostenibile



UNIVERSITÀ
DEGLI STUDI
DI NAPOLI
"PARTHENOPE"



UNIVERSITÀ
DEGLI STUDI
DI PERUGIA

AB. COD.	AUTHOR and TITLE	PAGE
EFC19001	Abad Correa David <i>Design and development of a hydrogen production system based on solid oxide electrolysis technology</i>	13
EFC19002	Milewski Jaroslaw <i>Theoretical investigation of using molten nitrates as electrolytes for fuel cells</i>	15
EFC19003	Beneito Ruben <i>Integration of a Solid Oxide Fuel Cell for the sustainable power generation from wastes in a winery industry</i>	17
EFC19004	Misz Ulrich <i>Development of standardized test methods for in-situ validation of system materials for the use in automotive fuel cell systems</i>	19
EFC19005	Papurello Davide <i>CFD model for tubular SOFC cells fed directly by biomass - a complete integrated system</i>	21
EFC19007	Ota Kenichiro <i>Green Hydrogen and Advanced PEFCs without NPGM and Carbon for Our Sustainable Growth</i>	23
EFC19008	Samsun Remzi Can <i>Compact and robust diesel fuel processing systems with quick-start capability for 5-10 kW fuel cell systems</i>	25
EFC19009	Nieto Gallego Emilio <i>Hyacinth project: cases of studies throughout samt tool</i>	27
EFC19010	Basso Peressut Andrea <i>Graphene oxide-based composite membranes as novel electrolytes for PEM fuel cells</i>	29
EFC19011	Chisaka Mitsuharu <i>Enhancement of Oxygen Reduction Reaction Activity on Phosphor and Nitrogen Co-doped TiO₂ catalyst for Polymer Electrolyte Fuel Cell Cathodes</i>	31
EFC19012	Ancona Maria Alessandra <i>Modelling and validation of a small-scale hybrid photovoltaic-battery-electrolyzer system</i>	33
EFC19013	Ballester Sierra Cristina <i>H2PORTS. Hydrogen refuelling system development in the port of Valencia</i>	35
EFC19014	Stoilova Anamarija <i>Estimating temperature in the catalyst layer of the PEM fuel cell</i>	37
EFC19015	Squizzato Enrico <i>Synthesis and characterization of Ca₂Fe_{1.95}Mg_{0.05}O₅: innovative low cost material for Reversible Solid Oxide Cell</i>	39
EFC19016	Baik Kyung Don <i>Development of cathode cooling fins with a multi-hole structure for open-cathode polymer electrolyte membrane fuel cells</i>	41
EFC19017	Lee Eunhye <i>Characteristics of activated carbon-supported Co-B and Co-P-B as a catalyst for hydrogen generation by NaBH₄ hydrolysis</i>	43
EFC19018	Chiche Ariel <i>Estimating the H₂ purge time for a PEM fuel cell working in dead-end mode in a closed environment</i>	45
EFC19019	Andersson Martin <i>System Level Modelling and Simulation of Transient Behavior for Polymer Electrolyte Fuel Cells</i>	47
EFC19020	Brendan Huitorel <i>Towards composite bipolar plates made by injection molding for PEMFC application: formulation, compounding and physical properties</i>	49
EFC19021	Gorelkov Stanislav <i>Effect of the cyclic frost exposure on the performance of PEM fuel cells</i>	51
EFC19022	Vladikova Daria <i>Impedance Studies of Ex-Situ Artificially Aged Ni-YSZ Anode for Accelerated Stress Tests</i>	53
EFC19024	Lee Yulho <i>Numerical modeling and performance optimization of a hybrid desiccant cooling system integrated with solid oxide fuel cell system</i>	55

AB. COD.	AUTHOR and TITLE	PAGE
EFC19028	Akabane Shunosuke <i>High electrical efficient SOFC generator for pure hydrogen with a multi-stage SOFC and regeneration system</i>	57
EFC19029	Mayuranathan Kishore Kumar <i>Evaluating Bauxite tailings for potential SOFC applications</i>	59
EFC19030	Verena Lukassek <i>Development of a compact μDMFC module with integrated gas-liquid separation</i>	61
EFC19031	Massaglia Giulia <i>N-doping modulation by plasma treatment in polyacrylonitrile derived carbon-based nanofibers for the oxygen reduction reaction</i>	63
EFC19032	Micoli Luca <i>Application of HTFC powered by LNG on a cruise ship: a case study</i>	65
EFC19033	Novalin Timon <i>Investigating iron release rate from metallic bipolar plates in proton exchange membrane fuel cells</i>	67
EFC19037	Crespi Elena <i>Comparison of humidification systems for flexible stationary PEMFC power systems</i>	69
EFC19038	Aimola Giorgia <i>The use of Microbial Fuel Cells for soil remediation: a preliminary study on DDE</i>	71
EFC19039	Quaglio Marzia <i>Integration of portable Sedimentary Microbial Fuel Cells in Autonomous Underwater Vehicles</i>	73
EFC19040	Wierzbicki Michał <i>CO assisted electrolysis of H₂O in quasi-symmetrical Ni-YSZ/YSZ/Ni-YSZ cell</i>	75
EFC19041	Kartouzian Dena <i>Impact of Porosity Gradients within Catalyst Layer and MPL of a PEM Fuel Cell on the Water Management and Performance: A Neutron Radiography Investigation</i>	77
EFC19042	Barale Jussara <i>DronHy: a Hydrogen Powered Drone at High Performances</i>	79
EFC19043	Crespi Elena <i>Supply of solar electricity to uninterruptible loads via seasonal storage with Power-to-Power systems</i>	81
EFC19044	Gagliardi Gabriele Guglielmo <i>Optimization of operating parameters on the direct methanol fuel cell using Nafion-graphene oxide multilayer membrane</i>	83
EFC19046	Tsiakaras Panagiotis <i>Oxygen reduction reaction on novel carbon supported pt-ir and pt-pd electrocatalysts</i>	85
EFC19047	Marra Eva <i>Evaluating thin-film model electrodes for AEMFC</i>	87
EFC19048	Mariani Marco <i>Enhancement of durability of microporous layers for PEM fuel cells based on graphene nanoplatelets.</i>	89
EFC19049	Linkov Vladimir <i>HySA Systems Fuel Cell Prototype Development and Demonstration for Stationary and Mobile Applications in South Africa</i>	91
EFC19051	Aricò Antonino Salvatore <i>High performance pem electrolyser for power-to-gas applications - hpem2gas</i>	93
EFC19054	Paritosh Kumar Mohanta <i>Effects of catalyst support materials and ionomer amounts in the cathode catalyst layers on membrane electrode assembly performances at high current loads</i>	95
EFC19055	Martino Marco <i>Chemical conversion coating technique in the preparation of structured catalysts for the CO-Water Gas Shift reaction</i>	97
EFC19056	Ruocco Concetta <i>Efficient catalysts for hydrogen production via ethanol reforming in a fluidized bed reactor</i>	99

AB. COD.	AUTHOR and TITLE	PAGE
EFC19058	Eguchi Koichi <i>Degradation Factors of Cathode during Operation of Solid Oxide Fuel Cells</i>	101
EFC19059	Giraldin Arianna <i>Solid Oxide Cells operating with C-containing fuels: overcoming the Ni based limitation</i>	103
EFC19062	Bove Dario <i>Simulation of Molten Carbonate Fuel Cells under dual-anion working conditions in carbon capture applications</i>	105
EFC19064	Stelitano Sara <i>Hydrogen Storage & ΔH Test Lab</i>	107
EFC19066	Fragiacomo Petronilla <i>Technical-Economic Analysis of Hydrogen Green Production and Storage for three Calabrian sites (Italy)</i>	109
EFC19067	Audasso Emilio <i>Detailed modelling of Internal Reforming Fuel Cells for process analysis and optimisation</i>	111
EFC19068	Bosio Barbara <i>A dual-anion mechanism in Molten Carbonate Fuel Cells for a dual-challenge: energy production and carbon capture</i>	113
EFC19069	Romagnoli Marcello <i>FCHGO: Fuel Cells HydroGen educatiOnal model for schools</i>	115
EFC19070	David Bernhard <i>Degradation Behavior of State of the Art PtCo Catalyst: An Ex- and In - Situ Analysis</i>	117
EFC19072	Skrzypkiewicz Marek <i>Experimental study of the performance of the anode supported solid oxide fuel cells (SOFC) fed with aerosol contaminated fuel</i>	119
EFC19074	Felli Andrea <i>Synthesis and Characterization of Ni-doped Double Perovskite $Sr_2FeNi_{0.4}Mo_{0.6}O_{6-\delta}$ as electrode for Symmetrical Solid Oxide Cell</i>	121
EFC19075	Colbertaldo Paolo <i>Sizing of integrated solar photovoltaic and electrolysis systems for clean hydrogen production</i>	123
EFC19076	Romagnoli Marcello <i>MAMA-MEA, Mass Manufacture of MEAs Using High Speed Deposition Processes</i>	125
EFC19077	Bianchi Fiammetta <i>Electrochemical modelling of Solid Oxide Fuel Cells</i>	127
EFC19080	Gonzalez Lola <i>Environmental monitoring of dissolved oxygen with floating photosynthetic microbial fuel cells</i>	129
EFC19081	Renda Simona <i>Study of the effect of Ru precursor in Ru-Ni/CeO₂-ZrO₂ catalysts for CO₂ methanation</i>	131
EFC19083	Grimaldi Amedeo <i>Simulation, analysis and control of Fuel Cell Electric Vehicle</i>	133
EFC19084	Gandiglio Marta <i>Solid oxide fuel cells as best practice for combined heat and power generation from biogas</i>	135
EFC19085	Messaggi Mirko <i>Experimental and numerical study of performance heterogeneities in a vanadium redox flow battery</i>	137
EFC19086	Ashurst Steven <i>The economics of hydrogen for residential heating: An assessment of how hydrogen and fuel cell systems fare compared to other low-carbon options across Europe</i>	139
EFC19087	Ashurst Steven <i>Fuel cell micro-CHP: European market status and future outlook</i>	141
EFC19088	Facci Andrea Luigi <i>Automotive derivative energy system: modelling driven pemfc chp prototype development</i>	143
EFC19090	Crespi Elena <i>GRASSHOPPER project: grid assisting modular hydrogen PEM power plant</i>	145

AB. COD.	AUTHOR and TITLE	PAGE
EFC19091	Cecchetti Marco <i>Exploiting through-plate reference hydrogen electrode to study cross-contamination and performance in Vanadium Redox Flow Battery</i>	147
EFC19092	Montaner Ríos Gema <i>Efficient thermal management strategies for cold start of automotive pemfc systems</i>	149
EFC19093	Oh Hwanyeong <i>Fault Diagnosis for Thermal Management System of a Residential Fuel Cell System</i>	151
EFC19095	Fragiacomo Petronilla <i>Renewable hydrogen production through the integration of an soec stack with a solar parabolic collector</i>	153
EFC19096	Osifo Peter <i>Development of chitosan membrane modified with 2-aminoethanesulfonic acid and silica nano-fillers for fuel cell applications</i>	155
EFC19099	Wachel Pawel <i>Strategies For Health Monitoring And Diagnostics Of Commercial Solid Oxide Fuel Cell Systems Based on Real-Time Modelling</i>	157
EFC19100	Bisello Andrea <i>The effects of platinum oxide species on performance degradation in polymer electrolyte fuel cells</i>	159
EFC19101	Colombo Elena <i>Local degradation study of pemfc during start-up and shut-down cycling</i>	161
EFC19102	Pivac Ivan <i>Characterization of PEM Water Electrolysis Cell with Electrochemical Impedance Spectroscopy</i>	163
EFC19103	Hornés Aitor <i>3D Printing of Functional Ceramics for the Industrial Fabrication of Solid Oxide Fuel Cells (SOFCs)</i>	165
EFC19104	Gonzalez Solino Carla <i>Non-invasive glucose/oxygen fuel cell for continuous monitoring of glucose</i>	167
EFC19107	Paoletti Claudia <i>Evaluation and selection of stable metallic materials for electrolysis processes in molten salts</i>	169
EFC19108	Barelli Linda <i>Definition of efficient and extended-lifetime-oriented power management for transportation fuel cell auxiliary power unit</i>	171
EFC19109	Tsiakaras Panagiotis <i>Poison-tolerant pd on nitrogen-doped 3d hierarchical ordered mesoporous electrocatalyst for the simultaneous detection of ascorbic acid, dopamine and glucose</i>	173
EFC19110	Tsiakaras Panagiotis <i>Pd10Co1 supported on ketjen black for the simultaneous detection of dopamine, uric acid, ascorbic acid in presence of glucose</i>	175
EFC19112	Chung Moon-sun <i>The design of a solid-state hydrogen storage system</i>	177
EFC19113	Bednarek Tomasz <i>A new parallel flow field single PEM fuel cell testing hardware for high power densities examination</i>	179
EFC19115	Frangini Stefano <i>Dual atmosphere corrosion of coated and uncoated aisi 441 and crofer 22 apu ferritic stainless steels under solid oxide electrolysis conditions</i>	181
EFC19116	Ivanova Mariya E. <i>ProtOMem Project: Achievements and challenges on the way to industrially relevant planar cell design</i>	183
EFC19117	Shirvanian Paige <i>Ultra-Low Loading Catalyst Layer Development for Anode Electrode in PEM Water Electrolyzer (PEMWE) Cells</i>	185
EFC19120	Bozic Mojca <i>Enzymatic cross-linked chitosan-based anion exchange membranes</i>	187

AB. COD.	AUTHOR and TITLE	PAGE
EFC19121	Litke Anton <i>Artificial neural networks for automatic detection and classification of functional defects in multilayered solid oxide membranes</i>	189
EFC19122	Bernuy-lopez Carlos <i>Sandvik Surface Technology: Mass manufacturing of coated metal coils for the rapid development of fuel cells, electrolyzers and batteries</i>	191
EFC19123	Aßmann Pia <i>Investigation of operando accelerated stress test for MEA components of PEM fuel cells</i>	193
EFC19124	Tomadini Simone <i>Electrodes for Reversible and Symmetrical solid oxide fuel cells based on Ruddlesden-Popper perovskites</i>	195
EFC19125	Rossetti Gabriele <i>Towards stable and low-PGM fuel cell cathode with Hierarchical Nanostructured Thin Film as non-carbon support</i>	197
EFC19127	Coquoz Pierre <i>Influence of spinel protective coating on Crofer interconnects conductivity</i>	199
EFC19128	Hwang Sang Soon <i>High temperature synthesis of TiO₂ nanoparticles as a catalyst for photochemical hydrogen generation using premixed flame burners</i>	201
EFC19129	Hwang Sang Soon <i>Combustion Synthesis of Binary TiO₂-SiO₂ Nanoparticles as Photochemical Catalyst for Hydrogen Production</i>	203
EFC19130	Ucar Nihat Ozer <i>Enhance of Direct Methanol Fuel Cell Performance By Adding SBA-3 Silica Material to the Nafion Membrane</i>	205
EFC19131	Ucar Nihat Ozer <i>Design and Optimization of Carbon Nanofiber Production by Carbondioxide Electrolysis</i>	207
EFC19132	Szablowski Lukasz <i>Mathematical model of steam reforming in anode channel of molten carbonate fuel cell</i>	209
EFC19133	Panto' Fabiola <i>High-pressure water electrolysis and corresponding safety issues: the role of platinum-based recombination catalyst</i>	211
EFC19134	Cipiti Francesco <i>Model-based investigation of biomass gasification in a fluidized bed reactor</i>	213
EFC19135	Tremouli Asimina <i>Performance assessment of MFC units fed with digestate</i>	215
EFC19136	Stamatakis Emmanuel <i>Integration of Metal Hydride Hydrogen Compressors (MHC) in Hydrogen Refueling Stations (HRS): Bench-marking & Market deployment aspects</i>	217
EFC19137	D'apolito Serafina <i>Comparative analysis of BEVs and FCEVs for the future development of the sustainable mobility in Italy</i>	219
EFC19138	You Jiseon <i>Different types of real household greywater and urine used in microbial fuel cell: power generation and treatment efficiency</i>	221
EFC19139	D'apolito Serafina <i>Energy and environmental performances assessment of MFCs applied to the animal-waste slurry treatment</i>	223
EFC19140	Monforti Ferrario Andrea <i>A techno-economic analysis of on-grid solar hydrogen production by electrolysis in the North of Chile and the case of exportation from Atacama Desert to Japan</i>	225
EFC19141	Sanna Caterina <i>LSCF/GDC co-electrospun nanofiber cathodes for application in IT-SOFCs</i>	227
EFC19142	Di Micco Simona <i>From biogas to bio-hydrogen for refueling stations: analysis on the plant availability and economic evaluations</i>	229

AB. COD.	AUTHOR and TITLE	PAGE
EFC19143	Gadducci Eleonora <i>Recovery procedure for 30kw PEM fuel cell stacks</i>	231
EFC19144	Lamberti Thomas <i>Hydrogen to Boat, fuel cell and hydrogen application for sailboats</i>	233
EFC19146	Gadducci Eleonora <i>Experimental assessment of FCS for marine application</i>	235
EFC19147	D'apolito Serafina <i>Assessing the bioelectricity production in Air-cathode MFCs using different organic substrates</i>	237
EFC19148	D'apolito Serafina <i>Influence of electrodes configurations on the air-cathode MFCs performances</i>	239
EFC19149	Barbera Orazio <i>A proper and effective choice of the voltage of a fuel cell stack: a study on the correlation between the electrical parameters and geometrical shape</i>	241
EFC19151	Squadrito Gaetano <i>Reducing electrolytic hydrogen costs by oxygen co-production</i>	243
EFC19152	Low Derek <i>Diagnosis of Electrocatalyst Degradation in Polymer Electrolyte Fuel Cells Under Automotive Conditions</i>	245
EFC19154	Malek Arkadiusz <i>Optimization of energy management in a city bus powered by hydrogen fuel cells</i>	247
EFC19155	Tsiakaras Panagiotis <i>Oxygen reduction reaction on fem@ptfe/c (m=mo, v, w) core-shell electrocatalysts: the role of compressive strain effect of fem core on ptfе shells</i>	249
EFC19156	Testi Matteo <i>HyCARE: Hydrogen CArrier for Renewable Energy storage</i>	251
EFC19157	Bocci Enrico <i>First results of the H2020-LC-SC3-RES-II BLAZE project: Biomass Low cost Advanced Zero Emission small-to-medium scale integrated gasifier fuel cell combined heat and power plant</i>	253
EFC19158	Tsiakaras Panagiotis <i>Molybdenum-modified and vertex-reinforced quaternary hexapod nano-skeletons as efficient electrocatalysts for methanol oxidation and oxygen reduction reaction</i>	257
EFC19159	Hribernik Silvo <i>Design of bio-based carbonaceous fibrous structures as catalysts in fuel cells</i>	259
EFC19160	Arena Federica <i>Bioelectrochemical TiN/FDH Catalyst for CO2 Reduction to HCOOH</i>	261
EFC19161	Taccani Rodolfo <i>Comparison of different plant layout and engineering solutions for fuel cells utilization on a small ferry</i>	263
EFC19162	Giacoppo Giosue <i>Design and implementation of a new concept of photoelectrochemical cell for solar water splitting</i>	265
EFC19163	Minutillo Mariagiovanna <i>Hydrogen refueling stations based on different renewable technologies: energy and economic assessments</i>	267
EFC19164	Funez Guerra Carlos <i>Viability analysis of trains hydrogen refueling stations using electrolyzers</i>	269
EFC19165	Funez Guerra Carlos <i>Viability analysis of green methanol production plant in chile and subsequently transport to japan</i>	271
EFC19167	Di Florio Giuseppe <i>LCA analysis of a SOFC-based cogeneration system with thermal energy storage</i>	273
EFC19168	Mugikura Yoshihiro <i>Performance analysis of SOFC stacks under severe operating conditions</i>	275

AB. COD.	AUTHOR and TITLE	PAGE
EFC19170	Yuan Haibo <i>Robust Voltage Control for DC-DC Boost Converter in Proton Exchange Membrane Fuel Cell Power System</i>	277
EFC19171	Blagoeva Darina <i>Fuel cells and hydrogen technologies: critical materials and supply chain</i>	279
EFC19173	Kang Haisu <i>Nanostructures of Nafion ultrathin film on the platinum and carbon surfaces in PEMFC catalyst layer: Molecular dynamics simulation approaches</i>	281
EFC19174	Lee Seung Geol <i>Electronic Properties of Nitrogen and Sulfur Doped Graphene: Density Functional Theory Approach</i>	283
EFC19175	Lee Seungbok <i>Nano-fabrication of a high-performance LaNiO₃ cathode for solid oxide fuel cells via an electrochemical route</i>	285
EFC19176	Crema Luigi <i>CH₂P: Cogeneration of Hydrogen and Power using solid oxide-based system fed by methane rich gas</i>	287
EFC19178	Di Lorenzo Mirella <i>Design optimisation of soil microbial fuel cells for energy harvesting in remote areas</i>	289
EFC19179	Di Lorenzo Mirella <i>Investigating the use of Soil Microbial Fuel Cells for sensing</i>	291
EFC19180	Rattazzi Diego <i>Preliminary Design of innovative low emissions systems for different maritime applications</i>	293
EFC19181	Andersson Martin <i>Simulation of a novel anode supported double-sided SOFC</i>	295
EFC19182	Robert Mylène <i>Conjoint effects of chemical and mechanical stress on fuel cell PFSA membranes</i>	297
EFC19183	Vaze Mahesh <i>Pressure Gradient Method to Resolve Water Flooding in PEMFC</i>	299
EFC19184	Kravos Andraž <i>Parameter sensitivity analysis of a thermodynamically consistent electrochemical PEMFC model for virtual observers</i>	301
EFC19185	Bargiacchi Eleonora <i>Life Cycle Assessment of synthetic natural gas production from different CO₂ point sources: a Cradle-to-Gate study</i>	303
EFC19186	Roncaglia Fabrizio <i>Investigation of molding parameters on graphite/epoxy composite-based Bipolar plates</i>	305
EFC19187	Baricci Andrea <i>Experimental characterization of Polymer Electrolyte Membrane Fuel Cells with low platinum loading operated under dry gas feed</i>	307
EFC19188	Piccardo Paolo <i>Characterization of interconnects operated in stacks up to 20k hours</i>	309
EFC19189	Cavana Marco <i>Assessment of the hydrogen receiving potential of a distribution gas network using a multi-component and transient gas network model</i>	311
EFC19190	Sietmann Michael <i>Quality assurance of bipolar plates using X-Ray tomography</i>	313
EFC19191	Gaele Maria Felicia <i>The effect of different additives on KOH/ Xanthan hydrogels proposed as electrolytes for Al-air primary cells</i>	315
EFC19192	Bochentyn Beata <i>Ce_{0.8}Ln_{0.2}O_{2-δ} (Ln= Gd, Sm, La, Nd, Pr) compounds applied as effective anode catalytic layers for biogas fueled SOFCs</i>	317

AB. COD.	AUTHOR and TITLE	PAGE
EFC19193	Cooper Ross <i>A feasibility assessment of a retrofit molten carbonate fuel cell coal-fired plant for flue gas CO₂ segregation</i>	319
EFC19194	Linhart Andreas <i>Overview of the developments and results of the Design2Service project</i>	321
EFC19195	Daletou Maria <i>Development of core components for high temperature pem fuel cells</i>	323
EFC19196	Campana Roberto <i>Fabrication and characterization of a planar Solid Oxide Fuel Cell by tape casting and spraying techniques</i>	325
EFC19197	Bermúdez Agudelo María Catalina <i>Development and Investigation of a tubular HT-PEM-Fuel cell with 3D-printed anode GDL</i>	327
EFC19199	Bochentyn Beata <i>New Cu/MexOy and Cu/SrTiO₃ catalytic materials for dry reforming and synthesis of methane</i>	329
EFC19200	Michel Cassir <i>Interface reactivity of oriented or polycrystalline ALD-processed ultra thin layers for single or hybrid high temperature fuel cells</i>	331
EFC19201	Aguilar Plazaola José Agustín <i>Modelling liquid water effect on Proton-Exchange Membrane Fuel Cells</i>	333
EFC19202	Bochentyn Beata <i>Promising Ni-containing catalysts for effective conversion of CO₂ within co-electrolysis process in SOEC</i>	335
EFC19203	Lee Seung Geol <i>Effect of Ionomer Distribution upon Surface Functionalization of the Carbon Support in the Catalyst Layer: Molecular Dynamics Simulation approach</i>	337
EFC19204	Zhou Xiao-dong <i>Solid Oxide Cells for Energy Conversion and Storage: Challenges and Opportunities</i>	339
EFC19205	Buono Andrea <i>Hydrogen-bike equipped with hybrid power unit: energy performance analysis and electromagnetic emissions test</i>	341
EFC19206	Migliarese Caputi Michele Vincenzo <i>Use of hydrogen trains on non-electrified railway sections: assessment of costs and emissions and comparison with alternatives</i>	343
EFC19207	Perfetto Giuseppe <i>Energy transition by means of “bottom-up” approach: pyrosludg_en for sustainability and local development</i>	345
EFC19208	Nastro Rosa Anna <i>Re-directing microbial metabolism: bioelectrochemical systems improve CO₂ assimilation in Clostridium spp. and Cupriavidus necator</i>	349
EFC19209	Nastro Rosa Anna <i>Energy harvesting from wastewater by in-bach feeding systems</i>	351
EFC19210	Georg Siestrup <i>Development of a modularly designed standard test system for high-temperature polymer electrolyte fuel cells with hydraulic single cell compression</i>	353
EFC19212	Meyer Yann <i>Comparative Study by Design of Experiments of linear and nonlinear constitutive models and geometric parameters effects on PEMFC performances</i>	355
EFC19213	Jung Chiyong <i>An ultra-light-weight polymer electrolyte fuel cell based on 0.1 mm thick carbon fiber bipolar plate</i>	357
EFC19214	Cinti Giovanni <i>Ammonia as a fuel in sofc: technology study and system design</i>	359
EFC19215	Foglia Fabrizia <i>Advanced neutron scattering to reveal structure-dynamics correlation in membrane technology</i>	361

AB. COD.	AUTHOR and TITLE	PAGE
EFC19216	Baldinelli Arianna <i>MicroCHP in rural areas: market opportunities for Solid Oxide Fuel Cells</i>	363
EFC19218	Chinannai Muhammad Faizan <i>Analysis of performance improvement of hydrogen/bromine flow batteries by using bromate electrolyte</i>	365
EFC19219	Alam Afroz <i>Multi-dimensional transient modelling of alkaline water electrolyser</i>	367
EFC19220	Chinannai Muhammad Faizan <i>Effects of water transport on performance behaviors of hydrogen bromine redox flow batteries</i>	369
EFC19221	Lee Jaeseung <i>A transient, two-phase model of pem fuel cell - performance analysis under coolant flow variation</i>	371
EFC19222	Lee Jaeseung <i>A transient parametric study for passive air-cooled polymer electrolyte membrane (pem) fuel cell</i>	373
EFC19223	Kang Yoon Seung <i>Modeling and analysis of complex multi-hub PAFC system for heat, power and hydrogen generation</i>	375
EFC19224	Cigolotti Viviana <i>Fuel Cell and Hydrogen technologies as an effective solution for the community energy storage: ComESto project</i>	377
EFC19225	Molognoni Daniele <i>Low-cost oxygen reduction cathodes for bioelectrochemical systems: application in microbial desalination cells</i>	379
EFC19226	Buaki-Sogo Mireia <i>Enzymatic BIOelectrodes for BioSENSors and Biofuel CELLS - BIOSENCELL</i>	381
EFC19227	Aliaguilla Martí <i>Low energy desalination in Microbial Desalination Cells using new ion exchange membranes</i>	383
EFC19228	Polverino Pierpaolo <i>Advanced Model-Based aging estimation of Solid Oxide Fuel Cell stacks</i>	385
EFC19229	Polverino Pierpaolo <i>Development of a model-based algorithm for online degradation estimation of Solid Oxide Fuel Cells</i>	387
EFC19230	Frédéric Fouda-onana <i>Impact of GDL modifications on the gas transport properties and PEMFC performances</i>	389
EFC19231	Alemu Molla Asmare <i>Numerical Investigation of a Direct Ammonia Tubular Solid Oxide Fuel Cell in Comparison with Hydrogen using Different Supports</i>	391
EFC19232	Sarruf Bernardo <i>Solid Oxide Fuel Cells with Ni-Free Anodes for the direct utilization of carbonaceous fuels and special balance of plant</i>	393
EFC19233	Tucci Matteo <i>Influence of environmental factors on mfc-based sensor for wastewater monitoring</i>	395
EFC19234	Tchorek Grzegorz <i>Different Modes of the Hydrogen Value Chain - how far from LNG to liquid H2</i>	397
EFC19236	Cinti Giovanni <i>HySchools: Hydrogen in Schools</i>	399
EFC19237	Avignone Rossa Claudio <i>The assembly of the anodic microbial community in microbial fuel cells is controlled by incremental changes in the external load control</i>	401
EFC19238	Mohseninia Arezou <i>Tailored Catalyst Layer and Micro-Porous Layer Porosity and the Effect on the Performance and Water Content in PEMFC</i>	403

AB. COD.	AUTHOR and TITLE	PAGE
EFC19240	Ghanam Abdelghani <i>Copper-adapted biofilms for cu²⁺ ions monitoring with microbial fuel cell based biosensors</i>	405
EFC19241	Franzetti Andrea <i>Functional characterisation of hydrocarbon degrading microbial communities in bioelectrochemical systems</i>	407
EFC19242	Salar García María José <i>Effect of pedot-pss modified anodes on the power output by urine-fed microbial fuel cells</i>	409
EFC19243	Squadrito Gaetano <i>Testing electro-stimulation of thermotoga neapolitana metabolism</i>	411
EFC19244	Walter Xavier Alexis <i>MFCs running low-power applications without any power-management circuitry</i>	413
EFC19246	Minutillo Mariagiovanna <i>High efficiency reversible technologies in fully renewable multi-energy system</i>	415
EFC19248	Goryanin Igor <i>Long-term operation of a bio electrical systems treating distillery wastewater</i>	417
EFC19249	Milewski Jaroslaw <i>A reduced order model of proton conducting solid oxide fuel cell: a proposal</i>	419
EFC19252	Imen Elferjani <i>Modelling polymer electrolyte membrane degradation: from bipolar plates to membrane</i>	421
EFC19253	Mcp hail Stephen <i>Developing Accelerated Stress Test Protocols for Solid Oxide Fuel Cells and Electrolysers: the European project AD ASTRA</i>	423
EFC19254	Chalkidis Thomas <i>Development of a 50m³/h high purity hydrogen system and integration with an automotive derivative low temperature PEM fuel</i>	425
EFC19255	Cigolotti Viviana <i>H₂Ports - Implementing Fuel Cells and Hydrogen Technologies in Ports</i>	427
EFC19256	Mendis Arjuna <i>Adaptive Dynamic Cell Reconfiguration of Microbial Fuel Cells for Power Stability</i>	429
EFC19258	Santonocito Gaetano <i>Purity 3.0 - Energy island system in marginal areas</i>	431
EFC19260	Cristiani Pierangela <i>Terracotta and biochar derived electrodes for bioelectrochemical systems</i>	433
EFC19263	Di Giorgio Paolo <i>Hybrid energy storage system for a plug-in fuel cell electric scooter</i>	435
EFC19264	Di Trolio Pasquale <i>Fully integrated power system for lightweight plug-in fuel cell electric vehicles</i>	437



EUROPEAN FUEL CELL

CONFERENCE & EXHIBITION

NAPLES Hotel Royal Continental

9 > 11 December, 2019

TOPICS

TRANSPORT: New materials and catalysts / Modelling from molecular to system scale / Stacks, cells and component manufacture and testing / Diagnostics and Process control, system engineering, hybridization / Market and Deployment, demonstration and real-world experience

INFRASTRUCTURES: New materials and composites / Modelling from molecular to system scale / Tanks, valves and component manufacture and testing / Diagnostics and Process control, system engineering, hybridization / Market and Deployment, demonstration and real-world experience / Hydrogen safety

ENERGY STORAGE: New materials and catalysts / Modelling from molecular to system scale / Stacks, cells and component manufacture and testing / Diagnostics and Process control, system engineering, hybridization / Market and Deployment, demonstration and real-world experience

ENERGY GENERATION: New materials and catalysts / Modelling from molecular to system scale / Stacks, cells and component manufacture and testing / Diagnostics and Process control, system engineering, hybridization / Market and Deployment, demonstration and real-world experience

MICROBIAL & ENZYMATIC BIOELECTROCHEMICAL SYSTEMS: Energy harvesting / Biofuel production (biohydrogen and biomethane) and other valuable products (including electrosynthesis, electrolysis and desalination processes) / Bioremediation / Resource recovery / Biophotovoltaics / Biosensors / Wearable and implantable technologies

CROSS-CUTTING AND OVERARCHING: Roadmaps, strategy, national plans / Applications in Developing Countries / Market studies and LCA / Hydrogen valleys / Education and training / Public Awareness and Acceptance / Legal and administrative practice / Regulation, Codes and Standards (RCS) / Safety

Special session dedicated to:

Poster Session - Dissemination of European project on Fuel Cell and Hydrogen Authors and presenters are invited to present European project on Fuel Cell and Hydrogen and their result

presented at: European Fuel Cell 2019 / Piero Lunghi Conference & Exhibition
December 9-11, 2019 / Naples, Italy



ATENA
FUTURE TECHNOLOGY



UNIVERSITÀ
DEGLI STUDI
DI NAPOLI
"PARTHENOPE"



UNIVERSITÀ
DEGLI STUDI
DI PERUGIA



SUPPORTING INSTITUTIONS



MAIN SPONSOR



SPONSORS



EXHIBITORS



SUPPORTED BY

